

11/1/79
11/1/79

Environmental Assessment of the Alaskan Continental Shelf

Final Reports of Principal Investigators

Volume 2. Physical Science Studies

Outer Continental Shelf Environmental Assessment Program
Boulder, Colorado

DECEMBER 1979



U.S. DEPARTMENT OF COMMERCE
National Oceanic and Atmospheric Administration



U.S. DEPARTMENT OF INTERIOR
Bureau of Land Management

Environmental Assessment of the Alaskan Continental Shelf

Final Reports of Principal Investigators

Volume 2. Physical Science Studies

Outer Continental Shelf Environmental Assessment Program
Boulder, Colorado 80303

DECEMBER 1979



U.S. DEPARTMENT OF COMMERCE

National Oceanic and Atmospheric Administration

The facts, conclusions and issues appearing in these reports are based on interim results of an Alaskan environmental studies program managed by the Outer Continental Shelf Environmental Assessment Program (OCSEAP) of the National Oceanic and Atmospheric Administration (NOAA), U.S. Department of Commerce, and primarily funded by the Bureau of Land Management (BLM), U.S. Department of Interior, through interagency agreement.

DISCLAIMER

Mention of a commercial company or product does not constitute an endorsement by National Oceanic and Atmospheric Administration. Use for publicity or advertising purposes of information from this publication concerning proprietary products or the tests of such products is not authorized.

CONTENTS

RU #	INVESTIGATOR(S)	AGENCY	TITLE	PAGE
59	Miles O. Hayes C.H. Ruby	U. of South Carolina, Columbia, SC	Oil Spill Vulnerability, Coastal Morphology, and Sedimentation of the Kodiak Archipelago	1
98	Roger Colony	Polar Science Ctr. U. of Washington, Seattle, WA	Dynamics of Near Shore Ice	156
206	J.V. Gardner T.L. Vallier et al.	U.S. Geological Survey, Menlo Park, CA	Sedimentology and Geo- chemistry of Surface Sediments and the Dis- tribution of Faults and Potentially Unstable Sediments, St. George Basin Region of the Outer Continental Shelf, Southern Bering Sea	181
244	R.G. Barry	Inst. of Arctic & Alpine Res., U. of Colorado, Boulder, CO	Study of Climatic Effects on Fast Ice Extent and Its Seasonal Decay along the Beaufort-Chukchi Coasts	272
257	William J. Stringer	Geophysical Inst., U. of Alaska, Fairbanks, AK	Morphology of Beaufort, Chukchi and Bering Seas Nearshore Ice Conditions by Means of Satellite and Aerial Remote Sensing.	376
431	A.H. Sallenger, Jr. J.R. Dingler	U.S. Geological Survey, Menlo Park, CA	Coastal Processes and Morphology of the Bering Sea Coast of Alaska	377
436	R. Schlueter	Dames & Moore Los Angeles, CA	Oil Spill Trajectory Analysis, Lower Cook Inlet, Alaska	442

FINAL REPORT
Research Unit - 59

Task D-4

OIL SPILL VULNERABILITY, COASTAL MORPHOLOGY, AND SEDIMENTATION
OF THE KODIAK ARCHIPELAGO

Co-principal investigators: Miles O. Hayes
Christopher H. Ruby

Coastal Research Division
Department of Geology
University of South Carolina
Columbia, S.C. 29208

Submitted: July 10, 1979

- I. Abstract - This report contains our Oil Spill Vulnerability Index, as it applies to the Kodiak Archipelago. Included under separate cover with this text is a set of 47 standard U.S.G.S. Quadrangle Maps with the color coded OSVI. Each of the maps also shows the position of the 127 sample and profile sites established in the study area, as well as longshore sediment transport direction arrows. A complete set of Appendices follows the body of the report. Data from these Appendices is available in total from the NODC. This is our Final Report for Kodiak.
- II. Task Objectives - The major emphasis of this project falls under Task D-4 which is to: evaluate present rates of change in coastal morphology, with particular emphasis on rates and patterns of man-induced changes, and locate areas where coastal morphology is likely to be changed by man's activities, if any. The relative susceptibility of different coastal areas will be evaluated, especially with regard to potential oil spill impacts.
- III. Field and Laboratory Activities - Included in the body of this report.
- IV. Results - The results have been summarized in the text and appendices of this report as well as on the set of basemaps being sent under separate cover.
- V. Preliminary Interpretations - Does not apply.
- VI. Auxiliary Material - Set of 47 U.S.G.S. Quadrangle Maps with the color coded Oil Spill Vulnerability Index and station locations.
- VII. Problems Encountered - None.

TABLE OF CONTENTS

Table of Contents.....
List of Figures.....
Geomorphic Setting.....
Island Arc System.....
Geologic Setting.....
Lithologies.....
Shuyak Formation.....
Kodiak Island Schist Terrane.....
Uyak Complex.....
Kodiak Formation.....
Ghost Formation, Sitkalidak Formation & Narrow Cape Formation.....
Oceanographic and Meteorologic Setting.....
Tides.....
Meteorology.....
Oceanography.....
Sedimentology.....
Coastal Morphology.....
Profile Site Analysis.....
Beach Sediments.....
Oil Spill Vulnerability.....
Introduction.....
Cold Water Spills.....
Environmental Vulnerability to Oil Spills.....
Oil Spill Vulnerability Scale.....
Rocky headlands.....
Wave-cut platforms.....
Fine-grained sandy beaches.....
Medium-coarse grained sandy beaches.....
Exposed tidal flats.....
Sand and gravel beaches.....
Gravel beaches.....
Sheltered rocky headlands.....
Protected estuarine tidal flats.....
Protected estuarine salt marshes.....
Applications to Kodiak Archipelago.....
References.....

Appendix 1.....
Appendix 2.....
Appendix 3.....
Appendix 4.....

LIST OF FIGURES

1. Study area location.....
2. Geologic cross section of Kodiak.....
3. Geologic map of Kodiak.....
4. Wind frequency and wave energy flux.....
5. Coastal Morphology - Sandy pocket beach.....
6. Coastal Morphology - High bedrock headland.....
7. Coastal Morphology - High bedrock headland & gravel beach.....
8. Coastal Morphology - Fjord head system.....
9. Coastal Morphology - Low sheltered rock headland.....
10. Coastal Morphology - Low sheltered rock headland.....
11. Coastal Morphology - Moderate energy gravel beach.....
12. Coastal Morphology - Fan delta.....
13. Profile Analysis - Profile KDP-73, Coarse grained cusped spit.....
14. Profile Analysis - Profile KDP-63, Coarse grained transgressive washover.....
15. Profile Analysis - Profile KDP-115, Fine gravel tombolo.....
16. Profile Analysis - Profile KDP-27, Moderate energy rock scarp.....
17. Profile Analysis - Profile KDP-81, Bedrock platform.....
18. Profile Analysis - Profile KDP-89, Gravel cusped spit.....
19. Profile Analysis - Profile KDP-29, Moderate energy pocket beach.....
20. Profile Analysis - Profile KDP-35, Low energy gravel beach.....
21. Profile Analysis - Profile KDP-67, Sand and gravel beach.....
22. Profile Analysis - Profile KDP-31, Low energy rock scarps.....
23. Profile Analysis - Profile KDP-1, Low energy sand and gravel beach.....
24. Grain Size Analysis - Mud flat.....
25. Grain Size Analysis - Sand beach.....
26. Grain Size Analysis - Well sorted fine gravel.....
27. Grain Size Analysis - Well sorted boulders and cobbles.....
28. Grain Size Analysis - Immature boulders.....
29. Grain Size Analysis - Sand and gravel.....
30. Grain Size Analysis - Immature boulders and gravel.....
31. Grain Size Analysis - Mature boulders.....
32. Grain Size Analysis - Immature gravel and granules.....

LIST OF TABLES

1. Coastal classification.....
2. Chemical and physical degradation of residual oils.....
3. Oil spill vulnerability.....

GEOMORPHIC SETTING

Kodiak Island is a mountaneous island in the western Gulf of Alaska covering an area of approximately 25000 sq km (Fig. 1). Composed of igneous and metasedimentary rocks derived from uplifted subduction zone complexes, the mountains are very rugged in character. Trending in a northeast-southwest direction, the Kodiak mountains have maximum elevations of 600-1200 m. During the Pleistocene, the mountains were very heavily glaciated. The area differs from one side of the island to the other, these differences are a function of differing geologic controls.

The northwest side shows dramatically the effects of glaciation. Long narrow fjords and U-shaped valleys predominate. Trending in a northwest-southeast direction, the valleys lie perpendicular to the axial trend of the mountains. Shorelines are straight, having narrow gravel beaches butted against steep valley walls. On the sides of the valley walls are elevated kame terraces formed during the last period of glaciation. At present there is no active glaciation occurring on the islands.

The southwest corner of Kodiak Island and all of Tugidak Island have a morphology somewhat different. Although still controlled by glaciation, the flatter topography reflects a continental form of glaciation rather than the valley glaciation of the NW. Deposits of glacial till blanket the entire area with thick deposits in the valleys and thin deposits on the ridges. The shorelines are generally long and continuous with a few crenulate bays eroding back into the glacial till. The till outcrops in a 15 m scarp along much of the coast and contributes large erratics as well as sand and gravel to the beach sediments.

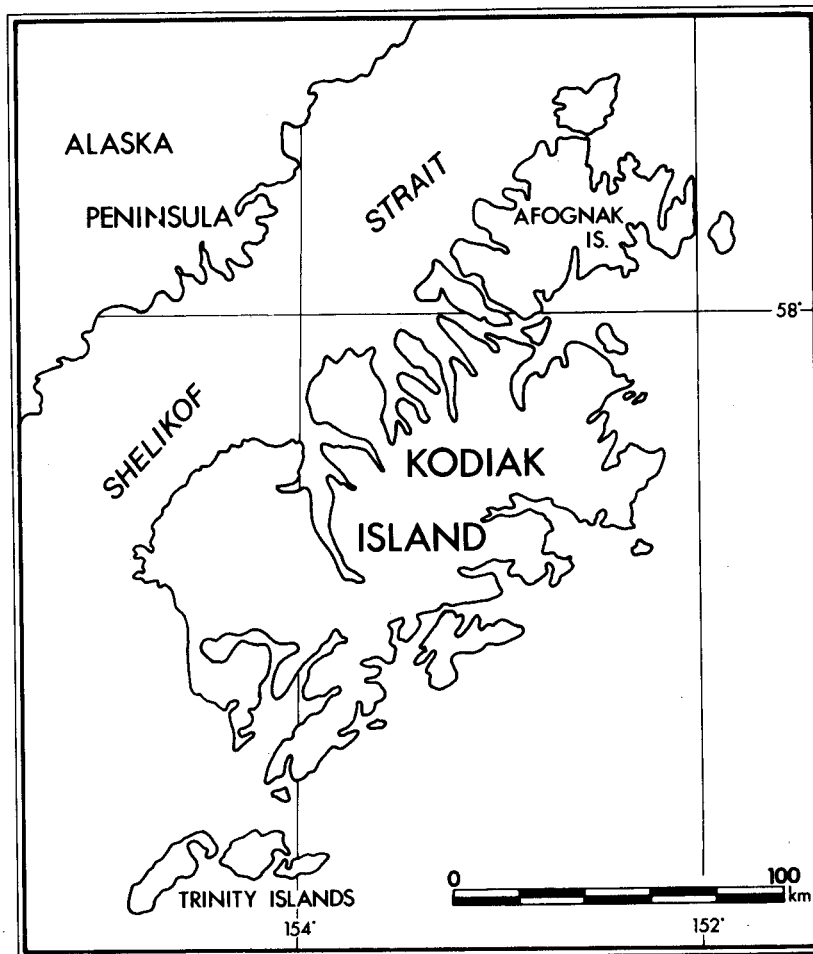
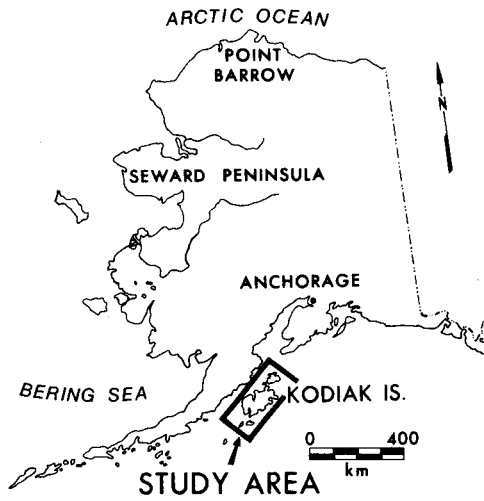


Figure 1. The study area includes all of the marine shoreline of Kodiak, Afognak and the Trinity Islands. It encompasses about 4300 shoreline kilometers (see Appendix 3 for breakdown).

The southeast side of the island is characterized by short wide estuary type embayments. The trend of most of these embayments is northeast-southwest running parallel with the major thrust faults on the island. They appear to be rift valleys or down dropped blocks formed when subduction complexes are thrust up over the existing rocks, (Fig. 2).

Afognak Island is somewhat similar to the southeast side of Kodiak. Smaller pocket beaches predominate where wave energy has eroded back into less resistant units of a wacke-shale interbedded subduction complex. The topography is less rugged than Kodiak and consists of hilly lowlands.

Drainage patterns on the islands tend to be short straight streams running northwest or southeast from a divide that trends northeast-southwest along the Kodiak Batholith. All the streams debouch into the heads of the fjords or small embayments. A few lakes occupy alpine valleys on the southwest side of the island. In addition, a few small ponds associated with drainage streams are found in the glacially scoured topography.

Island Arc System

The theory of plate tectonics has been able to explain a wide variety of large scale geographic forms on our planet. Southwestern Alaska is a dynamic area where plate tectonics plays a major role in the general formation of the physiography.

Using the geophysical classification of coasts in terms of plate tectonics (Inman & Nordstrom, 1971; Davies, 1973), Kodiak Alaska would be classified an island arc collision coast where relatively thin dense oceanic crust is being thrust under a less dense continental plate. A long linear subduction zone results and parallels an island arc system with andesitic island volcanoes. Major thrust fault systems trend parallel with the island arc system and exert a strong control on local morphology.

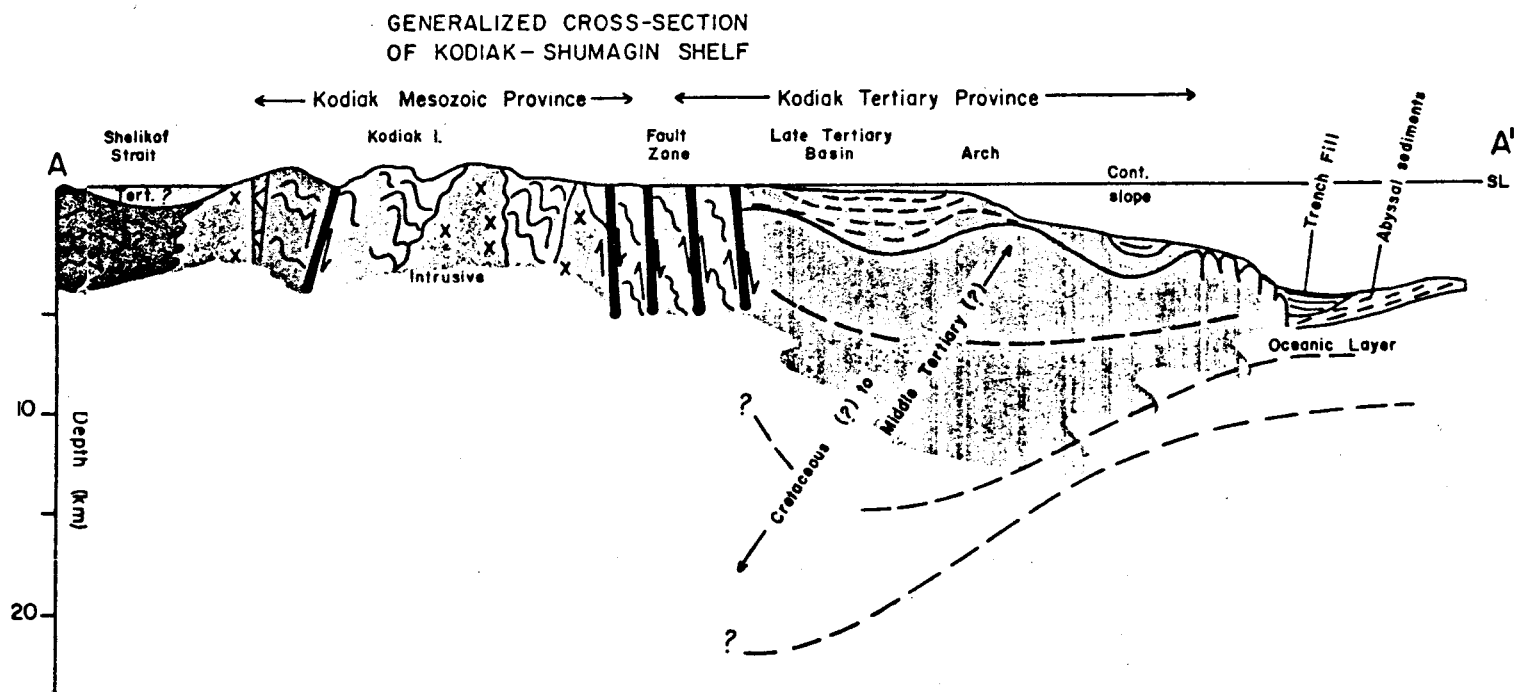


Figure 2. Generalized Cross-Section of Kodiak Island taken from Alaska Regional Profiles: South Central Region (1974). See Figure 3 for Cross-Section A-A'.

Island arc systems are highly active tectonically and are by far the major loci of world seismic activity. Coastlines along island arcs are typically straight with high rugged cliffs and narrow continental shelves. Deep earthquakes centered around the trench are instrumental in causing catastrophic changes to coastal shorelines. Stanley (1968) described those changes created by the 1964 Good Friday Earthquake and illustrated the effects of submergence and uplift on coastal morphology. On the island of Kodiak, an axial line running south from Narrow Cape of Sitkalidak Island to the west of Sitkidak Island separates a zone of submergence from a zone of uplift. Submergence occurred to the northwest of the axial line. Increasing in a northerly direction, a maximum of 2 m of submergence occurred on the northeast corner of Kodiak. Uplift occurred to the southwest of the axial line with maximum uplift of 1 m occurring at Narrow Cape. Plafker and Kachadoorian (1966) described in detail other geologic effects created by the Good Friday Earthquake. In addition to vertical displacements, landslides and tidal waves created noticeable changes on the coastal shorelines on Kodiak.

Thus, today, 15 years after the earthquake, there are very numerous geomorphic indicators still present on the shorelines. Some of the indicators of downwarp are 1) wave cut notches into bedrock scarps backing narrow intertidal beaches of gravels and cobbles on a bedrock platform, 2) dead tree lines on narrow spits and along low scarps into bedrock or unconsolidated material, 3) washover fans of unconsolidated sediments backing highly vegetated spits and beach ridge pocket beaches, 4) bedrock platforms which are never exposed at low tide. Indicators of uplift are 1) highly vegetated storm berms, now above the "reach" of storms, 2) infilled lagoons, 3) cut off inlets, sometimes with lakes

occupying abandoned lagoon channels, 4) elevated bedrock platforms, often with barnacle or mussel covered boulders above the normal tidal range, 5) dead and vegetated scarps sometimes found with beach ridges fronting them, 6) multiple swash lines of storm debris, 7) deeply incised river channels at delta mouths at the heads of fjords. These and many more indicators of the Good Friday Earthquake are found in the Kodiak Archipelago.

Kodiak has undergone tectonic change (primarily uplift) for millions of years. Thus we find on the island broad areas of wave-cut platforms sometimes over 300 m above the present sea level. Often times these areas will have a terraced or stair-stepped appearance, with each terrace indicating a relict stillstand of the island with respect to sea level. It is clear that tectonics plays a major role in the formation and modification of the island shorelines both in the long term geologic sense and on a much shorter historical time scale.

Today we find an island dominated by the tectonic uplift which pushed it out of the sea, and modified by periods of glaciation which are responsible for the second order features on the islands. The valley glaciers formed the fjords and sculpted the mountains into their present form. They also left behind vast amounts of semiconsolidated and unconsolidated materials which play a major role in the formation of the beaches. Where glacial outwash or till is present backing the coast, these deposits act as a sediment supplier to the shoreline. The beaches tend to be wide and generally flatter than in sediment starved areas. Beach sediments range from sand to gravel and boulders generally, dependent on the original make-up of the glacial deposit and the wave energy at the beachface. The only other broad depositional beaches on the island are associated with the fjord head rivers and rivers draining glacial deposits. At the fjord heads,

deltas dominated by tides are common. These areas are characterized by fan deltas of sand and fine gravel with highly developed bifurcating river channels and bars. Where rivers drain glacial deposits and empty onto the open coast, sand and gravel beaches occur downdrift. Sometimes, cusped deltas and spits are developed. Thus, glaciation plays a very major role as a general modifier of regional topography and a sediment supplier to the rivers and shorelines.

The third order features of the island are those associated with marine modification. These features are the subject of this report.

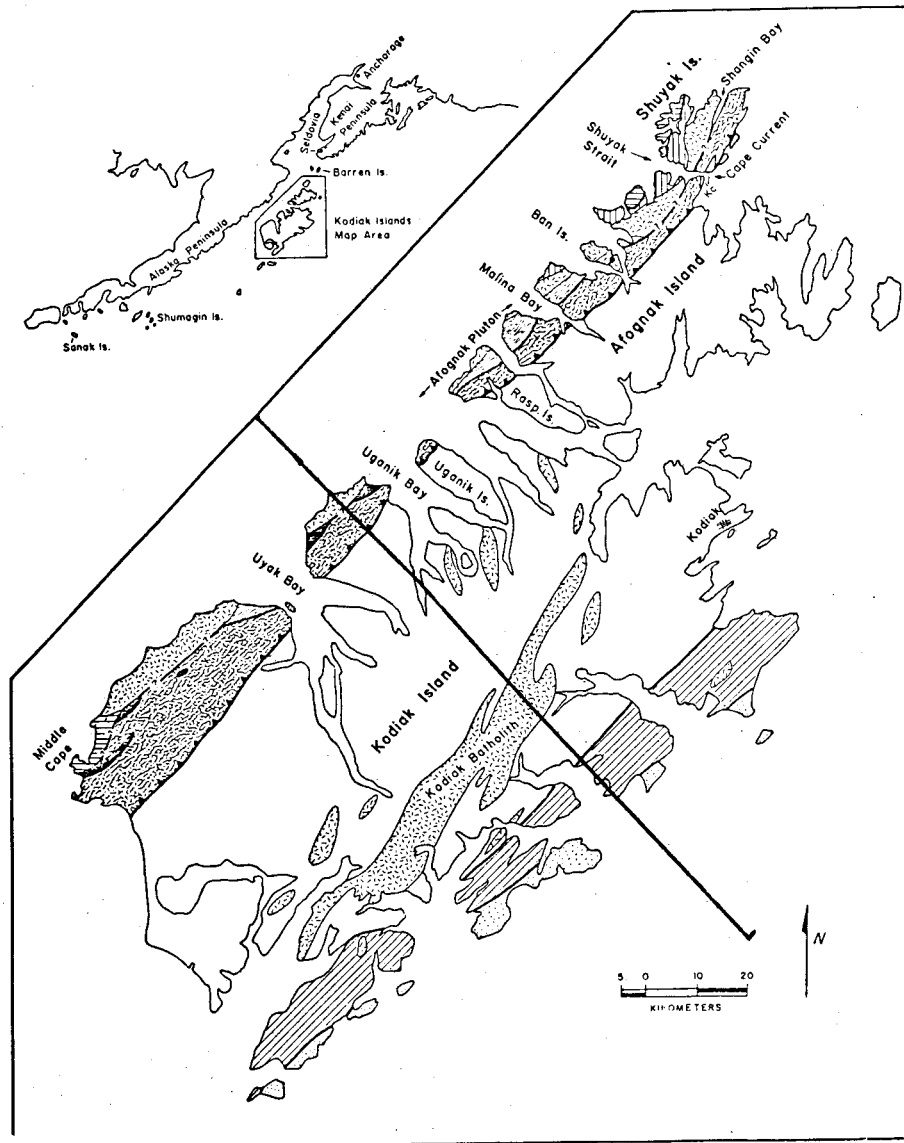
GEOLOGIC SETTING

Kodiak and surrounding islands in the southwestern Gulf of Alaska constitute a Cretaceous subduction complex within a tectonically active plate margin. Located at the southern most margin of the continuous Kodiak-Kenai-Chugach mountain belt, Kodiak Island is composed of highly deformed and uplifted marine sediments and ultramafic rocks. The Uganik thrust marks the boundary between a younger belt of deep sea rocks seaward and an older belt landward showing the accretion that continues today within the Aleutian trench (Burk, 1965; Plafker, 1972; Connelly, 1978; Moore, 1978). Seven major lithologic units occur on Kodiak Island, (Fig. 3).

Lithologies

Shuyak Formation

The oldest rocks are found on the northwest side of Afognak and Shuyak Islands. Composed of pillowed greenstones and volcanoclastic turbidites, they form the upper Triassic Shuyak Formation (Connelly, 1978). The pillowed



EXPLANATION

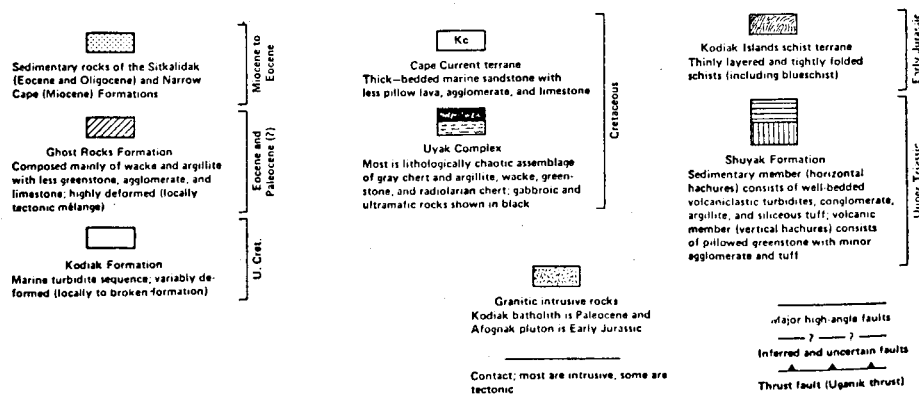


Figure 3. Generalized geologic map of Kodiak Islands; after Connelly and Moore (1977), Moore (1967), and Capps (1937).

greenstones have been interpreted by Jakes and Gill (1970) and by Connelly (1978) to be an island arc basalt formed at the early stages of volcanism. The upper sedimentary member consists of bedded turbidites with complete Bouma sequences indicating deposition by density currents at the seaward margin of the early arc basin (Connelly, 1978).

Kodiak Island Schist Terrane

To the southeast of and structurally beneath the Shuyak Formation lies the early Jurassic, Kodiak Island Schist Terrane. Consisting of quartz mica schists, greenschists, epidote schists and epidote amphibolites, the rocks are thinly layered and highly folded (Carden, et.al., 1977). Carden (1977) believes the schists were formed under extremely high pressures and temperatures as part of a subduction complex altered slightly to intensely by the intrusion of the Afognak pluton. The long narrow pluton is early Jurassic in age and is composed of foliated diorites and quartz diorites with abundant hornblende and little or no biotite (Connelly, 1978).

Uyak Complex

To the southeast of and structurally beneath the Kodiak Island Schist Terrance, the Uyak complex comes in contact along the Raspberry Fault (Moore, G.W., 1969). Connelly (1978) has modified the formerly Uyak formation to be called the Uyak Complex because of the complicated and disorderly assemblage of rocks within the unit. The complex is Cretaceous in age and consists mainly of gray and radiolarian cherts, wackes, greenstones and ultramafic rocks. A sedimentation model of this unit has been proposed by Connelly (1978) and described as being oceanic crust, subducted then uplifted.

The ultramafic rocks consist of gabbros, clinoproxinite, dunites and plagioclase peridotite. They constitute 6% of the unit. Hill (1975) has interpreted these rocks as being fragmented oceanic crusts, fractures at the subduction zone then uplifted with the overlying rocks.

Radiolarian cherts are found in small bedded tectonic blocks scattered throughout the unit. They are red in color, very homogeneous, and thinly bedded. The cherts amount to 2% of the unit. They have been interpreted as being a redeposition of radiolaria on the flanks of the mid-ocean rise by turbidity currents (Matthews, 1971; Nisbet & Pierce, 1974).

The gray cherts, thinly interbedded with deep sea sediments, account for 45% of the Uyak complex. Deposited above the radiolarian chert, they are believed to be the opalene skeletal remains of microplankton deposited as deep sea sediments (Wise & Weaver, 1974). The gray chert along with the radiolarian cherts are fractured and have been uplifted with the oceanic crust at the subduction zone.

Massive units of wacke are found within the Uyak complex. Connelly theorized that the wackes were derived from an arc-derived adesitic source, mixed with recycled cherts and then deposited as a normal trench turbidite sequence. The entire Uyak sequence was then underthrust and uplifted along the Uganik thrust fault by the Kodiak formation (Copps, 1937; Moore, G.W., 1969).

Kodiak Formation

The Kodiak Formation is the principle unit on Kodiak, underlying approximately 60% of the islands. It consists of arkosic wackes interbedded with shales and scattered pebbly conglomerates (Moore, G.W., 1969). The rocks

comprise a widespread turbidite sequence accreted at the continental margin (Clark, 1972; Moore, 1973; Budnick, 1974; Nelson & Bouma, 1977). The formation has been interpreted as a typical trench and deep sea sequence deposited during the late Cretaceous subduction (Plafker, 1972; Moore, 1973a; Moore, 1973b; Jones & Clark, 1973; Budnik, 1974).

Ghost Formation, Sitkalidak Formation & Narrow Cape Formation

Minor outcrops underlie the southeastern margin of Kodiak and make up the youngest rocks on the island. Predominately wackes and argillites they make up another subduction complex (Moore, G.W., 1969) that grades into younger sediments seaward of Kodiak. This gradation change indicates a continued accretion up to Holocene time (von Huene, 1972).

The rock type backing a section of shoreline can play a major role with regard to the shape of the beachface and the shape and quantity of sediments available to form beaches.

Highly bedded rock types like slates and shales can form a variety of scarp configurations, dependent on the dip of the bedding planes. Where bedding planes are nearly horizontal, the scarps will be very irregular and wave cut platforms will be quite flat and uniform. If the bedding planes are near vertical, the scarps will be uniform and wall-like, broken and displaced by fracture and fault patterns, while associated wave-cut platforms will be very irregular containing numerous tidal pools. Bedding planes dipping from near vertical to about 50 or 60° will often result in a dip-slope scarp. These scarps are flat and slope downward at the angle to dip of the bedding. Dips from 50° to about 20° will usually result in an irregular scarp and an irregular wave cut platform.

Bedded rock types yield platy fragments to the beachface. Thus gravels, cobbles and boulders will generally be flat regardless of their degree of rounding. Very well rounded gravels will look like discs and are referred to as discoidal gravels.

Unbedded rock species like quartz diorite have a more uniform strength and thus the shape of scarps and wave cut platforms becomes a function of fracture and fault patterns in the rock rather than their own internal structure. The scarps usually appear rather massive and rather steep. The wave cut platforms at their base are moderately uniform with undulatory surfaces and scattered tidal pools.

Gravels and boulders of this rock type will usually be equant in shape regardless of the degree of rounding. Well rounded gravels will be spherical.

The slate and quartz diorite are two end members of rock species control of scarp and platform shapes as well as gravel shapes. Most other rock types will fall, behaviorally, somewhere between them. Thus, scarps, platforms and beach sediment can take an extremely wide variety of shapes.

OCEANOGRAPHIC AND METEOROLOGIC SETTING

Tides

Mean tidal range, recorded in the Climatic Atlas of the Outer Continental Shelf Waters and Coastal Regions of Alaska, Volume 1 (1977), is variable along the Kodiak and Afognak coastline. Diurnal range, or the average difference in height between mean higher high water and mean lower low water in feet on a single day ranges from 7.5 at Sitkinak Lagoon on the southwestern coastline of Kodiak Island to 13.7 at Redfox Bay located on northeast Afognak Island. The harbor at Kodiak has a diurnal range of 8.5 feet; while Larson Bay, a small

fjord adjacent to Uyak Bay on the north side of Kodiak Island shows a tidal range of 13.7 feet. It is apparent from this data and field observation that tidal range increases from southwestern Kodiak Island to northeastern Afognak Island. Tidal range further increases in a northeasterly direction into Cook Inlet where funneling of the tidal wave contributes to an amplification of the tidal range. Seldovia on the Kenai Peninsula exhibits a tidal range of 17.8 feet while Anchorage in upper Cook Inlet has 29.0 foot diurnal range (Fig. 1).

Kodiak Island has a large number of fjords, especially along the northern shoreline. These fjords formed during the Pleistocene by valley glaciers over-deepening and widening pre-existing river valleys. Usually, fjords have well developed terminal moraines which lie submerged at the fjord mouth (Dyer, 1973). However, the fjords on Kodiak are generally unrestricted, the moraine deposits are either absent or lie submerged deep enough to permit easy passage of the tidal waves. In general, there is a free exchange of water with the seas. The funnel shape of the fjords along with their lack of restriction to flow provides an amplification of the tidal range. Thus, Larson Bay shows the 13.7 foot tidal range which is unusually large for that section of Kodiak Island. Many of the fjord heads contain well developed delta-marsh systems which appear to be tide dominated.

Meteorology

Weather conditions in the Kodiak Archipelago are regulated by the maritime environment of the southwestern Gulf of Alaska. Winter temperatures range between 26° and 45° F. Precipitation is heavy with 47" of rain and 71" of snow annually, but varies locally. Considerably more precipitation occurs on the eastern side of the island.

Wind and wave data taken from the Survey of Synoptic Meteorological Observations (1970) and the Climatic Atlas of the Outer Continental Shelf Waters and Coastal Regions of Alaska, Volume 1 (1977) indicate a prevailing and predominant northwesterly and westerly wind frequency, wind velocity, and associated wave energy flux (Fig. 4). The average wind direction is from the northwest at five knots. A counterclockwise flow associated with low pressure cells in the Gulf of Alaska during winter storms causes this prevailing and predominant wind and wave setup for Kodiak Island. During the summer months the major storm track is to the west of Kodiak Island, hence strong and frequent easterly winds are common. During January, 53% of the winds arrive from the west and northwest. During July, 38% of the wind is from the east and northeast, while only 25% is from the northwest and west. Thus wind velocities and directions and associated wave height and approach directions vary on a seasonal basis.

Kodiak Island weather observations show wind speeds greater than 22 knots 32% of the time in January as compared to 10% during July. 15% of the measured waves approaching Kodiak and Afognak Island during January are greater than 4 meters; while only 2% of the July waves are greater than 4 meters. Wave period is longer during January with 23% of the waves 7 seconds or longer. July waves are much shorter with only 6% greater than 7 seconds. These figures demonstrate a definite winter storm condition.

Oceanography

Ocean bathymetry rapidly deepens off the coastline within both the Gulf of Alaska the Shelikof Strait and the Island's numerous fjords and estuaries. Depths of 120 to 300 m are common within one kilometer of the shoreline. There is tremendous variability in relative wave energy from one area in the Kodiak Archipelago

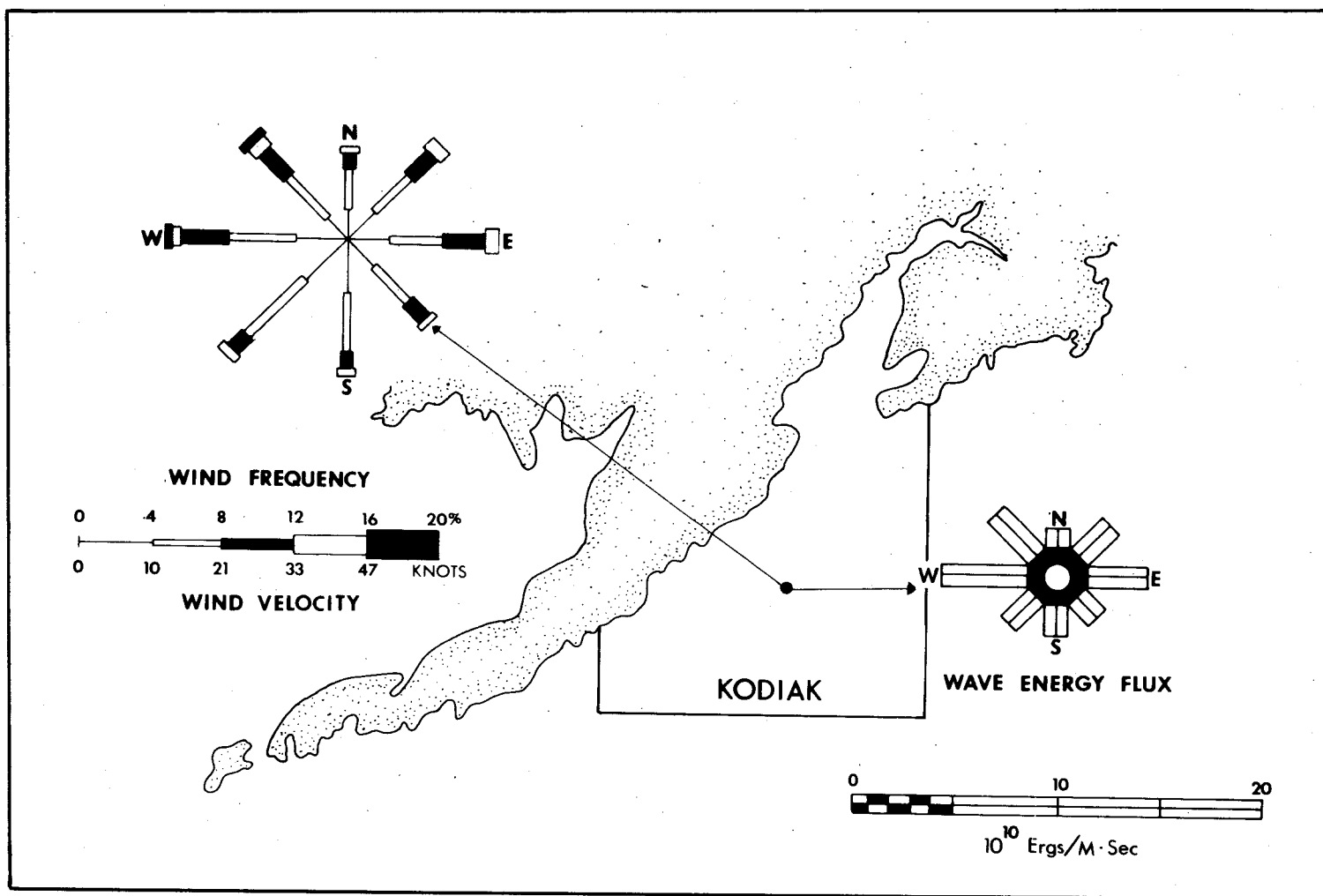


Figure 4. Wind and wave data taken from the Survey of Synoptic Meteorological Observations (1970). Note the predominance of the westerly and northwesterly wind and resultant wave energy flux.

to another. This is due to the variable fetch distance as well as the orientation of the shoreline with respect to incoming waves. As seen in Figure 4, predominant wind and resultant wave energy flux is from the northwest. However, the Shelikof Strait, which abuts the western side of Kodiak, is only 60 km wide. The narrowness of the Strait limits the maximum wave size which can be generated by a given wind velocity. For example, a 40 kt. wind blowing for two days across the Strait, will generate a maximum wave of 7 second period and 10 ft. height. If the same wind blows for two days across a 1000 mile wide section of the Gulf of Alaska, it will generate a wave of 12 second period and 30 ft. wave height, (Coastal Engineering Research Center, Shore Protection Manual, Vol. I). Thus, it is apparent that even though higher overall wind velocities are greater from the west, larger waves can be generated from the east due to the much greater fetch distance. By far the largest waves occur along the shorelines on the eastern side of the islands.

Many of the fjords tend to generate local wind systems, especially near their heads. They are usually backed by relatively high mountains which can generate catabatic winds which blow down slope toward the mouth of the fjord. In some of the inner parts of fjords, midbay spits and cusped spits indicate transport out of the bays as a result of these wind systems. In general, there is a uniform decrease in wave energy as the fjord heads are approached. The fjords have wave energies only a fraction as large as the wave energies on either the exposed east or western shorelines. The exposed shorelines usually have well developed high storm berms indicative of frequent large storms whereas the more protected fjords have much lower generally vegetated storm berms, indicative of milder very infrequent storms. The heads of the fjords as well as the very numerous protected areas on Afognak Island have exceptionally low wave energy.

SEDIMENTOLOGY

Tectonic activity has had a profound effect on the sedimentology and coastal geomorphology of Kodiak and Afognak Islands. Most of both islands show evidence of downwarping such as erosional scarps, washovers and drowned forests. Although the shoreline of the study area is predominantly erosional, depositional features such as tombolos, spits, beach ridge plains, mid bay bars and crenulate bays do occur. Salt marshes and tidal flats are found rarely, usually at the fjord heads. The absence of these features is related to the generally steep nearshore topographic slope and a lack of fine grained sediments (silts and clays). There is also considerable evidence of uplift in the form of raised beaches, vegetated storm berms, wave cut platforms well above sea level and incised river channels. Uplift features are especially evident along the southern and southeastern shoreline of the islands.

The last glaciation during the Pleistocene has played a major role in shaping both the coastal geomorphology and the sedimentology of Kodiak beaches. Beaches within much of the western half of Kodiak Island, northern coast of Afognak Island, and the Trinity Islands are backed by scarps into glacial till. A coarse-grained beach material with a complex composition is supplied by the glacial deposits. The eastern beaches of Kodiak Island and most of Afognak Island are backed by more homogeneous bedrock outcrops. Composition of beach sediment within these areas is highly homogeneous and very coarse grained due to the supply by local bedrock. The shape of the western beach cobbles and pebbles is mostly bladed to equant with very good rounding. Their well rounded character is the result of both the glacial abrasion and later reworking by marine processes. They are more mature than gravels and cobbles fronting bedrock

scarps. Gravel composition of schist and slate on the central and eastern shorelines results in a bladed to disc shape with fair to good rounding.

Most of the beaches along the coastline of both islands are very coarse grained ranging from cobbles and gravel to granules and coarse sand. A predominance of sandy beaches appear on the western coast of Kodiak Island and within the Trinity Islands due to an abundance of unconsolidated glacial material with a high percentage of sand. Thus on Tugidak Island, a till and outwash sediment source and a shallow shelf has resulted in the development of a very long recurved spit complex.

Overall mean grain size (see Appendix 1 for Kodiak and Afognak Island beach samples) generally ranges between 0.0ϕ (very coarse sand) and -3.5ϕ (pebbles). With a mix of large grain sizes and sand, sorting is relatively poor. Standard deviations of 2ϕ or greater are common. The very coarse material is supplied by glacial deposits as well as bedrock scarps and this results in the poor sorting of the sediments.

Beach material in southwest Kodiak Island and the nearby Trinity Islands is relatively fine. Tugidak Island, the westernmost Trinity Island is composed of 2.2ϕ fine sand to -0.2ϕ very coarse sand. Again, this grain size is a function of the size of the material supplied by the glacial deposits. The more distal glacial deposits (outwashes) are finer grained and more uniform than the proximal deposits (moraines and tills) and thus yield a finer grained beach material.

The beaches within the fjords are quite variable, but tend to be quite coarse due to their local bedrock sediment sources. However, at the fiord heads, rivers often introduce a fine sediment suite ranging from clays to granules. Sand size at the head of Terror Bay is 1.37ϕ .

Long term transport directions can sometimes be determined by a close analysis of grain size. In general, there is an expected fining trend away from sediment source in the direction of dominant transport. However, Kodiak Island shorelines are so complex and the sediment sources are so variable that no clear trends have been noted in this study. Grain size and sorting is primarily a function of the local geology and wave energy. Transport directions were determined by analysis of local coastal morphologic features such as spits, crenulate beaches, cusped forelands, tombolos, ridge and runnel systems and natural grain development. As a very general rule, there is a dominance of southerly transport along the southwestern side of Kodiak Island. Other than that area, transport direction is a function of shoreline orientation into prevailing wave approach direction and thus is highly variable over most of the island.

In general, the extreme complexity of the Kodiak Archipelago results in very complex and variable sedimentological characteristics which change rapidly from one shoreline section to another. Grain size, sorting and composition cannot be used as process indicators as on straight more homogeneous shorelines. Only local conditions determine the sediment character and behavior.

COASTAL MORPHOLOGY

The Kodiak Archipelago is an extremely diverse area. Almost any type of coastal environment can be found somewhere on the islands. High winds and waves have interacted with the rugged tectonically active geography to produce an incredibly beautiful and complex coastal morphology.

In general, the islands are erosional. High and low rock scarps and scarps into glacial material occur over much of the shoreline. Of the 4270 km of shoreline classified in this study, 1084.2 km or 25.3% falls into the categories of shear exposed rock scarps or exposed rock scarps with wave cut platforms (see Appendix; Coastal Classification and Oil Spill Vulnerability). In addition to the exposed rock scarps, there are 1462 km of protected rocky headlands representing 34.2% of the total study area. Further, many of the beaches which fall into the sand and gravel class (942 km or 22.1%) and the pure gravel class (634 km or 14.9%) are, in reality, erosional beaches cut into bedrock or semiconsolidated tills and covered by thin sediment accumulations. Thus, the upper limit on actively eroding shorelines is 4122 km or 96.5% of the total shoreline. This is an upper limit only. Some of the gravel and sand and pure gravel beaches are depositional in nature; perhaps as much as 20 or 30%. This reduces the total erosional beaches by 10% (down to approximately 86%).

Of the depositional shorelines, there are 60 km of sheltered tidal flats and 50 km of marshes. Together these two classes represent only 2.6% of the total shoreline. They are found most commonly at the fjord heads and major river mouths. An additional 40 km of shoreline falls into the classes of fine sand beaches, medium to coarse sand beaches and exposed tidal flats. These areas,

representing only 0.9% of the total study area are also depositional in nature. Thus, given that 30% of the gravel and sand and pure gravel beaches are depositional, the study area has only 14% depositional shoreline. For details pertaining to the actual shoreline kilometers and percents of each coastal type see Table 1 and the Appendix.

Figures 5 through 12 show some of the typical coastal types in the Kodiak area. They range from highly erosional to highly depositional. Following this section, is a more detailed analysis of specific study sites visited during the summer of 1978.

TABLE 1
COASTAL CLASSIFICATION
KODIAK ARCHIPELAGO

Class Description	Shoreline Kilometers	% Total Study Area
1. Straight Rocky Headlands	376.6	8.8
2. Eroding Wave-cut Platforms	706.6	16.5
3. Flat, Fine-grained Sandy Beaches	30.0	0.7
4. Steeper, Medium-to-Coarse Grained Sandy Beaches	5.4	0.1
5. Impermeable Exposed Tidal Flats	3.2	0.1
6. Mixed Sand and Gravel Beaches	942.4	22.1
7. Pure Gravel Beaches	634.2	14.9
8. Sheltered Rocky Headlands	1462.0	34.2
9. Protected Estuarine Tidal Flats	60.1	1.4
10. Protected Estuarine Salt Marshes	49.7	1.2
	4270.2	100.0

NOTE: In general, classes 1 and 2 are highly erosional in nature. Classes 5, 9 and 10 are depositional. Classes 3, 4, 6, 7 and 8 can be either erosional or depositional but in this area they tend to be more erosional.

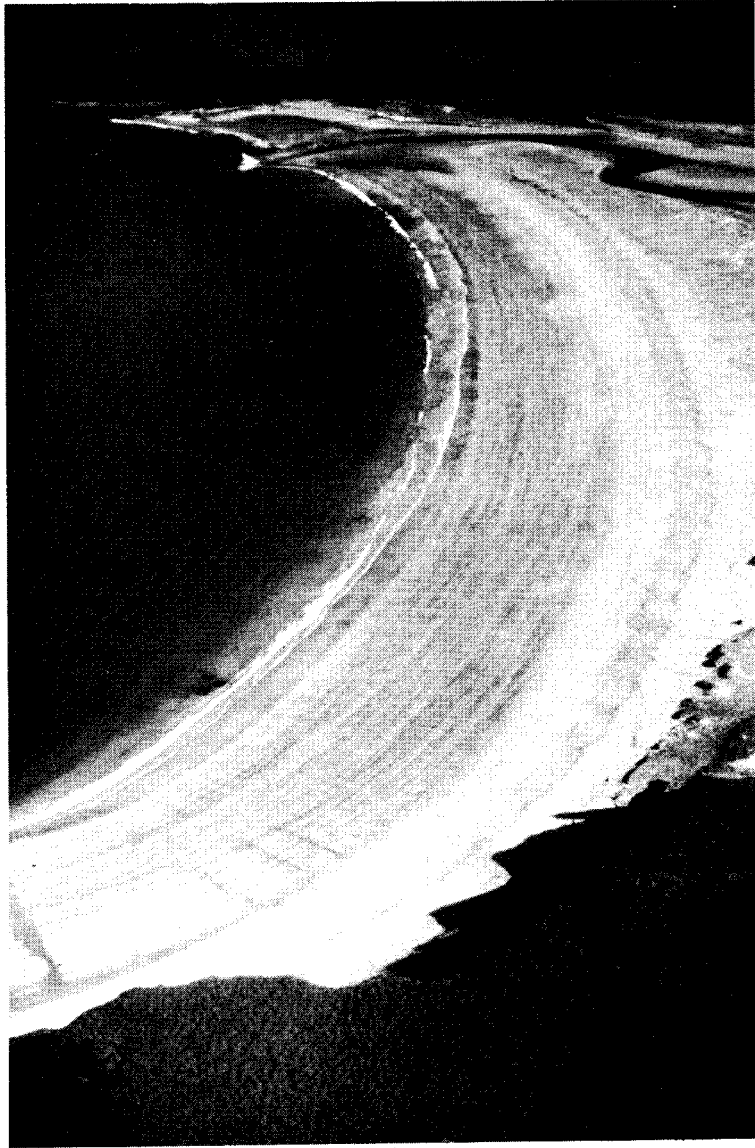


Figure 5. Typical sandy pocket beach. This coastal class is very rare in the Kodiak area due to a very low sand supply. This particular beach has a ready sand supply from the river backing the shoreline. The protected nature of this pocket beach is ideal for the deposition of sand. In general, these sandy beaches do not permit deep penetration of oil and will clean by natural processes rather rapidly. They are a very low #3 on the Oil Spill Vulnerability Index.



Figure 6. A typical high bedrock headland exposed to direct wave attack even at low tide. These areas, in this case on the western side of Kodiak Island, are exposed to very high wave energy and will clean themselves, in the event of an oil spill, within a few weeks. Further, the waves reflect off of the scarps and generate a return flow of water which tends to keep floating oil away from the rocks (note white foam line). These areas will fall into the #1 class of the Oil Spill Vulnerability Index, the lowest class.



Figure 7. This shows another type of bedrock headland. In this case a very poorly sorted boulder and gravel beach is developed at the base of the scarp. At high tide, waves break directly out the face of the scarp, but at low tide, the beach is exposed. Thus, the area becomes more vulnerable to oil spills at low tide. Usually these areas have very high wave energy and are thus generally classed #1, however, if the beach is broad enough to remain exposed at high tide, they are classified as #7 on the Oil Spill Vulnerability Index (pure gravel beaches).



Figure 8. A typical fjord head system. Most of the fjords have rivers which drain into their heads. Usually this results in a delta-tidal flat complex. The fjords tend to amplify the normal tides, thus the fjord heads display many macrotidal characteristics. In this figure we see a typical braided stream river delta of sands and gravels fronted by large swash and tidal bars of coarse sand and granules, covered with mussels. These areas are generally backed by a narrow marsh system and fall into the two most vulnerable classes on OSVI, #9 (protected estuarine tidal flat) and #10 (protected estuarine marsh).



Figure 9. This area, located on the northern Afognak shoreline, shows a typical low energy low irregular rock scarp. These areas are usually classified as #8 on the OSVI. Very abundant intertidal life covers the intertidal and subtidal rocks. The low wave energy results in heavy oil coating in the event of an oil spill. It also results in very slow natural cleaning. More than 40% of Afognak Island is of this highly vulnerable class.



Figure 10. This is a ground level photograph of an area classed #8 (protected rock headlands). The headlands are associated with very numerous poorly sorted gravel accumulations perched on bedrock. Intertidal life is extremely abundant and wave energy is very low. Oil introduced into these areas will do great damage and remain for long periods. These systems will tend to hold floating oil, once it has been introduced.

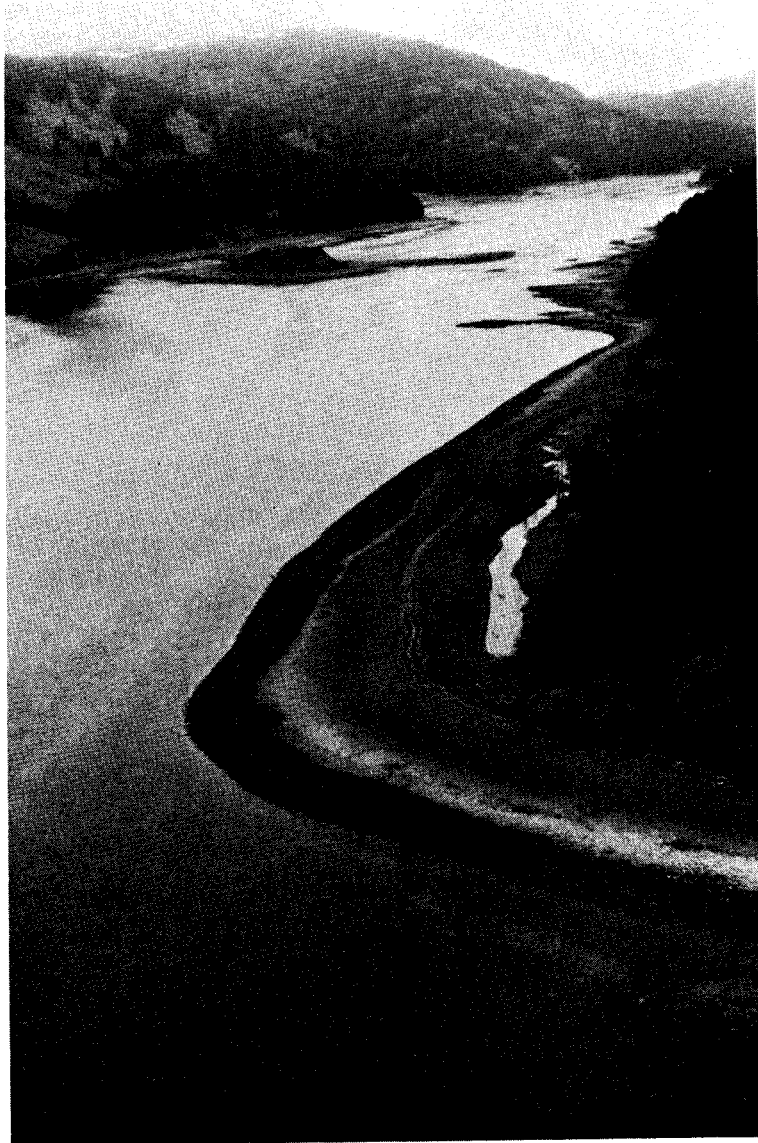


Figure 11. This shows a characteristic moderate energy pure gravel beach. In the background there are two gravel spits indicating transport into the fjord. The beach in the foreground shows a number of features. At the base of the beach face there is a dark boulder-cobble low tide terrace which appears darker due to heavy algal coating on the rocks (this indicates that the wave energy is not high enough to move the coarse sediment on the L.T.T. The middle beach face is mostly coarse gravel (clean). Above that, there are storm swash lines of logs and debris, backed by a storm berm and scarp. This is a very typical pure gravel beach. OSVI = 7. These areas permit deep penetration of spilled oil.



Figure 12. Well developed fan delta in the inner portion of Uyak Bay. Note two fan deltas in background. This delta displays a prominent zonation. At the outer funge of the delta are wave and tidal bars of fine gravel and sand with a heavy coating of mussels. Landward of that zone is a sandy flat usually with considerable infauna. At the top of the intertidal zone is a marsh which is backed by a low fresh water brushy vegetation. These areas, because of their sensitive marsh zones, are very vulnerable to oil spills, however they represent less than 1/10% of the shoreline.

Profile Site Analysis

This section describes, in a more detailed format, a variety of the shoreline types studied on Kodiak and Afognak Islands. During the summer of 1978, 127 stations were established. The even numbered stations consisted of the following:

1. Detailed taped description of beach morphology, back beach morphology, oil spill vulnerability, sediment characteristics, wave and tidal energy, and general biotic abundance.
2. Aerial photographs.
3. Ground photographs.
4. Description of rock type in scarps, and sediment composition on beach face.

The odd numbered stations consisted of all of the above plus:

1. A detailed line transit (profile) of the active beach face and any relevant back beach morphology.
2. Sediment samples taken from the upper, mid and lower beach face as well as any dunes or other interesting depositional features.
3. A sketch of the entire profile and surrounding area.
4. Measures of wave height and approach direction.
5. Temperature, wind speed and direction, general weather.

Later, coastal flights were made to fill in the shoreline between stations and to get a good overall picture of the study area. The Oil Spill Vulnerability Index is applied at that time.

Finally, laboratory analysis is conducted as follows:

1. All profiles are reduced to digital form and run on to computer tape. The tape is then used to plot the profiles (at a 1:5 vertical exaggeration) and then sent to the National Ocean Data Center.
2. All sediment samples are split, washed and either analyzed using sieves and a ro-tap machine, or sent down a settling tube. In either case, the data is reduced to digital form and run and plotted by computer. Magnetic tapes are then sent to the NODC.
3. All taped descriptions are transcribed.

The Appendix of this report contains a section labeled "Profile Sites". This section gives the details of each of the odd numbered stations. Each station is located both by longitude and latitude and by geographic position. The station is then described as to wave energy, sediment type, beach morphology, storm activity etc. Below that the general wave and tidal energy is characterized as well as the rock type of scarps and beach sediments. Finally the sediment samples which were taken are described. For further information regarding sediment samples, see the Appendix (Grain Size Analysis).

Figures 13 through 23 follow. Each figure describes a particular profile site, with photos, a beach sketch and a caption. These 11 figures will demonstrate some of the variability of coastal morphology found in the Kodiak Archipelago. They are not in any particular order and should not be viewed as representative of any percentage of shoreline in the study area.



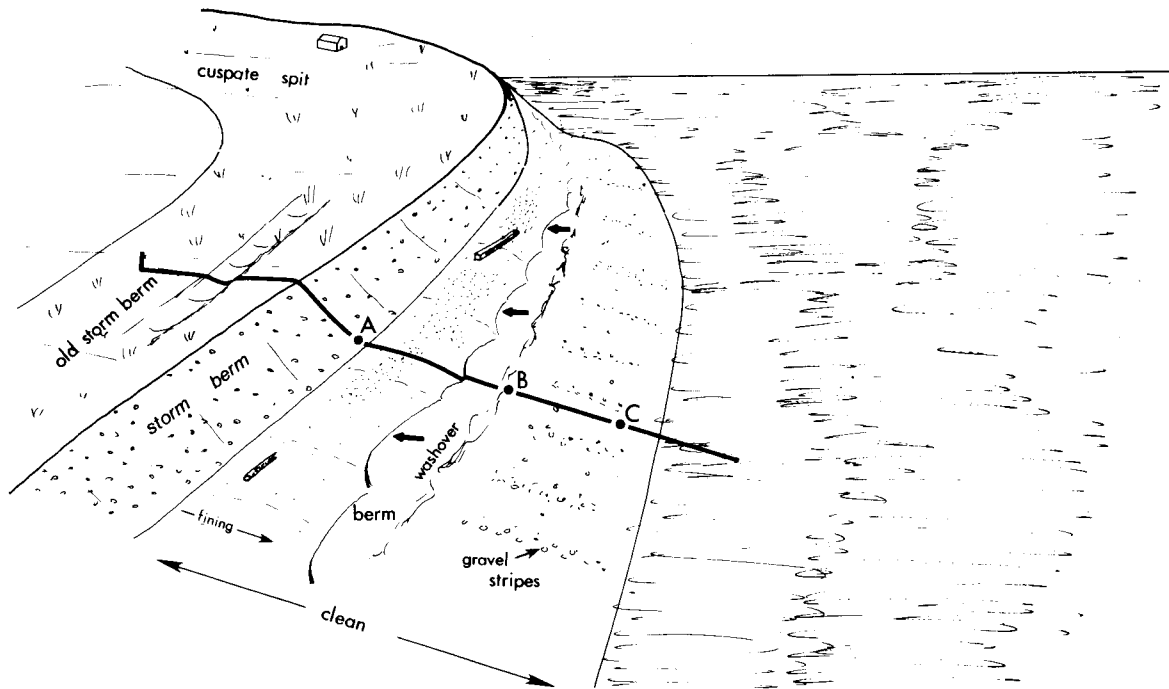
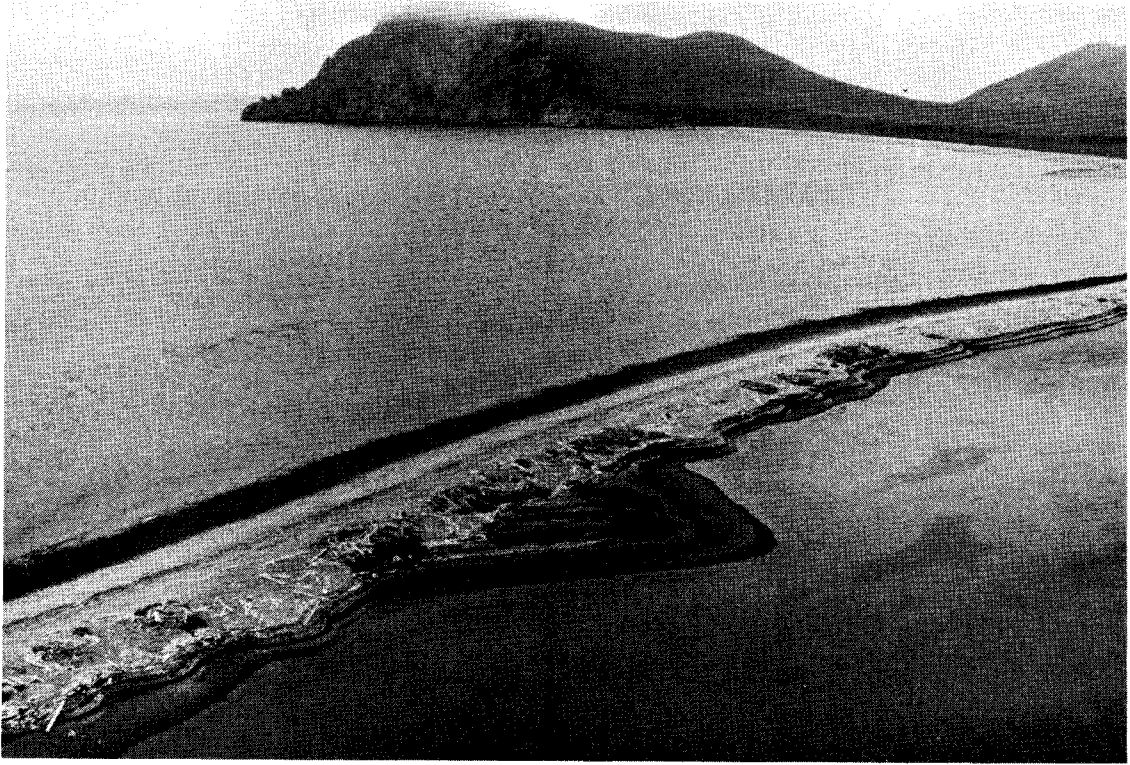


Figure 13. Profile site KDP-73 located in Dead Man Bay. The profile is set on the more exposed southern side of a very well developed cusped spit composed mostly of gravel and granules. The aerial photo shows the multiple vegetated storm berms at the top of the beach face. These either indicate uplift or very infrequent storms, or both. The beach face has a uniform convex upward shape and a strong fining trend toward the water line. Thus the top of the beach face is composed of coarse discoidal gravel while the base of the beach face has finer, more equant gravel. There are prominent gravel stripes on the lower 1/3 of the beach face, evident in the ground photo as well as the sketch. Wave energy is moderate with occasional high storm waves. The letters A, B and C on the sketch refer to sediment sample locations.



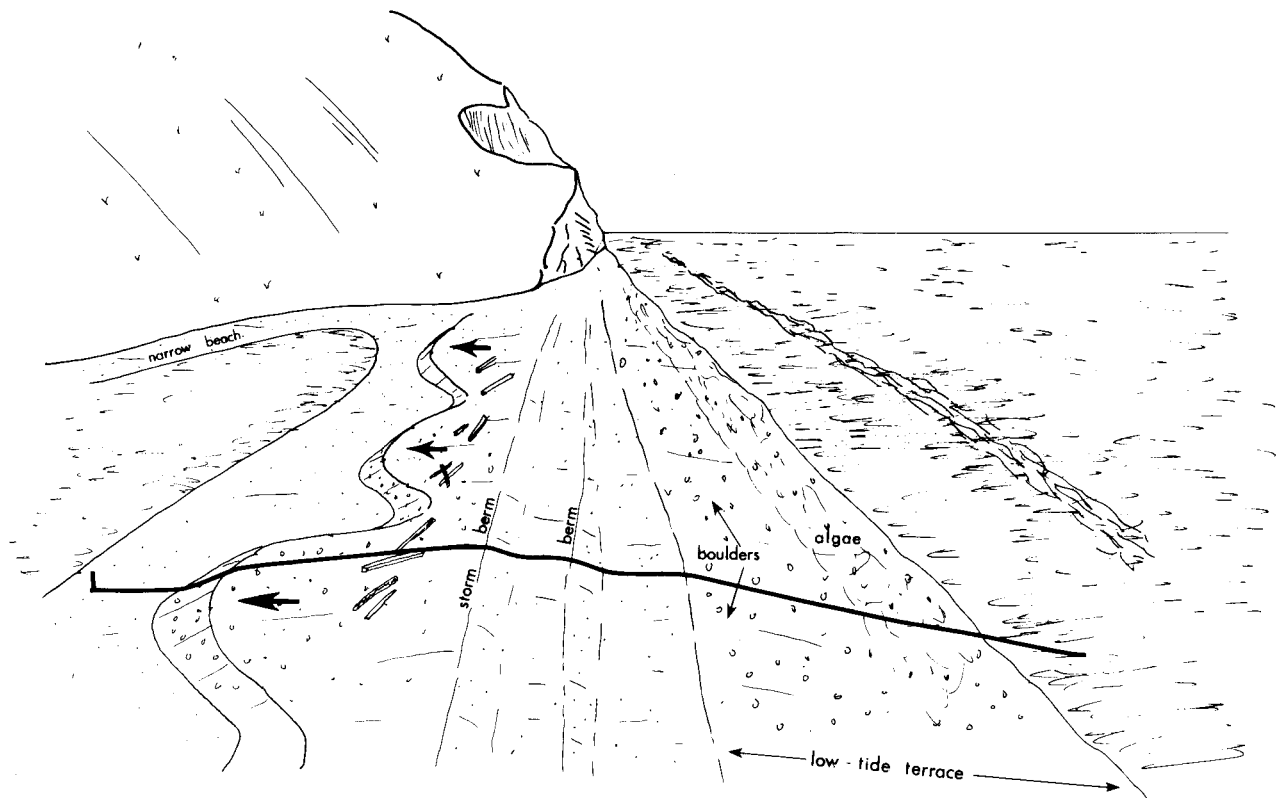
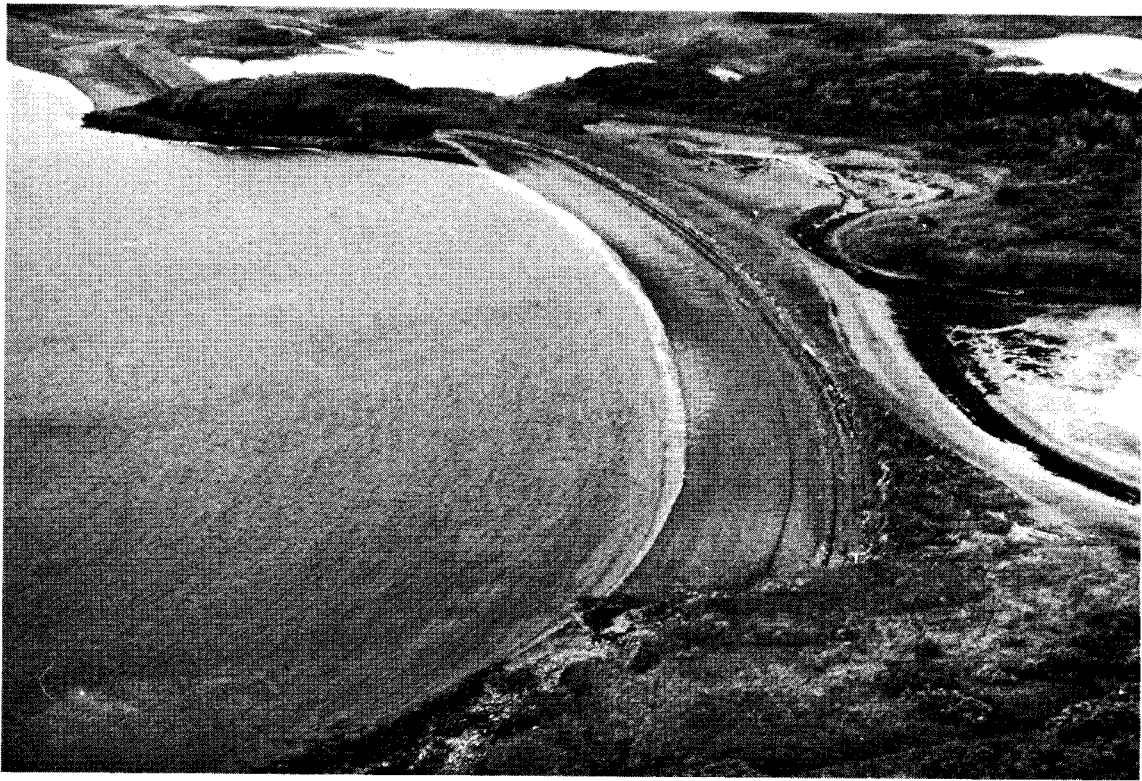


Figure 14. Profile site KDP-63 located on the spit fronting the Sturgeon River. This is one of the best examples of a very coarse grained transgressive washover profile in the study area. This narrow spit is composed of almost pure coarse gravel and cobbles and boulders. The aerial photograph shows a dark band across the base of the beach face. That band is an algal coating covering the boulder-cobble low tide terrace, illustrated in the ground photo. The beach face is narrow, clean, and composed of gravel. There are two berms up high and then a well developed washover terrace, active only during violent storms. The scalloped nature of the washover terrace is especially evident in the aerial photo and sketch. The coarse gravel is transported over the top of the spit and then deposited on the accreting face of the washover (lagoon side) by high velocity sheet flow caused by large breaking waves. Thus the spit migrates landward. The lagoon side beach has a narrow flat low tide terrace at the base of the washover slip face. This type of beach will hold oil for long periods due to its great porosity.



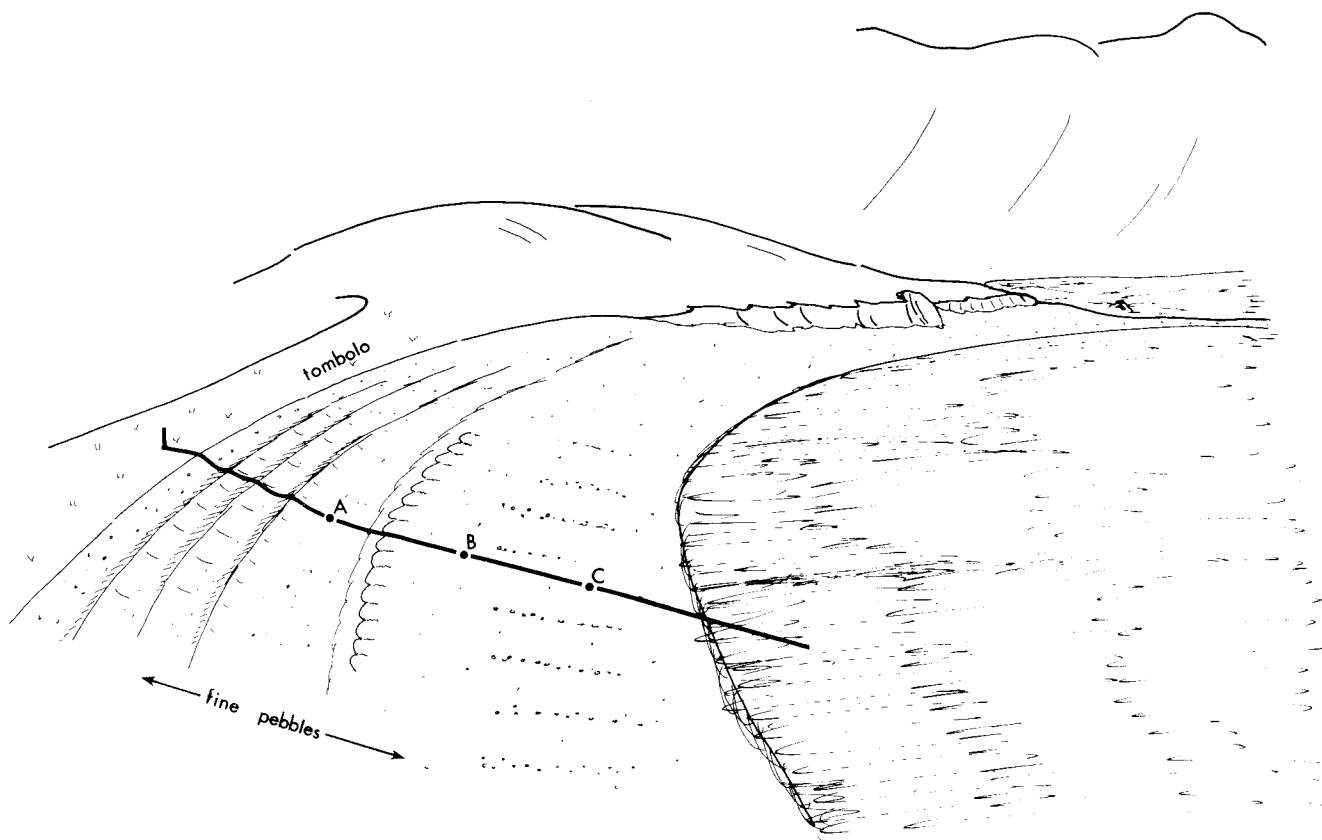


Figure 15. Profile site KPD-115 located on the Southern Uganik Passage. This profile is composed of nearly pure fine gravel and granules. It is quite simple with a slightly convex upward shape. There are four separate small berms (visible as algal swashlines on the ground photo). Above the berms is a partly vegetated low storm berm. The lower beach face has well developed gravel stripes. This type of gravel beach is very common in the better developed pocket beaches exposed to moderate to low energy. These beaches are usually quite well sorted. The relatively coarse nature of the sediments makes these beaches vulnerable to oil spills due to percolation of oil into the substrate and retention there. Note the very poorly developed beach on the lagoon side of the tombolo, with very low wave energy, (aerial photo).



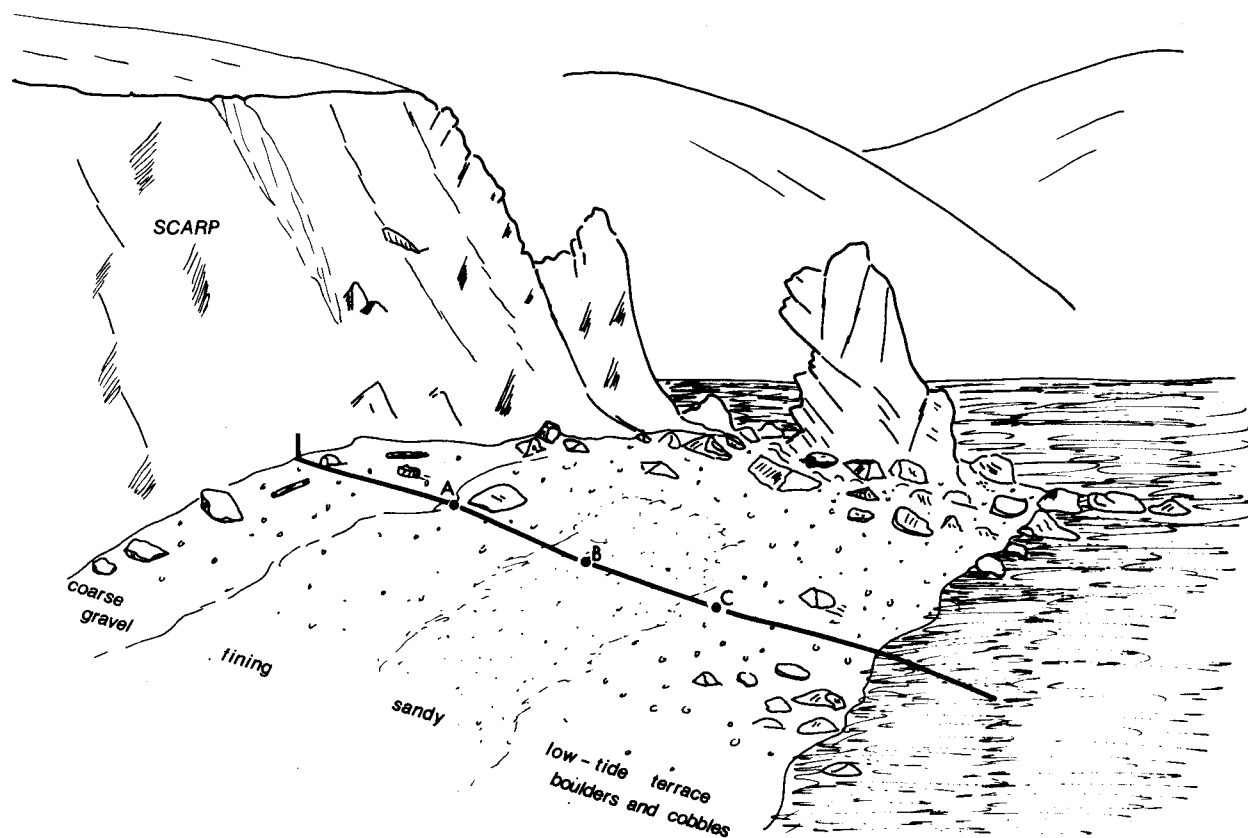


Figure 16. Profile site KPD-27 located in Malina Bay. This is a low to moderate energy rock scarp into quartz diorite with a poorly sorted beach face. The beach face is finest in the center (mostly sand) and coarsens toward the top (coarse gravel berm) and toward the water line where there is a steep short boulder-cobble low tide terrace. The lower energy is not great enough to move the sediments at the base of the beach face and thus they have a very heavy coating of algae and encrusting intertidal fauna. The rock stack behind the helicopter appears black at its base due to heavy mussel accumulations. The low wave energy and coarse grain size make this beach vulnerable to oil spills. However, during major storms, most of the beach sediment, will be moved about, aiding natural cleaning. There is a large kelp bed just offshore.



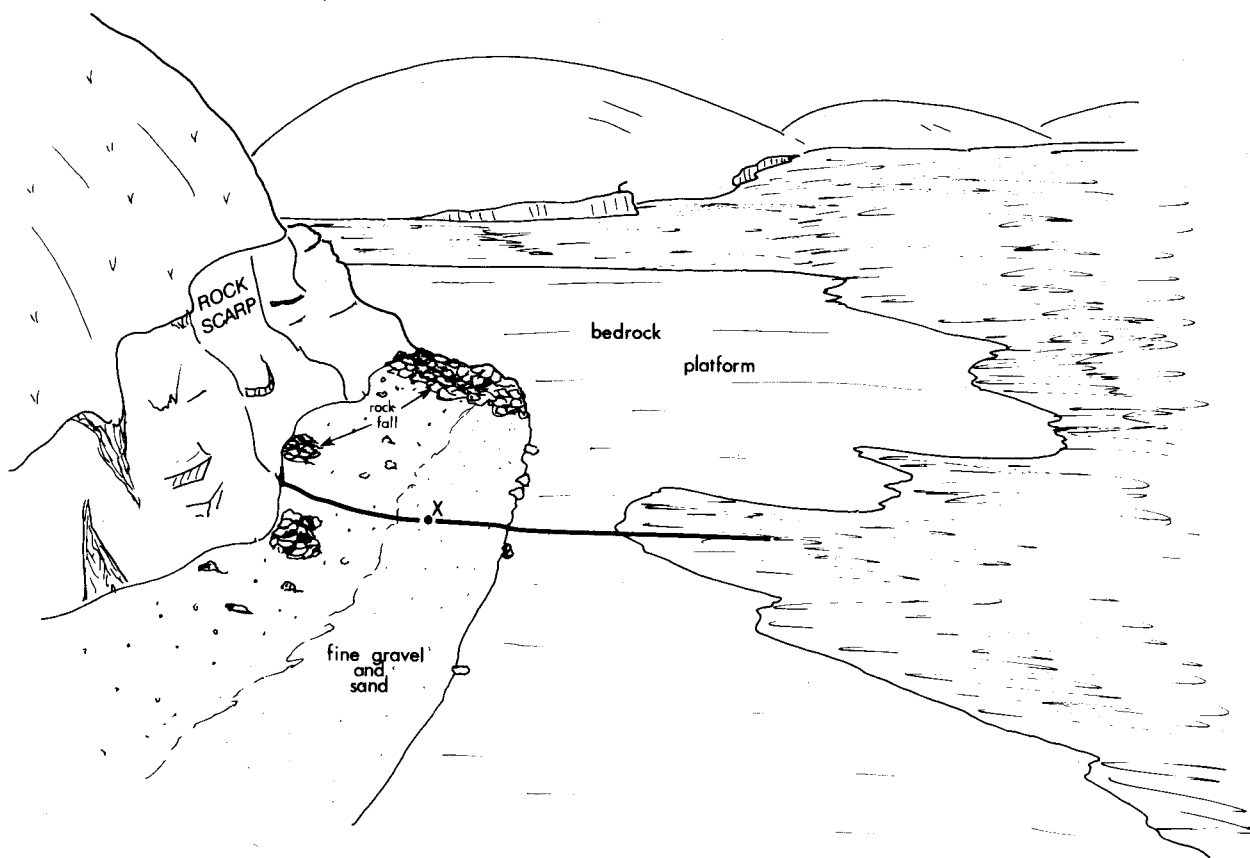


Figure 17. Profile site KDP-81 located on the Geese Channel. This location has one of the best developed wave cut platforms into bedrock in the Archipelago. The rock type is greywacke standing at a relatively steep angle. That results in a very irregular platform, with numerous tidal pools (see ground photo). The bedding planes in the rock are particularly evident in the aerial photograph. Note that about 90% of the intertidal zone is on the platform. Just below the scarp is a poorly sorted beach face of boulders, gravels and sand. Most of these sediments are rounded indicating fairly high wave energy. The entire beachface is less than 30 m wide. Rock platforms of this type generally have quite low oil residence times due to their impermeable character and high wave energy. The coarse beach face is more sensitive. Very heavy intertidal biota coats the bedrock.



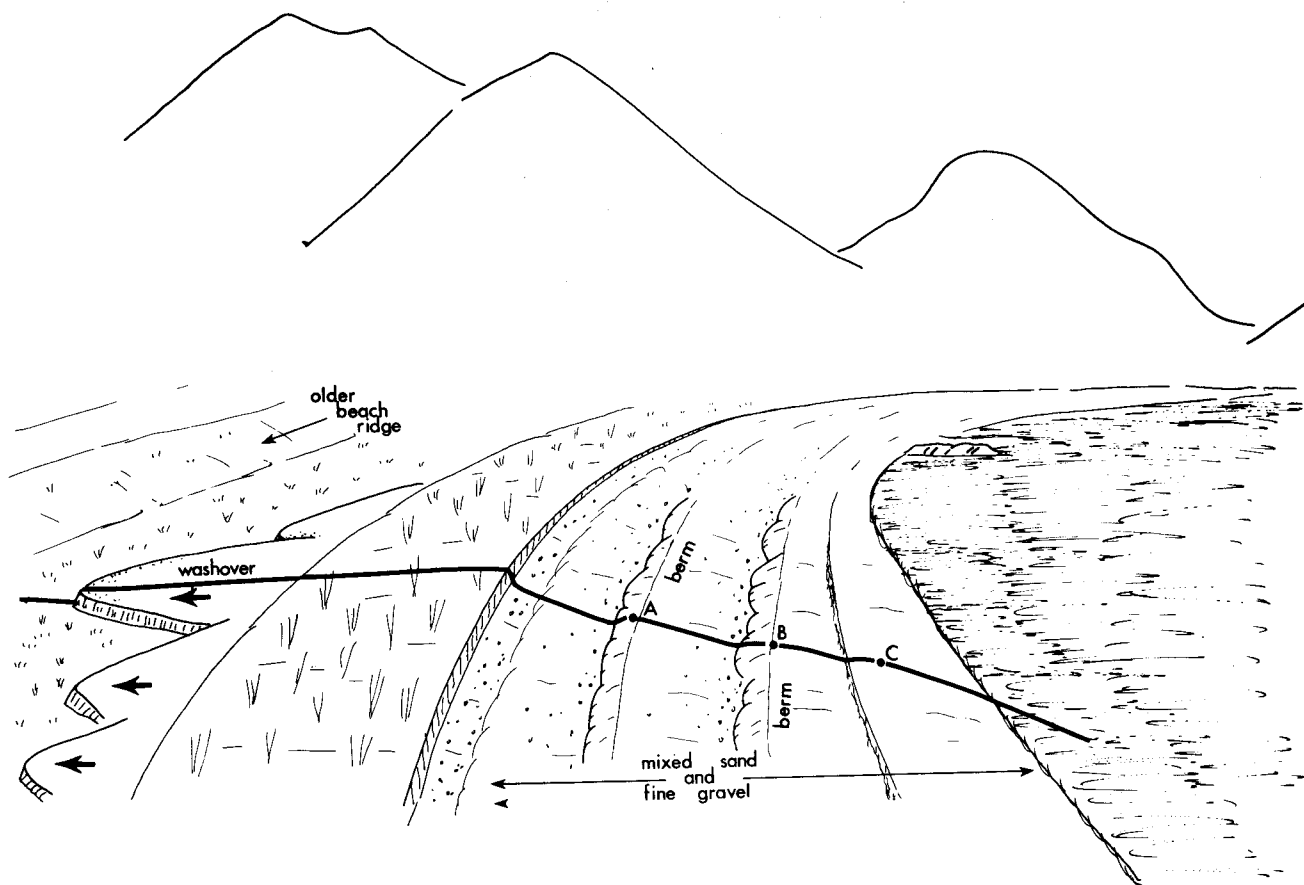
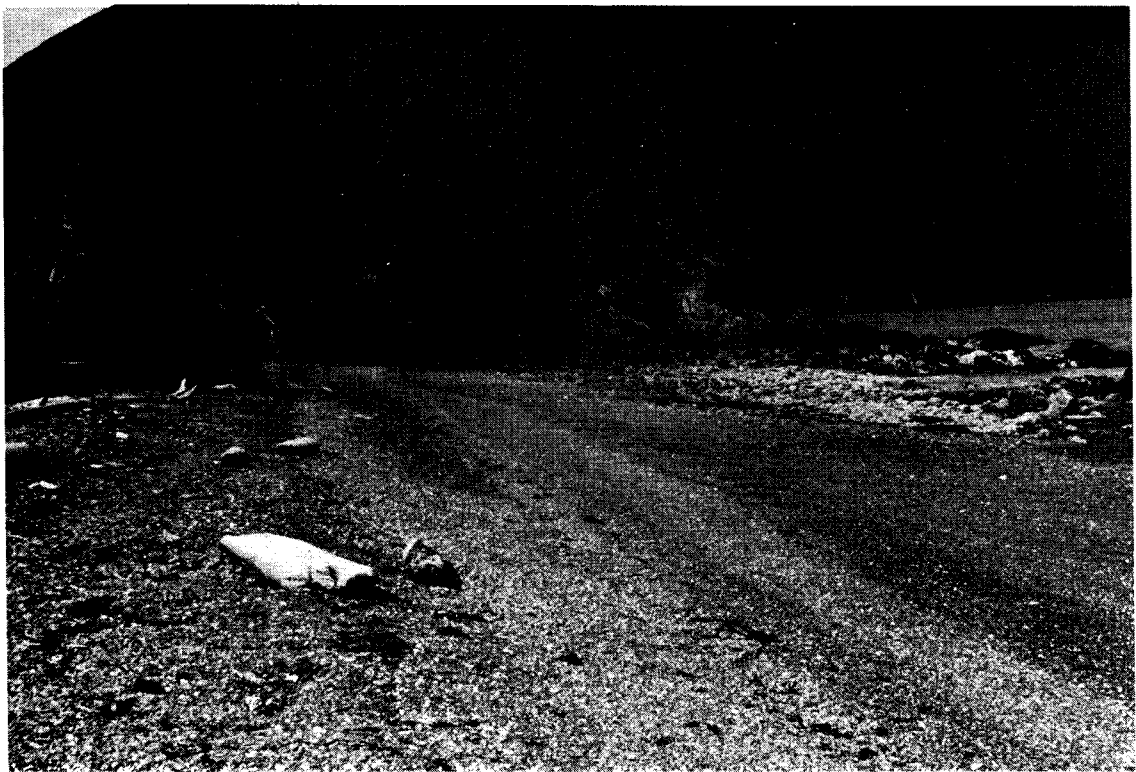


Figure 18. Profile site KDP-89 located on the Sitkalidak Strait. The profile is located on the seaward side of a large cusped spit. The area is very interesting with a nicely developed washover terrace backing a gravel and sand beach face. The washover, composed mostly of gravels and granules is migrating landward over a marsh behind the active beach face. It appears that the washover material has been transported over the top of the spit without being deposited on the vegetated top. Well behind the active beach face is a series of earlier beach ridges associated with a relict recurved spit complex. The beach face itself has three berms on it, each one with a very steep landward face. Oil Spill Vulnerability is about 6 or 7 due to the coarse grain size and thus long term retention potential.



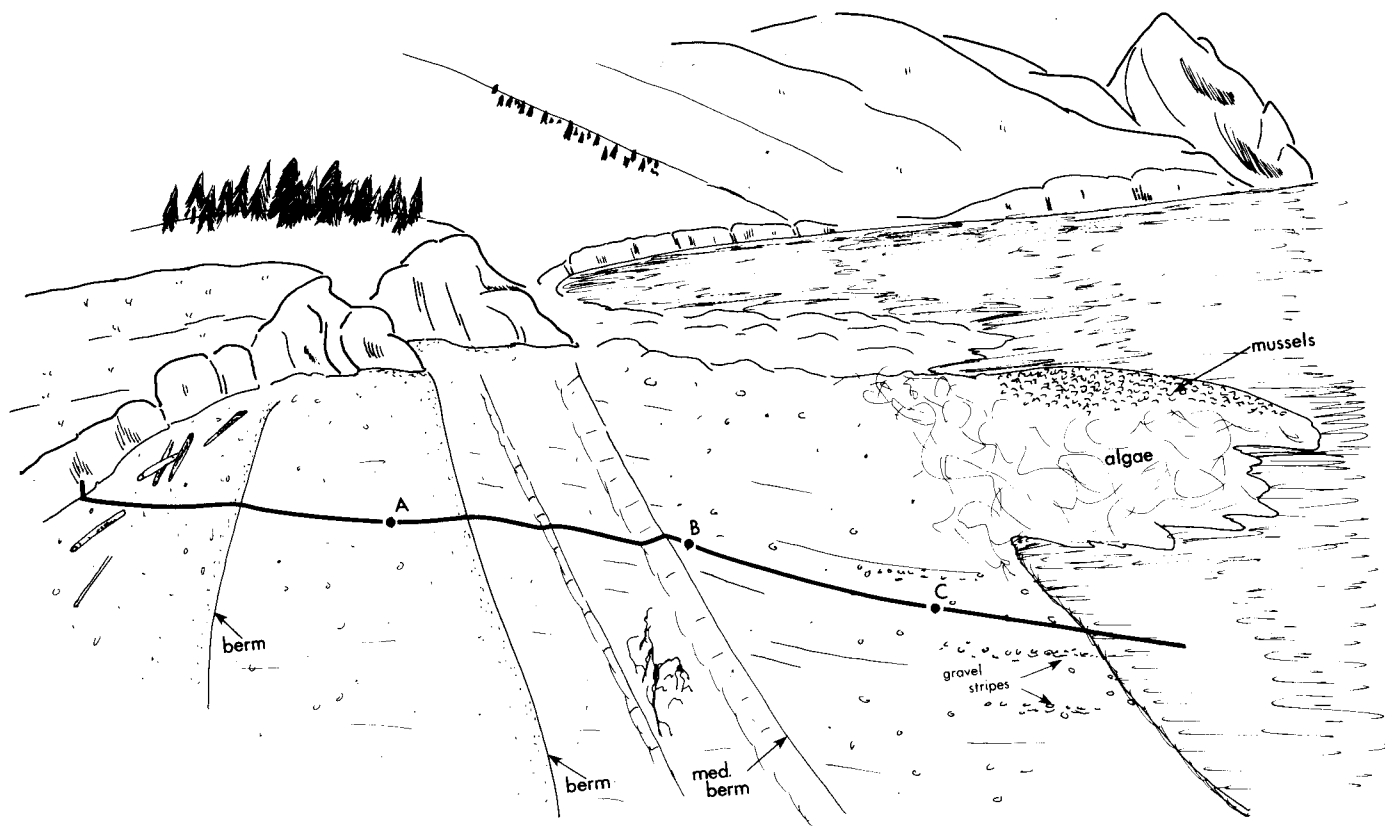


Figure 19. Profile site KDP-29 located in Malina Bay. This profile shows a very typical moderate energy gravel pocket beach. The pocket is located between two rocky headlands. Bedrock outcrops at the base of the beach face across most of the pocket beach indicating that the gravel is in fact only a thin veneer of sediment on bedrock. All exposed bedrock has a heavy biotic cover. Fronting the scarp is a high level storm berm composed mostly of discoidal gravels and granules. As usual, there is a log accumulation on top of the storm berm. The beach face is quite uniform and gets coarser as the water line is approached. Prominent gravel stripes occur at the base of the beach face where it intersects the rock platform. The OSVI is about 6 or 7 due to the coarse grain size.



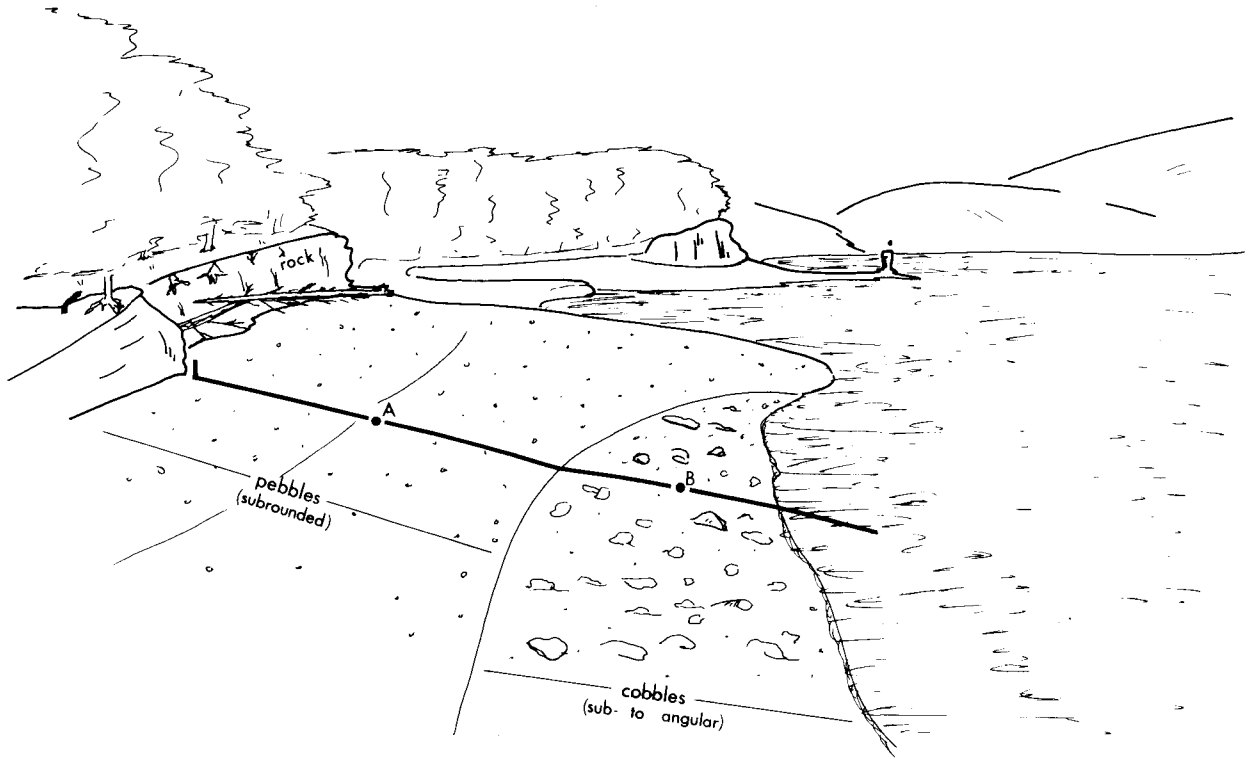


Figure 20. Profile site KDP-35 located on Lost Timber Point. This profile shows a low energy gravel beach. The low energy is attested to be the vegetation growing almost to the spring high tide line. Further, all of the gravels on the beach face are subangular to angular and, in general, covered with barnacles and algae (indicating very little movement by waves). The beach sediments ranging from sand to gravels with some larger, are perched on a bedrock platform. A scarp into that bedrock is present behind the beach face. The profile is narrow and simple. Dead trees backing the profile indicate earthquake downwarp. Most areas of this type are classified as OSVI 6 - 8 depending on grain size of beach sediment and wave energy.



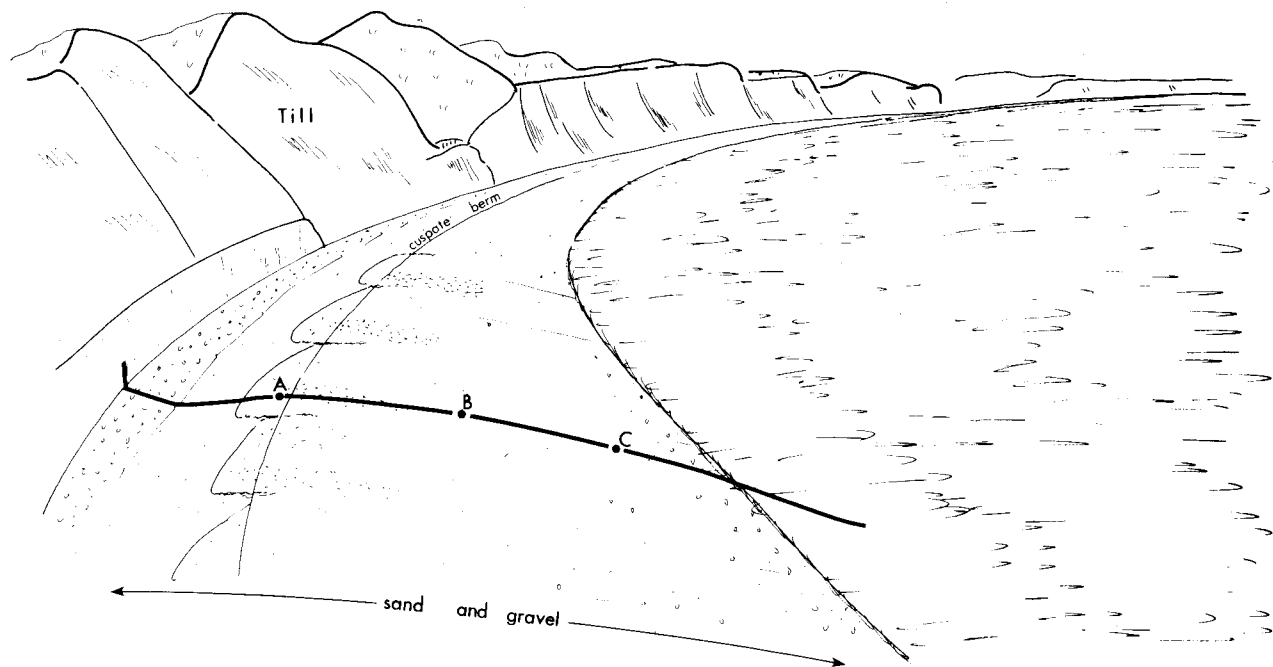


Figure 21. Profile site KDP-67 located just east of Ayakulik Island. This profile shows a typical sand and gravel beach face fronting a till scarp. Wave energy here is high, thus the finer sediments (clays and silts) have been removed. Beach faces in these areas are broad and strongly convex upward. In general, they are coarser at the top of the beach face and finest in the middle. These beaches are the most uniform and long in the study area, stretching for many miles with very little change. Shoreline environments of this type fall in the #6 slot of the OSVI and have very low biota populations.

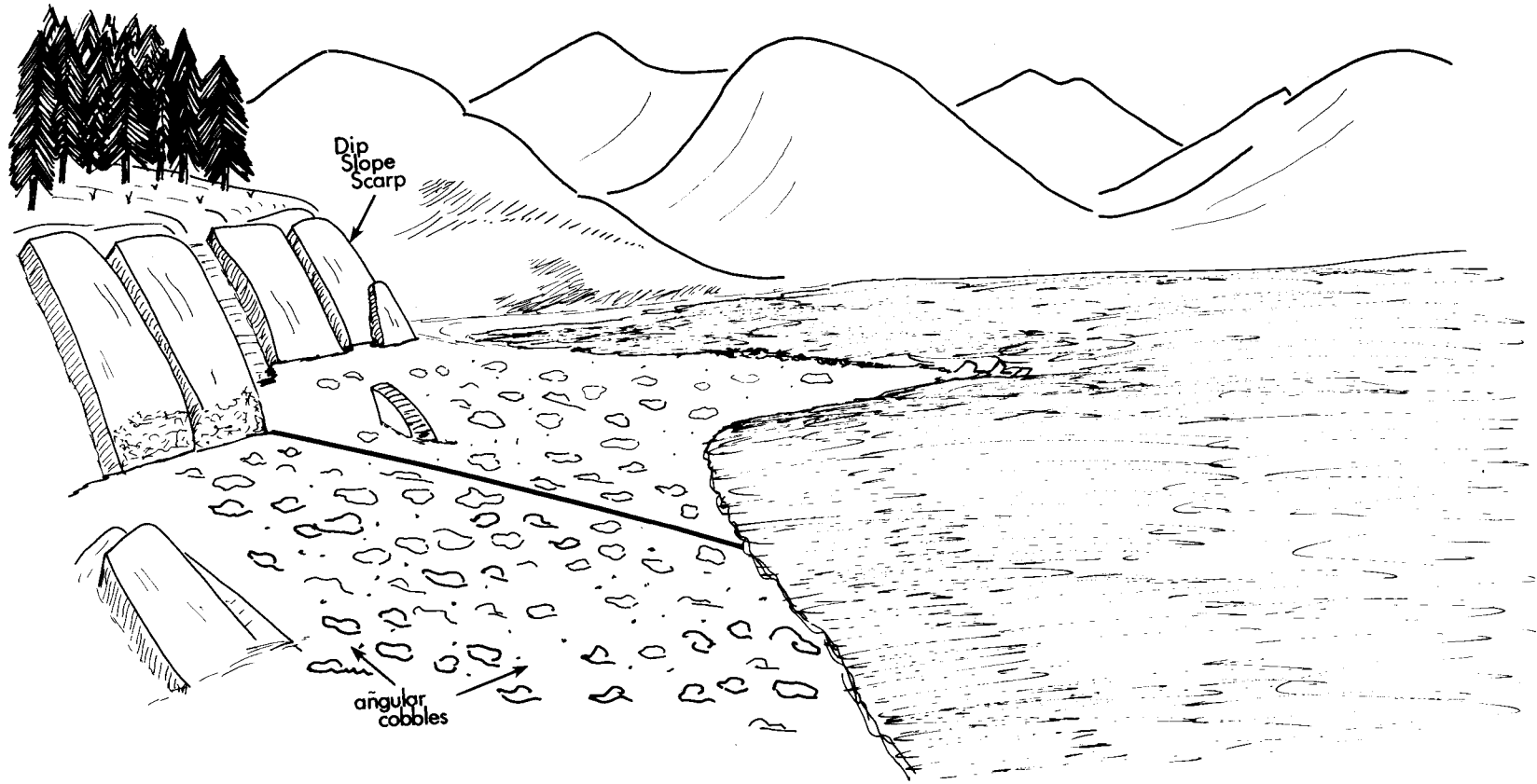




Figure 22. Profile site KDP-31 located on the Raspberry Strait. This is a very simple, very coarse grained, low to moderate energy beach fronting a "Dip Slope" scarp into slate and argillite. This particular rock unit is standing nearly vertically and breaks very easily along bedding planes forming large angular boulders and gravel. Wave energy then smooths them to be mostly sub-angular. Note the very distinct fining trend in boulder-gravel size from the base of the scarp to the water line. Intertidal communities have almost completely covered the sediments on the lower beach face. The profile is quite short and very steep. The oil spill vulnerability of an area like this will depend on the wave energy. In general these areas fall into classes 7 and 8. If exposed, they tend to fall into 1 or 2.

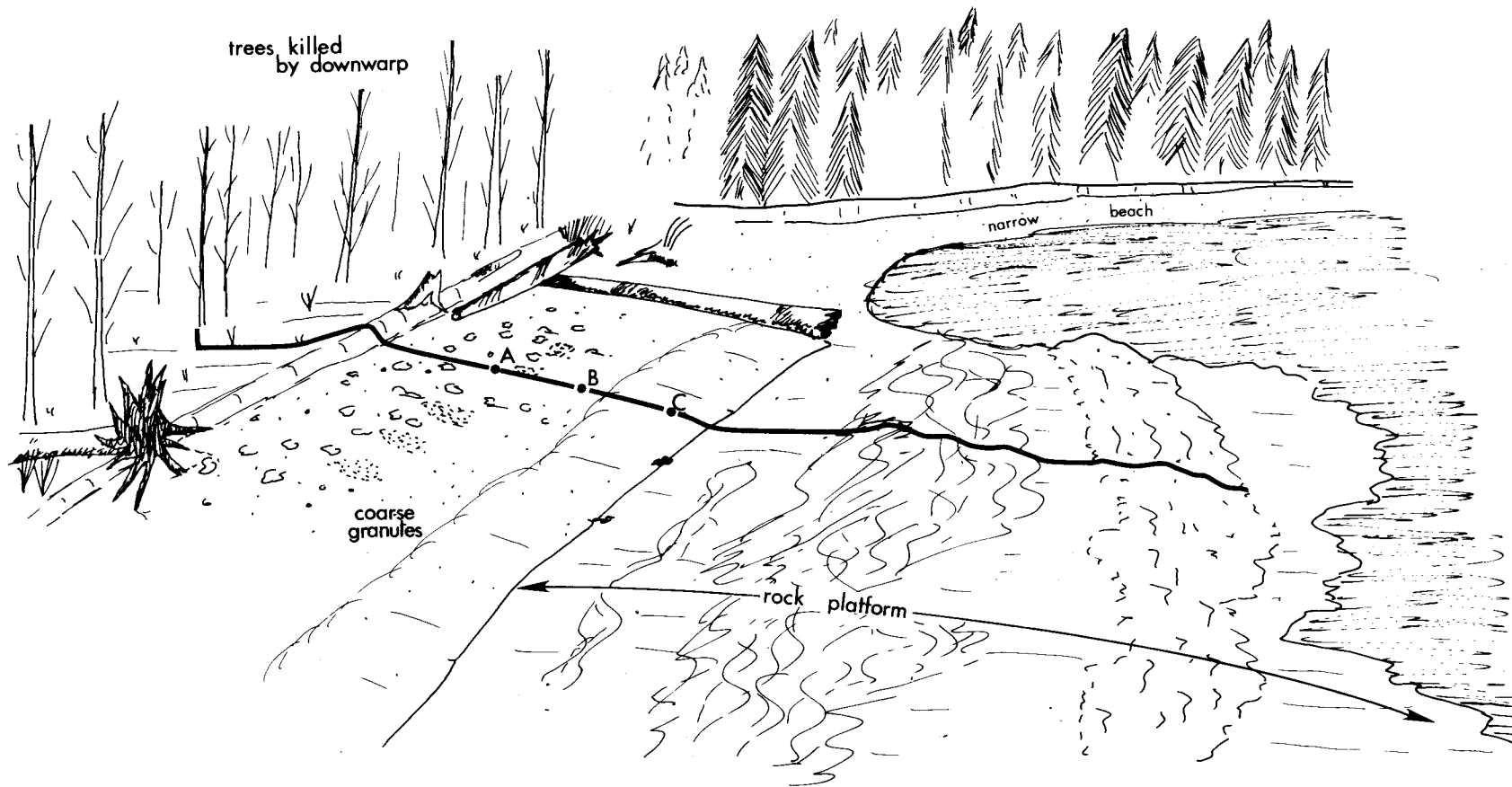




Figure 23. Profile site KDP-1 located on Afognak Point. This profile is a low energy gravel and sand beach on a bedrock platform. The back part of the profile has a developing storm berm which is actively migrating into the forest. It has not yet reached equilibrium following the downwarp of the Good Friday Earthquake of 1964. Many dead trees line the top of the profile, attesting to salt water intrusion. The upper beach face is a poorly sorted featureless sand and gravel accumulation which abuts a boulder-cobble covered bedrock platform at the base of the beach face. Although this area has rather low energy, especially during the summer, it still has been classified as a wave cut platform and given a #2 OSVI rating. Storms evidently impact this area rather frequently.

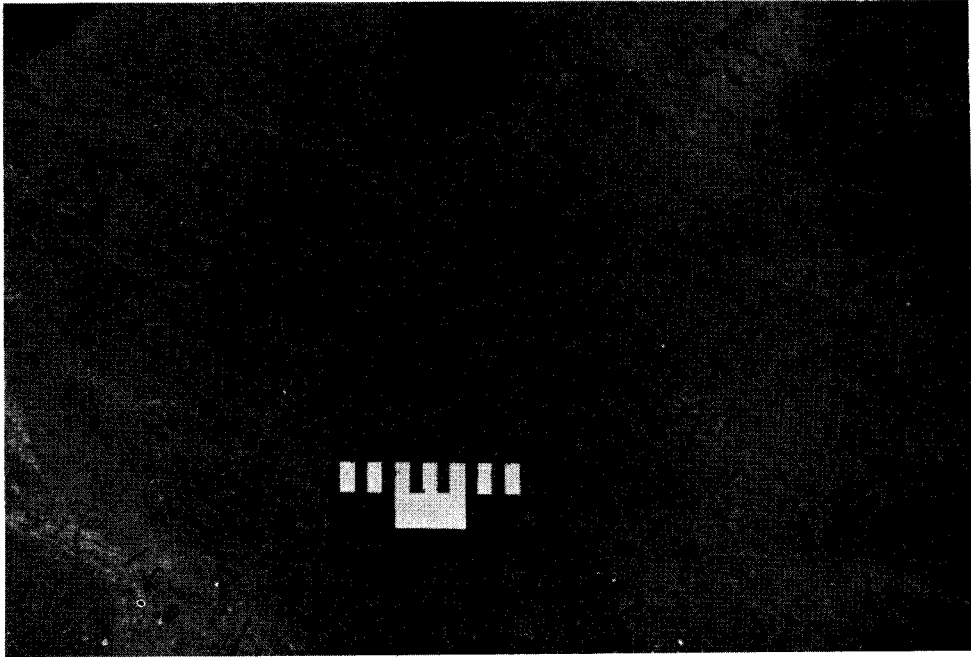
Beach Sediments

Since the Oil Spill Vulnerability Index is partly a function of beach sediment grain size, and since the Kodiak Archipelago has such an incredible variety of sizes and shapes of sediments, this section will, very briefly, depict some of that variety. Sediment grains size is a function of a number of parameters:

1. Source; whether it is a source rock in a scarp, like slate yielding boulders and gravel or a till deposit yielding unconsolidated clays, sands and gravels or a river yielding mature sands and gravels. Source is the most important single factor. It will dictate the range of sediment sizes available.
2. Wave energy; high wave energies will eliminate, through winnowing, the finer grain sizes of silts, clays and sometimes fine sand. In the same context, very low wave energies will permit the deposition of these finer sediments forming tidal flats and marshes. In some cases, a consistent wave approach active on a variable source (glacial till) will form a series of different beach types down drift of the source. There will generally be a fining trend away from the source. Thus a pure gravel-cobble beach occurs just down drift; a fine gravel beach further down drift and eventually a gravel and sand beach. In essence, wave energy will act as a sorting mechanism, separating grain sizes and depositing them in areas where they are in equilibrium with the incoming wave energy.
3. Rock type; certain rock types, due to their physical properties, behave in specific, predictable patterns once on a beach face. Slates

and bedded metamorphic and sedimentary rocks will always yield platy gravel shapes, while intrusive rocks will usually yield equant shapes. Certain rock species, like quartz, due to their extreme hardness, have very long life spans while others, less resistant to abrasion, like feldspar, are rapidly eliminated from active beaches.

The following 9 figures illustrate most of the sediment types found on Kodiak area beaches.



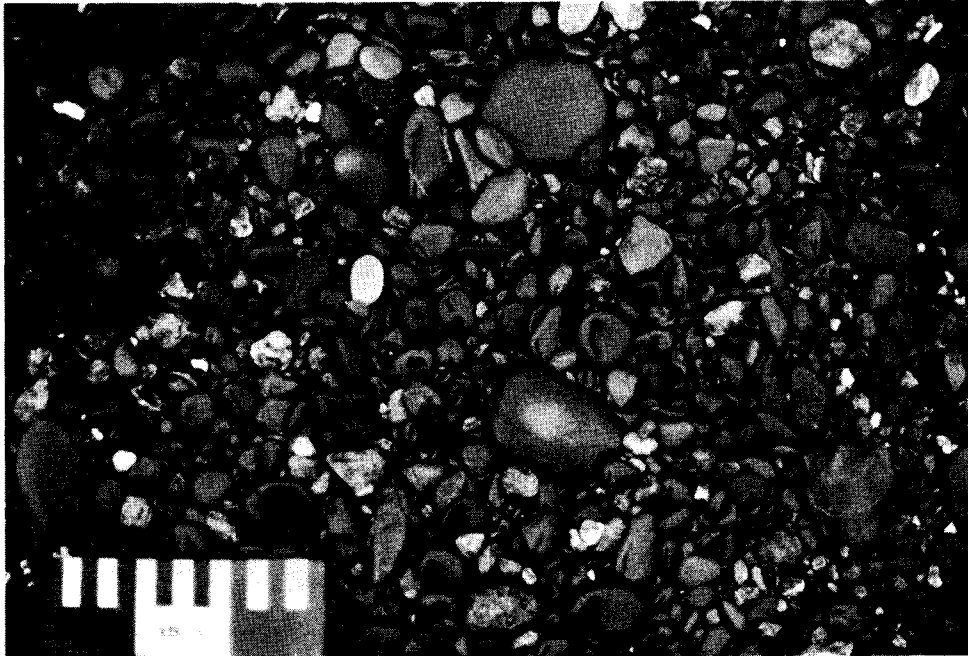


Figure 24 (above left). Typical mud flat sediments. These areas are composed of silts, clays and sometimes fine sand. They often have heavy infaunal communities, as in this photo. The very fine grain size does not permit the penetration of heavier fuel types during a spill. In general, the contaminants are refloated with each tide. Scale is 15 cm long.

Figure 25 (opposite left). Sandy beach face fronting a till source. These beaches are usually quite wide and strongly convex upward. Since the sediment is quite fine, and these areas are often exposed to high wave energy, the continual movement of sediments results in fairly rapid cleaning by natural processes. Oil can however percolate into the beaches and become buried during depositional beach cycles.

Figure 26 (above). A fairly well sorted fine gravel and granule beach. The good sorting will permit deep penetration of spilled oil and fairly long retention periods. Note the equant, round to subround character of these gravels (greywacke).

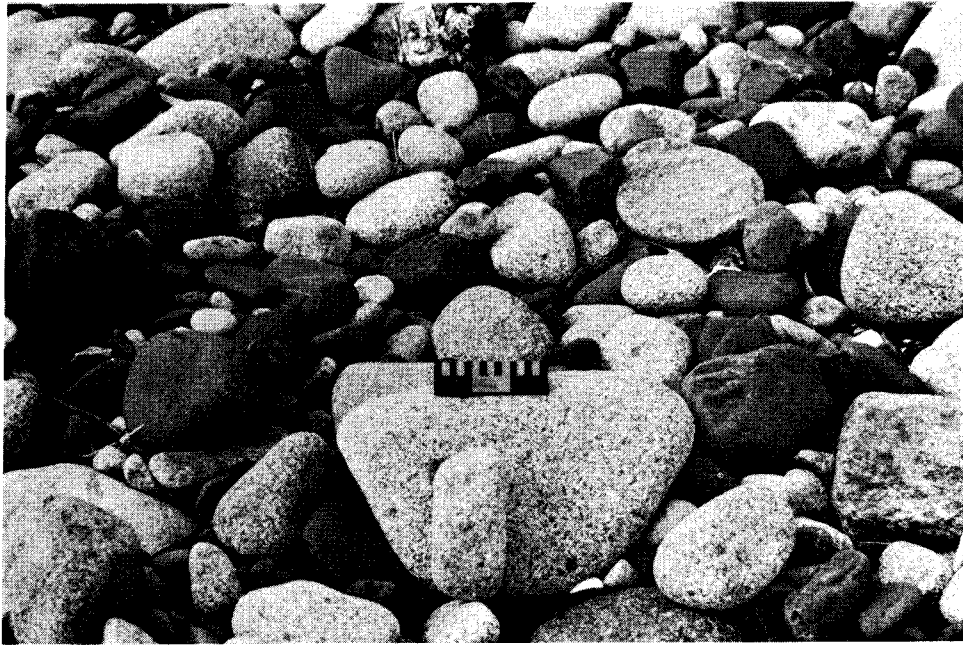




Figure 27 (above left). A typical fairly well sorted boulder-cobble coarse gravel beach sediment. Note the rounded to well rounded nature of most of the material and to total lack of fine sediment. This type of beach will absorb enormous quantities of spilled oil and hold them for long periods. These beaches fall into the #7 slot on the OSVI regardless of their exposure to waves.

Figure 28 (left). A boulder beach perched on bedrock. Fairly low wave energy is responsible for the angular to subangular shape of the boulders. Boulders of this size are generally not moved by wave activity and thus are usually covered with intertidal biota when near the low water line. All these boulders are locally derived.

Figure 29 (above). An example of a sand and often gravel beach face. Sometimes these sediments are mixed randomly but more often there is a coarsening of sediment with depth and in many cases a coarsening toward the top and bottom of the beach face. The OSVI would be #6.





Figure 30 (above left). Very immature locally derived boulders and gravel. Their angular shape and barnicle and algal coatings indicate very low wave energy. The combination of low energy and coarse porous grain size would give this area a high OSVI of 7 or 8. Beaches of this type are very common on Afognak Island.

Figure 31 (left). This shows the effect of very high wave energy on a boulder-cobble beach face. Note the well rounded character of the boulders and the coarsening of the boulders toward the water lines. Again, coarse grain size and resultant percolation and retention of spilled oil give this beach face a #7 OSVI rating.

Figure 32 (above). A very low wave energy mixed gravel and granule beach face. The low energy has resulted in only slight rounding of the gravels which have a considerable barnicle encrustation indicating that they are moved infrequently. This type of beach is common in many of the fjords and sheltered areas.

OIL SPILL VULNERABILITY

Introduction

With the ever increasing demand for petro-products, and the continued pricing policy of the OPEC, Alaska will remain in the forefront of petroleum exploration. With oil prices rising at their current rates, even the very hard to produce "deeper shelf" oil will become economically feasible. Thus, if there are economic quantities of oil on the Kodiak Archipelago shelf, they will soon be found and produced. This will place the shoreline of Kodiak and surrounding islands in a position to receive potential oil spills. The extreme weather and tectonic setting of the area makes it even more likely to suffer the effects of blowouts, pipeline ruptures, tanker groundings and so forth.

The primary purpose of this study has been to supply baseline data regarding shoreline geomorphology and how that morphology may interact with potential oil spills. Of primary importance is the ranking of coastal environments with regard to the longevity of spilled contaminants. Thus, the primary product of our research is a set of 47 standard U.S.G.S. Quadrangle base maps at a 1:63,360 scale. These 47 topo sheets cover all of Kodiak, Afognak and the Trinity Islands. Each map has a color coded overlay which classifies the shoreline into 1 of 10 subclasses, described in this section. Even at that scale (1 inch = 1 mile) there are considerable areas left open to question since the coastal morphology of this diverse study area can change dramatically in a few tens of feet. Due to this extreme complexity (4,270 km of shoreline where classified), it is impossible to display the classification adequately in a report of this size without raising printing and drafting costs to an unreasonably high figure.

In Appendix 3, of this report, all 47 base maps have been listed. Under each base map, the 10 subclasses of the "Oil Spill Vulnerability Index" are listed with the number of shoreline kilometers falling into each class for that base map. There is also a summary section which lists the totals for each OSVI for the larger 1:250,000 topographic sheets (there are 5 for this study area). In addition to the total shoreline kilometers in each of the OSVI ratings, this summary section gives the percentages of these figures for both that base map and the total study area. Thus, we find that Afognak base map (1:250,000 scale) has 189.1 km of shoreline of class #1 (exposed rock headlands). That figure represents 14.7% of the Afognak shoreline but it represents 50.2% of all the #1 OSVI shorelines. Another example: On Kodiak we find that 5.4 km are classified as #5 (exposed tidal flats), which is only 0.2% of the Kodiak shoreline but 100% of class #5 for the study area. Finally, there follows a "Grand Total" sheet. This page lists the total shoreline kilometers for each base map and the percent of the total study area. It then lists the total shoreline kilometers for each class and the percent of the total study area. Even though detailed maps do not accompany this report, inferences regarding the vulnerability of various areas can be obtained from the Appendix 3.

Our group has been studying oil spills and doing baseline analysis of various coastal areas for about 4 years. There is currently available a large number of publications dealing with specific spills (Blount, 1978; Blount and Gundlach, 1977; Gundlach and Hayes, 1977; Gundlach, Fischer and Stein, 1977; Gundlach, Ruby and Blount, 1977; Gundlach et. al., 1977; Hayes and Gundlach, 1975; Hayes et. al., 1976; Ruby et. al., 1977) as well as many dealing specifically with our

coastal work in parts of Alaska (Gundlach et.al., 1977; Hayes, Michel, and Brown, 1977; Ruby and Hayes, 1978; Hayes et.al., 1976; Nummedal and Stephen, 1976; Nummedal, Stephen and Ruby, 1977; Nummedal and Ruby, 1979; and a number of Annual and Progress Reports to OCSEAP). Those reports detail the controls that beach morphology, grain size and incoming energy can have on oil spill behavior and longevity. A number of the reports address the potential impacts of spills on various of the Alaskan marine assemblages. These earlier results will not be repeated in this report. They strongly support the concept that physical degradation of spilled oil is directly related to the marine energy in the spill environment. Table 2 from Rashid (1974), gives strong supportive quantitative data in this regard.

Table 2 Chemical and physical characteristics of original and residual Bunker C oils extracted from sediments collected in Chedabucto Bay 3½ years after the Arrow spill (from Rashid, 1974).

Characteristics	Bunker C oil		Low energy coast	Moderate energy coast	High energy coast
	Original ^a	Stored sample			
Hydrocarbons (%)					
Saturated	--	26	25	23	18
Aromatic	--	25	24	24	16
Total hydrocarbons	73.1	51	49	47	34
Ratio of saturate to aromatic	--	1.04	1.04	0.96	1.12
Non-hydrocarbons (%)					
Asphaltenes	16.3	20	22	23	22
Resins and NSOs	10.6	29	29	30	44
Total of non-hydrocarbons	26.9	49	51	53	66
Hydrocarbons/. non-hydrocarbons	2.72	1.04	0.96	0.88	0.52
Physical properties					
Specific gravity	0.950	0.963	0.9953	0.9765	0.9823
Viscosity (cP)		19.584	28.600	1210.000	3640.000

^a Task Force Operation Oil Report, 1970

Cold Water Spills

There is abundant literature dealing with case studies of the numerous major and minor oil spills that have taken place in the coastal waters of the lower 48 states and around the world. Predictive models for oil spill dispersal, spreading, bio-degradation and physical degradation have been developed from these studies. The sub-arctic areas, however, have been to a large extent omitted due to the difficulties inherent in any study of these environments and a general lack of actual oil spills in these environments from which to base detailed case studies. The Arrow oil spill in Chedabucto Bay, Nova Scotia, probably comes closest to a comparative model for the sub-Arctic. However, the clean-up effort and later studies (Owens and Drapeau, 1973; Owens, 1973; Drapeau, 1973; Owens, 1971; Owens and Rashid, 1976), made very little reference to the special problems encountered as a result of the colder environment (i.e. oil on ice and snow; ice-oil interaction with beach sediments; oil dispersal in heavily iced environments, etc.). Our investigation of the Buzzards Bay oil spill (Ruby et.al., 1977) and the Ethyl H. spill in the frozen Hudson River, have given new insight into the extremely limiting effects of oil spills in ice-choked waters.

Further, evaporation losses and biodegradation are slower in colder environments. Biodegradation can be reduced as much as 90% in water of 0°C when compared to water of 25°C (Robertson, 1972). Isakson et.al., (1975) states that burning may be the only feasible method of cleaning oil spills in iced areas; however, this may represent a trade of one type of pollution for another. During the Buzzards Bay spill clean-up, burning was an effective method for cleaning oil which was not accessible from the shore. Only a small amount of particulate matter resulting from the fires was noticed.

Finally, intense tidal currents and winds in the study area can disperse the spilled oil in an unpredictable manner, making it nearly impossible to recover before it impacts on nearby shorelines. Drapeau et.al., (1970) concluded that it is not feasible to recover or disperse oil slicks in regions of high tidal currents.

Environmental Vulnerability to Oil Spills

This scale has been devised on the basis of actual spill analysis and a careful study of the literature. It is based primarily on the longevity of oil in each sub-environment, which is generally a function of the intensity of the marine processes, sediment grain size and transport trends. The biologic sensitivity has also been utilized to modify the ratings of various environments.

Coastal environments are listed and discussed below in order of increasing vulnerability to oil spills.

Oil Spill Vulnerability Scale

1. Straight rocky headlands:

Most areas of this type are exposed to maximum wave energy. Waves reflect off of the rocky scarps with great force, readily dispersing the oil. In fact, waves reflecting off the scarps at high tide tend to generate a surficial return flow that keeps the oil off the rocks (observed at the Urquiola site in Spain and the Amoco Cadiz spill in France, see Figure 6). Even if oiled, natural cleaning will only require a few days or weeks. No human intervention is necessary. Almost 9% of the study area falls into this class. They occur in many different areas, always exposed.

2. Eroding wave-cut platforms:

These areas are also swept clean by wave action. All of the areas of this type at the Metula site had been cleaned of oil after one year. The rate of removal of the oil is a function of wave climate and the irregularity of the platform. In general, no clean-up measures are needed for this type of coast. However, there are large biologic populations in these areas. Most of these areas, 16.5% of the study area occur on Kodiak and Afognak Islands in highly exposed areas.

3. Flat, fine-grained sandy beaches:

Beaches of this type are generally flat and hard packed. Oil that is emplaced on such beaches will not penetrate more than a few centimeters at most. Usually the oil will be deposited on the surface of the sand where it can be removed by elevated scrapers or other road grading machinery. Furthermore, these types of beaches change slowly, so sand deposition and resultant burial of oil will take place at a slow rate. If left to natural processes, these beaches will be cleaned within several months. This type of beach is very rare in the study area representing only 0.7% of the shoreline.

4. Steeper, medium to coarse-grained sandy beaches:

On these beaches, the depth of penetration would be greater than for the fine-grained beaches (though still only a few centimeters), but rates of burial of the oil would be greatly increased. Based on our earlier studies, it is possible for oil to be buried as much as 50-100 cm within a period of a few days on beaches of this class. In this situation, removal of the oil becomes a serious problem, since removal of the oiled sediments will often result in large scale

erosion, as the beach changes into a new equilibrium state. This was a common problem encountered during the cleanup of the Arrow spill in Chedabucto Bay, Nova Scotia (Owens and Rashid, 1976). Another problem is that burial of the oil preserves it for release at a later date when the beach erodes as part of the natural beach cycle, thus causing longer term pollution of the environment. This class represents only 0.1% of the study area.

5. Impermeable exposed tidal flats:

One of the major surprises in the study of the Metula site was the discovery that oil had not remained on the mud flats. At the Urquiola site, oil was observed as it became refloated with rising tides on the mud flats. Penetration of the oil is prevented by the extremely fine sediment size, saturated with water. Therefore, if an oiled tidal flat is subject to winds and currents, the oil will tend to be removed, although not at the rapid rate encountered on exposed beaches. Mechanized clean-up is considered impossible. These are often areas of high biologic importance. These areas are very rare in the study area due to a lack of fine sediment. They represent only 0.1% of the total study area.

6. Mixed sand and gravel beaches:

On beaches of this type, the oil may penetrate several centimeters, and rates of burial are quite high (a few days in Spain). Any attempt to remove the oiled sediment will result in considerable erosion. This type of beach is the second most common in the study area, representing 22.1%. These beaches occur where till or glacial deposits are being reworked by marine processes and as pocket beaches between headlands. The longevity of the oil at the Metula site, particularly on the low-tide terraces and berm top areas, attests to the high susceptibility of this type of beach to long-term oil spill damage. Natural cleaning may require many years.

7. Gravel beaches:

Pure gravel beaches allow the oil to penetrate to considerable depth (up to 45 cm in Spain). Furthermore, rapid burial is also possible. A heavily-oiled gravel beach will be impossible to clean up without completely removing the gravel. Natural cleaning will be quite slow for this type of beach; the exact time required will depend on the intensity of the marine processes. Pure gravel beaches are quite common in the study area representing almost 15% of the shoreline. They occur mostly as pocket beaches and fronting rock scarps. In some cases they can be quite long.

8. Sheltered rocky headlands:

Our experience in Spain indicates that oil tends to stick to rough rocky surfaces. In the absence of abrasion by wave action, oil could remain on such areas for years, with only chemical and biological processes left to degrade it. They usually have gravel beaches associated with them and for the purposes of this study, sheltered gravel beaches are classified with sheltered rocky headlands. They represent the largest single class or 34.2% of the study area. Most of these areas are on Afognak Island and in the fjords on Kodiak Island.

9. Protected estuarine tidal flats:

If oil reaches a quiet, protected estuarine tidal flat, it will remain there for long periods because natural cleaning progresses at an extremely slow rate. Because of the low intensity of marine process parameters, removal of the oil will have to be accomplished by natural chemical and biogenic processes. This will take many years, dependent on the amount of oil deposited. Because of their high biologic populations, these environments are very sensitive to the toxic effects of oil. These areas are rare in the study area occurring only at fjord heads and at river mouth estuaries.

10. Protected estuarine salt marshes:

In sheltered estuaries, oil from a spill may have long-term deleterious effects. We observed oil from the Metula on the salt marshes of East Estuary, in the south shore of the Strait of Magellan, that had shown essentially no change in 1½ years. We predict a life span of at least 10 years for that oil. These areas are extremely important biologically, supporting large communities of organisms. These areas are generally associated with the protected tidal flats (#9) and are also rare, representing only 1.2% of the study area.

Applications to the Kodiak Archipelago

Using the vulnerability classification just described, it is possible to make a few generalizations regarding the Kodiak area and its reaction to potential oil spills. In general, the area is quite high risk. More than 73.8% of the shoreline falls in classes 6 - 10. These classes will have a spill longevity of a year or two to more than 10 years. The remaining 26.2% of the shorelines fall into classes 1 - 5 which are considerably lower risk areas where spilled oil would generally be expected to be cleaned by natural processes within a year. A closer analysis (see Table 3) shows that actually the shoreline classification is bimodal. In other words a large percent of the shoreline falls into classes 6, 7 and 8 while most of the remainder falls into classes 1 and 2. Classes 3, 4, 9 and 10 represent only 3.5% of the shoreline combined. Thus, there is a clustering of very low risk shorelines and moderately high risk shorelines.

Unfortunately, the Kodiak system is very complex and the higher risk areas do not lend themselves well to being protected during a spill. In many instances,

a low risk rock scarp will lie just seaward of a large embayment with high risk pure gravel beaches. The fact that the environments change so frequently and rapidly along the shoreline, makes the entire island a fairly high risk area. The indented (fjord) character of the islands will act as "oil traps" for floating oil. Oil will tend to be moved deeper into the fjords rather than to be flushed out. In general this will result in an oiling of increasingly sensitive environments, since higher risk, lower energy classes are located deeper in fjords and embayments. Additionally, there are long periods of relatively low wind and wave energy, especially during the summer. A spill during one of these periods could prove particularly devastating since many of the areas classed 1 and 2 would become 7 and 8. Thus, Table 3 should be viewed as a "minimum" spill damage in the event of a large spill.

Since the Oil Spill Vulnerability Index is based partly on the longevity of potential oil spills within each of the subenvironments, the following guidelines are given:

<u>OSVI</u>	<u>Spill Longevity</u>
1 + 2	A few days to a few weeks
3 + 4	A month to six months
5 + 6	Six to 24 months
7 + 8	A year or two to as much as 8 years
9 + 10	Up to ten years

These figures are highly dependent on the wave energy during the spill and partly dependent on the temperature. They can vary and are meant to be estimates only. They give a relative indication of the longevity from one environment to another.

TABLE 3

<u>Km of Shoreline</u>	<u>% of Shoreline</u>	<u>Discussion</u>	<u>Classes</u>
1083.2	25.3	Oil easily removed by wave action. Some problems in areas of gravel accumulation and in tidal pools. Pocket beaches may be particularly hard hit. Do not recommend human intervention once oil is on beach.	1 + 2
38.6	0.9	Generally low risk areas and quite rare in the study area. Fine sands and mud tidal flats will not permit much penetration of oil. Low wave energy areas will require as much as a year for natural cleaning. Mechanized cleaning on sand beaches is quite feasible but represents a very small area. Recommend no human effort in these areas.	3 - 5
942.4	22.1	Sand and gravel beaches represent a large percent of the shoreline and tend to be relatively high risk beaches. They permit rather deep burial of oil and can retain oil for about 2 years, especially if it is emplaced high on the beach face (as during a spring tide). Mechanized clean up can be very difficult due to low bearing strength of the sediments. Removal of sediments may accelerate erosion.	6
634.2	14.9	Pure gravel beaches will permit immediate deep burial of oil. Retention periods, especially in a lower wave energy area can be many years. Mechanized clean up will be impossible without removal of sediment and increased erosion. The increased erosion, may not be of particular importance in uninhabited areas.	7
1462.0	34.2	Sheltered rock headlands and their associated gravel pocket beaches will be highly damaged in the event of a spill. They occur primarily in fjords and on the very irregular areas on Afognak Island. These areas should receive first protection priority in the event of a	8

TABLE 3 (cont)

<u>Km of Shoreline</u>	<u>% of Shoreline</u>	<u>Discussion</u>	<u>Classes</u>
		spill. All possible means should be used to prevent oil from entering these areas (booms, skimmers, etc). Once these beaches are oiled, expect severe biological damage, deep penetration, difficult clean up and longevity up to 8 years.	
109.8	1.6	These bayhead and river mouth systems are highly vulnerable. They are, however, rare in the study area. Further, they occur in areas which will receive maximum protection as discussed above. If oiled, bio-damage will be extreme, recovery slow and spill longevity up to 10 years.	9 + 10

REFERENCES

- Alaska Regional Profiles, Southcentral Region, 1975, L.L. Selkregg (Coordinator), The University of Alaska, 255 p.
- Blount, A.E., 1978, Two years after the Metula oil spill, Strait of Magellan, Chile: Oil interaction with coastal environments: Tech. Rept. No. 16-CRD, University of South Carolina.
- Blount, A.E., and Gundlach, E.R., 1977, Response of coastal environments to the Metula oil spill in the Strait of Magellan, southern Chile: Geol. Soc. Am. Annual Meeting, Seattle, Washington, pp. 902-903.
- Budnik, R., 1974, The geologic history of the Valdez Group, Kenai Peninsula, Alaska: Deposition and deformation at a Late Cretaceous compressive plate margin (Ph.D. thesis): Los Angeles, University California, Los Angeles, 139 p.
- Burk, C.A., 1965, Geology of the Alaska Peninsula-Island arc and continental margin: Geol. Soc. America Mem. 99, 250 p.
- Carden, J.R., 1977, The geology and comparative petrology and geochemistry of the Seldovia/Kodiak and Brooks Range blueschist terranes, Alaska (Ph.D. thesis): Fairbanks, Univ. Alaska.
- Carden, J.R., Connelly, W., Corbes, R.B., and Turner, D.L., 1977, Blueschists of the Kodiak Islands, Alaska: An extension of the Seldovia schist terrane: Geology, v. 5, pp. 529-533.
- Clark, S.H.B., 1972, Reconnaissance bedrock geologic map of the Chugach Mountains near Anchorage, Alaska: U.S. Geol. Survey Misc. Geol. Inv. Map MF-350.
- Climatic Atlas of the Outer Continental Shelf Waters and Coastal Regions of Alaska, Volume 1, 1977, U.S. Department of Commerce, National Oceanic and Atmospheric Administration, Alaska Outer Continental Shelf Environmental Assessment Program, 439 p.
- Davies, J.L., 1973, Geographical Variation in Coastal Development: Hafner publishing company, New York, New York, 204 p.
- Drapeau, G., Harrison, W., Bien, W., and Leinonen, P., 1974, Oil slick fate in a region of strong tidal currents: Proc. 14th Coastal Eng. Conf., pp. 2245-2259.
- Dyer, K.R., 1973, Estuaries: A Physical Introduction: John Wiley and Sons, London, 140 p.

- Gundlach, E.R., Fischer, I.A., and Stein, R.J., 1977, The black tide of La Coruna: Oceans, Vol. 10, No. 2, pp. 56-60.
- Gundlach, E.R., and Hayes, M.O., 1977, The Urquiola oil spill: Case history and discussion of clean-up and control methods: Marine Pollution Bull., Vol. 8, pp. 132-136.
- Gundlach, E.R., Hayes, M. O., Ruby, C.H., and Nummedal, D., 1977, Application of a shoreline vulnerability index for predicting oil spill impact: Abstr., Poster Session, Coastal Soc., Annual Meeting, Seattle, Washington.
- Gundlach, E.R., Hayes, M.O., Ruby, C.H., Ward, L.G., Blount, A.E., Fischer, I.A., and Stein, R.J., 1977, Some guidelines for oil spill control in coastal environments, based on field studies of four oil spills: ASTM Symposium on Chemical Dispersants for the Control of Oil Spills, Williamsburg, Va. pp. 98-118.
- Gundlach, E.R., Ruby, C.H., and Blount, A.E., 1977, Massive oil spill in La Coruna, Spain; Short-term impact on beaches and rocky coasts as a function of coastal geomorphology and marine processes: Abstr., Geol. Soc. Am. Annual Meeting, Seattle, Washington, p. 999.
- Hayes, M.O. and Gundlach, E.R., 1975, Coastal geomorphology and sedimentation of the Metula oil spill site in the Strait of Magellan: Rept. National Science Foundation, Washington, D.C., 103 p.
- Hayes, M.O., Gundlach, E.R., and Perhac, R.M., 1976, The great Patagonian oil spill: Abstr., AAPG-SEPM Annual Meeting.
- Hayes, M.O., Michel, J., and Brown, P.J., 1977, Lower Cook Inlet, Alaska: Application of oil spill vulnerability index: 4th Inter. Conf. on Port and Ocean Eng. under Arctic Conditions, St. Johns, Newfoundland, pp. 828-843.
- Hayes, M.O., Ruby, C.H., Stephen, M.F., and Wilson, S.J., 1976, Geomorphology of the southern coast of Alaska: Abstr., 15th Inter. Coastal Eng. Conf., Hawaii, p. 530.
- Hayes, M.O., Ruby, C.H., Stephen, M.F., and Wilson, S.J., 1976, Geomorphology of the Southern coast of Alaska: Proc. 15th Inter. Coastal Eng. Conf., Hawaii, pp. 1992-2008.
- Hill, B.B., 1975, Layered gabbroic and ultramafic rocks in a tectonic melange, Kodiak Islands, Alaska: Geol. Soc. America Abs. with Programs, v. 7, p. 1116.
- Innman, D.L. and Nordstrom, C.E., 1971, On the tectonic and morphologic classification of coasts: Jour. of Geol., Vol. 79, pp. 1-21.

- Isakson, J.S., et al., 1975, Comparison of ecological impacts of postulated oil spills at selected Alaskan locations: USGS Rept. No. CG-D-155-75, Vol. 1, 633 p., Vol. 2, 865 p.
- Jakes, P., and Gill., 1970, Rare earth elements and the island arc series: Earth and Planetary Sce. Letters, v. 9, pp. 17-28.
- Jones, D.L., and Clark, S.H.B., 1973, Upper Cretaceous (Maestrichtian) fossils from the Kenai-Chugach Mountains, Kodiak and Shumagin Islands, southern Alaska: U.S. Geol. Survey Jour. Rsearch, v. 1, pp. 125-136.
- Matthews, D.H., 1971, Altered basalts from Shallow Bank, an abyssal hill in the NE Atlantic and from a nearby seamount: Royal Soc. London Philos. Trans. v. 268, pp. 551-572.
- Moore, G.W., 1967, Preliminary geologic map of Kodiak Island and vicinity, Alaska: U.S. Geol. Survey Open-File Rept. 271.
- Moore, G.W., 1969, New formations on Kodiak and adjacent Islands, Alaska: U.S. Geol. Survey Bull. 1274-A, pp. A27-A35.
- Moore, J.C., 1973a, Cretaceous continental margin sedimentation, southwestern Alaska: Geol. Soc. America Bull., v. 84, pp. 595-614.
- Moore, J.C., 1973b, Complex deformation of Cretaceous trench deposits, southwestern Alaska: Geol. Soc. America Bull., v. 84, pp. 2005-2020.
- Moore, J.C., 1978, Orientation of underthrusting during latest Cretaceous and earliest Tertiary time, Kodiak Islands, Alaska: Geology, v. 6, pp. 209-213.
- Nilsen, T.H., and Bouma, A.H., 1977, Turbidite sedimentology and depositional framework of the Upper Cretaceous Kodiak Formation and related stratigraphic units, southern Alaska: Geol. Soc. America Abs. with programs, v. 9, p.1115.
- Nisbet, E.G., and Price, I., 1974, Siliceous turbidites: Bedded cherts as redeposited, ocean ridge-derived sediments, in Hsu, K.J., and Jenkins, H.C., (eds.) Pelagic sedimentation: On land and under the sea: Internat. Assoc. Sedimentologists Spec. Pub. 1, pp. 351-366.
- Nummedal, Dag, and Ruby, Christopher, H., 1979, Spilled Oil Retention Potential Beaufort Sea, Proc. 5th Inter. Conf. on Port and Ocean Eng. Under Arctic Conditions, Trondheim, Norway, August 13, 1979 (in press).
- Nummedal, D. and Stephen, M.F., 1976, Coastal dynamics and sediment transportation: Northeast Gulf of Alaska: Tech. Rept. No. 9-CRD, Univ of South Carolina, 148 p.
- Nummedal, D., Stephen, M.F., and Ruby, C.H., 1977, Reconnaissance Evaluation of Longshore Sediment Transport, Northeast Gulf of Alaska: Proceedings 4th Int. Conf. on Port and Ocean Eng. Under Arctic Conditions, St. Johns, Newfoundland, September, pp. 892-903.

- Owens, E.H., 1971, The restoration of beaches contaminated by oil in Chedabucto Bay, Nova Scotia: Marine Sci. Branch, Ottawa, Can., Manus, Rep., Serv., No. 19, 75 p.
- Owens, E.H., 1973, The cleaning of gravel beaches polluted by oil: Proc. 13th Coastal Eng. Conf., Vancouver, B.C., pp. 2543-2556.
- Owens, E.H., and Drapeau, G., 1973, Changes in beach profiles at Chedabucto Bay, Nova Scotia, following large scale removal of sediments: Can. Jour. Earth Sci., 10, pp. 1226-1232.
- Owens, E.H., and Rashid, M.A., 1976, Coastal environments and oil spill residues in Chedabucto Bay, Nova Scotia: Can. Jour. Earth Sci., 13, pp. 908-928.
- Plafker, G., 1972, Alaskan earthquake of 1964 and Chilean earthquake of 1960: Implications for arc tectonics: Jour. Geophys. Research, v. 77, pp. 901-925.
- Plafker, G., and Kachadoorian, R., 1966, Geologic effects of the March 1964 earthquake and associated seismic sea waves on Kodiak and nearby islands, Alaska: Geological Survey Prof. Paper 543-D, 45 p.
- Rashid, M.A., 1974, Degradation of bunker C oil under different coastal environments of Chedabucto Bay, Nova Scotia: Estuarine and Coastal Marine Sci., 2, pp. 137-144.
- Robertson, B., Arhelger, S., Kinney, P.J., and Button, D.K., 1973, Hydrocarbon biodegradation in Alaskan waters: Center for Wetlands Resources, Louisiana State Univ., LSU-SG 73-01.
- Ruby, C.H., and Hayes, M.O., 1978, Application of an oil spill vulnerability index to the Copper River Delta, Alaska: Proceedings, Coastal Zone 1978, San Francisco, Cal., March, pp. 2204-2220.
- Ruby, C.H., Ward, L.G., Fischer, I.A., and Brown, P.J., 1977, Buzzards Bay oil spill - an Arctic analogue: 4th International Conf. on Port and Ocean Eng. under Arctic Conditions, St. Johns, Newfoundland, September, pp. 844-855.
- Silvester, R., 1970, Growth of crenulate shaped bays to equilibrium: Proc. ASCE. 96 (WW2), pp. 275-287.
- Stanley, K.W., 1966, Effects of the Alaska earthquake of March 27, 1964 on shore processes and beach morphology: Geological Survey Prof. Paper 543-J, 21 p.
- U.S. Army Coastal Engineering Research Center, 1975, Shore Protection Manual, Vol. 1, Second Edition.
- U.S. Naval Weather Service Comman, 1970, Summary of Synoptic Meteorological Observations, North American Coastal Marine Areas: National Climatic Center, Asheville, North Carolina.

von Huene, R., 1972, Structure of the continental margin and tectonism at the eastern Aleutian trench: Geol. Soc. America Bull., v. 83, pp. 3613-3626.

Wise, S.W., Jr., and Weaver, F.M., 1974, Chertification of oceanic sediments, in Hsu, K.J., and Jenkyns, H.C., (eds.) Pelagic sedimentation; On land and under the sea: Internat. Assoc. Sedimentologists Spec. Pub. 1, pp. 301-326.

APPENDICES

- APPENDIX 1. Grain Size Analysis - shows results of both sieve and settling tube grain size analysis and later computer synthesis.
- APPENDIX 2. Profile Site Descriptions - describes the location, sediment composition, bedrock composition, wave energy, sample types and locations as well as the general beach morphology, depositional and erosional features and biotic abundance of each of the profile sites.
- APPENDIX 3. Oil Spill Vulnerability and Coastal Morphology - shows numerically the kilometers of shoreline which fall into each of the 10 sub environments described in the text of this report. The first section shows a breakdown of each topographic sheet (1:63,360 scale). The second section shows the totals for each full scale topographic sheet (1:250,000) and the grand totals for the entire study area.
- APPENDIX 4. Profile Plots - computer plots of all profile sites at a 1:5 vertical exaggeration.

APPENDIX 1

Kodiak and Afognak Island Beach Sediment Samples

<u>Station Number</u>	<u>Mean Grain Size (ϕ)</u>	<u>Standard Deviation (ϕ)</u>
KDP1a	1.413	0.749
KDP1b	0.568	0.748
KDP1c	0.524	0.678
KDP1 mean	0.835	0.725
KDP3a	1.876	1.418
KDP3b	2.509	1.235
KDP3c	0.470	1.666
KDP3 mean	1.618	1.106
KDP5a	1.745	0.473
KDP5b	2.273	1.142
KDP5c	0.810	0.649
KDP5 mean	1.609	0.754
KDP7b	-2.413	1.926
KDP9	Rocky headland - no samples	
KDP11	Rocky headland - no samples	
KDP13a	2.314	1.644
KDP13b	2.937	2.322
KDP13c	1.276	1.748
KDP13 mean	2.176	1.905
KDP15b	1.402	1.589
KDP17a	1.035	0.697
KDP17b	2.200	0.744
KDP17c	1.532	1.070
KDP17 mean	1.589	1.837
KDP19	Rocky headland - no samples	
KDP21b	-3.700	0.867
KDP23a	-1.516	1.182
KDP23c	-1.265	0.489
KDP23 Dune sample	0.792	1.273
KDP 23 mean (excluding dune sample)	-1.391	0.836
*KDP25a	-1.794	1.097
*KDP25b	-2.615	0.929
*KDP25c	-2.733	1.057
KDP25 mean	-2.381	1.03

<u>Station Number</u>	<u>Mean Grain Size (ϕ)</u>	<u>Standard Deviation (ϕ)</u>
KDP27a	1.469	1.415
KDP27b	-2.405	1.321
KDP27c	-2.428	1.272
KDP27 mean	-1.123	1.336
KDP29a	-3.502	0.598
KDP29b	-2.235	0.690
KDP29c	-2.942	1.708
KDP 29 mean	-2.893	0.999
KDP31	Rocky headland - no samples	
KDP33a	-3.322	0.922
KDP33b	-2.575	0.868
KDP33c	-3.513	0.712
KDP33 mean	-3.136	0.834
KDP35a	-2.161	1.337
KDP35b	-1.801	2.268
KDP35 mean	-1.981	1.803
KDP37b	-2.429	1.982
KDP39b	-2.004	1.507
KDP41a	3.925	0.245
KDP41b	-1.956	1.273
KDP41c	2.129	1.097
KDP41 mean	1.366	0.872
KDP43a	-4.620	0.349
KDP43b	-3.406	0.841
KDP43 mean	-4.013	0.595
KDP45a	-4.560	0.468
KDP45b	-4.835	0.418
KDP45c	-2.793	1.947
KDP45 dune	-2.821	0.721
KDP45 mean (excluding mean dune sample)	-4.063	0.944
KDP47a	-2.610	2.008
KDP47b	-2.098	1.135
KDP47c	-1.853	2.014
KDP47 mean	-2.187	1.719
KDP49	Rocky headland - no samples	
KDP51a	-1.805	1.702
KDP51b	-2.066	1.834
KDP51c	-0.884	2.027
KDP51 mean	-1.585	1.854

<u>Station Number</u>	<u>Mean Grain Size (ϕ)</u>	<u>Standard Deviation (ϕ)</u>
KDP53	Rocky headland - no samples	
KDP55b	-2.331	0.989
KDP57a	-2.296	0.590
KDP57b	-2.154	0.649
KDP57c	-2.116	0.860
KDP57 mean	-2.189	0.700
KDP59a	-2.397	1.575
KDP61a	-3.113	1.782
*KDP61b	-2.571	1.170
KDP61 mean	-2.842	1.476
KDP63	Cobble spit - no samples	
KDP65b	2.611	1.532
		1.002
KDP67a	-0.844	1.208
*KEP67b	-1.686	1.105
KDP67 mean	-1.265	
KDP69a	2.122	0.687
KDP69b	1.514	0.532
KDP69c	0.024	0.827
KDP69 mean	1.220	0.682
KDP71a	0.824	0.525
KDP71b	1.325	0.545
KDP71c	1.209	0.731
KDP71 mean	1.119	0.600
KDP73a	-1.183	2.241
KDP73b	-1.942	1.048
KDP73c	-2.517	1.454
KDP73 mean	-1.880	1.581
KDP75a	-3.476	0.449
KDP75b	-2.976	0.700
KDP75 mean	-3.226	0.576
KDP77	Rocky headland - no samples	
KDP79a	2.168	0.080
KEP79b	0.366	1.443
KDP79c	1.386	0.981
KDP 79 mean	1.307	0.834
KDP81b	-1.855	1.726

<u>Station Number</u>	<u>Mean Grain Size (ϕ)</u>	<u>Standard Deviation (ϕ)</u>
KDP83a	-3239	2.065
KDP83b	-1.923	2.003
KDP83 mean	-2.581	2.034
KDP85b	0.560	0.733
KDP87	Rocky headland - no samples	
KDP89a	-1.846	1.146
KDP89b	-1.527	0.853
KDP89c	-1.557	1.353
KDP89 mean	-1.643	1.117
*KDP91a	-2.975	1.-09
*KDP91b	-3.068	1.555
KDP91 mean	-3.020	1.310
*KDP93a	-2.603	1.294
KDP93b	-2.807	0.392
*KDP93c	-1.958	1.590
KDP93 mean	-2.450	1.094
*KEP95a	-1.903	2.260
KDP95b	-2.893	1.083
*KEP95c	-1.940	1.367
KDP95 mean	-2.250	1.570
KDP97a	0.586	0.554
KDP97b	1.169	1.141
KDP97c	-0.075	1.367
KDP97 mean	0.840	1.020
*KDP99a	-2.170	1.885
KDP99b	-1.330	1.713
KDP99c	-1.864	0.878
KDP99 mean	-1.788	0.825
KDP101b	-1.640	1.868
KDP103b	-2.043	1.610
*KDP105a	-2.328	1.877
*KDP105b	-1.912	1.760
KDP105 mean	-2.120	1.318
KDP107	Rocky headlands - no samples	
KDP109a	-1.843	1.030
KDP109b	-1.600	1.210
KDP109 mean	-1.722	1.120
KDP111	-3.803	

<u>Station Number</u>	<u>Mean Grain Size (o/)</u>	<u>Standard Deviation (ϕ)</u>
KDP113a	-3.803	1.008
KDP113b	-0.744	0.894
KDP113c	-2.080	0.863
KDP133 mean	-2.209	0.922
*KDP115a	-1.847	1.021
KDP115b	-2.002	1.431
KDP115 mean	-1.925	1.226
KDP117a	0.743	0.976
KDP117b	3.309	0.560
KDP117c	2.542	1.159
KDP117 mean	2.198	0.897
KDP119a	0.887	1.269
KDP119b	0.354	0.728
KDP119c	-2.085	1.840
KDP119 mean	-0.281	1.279
KDP121a	-1.810	0.479
KDP121b	-1.885	1.021
KDP121c	-2.059	0.604
KDP121 mean	-1.918	0.701
KDP123a	-1.425	0.525
KDP123b	-1.371	1.035
KDP123c	-1.651	0.857
KDP 123 mean	-1.482	0.806
KDP125b	-2.735	1.583
KDP127a	-2.915	0.974
*KDP127b	-2.838	1.762
KDP127c	-2.523	1.213
KDP127 mean	-2.759	1.316

* Indicates a polymodal sample.

APPENDIX 2

KDP1:

1. Location:

0.5 km east of Afognak Point, 57°51'30"N, 152°47'30"W.

2. Body:

Basically, a low energy rock platform with a veneer of granule-gravel beach on the landward one half of the platform. An active low, poorly developed storm berm is currently building and migrating landward into the forest. That action is the result of the downwarp associated with the Good Friday Earthquake of 1964. Numerous dead trees line the upper beachface - resulting from salt water intrusion due to downwarping. Beach is quite narrow and of only moderate steepness. Two primary zones 1) Granules on bottom ½ of beachface; 2) Granules and medium to coarse discoid gravel. Rock platform is generally devoid of sediment and covered with very heavy intertidal life.

3. Energy and Rock Type:

Generally rather low energy. Rock type and beach sediments - shale, slate and greywacke.

4. Sample Index:

At the upper storm berm - cobbles and some large pebbles. Discs abundant. Black metamorphic sand underneath. At the high tide swash line, gravel 2-5 cm with a few large, 30 cm, cobbles.

A Sample - taken from the base of the cobble toe and gravel zone. Some sand here mixed in with the pebbles and very small cobbles.

B Sample - Loose 1/2 cm pebbles here with black sand underneath.

C Sample - Larger pebbles, 1-2 cm, black sand underneath. Also much shell material.

The shape changes from disc to bladed (from top to base of beachface), not dramatically as discs do show up near LTT. Everything is fairly angular, not equant.

KDP3:

1. Location: West side of Kazakof Bay.

2. Body:

This side of the bay is composed of steep low rock scarps (10-15 ft. high) and small pocket beaches. Rock scarps have well developed biotic zonation. There are many sea caves and arches. The profile runs across a nicely developed, moderately sloping beach of platy, black, low-ranked metamorphic rock. The beach has a grain size zonation with a fine zone between the spring high tide swash and the last high tide swash. It then coarsens

to the waterline where there is a step. It also coarsens toward the upper beachface. Very abundant intertidal life on the low tide terrace and rocks.

3. Energy and Rock Type:

Generally quite low energy. Sediment and rock type - low-ranked metamorphic.

4. Sample Index:

Sediment sample - black sand with about 25% coverage of gravels of shale or greywacke and a little sandstone. L = 2-3 cm. 2 samples taken at 2 depths. Top 5 cm, KDP3A; 5-10 cm, KDP3A2. The bottom sample is much coarser, about 60% pebbles and cobbles - medium sand. All pebbles platy and disc shaped. The deeper part is coarser. Sand deposited on top.

B Sample - No change with depth. The sand is medium and covers 75% of this area. Pebbles and cobbles make up the other 25%. Still platy but better rounded than A. Cobbles' long axis up to 5 cm in size. Pebbles 1/2 cm, max. L axis.

C Sample - No change with depth. Sand is medium with some shell material - 70% sand, covered with small pebbles, I = 3 cm and cobbles, I = 13 cm, making up remaining 25%.

KDP5:

1. Location: 3 km north of Cape Kostromitinof.

2. Body:

This profile is located on an open seaward facing headland. Most of the shoreline has high scarps (approx. 50' high). The profile is located on a pocket beach of medium-coarse sand. The surface is covered by scattered discoidal pebbles. There is a high berm and storm berm, both covered with logs. Basically, this is a slightly erosional pocket beach at the head of the embayment. Profile backed by dense forest. Not much biotic population.

3. Energy and Rock Type:

Relatively high energy - Sediment and rock type - low-rank metamorphic-shale and slate.

4. Sample Index:

The sand is medium to coarse, 1 ϕ . 15 cm = L shale or slate discs scattered on surface. Fairly well rounded. Sample A - medium to coarse sand with some 15 cm = L discs, slate or shale. Sample B - same as A, but pebbles only 5 cm = I. Sample C - same as B, but pebbles better rounded.

KDP7:

1. Location: 5 km northwest of Peril Cape, $58^{\circ}10'18''N$, $152^{\circ}10'50''W$.

2. Body:

Photo station only - high scarps with no landing potential even for helicopter. High vertical scarp. Scarp is very irregular. Very low energy rocky shoreline. Small pocket beaches are poorly sorted and coarse grained. Some lower scarp areas with sea caves and stacks. There are numerous rock slides introducing very coarse and immature (angular) material onto the beach.

3. Energy and Rock Type:

Low energy area - Rock type, low-rank metamorphic rocks.

KDP9:

1. Location: East side of Izhut Bay, $58^{\circ}12'28''N$, $152^{\circ}12'20''W$.

2. Body:

Located in a crenulate bay composed of pure gravel, with a variety of grain sizes. Coarsest up high on storm berm and at low tide terrace near step. Fines in middle beachface. Large number of dead trees backing profile, killed by downwarp salt water intrusion. Gravel is very homogeneous in composition - hard black low-rank fine-grained metamorphic rock. Granules generally elongated and discoidal. Not much biotic population. Very clean and well-sorted gravels will result in great oil penetration. Some small washovers backing storm berm. Multiple berms on beachface.

3. Energy and Rock Type:

Generally lower energy - Rock type, low-rank metamorphic.

4. Sample Index:

A sample - 5 cm to 2 cm L axis, some larger at high tide swash line. B sample - slightly smaller. C sample - similar to A, butter rounded and more bladed. With depth here, no sand - a little gravel, 5%. But the cobbles are smaller as we dig below the surface.

KDP11:

1. Location: Western exposed side of Tonki Cape Peninsula, $58^{\circ}16'15''N$, $151^{\circ}57'50''W$.

2. Body:

Very irregular section of low rock scarps (10-15 ft. high) exposed to open Gulf of Alaska waves. Mostly coarse poorly developed beaches up high, perched on bedrock platforms. Profile runs across a berm composed of pebbles with a boulder-cobble low-tide terrace covered with algae. Irregular bedrock

knobs stick up through the beach and all over the platform. The beach is steep and very clean due to high energy. All gravels and cobbles are well rounded.

3. Energy and Rock Type:

Relatively high energy - Rock type - slate.

4. Sample Index:

Sample A - taken from in front of the berm at the upper beachface. Generally pebble and cobble with some boulders. I = 6 cm. Sample B - from the middle beachface is much the same, except some smaller pebbles and larger cobbles are found here. Also a gravel underneath this sample. Poor sorting. Sample C - this is from the low tide terrace. Cobbles, boulders and pebbles. Very large grain size and poor sorting. Underneath the later material is some granule and coarse sand. The low tide terrace has bedrock outcropping. All sediments are very well rounded with the berm being more disc-like and the beachface and low tide terrace more bladed.

KDP13:

1. Location: East side of Tonki Bay, 58°20'19"N, 152°07'00"W.

2. Body:

Located in a small embayment with a mixed sand - cobble beach fronting a rock scarp. There is a small stream and valley just off the profile to the north with a cobble beach just past that. The profile itself is very straight and simple, showing no distinctive patterns. Irregular patches of coarse gravel, fine cobbles, pebbles and sand cover the surface. The sediments are very well rounded and black. There is a small storm berm with logs on it just behind the stream. A step is apparent at the base of the beachface and a spectacular arch just to the south. Low biotic population on this profile except for the rock arch.

3. Energy and Rock Type:

Moderate energy - Rock type - slate-greywacke.

4. Sample Index:

Sample A is from the upper beachface and it is entirely large to small pebbles, well rounded with a granule and coarse (1.5 ϕ) sand base. A few boulders and cobbles outcrop here. Sample B is from the middle beachface and is much like A, except smaller pebbles, but more cobbles and boulders, also more sand and granule material, poorly sorted. Sample C is from the lower beachface. This is pure pebbles, granule and 1.0 to 0.5 ϕ coarse sand. Better sorting than A or B.

There is a loose step in front of the beachface that is comprised of well-rounded pebbles and granule. Very little sand there. The low tide terrace is similar to the beachface with many boulders. The cobbles and boulders on the beachface average $I = 15$ cm, with some much larger. There is not much of a shape change on the beach; all sediments are fairly well rounded, especially on the beachface. Many bladed with some equant shapes. Some well rounded discs on and behind the berm up against the scarp.

KDP15:

1. Location: 1 km west of Posliedni Point, $58^{\circ}25'43''N$, $152^{\circ}17'50''W$.

2. Body:

This is a typical rock headland in the Seal Islands area, facing the open Gulf of Alaska. The profile is very simple; it runs down this steep, very coarse-grained beach which is perched on a bedrock platform outcropping at the waterline. The beachface is covered by boulders with a mean size of 100 cm. Most are subangular to subround. Heavy algal coating on bottom 1/3 of profile. The rock scarp backing the profile is quite irregular, with mounds of dipping bedrock.

3. Energy and Rock Type:

High energy - Rock type, higher grade metamorphic rocks, schist and turbidites.

KDP17:

1. Location: Big Waterfall Bay, $58^{\circ}24'19''N$, $152^{\circ}31'40''W$

2. Body:

This is a small pocket beach between two rock headlands. There are a number of bedrock outcrops in the beachface indicating that the beachface is perched on a bedrock platform. There is a small stream which crosses the profile to the southeast. The area is backed by a dense forest on a high (30') rock scarp. There is a narrow perched berm covered with logs up high, just forward of the scarp. Then a coarser upper beachface composed of granules with scattered mixed gravel and some sandy patches. There is a sharp toe onto a low tide terrace of granule and fine gravel with considerable medium and coarse gravel. Relatively light biota covering the rocks, even on the lower part of the low tide terrace. The headlands surrounding this pocket beach have a very heavy covering of algae, mussels, barnacles, limpets, snails etc.

3. Energy and Rock Type:

Moderate energy - rock type, slatey shale.

4. Sample Index:

Sample A - zone of pure 0.5 ϕ sand. Sample B - on the broad low tide terrace - an unsorted mixture of pebbles, granules and coarse sand. The lower low tide terrace is mostly granule, sand and small pebbles. Grain size is smaller here than the upper and mid low tide terrace. The rounding is fair throughout, and there is no shape change. The composition is mostly of argillite or slate. Many other rock types are found though - greenstone and quartz. Only barnacles are found as the wave energy is moderate to high.

KDP19A:

KDP19B:

1. Location: Perevalnie Islands,

19A - 58^o39'05"N, 152^o18'45"W
19B - 58^o38'25"N, 152^o20'00"W.

2. Body:

These are very high shear rock scarps. They have a heavy algal coating. Not many barnacles or mussels - just algae. There are very large "house size" boulders at the base of these scarps. No pocket beaches. This area is highly exposed.

3. Energy and Rock Type:

Very high energy - Rock type, metamorphic (slate and shales).

KDP21

1. Location: Cape Newland, 58^o39'05"N, 152^o39'05"W.

2. Body:

This is a purely rock profile, run across a rock headland which protects a pocket beach to the south. The profile starts on clean dry rock with effluent of ground water from bedding planes. It then crosses a band of snails, then there is a very sharp contact with a Fucus zone, which is 1 m wide (vertically). Below that is a 1.5 m wide band of barnacle sand mussels. Then, below that, the rocks are totally covered by algae. There is a series of these small pocket beaches and rock projections along this shoreline section. Most of the pocket beaches are perched on bedrock platforms. The area is relatively sheltered. Productivity here is very high.

3. Energy and Rock Type:

Low energy - Rock type, greenstone with chert.

4. Sample Index:

Sample X - taken from a granule zone in a small tide pool. This sample approximates the sediment type of the pocket beach to the south.

KDP23:

1. Location: 1 km south of Black Cape, $58^{\circ}24'14''\text{N}$, $152^{\circ}52'55''\text{W}$.

2. Body:

A gravel-sand pocket beach with headlands on both sides. Behind the profile is a scarp into bedrock capped by a section of glacial outwash. There is a well-developed storm accumulation of coarse gravel, boulders, and logs at the base of the scarp. The broad middle beachface is composed of sand and granules with scattered gravels and cobbles. There are numerous algae swash lines on the beach. At the base of the beachface is a low tide terrace cut into bedrock (wave cut platform) with scattered gravels and boulders on it. Biota is not too high due to continued movement of the sediments. The rock headlands have very heavy accumulations of mussels. There is a large kelp bed offshore. Sediment size coarsens and becomes better rounded as the base of the beachface is approached.

3. Energy and Rock Type:

Moderate energy - Rock type, mostly pillow lava, quartz diorite, chert, greenstone, volcanics and various intrusives.

KDP25:

1. Location: Inner southern shore - Paramanof Bay, $58^{\circ}17'13''\text{N}$, $152^{\circ}50'15''\text{W}$.

2. Body:

Profile is run at the perimeter of a pocket beach below a 100' rock cliff. There has been a large rock fall onto the beachface and into the water, where it is covered with algae, etc. The beachface is mostly mixed gravel and granules. It is very short and very steep. There are large boulders from rock fall all over the beach. There are no sediment trends on this beach.

3. Energy and Rock Type:

Low to moderate energy - Rock type, volcanics and metamorphics.

KDP27:

1. Location: North side Malina Bay, $58^{\circ}14'25''\text{N}$, $153^{\circ}04'30''\text{W}$.

2. Body:

The profile is backed by a high (greater than 300 ft.) scarp into quartz diorite with well-rounded zeolites. At the base is a perched berm of coarse gravel and cobbles with scattered logs. From there, the sediments fine to the center of the beachface where it is mostly sand and fine gravel. All gravel is equant and subround to well rounded. Toward the toe of the beachface, the sediments get coarser very rapidly. Then there is a boulder-cobble low tide terrace, which is quite steep and short. There are rock falls to the east and west, and a large stack to the east. The rocks on the rock falls and low tide terrace have heavy algae and barnacle cover. A kelp bed is just offshore. Sediment rounding is very good throughout the entire beachface and a typically good shape gradation exists. Disc to rollers as one approaches the waterline.

3. Energy and Rock Type:

Low to moderate energy - Rock type, mostly quartz diorite.

KDP29:

1. Location: South shore - Malina Bay, $58^{\circ}11'52''\text{N}$, $153^{\circ}02'42''\text{W}$.

2. Body:

A classic gravel profile perched on a bedrock platform. There is a high level storm berm fronting a low scarp. The storm berm is composed of granules and pebbles (4-5cm diameter), mostly discoidal with some scattered logs on top. There are a few very minor berms on the upper beachface. Then it levels out, and gets coarser with well-developed gravel stripes. It is quite coarse and equant - to roller shaped at the waterline. The rock platform projects out from beneath the beachface just to the west of the profile. It has a heavy mussel and algal coating.

3. Energy and Rock Type: Moderate energy, rock type is variable.

4. Sample Index:

Sample A is taken from behind the largest berm in front of the storm berm and about 15 yards from the scarp. It is mainly pebbles of all sizes and shell material, also a little coarse gravel and small ($I = 6$ cm) cobbles. Pebbles are all well-rounded and are mainly disc-shaped with a few equant, bladed and rollers mixed in.

Sample B is taken from the last high tide line which is a small berm. It is entirely small pebbles and large gravel - good sorting here.

Sample C is taken from the lower middle beachface where the profile has flattened out. The shape here is mainly equant and rollers with some bladed. Sorting is poor with small cobbles, pebbles, granule and coarse (0.5 ϕ) sand shell material.

The grain size gets larger toward the waterline. Larger cobbles in the water, but the sorting gets poorer. Behind the largest berm, grain size gets larger, but sorting also gets poorer. Behind the large berm, there is no sand, only gravel pebbles and small cobbles. Much shell material is also found there.

KDP31:

1. Location: Raspberry Strait, north shore, 58°06'15"N, 153°04'00"W.

2. Body:

A small rock headland with the bedrock nearly vertical. This is a dip-slope type of beach. The profile is made up of angular to subangular cobbles (25-30 cm in diameter). There is a zone of barnacles up high, then a clean zone, then a thick zone of Fucus. The beach is very steep and homogeneous. Very simple profile. Uniformly coarse grained.

3. Energy and Rock Type:

Moderate energy - Rock type, argillite, slate and some schist.

KDP33:

1. Location: Malina Point, 58°02'25"N, 153°21'53"W.

2. Body:

There is a large headland here with a beautiful multi-berm gravel beach just to the north where we ran the profile. The beachface has three primary pebble berms. Sediments are slightly coarser in the berm runnels and at the toe of the beach. All gravels are pure, well rounded, well sorted and fine. Beach is quite steep. Gravel composition is variable. The storm berm is covered with logs and coarse gravel. Most gravel is disc shaped.

3. Energy and Rock Type:

Moderate energy - Rock type, quartz diorite and argillite.

4. Sample Index:

Sample A - between middle and seaward berm - large pebbles, small pebbles, well rounded, disc-shaped. Sample B - upper beachface - pebbles and granule. Sample C - lower beachface - sandy gravel, loose pebbles and small pebbles.

KDP35:

1. Location: Lost Timber Point, $57^{\circ}59'25''\text{N}$, $152^{\circ}59'10''\text{W}$.

2. Body:

A low bedrock scarp with narrow flat stretches of beach. Beach material is mixed sand and gravel. Gravel is subangular to subround, black and platy. Beach has two zones: 1) a flat beachface zone and, 2) a flatter low tide terrace made of cobbles to sand. The cobbles are angular and covered with barnacles, mussels and algae. Very simple profile backed by 10' scarp into sedimentary rock. Trees are falling off of the scarp indicating downwarp effect of earthquake.

3. Energy and Rock Type:

Low energy - Rock type, argillite and slate.

4. Sample Index:

Sample A - upper beach, has large and small pebbles underlain by a gravel and coarse sand made up of rock fragments. Sample B - lower beachface, is cobbles, pebbles and boulders of various sizes. The boulders are small. This is underlain by gravel and 1.0 ϕ sands. Very poor sorting. The shape is mainly rollers with a few equant and bladed.

KDP37:

1. Location: 2 km north of Seiba Point, $57^{\circ}58'15''\text{N}$, $153^{\circ}16'45''\text{W}$.

2. Body:

Profile on a small gravelly spit indicating transport to the SW. The top of the spit is grassy with some overwash material. There is a very low scarp into argillite slate next. Then there is a high level berm of medium gravel and an upper beachface of sand. There is a smaller berm next, made of pure gravel, all well rounded, platy to discoidal in shape. This berm is cusped with sandy patches in the bays. The grain size increases from there to the waterline (about 15-20 cm in diameter at waterline). Then they are roller shaped, well rounded argillite fragments. Rock headlands have typical heavy bio-coatings.

3. Energy and Rock Type:

Moderate to high energy - Rock type, argillite slate - low rank metamorphics.

4. Sample Index:

Sample A - just above high water mark - berm. Discs and bladed, large pebbles with a gravel and sand underneath. Sample B - just below high water mark - berm - large and small pebbles with gravel and sand underneath. Sample C - lower beachface - slate cobbles with a few dioritic cobbles. Small and

large pebbles with gravel and sand underneath.

KDP39:

1. Location: Just southeast of Rolling Point, $57^{\circ}51'20''N$, $153^{\circ}06'45''W$.
2. Body:

This profile is on the sheltered side (east) of the point. It is a small pocket beach in a receded bedding plane erosion zone. There are a number of them in the area. The profile is moderately steep, composed of angular to subangular platy cobbles. Very homogeneous composition (slate - argillite). There is a prominent sandy zone in the middle beach. The lower half of the beachface is covered with the typical intertidal life. This is a poorly-sorted beach.

3. Energy and Rock Type:

Low energy - Rock type, slate, argillite.

4. Sample Index:

Beachface is large platy boulders and cobbles on a coarse (1.0 to 0.5 ϕ) sand - Sample A. The sand is also platy rock fragments and shell material. Sample A was taken from there. Sample B - the middle beachface is large pebbles with a coarse sand and small pebble base. Some loose cobbles are also mixed in. Sample C - the lower beachface is all cobbles and boulders with pebbles and shell material. Underneath is some coarse sand rock fragments.

KDP41:

1. Location: lower west side of Terror Bay, $57^{\circ}42'12''N$, $153^{\circ}10'35''W$.
2. Body:

This station is located at the head of Terror Bay. There is a large fan delta and tidal flat complex associated with the Terror River. There are very broad mussel flats on swash bars fronting the river. The station has heavy marsh grass all over the surface of the inner bars (the high parts); the lower parts are covered with an algal mat layer. Beneath the algal cover is a sand and gravel river bar. The sediments are coarser than expected down low (mud would be more typical, but this is sands and granules). There is a definite decrease in grain size as you approach the delta edge. There is not much infauna here, surprisingly.

3. Energy and Rock Type:

Low energy - Rock type, highly mixed river sediments.

4. Sample Index:

Sample A is from the algal mat. Sample B is from the coarse material below it. Sample C is from the lower part of the marsh. Closer to the river mouth, the marsh sediment is much finer here and mussels and Fucus growth

are very extensive.

KDP43:

1. Location: Uganik Bay, 4 km north of Rock Point on outer Northeast Arm
57°48'03"N, 153°27'45"W

2. Body:

This is a small pocket beach about 100 m wide. It is narrow and uniform, located between two rock headlands. Backing the beachface is a rock scarp into slate (5' high). There is a high level berm of coarse discoidal gravel, then on the middle beachface there are a number of smaller berms of fine gravel with algal swash lines on them. From there, the material coarsen again to the water line; where there are scattered larger boulders. The rock headlands are heavily coated with typical intertidal algae and encrusting life. Most sediments are well sorted and well rounded.

3. Energy and Rock Type:

Moderate energy - Rock type - mostly slate - argillite with chert, greenstone, and quartz diorites.

4. Sample Index:

Sample C - lower beachface - granules, fine gravel and some larger gravel and cobbles.

KDP45:

1. Location: Uganik Bay, south shore of East Arm, 57°42'25"N, 153°28'55"

2. Body:

This is a small crenulate beach indicating transport to the NE. The profile is very highly concave upward, being very steep on the landward side. There is a low scarp up high with some aeolian activity behind it (mostly carbonate fragments, barnacle frags.). There is minor storm overwash gravel up there also. The entire profile has discoidal gravel scattered on the surface. Mostly black sand and gravels. The most striking feature is the

very discoid shape of gravels. The coarsest gravels occur on the low flat portion of the profile, finer in mid-beachface then coarse up high. Heavy algal cover on bottom $\frac{1}{4}$ of profile. Under the lower beach is a sand - gravel mix. Most of the sand is 0.0 to 1.5 \emptyset rock fragments.

3. Energy and Rock Type:

Low-moderate energy. Rock type: quartz diorite, slate and schist.

4. Sample Index:

Sample A - The top unit was a pure pebble unit, below it, a mixture of coarse unsorted fragments that make up a coarse sand. Some pebbles were also mixed in sample KDP45, top; and bottom KDP45 1 and 2; this sample was taken from the small loose pebble interface. Sample B - is mostly pebbles with a gravelly sand underneath mixed with pebbles. Sample C - is a mixture of large and small pebbles and gravel with a coarse sand and gravel underneath which is also mixed with pebbles.

We sampled the pebble berm and upper smaller pebble beachface, also a relict dune KDP45D.

KDP47:

1. Location: 3 km west of Broken Point, $57^{\circ}52'35''N$, $153^{\circ}39'35''W$.

2. Body:

Located in a small embayment which has a highly indented shoreline eroding into glacial till. It is flanked on both sides by bedrock headlands. The beach is steep, a mix of sand and gravel typical of reworked glacial material. There are two gravel berms at the base of the scarp. From there, the profile slopes off uniformly in a long gentle slope with a step that was above water when the profile was run. The rock headlands have heavy intertidal biota.

3. Energy and Rock Type:

Moderate to high energy - Rock type - quartz diorite and schist, greenstone, slate. Very variable gravel composition.

4. Sample Index:

Sample A - appears to be pure pebbles. Av. I = 1-2 cm, but under the surface layer is a mixture of pebbles and sand. Volumetrically about 75% cobbles; 25% sand. The sand is about 1 ϕ .

Sample B - located mid-beachface, we go from pebbles to gravel and pebbles. Sand is also found here (1.0 ϕ).

Sample C - the grain size of the sand is slightly coarser than the berm on upper beachface 0.5 ϕ . Scattered small and medium pebbles as well as much gravel here, about

60% sand

30% gravel

10% pebble

KDP49:

1. Location: 3 km north of Chief Point, 57^o43'50"N, 153^o55'40"W

2. Body:

Profile is run in a pocket beach backed by a lower rolling topography. This particular pocket is rather sheltered. There is a low scarp up high fronted by a coarse gravel zone. Then there is a zone of coarse sand over cobbles all perched on a bedrock platform. The rest of the profile is a long irregular rock platform covered with subangular to subround cobbles all covered with zoned epifauna. Start with a zone of Fucus and numerous small snails, then heavy mussel accumulation, getting larger seaward with a Mya looking clam burrowed in. Further out there is a pink bryozoan and many starfish, limpets, urchins, snails, hermit crabs, etc.

3. Energy and Rock Type:

Low to moderate energy - Rock type: schist, greenstone and slate.

4. Sample Index:

Sample A - mixed coarse sand and shell fragments with moderate sized

cobbles lying on top. Average cobbles I = 7 cm; L = 15 cm. The sand is black.

Sample B - large cobbles and schist bedrock. The cobbles mainly schist and greenstone with some slate. Cobbles are I = 15 cm.

Sample C - same as B.

All the cobbles are subangular. Cobbles and rocks on the berm are also subangular, but not that disc like. No shape change but a size change from small cobbles on the berm to sand and cobbles and pebbles on the upper beachface to coarse gravel and cobbles and bedrock on the lower beachface.

KDP51:

1. Location: Inner Spiridon Bay, $57^{\circ}36'15''N$, $153^{\circ}35'50''W$
2. Body:

A small pocket beach opposite two rock islands with connecting tombolos and gravel beaches. Thus this beach is highly protected. The gravels on the beach are very immature (discoid and angular to the water line). The pocket is partly protected by the rock scarps. The profile starts at the base of a low scarp backed by a valley. It crosses a narrow berm of fine and medium gravel with scattered logs. Then it crosses a steep beachface with numerous algal swash lines. Heavy intertidal life on bottom 1/3 of profile.

3. Energy and Rock Type:

Very low energy - Rock type: slate

4. Sample Index:

Sample A - beachface, small gravel with granule base. Most of beachface is similar.

KDP53:

1. Location: North side of Zachar Bay, $57^{\circ}35'35''N$, $153^{\circ}48'30''W$

2. Body:

This beach has three sharp zones. The beach is backed by a partly vegetated scarp into slate. Fronting this is a fine gravel-sand zone, then a coarse gravel-boulder mid-beach, then a boulder-cobble lower beachface covered with typical biota. The pocket is 100 m long and 30 m in width. It is not steep due to very poor sorting.

3. Energy and Rock Type:

Low to moderate energy - Rock type: argillite - slate

4. Sample Index:

The entire mid and lower beachface covered with barnacles. Sub-angular slate and/or argillite cobbles. The sorting is poor. A distinct grading of material toward the sea is obvious. Grain size gets larger seaward. Under the cobbles is mainly granule and small pebbles. Some qtz, greenstone and possibly sandstone cobbles are found in very small numbers on the beachface. A smooth steady slope exists along the entire beach.

KDP55:

1. Location: Southern eastern shore of Amook Bay, $57^{\circ}25'22''N$, $153^{\circ}48'40''W$

2. Body:

This is a very well developed discoid gravel beach. The beach is broad and steep. There is a scarp into slate backing the beach. Upper beachface is fine and medium gravel, then medium to coarse gravel then coarse gravel, finally near the water line its mostly boulders. The biota is highly zoned: 1) Barnacles, 2) mussels and barnacles, 3) mussels, 4) algae, 5) total coverage with many starfish. The gravel at the base of the beachface is slightly better rounded, still very platy.

3. Energy and Rock Type:

Low energy - Rock type: slate.

4. Sample Index:

The upper beachface and berm is well sorted - small discoid pebbles with a granule base. Some qtz is mixed in at the mid beachface. Only sample was A - upper beachface. B and C are photo samples.

KDP57:

1. Location: Inner west shore of Uyak Bay, $57^{\circ}20'50''N$, $153^{\circ}48'34''W$

2. Body:

Located on a small mid-bay-spit. This spit is very high and very steep, composed of fine to medium gravel. The beachface is quite uniform. Transport is out of the bay. The opposite side of the spit (facing north) is composed of coarser gravel on a rock platform. This beach has quite high energy considering its location. There are a few relict beach ridges on storm berms on the top of the spit, heavily vegetated. May be indicators of uplift. Most of this beach is well sorted and underlain by granules.

3. Energy and Rock Type:

Moderate energy - Rock type: shale, slate and argillite.

4. Sample Index:

Sample A - upper beachface - pure gravel

Sample B - mid-beachface - pure fine gravel

Sample C - lower beachface - pure gravel - slightly coarser.

KDP59:

1. Location: Middle west shoreline of Uyak Bay, $57^{\circ}35'22''N$, $153^{\circ}58'00''W$

2. Body:

Small pocket beach between two bedrock projections, backed by a low scarp into slate. Just at the base of the scarp is an accumulation of fine gravel and sand. The sediment coarsens toward the waterline. There are a lot of boulders on the beachface. Down low, its mostly coarser gravel on a gravel-granule foundation. The rock projections have heavy biotic coating. This section of shoreline has relatively high wave energy. In general beaches on the western shorelines of these fjords have broader beaches, better sorted, better developed berms and less encrusting biota; all indicators of higher energy than the east sides.

3. Energy and Rock Type:

Moderate energy - Rock type - slate

4. Sample Index:

Sample A - upper beachface - 1.0 ϕ sand and granule mix with gravel on surface.

Sample B - photo sample - platy subangular cobbles and mixed gravel.

Sample C - photo sample - same as B but coarser.

KDP61:

1. Location: 4.5 km southwest of Rocky Point, 57 $^{\circ}$ 38'28"N, 154 $^{\circ}$ 17'00"W

2. Body:

Profile is backed by a 150-200' granodiorite scarp, which is vegetated in some places. There is no indication of recent rock fall at the base of the scarp. There is a small stack 150 m to west. Fronting the scarp is a gravel zone, then a sandy zone, followed by a fine to medium gravel berm. In front of the berm is another sandy area which intersects a mixed gravel berm top overwash of a second gravel berm. From that point to the water line, the sediments coarsen rapidly. At the water line are mostly large boulders (0.5 - 1.0 m

diameter), with coarse gravel and cobbles. There is a large kelp bed offshore. Much less biota on the rocks here, due to wave energy and sediment supply.

3. Energy and Rock Type:

High energy - Rock type - granodiorite and some slate.

4. Sample Index:

The beach material is well rounded with many equant and roller shaped gravels and cobbles at the lower beachface, and bladed and discs on the berms.

Sample A - sandy area up high.

Sample B - 2nd berm top overwash - gravel on granule - sand mix.

Sample C - boulder - cobble terrace with considerable granules and gravel.

KDP63:

1. Location: Spit fronting - Sturgeon River, $57^{\circ}32'05''N$, $154^{\circ}33'05''W$

2. Body:

Open beach is pure gravel and cobbles. Profile is backed by shallow lagoon - tidal flat with heavy ell-grass and an organic mud bottom. The beach on the lagoon side is fine gravel and organic mud; from there it slopes up on a steep slip face of the washover terrace. On the top of the washover is a storm berm covered with logs. The beachface has three berms. The top one is the largest, composed of pure gravel. Middle one is finer and bottom one is coarsest (medium to coarse gravel). The final berm intersects a boulder-cobble low tide terrace. There is a kelp bed offshore. All sediments are well rounded quartz diorite.

3. Energy and Rock Type:

Very high energy with occasional violent storms - Rock type - quartz diorite.

4. Sample Index:

Samples - all gravel of various sizes.

KDP65:

1. Location: 5 km north of Gurney Bay, 57°19'48"N, 154°45'05"W

2. Body:

This is a slightly sheltered rocky coast, however, it does get high energy at times. The beach is fairly complex but basically dominated by large boulders on a narrow wave cut platform with bedrock outcropping all over. There are scattered pockets of gravels, cobbles and sand. The rock scarp backing the profile is very irregular with many stacks. Intertidal life coats these scarps heavily. The profile is relatively flat and littered with boulders (3-4 m long axis). The boulders have considerable biota: mussels, large and small barnacles, starfish, limpets, algae, snails and so forth, very diverse.

3. Energy and Rock Type:

Moderate energy - Rock type - quartz diorite, slate and greenstone.

4. Sample Index:

The beach material under the boulders and cobbles is all pebbles, granules and 0.0φ coarse sand.

Sample X - taken midway through the profile. It is a sample of pebbles, gravel and coarse sand. The average size of the beach material is 2-3 cm, pebbles and all sizes down to sand. Cobbles and boulders are very abundant also.

KDP67:

1. Location: Just landward of Ayakulik Island, 57°12'40"N, 154°33'00"W

2. Body:

Located on a wide glacial till plain. The scarp is high (70-80') into muddy till. The profile contains one simple convex upward berm with incipient

cusps. There is a complex zone of sand, granules and gravel on the berm surface. The bays of the cusps are sand and granules, the horns are coarser gravels. There is also a zone of coarser gravel just beneath the scarp, and at the step. There appears to be a wave cut platform just offshore with a sandy ridge on it. Relatively steep profile.

3. Energy and Rock Type:

High energy - Rock type - highly varied of glacial origin.

4. Sample Index:

Sample A - berm top - sand, granules and fine gravel.

Sample B - mid-beachface - mostly granules with scattered mixed gravel.

Sample C - lower beachface - granules and mixed gravel and cobbles all are well rounded and generally equant.

KDP69:

1. Location: 3 km southeast of Low Cape, $56^{\circ}59'00''N$, $154^{\circ}28'15''W$

2. Body:

This profile is basically a wave cut platform into till with a well developed beach on top of it. The profile is backed by a low (10' high) scarp into outwash sediments (distal, mostly silts). At the base of the scarp is a narrow upper beachface of boulders and cobbles with logs on top. Then there is a sandy zone with fine and medium gravel. This zone intersects the low tide terrace which has sandy incipient ridges on it. The low tide terrace is covered with boulders and cobbles (left by the retreating scarp) on a sand base. Relatively light biota. This beach is quite broad and highly zoned with regard to grain size.

3. Energy and Rock Type:

High energy - Rock type - very variable-glacial source

4. Sample Index:

Sample A - upper beachface - fine sand

Sample B - mid-beachface - fine sand with gravels on top.

Sample C - lower beachface on ridge - medium sands.

All sediments are well rounded especially at the base of the beachface.

KDP71:

1. Location: Akhiok Bay near Sea Plane Base, $56^{\circ}56'20''N$, $154^{\circ}10'22''W$

2. Body:

This area is extremely sheltered. There are many flat islands just offshore. This peninsula is flat topped and covered with tundra. There is a low scarp into slate and shale. The beachface is very narrow. Sediments tend to fine toward the waterline. There is a uniform offshore slope. The bottom is muddy with many shale clasts. All sediments are angular indicating no reworking - no energy. Very numerous clams offshore. The islands are very similar to this area.

3. Energy and Rock Type:

Very low energy - Rock type - slate and shale.

4. Sample Index:

All beach material is angular, mostly coarse gravel and cobbles (10-15 cm = I).

KDP73:

1. Location: East side Moser Peninsula just west of Fox Islands, $56^{\circ}59'30''N$, $154^{\circ}03'05''W$.

2. Body:

This profile is located on a small cusped spit. The top of the spit is highly vegetated with a relict storm berm. The present storm berm is also vegetated, indicating infrequent but violent storms. The beachface is pure gravel with some sand behind neap berm, which has a well developed berm top overwash. There is a strong fining trend from the top to the bottom of the

beachface. The top has coarse discoid argillite gravel. The bottom has fine equant gravel. The beach is clean, very low biota due to active sediment movement.

3. Energy and Rock Type:

Moderate to high energy - Rock type - argillite and quartz diorite.

4. Sample Index:

Sample A - just seaward of storm berm - coarse gravel and cobbles.

Sample B - neap berm crest - fine gravel.

Sample C - coarse gravel and cobbles with gravel ribbons.

KDP75:

1. Location: North shoreline of Alpine Cove, $57^{\circ}08'30''N$, $153^{\circ}45'35''W$

2. Body:

This is a small low wave energy pocket beach. It has a very narrow beachface (25 m). The beachface is composed of fine and medium platy subangular greywacke gravel, with granules beneath. There is a small scarp cut into a vegetated flat at the top of the profile. The beachface has numerous algal swash lines. The gravels are very well sorted. Offshore slope is quite steep. Relatively low biota.

3. Energy and Rock Type:

Low energy - Rock type - greywacke and some quartz diorite.

KDP77:

1. Location: Southern Hepburn Peninsula; Portage Bay, $56^{\circ}47'48''N$, $153^{\circ}53'50''W$

2. Body:

The profile is backed by a low scarp into till. At the base of the scarp is a layer of reducing algae which is decaying on top of a wave cut platform into

the till. The middle beachface has boulders and gravel resting on bedrock. So this profile is very simple: a wave cut platform cut into till which overlies bedrock. Relatively high biota.

3. Energy and Rock Type:

Moderate energy - Rock type - bedrock is slate; gravels and cobbles are shale, argillite and diorite.

4. Sample Index:

Sample A - Till scarp with slate and argillite gravels.

Sample B - boulders and cobbles and gravel on bedrock platform. Most are subround.

KDP79:

1. Location: Alitak Bay just north of Seaborg Bay, $56^{\circ}53'28''N$, $154^{\circ}58'40''W$

2. Body:

This profile runs across a small spit that encloses a stream. There is a 2 m high scarp down to the stream from the spit top. The spit slopes gently upward to the crest. The beachface has considerable algal swashes on it. Beach composed of sand and gravels. Lower beachface is mostly gravel and granules. There is a low ridge on the low tide terrace. This is a broad depositional beach. Relatively low biota due to sediment and wave energy. Steep beachface, flat low tide terrace.

3. Energy and Rock Type:

Moderate energy - Rock type - variable, introduced from stream.

4. Sample Index:

Sample A - spit crest, mostly sand with some scattered mixed gravel.

Sample B - mid-beachface - mostly pure granule.

Sample C - low tide terrace - fine gravel, granules and 1.0 ϕ sand.

Most of the beach is underlain by sand. Gravels are mostly fine and well rounded.

KDP81:

1. Location: Geese Channel about 15 km southwest of Old Kaguyak Bay,
56°49'55"N, 153°46'25"W

2. Body:

Profile backed by high rock scarp, partly vegetated. The profile is on a very broad bedrock platform. Bedrock is standing vertically to 45° angle. There is a rock fall at the base of the scarp (boulders and cobbles are well rounded indicating high wave energy). There is a series of algal swash lines on a fine and medium gravel and sand lower beachface. There is a prominent toe down to the rock platform. The beachface is only 30 m wide. The platform has very heavy intertidal life and numerous very rich tidal pools.

3. Energy and Rock Type:

Moderate to high energy - Rock type - greywache.

4. Sample Index:

Sample X - taken from gravel - sand lower beachface. Mostly subangular gravel.

KDP83:

1. Location: Kaguyak Bay - north shoreline, 56°54'55"N, 153°41'25"W

2. Body:

Profile is backed by a high vegetated scarp. At base is a poorly developed storm berm composed of boulders and gravel which fines seaward. Logs are scattered on storm berm. Storm berm face is composed of medium and coarse well rounded gravel. The beachface is mostly medium and fine gravel and sand. There is a

well developed step onto a boulder-cobble low tide terrace covered with abundant fauna. The profile is bounded on both sides by rock ramparts with stacks.

There are islands just offshore.

3. Energy and Rock Type:

Moderate energy - Rock type - slate.

4. Sample Index:

Sample A - high tide swash line, gravels and cobbles with coarse sand.

Sample B - mid beachface medium and fine gravel and sand.

Sample C - lower beachface, fine and medium gravel and sand.

B and C are mostly 0.0 ϕ sand. Scattered bedrock boulder outcrops all over.

KDP85:

1. Location: Kiavak Bay, 57^o01'50"N, 153^o35'15"W

2. Body:

Very high scarp backs the profile. At base is a high level berm of very coarse gravel and cobbles and boulders with scattered logs. There is a cusped berm with coarse gravel horns and sandy bays. Bedrock platform outcrops at the base of the beachface. The bedrock has fairly heavy biota. Very poor sorting on the beachface. All gravels etc. are subrounded.

3. Energy and Rock Type:

Moderate to high energy - Rock type - greywacke.

4. Sample Index:

Sample B - mid beachface in a sandy area (1.0 ϕ).

KDP87:

1. Location: 2 km north of Cape Kasiak, 57^o04'33"N, 153^o29'00"W

2. Body:

Profile is backed by a high vegetated scarp. There are two berms of granules with fine to coarse gravels. There are large angular boulders (1-3 m

diameter) at the base of the scarp from rock falls. The beachface has incipient cusps with zones of coarse gravel and sandy areas. The beachface is steep until it intersects the low tide terrace which is quite flat and composed of boulders and cobbles. There is a prominent zonation of the biota on the L.T.T. (very heavy and diverse).

3. Energy and Rock Type:

Moderate to high energy - Rock type - greywacke and argillite.

4. Sample Index:

Sample A - upper berm face - mixed gravel.

Sample B - mid lower beachface - sandy patch in horn.

Sample C - lower beachface - sand, granule and mixed gravel.

Most gravels are subangular.

KDP89:

1. Location: Sitkalidak Strait, north shoreline, near Three Sisters Rocks,
57°12'55"N, 153°09'10"W

2. Body:

Profile located on seaward side of large cusped spit. This profile is very interesting with a large washover sequence on the back side, possibly a function of the earthquake downwarp. The washover terrace has migrated landward over a low marsh area. Most of the washover material has gone over the top of this spit without being deposited on top. The beachface is quite complex. There is a minor berm up high composed of medium gravel. There are two other larger berms on the mid beach face. Then two have very steep landward faces. Then there is a very minor granule berm just above the waterline. Most of the material is mixed sand and gravel with granules predominating. There are

three zones of coarser material. One just below a low scarp cut into the vegetated spit top, and then two behind the larger berms. A classic transgressive profile.

3. Energy and Rock Type:

Low to moderate energy - Rock type - slate with some schist and diorite.

4. Sample Index:

Sample A - upper large berm - subround platy to discoidal gravel.

Sample B - lower large berm - subround mixed gravel (I = 6 cm).

Sample C - lower beachface - mostly granules.

KDP91:

1. Location: Inner southern shoreline of Kiliuda Bay, $57^{\circ}18'15''N$, $153^{\circ}10'35''W$

2. Body:

Profile is run on a small spit composed of discoidal platy gravel.

There is a small scarp down to a lake behind the spit. The spit top is made of pure discoid gravel, mostly fine. The beachface has a series of small berms with algae swash lines. Most of the beachface is uniform of slope and grain size. There is a slight coarsening trend as the waterline is approached. At the base of the beachface there is a narrow low tide terrace. There is a light algal cover on the larger gravels and cobbles on the low tide terrace.

3. Energy and Rock Type:

Low energy - Rock type - slate and argillite.

4. Sample Index:

Sample A - upper berm - mostly fine discoid gravel, well sorted and angular.

Sample B - mid beachface - coarse angular gravel, fine gravel and granules.

Sample C - coarse gravel and granules. Grain size increases seaward but sorting decreases.

KDP93:

1. Location: Western outer shoreline of Boulder Bay, $57^{\circ}16'45''N$, $152^{\circ}47'30''W$
2. Body:

This profile is exposed to open Gulf of Alaska waves. There is a high shear rock scarp (500' high) backing the profile with "room size" boulders at its base (rock fall). There is considerable fine and medium gravel thrown up between the boulders. Fronting this is a berm of medium very well rounded gravel. The beachface is steep, composed of sand and granules. There are two large rock falls into waterline on each side of this beach. They have a moderate coating of biota, but the beach here is quite clean due to energy and sediment.

3. Energy and Rock Type:

Very high energy - Rock type - greenstone and argillite.

4. Sample Index:

Sample A - berm, medium gravel, well rounded.

Sample B - mid beachface - coarse gravel on a granule base.

Sample C - lower beachface - fine well sorted and rounded gravel.

KDP95:

1. Location: Middle southern shoreline of Ugak Bay, $57^{\circ}27'40''N$, $152^{\circ}46'50''W$
2. Body:

Profile is located on the updrift end of a large cusped spit-delta complex. The profile is backed by a low scarp cut into an old alluvial fan terrace, highly vegetated. The profile is complicated, starting with a sandy high berm, followed by a well developed gravel berm. Fronting that is another sandy zone and then a sharp crested fine gravel berm. The profile then flattens

out across a gravel-sand ribbon area. It then coarsens to the water line.

3. Energy and Rock Type:

Moderate to low energy - Rock type - variable, shale, slate, argillite, diorite.

4. Sample Index:

Sample A - upper fine gravel, granule sand berm.

Sample B - sharp crested gravel granule berm.

Sample C - lower beachface, mixed sand and gravel.

KDP97:

1. Location: Large pocket beach 2 km east of Shark Point, $57^{\circ}27'15''N$,
 $152^{\circ}33'50''W$

2. Body:

Profile has a small river backing it with a large washover terrace into the river. There are two major log accumulations on the profile - one vegetated storm berm and one on the river side probably the result of storm surge during storms. The overwash terrace has a pea gravel ablation surface on a black volcanic - metamorphic sand. The beachface is steep at the top, then flattens out in an area of ground water rills. Most sediment is black sand with scattered mixed gravels. There is a general fining trend from the washover terrace to mid beachface, then a coarsening trend to the waterline.

3. Energy and Rock Type:

Moderate energy - Rock type - metamorphic rock fragments.

4. Sample Index:

Sample A - upper beachface - sand and granules.

Sample B - mid beachface - same.

Sample C - lower beachface - same.

Most sand is about 1.5 ϕ .

KDP99:

1. Location: 1.5 km north of Sequel Point, $57^{\circ}34'15''\text{N}$, $152^{\circ}11'55''\text{W}$

2. Body:

Profile is a very simple narrow beach fronting a high rock scarp. The beachface has three zones, 1) mixed gravel beneath scarp, 2) granule area in mid beachface and, 3) mixed gravel lower beachface. All this is perched on a bedrock platform which outcrops at the waterline.

3. Energy and Rock Type:

Very high energy - Rock type - argillite.

4. Sample Index:

Sample A - base of scarp - mixed gravel on a granule - coarse sand base.

Sample B - the mid beachface pure granule with some very coarse sand. Well sorted.

Sample C - lower beachface, similar to upper beachface. Pebbles with a granule base. Good overall sorting on this beach, also well rounded.

KDP101:

1. Location: 1 km southwest of Broad Point on the Gulf of Alaska shoreline,
 $57^{\circ}40'45''\text{N}$, $152^{\circ}24'20''\text{W}$

2. Body:

Profile is backed by a high scarp into interbedded shale, slate and sandstone. Beachface is short and steep. There is discoid gravel up high, it fines in the middle of the beachface and becomes coarser and more equant at the base of the beachface. There is a large stack to the south. Only a moderate coating of biota.

3. Energy and Rock Type:

Low energy - Rock type - slate, shale, sandstone.

4. Sample Index:

Sample A - coarse - fine gravel, angular and discoid.

Sample B - mid beachface - mixed gravel with granules and sand.

Sample C - lower beachface - slightly coarser than B.

KDP103:

1. Location: 250 m south of Gibson Cove, $57^{\circ}46'30''N$, $152^{\circ}26'50''W$

2. Body:

This profile is partly man-altered, located near the Gibson Cove Cannery. There is a high scarp into slate and a beachface which is mostly a bedrock platform covered with the typical intertidal life of these protected areas. The platform is partly covered at the top and middle by angular gravel to boulders of slate, all locally derived.

3. Energy and Rock Type:

Low energy - Rock type - slate.

4. Sample Index:

Samples - all photos - coarse gravel to boulders of angular to subangular discoidal slate.

KDP105:

1. Location: Course Point, $57^{\circ}53'45''N$, $152^{\circ}28'00''W$

2. Body:

This is a small pocket beach opposite Spruce Island. It is surrounded by a 60' high rock scarp. The beachface is narrow, covered with logs and algae swashlines. It is composed mostly of mixed gravel to sand on bedrock. Beachface is very steep. Rock scarps and stacks have zoned biotic cover. Large kelp bed offshore.

3. Energy and Rock Type:

Low to moderate energy - Rock type - argillite with shale interbeds.

4. Sample Index:

Sample A - upper beachface, subround discoid gravel with some granules and sand.

Sample B - mid beachface, slightly coarser and covered with algae swash.

Sample C - lower beachface, well sorted, well rounded gravel, mostly bladed and roller shaped.

KDP107:

1. Location: East side of Sharatin Bay, 1 km south of Three Pillar Point,
57°50'43"N, 152°42'55"W

2. Body:

The profile is backed by a low scarp into phyllite-slate which is overlain by outwash sand and gravel. The beachface is mostly mixed gravels and boulders of slate, some scattered intrusive gravels (glacially derived). Rounding increases sharply toward the waterline. Mostly subangular at base of scarp. This is a small delta just to the south of the profile and a stack to the north. The biota is not particularly rich here, rather low energy. The beachface sediments form a veneer on a bedrock platform.

3. Energy and Rock Type:

Low energy - Rock type - slate-phyllite with variable glacially derived gravel.

4. Sample Index:

All photo samples of mixed gravels and boulders.

KDP109:

1. Location: Western shore of Kizhuyak Bay, 57°50'07"N, 152°53'35"W

2. Body:

Profile backed by a low (10' high) scarp into slate and shale which is overlain by till and outwash sediments. Fronting the scarp is an upper beachface of fine gravel and sand overlain by angular boulders and cobbles which become better rounded toward the waterline. There are numerous large boulders (1 m diameter) which are very heavily coated with encrusting biota. This beach is perched on a wave cut platform into bedrock. Sediments are generally quite coarse, mostly coarse gravel and cobbles.

3. Energy and Rock Type:

Low energy - Rock type - slate, shale and glacial variety (quartz, quartz diorite, intrusives).

4. Sample Index:

All samples are photos. Mostly boulders, cobbles and mixed gravel with some granules beneath, all on bedrock. Most beach sediments are platy and sub-angular.

KDP111:

1. Location: Eastern shore of Whale Island, 57°57'30"N, 152°44'05"W

2. Body:

Profile backed by a 4m scarp into argillite with intrusive dikes and bedded welded tufts. There is a prominent bedrock projection to the north, all covered with heavy intertidal life. About 90% of this profile is on bedrock covered in places with a thin veneer of gravels. There is strong evidence of downwarp here, dead trees at top of scarp falling onto upper beachface. The larger boulders are covered with algae etc. There are many small gravel - sand pocket beaches in this area, which are very clean. The area shows many signs of the Good Friday Earthquake downwarp.

3. Energy and Rock Type:

Moderate to high energy - Rock type - argillite and intrusives

4. Sample Index:

All samples are photos. Mostly cobbles and gravels on the bedrock with some pockets of sand or granules.

KDP113:

1. Location: Eastern, north shore of Marmot Island, $58^{\circ}14'45''N$, $151^{\circ}47'20''W$

2. Body:

The profile is fairly typical of this area, being backed by a low scarp into low ranked metamorphic rock. The beachface is quite narrow and steep, composed of sand and gravel. It is coarser up high at the berm just below the scarp. The berm has incipient cusps on its face. There is a well developed step onto the bedrock platform at the base of the profile. Large knobs of bedrock protrude through the beachface. The bedrock platform is very irregular, and knobby with many tidal pools. It is coated with heavy intertidal life, Fucus is most common; not too much encrusting forms.

3. Energy and Rock Type:

Moderate to high energy - Rock type - slate, greywacke.

4. Sample Index:

Sample A - just below berm - rounded bladed pebbles and small cobbles.

Under this is a coarse sand and granules.

Sample B - mid beachface, granule and very coarse sand.

Sample C - lower beachface. Pebbles and granule.

The pebbles and small cobbles are well rounded and bladed. There is little change along the profile. Below the berm, the pebbles get smaller and the middle beachface is granule and very coarse (0.0 to 0.5 ϕ) sand.

The lower beachface is pebbles and granules with some bedrock boulders outcropping.

KDP115:

1. Location: North shoreline of the Southern Uganik Passage, $57^{\circ}49'45''N$,
 $153^{\circ}19'15''W$

2. Body:

This area is occupied by a series of relict drumlins which have been eroded. Some are rock covered. The shoreline has been straightened out and faces the Alaska Peninsula. The profile itself is located on a tombolo. The beachface is composed of pure fine gravel with some sand. There are four separate small berms. the highest is composed of medium discoidal gravel (10 cm diameter). The lowest berm is very cusate. Below that berm, the beachface flattens out and is covered by very well developed gravel stripes or ribbons (wave length 4.8 m and about 30 cm high).

3. Energy and Rock Type:

Low to moderate energy - Rock type - argillite and slate.

4. Sample Index:

Sample A - the seawardmost berm, the smallest berm. It is mostly pebbles - small ones and composed of mostly argillite or slate and a few qtz pebbles. 1.0ϕ sand and gravel underneath.

Sample B - from the coarse part of a gravel striation. Pebbles on top with sand, granule and shell material below.

Sample C - lower beachface, sand and pebbles with a few small pebbles. Some granule material. The sand is coarser (1.5ϕ) but more abundant than the upper beachface. The sorting is very poor.

The pebbles at the 4 berms are all subrounded and disc shaped with good sorting.

The beachface is sand and pebbles with many gravel and pebble striations.

KDP117:

1. Location: Northwest shoreline of Tugidak Island, $56^{\circ}32'25''\text{N}$, $154^{\circ}38'50''\text{W}$

2. Body:

Profile fronting a till scarp. The beachface is dominated by sand with scattered gravels and cobbles on surface. Profile starts at berm at the base of the scarp. There is an accumulation of logs on this berm. There is an irregular berm below the high berm. The berm face has well developed ground water rills. Below that berm, the beachface intersects a wave cut platform into till which is littered with erratics. The till has a good percentage of sand, granules and gravel. It is a very wide platform and quite irregular with algae growing on the outer edge.

3. Energy and Rock Type:

Moderate to high energy - Rock type - very variable.

4. Sample Index:

Sample A - upper beachface - mostly sand with scattered gravel.

Sample B - middle beachface - mostly sand (1.5 ϕ) and gravel.

Sample C - lower beachface - same as B.

Most gravel is well rounded and equant. There are no grain size trends on the beachface.

KDP119:

1. Location: Southern shoreline of Tugidak Island, $56^{\circ}29'45''\text{N}$, $154^{\circ}33'45''\text{W}$

2. Body:

This a depositional profile. There is a broad series of beach ridges over a dead scarp, well behind the active beachface. The beach ridges are very long parallel just like the present berms, and ridge and runnel system.

The profile is very complex with three berms and a well developed ridge and runnel system. The high storm berm is composed of sand and gravel with a sharp face. There are low dunes behind the berm. The second berm is large and highly cusped with gravelly horns. The lowest berm is sandy and not too high. There is a deep runnel with a high ridge just seaward.

3. Energy and Rock Type:

High energy - Rock type - mixed sand.

4. Sample Index:

Sample A - upper berm face - sand.

Sample B - cusped berm face - coarse sand with some fine gravel.

Sample C - lower beachface - sand with granules.

The beachface below the third berm is about 90% sand and 10% well rounded equant to bladed pebbles. Some pebbles are quite large here.

KDP121:

1. Location: Northwest side of Sitkinak Island, $56^{\circ}36'12''N$, $154^{\circ}04'25''$

2. Body:

This profile is a strong indicator of uplift. The profile starts at a small lake, fronting a large vegetated hill with a relict scarp in it. Fronting the lake is a relict beach ridge spit of gravel and granules, all heavily vegetated. Seaward of that are three other vegetated beach ridges. The lake occupies what used to be a lagoon. Transport was toward the north. The beachface has a well developed storm berm covered with logs and fine and medium gravel (equant). The beachface is made of gravel and granules with a few algae swashlines. There is a broad spring tide berm in the middle beachface. The lower beachface is almost pure granules.

3. Energy and Rock Type:

High energy - Rock type - variable.

4. Sample Index:

Sample A - storm berm, pure gravel and granules.

Sample B - lower berm, sand with scattered mixed gravel and granules.

Sample C - lower beachface, well sorted fine gravel and granules.

KDP123:

1. Location: Southeastern Sitkinak Island, $56^{\circ}29'50''N$, $154^{\circ}03'00''W$

2. Body:

The profile is backed by a high rock scarp into argillite and greywacke, with numerous rock falls at its base. There is a poorly developed mixed gravel berm fronting the scarp. Many angular cobbles and boulders are found on the berm. The beachface slopes steeply to a boulder-cobble low tide terrace. The boulders are large (1 m diameter) and well rounded. The terrace is quite narrow.

3. Energy and Rock Type:

High energy - Rock type - argillite, sandstone, greywacke.

4. Sample Index:

Beach material is very variable, poorly sorted and of variable shape.

KDP125:

1. Location: Southeast shore of Sitkalidak Island, $57^{\circ}00'18''N$, $153^{\circ}14'30''W$

2. Body:

This profile is backed by a very broad uplifted terrace about 80' higher than the present one. It goes on for many kilometers. There is a sharp scarp into the bedrock to the upper beachface. At the base is a perched berm of coarse gravel and boulders with logs. Then there is a very steep beachface of poorly sorted boulders to sand and mixed gravel. At its base is a narrow zone of well rounded boulders and cobbles on a bedrock platform. The bedrock platform is

irregular with many tidal pools and very abundant intertidal life.

3. Energy and Rock Type:

High energy - Rock type - argillite.

4. Sample Index:

Sample A - upper berm, gravel and cobbles.

Sample B - mid beachface - finest material, coarse sand and mixed gravel.

Sample C - boulder cobble zone - all well rounded and equant.

KDP127:

1. Location: Cape Barnabas, $57^{\circ}09'00''N$, $152^{\circ}52'00''$

2. Body:

Profile is backed by a high scarp into mudstone. There is a perched berm at the base of mixed gravel (well rounded). The berm is highly irregular. This pocket beach is about 200 m wide. Beachface is narrow and perched on a bedrock platform. Very heavy life on platform.

3. Energy and Rock Type:

Very high energy - Rock type - mudstone and greywacke.

4. Sample Index:

Sample A - upper beachface - medium and coarse gravel.

Sample B - mid beachface - sand and granules with mixed gravel.

Sample C - lower beachface - same as B.

APPENDIX 3

Afognak A-0 + B-0
Class Km of Shoreline

1	11.7
2	32.5
3	
4	
5	
6	13.3
7	12.5
8	
9	
10	

Afognak A-1
Class Km of Shoreline

1	36.6
2	
3	
4	
5	
6	5.8
7	12.5
8	55.8
9	
10	

Afognak A-2
Class Km of Shoreline

1	27.4
2	
3	
4	
5	
6	10.8
7	14.2
8	54.1
9	
10	

Afognak A-3
Class Km of Shoreline

1	10.8
2	
3	
4	
5	
6	
7	40.0
8	54.9
9	
10	

Afognak A-4
Class Km of Shoreline

1	29.1
2	
3	
4	
5	
6	25.8
7	75.8
8	5.0
9	
10	

Afognak A-5
Class Km of Shoreline

1	5.0
2	
3	
4	
5	
6	13.4
7	
8	
9	
10	

Afognak B-1
Class Km of Shoreline

1	
2	45.8
3	
4	
5	
6	
7	16.7
8	94.9
9	1.7
10	

Afognak B-2
Class Km of Shoreline

1	14.2
2	14.2
3	
4	
5	
6	
7	32.5
8	76.6
9	
10	

Afognak B-3
Class Km of Shoreline

1	23.4
2	25.9
3	
4	
5	
6	
7	30.9
8	126.9
9	
10	

Afognak B-4
Class Km of Shoreline

1	8.3
2	
3	
4	
5	
6	
7	7.5
8	
9	
10	

Afognak C-1 + C-2
Class Km of Shoreline

1	22.6
2	15.0
3	
4	
5	
6	
7	6.7
8	20.0
9	
10	

Afognak C-2 + C-3
Class Km of Shoreline

1	
2	47.6
3	
4	
5	
6	
7	3.3
8	108.6
9	
10	

Kodiak A-3
Class Km of Shoreline

1	9.2
2	12.5
3	
4	
5	
6	11.7
7	7.5
8	
9	
10	

Kodiak A-4
Class Km of Shoreline

1	
2	42.6
3	5.9
4	3.3
5	
6	87.7
7	25.1
8	
9	11.7
10	10.9

Kodiak A-5
Class Km of Shoreline

1	13.4
2	30.9
3	
4	
5	
6	44.3
7	10.0
8	24.5
9	
10	1.6

Kodiak A-6
Class Km of Shoreline

1	
2	1.7
3	
4	
5	
6	22.5
7	
8	60.7
9	1.7
10	8.3

Kodiak B-1 + B-2
Class Km of Shoreline

1	
2	55.1
3	
4	
5	
6	29.2
7	
8	
9	
10	

Kodiak B-3
Class Km of Shoreline

1	1.2
2	36.7
3	
4	1.0
5	0.7
6	43.4
7	34.2
8	
9	2.5
10	1.7

Kodiak B-4
Class Km of Shoreline

1	
2	3.3
3	
4	
5	
6	21.7
7	23.9
8	
9	2.2
10	5.0

Kodiak B-5
Class Km of Shoreline

1	
2	
3	
4	
5	
6	
7	
8	
9	8.4
10	2.5

Kodiak B-6
Class Km of Shoreline

1	
2	
3	
4	
5	
6	
7	49.3
8	41.8
9	2.2
10	

Kodiak C-1
Class Km of Shoreline

1	1.7
2	23.3
3	
4	
5	
6	15.0
7	
8	
9	
10	

Kodiak C-2
Class Km of Shoreline

1	10.9
2	22.2
3	
4	
5	2.5
6	25.1
7	
8	20.0
9	5.0
10	5.0

Kodiak C-3
Class Km of Shoreline

1	
2	1.7
3	
4	1.1
5	
6	2.5
7	23.5
8	
9	2.2
10	3.7

Kodiak C-4
Class Km of Shoreline

1	
2	
3	
4	
5	
6	
7	1.7
8	25.9
9	1.2
10	

Kodiak C-5
Class Km of Shoreline

1	3.3
2	2.7
3	
4	
5	
6	10.9
7	5.0
8	67.7
9	6.7
10	6.7

Kodiak C-6
Class Km of Shoreline

1	20.9
2	12.5
3	
4	
5	
6	27.6
7	46.3
8	60.1
9	1.7
10	3.3

Kodiak D-1
Class Km of Shoreline

1	
2	25.1
3	
4	
5	
6	4.5
7	
8	5.3
9	
10	

Kodiak D-2
Class Km of Shoreline

1	1.7
2	53.4
3	
4	
5	
6	24.2
7	8.4
8	93.5
9	1.2
10	4.5

Kodiak D-3
Class Km of Shoreline

1	
2	44.3
3	
4	
5	
6	7.0
7	77.7
8	23.4
9	
10	2.3

<u>Kodiak D-4</u>	
Class	Km of Shoreline
1	18.4
2	17.9
3	
4	
5	
6	53.8
7	9.2
8	79.3
9	
10	

<u>Kodiak D-5</u>	
Class	Km of Shoreline
1	
2	34.2
3	
4	
5	
6	45.1
7	19.2
8	20.0
9	
10	

<u>Kodiak D-6</u>	
Class	Km of Shoreline
1	11.7
2	2.5
3	
4	
5	
6	9.2
7	8.3
8	
9	
10	

<u>Kaguyak C-6</u>	
Class	Km of Shoreline
1	
2	22.5
3	
4	
5	
6	17.4
7	
8	
9	5.0
10	

<u>Kaguyak D-5</u>	
Class	Km of Shoreline
1	8.3
2	11.7
3	
4	
5	
6	5.0
7	2.5
8	
9	
10	

<u>Kaguyak D-6</u>	
Class	Km of Shoreline
1	31.6
2	
3	
4	
5	
6	89.0
7	
8	30.8
9	
10	2.6

Trinity Islands C-1
Class Km of Shoreline

1	
2	19.1
3	5.8
4	
5	
6	70.7
7	2.5
8	37.4
9	4.2
10	2.5

Trinity Islands B-2 + C-2
Class Km of Shoreline

1	
2	
3	18.3
4	
5	
6	39.9
7	
8	30.8
9	
10	

Trinity Islands B-3 + C-3
Class Km of Shoreline

1	
2	
3	
4	
5	
6	26.7
7	
8	
9	
10	

Trinity Islands D-1
Class Km of Shoreline

1	7.5
2	29.1
3	
4	
5	
6	45.0
7	
8	86.6
9	
10	

Trinity Islands D-2
Class Km of Shoreline

1	
2	
3	
4	
5	
6	15.5
7	
8	6.7
9	
10	

Karluk A-1
Class Km of Shoreline

1	
2	
3	
4	
5	
6	5.8
7	13.4
8	72.4
9	2.5
10	

Class	<u>Karluk A-2</u> Km of Shoreline
1	1.0
2	
3	
4	
5	
6	29.2
7	1.7
8	26.7
9	
10	

Class	<u>Karluk B-2</u> Km of Shoreline
1	
2	5.0
3	
4	
5	
6	6.7
7	1.0
8	7.0
9	
10	

Class	<u>Karluk B-3</u> Km of Shoreline
1	26.7
2	
3	
4	
5	
6	24.2
7	
8	11.2
9	
10	

Class	<u>Karluk C-1</u> Km of Shoreline
1	
2	15.0
3	
4	
5	
6	11.2
7	2.0
8	11.7
9	
10	

Class	<u>Karluk C-2</u> Km of Shoreline
1	20.0
2	0.6
3	
4	
5	
6	1.6
7	9.2
8	21.7
9	
10	

AFOGNAK

Class	Km	% Afognak	% Total Study Area
1	189.1	14.7	50.2
2	181.0	14.0	25.6
3			
4			
5			
6	69.1	5.4	7.3
7	252.6	19.5	39.8
8	596.8	46.3	40.8
9	1.7	0.1	2.8
10			
Total	<u>1290.3</u>	<u>100.0</u>	

KODIAK

Class	Km	% Kodiak	% Total Study Area
1	92.4	4.7	24.5
2	422.6	21.4	59.8
3	5.9	0.3	19.7
4	5.4	0.3	100.0
5	3.2	0.2	100.0
6	485.4	24.4	51.5
7	349.3	17.7	55.1
8	522.2	26.3	35.7
9	46.7	2.4	77.7
10	<u>44.6</u>	<u>2.3</u>	89.7
Total	1977.7	100.0	

KAGUYAK

Class	Km	% Kaguyak	% Total Study Area
1	39.9	17.6	10.5
2	34.2	15.1	4.8
3			
4			
5			
6	111.4	49.3	11.8
7	2.5	1.1	0.4
8	30.8	13.6	2.1
9	5.0	2.2	8.3
10	<u>2.6</u>	<u>1.1</u>	5.2
Total	226.4	100.0	

TRINITY ISLANDS

Class	Km	% Trinity Islands	% Total Study Area
1	7.5	1.7	2.0
2	48.2	10.8	6.8
3	24.1	5.3	80.3
4			
5			
6	197.8	44.1	21.0
7	2.5	0.6	0.4
8	161.5	36.0	11.0
9	4.2	0.9	7.0
10	<u>2.5</u>	<u>0.6</u>	5.0
Total	448.3	100.0	

KARLUK

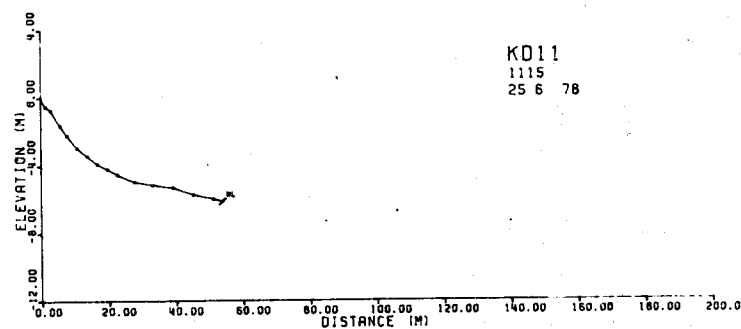
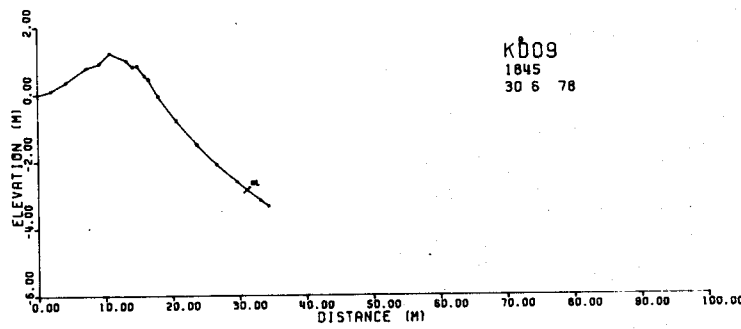
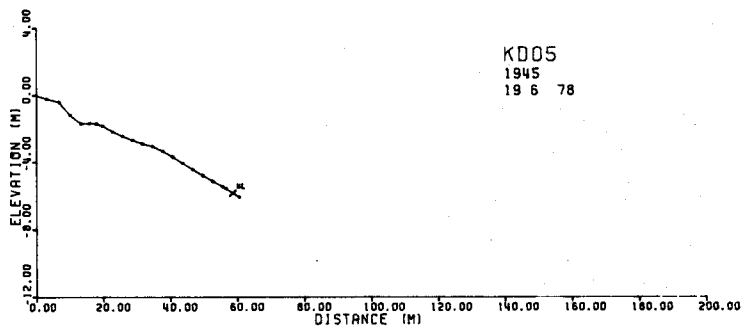
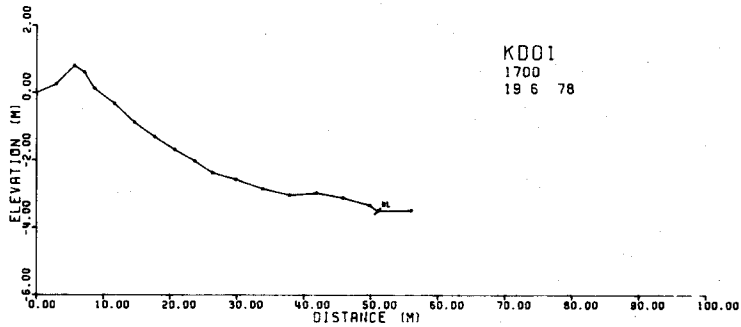
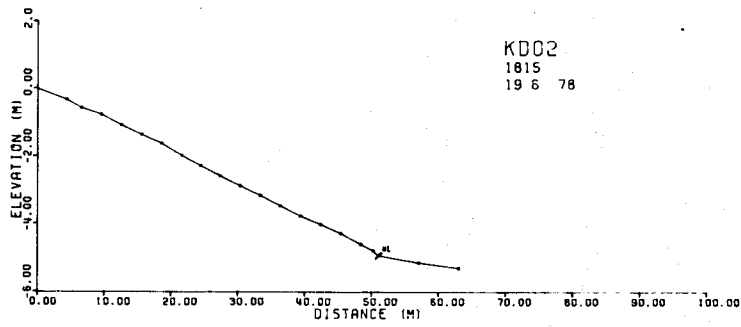
Class	Km	% Karluk	% Total Study Area
1	47.7	14.6	12.7
2	20.6	6.3	2.9
3			
4			
5			
6	78.7	24.0	8.4
7	27.3	8.3	4.3
8	150.7	46.0	10.3
9	2.5	0.8	4.2
10			
Total	327.5	100.0	

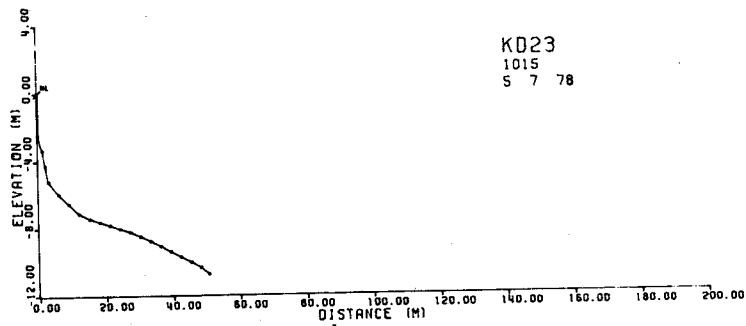
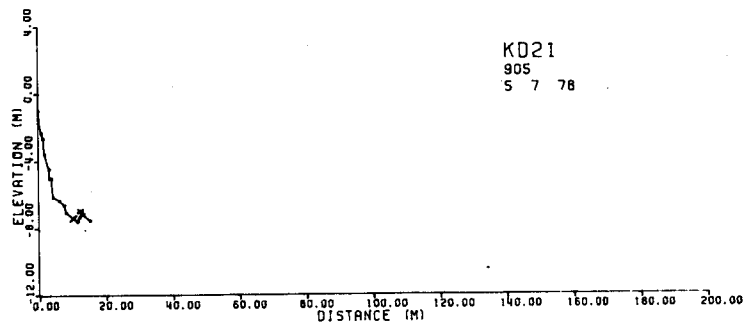
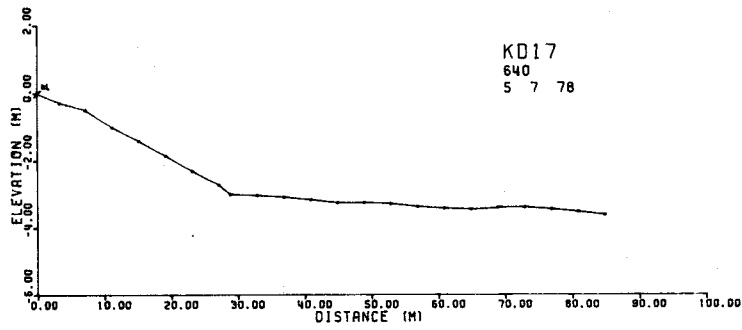
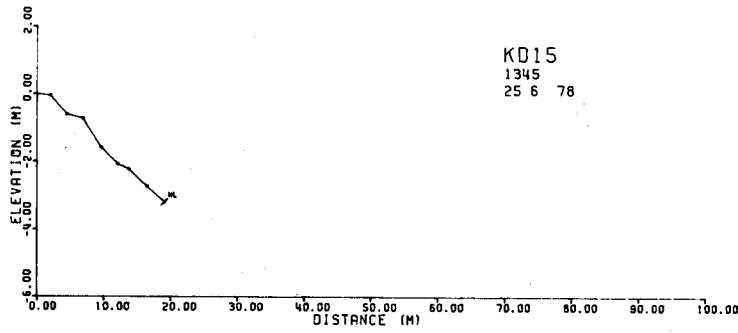
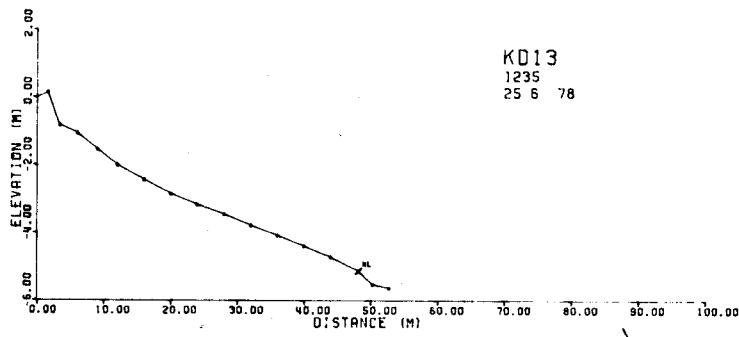
GRAND TOTALS

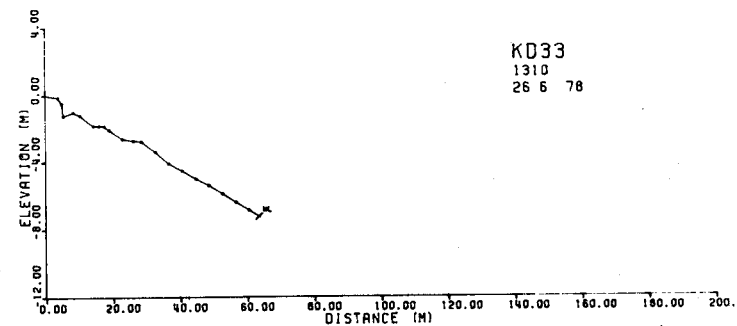
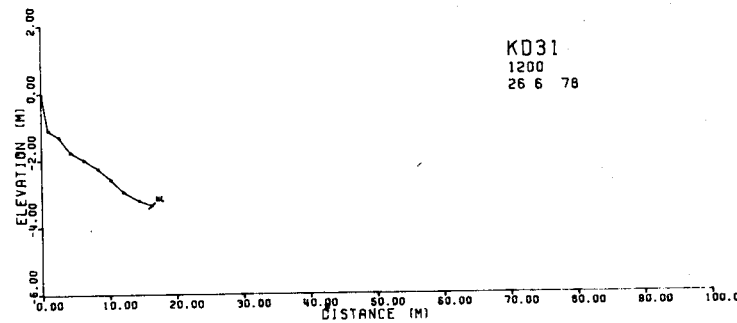
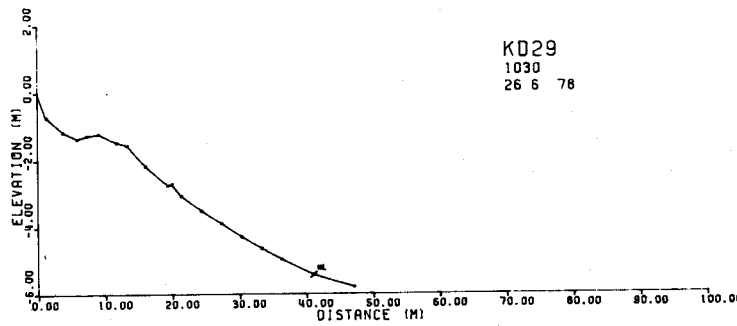
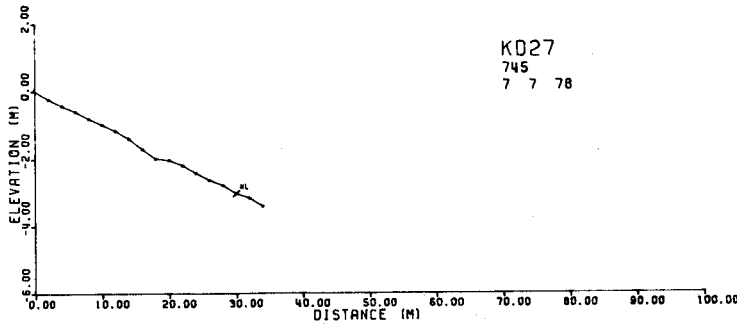
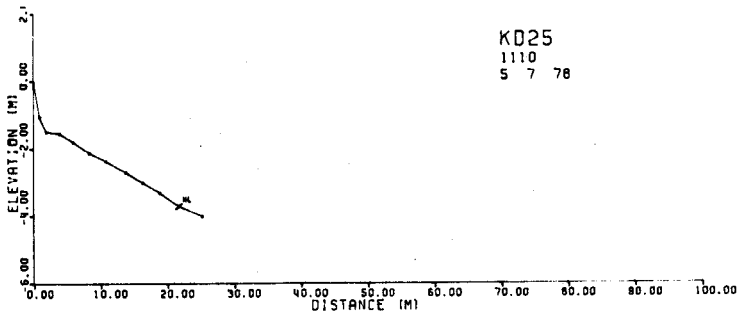
Base Maps	Total Shoreline Kms	% of Total
Afognak	1290.3	30.2
Kodiak	1977.7	46.3
Kaguyak	226.4	5.3
Karluk	327.5	7.7
Trinity Islands	<u>448.3</u>	<u>10.5</u>
Grand Total	4270.2	100.0

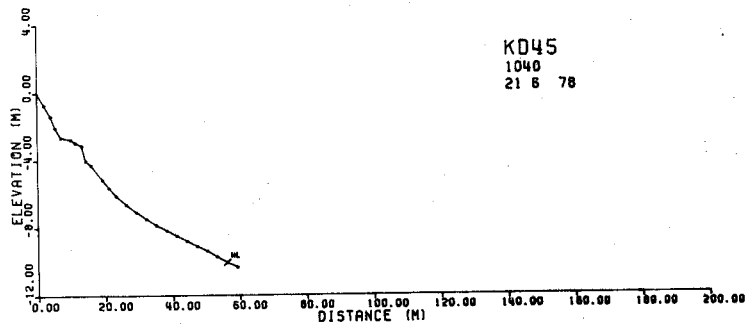
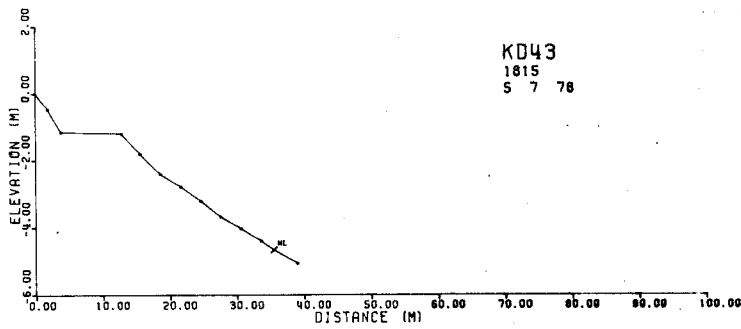
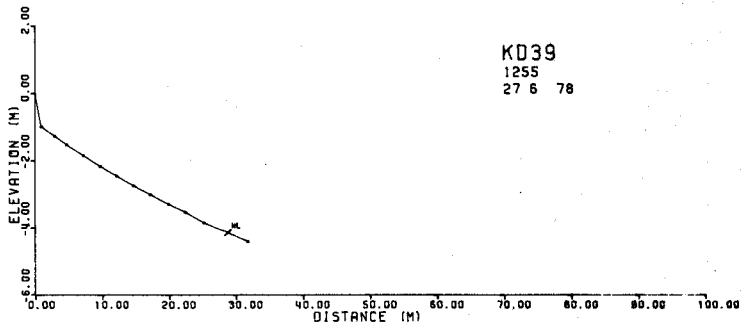
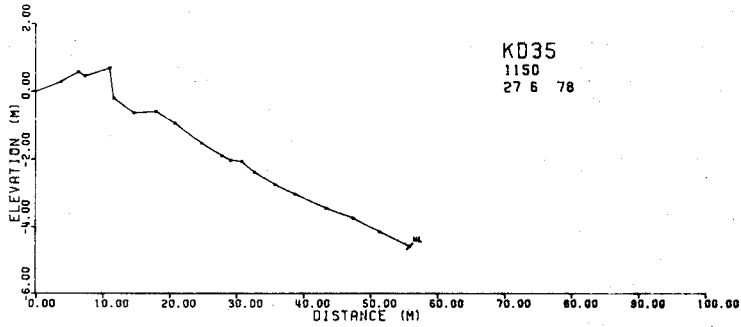
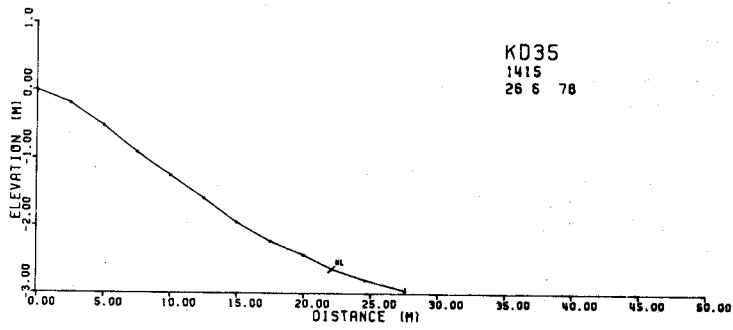
Class	Total Shoreline Kms	% of Total
1	376.6	8.8
2	706.6	16.5
3	30.0	0.7
4	5.4	0.1
5	3.2	0.1
6	942.4	22.1
7	634.2	14.9
8	1462.0	34.2
9	60.1	1.4
10	<u>49.7</u>	<u>1.2</u>
	4270.2	100.0

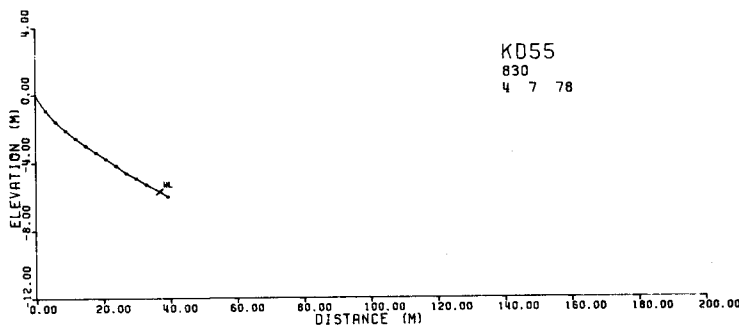
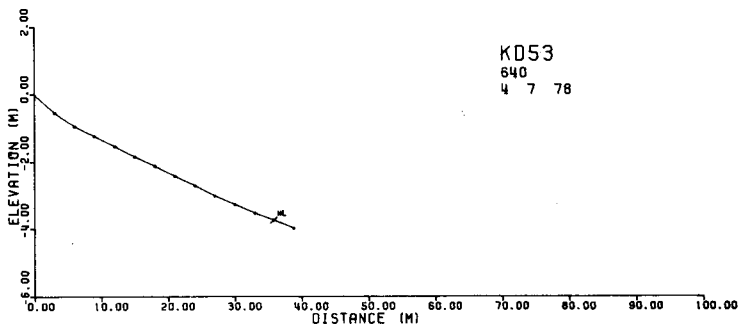
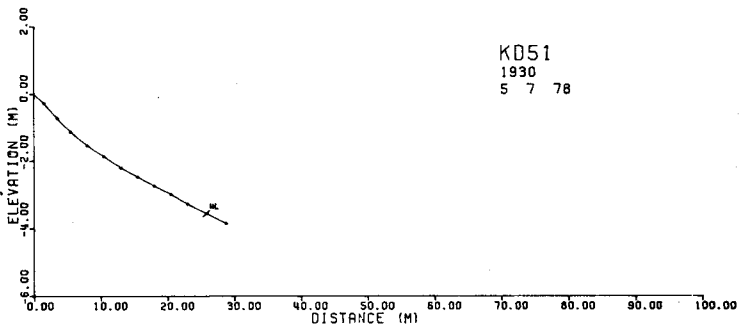
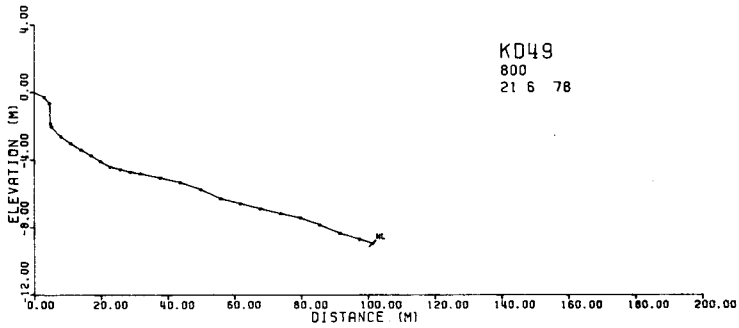
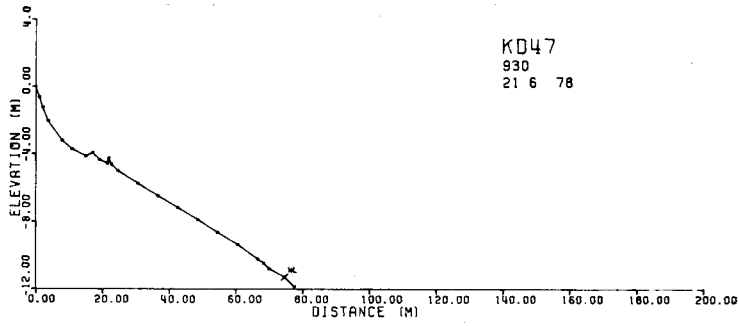
APPENDIX 4

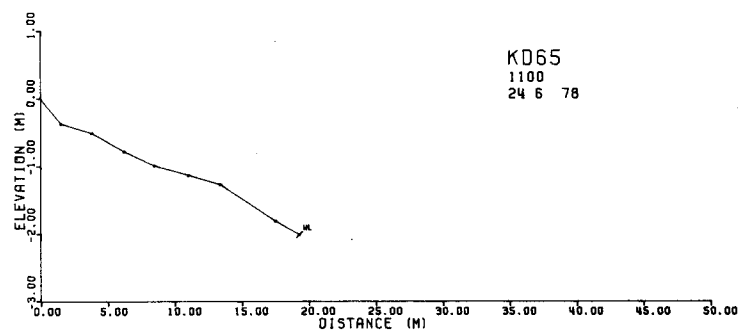
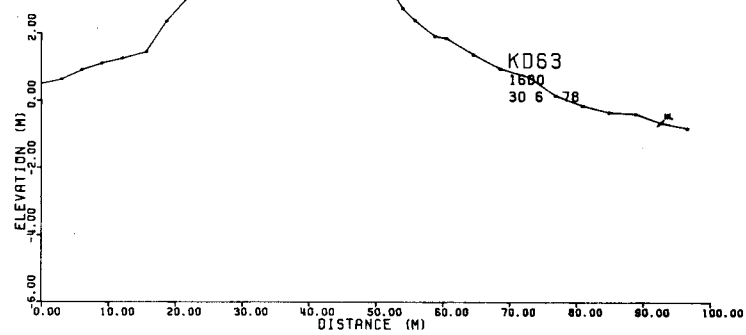
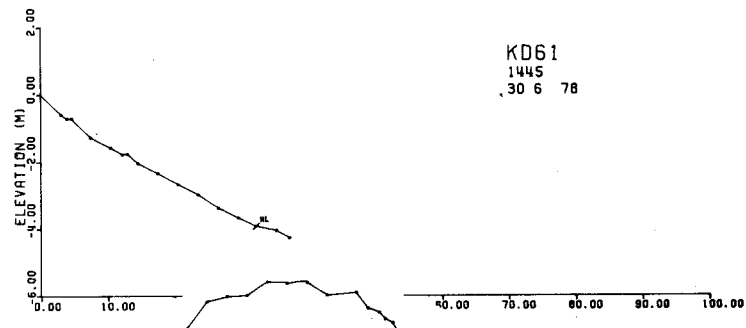
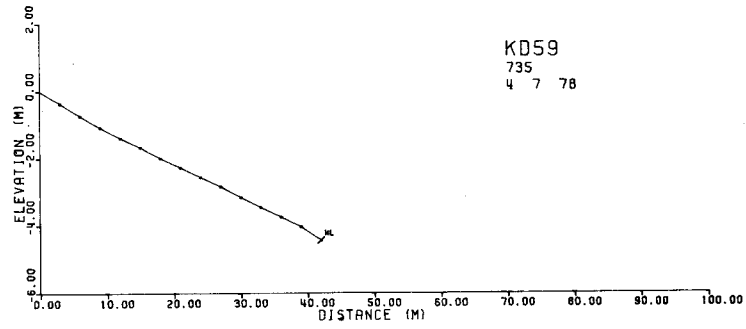
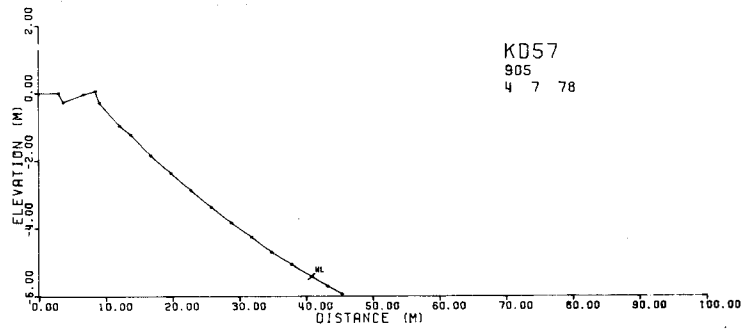


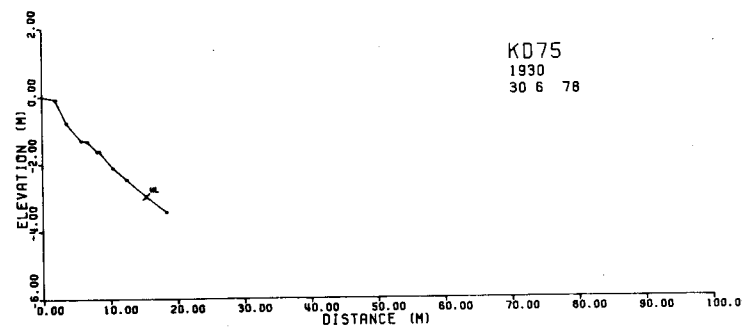
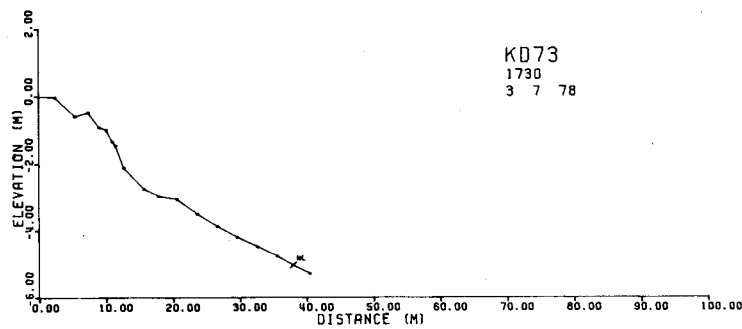
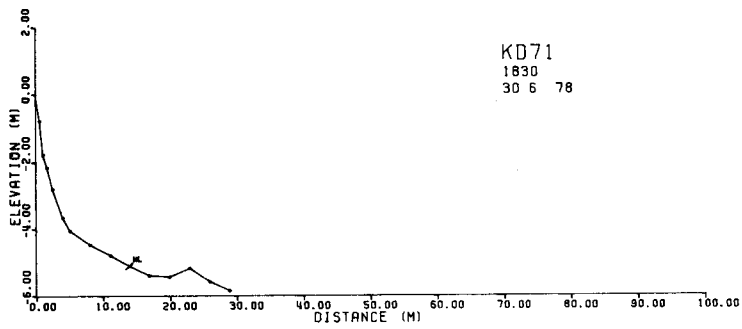
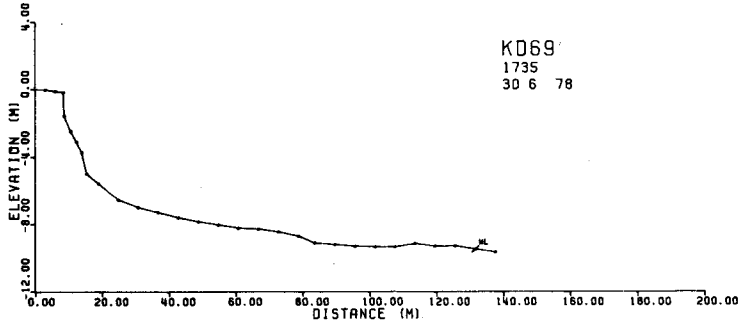
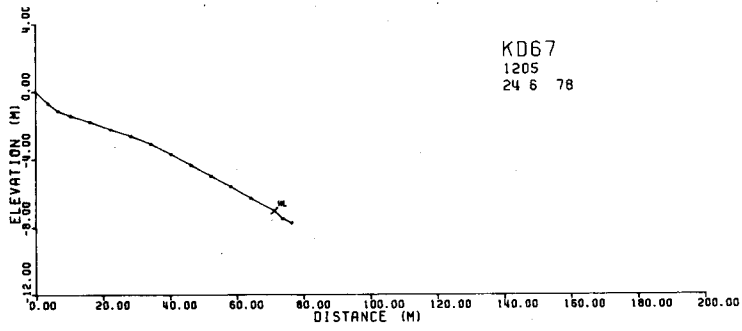


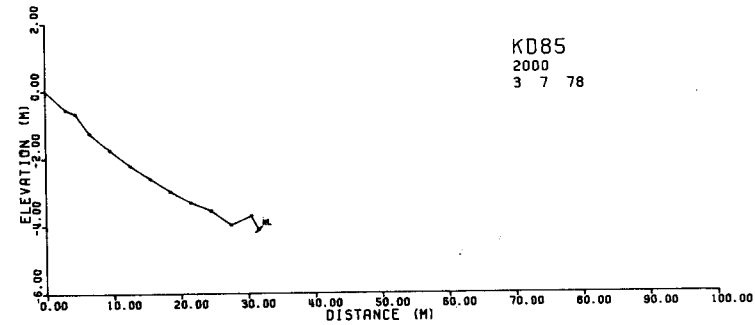
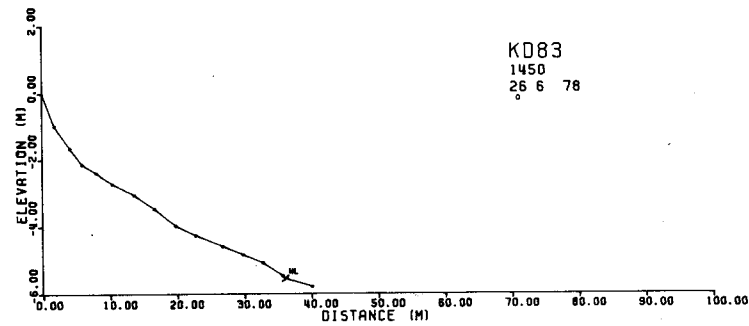
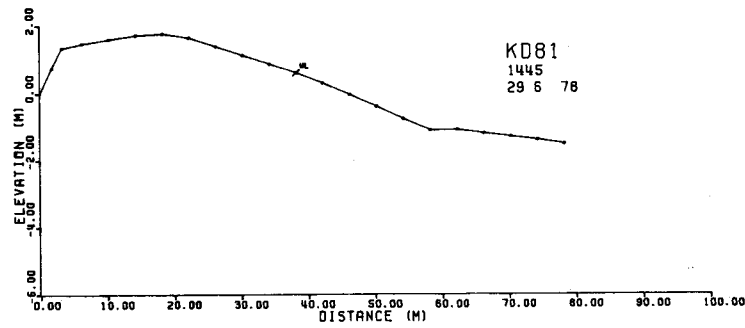
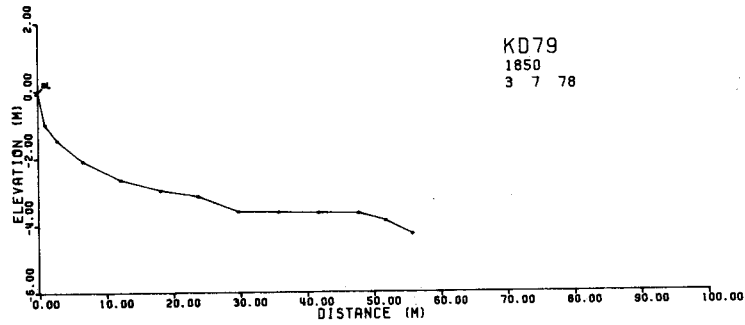
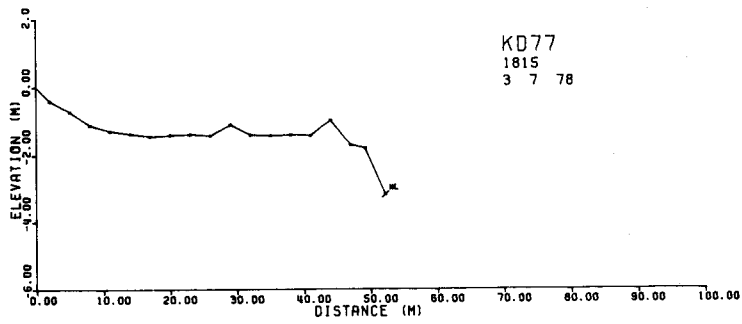


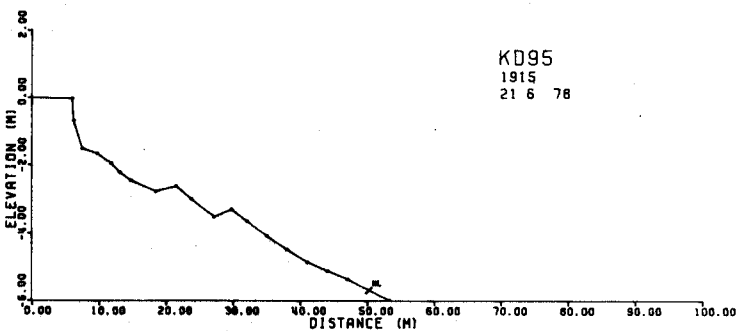
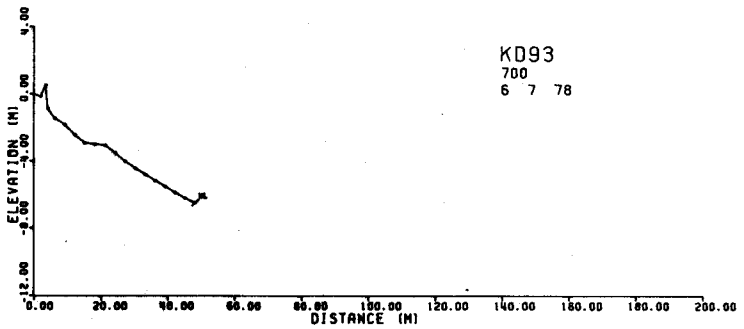
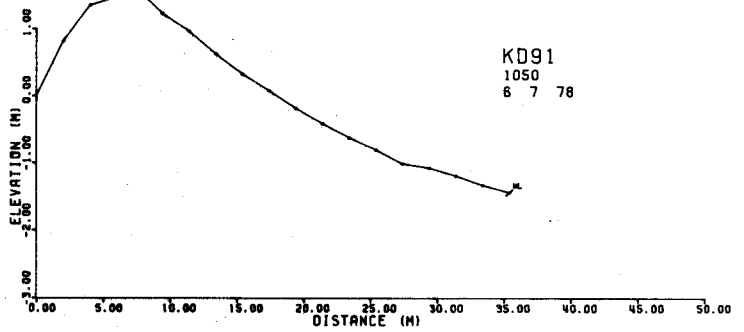
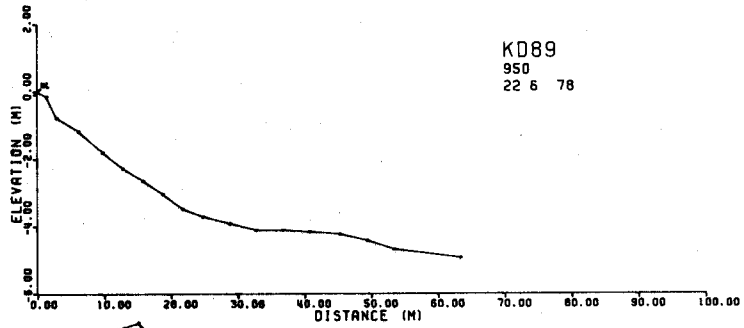
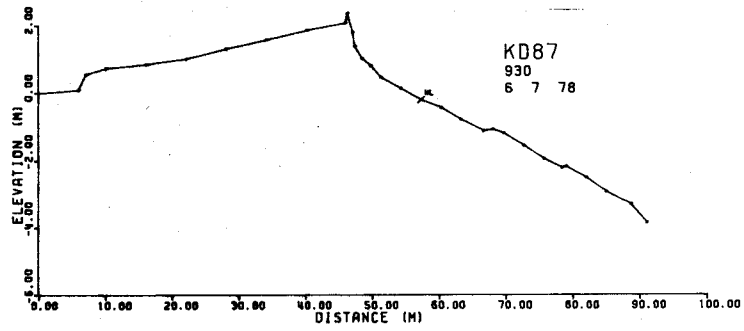


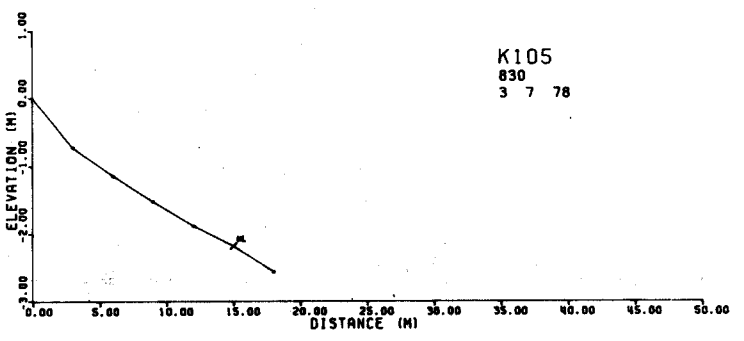
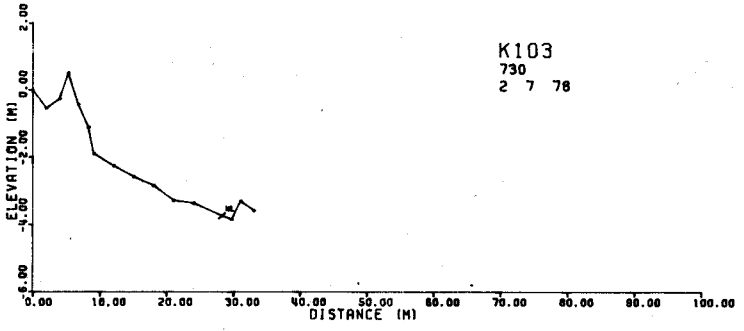
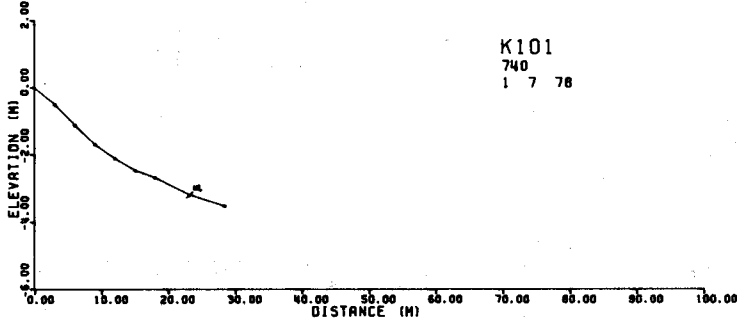
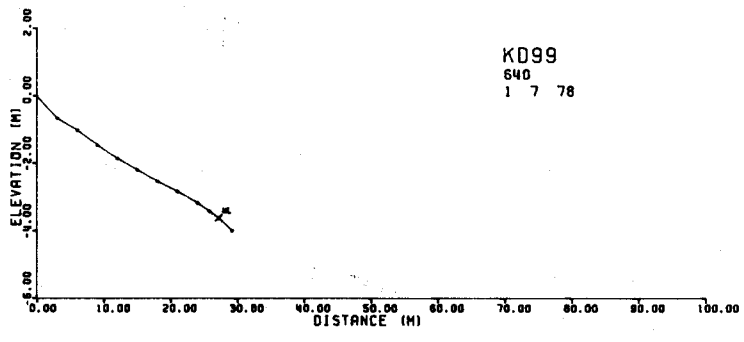
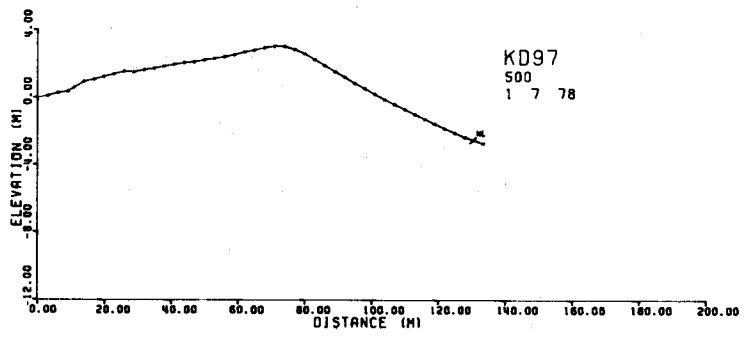


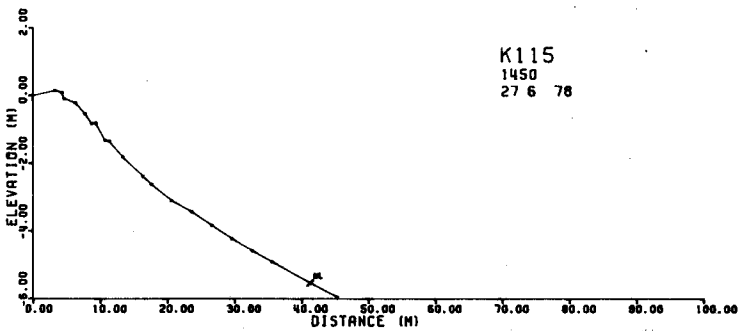
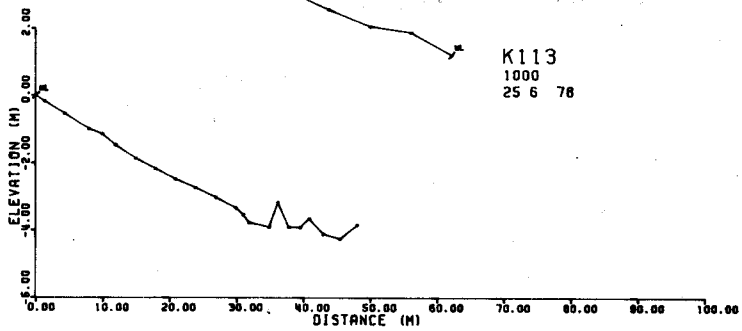
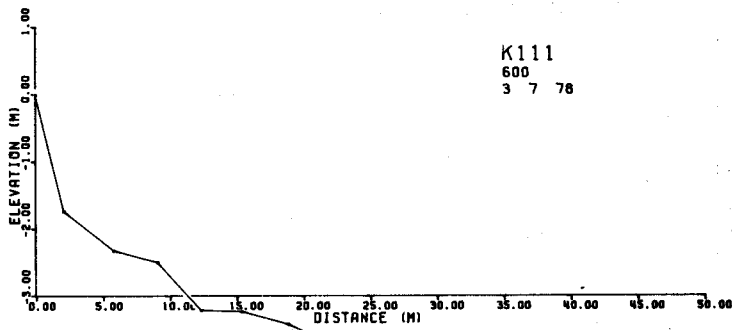
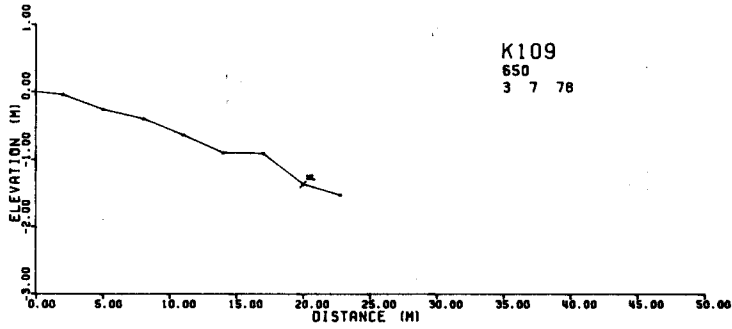
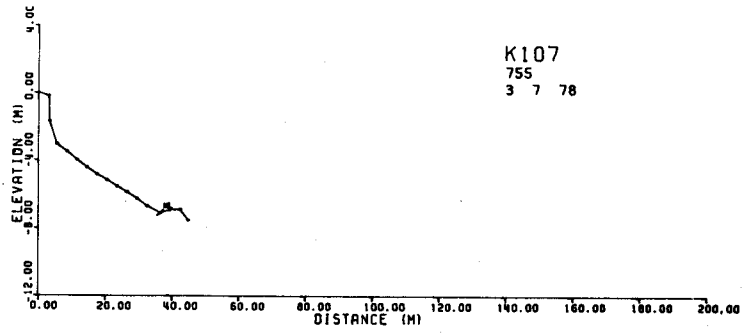


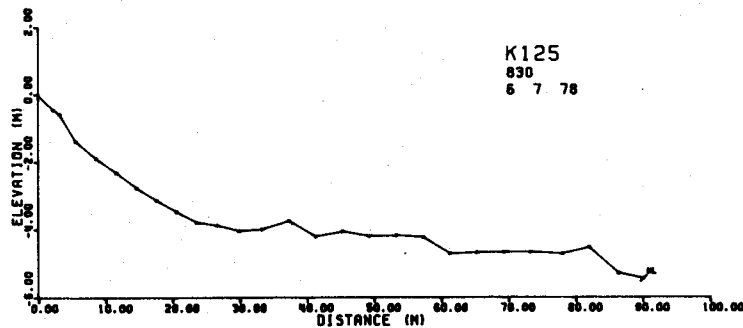
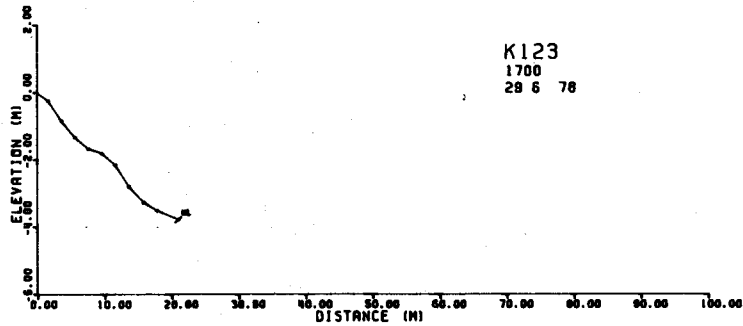
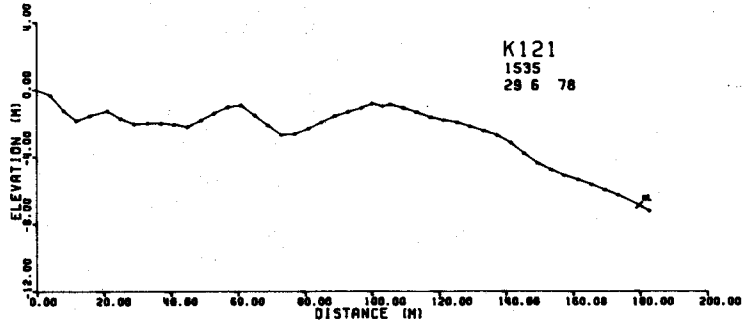
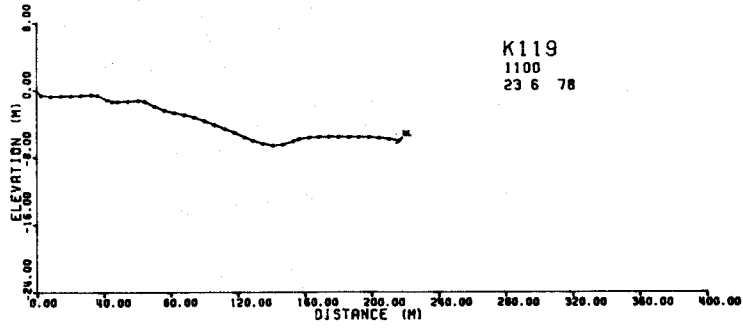
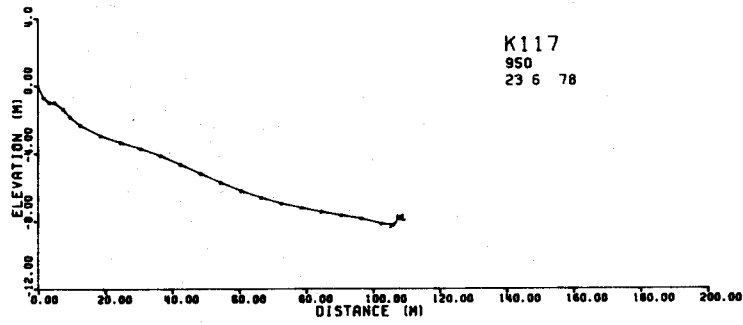


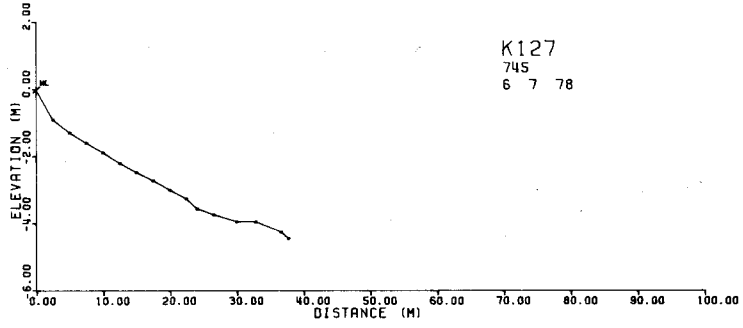












K127
745
6 7 78

FINAL REPORT

Contract: 03-5-022-67

Research Unit: 98

Number of Pages: 25

DYNAMICS OF NEAR SHORE ICE

Roger Colony

Polar Science Center
Division of Marine Resources
University of Washington
Seattle, Washington 98105

March 30, 1979

CONTENTS

	Page
I. Summary	1
II. Introduction	1
III. Current State of Knowledge	2
IV. Study Area	2
V. Sources, Methods and Rationale of Data Collection	2
VI. Results	3
VII. Discussion	3
VIII. Conclusions	9
Appendix I.10

I. Summary

The near shore pack ice of the Beaufort Sea and Chukchi Sea have a profound influence on the development of the gas and oil fields of Northern Alaska. Design of structures, security of sub-surface pipelines, and surface transport of oil is dependent on a knowledge of many of the properties of the near shore pack ice. The motion of the ice pack has been investigated over the past several years. From October 1975 to December 1976 OCSEAP sponsored a number of drifting buoys initially deployed along the continental shelf from Banks Island to Pt. Barrow. In the spring of 1977 a number of drifting buoys were deployed in the central Chukchi Sea. In the spring of 1978 four buoys were deployed in the near shore ice pack from Pt. Barrow to Cape Lisburne. This final report is of the motion of the four buoys deployed in 1978.

The study of the ice pack can be undertaken from a number of different views. Of primary importance is an observational program oriented toward a description of the state and motion. Other methods of study include the description of physical processes, often through mathematical modelling, and the development of various simulations, important to forecasting the state of the ice pack. The primary task of this contract is to observe the motion of the near shore pack ice from Pt. Barrow to Cape Lisburne. This program expands the geographic coverage and offers some indication of year-to-year variability of the ice behavior.

Previous studies have shown the near shore ice between the Mackenzie Delta and Pt. Barrow tends to be guided by the coast in its westward drift. Oil or other pollutants entered into the pack ice would probably be advected to some location off Pt. Barrow. Then depending on local conditions the pack can move northward and be reincorporated into the Beaufort Gyre or it can move southward, still guided by the Alaska coast, into the Chukchi Sea. The current study shows the near shore ice pack between Pt. Barrow and Cape Lisburne to move into the central Chukchi Sea during early summer and then to move north and west; probably to be incorporated into the transpolar drift stream. Once the ice moved toward the central Chukchi the mean motion was very similar to the drift of the summer of 1977.

II. Introduction

A. General Nature and Scope of Study

The purpose of the project was to determine from drifting buoys the motion of the near shore ice pack from Pt. Barrow to Cape Lisburne. In March of 1978, four RAMS (Random Access Measurement System) buoys were deployed within 100 km of the coast. This study extends the geographical area and provides some indication of year-to-year variations of the motion of sea ice. Of particular importance is the relation between the buoys and the margin between the pack ice and season open water. Also of interest is the frequency of very high speed events along the coast as observed in January of 1976. At this time one buoy recorded speeds to 140 cm sec^{-1} and net motions of several hundred kilometers within a week's time.

B. Specific Objectives

The primary objective of this report is to present the motion of the four buoys during March - October 1978. One buoy was instrumented with a barometer to record surface atmospheric pressures. This time series is also reported.

C. Relevance to Problems of Petroleum Development

Observations of ice motions are relevant to problems of petroleum development for three broad reasons: 1) the ice cover will serve as a carrier of any petroleum products spilled in the Beaufort or Chukchi Sea so that the ice trajectories serve as a first estimate of the paths to be taken by the oil 2) the observations are necessary to identify the important physical processes at work within the ice pack and 3) the ice motion is an observable quantity that may be compared with a simulation of pack ice dynamics or used to tune the simulation.

III. Current State of Knowledge

The RAMS buoys are reliable off-the-shelf items at a reasonable cost (\$5000) and usually survive for the design life of the batteries. The NIMBUS satellite relays data between the buoy and NASA data processing. The data processing of the NASA data tapes is a capability to be developed at each user's site. The University of Washington has the data processing capability.

The buoys deployed in March 1978 are the third set deployed as part of OCSEAP. The first set provided drift data in the southern Beaufort Sea in conjunction with the AIDJEX project during October 1975 - December 1976. These trajectories were reported in the 1977 Annual Report, Vol. XVI, by Untersteiner and Coon (RU 98). The second set were deployed in the central Chukchi Sea during March 1977 - September 1977 and the data is given in the Annual Report 1978 by Pritchard. The buoys reported here were deployed in the Chukchi Sea near the Alaskan coast in March 1978. Other ice drift data are the ice island T-3, the ship *Maud*, and a number of the Soviet North Pole ice stations.

IV. Study Area

The study area is the Chukchi Sea with emphasis on the near shore ice pack.

V. Sources, Methods, and Rationale of Data Collection

The measurements were made with the Random Access Measurement System (RAMS) which uses the techniques of Doppler Satellite navigation. The raw measurement is the frequency of a signal transmitted from the ice station to the satellite. The measured frequency is affected by a Doppler shift related to the rate of change in distance between the satellite and the ice station, which is itself related to the unknown ice coordinates and the known satellite orbit. During each satellite orbit several frequency measurements were made and from them an

over-determined solution was found for the unknown coordinates. The Doppler counts were made for discrete 1-second bursts transmitted from the buoy each minute. Typically, 20 measurements per pass were collected, stored, and transmitted to a receiving station on the ground. Fix calculations were done at NASA and mailed to the users in the form of magnetic tapes and printed output.

The user must edit the data for bad position fixes. The algorithm employed compares each fix latitude with the median of the latitude of the ten fixes preceeding and the ten fixes following it. When the differences exceed a preset tolerance, the fix is discarded. The algorithm is applied twice, with a smaller tolerance the second time. The same procedure was then applied for longitude.

The barometer was a Paroscientific Digiquartz sensor having superior accuracy, low sensitivity to temperature and low power consumption. This type of barometer has previously been used with RAMS buoys. The frequency of the quartz oscillator is encoded, radioed to the NIMBUS satellite, relayed to NASA, and later decoded by the user. Calibration charts are used to convert the frequency to atmospheric pressure.

VI. Results

Positions of the four buoys deployed in March 1978 have been edited. The results are shown in Figures 1-4 and in Appendix I. Figures 1-4 show at most one position fix per day as indicated by the small ticks. The large dots show the position near the first of each month.

The data was collected by the NIMBUS 6 satellite. The testing and launching of the NIMBUS 7 satellite disrupted the NASA data collection center. Over some periods the data was lost and over much of the time beginning in August the data was not available on magnetic tapes. By September the number of fixes was down to one every other day. This is in contrast to the usual number of twenty per day for the period March - June. Hand analysis provided the position data shown by the solid line in Figures 1-2.

The lifetime of the buoys was five to seven months. All available data is shown. Figure 5 shows the position of the ice edge for the summer of 1978. The ice edge analysis was obtained from NOAA satellite images.

VII. Discussion

The trajectories of the buoys are northward and westward during the spring and summer months. This is in accordance with the climatological drift as evidenced by T3, *Maud*, and several Soviet ice stations. The speed and direction of the 1978 buoys is very similar to the speed and direction of the 1977 buoys. It is interesting to note that the slight motion toward the Bering Straits during March was also seen in the 1977 buoy data.

A comparison of the drift data and the ice edge charts indicates that the buoys were always in the multi-year ice zone. Figures 1-5 suggest the ice edge is driven by the winds rather than a result of simple thermodynamics.

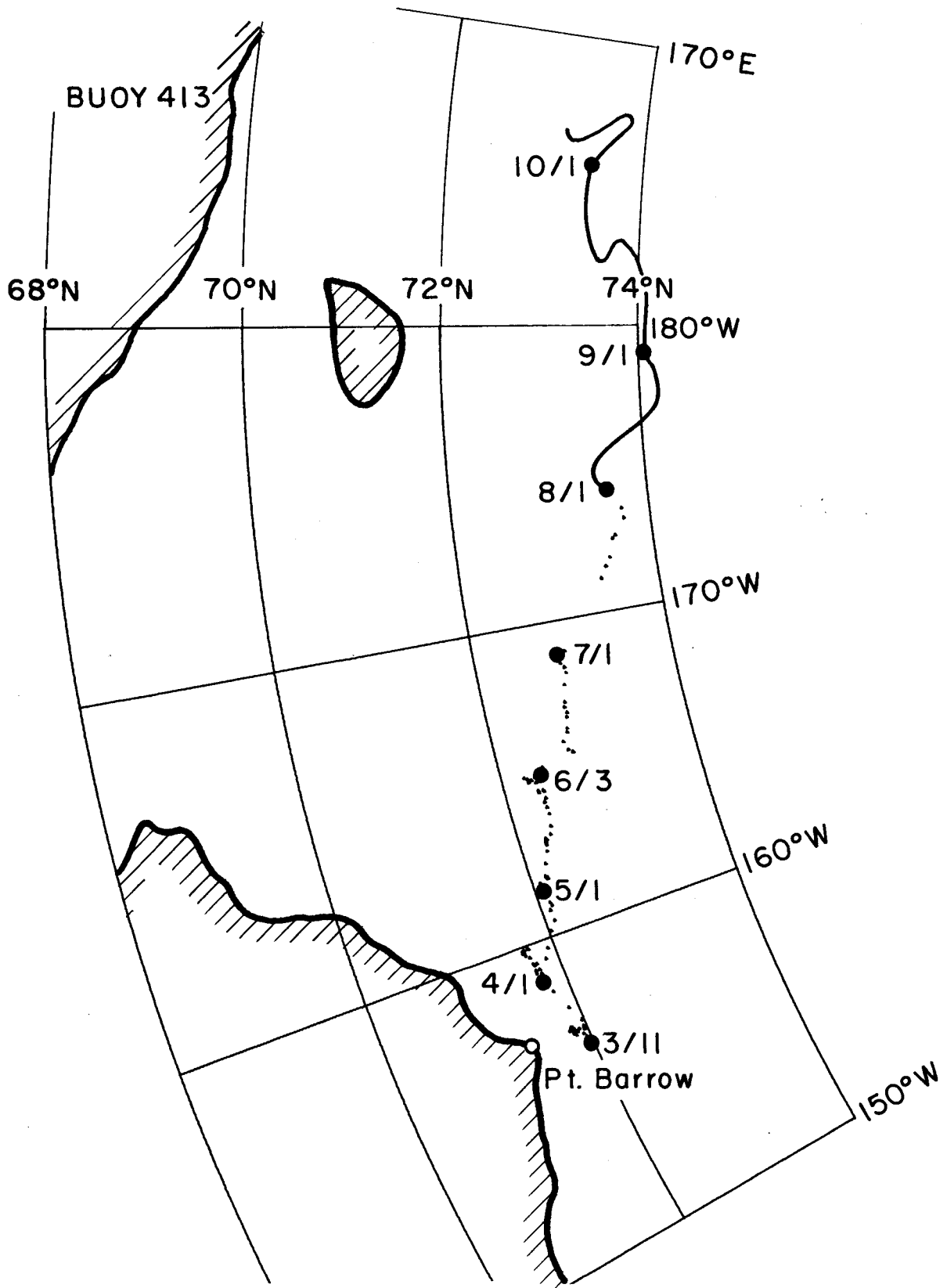


Figure 1: Trajectory of buoy 413

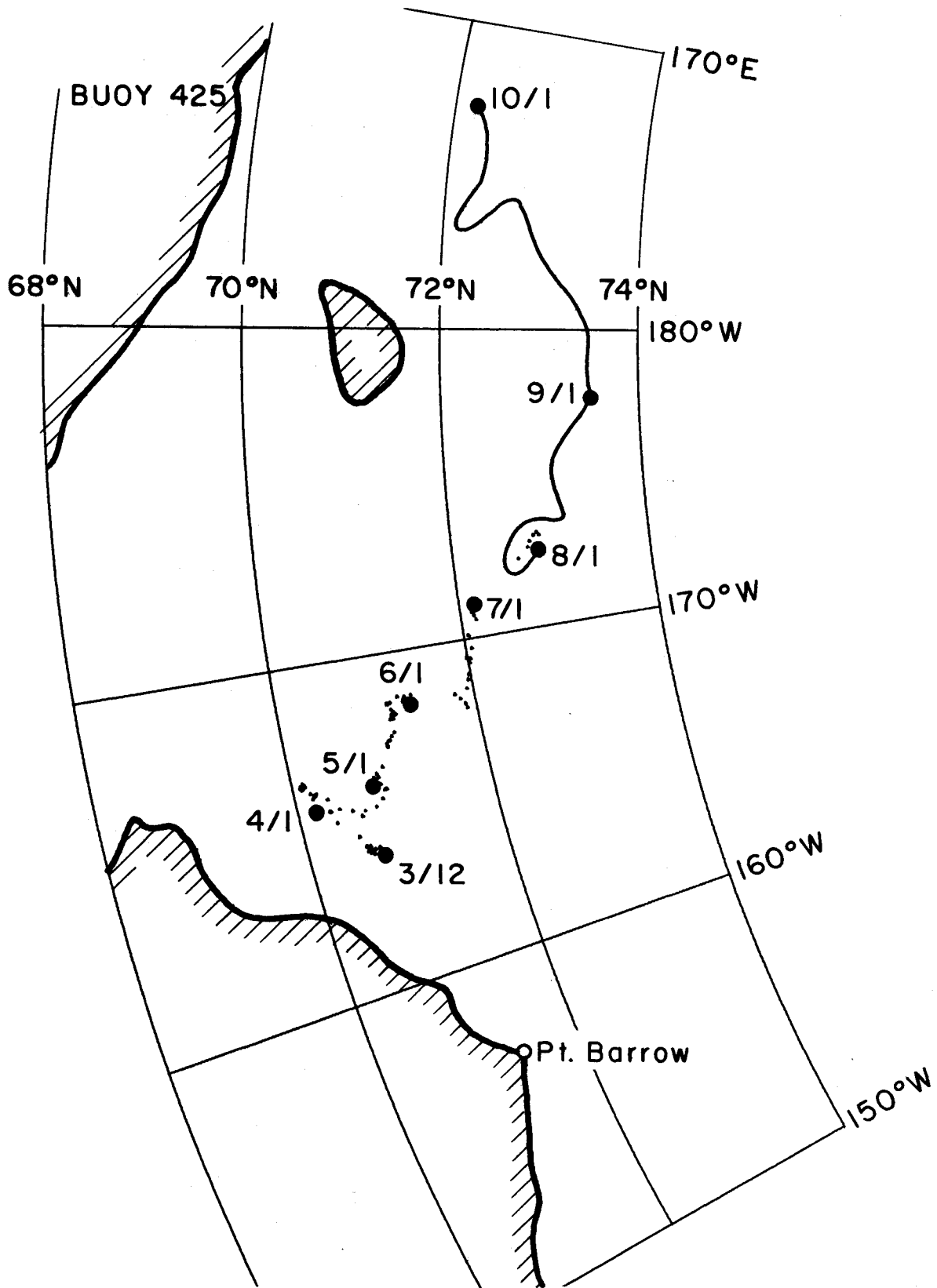


Figure 2: Trajectory of buoy 425.

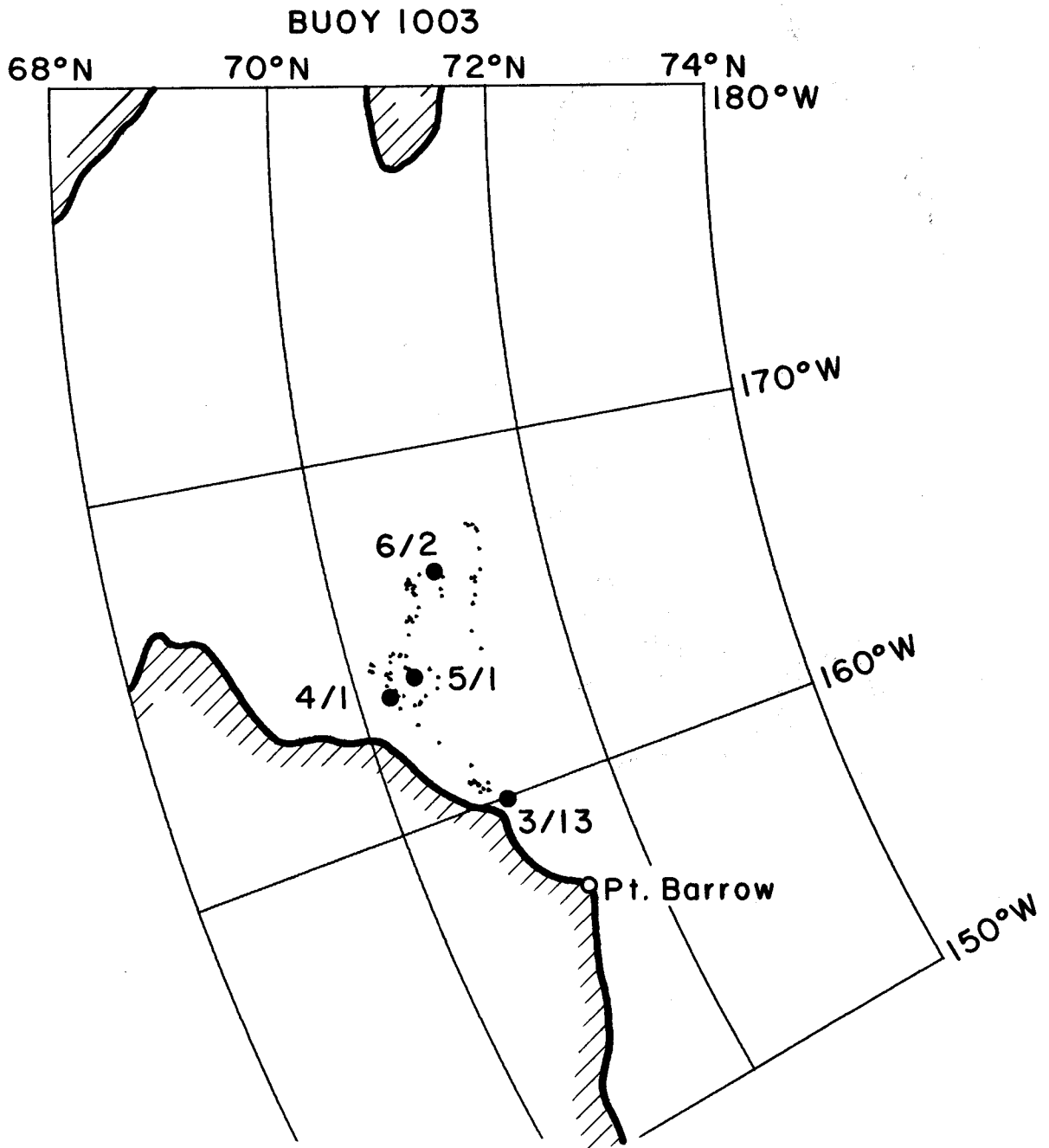


Figure 3: Trajectory of buoy 1003.

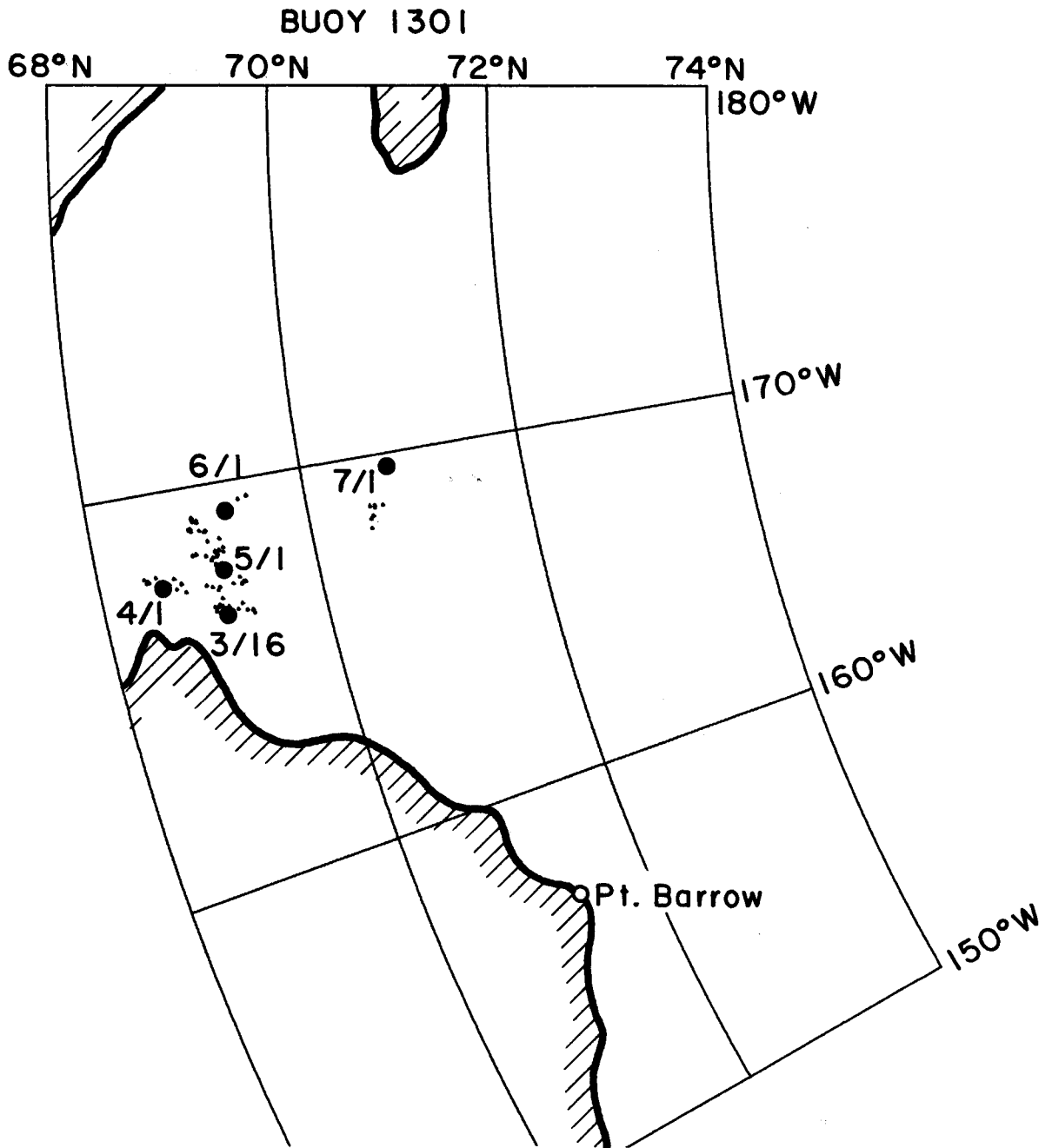


Figure 4: Trajectory of buoy 1301.

Oil spilled in the pack ice between Pt. Barrow and Cape Lisburne would be of no danger to Bering Sea for the year 1978. Although it is known that some ice from the Chukchi Sea has drifted through the Bering Straits and into the Bering Sea, this is not the norm. The years 1976-1978 all show the same summertime drift features; however sea ice is well known for producing anomalous events. The data of 1977-78 does not show the large jets of near shore pack ice motion that was recorded in January of 1976.

VIII Conclusions

Drift of the ice cover in the Chukchi Sea during March - October 1978 has been determined. The general northward and westward motion would have precluded oil spilled on or in the ice from being transported into the Bering Sea at this time. The drift for this time is very similar to the drift reported in 1977. The probable fate of the buoys is to be incorporated into the transpolar drift stream and exit into the Greenland Sea after two or three years.

DYNAMICS OF NEAR SHORE ICE

APPENDIX I

Measurements of Sea Ice Motion in the Chukchi Sea March-October 1978.

Four data buoys were deployed in the Chukchi Sea in March of 1978. Data has been processed to obtain position. Due to the preparation and launch of the NIMBUS 7 satellite some of the position data was analyzed by hand. The solid curves in the following figures indicate that analysis. The automatic data processing is described in AIDJEX Bulletin No. 35 by A. S. Thorndike and J. Y. Cheung (January 1977, University of Washington). The atmospheric surface pressure recorded at Buoy 425 is also reported in this appendix.

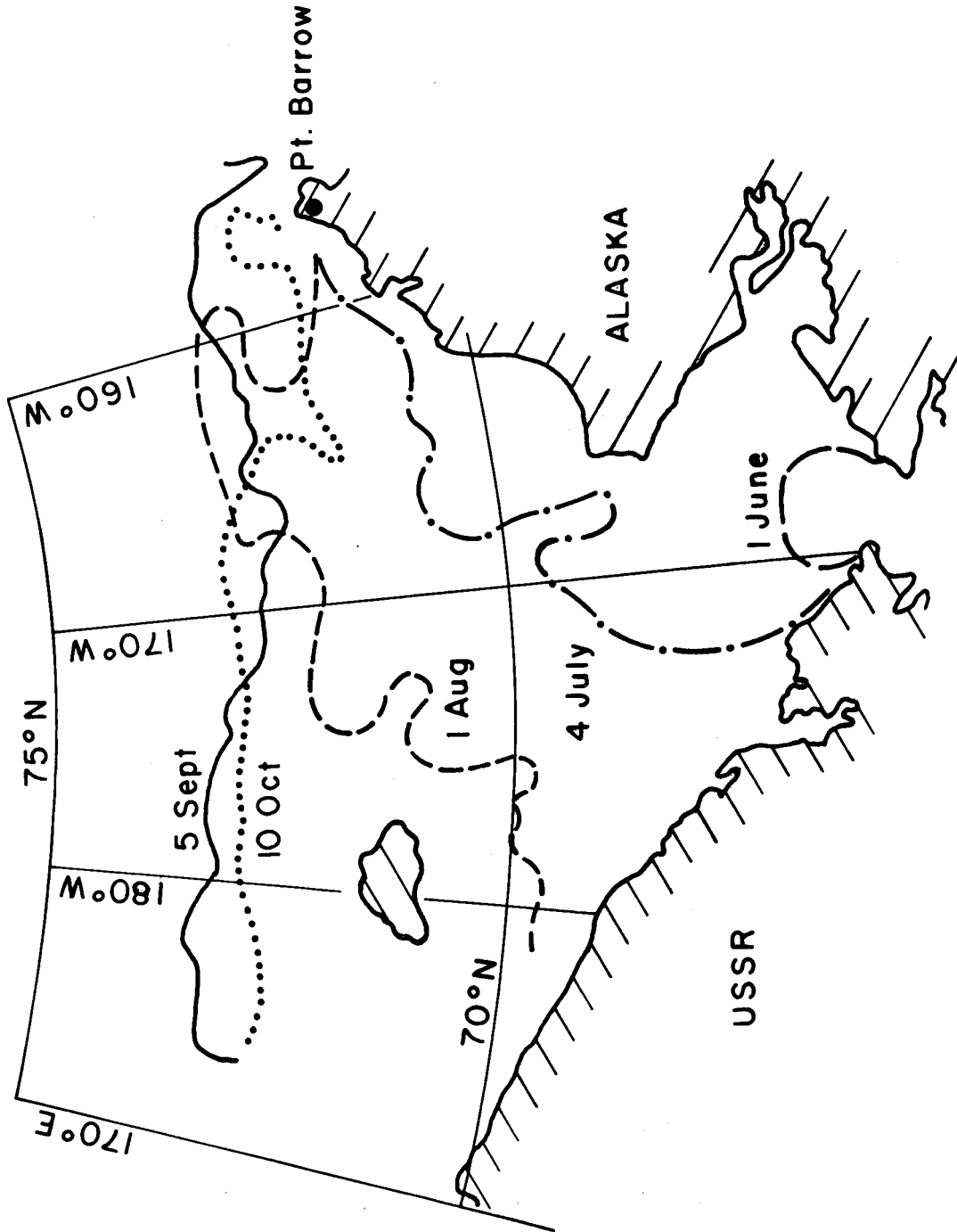
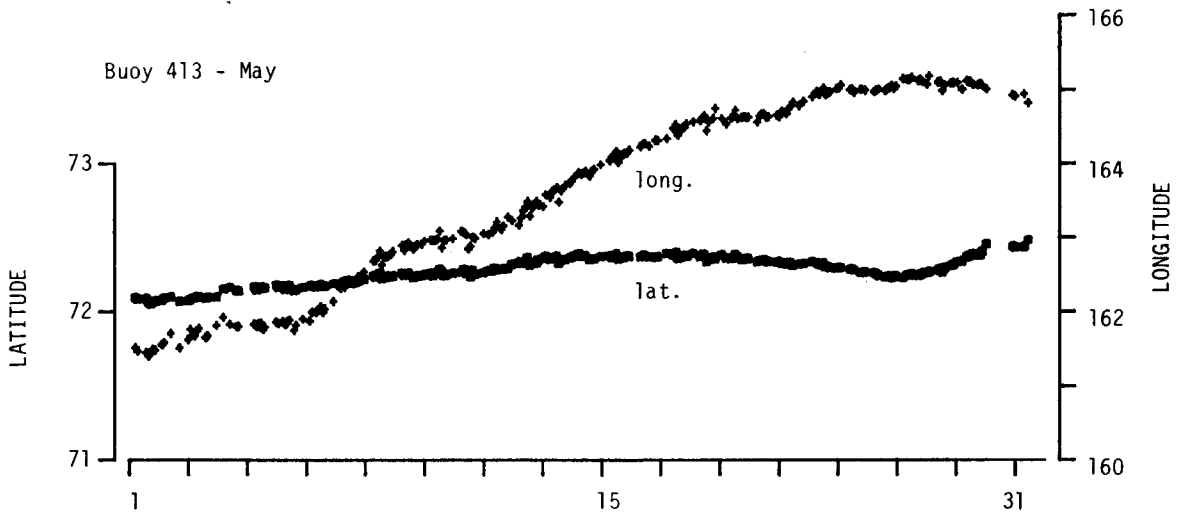
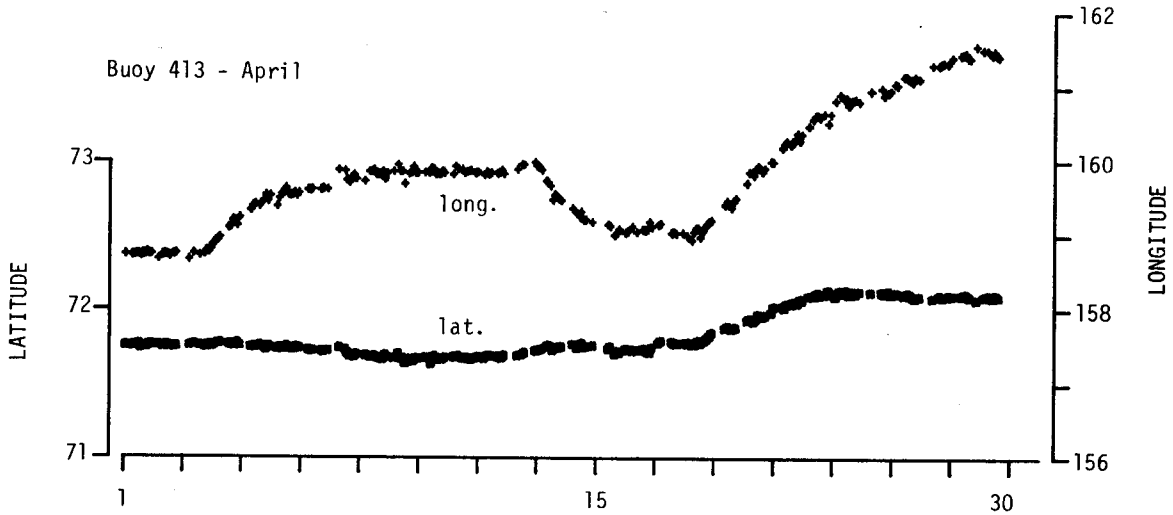
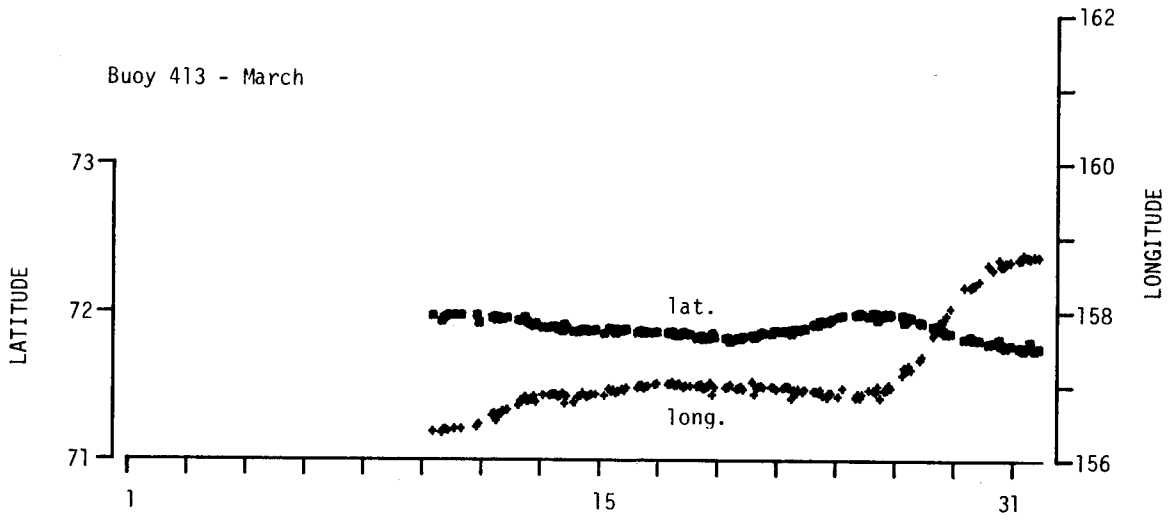
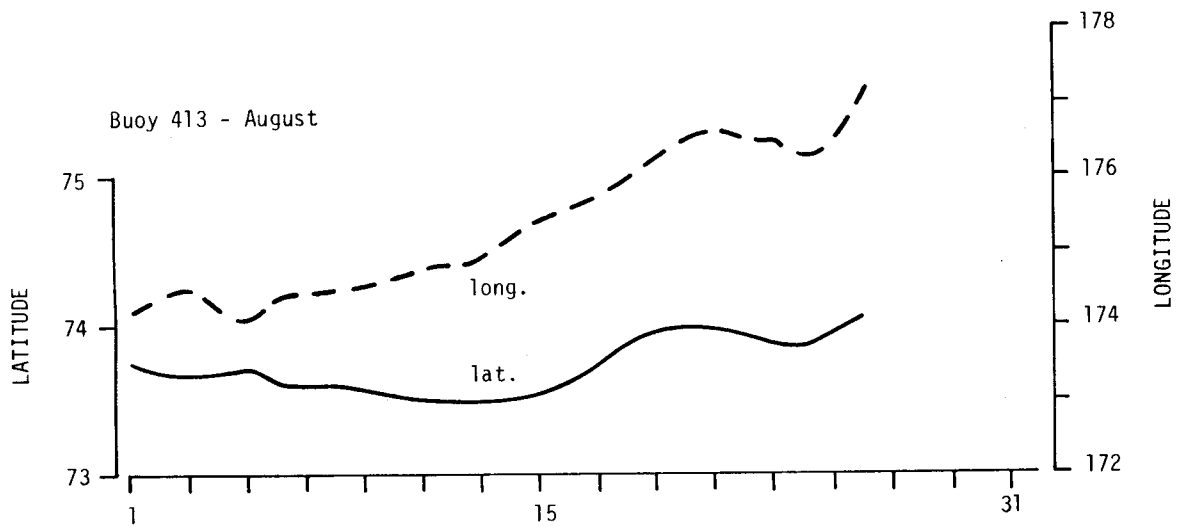
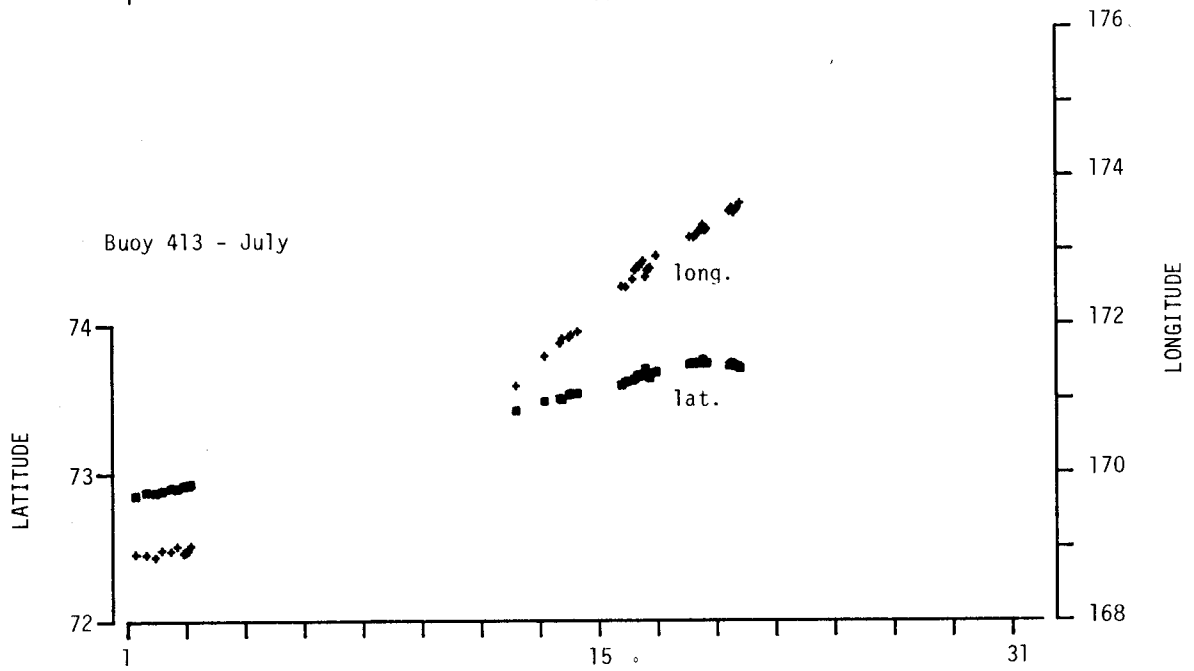
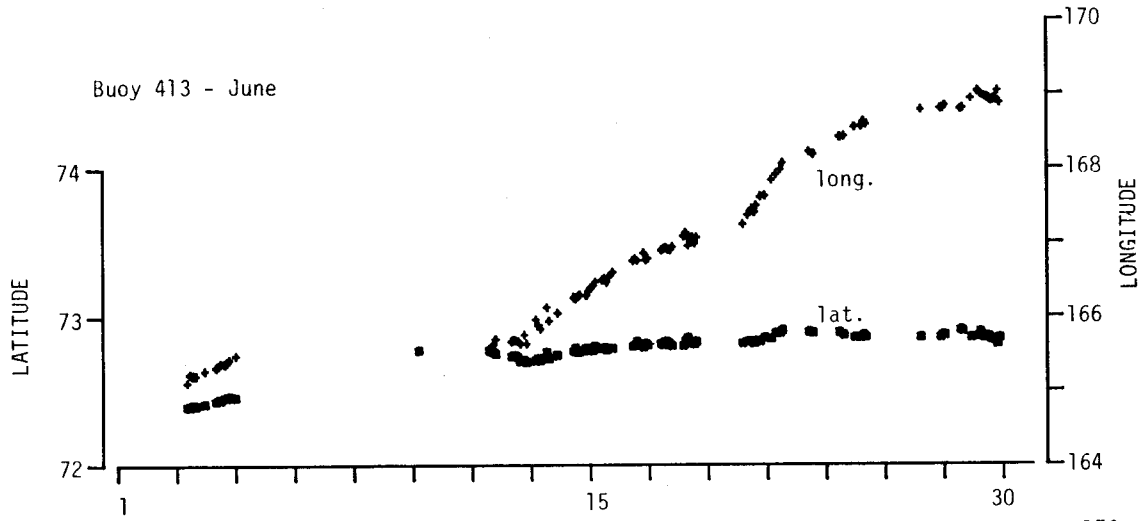
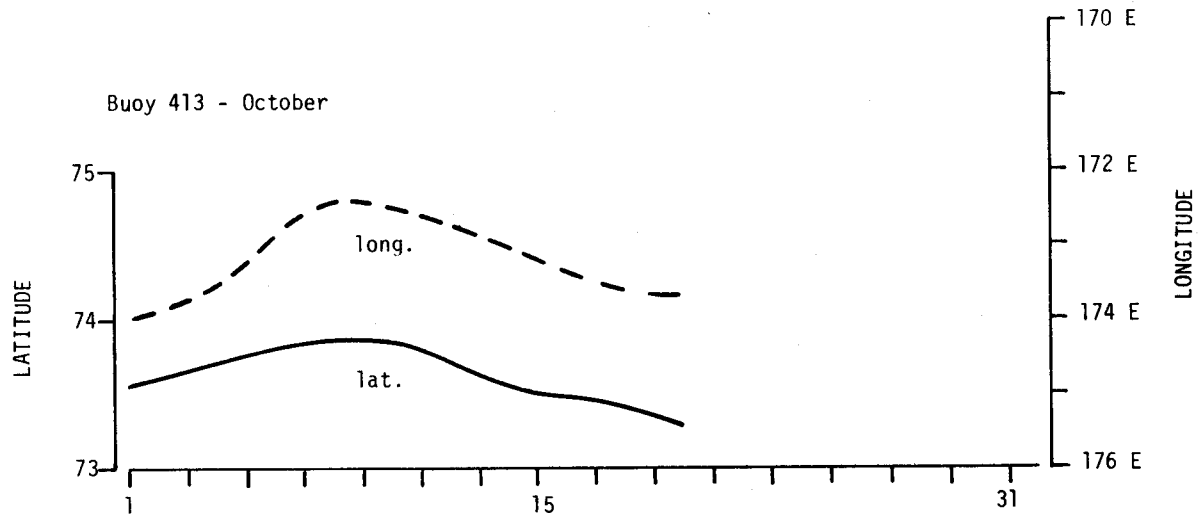
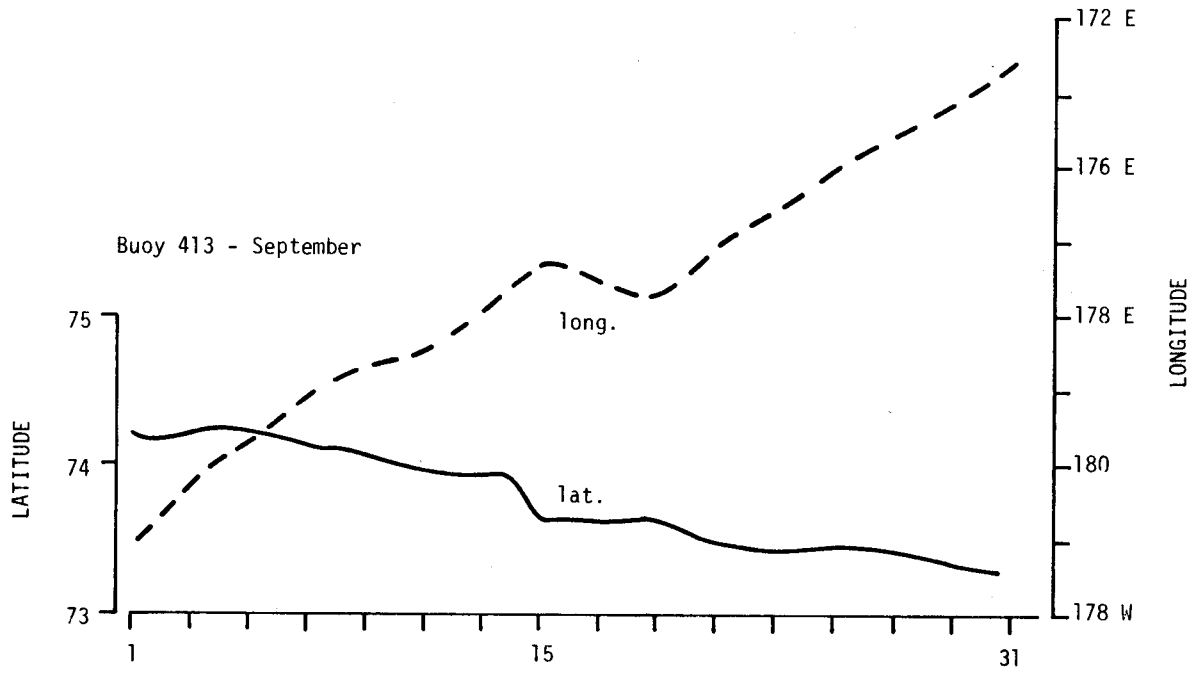
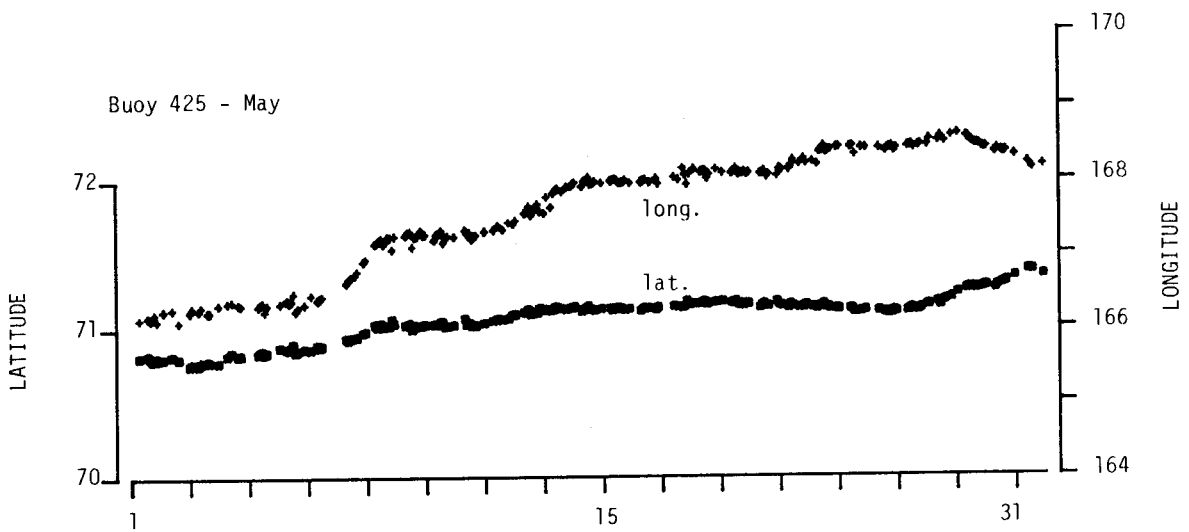
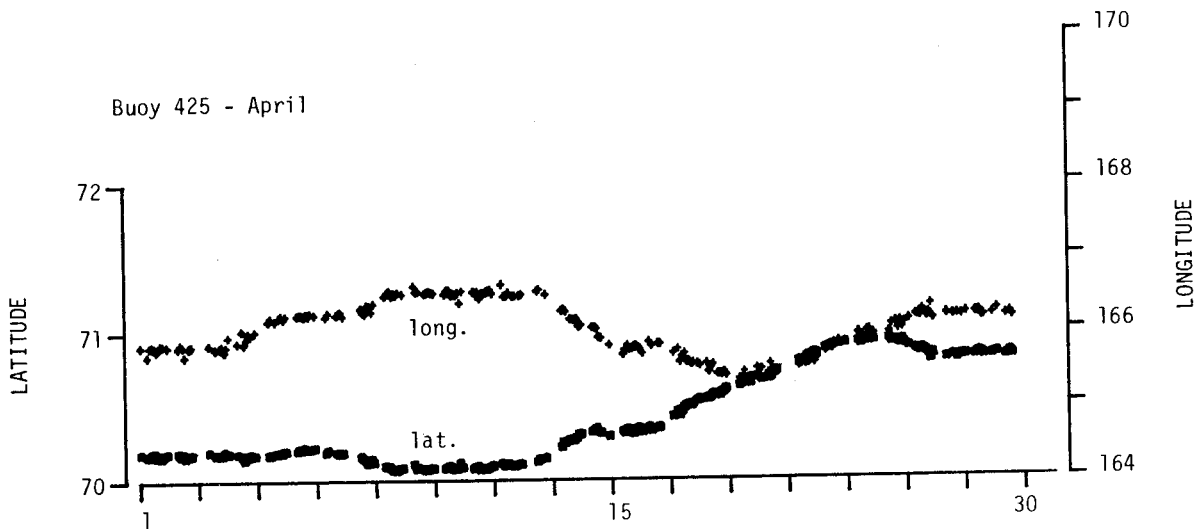
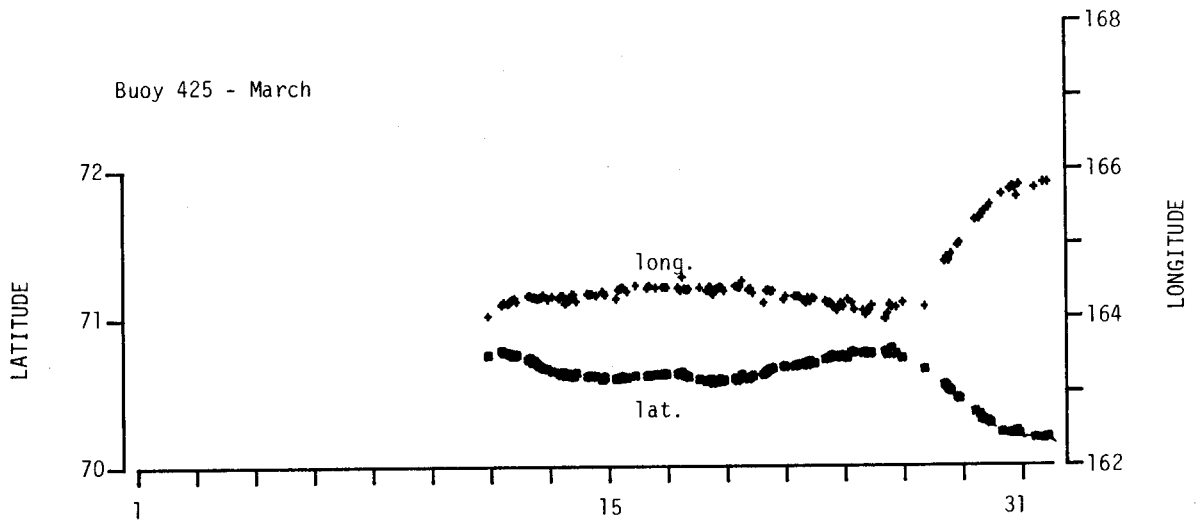


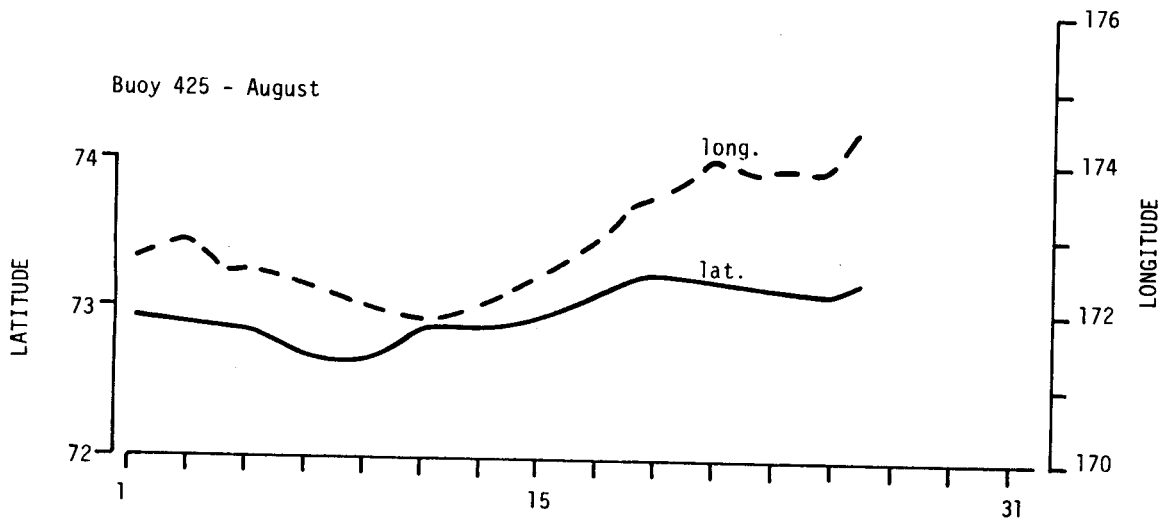
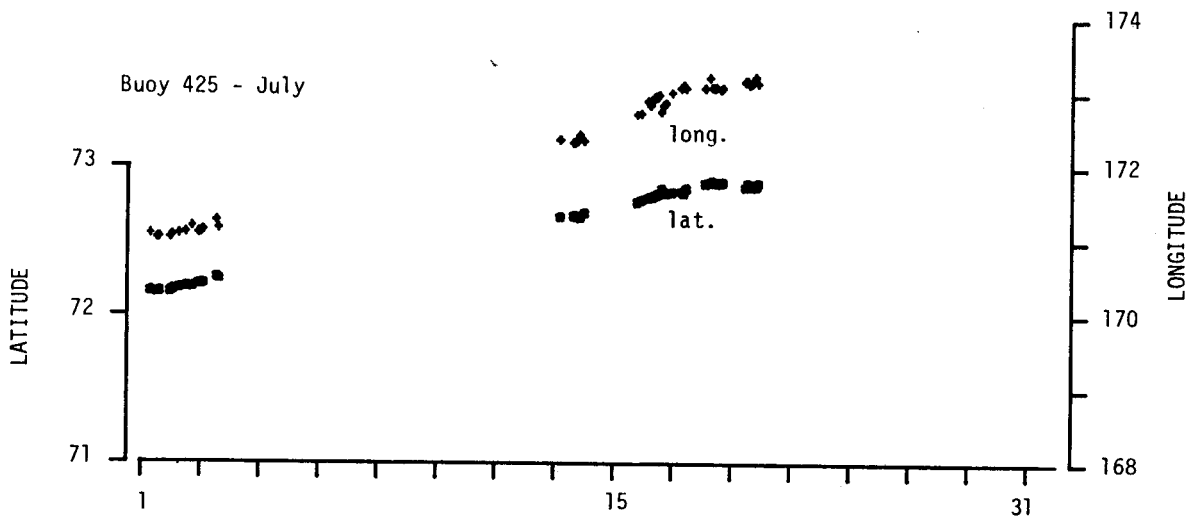
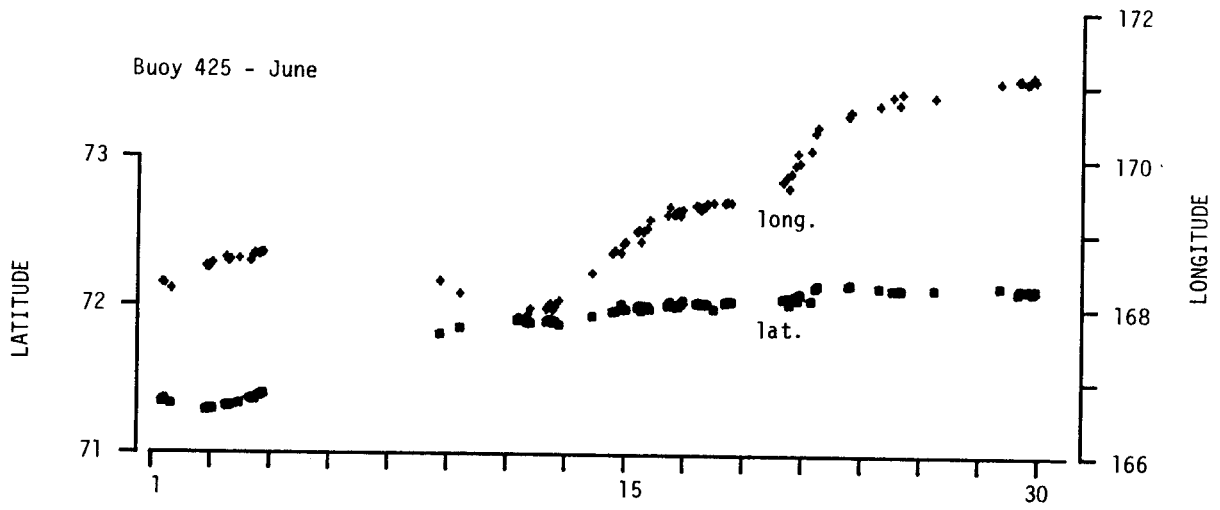
Figure 5: Ice edge margin from NOAA images, Summer 1978.

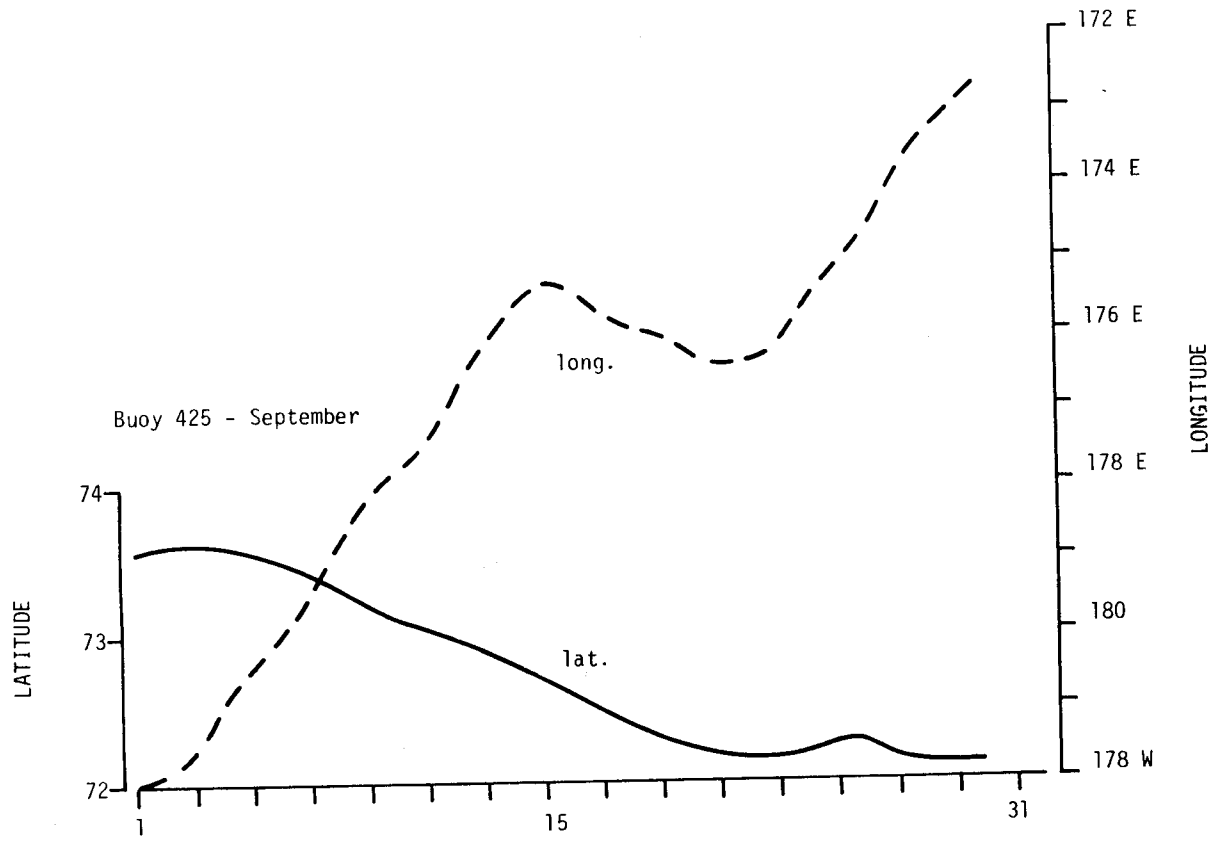


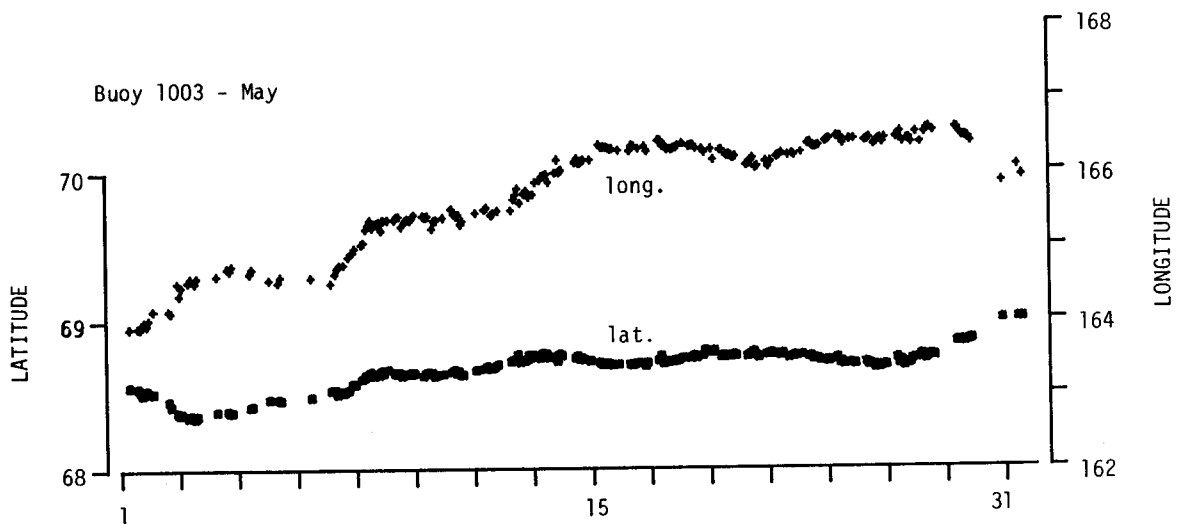
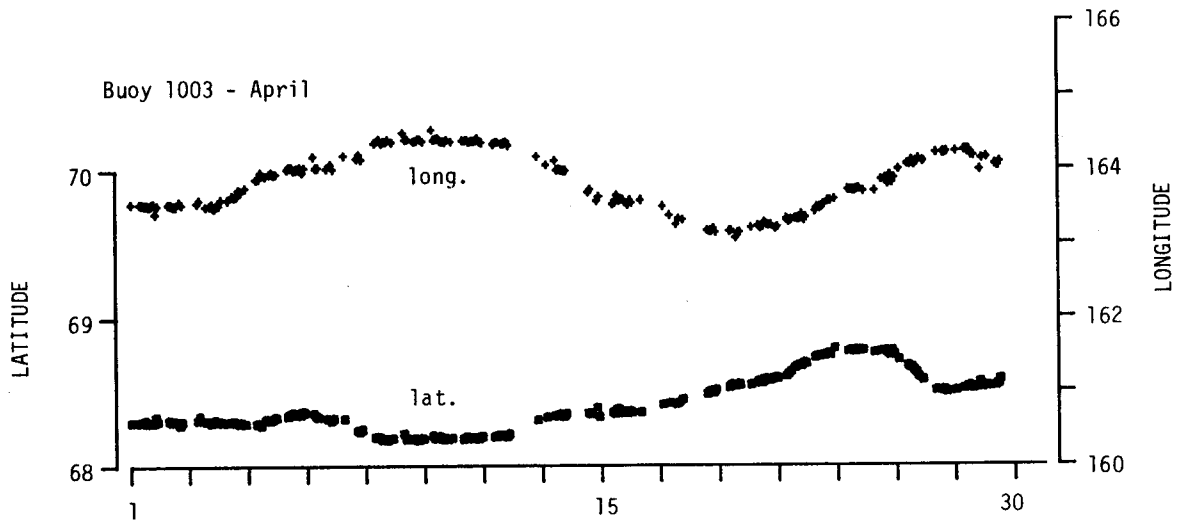
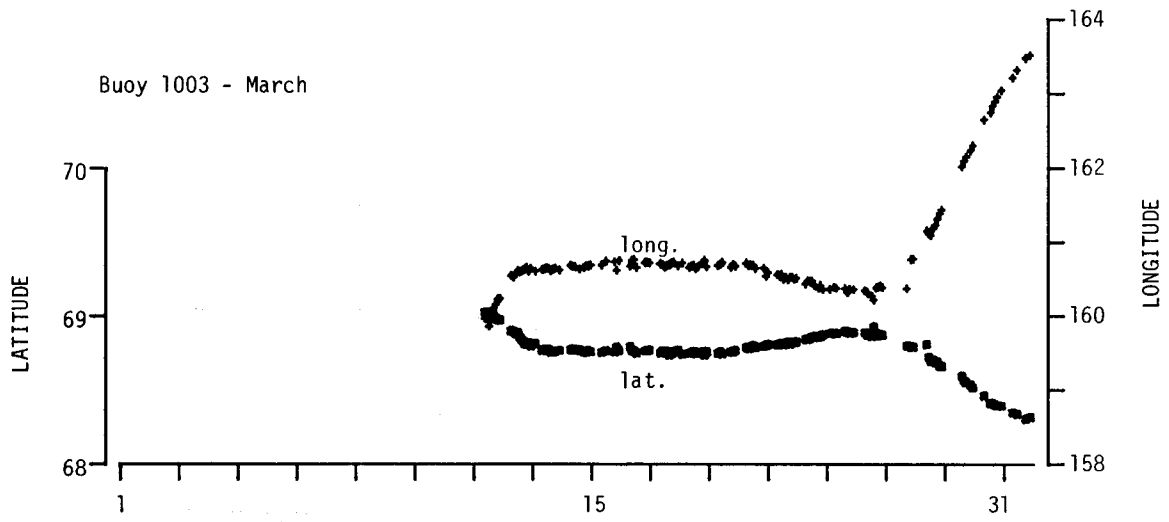


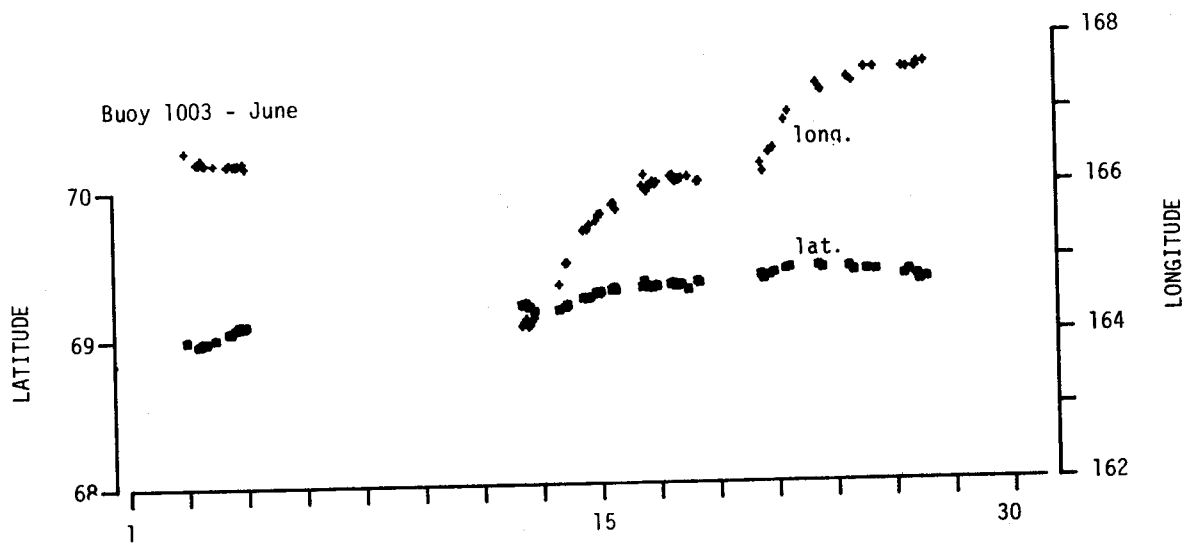


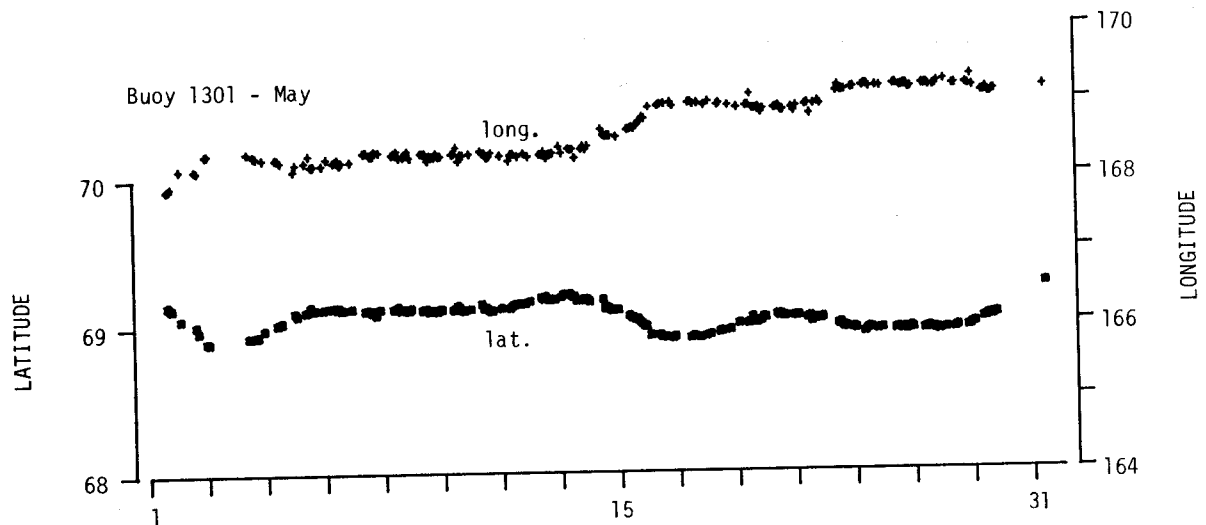
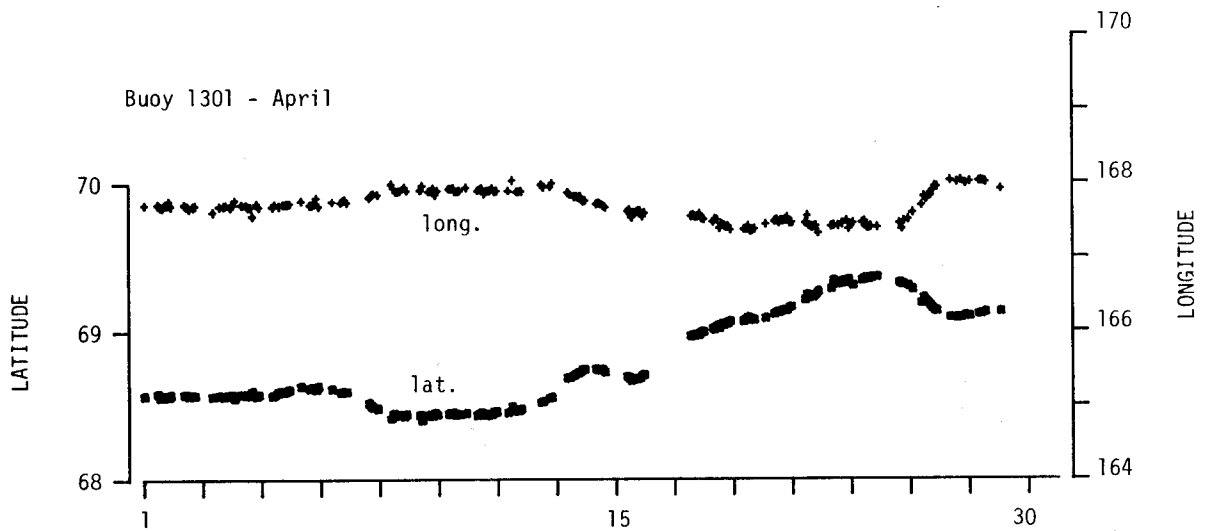
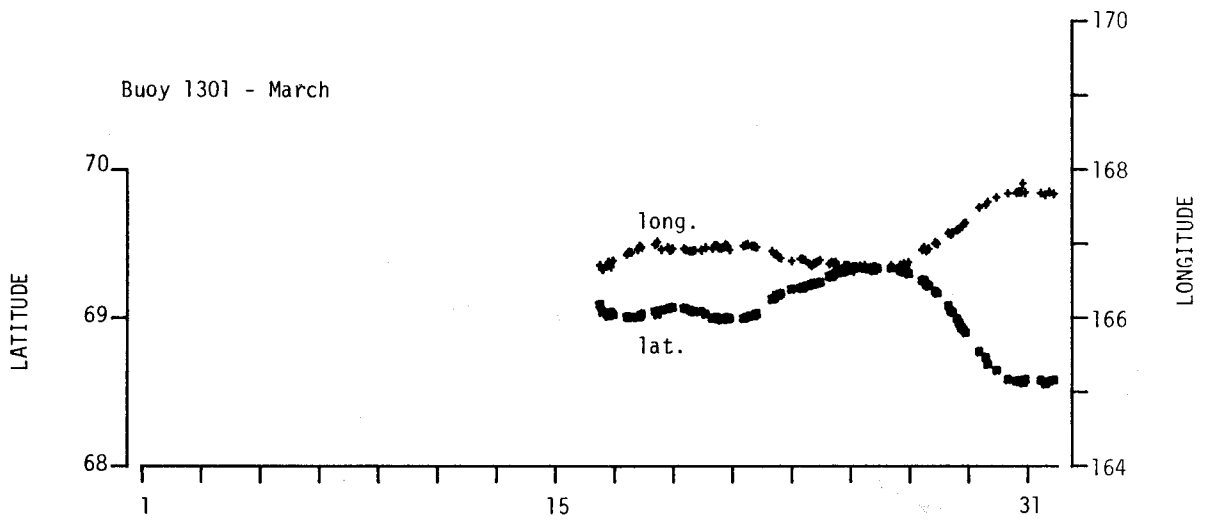


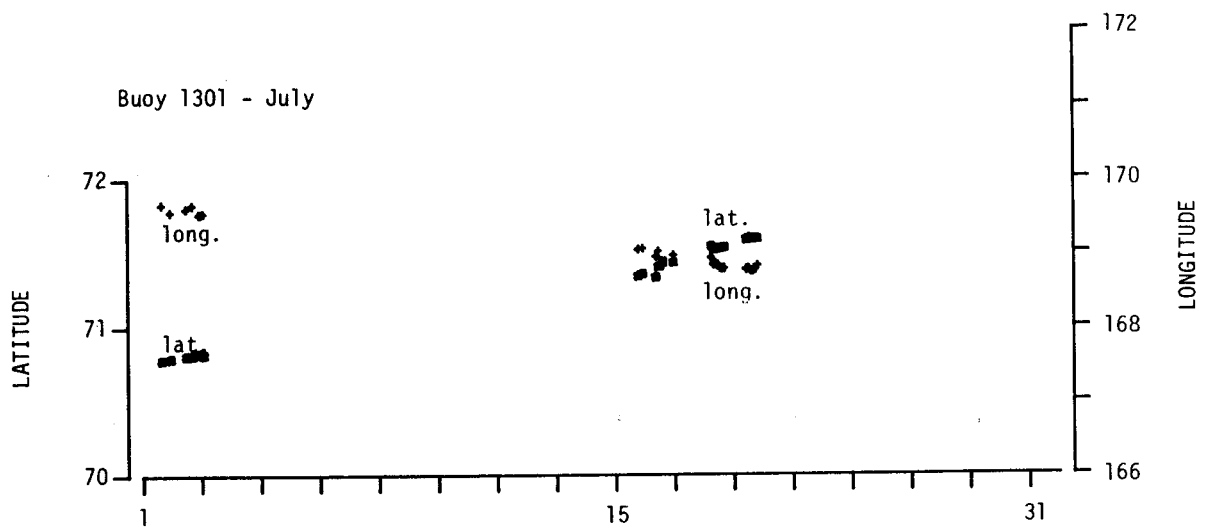
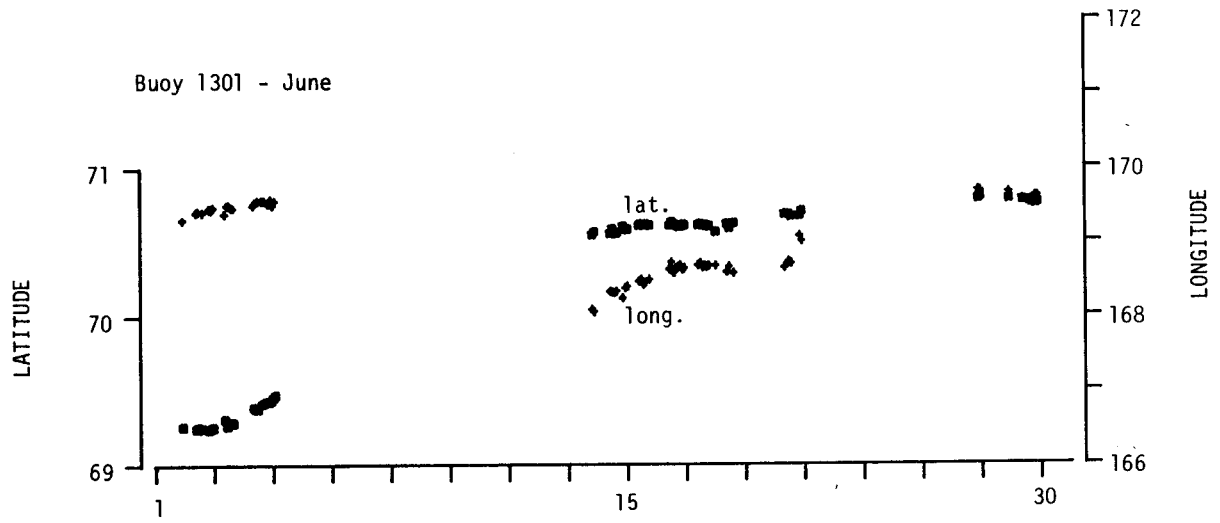






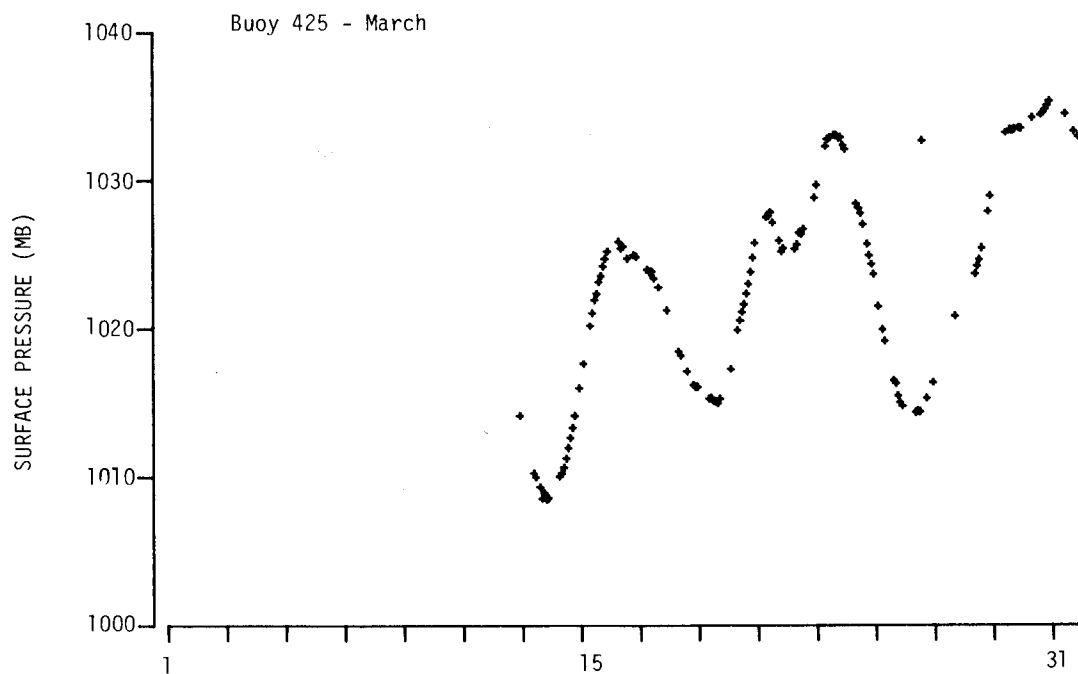


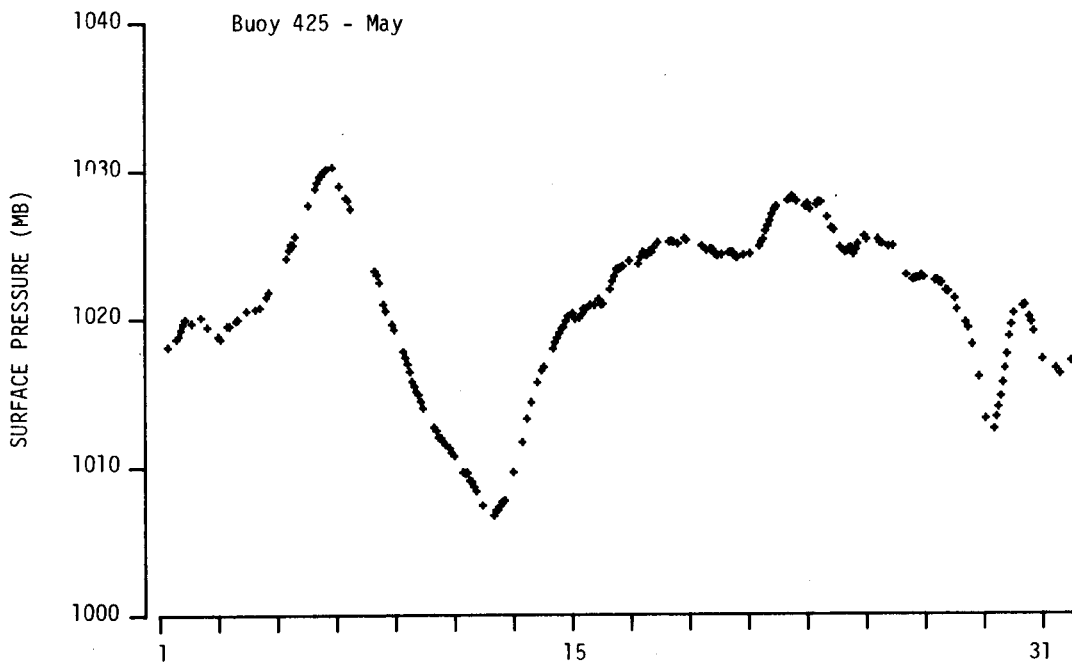
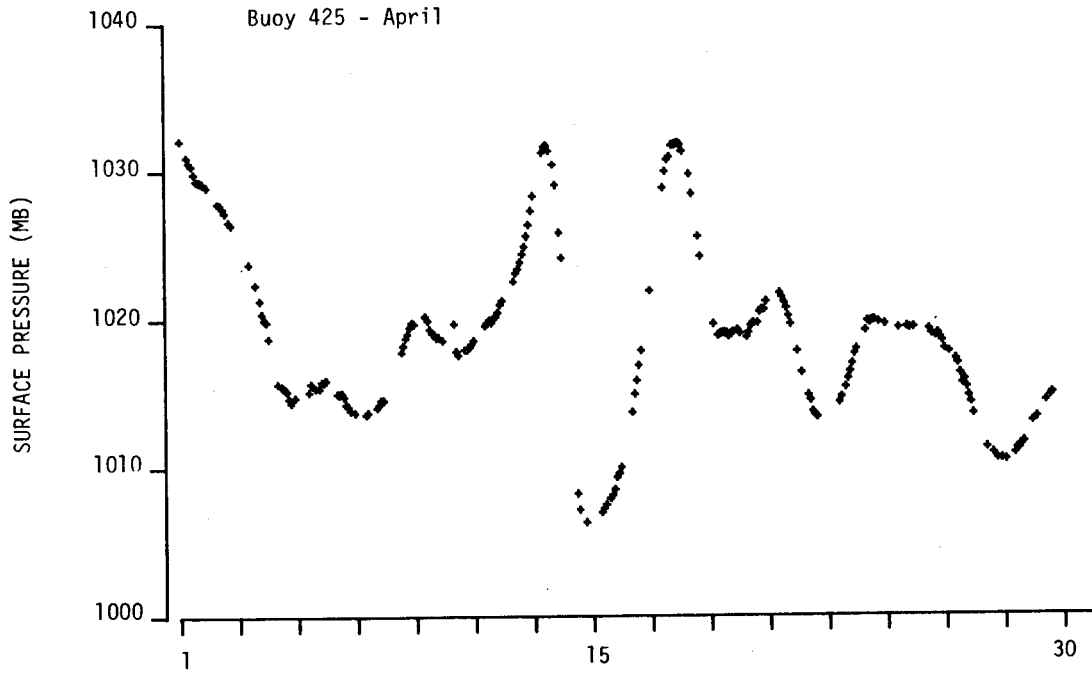


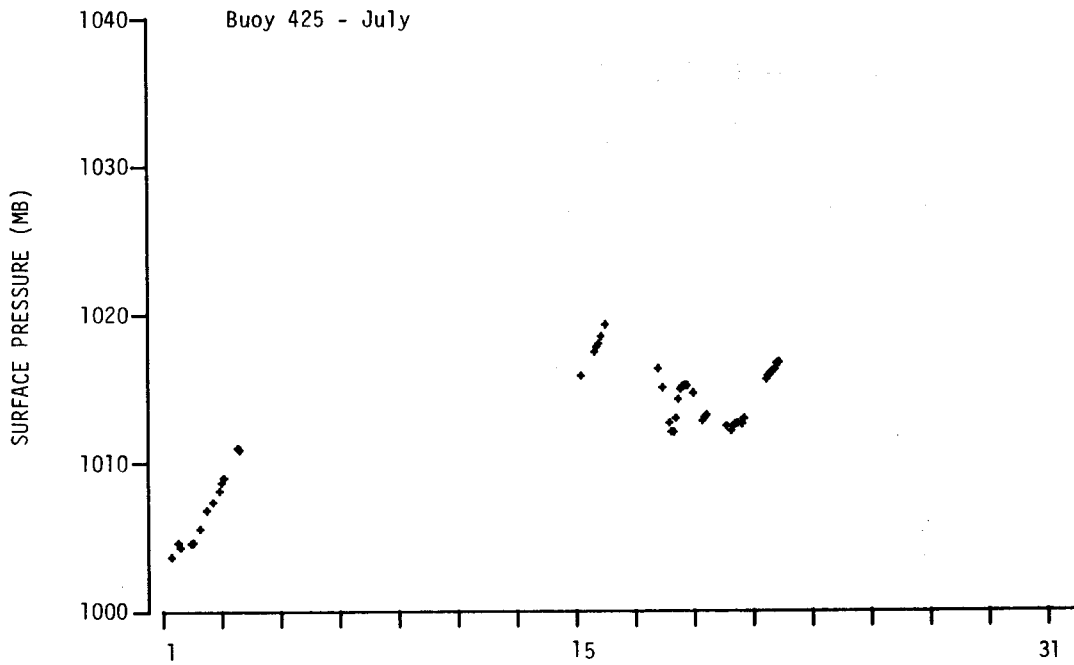
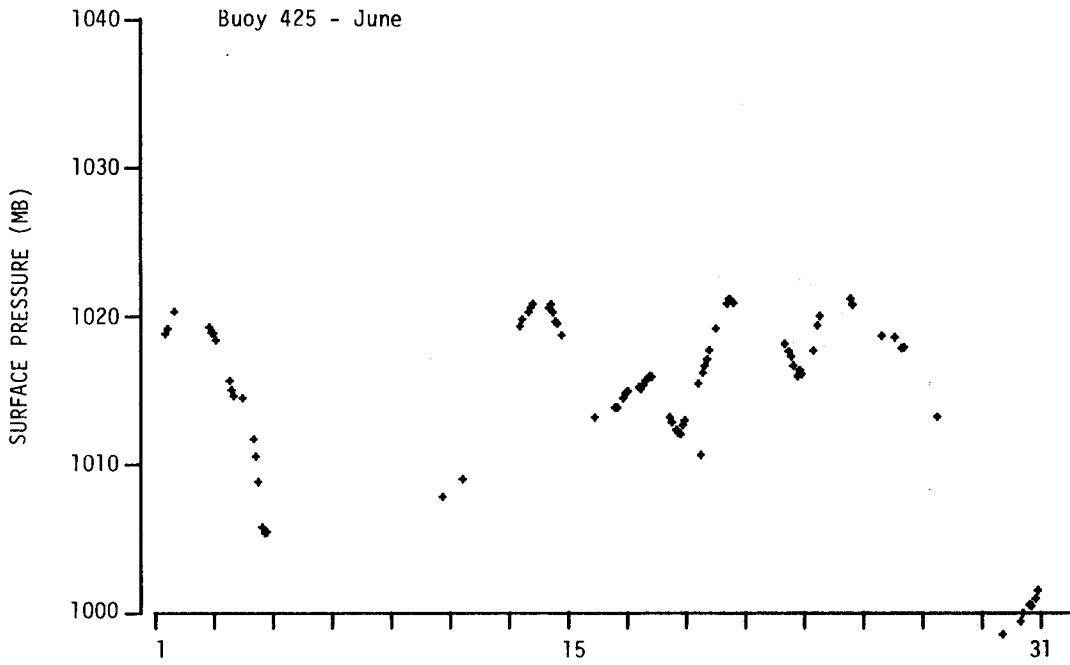


Time Series of Surface Pressure

Buoy 425 was instrumented with a Paroscientific Digiquartz pressure transducer to measure atmospheric sea level pressure. This instrument was checked at Barrow to insure correct calibration. Testing of this type of barometer is reported by P. Martin and M. Clarke, A Test of Barometric Pressure and Temperature Measurements from ADRAMS Buoys, AIDJEX Bulletin No. 40 (June 1978, University of Washington).







FINAL REPORT

Contract RK 6-6074
Research Unit 206
(Gardner & Vallier)
Research Unit 556 (Dean)

SEDIMENTOLOGY AND GEOCHEMISTRY OF SURFACE SEDIMENTS AND
THE DISTRIBUTION OF FAULTS AND POTENTIALLY UNSTABLE
SEDIMENTS, ST. GEORGE BASIN REGION OF THE
OUTER CONTINENTAL SHELF, SOUTHERN BERING SEA

PRINCIPAL INVESTIGATORS:

J.V. Gardner
T.L. Vallier
W.E. Dean

with organic geochemistry
section by

K.A. Kvenvolden
G.D. Redden

U.S. Geological Survey
Menlo Park, California

June, 1979

TABLE OF CONTENTS

Introduction

Purpose and organization -----	1
Shipboard data collection -----	1
Shore-based data collection -----	7

Sedimentology and Geochemistry of Surface Sediments

Summary -----	14
Regional setting -----	15
General description and texture -----	18
Petrology of surface sediments -----	20
Mineralogy of clays -----	28
Distribution of major, minor, and trace elements -----	28
Organic geochemistry (K. Kvenvolden and G. Redden)--	62
Discussion -----	65

Distribution of Faults and Potentially Unstable Sediments

Summary -----	74
Classification of faults -----	74
Fault distribution -----	75
Potentially unstable sediments -----	78
Discussion -----	80

Conclusions -----	82
-------------------	----

References -----	83
------------------	----

Appendix A -----	88
------------------	----

INTRODUCTION

Purpose and Organization

This final report summarizes data and interpretations from studies of surface sediments, faults, and areas of potentially unstable sediment masses in the St. George Basin region of the outer continental shelf, southern Bering Sea (Fig. 1). We have divided the report into four major parts: Part 1 is an introduction which reviews methods used and the quantity of data collected during the contract period; Part 2 deals with the sedimentology and geochemistry of surface sediments; Part 3 discusses distributions of faults and areas of potentially unstable sediment; and Part 4 is a review of the major conclusions. Information on other aspects of our studies can be found in our 1977 and 1978 annual reports to OCSEAP and in the various publications and reports tabulated in Appendix A.

Ship-board Data Collection

Most data used in this report (Table 1) were collected onboard the U. S. Geological Survey research vessels SEA SOUNDER and SAMUEL P. LEE. A small part of the single channel seismic reflection data was collected onboard the R/V STORIS. Navigation of R/V SEA SOUNDER and R/V LEE was by integrated satellite and Loran C which has a nominal position accuracy of $\pm 200\text{m}$ or better. In addition, the R/V LEE used doppler sonar integrated into the navigation system. Navigation on the R/V STORIS was by satellite with a position accuracy of $\pm 500\text{m}$ or better.

Acoustic data used to interpret distributions of reflectors, faults, and areas of potentially unstable sediments were collected by the following seismic-reflection equipment: 1) 3.5 kHz; 2) 2.5 kHz (Uniboom source); 3) single-channel seismic reflection (60KJ to 160KJ sparker and up to 1300 in³ air gun sources); and 4) 24-channel multichannel equipment using a 1300 in³ airgun array. The various types of seismic-reflection data and the cruises are shown in Table 2. Tracklines for cruises S4-76 and S6-77 of the R/V SEA SOUNDER are given in Figs. 2 and 3. In addition to seismic-reflection data, both gravity and magnetics were collected routinely while underway.

In general, the quality of the 3.5 kHz data is only fair, but the 2.5 kHz data are fair to good and the low-resolution seismic-reflection data are fair to excellent. The 3.5 kHz system generally penetrated only to the first subbottom reflector (0.005 sec; approximately 4 m), but in a few places it penetrated to 0.05 sec (approximately 35 m). The 2.5 kHz system typically penetrated to 0.05 sec or less. The single-channel seismic-

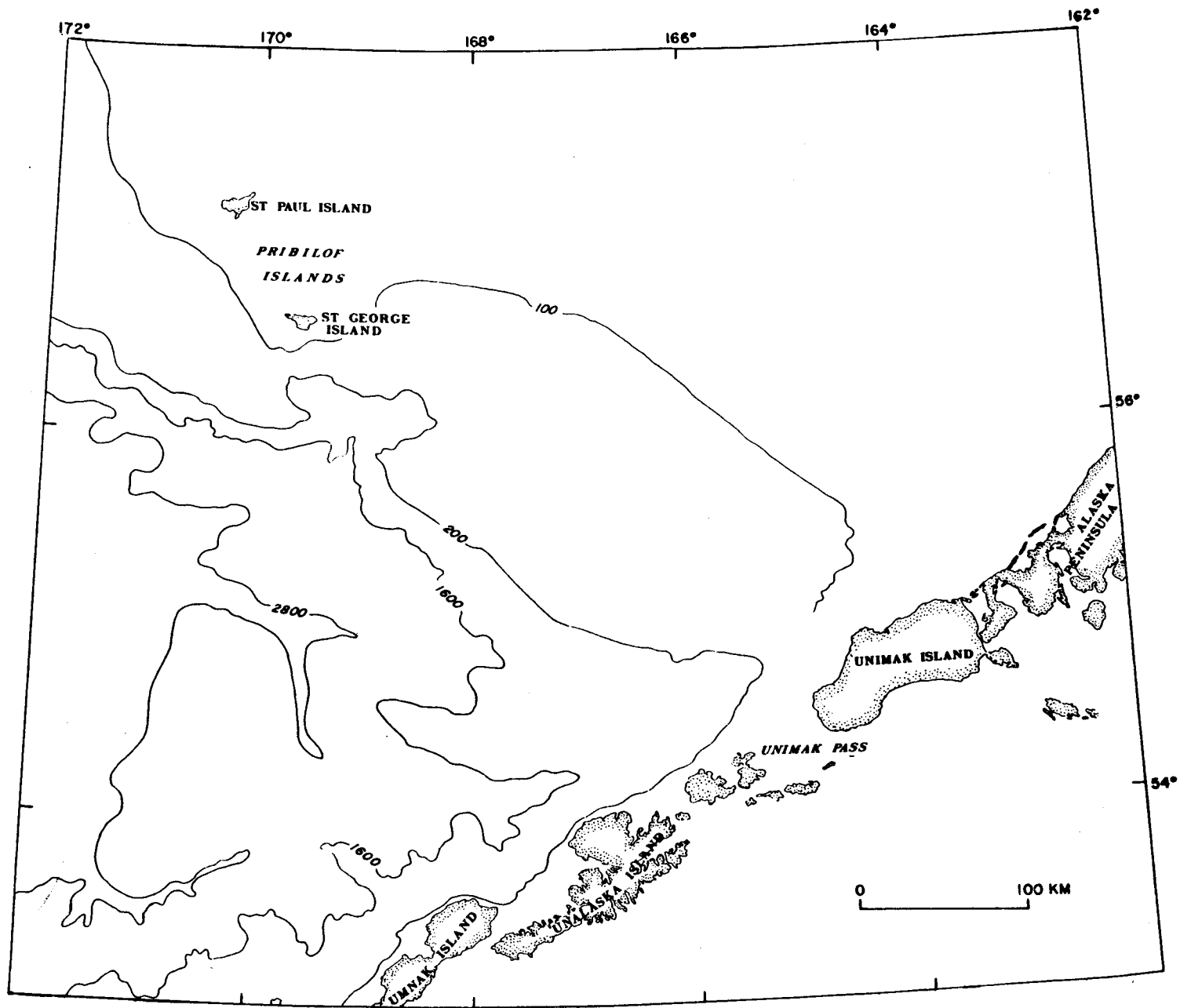
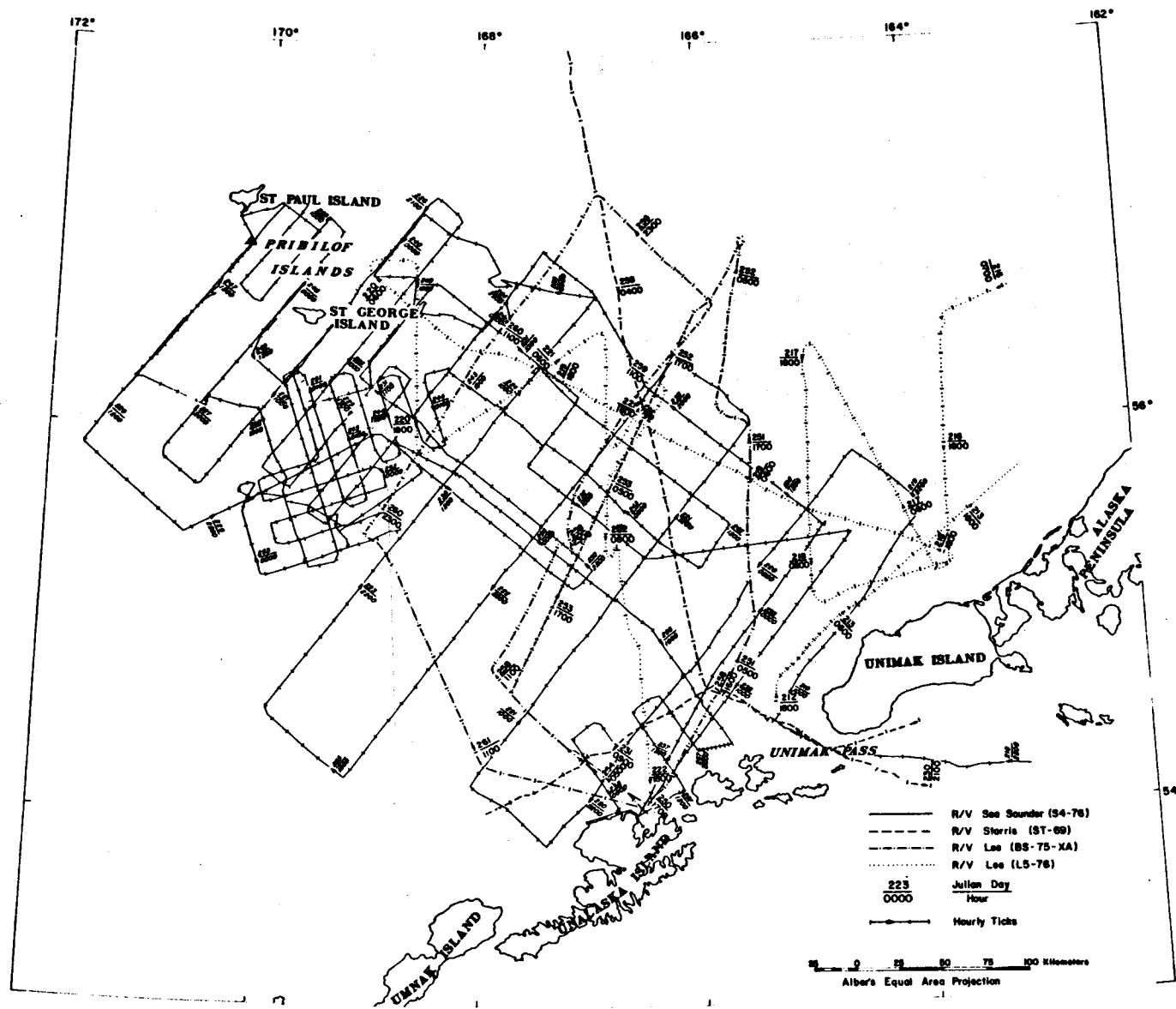


Figure 1. Index map of the southern Bering Sea.

Table 1. Summary of data collected on cruises S4-76 and S6-77 of the R/V SEA SOUNDER and multichannel data collected on the R/V LEE in St. George basin region, southern Bering Sea.

Data Type	Approximate Number of Kilometers	Number of Samples or Stations
12 kHz Profiles	6,500	
3.5 kHz Profiles	14,800	
2.5 kHz Profiles	5,900	
80-160 KJ Profiles	11,500	
Magnetometer Records	7,500	
Gravity Data	16,500	
Sea Surface T & S Profiles	13,000	
Side Scan Sonar Profiles	150	
Multichannel Reflection Profiles	2,800	
Gravity Cores		124
Piston Cores		8
Van Veen Samples		31
Dredge Hauls		5
XBT Stations		79
Current Meter Stations		27
Water Bottle Casts		143
CTD Profiles		41
Sea Floor TV (Hours)		6
Bottom Camera Stations		11



TRACK CHART

Figure 2. Track chart for cruises S4-76, L5-76, ST-69, and BS-75-XA.

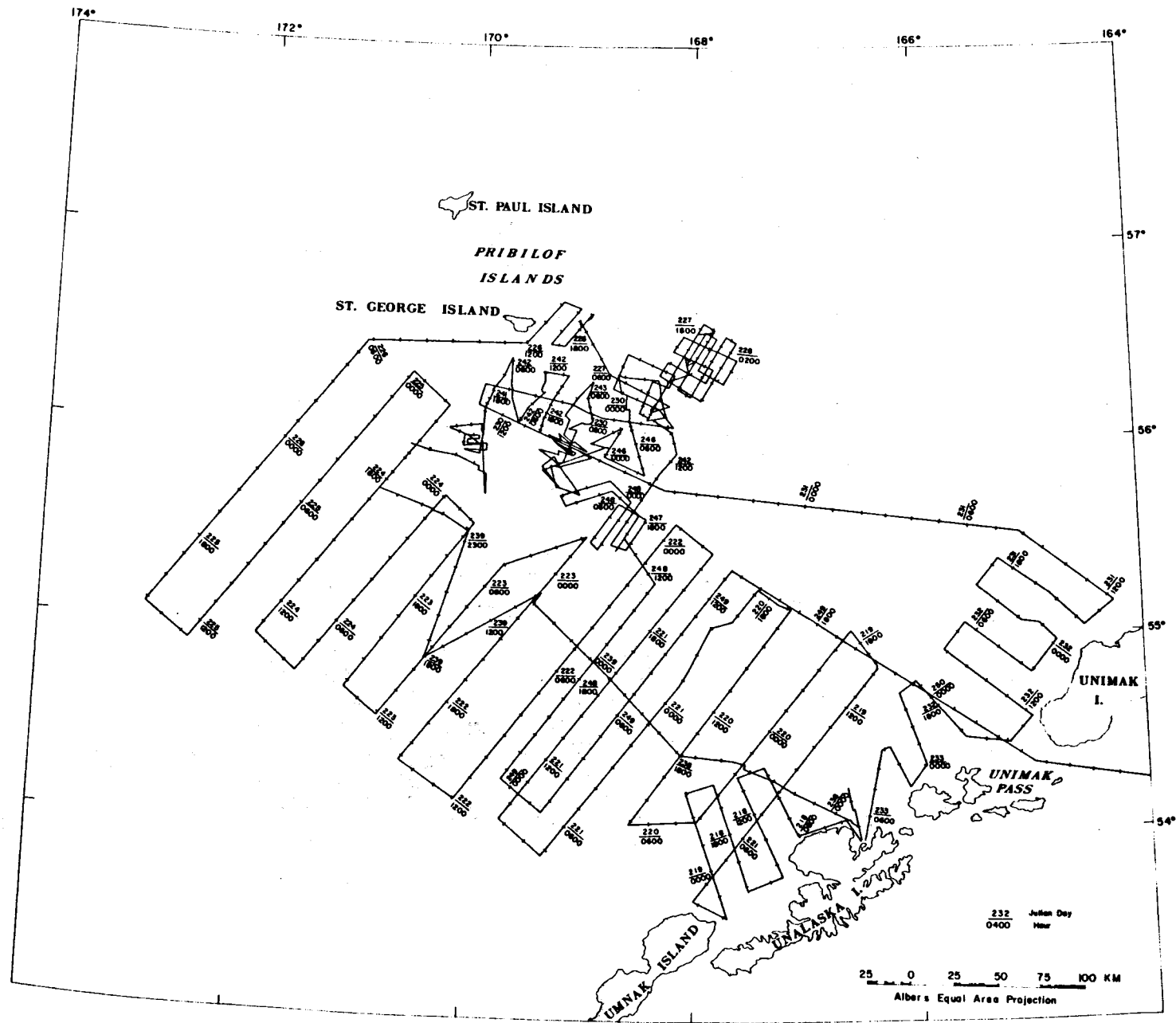


Figure 3. TRACK CHART FOR U.S.G.S. CRUISE S 6-77

reflection profiling systems penetrated to a maximum of about 2.0 sec in deep water and multichannel system was able to penetrate as much as 5.5 sec over the St. George basin (Marlow et al., 1976; 1977).

Table 2. Cruises and types of Seismic-Reflection Data

Ship	Cruise	Data Type				
		High Resolution		Low Resolution		
		3.5 kHz	2.5 kHz	single channel airgun	single channel sparker	multi-channel
R/V SEA SOUNDER						
	S4-76	X	X		X	
	S6-77	X	X		X	
R/V LEE						
BERS-	75-XA	X	X			X
	LS-76	X	X	X		X
R/V STORIS						
	ST-69				X	

Factors which affect the quality of the seismic data can be grouped in two broad categories: (1) the types of seismic systems used and their environments, and (2) the surface and subsurface geology. The environment of the seismic system includes the sea-state at the time of recording, ambient acoustic interference generated by the vessel, depth of water, and the watchstander overseeing the system. The first two factors affect the high-resolution systems much more than the low-resolution systems. Sea-state conditions during which most data were collected ranged between calm and Force 8, but were typically between Forces 1 and 4. Rough sea-states result in the decoupling of hydrophones and/or transducers from the water column, thus seriously reducing the quality of high-resolution records. Ambient acoustic interference generated by the vessel adds further to the noise level on all the data. The depth of water affects the high- and low-resolution systems in opposite ways. On the low-resolution single-channel systems, shallow water depths influence the records by producing a first harmonic (multiple) that on many records obliterates the signals beneath it. As the water depth increases, the interference by the first multiple is at deeper levels on the records, thus allowing more signals to be recorded. The high-resolution systems, however, performed well in shallow water because of the high repetition rates of the outgoing signals (generally 1/4 to 1 sec), but they did not perform well in deep water because of their relatively low power output. Reverberations create a "ringing" that also tends to mask out some signals.

Despite the weaknesses of the various systems and because of the coverage of the area and the large amount of good quality data collected, we feel that the data are more than adequate to interpret the regional surface and near-surface geology.

The resolution of the seismic systems (Table 3) were calculated using the velocity of sound in water and by following the procedure of Moore (1972) who showed that the resolution of seismic-reflection systems is between 0.25 and 0.75 the wavelength of the source. However, as we noted above, the actual resolution of a feature is not only a function of the outgoing frequencies but also is affected by the environments of the systems (e.g., sea-state, depth of water, acoustic interference, watchstander) and the surface and subsurface geology. There is a gap in the resolving range of our systems between about 0.5 m and 4 m which suggests that features with thicknesses or offsets in that range would not necessarily be resolved.

Table 3. Ranges of resolution for seismic systems.

Approximate Peak Frequency	Range of Minimum Resolution (m)
40 Hz (multichannel)	9.4 to 28.1
100 Hz (single channel)	3.2 to 11.2
2.5 kHz	0.15 to 0.5
3.5 kHz	0.1 to 0.3

Sampling stations are given in Figs. 4 and 5 and the data collected are given in Table 1. Sampling equipment included piston and gravity corers, van Veen samplers and dredge hauls. We photographed the sea floor using television, 35 mm, and 70 mm cameras. Physical oceanographic measurements were made by CTD profilers, water bottle casts, current meters, and expendable bathythermographs. We cut the cores onboard the R/V SEA SOUNDER into 1.5 m sections, sliced them in half, retaining one half for archiving and the other for sampling, and described the cores using megascopic and microscopic techniques. The archive halves were photographed, using an 8 x 10 camera, and X-rayed. Sampling of the cores for subsequent shore-based studies was done on the ship.

Shore-Based Data Collection

The upper 30 cm or more of piston and gravity cores were homogenized by mixing with sea water as a result of coring operations; consequently, analyses of surface samples represent average values for the upper 30 cm of the sediments. Samples collected using the van Veen sampler were undisturbed, and are representative of surface sediment to within a few centimeters below the sediment-water interface. Subsamples for analyses of

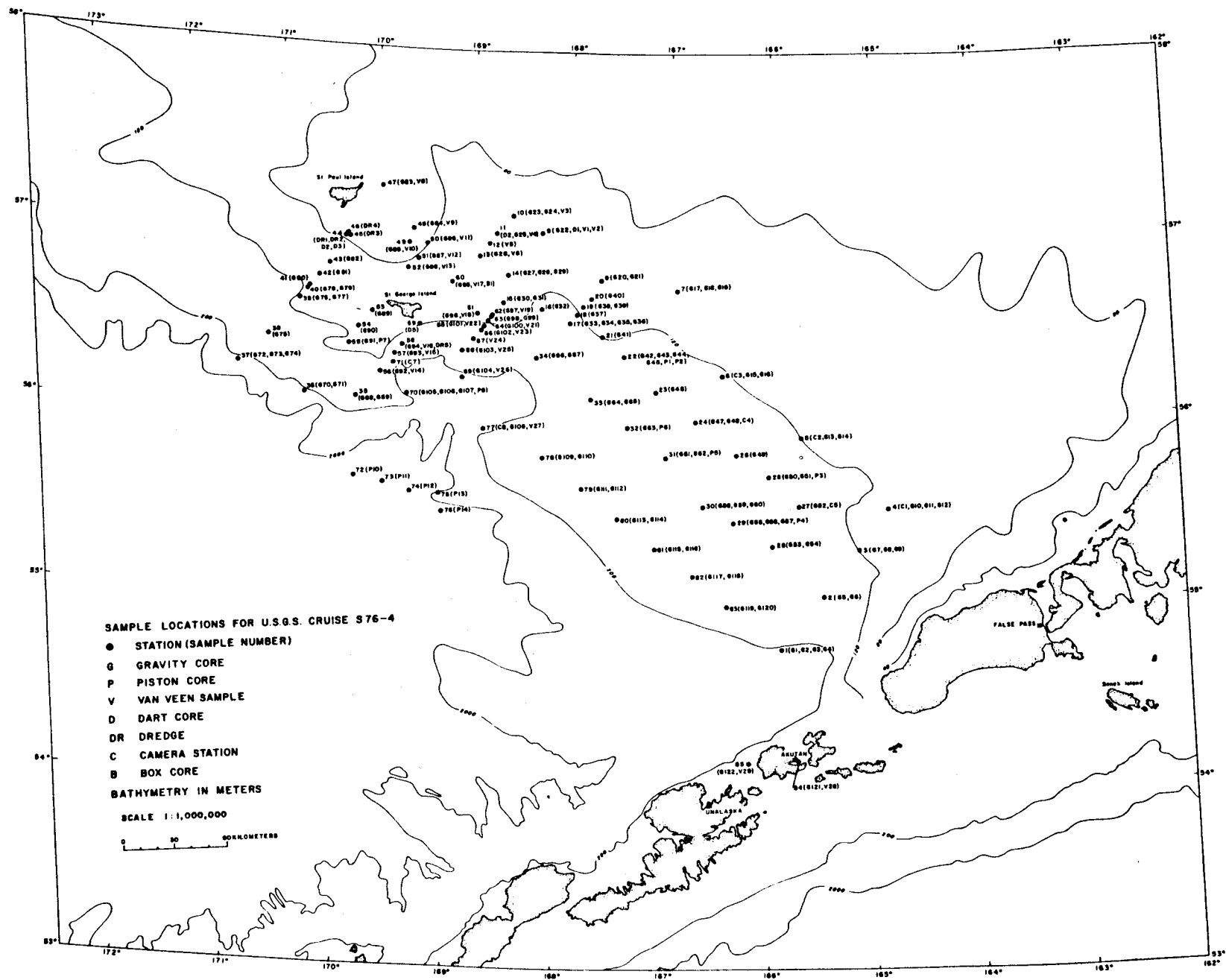


Figure 4. Sample locations for cruise S4-76.

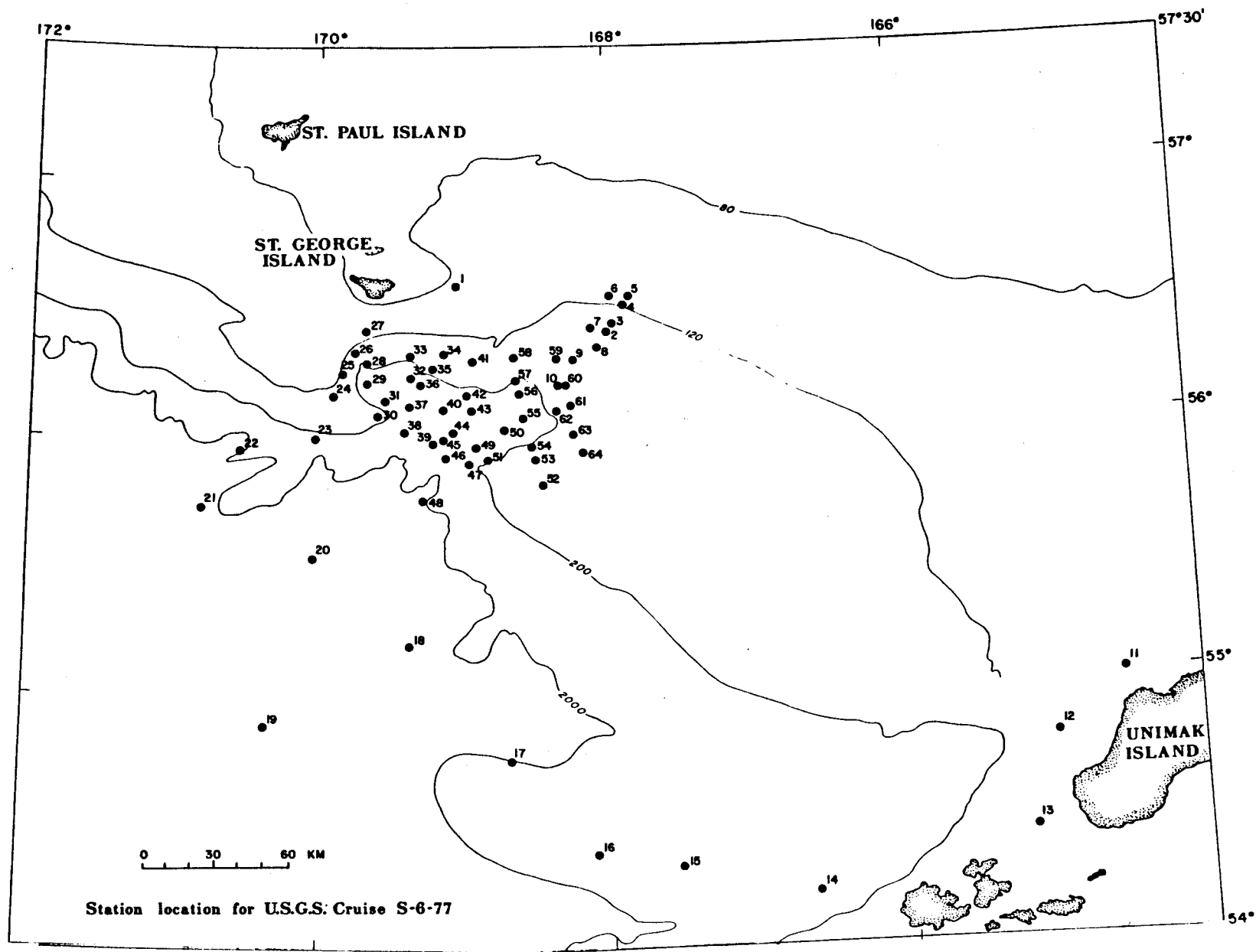


Figure 5. Sample locations for cruise S6-77.

grain-size composition of heavy ($\rho > 2.85$) and light ($\rho < 2.85$) minerals, clay minerals, and inorganic geochemistry were collected from the top 3 cm of van Veen samples, and from within the top 5 cm of gravity and piston cores (Table 4). The primary sampling network during the 1976 field season consisted of 51 stations centered over the St. George basin and the Pribilof Islands (Fig. 4). Duplicate cores were collected at 30 of these stations in order to measure local variability in major and minor elements. The duplicate cores were separated by as much as several hundred meters, depending upon drift of the ship while on station. In addition to samples collected on the St. George Basin grid, 18 samples were collected during the 1977 field season (Fig. 5) in the vicinity of the Pribilof Islands, from the adjacent continental slope, and near Unimak Island in the Aleutian chain. Sample locations used for our sediment analyses are plotted on a bathymetric chart of the area in Figure 6, which is keyed to Table 4.

Grain size was measured by first splitting samples into $>63\mu$ and $<63\mu$ size fractions. The $>63\mu$ fractions were analyzed using 2-m rapid sediment analyzers (Thiede et al., 1976) and the $<63\mu$ fractions were analyzed with a hydrophotometer (Jordan et al., 1971). Replicate analyses and calibration tests show that the rapid sediment analyzers have a precision of $\pm 5\%$ and accuracy of $\pm 5\%$. The hydrophotometer has a precision of $\pm 10\%$ and an accuracy of $\pm 1\%$. Total carbon was determined with a LECO model WR-12 carbon analyzer. Three analyses of total carbon per sample were averaged. The LECO has a precision of $\pm 2\%$ and an accuracy of $\pm 1\%$.

Bulk samples of sediment were sieved to retrieve the 63μ to 88μ fraction. This fraction was then floated on diluted tetrabromoethane ($\rho = 2.85$) to separate heavy minerals and rock fragments from light minerals and rock fragments. Random-mounted slides were prepared and a minimum of 300 counts were made covering the whole area of each slide using the line method.

All samples for clay mineralogy, as well as all samples for other studies reported here, were kept moist in air-tight sample vials at 3°C from the time of collection until the time of preparation. The $<2\mu$ fraction was used for clay mineral studies following the preparation procedures of Hein et al. (1975), and the semi-quantitative weighted-peak X-ray diffraction technique of Biscaye (1965). A polar planimeter was used to measure the areas under the peaks on the diffractograms. Barium saturation was attempted on several samples to help differentiate between chlorite and vermiculite. Although a peak at 7.8\AA commonly did appear as a result of this treatment, it was not well developed and was highly interpretive. Hence, barium saturation was not used routinely. Samples were glycolated to help identify the expandable clays. Diffractograms were run from 3° to 14° 2θ and measurements of peak areas were taken on the glycolated sample. X-ray diffraction peaks corresponding to d-spacings of 7\AA , 10\AA , and 17\AA were routinely measured for chlorite/kaolinite, illite,

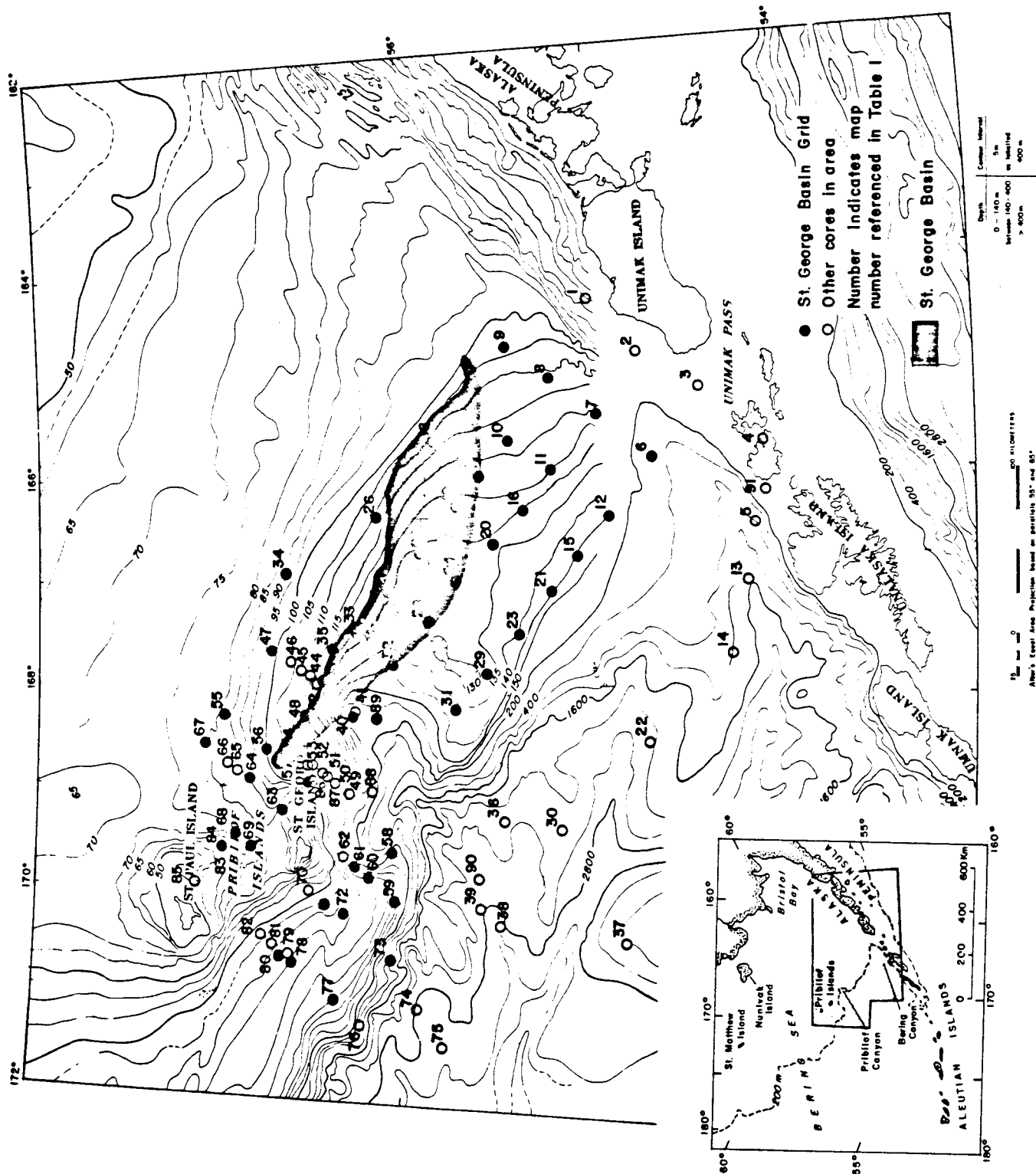


Figure 6. Bathymetric chart of the southern Bering Sea region with the St. George basin shaded. The number next to a circle or dot is a map reference number (see Table 4 for corresponding sample number).

Table 4. Summary of Analyses. Map number refers to numbers on Fig. 6. Letters in the sample column designate sample types; G = gravity core, P = piston core, and V = van Veen Sampler. X designates analysis performed.

Map Number	Core		Interval (cm.)	Grain Size	Clay	Heavy Mineral	Light Mineral	Inorganic Geochemistry		Carbon
	year	#						complete chemistry	6-step sig. only	
1	77	V05	0-3					X		X
2	77	V06	0-3	X		X	X	X		X
3	77	V07	0-3					X		X
4	76	G121	0-5	X	X	X	X	X		X
4	76	V28	0-3					X		
5	77	G014	0-5	X		X	X	X		X
6	76	G002	15-20	X		X	X	X		X
7	76	G005	0-5	X	X	X	X	X		X
7	76	G006	3-4					X		
8	76	G007	0-5							
8	76	G008	7-15	X	X	X	X	X		X
8	76	G009	4-5					X		
9	76	G010	0-10					X		
9	76	G011	13-18	X	X	X		X		X
9	76	G012	4-5					X		
10	76	G052	9-13	X	X	X	X	X		X
11	76	G053	0-1					X		
11	76	G054	0-3	X	X	X	X	X		X
12	76	G119	0-5	X		X	X	X		X
12	76	G120	4-5					X		
13	77	G016	0-5	X		X	X	X		X
14	77	G019	0-5	X		X	X	X		X
15	76	G117	0-1					X		
15	76	G118	6-11	X		X	X	X		X
16	76	G055	4-5					X		
16	76	G056	0-4	X		X	X	X		X
16	76	G057	0-5					X		
17	76	G050	0-1					X		
17	76	G051	6-11	X	X	X		X		X
17	76	P03	3-8					X		
18	76	G013	14-19	X	X	X	X	X		X
18	76	G014	4-5					X		
19	76	G049	0-5	X		X	X	X		X
20	76	G059	5-8	X	X	X		X		X
20	76	G060	0-2					X		
21	76	G115	4-5					X		
21	76	G116	0-5	X		X	X	X		X
22	77	G020	0-5	X		X	X	X		X
23	76	G113	3-8	X	X	X	X	X		
23	76	G114	0-1					X		
24	76	G061	4-5					X		
24	76	G062	0-5	X	X	X	X	X		X
24	76	P05	0-5					X		
25	76	G047	4-5					X		
25	76	G048	0-8	X		X	X	X		X
26	76	G015	4-5					X		
26	76	G016	7-9		X	X	X	X		
27	76	G046	11-16	X	X	X	X	X		X
28	76	G063	15-20	X	X	X		X		X
28	76	P06	6-11					X		
29	76	G111	1-5	X	X	X	X	X		X
29	76	G112	4-5					X		
30	77	G022	0-5	X		X	X	X		X
31	76	G109	3-8	X	X	X	X	X		X
31	76	G110	4-5					X		
32	76	G064	4-5					X		
32	76	G065	10-15	X	X	X	X	X		X
33	76	G042	0-1					X		
33	76	G043	0-6	X	X	X	X	X		X
34	76	G018	4-5					X		
34	76	G019	0-3	X		X	X	X		X
35	76	G041	6-11	X	X	X	X	X		X
36	76	P13	0-2	X	X	X	X		X	X
37	77	G023	0-5	X				X		X
38	77	G024	0-5	X				X		X
38	77	G025	0-10	X			X	X		X
39	76	P10	0-2	X	X	X	X		X	X

Table 4. (Continued)

Map Number	Core		Interval (cm.)	Grain Size	Clay	Heavy Mineral	Light Mineral	Inorganic Geochemistry		Carbon
	year	#						complete chemistry	6-step spec. only	
40	76	G066	4-5					X		
40	76	G067	5-10	X	X	X	X	X		X
41	77	G012	11-12					X		X
42	77	G007	0-1					X		X
43	76	G033	8-13	X				X		X
43	76	G034	4-5					X		
43	76	G036	2-7					X		
44	76	G037	2-8	X		X	X		X	X
45	76	G038	0-5	X					X	X
45	76	G039	0-5						X	
46	76	G040	6-10	X					X	X
47	76	G020	6-11	X	X	X	X	X		X
47	76	G021	4-5					X		
48	76	G032	6-11	X				X		X
49	76	G103	2-7	X	X	X	X		X	X
49	76	V25	0-3						X	
50	76	V23	0-3	X					X	X
51	76	V21	0-3	X				X		X
52	76	V20	0-3	X	X				X	X
53	76	V19	0-3	X					X	X
54	76	G030	1-6	X		X	X		X	X
54	76	G031	4-5						X	
55	76	V02	0-3	X		X	X	X		X
56	76	G027	14-19	X	X		X	X		X
56	76	G028	0-5					X		
56	76	G029	4-5					X		
57	76	V18	0-3	X	X	X	X	X		X
58	76	G105	10-15	X	X	X	X	X		X
58	76	G107	0-5					X		
58	76	P08	3-8					X		
59	76	G069	0-5	X		X		X		X
59	76	V07	0-3	X		X	X	X		X
60	76	V14	0-3	X		X	X	X		X
61	76	V15	0-3	X				X		X
62	76	G094	0-3	X		X			X	X
63	76	V17	0-3	X	X	X	X	X		X
64	76	V06	0-3	X	X	X	X	X		
65	76	V05	0-3	X					X	X
66	76	V04	0-3	X					X	X
67	76	V03	0-3	X	X	X	X	X		X
68	76	V11	0-3	X				X		X
69	76	V12	0-3	X	X	X	X	X		X
70	76	G089	0-3	X	X	X	X		X	X
71	76	G090	2-4	X				X		X
72	76	G091	0-1					X		
72	76	P07	5-10	X	X	X	X	X		X
73	76	G070	0-1					X		
73	76	G071	2-7	X	X	X	X	X		X
74	77	G029	0-5	X		X	X	X		X
75	77	G026	0-5	X		X	X	X		X
76	76	G072	4-5						X	
76	76	G074	0-5		X	X	X			
77	76	G075	6-10	X	X	X	X	X		
78	76	G077	0-5	X	X	X	X	X		X
79	76	G078	0-1						X	
79	76	G079	0-5	X		X			X	X
80	76	G080	0-5	X				X		X
81	76	G081	0-5	X			X		X	X
82	76	G082	0-5	X	X				X	X
83	76	V10	0-3	X					X	X
84	76	V09	0-3	X		X	X	X		X
85	76	V08	0-3		X					
86	76	V22	0-3	X	X	X	X		X	X
87	76	V24	0-3	X					X	X
88	76	V26	0-3	X						X
89	77	V04	0-3	X						
90	76	P11	0-5	X						X
91	76	V29	0-3	X		X				X

and mixed layer clays respectively. A slow scan (0.25° 2θ per min.) between 24° and 26° 2θ was used to differentiate kaolinite from chlorite. No internal standards were used in this study. Therefore, the values obtained by these techniques are relative within this study only and should not be taken as absolute percentages of clay minerals present.

A total of 103 samples from 65 stations in the 1976 St. George basin grid were analyzed for 31 major, minor, and trace elements using a combination of semiquantitative optical emission spectroscopy, X-ray fluorescence, atomic absorption spectrometry, and neutron activation analysis. The details of these analytical methods are described in sections by J. S. Wahlberg, Claude Huffman, Jr., J. I. Dinnin, Harriet G. Neiman, A. J. Bartel, and H. T. Millard, Jr., in Miesch (1976). Eighteen of these 103 samples were chosen at random for duplicate analyses in the analytical laboratories. All 121 analytical samples (103 samples plus 18 duplicates) were submitted in a randomized sequence to the analytical laboratories of the U.S. Geological Survey in Denver. An additional suite of 24 samples from 20 stations in the vicinity of the Pribilof Islands were analyzed for concentrations of 19 major, minor, and trace elements by semiquantitative optical emission spectroscopy.

Samples were air dried and ground in a ceramic mill to pass a 100-mesh (149 μ) sieve. Because the samples were air dried, analytical values of Na, S, and Mg will be too high due to Na^+ , $\text{SO}_4^{=}$, and Mg^{++} dissolved in interstitial water and left as a residue after evaporation. To correct these values, we assumed that all of the Cl determined by X-ray fluorescence was due to Cl dissolved in interstitial water, and that the interstitial water contained the same proportions of Na, S, Mg, and Cl as average sea water. Interstitial water contributions of Na, S, and Mg were then subtracted from the analytical values.

SEDIMENTOLOGY AND GEOCHEMISTRY OF SURFACE SEDIMENTS

Summary

Present-day sediment dynamics, combined with the dynamics associated with lowering of sea level during the Pleistocene, have created a mixture of sediments on the outer continental shelf of the southern Bering Sea that has been derived from the Alaskan mainland, the Aleutian Islands, and the Pribilof ridge. Concentrations of finer-grained, higher-organic sediments in the region of the St. George basin have further modified the regional distribution patterns of sediment composition. Q-mode factor analysis of 58 variables related to sediment size and composition--including major, minor, and trace elements, heavy and light minerals, and clay minerals-- reveals three dominant sediment associations.

Felsic sediment derived from the generally quartz-rich rocks of the Alaskan mainland forms a background over most of the

continental shelf. These sediments contain relatively high concentrations of Si, Ba, Rb, quartz, garnet, epidote, metamorphic rock fragments, K-feldspar, and illite. A second important association, superimposed on the felsic background, is andesitic sediment derived from the Aleutian Islands. These sediments contain relatively high concentrations of Na, Ca, Ti, Sr, V, Mn, Cu, Fe, Al, Co, Zn, Y, Yb, Ga, volcanic rock fragments, glass, clinopyroxene, smectite, and vermiculite. A local basaltic association, derived from the Pribilof Islands, factors out as a subset of the Aleutian andesite association. Concentrations of finer-grained sediment in St. George basin results in a sediment association containing relatively high concentrations of C, S, U, Li, B, Zr, Ga, Hg, silt, and clay.

Sediments of the Aleutian andesite association are concentrated mainly between the 100- and 200-meter isobaths; they exhibit a strong gradient, or "plume", decreasing away from Unimak pass and toward St. George basin. Lack of present-day currents sufficient to move even clay-size material and the presence of the Bering submarine canyon between the Aleutian Islands and the outer continental shelf and slope indicate that Holocene sediment dynamics cannot be used to explain the observed distribution of surface sediments derived from the Aleutian Islands. We suggest that this distribution pattern is relict and resulted from sediment dynamics during lower sea levels in the Pleistocene.

Regional Setting

The geologic history and structure of the region have been summarized by Scholl *et al.* (1968), Scholl and Hopkins (1969), Nelson *et al.* (1974), Marlow *et al.* (1975), Scholl *et al.* (1975), and Marlow *et al.* (1977a). The southeastern Bering Sea can be broadly subdivided into four major physiographic provinces: outer continental shelf, continental margin, Pribilof ridge, and the Bering and Pribilof canyons (Figure 7). The outer continental shelf is a broad, flat area that has a gradient of 1:2000 (0.03°) between the 100 m isobath and the shelf break at about 170 m. The Pribilof ridge is a prominent northwest-southeast-trending topographic high that is capped by the Pribilof Islands. The ridge is a relatively smooth surface cut by at least one terrace that may be a Pleistocene feature. The ridge plunges below the shelf at about $56^\circ 40' N$, $168^\circ 50' W$, but can be followed to the east in the subsurface to $55^\circ 40' N$, $165^\circ 30' W$. The continental slope to the northwest abruptly drops away from the shelf break with gradients of 1:20 (3°). Toward the southeast, however, the gradient decreases to 1:40 (1.4°). The continental slope is characterized by hummocky topography, scarps, and canyons on almost all scales. The continental margin in this region is incised by two giant submarine canyons, Bering and Pribilof canyons (Scholl *et al.*, 1970), which may have played significant roles in the transport of sediment to the Aleutian basin.

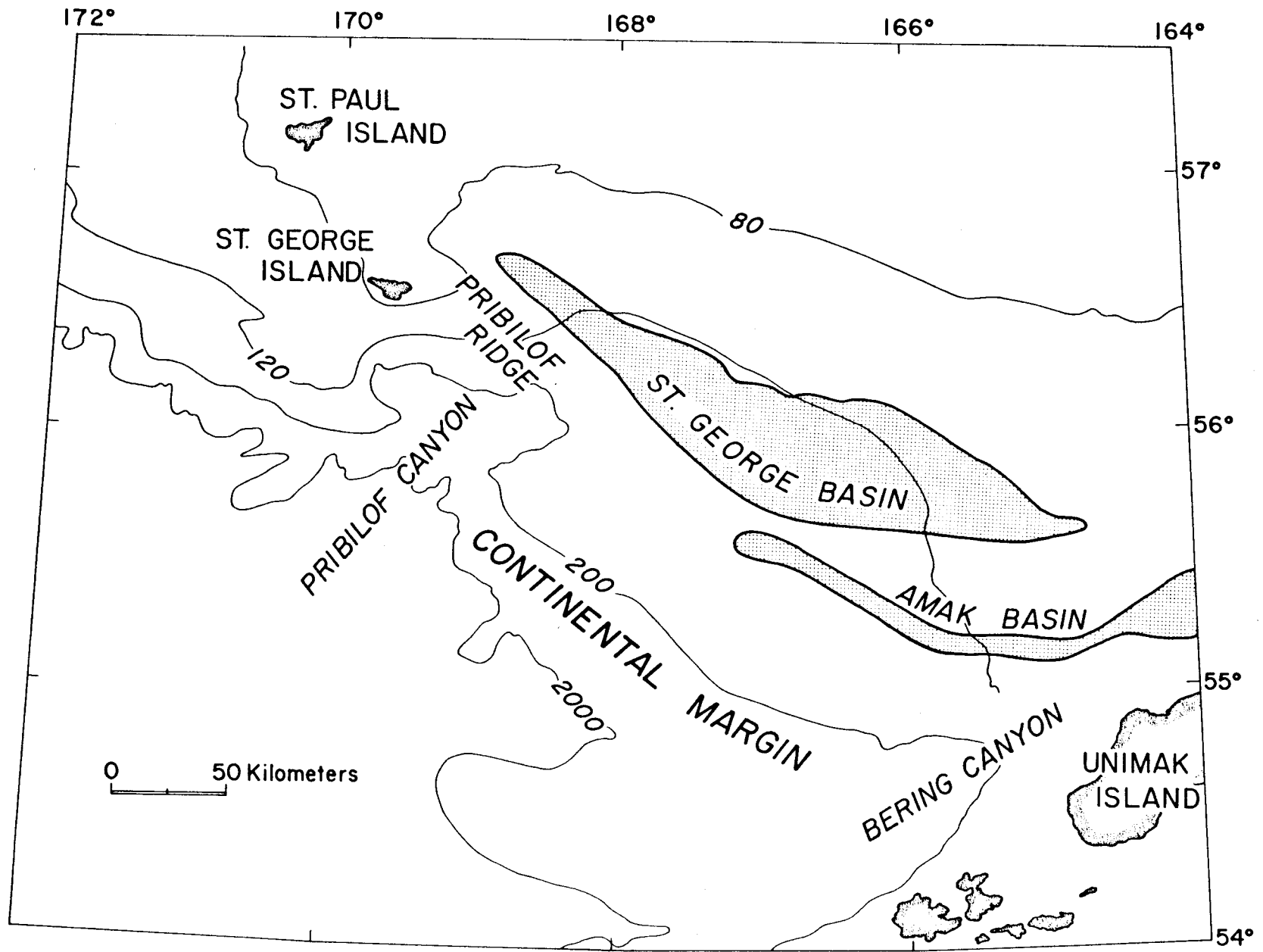


Figure 7. Physiographic provinces, southern Bering Sea.

Rock units underlying the continental shelf and slope can be broadly divided into an acoustically layered sequence of Cenozoic age and a Mesozoic unit that has been highly deformed and comprises the acoustic basement (Scholl *et al.*, 1968; 1975). The acoustic basement probably consists of deformed rocks of Mesozoic age that can be divided into two belts (Marlow *et al.*, 1977a; 1977b). A northeasterly belt of Upper Jurassic and younger Mesozoic rocks extends northwestward from the Black Hills region on the Alaska Peninsula to the northern part of the Pribilof ridge. A second belt lies basinward (southwest) of the first and consists of a younger (Campanian and younger assemblage of continental-margin rocks that extends, parallel to the inner belt of shallow-marine Jurassic rocks, from southern Alaska via the outer Bering shelf to eastern Siberia. Marlow *et al.* (1977a) speculated further that a Jurassic, Cretaceous, and earliest Tertiary magmatic arc extended parallel to and inside (landward) both deep-water and shallow-water depositional troughs.

The present-day deformational and sedimentological patterns in the southern Bering Sea were created after the growth of the Aleutian arc in late Mesozoic or earliest Tertiary time, when the old plate boundary shifted from an ancient Bering Sea margin to a site near the present Aleutian Trench, thereby trapping a large piece of the Kula Plate within the abyssal Bering Sea (Scholl, *et al.*, 1975; Cooper, *et al.*, 1976). After an initial episode of uplift and erosion in the early Tertiary, the margin underwent extensional collapse and differential subsidence that has continued to the present (Marlow *et al.*, 1976). Elongate basins formed in the vicinity of the modern outer shelf as a consequence of collapse. St. George basin is the largest of the southern basins. This basin is a graben of sedimentary fill encompassing an area of approximately 15,000 km² and containing a volume of at least 150,000 km³ (Marlow, *et al.*, 1976). The basin is a long (greater than 300 km) and narrow (30 to 50 km) structure that parallels the present continental margin and is, in places, filled with more than 10 km of upper Mesozoic (?) and Cenozoic sedimentary deposits.

Studies of the distribution of sediments on the continental shelf of the southern Bering Sea by Sharma *et al.* (1972) and Sharma (1974, 1975) have concentrated mainly on samples from Bristol Bay, located on the inner shelf. These authors characterize Bristol Bay as a classical graded shelf. Askren (1972) investigated sediments in a broad region to the northwest of our area but did include 12 samples from within the area of this study. He concluded that the shelf is mid-stage in the establishment of a graded condition.

The oceanographic circulation of the Bering Sea was first studied by Ratmanoff (1937) who described the exchange between the Bering Sea and the Pacific Ocean. Interpretations of the physical oceanography of the Bering Sea through 1974 (e.g. Favorite, 1974; Takenouti and Ohtani, 1974) suggest that surface waters move in a cyclonic gyre or semi-gyre eastward along the

north side of the Aleutians-Alaskan Peninsula, curve around to the northwest along the southwestern Alaskan coast, and eventually turn northward and flow through the Bering Strait. The presence of a return flow of bottom waters to the southwest and south over the shelf has not been documented. Recently, Schumaker et al. (in prep.) reported on current-meter moorings deployed to measure surface and near-bottom currents on the outer continental shelf of the southern Bering Sea. They report a predominantly east-west tidal flow with little net flow. The semi-gyre described above is suggested by their data but the circulation is very sluggish. Pulses of high-velocity flow do occur for a few days during storms, with peak flows up to 40 cm/sec, but these pulses show no net flow over a season.

General Description and Texture of Surface Sediments

The surficial sediments of the outer continental shelf are generally olive gray, greenish gray, to grayish olive green silt to silty sand. Evidence for extensive burrowing, such as color mottling, discrete burrows, and total homogenization with no internal structures, is common throughout all cores. Some cores have thin interbeds 5 to 15 cm thick of coarser-grained material, but this is not a general feature. Four cores from the outermost part of the continental shelf (cores G113, G116, G118, and G119) have an upper layer, 50 cm thick, of diatom-bearing greenish gray silt overlying a gray silty clay with very few diatoms. Almost all of the other cores show a uniform lithology. Askren (1972) reported benthonic foraminifera in sediments from this area. We examined 124 surface sediment samples and did not find any benthonic foraminifera. The reasons for this discrepancy remain a mystery.

The gray and greenish hues of the sediments indicate reducing conditions or at least reduced iron oxides in the clay minerals. The water column is certainly not anaerobic at any level; thus the reducing environment is diagenetic. Because the region is one of very high biological productivity (Hattori and Wada, 1974), it seems most likely that large volumes of organic debris from plankton and nekton settle to the sediment surface. Burrowing attests to high epifaunal and infaunal activity on and in the sediments. Organic debris that is supplied to anaerobic bacteria uses up all available oxygen by metabolizing the organic material. The sediments become reduced because of high biological oxygen demand within the sediments even though the bottom water is oxygenated.

The salient features of the distribution of grain sizes is a bull's-eye pattern of finer grain size over St. George basin, and a broad band of rapid size change around the head of Pribilof Canyon and the northwestern margin of Bering Canyon (Fig. 8). The bull's-eye pattern reflects the occurrence of finer grain sizes in the center of the graben that forms St. George basin.

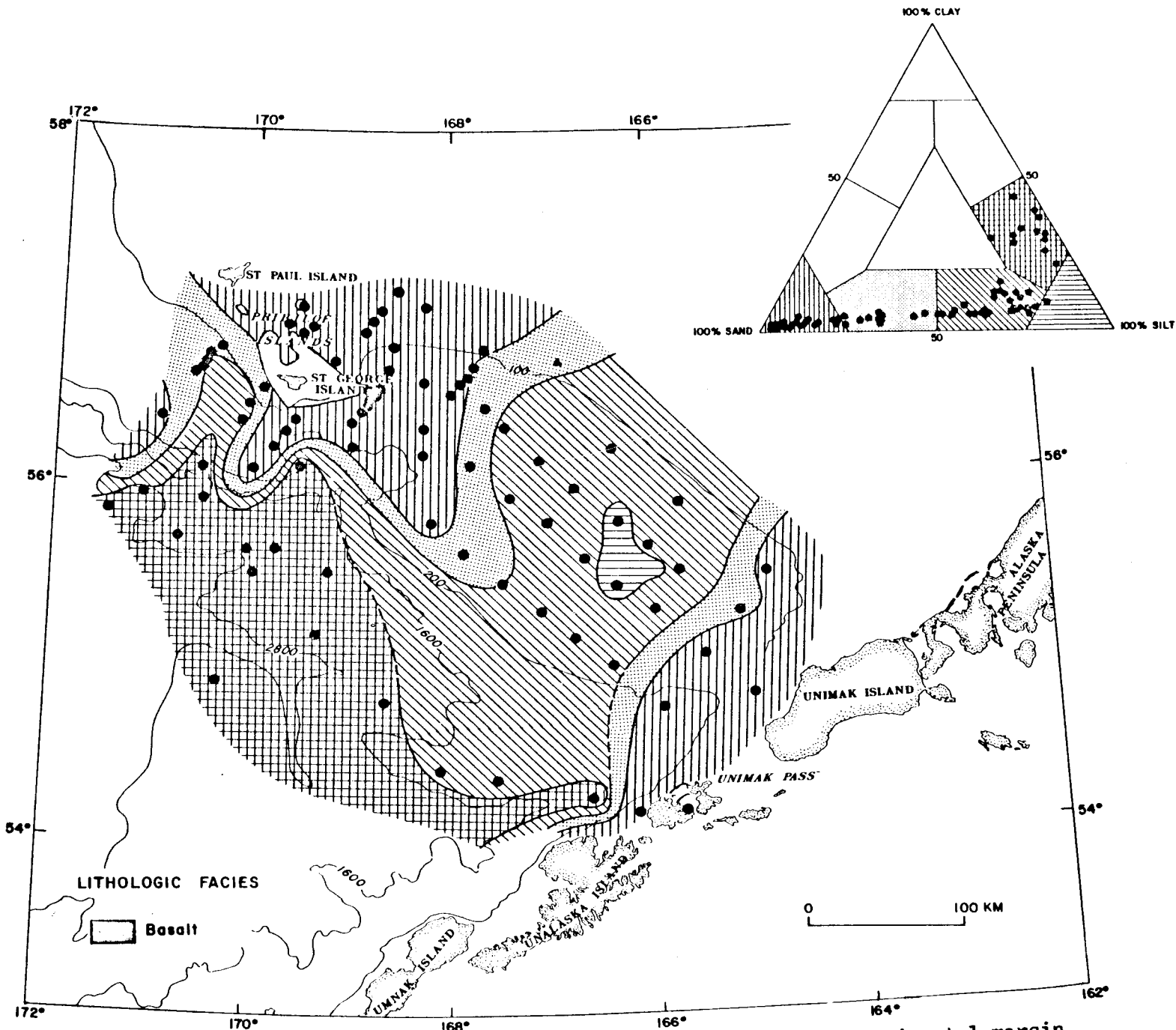


Figure 8. Map of lithologic facies of surface sediments from the continental margin.

The band of rapid size change coincides with areas of high topographic relief, with coarser sediments at the shallower depths.

The central portion of St. George basin is very poorly sorted (Fig. 9), which reflects the lack of significant winnowing. The northwestern border of the Bering Canyon, the head of Pribilof Canyon and the topographic high of Pribilof ridge all show moderately-sorted sediments. The size-frequency distribution for most sediments in St. George basin region are leptokurtic to very leptokurtic, but in the vicinity of the Pribilof Islands the distributions are mesokurtic. The distributions are fine to strongly fine-skewed throughout the region. Summary statistics of grain-size data (median grain size, mean grain size, sorting, skewness, and kurtosis) are given in Table 5.

Petrology of Surface Sediments

A subset of 32 samples, chosen to represent the whole region under study, was analyzed for heavy and light minerals. Those minerals and classes of rock fragments present in the study area, and their relative abundances, are listed in Table 6. Unidentifiable minerals and rock fragments account for only 1 to 10% of the counted grains.

The heavy minerals and rock fragments (those with specific gravity >2.85) fall into two major classes --metamorphic and volcanic. Metamorphic components occur as a low-concentration background ($<10\%$) over the entire area (Figure 10). Volcanic components in the heavy mineral fractions dominate the region and show a gradient away from the Aleutians and onto the continental rise (Fig. 11). The heavy-mineral data are plotted on a ternary diagram with percentages of amphiboles, pyroxenes, and volcanic-rock fragments as end members. Sediments from the Yukon and Kuskokwim Rivers were also analyzed and the results plotted on the ternary diagram for a comparison. The rivers are potential sources of sediment on the shelf and both rivers drain, in part, metamorphic terrains.

The light minerals and rock fragments (those with a specific gravity <2.85) include quartz, feldspar, volcanic glass, volcanic rock fragments and non-volcanic rock fragments. Relative concentrations within the three-component system of feldspars, quartz plus non-volcanic rock fragments, and volcanic glass plus volcanic rock fragments are shown in Figure 12. Analysis of samples from the Yukon River are also plotted in Fig. 12 but samples from Kuskokwim River sediments were not analyzed for light minerals.

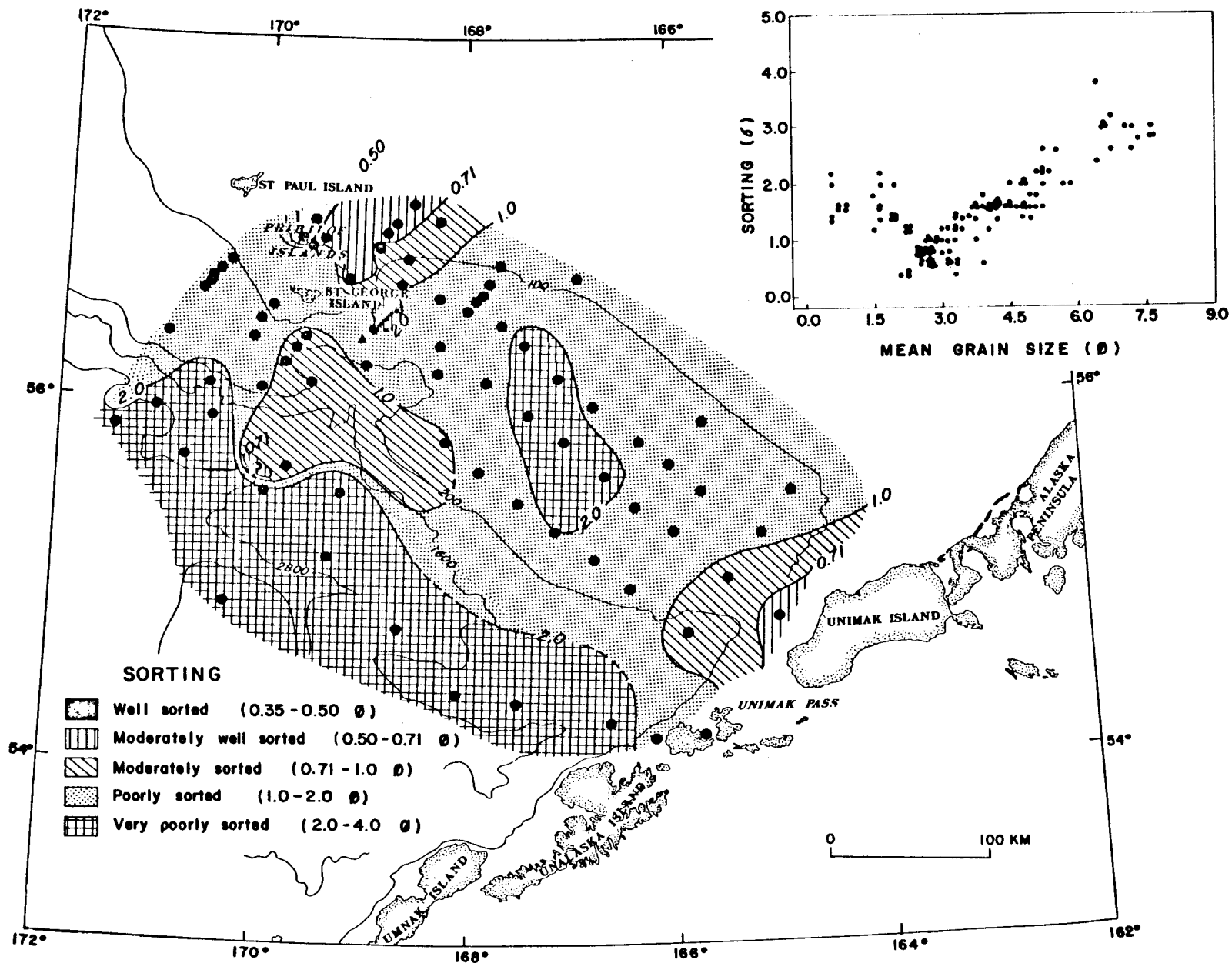


Figure 9. Distribution of sorting values from surface sediments. Inset is a plot of sorting vs mean grain size.

TABLE 5
 GRAPHICAL STATISTICS FROM GRAIN SIZE ANALYSIS
 (Folk and Ward, 1957)

SAMPLE	MAP INDEX NUMBER	MEDIAN (M_d) (ϕ)	MEAN (M_z) (ϕ)	SORTING (σ)	SKEWNESS (S_{k_i})	KURTOSIS (K_g)
76-G4	6	3.54	3.81	1.05	0.63	2.71
76-G5	7	3.72	3.88	0.69	0.55	3.02
76-G8	8	3.66	3.98	1.20	0.46	1.27
76-G10	9	3.20	3.52	1.32	0.43	1.66
76-G19	34	3.45	3.85	1.52	0.46	1.16
76-G20	47	3.01	3.33	1.32	0.49	1.44
76-G28	56	3.18	3.53	1.36	0.55	2.06
76-G30	54	3.18	3.29	1.05	0.38	2.38
76-G32	48	3.06	3.29	1.19	0.49	2.12
76-G33	43	3.14	3.71	1.68	0.59	1.54
76-G36	43	3.21	3.83	1.70	0.62	1.20
76-G37	44	3.04	3.32	1.30	0.46	1.48
76-G38	45	3.28	3.70	1.47	0.52	1.42
76-G39	45	3.29	3.75	1.52	0.53	1.35
76-G40	46	3.15	3.39	1.26	0.40	1.25
76-G43	33	4.84	4.80	2.06	0.13	1.08
76-G48	25	5.63	5.80	1.97	0.25	1.71
76-G51	17	4.92	4.81	1.69	0.07	1.37
76-G52	10	4.91	4.89	1.45	0.10	1.61
76-G54	11	4.60	4.52	1.66	0.07	1.30
76-G56	16	4.85	4.89	1.60	0.19	1.56
76-G57	16	5.12	5.26	1.57	0.28	1.72
76-G59	20	5.35	5.32	1.90	0.16	1.48
76-G60	20	5.26	5.11	2.17	0.06	1.16
76-G62	24	5.34	5.25	2.27	0.09	1.15
76-G67	40	2.00	1.93	1.45	0.19	5.24
76-G69	59	2.90	3.05	1.12	0.50	2.45
76-G71	73	6.52	6.76	3.27	0.17	0.93
76-G75	77	2.99	3.37	1.28	0.55	1.68
76-G77	78	3.79	4.15	1.60	0.43	1.16
76-G79	79	3.75	4.16	1.61	0.46	1.15
76-G80	80	4.60	4.64	1.67	0.16	1.05
76-G89	70	3.69	4.19	1.36	0.68	1.63
76-G90	71	4.94	5.01	1.70	0.20	1.44
76-G94	62	0.75	0.65	1.53	0.02	0.63
76-G103	49	1.72	1.77	2.06	0.19	2.27
76-G105	58	6.16	6.60	2.97	0.30	0.86
76-G107	58	5.36	6.66	3.08	0.60	0.97
76-G109	31	2.64	2.87	0.94	0.59	2.90
76-G111	29	3.02	3.71	1.59	0.69	1.06
76-G113	23	4.04	4.50	1.57	0.49	1.21
76-G116	21	4.68	4.80	2.04	0.12	1.34
76-G118	15	4.73	4.57	1.96	0.03	1.04

TABLE 5 cont.

SAMPLE	MAP INDEX NUMBER	MEDIAN (Md) (ϕ)	MEAN (Mz) (ϕ)	SORTING (σ)	SKEWNESS (S_{k_1})	KURTOSIS (K_g)
76-G119	12	4.48	4.57	1.50	0.22	1.27
76-G121	4	4.64	4.75	1.51	0.27	1.13
77-G14	5	6.56	6.77	2.61	0.21	1.14
77-G16	13	5.11	5.18	2.65	0.11	1.43
77-G19	14	5.34	5.48	2.69	0.17	1.32
77-G20	22	7.40	7.58	2.76	0.17	1.09
77-G22	30	7.08	7.30	2.74	0.19	1.13
77-G23	37	7.12	7.25	2.56	0.19	1.38
77-G24	38	7.36	7.61	2.84	0.19	0.85
77-G25	38	7.12	7.24	2.90	0.12	0.97
77-G26	75	6.23	6.51	2.35	0.30	1.19
77-G29	74	6.90	7.01	2.91	0.14	0.99
76-V2	55	2.58	2.59	0.76	0.26	2.41
76-V3	67	2.75	2.75	0.68	0.19	1.94
76-V4	66	2.59	2.66	0.68	0.36	1.79
76-V5	65	2.65	2.71	0.79	0.38	2.10
76-V6	64	2.80	2.99	0.72	0.48	3.34
76-V7	59	3.19	3.19	1.11	0.31	2.41
76-V9	84	2.14	2.13	0.43	0.14	2.22
76-V10	83	2.23	2.22	0.44	0.09	4.58
76-V11	68	2.80	2.80	0.66	0.11	1.66
76-V12	69	2.17	2.20	1.18	-0.03	3.13
76-V14	60	3.00	2.94	0.87	0.22	2.86
76-V15	61	1.42	0.93	1.56	-0.32	0.51
76-V16	62	0.45	0.65	2.10	0.36	1.07
76-V17	63	2.64	2.73	0.64	0.50	2.11
76-V18	57	2.84	2.81	0.64	0.06	1.33
76-V19	53	3.04	3.03	0.91	0.21	2.48
76-V21	51	2.93	2.90	0.89	0.21	2.42
76-V22	86	2.85	2.86	0.97	0.29	2.63
76-V23	50	2.66	2.67	0.93	0.33	2.96
76-V24	87	1.87	1.61	1.57	-0.12	1.86
76-V25	49	1.68	1.43	1.78	-0.01	2.36
76-V26	88	1.96	1.60	1.33	-0.34	2.11
76-V28	4	4.66	4.83	1.48	0.29	1.08
76-V29	91	1.86	1.93	1.33	0.12	3.64
77-V4	89	1.79	1.49	1.23	-0.32	1.94
77-V6	2	3.22	3.25	0.68	0.49	5.47
76-P3	26	5.02	5.06	1.75	0.17	1.56
76-P6	32	5.36	5.36	2.21	0.17	1.14
76-P7	55	5.13	5.14	1.69	0.15	1.16
76-P8	70	6.46	6.47	3.79	0.05	1.32
76-P11	73	7.73	7.72	3.08	0.06	0.89

TABLE 6

UNIVARIATE STATISTICS ON PERCENTAGES OF
HEAVY AND LIGHT MINERALS
AND CLASSES OF ROCK FRAGMENTS

MINERAL	MINIMUM	MAXIMUM	MEAN	STANDARD DEVIATION
v clinopyroxene	9.0	35.0	16.8	5.6
v orthopyroxene	5.0	19.0	11.4	3.9
v volcanic rock fragments	6.0	69.0	28.9	13.1
v amphibole	2.0	24.0	15.1	5.4
v olivine	0	7.0	1.1	2.0
opaques	2.0	18.0	7.3	3.8
m chlorite	0	8.0	2.9	2.1
m epidote	0	7.0	2.8	1.8
m garnet	0	4.0	1.2	1.1
m metamorphic rock fragments	0	8.0	3.3	2.2
plutonic rock fragments	0	6.0	1.7	1.6
fine-grained rock fragments	0	8.0	3.1	2.2
quartz	0.3	25.6	15.1	7.0
feldspar	1.6	50.4	36.1	7.0
v volcanic glass	2.9	30.6	11.2	8.3
v volcanic rock fragments	3.3	36.5	11.1	8.4
non-volcanic rock fragments	4.1	34.8	19.7	7.5
v = volcanic origin m = metamorphic origin				

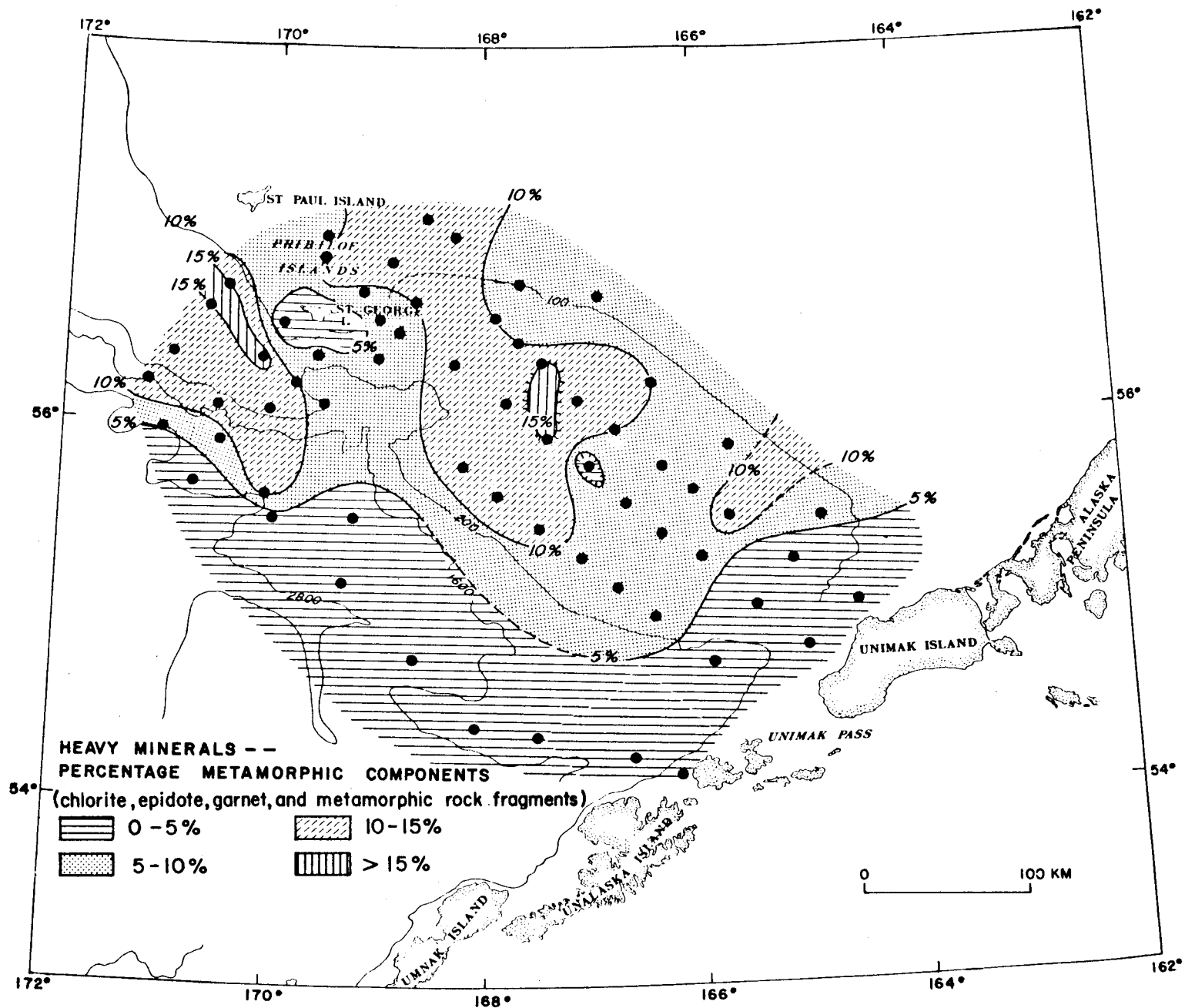


Figure 10. Distribution of the percentages of metamorphic components within the heavy mineral fraction of surface sediments.

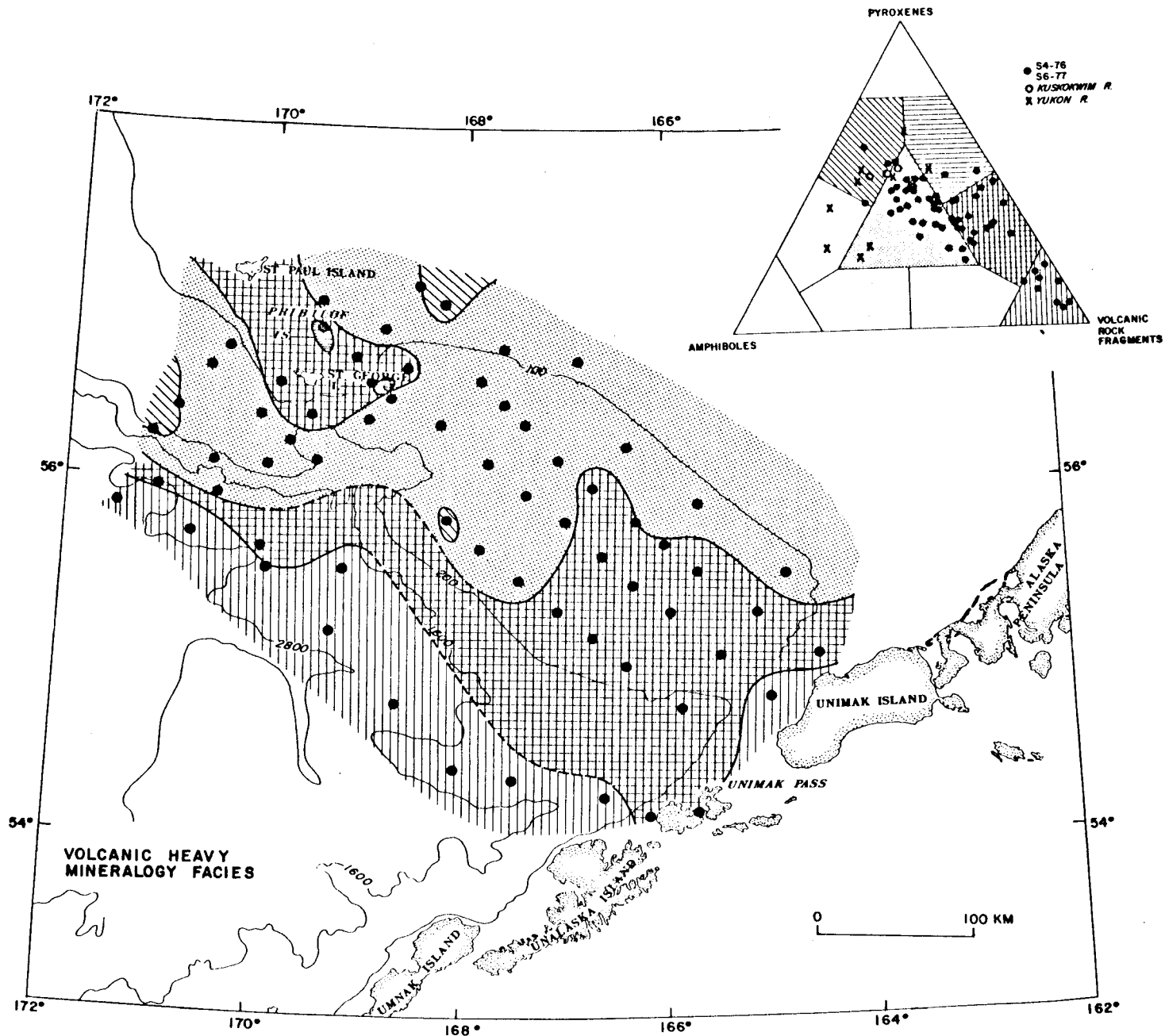


Figure 11. Distribution of the percentage of volcanic components within the heavy mineral fraction of surface sediments. Volcanic components include clinopyroxene, orthopyroxene, olivine, and volcanic rocks.

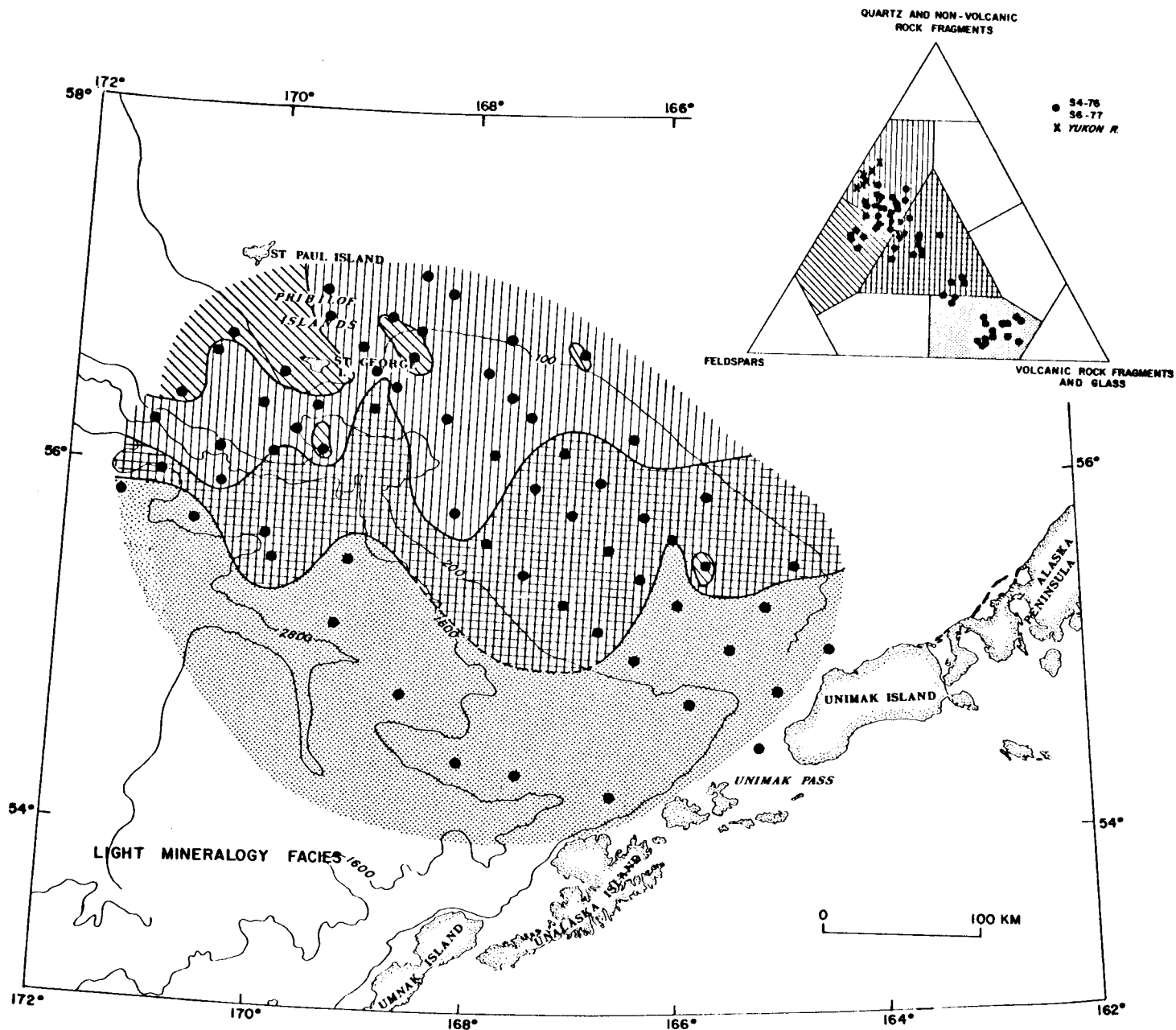


Figure 12. Distribution of light mineral components of surface sediments. Data on the ternary diagram include samples from the Yukon River as well as samples from the continental margin.

Mineralogy of Clays

The occurrences and relative abundances of the major clay mineral (chlorite, illite, smectite and vermiculite, illite crystallinity) and the expandable and non-expandable percentages of mixed-layer clays were determined; the univariate statistics for each clay mineral parameter are given in Table 7. Smectite and vermiculite are grouped together because of the difficulty of distinguishing one from the other on diffractograms. This grouping is reasonable because both clay minerals are the result of weathering of volcanic rocks (Biscaye, 1965). The aerial distributions of illite and kaolinite show no distinct gradients or concentrations. The distribution of smectite plus vermiculite (Fig. 13) shows a northwest-trending band of values that are greater than the mean. The highest values occur closest to the Aleutians and decrease with a northwest-trending gradient starting in the vicinity of Unimak Pass and Unimak Island. The distribution of chlorite also shows a northwest-trending band (Fig. 14), of lower-than-average values that may be the result of dilution within this zone by smectite plus vermiculite. Chlorite is derived from low-grade metamorphic rocks and is common in marine sediments in high latitudes (Biscaye, 1965).

Table 7. Univariate Statistics for the Relative Percentages of Clay Minerals

MINERAL	MINIMUM	MAXIMUM	MEAN	STANDARD DEVIATION
smectite + vermiculite	13.0	57.5	31.2	9.4
illite	17.0	47.0	29.8	6.9
kaolinite	0	11.8	6.0	3.5
chlorite	24.3	44.3	33.2	5.6

Distribution of Major, Minor, and Trace Elements

The distribution of total carbon shows a strong negative correlation with grain size (Fig. 15) throughout the region. For example, concentrations of total carbon are highest in the fine-grained central region of the St. George Basin and lowest in regions where coarser-grained sand occurs. The sediments that we investigated are almost completely devoid of carbonate, and therefore most of the total carbon is organic-carbon that has been absorbed by clay particles (Bader, 1963). A negative correlation between organic-carbon and grain size is almost universally observed in non-carbonate, fine-grained sediments in marine and lacustrine environments because of absorption of organic matter by clays (Trask, 1932; Van Straaten, 1954; Emery, 1960; Bordovskiy, 1965; Thomas, 1969; Kemp, 1971).

Values (wt. percent) for 32 elements are given in Table 8, and summary statistics for each of 31 elements in 103 samples

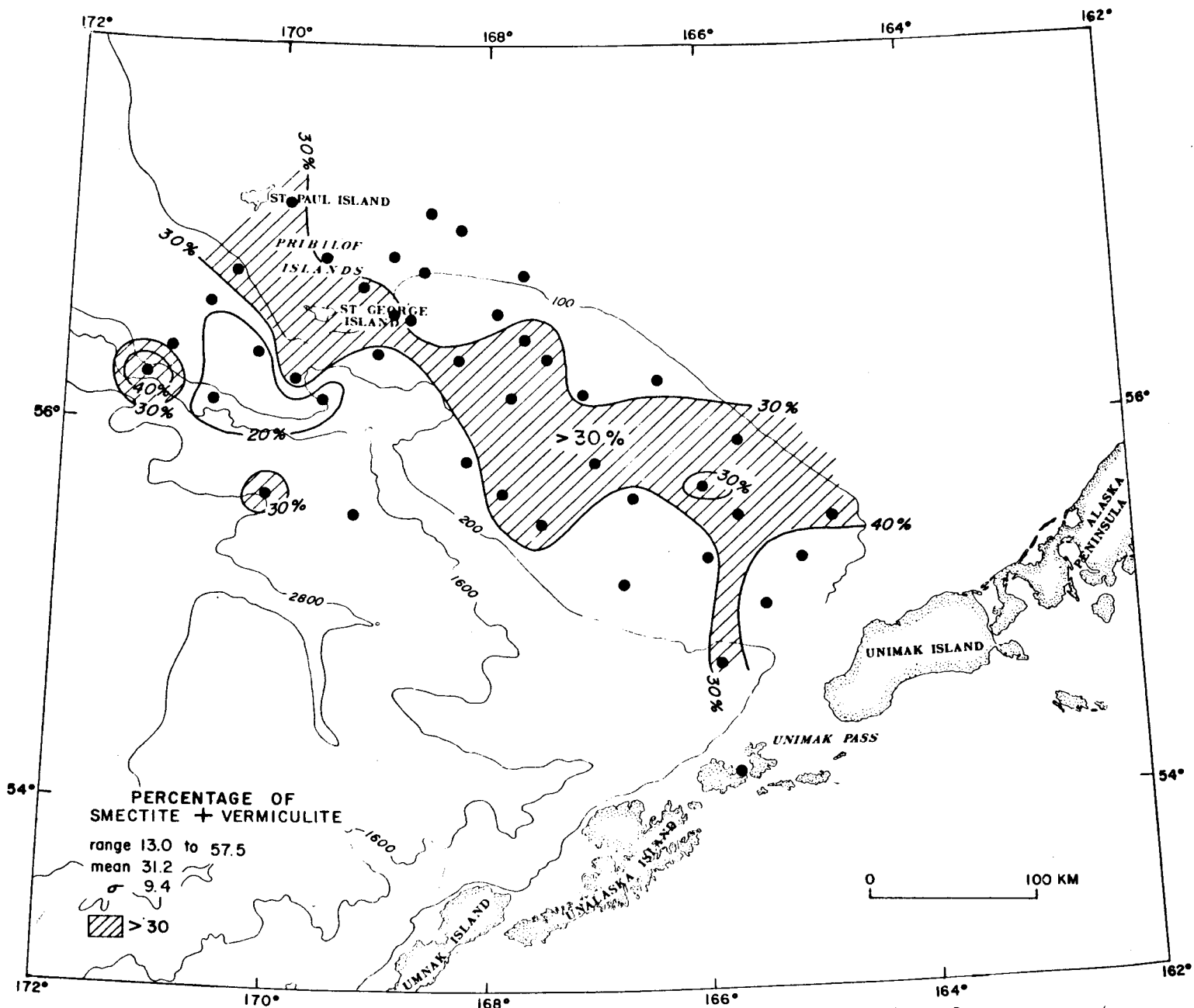


Figure 13. Map showing the distribution of the percentage of smectite plus vermiculite in the clay assemblage. The univariate statistics are also shown.

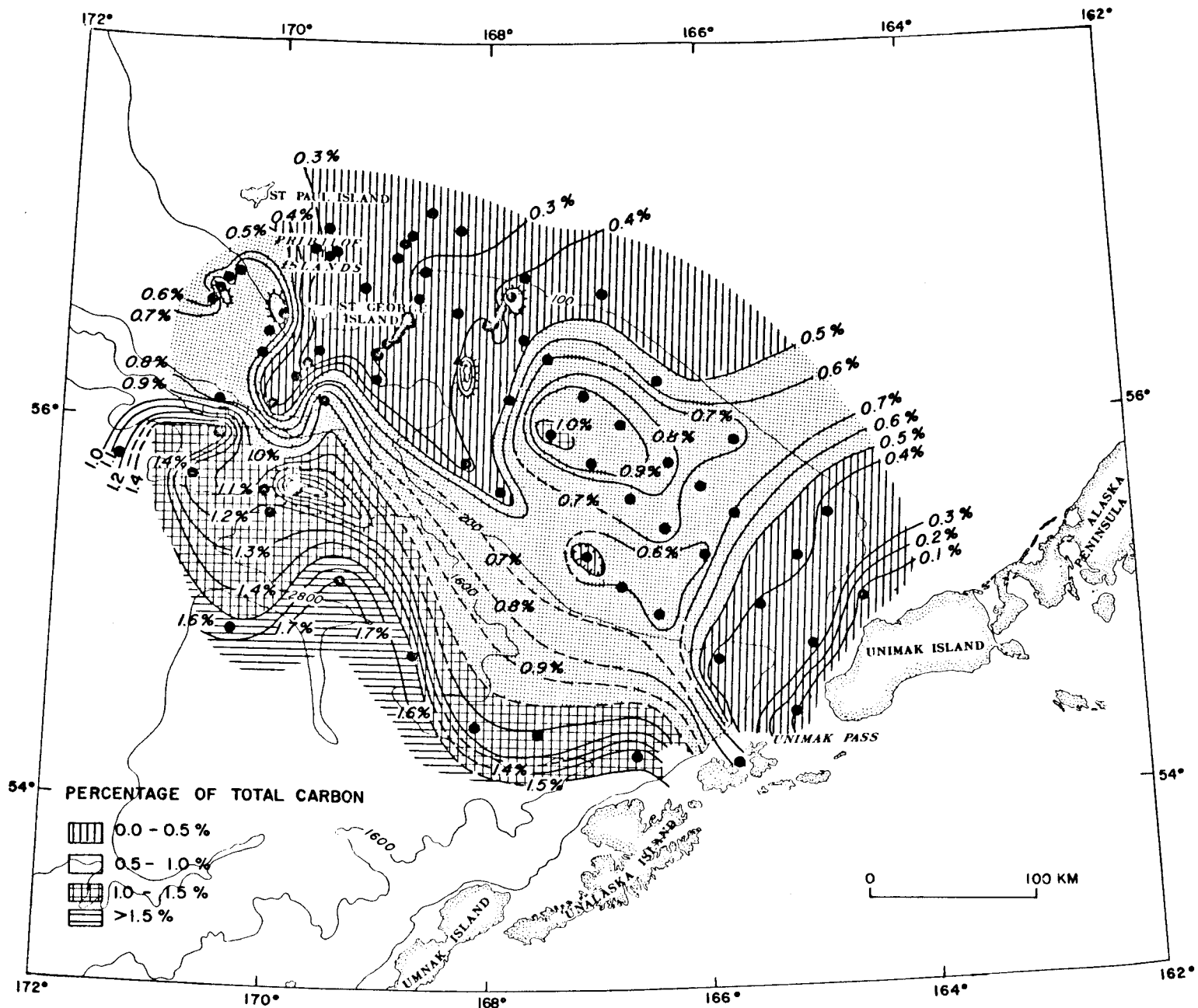


Figure 15. Map showing the distribution of the percentages of total carbon in bulk samples of surface sediments.

Table 8, Cruise S4-76. Values (in weight percent) for 32 elements determined by X-ray fluorescence (SRF or X), atomic absorption spectroscopy (aas or a), instrumental neutron activation (n), and emission spectroscopy (s) techniques.

CORE	INTERVAL (cm)										
		1 Si %-xrf	2 Al %-xrf	3 Ca %-xrf	4 K %-xrf	5 Fe %-xrf	6 Ti %-xrf	7 S %-xrf	8 Mg %-aas	9 Na %-aas	10 Hg ppm-a
G002	15-20	26.0000	7.0000	4.0000	1.0500	5.0000	0.7000	0.0200	1.5400	2.3100	0.0300
G005	0-5	24.0244	7.9282	4.6906	0.9747	5.6325	0.6475	0.1160	1.4600	2.5600	0.0400
G006	3-4	24.0945	7.2772	4.8357	1.0012	5.5919	0.6583	0.0070	1.5800	2.5800	0.0300
G008	7-15	31.7037	5.4672	2.1877	1.1643	2.2249	0.3825	0.0860	1.2400	2.4300	0.0400
G009	4-5	26.6231	6.4410	4.0624	1.0834	4.4519	0.5463	0.1210	1.1900	2.4000	0.0300
G010	0-5	30.1006	6.4251	3.0603	1.2005	3.1628	0.4405	0.1300	0.9700	2.3300	0.0500
G011	13-18	28.9928	5.6630	2.8738	1.1947	3.1495	0.4192	0.1460	0.9600	2.1100	0.0400
G012	4-5	28.3338	5.7741	2.9810	1.1540	3.1104	0.4109	0.1220	0.9600	2.1500	0.0400
G013	14-19	28.3011	5.6206	2.9053	1.1756	3.2160	0.4155	0.1100	1.0000	2.1700	0.0300
G014	4-5	28.6984	5.6577	2.8910	1.1947	3.2565	0.4321	0.1410	1.0000	2.0200	0.0400
G015	4-5	30.4651	5.3190	2.5822	1.2411	2.9138	0.4261	0.1410	0.9800	2.2600	0.0600
G016	7-9	27.6187	5.1724	2.4714	1.1158	2.9985	0.4310	0.1300	0.9700	1.9500	0.0500
G018	4-5	30.1847	5.2719	2.2106	1.2760	2.4410	0.3587	0.1540	0.9300	1.9600	0.0400
G018	4-5	31.3298	5.2835	2.2306	1.2677	2.4067	0.3809	0.0690	0.8300	1.9900	0.0400
G019	0-3	29.7640	5.0956	2.3349	1.2403	2.3865	0.3482	0.1310	0.8500	1.8500	0.0300
G020	6-11	30.6427	5.5465	2.0126	1.2503	2.3487	0.3435	0.1180	0.8700	2.0400	0.0600
G021	4-5	32.5123	5.5677	2.2084	1.2760	2.2452	0.3575	0.1230	0.8600	2.0400	0.0400
G021	4-5	30.6334	5.2470	2.0419	1.2229	2.3354	0.3586	0.1070	0.8200	2.0300	0.0400
G027	14-19	31.6617	4.9188	2.0955	1.2710	2.2445	0.3578	0.1630	0.8900	1.8900	0.0300
G028	cc	32.6432	5.1597	2.1034	1.2395	2.0165	0.3667	0.1200	0.7700	1.7900	0.0400
G029	4-5	31.6897	5.0628	2.0226	1.2088	2.0808	0.3133	0.0570	0.8400	1.9900	0.0400
G029	4-5	32.2272	5.5143	2.0971	1.2262	2.0871	0.3593	0.1170	0.8400	1.8000	0.0400
G032	6-11	31.4981	4.9993	1.9783	1.2561	2.1759	0.3276	0.1090	0.8600	1.8200	0.0300
G033	0-13	31.0167	4.8919	2.0934	1.2470	2.3375	0.3399	0.0880	0.8900	2.0900	0.0400
G034	4-5	32.8255	4.8749	2.1598	1.2810	2.2557	0.3459	0.1180	0.8200	1.9500	0.0300
G034	4-5	32.6432	5.4513	2.1834	1.2677	2.2046	0.3693	0.0990	0.8000	1.8400	0.0400
G036	2-7	31.0728	5.0438	2.0812	1.2096	2.2095	0.3303	0.0830	0.8200	1.8400	0.0400
G041	6-11	30.4231	5.1115	2.1227	1.2378	2.5179	0.3591	0.1350	0.8700	1.8600	0.0400
G042	0-1	28.5301	5.1274	2.4514	1.1631	2.9250	0.3950	0.0780	0.9900	1.9400	0.0400
G043	0-6	28.8386	5.3454	2.3020	1.1872	2.9425	0.3927	0.2509	0.9900	2.1100	0.0600
G046	11-16	28.3525	5.4830	2.5222	1.1905	3.4594	0.4282	0.2020	1.0600	2.0000	0.0400
G047	4-5	27.0531	5.8353	2.6408	1.1349	3.7601	0.4595	0.2340	1.1300	2.1100	0.0400
G048	0-8	26.2071	6.0493	2.6094	1.1125	3.7077	0.4558	0.1760	1.0900	2.0000	0.0400
G049	0-5	26.3754	5.7900	2.9510	1.1133	3.8769	0.4724	0.1490	1.1500	2.1700	0.0400
G049	0-5	25.6042	5.9911	2.8724	1.0842	3.7720	0.4586	0.1690	1.1000	2.1500	0.0500
G050	0-1	27.3195	6.0387	3.3376	1.0942	4.0070	0.4878	0.1150	0.9600	2.4800	0.0400
G050	0-1	22.5567	5.1231	2.6351	0.9215	3.2286	0.3651	0.1030	1.1500	2.4700	0.0800
G051	6-11	26.1043	5.8800	3.0954	1.0826	3.8525	0.4743	0.1840	1.2300	2.4600	0.0500
G052	9-13	24.9077	7.1502	3.4220	0.9929	4.2364	0.5161	0.2120	1.2300	2.4300	0.0400
G053	0-1	25.0573	5.9170	3.9566	1.0278	4.6386	0.5457	0.1790	1.2700	2.3900	0.0300
G054	0-3	25.7397	6.2769	3.9444	0.9954	4.5876	0.5463	0.2070	1.2400	2.4200	0.0500
G055	4-5	26.8241	6.6844	3.4977	1.0651	3.9854	0.5163	0.1040	1.2300	2.6000	0.0500
G055	4-5	27.1372	6.7850	3.5463	1.0776	4.1357	0.5435	0.1530	1.1700	2.2300	0.0400
G056	0-4	25.5574	6.4198	3.3048	1.0602	4.4750	0.5237	0.1200	1.1900	2.4100	0.0400
G057	0-5	26.3614	6.0864	3.4792	1.0560	4.2169	0.5055	0.0730	1.1900	2.3500	0.0400
G059	5-8	26.0809	6.1181	2.9103	1.0994	3.7329	0.4331	0.1220	1.0800	2.2100	0.0400
G060	0-2	26.0809	6.0753	2.6315	1.1482	3.6769	0.4272	0.3550	1.1900	2.3200	0.0600
G061	4-5	26.9302	5.3295	2.6844	1.1291	3.4230	0.4294	0.1650	1.0400	1.9700	0.0300
G062	0-5	28.6376	6.0070	2.6287	1.1714	3.3559	0.4609	0.1720	1.0500	2.1100	0.0400
G063	15-20	26.7587	4.8590	2.2835	1.1316	3.1929	0.4268	0.2080	1.0900	2.0600	0.0400

Table 8 (Continued), Cruise S4-76

CORE	INTERVAL (cm)	1	2	3	4	5	6	7	8	9	10
		Si %-xrf	Al %-xrf	Ca %-xrf	K %-xrf	Fe %-xrf	Ti %-xrf	S %-xrf	Hg %-aas	Na %-aas	Hg ppm-a
G064	4-5	29.1050	5.1972	2.0683	1.2071	2.4256	0.3313	0.1000	0.8500	1.8900	0.0500
G065	10-15	31.2130	5.4936	2.2442	1.2403	2.4046	0.3771	0.0930	0.8800	2.0300	0.0400
G066	4-5	29.3060	4.8659	2.7023	1.2470	3.2859	0.3722	0.0870	1.0900	1.9300	0.0400
G067	5-10	30.9325	5.2904	2.5493	1.2146	2.9866	0.3448	0.1000	0.9500	1.8300	0.0400
G069	cc	30.8437	4.7193	2.0105	1.2362	2.1326	0.3215	0.0710	0.8200	1.7400	0.0400
G070	0-1	26.2632	6.3933	2.0419	1.5716	3.8042	0.4244	0.4260	1.3600	1.8100	0.0900
G071	2-7	26.3567	6.5574	1.8211	1.6147	3.7930	0.4220	0.3840	1.2300	1.7500	0.0700
G075	6-10	32.7133	4.6701	2.0169	1.2146	1.9612	0.3150	0.0750	0.8000	1.9400	0.0300
G075	6-10	31.9842	4.9188	1.9926	1.2187	1.9584	0.3375	0.1000	0.7900	1.8200	0.0400
G077	0-5	31.8393	5.1073	2.0926	1.2021	2.0906	0.3843	0.1220	0.8600	1.9000	0.0400
G080	0-5	30.2361	4.5336	2.0769	1.1332	2.2109	0.3418	0.1070	0.9600	1.6600	0.0500
G090	2-4	29.6049	5.0464	2.3221	1.1100	2.7453	0.4318	0.1800	1.0500	1.9000	0.0500
G091	0-1	29.6799	4.9104	2.1613	1.1731	2.4459	0.4101	0.1570	1.0500	2.1400	0.0400
G105	10-15	27.2494	6.1975	1.8382	1.8771	3.9441	0.4496	0.2500	1.4300	1.5600	0.0800
G107	0-5	25.9828	6.2346	1.7903	1.8273	4.0042	0.4437	0.4570	1.5500	1.6000	0.1100
G109	3-8	31.9982	4.8172	2.5043	1.2279	2.4263	0.3363	0.0410	0.9000	2.0000	0.0200
G110	4-5	30.3576	5.1385	2.4121	1.2138	2.7159	0.3449	0.0610	0.9400	1.8800	0.0400
G111	1-5	31.3298	5.7106	2.5579	1.2353	2.5795	0.3876	0.1500	0.8900	2.1000	0.0400
G112	4-5	29.8341	5.4248	2.3957	1.2038	2.4935	0.3680	0.1060	0.8800	1.9700	0.0500
G112	4-5	30.6054	5.7683	2.5372	1.2046	2.4732	0.3000	0.0930	0.8900	2.1000	0.0400
G113	3-8	29.0957	5.9541	2.7766	1.1590	2.9950	0.4289	0.1120	0.9500	2.1100	0.0300
G114	0-1	29.3527	5.4724	2.8917	1.1224	3.1237	0.4095	0.0800	0.9000	2.0700	0.0500
G115	4-5	24.1365	6.9543	4.4876	0.9614	5.1016	0.5941	0.1580	1.1500	2.4000	0.0400
G115	4-5	26.7587	6.0546	3.3705	1.0851	3.9364	0.5098	0.2240	1.1100	2.2200	0.0500
G116	0-5	26.8848	6.2981	2.9939	1.1075	3.5426	0.4546	0.1360	1.0600	2.0800	0.0500
G117	0-1	26.1837	5.7159	3.5814	1.0635	4.0994	0.4976	0.1210	1.1100	2.3800	0.0300
G118	6-11	26.3099	6.6897	3.1726	1.0967	3.9217	0.4708	0.1870	1.1500	2.3700	0.0400
G119	0-5	26.2726	7.2454	3.9966	1.0344	4.6918	0.5705	0.1700	1.2800	2.4000	0.0500
G120	4-5	26.4595	6.4727	3.4649	1.1249	4.1308	0.5243	0.2380	1.2100	2.3400	0.0300
G120	4-5	25.9641	6.3192	3.4277	1.1332	4.1266	0.5227	0.1820	1.2100	2.3700	0.0500
G121	0-5	21.6032	7.0602	4.8928	0.8360	5.6143	0.5087	0.2600	1.8500	2.2500	0.1100
V002	0-3	33.6107	5.1485	1.9819	1.2138	2.0647	0.3939	0.0730	0.7400	1.6500	0.0300
V003	0-3	32.3160	4.0631	1.7603	1.1706	1.7500	0.2638	0.0360	0.6600	1.6300	0.0300
V006	0-3	31.3392	4.1996	1.7467	1.1847	1.8430	0.2901	0.0800	0.7500	1.7000	0.0200
V007	0-3	31.6477	4.6627	2.0898	1.2685	2.2431	0.3218	0.1570	0.8000	1.8000	0.0300
V007	0-3	30.7549	4.5923	2.0305	1.2146	2.1906	0.3301	0.0790	0.8500	1.7500	0.0400
V009	0-3	32.6806	3.9318	1.6924	1.1639	2.2494	0.2767	0.0640	1.4200	1.5200	0.0400
V011	0-3	31.5168	4.3399	2.1219	1.2129	2.5571	0.3993	0.1180	1.0600	1.7000	0.0400
V012	0-3	32.9564	3.9509	1.8060	1.1432	2.1829	0.3100	0.0630	1.0100	1.5500	0.0300
V014	0-3	32.7928	5.3034	2.1470	1.2378	2.2927	0.3352	0.0760	0.8400	1.9100	0.0400
V014	0-3	31.7411	4.5256	2.1343	1.2669	2.2710	0.3307	0.0710	0.8300	1.8000	0.0400
V015	0-3	31.1756	5.2062	2.5872	1.2318	3.3729	0.4710	0.0880	1.5600	1.9200	0.0300
V017	0-3	29.8108	5.2364	2.9860	1.1963	3.6042	0.5651	0.0400	2.1400	1.8700	0.0400
V018	0-3	30.4838	5.0146	2.3192	1.2528	2.7425	0.4252	0.1030	1.3100	1.7800	0.0300
V018	0-3	32.0590	4.7368	2.4214	1.2287	2.7397	0.4330	0.1160	1.2500	1.8400	0.0300
V021	0-3	29.8762	4.8289	2.0133	1.2196	2.3872	0.3559	0.0900	1.0700	1.7900	0.0300
V028	0-3	23.3934	6.9332	5.0879	0.8626	5.6290	0.5179	0.1420	1.9400	2.5400	0.0800
P003	3-8	26.7960	5.8112	3.3941	1.0419	3.9651	0.4990	0.1220	1.0900	2.2500	0.0400
P005	0-5	27.2588	5.1305	2.4843	1.1614	3.4125	0.4364	0.1780	1.0700	2.1300	0.0500
P005	0-5	25.6743	5.5677	2.3992	1.0934	3.3838	0.4098	0.1870	1.0600	2.1700	0.0500
P006	6-	27.0999	5.2655	2.3821	1.0950	3.1279	0.4065	0.1210	1.0400	2.1000	0.0500
P007	5- 0	28.9928	4.6293	2.2291	1.1282	2.5375	0.3770	0.1260	1.0000	1.8400	0.0500
P008	3-8	24.7629	6.3775	1.6738	1.7260	4.7281	0.4518	0.5480	1.6000	1.8900	0.0900

Table 8 (Continued), Cruise S4-76

CORE	INTERVAL (cm)	11	12	13	14	15	16	17	18	19	20
		L1 ppm-a	Pb ppm-a	Zn ppm-a	As ppm-x	Ce ppm-x	Sn ppm-x	B ppm-s	Ba ppm-s	Co ppm-s	Cr ppm-s
G002	15-20	15.0000	25.0000	116.0000	4.0650	0.6618	0.4058	14.0000	500.0000	15.0000	15.0000
G005	0-5	16.0000	20.0000	107.0000	0.0000B	0.0000B	0.0000B	20.0000	300.0000	20.0000	20.0000
G006	3-4	15.0000	25.0000	119.0000	3.7730	1.4530	1.0250	30.0000	500.0000	15.0000	70.0000
G008	7-15	16.0000	23.0000	91.0000	6.0230	1.8260	1.6030	30.0000	500.0000	15.0000	30.0000
G009	4-5	17.0000	14.0000	97.0000	4.5200	1.2590	1.3840	20.0000	500.0000	15.0000	30.0000
G010	0-5	18.0000	40.0000	72.0000	0.0000B	0.0000B	0.0000B	20.0000	700.0000	10.0000	30.0000
G011	13-18	18.0000	25.0000	71.0000	0.0000B	0.0000B	0.0000B	30.0000	700.0000	10.0000	50.0000
G012	4-5	19.0000	30.0000	71.0000	5.3250	1.5900	1.0170	20.0000	500.0000	10.0000	50.0000
G013	14-19	19.0000	25.0000	83.0000	0.0000B	0.0000B	0.0000B	50.0000	500.0000	10.0000	50.0000
G014	4-5	20.0000	35.0000	79.0000	5.9270	1.4270	1.0270	50.0000	500.0000	10.0000	30.0000
G015	4-5	20.0000	41.0000	77.0000	5.6120	1.2730	1.0980	50.0000	700.0000	10.0000	50.0000
G016	7-9	22.0000	30.0000	82.0000	0.0000B	0.0000B	0.0000B	50.0000	700.0000	10.0000	100.0000
G018	4-5	21.0000	40.0000	70.0000	6.2890	1.6820	1.1570	30.0000	700.0000	7.0000	30.0000
G018	4-5	20.0000	50.0000	68.0000	0.0000B	0.0000B	0.0000B	30.0000	700.0000	10.0000	70.0000
G019	0-3	20.0000	30.0000	65.0000	5.7190	1.3830	1.7780	50.0000	700.0000	7.0000	50.0000
G020	6-11	20.0000	50.0000	63.0000	0.0000B	0.0000B	0.0000B	30.0000	500.0000	10.0000	30.0000
G021	4-5	20.0000	43.0000	63.0000	6.0840	1.6380	0.9185	30.0000	700.0000	7.0000	70.0000
G021	4-5	20.0000	35.0000	63.0000	0.0000B	0.0000B	0.0000B	30.0000	700.0000	10.0000	50.0000
G027	14-19	20.0000	45.0000	62.0000	0.0000B	0.0000B	0.0000B	30.0000	700.0000	7.0000	50.0000
G028	cc	17.0000	43.0000	58.0000	0.0000B	0.0000B	0.0000B	20.0000	500.0000	10.0000	50.0000
G029	4-5	18.0000	48.0000	58.0000	0.0000B	0.0000B	0.0000B	30.0000	700.0000	10.0000	50.0000
G029	4-5	19.0000	39.0000	56.0000	0.0000B	0.0000B	0.0000B	30.0000	700.0000	7.0000	50.0000
G032	6-11	18.0000	45.0000	58.0000	0.0000B	0.0000B	0.0000B	30.0000	700.0000	7.0000	50.0000
G033	8-13	19.0000	41.0000	65.0000	0.0000B	0.0000B	0.0000B	30.0000	500.0000	7.0000	30.0000
G034	4-5	18.0000	44.0000	57.0000	4.6970	1.4040	0.9374	30.0000	700.0000	7.0000	50.0000
G034	4-5	20.0000	45.0000	61.0000	0.0000B	0.0000B	0.0000B	20.0000	500.0000	10.0000	70.0000
G036	2-7	19.0000	40.0000	55.0000	0.0000B	0.0000B	0.0000B	50.0000	700.0000	7.0000	70.0000
G041	6-11	21.0000	35.0000	70.0000	5.7260	1.4730	1.1610	30.0000	700.0000	10.0000	30.0000
G042	0-1	22.0000	40.0000	85.0000	4.5660	1.2820	0.8684	70.0000	700.0000	10.0000	100.0000
G043	0-6	23.0000	35.0000	84.0000	0.0000B	0.0000B	0.0000B	50.0000	500.0000	10.0000	50.0000
G046	11-16	23.0000	40.0000	94.0000	0.0000B	0.0000B	0.0000B	50.0000	500.0000	10.0000	50.0000
G047	4-5	22.0000	43.0000	101.0000	6.2650	1.3220	0.7828	50.0000	500.0000	10.0000	50.0000
G048	0-8	22.0000	38.0000	100.0000	0.0000B	0.0000B	0.0000B	50.0000	500.0000	10.0000	50.0000
G049	0-5	21.0000	35.0000	107.0000	0.0000B	0.0000B	0.0000B	50.0000	500.0000	15.0000	30.0000
G049	0-5	21.0000	33.0000	98.0000	0.0000B	0.0000B	0.0000B	30.0000	500.0000	10.0000	30.0000
G050	0-1	19.0000	31.0000	102.0000	0.0000B	0.0000B	0.0000B	30.0000	500.0000	15.0000	30.0000
G050	0-1	20.0000	25.0000	115.0000	0.0000B	0.0000B	0.0000B	50.0000	500.0000	15.0000	30.0000
G051	6-11	20.0000	20.0000	106.0000	0.0000B	0.0000B	0.0000B	30.0000	500.0000	15.0000	50.0000
G052	9-13	17.0000	35.0000	96.0000	0.0000B	0.0000B	0.0000B	20.0000	500.0000	15.0000	30.0000
G053	0-1	18.0000	20.0000	112.0000	5.1080	1.6680	2.5160	50.0000	500.0000	15.0000	30.0000
G054	0-3	18.0000	14.0000	108.0000	5.8430	1.4860	1.3530	30.0000	500.0000	15.0000	50.0000
G055	4-5	19.0000	28.0000	99.0000	5.5940	1.5160	0.8951	30.0000	500.0000	15.0000	30.0000
G055	4-5	20.0000	25.0000	99.0000	0.0000B	0.0000B	0.0000B	30.0000	500.0000	15.0000	30.0000
G056	0-4	19.0000	33.0000	99.0000	5.7260	1.3850	1.1080	30.0000	500.0000	15.0000	30.0000
G057	0-5	18.0000	36.0000	101.0000	0.0000B	0.0000B	0.0000B	50.0000	500.0000	15.0000	30.0000
G059	5-8	20.0000	38.0000	93.0000	0.0000B	0.0000B	0.0000B	30.0000	500.0000	10.0000	30.0000
G060	0-2	22.0000	45.0000	99.0000	0.0000B	0.0000B	0.0000B	30.0000	500.0000	10.0000	50.0000
G061	4-5	22.0000	30.0000	108.0000	6.0430	1.2730	2.2650	70.0000	500.0000	15.0000	50.0000
G062	0-5	22.0000	40.0000	94.0000	0.0000B	0.0000B	0.0000B	30.0000	500.0000	10.0000	50.0000
G063	15-20	23.0000	35.0000	102.0000	3.4840	0.8798	0.6366	50.0000	700.0000	10.0000	50.0000

Table 8 (Continued), Cruise S4-76

CORE	INTERVAL (cm)	11	12	13	14	15	16	17	18	19	20
		Li ppm-a	Rb ppm-a	Zn ppm-a	As ppm-x	Ge ppm-x	Sn ppm-x	B ppm-s	Ba ppm-s	Co ppm-s	Cr ppm-s
G064	4-5	20.0000	43.0000	68.0000	4.2730	1.3600	0.5784	30.0000	500.0000	10.0000	50.0000
G065	10-15	20.0000	44.0000	69.0000	0.0000B	0.0000B	0.0000B	30.0000	700.0000	10.0000	50.0000
G066	4-5	17.0000	30.0000	73.0000	4.9450	1.1650	1.0010	50.0000	700.0000	15.0000	70.0000
G067	5-10	16.0000	45.0000	72.0000	0.0000B	0.0000B	0.0000B	50.0000	500.0000	15.0000	50.0000
G069	cc	13.0000	40.0000	58.0000	0.0000B	0.0000B	0.0000B	30.0000	700.0000	7.0000	50.0000
G070	0-1	42.0000	70.0000	111.0000	3.5490	1.3810	0.9752	50.0000	700.0000	15.0000	100.0000
G071	2-7	44.0000	38.0000	118.0000	0.0000B	0.0000B	0.0000B	50.0000	500.0000	15.0000	70.0000
G075	6-10	17.0000	48.0000	55.0000	0.0000B	0.0000B	0.0000B	30.0000	500.0000	7.0000	50.0000
G075	6-10	17.0000	43.0000	59.0000	0.0000B	0.0000B	0.0000B	30.0000	500.0000	10.0000	50.0000
G077	0-5	20.0000	36.0000	62.0000	4.0650	1.4320	0.7464	30.0000	500.0000	7.0000	50.0000
G080	0-5	20.0000	40.0000	72.0000	0.0000B	0.0000B	0.0000B	50.0000	700.0000	7.0000	70.0000
G090	2-4	21.0000	30.0000	79.0000	0.0000B	0.0000B	0.0000B	50.0000	700.0000	10.0000	100.0000
G091	0-1	20.0000	40.0000	79.0000	4.0490	1.4280	0.7971	50.0000	700.0000	10.0000	100.0000
G105	10-15	43.0000	65.0000	134.0000	18.5300	1.6980	1.4940	70.0000	700.0000	15.0000	100.0000
G107	0-5	45.0000	75.0000	140.0000	13.3100	1.6660	1.4360	50.0000	1500.0000	15.0000	100.0000
G109	3-8	16.0000	43.0000	57.0000	0.0000B	0.0000B	0.0000B	50.0000	700.0000	10.0000	70.0000
G110	4-5	16.0000	43.0000	60.0000	4.9950	1.5620	1.0920	20.0000	500.0000	7.0000	50.0000
G111	1-5	17.0000	40.0000	66.0000	0.0000B	0.0000B	0.0000B	30.0000	700.0000	10.0000	50.0000
G112	4-5	13.0000	35.0000	66.0000	4.0130	1.6690	0.8168	50.0000	700.0000	10.0000	30.0000
G112	4-5	17.0000	25.0000	65.0000	0.0000B	0.0000B	0.0000B	50.0000	500.0000	10.0000	50.0000
G113	3-8	20.0000	33.0000	82.0000	5.6080	1.6280	1.3620	50.0000	500.0000	10.0000	30.0000
G114	0-1	19.0000	14.0000	82.0000	3.8160	1.3790	1.4470	50.0000	700.0000	10.0000	70.0000
G115	4-5	18.0000	30.0000	97.0000	4.8970	1.3140	1.2440	50.0000	500.0000	15.0000	30.0000
G115	4-5	19.0000	20.0000	104.0000	0.0000B	0.0000B	0.0000B	30.0000	500.0000	15.0000	30.0000
G116	0-5	20.0000	40.0000	90.0000	0.0000B	0.0000B	0.0000B	30.0000	500.0000	10.0000	30.0000
G117	0-1	13.0000	14.0000	110.0000	0.0000B	0.0000B	0.0000B	50.0000	500.0000	15.0000	50.0000
G118	6-11	20.0000	25.0000	97.0000	0.0000B	0.0000B	0.0000B	30.0000	500.0000	15.0000	30.0000
G119	0-5	17.0000	25.0000	99.0000	0.0000B	0.0000B	0.0000B	30.0000	500.0000	20.0000	30.0000
G120	4-5	19.0000	25.0000	108.0000	0.0000B	0.0000B	0.0000B	30.0000	500.0000	15.0000	50.0000
G120	4-5	19.0000	35.0000	108.0000	0.0000B	0.0000B	0.0000B	30.0000	500.0000	15.0000	30.0000
G121	0-5	17.0000	25.0000	102.0000	0.0000B	0.0000B	0.0000B	20.0000	300.0000	15.0000	30.0000
V002	0-3	15.0000	40.0000	45.0000	5.1910	1.6670	1.0290	20.0000	500.0000	7.0000	70.0000
V003	0-3	16.0000	35.0000	45.0000	5.4190	1.3980	0.5711	30.0000	700.0000	7.0000	200.0000
V006	0-3	16.0000	45.0000	46.0000	6.3580	1.5700	0.9425	30.0000	700.0000	7.0000	50.0000
V007	0-3	18.0000	35.0000	59.0000	0.0000B	0.0000B	0.0000B	50.0000	700.0000	7.0000	50.0000
V007	0-3	19.0000	45.0000	113.0000	0.0000B	0.0000B	0.0000B	30.0000	500.0000	7.0000	70.0000
V009	0-3	16.0000	48.0000	55.0000	0.0000B	0.0000B	0.0000B	50.0000	500.0000	15.0000	70.0000
V011	0-3	16.0000	30.0000	55.0000	6.7000	1.4220	0.6229	30.0000	700.0000	15.0000	70.0000
V012	0-3	15.0000	30.0000	48.0000	6.9840	1.4380	1.3300	50.0000	700.0000	10.0000	100.0000
V014	0-3	17.0000	38.0000	61.0000	5.2570	1.8520	1.1620	20.0000	500.0000	10.0000	50.0000
V014	0-3	18.0000	40.0000	53.0000	0.0000B	0.0000B	0.0000B	50.0000	500.0000	7.0000	50.0000
V015	0-3	16.0000	44.0000	68.0000	0.0000B	0.0000B	0.0000B	30.0000	500.0000	15.0000	150.0000
V017	0-3	13.0000	33.0000	71.0000	5.6390	1.5530	0.8603	20.0000	500.0000	20.0000	150.0000
V018	0-3	13.0000	40.0000	63.0000	5.5590	1.4630	1.0490	20.0000	700.0000	15.0000	70.0000
V018	0-3	16.0000	43.0000	62.0000	0.0000B	0.0000B	0.0000B	30.0000	500.0000	15.0000	100.0000
V021	0-3	18.0000	40.0000	58.0000	3.4330	1.0590	0.6202	30.0000	700.0000	10.0000	70.0000
V028	0-3	16.0000	23.0000	102.0000	0.0000B	0.0000B	0.0000B	30.0000	300.0000	30.0000	30.0000
V028	0-3	19.0000	14.0000	102.0000	0.0000B	0.0000B	0.0000B	50.0000	500.0000	15.0000	50.0000
P003	3-8	22.0000	25.0000	109.0000	0.0000B	0.0000B	0.0000B	30.0000	700.0000	10.0000	50.0000
P005	0-5	22.0000	35.0000	97.0000	0.0000B	0.0000B	0.0000B	30.0000	500.0000	10.0000	50.0000
P005	0-5	22.0000	35.0000	97.0000	0.0000B	0.0000B	0.0000B	30.0000	500.0000	10.0000	50.0000
P006	6-7	23.0000	40.0000	96.0000	0.0000B	0.0000B	0.0000B	50.0000	500.0000	10.0000	50.0000
P007	5-10	21.0000	45.0000	85.0000	0.0000B	0.0000B	0.0000B	70.0000	700.0000	10.0000	100.0000
P008	3-8	48.0000	90.0000	130.0000	8.3310	1.4770	1.4390	30.0000	700.0000	15.0000	70.0000

Table 8 (Continued), Cruise S4-76

CORE	INTERVAL (cm)	21	22	23	24	25	26	27	28	29	30
		Cu ppm-s	Ga ppm-s	In ppm-s	Ni ppm-s	Sc ppm-s	Sr ppm-s	V ppm-s	Y ppm-s	Yb ppm-s	Zr ppm-s
G002	15-20	70.0000	20.0000	700.0000	15.0000	20.0000	500.0000	150.0000	30.0000	3.0000	70.0000
G005	3-5	70.0000	20.0000	700.0000	10.0000	20.0000	500.0000	200.0000	50.0000	5.0000	100.0000
G006	3-4	70.0000	15.0000	700.0000	15.0000	30.0000	700.0000	300.0000	30.0000	5.0000	70.0000
G008	7-15	50.0000	20.0000	700.0000	15.0000	20.0000	500.0000	200.0000	30.0000	3.0000	70.0000
G009	4-5	70.0000	30.0000	700.0000	15.0000	20.0000	500.0000	200.0000	20.0000	3.0000	100.0000
G010	0-5	30.0000	20.0000	700.0000	15.0000	15.0000	500.0000	150.0000	20.0000	3.0000	70.0000
G011	13-18	30.0000	15.0000	500.0000	15.0000	15.0000	500.0000	150.0000	30.0000	3.0000	100.0000
G012	4-5	30.0000	20.0000	500.0000	15.0000	15.0000	500.0000	100.0000	30.0000	3.0000	100.0000
G013	14-19	30.0000	20.0000	500.0000	20.0000	15.0000	500.0000	150.0000	30.0000	3.0000	100.0000
G014	4-5	30.0000	15.0000	500.0000	15.0000	15.0000	300.0000	100.0000	30.0000	3.0000	150.0000
G015	4-5	20.0000	20.0000	500.0000	30.0000	15.0000	300.0000	150.0000	20.0000	3.0000	100.0000
G016	7-9	50.0000	20.0000	500.0000	15.0000	15.0000	500.0000	150.0000	30.0000	3.0000	150.0000
G018	4-5	20.0000	15.0000	300.0000	15.0000	10.0000	300.0000	70.0000	20.0000	3.0000	100.0000
G018	4-5	30.0000	15.0000	300.0000	20.0000	15.0000	300.0000	100.0000	20.0000	2.0000	200.0000
G019	0-3	15.0000	15.0000	500.0000	30.0000	15.0000	300.0000	150.0000	20.0000	3.0000	100.0000
G020	6-11	15.0000	15.0000	500.0000	20.0000	15.0000	200.0000	100.0000	20.0000	2.0000	70.0000
G021	4-5	15.0000	15.0000	500.0000	20.0000	10.0000	300.0000	70.0000	20.0000	3.0000	70.0000
G021	4-5	15.0000	15.0000	500.0000	15.0000	15.0000	300.0000	100.0000	20.0000	3.0000	100.0000
G027	14-19	15.0000	15.0000	300.0000	20.0000	10.0000	300.0000	100.0000	20.0000	3.0000	100.0000
G028	cc	15.0000	15.0000	500.0000	15.0000	15.0000	200.0000	70.0000	30.0000	3.0000	150.0000
G029	4-5	20.0000	15.0000	500.0000	20.0000	15.0000	300.0000	70.0000	15.0000	1.5000	100.0000
G029	4-5	15.0000	15.0000	500.0000	20.0000	15.0000	300.0000	70.0000	15.0000	2.0000	70.0000
G032	6-11	15.0000	15.0000	300.0000	20.0000	10.0000	300.0000	100.0000	20.0000	3.0000	100.0000
G033	8-13	20.0000	15.0000	500.0000	20.0000	15.0000	200.0000	70.0000	15.0000	1.5000	70.0000
G034	4-5	15.0000	15.0000	500.0000	30.0000	15.0000	300.0000	100.0000	15.0000	2.0000	100.0000
G034	4-5	15.0000	15.0000	700.0000	15.0000	15.0000	300.0000	100.0000	20.0000	2.0000	70.0000
G036	2-7	15.0000	20.0000	500.0000	20.0000	15.0000	300.0000	70.0000	20.0000	2.0000	70.0000
G041	6-11	20.0000	15.0000	500.0000	20.0000	15.0000	300.0000	100.0000	20.0000	3.0000	150.0000
G042	0-1	30.0000	20.0000	500.0000	20.0000	15.0000	500.0000	150.0000	20.0000	3.0000	100.0000
G043	0-6	50.0000	20.0000	500.0000	20.0000	15.0000	300.0000	100.0000	30.0000	3.0000	200.0000
G046	11-16	30.0000	20.0000	500.0000	30.0000	15.0000	300.0000	150.0000	20.0000	2.0000	100.0000
G047	4-5	50.0000	20.0000	500.0000	20.0000	15.0000	300.0000	150.0000	30.0000	3.0000	100.0000
G048	0-8	50.0000	20.0000	500.0000	20.0000	20.0000	500.0000	150.0000	30.0000	3.0000	100.0000
G049	0-5	70.0000	20.0000	700.0000	15.0000	15.0000	300.0000	150.0000	30.0000	3.0000	100.0000
G049	0-5	50.0000	20.0000	500.0000	15.0000	15.0000	300.0000	150.0000	30.0000	3.0000	100.0000
G050	0-1	50.0000	20.0000	700.0000	15.0000	20.0000	500.0000	150.0000	30.0000	3.0000	70.0000
G050	0-1	50.0000	20.0000	500.0000	15.0000	15.0000	500.0000	200.0000	50.0000	5.0000	70.0000
G051	6-11	50.0000	20.0000	700.0000	20.0000	20.0000	500.0000	200.0000	30.0000	5.0000	100.0000
G052	9-13	50.0000	20.0000	500.0000	10.0000	20.0000	300.0000	150.0000	30.0000	3.0000	150.0000
G053	0-1	70.0000	20.0000	700.0000	15.0000	20.0000	500.0000	200.0000	30.0000	3.0000	100.0000
G054	0-1	70.0000	30.0000	700.0000	15.0000	30.0000	700.0000	200.0000	30.0000	3.0000	70.0000
G054	0-3	50.0000	20.0000	700.0000	15.0000	20.0000	500.0000	200.0000	30.0000	3.0000	100.0000
G055	4-5	50.0000	20.0000	500.0000	20.0000	20.0000	500.0000	200.0000	30.0000	3.0000	100.0000
G055	4-5	50.0000	20.0000	500.0000	15.0000	20.0000	500.0000	200.0000	30.0000	3.0000	100.0000
G056	0-4	50.0000	20.0000	500.0000	15.0000	20.0000	500.0000	200.0000	30.0000	3.0000	70.0000
G057	0-5	50.0000	30.0000	700.0000	15.0000	20.0000	500.0000	200.0000	30.0000	3.0000	70.0000
G059	5-8	50.0000	20.0000	500.0000	15.0000	15.0000	300.0000	150.0000	30.0000	3.0000	100.0000
G060	0-2	50.0000	20.0000	500.0000	15.0000	20.0000	300.0000	150.0000	30.0000	3.0000	70.0000
G061	4-5	50.0000	20.0000	500.0000	30.0000	15.0000	500.0000	150.0000	30.0000	3.0000	100.0000
G062	0-5	50.0000	20.0000	500.0000	15.0000	15.0000	300.0000	150.0000	20.0000	3.0000	100.0000
G063	15-20	50.0000	15.0000	500.0000	15.0000	15.0000	300.0000	150.0000	30.0000	3.0000	70.0000

Table 8 (Continued), Cruise S4-76

CORE	INTERVAL (cm)	21	22	23	24	25	26	27	28	29	30
		Cu ppm-s	Ca ppm-s	Mn ppm-s	Ni ppm-s	Sc ppm-s	Sr ppm-s	V ppm-s	Y ppm-s	Yb ppm-s	Zr ppm-s
G064	4-5	20.0000	15.0000	500.0000	15.0000	15.0000	300.0000	100.0000	30.0000	3.0000	70.0000
G065	10-15	20.0000	15.0000	500.0000	20.0000	15.0000	300.0000	150.0000	20.0000	3.0000	70.0000
G066	4-5	30.0000	15.0000	700.0000	30.0000	15.0000	500.0000	150.0000	20.0000	3.0000	100.0000
G067	5-10	20.0000	15.0000	700.0000	15.0000	15.0000	200.0000	100.0000	20.0000	2.0000	70.0000
G069	cc	15.0000	15.0000	300.0000	15.0000	10.0000	200.0000	100.0000	20.0000	3.0000	100.0000
G070	0-1	50.0000	20.0000	500.0000	20.0000	15.0000	300.0000	200.0000	30.0000	3.0000	100.0000
G071	2-7	50.0000	30.0000	500.0000	20.0000	15.0000	300.0000	150.0000	30.0000	3.0000	70.0000
G075	6-10	15.0000	15.0000	500.0000	20.0000	10.0000	200.0000	70.0000	15.0000	1.5000	100.0000
G075	6-10	15.0000	15.0000	500.0000	20.0000	15.0000	300.0000	100.0000	15.0000	2.0000	100.0000
G077	0-5	15.0000	15.0000	500.0000	20.0000	15.0000	300.0000	100.0000	30.0000	3.0000	150.0000
G080	0-5	20.0000	15.0000	500.0000	20.0000	10.0000	300.0000	100.0000	20.0000	3.0000	100.0000
G090	2-4	30.0000	15.0000	300.0000	30.0000	15.0000	500.0000	100.0000	30.0000	3.0000	100.0000
G091	0-1	20.0000	15.0000	500.0000	30.0000	15.0000	500.0000	150.0000	20.0000	3.0000	100.0000
G105	10-15	70.0000	30.0000	500.0000	50.0000	15.0000	200.0000	150.0000	20.0000	3.0000	70.0000
G107	0-5	70.0000	20.0000	300.0000	50.0000	15.0000	300.0000	200.0000	30.0000	3.0000	100.0000
G109	3-8	30.0000	15.0000	500.0000	15.0000	15.0000	300.0000	100.0000	20.0000	2.0000	70.0000
G110	4-5	15.0000	15.0000	500.0000	15.0000	15.0000	300.0000	100.0000	20.0000	3.0000	100.0000
G111	1-5	30.0000	20.0000	500.0000	15.0000	15.0000	300.0000	150.0000	20.0000	3.0000	150.0000
G112	4-5	20.0000	15.0000	500.0000	15.0000	15.0000	300.0000	150.0000	20.0000	3.0000	70.0000
G112	4-5	20.0000	15.0000	500.0000	15.0000	15.0000	300.0000	150.0000	20.0000	3.0000	100.0000
G113	3-8	50.0000	20.0000	700.0000	15.0000	15.0000	300.0000	150.0000	30.0000	3.0000	100.0000
G114	0-1	50.0000	15.0000	500.0000	15.0000	15.0000	500.0000	150.0000	20.0000	3.0000	100.0000
G115	4-5	50.0000	15.0000	500.0000	15.0000	15.0000	500.0000	150.0000	30.0000	3.0000	70.0000
G115	4-5	50.0000	20.0000	500.0000	15.0000	15.0000	500.0000	150.0000	30.0000	3.0000	100.0000
G116	0-5	50.0000	20.0000	500.0000	15.0000	15.0000	300.0000	150.0000	30.0000	3.0000	100.0000
G117	0-1	70.0000	20.0000	500.0000	15.0000	15.0000	500.0000	200.0000	30.0000	3.0000	70.0000
G118	6-11	50.0000	15.0000	700.0000	15.0000	15.0000	300.0000	150.0000	30.0000	3.0000	70.0000
G119	0-5	70.0000	20.0000	700.0000	15.0000	20.0000	500.0000	200.0000	30.0000	3.0000	70.0000
G120	4-5	70.0000	20.0000	700.0000	20.0000	20.0000	700.0000	200.0000	30.0000	5.0000	70.0000
G120	4-5	50.0000	15.0000	700.0000	15.0000	15.0000	500.0000	150.0000	30.0000	3.0000	100.0000
G121	0-5	70.0000	20.0000	700.0000	15.0000	15.0000	500.0000	200.0000	30.0000	3.0000	70.0000
V002	0-3	7.0000	15.0000	500.0000	15.0000	10.0000	200.0000	70.0000	15.0000	2.0000	70.0000
V003	0-3	7.0000	15.0000	300.0000	15.0000	10.0000	200.0000	70.0000	20.0000	2.0000	70.0000
V006	0-3	7.0000	10.0000	300.0000	15.0000	7.0000	200.0000	70.0000	20.0000	2.0000	70.0000
V007	0-3	15.0000	15.0000	300.0000	15.0000	10.0000	300.0000	100.0000	15.0000	2.0000	70.0000
V007	0-3	20.0000	15.0000	300.0000	20.0000	10.0000	300.0000	70.0000	20.0000	3.0000	100.0000
V009	0-3	7.0000	15.0000	500.0000	50.0000	7.0000	200.0000	70.0000	15.0000	1.5000	70.0000
V011	0-3	15.0000	15.0000	300.0000	30.0000	10.0000	500.0000	100.0000	20.0000	3.0000	150.0000
V012	0-3	10.0000	10.0000	300.0000	30.0000	10.0000	300.0000	100.0000	15.0000	1.5000	70.0000
V014	0-3	15.0000	15.0000	500.0000	20.0000	15.0000	300.0000	100.0000	20.0000	2.0000	100.0000
V014	0-3	15.0000	15.0000	300.0000	30.0000	10.0000	300.0000	70.0000	15.0000	2.0000	100.0000
V015	0-3	15.0000	15.0000	500.0000	50.0000	15.0000	300.0000	150.0000	20.0000	3.0000	70.0000
V017	0-3	20.0000	20.0000	500.0000	150.0000	15.0000	300.0000	100.0000	15.0000	2.0000	150.0000
V018	0-3	15.0000	15.0000	300.0000	50.0000	15.0000	300.0000	150.0000	20.0000	3.0000	70.0000
V018	0-3	15.0000	15.0000	500.0000	30.0000	15.0000	300.0000	150.0000	15.0000	1.5000	100.0000
V021	0-3	15.0000	15.0000	300.0000	30.0000	10.0000	300.0000	100.0000	20.0000	2.0000	100.0000
V021	0-3	100.0000	20.0000	700.0000	70.0000	30.0000	500.0000	200.0000	20.0000	3.0000	70.0000
V028	0-3	15.0000	15.0000	300.0000	30.0000	10.0000	300.0000	100.0000	20.0000	2.0000	100.0000
F003	3-8	70.0000	20.0000	700.0000	15.0000	20.0000	500.0000	200.0000	30.0000	3.0000	100.0000
P005	0-5	50.0000	15.0000	500.0000	20.0000	15.0000	500.0000	150.0000	30.0000	3.0000	70.0000
P005	0-5	50.0000	15.0000	500.0000	15.0000	15.0000	300.0000	150.0000	30.0000	3.0000	70.0000
P006	6-	50.0000	20.0000	500.0000	20.0000	15.0000	500.0000	150.0000	30.0000	3.0000	100.0000
P007	5-0	30.0000	15.0000	500.0000	30.0000	15.0000	500.0000	150.0000	20.0000	3.0000	100.0000
P008	3-6	50.0000	20.0000	500.0000	30.0000	15.0000	200.0000	200.0000	30.0000	3.0000	70.0000

Table 8 (Continued), Cruise S4-76

CORE	INTERVAL (cm)	31		32		CORE	INTERVAL (cm)	31		32	
		Th	ppm-n	U	ppm-n			Th	ppm-n	U	ppm-n
G002	15-20	1.9400	1.5300			G064	4-5	3.3600	2.0500		
G005	0-5	3.5900	1.4600			G065	10-15	1.9400	2.3500		
G006	3-4	5.1000	1.2800			G066	4-5	1.9400	2.6100		
G008	7-15	1.9400	1.8800			G067	5-10	3.9400	1.6600		
G009	4-5	1.9400	1.9200			G069	cc	3.6500	1.6800		
G010	0-5	1.9400	2.2200			G070	0-1	6.6500	2.9100		
G011	13-18	1.9400	1.9700			G071	2-7	7.7300	3.9400		
G012	4-5	3.2300	1.6200			G075	6-10	5.7600	1.6400		
G013	14-19	5.7800	1.9400			G075	6-10	4.3600	1.9200		
G014	4-5	5.7000	2.1600			G077	0-5	5.6700	2.0800		
G015	4-5	5.1700	2.3700			G080	0-5	1.9400	2.5200		
G016	7-9	1.9400	2.6400			G090	2-4	4.5400	2.6000		
G018	4-5	4.9000	2.5900			G091	0-1	4.9000	2.0900		
G018	4-5	3.7800	2.6900			G105	10-15	7.1300	3.4000		
G019	0-3	1.9400	2.2600			G107	0-5	6.9900	2.8200		
G020	6-11	4.9400	2.0900			G109	3-8	4.3000	1.9000		
G021	4-5	5.8100	2.1900			G110	4-5	5.4600	1.8100		
G021	4-5	5.4700	2.1600			G111	1-5	4.6600	2.0900		
G027	14-19	1.9400	2.8700			G112	4-5	1.9400	2.0900		
G028	cc	4.1700	1.7700			G112	4-5	1.9400	1.9800		
G029	4-5	4.7300	2.0900			G113	3-8	3.9400	1.8800		
G029	4-5	3.9200	2.0300			G114	0-1	1.9400	2.1000		
G032	6-11	3.7500	2.2500			G115	4-5	1.9400	2.1300		
G033	8-13	3.8700	2.2100			G115	4-5	1.9400	2.3500		
G034	4-5	5.2600	1.8100			G116	0-5	5.2500	2.0100		
G034	4-5	1.9400	2.0800			G117	0-1	1.9400	1.9900		
G036	2-7	4.5800	1.5700			G118	6-11	1.9400	2.4200		
G041	6-11	1.9400	2.2600			G119	0-5	1.9400	2.1900		
G042	0-1	5.2700	2.0700			G120	4-5	1.9400	2.7000		
G043	0-6	5.5200	3.2900			G120	4-5	1.9400	2.5700		
G046	11-16	6.4300	2.4500			G121	0-5	1.9400	1.6000		
G047	4-5	1.9400	3.0200			V002	0-3	3.6600	1.7600		
G048	0-8	4.4900	2.4000			V003	0-3	2.7700	1.5100		
G049	0-5	1.9400	2.7700			V006	0-3	4.9700	1.4700		
G049	0-5	1.9400	2.4200			V007	0-3	1.9400	1.7900		
G050	0-1	1.9400	2.9000			V007	0-3	3.7600	1.6500		
G050	0-1	1.9400	2.7300			V009	0-3	3.8300	1.3300		
G051	6-11	1.9400	2.5800			V011	0-3	4.8100	1.6700		
G052	9-13	1.9400	2.2600			V012	0-3	2.8700	1.5200		
G053	0-1	5.1800	1.8900			V014	0-3	4.5100	1.4200		
G054	0-3	1.9400	2.3700			V014	0-3	3.5700	1.4300		
G055	4-5	4.4100	2.2200			V015	0-3	4.4600	1.4200		
G055	4-5	1.9400	2.4700			V017	0-3	4.4400	1.4300		
G056	0-4	1.9400	2.1200			V018	0-3	3.6400	1.7400		
G057	0-5	4.5000	1.7600			V018	0-3	4.2300	1.5900		
G059	0-2	1.9400	2.4000			Y021	0-3	2.8600	1.6900		
G060	0-2	1.9400	3.6200			Y028	0-3	1.9400	1.2100		
G061	4-5	4.8800	2.5900			P003	3-8	6.1600	2.2200		
G062	0-5	1.9400	2.6500			P005	0-5	1.9400	2.6600		
G063	15-20	1.9400	2.1600			P005	0-5	1.9400	3.0300		
						P006	6-	1.9400	2.3500		
						P007	5-0	1.9400	2.3200		
						P008	3-8	6.3700	3.8100		

Table 8 (Continued), Cruise S6-77.

S6-77 data, seawater corrected											
CORE	INTERVAL (cm)	S6-77 data, seawater corrected									
		Si X-xf	Al X-xf	Ca X-xf	K X-xf	Fe X-xf	Ti X-xf	X S-swc	X Mg-swc	X Na-swc	Hg ppm-a
V05	0-4	24.7743	6.8802	3.7164	0.8302	6.9943	0.8393	0.0861	2.8748	2.5240	0.0400
V06	0-4	24.3069	7.9387	4.0737	0.7471	5.3856	0.7194	0.1674	1.8529	2.9218	0.0400
V06	0-4	24.3069	7.4095	4.0023	0.7471	5.2457	0.7194	0.1674	1.8649	2.9960	0.0100
V07	0-4	24.7743	7.9387	4.2882	0.8302	5.3156	0.6595	0.0861	2.0907	2.8949	0.0300
G07	0-1	33.6557	5.1337	1.5723	1.0792	1.8884	0.2998	0.0768	0.8410	2.0701	0.0400
G12	11-12	28.5138	6.8802	1.3579	1.5773	3.5670	0.4196	0.1767	1.4501	2.0330	0.0800
G12	11-12	28.9813	7.4095	1.2864	1.6603	3.5670	0.4796	0.1767	1.5285	1.9588	0.0900
G14	0-5	26.6441	5.8217	2.7158	0.7471	3.6370	0.4196	0.1559	1.4146	2.3417	0.0100
G16	0-5	26.1766	6.3510	3.0017	0.9132	4.0566	0.4796	0.3116	1.5433	2.7060	0.0400
G19	0-5	26.6441	6.3510	3.0017	0.7471	4.0566	0.4796	0.1163	1.5801	2.5323	0.0100
G20	0-5	29.4487	3.9164	1.5008	0.7471	2.3081	0.2998	0.1140	0.9804	2.3467	0.0400
G22	0-5	29.4487	3.7576	1.5008	0.7471	2.1682	0.2998	0.0489	0.8685	1.9589	0.0100
G23	0-5	30.3836	2.9638	1.3579	0.5811	1.8185	0.2398	0.0372	0.8450	2.8138	0.0100L
G24	0-5	28.5138	3.1755	1.1435	0.7471	1.9584	0.2398	-0.0953	0.9187	2.2489	0.0800
G25	0-10	30.3836	3.9693	1.3579	0.8302	2.0982	0.2998	0.2930	1.0762	3.2522	0.1200
G25	0-10	28.5138	3.9164	1.2864	0.7471	2.0283	0.2398	0.0605	0.9750	2.6874	0.0400
G26	0-5	27.1115	5.2925	2.1441	0.9132	3.2873	0.4196	0.1745	1.3992	2.3890	0.1000
G29	0-5	28.0464	4.3398	1.2864	0.8302	2.4480	0.2998	0.3884	1.1358	2.7582	0.0300
CORE	INTERVAL (cm)	S6-77 data, seawater corrected									
		Li ppm-a	Rb ppm-a	Zn ppm-a	As ppm-x	Ge ppm-x	Sn ppm-x	B ppm-s	Ba ppm-s	Co ppm-s	Cr ppm-x
V05	0-4	6.0000	15.0000	135.0000	14.0000	1.6000	0.7000	20.0000	300.0000	30.0000	50.0000
V06	0-4	6.0000	15.0000	0.0000B	0.0000B	0.0000B	0.0000B	20.0000	500.0000	30.0000	20.0000
V06	0-4	5.0000	15.0000	107.0000	4.6000	1.2000	0.6000	20.0000	500.0000	30.0000	15.0000
V07	0-4	5.0000L	15.0000	102.0000	86.0000	0.2000L	0.3000	15.0000	500.0000	30.0000	30.0000
G07	0-1	7.0000	25.0000	56.0000	4.9000	1.5000	1.3000	30.0000	700.0000	15.0000	70.0000
G12	11-12	20.0000	40.0000	121.0000	4.8000	0.6000	1.0000	70.0000	700.0000	20.0000	100.0000
G12	11-12	21.0000	40.0000	126.0000	9.0000	1.3000	0.8000	70.0000	700.0000	20.0000	70.0000
G14	0-5	7.0000	15.0000	101.0000	0.0000B	0.0000B	0.0000B	70.0000	500.0000	20.0000	30.0000
G16	0-5	8.0000	15.0000	119.0000	5.2000	1.0000	1.1000	70.0000	500.0000	30.0000	30.0000
G19	0-5	7.0000	15.0000	110.0000	3.4000	1.0000	0.5000	70.0000	700.0000	30.0000	30.0000
G20	0-5	8.0000	15.0000	95.0000	0.0000B	0.0000B	0.0000B	150.0000	1000.0000	15.0000	30.0000
G22	0-5	7.0000	15.0000	88.0000	0.0000B	0.0000B	0.0000B	150.0000	1000.0000	15.0000	30.0000
G23	0-5	6.0000	10.0000	0.0000B	0.0000B	0.0000B	0.0000B	150.0000	1500.0000	15.0000	30.0000
G24	0-5	8.0000	15.0000	89.0000	0.0000B	0.0000B	0.0000B	150.0000	1500.0000	15.0000	30.0000
G25	0-10	7.0000	15.0000	83.0000	0.0000B	0.0000B	0.0000B	150.0000	700.0000	15.0000	30.0000
G25	0-10	8.0000	15.0000	84.0000	0.0000B	0.0000B	0.0000B	150.0000	700.0000	15.0000	30.0000
G26	0-5	10.0000	20.0000	105.0000	0.0000B	0.0000B	0.0000B	70.0000	700.0000	15.0000	50.0000
G29	0-5	10.0000	20.0000	99.0000	0.0000B	0.0000B	0.0000B	150.0000	700.0000	15.0000	50.0000

Table 8 (Continued), Cruise S6-77

S6-77 data, seawater corrected-continued

CORE	INTERVAL (cm)	Cu ppm-s	Ga ppm-s	Mn ppm-s	Ni ppm-s	Sc ppm-s	Sr ppm-s	V ppm-s	Y ppm-s	Yb ppm-s	Zr ppm-s
V05	0-4	20.0000	50.0000	700.0000	30.0000	30.0000	300.0000	300.0000	50.0000	5.0000	150.0000
V06	0-4	70.0000	30.0000	1500.0000	15.0000	30.0000	700.0000	300.0000	50.0000	5.0000	150.0000
V06	0-4	70.0000	30.0000	1500.0000	15.0000	30.0000	700.0000	150.0000	50.0000	5.0000	150.0000
V07	0-4	70.0000	30.0000	1500.0000	15.0000	70.0000	700.0000	300.0000	70.0000	5.0000	150.0000
G07	0-1	15.0000	20.0000	300.0000	30.0000	30.0000	300.0000	150.0000	30.0000	3.0000	200.0000
G12	11-12	70.0000	30.0000	500.0000	70.0000	30.0000	300.0000	300.0000	30.0000	3.0000	150.0000
G12	11-12	70.0000	30.0000	700.0000	70.0000	30.0000	300.0000	150.0000	30.0000	3.0000	150.0000
G14	0-5	100.0000	30.0000	700.0000	50.0000	30.0000	300.0000	200.0000	30.0000	3.0000	100.0000
G16	0-5	150.0000	30.0000	700.0000	30.0000	30.0000	300.0000	200.0000	30.0000	3.0000	150.0000
G19	0-5	150.0000	30.0000	700.0000	30.0000	30.0000	500.0000	150.0000	30.0000	3.0000	100.0000
G20	0-5	100.0000	10.0000	300.0000	50.0000	30.0000	300.0000	150.0000	30.0000	3.0000	100.0000
G22	0-5	100.0000	15.0000	300.0000	30.0000	15.0000	300.0000	150.0000	15.0000	2.0000	70.0000
G23	0-5	70.0000	15.0000	300.0000	30.0000	15.0000	200.0000	70.0000	15.0000	1.5000	70.0000
G24	0-5	100.0000	15.0000	300.0000	50.0000	20.0000	300.0000	100.0000	20.0000	2.0000	70.0000
G25	0-10	70.0000	15.0000	500.0000	30.0000	20.0000	300.0000	150.0000	20.0000	3.0000	70.0000
G25	0-10	70.0000	20.0000	300.0000	30.0000	15.0000	300.0000	150.0000	20.0000	2.0000	150.0000
G26	0-5	100.0000	30.0000	700.0000	30.0000	30.0000	300.0000	150.0000	30.0000	3.0000	100.0000
G29	0-5	70.0000	20.0000	300.0000	30.0000	20.0000	300.0000	150.0000	30.0000	3.0000	100.0000

Table 8 (Continued)

s4-76 Misc. Seds, Pribilof Isl

CORE	INTERVAL (cm)	1		2		3		4		5		6		7		8		9		10	
		Ca % - s	K % - s	Fe % - s	Ti % - s	Hg % - s	Na % - s	R ppm-s	Ba ppm-s	Co ppm-s	Cr ppm-s										
G030	1-6	3.0000	3.0000	5.0000	0.3000	1.5000	2.0000	30.0000	700.0000	10.0000	70.0000										
G031	4-5	3.0000	2.0000	5.0000	0.3000	1.5000	3.0000	30.0000	700.0000	10.0000	70.0000										
G037	2-7	3.0000	3.0000	3.0000	0.5000	1.0000	2.0000	20.0000	1000.0000	7.0000	50.0000										
G037	2-7	3.0000	2.0000	3.0000	0.3000	1.5000	3.0000	30.0000	700.0000	7.0000	50.0000										
G038	0-5	3.0000	2.0000	5.0000	0.3000	1.5000	3.0000	30.0000	700.0000	10.0000	30.0000										
G039	0-5	3.0000	3.0000	5.0000	0.3000	1.5000	3.0000	30.0000	700.0000	10.0000	100.0000										
G040	6-10	3.0000	3.0000	3.0000	0.3000	1.5000	3.0000	30.0000	1000.0000	7.0000	50.0000										
G040	6-10	3.0000	3.0000	3.0000	0.3000	1.5000	3.0000	30.0000	700.0000	10.0000	50.0000										
G072	4-5	5.0000	3.0000	5.0000	0.5000	2.0000	3.0000	30.0000	700.0000	15.0000	100.0000										
G072	4-5	3.0000	2.0000	5.0000	0.3000	2.0000	2.0000	50.0000	500.0000	15.0000	70.0000										
G078	0-1	3.0000	2.0000	3.0000	0.3000	1.5000	3.0000	30.0000	700.0000	10.0000	70.0000										
G079	0-5	3.0000	3.0000	3.0000	0.3000	1.5000	3.0000	30.0000	700.0000	10.0000	70.0000										
G081	30-35	5.0000	3.0000	5.0000	0.5000	2.0000	5.0000	70.0000	700.0000	10.0000	70.0000										
G082	20-25	5.0000	3.0000	5.0000	0.5000	1.5000	3.0000	50.0000	1000.0000	10.0000	70.0000										
G089	0-3	5.0000	2.0000	5.0000	0.5000	2.0000	3.0000	30.0000	700.0000	15.0000	100.0000										
G094	cc	5.0000	2.0000	7.0000	0.7000	5.0000	2.0000	30.0000	500.0000	30.0000	150.0000										
G103	2-7	5.0000	3.0000	7.0000	0.5000	2.0000	2.0000	70.0000	700.0000	15.0000	100.0000										
V004	0-3	3.0000	2.0000	3.0000	0.3000	1.0000	3.0000	50.0000	700.0000	7.0000	70.0000										
V005	0-3	3.0000	2.0000	3.0000	0.3000	1.5000	3.0000	30.0000	500.0000	7.0000	150.0000										
V010	0-3	3.0000	2.0000	3.0000	0.2000	3.0000	2.0000	30.0000	500.0000	15.0000	70.0000										
V019	0-3	5.0000	2.0000	3.0000	0.3000	1.5000	3.0000	30.0000	700.0000	10.0000	70.0000										
V020	0-3	5.0000	3.0000	3.0000	0.5000	2.0000	3.0000	30.0000	700.0000	10.0000	100.0000										
V022	0-3	3.0000	2.0000	3.0000	0.3000	1.5000	3.0000	50.0000	500.0000	10.0000	70.0000										
V022	0-3	3.0000	3.0000	5.0000	0.3000	2.0000	3.0000	50.0000	700.0000	10.0000	100.0000										
V023	0-3	3.0000	3.0000	3.0000	0.3000	2.0000	3.0000	30.0000	700.0000	10.0000	70.0000										
V023	0-3	5.0000	2.0000	5.0000	0.5000	1.5000	2.0000	30.0000	1000.0000	10.0000	70.0000										
V025	0-3	5.0000	3.0000	7.0000	0.5000	2.0000	3.0000	50.0000	700.0000	15.0000	100.0000										
P010	107-109	3.0000	2.0000	5.0000	0.3000	1.5000	5.0000	100.0000	1000.0000	10.0000	50.0000										
P013	25-27	5.0000	2.0000	5.0000	0.3000	1.5000	7.0000	100.0000	1000.0000	7.0000	30.0000										

CORE	INTERVAL (cm)	11		12		13		14		15		16		17		18		19	
		Cu ppm-s	Ga ppm-s	Mn ppm-s	Sc ppm-s	Sr ppm-s	V ppm-s	Y ppm-s	Yb ppm-s	Zr ppm-s									
G030	1-6	15.0000	15.0000	30.0000	15.0000	500.0000	100.0000	20.0000	3.0000	200.0000									
G031	4-5	20.0000	15.0000	30.0000	15.0000	500.0000	100.0000	30.0000	3.0000	150.0000									
G037	2-7	15.0000	15.0000	20.0000	10.0000	500.0000	100.0000	20.0000	3.0000	70.0000									
G037	2-7	15.0000	15.0000	15.0000	10.0000	300.0000	70.0000	20.0000	2.0000	100.0000									
G038	0-5	20.0000	15.0000	20.0000	15.0000	300.0000	100.0000	20.0000	3.0000	100.0000									
G039	0-5	30.0000	15.0000	30.0000	15.0000	500.0000	150.0000	30.0000	3.0000	100.0000									
G040	6-10	15.0000	15.0000	20.0000	15.0000	500.0000	100.0000	20.0000	3.0000	150.0000									
G040	6-10	20.0000	15.0000	20.0000	10.0000	300.0000	70.0000	20.0000	3.0000	70.0000									
G072	4-5	50.0000	20.0000	50.0000	15.0000	500.0000	150.0000	30.0000	3.0000	150.0000									
G072	4-5	50.0000	15.0000	50.0000	15.0000	300.0000	150.0000	30.0000	3.0000	100.0000									
G078	0-1	15.0000	15.0000	20.0000	15.0000	300.0000	70.0000	30.0000	3.0000	150.0000									
G079	0-5	15.0000	20.0000	20.0000	15.0000	500.0000	70.0000	30.0000	3.0000	150.0000									
G081	30-35	30.0000	15.0000	30.0000	15.0000	500.0000	150.0000	30.0000	3.0000	300.0000									
G082	20-25	30.0000	15.0000	30.0000	15.0000	500.0000	150.0000	20.0000	3.0000	100.0000									
G089	0-3	20.0000	20.0000	50.0000	15.0000	500.0000	150.0000	30.0000	3.0000	200.0000									
G094	cc	70.0000	20.0000	100.0000	20.0000	500.0000	200.0000	30.0000	3.0000	150.0000									
G103	2-7	20.0000	15.0000	50.0000	15.0000	500.0000	150.0000	30.0000	3.0000	70.0000									
V004	0-3	10.0000	15.0000	15.0000	10.0000	500.0000	70.0000	20.0000	2.0000	100.0000									
V005	0-3	15.0000	15.0000	20.0000	10.0000	300.0000	70.0000	15.0000	2.0000	100.0000									
V010	0-3	10.0000	10.0000	70.0000	7.0000	300.0000	70.0000	20.0000	2.0000	70.0000									
V019	0-3	15.0000	15.0000	30.0000	15.0000	300.0000	70.0000	20.0000	3.0000	100.0000									
V020	0-3	15.0000	15.0000	30.0000	15.0000	500.0000	100.0000	30.0000	3.0000	70.0000									
V022	0-3	20.0000	15.0000	30.0000	10.0000	300.0000	70.0000	20.0000	3.0000	150.0000									
V022	0-3	15.0000	20.0000	30.0000	15.0000	500.0000	100.0000	30.0000	3.0000	70.0000									
V023	0-3	15.0000	15.0000	30.0000	15.0000	500.0000	70.0000	20.0000	3.0000	70.0000									
V023	0-3	15.0000	15.0000	30.0000	15.0000	500.0000	150.0000	20.0000	3.0000	70.0000									
V025	0-3	20.0000	15.0000	50.0000	15.0000	500.0000	200.0000	30.0000	3.0000	100.0000									
P010	107-109	70.0000	20.0000	30.0000	15.0000	500.0000	150.0000	20.0000	3.0000	70.0000									
P013	25-27	100.0000	20.0000	30.0000	15.0000	300.0000	100.0000	20.0000	3.0000	50.0000									

Table 8 cruise s4-76
(semiquant. emission
spectroscopy only)

(including 18 analytical duplicates) are given in Table 9. Skewness and kurtosis statistics, histograms of raw and log-transformed data, chi-square tests, analysis of variance, and correlation analysis indicate that the frequency distributions for most of the 31 elements listed in Table 9 are more closely approximated by a lognormal than a normal distribution. Consequently, all statistical analyses are based on log-transformed data.

Estimates of the central and expected ranges of concentrations of a particular element in outer continental shelf sediments from the southern Bering Sea can be obtained using the geometric means (GM) and geometric deviations (GD) given in Table 9. The central range of a lognormal distribution is the range in which approximately 68% of the population is estimated to occur and is within the range of GM/GD to GMxGD. The expected range of a lognormal population is the range in which approximately 95% of the population is estimated to occur, and is defined as the ratio of GM/GD² to GMxGD².

A three-level, nested analysis of variance was performed on the 31 elements in 103 samples from St. George basin in order to compare the variances caused by analytical imprecision, within station variability, and regional (between-station) variability. The statistical model used was:

$$X_{ijk} = \mu + \alpha_i + \beta_{ij} + \epsilon_{ijk}$$

where X_{ijk} is the k^{th} analytical determination of the j^{th} sample from the i^{th} station, μ is the grand mean for the entire population, α_i is the difference between the grand mean and the mean for the i^{th} station, β_{ij} is the difference between the mean for the i^{th} station and the mean analysis of the j^{th} sample, and ϵ_{ijk} is the error in the k^{th} determination on the j^{th} sample from the i^{th} station. There are 51 stations ($1 \leq i \leq 51$), and a maximum of three samples per station ($1 \leq j \leq 3$), and a maximum of two replicate analyses per sample ($1 \leq k \leq 2$).

The computation of variance components at each of the three levels within the sampling design follows the techniques described by Anderson and Bancroft (1952). Results of the analysis of variance are presented in Table 10. The variance components at each level are given as percentages of the total logarithmic variance. Those variance components that are significantly different from zero at the 0.05 level of probability are marked with an asterisk (*) in Table 10.

Table 10 shows that most of the geographic variability in surface sediments from St. George basin occurs among sampling stations, with only a few elements exhibiting significant variability within stations. That is, chemical analyses of cores from the same station tend to show similar results, whereas analyses from different stations vary significantly. This indicates a component of compositional variability on a scale of greater than 50 km.

TABLE 9

Summary statistics for concentrations of major, minor, and trace elements in 103 samples or surface sediments from the St. George Basin, Outer Continental Shelf, Southern Bering Sea. N* refers to the total number of samples, out of 103, which contained measured element concentrations greater than the detection limit for that element. For subsequent statistical analyses, values less than the detection limit for a particular element were replaced by a value of 0.7 times the detection limit (e.g., the detection limit for both B and Rb is 20 ppm; values <20 ppm were replaced by $0.7 \times 20 = 14$ ppm). Analytical methods used are: (1) 6-step semiquantitative optical emission spectroscopy; (2) X-ray fluorescence; (3) Atomic Absorption Spectrophotometry; (4) Neutron Activation Analysis.

1/ values for Mg, Na, and S have been corrected for interstitial sea water containing dissolved Mg^{++} , Na^+ , and SO_4^- .

Element	Method	Observed Range	Arithmetic Mean	Standard Deviation	Coefficient of Variation (%)	(GM) Geometric Mean	(GD) Geometric Deviation	N*
Al (%)	2	3.9 - 7.9	5.6	0.79	14	5.5	1.15	103
Ca (%)	2	1.7 - 5.1	2.7	0.76	28	2.6	1.29	103
Mg (%) <u>1/</u>	3	0.66- 2.1	1.1	0.26	24	1.0	1.24	103
Fe (%)	2	1.7 - 5.6	3.2	0.96	30	3.0	1.34	103
K (%)	2	0.84- 1.9	1.2	0.15	13	1.2	1.12	103
Si (%)	2	22 - 34	29	2.8	10	29	1.10	103
Na (%) <u>1/</u>	3	1.5 - 2.6	2.1	0.26	12	2.0	1.14	103
Ti (%)	2	0.26- 0.70	0.42	0.084	20	0.41	1.21	103
B (ppm)	1	<20 - 70	37	13	34	35	1.42	102
Ba (ppm)	1	300 - 1,500	580	141	24	570	1.24	103
Co (ppm)	1	7.0 - 30	12	3.8	33	11	1.37	103
Cr (ppm)	1	15 - 200	55	29	52	50	1.57	103
Cu (ppm)	1	7.0 - 100	36	21	58	30	1.92	103
Ga (ppm)	1	10 - 30	18	3.8	22	17	1.22	103
Ge (ppm)	2							
Hg (ppm)	3	0.02- 0.11	0.044	0.016	36	0.041	1.36	103
Li (ppm)	3	13 - 48	20	5.9	30	19	1.25	103
Mn (ppm)	1	300 - 700	520	124	24	500	1.30	103
Ni (ppm)	1	10 - 150	22	16	73	20	1.51	103
Rb (ppm)	3	<20 - 90	38	11	29	35	1.40	98
Sc (ppm)	1	7.0 - 30	15	3.9	26	15	1.29	103
Sn (ppm)	2							
Sr (ppm)	1	200 - 700	370	120	33	350	1.39	103
V (ppm)	1	70 - 300	140	46	33	130	1.42	103
Y (ppm)	1	15 - 50	25	6.8	28	24	1.32	103
Yb (ppm)	1	1.5 - 5.0	2.8	0.69	24	2.8	1.28	103
Zn (ppm)	3	45 - 140	83	22	30	80	1.30	103
Zr (ppm)	1	70 - 200	94	27	29	91	1.29	103
U (ppm)	4	1.2 - 3.9	2.2	0.54	25	2.1	1.27	103
Th (ppm)	4	<2 - 7.7	3.5	1.6	46	3.2	1.59	58
S (%) <u>1/</u>	2	0.007 - 0.55	0.14	0.08	57	0.12	1.80	103

TABLE 10

Analysis of variance of surface sample chemistry, St. George Basin, outer continental shelf, southern Bering Sea. Asterick (*) indicates that a variance component is significantly different from zero at the 0.05 probability level; v is the observed variance ratio. See text for explanation.

Element	Total Logarithmic Variance	variance components as percentage of total variance			v
		Between Ship Stations	Between Samples Within Stations	Analytical Error	
Al	0.00393	82*	0	18	4.56
Ca	0.01269	88*	5	7	7.33
Mg	0.00887	97*	2*	1	32
Fe	0.01641	90*	6*	4	9.00
K	0.00292	88*	0	12	7.33
Si	0.00192	79*	0	21	3.76
Na	0.00470	93*	5*	2	13
Ti	0.00719	87*	0	13	6.69
B	0.02336	30*	11	59	0.43
Ba	0.00906	32*	29	39	0.47
Co	0.02041	71*	0	29	2.45
Cr	0.03900	54*	18	28	1.17
Cu	0.08124	90*	6*	4	9.0
Ga	0.00763	41*	46*	13	0.69
Ge					
Hg	0.01758	50*	7	43	1.00
Li	0.00919	96*	1	3	24
Mn	0.01448	58*	0	42	1.38
Ni	0.03239	59*	14	27	1.44
Rb	0.02168	49*	28*	23	0.96
Sc	0.01352	62*	0	38	1.63
Sn					
Sr	0.02053	46*	37*	17	0.85
V	0.02323	74*	4	22	2.85
Y	0.01427	52*	22	26	1.08
Yb	0.01633	42*	0	58	0.72
Zn	0.01633	82*	0	18	4.56
Zr	0.01254	16	9	75	0.19
U	0.01102	61*	33*	6	1.56
Th	0.04087	19	44*	37	0.23
S	0.03932	76*	0	24	3.17

The significant variation among stations for most elements suggests that regional baselines for these elements must be described by maps based on station means rather than by grand means for the entire region. According to Connor et al. (1972; see also Miesch, 1976), data are adequate for constructing maps when the variance among categories (stations in this study) exceeds the error variance for the category means. Because only one sample was taken at most stations and only one analysis was made for most samples, the error variance for station means is simply the sum of the variances due to analysis and the variance within stations (Table 10). The ratios of the variances among stations to the error variance are given as the variance ratio, v , in Table 10.

The variance ratio, v , is a relative measure of the adequacy of the sampling design for construction of maps. Where the ratio is large, no additional sampling is required to describe compositional differences among stations. Where the ratio is small, more sampling and (or) analytical work is required. Maps of element concentration for selected elements with values of $v > 1.0$, the minimum suggested by Connor et al. (1972), are shown in Figs. 16 through 25.

Elements that exhibit a concentration gradient decreasing from southeast to northwest, similar to the gradients observed in the volcanic components of the light and heavy mineral fractions, include Al, Ca, Mg, Fe, Na, Ti, Co, Cu, Mn, V, and Zn. Maps of concentration of Si and K exhibit an increasing concentration gradient in the same southeast to northwest direction. Maps for U, S, and Li exhibit a bull's-eye pattern centered over St. George basin, similar to the pattern exhibited by maps of total-C and grain size. Local concentrations of basaltic material contributed to the shelf from the Pribilof Islands, suggested by the distributions of heavy minerals, is further supported by relatively high concentrations of Mg, Ti, Co, Cu, Cr, Ni, and V in sediments in the vicinity of the Pribilof Islands.

A Q-mode factor analysis was used to determine regional groupings of similar sediment based on all measured composition variables, and to examine inter-relationships among variables. The data set used consisted of 50 compositional variables that include grain size, clay minerals, heavy and light minerals, and inorganic geochemistry of sediments from 30 stations. The computer program used for the Q-mode analysis was adapted from the CABFAC program of Klován and Imbrie (1971). A program option was used to scale all variables to range from zero to one so that those variables with larger means and variances would not determine the outcome. After scaling, the program normalizes the data so that the sum-of-squares of each row is unity. Rotated principal component (variance) also was used.

We found that 90% of the variance in the scaled and row-normalized data could be accounted for by only three factors. Varimax loadings for the 30 samples on each of the three factors

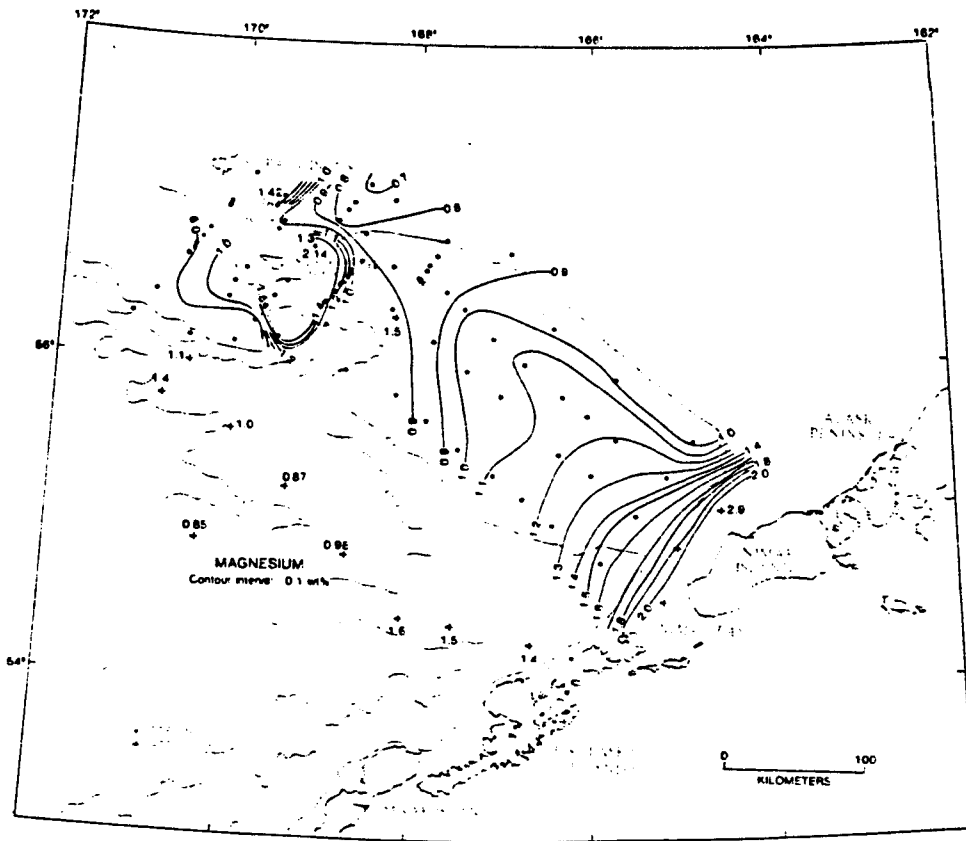


Figure 16. Distribution of magnesium (sea-water corrected) in surface sediments.

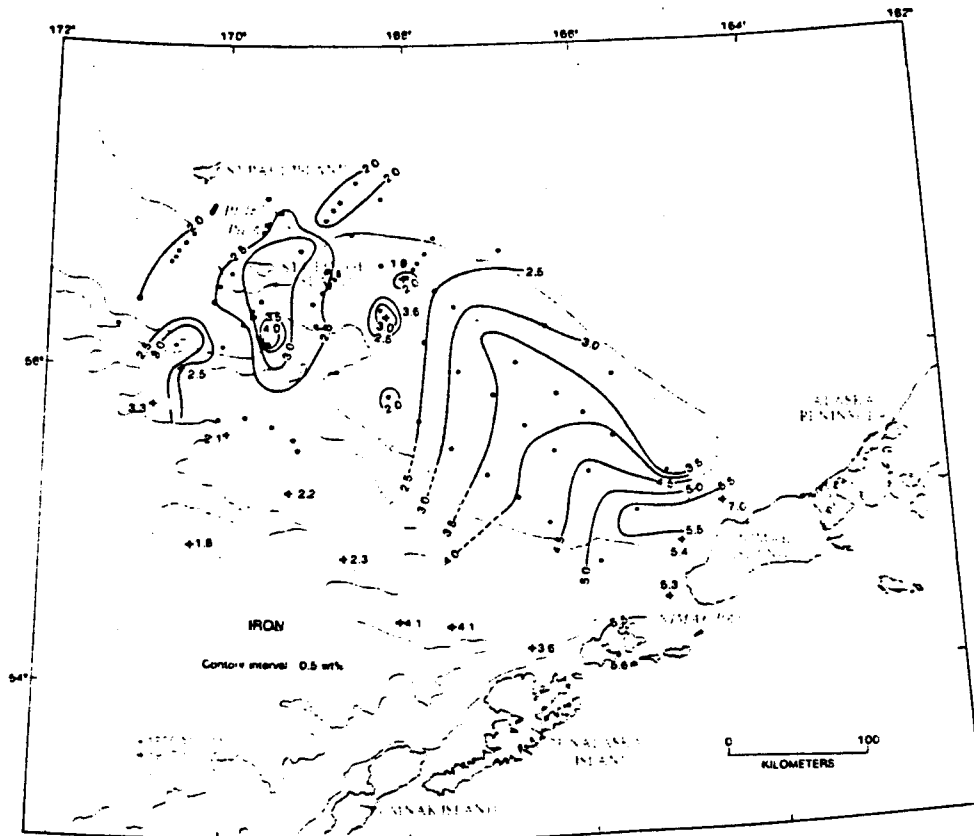


Figure 17. Distribution of iron in surface sediments.

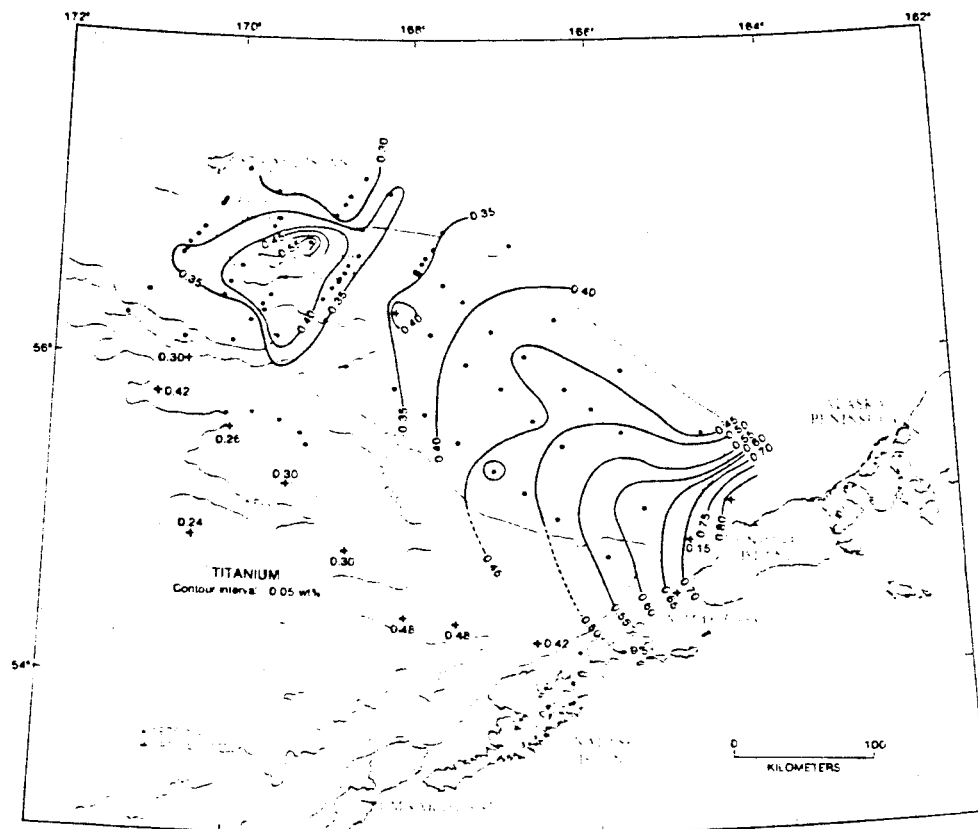


Figure 18. Distribution of titanium in surface sediments.

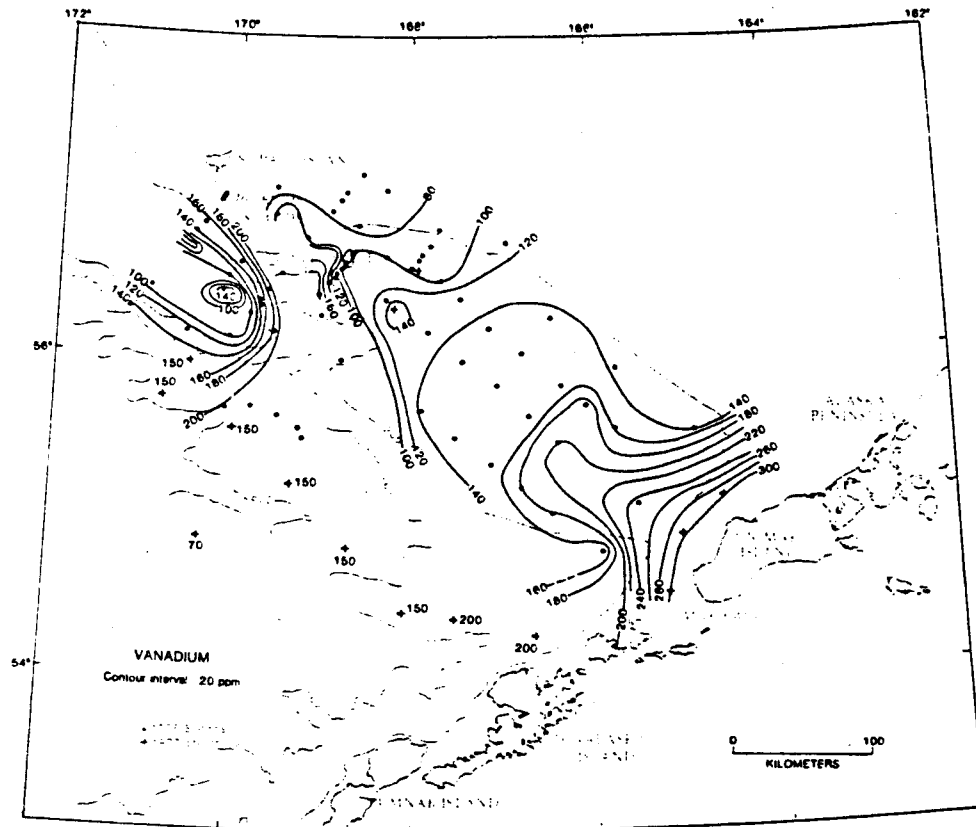


Figure 19. Distribution of vanadium in surface sediments.

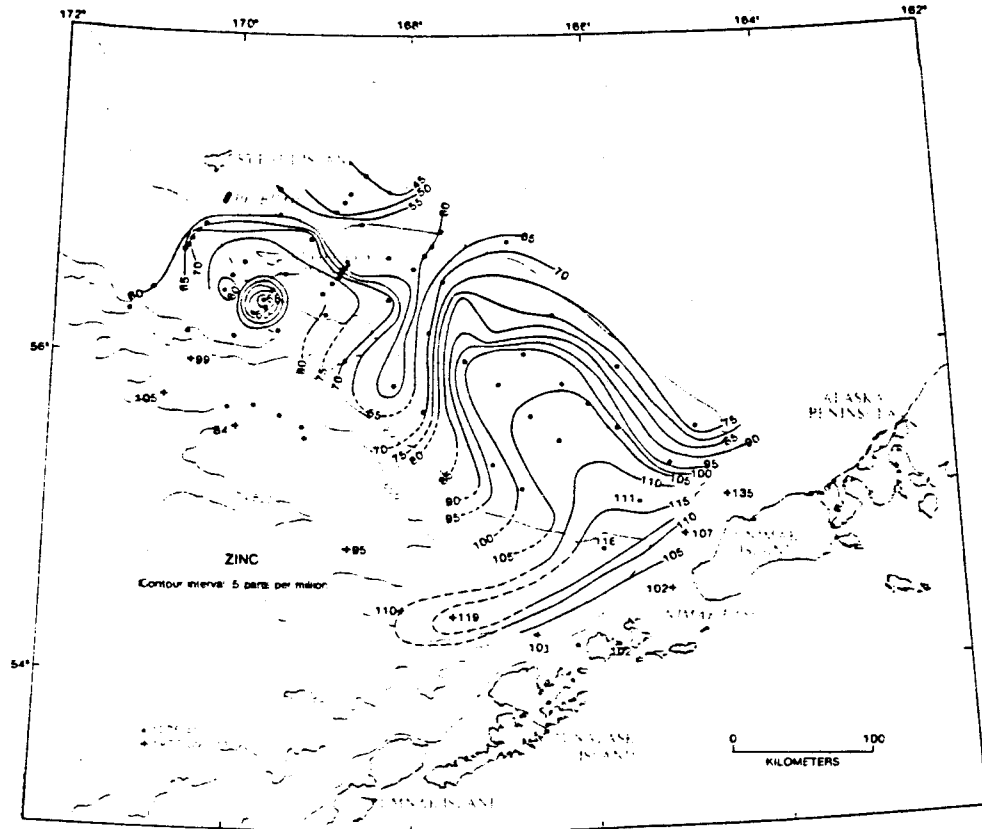


Figure 20. Distribution of zinc in surface sediments.

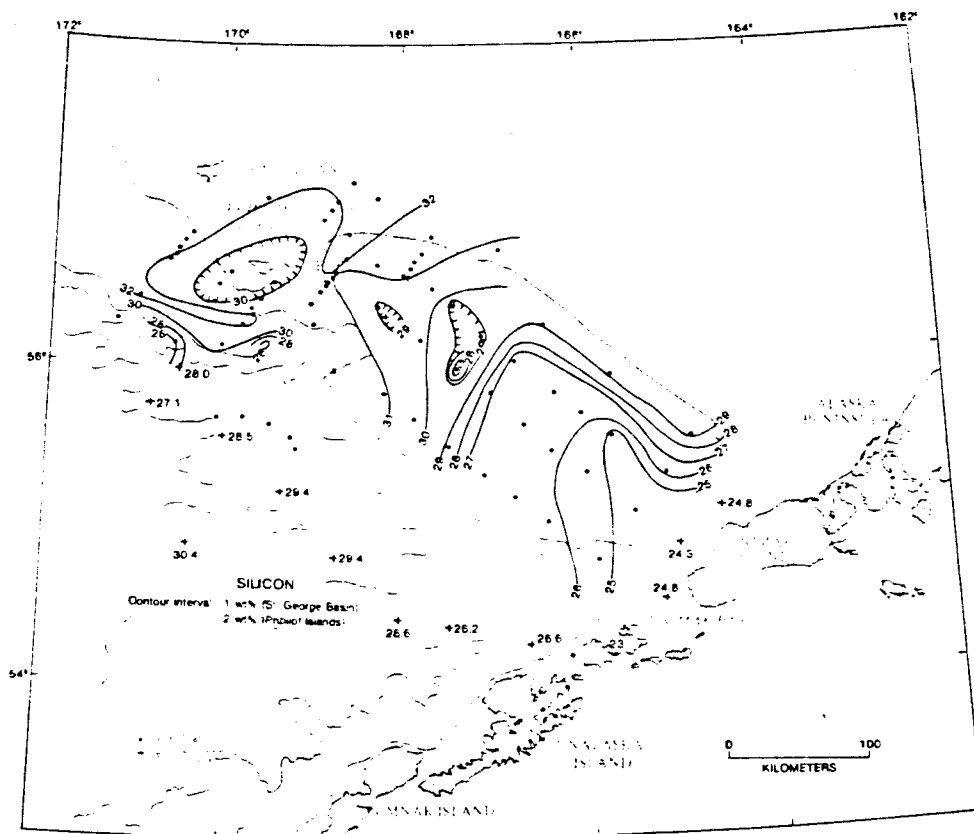


Figure 21. Distribution of silicon in surface sediments.

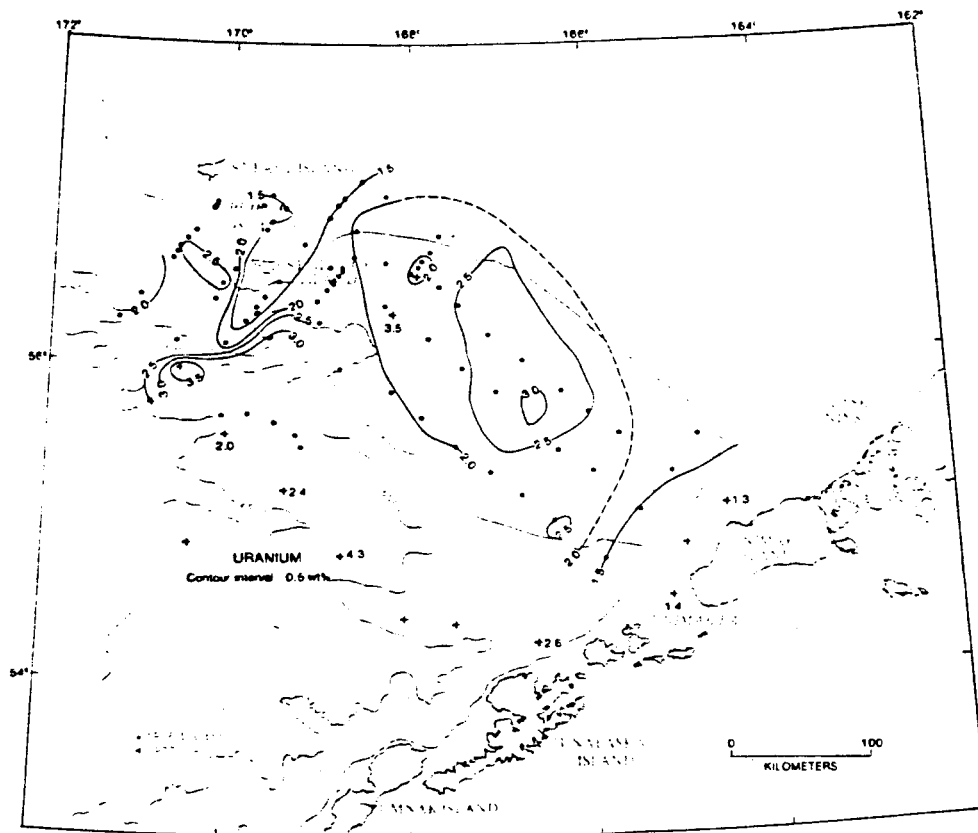


Figure 23. Distribution of uranium in surface sediments.

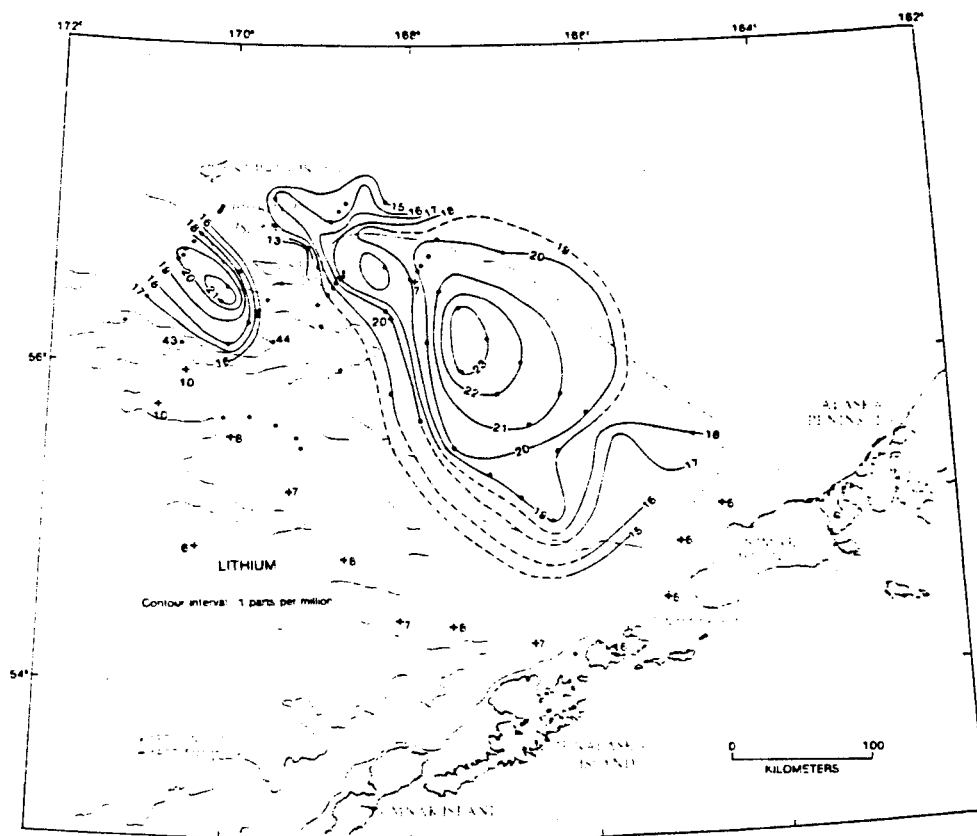


Figure 25. Distribution of lithium in surface sediments.

are listed in Table 11 and plotted in Figs. 26 through 28. These loadings can be thought of as composite compositional variables. In other words, the 50 compositional variables used as input to the Q-mode model have been reduced to 3 composite variables, each expressing some compositional attribute of the sediments based on a synthesis of a number of measured compositional variables. However, the loadings provide no indications as to which compositional variables were synthesized into which factor (composite variable). The factor loadings were treated as composite compositional variables in order to determine the relative contributions of each variable to the Q-mode model, and correlation coefficients between the loadings and the 50 observed variables were computed. Results are given in Table 12.

Table 12 indicates that loadings on factor 1 correlate positively with Na, Ca, Ti, glass, volcanic rock fragments, Sr, V, Mn, Cu, Fe, Al, smectite and vermiculite, Co, Y, Zn, Ga, clinopyroxene, and illite and kaolinite (i.e. factor 1 samples tend to be enriched in these components). Factor 1 loadings correlate negatively with Si, quartz, epidote, non-volcanic rock fragments, illite, k-feldspar, Rb, Ba, k. garnet, and orthopyroxene (i.e. factor 1 samples tend to be depleted in these components). Therefore, the compositional variables indicative of mafic volcanic material have all been synthesized into "factor 1".

Figure 26 shows that sediments with highest loadings for factor 1 occur closest to the Aleutian Islands. The distribution of sediments with high loadings for factor 1 is thus a measure of the distribution of sediments containing a relatively high input of volcanic material from the Aleutian Islands. The best "indicator" variables for Aleutian andesite are Na, Ca, Ti, glass, volcanic rock fragments, Sr, V, and Mn in roughly that order of importance.

Samples with highest loadings for factor 2 tend to have relatively high concentrations of Si, quartz, garnet, sand, epidote, orthopyroxene, metamorphic rock fragments, k-feldspar, and Ba. A map of sample loadings on factor 2 sediments (Fig. 27) indicates that these sediments occur as a "background" over most of the outer shelf, except near the Aleutian Islands where they are diluted by andesitic material. Sediment samples with high loadings on factor 2 tend to be coarser-grained, more felsic, mainland-derived materials that blanket most of Bristol Bay shelf (Sharma *et al.*, 1972). The best indicator variables for the mainland component are Si, quartz, garnet, sand, epidote, orthopyroxene, and metamorphic rock fragments in roughly that order of importance.

The distribution of sediment samples with high loadings on factor 3 (Fig. 28) reflects the distribution of finer-grained, higher-organic sediments concentrated in a bull's-eye pattern in the St. George Basin, and at the head of Pribilof Canyon south of

Table 11. Varimax factor loadings for three factors used in the Q-mode factor analysis of 50 variables in 30 samples of sediment from the outer continental shelf, southern Bering Sea.

CORE	COMM.	FACTOR 1	FACTOR 2	FACTOR 3
G11	0.9080	0.7587	0.4796	0.3201
G13	0.9008	0.5294	0.5074	0.6026
G16	0.9392	0.4767	0.5685	0.6236
G20	0.9240	0.3783	0.7593	0.4521
V03	0.8658	0.0877	0.9068	0.1894
V06	0.9359	0.0979	0.9325	0.2382
G41	0.8962	0.3859	0.6815	0.5317
G43	0.9065	0.3532	0.5077	0.7238
G46	0.8967	0.3406	0.4349	0.7691
G51	0.9267	0.6536	0.3418	0.6186
G52	0.8598	0.5680	0.3120	0.6632
G08	0.9467	0.8505	0.3004	0.3650
G05	0.9506	0.9386	0.1507	0.2166
G54	0.8910	0.7716	0.2190	0.4976
G59	0.9276	0.5470	0.3312	0.7202
G62	0.9134	0.5844	0.3052	0.6919
G63	0.9005	0.4297	0.4048	0.7430
G65	0.9308	0.3972	0.7326	0.4861
G67	0.8358	0.4346	0.7347	0.3273
V18	0.8028	0.4316	0.7473	0.2410
V12	0.8488	0.0976	0.8758	0.2687
G10	0.9443	0.3510	0.8605	0.2839
G11	0.8869	0.4319	0.7022	0.4552
G11	0.9474	0.6019	0.5320	0.5496
G10	0.7719	0.2832	0.3057	0.7735
P07	0.8830	0.3248	0.5012	0.7255
G77	0.9160	0.2168	0.7168	0.5960
G75	0.8905	0.1695	0.8172	0.4403
G71	0.8705	0.3085	0.3183	0.8210
G12	0.9116	0.8900	0.0309	0.3442
* Cumulative Variance		25.904	60.168	89.765

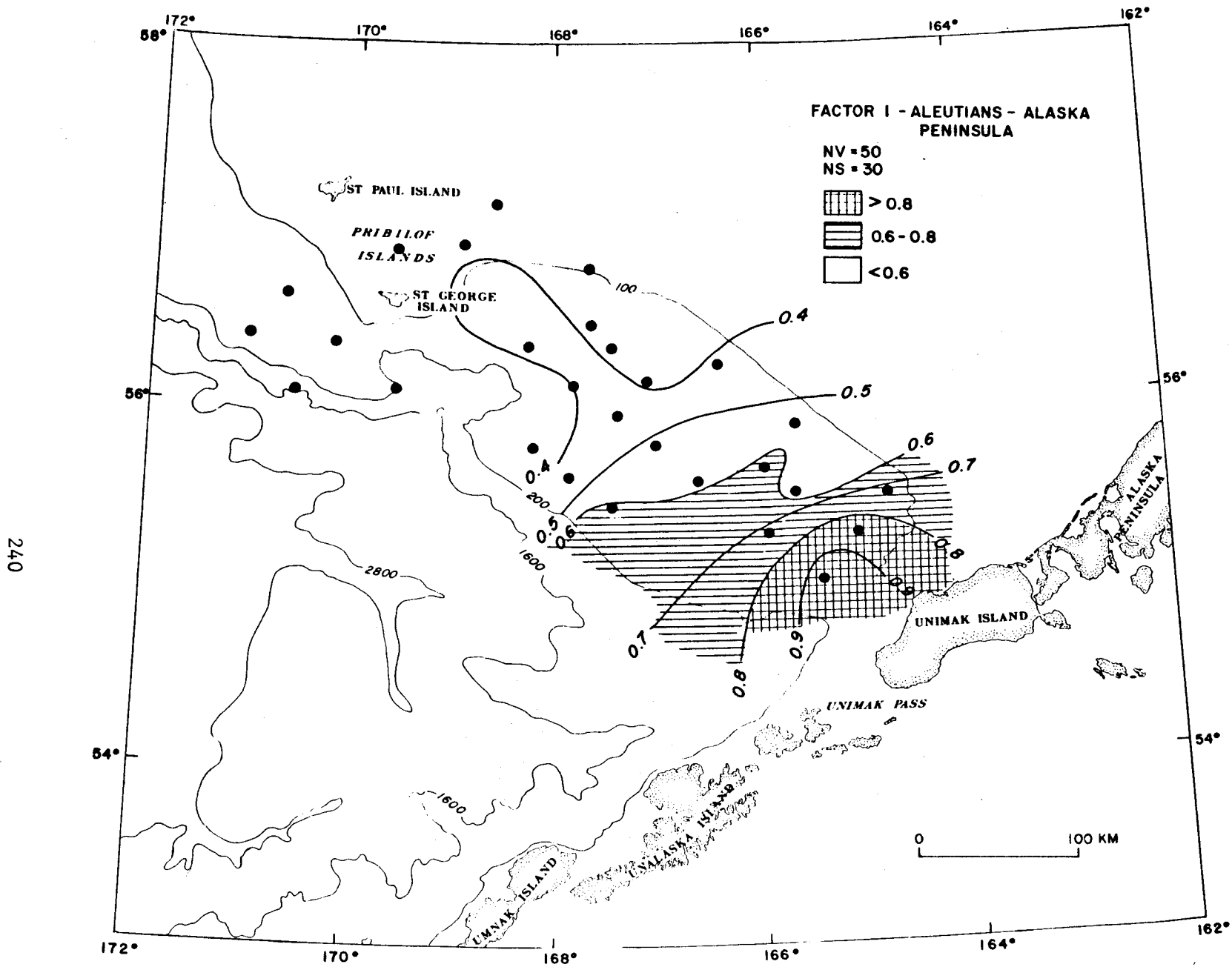


Figure 26. Map of the distribution of factor loadings for Factor I, the Aleutian-Alaska Peninsula factor.

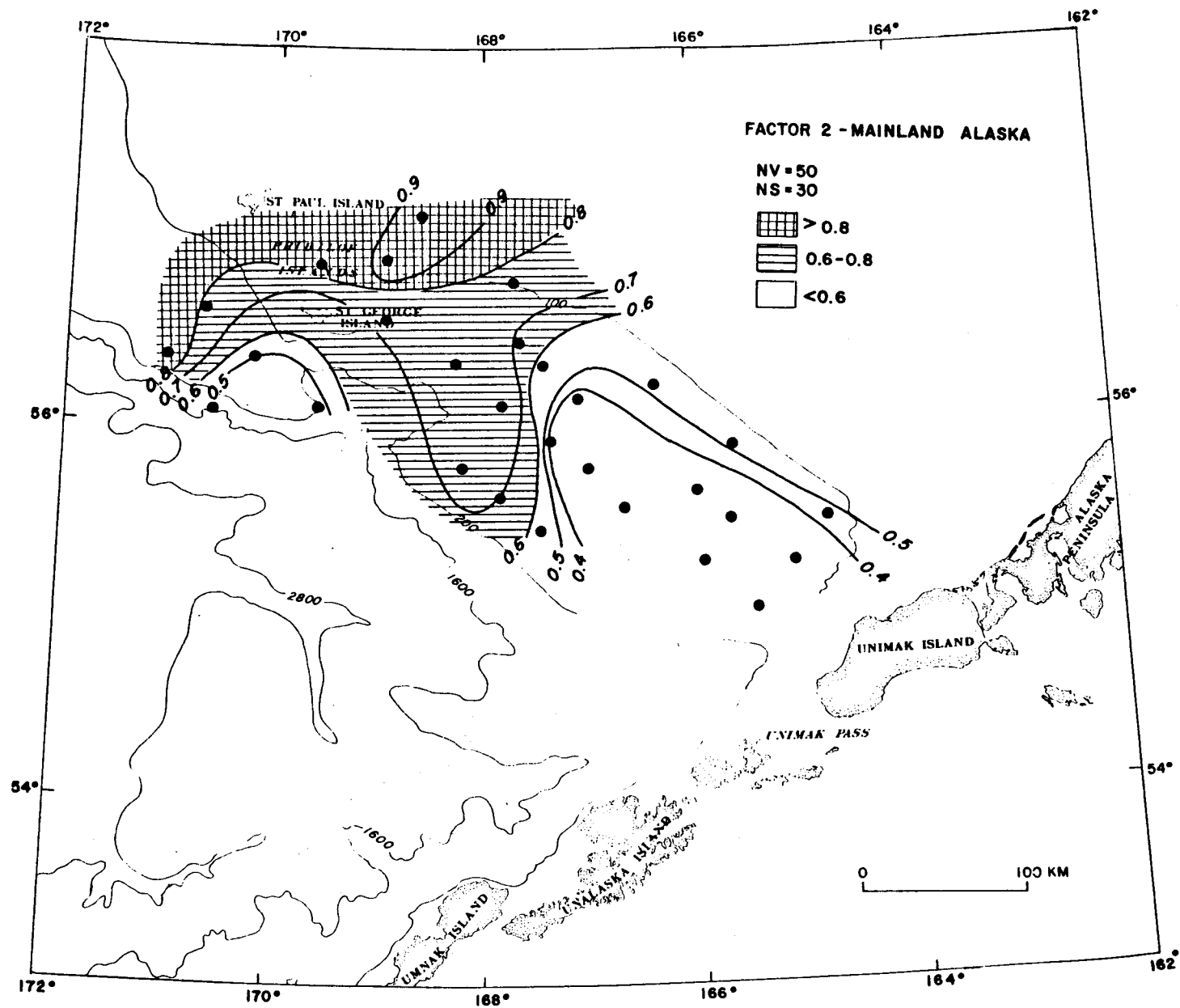


Figure 27. Map of the distribution of factor loadings for Factor II, the Alaska mainland factor.

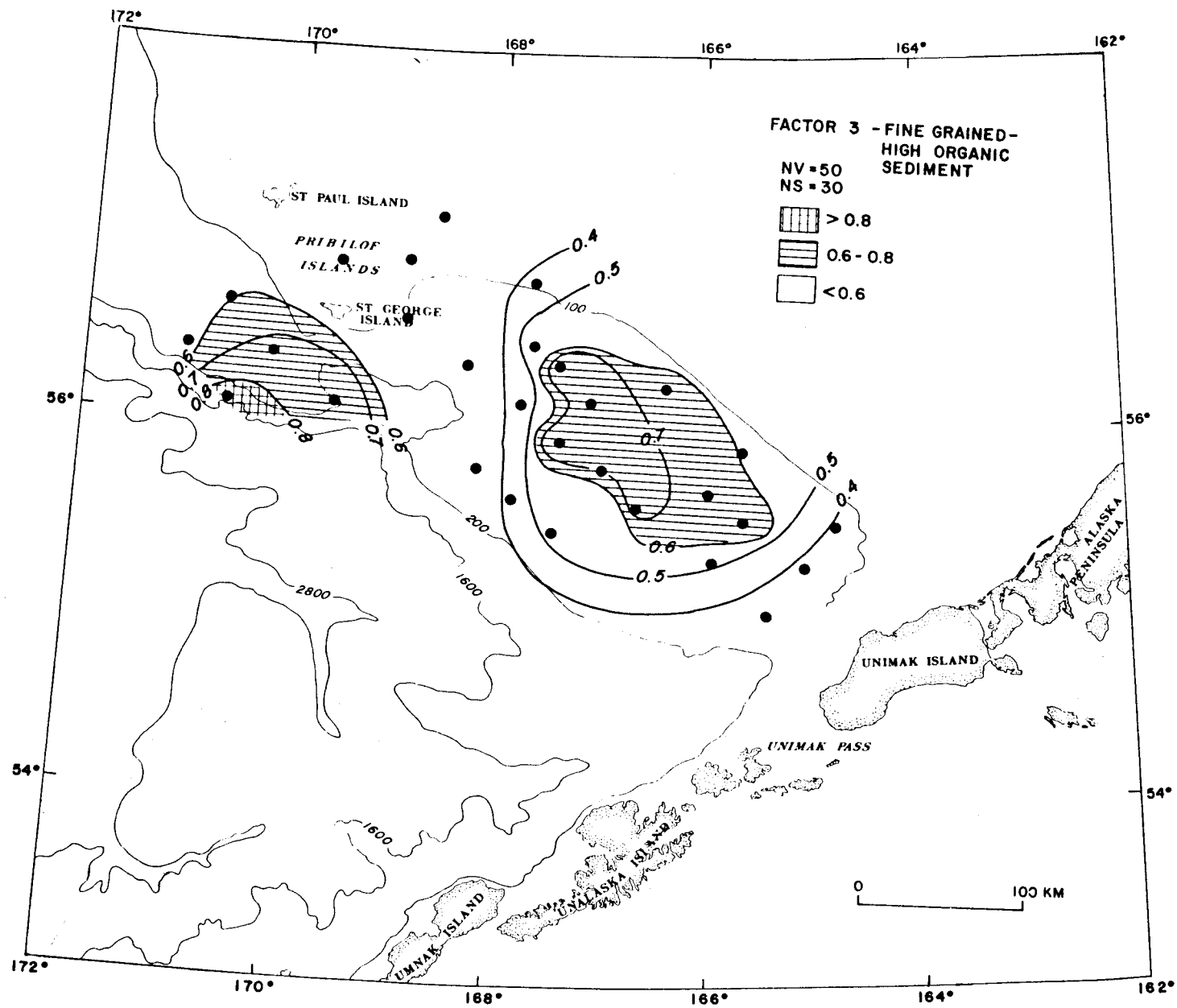


Figure 28. Map of the distribution of factor loadings for Factor III, the fine-grained high organic sediments factor.

Table 12: Correlation coefficients among factor loadings for each of the three factors used in the Q-mode factor analysis and the 50 observed compositional and size variables. Correlation coefficients significant at the 99% confidence level ($r > |0.41|$) are indicated by an asterick (*); correlation coefficients $> |0.60|$ are indicated by a double asterick (**).

VARIABLES	LOADINGS		
	factor 1	factor 2	factor 3
smect+ver	0.7007**	-0.4660*	-0.1331
illite	-0.6214**	0.4047*	0.0123
chlorite	-0.4535*	0.2027	0.2483
clinopx	0.5492*	-0.2751	-0.5591*
orthopx	-0.4779*	0.6088**	-0.2799
vol rx f	0.6894**	-0.8223**	0.2183
amphibol	-0.4557*	0.4326*	0.2786
opaques	0.0061	0.3379	-0.5101*
chlorits	-0.4332*	0.0392	0.6708**
epidote	-0.6736**	0.6454**	-0.1915
garnet	-0.4902*	0.7471**	-0.4466*
met rx f	-0.5803*	0.5813*	0.0502
plutonic	-0.3946	0.2686	0.2886
fine gr	-0.6321**	0.4728*	0.0957
ill klin	0.5297*	-0.2419	-0.0072
mean gz	0.1890	-0.7059**	0.8642**
% sand	-0.2569	0.7249**	-0.8970**
% silt	0.3396	-0.7147**	0.8319**
% clay	-0.1139	-0.4238*	0.6854**
Si (%)	-0.7361**	0.9612**	-0.3606
Al (%)	0.7604**	-0.8411**	0.2298
Ca (%)	0.8870**	-0.7124**	-0.1856
Fe (%)	0.7691**	-0.9097**	0.1764
K (%)	-0.4992*	0.2073	0.3131
Ti (%)	0.8559**	-0.8744**	0.1581
B	-0.2959	-0.0078	0.5395*
Ba (ppm)	-0.5918*	0.4403*	0.1044
Co (ppm)	0.6414**	-0.7061**	-0.0122
Cr (ppm)	-0.5604*	0.3894	-0.1697
Cu (ppm)	0.7720**	-0.9448**	0.3035
Ga (ppm)	0.5645*	-0.7997**	0.5064*
Hg (ppm)	0.2292	-0.5753**	0.4471*
Li (ppm)	-0.1790	-0.3222	0.6532**
Mn (ppm)	0.8021**	-0.6240**	0.0521
Ni (ppm)	-0.3997	0.1359	0.1963
Rb. (ppm)	-0.6067**	0.2520	0.3170
Sr (ppm)	0.8248**	-0.6717**	-0.0016
V (ppm)	0.8171**	-0.8584**	0.1649
Y (ppm)	0.6112**	-0.7218**	0.3289
Yb (ppm)	0.6987**	-0.6502**	0.1952
Zn (ppm)	0.5748*	-0.9095**	0.5649*
U (ppm)	-0.0571	-0.3118	0.8416**
T-C (%)	0.1606	-0.6109**	0.8256**
Na (%)	0.9008**	-0.7325**	0.0850
T-S (%)	0.1006	-0.6207	0.6796**
% quartz	-0.8025**	0.8392**	-0.0960
% K-spar	-0.6196**	0.4688*	0.1237
% glass	0.8384**	-0.6712**	-0.1790
% vol rx	0.8382**	-0.6673**	-0.2911
% nonvol	-0.6559**	0.4082	0.3993

the Pribilof Islands. Samples with high loadings on factor 3 tend to be finer grained and relatively rich in C, U, S, Li, and B (Table 12).

Hydrocarbon Gas in Sediments (Keith A. Kvenvolden and George D. Redden)

Studies of hydrocarbon gases in near-surface sediments of the southern Bering shelf and slope were conducted during the 1976 and 1977 field seasons. The general objectives of this work were (1) to determine the distribution of hydrocarbon gases in surface and near-surface sediments, and (2) to interpret possible sources for the gas. During the 1976 season, 33 stations were occupied where hydrocarbon gases were extracted from 108 sediment samples recovered from gravity cores (maximum depth, 1.4 m), or van Veen grabs. The stations were part of a network of 85 stations established to evaluate the general geology of the southern Bering shelf between Unimak Island and the Pribilof Islands including the area of the St. George basin. The gas analysis results from this season are summarized briefly here. Small quantities of methane (C_1), ethane (C_2), propane (C_3), *n*-butane (*n*- C_4), isobutane (*i*- C_4), ethene ($C_2:1$) and propene ($C_3:1$) were found in all samples. C_1 was the most abundant hydrocarbon, having an average concentration of about 5700 nL/L of wet sediment. The concentrations of C_1 usually increased slightly with depth. The other hydrocarbon gases were present at lower concentrations than methane, and these gases showed no identifiable trends with depth. No anomalous distribution or concentrations of hydrocarbon gases were observed that would suggest possible hydrocarbon seeps or potential hazards.

Between the 1976 and 1977 field seasons, examination of multi-channel, seismic profiles across St. George basin indicated the presence of a number of acoustic anomalies where reflectors abruptly terminate leaving regions of acoustic turbidity beginning at depths of about 200-300 m (Marlow, personal communication). Single-channel seismic records showed these same features, but they were not as well defined. The cause of these anomalies is not known, but it is commonly assumed that they may result from gas occupying a portion of the pore space. Although the features are deep, we reasoned that if hydrocarbon gases are involved, these gases may leak to the surface, giving rise to anomalous concentrations of hydrocarbon gases that would correlate with the acoustic features. Furthermore, the composition of the gases might provide a clue to their sources. Part of the 1977 field season was devoted to testing this idea.

During the 1977 field season two sets of samples were collected for hydrocarbon gas analysis (Fig. 29). The first set consisted of 22 samples from 9 gravity cores. These cores were taken on the southern Bering shelf in a region where acoustic anomalies had been noted on the seismic records. Four of these cores were located over the anomalies, and five were at positions not associated with anomalies. The second set of 22 samples came

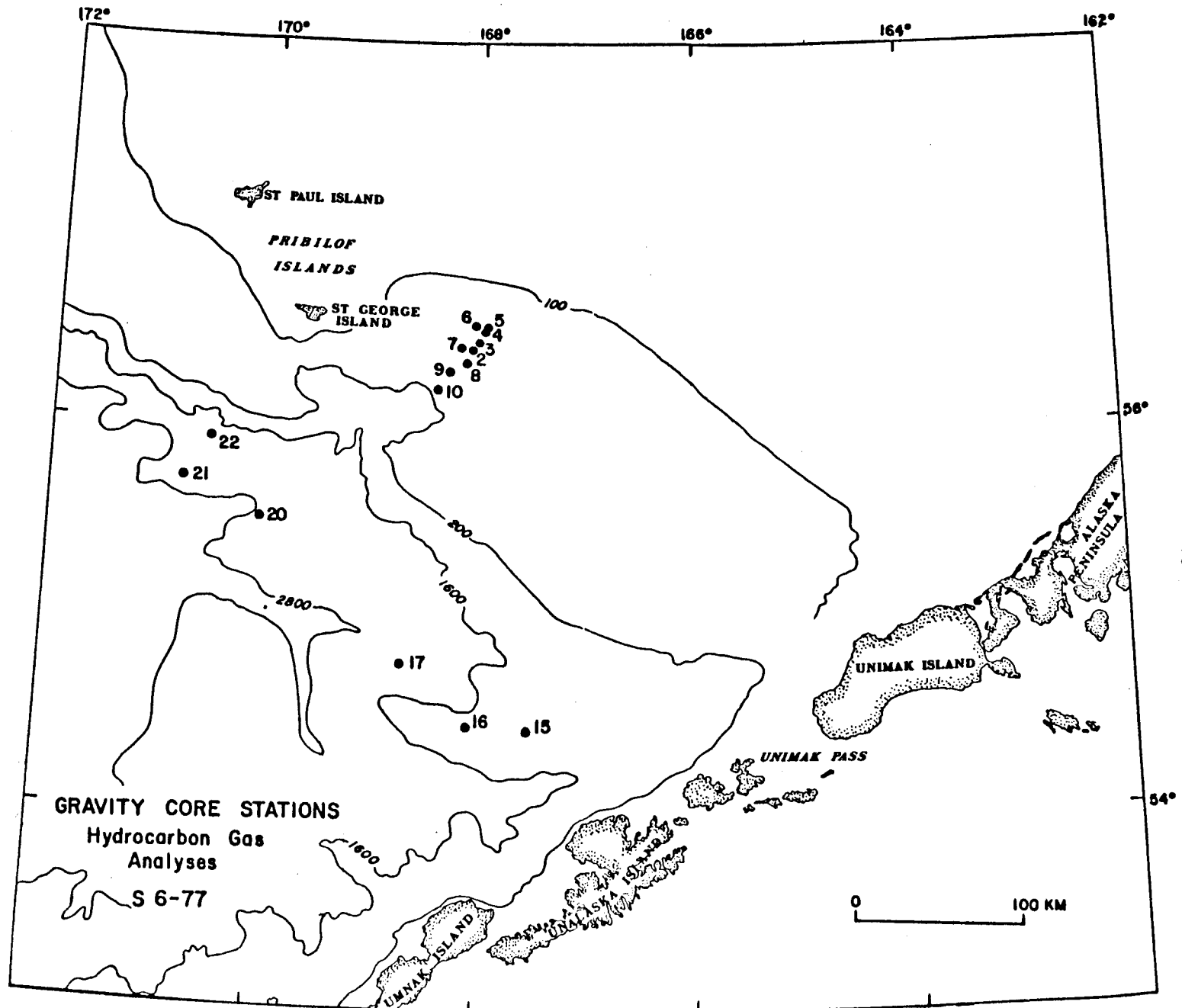


Figure 29. Map showing locations of samples that were collected for hydrocarbon gas analysis

from 6 gravity cores taken on the southern Bering slope. From these two sets of samples, comparisons were made between the occurrence of hydrocarbon gases from these two regions of the continental margin.

The following procedure was used for gas analysis. The 8-cm internal diameter core liner from the gravity core was cut at intervals (usually 0-10, 50-60, 100-110 cm). The sediment core was extruded from each of these intervals into a preweighed, 1 qt. can. The can had been pre-prepared with two small holes near the top and septa had been fixed over the holes. The can was filled with distilled water that had been purged with helium to remove any dissolved hydrocarbon gases. From the can 100 ml of water was removed. A double friction top was sealed in place, and the 100 ml headspace was purged with the helium through the septa. The cans were shaken for 10 minutes. From the can about 5 ml of gas was removed. Exactly one ml of this gas was injected into a modified Carle 311 Analytical Gas Chromatograph equipped with both flame ionization and thermal conductivity detectors. The instrument was calibrated by means of a standard mixture of hydrocarbon gases prepared by Matheson Gas Company. Calculations of concentrations of gases were determined from chromatograms by measuring the heights of peaks representing the gases. Partition coefficients were used to correct for the varying solubilities of the gases. Concentrations are reported as nL/L of wet sediment.

Results obtained during the 1977 field season are recorded in Table 13 (shelf) and Table 14 (slope). On the shelf, cores G-1, G-4, G-7, and G-10 were obtained in sediments over acoustic anomalies. The remaining cores were taken in areas where no anomalies were evident. There appears to be no correlation between gas concentrations and the presence of acoustic anomalies; that is, no hydrocarbon gas anomalies are associated with acoustic anomalies. If the acoustic anomalies are indeed caused by high concentrations of hydrocarbon gases, our data suggest that these gases do not leak to the surface to produce unusual concentrations of gases. The thick (200-300 m) of sediment cover may obscure or prevent gas migration.

Concentrations and compositions of the gases from the shelf and slope are generally similar. Average concentrations of C_1 differ slightly only because deeper samples with higher C_1 contents were recovered on the slope and are included in the average. For example, on the shelf, the average concentration of C_1 is about 2800 nL/L while on the slope the samples have an average C_1 concentration of about 3400 nL/L. The concentrations of the higher molecular weight hydrocarbons are similar for sediments from both shelf and slope.

Shelf sediments have an average $c_1(C_2 + C_3)$ ratio of 34 in contrast to the slope sediments with an average ratio of 107. Samples from the slope, however, include deeper intervals with higher C_1 contents and thus higher $C_1(C_2 + C_3)$ ratios. This ratio has been used in the past to interpret sources of hydrocarbon

gases (Bernard, Brooks, and Sackett, 1977, Earth and Planetary Science Letters, 31, 48-54). Ratios less than 50 were interpreted to indicate the presence of thermogenically-derived gases. Ratios greater than 50 suggested mainly biogenically-produced gases. Although this ratio may be a useful guide when high concentrations of gases are being considered, in the present study involving relatively low concentrations of gases, this ratio probably is not indicative of sources of hydrocarbon gases. It is quite likely that most of the hydrocarbon gases measured here are biologically-derived. The fact remains however, that in the first 60 cm of the cores, the C_1 ($C_2 + C_3$) ratios for southern Bering shelf and slope sediments are generally low as indicated on Table 13 and 14, and as also observed for the samples examined from the 1976 field season.

Two cores show usual concentrations of single components. C_2 is higher in samples from core G-12 than in other cores from both the shelf and the slope. In core G-28, the intervals from 100 cm and deeper show unusually high amounts of $i-C_4$. The significance of these observations is not clear at present.

The data shown in Tables 13 and 14 were obtained from analyses performed on shipboard immediately after core recovery. After gases were analyzed, these samples were frozen. A number of samples were thawed later and reanalyzed. This process tends to increase the amount of hydrocarbon gases that can be extracted. Most of the hydrocarbon gases are probably dissolved in the interstitial water of the sediments, and these are partially removed during the first extraction. Freezing and thawing release additional hydrocarbon gases that are held in the sediment in unknown ways. For these kinds of analyses, it is evident that comparisons of results can be made only with samples which have been processed in the same way. Because analyses of unfrozen samples recovered immediately after coring involves least sample manipulation, results of these analyses have been given here.

This work has shown that hydrocarbon gases are present in surface and near-surface sediments of the southern Bering shelf and slope. Concentrations of hydrocarbons are about the same in shelf and slope sediments in the interval from 0 to about 60 cm. On the shelf, acoustic anomalies at 200-300 m depth do not produce hydrocarbon gas anomalies in the near-surface sediments above them. The concentrations and distributions of hydrocarbon gases in the sediments examined here do not indicate that gas seeps are active in the areas sampled or that the gas in the sediments constitutes a geologic hazard because of high concentrations.

Discussion

The petrology of the surface sediments suggests that small amounts of material from mainland Alaska has been transported to the outer shelf relative to the volcanic material derived from

Table 13. Hydrocarbon Gases - Southern Bering Shelf S6-77

Sta.	Sample	Interval (cm)	Water Depth (m)	Concentrations (nL/L wet sediment)							$\frac{C_1}{C_2 + C_3}$
				C ₁	C ₂	C ₂ : 1	C ₃	C ₃ :1	i-C ₄	n-C ₄	
2	G -1	0-10	136	810	30	34	17	11	-	-	17
	"	50-60		4480	42	28	22	5	6	9	70
	"	92-102		5160	63	44	43	14	9	12	49
3	G -2	0-10	129	890	18	22	13	6	-	-	29
	"	42-52		2150	42	28	24	8	9	9	33
4	G -4	0-10	110	1040	27	34	13	17	-	9	26
	"	55-65		3230	39	31	22	11	-	9	53
5	G -6	0-10	108	1040	27	38	19	11	-	6	23
	"	50-60		3930	48	28	28	8	6	9	52
6	G -7	0-10	109	790	24	22	15	6	-	-	19
	"	27-37		2070	51	50	34	17	12	12	24
7	G-10	0-10	130	750	15	25	9	8	-	2	31
	"	34-44		2300	36	38	24	14	-	-	38
8	G-11	0-10	145	1860	47	45	26	14	6	9	25
	"	50-60		2680	29	18	17	8	6	8	58

Table 13 (Cont.)

9	G-12	0-10	154	8330	204	75	106	19	29	32	27
	"	50-60		3160	117	6	30	5	-	-	21
	"	100-110		4820	333	6	95	16	15	9	11
10	G-13	0-10	166	1170	47	39	25	14	9	9	16
	"	50-60		3170	35	9	11	11	-	-	69
	"	100-110		3100	79	9	7	27	-	-	36
	"	150-160		3950	158	12	9	49	-	-	24

Table 14. Hydrocarbon Gases - Southern Bering Slope S6-77

Sta	Sample	Interval (cm)	Water Depth (m)	Concentrations (nL/L wet sediment)							$\frac{C_1}{C_2 + C_3}$
				C ₁	C ₂	C _{2:1}	C ₃	C _{3:1}	i-C ₄	n-C ₄	
15	G-15	0-10	825	970	26	47	16	14	6	9	23
	"	100-110		925	43	62	30	26	6	9	13
16	G-18	0-10	1195	815	23	32	16	14	-	6	21
	"	50-60		2880	23	24	14	9	-	-	79
	"	100-110		4090	26	29	14	11	-	6	104
17	G-21	0-10	2224	1290	31	32	25	9	6	9	23
	"	50-60		1610	17	18	9	6	-	-	62
	"	100-110		2090	17	15	5	6	-	-	95
	"	150-160		4070	23	9	9	-	-	-	127
20	G-25	10-20	2900	1010	11	26	9	9	-	-	51
	"	70-80		4600	17	14	7	6	-	-	192
	"	110-120		5330	23	14	9	9	-	-	167
	"	160-170		7730	23	20	9	12	-	-	242
	"	200-210		6650	28	20	9	15	-	-	180
21	G-27	0-10	3158	5120	20	23	9	6	-	-	177
	"	50-60		4740	17	14	5	6	-	-	215
	"	102-112		7920	20	17	7	-	-	-	293

the Aleutian Islands and Alaskan Peninsula. The present-day continental shelf of the southern Bering Sea is extremely flat and broad. Bottom gradients typically are much less than 0.25° (1:13,000) and the mouths of large rivers that feed sediment into the Bering Sea, the Yukon, Kuskokwim, Kvichak, and, to a lesser extent, the Nushagak Rivers, are over 500 km away from the outer shelf. Sediment is transported from these rivers into Bristol Bay, but has almost no opportunity to be advected to the outer shelf because of the extremely low topographic gradients and insufficient watermass movement. Structural fronts in the water-column are parallel to the 50-m isobath (Schumacher *et al.*, in prep.). These fronts may have some effect in impeding the seaward dispersal of detritus toward the outer continental shelf.

The Aleutian Islands and the Alaskan Peninsula are obvious sediment sources for the volcanic components today but the Bering Canyon (Figure 6) provides a topographic depression that traps sediment before it can get to the outer shelf. The sluggish, semi-gyre cyclonic circulation pattern that characterizes surface flow in the southern Bering Sea (Favorite, 1974; Takenouti and Ohanti, 1974) is only on the order of 2 to 3 cm/sec (Schumacher, *et al.*, in prep.), too slow to transport even clay-sized particles.

The Pribilof Islands and Pribilof Ridge also are potential sediment sources for some of the volcanic components but the low relief and small area of the features preclude any large contributions. Lack of a dominant circulation and very low current velocities also eliminate the Pribilof Ridge as a major source. Thus, today, the source areas are isolated from the site of deposition.

Consequently, it seems unlikely that sediments are presently being transported to and deposited on the outer continental shelf of the southern Bering Sea in significant quantities, and the uppermost deposits must be relict from a previous depositional environment. Diatom floras from the bottom of each of our cores all fall within the *Denticula semina* zone (J. Barron, personal communication, 1976 and 1977), which ranges from 260,000 years BP to present (Koizumi, 1973). Although we believe that the sediments are relict and not modern, about all we can say about their age from existing data is that they are late Quaternary in age.

The dominant influence on Quaternary continental shelves has been glacioeustatic lowering of sea level, and it seems probable that this influence was magnified on the broad, flat shelf of the Bering Sea. Estimates of the lowering of sea level during the Pleistocene glacial periods are all about 130 m (Curry, 1960, 1965; Bloom, 1971). We have drawn a shoreline in Fig. 30 along the present-day 130-m isobath and subtracted 130 m from each of the isobaths to yield a schematic bathymetric chart of a low sea level period. Several features of this chart are worth noting. The region landward of the shoreline is featureless and flat with gradients much less than 0.25° . Any streams that flowed across

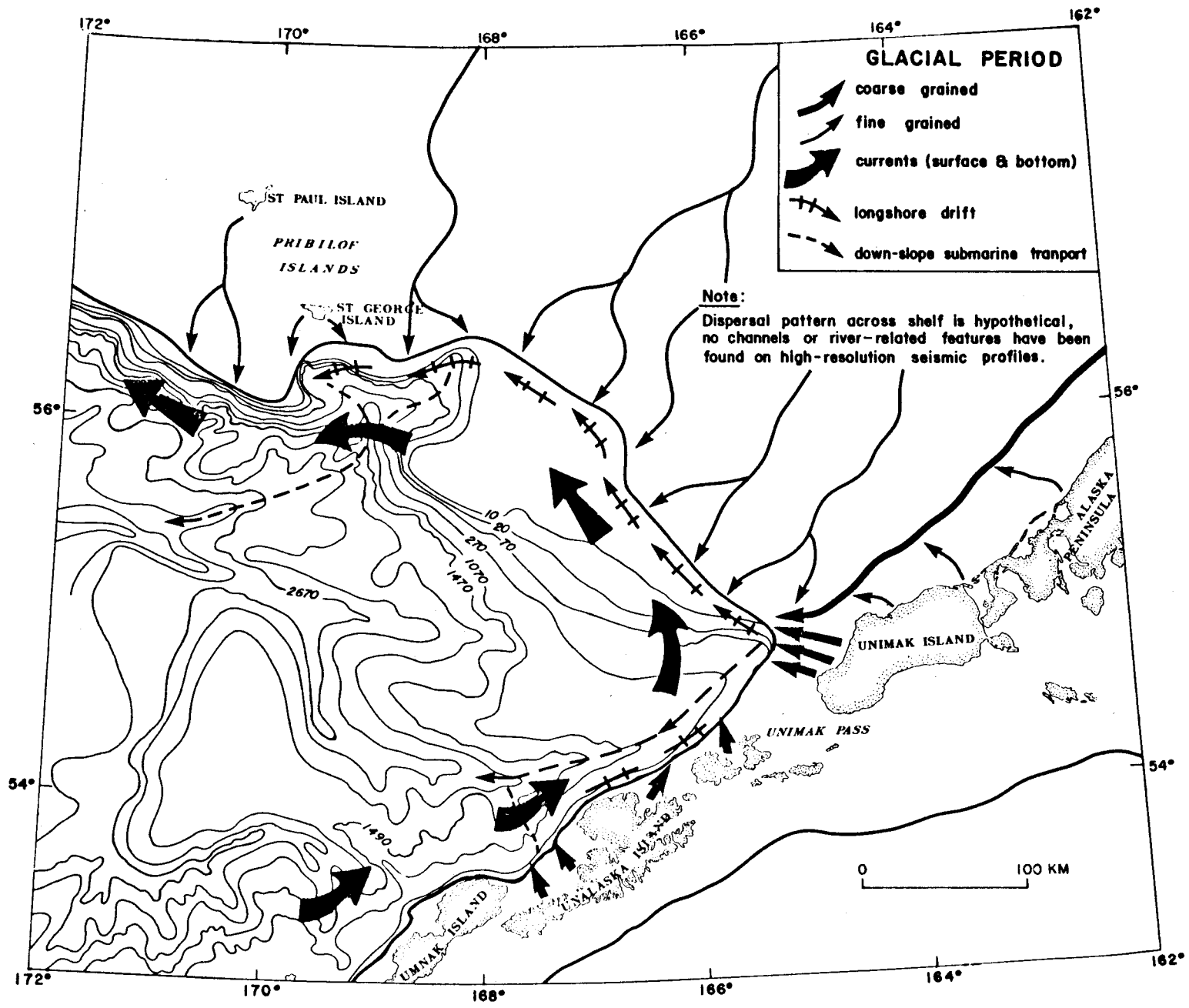


Figure 30. A paleobathymetric map of the continental margin of the southern Bering Sea during a period of worldwide glacial conditions.

this emerged shelf must have been very meandering with a large dendritic distributary system. This is especially important in light of speculations by Scholl et al. (1970) that the Yukon and (or) Kuskokwim Rivers cut the Pribilof Canyon during the Pleistocene. We see no evidence of buried or surface stream channels on more than 10,000 km of high-resolution seismic data (12 kHz, 3.5 kHz, and 1.5 kHz), and so we conclude that no rivers cut channels across this portion of the continental shelf during Pleistocene lower sea levels and that Pribilof Canyon was formed much earlier than the Pleistocene. Streams that debouched into the southern Bering Sea during glacial periods were not competent to transport much coarse-grained sediment. The mainland components (factor 2 of the Q-mode analysis) are represented by quartz, garnet, epidote, orthopyroxene, metamorphic rock fragments, Si, K, and Ba. However, all of these components are distributed as background with relatively low concentrations over the outer shelf.

Superimposed on this background of mainland materials are northwest-trending gradients of sediments that contain relatively high concentrations of andesitic components (factor 1), decreasing away from the Aleutian Islands in the vicinity of Unimak Pass. This Aleutian component is represented by clinopyroxene, volcanic glass, volcanic rock fragments, smectite + vermiculite, Na, Ca, Mg, Fe, Ti, Al, Co, Cu, Mn, V, and Zn. Volcanic debris is also distributed as an aureole of local extent around the Pribilof Islands. The northwest-trending gradients away from the Aleutian Islands reflect longshore transport of clay- to sand-size material from the Aleutians during periods of low sea levels. Much, and perhaps the vast majority, of the detritus shed off the Aleutians and Alaskan Peninsula was trapped by the Bering Canyon and funneled onto the continental rise. However, apparently material was periodically captured by longshore currents and transported onto and along the narrow shelf. Possibly the head of Bering Canyon may have periodically filled up, which allowed sediment to be transported across to the shelf. The strong gradients seen especially in the geochemical data suggest that a relatively strong, cyclonic, nearshelf circulation may have existed that was competent to transport coarse sediment along the shelf.

When sea level rose during periods of glacial to interglacial transition, the shift in the position of the shoreline must have been rapid because of the very low topographic gradients (Fig. 31). If we use the Pleistocene to Holocene transgression as a model, then the initial retreat of the shoreline was slow with a 50-m rise in sea level producing a transgression of about 70 km. Sea level curves (Curry, 1960, 1961; Morner, 1971; Bloom, 1971) indicate that the first 50-m rise in sea level took about 5,000 years. However, the next 10-m rise in sea level produced a 175-km retreat of the shoreline in only about 1,000 years. The remaining 70-m rise in sea level caused a 250-km transgression in the remaining 6,000 to 8,000 years. Therefore, when the shoreline began to retreat, it did so

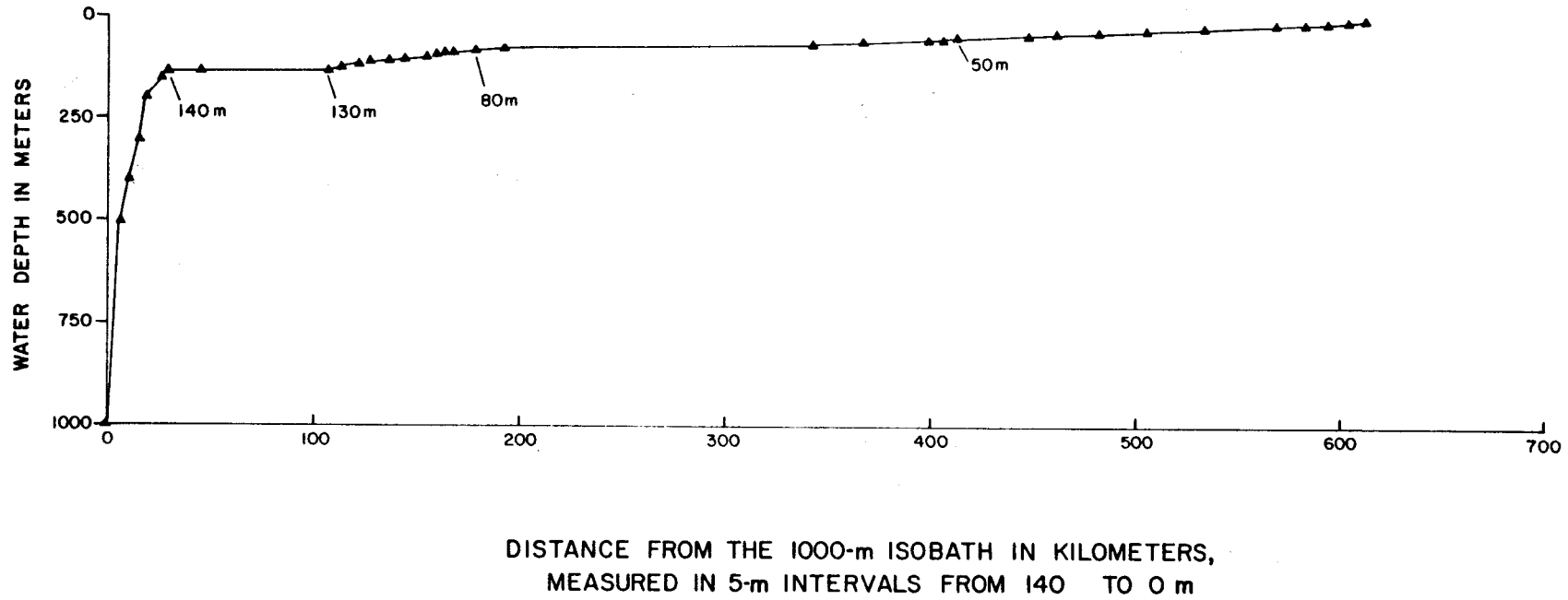


Figure 31. A profile of the continental margin of the southern Bering Sea drawn as distance from the 1000 m isobath. Each solid triangle from 140 to 0 m represents a 5-m sea level rise.

rapidly and, in effect, deserted a sediment distribution pattern with little modification. The result is a glacial-period sediment distribution pattern and an interglacial-period oceanographic circulation, as is observed today.

Present-day oceanographic conditions have modified the distribution and character of the sediments to a small degree, and in this context they are palimpsest (Swift, *et al.*, 1971). Maps of lithofacies and sorting (Figs. 8 and 9) show that a tongue of moderately sorted, coarse sediments extends along the shelf break south of Pribilof Canyon and along the northern flank of Bering Canyon. The tongue of Pribilof Canyon seems to be restricted in extent and this restriction coincides with the steepest portion of the continental slope. Conversely, the poorest sorted and finest-grained sediments, with relatively high concentrations of absorbed organic material (Q-mode factor 3), are found in the center of St. George basin. This distribution of textures can be explained by a combination of long-period storm waves and a gravity potential, i.e. a change in bathymetry significant enough to provide the energy necessary to keep sediment in transit. Komar *et al.* (1972) show that waves with a 15-sec period cause rippling of sandy sediments off the Oregon coast in water depths down to 149 m. Thus, high sea states that commonly occur in the southern Bering Sea during the late summer and fall can affect bottom sediments of the outer shelf. Resuspension of surface sediments by long-period storm waves would increase the density of the shelf-bottom boundary layer with the incorporation of clay and silt. The coarser sediment would probably fall out of suspension quickly. If this dense boundary layer were located in an area closely adjacent to a gravity potential (i.e. a region with a slope of perhaps 2° or more), then the dense boundary layer would flow down slope and out of the area. This mechanism would tend to winnow out the fine-grain sizes and impart a better sorting to the sediment than remains behind. The patterns of textural parameters (Figs. 8 and 9) show this result. The broad continental slope north of Bering Canyon has gradients of about 1.5° and apparently is too gentle to provide the critical gravity potential, thus little winnowing is occurring there. However, the slope just south of Pribilof Canyon has gradients in excess of 3° and evidence of winnowing is suggested by better sorting and coarser grain sizes.

Sediments in St. George basin also are affected by these long-period storm waves but, because of lack of a gravity potential, the shelf-bottom boundary layer is restricted to the limits of the basin and the sediment is redeposited in the same general area. The fact that St. George basin is a surface graben also helps to explain the general lack of transport of sediment out of this area. Storm waves mix sediments in St. George basin, but the only apparent effect is to obscure the boundaries between the textural provinces and to concentrate finer-grained and more poorly-sorted sediment into a bull's-eye pattern.

Distribution patterns of grain size do not reflect the graded-shelf size distribution described by Sharma et al. (1972). However, their sampling stations stop along the northern boundary of the area covered by our data. When the data of Sharma et al. (1972) are joined to our data, the two complement each other very well, yet each tells a different story. Their data are concentrated in the shallow (<100m) reaches of Bristol Bay and reflect a gradual decrease in grain size with distance from shore. Our data are concentrated in depths greater than 100m, and show the overprints of the effects of topography (gravity) controls on the redistribution of sediment. Sediments in Bristol Bay are presently affected by storm waves because even the relatively short-period waves can affect the sediment surface. The outer shelf is immune to the normal sea state because of depth and only periodic large storm waves affect the sea floor in this region and only for short durations.

DISTRIBUTION OF FAULTS AND POTENTIALLY UNSTABLE SEDIMENTS

Summary

Seismic-reflection data are used to identify and map faults beneath the outer continental shelf of the southern Bering Sea. We studied more than 10,000 km of single-channel and 600 km of multichannel seismic-reflection profiles. Our seismic systems can resolve offsets that range from a fraction of a meter to several kilometers. Faults are classified as major, minor, and surface based on the type and amount of displacement. Major faults are those resolved on both multi-channel and single-channel seismic-reflection records. These faults generally penetrate from several hundred meters to several kilometers beneath the sea floor and some displace reflectors more than 60 meters. Major faults are principally distributed along or near the borders of St. George basin and they trend NW-SE parallel to the basin's long axis. Major faults often offset the seafloor and as surface faults, are most abundant along the boundaries of St. George basin. Minor faults are widely distributed throughout the outer shelf; however, to the east they are concentrated in the middle of St. George basin. Most minor faults exhibit displacements of 5 m or less and almost all approach the sea floor to within 4 or 5 m. The precise age of faulting is not known although both surface and minor faults do offset upper Pleistocene sediment. Major faults are probably related to stress fields established by Mesozoic and Cenozoic plate motions and minor faults are related to high seismicity in the nearby Aleutian subduction zone.

Classification of Faults

We classify faults in this study by their relative amount of vertical displacement. The resolutions of the seismic systems, which determine the minimum offset we can detect with each system, are shown in Table 3 and were calculated using the velocity of sound in water and by following the procedure of

Moore (1972). The following seismic-reflection data were used to map the distribution of faults: 1) 3.5 kHz; 2) 2.5 kHz; 3) single-channel seismic-reflection (60 KJ to 160 KJ sparker, and up to 1326 in³ air-gun sources); and 4) 24-channel system using a 1326 in³ air-gun array.

A gap may exist in the resolving range of our systems between about 0.5 m and 3 m, which suggests that offset features in that range may not be resolved. Our studies concentrate on faults cutting strata above the acoustic basement as resolved on our single-channel seismic-reflection system. However, our multichannel data also indicate that many faults occur within the acoustic basement.

Faults are classified as surface, minor, and major faults. Surface faults offset the surface of the sea floor regardless of the recording system. They offset the sea floor no more than a few meters. Minor or near-surface faults are resolved on 2.5 kHz and/or 3.5 kHz records, but not on single or multichannel seismic-reflection profiles. These faults typically displace reflectors less than 0.006 sec (5 m); most minor faults are close to but do not break the sea floor. Sediment can be seen in places to drape over near-surface faults. Major faults are defined as those resolved on multichannel and single-channel seismic-reflection profiles. These faults generally are growth structures and many offset acoustic basement. Boundary faults are major faults that mark the boundaries of St. George basin.

Fault Distributions

Distribution of faults is shown in Fig. 32. The true orientation of most faults is unknown because of the relatively wide spacing of tracklines. Faults found on northeast-southwest tracklines, perpendicular to the long axis of St. George basin, greatly outnumber those observed on northwest-southeast tracklines which indicates that the majority of the faults have a northwest-southeast trend and parallel the trend of the basin. Faults bounding St. George basin can be confidently traced between tracklines. We believe that most faults beneath the shelf and those in St. George Basin in particular, trend northwest-southeast parallel to the basin and to the margin.

Boundary faults clearly delineate St. George basin and the north side of the Pribilof ridge. These faults are normal faults, occur in groups, and exhibit increased offset with depth, which indicates growth-type structures. These faults in many places cut nearly all of the sedimentary section, and often offset acoustic basement, but rarely offset the sea floor.

Major faults (other than boundary faults) principally occur within St. George basin, although a few occur within Amak basin (Figure 33). This class of fault decreases in abundance near the

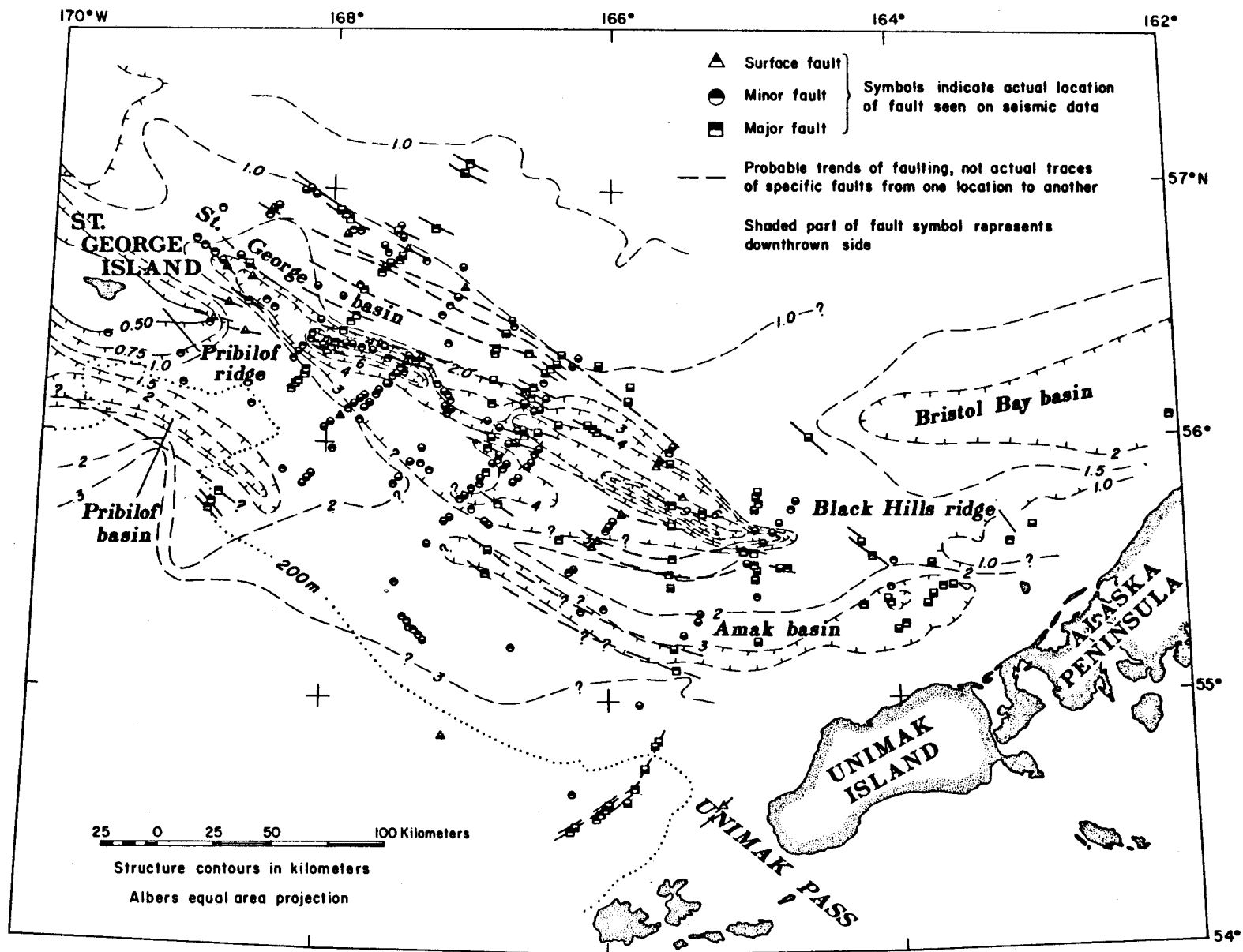


Figure 32. Map of distribution of faults in the southern Bering Sea. Lines through fault symbols are inferred trend of the fault, not any known strike. Structure contours of acoustic basement from Marlow et al. (1976, 1977a).

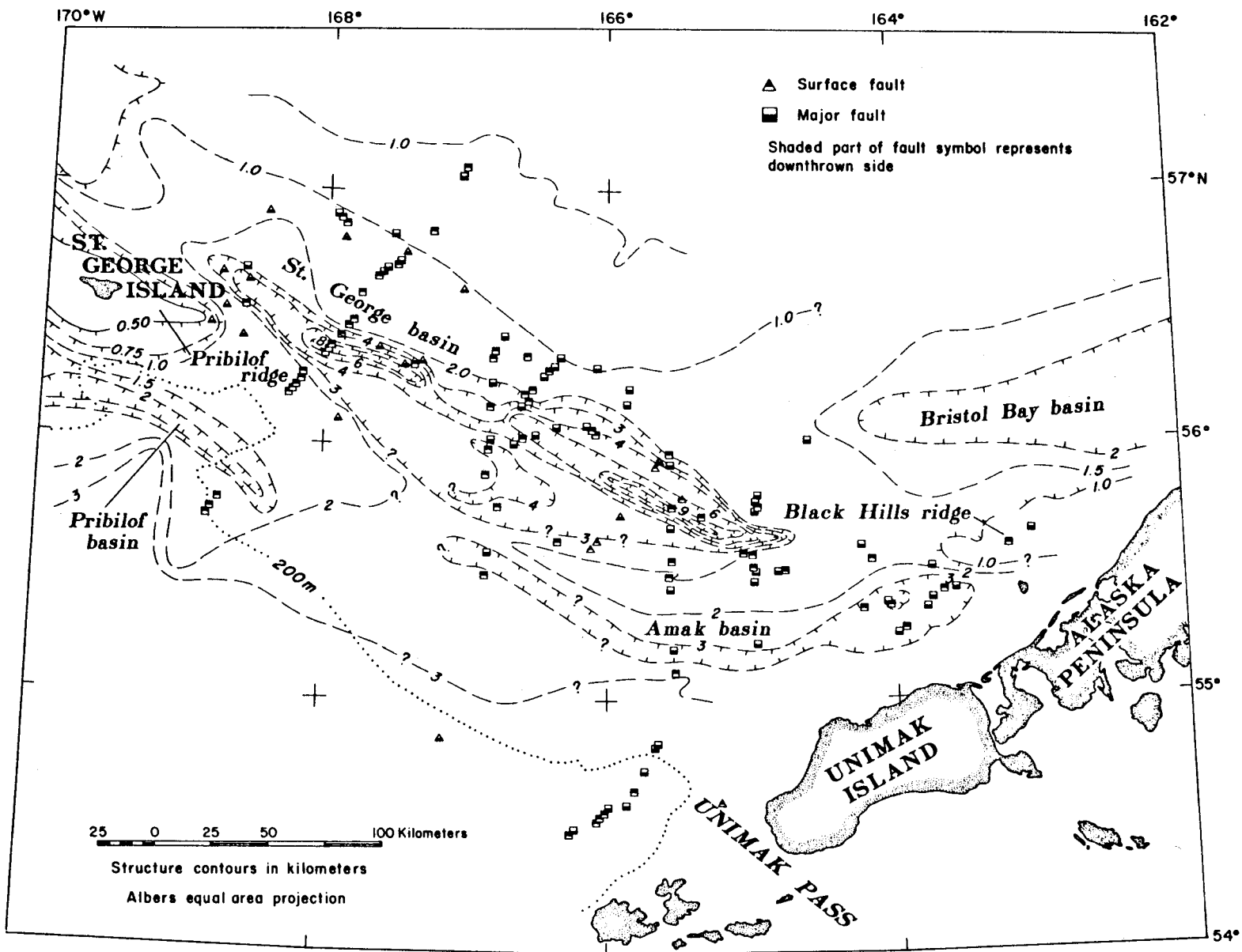


Figure 33. Distribution of surface and major faults. Structure contours on acoustic basement from Marlow *et al.* (1976, 1977a, 1977b).

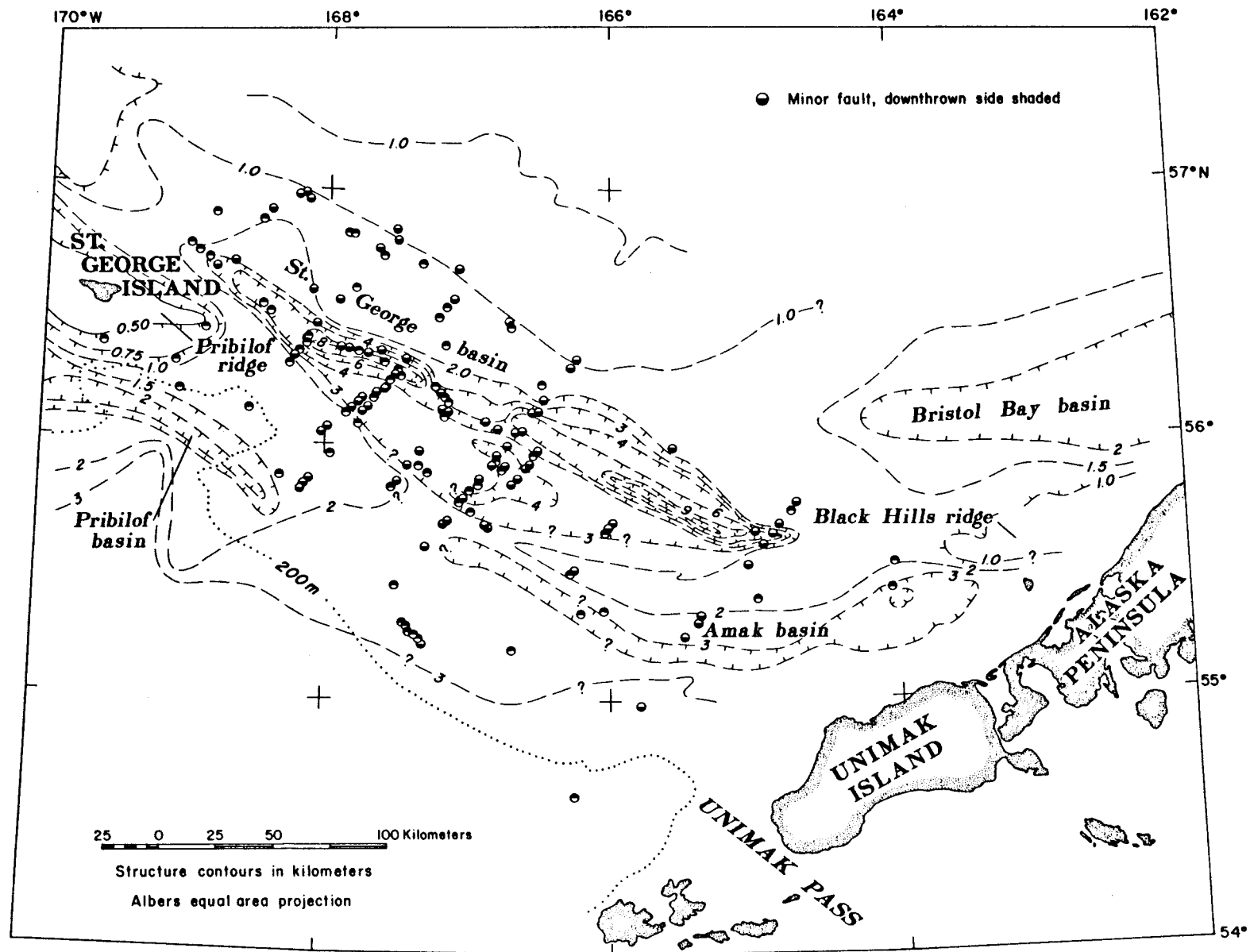
Pribilof Islands. Major faults show displacements that generally are less than the larger boundary faults but offsets greater than 0.08 sec (60 m) occur in the central region of St. George basin. Major faults are not always offset in the same sense as adjacent boundary faults, which suggests that deformation of the outer shelf has involved more than simple subsidence.

Surface faults tend to be more abundant along the outer margin of St. George basin and along Pribilof ridge than in the center of the basin (Figure 33). Most surface faults can be traced from high-resolution to low-resolution records, which suggests that most surface faults are expressions of major faults and of boundary faults.

Minor faults (Figure 34) occur throughout the southern outer shelf, although, like other classes of faults, they are also concentrated in the middle region of St. George basin, away from the Pribilof ridge. Minor faults are more frequent south of the ridge than to the north (Figure 34). Most minor faults offset reflectors less than 0.006 sec (5 m) and almost all these faults cut the top 0.005 sec (approximately 4 m) of the sedimentary section. Diatoms recovered in sediment from gravity cores up to 2m long are younger than 260,000 years (all within the Denticula seminae Zone; John Barron, pers. commun., 1976, 1977). If we assume that a 2m core just penetrated the entire Denticula seminae Zone, then the minimum accumulation rate is $0.8 \text{ cm}/10^3 \text{ yr}$. If we assume that this minimum accumulation rate is typical for the top 4 m of sediment (the thickness generally affected by minor faults), then the maximum age of the sediment, calculated at $0.8 \text{ cm}/10^3 \text{ yr}$ is 520,000 YBP. Thus, minor faulting may be no older than Pleistocene in age. Accumulation rates may be much greater, for example $10 \text{ cm}/10^3 \text{ yr}$ as suggested by C^{14} dates from areas farther north (Askren, 1972), in which case the minor faults could cut sediment as young as 40,000 YBP.

Potentially Unstable Sediments

Areas of potentially unstable sediment masses (Fig. 32) were determined from the seismic reflection records by using one or more of the following criteria: 1) surface faults with steep scarps and rotated surfaces; 2) deformed bedding and/or discontinuous reflectors; 3) hummocky topography; 4) anomalously thick accumulation of sediment; and 5) acoustically-transparent masses of sediment. Regions that show unstable sediments (e.g. gravity slides, slumps, creep, scarps, etc.) are confined to the continental slope and rise and the Pribilof and Bering canyons. Zones of creep, as shown by irregular, hummocky topography, begin near the shelf break at depths of about 170 m and continue onto the upper continental slope. Hummocky topography occurs on the continental slope on a large scale and mass movement is a common feature. We regard the entire continental slope and the walls of the major submarine canyons to be zones of potentially unstable sediment. Regimes of active



261

79

Figure 34. Distribution of minor faults. Structure contours from Marlow et al. (1976, 1977a, 1977b).

sediment movement could respond to a variety of energy sources including earthquakes, storms, internal waves, and gravity.

Discussion

Faults of the outer continental shelf of the southern Bering Sea are concentrated in St. George basin. Many faults cut upper Pleistocene sediment and some offset the sea floor, indicating that the area is tectonically active. The processes that initially formed St. George basin are presently active. Principal structural features along the outer continental shelf, e.g. St. George and Amak basins, as well as other minor basins (see Marlow *et al.*, 1976), probably all had a common origin and tectonic history. Subduction between the Kula (?) and North American plates along the Bering Sea margin is thought to have been oblique during the Mesozoic (Marlow *et al.*, 1976). However, reconstructions by Cooper *et al.* (1976), indicate that the ancient margin may have been a transform fault separating two plates. Nevertheless, structural patterns were developed parallel to the margin. The Mesozoic stress field and thermal regime changed when subduction jumped from the Siberian margin to near the present Aleutian trench. If oblique subduction did occur along the Bering Sea margin, then a southward shift of the site of compression would have isolated the margin in late Mesozoic time. A relaxation of compression would then give way to extension and thus to formation of grabens beneath the outer shelf. The complementary horst structures hypothesized by Bott (1976) for this type of model may be represented by the Pribilof ridge. If the Bering margin was instead a transform fault zone during the Mesozoic, then some complex model such as a combination of sediment loading (Watts and Ryan, 1976), mantle metamorphism (Falvey, 1974) and mantle flowage (Bott, 1976) may have lead to the collapse of the margin and formation of large grabens along the outer shelf. Whatever the tectonic stresses are that caused extension, they are presently active as evidenced by large growth faults bounding St. George basin. Second-order structures such as minor faults are probably superimposed features which resulted from subduction beneath the arc during the Cenozoic.

The southern Bering Sea margin is within 500 km of the Aleutian Trench, the present site of subduction between the Pacific and North American plates. Several intermediate - to deep-focus (71 to 300 km deep) and many shallow-focus (less than 71 km deep) earthquakes were recorded beneath the southern Bering Sea margin from 1962 to 1969 as shown in Figure 35. The St. George basin and surrounding areas have been subject to earthquakes with intensities as high as VIII (modified Mercalli scale), which corresponds to a magnitude 5.7 earthquake (Meyers and others, 1976). Recurrence rates of earthquakes for the area bounded by latitudes 50° and 60° N and longitudes of 160° to 175° W have been as high as 6.4 earthquakes per year from 1963 to 1974 for magnitudes of 4.0 to 8.4, and 0.013 earthquakes per year of

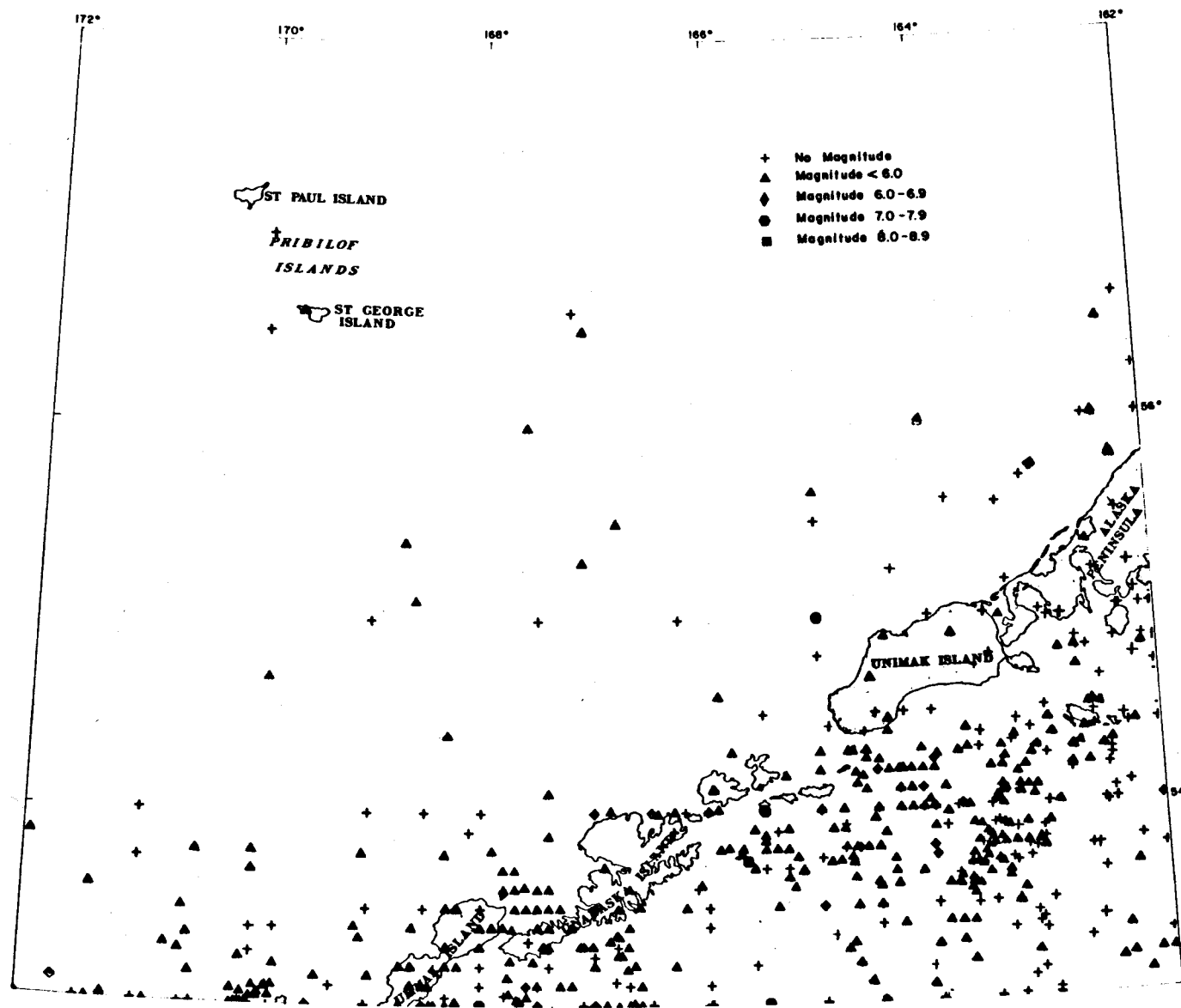


Figure 35. EPICENTERS UP THRU 1964
(DEPT. OF COMMERCE, 1970)

magnitude 8.5 to 8.9 (1 every 130 years) from 1899 to 1974 (Meyers and others, 1976).

The correlation of earthquakes to shallow faulting is not well understood (Page, 1975). We believe, however, that many of the faults in the southern Bering Sea are active and that they probably respond to earthquake-induced energies and possibly to sediment loading in St. George basin.

CONCLUSIONS

Detailed conclusions are given in the discussion sections of parts 2 and 3. Some of the major conclusions are repeated in this section.

The large number of faults, evidence for recent movement along some, and the high seismicity indicate that faulting is a major environmental concern in the outer continental shelf region of the southern Bering Sea, especially in St. George basin. All faults are potentially active, their movement probably influenced by seismic energies and the local geology, including basement structures and sediment loading. Unstable sediment masses pose potential threats to developments on the continental slope and walls of the submarine canyons.

Mineralogical and inorganic geochemical data show three major sources of sediments and one sediment sink. The Alaska mainland source forms a mineralogical and chemical background to most samples from the shelf. The dominant source is the Aleutian Islands and a third, very local source, is the Pribilof Islands. St. George basin has served as a sink for fine-grained sediment.

Sediment distributions do not appear to reflect present-day deposition. Rather, we believe that the distributions are the result of accumulation during periods of lower sea level in the Pleistocene, modified by present-day processes. Evidence for this conclusion is shown by a concentration of Aleutian sediments, between the 100 m and 200 m isobaths, which exhibit a strong gradient, or "plume", that decreases away from Unimak Pass into St. George basin. Lack of present-day currents sufficient to move even clay-size material and the presence of the Bering submarine canyon between the Aleutian Islands and the outer continental shelf and slope indicate that Holocene sediment dynamics cannot be used to explain the observed distribution of surface sediments derived from the Aleutian Islands. We believe it is logical to suggest that this distribution pattern is relict and is the result of sediment dynamics during lower sea levels.

REFERENCES

- Anderson, R. L. and Bancroft, T. A., 1952, Statistical theory in research: New York. McGraw-Hill Book Co., 399 p.
- Askren, D. R., 1972, Holocene stratigraphic framework-southern Bering Sea continental shelf: MS Thesis, Univ. of Washington, 104 p.
- Bader, R. G., 1962, Some experimental studies with organic compounds and minerals: Univ. Rhode Island, Graduate School of Oceanography Occasional Pub. No. 1, 85 p.
- Biscaye, P. E., 1965, Mineralogy and sedimentation of Recent Deep-sea clay in the Atlantic Ocean and adjacent seas and oceans: Geol. Soc. Amer. Bull., v. 76. p. 803-831.
- Bloom, A. L., 1971, Glacial-eustatic and isostatic controls of sea level since the last glaciation: in Turekian, K. K. (ed.) Late Cenozoic Glacial Ages, Yale Univ. Press, New Haven, p. 355-379.
- Bordovskiy, O. K., 1965, Accumulation and transformation of organic substances in marine sediment: Marine Geology, v. 3, P. 3-114.
- Bott, M. H. P., 1976, Formation of sedimentary basins of graben type by extension of the continental crust: Tectonophysics, v. 36, p. 77-86.
- Connor, J. J., Feder, G. L., Erdman, J. A., and Tidball, R. R., 1972, Environmental geochemistry in Missouri - a multiplinary study, in Earth science and the quality of life--Symposium 1: Internat. Geol. Cong., 24th, Proc., p. 7-14.
- Cooper, A. K., Scholl, D. W., and Marlow, M. S., 1976, Plate tectonic model for the evolution of the eastern Bering Sea Basin: Geol. Soc. Amer. Bull., v. 87, p. 199-1126.
- Creager, J. S., Scholl, D. W., et al., 1973, Initial Reports of the Deep Sea Drilling Project, V. 19: Washington (U. S. Government Printing Office), 913 p.
- Curray J. R., 1960, Sediments and history of Holocene trans-gression, continental shelf, northwest Gulf of Mexico:- in Shepard, F. P., Phleger, F. B., and van Andel, T. H. (eds.), Recent Sediments, Northwest Gulf of Mexico, Tulsa, Oklahoma, Am. Assoc. Petroleum Geologists, p. 221-266.
- _____, 1961, Late Quaternary sea level: a discussion: Geol. Soc. Amer. Bull., v. 72, p. 1707-1712.

- 1965, Late Quaternary history, continental shelves of the United States: in Wright, H. E., Jr., and Frey, D. G. (eds.), The Quaternary of the United States, Princeton, N. J., Princeton University Press, p. 723-735.
- Emery, K. O., 1960, The sea off southern California. A modern habitat of petroleum: New York, John Wiley and Sons, 366 p.
- Favorite, F., 1974, Flow into the Bering Sea through Aleutian passes: in Hood, D. W. and Kelley, E. J (eds.), Oceanography of the Bering Sea, Inst. of Marine Science, Univ. of Alaska, Occasional Pub. 2, p. 3-37.
- Folk, R. L., and Ward, W. C., 1957, Brazos River bar: a study in the significance of grain size parameters: Jour. Sed. Petrology, v. 17, p. 3-27.
- Hein, J., Scholl, D. W., and Gutmacher, C., 1975, Neogene clay minerals of the far northwest Pacific and Southern Bering Sea: Sedimentation and diagenesis, in Bailey, S. W. (ed.) AIPEA proceedings, International Clay Conf., Mexico City, p. 71-80.
- Jordon, C. F., Jr., Fryer, G. E., and Hemmen, E. H., 1971, Size analysis of silt and clay by hydrophotometer: Jour. Sed. Petrology, v. 41, p. 489-496.
- Kemp, A. L. W., 1971, Organic carbon and nitrogen in the surface sediments of Lake Ontario, Erie, and Huron: Jour. Sed. Petrology, v. 41, No. 2, p. 537-548.
- Klovan, J. E., and Imbrie, J., 1971, An algorithm and FORTRAN IV program for large scale Q-mode factor analysis and calculation of factor scores: Jour. Internat. Assoc. Mathematical Geology, v. 3, no. 1, p. 61-77.
- Koizumi, J., 1973, The Late Cenozoic diatoms of sites 183-193, Leg 19, Deep Sea Drilling Project: in Creager, J. S., Scholl, D. W., and others, Initial Reports of the Deep Sea Drilling Project, v. 19: Washington, D. C., p. 805-856.
- Komar, P. D., Neudeck, R. H., and Kulm, L. D., 1972, Observations and significance of deep-water oscillatory ripple marks on the Oregon continental shelf: in Swift, D. J. P., Duane, D. B., and Pilkey, O. H., Shelf Sediment Transport Process and Patterns, Dowden, Hutchinson, and Ross, Inc., 601-619.
- Marlow, M. S., Scholl, D. W., and Cooper, A. K., 1975, Structure and evolution of the Bering Sea Shelf south of St. Lawrence Island: Am. Assoc. of Petroleum Geologists Bull., v. 60, p. 161-183

- Marlow, M. S., Scholl, D. W., Cooper, A. K., and Buffington, E. C., 1976, Structure and evolution of Bering Sea shelf south of St. Lawrence Island: Amer. Assoc. Petroleum Geologists Bull. v. 60, P. 161-183.
- Marlow, M. S., Scholl, D. W. and Cooper, A. K., 1977a, St. George Basin, Bering Sea shelf: a collapsed Mesozoic margin: in Island Arcs, Deep Sea Trenches, and Back-Arc Basins, Maurice Ewing series, Amer. Geophysical Union, v. 1. p. 211-220.
- Marlow, M. S., Cooper, A. K., and Scholl, D. W., 1977b, Mesozoic structural trends beneath the southern Bering Sea shelf: (abs.) Geol. Soc. Amer. Ann Mtg, 1977, v. 9, p. 460-461.
- Meyers, H., Brazee, R. J., Coffman, L. L., and Lessig, S. R., 1976, An analysis of earthquake intensities and recurrence rates in and near Alaska: N.O.A.A. Tech. Memorandum, EDS NGSDC-3, 101 p.
- Miesch, A. T., 1976, Geochemical Survey of Missouri, Methods of sampling, laboratory analysis, and statistical reduction of data: U. S. Geol. Survey Prof. Paper, 954-A, 39 p. Moore, D. G., 1972, Reflection profiling studies of the California continental borderland: structure and Quaternary turbidite basins: Geol. Soc. Amer. Spec. Paper 197, 142 p.
- Morner, N., 1971, Eustatic changes during the last 20,000 years and a method of separating the isostatic and eustatic factors in an uplifted area: Paleogeography, Paleoclimatology, Paleoecology, v. 9, p. 153-181.
- Nelson, C. H., Hopkins, D. M., and Scholl, D. W., 1974, Cenozoic sedimentary and tectonic history of the Bering Sea: in Hood, D. W., and Kelley, E. J. (eds.), Oceanography of the Bering Sea, Inst. of Marine Science, Univ. of Alaska, Occasional Publ. 2, P. 485-516.
- Page, R. A., 1975, Evaluation of seismicity and earthquake shaking at offshore sites: Offshore Technology Conference Proceedings, p. 179-190.
- Ratmanoff, G. E., 1937, Explorations of the seas of Russia: Publ. Hydrol. Inst. 25, p. 1-175.
- Scholl, D. W., Buffington, E. C., and Hopkins, D. M., 1968, Geologic history of the continental margin of North America in Bering Sea: Marine Geology, v. 6, p. 297-330.
- Scholl, D. W., and Hopkins, D. M., 1969, Newly discovered Cenozoic basins, Bering shelf, Alaska Amer. Assoc. Petroleum Geologists, Bull., v. 53, p. 2067-2078.

- Scholl, D. W., Buffington, E. C., Hopkins, D. M., and Alpha, T. R., 1970, The structure and origin of the large submarine canyons of the Bering Sea: *Marine Geology*, v. 8, p. 187-210.
- Scholl, D. W., Buffington, E. C., and Marlow, M. S., 1975, Plate tectonics and the structural evolution of the Aleutian-Bering Sea region: in Forbes, R. B., (ed.), *Contributions to the Geology of the Bering Sea Basin and Adjacent Regions*: Geol. Soc. America Spec. Paper 151, p. 1-32.
- Schumacher, J. D., Kinder, T. H., Pashinski, D. J., and Charnell, R. L., in prep., Structural fronts over the continental shelf of the eastern Bering Sea: submitted to *J. Physical Ocean*.
- Sharma, G. D. 1974, Contemporary depositional environment of the eastern Bering Sea: in Hood, D. W. and Kelley, E. J., (eds.), *Oceanography of the Bering Sea*, Inst. of Marine Science, Univ. of Alaska, Occasional Publ. 2, p. 517-540.
- _____ 1975, Contemporary epicontinental sedimentation and shelf grading in the southeast Bering Sea: in Forbes, R. B. (ed.), *Contributions to the geology of the Bering Sea Basin and adjacent Regions*, Geol. Soc. Amer. Spec. Pap. 151, p. 33-48.
- Sharma, G. D., Nardu, A. S., and Hood, D. W., 1972, Bristol Bay: A model contemporary graded shelf: *Amer. Assoc. Petroleum Geologists*, v. 56, p. 2000-2012.
- Swift, D. J. P., Stanley, D. J., and Curray, J. R., 1971, Relict sediments on continental shelves: a reconsideration: *J. Geol.*, v. 79, p. 322-346.
- Takenouti, A. Y., and Ohtani, K., 1974, Currents and water masses in the Bering Sea: A review of Japanese work: in Hood, D. W. and Kelley, E. J., (eds.), *Oceanography of the Bering Sea*, Inst. of Marine Science, Univ. of Alaska, Occasional Publ. 2, p. 39-57.
- Thiede, J., Chriss, T., Clauson, M., and Swift, S. A., 1976, Settling tube for size analysis of fine and coarse fractions of oceanic sediments: Oregon State Univ., School of Oceanography, Reference 76-8, 87 p.
- Thomas, R. L., 1969, A note on relationship of grain size, clay content, quartz and organic carbon in some Lake Erie and Lake Ontario Sediments: *Jour. Sed. Petrology*, v. 39, p. 803-809.

- Trask, P. D., 1932, Origin and environment of source beds of petroleum: Houston, Gulf Pub. Co., 323 p.
- U. S. Department of Commerce, 1970, Seismicity of Alaska NEIC Map 3011: Environ. Science Adm., U. S. Coast and Geol. Survey, Washington, D. C., 1 ed.
- Van Straaten, L. M. J. V., 1954, Composition of recent marine sediments in the Netherlands: Leid. Geol. Meded., v. 19, p. 1-108.
- Watts, A. B. and Ryan, W. B. F., 1976, Flexure of the lithosphere and continental margin basins: Tectonophysics, v. 36, p. 25-44.

APPENDIX A. List of Publications and Major Reports

- Marlow, M., McLean, H., Vallier, T., Scholl, D., Gardner, J., and Powers, R., 1976, Preliminary report on the regional geology, oil and gas potential, and environmental hazards of the Bering Sea shelf south of St. Lawrence Island, Alaska: U. S. Geological Survey Open-File Report 76-785, 60 p.
- Gardner, J. V. and Vallier, T. L., 1977, Faulting, unstable sediments and surface sediments in the southern Bering Sea outer continental shelf and slope: EOS Transactions, Amer. Geophys. Union, v. 58, No. 6, p. 404.
- Gardner, J. V., Vallier, T. L. and others, 1977, Distribution and carbon content of surface sediments in the outer continental shelf of the southern Bering Sea: Geol. Soc. Amer. Abs. with Programs, Annual Mtg., p. 985.
- Kvenvolden, K. A., and Redden, G. D., 1977, Low molecular weight hydrocarbons in sediments of the southern Bering shelf: Geol. Soc. Amer. Abs. with Programs, Cordilleran Section Mtg., v. 9, p. 449.
- Vallier, T. L., Gardner, J. V., and others, 1977, Heavy minerals and clay mineralogy of surface sediments, southern Bering Sea continental margin: Geol. Soc. Amer. Abs. with Programs, Annual Mtg. p. 1207.
- Vallier, T. L. and Gardner, J. V., 1977, Maps showing types and data of faults interpreted from seismic profiles in the St. George Basin, southern Bering Sea: U. S. Geol. Survey Open-File Report 77-591, 14 p. plus maps.
- Gardner, J. V. and Vallier, T. L., 1977, Underway geophysical data collected on U. S. G. S. Cruise S4-76, southern Beringian shelf: U. S. Geol. Survey Open-File Report 77-524, 4 p. plus microfilm copies of the records.
- Gardner, J. V., Vallier, T. L., and Dean, W. E., 1978, Grain size, total carbon, mineralogy, and inorganic geochemical data from surface sediments of the southern Bering Sea continental shelf: U. S. Geological Survey Open-File Report 78-923, 31 p.
- Gardner, J. V., and Vallier, T. L., 1978, Underway seismic data collected on U. S. G. S. Cruise S6-77, southeastern Bering Sea: U. S. Geol. Survey Open-File Report 78-322, 5 p. plus microfilm copies of records.

- Underwood, M. B., Vallier, T. L., Gardner, J. V., and Barron, J. A., 1979, Age, grain size, mineralogy, and carbon/carbonate content of Miocene and Pliocene samples from dredge hauls, DSDP Holes 184 and 185, and the Sandy River well, southern Bering Sea continental margin and Alaska Peninsula: U. S. Geol. Survey Open-File Report 79-450, 34 p.
- Vallier, T. L., Underwood, M. B., Jones, D. L., and Gardner, J. V., submitted, Upper Jurassic rocks from the continental shelf, southern Bering Sea; Amer. Assoc. Petrol Geol. Bull.
- Gardner, J. V., Dean, W. E., and Vallier, T. L., in press. Sedimentology and geochemistry of the surface sediments, outer continental shelf, southern Bering Sea: Marine Geology.
- Gardner, J. V., and Vallier, T. L., in press, Distribution of faults in the outer continental shelf, southern Bering Sea: Amer. Assoc. Petroleum Geology Bull.
- Simpson, G. L., Vallier, T. L., Pearl, J. E., and Lee-Wong, F., in press, K-Ar ages and geochemistry of basalt dredged near St. George Island, southern Bering Sea: U. S. Geol. Survey Circular.
- Lee-Wong, F., Vallier, T. L., Hopkins, D. M., and Silberman, M. L., in press, Preliminary report on geochemical data for basalt from the Pribilof Islands and vicinity, southern Bering Sea: U. S. Geol. Survey Open-File Report 79- .
- Vallier, T. L., Underwood, M. B., Gardner, J. V., and Barron, J. A., submitted, Neogene sedimentation on the outer continental margin, southern Bering Sea: Marine Geology.
- Dean, W. E., and Gardner, J. F., in preparation, An oxidizing event which affected sediments in the Aleutian Basin, southern Bering Sea: Geology.
- Lee-Wong, F., Vallier, T. L., Hopkins, D. M., and Silberman, M. L., in preparation, Petrology of basalt from the Pribilof Islands and adjacent dredge hauls, southern Bering Sea: Jour. Petrology.
- Gardner, J. V., and Klise, D. A., in preparation, Late Quaternary paleoclimate of the southern Bering Sea outer continental shelf: Marine Geology.

FINAL REPORT

Contract #03-5-022-91

Research Unit #244

Number of Pages: ii + 60 pp. + appendices

STUDY OF CLIMATIC EFFECTS ON FAST ICE EXTENT
AND ITS SEASONAL DECAY ALONG THE
BEAUFORT-CHUKCHI COASTS

Principal Investigator

R.G. Barry

Associate Director, Professor of Geography

Institute of Arctic and Alpine Research

University of Colorado 80309

31 March 1979

TABLE OF CONTENTS

	<u>Page</u>
Project Personnel	ii
I. Summary	1
II. Introduction	3
A. General Nature of the Study	3
B. Specific Objectives	3
C. Relevance to Problems of Petroleum Development	4
III. Current State of Knowledge	5
IV. Study Area	5
V. Data	6
A. Remote Sensing	6
B. Meteorological Data	6
C. Climate - Ice Interaction Case Studies	7
VI. Results	7
A. Remote Sensing Interpretation and Ice Mapping	7
B. Synoptic Climatology	11
C. Climate - Ice Interaction	20
VII. Discussion	25
VIII. Conclusions	28
Tables	36
Figures	42
References	56
Appendix 1	
Appendix 2	
Appendix 3	

Project Personnel

Roger G. Barry: Principal Investigator

Andrew Carleton: Graduate Research Assistant (October 1978-March 1979)

Margaret Eccles: Programming Consultant

Richard Keen: Graduate Research Assistant (March-April 1976)

Charlene (Wright) Locke: Professional Research Assistant (July-August 1977)

Richard E. Moritz: Graduate Research Assistant (April 1975-August 1977)

A. Jane (Reynolds) Quinlan: Graduate Research Assistant (June 1977-May 1978)

Jeffery C. Rogers: Graduate Research Assistant (January 1976-March 1979)

Barry F. Warmerdam: Graduate Research Assistant (June 1977-August 1978)

Ronald L. Weaver: Graduate Research Assistant (September 1975-March 1976)

Gary M. Wohl: Graduate Research Assistant (July 1976-August 1978)

I. SUMMARY.

The most significant hazard to offshore petroleum development along the Beaufort-Chukchi Sea coasts of Alaska is posed by the occurrence of sea ice for at least nine months of the year. As a basis for assessment of this hazard, the project had the following objectives: (1) to delimit the extent of fast ice along the Beaufort and Chukchi coasts prior to and during the decay season; (2) to define and characterize the nature of the summer decay of fast-ice from remote sensing data; (3) to determine climatic processes and meteorological synoptic events contributing to the spatial and temporal characteristics of fast-ice breakup and to examine their amenability to predictive assessment.

Ice conditions were mapped for 1973-76, primarily from Landsat satellite imagery; climatic conditions were studied for the available period of continuous records (since 1921 at Barrow).

Major findings are as follows:

- (1) The rate and pattern of summer breakup of the fast ice in the Beaufort Sea is strongly influenced by the history of ice events during the preceding winter, and especially by the occurrence of grounded ridges between about 15 m and 30 m water depth. Along the Chukchi Sea coast a recurrent flaw lead south of Barrow facilitates ice movement once melt and cracking begins.
- (2) The stages of fast ice decay and northward pack ice retreat on the Beaufort Sea coast can be correlated with the accumulated thawing-degree days (TDDs).

- (3) In order of importance, air temperature, sea-level pressure distribution, and surface wind direction account for most of the year-to-year variance in northward pack ice retreat in the Beaufort Sea; their correlation with ice retreat increases as the summer progresses.
- (4) Light-ice summers in the Beaufort Sea are associated with southerly surface winds and a tendency for higher than normal pressure over the Arctic Basin centered about 80°N , 120°W , and lower than normal pressure over the East Siberian Sea, centered on 75°N , 170°E . The reverse is true for heavy-ice summers.
- (5) The trends in sea-level pressure at 80°N , 120°W and 75°N , 170°E since 1939 and summertime TDDs since 1921 at Barrow indicate a decline in favorable mean ice conditions. Since 1953, 13 of 24 summers have accumulated over 400 TDDs (required for a northward retreat of the pack ice) while 28 of 32 summers from 1921 to 1952 did so. Heavy-ice conditions, such as those during 1955, 1975, and other recent summers, may not have occurred since before the mid-1920's.
- (6) Monthly temperatures at Barrow in summer show some persistence that may be applied to forecasting breakup conditions. Summers with a predominance of monthly mean temperatures below normal, even with some normal months, will become severe ice years. Temperature persistence increases in late summer-autumn, implying applicability also to the timing of freeze up.

II. INTRODUCTION

A. General Nature of the Study

Nearshore ice along Alaska's Beaufort Sea and Chukchi Sea coasts undergoes an annual cycle of formation, extension, modification, ablation, and breakup. Many of the processes which contribute to this cycle are poorly understood, although it is generally recognized that meteorological and climatological factors are important influences for ice formation, motion, deformation, ablation, and breakup. This study has attempted to interpret ice characteristics and their time variations from remote sensing data supplemented by aircraft and field observations. This derived information covering both the Beaufort and Chukchi coasts has been compared with concurrent coastal weather conditions and regional atmospheric circulation patterns. On this basis, a systematic set of weather-ice relationships has been derived which, apart from their description of some anomalous conditions, can also provide a framework for predictive schemes.

B. Specific Objectives

- (1) Map ice characteristics and behavior during the decay season of 1973-76 from available remote sensing data.
- (2) Investigate surface weather data from the coastal stations and synoptic-scale atmospheric pressure patterns over the region to determine relationships between important ice-related weather "events" and the atmospheric circulation.
- (3) Examine the possibilities for predictive assessments of climatic factors influencing fast-ice decay and pack ice retreat.

C. Relevance to Problems of Petroleum Development

Offshore petroleum development may involve temporary operations on the winter fast-ice surface or in the open waters during summer. Alternately, large, ice-resistant structures may be used year-round. An accurate assessment of the best operational modes and of the seasonal distribution of ice hazards requires that the normal patterns of fast-ice characteristics and breakup processes and their interannual variability be specified. Also, the pathways of pollutants deriving from oil spills or blowouts are dependent to some degree on the season, and, in summer, on the relative progression of the breakup. It also seems significant that various faunal populations utilize the coastal environment, above and below the ice and in the open water areas. Seasonal and interannual variations in the weather and ice characteristics are important factors affecting the distribution and movements of these populations. These questions are elaborated in the report of the Beaufort/Chukchi Synthesis Meeting (Arctic Project Office, 1978).

The timing of major phases of the seasonal ice regime in the near-shore zone (i.e. melt in situ, first openings and movement, clearance along coast, etc.) and their interannual variability are of primary and most direct importance to offshore operations. The results summarized below address these questions. Also, the basis for a long-range ice forecasting technique has been developed, using air temperature at Barrow. This technique can be used to determine (i) when shipping can be expected to begin; (ii) the approximate length of the shipping season; (iii) the relative severity of summertime ice conditions.

III. CURRENT STATE OF KNOWLEDGE

The general characteristics of fast ice have been known for some time (e.g. Zubov, 1943), while more recent review of conditions in the Beaufort Sea fast-ice zone are given by Kovacs and Mellor (1974) and Reimnitz et al. (1976). The regional-scale dynamics of the fast-ice zone could not be effectively studied in detail until the launch of Landsat (formerly ERTS) in 1972. A good deal of literature has emerged since that time treating the information content of Landsat imagery of sea ice, but the OCSEAP Project represents the first systematic applied study of the regional scale surface morphology, composition and dynamics of fast-ice along the Beaufort and Chukchi Sea coasts. Our analysis complements the ice mapping studies of Stringer (OCSEAP Research Unit #258).

Weather and climate have been studied by a number of authors (see e.g., Watson, 1968; Selkregg, 1974; Holmgren and Weller, 1974) for the Alaska region, and the Arctic atmospheric circulation has likewise been treated (e.g. Keegan, 1958; Reed and Kunkel, 1960; Wilson, 1967, Hare, 1968; Weller and Bowling, 1974). However, the relationships between ice decay processes and weather variations has hitherto received little attention, especially on the detailed scale required for BLM planning.

IV. STUDY AREA

The fast ice zone along the Beaufort and Chukchi Sea coasts between Demarcation Point and the Bering Strait represents the study area for this project. The seaward extent is variable according to season and location, but is generally about 50 km from the coast.

V. DATA

A. Remote Sensing

Regional scale mapping of the ice characteristics and behavior for 1973-76 has been carried out from Landsat imagery. Details of frames interpreted are given in the Quarterly Reports. Interpretation of categories of age, deformation, puddling of the ice, etc., has been performed with the aid of other remote sensing products (particularly aircraft SLAR and CIR) as well as reconnaissance observations and hand-held photography of the ice from aircraft.

B. Meteorological Data

The sources of data for the studies included here are as follows:

- (1) National Weather Service station meteorological data for Kotzebue (1953-76), Barrow (1953-75) and Barter Island (1958-75) respectively. These data are published as Local Climatological Data. Parameters used are temperature (sometimes converted into thawing degree days), wind speed and direction, barometric pressure, cloud cover. Synoptic weather data for DEW-line stations (Deadhorse, Lonely, Oliktok) are also used for case studies.
- (2) Daily (1200 GMT) grid-point data on MSL pressure for 1946-74 analyzed by NMC, NOAA (provided by NCAR, Boulder). These are used in the pressure pattern classifications and for computing geostrophic winds.
- (3) Sea-level pressure maps for the Beaufort Sea prepared by AIDJEX for summer 1975.

C. Climate-Ice Interaction Case Studies

These studies utilised the above data sources and also tabulations of the retreat of fast-ice and pack ice off Barrow on September 15 of each year since 1953 (Barnett, 1976). Each summer is ranked according to its ice severity.

The analytical methods used in the case studies involved the characterization of particular ice events identified on Landsat imagery in terms of preceding and concurrent meteorological conditions. Indices employed in the analysis include cumulative thawing degree days (sums of positive departures of daily average temperature above 0°C).

The research strategy focussed on identifying links between climatological parameters, synoptic patterns of atmospheric circulation and processes of ice decay in the near-shore zone. This has also necessitated the determination of the initial state of ice conditions in spring. Mapping of winter ice events would necessitate repetitive SLAR imagery and supporting ground-truth information which were not available.

VI. RESULTS

A. Remote Sensing Interpretation and Ice Mapping

1. Ice Maps

The mapping of shorefast ice extent and morphological characteristics, as inferred primarily from available cloud-free Landsat imagery, has been carried out for the entire Beaufort Sea and Chukchi Sea coasts for the spring-summer seasons of 1973 through 1976.

For convenient references, a summary is given of the Annual Reports (AR) and Quarterly Reports (QR) containing these ice maps:

	<u>1973</u>	<u>1974</u>	<u>1975</u>	<u>1976</u>
A. <u>Beaufort Sea:</u>				
Barrow Sector	QR Sep.77	AR Mar.77	QR Sep.77	QR Dec.77
Prudhoe Sector	AR Mar.77	AR Sep.76	QR Sep.77	AR Mar.78
Barter Is. Sector	QR Sep.77	QR Sep.77	QR Sep.77	AR Mar.78
B. <u>Chukchi Sea:</u>				
Barrow Sector	AR Mar.77	AR Mar.77	AR Mar.77	QR Sep.77
Pt. Hope Sector	AR Mar.77	AR Mar.77	AR Mar.77	QR Sep.77
Kotzebue Sector	QR Dec. 76	AR Mar.77	AR Mar.77	QR Sep.77

Summary maps showing the fast ice extent in early summer 1973-76 along both coasts are reproduced in Appendix 1.

The study necessitated the development of interpretive keys of ice conditions based on the remote sensing data. These included Landsat, some limited SLAR (side looking radar) imagery and high-level aircraft infrared photography. In addition, project personnel carried out low-level aircraft reconnaissance along the Beaufort coast in early summer 1975, 1976, 1977, and along the Chukchi coast in 1976 and 1977. Correlative analysis of Landsat images, SLAR imagery, and CIR photography, supplemented by field observations, shows that the following ice features can be located and identified:

- (1) Large fields of level, hummocked, and ridged ice.
- (2) Differentiation of first-year and older age categories, if the older ice inclusions are vast-floe (2-10 km) size or greater.
- (3) Ice puddling characteristics: the integrated effects of puddle depths and percent areal coverage.
- (4) Large, well-grounded ice features in the fast-ice.

- (5) Ice concentration vs. open water.
- (6) Time changes in the ice (motions, puddling increases, drainage, breakup).

A test of the spectral information content of Landsat data using the LARSYS system at Purdue University (through a subcontract with Laboratory for the Application of Remote Sensing, Purdue University) shows that during the melt season these data are mainly useful in determining the coverage and relative depth of surface melt pools on the ice.

A major problem with the Landsat data is the infrequent coverage and the high probability of cloud cover in the study area.

The average dates of significant ice decay events based on the Landsat analysis are summarized in Table 1. It should be stressed that these phenomena are large-scale ($\geq 10 \text{ km}^2$) because of the satellite resolution. Motions can occur on various scales in the "fast" ice during winter, for example, but these motions are too small for Landsat to resolve. These dates can be viewed as climatological averages, with a probable variability (between years) of ± 10 days. The ≥ 14 -day data gaps caused by the Landsat orbit do not permit better time resolution.

An overview of ice breakup processes along both coasts is given in Appendix 1. Some additional details for the Beaufort Coast are, however, appropriate here. The spring flooding of estuarine ice areas is most prominent along a short section of the coast including the Colville, Kuparuk and Sagavanirktok rivers. Other rivers showing some evidence of this phenomenon include the Canning, Sadlerochit, Hulahula, Jago and Aichikik rivers. Around mid-to-late June, the areas previously flooded

by these rivers begin to develop shore-polynyi which spread laterally and seaward through mid-July. The largest of these (Colville) appears to allow an avenue of motion for shoreward-moving ice when breakup starts. Although the Meade, Chipp and Alaktok rivers do not exhibit large-scale flooding over the ice in May, they appear to enhance the ice melt in Dease Inlet and Smith Bay through the creation of shore polynyi in late June. Polynyi off Point Hope are discussed in Section VI C.

Surface meltwater on the ice shows considerable variations, both spatially in a given year and interannually at a given site. First-year ice with relatively light deformation appears to pond the most melt-water. These areas often drain in late June or early July. Nevertheless, they are usually the first areas to melt through completely and break up. When older ice floes are incorporated into the fast-ice, they tend to persist late into the melt season. After the interstitial matrix of first-year ice has melted, however, these floes become mobile.

Large, grounded ice masses can be found in the fast-ice in any given year. Depending on the depth at which they become grounded, they may or may not represent the seaward edge of fast ice. It is certain, however, that well-grounded ice masses do not form a continuous, shore-parallel strip along the coast, but are separated by ice which is either poorly-grounded or floating. In some years they may be absent along major sections of the coast. The elevated ice deformation features which comprise the groundings persist later into the melt season than any other component of the fast-ice. In at least one year (1975), several of these large, grounded masses survived the summer and could be seen in the spring-summer fast-ice of 1976.

In 1973, 1974 and 1976 a coastwise parallel strip of open water and loose pack ice was present in August along most of the coast. In 1975, the fast-ice melt was retarded by extremely low summer temperatures, and the polar pack ice was held close to shore. This was also a year when several extensive, grounded ridge fields occurred in the eastern part of outer Harrison Bay to Cross Island. Landsat imagery from August and September, 1975, indicates these ice structures may have shielded the inner shelf from even more pack ice impingement than was observed. November, 1975, imagery indicates that the presence of these ice structures stabilized the incipient fast-ice sheet at a very early date.

B. Synoptic Climatology

1. Beaufort Sea

Daily MSL pressure grids for the sector 57° - 80° N, 125° - 170° W, have been classified for January 1966-August 1974 by Moritz (1978) using an objective technique based on Kirchhofer (1973). The method focuses on the location of pressure systems and their shape; the pressure gradient is normalized for each daily map removing intensity effects. Moritz derived 21 discrete characteristic patterns (CPs) which accounted for 97 percent of all days during the period. The order of identification of the types corresponds to their total frequency (i.e. CP1 is most frequent, CP21 least frequent). The most frequent patterns are those with low pressure over the southern part of the grid and highs or ridges to the north. Analyses of daily surface pressure charts in relation to the synoptic catalog of nominal pressure pattern types showed that some variation in qualitative features of the pressure field is to be expected among the individual daily grids grouped with a given CP.

The time series of nominal pressure patterns was analyzed for seasonal changes. In winter (mid-September to mid-May) CP1 dominates the surface circulation, with lows to the south and highs to the north (see Figure 1 a-d). CPs 3, 4, 7 and 9, which have their highest pressure somewhere near the northern coast with lower pressures to the southwest, south or southeast, are also important in winter. A pronounced shift in mean monthly pressure pattern frequencies occurs from mid-May to June, characterized by more frequent occurrence of CPs 2, 5, 6, 8, 10, 14, 15 and 21, and a corresponding decrease in frequency of the main winter CPs (see Figure 2). The summer regime, consisting of these patterns, is well developed during July through late August. This regime has frequent low pressure features over the central, western and northern portions of the grid sector. To the south, the Pacific High often extends northward as a ridge over the Gulf of Alaska at this season. The summer regime has a greater variety of patterns than does the winter regime. A second transition occurs from late August to mid-September, when the winter patterns begin to dominate again. During January, CPs 2 and 4 undergo a one-month frequency increase, leading to small "kinks" in the seasonal cooling curves at Barrow and Barter Island. This phenomenon is similar to, but less pronounced than the Antarctic coreless winter, and is caused by increased temperature advection when the two patterns occur.

On the interdiurnal time scale, persistence is the most important characteristic of the pressure pattern time series. All CPs persist significantly more often than at random. Non-persistence transition probabilities are generally too small to be of forecasting value, but are nonetheless highly significant in a statistical sense. Persistence

is most pronounced for CP1 and for winter patterns in general. Non-persistence transitions indicate eastward progression of low pressure systems through the southern part of the grid sector in winter. Beaufort Sea highs and ridges often tend to be displaced south or southeast at this season. In spring, the southwest lows often move over central Alaska rather than skirting the state to the south, while in summer Pacific cyclone systems move northward along the west coast and into the Arctic Basin.

Coastal weather data are serially correlated on a day to day basis in the region, leading to reductions in the per-month degrees of freedom for the series. Nonetheless, daily temperature departures, wind speeds, and wind directions all show highly-significant associations with the CP categories in all seasons. Weather variables which have significant inter-CP differences in some, but not all, seasons include daily sky cover, dew-point depression and precipitation amount. Tests demonstrate conclusively that a portion of the variance in weather data series is due to the sea level pressure patterns.

Although any study of this size cannot completely characterize all aspects of the regional climatology, several important features were identified by our methods. In all seasons the surface wind directions are largely determined by the prevailing surface pressure pattern on the Beaufort Sea coast. Generally good agreement was found between the Barrow surface wind directions and the geostrophic directions on the CP synoptic maps. Daily temperature departures have three major regimes through the year. In winter the overall variance of temperature is

largest. Screen temperatures are largely determined by the surface net radiation and the three dimensional temperature advection by the circulation. Thus extreme warmings are associated with influx of moist Pacific air, high wind speeds and relatively heavy cloud cover when CP2 occurs (see Table 2). By contrast, CPs 3 and 7 bring cold, clear, dry air from the central Arctic or Siberia, and cut off the Pacific influence at the surface. The normal winter pattern, CP1, lies between these two extremes with an intermediate rate of temperature advection from the south. Temperature departures with CP1 are, however, substantially closer to those of CP3 and CP7 than to those of CP2, which is a relatively rare pattern in winter. These relationships lead to a right-skew frequency distribution of screen temperatures in winter, especially in January when CP2 occurs more frequently.

During the spring transition the large-scale surface temperature contrasts between the Pacific heat source region and the Beaufort Coast are at an annual minimum, leading to a minimum in the variance of daily temperature departures. In some cases, notably CP6, the positive effects of large scale southerly advection begin to be balanced by local ocean/tundra heating differences. In summer these local contrasts are paramount, leading to positive temperature departures with offshore flow and negative departures for onshore flow (Table 3). Since the surface winds are largely determined by the synoptic pressure pattern, there is a high degree of correspondence between the CPs and their temperature departures in summer. CPs 2, 4, 10, 15 and 21 have southerly components to their mean wind directions, bringing positive temperature departures and relatively large

dew-point depressions to Barrow in July. By contrast, CPs 1, 5, 6, 8 and 14 have wind directions between west and east-northeast at Barrow, bringing negative temperature departures up to -3°C and near-saturated air.

The wind directions at Barrow are in general agreement with the CP synoptic map isobars in the majority of cases. As one might expect, wind direction is the most consistent weather characteristic of the CPs from season to season.

Barrow wind speeds show significant inter-CP differences in all seasons (see Tables 2 and 3). In winter speeds are low with the ridge patterns (CPs 3 and 7), while the cyclonic storms from the Pacific bring quite strong winds. These strong winds would be expected to develop in the presence of the strong surface baroclinicity which characterizes the region in winter. During the spring transition season most of the patterns have wind speeds around 5 ms^{-1} , but CP1 is one to two ms^{-1} faster. This increase occurs at the same time that the standard deviation of pressure over the daily maps is falling sharply for CP1, indicating weaker geostrophic flow. The implication is that the synoptic station network is inadequate to measure the true pressure gradient near the coast. This problem continues into the summer, when sea breeze effects are probably present (Moritz, 1977), as indicated by strong easterly patterns and weak westerly patterns. Even during summer the patterns with northerly flow tend to have lower mean wind speeds. In the fall the cyclonic storms begin to become more intense, leading to higher winds.

Precipitation is primarily a function of the vertical motion field and the humidity of the air. During winter the patterns with advection

from the Pacific tend to be cyclonic, implying positive vertical circulations near the Beaufort coast. Moist, marine air is brought into the region under these CPs. Thus CP2 is associated with measureable precipitation in over half its winter occurrences. However, the overall high frequency of CP1 and the small seasonal precipitation totals along the coast make CP1 the major winter precipitation pattern. By contrast, the west-coast cyclonic patterns are most frequent in summer, and the majority of the annual catch falls in association with these CPs during June-September.

In presenting these results and the synoptic catalog (available on tape via NODC), a qualification must be noted above the reliability of the pressure data over the Beaufort Sea. Comparison of the summer 1975 pressure data provided by AIDJEX with NMC analyses shows a significant degree of discrepancy (Wohl, 1978). However, when Wohl attempted to modify the synoptic classification using only data over northern Alaska and the Beaufort Sea, in order to eliminate the effect of Gulf of Alaska circulation systems on the CP categories, he found that the resulting revised classification was less satisfactory than the original one due to the poor data over the Beaufort Sea.

2. Chukchi Sea

An identified typing scheme was also developed for the Chukchi Sea for January 1946-August 1974 in order to ensure a sufficient extension to the west. The grid covers the sector approximately 57°N , 155°W -- 57°N , 175°E -- 77°N , 135°W -- 77°N , 155°E . A synopsis of the basic results and of the application of the catalog to an analysis of daily climatic data for Kotzebue is given in Figures 3 a-d, 4-7.

- (i) Winter - Type 1 (Arctic High Pressure with subpolar easterlies at Kotzebue) is dominant, bringing near normal weather characteristics. Interruptions by anticyclonic (the most common) systems bring cold, dry weather to Kotzebue because they are associated with cold, continental air masses with weak northerly winds and little cloud cover which tend to reinforce the Arctic inversion. Cyclonic interruptions (less common) bring warmer than average, moist weather to Kotzebue because they are associated with warm maritime airmasses with strong southerly to easterly winds that tend to break-up the Arctic inversion and large cloud amounts that influence the net radiation budget by absorbing and re-radiating (terrestrial) radiation.
- (ii) Summer - In summer there is a greater variety of types and the difference between cyclonic and anticyclonic types is not readily apparent. The main factor influencing temperature is geostrophic wind direction, with easterly winds causing continental outflow of warm air and westerly winds causing cool air advection from the Chukchi Sea. Because ice conditions are closely related to temperature conditions, warm types with easterly flow (1, 2, 13, 17) are probably important in helping force summer ice break-up. Cold westerly types (3, 10, 15) are probably important for delaying that breakup. Type 3 which is closest to the mean pressure pattern is the most common type in July.
- During summer, a mean storm track is established from south to north up the Bering Sea and through the Bering Strait,

following the northwest coast of Alaska in the Chukchi Sea. Hence, summer is a time of heightened cyclonic activity, with cyclonic types 2, 7, 12, 17 bringing considerable precipitation. It is likely that the role of open water in the Bering and Chukchi seas is important in supplying latent heat and moisture to storms moving along this track, which are less frequent during the frozen winter period.

A relationship between the onset of "monsoon" westerly winds and accumulated thawing degree days (TDDs) in summer has been established (Figure 8). Probably because of the influence of interior high temperatures and resultant thermal low, westerlies tend to blow inland at Kotzebue during summer, unless interrupted by strong opposing pressure types. The earlier these winds set in, the lower the total TDDs at Kotzebue.

Based on analyzes for Kotzebue described in the Annual Report for 1978 (p. 49), a general model of a cold July on the Chukchi Sea coast can be outlined.

- 1) Major cyclonic types (2, 7, 12, 17) decrease in frequency, from 77 days in 7 warm Julys to 38 days in 7 cold Julys, indicating that the normal storm track up the Bering Sea, Bearing Strait, and eastern Chukchi Sea does not become well established.
- 2) Marginally cyclonic types increase (types 5, 10, 11, 15) in frequency from 29 days in warm years to 57 days during cold years. This may indicate a shift of the normal storm track to the east, over continental Alaska. This track tends to advect cool air from the Chukchi Sea to Kotzebue by reinforcing the prevailing NW and N winds.

- 3) A logical reason for such a shift would be the establishment of a mean upper trough over the Chukchi Sea tending to "steer" surface storms to the east of Kotzebue. Such a trough would also bring cold Arctic air over the Chukchi Sea, tending to delay ice breakup. It would be associated with upper divergence over the Beaufort Sea, which favors the development of lower pressure in this key area. Low pressure in the Beaufort Sea brings northwest surface flow at Kotzebue, again strengthening the prevailing westerlies.
- 4) Delayed ice breakup in the Chukchi Sea tends to bring about the lower sea surface temperature and cooler conditions in general at Kotzebue, as indicated by the decrease in average temperature of most of the other types at Kotzebue.

There is some relationship between the winds over the Chukchi coast and ice conditions at Barrow. The five years of earliest westerly onset were also the years with most severe summer ice conditions at Barrow. The causal mechanism behind this association is not yet established, but the relationship has some predictive value. If the westerlies set in prior to May 4 at Kotzebue, it is likely to be a severe ice summer on the Beaufort Sea coast.

The warmest weather at Barrow during summer is associated with Chukchi types 2 and 12, which are characterized by cyclones in the Bering Sea and Bering Strait region, which steer very warm air toward Barrow from the North Pacific. These types occur on about 30 percent of the days during warm July, but only about one-half that during cold Julys. Types 3 and 10 are the cold types which occur on 26 percent of the days during cold

Julys and only one-half that during warm Julys. They are characterized by cyclones in the Beaufort Sea that steer cold air southward and westward from the Arctic pack ice to Barrow.

C. Climate-Ice Interactions

1. General Relationships

A central objective of the project has been to determine the role of the seasonal climatic regime and synoptic weather events on the course of the fast ice decay. This has included case studies and statistical analysis of long-term climatic data at Barrow. The details of our results are presented in Appendices 1-3 and only a brief summary is given here.

From analysis of Landsat imagery and Barrow temperature data the following general relationships have been established with thawing degree-days (TDDs) for the Beaufort Sea ice off Barrow:

	<u>TDDs (°C)</u>	<u>Ice Event</u>
(i)	<55	- initiation of ponding and rapid thawing of ice
(ii)	55 - 140	- initial breakup, some open water
(iii)	140 - 220	- fast ice largely gone, melting on pack ice
(iv)	220 - 300	- pack ice retreats, up to 80 km north of Pt. Barrow
(v)	>300	- pack ice retreats more than 80 km

From more limited data for Kotzebue and ice conditions off Kivalina, in situ melt begins with about 10 TDDs, first breakup with 55, and the nearshore zone is largely clear with 200 TDDs.

The frequency of these categories shows a significant change over time, based on climatic data at Barrow:

<u>TDD categories</u>	<u>1921 to 1952</u>	<u>1953 to 1975</u>
(i)	0	0
(ii)	1	1
(iii)	3	10
(iv)	12	4
(v)	16	8

The number of summers in which the pack ice did not retreat jumped from 4 in 32 years (12%) to 11 in 23 years (48%) in the last 55 years. There has been an average loss of 37 TDDs (a decrease from 311 for 1921-52 to 274 for 1953-75) or about 0.5°C in the mean summer temperature over the same time intervals.

Since Landsat data on ice conditions have only been examined for the 1973-76 summers, it is important to compare the climatic conditions during these years with long-term averages. This is done in Table 4, which shows mean thawing degree-days totals for Kotzebue, Barrow and Barter Island and a ranking of the 1973 to 1976 summers in terms of standard deviation (S.D.) departures. At Barter Island, all four years are within the ± 1 S.D. range about the mean.

Analysis of early weather records at Barrow for 1882, 1883, 1902, 1903, 1911, and 1916, and comparison with the interpretations of data on ice conditions in ships' logs by Hunt and Naske (R.U. #261) indicates mixed results. Both sources agree on light-ice conditions in 1902 and 1911, the data for 1883 and 1916 are too sparse to make definitive comparisons, and for 1882 and 1903 there appears to be some element of disagreement.

Regression analysis of summertime climatic parameters and pack ice retreat by mid-September tabulated by Barnett (1976) shows that geostrophic winds are not the best indicator of the distance off Barrow to the limit of 4/8 ice concentration. Surface wind direction makes a small contribution to the variance, but thawing degree-day totals alone account for 65 percent of the variance of ice distance. This

dominant temperature effect makes the role of other variables seem largely irrelevant at the present stage of our understanding of ice decay and breakup processes.

This finding raises the question of the role of wind direction in determining the summer temperature. An earlier analysis by Weaver (1970) shows that at Barrow, southerly winds bring significantly higher summer temperatures (10.6°C in July 1966) than onshore winds (2.7°C). It remains to be determined how much of the temperature-explained variance derives from this effect. Also, it is not clear how far the occurrence of open water off Pt. Barrow helps to determine the station temperature instead of the reverse, as we are assuming. Since water temperature remains close to freezing point the former effect should be limited.

2. Synoptic Climatology - Ice Interactions

The synoptic typing catalog developed for the Beaufort Sea area has been examined by Wohl (1978) in terms of its usefulness for discriminating coastal ice conditions. Individual synoptic types and groups of types, according to their geostrophic wind direction at Barrow, have been analyzed against Barnett's index¹ of ice conditions off Barrow on September 15 during 1953-77 by stepwise regression. Groups of northerly and southerly flow types account for about 42% of the variance but their average summer frequency is only 6 and 17 days, respectively. Re-definition of the circulation patterns using only grid points north of 65°N

¹ This score is the sum of the distance from Pt. Barrow to the ice edge and to the boundary of 4/8 ice concentration on September 15, the initial date that the sea route from Barrow to Prudhoe Bay has \leq 4/8 ice, the number of days this route is ice free, and the number of days it has \leq 4/8 ice.

and subsequent re-analysis along the same lines gave no significant improvement. Apart from the problems of unreliable pressure data over the Beaufort Sea already noted, there is the basic problem of attempting to determine the net effect of the season's climatic characteristics on ice conditions late in the season. While individual seasons, such as 1975, may show clear relationships to atmospheric circulation in terms of pack ice movement (Wendler and Jayaweera, 1976), most seasons show less persistent circulation patterns.

Preliminary work by Warmerdam on 500 mb pressure patterns and May-September air mass characteristics at Barrow (based on mean daily equivalent potential temperature at the surface) suggest some potentially useful relationships with ice conditions at Barrow. These results are as follows:

- (1) Air mass frequency is closely associated with ice conditions.

Severe ice years occur in summers with a dominance of Arctic air at Barrow (80% in August), while light ice years occur in association with infrequent Arctic air (20% in August) and its displacement by warmer Pacific air masses from the south.

- (2) August is the key month. There are large significant differences in Arctic air frequency during this month between severe and light ice years. Differences are also notable in July, but are not as great, and there are no significant differences in May, June, or September. This implies difficulty in long-range prediction of ice severity.

- (3) The 500 mb patterns responsible for displacing Arctic air with Pacific air seem to be mostly those with ridging over Alaska and/or Canada, leading to southerly flow over the North Slope. If such ridging is not present during August, it will be a moderate to severe ice summer.
- (4) Severe ice years seem to be associated with the formation of a large upper trough over the Alaskan region, effectively blocking Pacific air from reaching the North Slope.

3. Polynyi Near Point Hope

A special analysis of the occurrence of polynyi in the vicinity of Point Hope on Chukchi Sea coast has been carried out. Areas of open water and thin ice have been mapped from Landsat imagery for March-June 1973-77 (Table 5). The thin ice areas show up by their proximity to open water and from their usually much lower reflectance.

The development of polynyi and interannual differences in extent have been examined in relation to wind and temperature data. Onshore and alongshore components of geostrophic wind are determined from MSL pressure at six NMC grid points in proximity to Point Hope. Temperature data are for Kotzebue, but should be generally representative.

Rapid polynya development in spring is favored by strong offshore winds causing frictional divergence. Both 1974 and 1976 illustrate this effect (Table 5). The average wind is NE, 9.5 m s^{-1} in March 1974. The decrease in size from April to May apparently reflects the decrease in wind speed and the small accumulation of TDDs. The expansion during June, however, seems to be related to the rapid increase in temperature.

The reduction in polynya size from March to April 1976 is probably attributable both to the slight decrease in wind speed and to the low temperatures. From April to May, wind speeds show some increase and TDDs are also accumulating.

It is concluded that early polynya development is favored by strong offshore (Northeasterly) winds. This dynamic effect seems to be important if wind speeds increase during the season. Advection of warm air from the land appears to become equally important as the season progresses, but there are too few cases at present to quantify this effect.

VII. DISCUSSION

The picture of the ice regime and its response to climatic conditions developed in this study must still be regarded as tentative. The period of detailed record provided by the Landsat imagery is too short to be confident that a range of conditions representative of, say, a 10-20 year period has occurred. Several other factors introduce additional uncertainties into the interpretations. The infrequent Landsat coverage, due to the orbit mode and cloud cover, makes the timing of many ice events and the melt stages imprecise. Moreover, the limited ground truth available to assist the interpreter makes the reliability of the ice maps dependent on subjective judgement. It is believed that the mapping was at least internally consistent for each coast, since the interpretation was carried out in each case by a single individual with field experience in the area in summers 1975-77. Another problem, already referred to, is the unreliability of the pressure data in the Beaufort Sea.

In terms of analytical methods, it is considered that the combination of synoptic and statistical climatological approaches has proved worthwhile.

The synoptic catalogs provide a useful statistical description of the dominant seasonal circulation patterns and their weather characteristics in the two areas. The fact that a simple temperature index proves more effective in accounting for ice variability than the synoptic type frequencies reflects several problems. First, there is only one value of the ice index per year to be related to the total effect of a large complex of weather conditions over the summer, some positive, some negative. Second, each type is subject to internal variability in the actual weather conditions that occur, especially as no account is taken of pressure gradient. Third, the type catalogs are imperfect descriptions of the actual pressure fields due to the basic data limitations over the Beaufort and northern Chukchi seas. Even so, the type catalogs and the quantitative type descriptions provide a basis for assessing the likely effect of given circulations on the coastal climate. It must also be cautioned that the statistical associations imply linear relationships whereas most of the processes involve complex feedbacks and are likely to be non-linear.

Ice decay and breakup is determined partly by the ice history, in terms of the frequency of grounded ridges. River flooding causes local polynyi to develop. These assist the melt and breakup process by facilitating movement, which may initially be shoreward. However, it remains uncertain as to the relative importance of thermodynamic processes, especially associated with warm air advection, and mechanical wind stress on the fast ice breakup. Obviously warm offshore winds (southerly on the Beaufort Sea coast, easterly on the Chukchi Sea coast) will assist in accelerating the melt process and in breaking off ice floes if there is a flaw lead in the shear zone. The statistical relations, at least,

imply that the thermal effect is more important, but more work is needed to examine this question of process thoroughly.

On the time-scale of a few days, for example, there is a good correspondence between the timing of breakup between Pt. Barrow and Cape Halkett, as determined from the Landsat imagery, and the occurrence of southerly geostrophic winds. Beaufort synoptic types CP2 and 5 occur on a majority of these days. The relationship is less clear, however, if examined in terms of observed southerly surface winds.

Relationships between the weather characteristics and pressure patterns suggest some possibly useful applications. The establishment of the Pacific High in its summer position should lead to the regime dominated by Beaufort type CP2. If monthly forecasts of the pressure field can be made by numerical, analog, or other means, then a forecast for the early displacement of the high in spring implies an early onset of southerly winds, positive temperature departures, and possibly a light sea ice year along the coast. The occurrence of high winds in winter with incursions of cyclonic patterns implies that the near-shore ice may be subject to false freezeups and subsequent disturbance by such storms before, say, January or February. A case of such ice disruption has been documented by Shapiro (1976) for December 1973 near Barrow. The general seasonal character of pressure pattern occurrence, and their associated weather characteristics will also be useful as an introduction to forecasters in the region, although the major application of the data should be as an information resource for planning and decision-making involving the Beaufort Sea Coastal region.

VII. CONCLUSIONS

The results of this project allow two broad sets of conclusions to be drawn. The first group are direct products of the ice mapping and climate-ice interaction studies. The second set are more general, tentative, inferences of significance for planning with regard to offshore petroleum development.

A. The Seasonal Fast-Ice Regime

The results of our program, combined with other OCS studies, provide a scenario of the fast-ice regime that can serve as a framework for seasonal scheduling of operations in the nearshore zones (see Appendix 1 for details).

1. Beaufort Sea Coast

- (i) new ice formation - late September/early October
- (ii) first continuous fast-ice sheet - mid/late October
Unstable outside bays and the barrier islands
- (iii) extension and modification of fast-ice - November to February

No direct observations cover this period. The general sequence involves:

- seaward fast-ice progression of the ice edge
- ridging of successive ice edges
- incursions of older ice
- grounded ice masses, formed in situ or driven shoreward

- (iv) stable fast-ice inside about the 15m isobath - February to April/May
- (v) estuarine flooding of ice - late May
- (vi) puddling on ice - early June
- (vii) melting and weakening of ice - June (Attached ice decays April/June)
- (viii) breakup - late June to August
- (ix) nearshore area largely free of fast-ice - early August
Some deep-draft older ice and ridge fragments remain in the nearshore zone.

2. Chukchi Sea Coast

The fast-ice on the Chukchi coast is generally less extensive than on the Beaufort Sea coast (see Figures in Appendix 1). The sequence is similar to that above except that, for the central section, freeze-up occurs about two weeks later, and breakup 3-4 weeks earlier. Sections such as Peard Bay, in the north, where the coastline is oriented roughly east-west and there are barrier islands, tend to have breakup characteristics similar to the Beaufort coast east of Barrow. Polynyas are a prominent feature south of Point Hope in spring-early summer when they assist in accelerating the breakup. The fast-ice/pack-ice boundary south of Barrow is the frequent site of a flaw lead in winter and the ice in this sector is generally less stable and more subject to disruption and ridging by pack-ice pressure.

B. Ice Conditions and Climatic Effects

(1) Summer temperature conditions, as indicated by accumulated thawing degree-days, account for 65 percent of the variance in the distance off Pt. Barrow of the southern limit of 4/8 concentration of pack-ice on September 15. If windspeed and pressure data are incorporated in the regression, 80 percent of the variance is accounted for. Variability in ice extent by late summer is related to the sea level pressure distribution, surface wind direction at Barrow, and maximum accumulated thawing degree days at Barrow. Winds are more frequent from the south-southeast (135° - 195°) during light-ice summers while winds from the north-northeast (345° - 45°) are more frequent during severe ice summers (Rogers, 1978). These winds and pressure distributions are probably indicative of the fact that warm and cold air advection over the ice plays a primary role in determining whether a light- or severe- (respectively) ice summer will occur. This in turn is reflected in the thawing degree day accumulation which is the parameter most highly correlated to the distance which the ice retreats northward. (See Appendix 2.)

(2) An accumulation of 140-220 thawing degree days ($^{\circ}$ C) is required to remove the fast ice and 220-300 TDDs for open water to extend up to 80km off Pt. Barrow on September 15. Along the Chukchi coast, the ice data are less precise as to the timing of events due to the satellite coverage. For the Kivalina sector, using Kotzebue temperatures, approximately 200 TDDs are required to remove the fast.

(3) The high correlation between accumulated TDDs and ice retreat has been used by Rogers (1977) to develop the basis of a scheme for long-range forecasting of ice conditions in summer-early autumn along the Beaufort Sea coast (Appendix 3). The results suggest that forecasts could be made with reasonable success based upon persistence of air temperature anomalies from month to month. Persistence occurs between all months with greater frequency than would be expected by chance. In general, the anomaly of air temperature in July is most likely to recur in August, and the anomaly in August is very frequent again in September.

(4) The synoptic pressure pattern types can be characterized seasonally in terms of broadly distinctive combinations of temperature and wind conditions. Thus, CP 1 for the Beaufort Sea sector represents a pattern of polar easterly circulation, resembling the mean winter pattern, with strong NE winds and temperatures about or slightly below average. Types CP 2 and 5, which are frequent summer patterns, give rise to southerly geostrophic (southwesterly surface) winds and positive temperature departures. The summertime shift to these types is the underlying determinant of ice breakup. The available data indicate that frequencies of surface types with northerly and southerly flow components account for about 40% of the variance in the Barnett ice index. However, the TDD index is a simpler and more successful descriptor. Preliminary analysis

of mid-tropospheric circulation patterns suggests that these may be a more useful index than surface pressure fields. Further work on this would be necessary to provide definite results.

(5) Climatic data at Barrow indicate a drop in summer temperature of about 0.5°C for 1953-75 compared with 1921-52. Correspondingly, the number of summers in which >220 thawing degree days ($^{\circ}\text{C}$) were attained has declined from 88 percent for 1921-52 to 52 percent for 1953-75. This implies that fewer summers with good shipping conditions have been experienced since the 1950's compared with the three preceding decades. In climatic terms, at least, the 1975 summer was not a rare event. The limited climatic data for the 1892-1916 interval at Barrow suggest that ice conditions inferred from ship's logs should be interpreted with caution.

(6) The movement of pack ice, or broken fast-ice, along the Beaufort Sea coast in summer is almost always in the same direction as the wind at Barrow and Barter Island, even though the moving ice may be hundreds of kilometers from these stations. However, the ice at Barrow moves with lighter winds than at Barter Island. Movement and breaking of ice observed on Landsat imagery in the vicinity of Barter Island usually occurs with wind speeds averaging twice those during ice motion off Barrow. This may relate to the tendency for more open water in the Barrow area and the ice outlet via the Chukchi Sea.

C. Ice Hazards in Relation to Offshore Petroleum Development

(a) Ice deformation features. Ridges and hummocks show more or less preferred locations from year to year (cf. maps prepared by W. Stringer RU #257), probably in relation to the location of shoals (see Reimnitz, et al., 1978). Examples are: offshore and west of Barter Island, in a line from Narwhal Island to a point approximately 80km due north of Atigaru Point in Harrison Bay, and approximately along the 20m isobath arcing around Pt. Barrow in the Chukchi Sea and Beaufort Sea. These areas are the scene of enormous shear and pressure forces, most of which seem to occur during the dark period November through February.

The edge of contiguous fast-ice appears to be displaced progressively seaward through the winter months, based on interpretation of ice edges and puddling features on summer imagery. Each successive winter ice edge can be a site for ice deformation so that large grounded ice masses can occur well inside the 20m isobath. In general, however, the areal extent and intensity of ice deformation seems to be greatest near the late-winter fast-ice edge in the so-called stamukhi zone (Reimnitz, et al., 1978). This may be a consequence of the involvement of more massive polar floes and thicker first-year ice in ridge formation late in the season. Our case-study of ridging off Oliktok in late March - early April, 1975 illustrates the anomalously large and well-grounded field of shear ridges that may form in this manner.

The implication is that permanent offshore structures may be subject to relatively large ice forces, even well inside the 20m isobath, but these forces would occur further seaward by late winter. Recent work by Kovacs and Sodhi (1978) also shows that the entire Beaufort Sea and northern Chukchi Sea coasts may be subject to shore pile-up or ride-up, especially in spring and autumn. Such events may occur within 15-30 minutes with ice mounting steep coastal bluffs up to 10m high.

(b) Grounded ice. As noted above, remote sensing data can be used to locate well-grounded ice because it remains in situ late into the melt season. This type of ice is very discontinuous along the coast. During the decay season, therefore, under-ice oil spills occurring within the fast ice zone would not necessarily be contained within a band of grounded ice parallel to the coast. Nevertheless, the elongate ridges which parallel extensive segments of the Beaufort Sea coast in late winter have keels extending well below the level ice, even though they may be floating or only weakly grounded. These ridges might be effective in temporarily containing most of an under-ice oil spill during February through May. Such trapping capability would rapidly diminish after late June as the fast ice begins to disintegrate leaving only well-grounded ridges in situ. This decay date also marks the end of the period when trapping could occur in the irregular bottom topography of the floating fast ice.

Our mapping has shown that well-grounded, deformed ice masses are occasionally found in waters $\leq 10\text{m}$ deep. Structures and lines on the near-shore bottom must be able to withstand the forces generated by such features and associated bottom scour, even though the frequency and intensity of such events are much less than in the stamukhi zone.

TABLE 1. AVERAGE SEASONAL REGIMES IN ALASKAN SHOREFAST ICE

<u>Ice Phase</u>	<u>Central Beaufort Sea Coast</u>	<u>Central Chukchi Sea Coast</u>
New ice forms	3 Oct.	10 Oct.
First continuous fast ice	Mid October	Early November
Extension/modification of fast ice	Nov. - Jan./Feb.	Nov./Dec. - Jan./Feb.
Stable ice sheet inside 15 m isobath	Jan./Feb. - Apr./May	Feb. - Apr./May
River flooding fast ice	25 May	1 May
First melt pools	10 June	10 May
First openings and movement	30 June	10 June
Nearshore area largely free of fast ice	1 August	1 July

¹ These dates are based on available Landsat imagery for 1973-1977. An identifiable event may occur anywhere between the dates of available clear frames which bracket the latest date of recognized non-occurrence and the earliest date of its identified occurrence; the average of these dates is used here.

TABLE 2

JANUARY CP WEATHER CHARACTERISTICS

CP	$\overline{dT_1}$ (°C)	$\overline{dT_2}$ (°C)	\overline{WD} (°)	\overline{U} (m/s)	\overline{SC} (1/10)	$\overline{dT_D}$ (°C)	r^* (mm)	%-1 (%)	%-2 (%)
1	-1.8	-2.4	73	5.6	5.2	4.5	66.3	20	11
2	+13.5	+15.1	226	7.5	7.9	2.3	46.2	14	58
3	-3.6	-3.4	304	4.0	5.2	4.1	19.0	6	11
4	+3.0	+2.8	104	5.4	5.9	3.9	46.5	14	19
5	+2.7	+5.6	267	6.9	6.1	5.3	29.5	9	29
6							16.0	5	46
7	-2.5	-3.3	315	3.2	4.1	3.8	0.5	0	2
8							8.1	2	53
9	+1.4	-1.5	154	5.6	6.4	3.5	26.2	8	23
10							41.9	13	44

*Precipitation data are for season I (January-March) rather than for January.

TABLE 2a
KEY FOR WEATHER CHARACTERISTIC TABLES

<u>Symbol</u>	<u>Explanation</u>
CP	Characteristic pattern
$\overline{dT_1}$	Mean of the daily temperature departures at Barrow
$\overline{dT_2}$	Mean of the daily temperature departures at Barter Island
\overline{WD}	Mean of the daily wind directions at Barrow
\overline{U}	Mean of the daily wind speeds at Barrow
\overline{SC}	Mean of the daily sky covers at Barrow
$\overline{dT_D}$	Mean of the daily dew point depressions at Barrow
r	Total precipitation catch (water equivalent) at Barrow 1956-1974, for the given season and CP
%-1	r as a percentage of the unstratified seasonal catch at Barrow, 1956-74
%-2	Number of days with measureable precipitation at Barrow, as a percentage of the number of daily occurrences of the given CP

TABLE 3

JULY CP WEATHER CHARACTERISTICS

CP	$\overline{dT_1}$ (°C)	$\overline{dT_2}$ (°C)	\overline{WD} (°)	\overline{U} (m/s)	\overline{SC} (1/10)	$\overline{dT_D}$ (°C)	$\overline{r^*}$ (mm)	$\overline{\% -1}$ (%)	$\overline{\% -2}$ (%)
1	-1.7	-1.5	68	6.3	6.4	1.7	49.5	5	15
2	+1.0	+1.6	227	5.1	8.5	2.1	329.7	35	46
4	+2.0	+0.2	89	5.5	6.9	2.5	28.4	3	21
5	-2.1	-1.4	262	5.0	8.9	1.8	115.6	12	46
6	-0.3	-1.2	71	5.4	8.0	1.8	77.7	8	34
8	-2.5	-3.0	9	4.6	8.9	0.9	64.3	7	39
14	-3.2	-2.6	308	3.9	8.2	1.4	15.0	2	30
15	+1.3	+0.1	196	5.0	8.9	2.1	156.0	17	54
21	+0.6	-1.8	91	5.3	8.0		1.5	0	23

*Precipitation data are for season IV (July-August) rather than for July.

TABLE 4. AVERAGE THAWING DEGREE-DAYS ($^{\circ}\text{C}$) AND 1973-76 SUMMER CONDITIONS

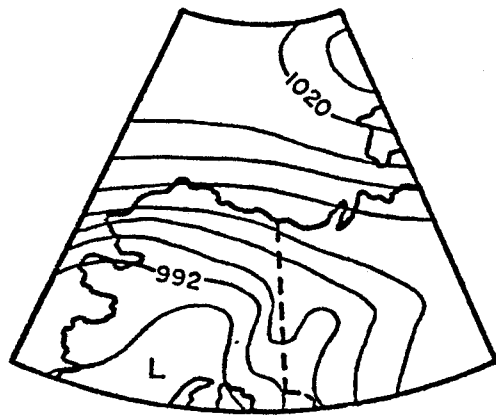
<u>Parameter</u>	<u>Kotzebue</u>	<u>Barrow</u>	<u>Barter Island</u>
Mean TDDs	1080 (1943-76)	296 (1921-75)	324 (1948-75)
S.D.	113	101	98
Median	1059	275	317
± 1 S.D. range	967-1193	194-397	226-422
1973	below avg. ¹ (971)	above avg. (358)	above avg. (398)
1974	above avg. ¹ (1170)	above avg. (364)	below avg. (328)
1975	>2 S.D. colder (845)	>1 S.D. colder (192)	below avg. (256)
1976	near avg. (1086)	near avg. (273)	near avg. (320)

¹Denotes a total within 1 S.D. of the mean value.

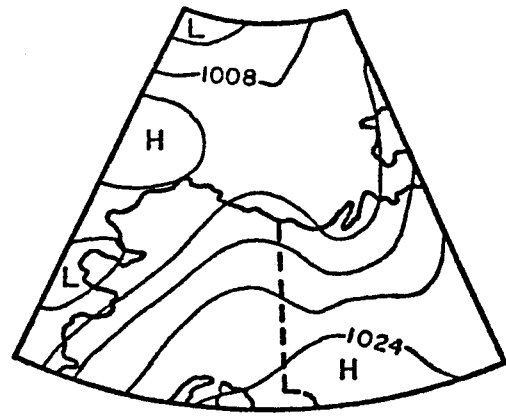
TABLE 5. POLYNYA EXTENT AND CLIMATIC PARAMETERS

<u>Year</u>	<u>Date</u>	<u>Polynya Area (Km²)</u>	<u>Monthly Rate of Change (Km²)</u>	<u>Cumulative TDDs ($^{\circ}\text{C}$)</u>	<u>Mean Vector Wind for NMC Grid Points Near Point Hope (ms⁻¹)</u>
1973	11 April	900		1	ENE 7.5
	17 May	1025	+ 125	53	ENE 6.5
1974	20 March	2280		0	ENE 9.5
	7 April	4125	+1845	0	ENE 11.0
	*13 May	1450	-2675	26	ENE 5.5
	17 June	4500	+3050	162	E 1.5
1975	*12 April	560		0	E 3.0
	*16 May	1290	+ 730	30	ENE 6.0
	*3/5 June	1650	+ 360	127	NNE 2.0
1976	17 March	4235		0	E 5.0
	22 April	475	-3760	2	ENE 4.5
	10 May	1850	+1375	35	NE 6.0
	15 June	2660	+ 810	162	SE 0.2
1977	17 April	663			ENE 3.0
	23 May	2113	+1450		E 4.0

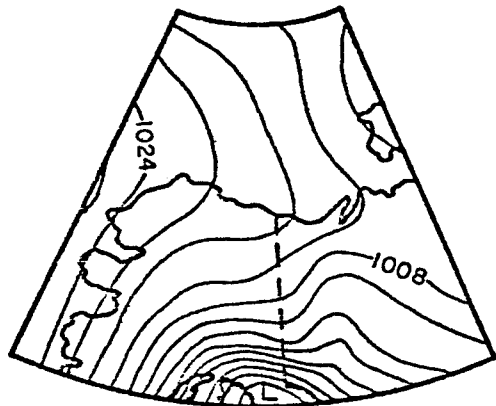
*Restricted coverage by satellite, polynya area may be underestimated .



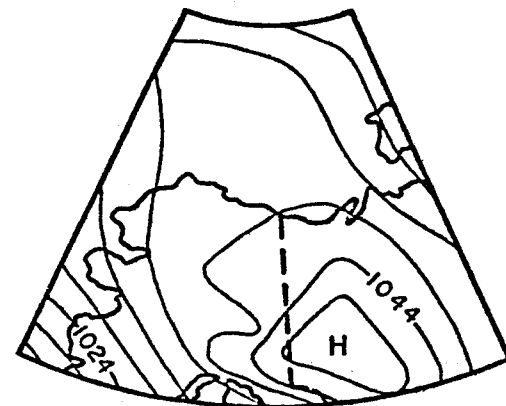
CP1



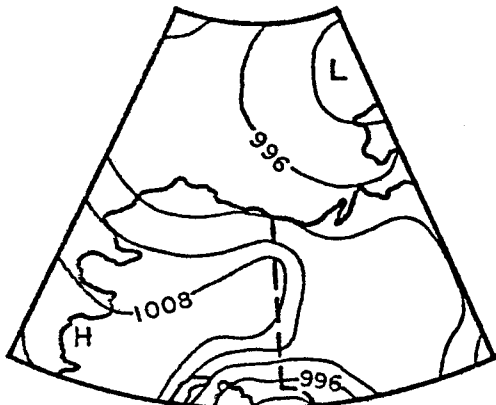
CP2



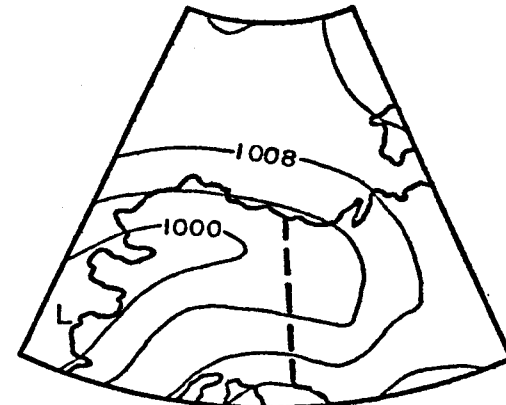
CP3



CP4

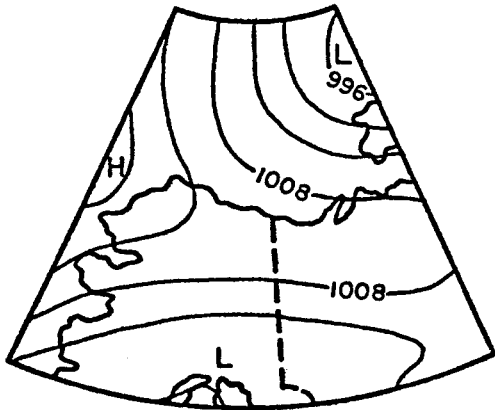


CP5

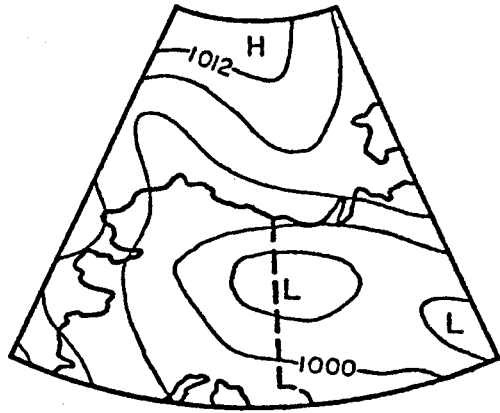


CP6

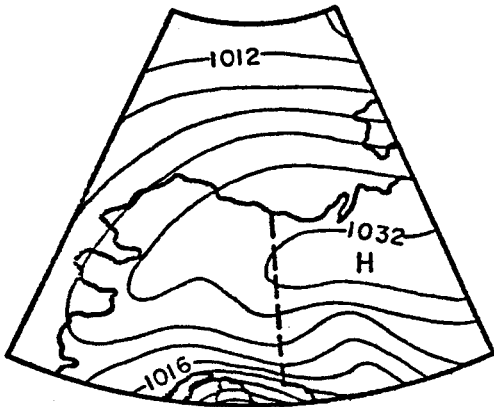
Figure 1a. Characteristic Patterns 1-6



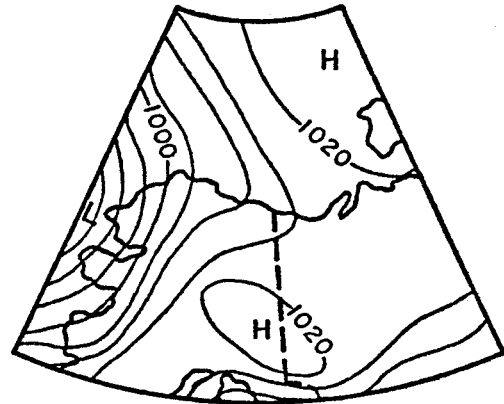
CP7



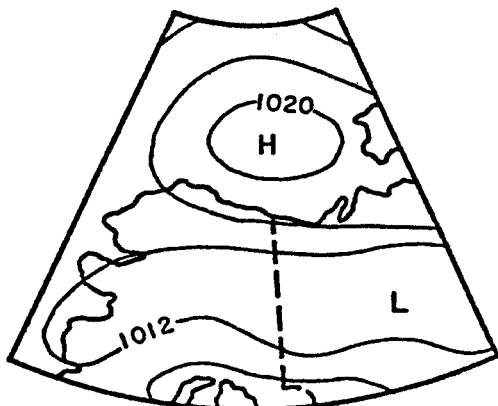
CP8



CP9



CP10

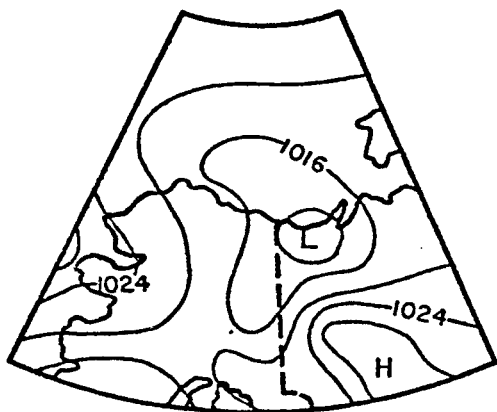


CP11

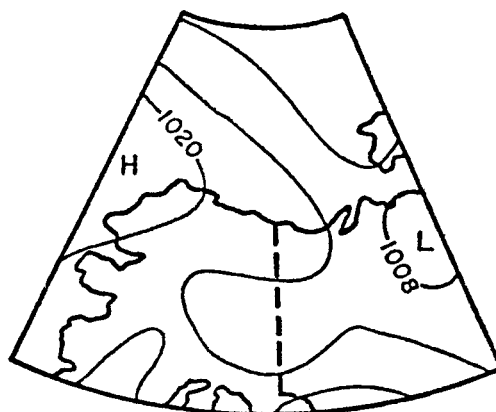


CP12

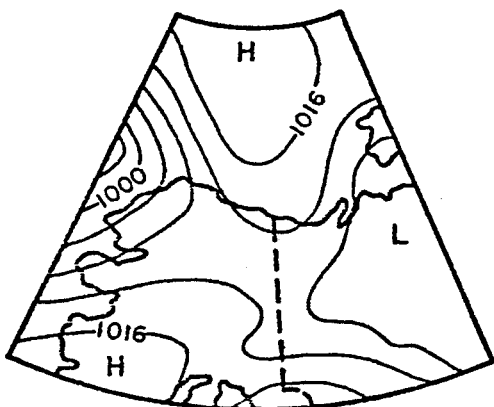
Figure 1b. Characteristic Patterns 7-12



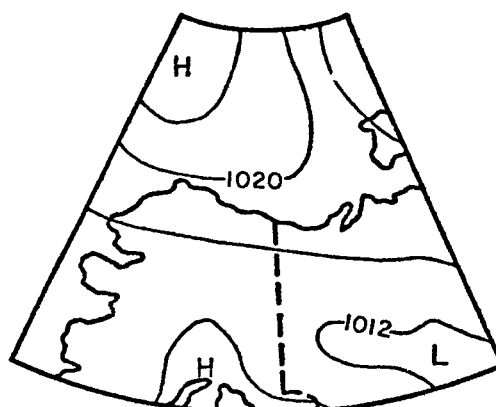
CPI3



CPI4



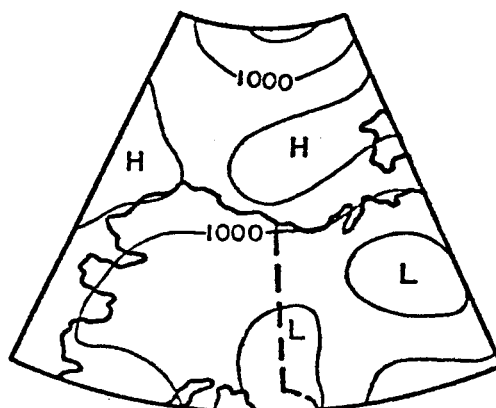
CPI5



CPI6

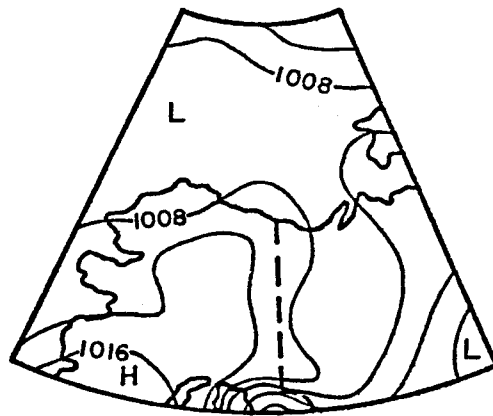


CPI7

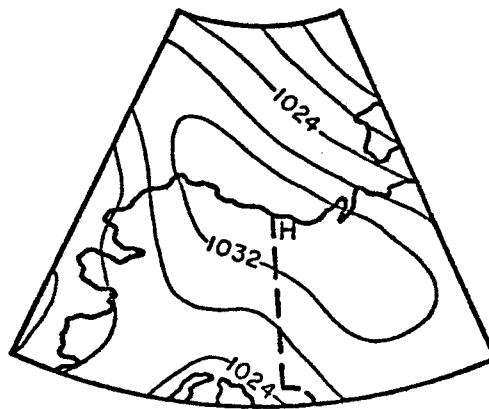


CPI8

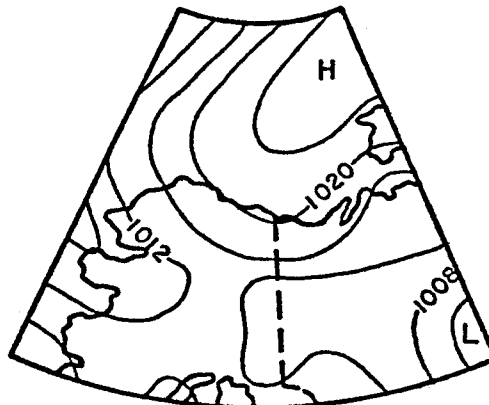
Figure 1c Characteristic Patterns 13-18



CP19



CP20



CP21

Figure 1d Characteristic Patterns 19-21

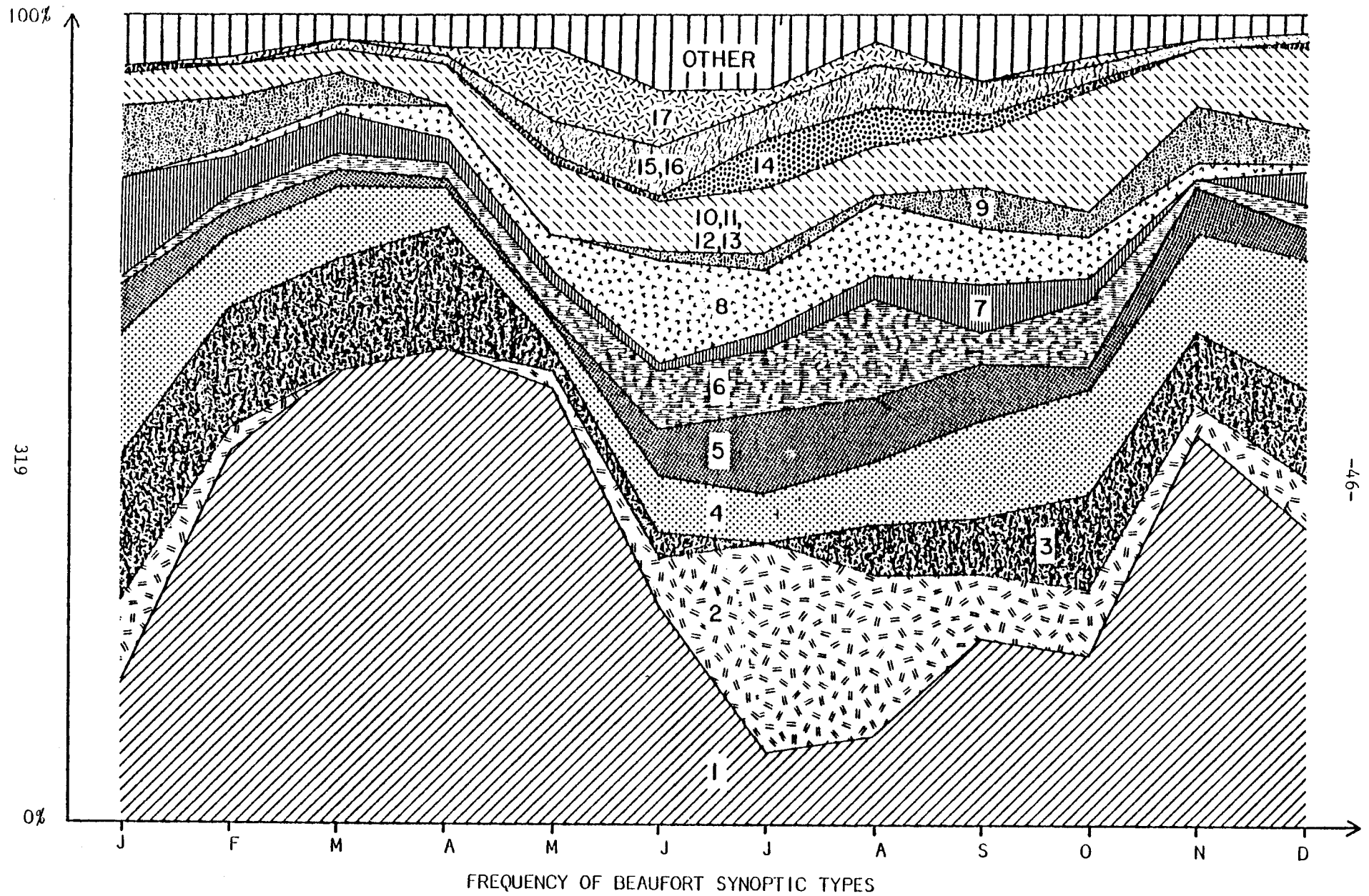
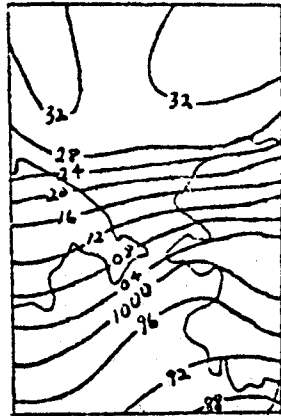
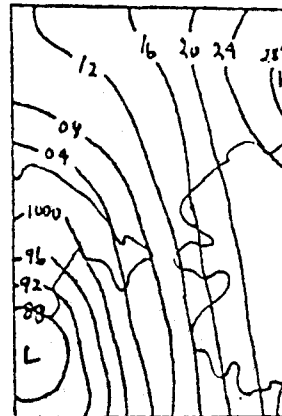


Fig. 2.

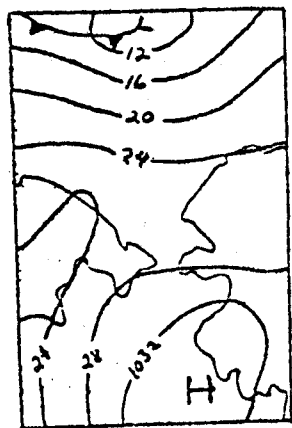
September, 1968 to August, 1974



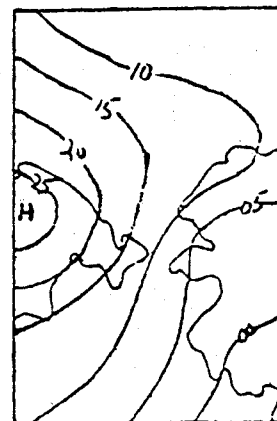
Type 1. 14 March 1970



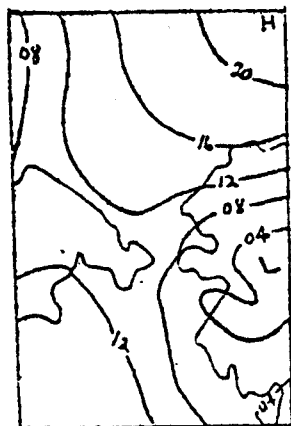
Type 2. 7 August 1968



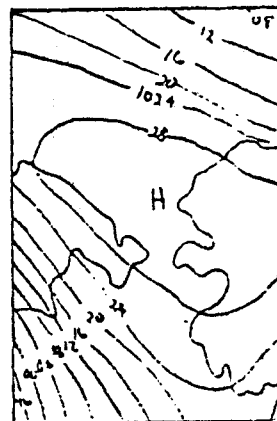
Type 3. 20 March 1967



Type 4. 2 February 1961

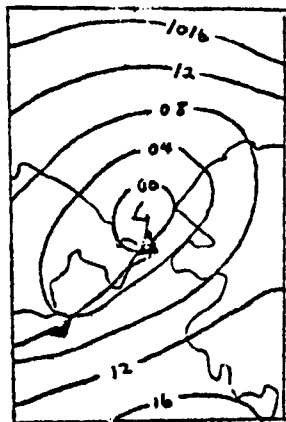


Type 5. 23 June 1969

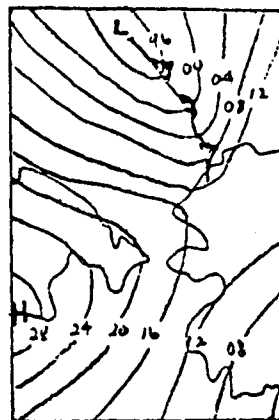


Type 6. 12 March 1955

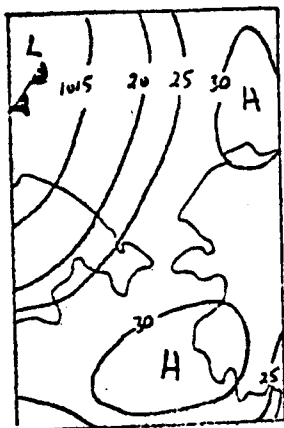
Figure 3a Chukchi Synoptic Types 1 - 6 (isobars in mb, omitting 1000 or 900)



Type 7. 16 July 1966



Type 8. 26 September 1957



Type 9. 17 April 1948



Type 10. 28 August 1948

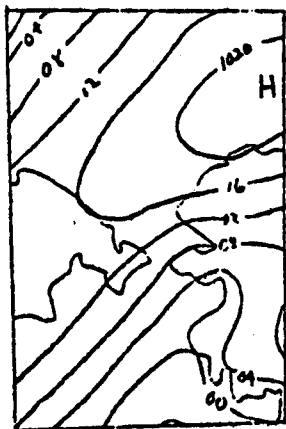


Type 11. 4 February 1955



Type 12. 8 September 1946

Figure 3b Chukchi Synoptic Types 7 - 12 (isobars in mb, omitting 1000 or 900)



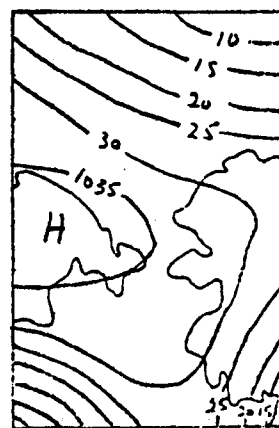
Type 13. 16 June 1969



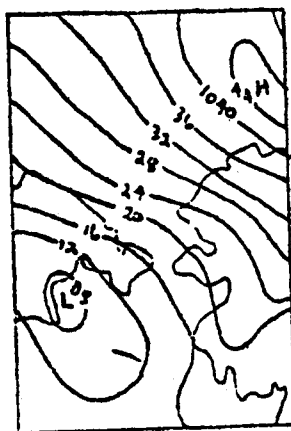
Type 14. 19 December 1966



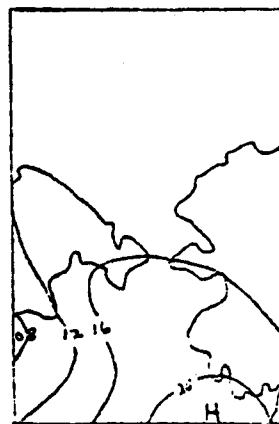
Type 15. 16 June 1960



Type 16. 4 March 1956

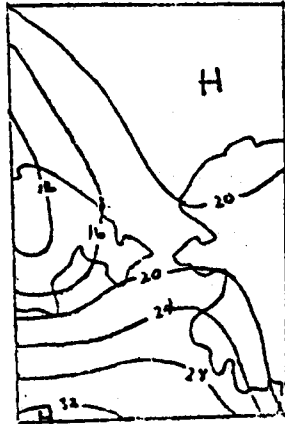


Type 17. 26 December 1968

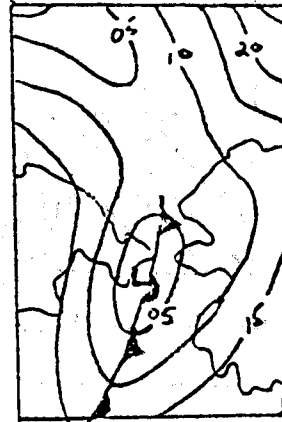


Type 18. 19 July 1963

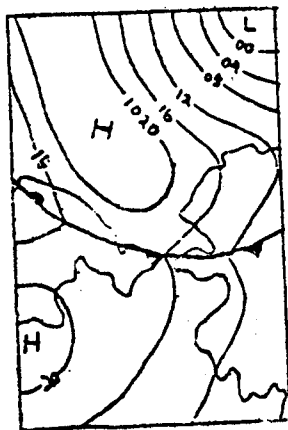
Figure 3c Chukchi Synoptic Types 13 - 18 (isobars in mb, omitting 1000 or 900)



Type 19. 17 October 1964



Type 20. 24 April 1959



Type 21. 7 June 1970



Type 22. 1 January 1956

Figure 3d Chukchi Synoptic Types 19 - 22 (isobars in mb, omitting 1000 or 900)

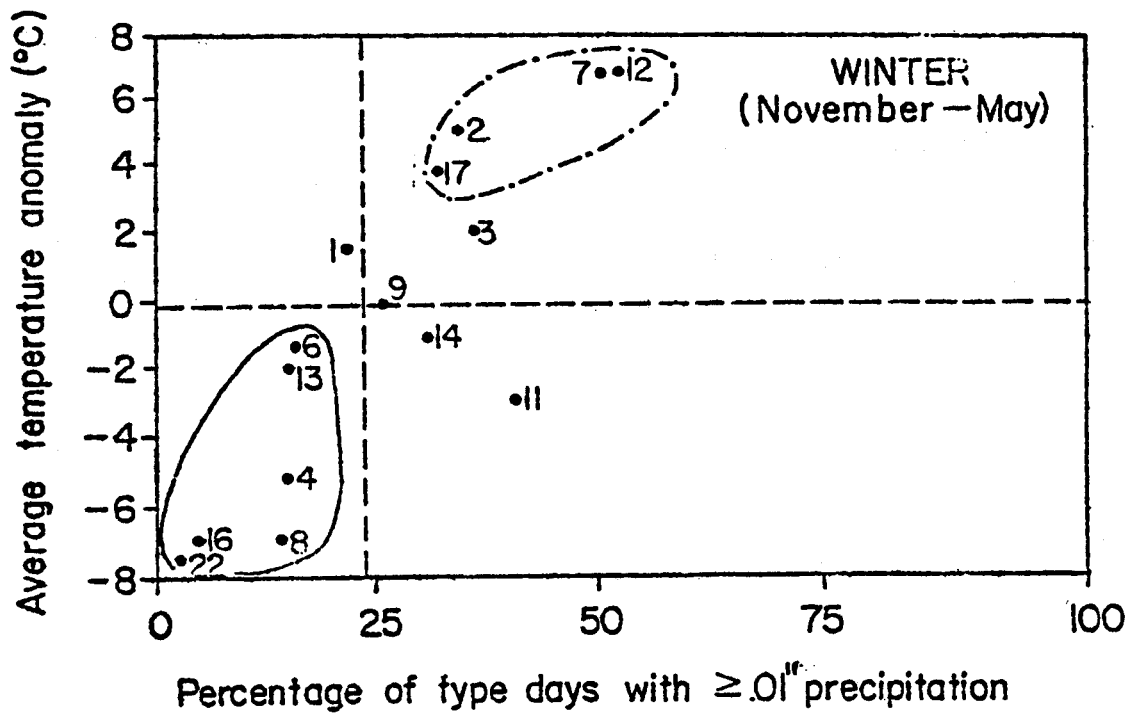


Figure 4 Temperature and precipitation characteristics of winter types at Kotzebue

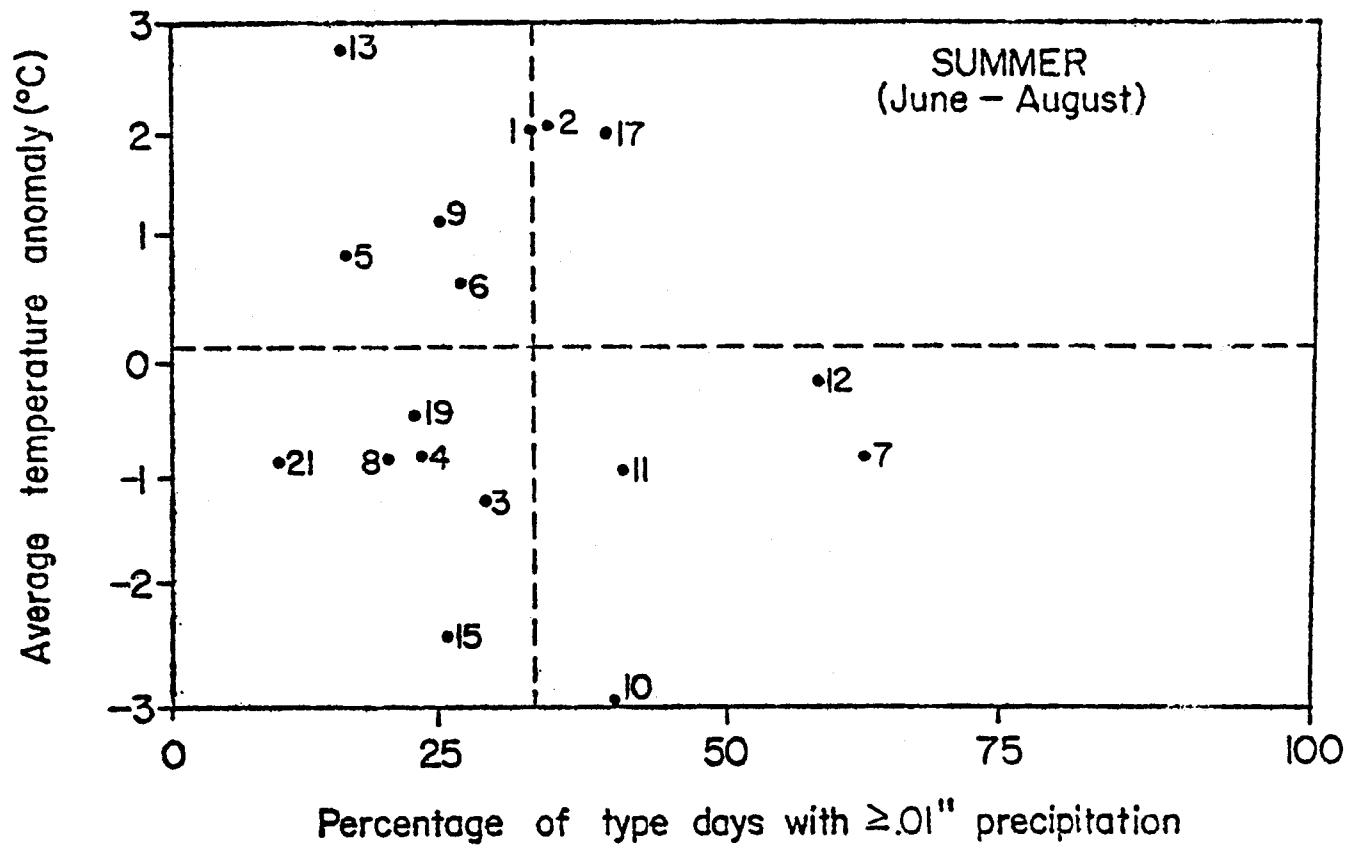


Figure 5 Temperature and precipitation characteristics of summer type at Kotzebue

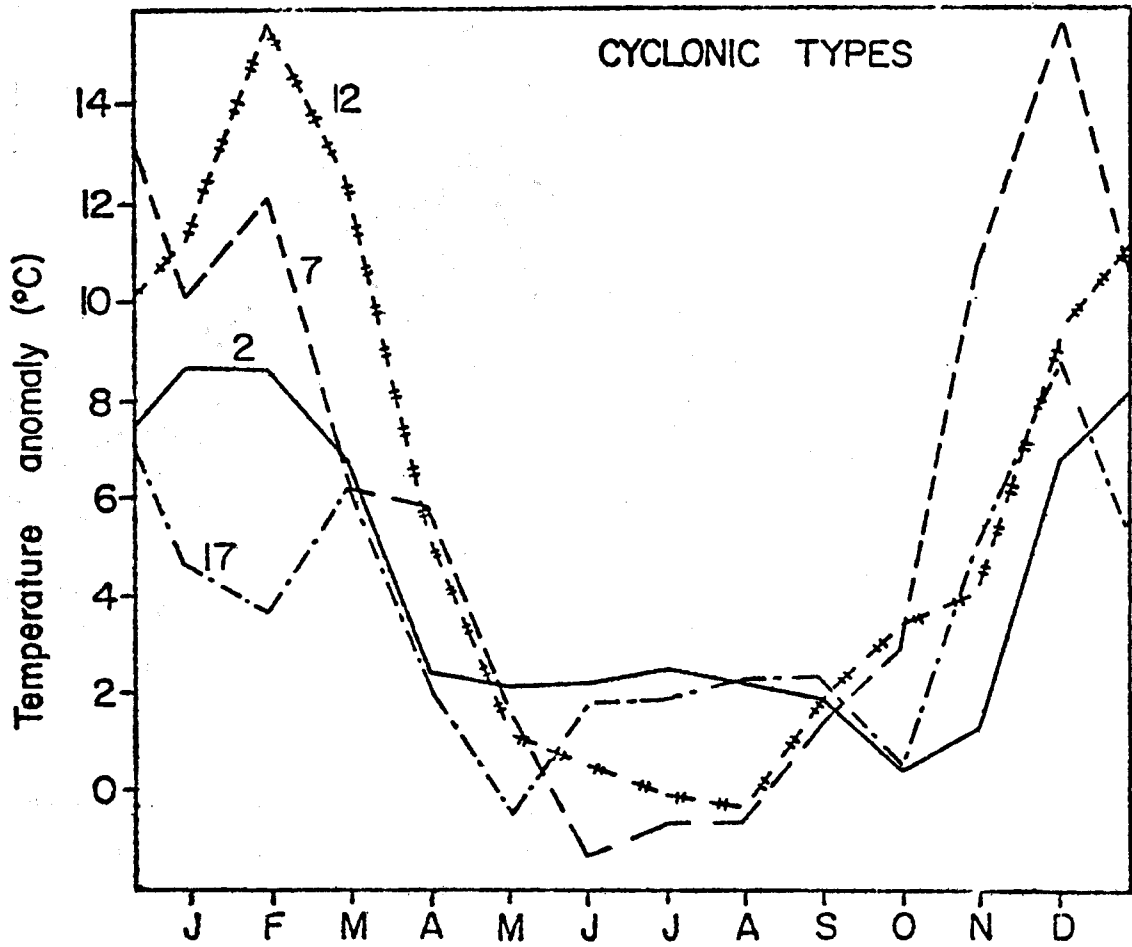


Figure 6 Temperature departure characteristics of the major cyclonic types, at Kotzebue, 1955-1974.

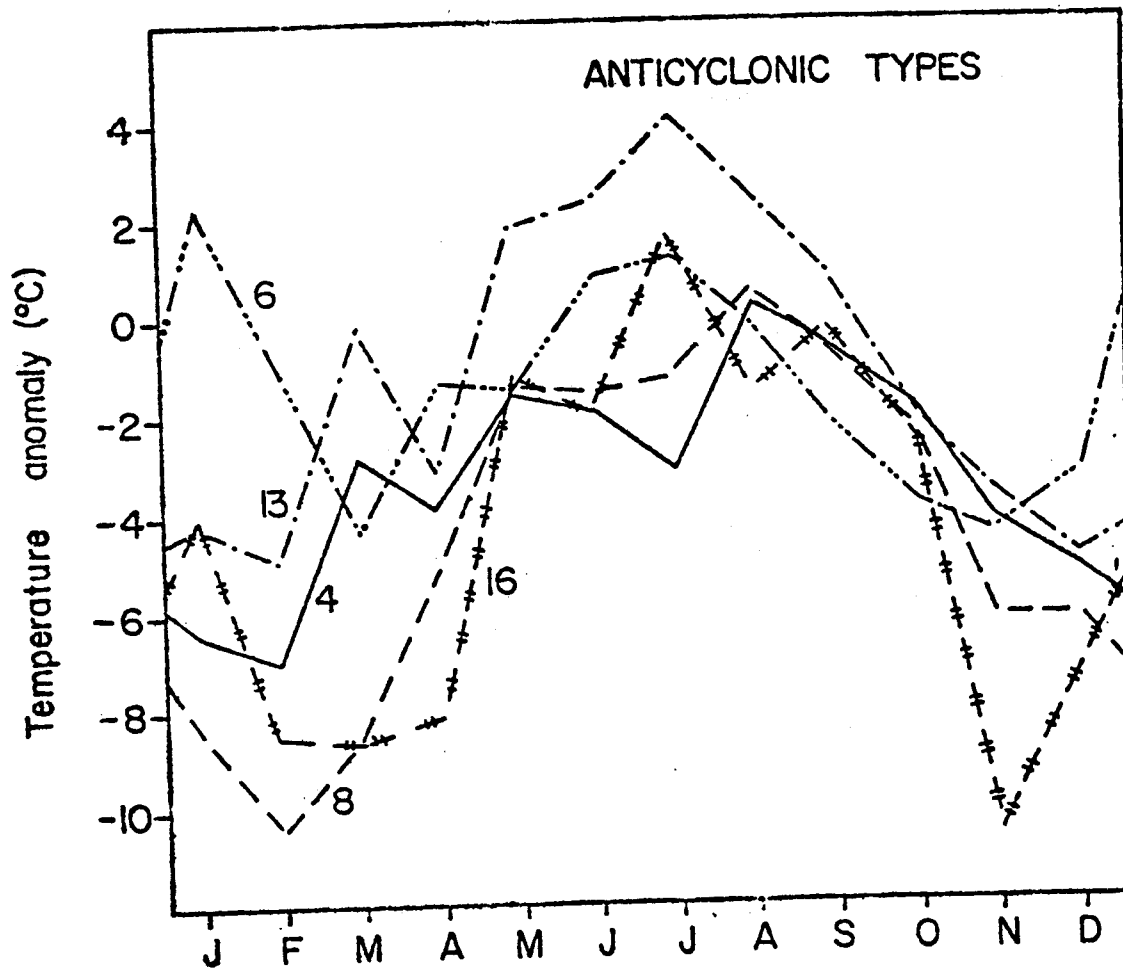


Figure 7 Temperature characteristics of the major anticyclonic types, at Kotzebue, 1955-1974.

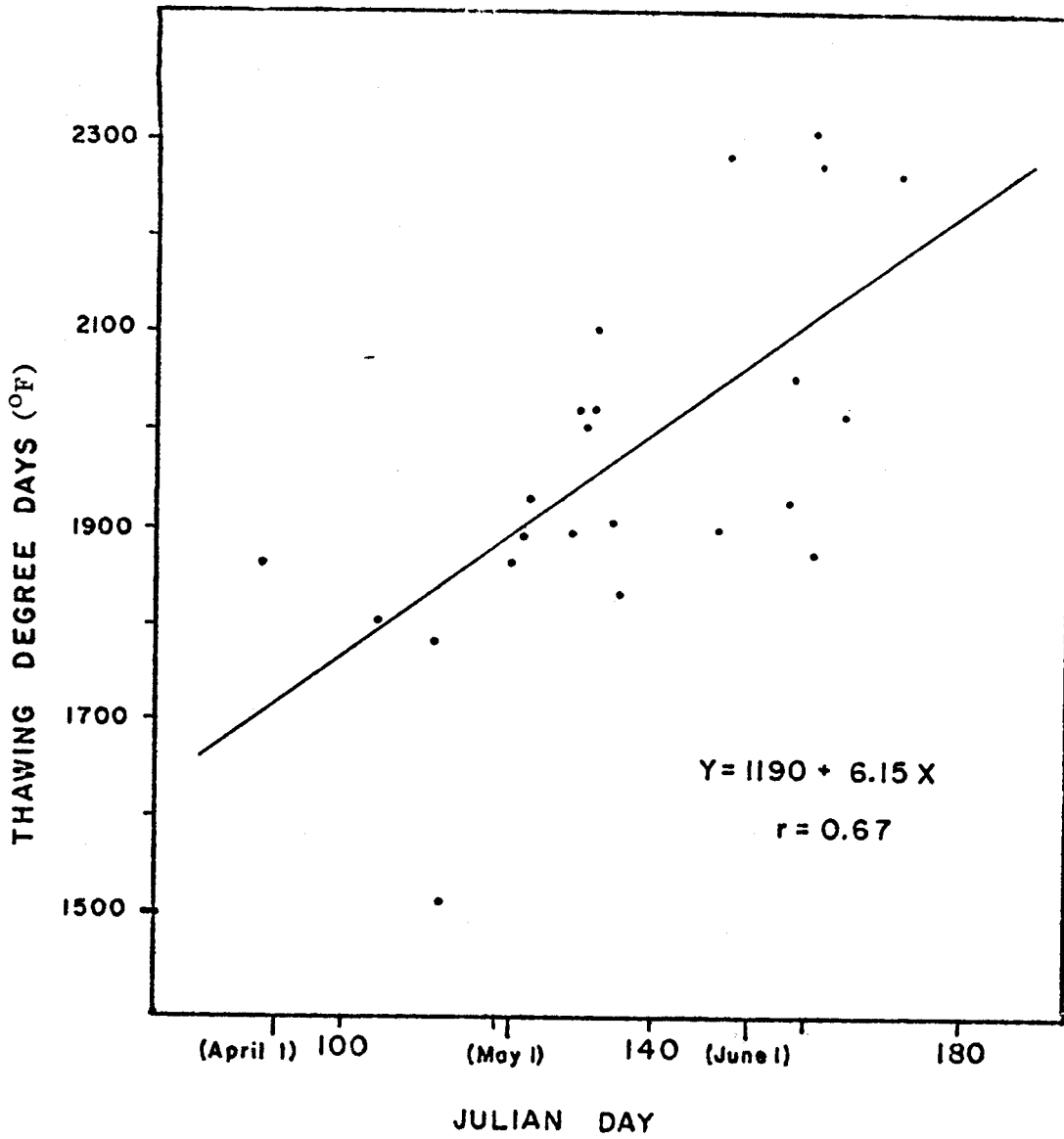


Figure 8 Date of westerly wind onset and accumulated thawing degree days at Kotzebue, 1953-1976 (except 1973). The outlier at approximately 1500 TDD represents the severe summer of 1975.

REFERENCES

- Arctic Project Office 1978. Environmental Assessment of the Alaskan Continental Shelf: Interim Synthesis: Beaufort/Chukchi. Environ. Res. Labs., NOAA, Boulder, 362 pp.
- Barnett, D. G. 1976. A Practical Method of Long Range Ice Forecasting for the North Coast of Alaska, Pt. 1. FLEWEFAC Tech. Rept. #1, Suitland, Md. 16 pp.
- Hare, F. K. 1968. The Arctic. Quart. J. Met. Soc., 94:439-458.
- Holmgren, B., Benson, C. and Weller, G. 1975. A Study of Breakup on the Arctic Slope of Alaska by Ground, Air and Satellite Observations. In: Climate of the Arctic, 24th Alaska Science Conf. (G. Weller and S. Bowling, eds.) Geophysical Inst., Fairbanks, 358-366.
- Hunt, W. and Naske, C. M. 1979. A baseline study of historic ice conditions in the Beaufort Sea, Chukchi Sea and Bering Strait. Final Report. Research Unit 261. Outer Continental Shelf Environmental Assessment Program. Environmental Assessment of the Alaskan Continental Shelf. Environ. Res. Labs., NOAA, Boulder.
- Keegan, T. J. 1958. Arctic Synoptic Activity in Winter. J. Met., 15: 513-521.
- Kovacs, A. and Mellor, M. 1974. Sea Ice Morphology and Ice as a Geologic Agent in the Southern Beaufort Sea. In: The Coast and Shelf of the Beaufort Sea (J. C. Reed and J. Sater, eds.) Arctic Institute of North America, Washington, D.C. 113-161.
- Kovacs, A. and Sodhi, D. S. 1978. Shore ice pile-up and ride-up: Field observations, models, theoretical analyses Mimeo Report, R.U. #88, OCSEAP, NOAA/BLM, 59 pp.
- Moritz, R. E. 1977. On a possible sea-breeze circulation near Barrow, Alaska. Arct. Alp. Res., 9:427-31.
- Moritz, R. E. 1978. Synoptic climatology of the Beaufort Sea Coast of Alaska. M.A. Thesis, Univ. of Colorado, Boulder, 238 pp.
- Reed, R. J. and Kunkel, B. 1960. The Arctic Circulation in summer. J. Met., 17:489-506.
- Reimnitz, E., Toimil, L. J. and Barnes, P. W. 1978. Arctic continental shelf processes and morphology related to sea ice zonation, Beaufort Sea, Alaska. Marine Geol., 28:179-210.
- Rogers, J. C. 1978A. Meteorological Factors Affecting Interannual Variability of Summertime Ice Extent in the Beaufort Sea. Mon. Weath. Rev., 106:890-97.

- Rogers, J. C. 1978B. A Meteorological Basis for Long-range Forecasting of Summer and Early Autumn Sea Ice Conditions in the Beaufort Sea. In: Muggerridge, D. B. (ed.) POAC 77. Fourth International Conference on Port and Ocean Engineering Under Arctic Conditions, Vol. 2. Memorial Univ., St. John's, Newfoundland. 952-62.
- Selkregg, L. 1974. Alaska Regional Profiles: Arctic Region. University of Alaska AEIDC, Anchorage. 28 pp.
- Shapiro, L. H. 1976. Preliminary Study of Ridging in Landfast Ice at Barrow, Alaska, Using Radar Data. In: Proceedings, Third International Conference on Port and Ocean Engineering Under Arctic Conditions, Vol. 1. Inst. Marine Sci., Univ. of Alaska, Fairbanks. 417-25.
- Shapiro, L. H., Barry, R. G. (eds.) 1978. The Sea Ice Environment. In: Environmental Assessment of the Alaskan Continental Shelf: Interim Synthesis: Beaufort/Chukchi. (Arctic Project Office, OCSEAP), Environ. Res. Labs., NOAA, Boulder. 3-55.
- Stringer, W. 1978. Nearshore ice conditions by means of satellite and aerial remote sensing. Final Report. Research Unit 257. Outer Continental Shelf Environmental Assessment Program. Environmental Assessment of the Alaskan Continental Shelf, Environ. Res. Labs., NOAA, Boulder.
- Watson, C. E. 1974. The Climate of Alaska. In: Climates of the States, NOAA Water Information Center, 481-501
- Wendler, G. and Jayaweera, K. O. L. F. 1976. Some remarks on the unusual Beaufort Sea ice conditions in summer 1975. Rep. UAG-R-246, Geophys. Inst., Univ. of Alaska, Fairbanks, 28 pp.
- Weller, G. and Bowling, S. (eds.) 1975. Climate of the Arctic, 24th Alaska Science Conference, Geophysical Inst., Fairbanks, 436 pp.
- Wilson, C. 1967. Climatology. Introduction, Northern Hemisphere I. CRREL Report IA3, Cold Regions Research and Eng. Lab., Hanover, 141 pp.
- Wohl, G. M. 1978. A study of sea ice conditions and synoptic climatology for the Beaufort Sea coast of Alaska. M.A. Thesis, Univ. of Colorado, Boulder. 166 pp.
- Zubov, N. N. 1943. Arctic Ice. Translation by U.S. Navy Oceanographic Office and Amer. Met. Society. 491 pp.

PROJECT PUBLICATIONS

Articles

- Barry, R.G., Moritz, R.E. and Rogers, J.C. 1979. Studies of climate and fast ice interaction during the decay season along the Beaufort Sea coast. In: Proc. 27th Alaskan Science Conference, Vol. 2 (Technical Papers), in press.
- Barry, R.G., Moritz, R.E. and Rogers, J.C. 1979. The fast ice regimes of the Beaufort and Chukchi sea coasts, Alaska. Cold Regions Sci. Technol. (in submission).
- Moritz, R.E. 1977. On a possible sea-breeze circulation near Barrow, Alaska. Arct. Alp. Res., 9: 427-31.
- Rogers, J.C. 1978. A meteorological basis for long-range forecasting of summer and early autumn sea ice conditions in the Beaufort Sea. In: D.B. Muggerridge (ed.), Proceedings of the Fourth International Conference on Port and Ocean Engineering Under Arctic Conditions, Vol. 2: 952-62.
- Rogers, J.C. 1978. Meteorological factors affecting interannual variability of summertime ice extent in the Beaufort Sea. Mon. Weath. Rev., 106: 890-97.
- Shapiro, L. and Barry, R.G. (eds.) 1978. The sea ice environment. In: Environmental Assessment of the Alaskan Continental Shelf. Interim Synthesis: Beaufort/Chukchi, Arctic Project Office, OCSEAP, NOAA (BLM) Environmental Research Labs., NOAA, Boulder: pp. 3-55.

Abstracts

- Barry, R.G. Moritz, R.E. and Rogers, J.C. 1977. Studies of climate and fast-ice interaction in relation to offshore petroleum development along the Beaufort and Chukchi sea coasts. Bull. Amer. Met. Soc., 58 (10): 1131.
- Barry, R.G. and Moritz, R.E. 1978. Synoptic climatological studies of the Beaufort Sea coast, Alaska. AAAG Program Abstracts. New Orleans 1978, p. 167.

Moritz, R.E. and Bartolucci, L.A. 1977. A multiband remote sensing study of melting shorefast sea ice. In: D.B. Morrison and D.J. Scherer (eds.) Symposium Proceedings, Machine Processing of Remotely Sensed Data, Laboratory for the Application of Remote Sensing, Purdue University, W. Lafayette, Ind., p. 238.

Warmerdam, B. 1978. Synoptic climatology of the Chukchi Sea coast, northwest Alaska. AAAG Program Abstracts. New Orleans 1978, p. 167-8.

Theses

Moritz, R.E. 1978. Synoptic climatology of the Beaufort Sea coast of Alaska. M.A. Thesis, Univ. of Colorado, Boulder. 238 pp.

Wohl, G.M. 1978. A study of sea ice conditions and synoptic climatology for the Beaufort Sea coast of Alaska. M.A. Thesis, Univ. of Colorado, Boulder. 166 pp.

Annual Reports. R.U. #244

Barry, R.G. 1976. Study of climatic effects on fast ice extent and its seasonal decay along the Beaufort Sea coast. In: Environmental Assessment of the Alaskan Continental Shelf. Vol. 14, Ice, Environmental Research Labs., NOAA, Boulder, pp. 58-116.

Barry, R.G. 1977. Study of climatic effects on fast ice extent and its seasonal decay along the Beaufort-Chukchi coasts. In: Environmental Assessment of the Alaskan Continental Shelf. Vol. 14, Transport, Environmental Research Labs., NOAA, Boulder, pp. 574-743.

Barry, R.G. 1978. Study of climatic effects on fast ice extent and its seasonal decay along the Beaufort-Chukchi coasts. In: Environmental Assessment of the Alaskan Continental Shelf, Vol. 9, Transport, Environmental Research Labs., NOAA, Boulder, pp. 604-719.

Quarterly Reports. R.U. #244

	<u>Beaufort Sea</u>		<u>Chukchi Sea</u>
December 1975	19 pp		
June 1976	6 pp	June 1976	5 pp
September 1976	98 pp	September 1976	27 pp
		December 1976	59 pp
		June 1977	4 pp
		September 1977	194 pp
		December 1977	35 pp
		June 1978	2 pp
		September 1978	13 pp
		December 1978	12 pp

APPENDIX 1

The Fast Ice Regimes of the Beaufort
and Chukchi Sea Coasts, Alaska

R. G. Barry, R. E. Moritz and J. C. Rogers

Introduction

The ice along the Beaufort and Chukchi Sea coasts of Alaska is the dominant coastal feature for approximately nine months of the year and is receiving intensive study prior to the proposed leasing of continental shelf tracts for petroleum exploration. Drilling operations face major problems due to the severity of the sea ice conditions, and environmental impact assessments therefore require a detailed understanding of the behavior of the ice. In connection with the Offshore Continental Shelf Environmental Assessment Program (OCSEAP) of NOAA-BLM, the seasonal regimes of the near-shore ice have been studied, primarily from remotely sensed data for 1973 to 1976, with special emphasis on the decay season. A major aim of this research is to determine the rate and spatial pattern of the ice decay processes, and to assess the role of climatic factors in determining them. The objective here is to bring together the principal results concerning the seasonal ice regimes of these coastal areas, incorporating the findings of earlier investigations, and to examine the links between the ice cycle and coastal climate. Detailed findings on coastal climatology are presented elsewhere (Barry, 1976; 1977; 1978; Moritz, 1978; Rogers, 1978A; 1978B).

Nearshore ice in the Beaufort Sea has received considerable study in the past few years, although much less attention has been paid to conditions in the Chukchi Sea. Surveys of the nearshore ice environment have been prepared by Kovacs and Mellor (1974) with emphasis on ice surface morphology and sea-floor gouging, and by Reimnitz et al. (1978), who introduced a modified scheme of cross-shelf ice zonation. The latter also gave special attention to the role of shoals and pack ice drift in producing the observed patterns

of shear lines and bottom scour. Ice extent and ridging along both the Beaufort and Chukchi coasts have been mapped by Stringer (1974; 1978A) under the OCSEAP, while shore-based radar studies of motion in the nearshore ice have been carried out by Shapiro (1976) at Barrow and by Weeks, et al. (1978) near Prudhoe Bay. Deformation studies from strain gauge networks have been made by Cooper (1975), and investigators of the Beaufort Sea Project (Environment Canada) have conducted remote sensing and other analyses of ice conditions with emphasis on the Canadian sector (Markham, 1975; Marko, 1975; Ramseier, et al., 1975).

Ice Zonation and the Annual Ice Cycle

Fast ice is formally defined as "sea ice which forms and remains fast along the coast, where it is attached to the shore, ... or between shoals or grounded icebergs" (World Meteorological Organization, 1970). However, the characteristics of ice in the nearshore zone of the Beaufort Sea differ markedly from those in Davis Strait, for example (Jacobs, et al., 1975). The cross-shelf ice zonation on the Beaufort Sea coast has been characterized by Kovacs and Mellor (1974) and Reimnitz, et al. (1978) as comprising zones of fast ice, grounded ridges and seasonal pack ice. The fast ice itself consists of an inner zone of bottom-fast ice, including the ice foot near the beach, and an outer zone of floating fast ice beyond the 2m isobath (approximately). Along much of the coast the seaward limit of the fast ice is fixed at any given time by a zone of grounded pressure and shear ridges, termed "stamukhi" (Transehe, 1928). Free-floating ice may become temporarily attached as a sheet-like extension on the seaward edge of these grounded ridges (cf. Stringer, 1974), which first form in about 8 to 15m deep water, but by late winter may occur beyond the 20m isobath. Since the boundaries of the ice zones and their characteristics change

through the year, it has proved difficult to develop a comprehensive, universally-accepted ice nomenclature for the nearshore zones (see Cooper, 1974; Reimnitz, et al., 1978; Stringer, 1978B). Different authors emphasize different aspects of the ice conditions according to the particular objectives of their study (bottom scour, ice dynamics, navigation hazards, and so on) and their various research tools (field measurements, ground, airborne or satellite remotely sensed data), although all of the proposed zonation schemes are most applicable to late winter/spring conditions.

Three criteria which are of general use in distinguishing fast ice from other sea ice are as follows: (i) the ice remains immobile near the shore for a specified time interval; (ii) it extends seaward from the coast as a continuous sheet with no open water; (iii) the ice is grounded, or forms a continuous sheet which is bounded at the seaward edge by grounded ice (ridges, ice island fragments, etc.). At certain times during winter, ice on the Beaufort coast may be immobile and continuous for a hundred km offshore (within the resolution of LANDSAT imagery \approx 100 meters). Such occurrences, involving attached ice and seasonal pack ice, do not meet the third criterion above, although they are an important aspect of the coastal ice environment. A well-defined zone of horizontal ice velocity shear can be used as an indicator of the fast ice edge when the pack is in motion (cf. Stringer, 1974).

The nearshore ice undergoes an annual cycle of formation, growth, extension and decay, finally giving way to open water after breakup. The stages of this cycle can be characterized by a sequence of recurrent ice "events" that can be identified through interpretation of remotely sensed data. These events, which are discussed further below in conjunction with Table 1, are as follows:

(1) new ice formation in the near shore area, (2) freeze-up in bays and lagoons, (3) extension of fast ice seaward of lagoons with modification of the ice sheet by storms and by pack ice stress, (4) over-ice flooding at the river mouths in spring, (5) melt pools forming in situ on the ice surface, (6) openings in previously continuous ice sheets, (7) movements in previously immobile nearshore ice (end of stable fast ice), (8) near-shore area largely free of fast ice. It should be pointed out that "breakup" as defined by Kniskern and Potocsky (1965) for coastal observations, refers to $\leq 1/10$ ice concentration in the harbor. They note that much higher concentrations may exist outside. Consequently, their tabulations, which are included in other sources (National Ocean Survey, 1977) correspond to our phase 8.

The timing of these recurrent ice events and the duration of the major ice stages have been investigated for both coastal areas. To some extent they are dependent on weather conditions in a given season and the nature of this control has been a major topic of our research. The ice mapping has been based on LANDSAT multi-spectral scanner (MSS) imagery for 1973 to 1977, utilizing mainly bands 4 (wavelengths $0.5-0.6 \times 10^3 \mu m$) and 7 ($0.8-1.1 \times 10^3 \mu m$), supplemented by some X-band (wavelength $3 \times 10^{-2} m$) side-looking airborne radar (SLAR) imagery and color infrared (CIR) photography from aircraft underflights. Low-level aircraft reconnaissance flights, including hand-held photography, were carried out over the ice in early summer 1975, 1976 and 1977. LANDSAT MSS imagery has a spatial resolution capability of about 80 m and provides coverage of a given point on the earth's surface every 18 days, with up to three days consecutive coverage at high latitudes due to image overlap. However, the overcast conditions which prevail during the arctic summer, especially along coasts, render many of these images useless.

In addition to the regular annual cycle of ice formation and decay it is important to consider episodic ice processes which affect the ice canopy through one or more subsequent stages in its development. For example, brief but intense pressure and shear stresses at the fast ice margin can lead to massive ice ridge systems which stabilize the ice to shoreward when they become firmly grounded on the sea floor. Thus it is well to keep in mind that any two ice decay seasons may have similar weather conditions but different breakup rates and patterns, due to differences in the "initial state" of the ice at winter's end.

The Ice Growth Season

Ice conditions along the Alaskan coasts of the Beaufort Sea and the Chukchi Sea differ sufficiently to make it preferable to treat them separately in terms of their seasonal regimes. Points of similarity and contrast are examined later. Approximate dates of the major phases in the fast ice regimes on both coasts are shown in Table 1. However, it must be emphasized that since the satellite observations used in our study cover only five seasons, with frequent data gaps due to cloud cover, the long-term averages may differ from our estimates by about ± 7 to 10 days.

The Chukchi Sea Coast

During August surface water temperatures exceed 8°C along the coast south of Cape Lisburne (see Figure 1 for place names), although they drop to less than 4°C north of Wainwright (State of Alaska, 1975, Figure 48; Brower, et al., 1977). Consequently, new ice begins to form in the nearshore water at the beginning of October to the north, but not until late October at Kotzebue and some time in November nearer the Bering Strait (Table 1). The actual freeze-up date may vary by about ± 10 days from these averages, but towards the Bering Strait there is increased

variability, both spatially and interannually (cf. Kniskern and Potocsky, 1965).

High winds and waves cause intermittent rafting and destruction of the new ice. Storm surges of up to three meters have been recorded at Point Barrow in October, for example (Schaeffer, 1966). In general, wave heights and surge levels are higher in the Chukchi Sea than in the Beaufort Sea due to the greater fetch over open water that exists on the former coast in summer and autumn. Disruption of the fast ice sheet, with subsequent refreezing, continues into January when the ice has thickened to about one meter or more. According to Peyton and Behlke (1969) floes in the pack ice off the Chukchi coast have a late winter thickness of about 1.2 to 1.5 meters.

The fast ice is extensive in Kotzebue Sound, but in several sections of the coast it forms a narrow belt only a few kilometers wide, due to the relatively steep slope of the bottom near shore. Figure 2 shows these areas off Cape Lisburne, Point Franklin and Point Barrow. Long leads parallel much of the coast in winter and recurrent polynyai (open water areas enclosed by ice) are observed, especially in spring, south of Point Hope, Cape Lisburne, and off Icy Cape. These result from the combined effects of prevailing E-NE winds during winter and spring and occasional south-setting surface currents as inferred by Shapiro and Burns (1975) in March, 1973. Both mechanisms serve to displace the ice away from the coast. The normal water motion is northward (State of Alaska, 1975, Figure 41), except locally south of Point Lay and Point Hope.

The Beaufort Sea Coast

The ice regime on the Beaufort Sea Coast is considerably more complex than on the Chukchi Coast. In part this is due to the important role

played by the Arctic pack ice. The pack has a westward drift, averaging 20 km per month in winter and 80 to 100 km per month in summer (Untersteiner and Coon, 1977), through the agencies of the clockwise current gyre in the Beaufort Sea and the prevailing easterly winds over the continental shelf. A second major factor is the relatively gentle slope of the sea floor near the coast. The 20 m isobath is between 25 and 60 km offshore along much of the coast, so that grounded ice can establish itself relatively far from shore compared to the Chukchi Sea. Four discontinuous chains of barrier islands extend along 52 percent of the 800 km Beaufort coast of Alaska with river deltas taking up a further 16 percent (Short, et al., 1974). Landward of the islands, the near shore zone is protected from pack ice incursions, allowing the formation of a continuous, nearly smooth ice sheet. The extensive areas with water depth less than 2 m, especially in Harrison Bay, enable bottom-fast ice to account for as much as 75 percent of the total fast ice cover, according to Reimnitz et al., (1978).

Freezing begins in the lagoons and shallow waters over the inner shelf where salinities are lowest (Reimnitz, et al., 1978). Figure 3 illustrates newly-formed ice between Barter Island and Herschel Island on October 6, 1974. On this LANDSAT scene the light-toned areas near shore correspond to various thicknesses of young ice, which has a high spectral reflectance. The darkest of these near-shore ice areas are either local melting or puddling. Seaward of this fast ice, young ice (dark-grey intone) is forming and being deformed by the pack ice and currents. The roughness of the ice sheet depends on the wave conditions during the early growth phases and on the location of any fragments of multi-year ice, including pressure ridge remnants which survived the melt season (Kovacs 1976), or ice islands. On the open coast and seaward of the barrier islands, however, impingement of the moving pack ice, especially during early winter storms, leads to rafting and hummocking

of the growing fast ice sheet. The thin, newly-frozen ice in unprotected areas is free to move away from or along the coast, given only modest wind and water stresses. Figure 3 illustrates the result of this process, showing the jagged fast ice edge after floes have broken off.

There is little information on storm surges in the Beaufort Sea (Aagaard and Contributors, 1978). Reimnitz and Maurer (1978) estimate that surges of three meters or more, such as that of 13 September, 1970 associated with a northwesterly gale, have a recurrence interval of about 100 years during autumn when there is little ice in the nearshore area. However, there are also mid-winter surges, not necessarily linked to local storms, with heights of up to 1.5 meters (Henry and Heaps, 1976). These may cause flooding of the bottom-fast ice, with subsequent refreezing. Negative surges of 60 to 100 cm (cf. Aagaard and Contributors, 1978) also occur and in winter these can fracture the ice sheet. Moderate pressure due to pack ice impingement is sufficient to disrupt and deform the fast ice until it is at least 0.5 meters thick when it becomes less saline, through brine drainage, and stronger. The shoreward forces of the drifting pack ice are eventually checked by the fast ice sheet itself or by the grounding of pressure ridges on the sea bed (Kovacs and Mellor, 1974). Such grounded ridges often form the seaward boundary of the main fast ice sheet, although attached ice may occur beyond. There are almost no observations covering the period November through February, but it is considered that these ridges tend to form in 8 to 15 meters of water in November and December, and subsequently out to the 20 meter isobath as the ice sheet extends seaward (Fig. 4). Figure 5 is a hand-held, aerial oblique photograph of a typical ice-deformation zone during the early melt season in the fast ice off Barter Island. The pressure and shear ice structures in the figure are roughly 1 to 10 meters high.

From February to early May the ice shoreward of about the 15 m isobath is essentially stable, a factor of major significance for possible oil and gas exploration. Laser measurements of target displacements in the fast ice near Prudhoe Bay show generally small relative motions of about one meter during spring 1976 and 1977, with maximum values of tens of meters (Weeks, et al., 1978). The motion is predominantly outward from the coast and is attributed to thermal expansion, although near the outer margin of fast ice the drifting pack can cause slippage in the shear zone. Deformation of the fast ice diminishes in late winter-early spring as the ice sheet thickens to about two meters and is stabilized by grounding near its edge. However, tidal displacements and diurnal thermal stresses affect the tensile strength of the ice (Nelson, 1974). Tidal cracks are particularly common at the junction of the bottom fast and floating fast ice.

Figures 6 and 7 show a sequence of LANDSAT images which illustrates a striking example of late-winter ice deformation. On Figure 6 (20 April, 1975) dark gray lineations are evident, bounded by the meridians 149°W and 150°W (inside the narrow rectangle). The darkest tones to the north are areas of open water or very thin ice in leads. We interpret the gray lineations as heavy ice-deformation zones which show up because of shadows cast by the piled ice at the low sun elevation angle (30 degrees above the horizon). The ridges clearly were not in this area on March 25 (see LANDSAT MSS scene 1975-21163), so the deformation event must have occurred in late March or early April, much later than is often considered "normal" for such processes. Figure 7 (12 September, 1975) shows much of the 40-km long ridged zone still intact after the melt season. The breakup and removal of surrounding ice indicates that the feature is indeed firmly

grounded on the sea floor, without detectable displacement since at least 20 April. The dark gray lineations of 20 April match the brightest tones on the 12 September scene. This reversal of the "spectral signature" is attributed to the drainage of melt water from the elevated ice of the ridges and hummocks. Flatter ice areas with extensive melt puddles and thin, "rotten" ice which has almost melted through appear darker on the late summer imagery, especially in band 7.

The ice feature on these scenes was positioned in waters about 25 meters deep, indicating again the importance of interactions between the shallow inner shelf and the ever-present Arctic pack ice on the Beaufort Coast. Coastal ice conditions were especially severe during the 1975 navigation season (Barnett, 1976) with pack ice over parts of the continental shelf for the entire summer and extremely low coastal temperatures. The ice deformation feature in the figures probably limited the shoreward incursion of pack ice in Harrison Bay during summer, 1975, providing a protected lagoon environment to shoreward. In this way such ice features could be exploited as giant pack ice shields during the summer and fall, if their location and potential stability could be determined in the spring. However, the particular system illustrated in the figures is the largest and longest-lived such structure we observed on LANDSAT imagery for the decay seasons 1973-1976. The possibility of artificially creating ice barriers such as this is under serious consideration as a means of engineering stable operations platforms in the nearshore zone (Clarke, 1976). LANDSAT imagery (not reproduced here) in the same area on 3 November, 1975, shows the grounded ice feature is still in place, with new fast ice extending seaward around it. Again the feature plays the role of a giant ice barrier

island far offshore, with a lagoon of sheltered fast ice in Harrison Bay. Our aerial reconnaissance in early summer, 1976 confirmed this sheltering effect, most of the ice in the bay having little or no surface relief (Figure 8). The major ice relief inside the summer, 1976 fast ice edge occurred on fragments of older ice which remained in the nearshore area after the severe summer of 1975 (e.g. Figure 7). These conditions are in marked contrast to those of summer, 1974, when numerous ridge-like deformation systems were located in Harrison Bay using a combination of LANDSAT, CIR and SLAF data. Thus we stress that winter ice events of an episodic character can profoundly influence ice conditions in subsequent seasons.

The Ice Decay Season-General Characteristics

The temporal and spatial characteristics of the ice decay season have been the primary foci of our research. The beginning of the ice decay process is important because it signals the end of the period of stable fast ice, while the final ice clearance marks the start of the possible navigation season. The course of the decay process is determined by the pre-existing ice conditions, especially the occurrence of grounded ridges near the seaward edge of the fast ice, by the "normal" seasonal march of climatic conditions, and by departures from the seasonal norms due to synoptic weather events. Examples of the ways in which these various controls operate are discussed below.

Chukchi Coast

The decay and breakup of ice along the Chukchi coast is different in character from that in the Beaufort Sea due primarily to the orientation of the coastline with respect to the prevailing winds in spring, and to the physiographic character of the coast itself. Barrier islands, which are present along much of the Beaufort Sea coast, are less exten-

sive on the Chukchi Coast of Alaska, although they form numerous almost-closed lagoons along the Seward Peninsula and off Point Lay. These account for 32 percent of the 760 km coastline from Cape Prince of Wales to Point Hope and 37 percent of the 580 km coast between Point Hope and Point Barrow. Shallow waters are more restricted off the Chukchi coast where the 20 m isobath is generally 10 to 25 km offshore, which is less than half the average distance off the Beaufort Sea coast.

Along the margin of the shorefast ice (depicted in early summer in Figure 2) there are leads and polynyi. These continually open and refreeze during winter and spring and are the site of the first summer openings in the ice cover. Figure 9 illustrates the extent of open water and thin ice south of Point Hope in 1974 and 1976. The short-term changes indicated on these maps are due to refreezing and to changes in wind direction moving the pack; winds with a northeasterly component move the ice away from the flaw lead. Even north of Wainwright there may be significant openings paralleling the coast along the fast ice margin by mid-May. Since there are few major rivers along the Chukchi coast, flooding of the nearshore ice is not a dominant component of the decay process, although it is locally important, especially in Kotzebue Sound, due to the Noatak and Kobuk rivers.

Another factor in the Chukchi Sea which differs markedly from conditions on the Beaufort Coast is the role of ocean currents. Handlers (1977) summarizes current measurements and reports that there is generally a northward flow with a velocity of 1.5 m s^{-1} on the east side of Bering Strait, decreasing northward to $.2$ to $.3 \text{ m s}^{-1}$. His analysis of pack ice retreat data for 1972-75 shows that the mean current flows faster than the ice margin retreats northward, thereby extending low

salinity water below the ice. The role this advected water layer plays in the heat and mass budget of the ice remains to be determined. The decrease in pack ice concentration which progresses northward in June and July (Brower, et al., 1977) facilitates the clearance of fast ice from the coast by winds following its decay in situ during May (Table 1). During the summer months, however, the winds at Kotzebue are predominantly westerly, and this could retard the process. Also, in Kotzebue Sound and in the bay north of Cape Lisburne, local current gyres and the coastal configuration may keep ice trapped against the coast. North of Wainwright, the nearshore ice forms a narrow zone only two to three km wide containing many pack ice remnants. It is subject to considerable pressure ridging. Here the summer rise in temperature serves first to detach fast ice from the beach and later to detach grounded ridges from the sea bed (Shapiro, et al., 1977). During late July 1973, breakup started when winds began to move the floating ice between grounded ridges oriented parallel to the shore. Some ridges may remain in the nearshore zone along the northern section of the Chukchi coast throughout the summer.

Beaufort Sea

The course of a particular ice decay season along the Beaufort Sea Coast is determined by roughly constant factors, including the coastal geography and bathymetry, and the seasonal marches of temperature and incoming solar radiation, and more variable factors such as synoptic changes in regional weather patterns (especially when they involve wind direction anomalies) and prior history of the ice sheet. As noted above, the shallow inner shelf supports an extensive 2m-thick bottom fast ice sheet, especially in Harrison Bay (Reimnitz, et al., 1978, Figure 1). The numerous barrier islands protect much of the flat

first-year ice from pack ice impingement and consequent deformation. Figure 4 indicates that coast-to-shear-zone distances off Cross and Narwhal Islands and in Harrison Bay off Atigaru Point are similar from year to year, whereas east of Pt. Barrow and northwest of Prudhoe Bay there is considerable interannual variation. The larger variability west of Cross Island appears to be related to the distribution of shoals and the shear zones which can develop around ice grounded on them. Reimnitz, et al. (1978) report that the location of the fast ice margin is usually coincident with first-year pressure and shear ridge zones which can occur in the depth interval 10 to 30 meters. This pattern is modified by major coastal promontories (e.g. Barter Island, Cross Island, Point Barrow) where seaward fast ice extent is limited, while extensive fast ice exists in the intervening coastal "indentations." A similar pattern is also observed on the Chukchi coast. The fast ice margin is thus significantly affected by shoals, which are themselves altered by the gouging action of deep-draft ice, although the relevant time scale for this process is decades rather than seasons. However, grounded ridges do not necessarily occur in all sections of the coast in every winter season.

The first stage of the Beaufort decay season is major estuarine flooding of the nearshore ice in late May or early June. For example, Carlson (1977) reports that in early June, 1975 the areas of flooded ice on three major river mouths were: Colville 276 km², Sagavanirktok 208 km², and Kuparuk 101 km². In 1974 the flooding of these same estuaries was much less extensive, except in the Sagavanirktok area. On June 6, 1976 (Figure 10) Landsat imagery shows ice flooding extending seaward from several estuaries including the Colville and Sagavanirktok rivers with about 100 km² each. Other rivers showing evidence of this

phenomenon on Landsat imagery include the Canning, Sadlerochit, Hulahula, Jago and Aichikik. The floodwaters of the Colville River carry sediment onto the ice, reducing the surface albedo and thereby enhancing melt, although the Sagavanirktok River is apparently less sediment-laden (Reimnitz and Bruder, 1972; Carlson, 1977). Due to the flooding, the bottom fast ice begins to float and cracks develop in the ice, especially adjacent to areas of flooding or in situ ablation around the river mouths. The resultant shore polynyi spread laterally and seaward from mid June through early July, while the ice sheet thins and puddles, until wind and water stresses cause the initial openings and displacements in the ice sheet, often towards the shore polynyi. Cracks and openings also occur along the seaward fast ice margin (the flaw lead) due to displacements of the pack ice in the Beaufort Sea gyre.

Figures 11 to 13 comprise a sequence of Landsat MSS scenes in the vicinity of Prudhoe Bay during the decay season, 1974. The sequence illustrates the ice decay processes typical of the Beaufort Coast. Figure 14 is a map of the Prudhoe area containing ice information interpreted from Landsat scenes 1702-21093 and 1703-21151 (25 and 26 June, 1974, respectively). The fast ice sheet can be distinguished from pack ice on 26 June by noting the position of the shoreward-most open water spaces between floes. This line is plotted on Figure 14 as "A." The sheet of continuous ice need not, of course, be firmly grounded or attached to shore, based solely on this criterion. By overlaying image transparencies for different dates, using the coastline for geographic control, we find ice masses, denoted by "G" on Figure 14, which remained in place while surrounding ice broke up. We take these ice features to

be firmly grounded. SLAR imagery* flown 29 April, 1974 indicates that these areas contain ridged and hummocked ice with a very rough appearance. The surface roughness leads to a high X-band radar return, showing up as bright tones on the imagery (Dunbar, 1975; Campbell, et al., 1976). These three ice features are at or very near the 26 June continuous ice edge "A", indicating the role played by grounded ice in determining the fast ice edge. Shore polynyi are evident on the major rivers, and we have outlined these areas on Figure 14. The complex gray tone patterns on the 26 June scene are due to spatial variations in the areal coverage and depth of melt puddles on the ice surface. On this date, the pack ice is compacted along the fast ice margin. Overlay of 25 and 26 June scenes yields the ice displacement vectors plotted on Figure 14. The fast ice is immobile (to within Landsat resolution capability) inside the line "A", while the pack ice far from shore is moving westward at about 10 km per day. The average surface winds at the Oliktok DEW-Line station on 25 June is 6.2 m s^{-1} in the direction indicated by "OLI."

Thus the pack ice 20 km or so beyond the fast ice edge drifted as one would expect from "Zubov's rule" for steady, wind-induced ice drift: i.e., at 1/30th to 1/50th of the wind speed, at an angle about 30° to the right of the wind. More interesting are the vectors in the first 10 km seaward of the line "A". Evidently the pack ice here was nearly motionless, with the pronounced shear zone located some 15 km or more seaward of the fast ice edge. In this instance a buffer zone of immobile pack ice appears to shield the fast ice from shear stresses. It is possible that the coastal promontories or grounded ice areas off Figure 14 to the west stalled the

* The authors are grateful to J. Wayenberg, U.S. Geologic Survey Ice Dynamics Project, Tacoma, WA, for providing the 1974 SLAR data. The images are from the flights described in Campbell, et al. (1976).

motion of this pack ice, with the momentum of the moving pack dissipated as a normal stress (to the west) against such barriers. In any event, we see that it may be an oversimplification to equate the shear zone with the fast ice edge during the summer.

The 26 June scene illustrates ice conditions just prior to the onset of breakup, with well-developed shore polynyai extending from the major river mouths, a well-defined fast ice sheet including several major grounded ice masses, and a complicated pattern of surficial melt on the fast ice. Figure 12 shows the ice conditions on 14 July, 1974. The shore polynyai on the Colville, Kuparuk and Sagavanirktok rivers have expanded considerably by melting since 26 June. The pack ice is still compact against the near-shore ice. Despite the rapid drift observed on the 25-26 June sequence, several pack ice floes due north of Prudhoe Bay can be positively identified on the scenes of 26 June and 14 July. Their net 18-day displacements are less than 10 km, directed southwest, towards the Colville shore polynya. The fast ice sheet of 26 June has also been displaced by a similar amount between the two westernmost grounded ice features in eastern Harrison Bay. The displacements have large onshore components, the ice shearing away from the immobile grounded masses. The breakup mechanism here appears to be shoreward pressuring of the fast ice by the pack, indicating that offshore wind directions may not be a necessary prerequisite to breakup if the fast ice is sufficiently ablated and weakened. The somewhat more-uniform gray tones on the 14 July scene indicate that most of the fast ice has reached an advanced state of decay via melting at the surface. The 29 April SLAR imagery and 21 June CIR photos show many ice deformation features in the Harrison Bay fast ice. Such features are usually

associated with deep-draft keels which, however, must have been floating or grounded less-firmly than the three major ice masses mentioned earlier. As these keels move shoreward under pack ice pressure they can gouge the shallower sea floor, presenting yet another potential hazard for structures or lines along the bottom. Conditions on 14 July are representative of a mid-breakup situation.

By 2 August, 1974 (Figure 13) there is a coast-parallel strip of open water extending 10 to 15 km from shore. The continuous fast ice sheet of 26 June has essentially disintegrated at this time. The three major grounded ice masses which initially stabilized the fast ice edge have decreased in area, but are still located in the same positions as they were on 26 June, indicating once again the potential longevity of ice deformation features in the stamukhi zone.

Breakup in the sector between Point Barrow and Pitt Point lags areas further east by about one month, probably due to the limited freshwater inflow other than in the lagoons. Ice in Harrison Bay can also be slow to clear as a result of trapping of ice, due to the coastal configuration. Deep surface meltwater ponds often drain through cracks and thawholes in early July, although they ususally become the first sites of complete melt through later in the decay season. Following drainage, the spectral signature of flat first-year ice reverses on the MSS imagery, due to the increase in spectral reflectance of bare ice over puddled ice, especially in band 7. Older floes incorporated into the fast ice, plus the remains of grounded ridges and hummocks, and even ice island fragments, usually beyond the barrier islands, can

persist even after the first-year ice has largely melted out in late August. In August 1973, 1974 and 1976 a strip of open water paralleled most of the coast, bordered by loose pack ice, whereas in 1975, fast ice decay was retarded by low summer temperatures in the northwesterly airflow which also held the pack ice close to the coast (Wendler and Jayaweera, 1976; Wohl, 1978). The major shipping delays which accompanied severe ice conditions in August and September, 1975 were primarily caused by the ice accumulation just off Point Barrow, since a channel inside and just seaward of the Barrier Islands was essentially ice free to Prudhoe Bay. We also note that the early summer melt patterns were similar in the Barrow and Prudhoe Bay areas near shore in all four summers 1973-1976.

Climatic Controls

The climatic controls on the fast and pack ice of the Beaufort and Chukchi seas can be differentiated for two regions, one which includes the Beaufort Sea and the northern Chukchi Sea and the other for the southern Chukchi Sea to the Bering Strait. Different climatic controls result from the contrasting orientation of the two Alaskan coasts and the presence of the Brooks Range, although the actual boundary separating these regions is difficult to pinpoint. The Brooks Range, which crosses Alaska between latitudes 67° - 69° N, extends westward to Point Hope and it is nearest to the coast in the vicinity of Barter Island. From Icy Cape to Cape Bathurst, N.W.T., the orientation of the coast is roughly east-west and the severity of summertime ice conditions depends primarily upon the predominance of either northerly or southerly winds. South of Icy Cape the coastal orientation is such that easterly and westerly winds affect the nature of ice conditions.

For the Beaufort Sea, southerly and southeasterly surface winds at Barrow are more frequent during light-ice summers while northerly and northeasterly winds are more frequent during heavy-ice summers (Rogers, 1978). The predominance of winds from a particular direction is determined by anomalies in the atmospheric circulation over the Arctic Ocean. Markham (1975) used January, February, and March atmospheric pressure patterns over the Arctic Ocean to estimate the motion of the pack ice and to predict summertime ice conditions in the southeastern Beaufort Sea. His technique, which estimates the volume of ice entering or leaving the Beaufort Sea via the Beaufort Sea gyre, was found to be useful for the southeastern Beaufort Sea in predicting which summers would have extremes of ice conditions.

Between Icy Cape and Point Barrow, north-northeasterly and south-southeasterly surface winds are important in terms of ice movement and breakup. This is particularly true in the fast ice zones of Icy Cape and Peard Bay which have melt and breakup characteristics similar to those occurring along the Beaufort Sea coast. Summertime atmospheric features both north and south of the Brooks Range play an important role in determining the coastal wind regime over the southern Chukchi Sea (Warmerdam, 1978). At Kotzebue, surface winds from 255° - 315° occur on about 41 percent of days during June through September. The Pacific subtropical high pressure intensifies during colder summers at Kotzebue, and the pressure over much of the western Arctic Ocean and northern Alaska is lower than normal. This results in stronger westerly geostrophic flow over the southern Chukchi Sea, which may delay breakup in that area and keep air temperatures below normal. During warmer summers, the south-north pressure

gradient is weaker, allowing more occurrences of warm overland flow, but still resulting in mean westerly geostrophic flow. There is a clear correlation (0.67) between date of onset of the westerly regime at Kotzebue and the accumulated thawing degree-days (summers 1953-76, except 1973). The five years of earliest westerly onset were also the summers with the five most severe ice conditions off Barrow. During all summers in recent decades, however, it was warm enough to clear the southern Chukchi Sea coast and Kotzebue Sound of ice.

Northeasterly surface winds normally prevail along both coasts during winter. Along the Beaufort and northern Chukchi coasts this flow is due to a ridge of high pressure over the western Arctic Ocean while over the southern Chukchi Sea it results from the Aleutian low which appears on monthly mean pressure maps. This large-scale flow has considerable influence on the pack ice. Shapiro and Burns (1975) found that during early March 1973 a breakout of ice occurred from the southern Chukchi Sea to the northern Bering Sea through the Bering Strait. This event lowered the ice concentration in the Chukchi Sea by about 10 percent compared with 1974 according to Ahlnäs and Wendler (1977). They showed that during March 1973 the winds were largely from the northeast, which would detach ice from the Alaskan coast, whereas during March 1974 the winds over the Chukchi were from the northwest which would push the ice against the coast. Hibler, et al. (1974) showed that in March 1973 there was also drift of near-shore pack ice from the Beaufort Sea into the Chukchi Sea. These results indicate that strong northeasterly flow around a ridge of high pressure moves the ice from the Beaufort Sea to the Chukchi Sea and can lower the ice concentration near both these Alaskan coasts. During March 1973 this ice movement was facilitated by decreased ice concentration due to preceding ice drift into the Bering Sea.

Large-scale disruptions in the pack ice brought on by atmospheric conditions during winter have important implications for conditions in the fast ice zone. Pack ice movements invariably result in ridging along the edges of the fast ice zone, and they remove ice from the Beaufort Sea gyre (Markham, 1975). Both of these factors may in turn have an influence upon summertime ice conditions and breakup in the fast ice zone. Shapiro (1976) showed how an intense winter storm drove the pack ice into the fast ice zone of the Chukchi Sea coast near Barrow in late December 1973. Southwesterly winds of about 90 km hr^{-1} occurred for several hours and drove the pack parallel to the shore at speeds up to 8 km hr^{-1} .

Open water appears in the fast ice zone of the Beaufort Sea after sufficient melting of the ice, puddling, and melting of thaw holes. It is well known from the work of Zubov (1945) and Bilello (1961; 1977) that air temperature expressed as an accumulated freezing or thawing degree-day is the parameter most highly correlated with ice formation, growth, decay, and breakup. A freezing (thawing) degree day is the negative (positive) departure of 1°C in mean daily temperature from zero. In the Beaufort Sea, fast ice decay and disappearance and pack ice retreat are highly correlated with such temperature indices. Openings and movement in the ice occur with an accumulation of about 55-140 TDDs ($^{\circ}\text{C}$). With the accumulation of 140-220 TDDs the fast ice is gone and the pack ice starts melting.¹ Southerly winds may clear the nearshore zone by pushing the

¹ Less complete data for northwestern Kotzebue Sound-Kivalina, indicate that the accumulation of about 200 TDDs at Kotzebue approximates to fast ice clearance.

fast ice into the pack ice, which remains continually to the north of the 20 m isobath while the fast ice clears. After 220 TDDs the pack continues melting and retreats northward during southerly winds. The distance of the ice off Barrow on September 15 correlates highly (0.815) with accumulated thawing degree days. It is also affected by surface wind direction and mean surface pressure pattern, although the temperature is correlated with these in turn. Table 2 shows the mean maximum accumulation of summertime TDDs and wintertime freezing degree days. Despite being the northernmost station, and having the coldest winters in terms of accumulated freezing degree days, Sachs Harbor (72°N, 126°W) has warmer summers than those at Barrow and Barter Island. This is due to the high frequency of winds blowing across Banks Island, and to the appearance of open water in late May - early June in the southeastern Beaufort Sea (Markham, 1975). The median date of $\geq 2/10$ ice concentration in the vicinity of Sachs Harbor is about July 2, and it can occur in late May or early June in "good" years. Based on the climatic data and their correlation with the ice clearance, it is believed to have been sufficiently warm to have cleared the fast ice zone along the Beaufort Sea during all summers since 1921, when continuous meteorological data became available at Barrow (Rogers, 1978B).

Implications for Offshore Development

Until recently, marine transportation has been the primary activity in the Beaufort and Chukchi Seas for which ice hazards were a major concern. If petroleum exploration and development begin along the Alaskan continental shelf, activities related to exploratory drilling, such as determining the type and location of drilling platforms, and others related to development,

production, and transport of oil from offshore to pumping stations will also face problems with ice conditions and movement. Over-ice transport of equipment and supplies will be feasible and will depend upon ice conditions.

The degree of hazard posed by ice conditions to each of these activities depends upon where and how far from shore they are undertaken, i.e., on the type of sea ice (Weeks, 1978). The development of petroleum faces the least risk shoreward of the barrier islands and in the bottom-fast ice zone where wintertime ice motion is small (meters), or non-existent. Large (on the order of kilometers), and therefore hazardous, ice motions in this region occur primarily in autumn before ice becomes fast to the sea floor, and in late spring. However, recent studies by Taylor (1977), and Kovacs and Sodhi (1978) demonstrate that shore ice pile-up and ride-up is a common event on most arctic beaches. Ice ride-up may extend 50-150 m inland with both thick and thin sea ice. Such events appear to be most common in spring and early winter and may last only 15-30 minutes.

Increasingly greater risk to petroleum development would occur for activities undertaken in the floating fast ice zone and seaward. Large variations in ice conditions from year to year characterize the floating fast ice zone. These variations are dependent upon the forces and movements which can occur in this region during autumn before the fast ice is strong (thick) enough to resist deformation. There is evidence that colder winters are associated with less ice motion in this zone, although movement is always possible. The formation of small leads due to ice motion is hazardous to ice surface transportation particularly if the

lead rapidly refreezes and becomes snow covered. Hazards in the floating fast ice zone are considerably less shoreward of the 10-15 m isobath. Seaward of this there is greater potential of ice deformation and formation of grounded ridges. These are now discussed in more detail.

Ice deformation features. Ridges and hummocks show more-or-less preferred locations from year to year, probably in relation to the location of shoals (see Reimnitz, et al., 1978; Stringer, 1978A). Examples are: offshore and west of Barter Island, in a line from Narwhal Island to a point approximately 80 km due north of Atigaru Point in Harrison Bay, and approximately along the 20m isobath arcing around Pt. Barrow in the Chukchi Sea and Beaufort Sea. These areas are the scene of enormous shear and pressure forces, most of which seem to occur during the dark period November through February.

Since the edge of contiguous fast ice appears to be displaced progressively seaward through the winter months, each successive winter ice edge can be a site for ice deformation. Thus, large grounded ice masses may occur well inside the 20m isobath. In general, however, the areal extent and intensity of ice deformation seems to be greatest near the late-winter fast ice edge in the stamukhi zone. This may be a consequence of the involvement of more massive polar floes and thicker first-year ice in ridge formation late in the season. Our case-study illustrates the anomalously large and well-grounded field of shear ridges that may form in this manner.

Grounded ice. This type of ice is very discontinuous along the coast. During the decay season, therefore, under-ice oil spills occurring within the fast ice zone would not necessarily be contained within a band of grounded ice parallel to the coast. Nevertheless, the elongate ridges

which parallel extensive segments of the Beaufort Sea coast in late winter have keels extending well below the level ice, even though they may be floating or only weakly grounded. These ridges might be effective in temporarily containing most of an under-ice oil spill during February through May. Such trapping capability would rapidly diminish after late June as the fast ice begins to disintegrate leaving only well-grounded ridges in situ. This decay date also marks the end of the period when trapping could occur in the irregular bottom topography of the floating fast ice.

Our mapping has shown that well-grounded, deformed ice masses are occasionally found in waters $\leq 10\text{m}$ deep. Structures and lines on the near-shore bottom must be able to withstand the forces generated by such features and associated bottom gouging and scour, even though the frequency and intensity of such events are much less than in the stamukhi zone.

During virtually all summers, the fast ice zone clears of ice (Rogers, 1978) with pack ice retreat occurring during summers with more frequent southerly winds. While this is encouraging for setting up structures in the open water of the bottom fast ice and floating fast ice zones, there is always the danger of pack ice incursions due to wind shifts over the course of the summer. This problem may be alleviated by ice reconnaissance and improved ice forecasting, but structures or shipping operations must take account of this hazard.

Summary

The fast ice regimes of the Beaufort-Chukchi Sea coasts are described, based on LANDSAT imagery for 1973-76, in order to outline the timing of the seasonal states. The spring location of the outer fast ice margin is strongly influenced by the occurrence of grounded ridges along much of the Beaufort Sea coast. However, for about 2° longitude eastward from Point Barrow, and also north of Cape Lisburne and off Kotzebue, the limit is much more variable from year-to-year, apparently in response to the particular patterns of current gyres, pack ice drift, and shear. The significance of winter ridging events for the summer breakup process is illustrated by case studies. A flaw lead and polynyi are major features of the Chukchi coast. The decay process is closely related to thawing degree day accumulations; approximately 140-220 TDDs (°C) are required to remove the fast ice and 220-300 for open water to extend up to 80 km off Pt. Barrow on 15 September. Surface winds are more frequent from 135°-195° during light-ice summers on the Beaufort coast, and from 345°-045° during severe ice summers, reflecting the airflow direction-temperature association. Based on the climatic data at Barrow and their correlation with ice clearance, the fast ice in the nearshore zone of the Beaufort Sea coast should have cleared in all summers since 1921. Some implications of the characteristics of the fast ice zone in the Beaufort Sea for potential offshore developments are discussed.

ACKNOWLEDGEMENTS

This study was supported by the Bureau of Land Management through interagency agreement with the National Oceanic and Atmospheric Administration, under which a multi-layer program responding to needs of petroleum development of the Alaskan continental shelf is managed by the Outer Continental Shelf Environmental Assessment Program Office (Contract 03-5-022-91, RU 244).

We thank the following individuals: Marilyn Joel, for drafting the figures; Andrew Carleton, who analyzed the polynya information; and input to the project provided by R. Keen, C. W. Locke, A. J. Quinlan, B. Warmerdam, R. L. Weaver and G. Wohl, graduate research assistants, and Margaret Eccles, programming consultant.

REFERENCES

- Aagard, K. and contributors, 1978: Physical oceanography and meteorology. In: Environmental Assessment of the Alaskan Continental Shelf. Interim Synthesis: Beaufort/Chukchi. Environmental Research Laboratories, NOAA, Boulder, CO, pp. 56-100.
- Ahlnas, K., and Wendler, G., 1977: Arctic sea ice conditions in early spring viewed by satellite. Arctic and Alpine Res., 9(1):61-72.
- Barnett, D. G., 1976: A practical method of long-range ice forecasting for the north coast of Alaska, Part 1. Tech. Rep. No. 1, Fleet Weather Facility, Suitland, Md., 16 pp.
- Barry, R. G., 1976: Study of climatic effects on fast ice extent and its seasonal decay along the Beaufort Sea coast. In: Environmental Assessment of the Alaskan Continental Shelf, Vol. 14, Ice, Environmental Research Laboratories, NOAA, Boulder, CO, pp. 58-115.
- Barry, R. G., 1977: Study of climatic effects on fast ice extent and its seasonal decay along the Beaufort-Chukchi coasts. In: Environmental Assessment of the Alaskan Continental Shelf, Vol XIV, Transport, Environmental Research Laboratories, NOAA, Boulder, CO, pp. 574-743.
- Barry, R. G., 1978: Study of climatic effects on fast ice extent and its seasonal decay along the Beaufort-Chukchi coasts. In: Environmental Assessment of the Alaskan Continental Shelf, Vol. 9, Transport, Environmental Research Laboratories, NOAA, Boulder, CO, pp. 604-719.
- Bilello, M. A., 1961: Formation, growth, and decay of sea ice in the Canadian Arctic archipelago. Arctic, 14:3-24.
- Bilello, M. A., 1977: Decay patterns of landfast sea ice in Canada and Alaska. In: A Symposium on Sea Ice Processes and Models, Preprints, Vol. II, pp. 1-10, (Internat. Comm. Snow and Ice/AIDJEX), University of Washington Press, Seattle.
- Brower, W. A., Jr., Searby, H. W., Wise, J. L., Diaz, H. F. and Prechtel, A. S., 1977: Climatic Atlas of the Outer Continental Shelf Waters and the Coastal Regions of Alaska, Vol. III. Chukchi-Beaufort Sea, Arctic Environmental Information and Data Center, University of Alaska, Anchorage, 409 pp.
- Campbell, W. J., Gloersen, P., Webster, W. J., Wilheit, T. T. and Rainseir, R. O., 1976: Beaufort Sea ice zones as delineated by microwave imagery. J. Geophys. Res., 81:1103-10.
- Carlson, R. F., 1977: Effects of seasonability and variability of streamflow on nearshore coastal areas. In: Environmental Assessment of the Alaskan Continental Shelf, Vol. XIV, Transport, Environmental Research Laboratories, NOAA, Boulder, CO, pp. 96-250.

- Clarke, E. S., 1976: Development of a prototype Beaufort Sea technology scenario. Science in Alaska Proc. 27th Alaska Science Conf., Vol. 1, Alaska Division, AAAS, Fairbanks, pp. 169-70.
- Cooper, P. F., Jr., 1974: Landfast ice in the southeastern part of the Beaufort Sea. In: The Coast and Shelf of the Beaufort Sea (ed., J. C. Reed and J. F. Sater), Arctic Institute of North America, Arlington, VA, pp. 235-42.
- Dunbar, Moira., 1975: Interpretation of SLAR imagery of sea ice in Nares Strait and the Arctic Ocean. J. Glaciol., 73:193-213.
- Handlers, R. F., 1977: On the question of accumulation of ice-melt water south of the ice in the Chukchi. M.S. thesis, Naval Postgraduate School, Monterey, 47 pp.
- Henry, R. F. and Heaps, N. S., 1976: Storm surges in the southern Beaufort Sea. Journal of the Fisheries Research Board of Canada, 33:2362-76.
- Hibler, W. D., Ackley, S. F., Crowder, W. K., McKim, H. L. and Anderson, D. M., 1974: Analysis of shear zone ice deformation in the Beaufort Sea using satellite imagery. In: The Coast and Shelf of the Beaufort Sea, J. C. Reed and J. E. Sater (eds.), Arctic Institute of North America, Arlington, VA, pp. 285-296.
- Jacobs, J. D., Barry, R. G. and Weaver, R. L., 1975: Fast ice characteristics with special reference to the eastern Canadian Arctic. Polar Record, 17 (110):521-36.
- Kniskern, F. E. and Potocsky, G. J., 1965: Frost degree days, related ice thickness curves, and harbor freezeup and breakup dates for selected Arctic stations. U.S. Naval Oceanographic Office, Tech. Rep. TR-60, Washington DC, 123 pp.
- Kovacs, A., 1976: Grounded ice in the fast ice zone along the Beaufort Sea coast of Alaska. U.S. Army CRREL, Technical Report 76-32, Hannover, NH, 29 pp.
- Kovacs, A. and Gow, A. J., 1976: Some characteristics of grounded floebergs near Prudhoe Bay, Alaska. Arctic, 29:169-73.
- Kovacs, A. and Mellor, M., 1974: Sea ice morphology and ice as a geologic agent in the southern Beaufort Sea. In: The Coast and Shelf of the Beaufort Sea, J. C. Reed and J. E. Sater (eds.), Arctic Institute of North America, Arlington, VA, pp. 113-61.
- Markham, W. E., 1975: Ice climatology of the Beaufort Sea. Beaufort Sea Project Technical Report No. 26, Department of Environment, Victoria, British Columbia, 87 pp.
- Marko, J., 1975: Satellite observations of the Beaufort Sea ice cover. Beaufort Sea Project Technocak Report No. 34, Department of Environment, Victoria, British Columbia, 137 pp.

- Moritz, R. E., 1978: Synoptic climatology of the Beaufort Sea coast of Alaska, Unpublished M.A. thesis, University of Colorado, Boulder, CO, 238 pp.
- National Ocean Survey, 1977: United States Coast Pilot. Pacific and Arctic Coasts. Alaska. Cape Spencer to Beaufort Sea (8th ed.), Rockville, Md, 412 pp.
- Nelson, R. D., 1974: Measurements of tide- and temperature-generated stresses in shorefast sea ice. In: The Coast and Shelf of the Beaufort Sea, J. C. Reed and J. E. Sater (eds.), Arctic Institute of North America, Arlington, VA, pp. 195-204.
- Peyton, H. R. and Belke, C. E., 1969: A thickness survey of pack ice along the northwest Alaska Coast. Arctic Environmental Engineering Laboratory, University of Alaska, 20 pp.
- Ramseier, R. O., Vant, M. R., Arsenault, L. D., Gray, R. G. and Chudobiak, W. J., 1975: Distribution of sea ice thickness in the Beaufort Sea. Beaufort Sea Project, Technical Report No. 30, Department of Environment Victoria, British Columbia, 98 pp.
- Reimnitz, E. and Bruder, K. F., 1972: River discharge into an ice covered ocean and related sediment dispersal. Bull. Geol. Soc. Amer., 83:861-66.
- Reimnitz, E. and Maurer, D. K., 1978: Storm surges in the Alaskan Beaufort Sea. U.S. Geol. Surv. Open File Report 78-5893, 26 pp.
- Reimnitz, E., Toimil, L. and Barnes, P., 1978: Arctic continental shelf morphology related to sea ice zonation, Beaufort Sea, Alaska. Marine Geology, 28:179-210.
- Rogers, J. C., 1978A: A meteorological basis for long-range forecasting of summer and early autumn sea ice conditions in the Beaufort Sea. In: POAC 77, Proceedings (Fourth International Conference on Port and Ocean Engineering under Arctic Conditions), D. B. Muggerridge Memorial University of Newfoundland, St. Johns, pp. 952-62.
- Rogers, J. C., 1978B: Meteorological factors affecting interannual variability of summertime ice extent in the Beaufort Sea. Mon. Wea. Rev., 106:890-897.
- Sater, J. E., Walsh, J. E. and Wittmann, W. I., 1974: Impingement of sea ice on the north coast of Alaska. In: The Coast and Shelf of the Beaufort Sea, J. C. Reed and J. E. Sater (eds.), Arctic Institute of North America, Arlington, VA, pp. 85-105.
- Schaeffer, P. J., 1966: Computation of a storm surge at Barrow, Alaska. Archiv fur Meteorologie, Geophysik und Bioklimatologie, A15:372-93.
- Shapiro, L. H., 1976: A preliminary study of ridging in landfast ice at Barrow, Alaska, using radar data. In: Proceedings of the Third International Conference on Port and Ocean Engineering under Arctic Conditions, Institute of Marine Science, University of Alaska, pp. 417-25.

- Shapiro, L. H. and Burns, J. J., 1975: Satellite observations of sea ice movement in the Bering Strait region. In: Climate of the Arctic, G. H. Weller and S. A. Bowling (eds.), University of Alaska, Fairbanks, pp. 379-386.
- Shapiro, L. H. and Harrison, W. D., 1976: Mechanics of origin of pressure ridges, shear ridges and hummock fields in landfast ice. In: Environmental Assessment of the Alaskan Continental Shelf, Vol. 14, Ice, Environmental Research Laboratories, NOAA, Boulder, CO, pp. 117-153.
- Shapiro, L. H., Harrison, W. D. and Bates, H. R., 1977: Mechanics of origin of pressure ridges, shear ridges and hummock fields in landfast ice. In: Environmental Assessment of the Alaskan Continental Shelf, Vol. XV, Transport, Environmental Research Laboratories, NOAA Boulder, CO, pp. 1-41.
- Short, A. D., Coleman, J. M. and Wright, L. D., 1974: Beach dynamics and nearshore morphology of the Beaufort Sea coast, Alaska. In: The Coast and Shelf of the Beaufort Sea, J. C. Reed and J. E. Sater (eds.), Arctic Institute of North America, Arlington, VA, pp. 477-488.
- Short, A. D. and Wiseman, W. J., Jr., 1975: Coastal breakup in the Alaskan Arctic. Bulletin of the Geological Society of America, 86:199-202.
- State of Alaska, 1975: Alaska Regional Profiles. Vol. II, Arctic Region, L. L. Selkregg, coordinator, Arctic Environmental Information and Data Center, University of Alaska, 218 pp.
- Stringer, W. J., 1974: Morphology of the Beaufort Sea shorefast ice. In: The Coast and Shelf of the Beaufort Sea (ed. J. C. Reed and J. E. Sater). Arctic Institute of North America, Arlington, VA, pp. 165-72.
- Stringer, W. J., 1978A: Morphology of Beaufort, Chukchi and Bering seas nearshore ice conditions by means of satellite and aerial remote sensing. In: Environmental Assessment of the Alaskan Continental Shelf, Environmental Research Laboratories, NOAA, Boulder, CO.
- Stringer, W. J., 1978B: Fast ice terminology, Glaciological Data, Report GD-2, (World Data Center A for Glaciology, Boulder, CO), pp. 21-23.
- Transehe, N. A., 1928: The ice cover of the Arctic Sea, with a genetic classification of sea ice. In: Problems of Polar Research, American Geographical Society, Spec. Publ. No. 7, New York, pp. 91-123.
- Untersteiner, N. and Coon, M. D., 1977: Dynamics of nearshore ice. In: Environmental Assessment of the Alaskan Continental Shelf, Vol. XVI, Hazards, Environmental Research Laboratories, NOAA, Boulder, CO, pp. 164-332.
- Weeks, W. F. (ed.), 1978: Environmental hazards to offshore operations. In: Environmental Assessment of the Alaskan Continental Shelf. Interim Synthesis: Beaufort/Chukchi. Environmental Research Laboratories, NOAA, Boulder, CO, pp. 3335-55.

Weeks, W. F., Kovacs, A., Mock, S. J. Tucker, W. D., Hibler, W. D. and Gow, A. J., 1978: Studies of the movement of coastal sea ice near Prudhoe Bay, Alaska, U.S.A. Journal of Glaciology, 19(81):533-46.

World Meteorological Organization, 1970. WMO Sea-Ice Nomenclature: Terminology Codes and Illustrated Glossary, WMD Publication No. 259, Technical Publication No. 145, Geneva, 147 pp.

Zubov, N. N., 1945: L'dy Arktiki. (Translation: Arctic Ice, U.S. Navy Oceanographic Office, 1963, 491 pp.).

TABLE 1. Average seasonal regimes in Alaskan shorefast ice¹.

<u>Ice Phase</u>	<u>Central Beaufort Sea Coast</u>	<u>Central Chukchi Sea Coast</u>
New ice forms	3 October	10 October
First continuous fast ice	Mid October	Early November
Extension/modification of fast ice	Nov. - Jan./Feb.	Nov./Dec. - Jan./Feb.
Stable ice sheet inside 15 m isobath	Jan./Feb. - Apr./May	Feb. - Apr./May ²
River flooding fast ice	25 May	1 May
First melt pools	10 June	10 May
First openings and movement	30 June	10 June
Nearshore area largely free of fast ice	1 August	5 July

¹ These dates are based on available LANDSAT imagery for 1973-77. An identifiable event may occur anywhere between the dates of available clear frames which bracket the latest date of recognized non-occurrence and the earliest date of its identified occurrence; the average of these dates is used here.

² Locally, the ice may not achieve any prolonged stability.

TABLE 2. Average cumulative thawing and freezing degree-days ($^{\circ}\text{C}$).

	<u>Period</u>	<u>Thawing degree-days</u>		<u>Freezing degree-days</u>
		<u>Mean</u>	<u>Standard deviation</u>	<u>Mean</u>
Kotzebue	1943-76	1081	113	3414
Barrow	1921-75	296	101	4836
Barter Is.	1948-75	324	98	4877
Sachs Harbour	1956-75	364*	-	5382*

* based on mean monthly temperatures.

FIGURE CAPTIONS

1. Location map of the Beaufort-Chukchi Sea coasts.
2. Spring-early summer limits of the fast ice zone on the Chukchi coast, 1973-76.
3. LANDSAT scene showing nearshore ice conditions on 6 October, 1974, between Barter Island and Herschel Island.
4. Spring-early summer limits of the fast ice zone on the Beaufort coast, 1973-76.
5. Low-level aerial oblique photograph of the ice-deformation zone off Barter Island, June 1976.
6. LANDSAT scene showing a large ridge field in outer Harrison Bay, 20 April, 1975.
7. LANDSAT scene showing the same area as Fig. 6 on 12 September, 1975.
8. Low-level aerial view of flat ice in Harrison Bay, June, 1976.
9. The extent of polynyi off Point Hope in spring-early summer, (a) 1974, and (b) 1976, mapped from LANDSAT imagery.
10. LANDSAT scene showing rivers flooding over ice in the vicinity of Prudhoe Bay, 6 June, 1976.
11. LANDSAT scene showing pre-breakup conditions in the vicinity of Prudhoe Bay, 26 June, 1974. Polynyi are evident off the major river mouths.
12. LANDSAT scene showing mid-season nearshore ice breakup in the vicinity of Prudhoe Bay, 14 July, 1974.
13. LANDSAT scene showing post-breakup conditions in the vicinity of Prudhoe Bay, 2 August, 1974. A coastal strip of open water extends 10-15 km from shore. Three major grounded ice masses are located in the same positions as on 26 June.
14. Mapped interpretation of ice conditions in the vicinity of Prudhoe Bay on 25-26 June, 1974. The fast ice/pack ice boundary is marked 'A'. Grounded ice masses which persisted into August are marked 'G'. Ice displacement vectors have been determined between 25 and 26 June. Average surface wind direction at Oliktok on 25 June is denoted 'OLI'.

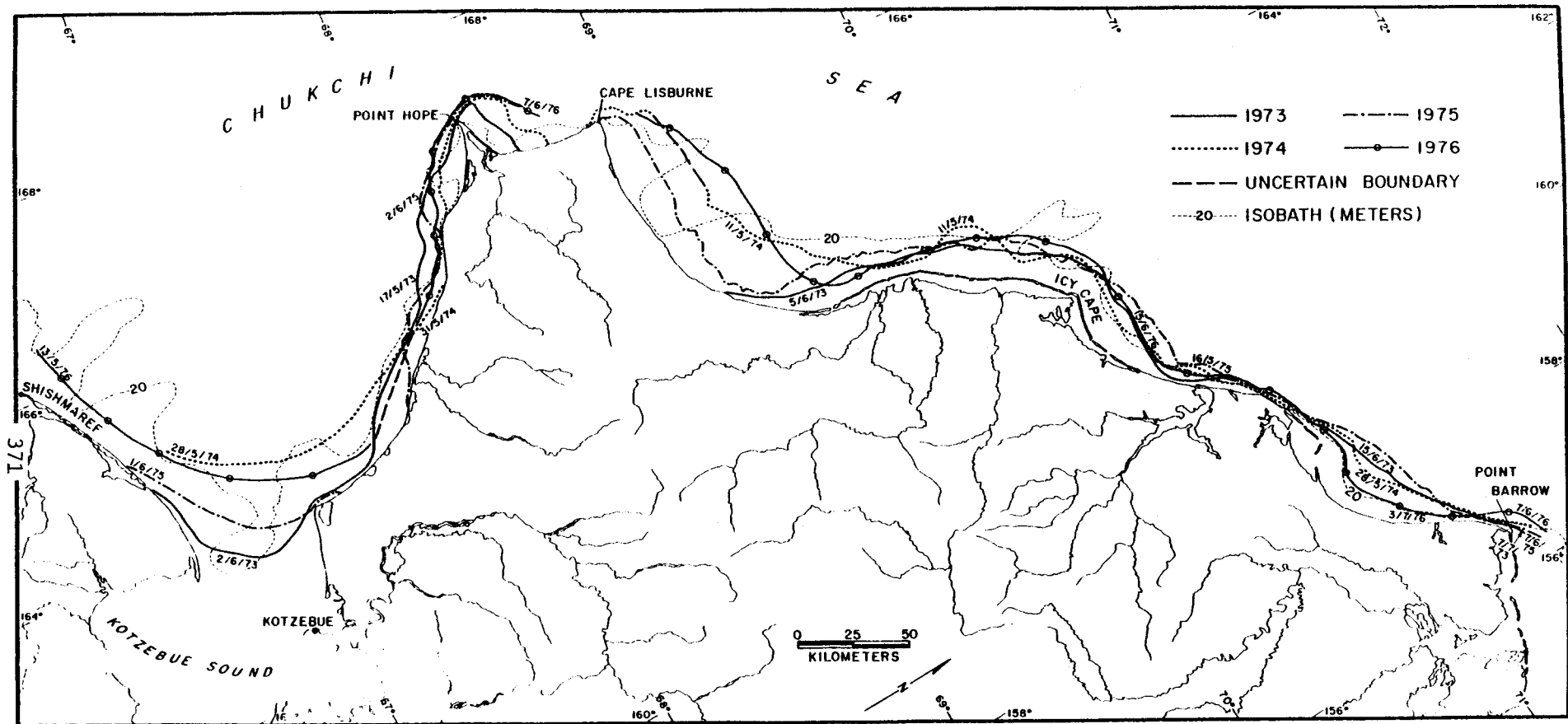


Fig. 2. Spring-early summer limits of the fast ice zone on the Chukchi coast, 1973-76.

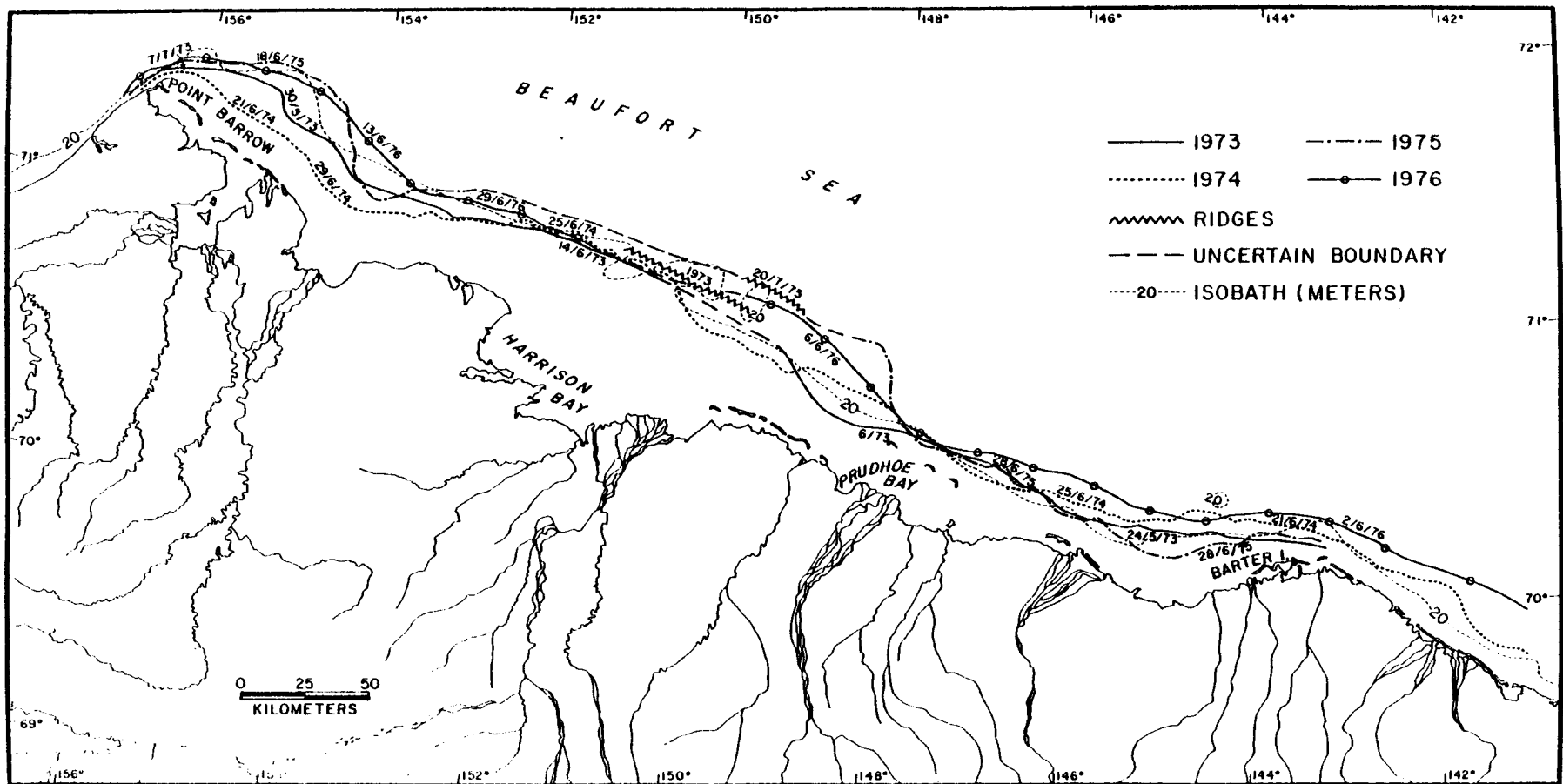


Fig. 4. Spring-early summer limits of the fast ice zone on the Beaufort coast, 1973-76.

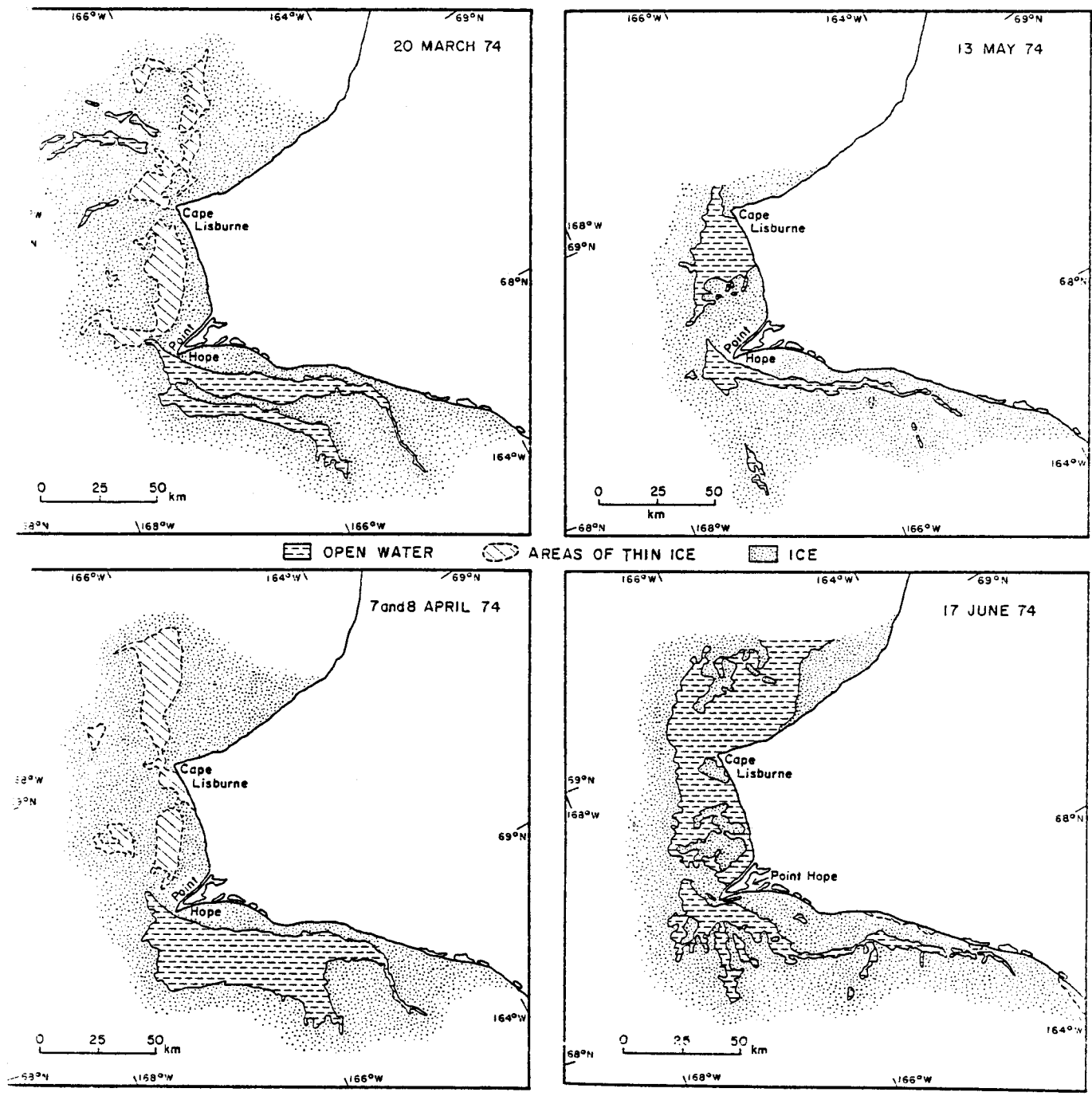


Fig. 9a. The extent of polynyi off Point Hope in spring-early summer, 1974, mapped from LANDSAT imagery.

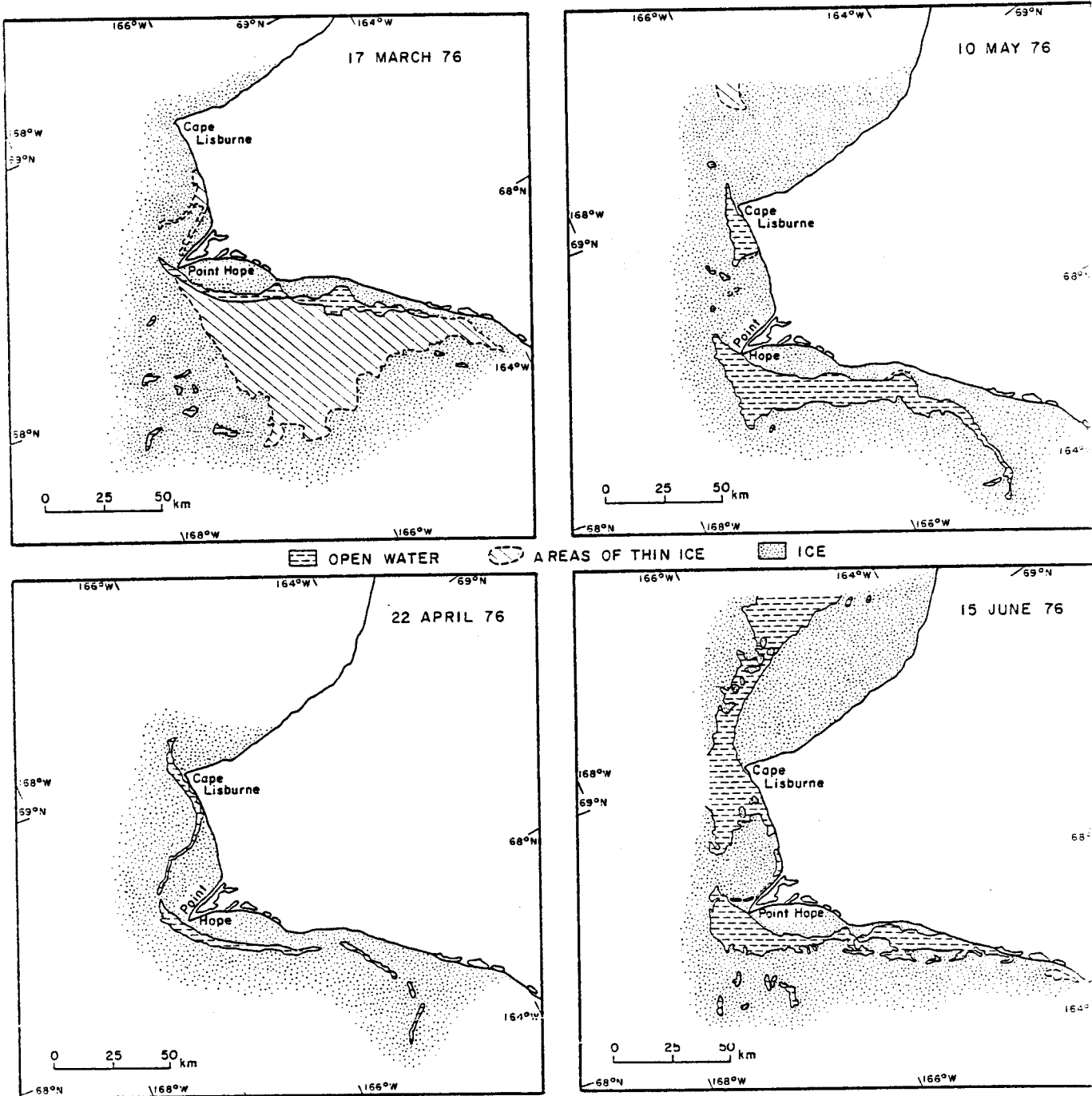


Fig. 9B. The extent of polynya off Point Hope in spring-early summer, 1976, mapped from LANDSAT imagery.

The following was submitted as Appendix 2:

Rogers, Jeffery C. (1978). "Meteorological Factors Affecting Inter-annual Variability of Summertime Ice Extent in the Beaufort Sea," Monthly Weather Review, Vol. 106, No. 6, pp. 890-897.

The following was submitted as Appendix 3:

Rogers, Jeffrey C. (1977). "A Meteorological Basis for Long-Range Forecasting of Summer and Early Autumn Sea Ice Conditions in the Beaufort Sea," POAC 77, Vol. 2, pp. 952-962.

Research Unit 257

The following were submitted as the final report for this research unit:

Stringer, William J. (1978) Morphology of Beaufort, Chukchi and Bering Seas Nearshore Ice Conditions by means of Satellite and Aerial Remote Sensing. Geophysical Institute, University of Alaska, Fairbanks, AK 99701.

VOLUME I - 218 pp.

VOLUME II - 576 pp.

FINAL REPORT

Research Unit No. 431
April 1, 1976 - September 31, 1978
Pages 66

COASTAL PROCESSES AND MORPHOLOGY OF THE
BERING SEA COAST OF ALASKA

Asbury H. Sallenger, Jr.
John R. Dingler

U.S. Geological Survey
Menlo Park, California 94025

I. SUMMARY OF OBJECTIVES, CONCLUSIONS, AND IMPLICATIONS WITH RESPECT TO OCS OIL AND GAS DEVELOPMENTS

Much of our effort during the first year of our study (FY 76) was involved in regional characterization of the physical environment of the Bering Sea coast of Alaska. This included determination of net long-shore transport directions (for the entire study area), characterization of coastal morphology, and reconnaissance of beach morphology and sediment characteristics (for the northern Bering Sea coast of Alaska and the Bristol Bay coast of the Alaska Peninsula). In FY 77, these types of studies were extended to Pavlov Bay and Cold Bay on the Pacific coast of the Alaska Peninsula. These potential deep water ports may serve offshore petroleum exploitation of the Bristol Bay area in the future. The results of these types of studies can be used to obtain qualitative assessments of coastal stability, in preparing preliminary siting studies for coastal developments, and in the determination of the long-term directions of transport of particulate pollutants in the littoral system.

Storms pose major hazards to coastal developments along the Alaskan Bering Sea coast. Shallow offshore depths that characterize much of the eastern Bering Sea shelf (particularly the northern Bering Sea) make coastal areas susceptible to storm surges of large magnitude. During FY 76, debris lines that resulted from a particularly severe storm in 1974 were measured at many locations along the northern Bering Sea coast of Alaska. Debris-line elevations provide a combined measure of sea-level rise due primarily to wind stress, drop in barometric pressure, wave set-up and runup. Measured elevations ranged generally between 3 and 4.75 m. The highest debris lines were found along the eastern side of Norton Sound. Ice had begun developing along the shore and in shallow areas prior to the storm. Ice blocks, which were lifted by the rise in sea level, were driven ashore by wind and breaking waves and caused damage in the village of Unalakleet. Large logs floating offshore and in debris lines could also be driven shoreward and be battered against coastal structures. These potential consequences of storms in this environment pose hazards to coastal developments in addition to hazards resulting from flooding and wave activity alone.

Our study on the coastal effects of this major storm continued in FY 77 with investigations on amounts of coastal change in the vicinity of Nome. Tundra bluffs were eroded as much as 45 m. This erosion was, however, irregular in plan view. Shoreline changes were also complex. Giant cusps with a longshore wavelength averaging 413 m were replaced during the storm by giant cusps spaced 853 m. The net effect of these changes was a complex pattern of shoreline erosion and accretion. For example, the shoreline accreted 50 m at one location while 150 m away the shoreline eroded 10 m. Interestingly, the net change was accretion. Similar changes were measured for a storm that occurred in 1950, but in this case the net change was erosion as expected. The accretion observed for the 1974 storm may be related to freeze-up processes, but the mechanisms are unknown.

A storm in September, 1977 caused a surge of nearly 2 m. Changes in beach and nearshore profiles that presumably resulted from this storm were again complex. One profile comparison indicated net accretion, whereas a profile located only 50 m away showed evidence of both substantial accretion and erosion. Coastal change is not, however, restricted to

storm conditions in this environment. Giant cusps were observed to migrate along the coast at 5-6 m/day during the period 6/23/51 - 7/30/51. This migration caused as much as 50 m accretion at a given location over a period of several weeks.

Preliminary analysis indicate that beach changes in the vicinity of Nome are much more dynamic (and complex) than beach changes for most other coastal areas along the northern Bering Sea coast.

A wave climate model for the northern Bering Sea was developed and used to simulate wave characteristics during the 1974 storm. Wave measurements during high energy conditions are needed, however, to verify some assumptions used in the model. Wave measurements were made near Nome during the summer of 1977. Unfortunately only fair weather conditions were encountered during the measurement period.

One use of the kind of data we have provided is to establish a coastal development set-back line. That is, the appropriate government body would prohibit developments within areas subject to inundation by storm surge or undermining by coastal erosion. Additional input into this analysis must include the long-term rate of erosion. This question needs more study. For structures that must cross the coastline (e.g. pipelines) the maximum scour depth must be established for both storms and over the long-term. Our investigations of these problems had only begun.

II. INTRODUCTION

A. General Nature and Scope of Study

Prior to FY 76, little information was available on the coastal processes of the Bering Sea coast of Alaska. This was a significant gap in our knowledge in view of anticipated coastal and nearshore developments in support of offshore petroleum exploitation.

During the first year of our study (FY 76), much of our effort was involved with regional characterization of the physical environment of the coast. This included determination of net longshore drift directions (areas 1, 2 and 3 on Fig. 1), classification of coastal morphology (areas 1 and 3) and detailed reconnaissance of beach morphology and sediment characteristics (areas 1 and 3). From these studies preliminary assessments have been made on coastal stability, sediment sources and sinks, and sediment transport pathways along the coast. These studies laid the groundwork for the more quantitative studies of coastal processes that followed.

During the second year of our study (FY 77), detailed investigations on coastal processes commenced in the Norton Sound area (Fig. 1 area 1). These studies generally followed two directions. First, historical studies of the effect of storms on coastal change from aerial photographs, debris-line elevations, and computer simulations of wave characteristics for the particularly severe November, 1974 storm. Second, direct measurements were made during the FY 77 field season of the amounts of coastal change and of the nearshore wave characteristics. The wave measurement program was intended to be a field verification of the computer model. The direct measurements of coastal change was a first step toward relating amounts of coastal change with computed wave characteristics.

The ultimate objective of the study was to develop a quantitative understanding of those processes controlling coastal erosion and accretion for the diverse coastal types found along the Bering Sea, coast of Alaska. Our work on the quantitative aspects of the problem, however, had only just begun when funding was terminated. Work during FY 78 dealt with reduction of data gathered during FY 77.

B. Specific Objectives

1. Determination of the net longshore transport directions for the Bering Sea coast of Alaska (Fig. 1, areas 1, 2, and 3).
2. Characterization of the coastal morphology for the Bristol Bay coast of the Alaska Peninsula and the northern Bering Sea coast of Alaska (Fig. 1, areas 1 and 3).
3. Reconnaissance of beach morphology and sediment characteristics for the Bristol Bay coast of the Alaska Peninsula and the northern Bering Sea coast of Alaska (Fig. 1, areas 1 and 3).

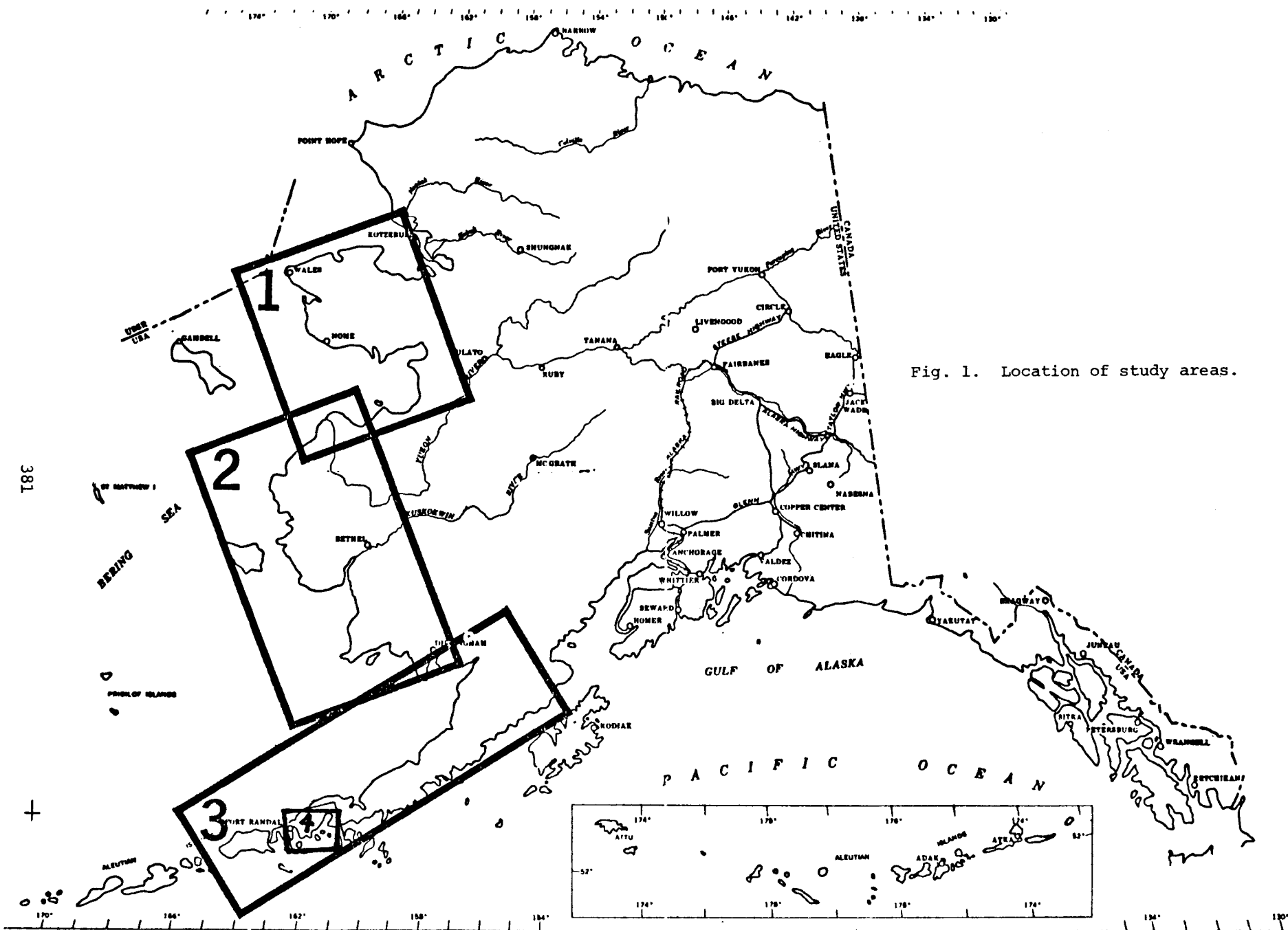


Fig. 1. Location of study areas.

4. Determination of net longshore transport directions, coastal morphology, and beach and sediment characteristics for Pavlov and Cold Bays on the Pacific coast of the Alaska Peninsula (Fig. 1, area 4).

5. Measurement of debris line elevations along the northern Bering Sea coast of Alaska that resulted from the November, 1974 storm (Fig. 1, area 1).

6. Computer simulation of wave characteristics in the north-east Bering Sea during the 1974 storm (Fig. 1, area 1).

7. Measurement of amounts of coastal change in the Nome area that resulted from the November, 1974 storm (Fig. 1, area 1).

8. Remeasure beach and nearshore profiles during FY 76 and FY 77 in the northern Bering Sea study area (Fig. 1, area 1).

9. Remeasure beach profiles during FY 76 and FY 77 in the southern portion of the Bristol Bay coast of the Alaska Peninsula study area (Fig. 1, area 3).

10. In situ measurements of wave characteristics and sea level variations in the vicinity of Nome (northern Bering Sea) (Fig. 1, area 1).

C. Relevance to Problems of Petroleum Development

One use of the type of data we present is in the establishment of a coastal development set-back line; that is, the appropriate government body would prohibit developments within areas subject to inundation by storm surge or undermining by coastal erosion. Additional input into this analysis must include the long-term rate of erosion of the coast. This is a question that needs more study. For structures that must cross the coastline (e.g. pipelines) the maximum scour depth must be established both for storms and over the long term. Our investigations of these problems had only begun.

III. CURRENT STATE OF KNOWLEDGE

Our previous work in the area has been briefly summarized in section II of this report (see also Sallenger, et al., 1977, 1978). Relevant work prior to FY 76 includes:

A. Greene (1970) observed longshore drift directions near Nome to be variable for June and July 1967, but predominantly to the east. Wave heights were generally low (≈ 30 cm), but storms during the late summer and fall were reported to produce high energy conditions.

B. The Draft E.I.S. for the Lost River Project reports that wave heights vary from approximately 30 cm in height up to 5 to 7 m with a theoretical maximum of 12 m off the mouth of the Lost River. Longshore transport is generally from west to east. Sediment transported during storm conditions greatly exceeds that transported under "normal" conditions.

C. The Corps of Engineers conducted several studies in the area including:

1. a report on flood protection and navigation improvement for Unalakleet.
2. National Shoreline Report which reports severe coastal erosion in Dillingham.

D. Several studies attempting to categorize coastal morphology at very small scales have been conducted (e.g. Putnam, 1960 and Dolan, 1967).

E. Additional studies include work on Quaternary marine transgressions and old strand lines (e.g. Hopkins, 1967) and several studies on beach placer deposits near Nome (e.g. Greene, 1970) and along the south shores of Bristol Bay (e.g. Berryhill, 1963).

IV. STUDY AREA

Our study area includes the Bering Sea coastal areas shown in Fig. 1. Also, some reconnaissance level studies have been done in Pavlov and Cold Bays on the south side of the Alaska Peninsula (Fig. 1, area 4). Most of our work, however, deals with the northern Bering Sea coast of Alaska (Fig. 1, area 1). See section IIB of this report for the locations of specific studies.

V. METHODS, RESULTS, DISCUSSION, AND CONCLUSIONS

Three separate reports have been prepared.

	<u>Page Number</u>
A. Coastal change along the northern Bering Sea coast of Alaska and the Bristol Bay coast of the Alaska Peninsula; by A. H. Sallenger.	7
B. Wave characteristics during the November, 1974 storm in the northern Bering Sea; by A. H. Sallenger.	38
C. Wave measurements and estimates of wave generated littoral transport; Nome, Alaska; by J. R. Dingler.	45

The first report (A) deals with objectives 5, 7, 8, and 9 (see section IIB). The second report (B) deals with objective 6. The third report (C) deals with objective 10. Our reconnaissance work (objectives 1-4) was discussed in detail in Sallenger, et. al., 1977.

A. COASTAL CHANGE ALONG THE NORTHERN BERING SEA COAST OF ALASKA AND THE BRISTOL BAY COAST OF THE ALASKA PENINSULA

A. H. Sallenger

STORM CHANGES IN THE NOME-SAFETY LAGOON AREA

NOVEMBER, 1974 STORM

Introduction

During the second week of November, 1974 a severe storm moved across the Bering Sea and caused extensive damage to communities along the northern Bering Sea coast of Alaska (Fig. 2). A detailed description of the meteorological characteristics of the storm is given in Fathauer (1975). At Nome, barometric pressure dropped 56 mb over a period of 26 hours and peak winds had a velocity of 111 km/hr from the south. Nearshore waves were reportedly 3-4 m in height. (See also "Wave characteristics during the November, 1974 storm in the northern Bering Sea", report B of this section)

The southerly winds and shallow offshore depths (e.g. mean depth of Norton Sound is approximately 20 m) contributed to a storm surge of large magnitude along the coast. Elevations of debris lines that resulted from this surge were measured at 30 locations distributed around the study area. Debris line elevation provides a measure of storm sea level rise due predominantly to the combined effects of drop in barometric pressure, wind set-up, wave set-up and run-up. Generally, the major portion of storm sea level rise can be attributed to wind set-up. The storm surge was superimposed on a spring high tide, but this was of relatively minor significance since the astronomical tide range for the region is low (e.g. the diurnal range at Nome is .49 m). Debris line elevations ranged from 3.25 m above mean sea level north of Norton Sound to nearly 5 m along the eastern flank of Norton Sound (Fig. 3) (data given in Sallenger, et. al., 1977). The maximum value is probably a result of the geometry of the Sound and compares in magnitude to disastrous storm surges caused by hurricanes on the Gulf of Mexico coast. At Nome, storm surge and waves overtopped a sea wall and caused nearly 15 million dollars in damage.

The storm occurred during freeze-up. The northern Bering Sea generally has greater than 80% ice coverage between late November and mid-May. This led to some interesting consequences in regard to coastal change and movement of coastal sediments.

Bluff Erosion

In the vicinity of Nome, bluffs 2-5 m in height extend along the coast for 40 km. These are generally composed of muds and are overlain by tundra vegetation. Vertical aerial photography is available for this region for June 17, 1974 and July 23, 1976. Except for the November, 1974 storm, no storm of sufficient magnitude to significantly erode the bluffs occurred during this period. Thus, comparisons of the relative positions of bluffs for these two times should yield the amount of change attributable to the 1974 storm. Using a zoom transfer scope, bluff positions were plotted for each time at a common scale of approximately 1:5700.

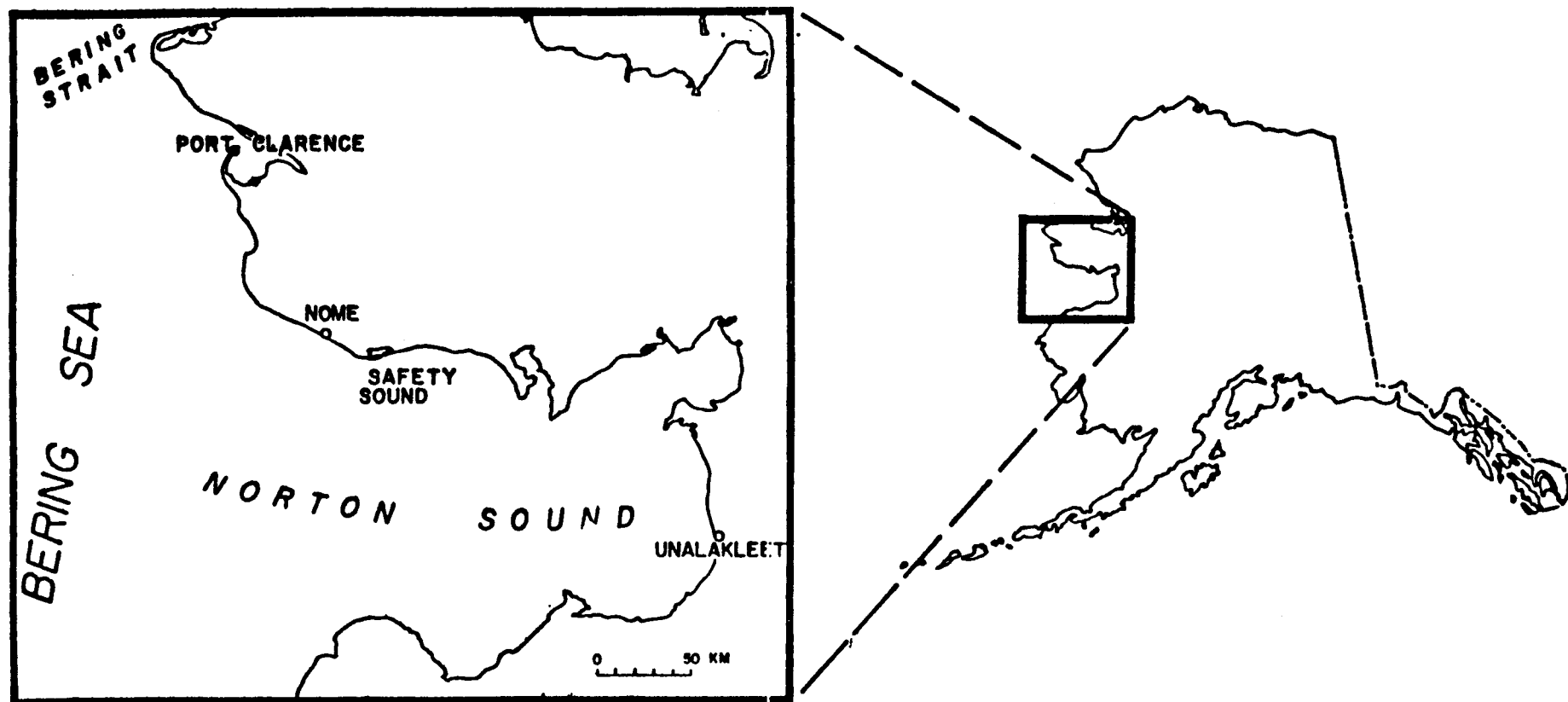


Fig. 2. Location of northern Bering Sea study area.

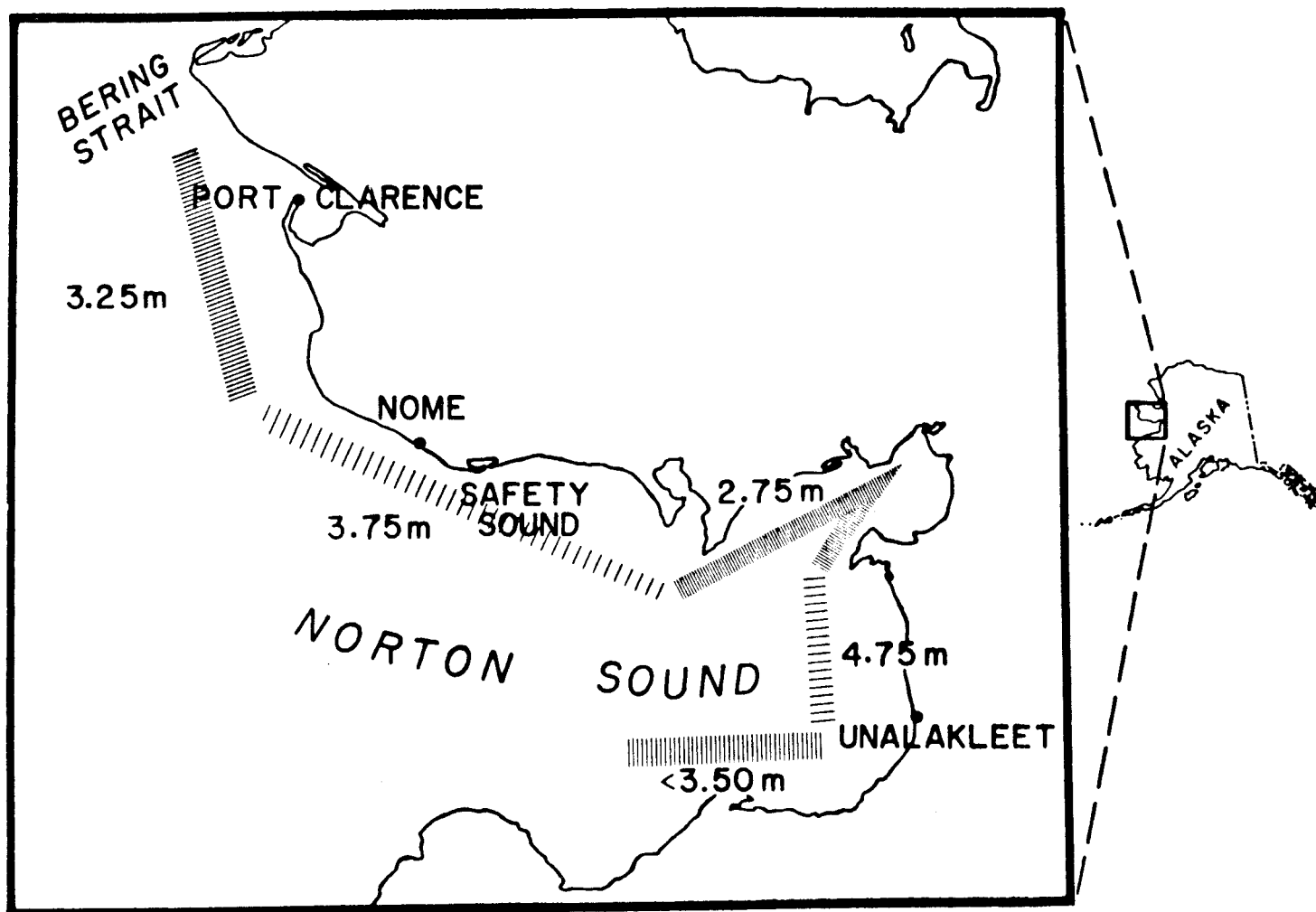


Fig. 3. Summary of measurements of debris line elevations. These are based on 30 measurements of debris line elevation distributed evenly around the study area. The elevations are referenced to observed sea level due to the paucity of predicted and measured tidal information for the area. This causes no large errors since the astronomical tide range for the region is relatively low. For example the diurnal range at Nome is .49 m. Consequently, to consider the measurements referenced to mean sea level would suggest maximum errors of approximately ± 25 cm.

Bluffs were eroded as much as 45 m. The erosion was, however, irregular in plan view, ranging from 0 to 45 m east of Nome where bluffs are 1.5 to 2 m high and 0-18 m west of Nome where bluffs are 3-5 m high. An example of this irregular pattern of erosion is shown in Fig. 4A where an embayment separated by two promontories was eroded into a once linear bluff. That the bluff was linear prior to the storm is confirmed by pre-storm photography. Depth to permafrost inland from the coast ranges from approximately .5 to .8 m depending on the composition of overlying material, but is much deeper near the coast and on the beaches (Greene, 1970). Variations in the lateral proximity of permafrost to the bluffs prior to the storm may have contributed to the observed non-uniform amount of erosion.

The surface of the platform to the left of the observer in Fig. 4B was presumably at or near the surface of permafrost prior to the storm. A .5-1.0 m thick layer of sediment and tundra that laid on top of the platform was stripped off by the storm waves whereas the frozen material below was resistant to modification. These platforms were best developed at the promontories discussed above. The photograph was taken in July, 1975 about one month of ice free conditions after the storm. No longer having the insulating protection of the overburden, the platform had eroded away by solifluction and other processes by the summer of 1976.

Shoreline Changes

Shoreline changes were complex. Along the barrier spit enclosing Safety Sound (Fig. 2), vertical aerial photographs are available for 17 June 1974 and 9 September 1975. In this area, nearshore ice generally protects the beaches from modification by waves until mid-June. Since the storm occurred during freeze-up, the ice-free interval between the storm and post-storm photographs was approximately three months. Except during storm conditions, wave energy in this environment is quite low. For example, during the summers of 1976 and 1977 wave heights were generally 0.3-0.6 m or less, except during the latter part of the ice free season (late September through November) when storms were frequent. Greene (1970) reported similar measurements. Furthermore, repetitive profile measurements during the summers of 1976 and 1977 showed that coastal change was minimal except during storms. No large storms occurred during the interval between the storm and post-storm photographs or during the pre-storm photographs and the storm. Thus, comparisons of shoreline positions between the two sets of photographs may provide a reasonable measure of shoreline change attributable to the major 1974 storm.

Prior to the storm, giant cusps with a longshore wavelength averaging 413 m were observed (Fig. 5). Giant cusps are crescentic and regularly spaced shoreline features similar in form to beach cusps, but are an order of magnitude or more larger and are generally associated with offshore bars. The pre-storm cusps observed, however, were not obviously associated with a bar. A bar was visible on aerial photographs through the sea surface, but it was sinuous and irregular in plan view with no apparent relation to the cusps. However, there may have been an inner bar present that was not visible in the photography. The pre-storm cusps were apparently destroyed by the storm and were replaced by

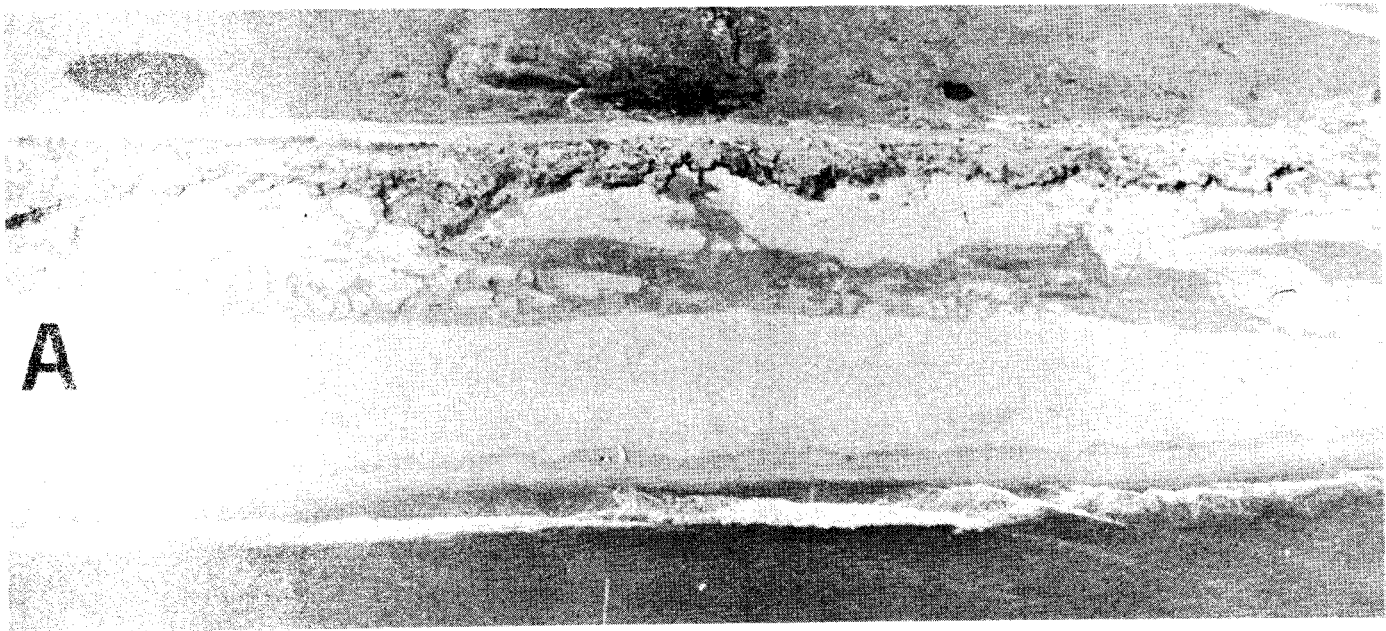


Fig. 4. A. Aerial view of the post-storm bluff. Note the embayment and two promontories on the left. This was a result of nonuniform erosion during the storm (see text). B. Ground view of one of the promontories shown in Fig. 3A. Note the platform to the left of the observer. Presumably, the surface of the platform was at the surface of permafrost prior to the storm. The unfrozen overburden was stripped off by storm waves.

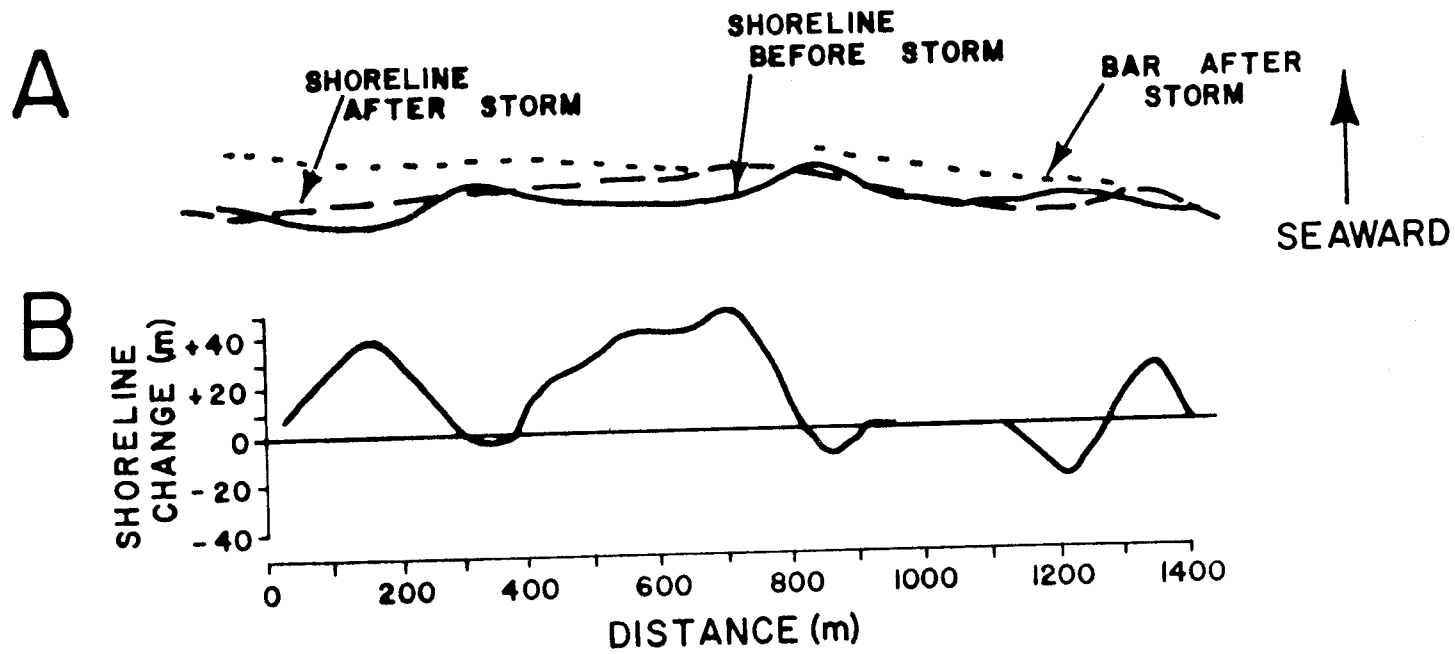


Fig. 5. An example of shoreline changes that resulted from the 1974 storm. Note the complex pattern and that the net change is accretion.

much larger giant cusps spaced 863 m (Fig. 5). Oblique bars that were obviously associated with the new cusps were observed on the post storm photography. The net effect of these changes was a relatively complex pattern of erosion and accretion. For example, the shoreline accreted 50 m at one location while 150 m away the shoreline eroded 10 m. Interestingly, the net change was accretional.

The giant cusps also controlled the location and extent of overwash; the overwash extending farther landward opposite embayments of the rhythmic shoreline topography (Fig. 6). In the same manner, giant cusps appeared to control the erosion of coastal vegetation. For example, in Fig. 6 it is seen that the beach grass closely parallels the form of the giant cusps. On the Outer Banks of North Carolina, Dolan (1971) made a similar observation. The regular spacing of breaches in a dune ridge following a storm matched the spacing of giant cusps.

COMPARISONS OF SHORELINE CHANGES BETWEEN THE 1974 AND NOVEMBER, 1950 STORMS

Shoreline comparisons based on photography from August 28, 1950 and June 22, 1951 showed similar changes in giant cusps. A relatively severe storm with southwesterly winds was recorded at Nome on November 10, 1950. On the pre-storm photography giant cusps spaced 363 m were observed (Fig. 7). These were replaced by very large cusps spaced 1.7 km, presumably as a result of the storm. Again a complex pattern of erosion and accretion resulted where at one location the shoreline eroded 41 m while 140 m away the shoreline accreted 12 m. In contrast to the 1974 storm, however, the net change was erosional.

The net accretion associated with the 1974 storm is perplexing. The comparisons of photography for both the 1950 and 1974 storms had good control. Numerous stable irregularities on the lagoon shoreline were used to match scales and orientation. Also, the trends for each storm were generally evident on all photographs compared.

It is interesting that air temperatures preceding each storm were quite different. They remained well below 0° C on the five days preceding the 1974 storm with daily minimums as low as -23° C (Fig. 8). Preceding the 1950 storm air temperatures were much warmer and generally above 0° C. When sea water temperature falls below its freezing point, an ice foot will begin to develop along the shoreline. An ice foot can form by a number of mechanisms (see for example Joyce, 1950). One of these is the freezing of spray and swash on the foreshore. By this process a rampart is built composed of ice and sediment which protects the foreshore from modification by waves. During storms, an ice foot of large proportions can be formed (Rex, 1964). For the 1974 storm, however, the optimum temperatures for ice foot formation existed prior to the storm. There may have been a thin covering of sea ice present in Norton Sound prior to the storm. The southerly winds could have pushed this ice against the south facing beaches. Perhaps these freeze-up processes contributed in some manner to the shoreline accretion observed for the 1974 storm. The mechanism is, however, unclear. The source of sediment may have been from the wide storm surf zone, but it is difficult to perceive

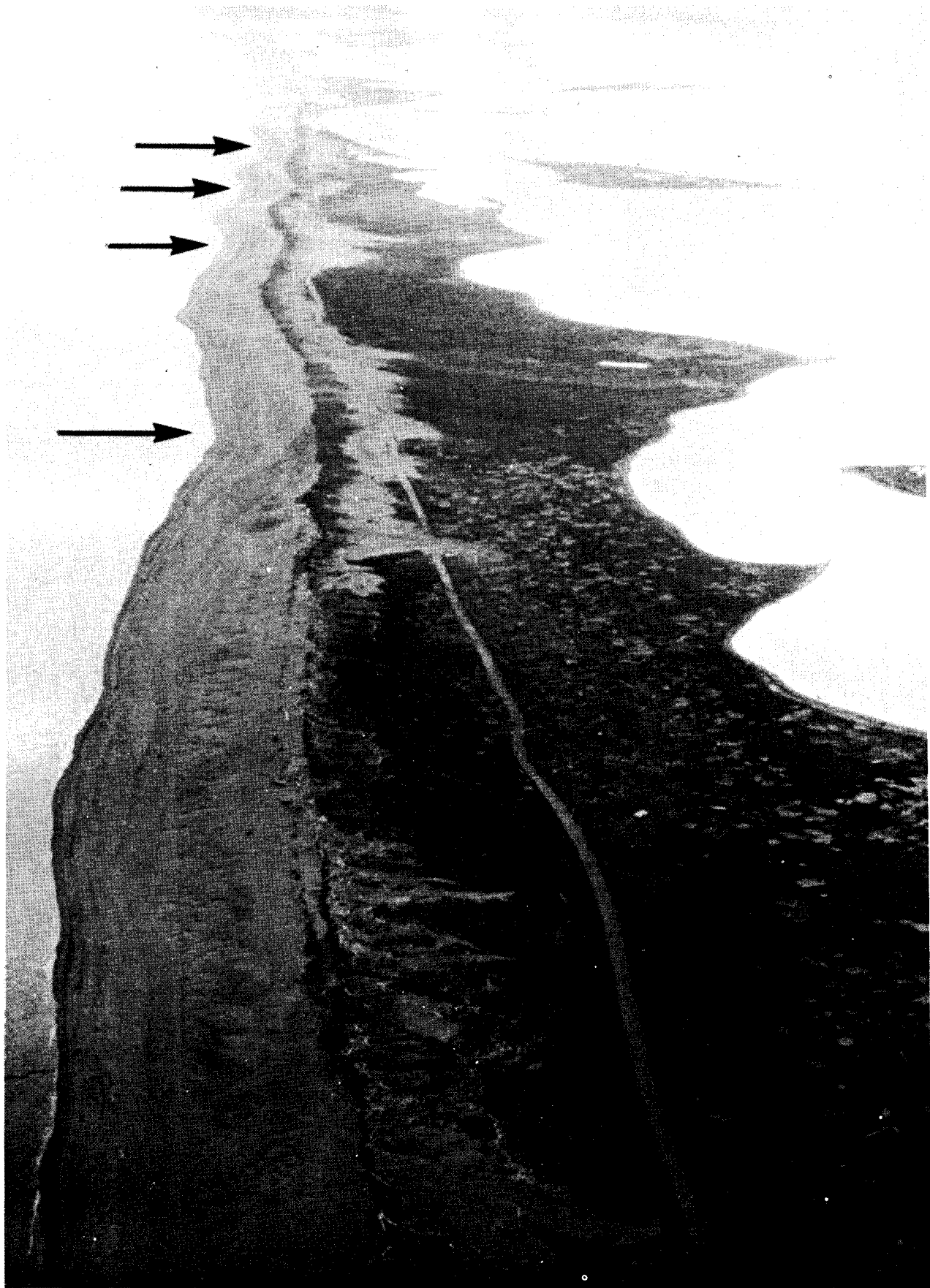


Fig. 6. Post-storm aerial view of the barrier spit enclosing Safety Sound. Note the maximum extent of overwash is opposite the embayments (arrows) of the rhythmic shoreline topography. Also, the beach grass line parallels the rhythmic shoreline.

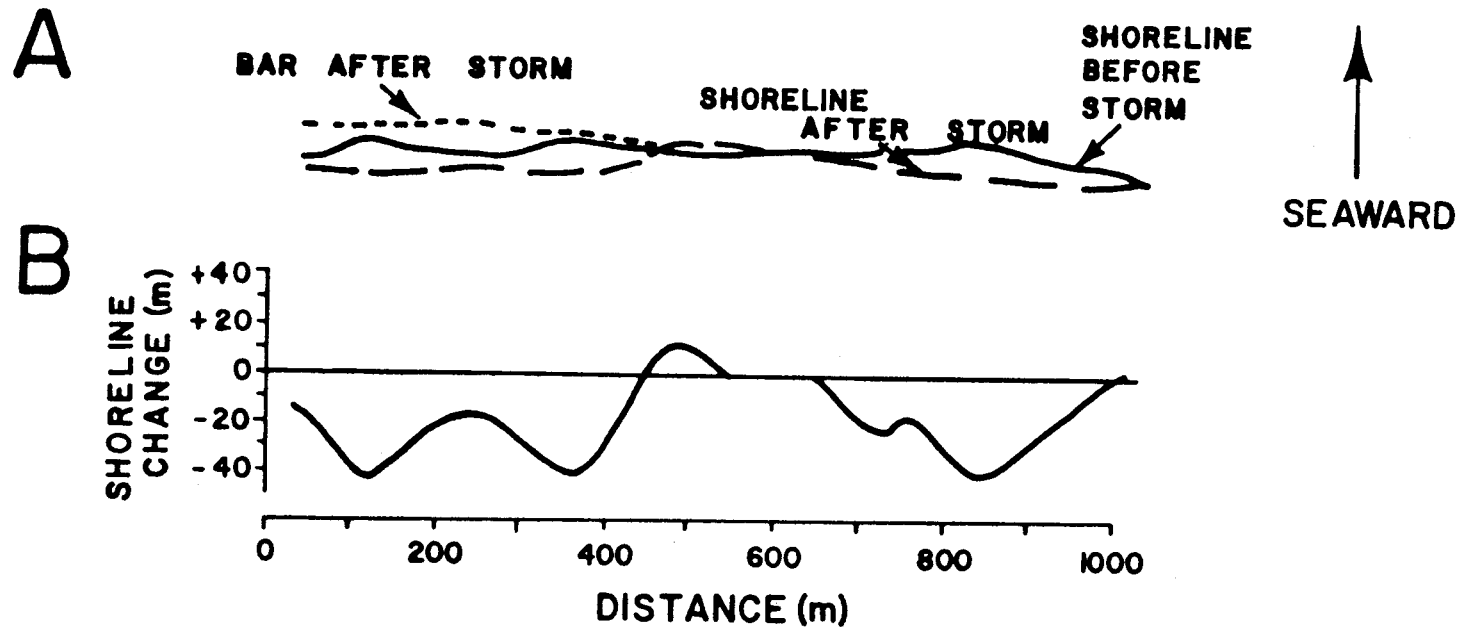


Fig. 7. An example of shoreline changes that resulted from the November, 1950 storm. Note the complex pattern and that the net change is erosion.

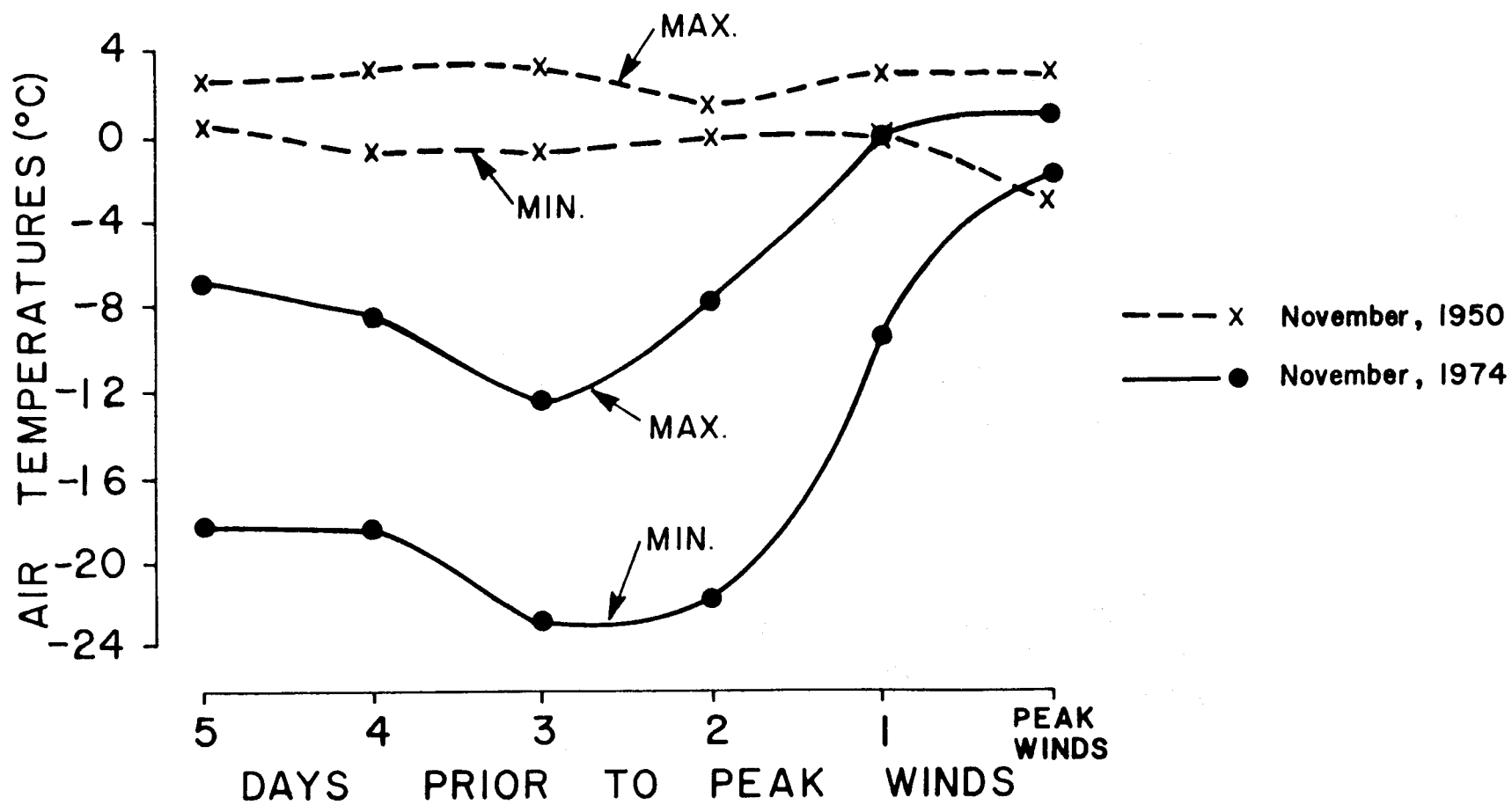


Fig. 8. Maximum and minimum daily air temperatures preceding the 1976 and 1950 storms.

how sufficient sediment would be displaced landward to account for the observed large scale changes. Furthermore, it appears that these potential ice effects were not capable of preventing modification of the landward parts of the barrier by storm surge and waves (Fig. 6).

Perhaps post-storm accretion occurred prior to the post-storm photography. Nearshore ice generally protects the beaches until mid-June. Thus, there was approximately a three month interval between the storm and the post storm photography during which the shoreline could prograde. However, it is questionable that there would be up to 50 m of accretion beyond the pre-storm shoreline as a result of normal rebuilding processes following the storm. Post-storm accretion cannot, however, be ruled out.

SEPTEMBER, 1977 STORM

A moderately severe storm was recorded at Nome in early September, 1977. A debris line at Nome harbor that resulted from this storm was approximately 2 m above MSL. Beach and nearshore profiles were measured in the Nome area during the third week of August and were remonitored during the second week of October. (Methods used in profiling are given in an appendix immediately following this report.) Comparisons of these profiles show the amount and character of coastal change that occurred during this period. Presumably, much of the change can be attributed to the September storm.

Two of these comparisons from Safety Lagoon are shown in Figs. 9 and 10. The locations of these profiles are shown in Fig. 11. The profile lines are parallel and 50 m apart, and are oriented approximately normal to the shoreline trend.

The comparison shown in Fig. 9 indicates that the net change was accretion. A bar was formed approximately 250 m seaward of the normal shoreline. In contrast, Fig. 10 shows that only 50 m away there was both substantial erosion and accretion. Again, a bar has formed. The sediment may have been supplied from erosional areas both seaward and shoreward of the bar. The foreshore slope has been decreased as would be expected during a storm, yet this decrease in slope was the result of accretion. Other profile comparisons in the area showed the same types of complex changes.

Obviously, nearshore changes in this environment are quite complex.

NON-STORM CHANGES IN THE NOME-SAFETY SOUND AREA

The wave climate of the northern Bering Sea is dominated by locally generated sea. Swell waves generated in the southern Bering Sea are greatly reduced in magnitude by refraction and frictional dissipation over the wide continental shelf before reaching the coast. Thus, in the absence of strong onshore winds, nearshore wave conditions can be quite low. This low wave energy probably accounts for the very small scale changes observed in profiles measured at the beginning and end of the 1976 field season, a period during which no storms occurred. (See Sallenger et. al., 1977)

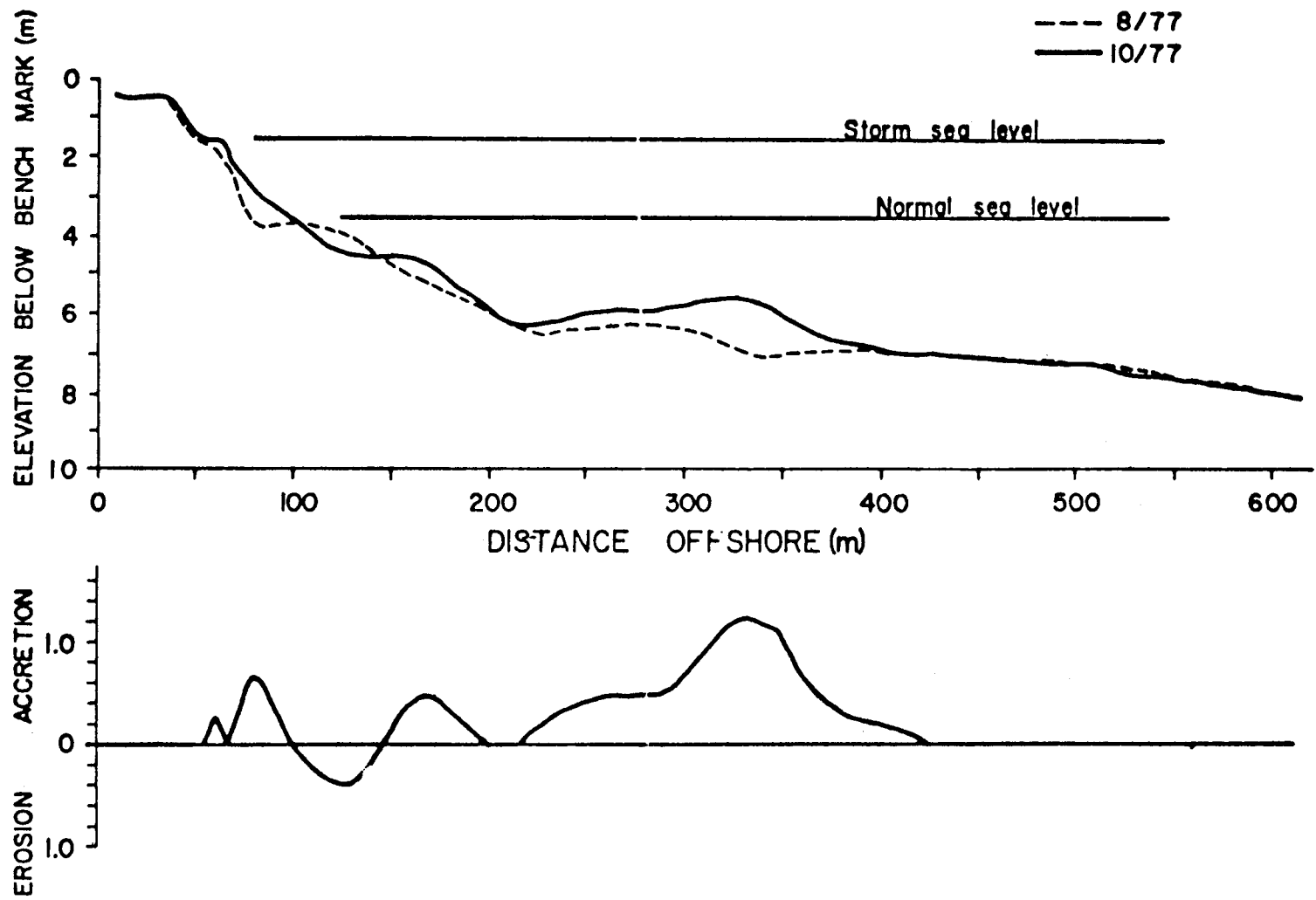


Fig. 9. Beach and nearshore profile comparison.

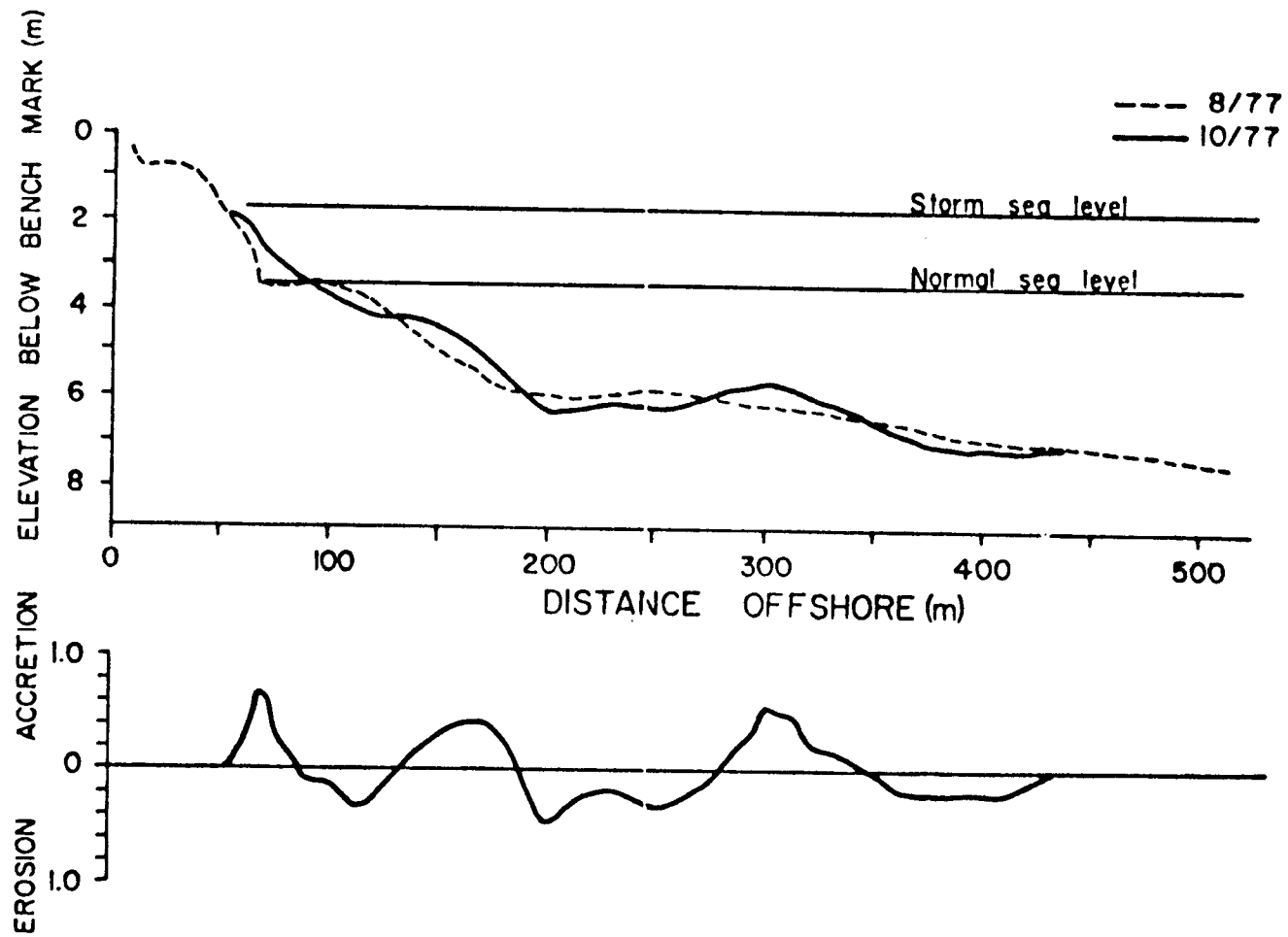


Fig. 10. Beach and nearshore profile comparison.

This is not to imply, however, that coastal change occurs only during severe storms. Vertical aerial photography is available for 6/23/51, 7/13/51 and 7/30/51 for a portion of Safety spit (Fig. 2). Giant cusps spaced 1.7 km were observed on the 6/23/51 photography. These cusps were apparently formed as result of the severe November, 1950 storm as has been discussed earlier. A comparison of shoreline positions in the vicinity of the cusp horns is shown in Fig. 12. Winds were dominantly from the southwest during the period covered by the photography. Locally generated waves caused a net transport to the east along the coast. In response to this transport, the cusps migrated along the coast at 5-6 m/day. This migration caused as much as 50 m accretion at a given location over a period of several weeks.

COMPARISON OF BEACH CHANGES IN THE NOME-SAFETY
LAGOON AREA TO OTHER BEACHES IN THE
NORTHERN BERING SEA

Beaches in the Nome-Safety Sound area are composed of sands and pebbly sands, whereas most other beaches along the northern Bering Sea coast are composed of coarser sediments (sandy gravels and coarser) (Sallenger, et. al., 1977). Examples of the coarse grained beaches are 1) the reach from the York Mountains (located in between Bering Strait and Port Clarence) to the entrance to Norton Sound, and 2) the east coast of Norton Sound.

The morphology of these coarse grained beaches is quite different than that of the finer grained beaches in the Nome-Safety Sound area

- 1) Giant cusps are generally absent so the response of these beaches can be considered a two dimensional problem relative to that of Nome-Safety Sound beaches.
- 2) Nearshore bars are generally absent.
- 3) These beaches are characterized by a very prominent storm berm (see Sallenger, et. al., 1977).

During the 1974 storm, these coarse beaches were built vertically to an elevation approximately equal to that of the storm-swash run-up. This was determined by comparing the elevations of debris lines, which approximate the elevation of storm run-up, with post-storm berm crest elevations (Fig.13). Under non-storm conditions, low wave heights (averaging approximately 30 cm) and the low tidal range (diurnal range is .5 m) essentially prevents the storm berms from being reworked. In fact, measurements of profiles located on coarse grained beaches at the beginning and end of the 1976 field season (a period during which no storms occurred) showed that there was essentially no change in the profiles, (Sallenger, et. al., 1977).

In the Port Clarence area, profiles were measured again during the 1977 field season. Comparative plots for two profiles are shown in Fig. 14 and Fig. 15. The locations of these profiles are shown in Fig. 16. (Methods used in measuring profiles are given in an appendix following this report) Most of the change in beach elevation is confined to the mid and lower foreshore (most of the change for the back-shore shown in B12 (Fig. 15) is spurious due to 1) the linear interpolation between data points and 2) the different densities of data

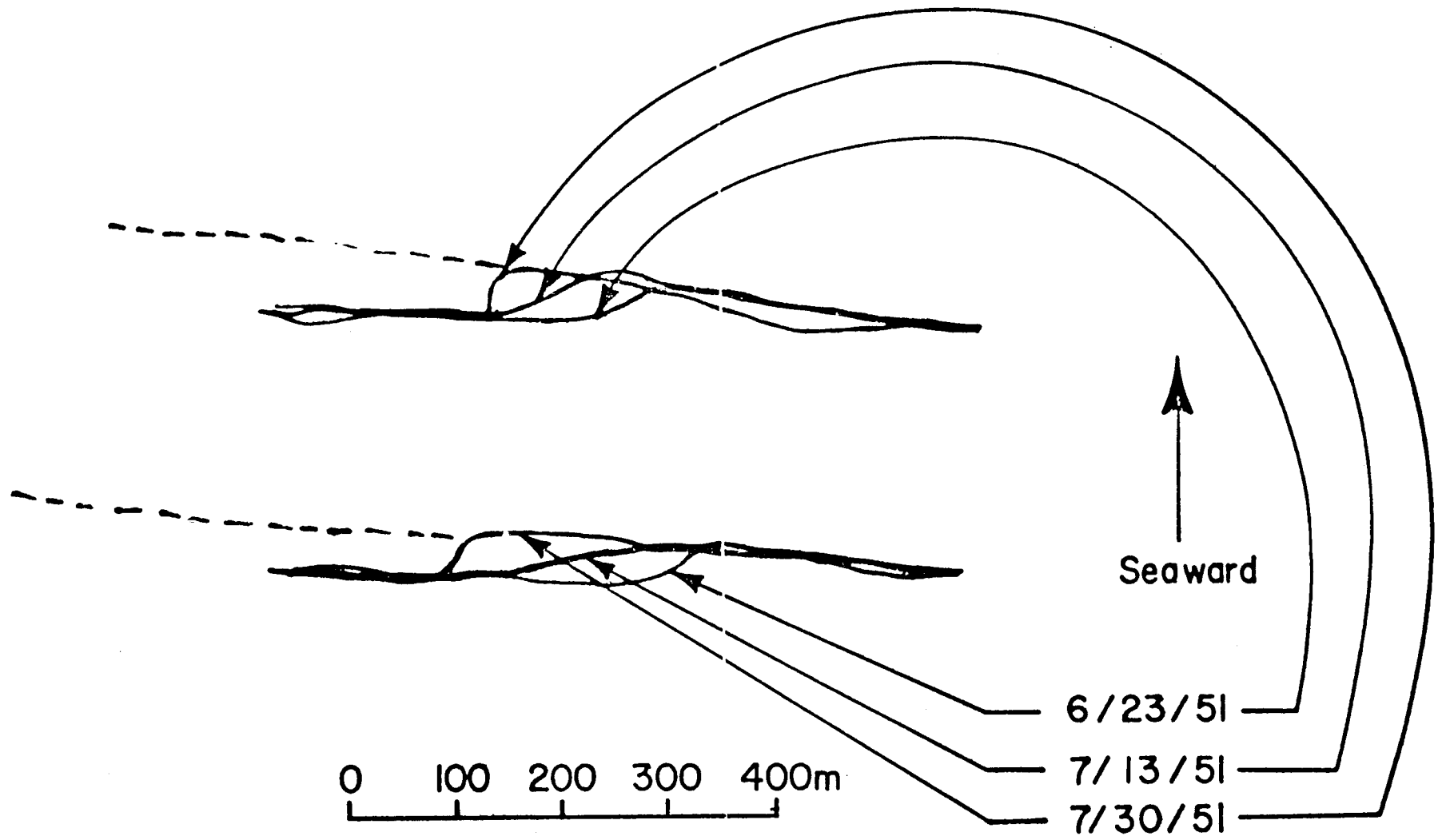


Fig. 12. Migration of giant cusps.

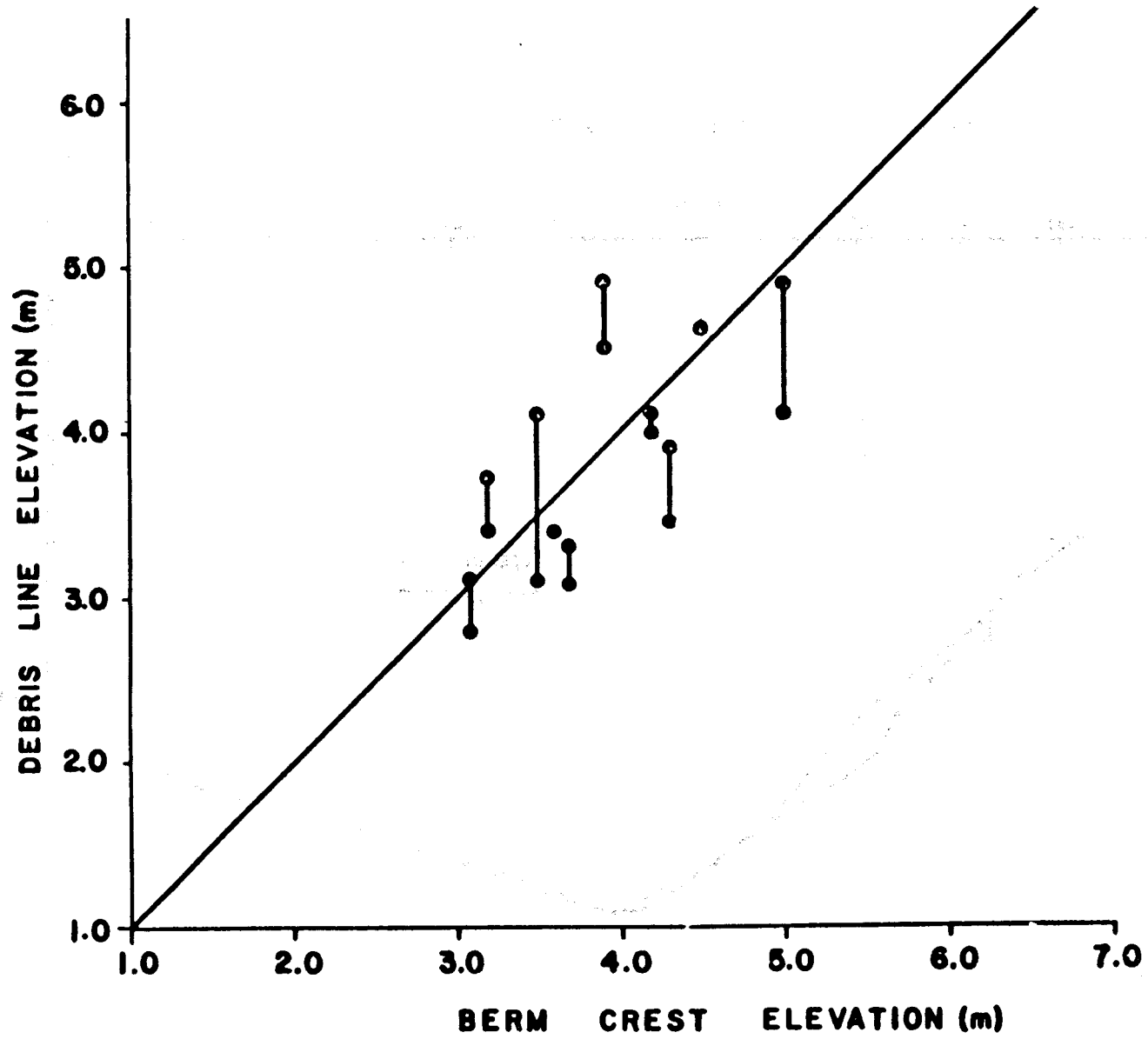


Fig. 13. Debris line elevations plotted versus berm crest elevations at the same locations.

401

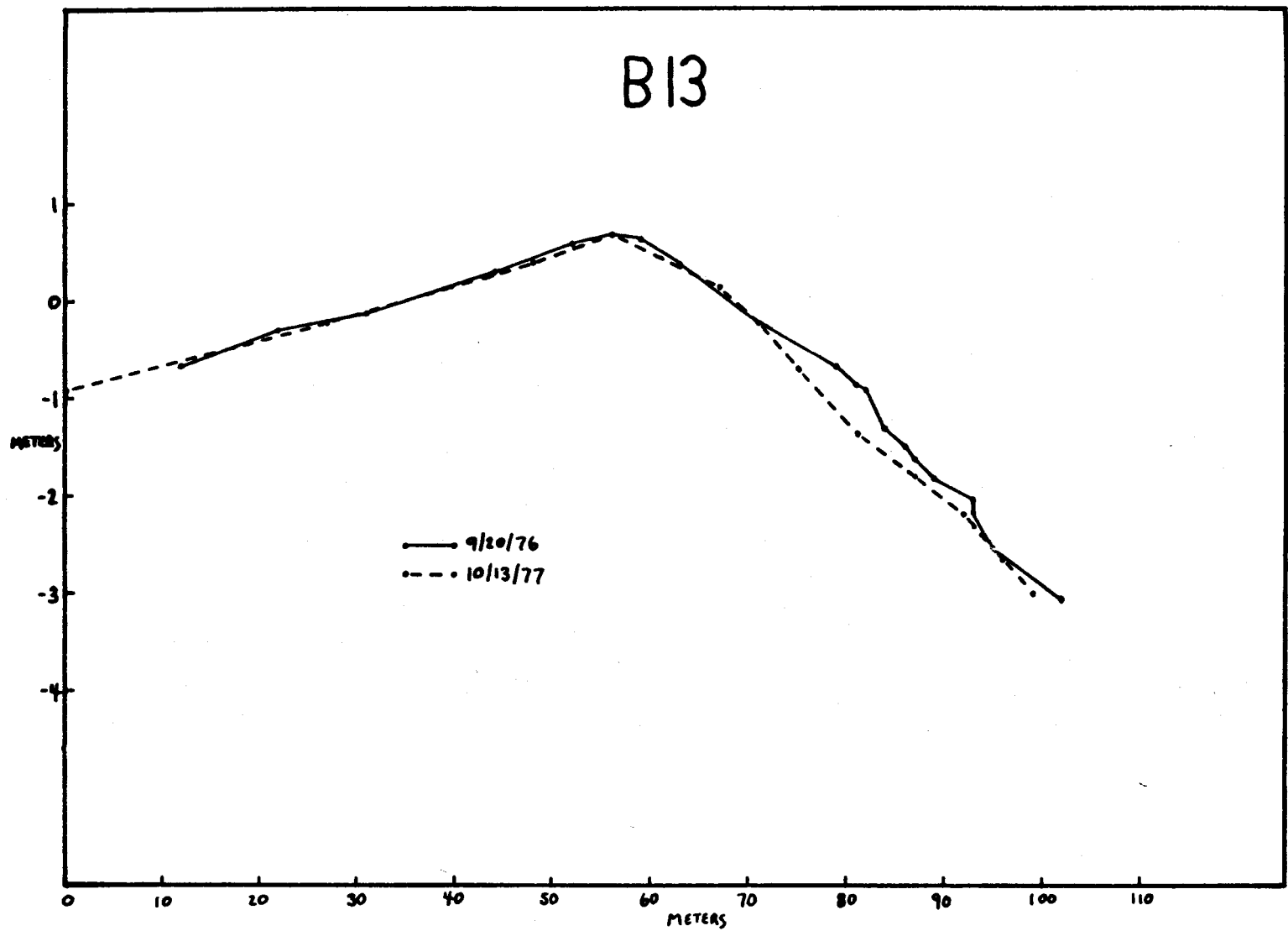


Fig. 14. Beach profile comparison from the Port Clarence area.

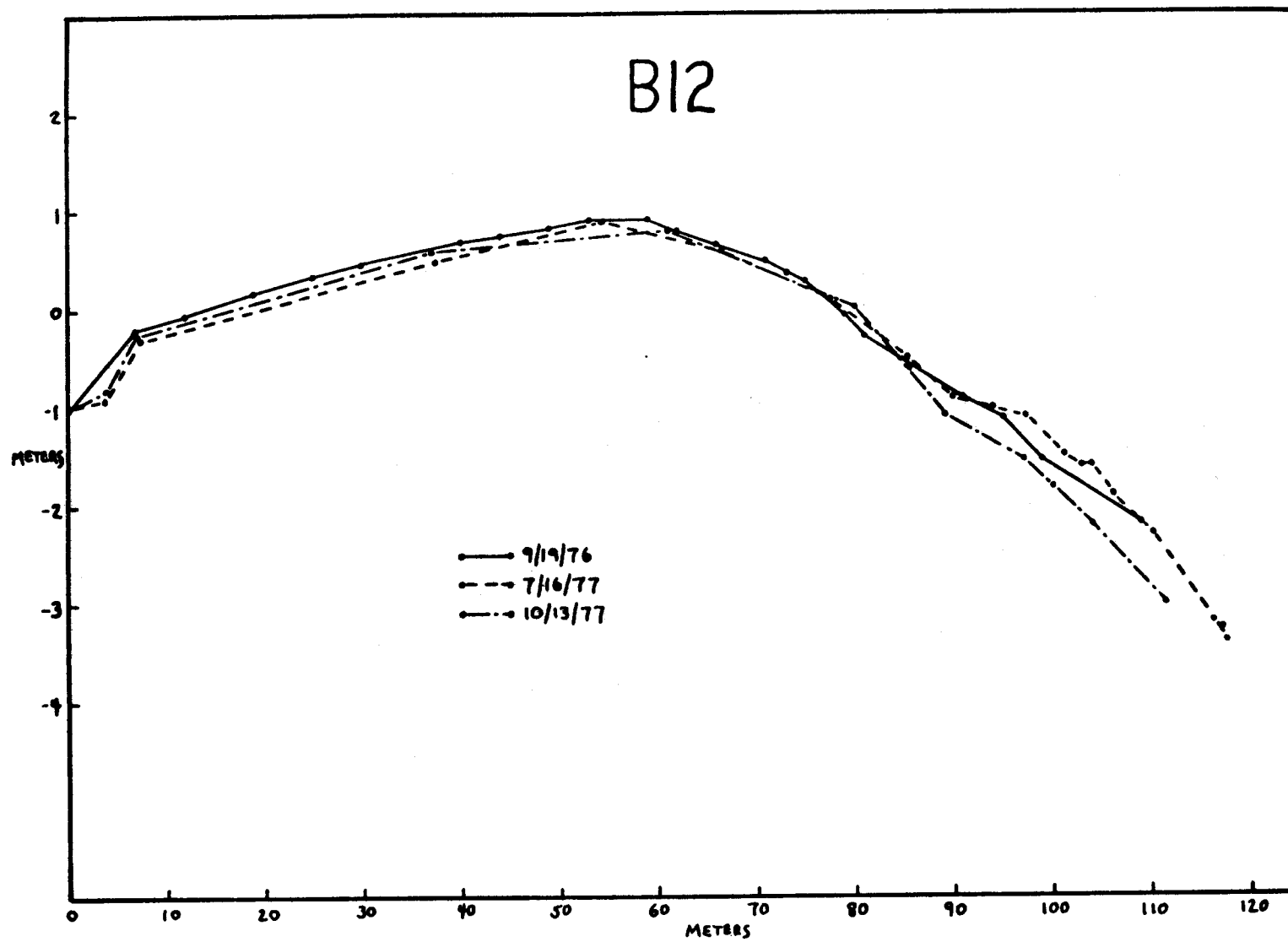
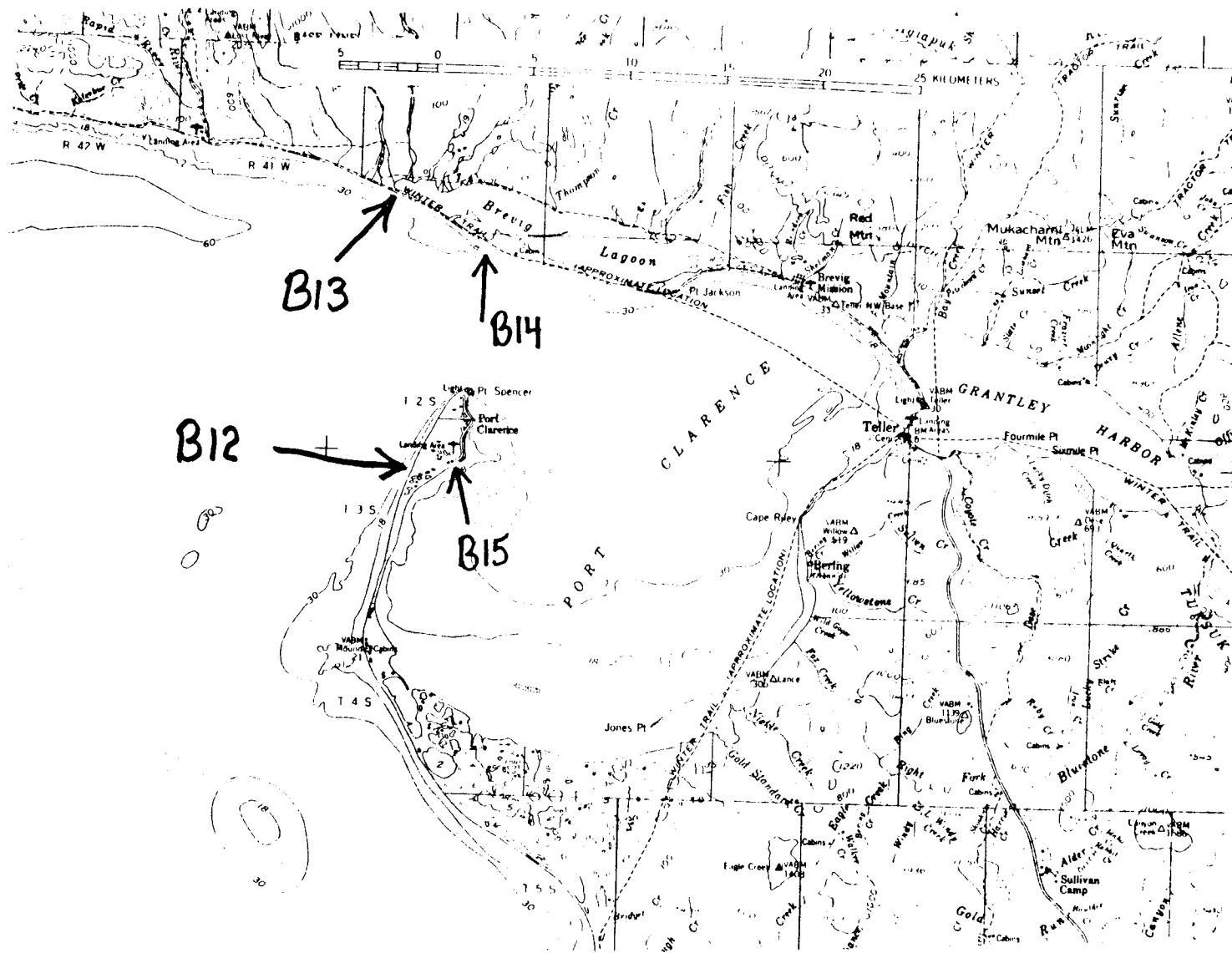


Fig. 15. Beach profile comparison from the Port Clarence area.



403

Fig. 16. Location of some of our Port Clarence area profiles. Locations of all profiles given in Sallenger, et. al., 1977.

on the backshore for different surveys). A relatively small amount of accretion is observed between the fall 1976 profile and the July 1977 profile (Fig. 15). This is probably a result of 1) ice foot formation during freeze-up of 1976 and 2) reworking by relatively small waves. Erosion of the foreshore is observed between the July and October 1977 profiles (Fig. 14 and Fig. 15). This is probably the result of the September, 1977 storm discussed in the previous section.

Large scale shoreline changes over short time periods, such as observed for the Nome-Safety Lagoon area, are not apparent for the coarse grained beaches (based on preliminary analyses of aerial photographs). This is due primarily to the absence of giant cusps along the fine grained beaches. The magnitude of long term change is, however, unknown.

COMPARISON OF BEACH CHANGES ALONG THE BRISTOL BAY COAST OF THE ALASKA PENINSULA TO THE NORTHERN BERING SEA COAST OF ALASKA

During our reconnaissance of the Bristol Bay coast of the Alaska Peninsula in September 1976, beach profiles were measured. Selected profiles south of Pt. Moller were remeasured during August, 1977.

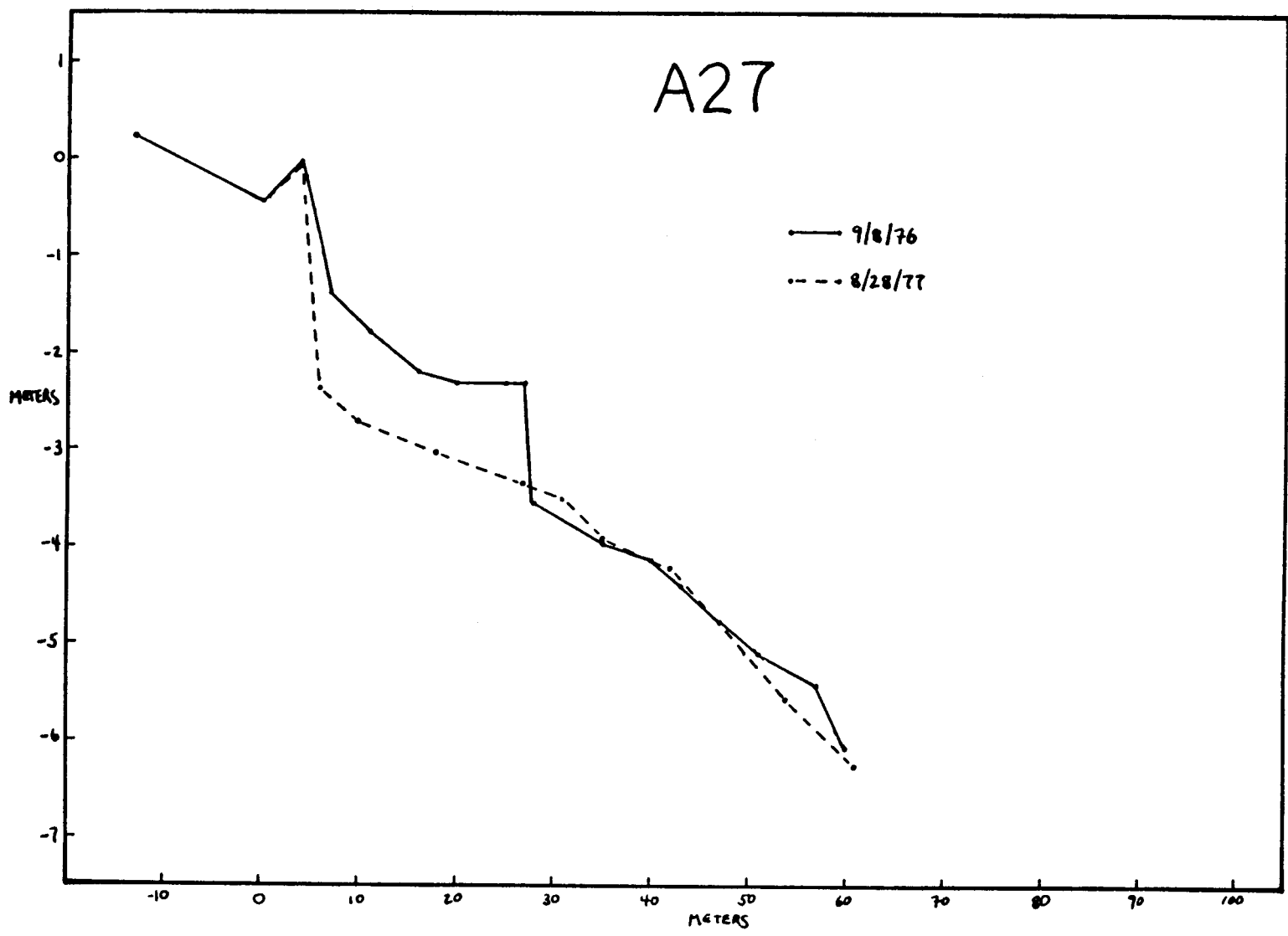
Similar to the Nome-Safety Sound area, beaches south of Port Moller are generally composed of sand sized material and giant cusps and nearshore bars are common (Sallenger, et. al., 1977). (Sediments, however, are volcanic rock fragments, whereas sediments in the Nome-Safety Sound area are primarily quartz and garnet sands)

In contrast to the coarse grained beaches of the northern Bering Sea, berm crests are between 1-2 m above mean higher high water (Sallenger, et. al., 1977). Wave energy appears to be higher along the southern portion of the Alaska Peninsula than Norton Sound (due to a greater effective fetch and deeper offshore bathymetry). Consequently, berms are probably reworked during spring tides, whereas berms of the coarse grained beaches in the northern Bering sea are reworked only during severe storms.

Examples of compared profiles are shown in Figs. 17-20. The locations of the profiles are shown in Fig. 21. Three of the profiles show erosion (Figs. 17, 19 and 20). The maximum amount of erosion is in excess of one meter. However one profile shows nearly 1 m of accretion. The same type of complex changes observed in the Nome-Safety Sound area (involving giant cusps) are probably also active in this environment.

In view of 1) the relatively high incident wave energy, 2) relatively frequent reworking of berms, and 3) analyses of compared profiles, beach changes appear to be much more dynamic along the southern Bristol Bay coast of the Alaska Peninsula than beach changes along the northern Bering Sea coast of Alaska. However, our data base is limited.

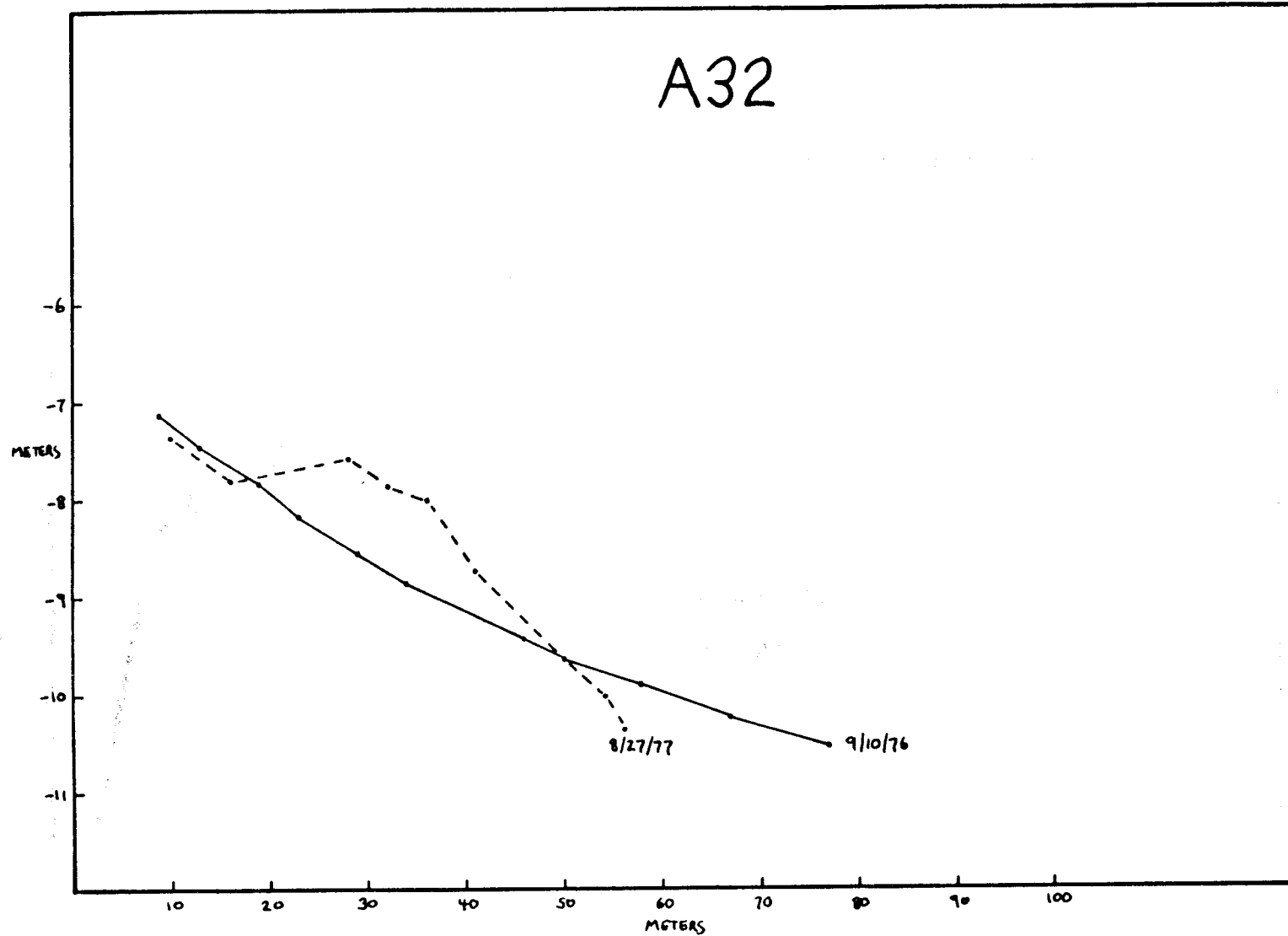
A27



405

Fig. 17. Beach profile comparison from the Alaska Peninsula.

A32



406

Fig. 18. Beach profile comparison from the Alaska Peninsula.

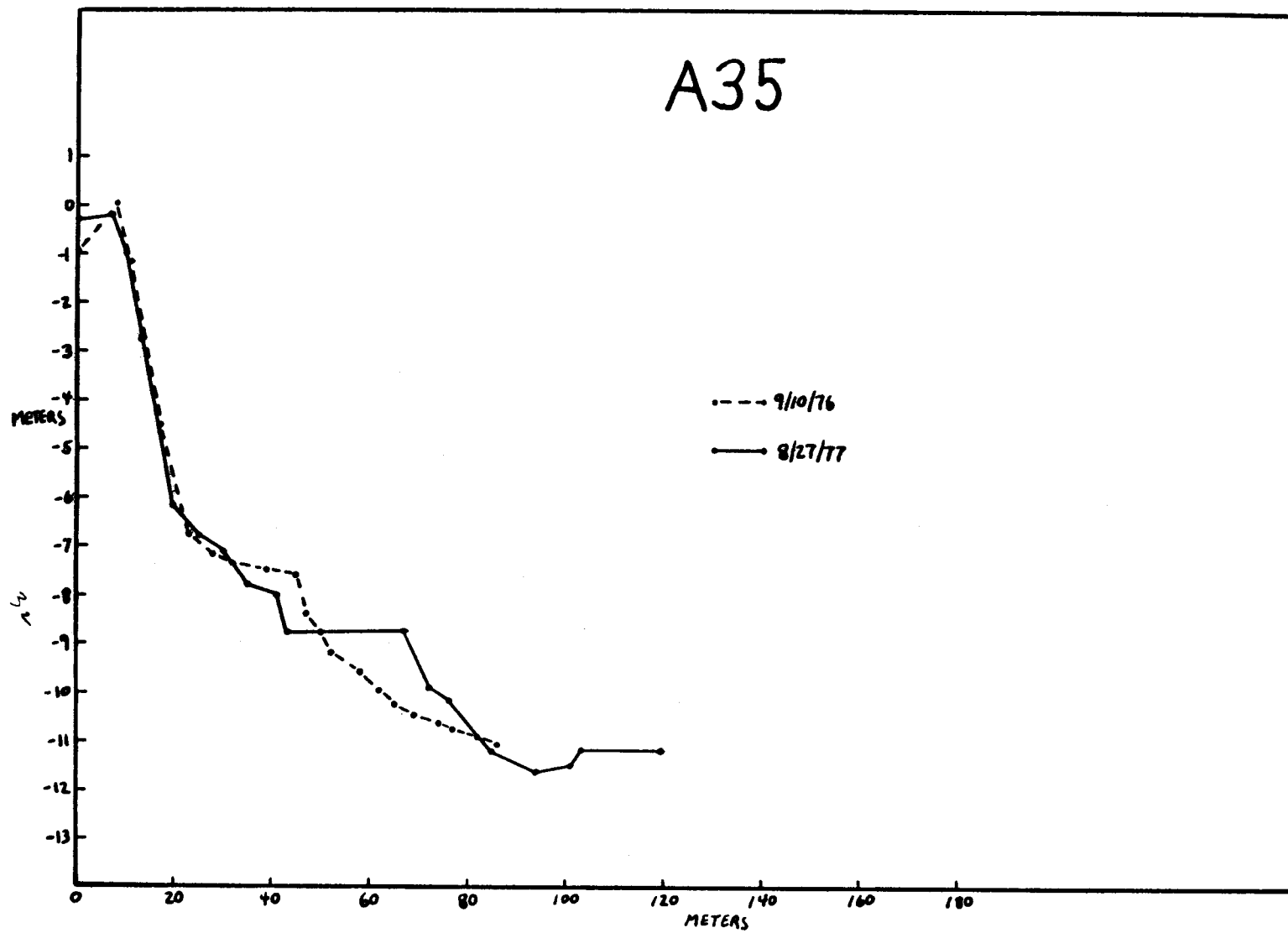


Fig. 19. Beach profile comparison from the Alaska Peninsula.

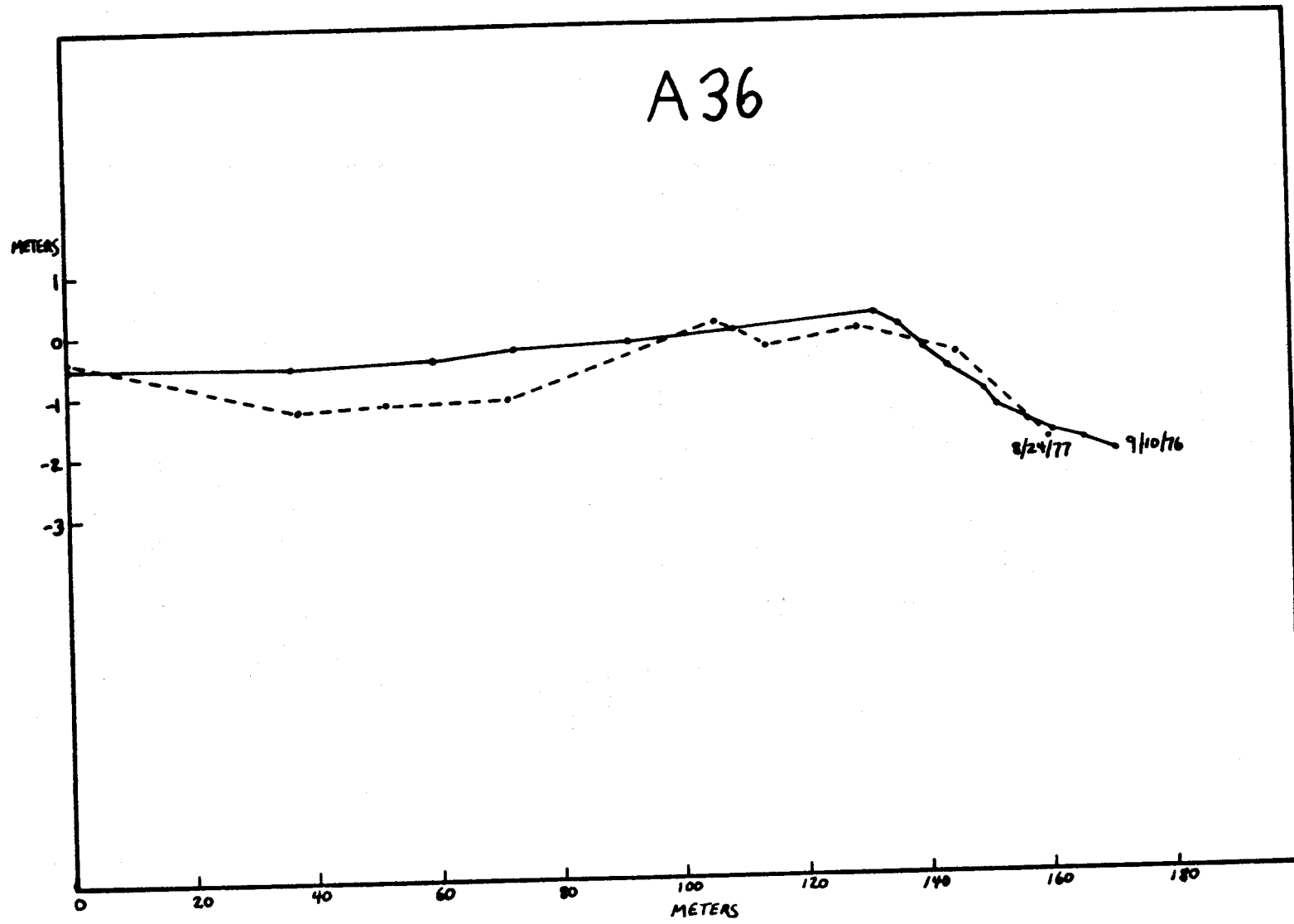


Fig. 20. Beach profile comparison from the Alaska Peninsula.

APPENDIX

METHODS USED IN MEASURING BEACH AND NEARSHORE PROFILES

Because of the acquisition of new and more accurate instrumentation for the 1977 field season, different techniques were used in the 1976 and 1977 field seasons for measuring beach and nearshore profiles. (Note: in some locations, e.g. Alaska Peninsula, only beach profiles were measured).

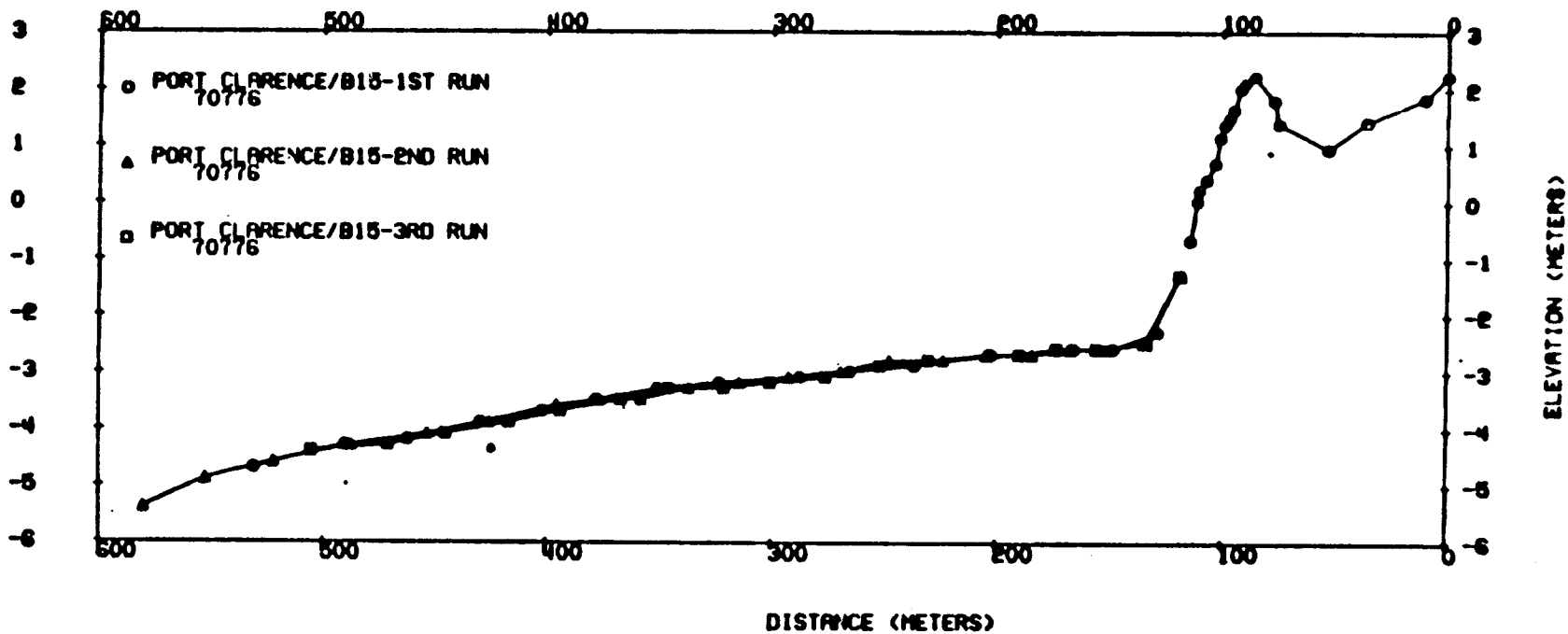
Methods used during 1976 field season

The onshore part of each profile was surveyed using a level and stadia rod. A permanent marker was driven into the ground at the shoreward end to each profile to permit reoccupation of the profiles on subsequent trips. Whenever possible, this stake was located behind the beach in the tundra to minimize the chance of loss. In all cases the stake height was measured so the profiles could be vertically referenced to a fixed point (the stake top). A second stake was placed seaward of the reference stake to serve as a backup marker and to keep the stadia rod carrier on the profile line. Horizontal distances were obtained using special range finding cross hairs in the level. With this technique horizontal resolution is at least ± 1 m at all distances. Elevations were read to 1 cm. The elevation of sea level with respect to the level was measured and used to tie together onshore and offshore parts of the profile.

After the onshore profile was completed, two navigation flags were also placed on the profile line. One flag was located at the level (usually at the berm crest), and the other was (generally) placed near the water line. A perpendicular to the profile line was shot from the level to locate a third flag down the beach. This last flag was situated on the order of 100 m from the level. Then the boat, with precision fathometer mounted amidships, slowly ran at constant speed toward the beach using the two navigation flags to stay on course. At intervals of a few to tens of seconds the angle to the third flag was measured with a sextant and corresponding mark made on the fathometer record. During the first trip (1976 field season) offshore profiles were run in triplicate; on the second trip multiple passes were made only on occasion. Sextant readings were made to the nearest 10 minutes; resolution, therefore, varies with position along the profile line. The fathometer record can be read to 0.1 m when the sea is perfectly calm. Superimposed wave motion adds uncertainty to this reading because it is not easy to completely remove the wave component from the fathometer record. A comparison of three beach and nearshore profiles run at the same location on the same day is shown in Fig. 22. It is clear the method produced reproducible results.

Methods used during 1977 field season

Nearshore portions of a profile were monitored with a precision fathometer mounted in a 5.8 m inflatable boat powered by twin 40 h. p. engines. The electro-optical distance measuring capacity of the Total



BEACH PROFILES - NORTON SOUND, ALASKA

Fig. 22. Beach Profile number B 15 (near Port Clarence, Alaska): 7 July 1976 profile. Offshore portion taken in triplicate to determine reliability of the profiling technique. Origin of the x-axis is the onshore reference stake. Origin of the z-axis is sea level. Gap indicates break between onshore and offshore parts of the profile.

Station (Model 3801A; Hewlett-Packard) was used for positioning the boat on profile lines. The Total Station measured the horizontal distance to the boat as the boat moved shoreward along a profile line. The instrument has a range of 1.6 km under average conditions and an accuracy of $\pm (4.9 \text{ mm} + 3 \text{ cm per } 300 \text{ m})$ for slope distance and $30''$ for zenith angle. The horizontal distance is computed internally from slope distance and zenith angle. The onshore portions of the profiles were measured using the vertical and horizontal distance capabilities of the Total Station.

B. WAVE CHARACTERISTICS DURING THE NOVEMBER 1974 STORM IN THE NORTHERN BERING SEA

Asbury H. Sallenger

Swell waves undergo extensive refraction and frictional dissipation as they propagate across the wide, shallow continental shelf of the northern Bering Sea. For example, eight-second swell waves, moving northeast from the southern Bering Sea, will begin to be influenced by the bottom nearly 300 nm south of Nome (Fig. 23). Thus, sea waves, those in the process of generation, dominate the coastal wave climate. During storms, these sea waves can apparently build to relatively large dimensions and the shallow shelf contributes to storm surges of large magnitude. For example, during a storm in November 1974, waves were reportedly 3 to 4 m at Nome and debris lines were left nearly 5 m above mean sea level in the Unalakleet area (see Sallenger, et al., 1977 and section V A of this report).

I have attempted to simulate the wave characteristics during the 1974 storm using the refraction program developed by Dobson (1967) and modified by Thrall (1973) to include the effects of continuous wave generation. To some extent, Thrall (1973) followed the computer logic outline by St. Denis (1969). I have modified the program further by incorporating the effects of frictional dissipation using the method of Bretschneider and Reid (1954).

The program is based on linear small-amplitude progressive wave theory. This leads to the following assumptions. 1) Wave amplitude is small relative to wave length. 2) Wave profile can be approximated by a sinusoid. 3) Flow is two-dimensional, irrotational, inviscid, incompressible, and fluid is of constant density. Other assumptions are: 1) bottom contours are smooth; 2) energy is not transmitted along wave crests; 3) water surface is a plane; 4) diffraction and reflection are negligible; 5) friction factor is equal to .01.

Inputs into the computer program were: 1) a 4.2 nm grid of depths of the northeastern Bering Sea, and 2) initial fetch length, wind velocity, and wind direction as determined from surface pressure weather charts. The initial fetch length was sufficiently small so that the waves would initially be in deep water (i.e., the ratio of water depth and wavelength was less than .5). The program propagates waves across the shelf to the shoreline in discrete increments incorporating the effects of refraction, shoaling, bottom friction, and wave generation.

Two conditions are presented: 1) southerly winds at 47 knots at 1800 BST on November 11, 1974 (interpolated from weather charts) and 2) south westerly winds (200°) at 57 knots at 0100 BST on November 12. As a first approximation, the increase in depth over the shelf due to storm surge was considered uniform. Two meters and three meters were used for condition 1 and 2, respectively. For each condition, waves were propagated over the maximum fetch length indicated on the respective surface pressure charts. This assumes that the fetch length and wind characteristics were fixed in time and space. Thus, results should provide the maximum wave heights that should result from an individual

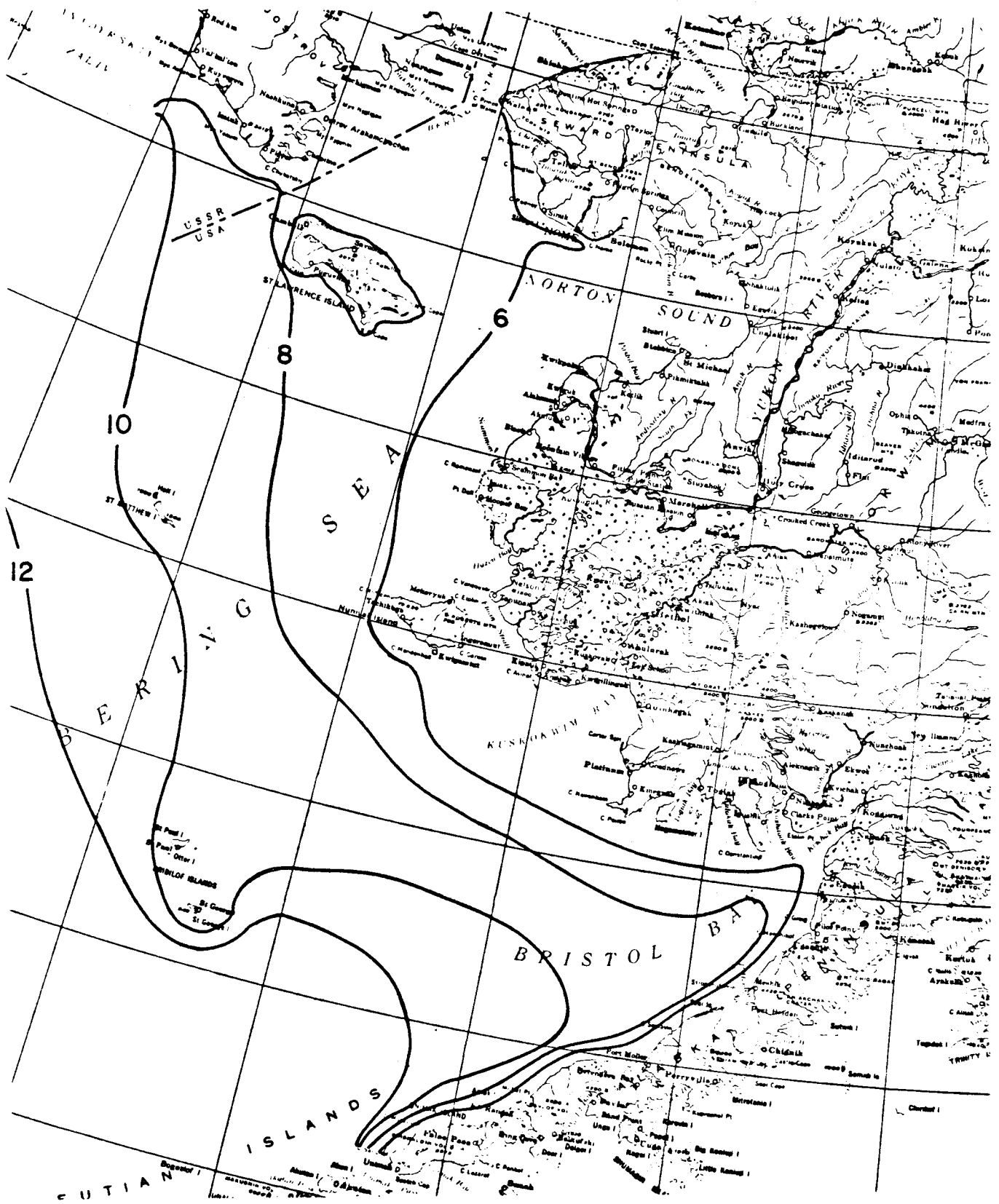


Fig. 23. Contours showing where waves of a given period will begin being influenced by the bottom (contours in seconds).

condition. One could change the wind velocity and direction in increments as the waves are propagated (that is, as the storm moves northward). This, in many cases, would decrease the wave height since the wind would no longer be blowing parallel to most orthogonals. As will be shown, this exercise did not appear to be warranted, since the resulting wave heights appeared to be lower than what was observed in nature even when using the maximum condition.

Plots of wave orthogonals (lines which are everywhere normal to wave crests) for the two conditions are shown in figures 24 and 26. An interesting feature of both these plots is the extensive convergence of orthogonals offshore of the Yukon Delta (see the areas where four adjacent orthogonals abruptly terminate). Here one would expect relatively large wave heights and confused seas which may pose hazards to navigation.

Wave heights along the shoreline for these two conditions are shown in figures 25 and 27. In figure 25 (wind 47 knots) wave heights reach a maximum of ≈ 2.5 m near the Bering Strait and then decrease to about one meter in the Nome area. For the higher winds (57 knots, fig. 27) wave heights in the Nome area were 2 m in height which, as expected, is substantially larger than those for condition 1, but is significantly lower than wave heights reported for Nome during the storm ($\approx 3-4$ m).

It is very difficult to obtain an accurate measurement of wave height from the shore by visual means alone. Thus, the difference in computed versus observed wave heights may not necessarily indicate a problem with the model. However, models such as the one used here have not, to my knowledge, been verified. This is particularly true, I believe, for the case of waves undergoing bottom influences and wave generation, simultaneously, over relatively long distances and shallow depths. Clearly, more field measurements are needed to substantiate these shallow water wave models. Changes may be required in both the basic equations and in the computer logic (i.e., how and in what sequence the equations are applied). We have obtained some wave measurements in the Nome area (see section V C of this report). Unfortunately, these were under relatively low energy conditions. There is a need for measurements both along the coast and in deep water under high wind (and well defined fetch) conditions.

'74' STORM • MAX FETCH. SURGE = 2.0M. 1800 BST. NOV 11. 1974

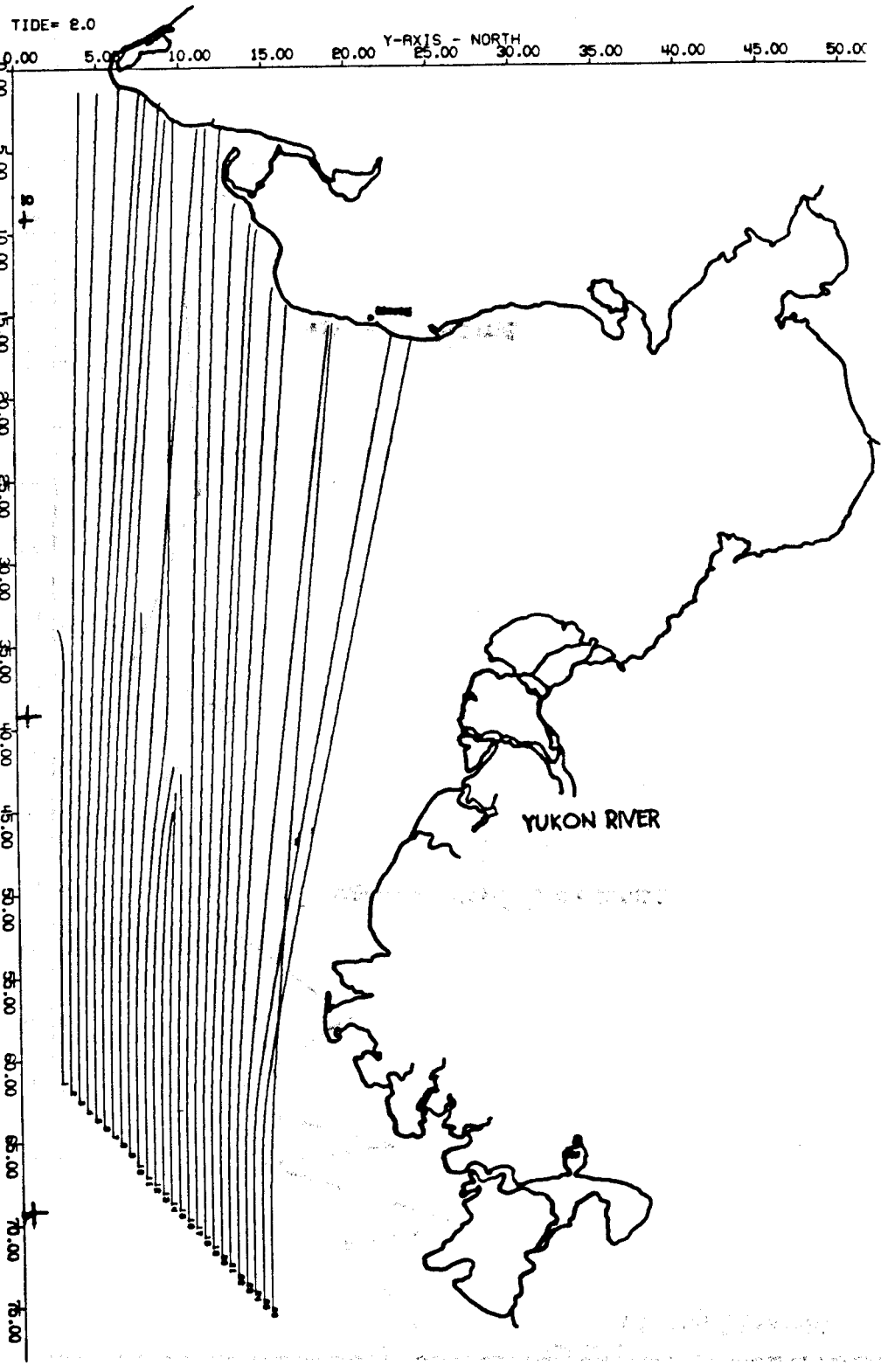


Fig. 24. Plot of wave orthogonals for condition 1 (see text).

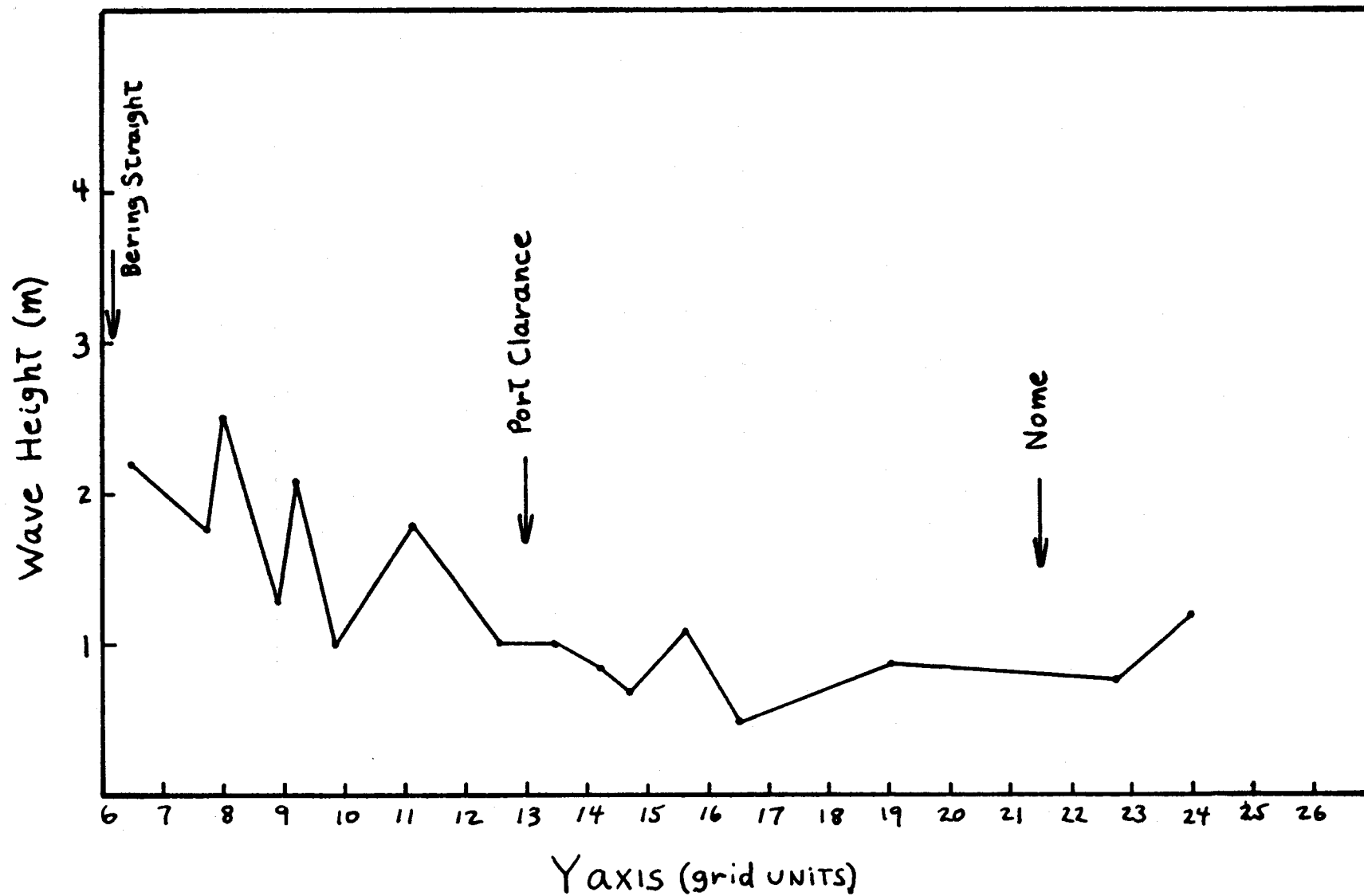


Fig. 25. Plot of computed wave heights along the shoreline for condition 1. Shoreline position is the intercept of the y-axis given here with the shoreline in fig. 24.

'74' STORM • MAX FETCH. SURGE = 3.0M. 0100 BST. NOV 12. 1974

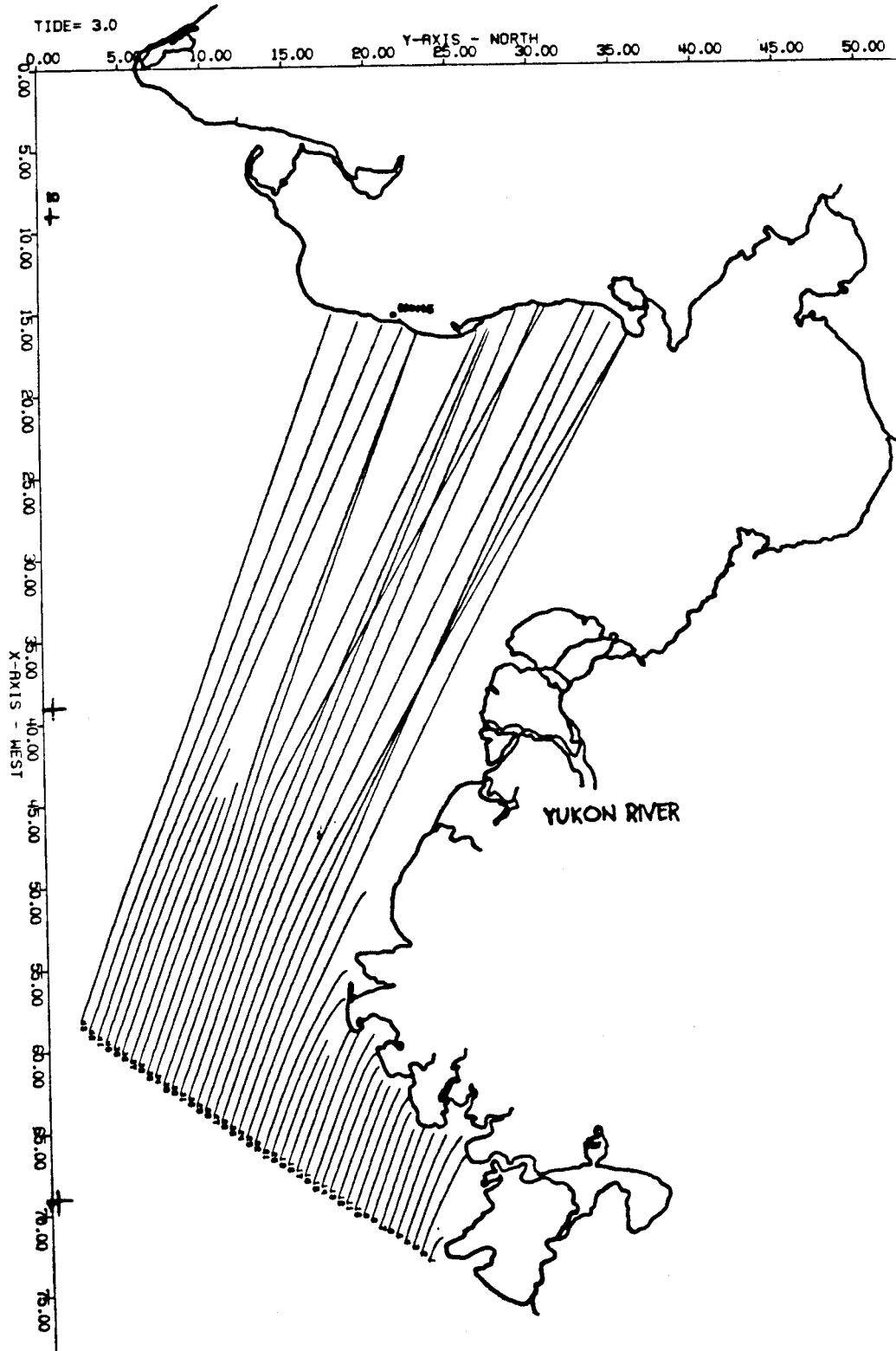


Fig. 26. Plot of wave orthogonals for condition 2 (see text).

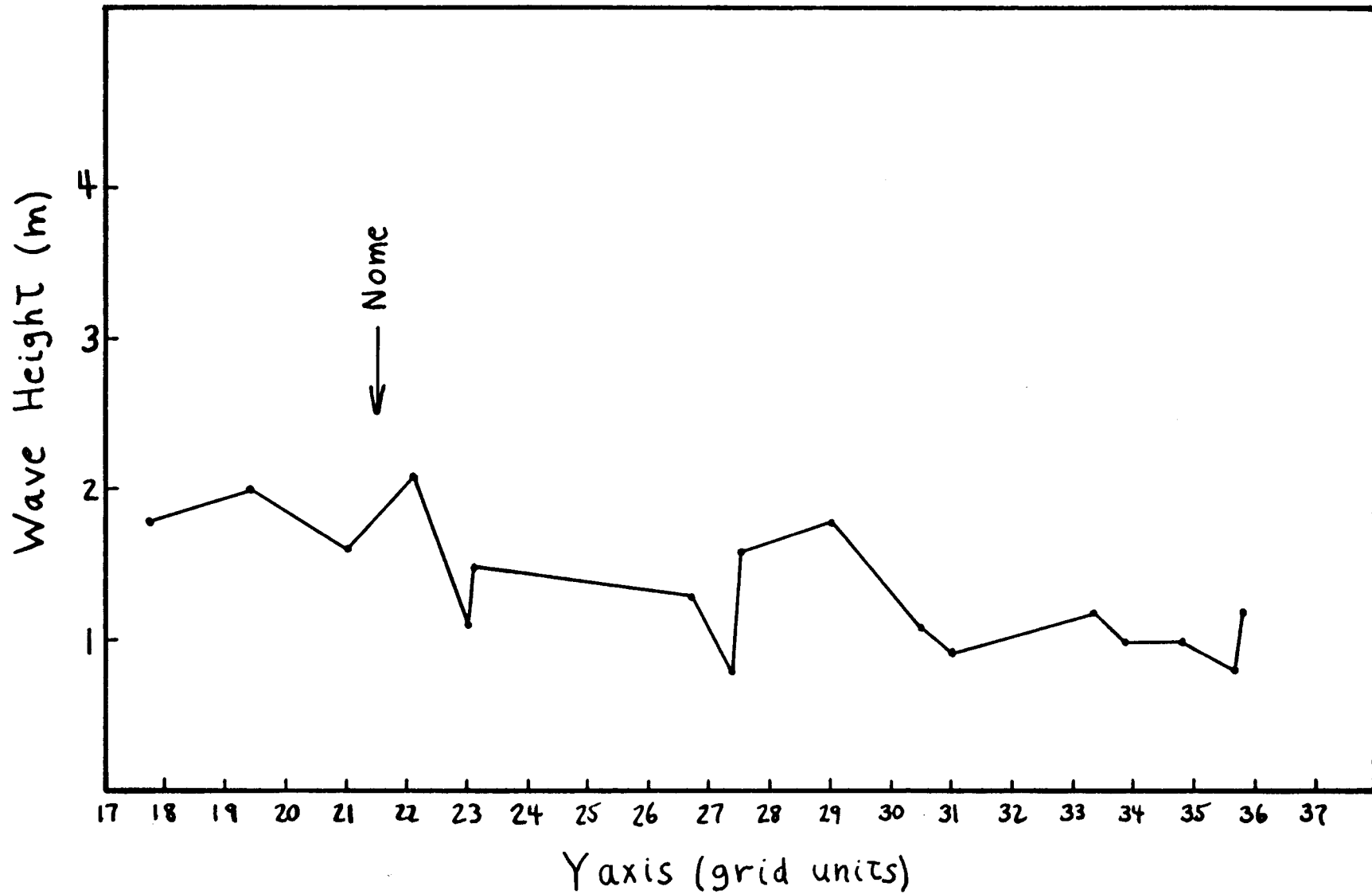


Fig. 27. Plot of computed wave heights along the shoreline for condition 2. Shoreline position is the intercept of the y-axis given here with the shoreline in fig. 26.

WAVE MEASUREMENTS AND ESTIMATES OF WAVE-GENERATED LITTORAL TRANSPORT;
NOME, ALASKA
John R. Dingler

Nome, Alaska is located on the coast of Norton Sound, a shallow arm of the northern Bering Sea (Figure 1). Because the area is remote, very little is known about local coastal processes. Recently, however, research in the region has increased dramatically in conjunction with the possibility of large-scale oil exploration and recovery. The purpose of this part of OCSFAP Research Unit 431 was to determine wave conditions and sediment transport rates in the nearshore during the ice-free months. It was hoped that the study period would include both fair and stormy weather, but only fair weather conditions were monitored the first field season (1977). The following season's field work was cancelled because of a paucity of funds.

The position of land forms around the Bering Sea (Figure 1) strongly suggests that most waves reaching the Nome area will be generated either locally or in the southern Bering Sea. Although waves could reach the area from the Pacific Ocean, the Aleutian Islands probably absorb most of that wave energy. The location of St. Lawrence and Nunivak Islands further restricts the amount of wave energy reaching Nome; only waves approaching from directions between 193° and 229° N will be able to enter Norton Sound.

Wave generation depends on three factors: wind speed, wind duration, and fetch. During the summer, measurements taken by the Corps of Engineers in Nome showed that wind speed was low and direction variable. This means that most locally generated waves will have short periods and small heights since fetch lengths are short except from the south.

During July and August, 1977, wave pressure measurements were made in 7 m of water near Nome in order to determine the littoral transport rate along the adjacent coastline (Figure 2). Data were collected from a four-sensor array and transmitted to a shore-based recording station using a Shelf and Shore (SAS) System (Lowe, et al., 1973). The SAS System operated every six hours, and a total of 796, 10 minute time series were recorded at four series per transmission (Table 1). A scan of the time series showed that the wave period was generally short and wave height low during the study period, but that occasional higher energy events occurred (Sallenger, et al., 1978).

Spectral analysis of 183 of the raw data records produced 420 wave trains (spectral peaks) for which wave period, height, and direction were calculated (Table 2). Peak wave periods ranged from 3.9 to 18 sec with a median of 6.7 sec. Wave heights ranged from 2 to 162 cm with a median of 16 cm. The total wave energy for each record, which was obtained by averaging the appropriate Fourier coefficients from the four sensors, ranged from 8 to 5500 cm^2 with a median of 130 cm^2 (Table 1).

Wave trains approached the study site from directions between 126° and 229° N (Figure 3). Waves of periods greater than 6 sec almost exclusively came from the window between the two islands (236 out of 259 wave trains), whereas shorter period waves came from a wider range of directions (only 63 out of 167 wave trains came from within the window). This wave pattern is reasonable, given the location of Nome and the summer wind patterns in the area. Locally generated waves, which come from a wide range of directions, are short in period: Longer period waves originate in the southern Bering Sea or, perhaps, in the Pacific Ocean.

The littoral transport rate, the rate at which sediment moves alongshore inside the surf zone is readily estimated from spectral wave parameters. The sediment transport rate, for reasons listed in Komar (1976, p. 206), is

expressed here as an immersed weight transport rate I_1 and is given by

$$I_1 = K(EN)_b \sin \alpha_b \cos \alpha_b. \quad (1)$$

In Equation 1, K is a dimensionless proportionality coefficient equal to 0.77, E is the wave energy, C_n is the wave group velocity, α is the angle between the wave crest and a line parallel to the shoreline, and b is a subscript that denotes breaking wave conditions. The equation

$$I_1 = (\rho_s - \rho)ga'S_1 \quad (2)$$

relates I_1 to the longshore volume transport rate of sand S_1 . In Equation 2, ρ_s is the sediment density, ρ is the fluid density, g is the acceleration of gravity, and a' is a correction factor for the pore space of the beach sand (taken as 0.6).

The computer, using wave parameters at the array, calculated I_1 for each of the 420 peak frequencies. The wave trains were not refracted to the breaker zone; in this situation, using wave parameters at the array does not change I_1 within experimental error. For the 420 wave trains, I_1 ranged from -7.5×10^8 to 7.2×10^7 dynes/sec with eastward transport occurring 78% of the time. The average sediment transport rate for the summer was 1.3×10^6 dynes/sec toward the east. Easterly transport is consistent with the transport direction determined from the coastal morphology that was observed by other members of this group.

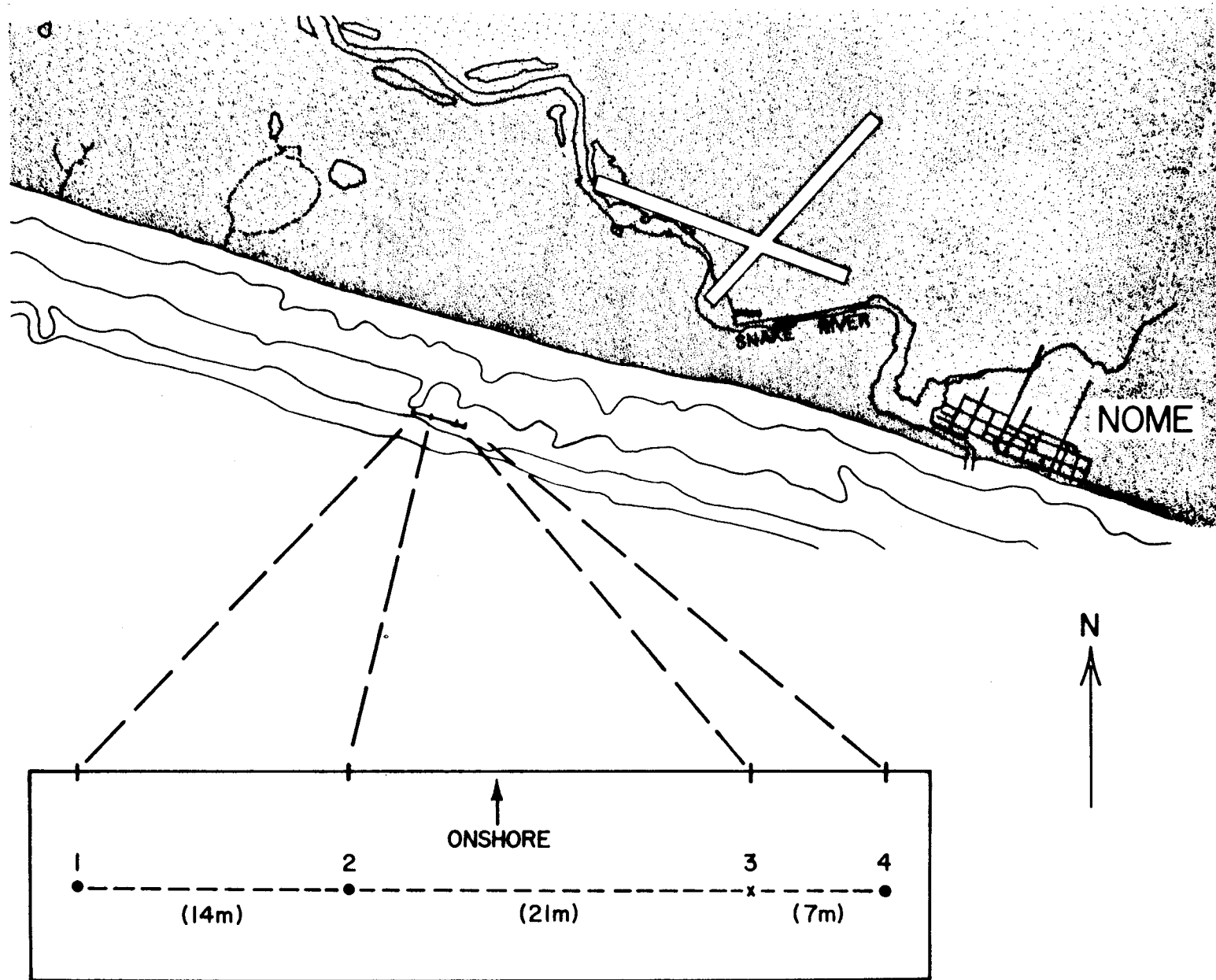


Figure 28. Wave array location relative to Nome, Alaska. Insert shows sensor locations with the "x" representing the spar location.

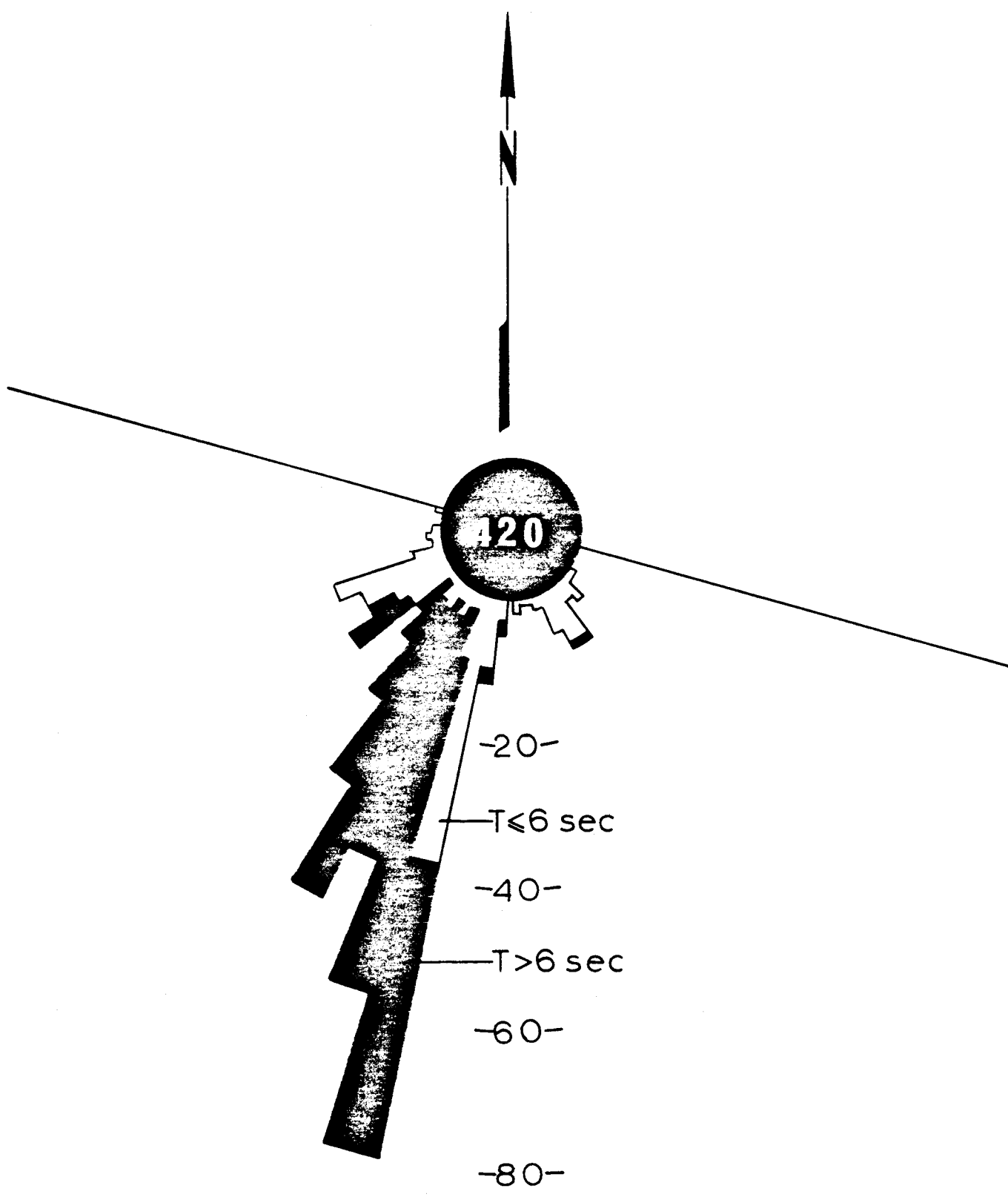


Figure 29. Rose diagram for wind directions as a function of period. Solid line at 106°N represents the array and shoreline orientation.

TABLE 1

Summary information for the 200 transmissions during July, August and September, 1977. Empty spaces in the last two columns mean that wave spectra were not run.

Column headers:

= Experiment number

D = Date

T = Time (Bering Standard Time)

h = Mean water depth (cm)

E_T = Average total energy for the four sensors (cm^2).

NO.	DATE	TIME (BST)	h (cm)	E_{T2} (cm^2)
N001	9JUL77	1630	716	15
N002	9JUL77	2230	700	16
N003	10JUL77	0430	716	26
N004	10JUL77	1030	674	30
N005	10JUL77	1630	707	42
N006	10JUL77	2230	707	87
N007	11JUL77	0430	712	55
N008	11JUL77	1030	691	27
N009	11JUL77	1630	719	22
N010	16JUL77	0040		
N011	16JUL77	0640	707	1610
N012	16JUL77	1240	696	3416
N013	16JUL77	1840	713	118
N014	17JUL77	0040	731	149
N015	17JUL77	0640	701	103
N016	17JUL77	1240	694	78
N017	17JUL77	1840	705	174
N018	18JUL77	0040	729	138
N019	18JUL77	0640	698	76
N020	18JUL77	1240		
N021	18JUL77	1840		
N022	19JUL77	0040	741	251
N023	19JUL77	0640	696	44
N024	19JUL77	1240		
N025	19JUL77	1840	698	4260
N026	20JUL77	0040	737	235
N027	20JUL77	0640	703	158
N028	20JUL77	1240		
N029	20JUL77	1840	716	130
N030	21JUL77	0040	754	149
N031	21JUL77	0640		
N032	21JUL77	1240	712	47
N033	21JUL77	1840	699	35
N034	22JUL77	0040	743	37
N035	22JUL77	0640	706	1028
N036	22JUL77	1240	708	8
N037	22JUL77	1840	700	9
N038	23JUL77	0040	726	12
N039	23JUL77	0640	694	16
N040	23JUL77	1240	692	637
N041	23JUL77	1840	691	970
N042	24JUL77	0040	707	80
N043	24JUL77	0640	681	1461
N044	24JUL77	1240	688	129
N045	24JUL77	1840	692	1633
N046	25JUL77	0040		
N047	25JUL77	0640		
N048	25JUL77	1240	692	1114
N049	25JUL77	1840	721	195
N050	26JUL77	0040	712	111
N051	26JUL77	0640	711	83

NO.	DATE	TIME (BST)	h (cm)	E_{T^2} (cm^2)
N052	26JUL77	1240	693	130
N053	26JUL77	1840	735	311
N054	27JUL77	0040	706	290
N055	27JUL77	0640	711	92
N056	27JUL77	1240	677	65
N057	27JUL77	1840	723	432
N058	28JUL77	0040	687	41
N059	28JUL77	0640	693	45
N060	28JUL77	1240	667	92
N061	28JUL77	1840	714	260
N062	29JUL77	0040	696	239
N063	29JUL77	0640	696	173
N064	29JUL77	1240	673	130
N065	29JUL77	1840	715	1225
N066	30JUL77	0040	717	2846
N067	30JUL77	0640	699	130
N068	30JUL77	1240	683	1258
N069	30JUL77	1840	710	611
N070	31JUL77	0040	720	35
N071	31JUL77	0640	698	808
N072	31JUL77	1240	695	73
N073	31JUL77	1840	705	45
N074	1AUG77	0040	730	3987
N075	1AUG77	0640	692	824
N076	1AUG77	1240		
N077	1AUG77	1840	683	540
N078	2AUG77	0040		
N079	2AUG77	0640	679	1208
N080	2AUG77	1240	702	1033
N081	2AUG77	1840	689	2194
N082	3AUG77	0040	746	1389
N083	3AUG77	0640	705	865
N084	3AUG77	1240	730	66
N085	3AUG77	1840	705	50
N086	4AUG77	0040	744	99
N087	4AUG77	0640	697	134
N088	4AUG77	1240	702	184
N089	4AUG77	1840	672	661
N090	5AUG77	0040	714	1208
N091	5AUG77	0640	679	1397
N092	5AUG77	1240	697	1824
N093	5AUG77	1840	683	2204
N094	6AUG77	0040	704	3228
N095	6AUG77	0640	684	2801
N096	6AUG77	1240	683	4782
N097	6AUG77	1840	701	1723
N098	7AUG77	0040	708	2988
N099	7AUG77	0640	698	1316
N100	7AUG77	1240	700	1133
N101	7AUG77	1840	732	3022
N102	8AUG77	0040	728	1928

NO.	DATE	TIME (BST)	h (cm)	E_{T2} (cm^2)
N103	8AUG77	0640	733	2315
N104	8AUG77	1240	732	855
N105	8AUG77	1840	763	189
N106	9AUG77	0040	740	28
N107	9AUG77	0640	725	166
N108	9AUG77	1240	700	93
N109	9AUG77	1840	716	2510
N110	10AUG77	0040	702	3022
N111	10AUG77	0640	699	1928
N112	10AUG77	1240	693	2315
N113	10AUG77	1840	733	855
N114	11AUG77	0040	718	189
N115	11AUG77	0640	709	245
N116	11AUG77	1240	691	916
N117	11AUG77	1840	722	267
N118	12AUG77	0040	711	1145
N119	12AUG77	0640	687	1208
N120	12AUG77	1240	683	1761
N121	12AUG77	1840	716	255
N122	13AUG77	0040	719	144
N123	13AUG77	0640	701	94
N124	13AUG77	1240	697	125
N125	13AUG77	1840	714	99
N126	14AUG77	0040	725	52
N127	14AUG77	0640	702	77
N128	14AUG77	1240	703	94
N129	14AUG77	1840	712	42
N130	15AUG77	0040	705	735
N131	15AUG77	0640		
N132	15AUG77	1240		
N133	15AUG77	1840		
N134	16AUG77	0040	658	275
N135	16AUG77	0640	677	884
N136	16AUG77	1240	677	267
N137	16AUG77	1840	674	766
N138	17AUG77	0040	703	843
N139	17AUG77	0640	670	2058
N140	17AUG77	1240	685	1140
N141	17AUG77	1840	694	2454
N142	18AUG77	0040	740	2061
N143	18AUG77	0640		
N144	18AUG77	1240		
N145	18AUG77	1840		
N146	19AUG77	0040	691	1947
N147	19AUG77	0640	651	5486
N148	19AUG77	1240	682	422
N149	19AUG77	1840	662	488
N150	20AUG77	0040	712	306
N151	20AUG77	0640	690	548
N152	20AUG77	1240	724	57
N153	20AUG77	1840	704	57

NO.	DATE	TIME (BST)	h (cm)	E_{T2} (cm^{-2})
N154	21AUG77	0040	717	22
N155	21AUG77	0640	680	11
N156	21AUG77	1240	699	28
N157	21AUG77	1840	701	1420
N158	22AUG77	0040	709	10
N159	22AUG77	0640	687	444
N160	22AUG77	1240	710	25
N161	22AUG77	1840	718	73
N162	23AUG77	0040	722	442
N163	23AUG77	0640	709	47
N164	23AUG77	1240	710	1086
N165	23AUG77	1840	736	120
N166	24AUG77	0040	714	26
N167	24AUG77	0640	712	21
N168	24AUG77	1240	704	16
N169	24AUG77	1840	733	25
N170	25AUG77	0040	704	18
N171	25AUG77	0640	702	33
N172	25AUG77	1240	697	193
N173	25AUG77	1840	743	53
N174	26AUG77	0040	713	36
N175	26AUG77	0640	723	23
N176	26AUG77	1240	699	80
N177	26AUG77	1840	746	22
N178	27AUG77	0040	723	24
N179	27AUG77	0640	728	31
N180	27AUG77	1240	701	18
N181	27AUG77	1840	735	15
N182	28AUG77	0040	724	14
N183	28AUG77	0640	708	105
N184	28AUG77	1240	686	210
N185	28AUG77	1840		
N186	29AUG77	0040		
N187	29AUG77	0640	687	199
N188	29AUG77	1240	678	82
N189	29AUG77	1840	691	82
N190	30AUG77	0040	715	56
N191	30AUG77	0640	690	112
N192	30AUG77	1240	692	60
N193	30AUG77	1840	685	67
N194	31AUG77	0040	721	78
N195	31AUG77	0640	690	71
N196	31AUG77	1240	707	56
N197	31AUG77	1840	693	34
N198	1SEPT77	0040	737	39
N199	1SEPT77	0640	696	24
N200	1SEPT77	1240	723	20

TABLE 2

Spectral parameters for the 420 wave trains. The frequencies corresponding with the listed frequency bands are given in Table 3.

Column headers:

EXP = The experiment number (see Table 1)

Bs = The frequency band on the low frequency side of a peak.

Be = The frequency band on the high frequency side of a peak.

Bp = The peak frequency.

T = The peak period (sec).

ANGLE = The approach angle ($^{\circ}$ N).

H = The rms waveheight for the peak frequency (cm).

H' = The rms wave height for the whole peak (cm)

I_l = The littoral sediment transport rate (dynes/sec).

EXP	Bs	Be	Bp	T (sec)	ANGLE (deg)	H (cm)	H' (cm)	I1 (dyn/sec)
N001	7	13	12	5.5	210	4.1	7.4	0.103e+07
N001	13	18	14	4.7	244	3.7	7.5	0.623e+06
N001	3	7	5	14.0	211	2.3	3.5	0.227e+07
N002	8	15	11	6.1	207	4.9	8.9	0.137e+07
N002	15	18	17	3.9	254	3.5	5.6	0.336e+06
N002	3	8	7	9.8	207	2.3	4.0	0.670e+06
N003	11	18	12	5.5	201	5.8	11.5	0.108e+07
N003	8	11	10	6.7	227	5.0	7.5	0.315e+07
N003	4	8	7	9.8	219	3.6	5.4	0.336e+07
N004	4	12	8	8.5	229	8.1	13.9	0.139e+08
N004	12	18	13	5.1	216	3.5	7.0	0.372e+06
N005	5	12	8	8.5	223	9.3	16.5	0.226e+08
N005	12	18	14	4.7	235	3.1	6.8	0.498e+06
N006	5	13	8	8.5	219	9.2	16.9	0.197e+08
N007	4	15	9	7.5	224	9.3	17.2	0.146e+08
N008	4	10	9	7.5	218	5.8	9.5	0.569e+07
N008	10	13	11	6.1	223	5.5	8.4	0.257e+07
N008	16	18	17	3.9	204	3.2	5.0	0.108e+06
N008	13	16	15	4.4	233	3.1	5.8	0.278e+06
N009	6	18	10	6.7	219	6.2	12.6	0.487e+07
N009	4	6	5	14.0	213	2.2	2.7	0.228e+07
N011	2	10	9	7.5	198	19.9	49.1	0.127e+08
N012	10	18	16	4.1	196	65.8	150.3	-0.521e+07
N012	4	10	7	9.8	197	31.0	64.8	0.843e+07
N013	5	12	9	7.5	235	9.8	19.3	0.181e+08
N013	12	18	13	5.1	253	9.0	23.0	0.560e+07
N014	11	18	15	4.4	235	14.3	29.1	0.197e+07
N014	4	11	9	7.5	209	10.5	18.8	0.173e+08
N015	16	18	17	3.9	245	10.5	16.8	-0.104e+05
N015	14	16	15	4.4	237	9.7	14.3	0.211e+07
N015	4	12	10	6.7	234	9.0	17.9	0.856e+07
N015	12	14	13	5.1	192	7.8	11.9	0.210e+07
N016	4	11	9	7.5	236	9.4	16.2	0.170e+08
N016	11	18	13	5.1	249	7.9	19.3	0.402e+07
N017	15	18	16	4.1	286	14.7	24.9	0.299e+07
N017	10	15	14	4.7	263	14.0	26.8	0.841e+07
N017	8	10	9	7.5	221	8.2	10.6	0.127e+08
N017	3	8	7	9.8	210	4.2	6.9	0.254e+07
N018	5	12	11	6.1	235	14.1	22.0	0.257e+08
N018	12	18	14	4.7	242	13.2	26.7	0.103e+08
N019	14	18	16	4.1	252	9.7	17.7	0.254e+07
N019	12	14	13	5.1	240	8.0	11.7	0.426e+07
N019	5	12	9	7.5	211	6.6	14.3	0.495e+07
N021	4	15	12	5.5	256	19.3	37.3	0.295e+08
N021	15	18	16	4.1	264	14.6	26.8	0.583e+07
N022	11	18	15	4.4	248	9.1	20.8	0.353e+07
N022	5	11	8	8.5	207	6.0	12.2	0.534e+07
N023	5	12	7	9.8	208	5.9	11.0	0.596e+07
N025	13	17	16	4.1	196	64.3	120.6	0.128e+08
N025	8	13	12	5.5	199	41.1	81.1	0.569e+08

EXP	Bs	Be	Bp	T (sec)	ANGLE (deg)	H (cm)	H' (cm)	I1 (dyn/sec)
N025	4	8	7	9.8	197	35.7	59.3	0.473e+08
N026	10	18	12	5.5	245	18.9	42.0	0.351e+08
N026	4	10	9	7.5	203	6.2	10.9	0.425e+07
N027	11	18	14	4.7	241	15.2	33.3	0.125e+08
N027	8	11	10	6.7	233	7.5	11.8	0.557e+07
N027	3	8	7	9.8	209	5.0	7.5	0.478e+07
N029	6	15	12	5.5	240	14.6	27.3	0.193e+08
N029	15	18	17	3.9	270	8.9	16.4	0.125e+07
N029	4	6	5	14.0	203	2.8	3.6	0.201e+07
N030	12	18	13	5.1	226	15.2	30.6	0.158e+08
N030	6	12	11	6.1	237	11.0	18.2	0.136e+08
N030	4	6	5	14.0	216	2.4	3.6	0.242e+07
N032	13	18	14	4.7	247	9.1	15.0	0.450e+07
N032	6	13	12	5.5	239	7.0	12.5	0.460e+07
N032	3	6	5	14.0	205	1.7	2.7	0.402e+06
N033	10	18	14	4.7	243	7.0	15.1	0.300e+07
N033	5	10	9	7.5	217	4.2	6.1	0.242e+07
N034	10	18	13	5.1	245	7.2	15.8	0.395e+07
N034	6	10	8	8.5	213	3.0	5.0	0.134e+07
N034	3	6	5	14.0	222	1.9	2.9	0.178e+07
N035	4	10	9	7.5	198	15.5	35.5	0.424e+07
N036	12	18	17	3.9	194	2.7	4.1	0.505e+05
N036	9	12	10	6.7	206	2.7	4.1	0.623e+06
N036	6	9	8	8.5	212	2.7	4.2	0.722e+06
N036	3	6	5	14.0	197	1.8	3.0	0.175e+06
N037	6	14	10	6.7	210	4.4	7.4	0.115e+07
N037	4	6	5	14.0	211	1.5	2.1	0.846e+06
N037	14	18	16	4.1	194	1.2	2.3	0.661e+04
N038	8	18	12	5.5	202	4.6	8.4	0.609e+06
N038	3	8	6	11.5	202	2.2	3.9	-0.201e+06
N039	4	9	7	9.8	201	3.9	6.3	0.558e+06
N039	9	18	12	5.5	197	3.8	8.5	0.193e+06
N040	2	11	10	6.7	198	13.1	33.2	0.728e+07
N041	14	16	15	4.4	193	28.2	44.4	-0.175e+07
N041	12	14	13	5.1	192	21.7	33.6	-0.874e+06
N041	3	12	11	6.1	194	17.6	43.2	-0.107e+07
N042	11	18	16	4.1	241	12.5	24.0	0.430e+07
N042	6	11	8	8.5	210	3.8	7.2	0.150e+07
N042	3	6	5	14.0	204	1.9	2.9	0.418e+06
N043	12	18	17	3.9	192	47.5	95.0	0.155e+07
N043	9	12	11	6.1	204	22.6	38.0	0.147e+08
N043	6	9	8	8.5	200	18.3	30.6	0.144e+08
N043	3	6	5	14.0	204	15.9	27.1	0.465e+08
N044	16	18	17	3.9	198	14.5	22.7	0.148e+06
N044	12	16	15	4.4	147	14.1	24.9	-0.463e+07
N044	4	12	10	6.7	207	4.2	8.4	0.813e+06
N045	8	18	12	5.5	199	35.2	108.6	0.114e+07
N045	6	8	7	9.8	200	21.8	28.5	0.587e+08
N045	3	6	5	14.0	195	11.4	21.8	-0.747e+07
N048	10	18	14	4.7	153	32.6	85.3	-0.353e+08

EXP	Bs	Be	Bp	T (sec)	ANGLE (deg)	H (cm)	H' (cm)	Il (dyn/sec)
N048	2	10	9	7.5	201	23.1	42.0	0.206e+08
N049	13	18	15	4.4	183	13.9	29.3	-0.279e+07
N049	6	13	9	7.5	207	13.3	26.7	0.138e+08
N050	4	15	9	7.5	205	14.2	26.2	0.179e+08
N050	15	18	16	4.1	175	8.2	14.9	-0.152e+07
N051	4	18	10	6.7	209	11.7	24.9	0.128e+08
N052	11	18	14	4.7	153	14.2	30.2	-0.105e+08
N052	4	11	9	7.5	217	7.2	12.5	0.553e+07
N053	4	18	14	4.7	147	17.6	49.7	-0.175e+08
N054	7	14	13	5.1	152	20.6	32.2	-0.324e+08
N054	14	18	16	4.1	157	20.4	37.6	-0.166e+08
N054	4	7	6	11.5	195	1.9	3.3	-0.560e+06
N055	12	15	13	5.1	149	8.9	15.5	-0.615e+07
N055	9	12	11	6.1	147	7.2	10.5	-0.388e+07
N055	5	9	8	8.5	214	3.2	5.9	0.135e+07
N056	10	18	17	3.9	156	10.1	21.3	-0.255e+07
N056	5	10	8	8.5	214	4.2	6.7	0.218e+07
N057	4	10	7	9.8	203	11.4	23.5	0.156e+08
N058	12	16	14	4.7	147	7.4	10.4	-0.280e+07
N058	4	12	8	8.5	205	5.5	10.6	0.388e+07
N059	4	14	8	8.5	209	8.3	14.6	0.124e+08
N060	11	18	15	4.4	197	13.1	25.3	-0.558e+06
N060	5	11	9	7.5	211	4.3	7.9	0.226e+07
N061	11	18	16	4.1	148	21.8	42.5	-0.462e+07
N061	4	11	8	8.5	215	11.0	16.2	0.238e+08
N062	9	15	11	6.1	204	19.6	36.3	0.100e+08
N062	6	9	8	8.5	214	9.6	13.3	0.173e+08
N063	14	18	17	3.9	151	15.6	30.0	-0.448e+07
N063	9	14	13	5.1	201	10.4	21.5	0.973e+06
N063	5	9	8	8.5	213	7.0	10.9	0.883e+07
N063	3	5	4	18.0	218	2.1	2.7	0.232e+07
N064	16	18	17	3.9	167	12.8	20.0	-0.109e+07
N064	12	16	15	4.4	197	12.0	20.9	-0.134e+07
N064	4	12	10	6.7	210	9.1	18.5	0.496e+07
N065	10	12	11	6.1	200	26.0	38.1	0.211e+08
N065	12	15	14	4.7	196	25.5	47.4	0.381e+07
N065	3	10	9	7.5	207	21.6	43.9	0.426e+08
N066	12	14	13	5.1	197	37.7	59.1	0.831e+07
N066	3	12	10	6.7	199	32.0	74.0	0.192e+08
N067	6	18	10	6.7	200	16.0	31.3	0.146e+08
N067	4	6	5	14.0	207	2.8	4.1	0.197e+07
N068	9	12	10	6.7	196	21.2	39.5	0.122e+07
N068	1	9	8	8.5	200	19.0	40.9	0.282e+08
N069	12	14	13	5.1	198	17.6	27.5	0.426e+07
N069	4	12	9	7.5	203	14.7	34.5	0.222e+08
N071	3	12	11	6.1	198	17.0	41.0	0.531e+07
N072	4	15	8	8.5	212	8.2	15.8	0.103e+08
N073	6	18	9	7.5	223	9.4	18.2	0.154e+08
N073	4	6	5	14.0	213	2.2	3.3	0.219e+07
N074	12	16	15	4.4	196	57.0	96.2	-0.272e+07

EXP	Bs	Be	Bp	T (sec)	ANGLE (deg)	H (cm)	H' (cm)	I1 (dyn/sec)
N074	10	12	11	6.1	197	37.9	54.0	0.211e+08
N074	6	10	8	8.5	197	30.1	56.4	0.156e+08
N074	2	6	4	18.0	196	28.1	45.1	-0.270e+08
N075	6	10	9	7.5	197	14.4	27.8	0.131e+08
N077	6	11	10	6.7	203	10.8	23.5	0.752e+07
N077	3	6	5	14.0	198	8.4	16.0	0.102e+08
N079	2	8	7	9.8	201	13.7	32.5	0.788e+07
N081	1	14	13	5.1	197	33.1	83.2	0.908e+07
N082	6	9	8	8.5	199	16.3	30.1	0.216e+08
N082	3	6	5	14.0	196	12.7	24.6	0.275e+07
N083	3	10	9	7.5	201	15.5	35.0	0.235e+08
N084	10	18	11	6.1	240	11.5	20.8	0.171e+08
N084	5	10	8	8.5	214	5.9	12.7	0.713e+07
N085	5	13	9	7.5	219	8.1	14.3	0.116e+08
N085	13	18	15	4.4	248	4.5	9.1	0.594e+06
N086	12	15	14	4.7	141	8.7	14.1	-0.106e+07
N086	4	12	10	6.7	220	8.2	14.6	0.877e+07
N087	5	12	9	7.5	216	6.6	12.7	0.762e+07
N087	12	14	13	5.1	241	6.0	8.6	0.170e+07
N088	12	18	16	4.1	184	16.3	35.8	-0.284e+07
N088	6	12	9	7.5	228	8.6	13.2	0.142e+08
N089	9	15	14	4.7	193	21.2	46.6	-0.327e+06
N089	3	9	8	8.5	207	11.1	24.8	0.922e+07
N090	3	16	15	4.4	196	33.1	74.9	-0.769e+07
N091	11	17	15	4.4	192	40.0	84.0	-0.161e+08
N091	4	11	7	9.8	196	21.8	47.1	0.193e+07
N092	11	16	15	4.4	197	41.1	80.3	-0.340e+08
N092	7	11	9	7.5	197	21.1	43.1	0.175e+08
N092	4	7	6	11.5	195	17.6	32.4	-0.364e+07
N092	1	4	3	25.0	197	15.7	29.4	0.238e+08
N093	10	13	12	5.5	194	32.6	51.5	-0.306e+08
N093	6	10	9	7.5	195	22.6	44.4	-0.413e+07
N093	4	6	5	14.0	195	19.0	29.8	-0.174e+08
N093	1	4	3	25.0	196	17.3	33.2	0.274e+06
N094	7	13	12	5.5	197	32.6	74.7	-0.264e+05
N094	2	7	5	14.0	197	22.5	51.5	0.512e+07
N095	8	12	11	6.1	190	31.4	62.3	-0.664e+06
N095	4	8	7	9.8	187	27.6	54.8	-0.111e+09
N095	1	4	3	25.0	185	24.7	46.3	-0.749e+09
N096	11	15	14	4.7	196	58.5	104.7	-0.361e+07
N096	6	11	10	6.7	198	38.5	80.1	0.134e+08
N096	3	6	5	14.0	197	34.4	56.6	0.206e+08
N097	6	12	10	6.7	198	23.0	51.7	0.136e+08
N097	1	6	4	18.0	196	15.5	36.4	0.811e+07
N098	15	18	17	3.9	196	71.7	118.5	-0.510e+07
N098	12	15	14	4.7	196	44.8	73.7	0.861e+06
N098	9	12	10	6.7	197	31.1	57.2	0.224e+08
N098	4	9	8	8.5	196	25.2	53.4	0.162e+07
N099	9	11	10	6.7	200	21.4	33.7	0.201e+08
N099	5	9	8	8.5	197	15.4	31.6	0.516e+07

EXP	Bs	Be	Bp	T (sec)	ANGLE (deg)	H (cm)	H' (cm)	I1 (dyn/sec)
N099	1	5	3	25.0	195	13.5	28.2	-0.156e+08
N100	3	11	10	6.7	198	18.8	42.6	0.933e+07
N101	2	11	10	6.7	199	19.0	45.8	0.117e+08
N102	8	11	10	6.7	196	28.4	50.0	0.484e+07
N102	6	8	7	9.8	198	23.5	37.6	0.239e+08
N102	1	6	5	14.0	196	21.7	47.2	0.134e+08
N103	2	7	6	11.5	196	18.0	41.4	-0.257e+07
N104	13	17	16	4.1	250	7.0	13.3	0.612e+06
N104	11	13	12	5.5	235	6.6	8.8	0.350e+07
N104	7	11	9	7.5	217	5.4	8.6	0.518e+07
N104	4	7	6	11.5	222	2.2	3.0	0.193e+07
N105	12	18	13	5.1	251	9.0	19.4	0.506e+07
N105	10	12	11	6.1	234	5.3	6.9	0.256e+07
N105	4	7	6	11.5	214	4.7	5.7	0.687e+07
N105	7	10	9	7.5	228	4.1	6.8	0.279e+07
N106	12	17	16	4.1	248	5.8	10.4	0.765e+06
N106	4	10	9	7.5	217	4.1	7.2	0.278e+07
N106	10	12	11	6.1	235	4.0	5.7	0.197e+07
N107	10	18	17	3.9	162	26.2	35.1	-0.187e+08
N107	8	10	9	7.5	207	4.3	6.1	0.172e+07
N107	4	8	7	9.8	212	3.8	6.4	0.321e+07
N108	11	18	16	4.1	154	13.4	25.8	-0.565e+07
N108	5	11	7	9.8	212	5.1	8.2	0.671e+07
N109	13	16	15	4.4	195	44.8	73.0	-0.180e+08
N109	10	13	12	5.5	197	28.4	49.5	0.241e+07
N109	6	10	9	7.5	198	22.4	44.5	0.204e+08
N109	4	6	5	14.0	196	20.3	30.4	-0.584e+07
N110	12	15	14	4.7	197	45.1	77.3	-0.231e+05
N110	9	12	11	6.1	196	36.9	58.9	0.559e+07
N110	6	9	8	8.5	197	31.2	49.5	0.402e+08
N110	3	6	5	14.0	196	25.3	41.4	0.711e+07
N111	5	13	11	6.1	197	27.2	62.6	0.280e+07
N112	2	8	7	9.8	197	19.9	47.6	0.146e+08
N113	5	7	6	11.5	202	14.2	21.0	0.555e+08
N114	4	8	7	9.8	213	13.3	18.3	0.489e+08
N115	5	11	9	7.5	202	9.6	21.7	0.122e+08
N115	1	4	3	25.0	197	6.2	10.5	0.404e+07
N116	10	18	17	3.9	196	41.8	78.6	-0.235e+08
N116	4	10	7	9.8	202	15.7	32.2	0.286e+08
N117	15	18	17	3.9	169	23.3	37.9	-0.116e+08
N117	11	15	14	4.7	176	15.7	25.1	-0.527e+07
N117	4	11	8	8.5	208	7.8	14.5	0.946e+07
N118	8	11	9	7.5	200	17.7	31.8	0.211e+08
N118	5	8	7	9.8	199	14.2	25.0	0.139e+08
N119	14	17	16	4.1	195	32.4	58.5	-0.285e+07
N119	11	14	12	5.5	197	22.2	39.4	-0.544e+07
N119	8	11	10	6.7	200	17.7	30.6	0.113e+08
N119	5	8	6	11.5	198	15.6	25.1	0.610e+07
N120	10	17	16	4.1	197	46.1	85.4	-0.188e+08
N120	8	10	9	7.5	198	23.9	35.0	0.185e+08

EXP	Bs	Be	Bp	T (sec)	ANGLE (deg)	H (cm)	H' (cm)	I1 (dyn/sec)
N120	6	8	7	9.8	198	21.7	31.0	0.181e+08
N120	4	6	5	14.0	198	19.1	27.5	0.332e+08
N121	13	15	14	4.7	149	21.0	27.9	-0.188e+08
N121	8	13	12	5.5	146	19.8	29.3	-0.199e+08
N121	5	8	7	9.8	221	9.2	11.0	0.227e+08
N122	12	18	16	4.1	134	13.4	28.3	-0.303e+07
N122	10	12	11	6.1	149	10.5	14.5	-0.571e+07
N122	4	10	8	8.5	212	8.8	15.1	0.128e+08
N123	9	16	14	4.7	147	9.8	20.4	-0.472e+07
N123	5	9	8	8.5	206	7.1	11.3	0.713e+07
N124	12	18	16	4.1	144	15.2	29.5	-0.881e+07
N124	4	12	8	8.5	217	5.8	11.6	0.724e+07
N125	16	18	17	3.9	183	11.7	18.1	-0.982e+06
N125	9	16	14	4.7	148	11.0	22.0	-0.480e+07
N125	4	9	8	8.5	218	7.7	9.5	0.123e+08
N126	4	10	8	8.5	209	7.6	12.4	0.106e+08
N126	10	13	11	6.1	196	6.4	11.1	0.212e+07
N126	13	17	15	4.4	132	5.3	11.0	-0.480e+06
N127	11	18	17	3.9	145	11.1	22.2	-0.345e+07
N127	8	11	9	7.5	215	5.0	8.6	0.427e+07
N127	4	8	7	9.8	208	4.9	6.9	0.374e+07
N128	12	18	15	4.4	143	13.2	23.9	-0.775e+07
N128	8	12	10	6.7	223	5.9	11.2	0.397e+07
N128	4	8	7	9.8	215	5.2	8.1	0.648e+07
N129	5	11	8	8.5	215	5.4	9.8	0.631e+07
N129	11	15	14	4.7	149	4.6	7.9	-0.609e+06
N130	14	18	15	4.4	139	34.5	60.3	-0.302e+08
N130	8	14	13	5.1	192	30.0	53.3	-0.271e+08
N130	4	8	7	9.8	211	5.3	8.3	0.431e+07
N134	10	16	14	4.7	196	25.1	41.5	-0.225e+07
N134	5	10	8	8.5	210	4.9	9.0	0.283e+07
N135	9	16	13	5.1	197	30.4	63.6	-0.289e+08
N135	3	9	8	8.5	200	11.6	25.6	0.685e+07
N136	9	18	13	5.1	194	19.5	45.6	-0.824e+07
N136	6	9	8	8.5	218	4.3	6.4	0.357e+07
N137	2	15	12	5.5	192	30.8	61.2	-0.398e+08
N137	15	17	16	4.1	196	29.2	44.9	-0.110e+08
N138	10	15	12	5.5	190	35.8	60.3	-0.389e+08
N138	4	10	9	7.5	195	12.6	25.7	0.162e+07
N139	4	12	11	6.1	194	34.7	71.1	-0.356e+07
N140	3	11	9	7.5	209	30.8	55.1	0.717e+08
N141	7	11	9	7.5	203	35.7	62.8	0.368e+08
N141	5	7	6	11.5	194	20.2	31.0	0.282e+08
N142	15	18	17	3.9	197	55.6	95.2	0.296e+07
N142	11	15	14	4.7	196	39.2	66.7	0.324e+07
N142	7	11	9	7.5	196	28.0	53.6	0.264e+08
N142	4	7	6	11.5	197	18.3	31.7	0.977e+07
N146	7	15	13	5.1	194	44.8	90.4	-0.125e+08
N146	4	7	6	11.5	196	14.2	26.3	0.114e+07
N146	2	4	3	25.0	199	13.0	21.3	0.480e+08

EXP	Bs	Be	Bp	T (sec)	ANGLE (deg)	H (cm)	H' (cm)	I1 (dyn/sec)
N147	6	13	12	5.5	191	82.0	119.5	-0.763e+08
N147	13	18	16	4.1	191	81.1	162.0	-0.484e+07
N147	3	6	5	14.0	163	32.3	49.7	-0.502e+09
N148	6	17	13	5.1	194	29.3	55.6	-0.114e+08
N149	7	18	10	6.7	211	34.3	62.0	0.709e+08
N149	3	7	6	11.5	209	3.3	6.5	0.166e+07
N150	5	18	11	6.1	192	27.7	49.2	0.112e+08
N151	12	14	13	5.1	194	17.9	28.4	0.128e+07
N151	3	12	11	6.1	198	17.2	34.8	0.141e+07
N152	5	13	11	6.1	212	8.3	15.2	0.413e+07
N152	13	18	16	4.1	155	7.5	15.0	-0.136e+07
N153	15	17	16	4.1	159	8.0	12.1	-0.120e+07
N153	5	13	11	6.1	200	7.8	13.6	0.185e+07
N153	13	15	14	4.7	149	6.7	9.9	-0.797e+06
N154	14	18	17	3.9	133	5.4	9.3	-0.456e+06
N154	8	14	12	5.5	196	4.5	8.5	0.293e+06
N154	4	8	7	9.8	210	1.7	2.9	0.346e+06
N155	4	10	7	9.8	205	4.1	6.2	0.271e+07
N155	10	15	13	5.1	219	1.9	4.0	0.170e+06
N156	3	11	7	9.8	212	6.8	9.0	0.914e+07
N157	3	8	7	9.8	196	16.7	35.8	0.276e+08
N158	4	10	6	11.5	207	4.1	6.4	0.350e+07
N158	14	18	17	3.9	242	2.4	4.3	-0.107e+05
N158	10	14	12	5.5	234	1.9	3.6	0.244e+06
N159	3	7	6	11.5	200	9.7	18.2	0.107e+08
N160	4	10	6	11.5	213	7.7	10.4	0.255e+08
N160	10	12	11	6.1	208	2.0	3.2	0.286e+06
N161	4	10	7	9.8	210	15.5	17.7	0.429e+08
N161	10	15	12	5.5	244	9.0	14.4	0.765e+07
N161	15	18	17	3.9	252	4.8	8.7	0.305e+06
N162	9	12	11	6.1	197	12.7	22.7	0.100e+08
N162	7	9	8	8.5	199	11.1	16.1	0.349e+07
N162	4	7	6	11.5	196	7.6	14.2	0.241e+07
N163	10	14	12	5.5	253	6.3	11.2	0.288e+07
N163	3	10	8	8.5	206	4.2	8.4	0.190e+07
N164	3	10	9	7.5	198	16.3	38.4	0.500e+07
N165	9	14	13	5.1	200	7.8	16.2	0.296e+07
N165	2	9	8	8.5	203	6.2	12.4	0.375e+07
N166	8	15	10	6.7	239	5.9	11.7	0.492e+07
N166	15	17	16	4.1	248	3.8	5.9	0.358e+06
N166	4	8	7	9.8	199	3.1	5.1	0.861e+06
N167	12	16	13	5.1	246	4.6	7.5	0.152e+07
N167	9	12	11	6.1	202	4.5	7.7	0.157e+07
N167	3	9	7	9.8	212	4.1	6.1	0.210e+07
N168	3	11	8	8.5	210	4.7	8.3	0.353e+07
N168	11	14	13	5.1	243	2.6	4.8	0.377e+06
N169	6	13	9	7.5	209	5.5	11.1	0.126e+07
N169	13	16	14	4.7	252	4.1	6.7	0.831e+06
N169	3	6	5	14.0	219	2.7	3.7	0.386e+07
N170	7	13	10	6.7	200	6.0	9.2	0.104e+07

EXP	Bs	Be	Bp	T (sec)	ANGLE (deg)	H (cm)	H' (cm)	I1 (dyn/sec)
N170	13	18	17	3.9	243	3.0	6.5	0.178e+06
N170	3	7	6	11.5	213	2.1	3.4	0.985e+06
N171	4	13	12	5.5	249	4.2	8.5	0.122e+07
N172	7	17	15	4.4	141	6.5	14.4	-0.728e+06
N172	4	7	6	11.5	217	3.1	5.1	0.310e+07
N173	15	18	17	3.9	251	5.3	8.9	0.470e+06
N173	3	9	7	9.8	201	3.9	7.3	0.154e+07
N173	9	12	11	6.1	200	3.6	5.9	0.311e+06
N173	12	15	14	4.7	261	3.6	6.8	0.342e+06
N174	12	18	16	4.1	126	4.9	10.0	-0.391e+05
N174	4	8	7	9.8	202	4.3	6.3	0.170e+07
N174	8	12	11	6.1	201	3.1	5.8	0.454e+06
N175	10	18	15	4.4	134	4.8	10.2	-0.493e+06
N175	3	10	7	9.8	203	3.6	6.9	0.195e+07
N176	9	17	15	4.4	248	5.0	11.0	0.595e+06
N176	4	9	7	9.8	198	3.6	5.9	0.162e+07
N177	4	10	8	8.5	204	4.9	8.0	0.209e+07
N177	10	17	16	4.1	248	2.9	6.6	0.151e+06
N178	10	17	15	4.4	251	4.3	8.5	0.507e+06
N178	4	10	8	8.5	205	3.6	6.9	0.135e+07
N179	5	11	8	8.5	204	3.6	7.2	0.106e+07
N179	11	14	13	5.1	137	2.7	4.8	-0.184e+06
N180	4	6	5	14.0	220	3.0	3.7	0.546e+07
N180	6	11	7	9.8	206	2.8	4.7	0.106e+07
N180	11	15	14	4.7	248	2.5	4.2	0.192e+05
N181	4	11	8	8.5	209	3.0	6.0	0.848e+06
N182	7	12	9	7.5	208	2.5	4.7	0.663e+06
N182	4	7	6	11.5	215	2.4	3.7	0.156e+07
N182	12	18	17	3.9	194	2.4	4.7	0.176e+04
N183	11	18	17	3.9	234	16.2	27.7	0.727e+07
N183	4	6	5	14.0	220	2.8	3.7	0.391e+07
N183	6	11	7	9.8	205	2.8	5.1	0.108e+07
N184	9	18	12	5.5	222	18.2	40.0	0.302e+08
N184	7	9	8	8.5	215	3.1	4.7	0.169e+07
N184	4	7	5	14.0	228	2.8	4.5	0.450e+07
N187	7	17	13	5.1	243	14.3	36.3	0.149e+08
N187	5	7	6	11.5	208	2.8	4.3	0.166e+07
N187	3	5	4	18.0	215	2.4	3.3	0.199e+07
N188	6	18	14	4.7	219	9.8	24.0	0.421e+07
N188	3	6	5	14.0	213	1.7	2.9	0.151e+07
N189	13	18	16	4.1	229	10.0	20.9	0.318e+07
N189	8	13	12	5.5	243	7.2	12.5	0.493e+07
N189	3	8	6	11.5	210	3.3	5.7	0.277e+07
N190	9	13	11	6.1	241	7.2	11.1	0.637e+07
N190	7	9	8	8.5	206	2.8	4.2	0.572e+06
N190	4	7	5	14.0	210	2.4	3.9	0.151e+07
N191	12	18	16	4.1	191	14.7	27.5	0.187e+07
N191	6	12	11	6.1	226	4.3	7.9	0.168e+07
N191	4	6	5	14.0	202	3.2	3.8	0.214e+07
N192	14	18	17	3.9	208	10.9	16.9	0.859e+06

EXP	Bs	Be	Bp	T (sec)	ANGLE (deg)	H (cm)	H' (cm)	Il (dyn/sec)
N192	7	14	11	6.1	241	5.8	11.5	0.346e+07
N192	4	7	6	11.5	213	2.1	3.2	0.104e+07
N193	12	18	17	3.9	245	10.7	20.1	0.170e+07
N193	9	12	11	6.1	230	4.5	7.1	0.206e+07
N193	4	9	5	14.0	204	2.6	5.0	0.868e+06
N194	8	14	13	5.1	238	8.6	15.3	0.518e+07
N194	4	8	7	9.8	205	2.2	4.4	0.547e+06
N195	12	18	17	3.9	202	11.3	21.1	0.208e+07
N195	8	12	11	6.1	223	6.3	10.2	0.425e+07
N195	4	8	6	11.5	207	3.3	5.1	0.271e+07
N196	8	13	12	5.5	224	7.5	14.0	0.424e+07
N196	13	18	15	4.4	206	7.3	15.7	0.101e+07
N196	4	8	6	11.5	213	3.5	5.6	0.379e+07
N197	13	18	16	4.1	211	5.5	11.7	0.771e+06
N197	11	13	12	5.5	218	5.3	8.7	0.214e+07
N197	9	11	10	6.7	237	5.2	7.6	0.392e+07
N197	3	9	7	9.8	212	3.7	6.6	0.224e+07
N198	8	13	12	5.5	226	6.9	11.3	0.416e+07
N198	13	17	15	4.4	212	5.2	10.7	0.630e+06
N198	4	8	7	9.8	209	3.7	5.3	0.236e+07
N199	9	14	11	6.1	237	5.7	10.0	0.372e+07
N199	14	17	16	4.1	215	4.6	7.9	0.421e+06
N199	4	9	8	8.5	209	2.2	4.2	0.559e+06
N200	9	18	11	6.1	232	5.3	11.3	0.319e+07
N200	4	9	7	9.8	208	2.9	5.2	0.163e+07

TABLE 3

Frequencies and periods associated with the 18 bands from the spectral analysis.

Column headers:

B = Band number

f = Frequency (sec^{-1})

T = Period (sec).

B	f	T
1	0.00879	113.8
2	0.02441	41.0
3	0.04004	25.0
4	0.05566	18.0
5	0.07129	14.0
6	0.08691	11.5
7	0.10254	9.8
8	0.11816	8.5
9	0.13379	7.5
10	0.14941	6.7
11	0.16504	6.1
12	0.18066	5.5
13	0.19629	5.1
14	0.21191	4.7
15	0.22754	4.4
16	0.24316	4.1
17	0.25879	3.9
18	0.27441	3.6

VI. NEEDS FOR FURTHER STUDY

A. Storms and their effects on the Bering Sea coast of Alaska should be studied in greater detail. These studies should include additional studies on the frequency and magnitude of storm surge and extreme wave conditions.

B. Long-term changes in shoreline position should be assessed in greater detail.

C. In order to properly evaluate the output of the wave model, we need direct measurement of a wide spectrum of wave energies. At least one more field season of wave measurement is necessary.

D. OCSEAP should consider maintaining a medium-level study on coastal processes of the southern portion of the Bristol Bay coast of the Alaska Peninsula. This is a critical area in view of its high biological productivity (e.g. Izembek Lagoon) and its proximity to potential deep water ports on the south side of the Peninsula.

VII. REFERENCES

Berryhill, R. V., 1963, Reconnaissance of beach sands, Bristol Bay, Alaska. U.S. Bureau of Mines, Report Inv. 6214:48 pp.

Bretschneider, C. L. and Reid, R. O., 1954, Modification of wave height due to bottom friction, percolation, and refraction: U.S. Army Corps of Engineers, Beach Erosion Board, T.M. 45, 36 p.

Dobson, R. S., 1967, Some applications of a digital computer to hydraulic engineering problems, Stanford Univ., Dept. of Civil Engineering, Tech. Report 80.

Dolan, R., 1971, Coastal landforms: crescentic and rhythmic, Geol. Soc. Am. Bull., 82:177-180.

Fathauer, T., 1975, The great Bering Sea storms of 9-12 November 1974, Weatherwise: 76-83.

Greene, H. G., 1970, Morphology, sedimentation and seismic characteristics of an arctic beach, Nome, Alaska -- with economic significance, M.S. thesis, San Jose State College, San Jose, CA: 139 pp.

Hopkins, D. M., 1967, Quaternary marine transgressions in Alaska, in Hopkins, D. M., ed. The Bering Land Bridge, Stanford Univ. Press: 495 p.

Joyce, J. R. F., 1950, Notes on ice-foot development, Meny Fjord, Graham Land, Antarctica, J. Geol. 58: 646-49.

Lowe, R. L., Inman, D. L., Brush, B. M., 1972, Simultaneous data system for instrumenting the shelf. Proc. Coastal Eng. Conf., 13:95-112.

Pawka, S. S., Inman, D. L., Lowe, R. L., Holmes, L., 1976, Wave climate at Torrey Pines Beach, California, U.S. Army Corps of Engineers, Coastal Eng. Research Center, Tech. Paper 76-5:372 pp.

St. Denis, M., 1969, On wind generated waves, Topics in Ocean Engineering, C. L. Bretschneider, ed., Gulf Pub. Co., Houston, Texas: 31 p.

Sallenger, A. H., Hunter, R., Dingler, J., 1977, Coastal processes and morphology of the Bering Sea coast of Alaska, FY 76 Annual Report, OCSEAP, NOAA, Research Unit-431: 66 p.

Sallenger, A. H., Hunter, R., Dingler, J., 1977, Coastal processes and morphology of the Bering Sea coast of Alaska, FY 77 Annual Report, OCSEAP, NOAA, Research Unit-431: 54 pp.

Thrall, D. E., 1973, Development of a computer program to simulate wind wave generation, refraction and shoaling in the Gulf of Maine, Engineering Design and Analysis Laboratory, Univ. of New Hampshire EDAL Rep. 113: 25 pp.

Komar, P. D., 1976, Beach Processes and Sedimentation; Prentice-Hall, Inc., Engelwood Cliffs, New Jersey. 429p.

Sallenger, A. H., J. R. Dingler, and R. Hunter, 1978, "Coastal processes and morphology of the Bering Sea Coast of Alaska"; NOAA-OCS Annual Report, Research Unit #431, 53p.

FINAL DRAFT
OIL SPILL TRAJECTORY ANALYSIS
LOWER COOK INLET, ALASKA
BERING SEA-GULF OF ALASKA PROJECT OFFICE
OUTER CONTINENTAL SHELF ENVIRONMENTAL
ASSESSMENT PROGRAM
NATIONAL OCEANIC AND ATMOSPHERIC ADMINISTRATION

DAMES & MOORE JOB NO. 6797-011-02
LOS ANGELES, CALIFORNIA
MARCH 9, 1979

CONTENTS

	<u>Page</u>
EXECUTIVE SUMMARY	v
I. INTRODUCTION	1
II. OIL SPILL MODEL	3
III. INPUT DATA PREPARATION	6
A. OIL SPILL SCENARIOS	6
B. GRID SYSTEM	7
C. OCEANOGRAPHIC AND METEOROLOGIC INPUT DATA	8
D. MISCELLANEOUS DATA	18
IV. SIMULATION RESULTS	19
A. BASE CASES	19
B. SYSTEMATIC PERTURBATION ANALYSIS	25
C. RANDOM PERTURBATION ANALYSIS	33
V. RECOMMENDATIONS	37
BIBLIOGRAPHY	41
APPENDIX A OIL SPILL MODEL DOCUMENTATION	
APPENDIX B BASE CASE TRAJECTORIES AND RESULTS	
APPENDIX C PERTURBATION CASE TRAJECTORIES	
APPENDIX D INPUT DATA FILES	

LIST OF FIGURES

Figure No.

ES-1	Potential Boundary Contact Zones
ES-2	Annual Percent Probability of Exposure
1	Grid System
2	Postulated Oil Spill Sites
3	Wind Patterns 1 and 2
4	Wind Patterns 3 and 4
5	Wind Patterns 5 and 6
6	Wind Pattern 7
7	Wind Pattern 8
8	Current Meter Station Location
9	Net Current Pattern
10	Net Current Vector Pattern
11	Tidal Current Phase Distribution
12	Tidal Current Pattern at T = 0.00 Hrs
13	Tidal Current Pattern at T = 3.11 Hrs
14	Tidal Current Pattern at T = 6.21 Hrs
15	Tidal Current Pattern at T = 9.32 Hrs
16	Potential Boundary Contact Zones
17	Annual Percent Probability of Exposure
18	Net Current Standard Deviation Distribution
19	Example Trajectory for Time-Dependent Winds
A-1	Analytic Solution-Verification Runs
A-2	Computed Solution-Verification Runs, $\Delta T = 0.1$ Hrs
A-3	Computed Solution-Verification Runs, $\Delta T = 0.4$ Hrs
A-4	Verification Run - Net Current Only
A-5 through A-7	Verification Run - Wind Only
B-1 through B-72	Base Case Trajectories
B-73 through B-81	Potential Boundary Contact Zones, Sites 1 to 8
B-82 through B-90	Annual Percent Probability of Exposure, Sites 1 to 8
C-1 through C-64	Systematic Perturbation Cases, Sites 1 and 7
C-65 through C-72	Systematic Perturbation Cases, Site 3
C-73 through C-78	Random Perturbation Cases, Site 7

LIST OF TABLES

Table No.

1	Direction, Speed, and Frequency of Eight Wind Patterns
2	PMEL and NOS Net Current Data
3	PMEL and NOS Tidal Current Data
4	Comparison of Predicted Tidal Current with M2 Constituent
5	Comparison of Measured and Predicted M2 Tidal Current Components
6	Base Case Boundary Contact Cells
7	Systematic Perturbation Boundary Contact Cells
8	Variability Between Base Case and Systematic Perturbation Trajectories
A-1	Verification Data Files
A-2	Sample Program Output

EXECUTIVE SUMMARY

A. INTRODUCTION

As part of its ongoing program, the Outer Continental Shelf Environmental Assessment Program (OCSEAP) contracted with Dames & Moore for continuing studies of the behavior of spilled oil in Lower Cook Inlet, Alaska. The primary purpose of this study was to update existing wind and water current fields using recently available data and to analyze the transport of postulated surface oil slicks under these fields.

This Executive Summary highlights the results and conclusions arising out of this study. Details and supporting evidence as well as recommendations for further work are contained in the main body of the final project report.

B. SCOPE AND METHODOLOGY

Behavior of a surface oil slick was represented by the trajectory of the centroid of the slick neglecting mass-dependent phenomena such as spreading, evaporation, sinking, etc. The velocity of the centroid was modeled as the linear, vectorial addition of wind velocity coupled to centroidal velocity by a coefficient of 3 percent and the total surface current velocity. A Dames & Moore oil spill numerical model embodying these concepts was used to carry out the analyses.

Wind fields in the area of interest were defined by eight spatially dependent flow patterns assumed to be constant over the simulation period. These patterns represent wind conditions observed two-thirds of the time on an annual basis, and include six patterns with winds typically parallel to the main axis of Cook Inlet and two with the predominant flow across the Inlet.

Surface currents were divided into two components, a time-dependent tidal flow and a constant net surface circulation. The tidal flow field

was developed from harmonic analyses of current measurements in combination with an existing tidal flow hydrodynamic model. The net current field was derived from analyses of current measurements, published literature, and a previously developed net circulation pattern.

Using these data sets as input to the oil spill model, three types of spill scenarios were examined:

1. Base Cases

Trajectories, shoreline impact locations, times to impact and probabilities of impact were computed for spills occurring at nine postulated sites within Lower Cook Inlet. The environmental fields discussed above, in combination with other parameters, such as spill time in relation to tidal phase, were the key inputs to each scenario.

Results of these scenarios were synthesized into two summary figures showing the shoreline distribution of location of impact, time to impact, and probability of impact given that a spill could occur at any one of the sites.

2. Systematic Perturbation Cases

Systematic perturbation runs were made to investigate the sensitivity of the base case results to small changes in the environmental fields. Each field was independently altered so that speeds were changed +25 percent from the base case while patterns (direction fields) were held constant. Spills driven by the perturbed fields were initiated at three of the nine base case sites.

Analyses of the perturbation results were based on a quantitative comparison of changes in the base case shoreline impact locations and times to impact. A qualitative analysis of the perturbation trajectories was also performed.

3. Random Perturbation Analysis

Using available information on the variability of the net current field, a stochastic analysis was performed to ascertain the effects of this variability on the base case results. Perturbation trajectories were computed in which base case net current vectors were augmented by vectors randomly drawn from a Gaussian distribution with zero mean and known standard deviations defined by field data.

Analysis of the random perturbation cases focused on the distribution of shoreline impact points about the base case result. In a subjective manner the behavior of the trajectories themselves were also analyzed.

C. RESULTS AND CONCLUSIONS

The results of this project include not only the predicted oil spill behavior, but also the input wind and current fields. The fields developed represent the most recent synthesis of current measurement and modeling results available in October 1978.

For purposes of oil spill simulation, the tidal current information is in the most satisfactory condition. To a great extent, this is due to the availability of a hydrodynamic tidal current model, Mungall, 1973, and the excellent agreement between predicted and observed data. Based on the results discussed below, which show predominantly weak dependence of spill movement on tidal currents, it is concluded that further work on tidal currents should be deemphasized.

Review of the net current data yields a considerably different result. Considerable current meter data has been collected and analyzed to the extent that the general hydrodynamics of Lower Cook Inlet are reasonably well understood. Attempts to translate this knowledge into the level of detail necessary to perform meaningful spill modeling

uncovered certain deficiencies. In particular, the spatial and temporal coverage of processed data was found to be very uneven. No winter season current meter data had been processed though measurements have been taken. The results reflect only the summer season current data and should be interpreted in that light.

Equally as important, data collected in 1974 in the northern portion of the study area would have been invaluable in defining the net current pattern in the vicinity of Kalgin Island and southward along the western side of the Inlet. Without these data, there is uncertainty concerning the magnitude and direction of net flow in areas that the results of this study indicate are subject to considerable exposure to spilled oil. A satisfactory modeling effort cannot be completed until the 1974 data have been analyzed and interpreted.

The meteorologic data base remained essentially unchanged as a result of this project. However, further refinement and treatment of the meteorological input data is of primary importance for two reasons. First, as discussed below, the wind fields tend to dominate the surface spill movement. Even in the systematic perturbation cases with weak winds, the general area of shoreline impact is usually determined by the prevailing winds. Secondly, the simulation period limits the range of applicability of the trajectory impact results. While persistence of the wind fields can occur, it is more likely that a changing sequence of wind fields corresponding to the progression of passing weather fronts will be observed over a period equal to that used here. Hence, the results of this project indicate that the wind fields and their simulated behavior are the most limiting aspect of the environmental data base.

Results of the base case simulations are summarized in Figures ES-1 and ES-2. Shoreline impact location, time to impact, and probability of impact are presented. These are key parameters in evaluating the impact of potential oil spills. Areas subject to impact in a short period are critical in two senses:

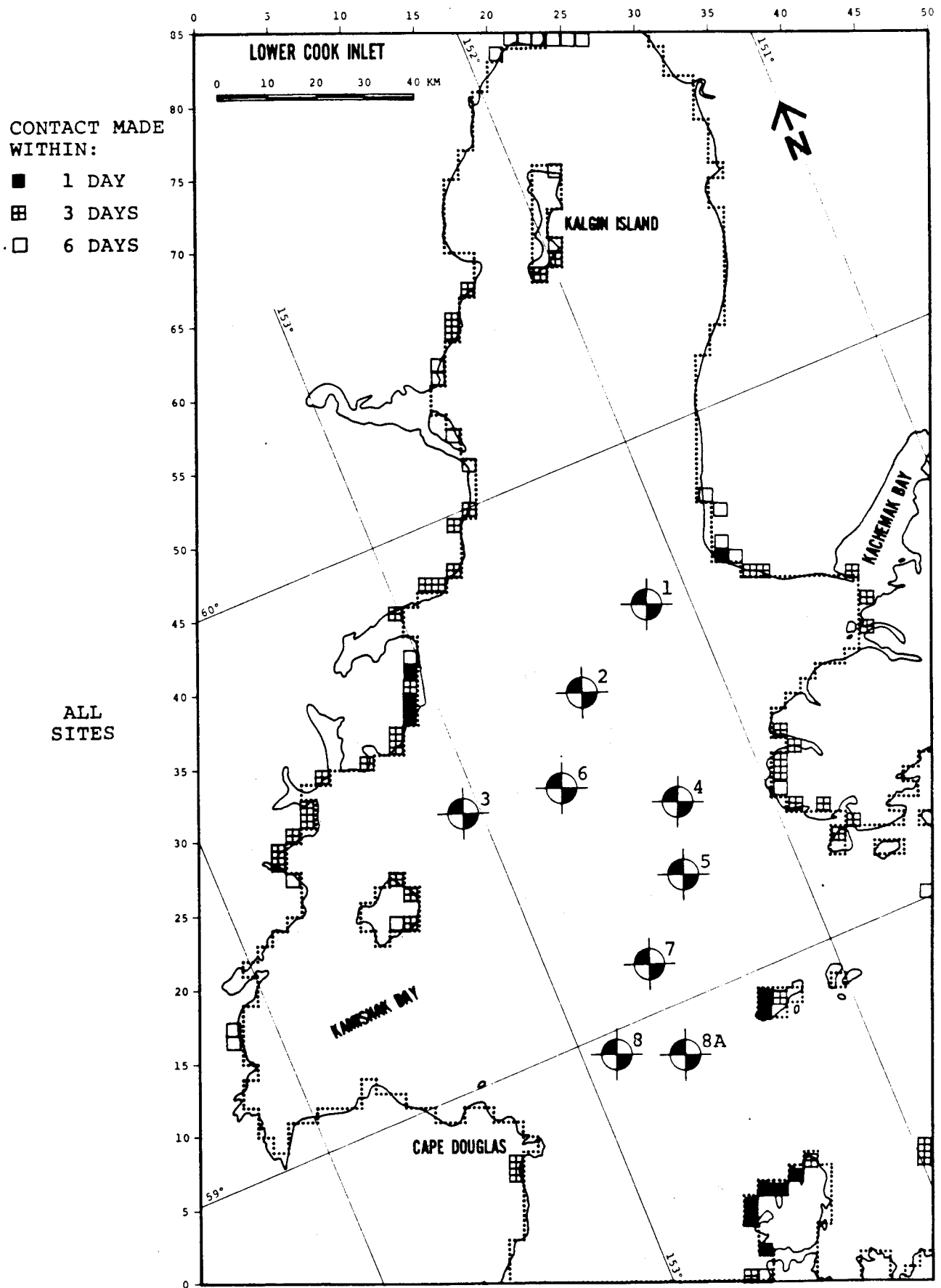


FIGURE ES-1: POTENTIAL BOUNDARY CONTACT ZONES

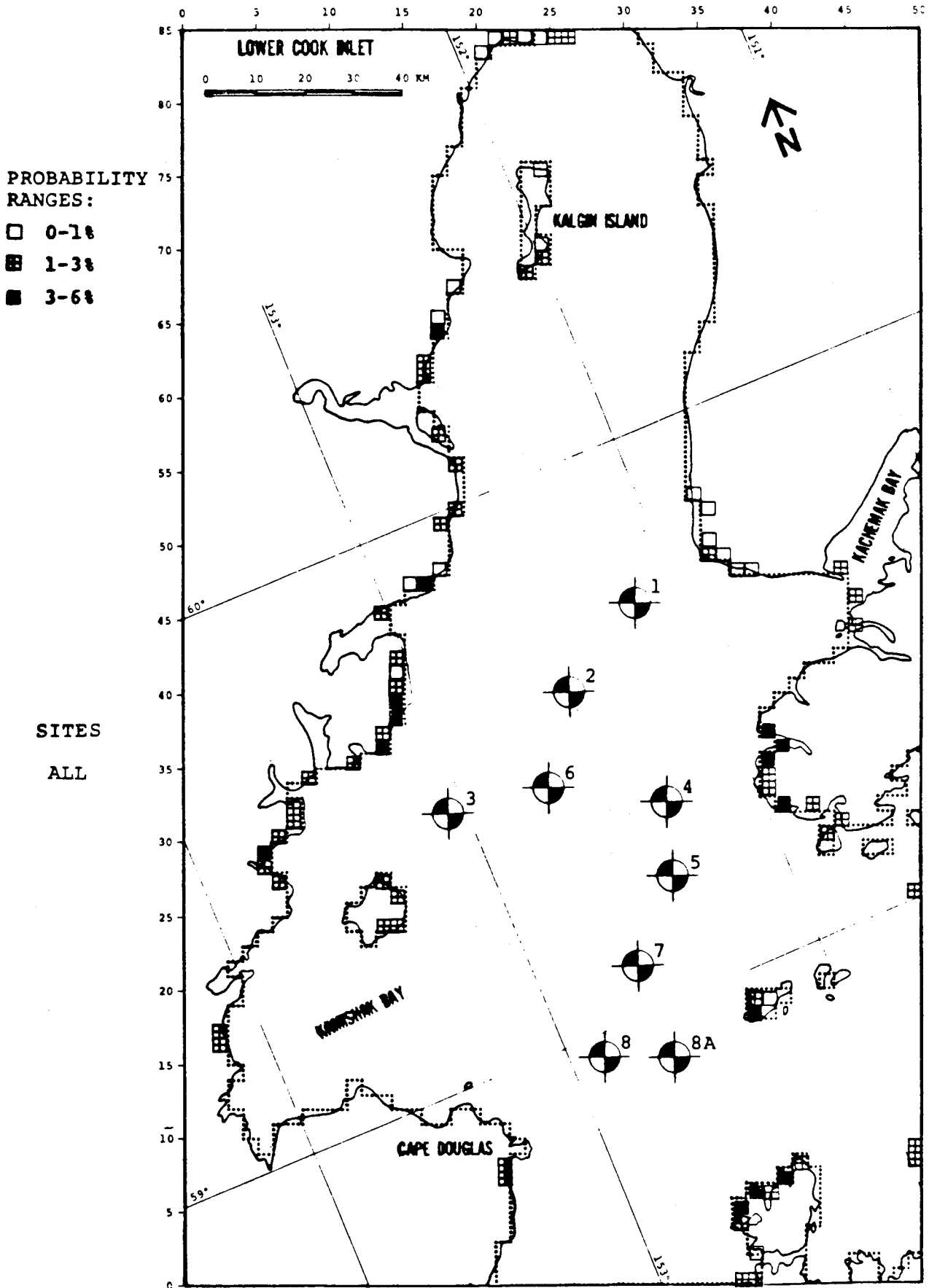


FIGURE ES-2: ANNUAL PERCENT PROBABILITY OF EXPOSURE

- 1) The rapid movement from spill site to shoreline impact makes containment and control difficult unless the necessary resources are in the immediate vicinity and are mobilized quickly once a spill release occurs.
- 2) For a given spill size, the shorter time to impact means that more oil is likely to be available for shoreline contamination and the more toxic constituents will have had less time to disperse.

The base case results show a broad area of shoreline impact points with two exceptions being the Cape Douglas and Cape Kasilof (east of Kalgin Island) areas. The most critical areas, both in terms of time to impact and probability of exposure are:

- 1) Iliamna Bay northward to Chinitna Bay on the west side of the Inlet.
- 2) Dangerous Cape to Cape Elizabeth
- 3) the Barren Islands
- 4) Shuyak Island at the northern end of Afognak Island.

To a lesser extent, Harriet Point, Anchor Point, and Augustine Island are also areas of concern.

These results are consistent with those presented in the Dames & Moore 1976 study. Two additional areas of exposure are suggested by the present study that were not apparent in the 1976 study:

- 1) The area north of the Forelands can be potentially exposed to spilled oil from Sites 1, 3, and 4 and to some extent from Sites 2 and 5, whereas the 1976 work showed no movement past the Forelands. This suggests that Upper Cook Inlet may also be an area of concern for oil impacts.

- 2) The Chugach Islands are impacted by trajectories from Site 5 and trajectories extend into the Gulf of Alaska from Sites 7 and 8A. These events, not seen in the 1976 study, suggest the possibility of exposure on the eastern side of the Kenai Peninsula as well as Kodiak Island.

The systematic perturbation analyses gave results that generally fall into two categories that can be defined by considering the shift in impact location resulting from the altered environmental conditions. One category, consisting of all perturbation trajectories impacting within 10 km of the corresponding base case, contains over 50 percent of all the perturbation case trajectories. This indicates that over half of the base case trajectory impact points would not be greatly affected by a 25 percent change in the environmental driving forces.

The remaining trajectories that had significantly different impact points from the base case generally correspond to cases where, for example, the base case trajectory impacted an island while the perturbation case did not and consequently took considerably longer to reach the shoreline. In these cases, the perturbation results should be interpreted to mean that the final impact point is sensitive to parameters defining the trajectory simulation case. These include not only the environmental forcing fields, but quantities such as the initial tidal current phase, wind drift angle, spill location, etc.

These results suggest that the spill scenarios investigated here can be evenly divided into two classes:

- 1) One class represents those cases where the simulation results are "stable," with respect to perturbations in the simulation parameters. Here, stable means small changes in the scenario result in small changes in the shoreline impact point.

- 2) The second class represents those "unstable" cases where small changes in the scenarios result in large changes in shoreline impact locations. These cases may require additional treatment of the environmental driving fields and advanced modeling methodologies to accurately predict the "real-world" behavior of an oil spill.

The random perturbation analyses generally reinforce the conclusions from the systematic analyses. That is, the random perturbations treated here do not significantly affect the base case results. However, there are cases where small, random deviations can lead to much larger changes in the shoreline impact distribution. These cases may require more sophisticated analysis to develop credible simulation results.

I. INTRODUCTION

PURPOSE

This study was initiated on request of the Outer Continental Shelf Environmental Assessment Program (OCSEAP) on behalf of the Bureau of Land Management. A previous oil spill trajectory analysis for Lower Cook Inlet was completed in March 1976 (Dames & Moore, 1976). That study provided information on probable shoreline impact areas and associated time to impact of hypothetical oil spills originating from 12 selected locations within Lower Cook Inlet. The results were based primarily on an oil spill trajectory model with winds, net, and tidal currents being the environmental driving forces.

The present study is an extension of the 1976 study in that the environmental data were updated to reflect more recent information and nine additional hypothetical spill locations in Lower Cook Inlet were investigated. This study also addressed certain questions regarding stochastic and deterministic aspects of the environmental data and their effects on the variability of the modeling results and conclusions drawn therefrom.

SCOPE

This study was conducted in accordance with the scope of work detailed in the Dames & Moore proposal, "Statement of Work, Oil Spill Analysis," RFX41-D&M-188, for National Oceanic and Atmospheric Administration, April 4, 1978 and "Revised Statement of Work, Oil Spill Trajectory Analysis," RFX41-D&M-346, June 1, 1978, and "Amendments to the Statement of Work, dated August 1, 1978, Oil Spill Trajectory Analysis," RFX41-D&M-346. In summary form, the primary elements of the scope of work presented in the above documents were as follows:

2. Trajectory Simulation: Calculate "base case" trajectories using the same overall approach employed in the 1976 study. Simulate spill trajectories from eight hypothetical spill sites specified by Outer Continental Shelf Environmental Assessment Program (OCSEAP), using a basic set of selected wind and current fields. Provide the point at which the trajectory intersects the shoreline, the time to impact and the probability of exposure for each site individually and all sites combined.
3. Environmental Data: Update the environmental input data base used in the 1976 study with data made available since the 1976 study.
4. Sensitivity Analysis: Perform a perturbation analysis on a limited number of base case trajectories in order to assess the effects of systematic and random fluctuations of the environmental data on the predicted shoreline impact distributions.

Section II contains an overview of the oil spill model used in this study and provides the general framework of the analytic approach used to determine shoreline exposure due to postulated oil spills at selected sites; details on the model itself are contained in Appendix A, Model Documentation. Similarly, details of the environmental input data are presented in Section III and a discussion of the methodology and results of the trajectory simulations follow in Section IV. Finally, based on the results of this study and their implications, recommendations for future studies are contained in Section V.

II. OIL SPILL MODEL

The physicochemical behavior and ultimate fate of oil spilled in the marine environment involve complex and, in most circumstances, poorly understood phenomena. In addition to the many oceanographic and meteorologic parameters of importance, characteristics of the oil itself play a major role in its transport and dispersion. In spite of the uncertainties associated with these parameters, several oil spill models have been developed that provide valuable information for contingency planning, environmental impact assessment, etc. The variety of simulation techniques and models that exist reflect, in part, the embryonic state-of-the-art and the range of modeling applications.

Reviews of generic approaches to oil spill modeling as well as selected oil spill models have been recently published (Fallah and Stark, 1976; Oceanographic Institute of Washington, 1977). These reviews focused on descriptions of the relevant physical processes, procedures for their simulation, and the uses and limitations of the various models. In general, these assessments indicate that present oil spill modeling efforts are limited by a meager understanding of the basic phenomena and the difficulties associated with accurately specifying the dominant environmental driving forces over a large area, such as Lower Cook Inlet.

For this study, trajectory simulation was used to track the centroid of a two-dimensional surface oil slick. Although the model has the capability to include surface spreading of a slick, this was not incorporated in the present study for several reasons. Since the ultimate extent of a surface slick depends strongly on spill volume, the absence of a comprehensive risk assessment defining appropriate spill sizes (most probable, maximum credible, worst-case, etc.) precluded the consideration of surface spreading. Secondly, the wind and current data bases available or anticipated at the outset of this effort were not sufficiently well defined to justify the use of more refined simulation techniques. These expectations have been fulfilled with a few notable exceptions; significant gaps in the environmental data bases do, in fact, remain to be filled. These are discussed in greater detail in Section III.

Consistent with the trajectory simulation approach, (neglecting the effects of spreading), other physicochemical processes affecting a marine oil spill have not been considered. These include evaporation, sinking, dissolution, emulsification, etc. While these processes may play important roles in determining the ultimate fate of an oil spill, they were assumed to be secondary to the primary surface transport mechanisms.

Movement of the spill centroid in the Dames & Moore model is considered to be governed by the independent effects of wind and water currents. Second-order forces such as waves and wind-wave-current interaction are neglected. The wind-induced velocity vector of the centroid is taken to be colinear with the wind vector and proportional to the wind speed. This "wind factor" has been experimentally found in the range from 1 to 5 percent (Oceanographic Institute of Washington, 1977) and is taken to be 3 percent for this study. There is some question as to whether the wind and slick vectors should be colinear due to the considerable scatter in relevant field data. However, the evidence is not conclusive on this issue and, hence, this study assumes colinearity.

The slick centroid is modeled to move at the same instantaneous velocity as the underlying current, neglecting the wind-driven component. As with the wind-driven component, there is no conclusive set of evidence which documents that this is the best approach. However, alternative schemes (i.e., Schwartzberg, 1971) have major flaws or have been subjected to limited validation.

For this study, the current field was divided into two components, a net surface component and a tidal component. Hence, the centroidal velocity vector can be written as:

$$\bar{U}_{oil} = 0.03 \bar{U}_{wind} + \bar{U}_{tidal} + \bar{U}_{net} \quad (1)$$

Using this basic model, both deterministic and probabilistic simulations have been run. In both the base case and systematic perturbation

analyses, deterministic wind and current fields are used to describe unique trajectories from each postulated spill site. These deterministic trajectories provide time to shoreline impact and, when combined with the annual average probability of the wind patterns, yield an average annual probability of exposure to an oil spill from any site.

The stochastic analyses were based on a knowledge of both the mean and standard deviation of the net surface current speeds at certain data measurement locations. Hence, a randomly selected vector was added to the deterministic net circulation field based on a Gaussian distribution with mean zero and known standard deviation. The resultant distribution of impact points provides a measure of the effect of variations in the net surface circulation field.

Operational implementation of the oil spill model is based on a grid system that overlaps the area of interest as illustrated in Figure 1. The grid system serves multiple purposes: 1) definition of the Cook Inlet geometry, 2) input of wind and current information, and 3) definition of shoreline impact locations. With the input available to the model, a trajectory is generated by evaluating Equation (1) over a sequence of finite time steps until the centroid reaches a boundary or exceeds an upper limit on time. Subsequent analyses are based on the trajectory termination point and, in a more subjective manner, on the nature of the trajectory itself.

NOTE:
 GRID
 NETWORK
 OUTLINED
 FOR EVERY
 FIFTH GRID
 INTERVAL

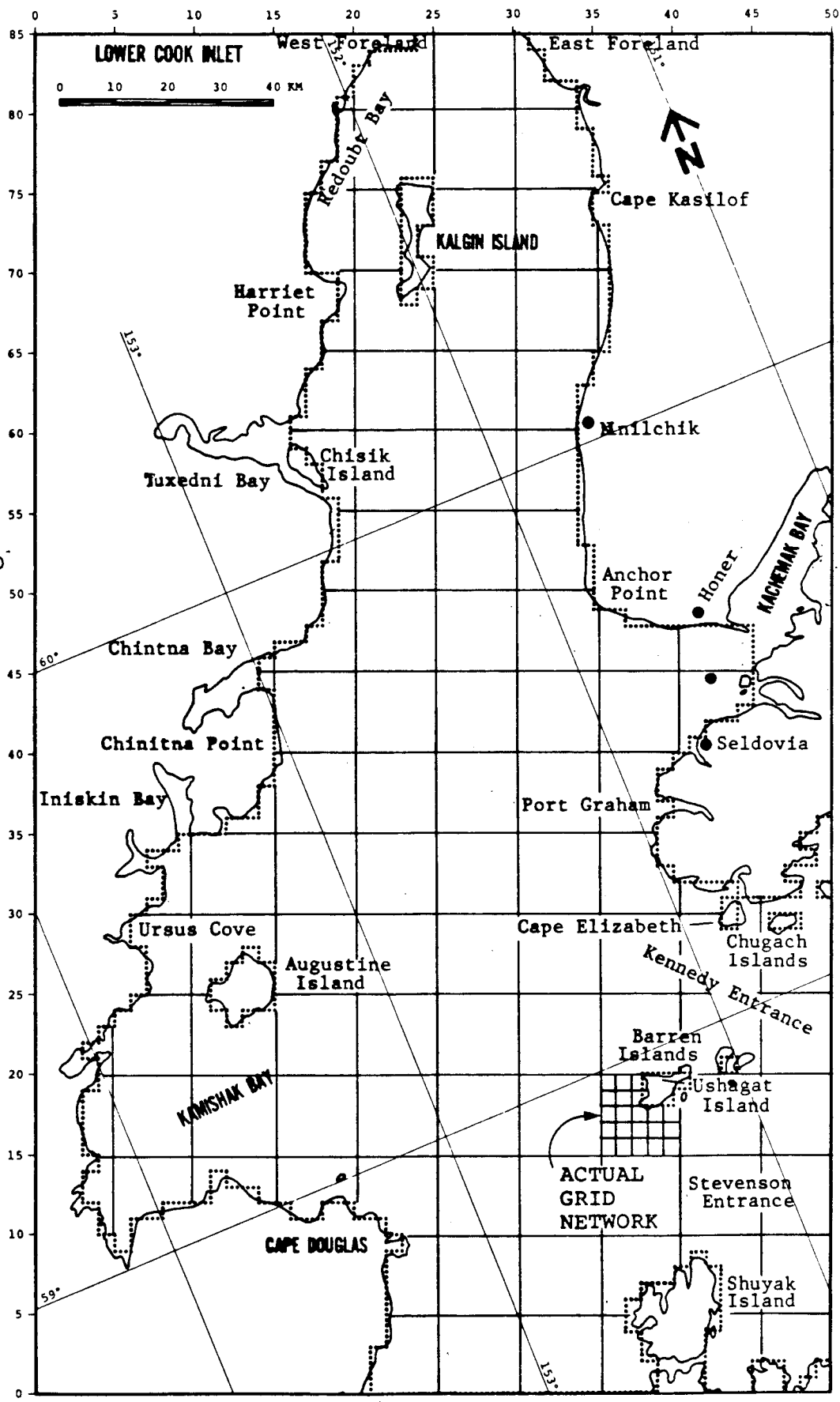


FIGURE 1: GRID SYSTEM

III. INPUT DATA PREPARATION

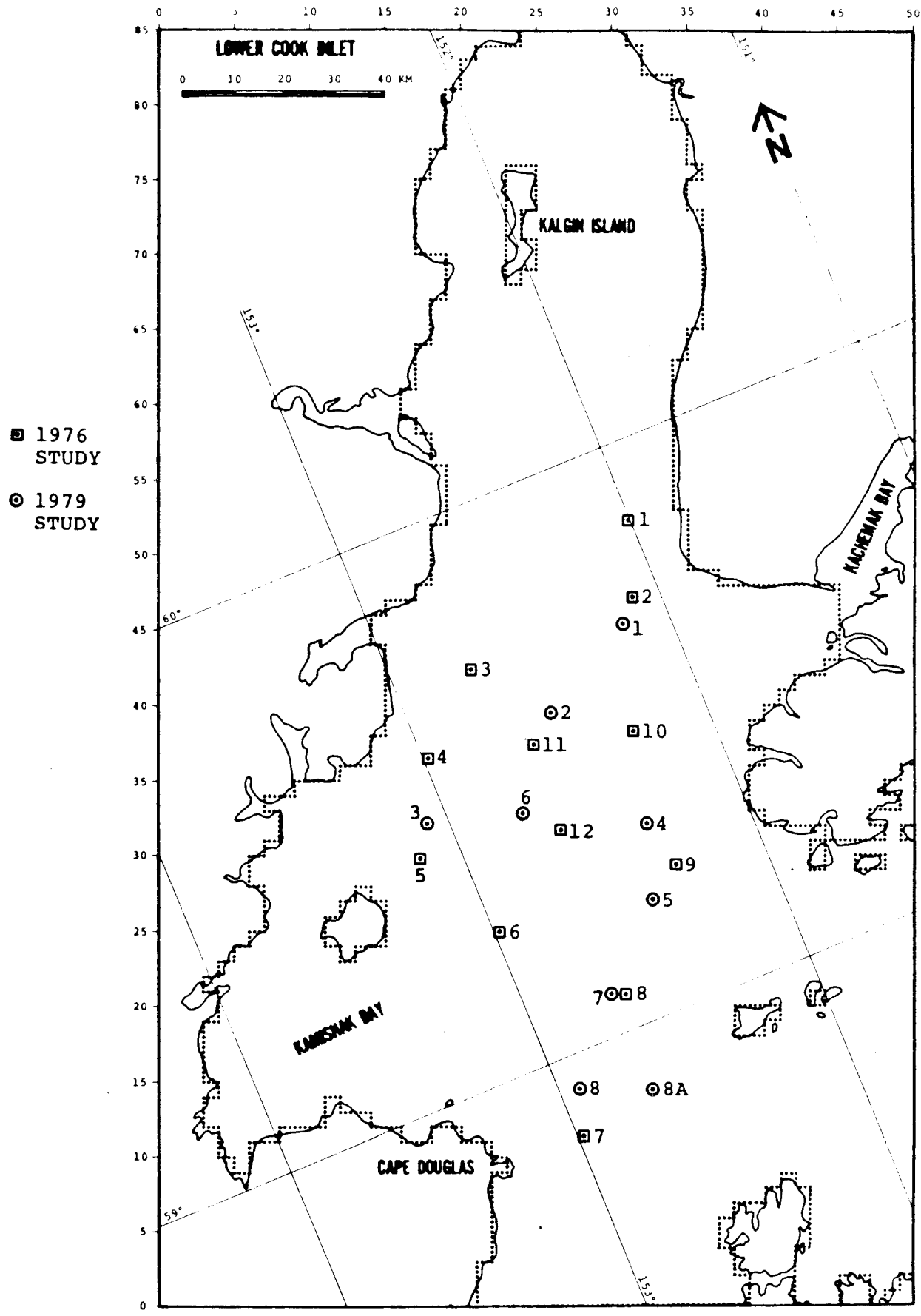
A. OIL SPILL SCENARIOS

The 1976 oil spill study evaluated the coastal exposure in terms of probabilities and times to impact from 12 postulated oil spill sites in Lower Cook Inlet. These 12 sites were selected as representative of areas where possible exploratory drilling would occur. In the present study, eight alternative sites were selected by the Bering Sea-Gulf of Alaska Project Office of OCSEAP to represent areas of more recently leased tracts and probable pipeline locations not evaluated in the 1976 study. Figure 2 shows the locations of the 12 hypothetical oil spill sites evaluated in the 1976 study and nine spill sites evaluated in the present study (one additional site was added by Dames & Moore to the original eight prescribed by OCSEAP).

Scenarios for potential oil spills at these locations were evaluated without consideration for volume or rate of release of oil. Further, all sites were treated independently, and the probability of a spill occurring at any location was considered equal. Based on these assumptions, the estimated time to impact and the probability of exposure for the coastal regions of Lower Cook Inlet were determined.

The 1976 study utilized existing information on the meteorologic and oceanographic conditions within Lower Cook Inlet. The present study has updated the meteorologic and oceanographic data using sources of information that have become available since the 1976 study. In addition, certain refinements were made to the analysis and interpolation of input data.

At each spill site, a separate centroidal trajectory was calculated for 32 postulated environmental events. These events were composed of eight wind patterns, a tidal current pattern (with spills occurring at four separate phases of the tide), and a net current pattern. Thus, the set of base case oil spill trajectories for the present study represented a



462 **FIGURE 2: POSTULATED OIL SPILL SITES**

total of 288 postulated spills. In addition, systematic variations on these base cases were run at Sites 1 and 7 for wind and net current fields having the same pattern (direction field) but with speeds ± 25 percent of the base cases. Site 3 was also investigated for a single systematic variation of the wind fields with speeds reduced by 25 percent of the base cases. Since the perturbation trajectories were initiated at a single phase of the tidal current cycle, a total of 72 systematic perturbation runs were made. Finally, a set of random perturbation cases was run at Site 7 for wind fields Nos. 1, 2, and 7. A total of 18 individual trajectories were computed for each wind field at one phase of the tidal cycle; hence, 54 random perturbation runs were made.

B. GRID SYSTEM

The grid system illustrated in Figure 1 was used as the framework to input both wind and current data as well as to define the geometry of Lower Cook Inlet itself. This grid system was oriented along the main axis of Cook Inlet with each cell being 3 km on a side. Characteristic features of the Inlet required by the model such as land and water areas and open water boundaries, were prescribed by assigning to each cell an index that defines the predominant feature of that cell. Land boundaries were chosen to represent the "best" approximation of the geometric extent of the inlet. The input data file defining the land and water areas and the open water boundaries is presented in Appendix D.

Note in Figure 1 that several bays were delimited from the main body of water within Lower Cook Inlet by "water boundary" cells. Within these bays, the detailed nature of the wind and surface current fields are not sufficiently well known to permit an accurate simulation of spill movement. For those cases where the trajectory intersected one of these boundary cells, the trajectory was terminated and it was concluded that oil would have, in fact, entered the bay, but its subsequent behavior was not determined.

C. OCEANOGRAPHIC AND METEOROLOGIC INPUT DATA

GENERAL

The model used to simulate the centroidal trajectory of hypothetical oil spills in Lower Cook Inlet presumes that the oceanographic and meteorologic fields are the primary driving forces. The meteorologic inputs were surface wind speed and direction, and the oceanographic inputs were tidal and net surface currents. The primary effort in this phase of the study was to review and upgrade the data bases used in the 1976 study with data that had subsequently become available. During the review process several areas of improvement were made in the quality of the input data as well as the assumptions involved in deriving the spatial and temporal distributions of the input data fields. The improvements and results are discussed in the following sections.

METEOROLOGIC DATA

The meteorologic input data used in the 1976 study were representative surface wind patterns developed from historical data. Eight wind patterns were developed based on the work of Putnins (1966 and 1969) and used as input to the oil spill model. For a discussion of the development of the eight wind patterns see Dames & Moore, 1976. Each wind pattern represented a spatial distribution of wind speed and direction over Lower Cook Inlet and was held constant with time during the trajectory simulation. With respect to assumptions imposed on the modeling effort, the treatment of the wind fields as constant with time may be the most limiting factor in the input data. This is due to the fact that, based on the results from the 1976 study, the winds were the major driving force in the trajectory movement. While recognizing this limitation in the input data, it was agreed that a similar treatment of the wind fields would be followed in the present study.

A review of the wind fields utilized in the 1976 study was conducted by Dames & Moore's meteorologists in Anchorage. This review was partially

based on a comparison of the 1976 wind fields with data taken from the semi-submersible drilling platform Ocean Ranger operating in Lower Cook Inlet approximately 40 miles southwest of Homer from June through September 1977. This information indicated that the wind speeds used in the 1976 study were essentially representative. However, the wind directions could not be refuted or confirmed by the 1977 data. In addition, a review of the literature available since 1976 did not uncover any significant additions to the knowledge of Lower Cook Inlet meteorology. Thus, based on this limited review, the wind patterns used in the 1976 study were retained for use in the present study.

Due to the extension of the grid system to cover the more southerly portion of Lower Cook Inlet, the wind fields were extended (manually) to provide the required coverage over this area. All wind fields were re-digitized to conform to the format of the shifted grid system with wind speed and direction specified at every third grid point. The input data files for all eight wind fields are presented in Appendix D.

The resulting wind fields are shown in Figures 3 to 7. Table 1 provides the frequency of occurrence for each of the eight wind patterns for the months of January, April, July, and October, plus the annual frequency.

OCEANOGRAPHIC DATA

Since the model simulates the centroidal trajectory of a surface oil spill, only those parameters that control and affect movement of the water surface were utilized in the simulation. As previously indicated in Section II, the simulation involved in this study neglects the effects of waves and wind-wave interaction directly, but assumes these mechanisms are included and represented in a simplified manner in the treatment of the wind-induced surface currents.

In the absence of any wind drift current component, surface currents in Lower Cook Inlet can be assumed to be comprised of two components: a net

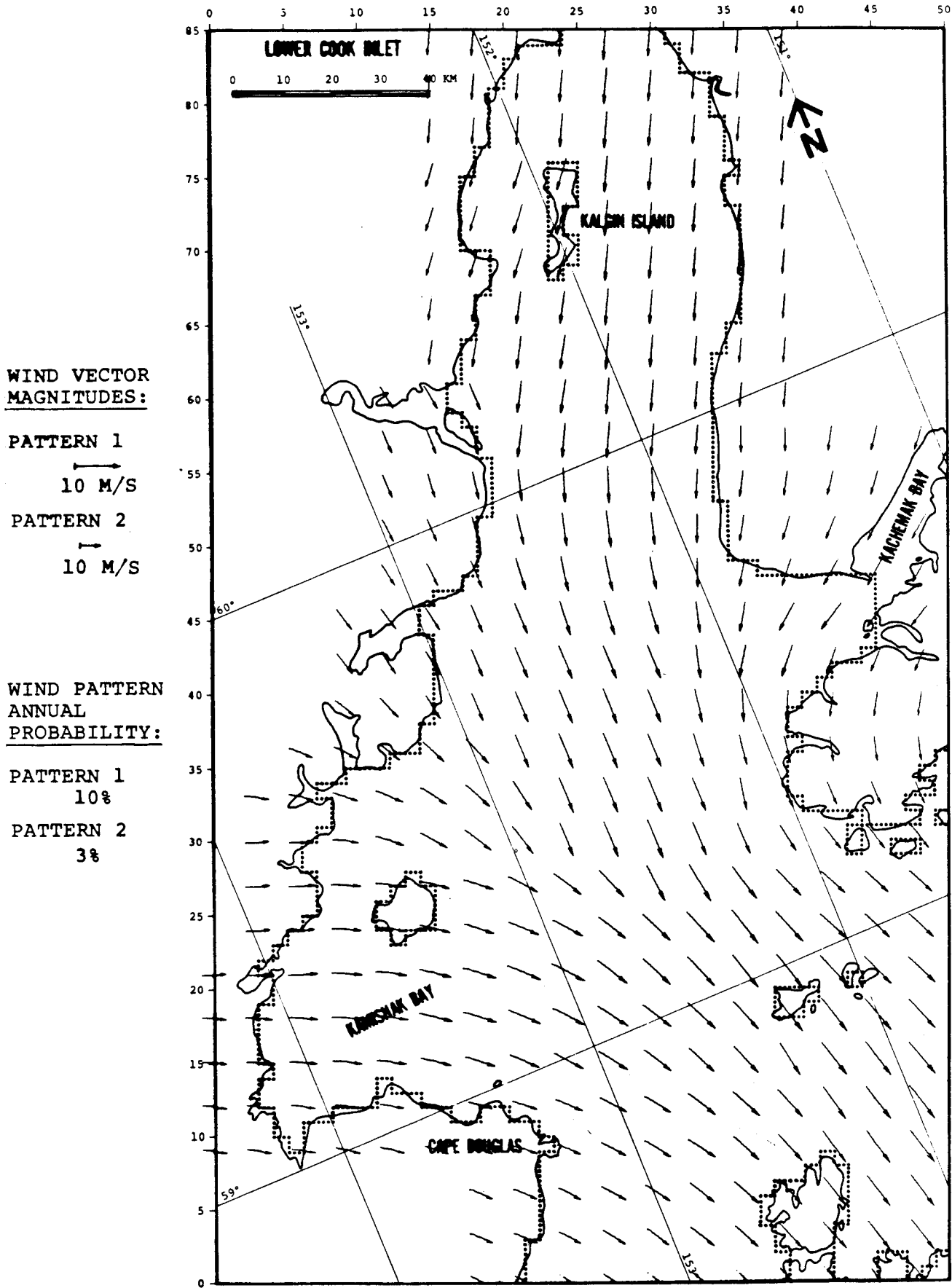


FIGURE 3: WIND PATTERNS 1 AND 2

WIND VECTOR
MAGNITUDES:

PATTERN 3

→
10 M/S

PATTERN 4

→
10 M/S

WIND PATTERN
ANNUAL
PROBABLIITY:

PATTERN 3
17%

PATTERN 4
6%

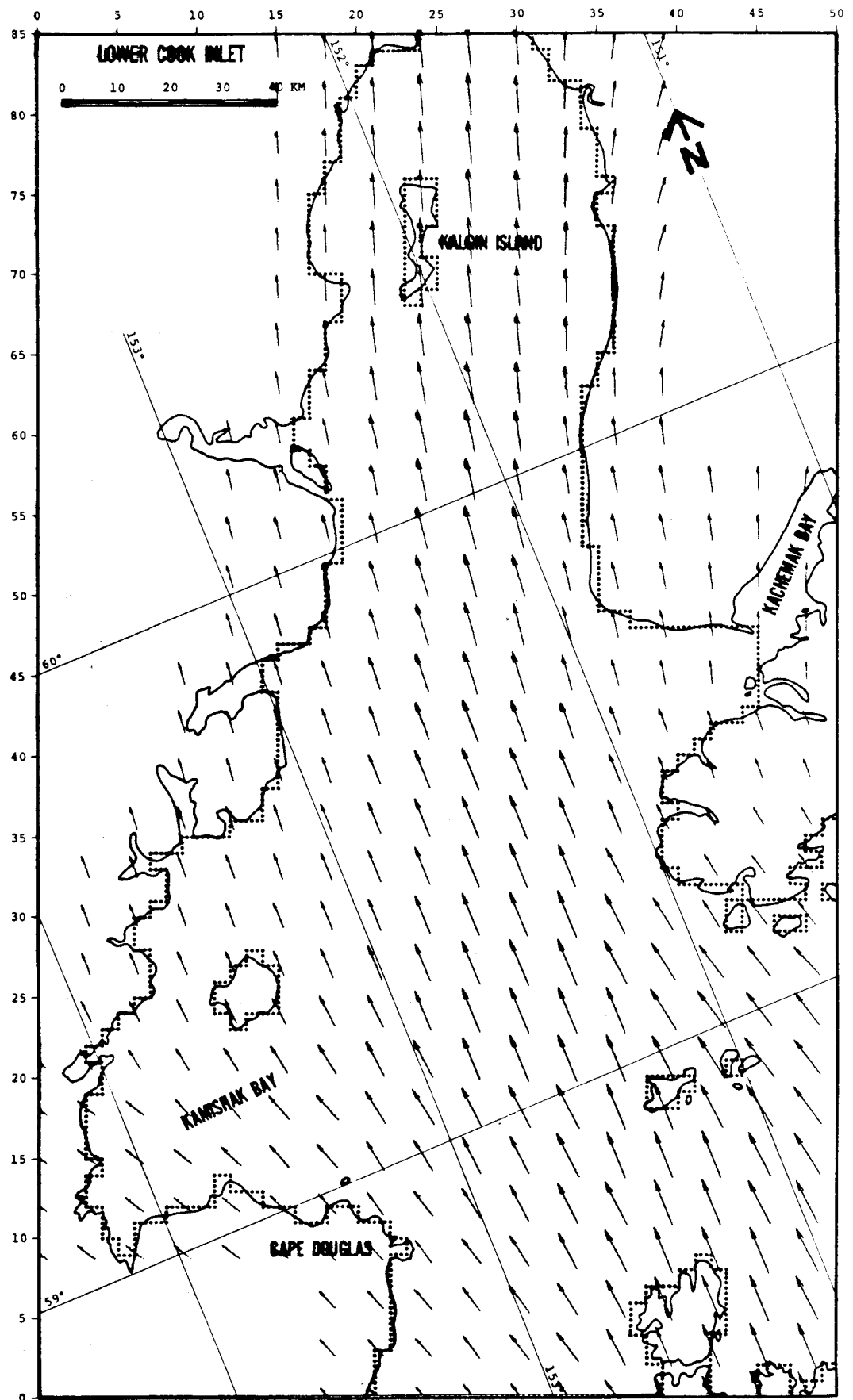


FIGURE 4: WIND PATTERNS 3 AND 4

**WIND VECTOR
MAGNITUDES:**

PATTERN 5
→
10 M/S

PATTERN 6
→
10 M/S

**WIND PATTERN
ANNUAL
PROBABILITY:**

PATTERN 5
3%

PATTERN 6
1%

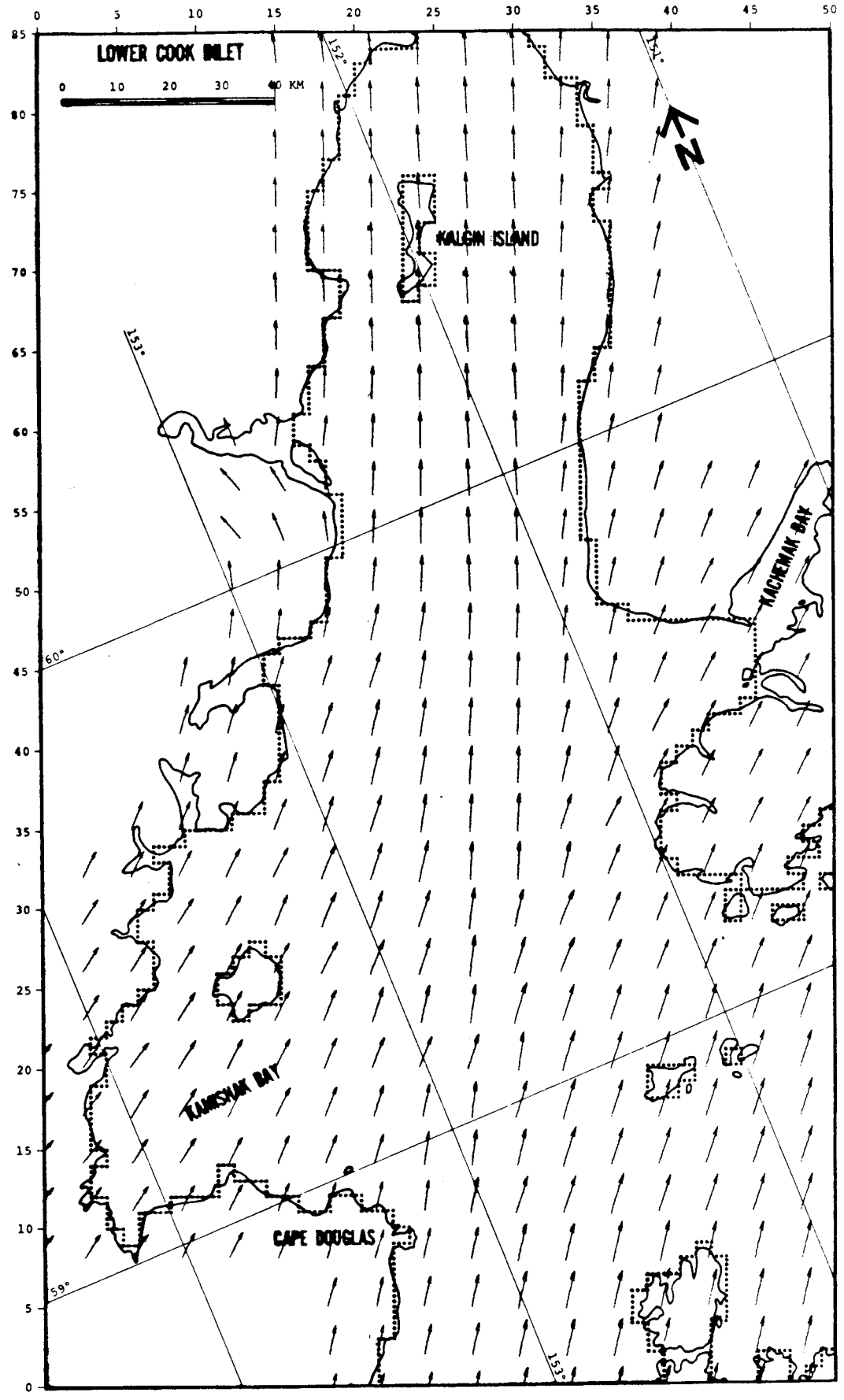


FIGURE 5: WIND PATTERNS 5 & 6

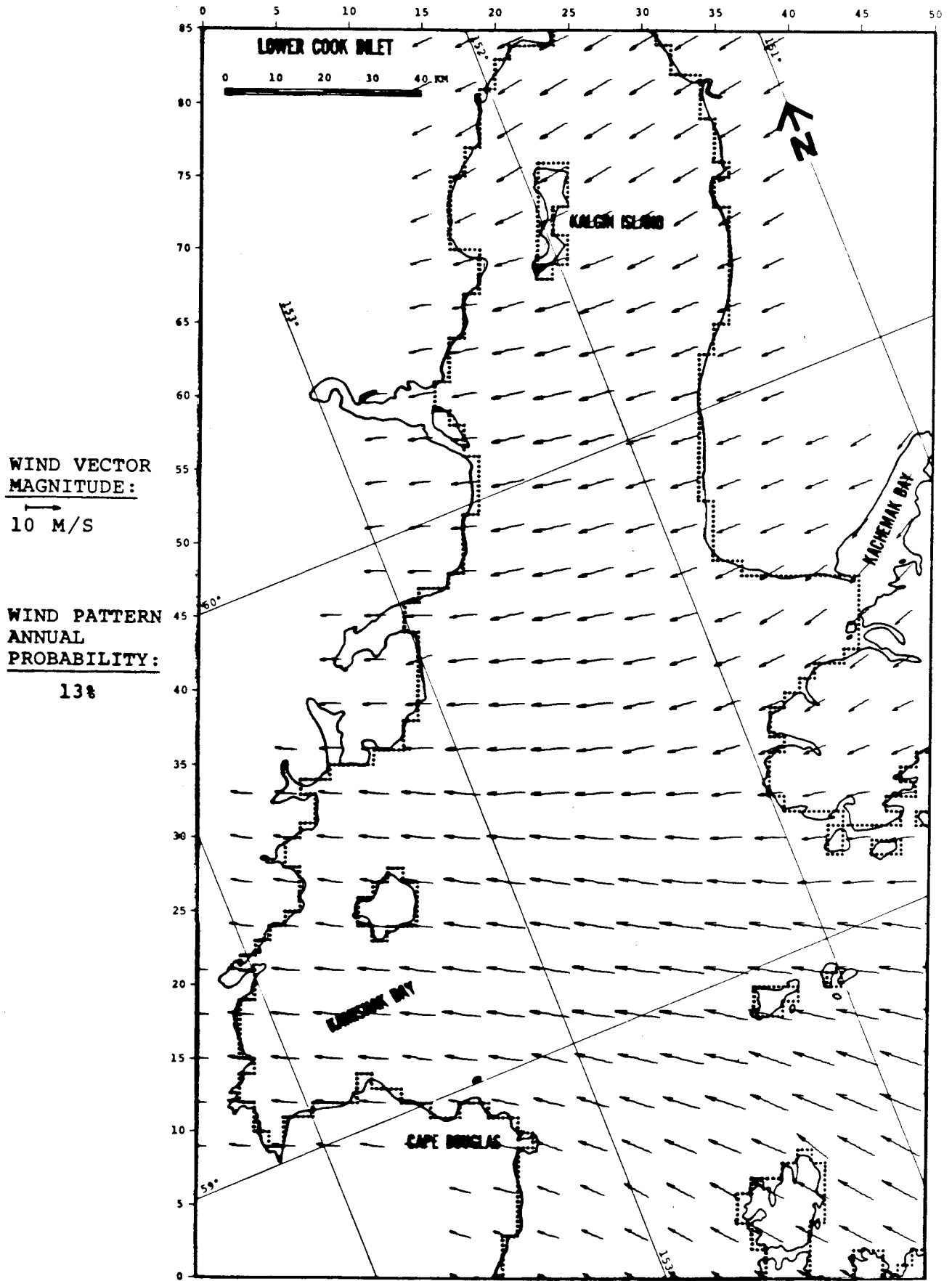


FIGURE 6: WIND PATTERN 7

WIND VECTOR
MAGNITUDE:
→
10 M/S

WIND PATTERN
ANNUAL
PROBABILITY:
15%

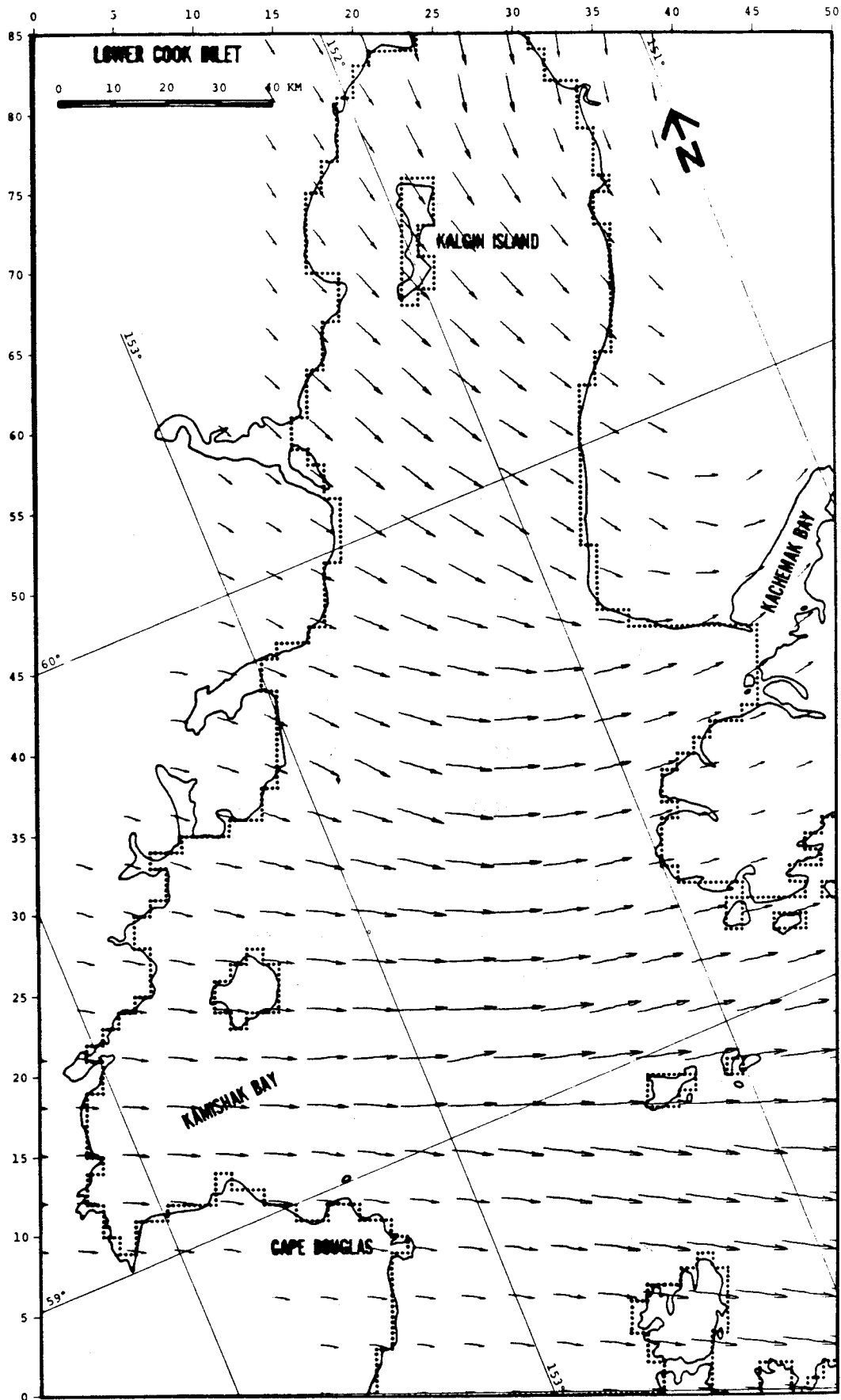


FIGURE 7: WIND PATTERN 8

TABLE 1

DIRECTION, SPEED, AND FREQUENCY OF EIGHT WIND PATTERNS

Pattern	Direction ^a	Speed ^b (knots)	Frequency (percent)				
			Jan	Apr	Jul	Oct	Annual
1	N	16-26	12	14	4	8	10
2	N	32-52	4	5	1	3	3
3	SE	10-25	15	12	26	10	17
4	SE	20-50	5	4	9	3	6
5	SW	11-16	0	2	7	3	3
6	SW	22-32	0	1	2	1	1
7	E	12-22	22	12	5	12	13
8	NW	11-27	<u>7</u>	<u>17</u>	<u>12</u>	<u>24</u>	<u>15</u>
Total Frequency			67	65	67	65	66

^aLower Cook Inlet--vicinity of Barren Islands

^bAnnual mean speed range

surface circulation component, and a tidally induced surface current component. The net circulation component was assumed to remain constant in time, while the tidal current component was phased with the tide and with location within Lower Cook Inlet.

The following sections provide details on the derivation and input of the net surface circulation and tidal current components.

NET SURFACE CIRCUCLATION

The net surface ciruclation pattern developed for the 1976 study was primarily based on previously published information contained in Burbank (1974) and Alaska Department of Fish and Game (ADF&G) (1975). In the 1976 study, the magnitude of the net circulation was estimated from the ADF&G work in Kachemak Bay and from the differences in average maximum flood and ebb tide currents measured by NOAA in Lower Cook Inlet. Adjustments to the data were made based on judgment and subjective interpretations.

Although it is generally agreed that surface circulation within Lower Cook Inlet is still not well defined, improvements to the 1976 circulation pattern have been obtained by utilization of data recently made available from the data sources described below:

PMEL Current Measurements - Mean currents at a 20-meter depth (below MLLW) at five locations in Lower Cook Inlet (see Figure 8). The duration of measurements ranged from 156 to 185 days during the months from May to October 1977.

NOS Current Measurements - Mean currents at a 6.7-meter depth (below MLLW) at 21 locations in Lower Cook Inlet (see Figure 8). The duration of measurements ranged from 5 to 60 days during the months from May to August 1973.

In addition, use was made of Meunch et al. (1977) and Burbank (1977) to delineate current patterns between the above current stations.

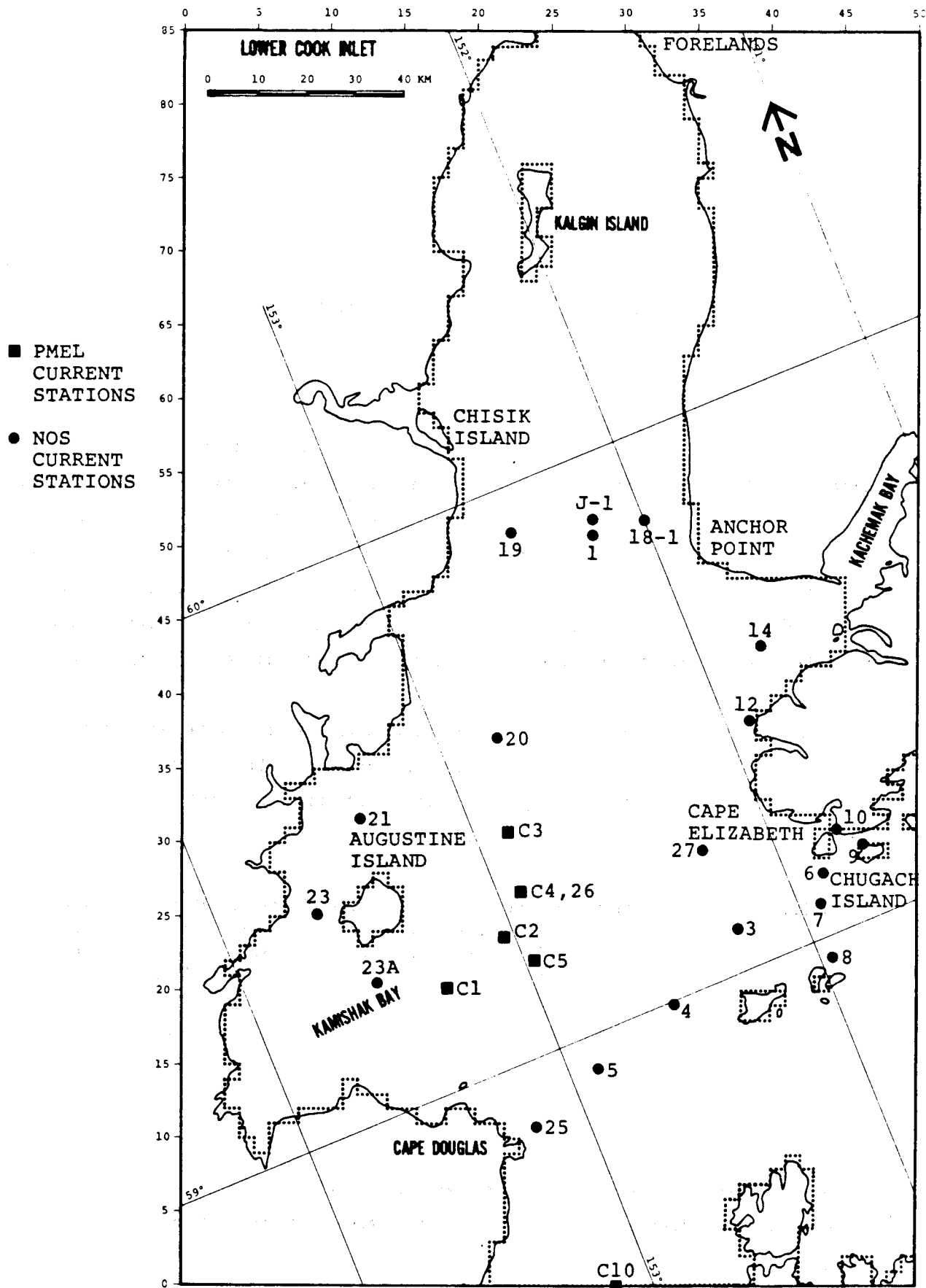


FIGURE 8: CURRENT METER STATION LOCATION

It should be pointed out that the circulation pattern derived from the use of these data is actually representative of average circulation conditions occurring during the summer months. Both the PMEL and NOS data were taken within the 6-month period from May to October. Therefore, the seasonal variations that would occur during the winter months are not included in the current measurement data. It can be hypothesized that during the summer months, surface circulation would be stronger and assume a different pattern than during winter months, due to the high runoff from snowmelt. Changes in seasonal circulation patterns, however, are not known nor easily estimated from presently available data.

Summary forms of the current data obtained from PMEL included data listings, current vector plots, and current histograms. The data represent 35-hour low pass, filtered mean currents. A summary of the data for those stations and depths used in this effort is presented in Table 2. Figure 8 shows the location of the current stations in relation to Lower Cook Inlet. It can be seen from Table 2 that the NOS current measurements were taken at a depth of 6.7 meters below MLLW and thus are not truly representative of surface current conditions. However, measurements taken at this depth will not respond to significant portions of the wind drift component that would be highly reflected in surface current measurements. This is important in that the wind drift surface current is handled separately in the model. The PMEL current measurements shown in Table 2 were taken at a depth of 20 meters. These are less representative of surface currents than the NOS measurements, but presently provide the best available data for estimating the net surface circulation in the complex central portion of Lower Cook Inlet between Augustine Island and Cape Elizabeth.

Figure 8 shows that the available current measurements cover that portion of Lower Cook Inlet from a line between Cape Douglas and Chugach Island northward to a line between Anchor Point and Chisik Island. Farther northward to the area of the Forelands, current measurement data were not available. NOS has taken extensive current measurements in that area from May through September 1974, however, summaries of the data were not

TABLE 2

PMEL AND NOS NET CURRENT DATA

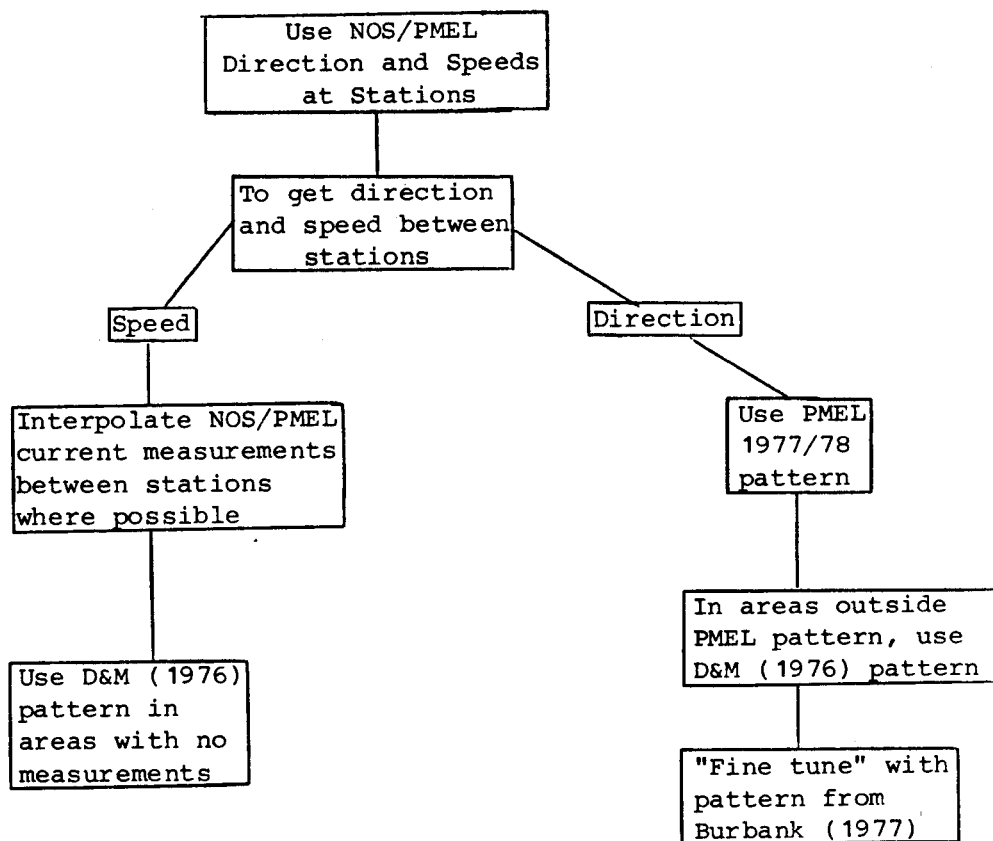
Station	Net Speed (cm/sec)	Net Direction (° North)	Standard Deviation		Station Depth	Measurement Duration	Installation Date
	\bar{u}	θ	(cm/sec) $\sigma_{\parallel}(1)$	(cm/sec) $\sigma_{\perp}(2)$	(m) Z	(days)	(m/d/y)
PMEL							
C1	15.92	201	10.07	4.71	20.0	156.3	5/10/77
C2	8.02	229	10.62	4.41	20.0	125.0	6/10/77
C3	8.17	238	6.08	3.40	20.0	155.0	6/10/77
C4	3.25	278	8.70	6.56	20.0	155.3	6/10/77
C5	20.70	251	14.49	8.75	20.0	155.3	6/10/77
C10	27.77	230	21.47	10.49	20.0	155.0	5/10/77
NOS							
1	3.08	268	4.03	5.41	6.7	59.6	6/16/73
J-1	3.68	295	4.50	4.15	6.7	24.8	5/8/73
3	23.16	291	10.28	11.00	6.7	27.0	6/23/73
4	2.12	118	11.39	9.63	6.7	25.5	7/21/73
5	4.43	231	12.97	11.06	6.7	23.0	7/10/73
6	12.66	282	8.71	7.88	6.7	26.8	7/21/73
7	4.17	232	7.49	4.34	6.7	11.3	8/22/73
8	12.62	147	10.73	7.91	6.7	10.3	8/10/73
9	14.01	276	14.52	9.49	6.7	12.0	6/22/73
10	14.13	74	2.95	3.74	6.7	10.0	7/2/73
12	4.97	331	2.82	17.47	6.7	11.5	8/27/73
14	5.74	190	1.55	2.06	6.7	12.0	6/5/73
18-1	9.46	39	3.28	1.29	6.7	20.3	5/22/73
19	13.20	66	3.06	2.13	6.7	26.0	5/21/73
20	4.94	30	1.77	2.90	6.7	5.8	5/18/73
21	4.33	217	2.42	4.05	6.7	6.3	8/6/73
22	8.37	210	8.36	3.61	6.7	12.5	8/23/73
23	6.90	264	1.16	1.19	6.7	4.5	7/27/73
25	62.80	166	16.96	4.88	6.7	10.3	7/25/73
26	1.91	243	20.97	15.31	6.7	13.5	8/23/73
27	2.21	355	7.18	7.51	6.7	27.0	6/18/73

(1) σ_{\parallel} : Standard deviation in direction of net current.

(2) σ_{\perp} : Standard deviation perpendicular to direction of net current.

available for this study. Therefore, the net surface circulation in this portion of Lower Cook Inlet was estimated without the benefit of current meter measurements; the net surface circulation input data for this region is, at best, a rough estimate.

Using the above data sources the net surface circulation pattern in Lower Cook Inlet was updated from that presented in the 1976 study utilizing the following approach:



Departures from the above approach were made in order to ignore the vortex currents presented by Burbank (1977), and to discount the results of Station 20 (NOS data) due to the short duration (6 days) of measurement (Pearson and Muench, 1978). Stations 19 and 20 indicate northerly flow along the western portion of Lower Cook Inlet. Due to lack of data, there

is no general agreement as to the net surface circulation above Station 19. However, a northerly surface current is possible due to the southerly extending shoal below Kalgin Island that may effectively separate flow.

Figure 9 shows the updated net current pattern that was developed using the above approach and the previously defined sources of data. To establish some measure of reliability in the interpretation and interpolation of the data, two independent investigators developed net circulation patterns and their results compared. Close agreement was obtained among the major features of the circulation patterns. Minor differences were resolved through further interpretation of the data.

This pattern was reviewed by PMEL on October 18, 1978 and based on their comments, minor revisions were made to current speeds at selected locations. Once agreement was attained regarding the pattern shown in Figure 9, the model grid was overlaid and the net current speed and direction were read off or interpolated at every other grid point. A vector plot of the interpolated net current input data is shown in Figure 10 and the input data file is presented in Appendix D.

TIDAL CURRENTS

The tidal currents developed for the 1976 study were based on preliminary results of the 1973 NOS current measurements for the southerly portion of Lower Cook Inlet and personal communication with Mr. Muirhead of the Oceanographic Division of the National Ocean Survey for selected peak values of the 1974 NOS current measurements for the northerly portion of Lower Cook Inlet. At that time, harmonic analyses of the tidal current measurements were not available. The change of phase of tidal currents throughout Lower Cook Inlet was not considered in the 1976 study.

In updating the tidal current data from the 1976 study, several areas of improvement were obtained. First, harmonic analyses were available for not only the 1973 NOS current data but also for current measurement data taken by PMEL in 1977. (Neither harmonic analyses nor summary results were

- NOTE:
- DIRECTION OF CURRENT GIVEN BY ARROWS
 - SPEED OF CURRENT GIVEN IN (KM/HR) NEXT TO ARROW

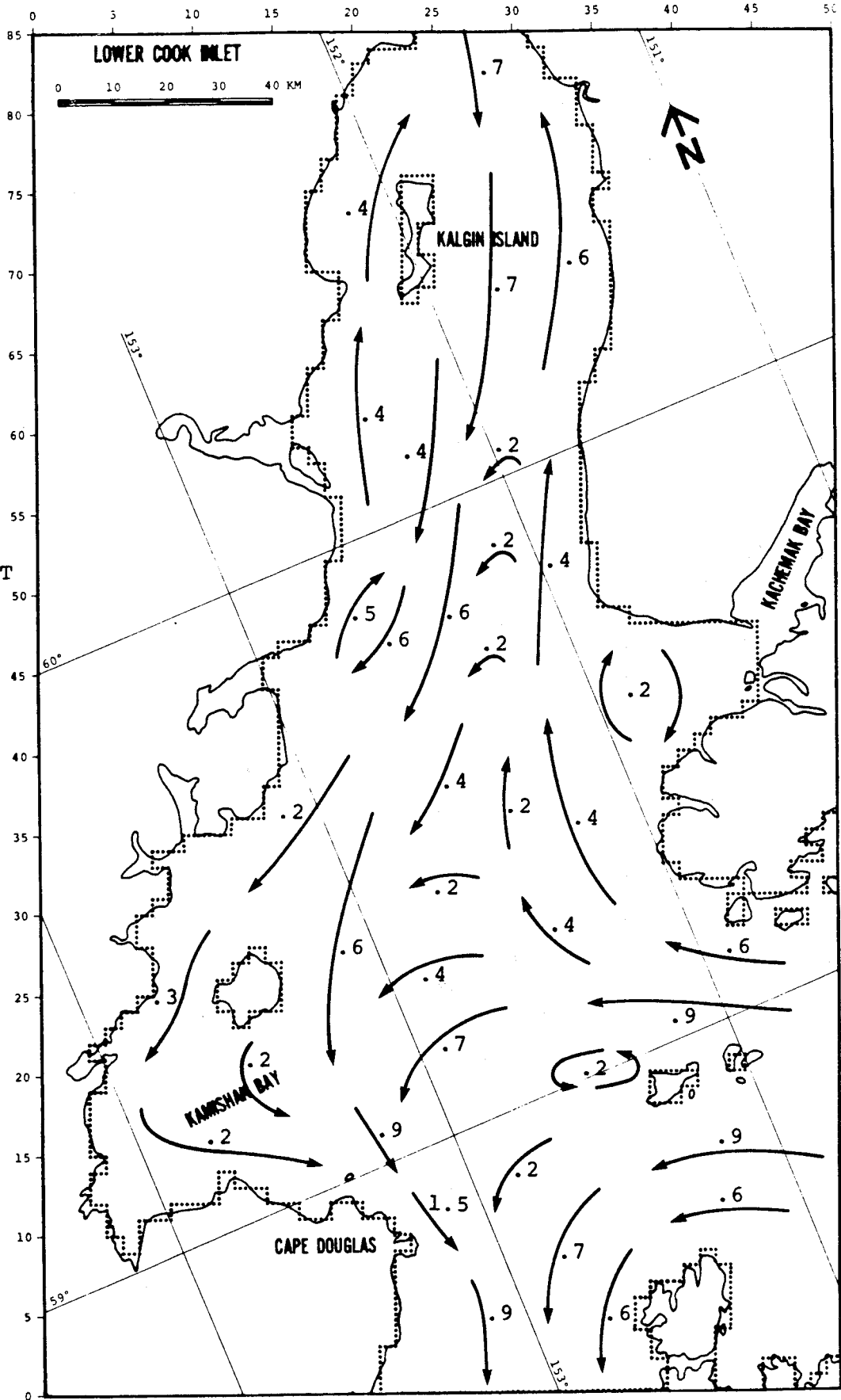


FIGURE 9: NET CURRENT PATTERN

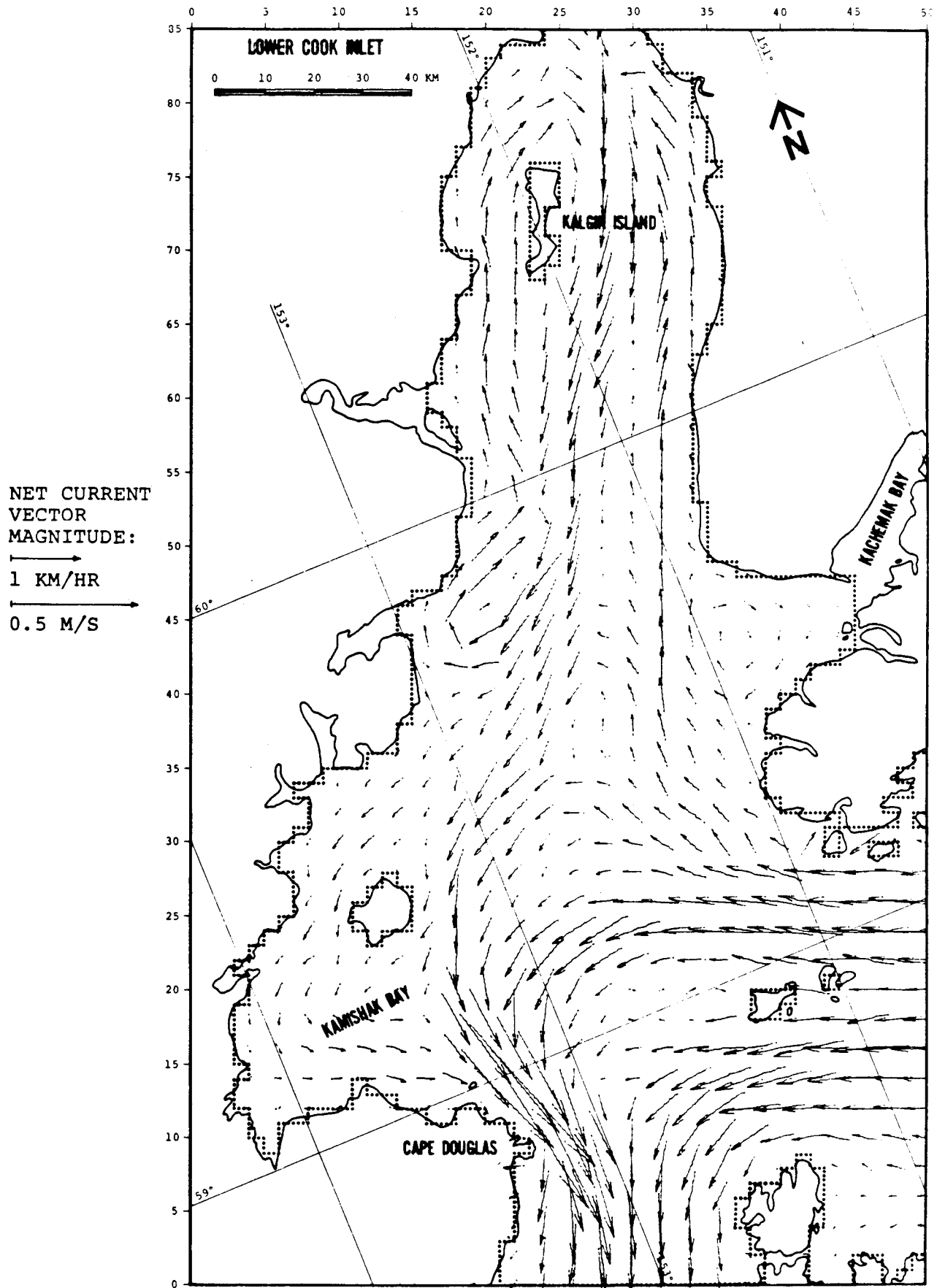


FIGURE 10: DIGITIZED NET CURRENT PATTERN

available for the 1974 NOS data (Muirhead, 1978)). Secondly, because harmonic analyses were available it was possible to compare measured results with results predicted from a hydrodynamic model of Cook Inlet (Mungall, 1978). If the comparisons were favorable, more confidence could be placed on the results of the hydrodynamic model, which, because of its ability to provide more detailed information on tidal currents, could be used to assess the spatial distribution of tidal currents in Lower Cook Inlet. Thirdly, the phasing of tidal currents within Lower Cook Inlet could be easily estimated from the hydrodynamic model and measurements, thus permitting a more realistic treatment of tidal currents.

The tidal current data were provided by PMEL in three basic formats. These were plots of the M2 tidal current ellipses, computer printouts of the east and north tidal current components of the M2 constituent with corresponding phase relationships, and listing of the tidal current harmonic components for the O1, K1, N2, M2, and S2 constituents. The above data were made available for the stations and depths presented in Table 3. Also included in Table 3 are the summarized data that were utilized in this analysis.

A review of the data revealed that tidal currents exhibit a large range of characteristics within Lower Cook Inlet. Rotary-type tidal currents (M2 constituent) were found to exist at PMEL Stations C1, C4, C5, C10, and NOS Stations 3 and 27. NOS Stations 1, 4, 6, and 19 exhibited more of a reversing type of current (M2 constituent) than a rotary-type current.

The direction of major axis and magnitude of the current speed varied widely throughout Lower Cook Inlet. The largest magnitudes occur in the eastern portion of the inlet, presumably due to the larger tidal ranges caused by the Coriolis affect within Cook Inlet. The lowest magnitudes occur in the southern and west-central areas of Lower Cook Inlet. No harmonic analyses of tidal current data were obtained for Lower Cook Inlet north of Anchor Point. Harmonic analysis of the current measurements taken in northern Lower Cook Inlet during 1974 will reportedly be available late in 1979 or early in 1980 (Muirhead, 1978).

TABLE 3

PMEL AND NOS TIDAL CURRENT DATA

Station	Constituent	East		North		Major Axis			Minor Axis	
		H (cm/s)	G°	H (cm/s)	G°	θ	H (cm/s)	G°	H (cm/s)	Rotation
PMEL C1	O1	2.7	296	3.6	203	354	3.6	199	2.6	C
	K1	4.4	352	5.9	259	354	5.9	255	4.4	C
	N2	4.6	55	4.7	298	317	5.6	269	3.4	C
	M2	29.4	57	30.4	300	317	36.1	271	22.1	C
	S2	11.5	93	11.9	336	317	14.1	307	8.6	C
PMEL C4	O1	2.1	254	5.2	183	9	5.3	186	2.0	C
	K1	3.5	310	8.6	239	9	8.7	242	3.2	C
	N2	3.0	36	7.3	298	356	7.3	296	3.0	C
	M2	19.4	38	46.8	300	356	46.9	298	19.2	C
	S2	7.6	74	18.4	336	356	18.4	334	7.5	C
PEML C5	O1	2.2	349	3.6	180	329	4.2	177	0.4	C
	K1	3.6	45	6.0	236	329	7.0	233	0.6	C
	N2	2.8	97	4.4	309	329	5.0	301	1.3	C
	M2	17.9	99	28.1	311	329	32.3	303	8.2	C
	S2	7.0	136	11.0	353	329	12.6	339	3.2	C
PMEL C10	O1	1.9	40	1.9	213	315	2.7	216	0.2	CC
	K1	3.1	96	3.1	269	315	4.4	272	0.3	CC
	N2	1.1	59	1.7	1	26	1.8	14	0.9	C
	M2	7.2	61	10.7	3	26	11.6	16	5.6	C
	S2	2.8	97	4.1	39	26	4.5	52	2.2	C
NOS 1	O1	1.4	45	13.0	202					
	K1	0.3	5	21.2	221					
	N2	3.2	15	25.9	283					
	M2	18.1	94	123.1	323					
	S2	4.0	123	40.0	347					
NOS 3	O1	3.9	14	3.1	149					
	K1	9.4	36	6.5	228					
	N2	16.2	84	6.8	321					
	M2	54.0	98	29.8	305					
	S2	23.8	140	10.6	316					
NOS 4	O1	4.4	34	1.0	157					
	K1	5.3	38	2.2	163					
	N2	3.1	23	6.4	229					
	M2	22.9	101	7.5	281					
	S2	11.7	132	3.5	354					
NOS 6	O1	6.1	351	7.5	214					
	K1	15.0	9	12.5	196					
	N2	14.2	59	15.1	227					
	M2	75.1	88	65.3	263					
	S2	31.3	115	29.0	284					
NOS 19	O1	4.2	150	5.6	171					
	K1	5.5	169	11.9	206					
	N2	6.6	254	18.6	265					
	M2	38.8	295	97.3	304					
	S2	11.5	319	32.0	330					

H = current speed

G° = tidal current constituent epoch (relative to Greenwich, Meridian)

 θ = direction of major axis (clockwise from north)

C = clockwise rotation

CC = counterclockwise rotation

The tidal current input data for the 1976 study was an estimate of average tidal current conditions based on preliminary tabulations of current measurements. In order to update the 1976 data with those made available for the present study, some measure of comparison was necessary. It was agreed that the basis for the tidal current input data for the present study remain the same as for the 1976 study; that is, tidal current input data should represent average tidal conditions. Therefore, a simplified approach was taken to provide a comparison between the harmonic tidal current constituents and average tidal conditions. January 5, 1978 was selected for which tidal predictions indicated a mean tidal range would occur in Lower Cook Inlet, using Seldovia, Alaska as the reference station. Using the results of the harmonic analyses, (five major tidal constituents: O1, K1, M2, N2, S2), tidal currents were predicted at three stations for this particular mean tidal range, based on the methods presented in Schureman, 1958. It was hypothesized that since the M2 constituent was the dominant constituent, perhaps it alone might be used to provide an estimate of average tidal current conditions within Lower Cook Inlet. Therefore, the M2 tidal current constituent was calculated separately for this particular mean tidal range. Summary results of these calculations are presented in Table 4.

Comparison of the results indicated that the magnitude of the peak M2 tidal current constituent would provide a reasonable approximation to average peak tidal currents in Lower Cook Inlet. For those stations examined, the magnitude of the peak M2 tidal current constituent fluctuates between being slightly larger and slightly smaller than the peak predicted tidal current. This would, over a series of tidal cycles, tend to cancel out and provide a reasonable approximation to average tidal current effects.

The oil spill model has the capability to accept rotary-type tidal current input. Some discussion in the early stage of the present study was centered around the possibility of utilizing rotary tidal currents. However, from the standpoint of available data distribution in the southern and west-central portions of Lower Cook Inlet and the lack of data in the northern section, it was decided that accurate specification of rotary

TABLE 4

COMPARISON OF PREDICTED TIDAL CURRENT WITH M2 CONSTITUENT

<u>Station</u>	<u>Predicted Peak Current Along Major Axis (cm/sec)</u>		<u>Predicted Peak M2 Component Along Major Axis (cm/sec)</u>	
	<u>Ebb</u>	<u>Flood</u>	<u>Ebb</u>	<u>Flood</u>
NOS-1	130	133	125	122
PMEL C-1	31	28	37	37
PMEL C-4	45	54	48	47

¹Predictions were made for January 5, 1978, when tidal predictions indicated a mean tidal range at Seldovia, Alaska. Predictions for tidal currents included the O1, K1, M2, N2, and S2 constituents.

²The major and minor axes refer to the axes of the tidal current ellipse used to represent tidal current characteristics in harmonic form, see Shureman, 1958. The orientation of the major axis of the ellipse is usually identical with the maximum flood-maximum ebb direction, the exception being at geographical bends where the difference in flood and ebb directions is not equal to 180°, the direction of the major axis of a constituent, say the M2 component, does not necessarily equal the direction of the major axis of the tidal current ellipse.

currents was beyond the credibility of the data base. Although greater refinement could be obtained by inputting the actual elliptical nature of the tidal currents observed at many of the stations, this refinement was not justified compared to the rather uncertain accuracy of other input parameters, such as the net current pattern and the assumption of constant wind patterns.

Thus, the peak M2 tidal current components for ebb and flood conditions were selected as the tidal current input to the oil spill trajectory model. The M2 current component was derived from a two-dimensional hydrodynamic model by Mungall; description of the model, its application, and results are well documented (for example, see Matthews and Mungall, 1972; Mungall and Matthews, 1973; Mungall, 1973). This numerical model, which includes Coriolis and frictional terms, has been applied to Cook Inlet for the prediction of tides and currents and the results have been shown to be in good agreement with the few available observations. Because the model is two-dimensional the predicted currents are depth-averaged. However, it has been shown that the predicted currents are in close agreement with observed surface currents. Further, it has been concluded that the relatively shallow waters of Cook Inlet respond as a whole to the tidal motion showing little variability with depth (Mathews and Mungall, 1972). Thus, it was felt that the use of Mungall's model to provide a tidal current distribution in Lower Cook Inlet would result in a more reliable set of tidal current input data than subjective interpolation from available tidal current measurements.

The model-generated tidal currents represented the M2 tidal current component for a mean tidal range in Cook Inlet. Thus, they provide a reasonably direct comparison with the results of the harmonic analyses from the PMEL and NOS current measurements, with the exception that the model predicted currents were depth-averaged while the PMEL and NOS current measurements were taken at 20.0 and 6.7 meter depths, respectively. Table 5 presents a comparison of PMEL and NOS M2 tidal current component characteristics with the predictions provided by Mungall's model at the closest output grid point to the measurement station. Based on this comparison it

TABLE 5

COMPARISON OF MEASURED AND PREDICTED M2 TIDAL CURRENT COMPONENTS

Station	Measured		Predicted			Difference			
	Major Axis Speed (cm/sec)	Direction (°N)	Minor Axis Speed (cm/sec)	Major Axis Speed (cm/sec)	Direction (°N)	Minor Axis Speed (cm/sec)	Major Axis Speed (%)	Direction (°)	Minor Axis Speed (%)
NOS-1	125	354	13	99	19	4	21	25	69
NOS-19	105	21	5	100	12	7	5	9	-40
NOS-27	95	340	15	85	11	22	11	31	-47
PMEL C-1	36	317	22	38	351	13	-6	34	41
PMEL C-4	47	356	19	43	8	13	9	12	32
PMEL C-5	32	329	8	37	10	10	-16	41	-25

¹Predicted from Mungall's hydrodynamic model of Cook Inlet based on mean tidal range (Mungall, 1978)

²The major and minor axes refer to the axes of the tidal current ellipse used to represent tidal current characteristics in harmonic form, see Schureman, 1958. The orientation of the major axis of the ellipse is usually identical with the maximum flood-maximum ebb direction, the exception being at geographical bends where the difference in flood and ebb directions is not equal to 180°. The direction of the major axis of a constituent, say the M2 component, does not necessarily equal the direction of the major axis of the tidal current ellipse.

was decided that the model predicted currents would be used to provide interpolation between the currents determined by NOS and PMEL measurements. In view of the absence of measurements in the northern portion of Lower Cook Inlet, the hydrodynamically predicted M2 current magnitudes and directions were used as input for this area. These were adjusted slightly based on the tidal current patterns developed in the 1976 study. The directions for ebb and flood currents for the southern portion of Lower Cook Inlet were based on the NOS and PMEL measurements and interpolated with the directions from the 1976 study.

As previously mentioned, the tidal current input data for the 1976 study did not account for phasing of tidal currents as a function of location within Lower Cook Inlet. Although the addition of tidal current phase relationships would not significantly alter the results of the oil spill trajectory model, it was felt that this improvement could rapidly be developed and implemented, resulting in a more realistic treatment of this oceanographic input parameter. Tidal current phase relationships were obtained from the publication of tidal current predictions (NOAA, 1978), the harmonic analyses of PMEL and NOS current measurements and results of Mungall's tidal model of Cook Inlet. The tidal current cophase lines derived from the results of Mungall's model were in general agreement with the trend of the tidal current phase relations that could be inferred from the measured and published tidal current sources. Figure 11 presents the approximate tidal current phase distribution within Lower Cook Inlet derived from the above sources. The phase relationships shown are representative of peak tidal currents occurring during a mean tidal range. A single phase is given in degrees and represents an average of the peak ebb and flood current phases. A zero phase was arbitrarily selected for the southern portion of Lower Cook Inlet on a line between Cape Douglas and Cape Elizabeth (see Figure 11). The lag of the peak ebb or flood currents within Lower Cook Inlet were then referenced to this arbitrary zero phase line.

PHASE GIVEN
IN DEGREES
RELATIVE
TO TIDAL
CURRENTS
AT ENTRANCE
TO COOK
INLET

360°=124 HRS.

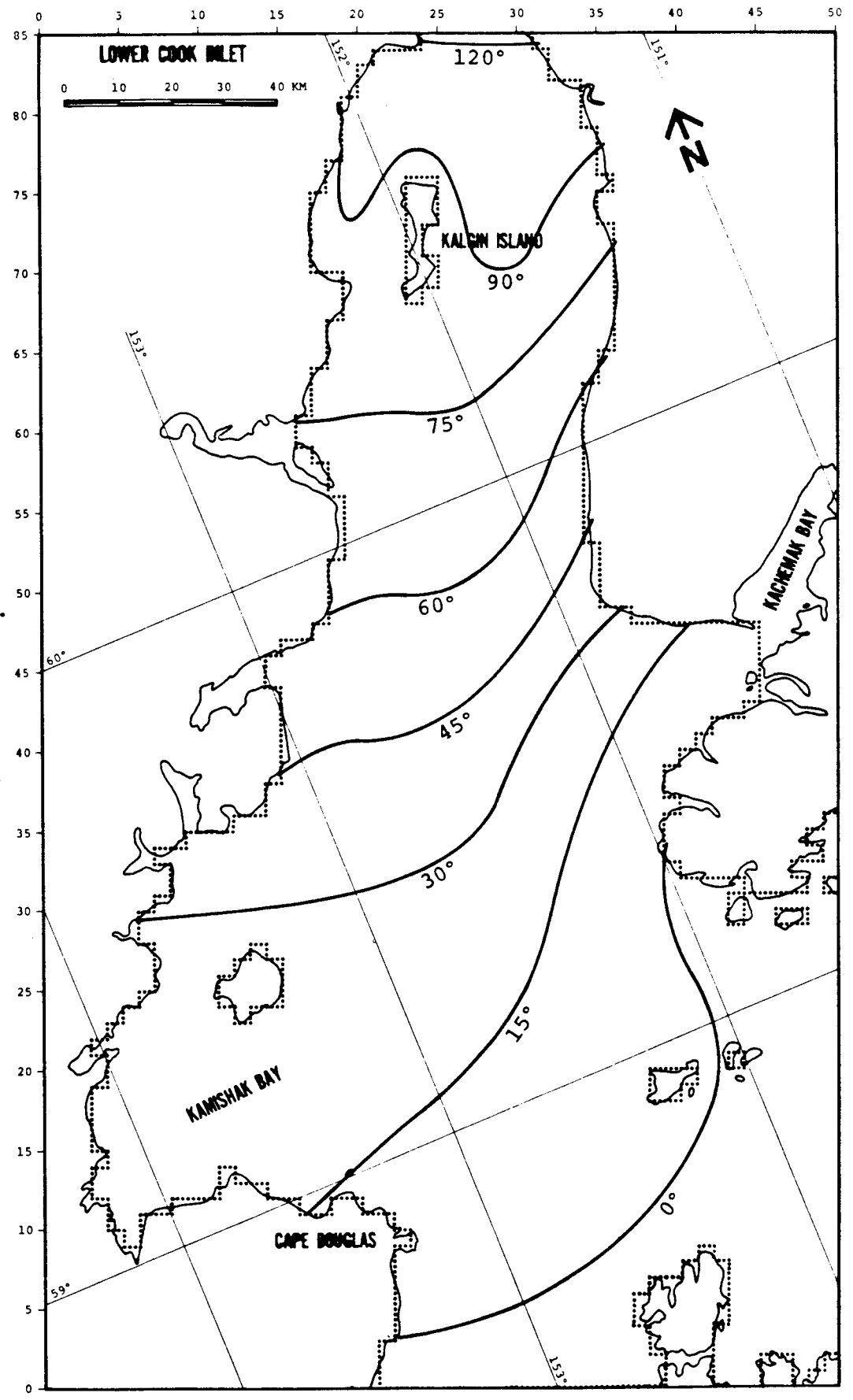


FIGURE 11: TIDAL CURRENT PHASE DISTRIBUTION
487

Using the results of PMEL and NOS harmonic analyses of tidal currents and the results of Mungall's model, distributions of peak ebb and flood M2 tidal current magnitudes and directions were developed for Lower Cook Inlet. Figures 12 to 15 show vector plots of tidal current input data with the current phase relationships included for various phases of the tidal cycle. Selected input data files are presented in Appendix D for tidal phases equal to 0, 90, 180, and 270 degrees.

D. MISCELLANEOUS DATA

Several other quantities must be input to the model in order to completely define the simulation parameters. Those that are of importance to the study are primarily control parameters that affect the numerical algorithms within the program and are described below.

- Time step - 0.5 hour
This is the time step used in Equation (1) (see Appendix A) to compute slick centroid movement. It was chosen so that the maximum centroid displacement in any one time step would not exceed one cell width.

- Stop time = 150 hours = 6.21 days
The stop time defines the period over which centroid movement is simulated. It was chosen to cover 12 complete tidal cycles or just over 6 days. The period of the predominant tidal cycle in Cook Inlet is 12.42 hours.

- Initial tidal phase
The ultimate disposition of the oil slick depends on the point in time within the tidal cycle at which the spill occurs. Four points along the tidal cycle, at the 0 phase line, previously defined, were selected for simulation: maximum flood, and ebb, and the two slack tides midway between the extreme.

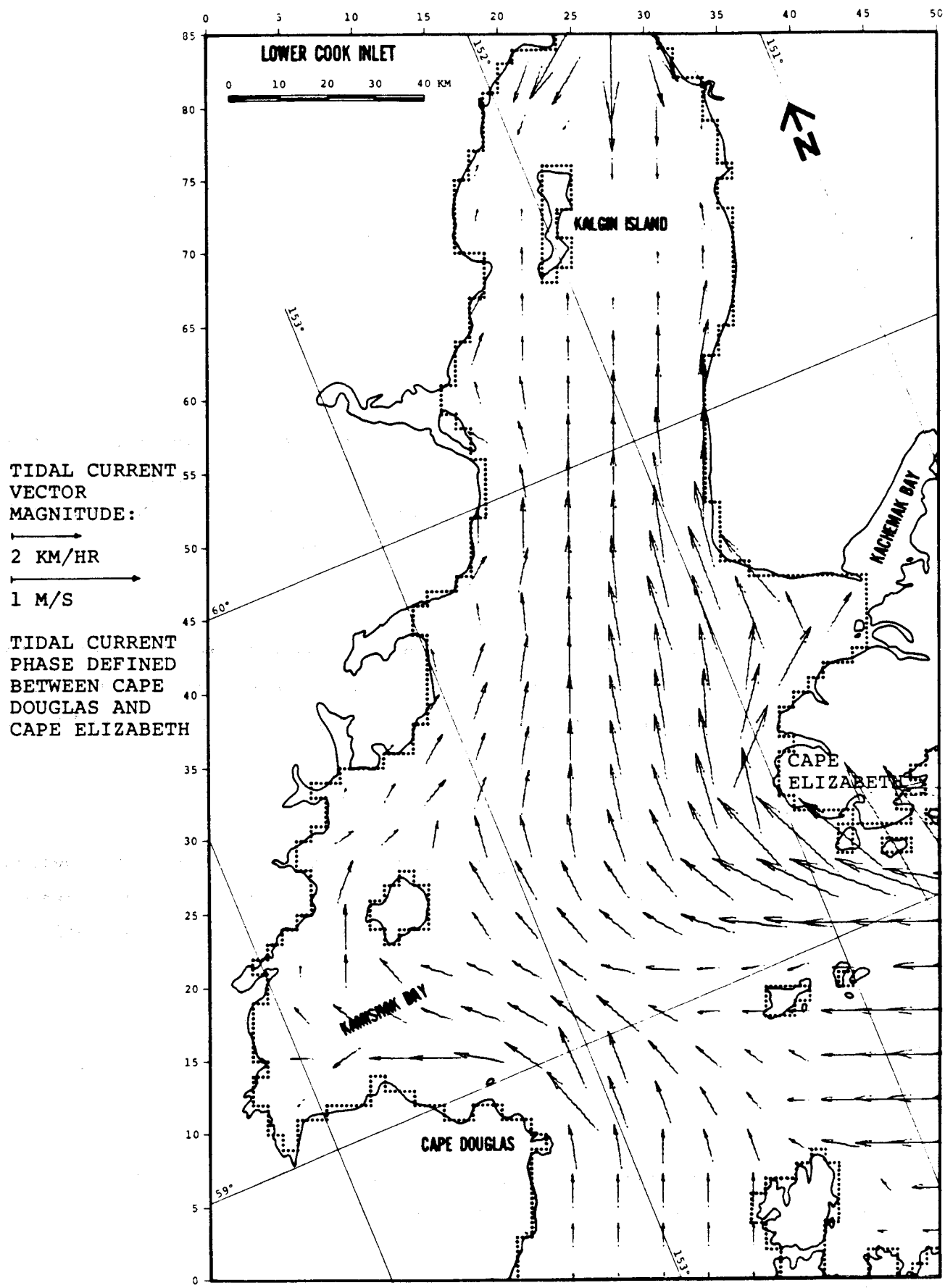


FIGURE 12: TIDAL CURRENT PATTERN AT T=0 HRS. (PHASE OF 0 DEG)

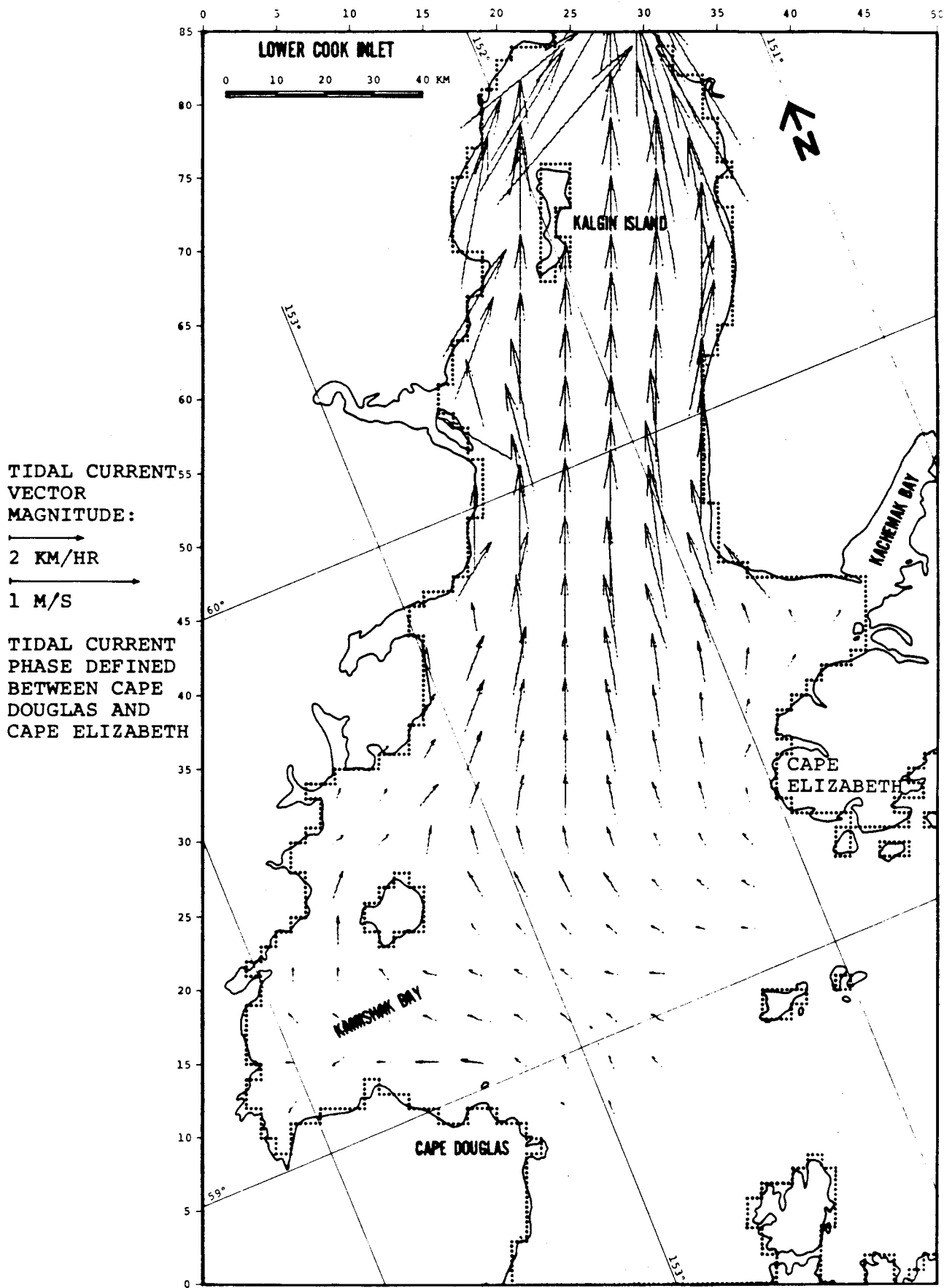


FIGURE 13: TIDAL CURRENT PATTERN AT T=3.11 HRS. (PHASE OF 90 DEG)

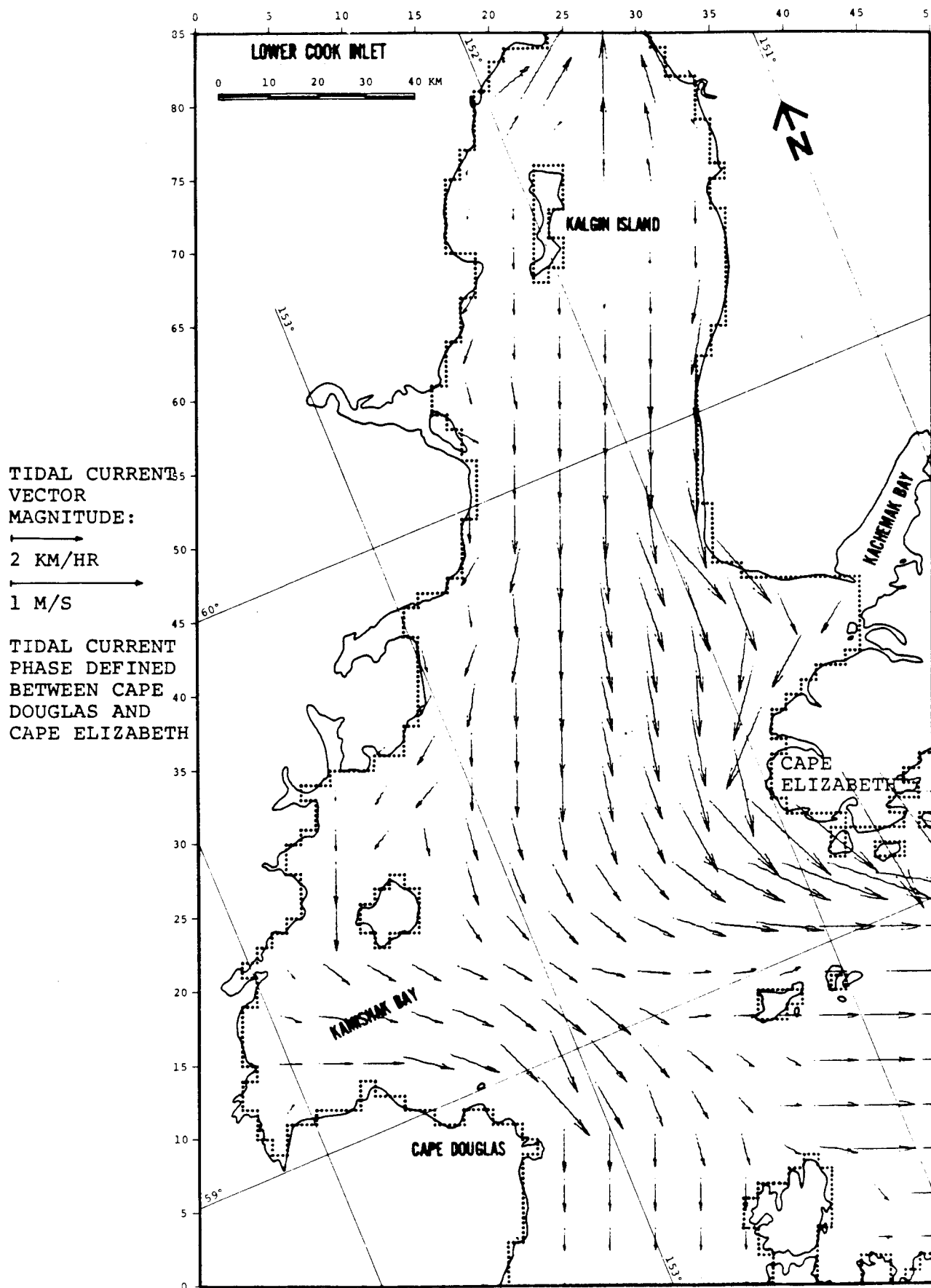


FIGURE 14: TIDAL CURRENT PATTERN AT T=6.21 HRS. (PHASE OF 180 DEG)

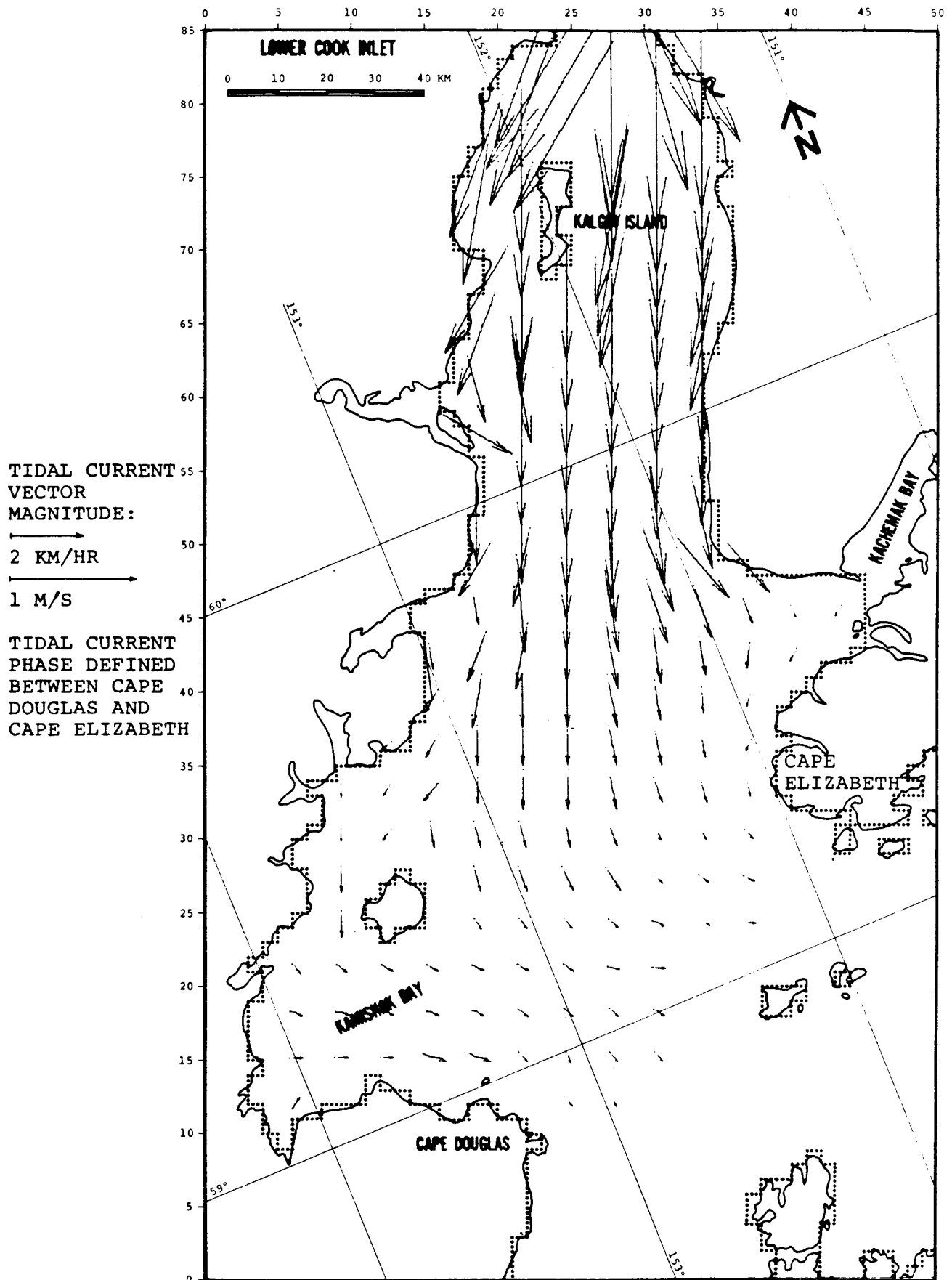


FIGURE 15: TIDAL CURRENT PATTERN AT T=9.32 HRS. (PHASE OF 270 DEG)

IV. SIMULATION RESULTS

A. BASE CASES

Using the methodology described in Section II and the hypothetical oil spill scenarios described in the previous section, a total of 288 trajectories simulations were run. These trajectories are denoted base case trajectories and are displayed in Appendix B. In reviewing the simulated trajectories for various starting phases of the tide at a given site, it was observed that they did not deviate significantly from each other. Therefore, the base case trajectories presented in Appendix B are shown for all sites and wind conditions for only one tidal phase (phase of 0 degrees). The trajectories are separated and presented in the order of the eight wind patterns simulated for each site, which shows the dominance of the wind drift current component over the net and tidal current components. The numbers printed along the trajectories represent the cumulative elapsed time in hours from the start time of the trajectory simulation.

Potential Boundary Contact Zones

When a trajectory terminates at a boundary cell, the termination cell and the elapsed time are known. These two items of information were summarized for each site and combined for all sites to give potential boundary contact zones. Graphical results for each site are presented in Appendix B, Figures B-73 to B-81. The termination cell for each trajectory has been identified for each postulated spill site by one or more numbers adjacent to the cell. The number represents the wind pattern(s) used to produce a trajectory termination at that cell. The dots over each number indicate the number of times that cell was contacted for each set of four trajectories for each wind pattern. The four trajectories correspond to the four different release phases of the tide. For example, in Figure B-73, the cipher "8" near Kachemak Bay indicates that shoreline cell was impacted by two of the four trajectories run for wind field Number 8.

Also provided for each contact cell are ranges of times to impact. These ranges are given as occurring within 1, 3, or 6 days and are distinguished by corresponding symbols defined in the figures. Table 6 presents a listing of the base case boundary contact cells and the termination times for all sites and simulated conditions. This table allows comparison of actual termination times rather than the previously described ranges of termination times. Figure 16 allows a graphical interpretation of the combination of the potential boundary contact zones for all nine sites. For the eight wind patterns and oceanographic conditions selected for use in this study, Figure 16 shows the potential distribution of centroid trajectory contact zones.

Figure 16 shows a wide distribution of potential contact zones within Lower Cook Inlet. It is interesting to note that the eastern shoreline of Lower Cook Inlet north of Anchor Point is free of potential contact zones. Due to the locations of the hypothetical oil spill sites, all south of Anchor Point, the meteorologic and oceanographic input data fields do not provide a driving force that would create impact on this area of the shoreline. The wind patterns, with the exception of wind pattern No. 8, are either directed parallel to, or away from this area. Wind pattern No. 8 could create an impact if a spill site was located somewhat above Anchor Point. The net and tidal currents in this area (the eastern shoreline north of Anchor Point) are essentially parallel to shore and could not easily force a trajectory to impact the shoreline. Likewise, the shorelines of Kamishak Bay are relatively free of potential contact zones. This appears to be the result of the absence of spill sites, with the exception of Site 7, in the central portion of Lower Cook Inlet below Augustine Island. The net current pattern would drive a trajectory out of Kamishak Bay and the tidal currents, being very weak in this area, could not significantly affect net transport of the centroid. However, wind pattern No. 7 could drive a trajectory directly into Kamishak Bay if the spill site were located in the central portion of Lower Cook Inlet reasonably close to and slightly south of Augustine Island.

TABLE 6

BASE CASE
BOUNDARY CONTACT CELLS

	SITE 1			SITE 2		
	Cell Location ¹		Time to Impact ² (hrs)	Cell Location ¹		Time to Impact ² (hrs)
	X	Y		X	Y	
Wind 1						
Tidal Phase 1	39	20	86	39	7	88
Tidal Phase 2	39	20	78	39	7	83
Tidal Phase 3	39	19	87	39	7	88
Tidal Phase 4	39	19	95	39	7	91
Wind 2						
Tidal Phase 1	40	20	39	42	9	43
Tidal Phase 2	40	20	36	42	9	41
Tidal Phase 3	40	20	38	42	9	43
Tidal Phase 4	40	20	41	42	9	45
Wind 3						
Tidal Phase 1	27	86	126	17	63	94
Tidal Phase 2	26	86	125	18	58	75
Tidal Phase 3	26	86	122	18	65	95
Tidal Phase 4	26	86	118	18	65	91
Wind 4						
Tidal Phase 1	24	69	38	18	65	49
Tidal Phase 2	25	70	37	18	66	52
Tidal Phase 3	25	70	35	18	65	50
Tidal Phase 4	25	70	32	18	66	48
Wind 5						
Tidal Phase 1	24	69	150	27	56	151
Tidal Phase 2	25	71	118	27	57	151
Tidal Phase 3	25	63	151	27	54	151
Tidal Phase 4	26	61	151	27	54	151
Wind 6						
Tidal Phase 1	25	70	75	25	70	127
Tidal Phase 2	25	75	87	25	70	132
Tidal Phase 3	25	70	73	25	70	127
Tidal Phase 4	25	70	78	25	70	120
Wind 7						
Tidal Phase 1	15	41	49	14	37	40
Tidal Phase 2	15	40	53	9	35	60
Tidal Phase 3	15	41	50	12	36	49
Tidal Phase 4	14	46	53	14	37	38
Wind 8						
Tidal Phase 1	45	49	50	46	45	67
Tidal Phase 2	46	47	47	46	44	72
Tidal Phase 3	45	49	47	46	45	70
Tidal Phase 4	36	50	17	46	46	64

¹Contact cell defined by X and Y location corresponding to the long and short grid axes, as shown on Figures 16 and 17.

²151-hour truncation employed on time to contact (≤ 150 hours contact was made; 151 hours no contact).

TABLE 6

BASE CASE
BOUNDARY CONTACT CELLS

	SITE 3			SITE 4		
	Cell Location ¹		Time to Impact ² (hrs)	Cell Location ¹		Time to Impact ² (hrs)
	X	Y		X	Y	
Wind 1						
Tidal Phase	39	1	94	41	8	70
Tidal Phase 2	39	1	91	41	8	63
Tidal Phase 3	39	1	94	39	19	40
Tidal Phase 4	39	1	96	41	8	73
Wind 2						
Tidal Phase 1	39	7	43	39	20	18
Tidal Phase 2	39	7	42	39	20	16
Tidal Phase 3	39	7	41	39	20	17
Tidal Phase 4	39	7	44	39	20	20
Wind 3						
Tidal Phase 1	15	39	37	25	83	151
Tidal Phase 2	14	38	43	26	84	151
Tidal Phase 3	15	39	37	24	79	151
Tidal Phase 4	15	39	38	23	79	151
Wind 4						
Tidal Phase 1	15	40	20	24	85	76
Tidal Phase 2	15	39	18	25	86	76
Tidal Phase 3	15	39	17	23	85	81
Tidal Phase 4	15	42	24	23	85	78
Wind 5						
Tidal Phase 1	25	56	151	36	50	51
Tidal Phase 2	22	47	151	36	50	61
Tidal Phase 3	24	50	151	36	50	57
Tidal Phase 4	26	54	151	36	50	52
Wind 6						
Tidal Phase 1	26	85	151	36	50	39
Tidal Phase 2	25	70	151	38	49	45
Tidal Phase 3	24	69	133	36	50	43
Tidal Phase 4	26	86	141	36	50	39
Wind 7						
Tidal Phase 1	8	32	38	6	30	86
Tidal Phase 2	6	30	48	7	28	81
Tidal Phase 3	7	31	42	6	29	86
Tidal Phase 4	8	33	37	6	30	86
Wind 8						
Tidal Phase 1	41	33	83	41	37	30
Tidal Phase 2	41	33	88	40	35	28
Tidal Phase 3	41	33	85	40	36	28
Tidal Phase 4	40	34	75	40	38	25

¹Contact cell defined by X and Y location corresponding to the long and short grid axes, as shown on Figures 16 and 17.

²151-hour truncation employed on time to contact (≤ 150 hours contact was made; 151 hours no contact).

TABLE 6

BASE CASE
BOUNDARY CONTACT CELLS

	SITE 5			SITE 6		
	Cell Location ¹		Time to Impact ² (hrs)	Cell Location ¹		Time to Impact ² (hrs)
	X	Y		X	Y	
Wind 1						
Tidal Phase 1	40	7	57	38	6	76
Tidal Phase 2	41	8	52	38	6	73
Tidal Phase 3	39	19	27	38	6	75
Tidal Phase 4	40	7	59	38	6	78
Wind 2						
Tidal Phase 1	39	20	12	41	8	39
Tidal Phase 2	39	20	10	41	8	38
Tidal Phase 3	39	19	12	41	8	38
Tidal Phase 4	39	19	14	41	8	40
Wind 3						
Tidal Phase 1	19	56	100	17	48	68
Tidal Phase 2	18	65	130	17	48	73
Tidal Phase 3	17	62	126	17	48	69
Tidal Phase 4	19	53	88	17	48	65
Wind 4						
Tidal Phase 1	19	68	65	17	48	32
Tidal Phase 2	22	85	87	19	53	38
Tidal Phase 3	23	85	83	18	49	32
Tidal Phase 4	21	84	88	18	52	34
Wind 5						
Tidal Phase 1	36	50	75	25	52	151
Tidal Phase 2	36	50	76	25	51	151
Tidal Phase 3	36	51	74	25	48	151
Tidal Phase 4	35	54	79	26	50	151
Wind 6						
Tidal Phase 1	36	50	52	25	69	151
Tidal Phase 2	39	49	59	25	69	151
Tidal Phase 3	39	49	55	25	68	151
Tidal Phase 4	36	50	51	25	70	150
Wind 7						
Tidal Phase 1	15	27	44	6	30	67
Tidal Phase 2	15	27	46	6	29	68
Tidal Phase 3	15	27	45	6	29	67
Tidal Phase 4	14	28	47	7	31	61
Wind 8						
Tidal Phase 1	43	33	51	40	38	46
Tidal Phase 2	44	31	54	41	37	53
Tidal Phase 3	45	32	53	40	38	48
Tidal Phase 4	41	33	38	40	39	45

¹Contact cell defined by X and Y location corresponding to the long and short grid axes, as shown on Figures 16 and 17.

²151-hour truncation employed on time to contact (≤ 150 hours contact was made; 151 hours no contact).

TABLE 6
 BASE CASE
 BOUNDARY CONTACT CELLS

	SITE 7			SITE 8		
	Cell Location ¹		Time to Impact ² (hrs)	Cell Location ¹		Time to Impact ² (hrs)
	X	Y		X	Y	
Wind 1						
Tidal Phase 1	38	6	42	38	1	40
Tidal Phase 2	39	7	42	38	1	37
Tidal Phase 3	38	6	41	38	1	39
Tidal Phase 4	38	6	43	38	1	43
Wind 2						
Tidal Phase 1	41	8	22	38	5	19
Tidal Phase 2	41	8	21	39	3	20
Tidal Phase 3	40	7	22	38	5	18
Tidal Phase 4	40	7	22	38	6	20
Wind 3						
Tidal Phase 1	15	39	98	15	25	67
Tidal Phase 2	15	43	120	14	25	76
Tidal Phase 3	15	40	101	14	25	80
Tidal Phase 4	14	37	90	14	25	79
Wind 4						
Tidal Phase 1	17	48	52	14	37	50
Tidal Phase 2	17	48	50	14	37	56
Tidal Phase 3	17	48	50	14	37	55
Tidal Phase 4	18	49	53	14	37	51
Wind 5						
Tidal Phase 1	26	53	151	27	49	151
Tidal Phase 2	27	58	151	28	51	151
Tidal Phase 3	26	50	151	27	45	151
Tidal Phase 4	26	48	151	25	38	151
Wind 6						
Tidal Phase 1	25	70	140	27	65	151
Tidal Phase 2	25	70	135	37	50	94
Tidal Phase 3	25	70	145	27	60	151
Tidal Phase 4	25	67	151	27	62	151
Wind 7						
Tidal Phase 1	3	18	98	22	8	38
Tidal Phase 2	3	17	103	22	8	43
Tidal Phase 3	3	17	102	22	9	38
Tidal Phase 4	3	18	97	22	8	38
Wind 8						
Tidal Phase 1	51	27	97	41	8	46
Tidal Phase 2	51	27	94	39	7	41
Tidal Phase 3	51	27	102	41	8	46
Tidal Phase 4	51	27	99	42	9	50

¹Contact cell defined by X and Y location corresponding to the long and short grid axes, as shown on Figures 16 and 17.

²151-hour truncation employed on time to contact (≤ 150 hours contact was made; 151 hours no contact).

TABLE 6

BASE CASE
BOUNDARY CONTACT CELLS

	Cell		Time to Impact ² (hrs)
	Location ¹		
	X	Y	
<u>SITE 8A</u>			
Wind 1			
Tidal Phase 1	38	6	27
Tidal Phase 2	38	6	24
Tidal Phase 3	38	6	26
Tidal Phase 4	38	5	29
Wind 2			
Tidal Phase 1	39	7	12
Tidal Phase 2	39	7	13
Tidal Phase 3	39	7	13
Tidal Phase 4	39	7	13
Wind 3			
Tidal Phase 1	14	37	111
Tidal Phase 2	14	37	110
Tidal Phase 3	14	37	111
Tidal Phase 4	14	37	107
Wind 4			
Tidal Phase 1	17	48	60
Tidal Phase 2	17	48	62
Tidal Phase 3	16	48	64
Tidal Phase 4	16	48	63
Wind 5			
Tidal Phase 1	36	50	125
Tidal Phase 2	36	51	128
Tidal Phase 3	35	54	135
Tidal Phase 4	36	53	139
Wind 6			
Tidal Phase 1	39	49	89
Tidal Phase 2	38	49	89
Tidal Phase 3	39	49	91
Tidal Phase 4	39	49	87
Wind 7			
Tidal Phase 1	22	8	52
Tidal Phase 2	22	8	52
Tidal Phase 3	22	9	49
Tidal Phase 4	22	8	50
Wind 8			
Tidal Phase 1	51	9	59
Tidal Phase 1	51	9	56
Tidal Phase 3	51	9	63
Tidal Phase 4	51	10	62

¹Contact cell defined by X and Y location corresponding to the long and short grid axes, as shown on Figures 16 and 17.

²151-hour truncation employed on time to contact (≤ 150 hours contact was made; 151 hours no contact).

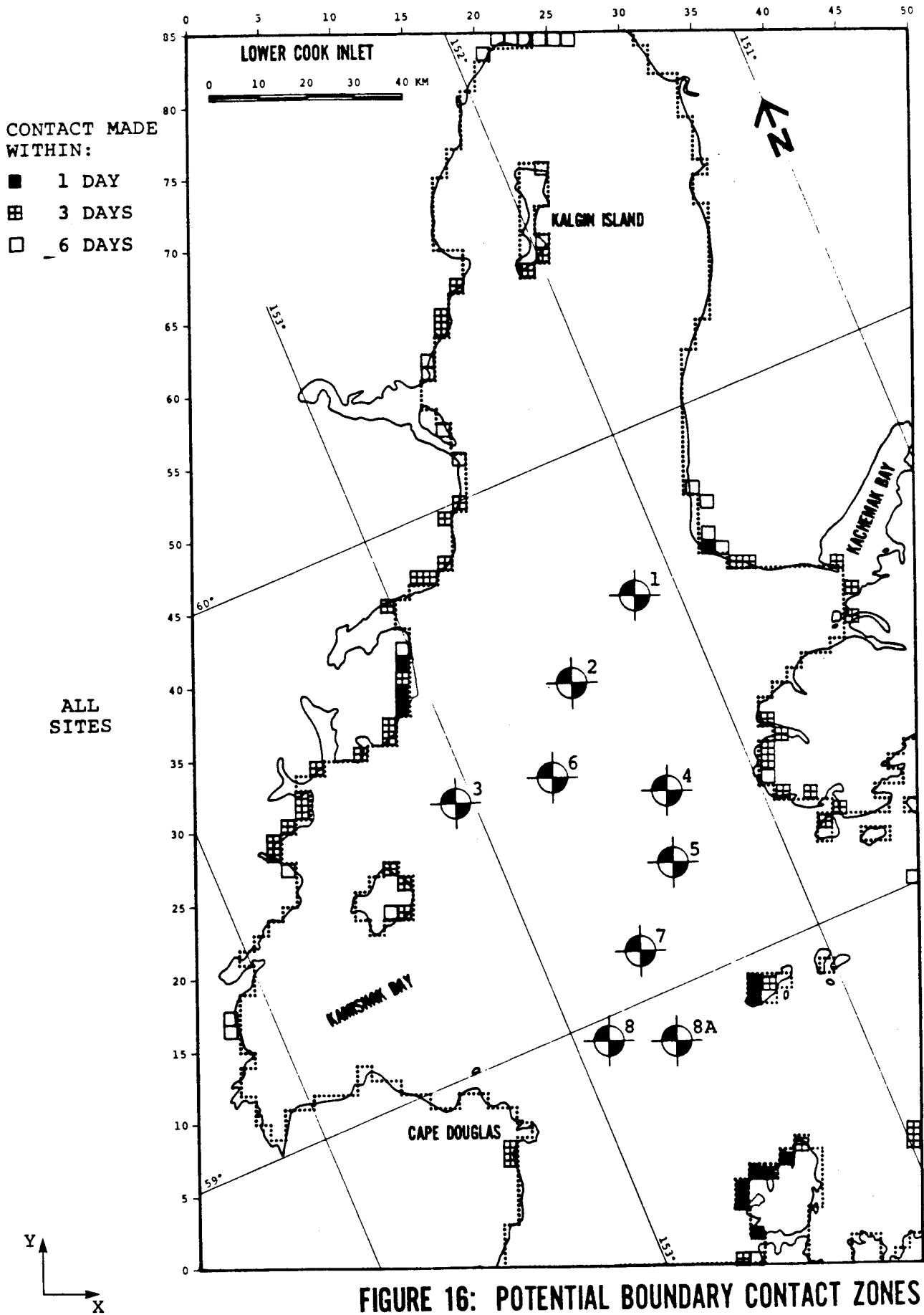


FIGURE 16: POTENTIAL BOUNDARY CONTACT ZONES

Given the specified meteorologic and oceanographic driving fields, the potential contact zones shown on Figure 16 are as expected for the distribution of the hypothetical spill sites investigated in this study. For example, consider Site 1. Under the influence of wind patterns Nos. 1 and 2, which have a predominant southerly direction in this area, the trajectories for both patterns impact Ushagat Island slightly to the west of south from spill Site 1 as shown in Figures B-1 and B-10. This indicates the dominance of the wind drift current component compared with the net and tidal current components. The net current moves the trajectories to the west as the trajectories pass south of Cape Elizabeth, which is consistent with the change in the net current direction from northerly to westerly. The effect of the tidal currents on the base case trajectories evidently does not significantly alter the impact zones.

Wind pattern No. 3 is primarily northerly and the trajectories from Site 1 show that again the wind drift current component dominates the net and tidal current components throughout this region. These trajectories come close to contacting Kalgin Island and pass just to the west of the island. The trajectories progress northeasterly as the wind drift and net current vectors parallel each other along the island. An eastward component of the net current north of Kalgin Island shifts the trajectory further to the northeast, moving it to the boundary of the Forelands as shown in Figure B-19.

Wind pattern No. 4 is similar to 3, except the magnitude of the wind is greater. The larger wind drift current component moves the trajectory from Site 1 through this region faster, which does not allow the net current component to affect the trajectory for as long a period of time as in wind pattern No. 3. The net current has a westerly component in this region, but because the trajectory moves more rapidly with wind pattern No. 4, the effect of the westerly component is diminished. The trajectory does not traverse the west shoreline of Kalgin Island as was the case with wind pattern No.3, but terminates on the southern shoreline of the island as shown in Figure B-28.

Wind patterns Nos. 5 and 6 consist primarily of winds moving directly up the northern portion of Lower Cook Inlet. The vectoral combination of the wind drift and net current components result in a northerly drift. The movement of the trajectories confirm this; impacts occurred along Kalgin Island and two trajectories were terminated just south of the island after 150 hours as shown in Figures B-37 and B-46.

Wind pattern No. 7 is directed to the northwest in the region of spill site No. 1. The vectoral combination of the wind drift and net current components provide a resultant westerly movement of the trajectory. The contact cells from wind pattern No. 7 are all located almost directly west of spill site No. 1 as shown in Figure B-55.

Wind pattern No. 8 has an easterly direction in the vicinity of spill site No. 1. The net current magnitude in this region is relatively small and does not significantly influence the trajectory movement. Thus, the trajectories move toward the east and are shown to contact the northern shoreline of Kachemak Bay as shown in Figure B-64. The effect of the tide can be seen to influence to some extent where the contact will occur along the shoreline.

Similar reasoning can be applied to the other spill sites to show that the resulting trajectory movements shown in Figures B-1 through B-72 are as expected given the specified environmental forcing fields. Careful examination of these figures will show the relative importance or dominance of the specified environmental forcing fields. Summarily, it can be stated that the wind drift current component provides the primary driving force for centroid movement. In certain areas, such as offshore Cape Douglas, the net current significantly influences trajectories. Although the tidal current, with few exceptions, does not significantly alter the net trajectory it should be noted that the specified wind patterns and to a degree the net current pattern are all rather uniform. The tidal currents or other environmental forcing fields could become more important if transient and nonuniform conditions were specified. For example, if a wind field was rotated and the wind speed varied with time, then the tidal current phase at time of release might become an important factor in trajectory movement.

Annual Percent Probability of Exposure

As was done in the 1976 study, an assessment was made of the annual percent probability of shoreline exposure. The exposure probabilities were based entirely on the annual percent frequencies assigned to each of the wind patterns as discussed in Section III. The annual probabilities of exposure were determined for a spill occurring at each site in the following manner:

1. For each boundary cell contacted, the wind pattern or patterns associated with that contact cell were identified.
2. The cumulative annual frequency of the wind pattern or patterns associated with that contact cell were computed. The annual frequency of a wind pattern was counted only once in determining a cumulative frequency, even if that wind pattern was identified as producing more than one contact for that cell.
3. The cumulative annual percent frequencies of the wind patterns associated with a contact cell were assumed to represent the annual probability of exposure for that cell.

Although the above assessment is a first-order approximation, it provides a means of evaluating or comparing the expected exposure level for the specified spill sites and environmental driving forces. Further refinement in assessing exposure probabilities is not justified given the limitations inherent in determining the contact cell locations.

Graphical representation of the annual percent probability of exposure given that a spill occurs at each site is presented in Appendix B, Figures B-82 through B-90. For each cell contacted, the range of probability of exposure calculated for that cell has been coded according to the legend given on the figures. No attempt has been made to smooth or add exposure probabilities between contact cells. However, it should be noted that the probability of exposure is not a discrete function, but in reality a continuous one.

A summary of the annual probability of exposure for all nine sites is presented in Figure 17. This figure represents the annual probability of exposure given that a single spill is equally probable from any of the nine potential spill sites. The probabilities were calculated by dividing the cumulative probabilities for each cell (the summation of probabilities for all sites) by the number of sites.

The relative exposure levels along the boundary cells thus provides within the limitations of the model and specified input data, an estimate of those portions of Lower Cook Inlet which are most likely to experience impact by the centroid of a hypothetical oil spill from the nine sites under consideration.

It should be noted that the annual probabilities expressed in this assessment are based on the assumption that, on the average, one spill would occur annually from any of the hypothetical spill sites. Therefore, since specific oil spill statistics were not used in this study, the exposure probabilities should be interpreted only from a comparative viewpoint. In addition, an assessment of shoreline exposure should include both the likelihood of exposure, and the time to exposure. Less likely exposure sites with shorter times to impact could be more significant due to greater volumes of oil likely to exist at the surface upon impact, dosage and toxicity considerations, and shorter response time available for spill containment, diversion, and cleanup operations.

The overall strategy in simulating the base case trajectories shown in Figures B-1 through B-72 was deterministic in that all quantities were uniquely specified. However, both systematic and random fluctuations may affect the base case shoreline impact distribution. The purpose of the following perturbation analyses is to determine the sensitivity of the shoreline distribution of contact cells and times to impact to perturbations in the base cases.

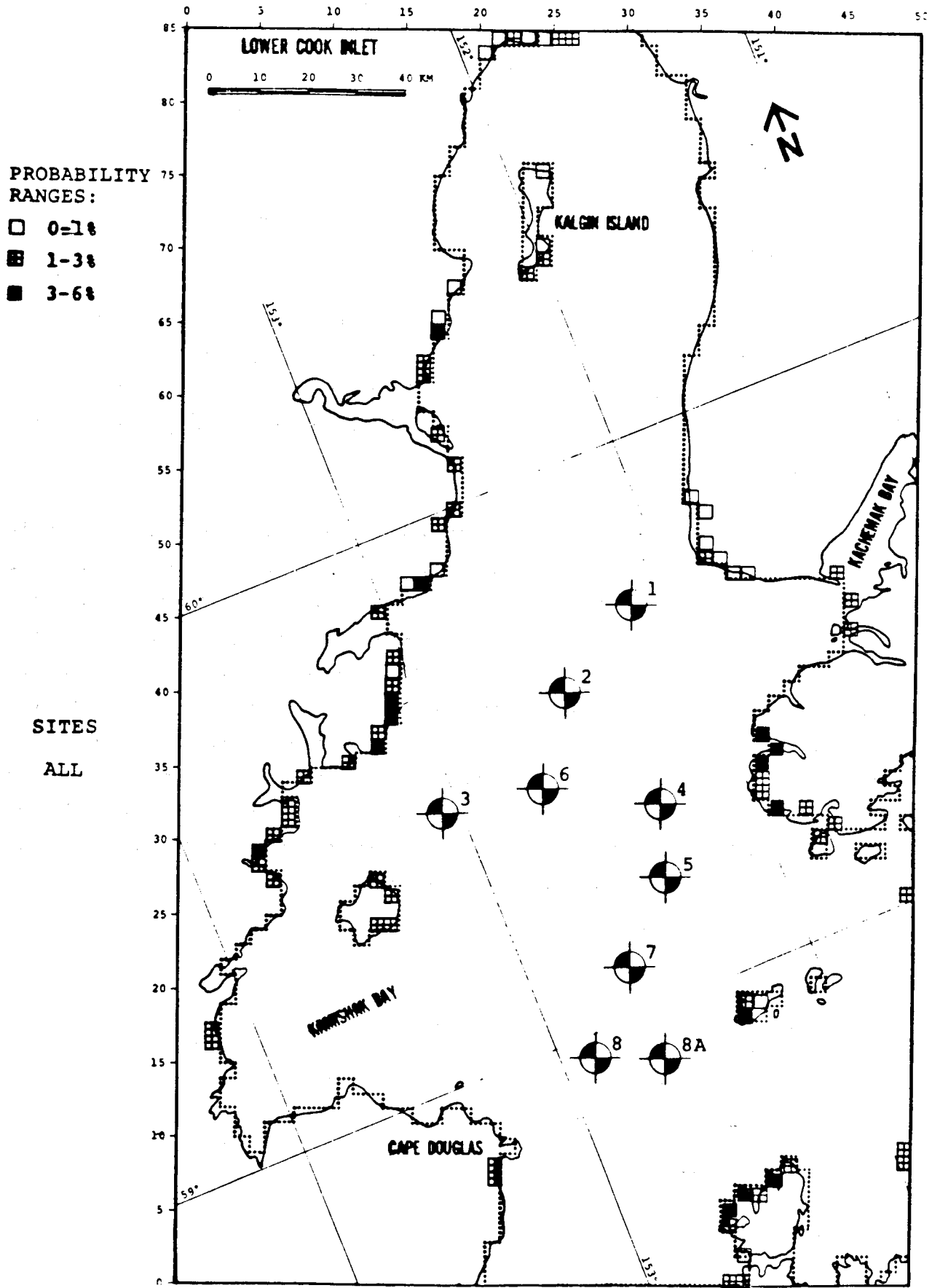


FIGURE 17: ANNUAL PERCENT PROBABILITY OF EXPOSURE

B. SYSTEMATIC PERTURBATION ANALYSIS

Sites 1, 3, and 7 were chosen to investigate the sensitivity of the results to variations on the wind and net current patterns because they yielded a fairly wide distribution of shoreline impact points for the base cases. A systematic perturbation was defined to be one where the wind and current exhibit the same directional distribution as in the base cases while the speed can be weaker (speeds less) or stronger (speeds greater).

For Sites 1 and 7, a set of four runs were made: 1) winds weaker by 25%, 2) winds stronger by 25%, 3) net current weaker by 25%, and 4) net current stronger by 25%. In each case, an initial tidal current phase of zero degrees was used. (As discussed for the base case trajectories, the starting phase of the tidal current was not found to significantly alter the resulting trajectories.)

Trajectories for the systematic perturbation analyses for Sites 1 and 7 are presented in Appendix C, Figures C-1 to C-64. The figures are arranged by wind patterns; that is, Figures C-1 to C-8 present the perturbation trajectories for wind pattern No. 1. Figures C-1 to C-4 present the perturbation trajectories for spill site No. 1 including trajectories for the systematic perturbation of the net current ($\pm 25\%$) and the wind drift current ($\pm 25\%$). Figures C-5 to C-8 present the trajectories for Site 7 with the same perturbation conditions specified above. This arrangement allows comparisons between trajectories from the same site and a particular wind pattern to be easily made.

Table 7 presents a summary listing of the termination cells and times to impact of the systematic perturbation analysis. Since only three sites were analyzed for the systematic perturbation analysis, development of potential contact zones was not made since comparison with the base case potential contact zones would be incomplete and possibly misleading. In order to provide some means of comparing the effect that the systematic perturbation has on the trajectory termination cells and times, Table 8 was developed. This table presents the variation in contact cell termination by means of the distance, (in kms), between the base case termination cell

TABLE 7

SYSTEMATIC PERTURBATION BOUNDARY CONTACT CELLSSite 1

<u>Wind Pattern</u>	<u>Net +25%</u>			<u>Net -25%</u>		
	<u>Cell Location</u>		<u>Time to Impact *</u> <u>(hrs)</u>	<u>Cell Location</u>		<u>Time to Impact *</u> <u>(hrs)</u>
	<u>X</u>	<u>Y</u>		<u>X</u>	<u>Y</u>	
1	39	20	80	39	20	69
2	41	20	36	51	4	56
3	24	69	106	24	69	85
4	24	69	36	24	69	36
5	36	50	21	37	50	23
6	35	57	27	36	53	23
7	14	38	62	15	39	66
8	46	48	42	46	48	42

<u>Wind Pattern</u>	<u>Wind +25%</u>			<u>Wind -25%</u>		
	<u>Cell Location</u>		<u>Time to Impact *</u> <u>(hrs)</u>	<u>Cell Location</u>		<u>Time to Impact *</u> <u>(hrs)</u>
	<u>X</u>	<u>Y</u>		<u>X</u>	<u>Y</u>	
1	40	20	59	39	20	105
2	51	6	44	40	20	48
3	24	69	70	24	69	147
4	25	70	30	25	70	51
5	36	51	20	36	50	25
6	35	54	16	36	50	21
7	15	39	47	12	36	105
8	46	48	34	46	47	105

* 151-hour truncation employed on time to contact (≤ 150 hours contact was made; 151 hours no contact).

TABLE 7

SYSTEMATIC PERTURBATION BOUNDARY CONTACT CELLSSite 7

<u>Wind Pattern</u>	<u>Net +25%</u>			<u>Net -25%</u>		
	<u>Cell Location</u>		<u>Time to Impact* (hrs)</u>	<u>Cell Location</u>		<u>Time to Impact* (hrs)</u>
	<u>X</u>	<u>Y</u>		<u>X</u>	<u>Y</u>	
1	38	5	43	39	7	40
2	40	7	21	41	8	20
3	13	37	100	18	49	120
4	17	48	55	18	49	52
5	27	52	151	36	51	49
6	26	67	151	36	50	74
7	12	14	73	4	20	88
8	48	24	151	51	23	69

<u>Wind Pattern</u>	<u>Wind +25%</u>			<u>Wind -25%</u>		
	<u>Cell Location</u>		<u>Time to Impact* (hrs)</u>	<u>Cell Location</u>		<u>Time to Impact* (hrs)</u>
	<u>X</u>	<u>Y</u>		<u>X</u>	<u>Y</u>	
1	39	7	33	39	3	61
2	41	8	17	39	7	29
3	17	48	98	13	37	141
4	18	49	42	18	51	79
5	28	63	151	26	41	151
6	36	50	61	28	61	151
7	3	19	73	14	13	91
8	51	24	58	48	23	151

* 151-hour truncation employed on time to contact (≤ 150 hours contact was made; 151 hours no contact).

TABLE 8

VARIABILITY BETWEEN BASE CASE AND
SYSTEMATIC PERTURBATION TRAJECTORIES

Site 1

<u>Wind Pattern</u> (Tidal Current Starting Phase = 0 Degrees)	<u>Perturbation Cases</u>							
	<u>Net +25%</u>		<u>Net -25%</u>		<u>Wind +25%</u>		<u>Wind -25%</u>	
	<u>ΔX</u> (km)	<u>ΔT</u> (hrs)						
1	0.0	6	0.0	17	3.0	27	0.0	-19
2	3.0	3	58.2	-17	53.4	-5	0.0	-9
3	51.8	20	51.8	41	51.8	56	51.8	-21
4	0.0	2	0.0	2	4.2	8	4.2	-13
5	67.4	129	69.1	127	64.9	130	67.4	125
6	49.2	48	60.7	52	56.6	59	68.5	54
7	9.5	-13	6.0	-17	6.0	2	17.5	-56
8	4.2	8	4.2	8	4.2	16	6.7	-55

Site 7

<u>Wind Pattern</u> (Tidal Current Starting Phase = 0 Degrees)	<u>Perturbation Cases</u>							
	<u>Net +25%</u>		<u>Net -25%</u>		<u>Wind +25%</u>		<u>Wind -25%</u>	
	<u>ΔX</u> (km)	<u>ΔT</u> (hrs)						
1	3.0	-1	4.2	2	4.2	9	9.5	-19
2	4.2	1	0.0	2	0.0	5	6.7	-7
3	8.5	-2	31.3	-22	27.7	0	8.5	-43
4	0.0	-3	4.2	0	4.2	10	9.5	-27
5	4.2	0	30.6	102	30.6	0	36.0	0
6	9.5	-11	68.5	66	68.5	79	28.5	-11
7	29.5	25	6.7	10	3.0	25	36.2	7
8	12.7	-54	12.0	28	9.0	40	15.0	-54

ΔX = radial distance from base case termination cell to perturbation termination cell

ΔT = difference in termination times between base case and perturbation case ($T_{base} - T_{perturbation}$). Positive ΔT indicates perturbation trajectory terminated sooner than base case trajectory.

developed. This table presents the variation in contact cell termination by means of the distance (in kms), between the base case termination cell and the systematic perturbation case termination cell. Table 8 also provides the time difference between base case times to impact and systematic perturbation case times to impact. A positive time indicates that the perturbation trajectory terminated sooner, a negative time indicates the perturbation trajectory took longer to terminate. This information provides direct comparison of the expected variability of the results of the oil spill simulation when subjected to the specified systematic perturbation of the input data.

For Site 1, wind pattern No. 1, Table 8 shows that all perturbation trajectories terminated close to or at the base case termination cell (see Figures C-1 through C-4). The times to impact are shown to be sooner than the base case for the perturbation cases net +25 percent and wind +25 percent, and later for wind -25 percent. In light of the wind and net current patterns, the only unexpected result is the shorter termination time for the perturbation case, net +25 percent. Comparison between the base case trajectory and the net +25 percent trajectory shows that the later trajectory is moved closer to Port Graham and into a weaker net current field, even after being increased 25 percent. This allows the wind to move the trajectory further south in the same period of time resulting in an earlier contact time compared to the base case.

As shown in Table 8 the distances and termination times for perturbation cases net +25 percent and wind -25 percent for Site 1 are similar for both wind patterns Nos. 1 and 2 (see Figures C-1, C-4, C-9, and C-12). However, large variations exist for perturbation cases net -25 percent and wind +25 percent for Site 1 wind patterns Nos. 1 and 2, (see Figures C-2, C-3, C-10, and C-11). The perturbation trajectories shown in Figures C-10 and C-11 do not impact Ushagat Island as the trajectories shown in Figures C-2 and C-3 do, but traversed slightly to the east between Ushagat and W. Amatuli Islands, and terminated on the grid boundary. This provides the large variations in these two similar sets of perturbation cases. The stronger winds associated with the perturbation case wind +25 percent for

wind patterns No. 2 drive the trajectory through the northwesterly flowing net current field in Kennedy Entrance faster, thus reducing the westerly component imparted to the base case trajectory by the net current. The increased wind velocity also reduces the westerly component of the resulting vectoral addition of the various current components, also aiding the more easterly perturbation trajectory.

The perturbation case for Site 1 wind pattern No. 2 net -25 percent generates the same effect. Reducing the net current in Kennedy Entrance reduces the westerly drift in that area, however, the time element is not as important. The trajectory passes through the Barren Islands slightly sooner than it took the base case to impact Ushagat Island. This is mainly attributed to the reduced northerly component of net current above Cape Elizabeth.

For Site 1 wind pattern No. 3 (see Figures C-17 through C-20), the results of all the perturbation cases show a difference in distance of 51.8 km from the base case trajectory termination cell. The base case trajectories narrowly passed Kalgin Island and terminated at the grid boundary between The Forelands. All perturbation trajectories for Site 1 wind pattern No. 3 terminated at the southern tip of Kalgin Island. The times to impact show the relative influence of the current field being systematically increased or decreased. The relative times to impact are also consistent with logical expectations given the relative magnitudes of the wind drift and net current component fields through this region of Lower Cook Inlet.

The trajectories for Site 1 wind pattern No. 4 show little variation in distance between termination cells compared with the base case trajectory termination cell (see Figures C-25 through C-28). All trajectories terminate along the southern portion of Kalgin Island. Since wind pattern No. 4 is the same as wind pattern No. 3, except for greater wind speeds, it becomes apparent that the wind drift current component dominates the trajectory for this site. The times to impact also show that the wind field dominates as perturbation cases wind +25 percent produce the only significant variation.

wind patterns No. 2 drive the trajectory through the northwesterly flowing net current field in Kennedy Entrance faster, thus reducing the westerly component imparted to the base case trajectory by the net current. The increased wind velocity also reduces the westerly component of the resulting vectoral addition of the various current components, also aiding the more easterly perturbation trajectory.

The perturbation case for Site 1 wind pattern No. 2 net -25 percent generates the same effect. Reducing the net current in Kennedy Entrance reduces the westerly drift in that area, however, the time element is not as important. The trajectory passes through the Barren Islands slightly sooner than it took the base case to impact Ushagat Island. This is mainly attributed to the reduced northerly component of net current above Cape Elizabeth.

For Site 1 wind pattern No. 3 (see Figures C-17 through C-20), the results of all the perturbation cases show a difference in distance of 51.8 km from the base case trajectory termination cell. The base case trajectories narrowly passed Kalgin Island and terminated at the grid boundary between The Forelands. All perturbation trajectories for Site 1 wind pattern No. 3 terminated at the southern tip of Kalgin Island. The times to impact show the relative influence of the current field being systematically increased or decreased. The relative times to impact are also consistent with logical expectations given the relative magnitudes of the wind drift and net current component fields through this region of Lower Cook Inlet.

The trajectories for Site 1 wind pattern No. 4 show little variation in distance between termination cells compared with the base case trajectory termination cell (see Figures C-25 through C-28). All trajectories terminate along the southern portion of Kalgin Island. Since wind pattern No. 4 is the same as wind pattern No. 3, except for greater wind speeds, it becomes apparent that the wind drift current component dominates the trajectory for this site. The times to impact also show that the wind field dominates as perturbation cases wind ± 25 percent produce the only significant variation.

Table 8 shows large variations between all perturbation cases for Site 1 wind pattern No. 5 and the base case termination cell and time to impact (see Figures C-33 through C-36). The base case trajectory slowly moves northward and impacts the southern tip of Kalgin Island (wind patterns Nos. 5 and 6 are similar in direction to Nos. 3 and 4 in the upper portion of Lower Cook Inlet). However, all perturbation trajectories for Site 1 wind pattern No. 5 move easterly and terminate along the shoreline in the vicinity of Anchor Point.

Since wind pattern No. 6 is similar to wind pattern No. 5, the results of the systematic perturbation analysis for Site 1 are also similar (see Figures C-41 through C-44). The base case trajectory for Site 1 under the influence of wind pattern No. 6 moved northward and terminated on Kalgin Island. As for wind pattern No. 5, the perturbation trajectories for wind pattern No. 6 moved eastward and terminated along the shoreline in the vicinity of Anchor Point.

The base case trajectories for Site 1 wind pattern No. 7 all move basically westward, making contact between Chinitna and Iniskin Bays (see Figures C-49 through C-52). Wind pattern No. 7 is predominantly westward in this section of the inlet. The net current changes from northeasterly to northwesterly to southwesterly as one moves from east to west across the inlet from spill site No. 1. The strongest net currents are the northeasterly and southwesterly flows. The perturbation cases for Site 1 wind pattern No. 7 show relatively small variations in termination cell distances. This indicates the dominance of the wind for these trajectories. The perturbation case net +25 percent terminates further south than the base case as expected due to the increased southwesterly flow near the western shoreline. The time to contact is increased over the base case as the trajectory moves further from Site 1.

The perturbation case net -25 percent for Site 1 wind pattern No. 7 allows the stronger tidal currents along the eastern side of Lower Cook Inlet to have a greater effect on the trajectory as it moves more southerly than the base case trajectory during its initial movement away from spill

site No. 1. This results in the perturbation trajectory terminating slightly south of the base case trajectory. Due to the reduced westerly component from the net current, the time to contact is increased.

The perturbation cases wind +25 percent for Site 1 wind pattern No. 7 also show termination cells and times to contact as expected (see Figures C-51 and C-52). The wind +25 percent perturbation case takes less time to contact and is slightly south of the base case, not being affected by the northerly component of net current in the southern edge of the net current eddy off of Chinitna Bay. The wind -25 percent trajectory takes longer to impact and makes contact south of the base case trajectory termination cell as the stronger tidal currents on the eastern side of the inlet have a longer period of time to affect the trajectory movement. The southwesterly flowing net current along the western portion of the inlet drives the trajectory further south.

The perturbation cases for Site 1 wind pattern No. 8 (see Figures C-57 through C-60), show relatively little variation in contact cell compared with the base case trajectory. The winds near spill site No. 1 from wind pattern No. 8 are easterly and because the net currents are small in magnitude, the winds dominate trajectory movement. This is readily apparent from the variation of the perturbation cases net +25 percent, which are identical. As expected, the perturbation case wind +25 percent arrives sooner and wind -25 percent arrives later.

Similar reasoning can be applied to the systematic perturbation trajectories run for Site 7 to provide insight to the variations in contact cell distances and termination times presented in Table 8. As can be seen from the values listed in the table and the trajectories shown in Figures C-1 through C-64, significant variation can exist from selected sites and wind patterns.

It should be emphasized that the systematic perturbations were applied to rather spatially uniform current fields with only one simplified time-dependent current component (tidal current). In reality, the current fields

would experience a wide range of spatially and temporally varying perturbations. However, the results of the systematic perturbation analysis show that trajectory variations do exist and can be quite large. Perturbation trajectories should be examined closely in order to understand the variation in termination cell distances and time differences presented in Table 8.

A special systematic perturbation analysis was conducted for postulated spill site Number 3. This site is the most westerly of all the postulated spill sites. Questions arose during the study regarding the impact that might occur along the shoreline of Kamishak Bay and Augustine Island due to a reduced wind field magnitude imposed on the trajectories originating from Site 3. A limited systematic perturbation analysis was performed for Site 3 using all eight wind patterns reduced in magnitude by 25 percent. An initial tidal current phase of zero degrees was selected for each run. The eight trajectories are presented in Appendix C, Figures C-65 through C-72.

Trajectories from Site 3 for wind patterns 1 and 2 would have the potential to impact Augustine Island if the wind vector magnitudes were reduced so that the wind drift current component was nearly equal to the net current component. As seen in Figures C-65 and C-66, the wind drift current component still dominates even after being reduced 25 percent and the trajectories move southerly and southeasterly away from Kamishak Bay.

If wind patterns Nos. 3 and 4 were reduced in magnitude so that the wind drift current component were equal to or less than the net current component, the resulting trajectories could be driven in a westerly or southwesterly direction. This would result in potential contact being made along the northern shoreline of Kamishak Bay or on Augustine Island. As shown on Figures C-67 and C-68, the 25 percent reduction in the wind magnitude did not result in contact being made along Kamishak Bay or Augustine Island. The winds still dominate the trajectory movements driving them into the shoreline between Iniskin and Chinitna Bays.

Due to the vectoral combinations of the wind drift and net current components, wind patterns Nos. 5 and 6 would need to be severely reduced in

magnitude to result in trajectory movement from Site 3 into Kamishak Bay. Figures C-69 and C-70 show that this situation was not created, even for a 25-percent reduction in the wind field magnitudes. The trajectory for wind pattern No. 5 moves slowly toward the southeast until it encounters the weaker net currents in the central portion of Lower Cook Inlet. The trajectory then moves toward the northeast until it exceeds the simulation time limit and terminates in the middle of the inlet. The trajectory driven by wind Pattern 6 shows a similar fate, with the influence of the wind field being more dominant and driving the trajectory further up the middle of the inlet.

Wind Pattern 7 is directed toward the northwest near Site 3, and the base case trajectory is shown on Figure B-57 to move almost due west making contact just north of Ursus Cove. If the winds were reduced, the net current might drive the trajectory further south into Kamishak Bay. As shown on Figure C-71, with the wind field reduced 25 percent in magnitude, the trajectory does move further south than the base case and takes nearly twice as long to make contact. However, with the 25-percent reduction in wind field magnitude, the trajectory terminates only 10 km from the base case trajectory and does not move into the southern portion of Kamishak Bay.

Wind Pattern 8 would need to be reduced to nearly zero magnitude before a trajectory from Site 3 would have even a remote chance of moving into and making contact along the shoreline of Kamishak Bay. However, for continuity this wind pattern was reduced in magnitude by 25 percent and a trajectory simulated. The base case trajectory for Site 3 wind Pattern 8 made contact near Cape Elizabeth. The reduction in the wind speed allows the trajectory, shown in Figure C-72, to be driven further south due to the increased influence of the net current component. As the trajectory approaches Kennedy Entrance the net current and wind drift current components become nearly equal in magnitude and opposite in direction. This results in the centroid of the trajectory oscillating with the tidal currents in a northwest and southeast direction until it exceeds the simulation time limit and terminates.

C. RANDOM PERTURBATION ANALYSIS

A random perturbation analysis was performed in recognition that the environmental forcing fields are not smooth and deterministic, but are affected by naturally occurring turbulent phenomena. As in the systematic error analysis, the purpose of the random perturbation analysis is to measure the sensitivity of the final shoreline distribution of impact points to these fluctuations.

To carry out this approach, the probability distribution functions for the wind and current fields are needed. The only data for which measurements of standard deviations were readily available were for net currents. These data were only available at a few stations, where the standard deviation was given parallel and perpendicular to the mean net current vector. The measured net current standard deviations were used to estimate a simplified distribution of the standard deviation for the entire net current field as shown in Figure 18.

The deviations are largest in the Kennedy Entrance area where the net current field exhibited considerable variability. While the net currents in Kamishak Bay are generally weak, they also appear to be relatively stable and consequently show small standard deviations in both components. Similarly, the net current field in the middle portion of Lower Cook Inlet west of Kachemak Bay is relatively well defined compared to the southern portion of the Inlet. The standard deviations are larger than in Kamishak Bay since the current field itself is stronger. The standard deviations of net currents in the vicinity of Kalgin Island are not defined since current meter data are not presently available. Hence, no random perturbation cases were run in this area.

At each time step, the net current was perturbed by adding vectors parallel and perpendicular to the mean net current. The magnitudes of these additional vectors were randomly drawn from a normal distribution with a mean of zero and the standard deviation as defined in Figure 18.

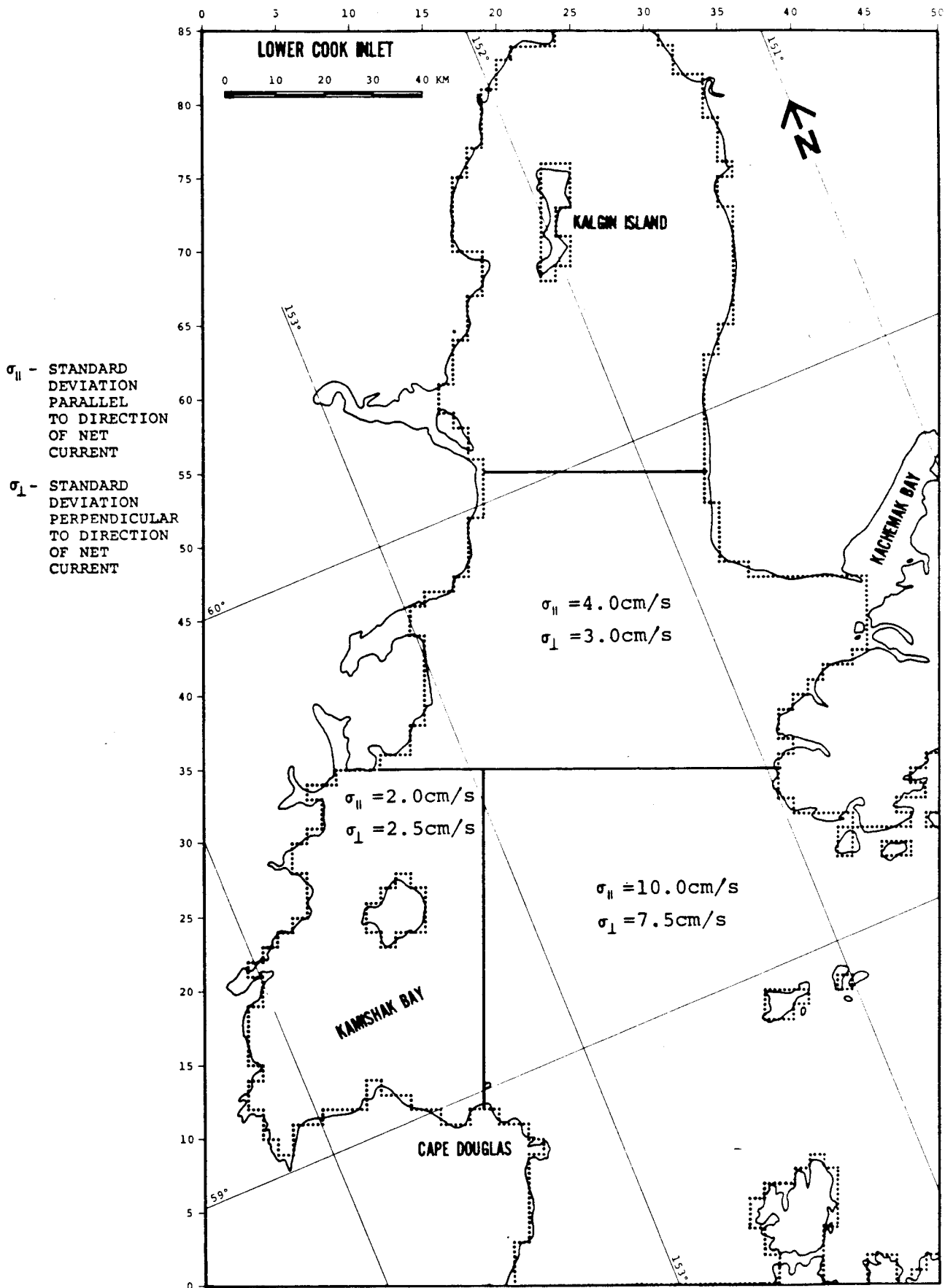


FIGURE 18: NET CURRENT STANDARD DEVIATION DISTRIBUTION

A series of 18 trajectories were run for each selected base case where the net current field was subjected to a random distortion throughout the entire period of simulation. These trajectories are shown in Appendix C, Figures C-73 through C-78, (note that, for purposes of clarity, only nine trajectories are plotted in each figure). By choosing 18 trajectories, it can be asserted that 90 percent of the trajectory population lies within the extremes of the observed shoreline distribution at the 75-percent confidence level.

The results of this perturbation analysis must be interpreted with some care. The computed distribution of shoreline impact points is not representative of any annual distribution. Rather, the distribution of shoreline impact points is what might possibly be expected, given that the base case simulation conditions are prevailing and assuming that the standard deviation derived from the current meter records are uncorrelated with space and time. Specifically, the net current standard deviations must be assumed to be uncorrelated with the wind and current fields. The trajectory deviations from the base cases, then, are due only to purely random phenomena acting to modify the base case environmental fields.

Adopting this point of view, an important conclusion can be drawn based on the relatively narrow range of shoreline impact points. This range--approximately three grid cells or 10 km--is less than what is believed to be attributed to unknowns in the base case data itself. For example, the range of impact points observed in the systematic perturbation analysis is much greater than that computed here.

Since the random deviations imposed on the net current field are selected from a Gaussian distribution, it is possible to derive approximate results that indicate the functional dependence of these results on step size. Consider an idealized case where:

- 1) $\sigma_{||} \equiv 0$
- 2) the base case net current field is uniform in space and constant in time.

The resultant distribution on a line perpendicular to the net current field would be normal with a standard deviation given by

$$\sigma_s = \sqrt{n} \cdot \sigma_1 \cdot \Delta t \quad (2)$$

where σ_s = standard deviation of the impact point distribution

n = number of steps required to reach the trajectory end point

Δt = time step

σ_1 = standard deviation of the random component of the net current distribution

The trajectories shown in Figures C-73 and C-74, remain in the region where σ_1 is a constant 7.5 cm/s (270 m/hr). Ignoring divergencies in the wind and current driving fields, and noting that the base case trajectory contacted the shoreline after 84 time steps, a value for σ_s of 1.2 km is obtained. Thus, it would be expected that two-thirds of the random perturbation cases would impact within approximately 2.5 km of the shoreline. This is less than one grid cell. Clearly, except for long trajectories or those moving through areas of high variability, the deviations in the base case trajectories introduced by random perturbations in the net current field are small.

The effect of the time step, Δt , on the shoreline distribution can be determined by rewriting Equation (2). Since, in the idealized case, there is no velocity perturbation parallel to the constant, uniform base case net current field, the number of time steps in the simulation is given by

$$n = \frac{T}{\Delta t}$$

where T = period of simulation, a constant. Using this result, Equation (2) can be written as

$$\sigma_s = \sqrt{T \cdot \Delta t} \cdot \sigma_1$$

Thus, the standard deviation of the distribution of shoreline impact points is proportional to the root of the time step.

Information on the persistence of the net current field from the field observations was not available during this study so Δt was chosen to be equal to the time step size used in the base case simulations, one-half hour. If, in fact, the persistence is greater than this value, the dispersion of shoreline impact points would be underestimated by the value of 1.2 km calculated for σ_s . If the persistence is, say, an order of magnitude larger than assumed here, then the value of σ_s would only be approximately 4 km, or just over one cell width. In order to have a major impact on the results presented, the net current persistence would have to be on the order of 100 hours. However, if this is true, then the basic assumptions inherent in this random perturbation analysis are not likely to be valid and an entirely different approach to the analysis of random fluctuations in the net current field would have to be taken.

Figures C-77 and C-78 illustrate the importance of the base case driving fields relative to their random deviations. The clear bifurcation of the 18 trajectories can be understood by noting the divergence of the tidal current field in the lower portion of Kamishak Bay as illustrated in Figure 12. The resulting direction each trajectory takes is determined by which of the divergent current vectors is first encountered due to the random fluctuations. The bifurcation results in larger trajectory deviations than introduced by random fluctuations alone.

This explanation suggests that the shoreline distributions shown in Figures C-77 and C-78 might be basically different if starting tidal phases other than zero degrees were selected for initiating the trajectory from Site 7. For example, the tidal current pattern for an assumed phase of 180 degrees, (see Figure 14), does not show the divergence that caused the observed bifurcation in Figures C-77 and C-78.

V. RECOMMENDATIONS

The results and conclusions arising from this project are summarized in the Executive Summary. Consequently, the following discussion focuses on recommendations for future work directed toward developing a more accurate, comprehensive understanding of the fate and behavior of oil spills, particularly in Lower Cook Inlet.

One primary area of concern is the nature, extent, and quality of the wind and current data used to develop the basic spill centroid driving forces. As indicated in the Executive Summary, winds dominate the oil spill movement simulated in this study. However, the meteorological data base has not been developed to the level of detail believed required for reliable oil spill simulation analyses. For example, using constant wind fields over a period of up to 150 hours does not accurately represent the expected wind persistence in the Lower Cook Inlet region.

An improved method is needed to simulate more representative wind fields that approximate the time histories and persistence of winds over Lower Cook Inlet. It is suggested that the same basic typology of wind patterns developed by Putnins (1966 and 1967) be used in conjunction with a first-order transition matrix, which would link the wind patterns in simulating a meteorological event. Such a matrix would give, for any wind pattern, the probability of transition to any other wind pattern.

In place of the deterministic base cases developed here, an ensemble of simulations from each site could be run to directly develop the equivalent of Figure ES-2, the annual percent probability of shoreline exposure. While the results of such an approach are difficult to predict, a much broader distribution of impact points would be generally expected due to the variability of wind patterns imposed. For example, realistic sequences of events could lead to impacts in, say, the Cape Douglas area that do not occur under the present approach (see Figure C-77).

An example trajectory generated by the implementation of a simplified version of such a scheme is shown in Figure 19. While this trajectory is based on a hypothetical sequence of events, it does illustrate that explicit inclusion of the time dependency of the winds can potentially lead to trajectories and impact points not attainable under the approach used in this study. This trajectory was generated in the following manner:

- 1) Net and tidal currents were unchanged from the base case simulations.
- 2) Wind fields were the same as the base case with the exception that they were (arbitrarily) assumed to persist for only 30 hours.
- 3) Wind field transition probabilities were taken to be 1/7. That is, given any wind field, the probability of transition to any other was equally likely.
- 4) Using random numbers, several sets of wind field sequences were generated until a "reasonable" one was available. Typically, the reasonable criteria was used to eliminate transition sequences such as 7-8-7.
- 5) The selected sequence of Patterns 6-5-7-7-2 was input to the oil spill model and the trajectory calculated.

The nature of the resultant trajectory makes evident the clear need to include the time-dependency to the meteorological data in future efforts.

It is proposed that a fundamentally different scheme might be considered which would link a meso-scale wind model directly to the oil spill model to provide direct input representation of wind fields. One noteworthy advantage of this approach would be its ability to more accurately represent local wind field disturbances than are presently available in the use of Putnins wind types. In addition, this methodology would permit the modeling of realistic meteorologic events such as the passage of a front across Cook Inlet.

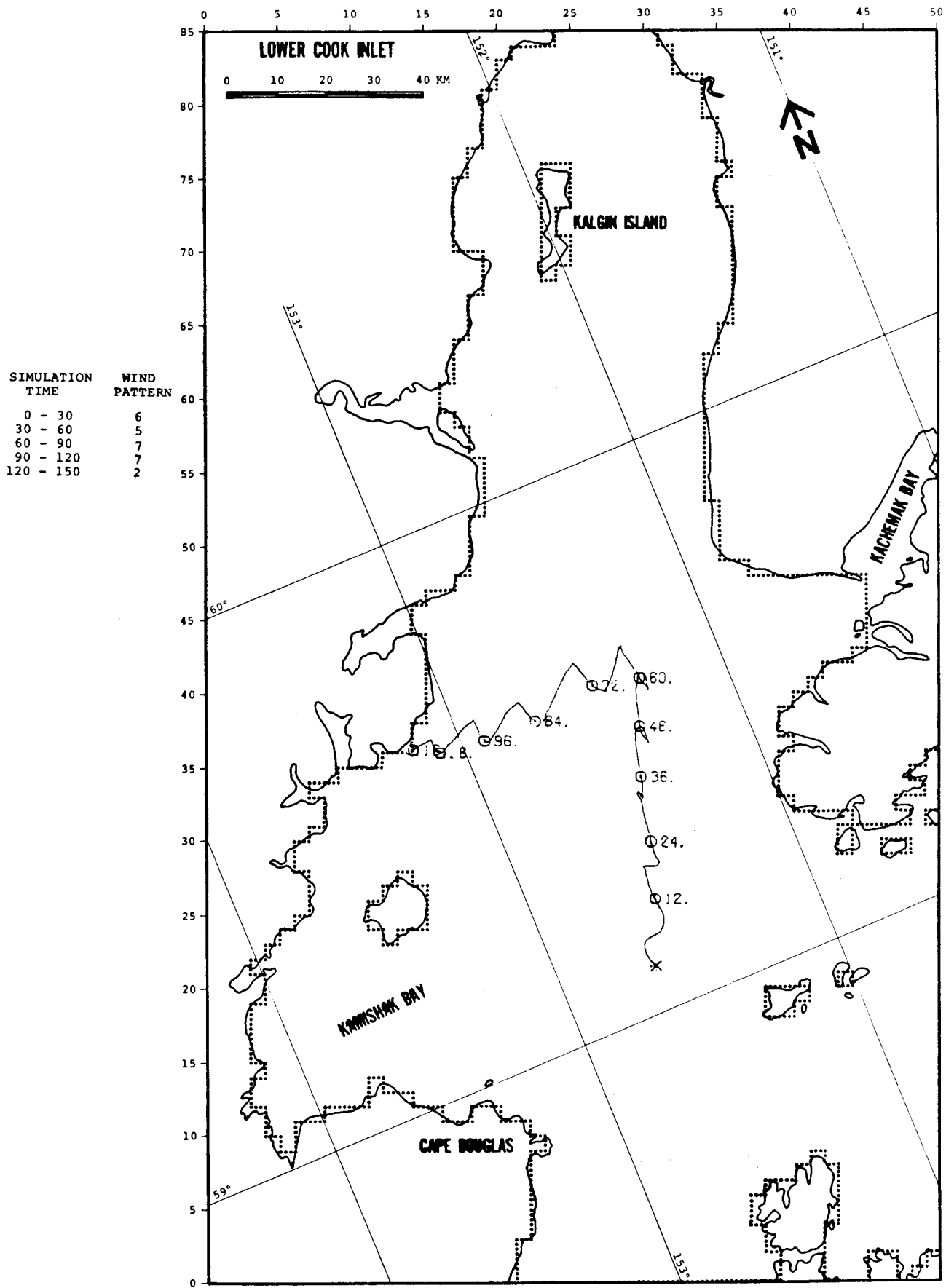


FIGURE 19: TIME DEPENDENT WINDFIELD TRAJECTORY

The use of such a meso-scale wind field model, while expensive to run repeatedly is a step toward the development of an operational real-time oil spill model. A bank of results could be developed for commonly observed meteorologic events and the results filed for quick recall or the model could be run when a spill occurred given the specified prevailing wind conditions.

Additional efforts to improve the net and tidal current information must also focus on more objective techniques to develop the requisite vector fields. However, the principal difficulty here is not the existence, but rather the availability of field data. As a result of several ongoing programs, a wealth of water column hydrodynamic data has been collected but largely remains unprocessed. The minimal hydrodynamic modeling work done on this project suggests that an expanded hydrodynamic modeling effort using the field data on hand, would likely be successful.

Completion of these proposed activities would increase the confidence placed in the results of future oil spill modeling efforts. Other areas of investigation will need to be addressed in the long-term. Several field observers have noted the important role that density fronts can play in retarding the movement and spread of an oil slick. Lower Cook Inlet in the heavy runoff season will likely exhibit such fronts. One potential means to deal with this facet of Cook Inlet hydrodynamics is through the use of satellite data.

In addition, the presence of ice in Cook Inlet can have a very significant effect on the distribution of spilled oil. For example, oil trapped in or beneath ice may be transported well beyond the region otherwise contaminated or may be held without significant decay for extended periods, possibly as long as several years. Oil spills entrained by ice is an area of research that has yielded little information to date for use by modelers.

The oil spill model used in this study is based on a relatively simple, well accepted methodology to predict spill centroid movement.

While sophisticated transport models are available, evaluations of the environmental data base weaknesses indicate that more sophisticated approaches are presently inappropriate.

As the quality and extent of the environmental data increase, more sophisticated numerical modeling efforts should initially focus on applying a two-dimensional surface transport model. Unfortunately, the strong shear exhibited by both the net and tidal currents (more realistic wind fields are also likely to exhibit more shear than the ones used in this study) may preclude the use of the Fay-Holt model (Fay, 1969 and Holt, 1972) for spreading in calm water as used by several previous investigators (Isakson, 1975; Premach and Brown, 1973; and Wang, 1974). A two-dimensional model that could realistically treat shearing forces would contribute to the state-of-the-art.

It is difficult to assess the importance and viability of applying three-dimensional hydrodynamic models. Presently, existing limitations on knowledge of the physical processes, as discussed in Section II, hamper progress toward a 3-D model of oil dispersion. In addition, obtaining carefully controlled verification data, particularly from field experiments, has proven difficult. As a result, limited model verification data are available.

Evaporation can be easily modeled, while wave-slick interaction, although recognized to be important in sinking, is very poorly understood. A prudent approach for future development would be to pursue two-dimensional modeling, accounting for forces known to play a dominant role in oil movement. The approach selected, however, should be easily extendable to three dimensional modeling when appropriate.

BIBLIOGRAPHY

- Alaska Department of Fish & Game, 1975. Miscellaneous data obtained from radar drogue study.
- Burbank, D.C., 1974. Suspended sediment transport and deposition in Alaskan coastal waters, University of Alaska, Masters Thesis, 222p.
- Burbank, D.C., 1977. Circulation studies in Kachemak Bay and Lower Cook Inlet, Alaska. Department of Fish & Game, Anchorage, Alaska (unpublished manual).
- Dames & Moore, 1976, Report, oil spill trajectory analysis, Lower Cook Inlet, Alaska, for National Oceanic and Atmospheric Administration, Job Number 6769-003-20.
- Fallah, M.H., and R.M. Stark, 1976. Literature Review: Movement of Spilled Oil at Sea, Marine Technology Society Journal, Vol. 10, No. 1, January.
- Fay, J.A., 1969. The Spread of Oil Slicks on a Calm Sea, Fluid Mechanics Laboratory, Publication No. 69-6, Department of Mechanical Engineering, Massachusetts Institute of Technology, August.
- Hoult, D.P., 1972. Oil Spreading on the Sea, in Annual Review of Fluid Mechanics, Vol. 4, pp. 341-368.
- Isakson, J.S., et al., 1975. Comparison of Ecological Impacts of Postulated Oil Spills at Selected Alaskan Locations, Mathematical Sciences Northwest, National Technical Information Service, Springfield, Virginia (Accession No. AD-A017-600), June.
- Matthews, J.B., and J.C. Mungall, 1972. A Numerical tidal model and its application to Cook Inlet, Alaska, Journal of Marine Research, Volume 30, Number 1, January 15, pp 27-38.
- Meunch, R.D., Mofjeld, H.O., Charnell, R.L., 1977. Oceanographic conditions in Lower Cook Inlet; spring and summer 1973. Contribution No. 351 from the NOAA ERL, Pacific Marine Environmental Laboratory.
- Muirhead, C., 1978. Personal communication regarding availability of analyzed net and tidal current summaries from 1974 summer data measurement program in Cook Inlet, National Ocean Survey, National Oceanic and Atmospheric Administration, Rockville, Maryland, November.
- Mungall, J.C.H., and J.B. Matthews, 1973. Numerical tidal models with unequal grid spacings, technical report F73-2, Institute of Marine Science, University of Alaska, Fairbanks, Alaska, January, 213 p.

BIBLIOGRAPHY (Continued)

- Mungall, J.C.H., 1973. Cook Inlet tidal stream atlas, technical report R73-6, Institute of Marine Science, University of Alaska, Fairbanks, Alaska.
- Mungall, J.C.H., 1978. Personal communication regarding interpretation of output data from runs of a hydrodynamic model of Cook Inlet. Runs made on Dames & Moore computer facilities and output maintained in job file, Los Angeles, California.
- National Oceanic and Atmospheric Administration, 1978. Tidal Current Tables, Pacific Coast of North America and Asia, 1978. National Ocean Survey, annual publication.
- Oceanographic Institute of Washington, 1977. Modeling Methods for Predicting Oil Spill Movement, submitted to Oceanographic Commission of Washington, Seattle, Washington. March.
- Pearson, C., and R.D. Muench, 1978. Personal communication regarding development of a net circulation pattern for Lower Cook Inlet, Pacific Marine Environmental Laboratory, National Oceanic and Atmospheric Administration, Seattle, Washington.
- Premack, J., and G.A. Brown, 1973. Prediction of Oil Slick Motions in Narragansett Bay, Proceedings Joint Conference on Prevention and Control of Oil Spills, Washington, D.C., 13-15 March 1973, pp. 531-540.
- Putnins, Paul, 1966. Studies on the Meteorology of Alaska: First Interim Report (The sequences of basic weather patterns over Alaska), U.S. Department of Commerce, ESSA, EDS, Silver Spring, MD 10910, 107 p.
- Putnins, Paul, 1969. Studies on the Meteorology of Alaska: Final Report (Weather situations in Alaska during the occurrences of specific basic weather patterns), U.S. Department of Commerce, ESSA, Research Laboratories, Boulder, CO 80302, 267 p.
- Schureman, Paul, 1958, Manual of Harmonic Analysis and Prediction of Tides, Coast and Geodetic Survey, U.S. Department of Commerce, Washington, D.C.
- Wang, S., 1974. A Numerical Model for Simulation of Oil Spreading and Transport and its Application for Predicting Oil Slick Movement in Bays, Tetra Tech., Inc., Report No. TT-P-345-74-1, February.

APPENDIX A

OIL SPILL MODEL DOCUMENTATION

A-1 OVERVIEW

This appendix is intended to expand on the discussion contained in Section II describing the oil spill model used in the study. Particular emphasis is placed on the numerical algorithms in the model and the schemes used to implement them. Also included are several verification cases that illustrate the correct operation of the model.

A-2 TRAJECTORY ALGORITHM

One key aspect of the model operation is the input and interpolation of the wind and current fields. Data defining the spatial and temporal variation of the wind and current fields are prescribed at the intersection of the grid lines. Since the number of intersection points can become large (there are over 45,000 for the grid used in this study, see Figure 1), the model has been designed to accept input only at every n th intersection point where " n " is any integer up to the maximum dimension of the grid. Selection of this quantity is based on the variability of the wind and current fields and the level of detail of the input data. For this study, the net current field were input at every second grid point and the tidal current and wind fields at every third grid point.

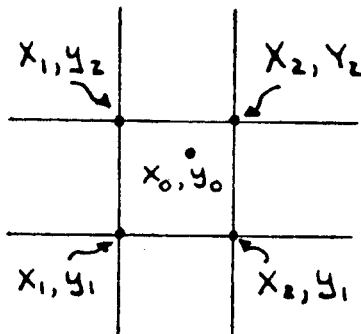
The temporal variation of each of these fields is defined by specifying the entire spatial distribution at one or more times. If only one distribution is given for a field, that field is taken to be constant throughout the period of simulation. This was, in fact, the case for both the net current and wind fields. The temporal variation of the tidal current field was defined by specifying tidally driven currents at 12 points in the tidal cycle.

Once this data is input, certain initialization and "housekeeping" functions are performed and the actual computations begin. The program interpolates the wind and currents to the location of the spill centroid. The interpolation scheme used is a three-way linear interpolation on the two spatial dimensions and on time. Each of the vectors, wind, tidal

current and net current is interpolated independently. For each vector the program interpolates speed and direction separately using the following expressions:

$$\begin{aligned}
 S(x_0, y_0, t) = & \frac{t_2 - t}{t_2 - t_1} \cdot \left[\frac{y_2 - y_0}{y_2 - y_1} \cdot \left(\frac{x_2 - x_0}{x_2 - x_1} \cdot S(x_1, y_1, t_1) + \frac{x_0 - x_1}{x_2 - x_1} \cdot S(x_2, y_2, t_1) \right) \right. \\
 & + \left. \frac{y_0 - y_1}{y_2 - y_1} \cdot \left(\frac{x_2 - x_0}{x_2 - x_1} \cdot S(x_1, y_2, t_1) + \frac{x_0 - x_1}{x_2 - x_1} \cdot S(x_2, y_2, t_1) \right) \right] \\
 & + \frac{t - t_1}{t_2 - t_1} \cdot \left[\frac{y_2 - y_0}{y_2 - y_1} \cdot \left(\frac{x_2 - x_0}{x_2 - x_1} \cdot S(x_1, y_1, t_2) + \frac{x_0 - x_1}{x_2 - x_1} \cdot S(x_2, y_1, t_2) \right) \right. \\
 & + \left. \frac{y_0 - y_1}{y_2 - y_1} \cdot \left(\frac{x_2 - x_0}{x_2 - x_1} \cdot S(x_1, y_2, t_2) + \frac{x_0 - x_1}{x_2 - x_1} \cdot S(x_2, y_2, t_2) \right) \right]
 \end{aligned}$$

where $S(x, y, t)$ = component of speed at a point (x, y) at time t
 x_0, y_0 = location of spill centroid at time t_0
 t_1, t_2 = times where input data are given where $t_1 \leq t \leq t_2$
and where x_1, y_1, x_2, y_2 are grid coordinates surrounding the spill centroid as shown in the following diagram.



The total drift vector is then computed using Equation (1) of Section II and the movement of the oil slick centroid is then determined by that drift vector.

For example, suppose that the centroid is at a location (x_0, y_0) at time t . The drift vector (u_0, v_0) computed at that point then determines the new location (x_n, y_n) at time $t + \Delta t$ by

$$x_n(t+\Delta t) = x_0(t) + u_0\Delta t,$$

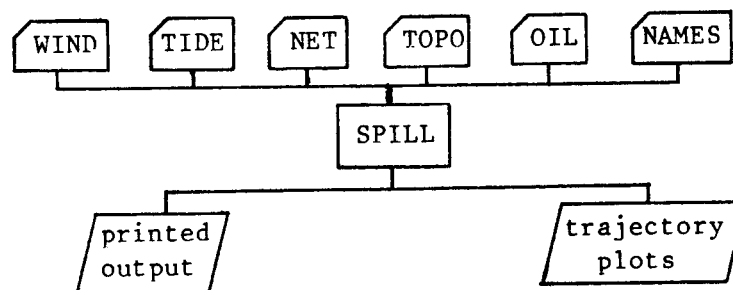
$$y_n(t+\Delta t) = y_0(t) + v_0\Delta t.$$

The trajectory is terminated when either the simulation time exceeds an upper limit or the trajectory intersects a land or water boundary cell.

The program produces a printed output which summarizes the input parameters and the location of the spill at the termination point of the trajectory. Apart from the printed results, a plot of the trajectories is also produced. Up to 13 different trajectories can be displayed on one plot with each marked by a different symbol at selected times along the trajectory.

A-3 MODEL INPUT

The operational structure of the model input and output is illustrated below.



where

	denotes input data
	denotes program
	denotes output.

A brief description of each entity follows:

<u>Entity</u>	<u>Description</u>
WIND	Data file describing the spatial and temporal behavior of the wind field
TIDE	Data files describing the spatial and temporal behavior of the tidal current field
NET	Data files describing the spatial and temporal behavior of the net current field
OIL	Data file containing information on the oil itself (i.e., spill location, density, etc.), and the spill area (i.e., grid size, direction of magnetic north, etc.)
TOPO	Data file containing gridded information on location of land, water, and boundary cells
NAMES	Data file containing control names for data files
SPILL	Program that combines movement and spreading algorithms to produce map of oil distribution
RESULTS	Final output file containing listing of input data and the location of the spill at specified time steps. This file may be sent directly to the printer.
PLOTS	Trajectory plot.

A detailed listing of the data in each of these files is given below:

OIL

<u>Variable</u>	<u>Units</u>	<u>Description</u>
RUN	--	80-character alphanumeric description of the case this data file represents
SOP	--	Spreading option: = 1 - spreading = 2 - trajectory
DOP	--	Display option: (valid for SOP = 2 <u>only</u>) = 0 - display trajectory termination only = 1 - display trajectory at every PSTEP = 2 - display trajectory at every time step (DT)

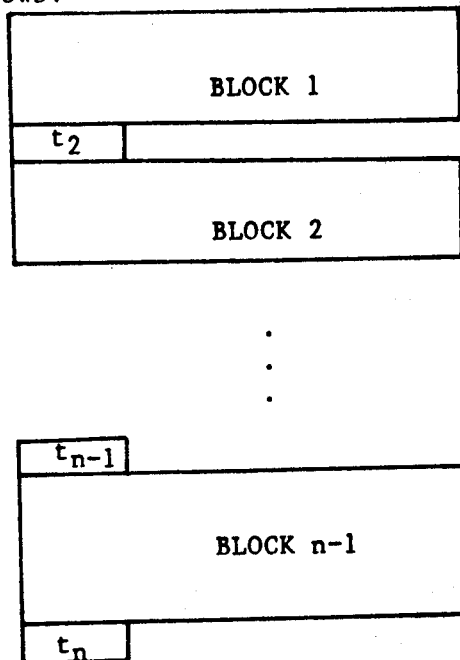
PSTEP	--	Printing frequency given as an integer multiple of the time step (DT).
RH20*	gm/cc	density of seawater
ROIL*	gm/cc	density of oil
SIG*	dynes/cm	net surface tension spreading coefficient
NU*	cm ² /se	kinematic viscosity of seawater
YSPILL	kilometers	y - coordinate of spill location
XSPILL	kilometers	x - coordinate of spill location
CW	--	wind coupling coefficient
C1*	--	inertial spreading coefficient
C2*	--	viscous spreading coefficient
C3*	--	surface tension spreading coefficient
ADEFL	degrees	angle between wind vector and resultant oil velocity vector
MAXDOSE*	gm/meter	maximum shoreline dosage
MINTHIK*	meters	minimum oil film thickness
IMAX	--	number of horizontal cells
JMAX	--	number of vertical cells
DS	kilometers	grid size

*These parameters were not used in this study, but are utilized in applications of the Dames & Moore oil spill model involving spreading as well as transport.

AGRID	degrees	angle from x-axis to magnetic north, measured positive clockwise
DT	hours	time step
ST	hours	simulated period
DCYCLE*	hours	simulation period for force calculation
CUTOFF*	--	first numerical constant for spreading calculation
RSALG*	--	second numerical constant for spreading calculation
CT(1)	hours	calculation start time in wind cycle
CT(2)	hours	calculation start time in tidal current cycle
CT(3)	hours	calculation start time in net current cycle
MFAC(1)	--	number of cells at which wind data are input
MFAC(2)	--	number of cells at which tidal current data are input
MFAC(3)	--	number of cells at which net current data are input
EVAPP*	percent	maximum percent evaporation loss
EVAPT*	hours	maximum period of evaporation
XAXIS	inches	length of x-axis on plot
YAXIS	inches	length of y-axis on plot
Q*	kiloliters	volume of spill

WIND, TIDE, NET

Both wind and current data are input in the same format. For any given parameter, the total set of data can be schematically represented as follows:



Block 1 data describe the spatial dependence of the wind or current fields at time $t = 0$. Block 2 describes the fields at t_2 , and so on. The last time, t_n , denotes the cycle time of that wind or current field. For times greater than t_n , the input file is rewound and reused with each time value increased by t_n .

Within each block, the wind or current fields are input at every n th grid intersection. They are specified in the order (speed, direction) with FORMAT (16F5.0). The direction is relative to magnetic north (positive clockwise) and speed is in meters per second.

INPUT DATA FILES: TOPO

The topographic data file uses the following convention:

<u>Cell</u>	<u>Value</u>
"valid" water	4
"invalid" water	3
land	2
water boundary	1

Here "valid" and "invalid" denote water areas where oil may and may not be allowed by the model. These areas must be separated by a line of cells having a value of 1, the water boundary cell value.

Each cell within the grid is assigned one value. For input convenience, each row may be specified by values in cells that are different from the adjacent cell in that row. The program will fill in the grid with the proper values.

The input is formatted so that the first five columns for each row is an identifier. Columns 6 to 80 correspond on a one-to-one basis with cells in a row. If there are more than 75 cells in a row, the same scheme is continued on the next record in columns 6 to 80.

INPUT DATA FILE: NAMES

Several sets of data may be processed in one run of the oil spill model. Input data file NAMES is the main control file for the spill model, directing it to the correct data files.

Each input line represents one case. The file names are input as follows:

<u>COLUMNS</u>	<u>FILE</u>
1 - 7	Name of the "OIL" data file
11 - 17	Name of the "TOPO" data file
21 - 27	Name of the "WIND" data file
31 - 37	Name of the "TIDE" data file
41 - 47	Name of the "NET" data file

The last card of this file must have the letter "END" in Column 1-3.

Examples of these input data files are included in the next section.

A-4 VERIFICATION

A series of test runs have been made where the trajectory can be analytically described from the solution of a set of differential equations. In addition, three test cases were run where the wind and net current fields were isolated to give a more qualitative the verification of the model.

The four analytic verification cases are all based on one set of driving forces, that are simplified analogies of the actual environmental forcing fields used for this study. A constant wind, a spatially varying net current field and a temporally varying tidal current field defined on a 13 x 13 grid were run singly or in combination to test the model. The necessary data files used to run the verification cases are shown in Table A-1.

The OIL data file shown is best understood by reading it left to right, line by line, in correspondence with the list of input parameters given above (also, see Table A-2 for a restatement of the input data by the program itself).

TABLE A-1

VERIFICATION DATA FILES

OIL data file

2.	0.	20.	7.769	7.769			
1.	.85	9.5	0.012	1000.	14.	5.	8.
0.03	1.14	1.45	2.3	0.0	0.0	0.0	30.
13	13.	1.5	270.	0.1	8.	0.3	
0.0	0.0	0.0	13.	13.	13.0	0.0	0.1

TOPO data file

13	2	2
12	23314	42
11	2314	42
10	214	41
9	24	42
8	24	42
7	24	42
6	24	42
5	24	42
4	24	42
3	24	42
2	24	42
1	1	1

WIND data file

6.	180.	6.0	180.
6.	180.	6.0	180.
30.			

NET data file

0.0	270.	0.6	270.
0.0	270.	0.6	270.
30.			

TIDE data file

.4	0.	.4	0.
.4	0.	.4	0.
2.0			
.4	90.	.4	90.
.4	90.	.4	90.
4.0			
.4	180.	.4	180.
.4	180.	.4	180.
6.0			
.4	270.	.4	270.
.4	270.	.4	270.
8.0			

TABLE A-2

SAMPLE OF PROGRAM OUTPUT

DAMES AND MOORE OIL SPILL MODEL

RUN IDENTIFICATION: VERIFICATION TEST TRAJECTORY MODE.

SPREADING OPTION 2	DISPLAY OPTION 0
PRINT FREQUENCY 5	DENSITY OF SEAWATER 1.000 (GM/CC)
DENSITY OF OIL .850 (GM/CC)	SPREADING COEFFICIENT 9.500 (DYNES/CM)
KINEMATIC VISCOSITY .012 (CM**2/SEC)	SPILL VOLUME 1000.00 (KLS)
WIND COUPLING COEFFICIENT .0300	INERTIAL SPREADING COEFFICIENT 1.14
VISCOUS SPREADING COEFFICIENT 1.45	SURFACE TENSION SPREADING COEFFICIENT 2.30
WIND/OIL DEFLECTION ANGLE 0.0 (DEG)	MAXIMUM SHORE DOSEAGE 0.00(GM/M)
MINIMUM FILM THICKNESS 0. (M)	NUMBER OF HORIZONTAL CELLS 13
NUMBER OF VERTICAL CELLS 13	GRID SIZE 1.50 (KM)
MAG. NORTH-HORIZONTAL AXIS ANGLE 270.0 (DEG)	TIME STEP .4000 (HRS)
STOP TIME 30.0 (HRS)	CUTOFF .30
SPREADING ALGORITHM 0	WIND START TIME 0.0000 (HRS)
PRIMARY CURRENT START TIME 0.0000 (HRS)	RESIDUAL CURRENT START TIME 0.0000 (HRS)
WIND GRID MULTIPLE 13	PRIMARY CURRENT GRID MULTIPLE 13
RESIDUAL CURRENT GRID MULTIPLE 13	X-COORDINATE OF SPILL LOCATION 1.40000E+01 (I)
Y-COORDINATE OF SPILL LOCATION 5.00000E+00 (KM)	MAXIMUM EVAPORATIVE LOSS 0. PERCENT
MAXIMUM PERIOD OF EVAPORATION .1 (HRS)	DRIFT COMPUTATION END TIME 8.0000 (HRS)
DATA CYCLE PERIOD 8.0000 (HRS)	X-AXIS LENGTH 7.77 (INCHES)
Y-AXIS LENGTH 7.77 (INCHES)	

FIELD LENGTH REQUIRED IS 05J502R

TRAJECTORY 1	TERMINATED AT CELL	10	13	AT TIME	20.400 HOURS.
TRAJECTORY 2	TERMINATED AT CELL	10	13	AT TIME	17.600 HOURS.
TRAJECTORY 3	TERMINATED AT CELL	2	10	AT TIME	13.600 HOURS.
TRAJECTORY 4	TERMINATED AT CELL	2	10	AT TIME	14.980 HOURS.

The TOPO data for this 13 x 13 grid was given a file name of TOPO. The first five columns are numbered 1 to 13 to correspond to the row numbers. Notice how the various areas are coded to represent land, water, and boundary cells.

The WIND file is very compact since a constant wind is easily specified. This file represents a wind with speed of 6 m/s and a direction of 180°. Since the grid is 13 x 13 and, by reference to the OIL data, input is specified at every 13th grid points, only four values are required to fill the entire grid.

The NET CURRENT file illustrates data varying in space. This data represents a current that gradually changes its speed along the X axis. At X = 0 the current is 0.0 m/s, at X = 13 cells, the current is 0.6 m/s. This current is at constant direction of 270 degrees (current toward west).

The TIDE CURRENT file illustrates data changing with time. This is a tide of constant speed of 0.4 m/s that periodically changes its direction in a circular manner from 0 degrees at t=0 to 360 degrees at t=8 hours.

The four verification cases run using these input data files are listed below:

CASE I. Constant Drift

This case shows the spill movement as a result of a constant wind. The analytic solution is:

$$\begin{aligned}\bar{V} &= C_w \cdot V_w \hat{j} = 0.648 \hat{j} \\ y(t) &= 0.648 \cdot t + y_0 \\ x(t) &= x_0\end{aligned}$$

where C_w = wind coupling coefficient = 0.03
 V_w = wind speed = 6 m/s
 x_0, y_0 = centroid starting position
 $x(t), y(t)$ = centroid position as a function of time

CASE II. Time-Dependent Drift

This case tests input data varying with time and shows the location of the spill centroid as a result of the wind and tide. The analytic solution is:

$$\begin{aligned}\bar{v} &= C_w \cdot V_w \hat{j} + V_t \cdot \cos\left(\frac{\pi}{4} \cdot t\right) \hat{j} + V_t \cdot \sin\left(\frac{\pi}{4} \cdot t\right) \hat{i} \\ &= 0.648 \hat{j} + 1.44 \cdot \cos\left(\frac{\pi}{4} \cdot t\right) \hat{j} + 1.44 \cdot \sin\left(\frac{\pi}{4} \cdot t\right) \hat{i}\end{aligned}$$

$$y(t) = 0.648 \cdot t + 1.44 \cdot \frac{4}{\pi} \cdot \sin\left(\frac{\pi}{4} \cdot t\right) + y_0$$

$$x(t) = -1.44 \cdot \frac{4}{\pi} \cdot \cos\left(\frac{\pi}{4} \cdot t\right) + x_0 + 1.44 \cdot \frac{4}{\pi}$$

where the same parameters as Case I are in use.

CASE III. Space-Dependent Drift

This case tests input data varying over space and shows the location of the spill centroid as a result of the wind and net current. The analytic solution is:

$$\begin{aligned}\bar{v} &= C_w \cdot V_w \hat{j} - V_n \cdot x \hat{i} \\ &= 0.648 \hat{j} - \frac{216}{1950} \cdot x \hat{i}\end{aligned}$$

$$x = x_0 \cdot e^{\frac{-216}{1950} t}$$

$$y = 0.648 \cdot t + y_0$$

CASE IV. Compound Drift

This case illustrates both time and spatially-dependent driving fields and is a combination of Cases II and III. The analytic solution is:

$$\begin{aligned} \bar{V} &= C_w \cdot V_w \hat{j} + V_e \cdot \cos\left(\frac{\pi}{4} \cdot t\right) \hat{j} + V_e \cdot \sin\left(\frac{\pi}{4} \cdot t\right) \hat{i} - V_n \cdot X \hat{i} \\ &= 0.648 \hat{j} + 1.44 \cdot \cos\left(\frac{\pi}{4} \cdot t\right) \hat{j} + 1.44 \cdot \sin\left(\frac{\pi}{4} \cdot t\right) \hat{i} - \frac{216}{1950} X \hat{i} \\ y(t) &= 0.648 \cdot t + 1.44 \cdot \frac{4}{\pi} \cdot \sin\left(\frac{\pi}{4} \cdot t\right) + y_0 \\ x(t) &= 0.2535 \cdot \sin\left(\frac{\pi}{4} \cdot t\right) - 1.7977 \cdot \cos\left(\frac{\pi}{4} \cdot t\right) + 15.7977 \cdot e^{-\frac{216}{1950} \cdot t} \end{aligned}$$

These four cases were run using the oil spill program with a time step of 0.1 and 0.4 hours. The printer output, plots of the analytic solution, and plots of the verification runs are shown in Table A-2 and Figures A-1 to A-3. The differences between the analytic and computed solutions are due to a finite time step and are summarized below.

Displacement (km) of Spill at t = 10 hrs

<u>Trajectory</u>	<u>Analytic Solution</u>	<u>Computed Solutions</u>		<u>Relative Difference</u>	
		<u>$\Delta t = 0.1$ hr</u>	<u>$\Delta t = 0.4$ hr</u>	<u>$\Delta t = 0.1$ hr</u>	<u>$\Delta t = 0.4$ hr</u>
1	6.48	6.48	6.48	0.0%	0.0%
2	8.51	8.57	8.72	0.7%	2.4%
3	11.40	11.42	11.49	0.17%	0.78%
4	11.91	12.03	12.38	1.00%	3.9%

These results provide confidence that the program correctly implements the basic movement algorithm and that a 0.4-hour time step was adequate for use in the remainder of the production runs.

The remaining verification runs were made after the input data for the actual current and wind data was ready for analysis. These runs, which consisted of using the net current and selected wind fields in isolation, serve to partially verify these data sets and to verify operation of the model under more complex conditions than the analytic verification cases. The results are shown in Figures A-4 through A-9. Hand calculations indicate that these trajectories are consistent with "eyeball" interpolation of the input data.

BY _____ DATE _____
CHECKED BY _____

REVISIONS BY _____ DATE _____
FILE _____

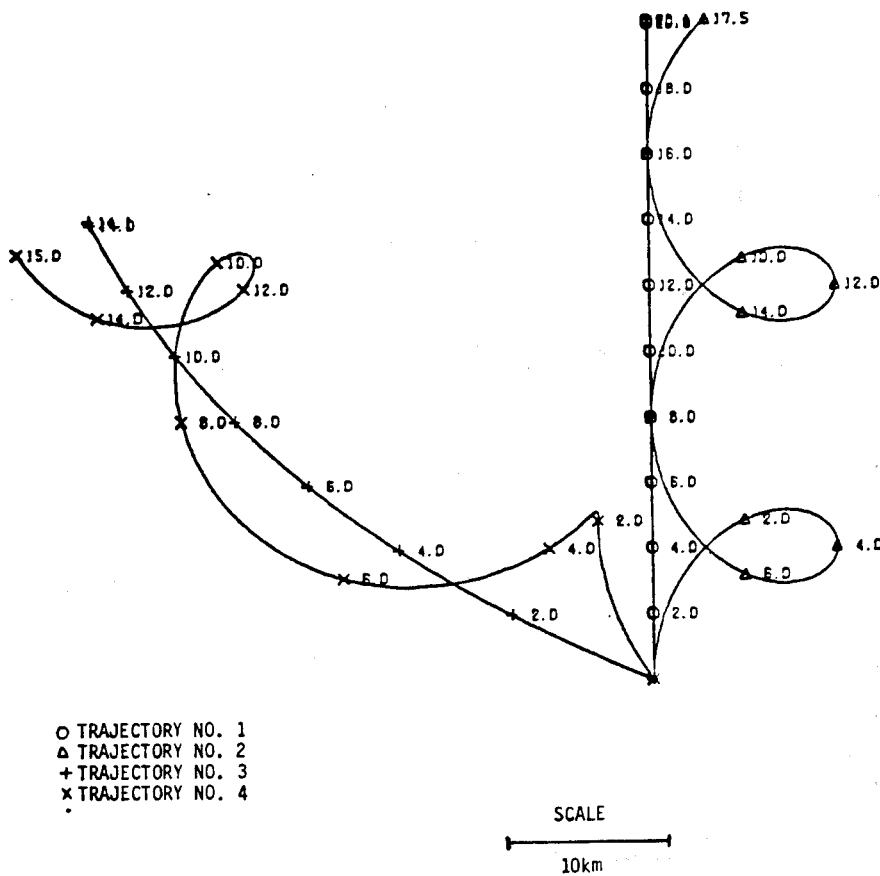


FIGURE A-1: ANALYTIC SOLUTION—VERIFICATION RUNS

DAMES & MOORE

BY _____ DATE _____
CHECKED BY _____
FILE _____
REVISIONS BY _____ DATE _____

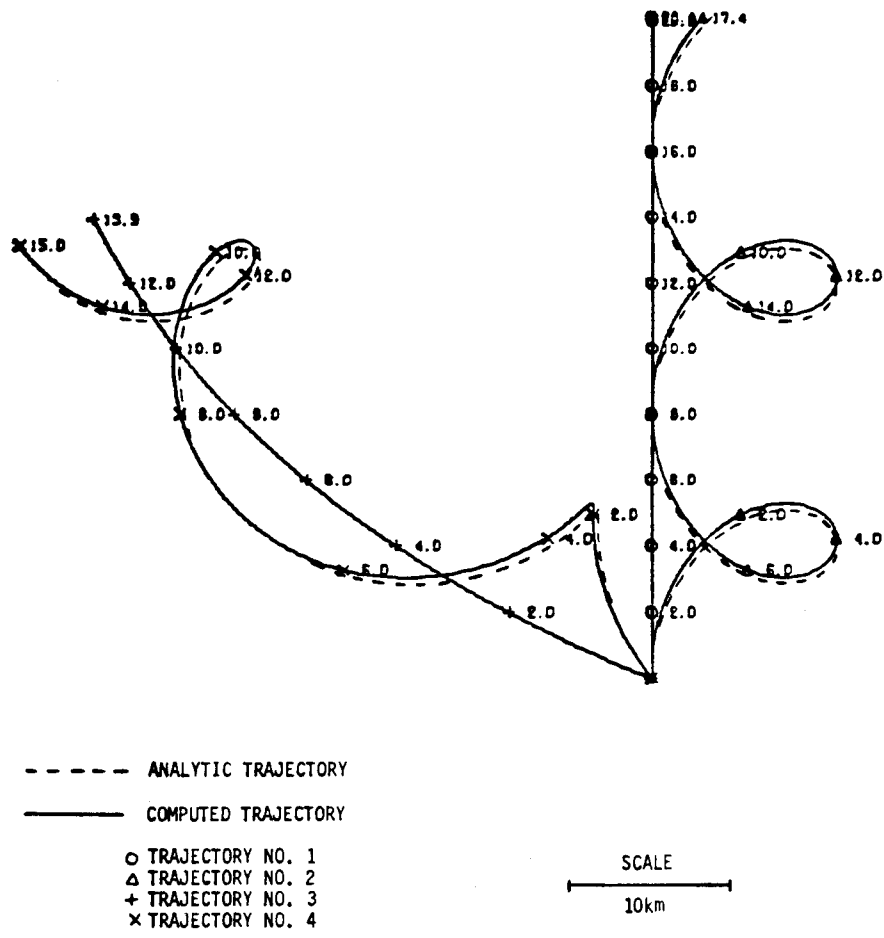


FIGURE A-2: COMPUTED SOLUTION—VERIFICATION RUNS, $\Delta T=0.1$ HRS

BY _____ DATE _____
CHECKED BY _____

FILE _____

REVISIONS BY _____ DATE _____

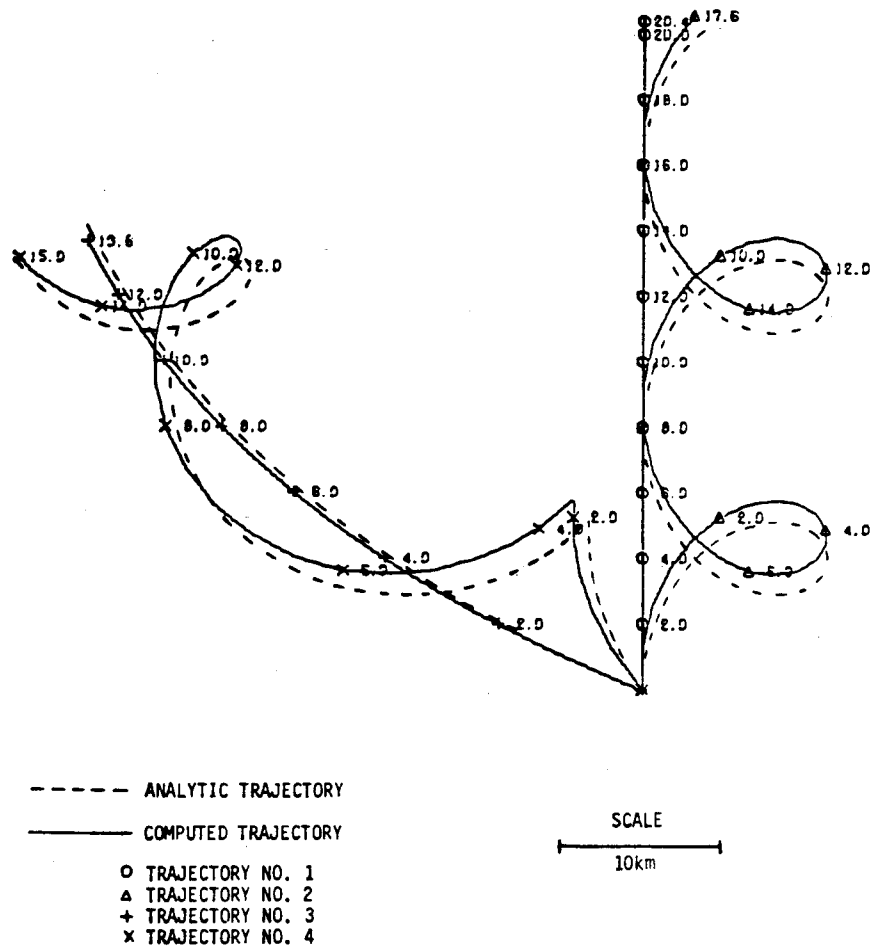


FIGURE A-3: COMPUTED SOLUTION-VERIFICATION RUNS, $\Delta T=0.4$ HRS

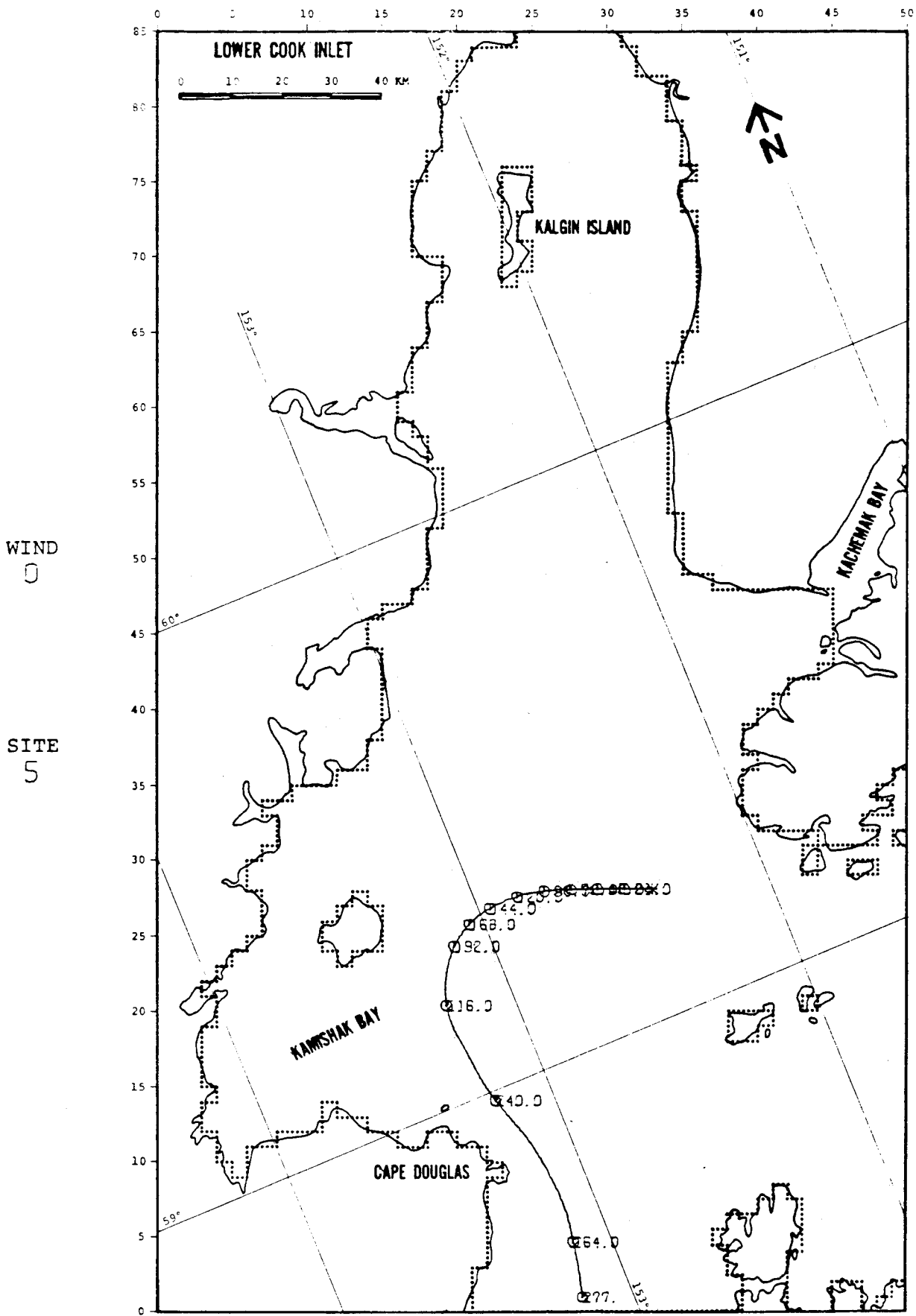


FIGURE A-4: VERIFICATION: NET CURRENT ONLY

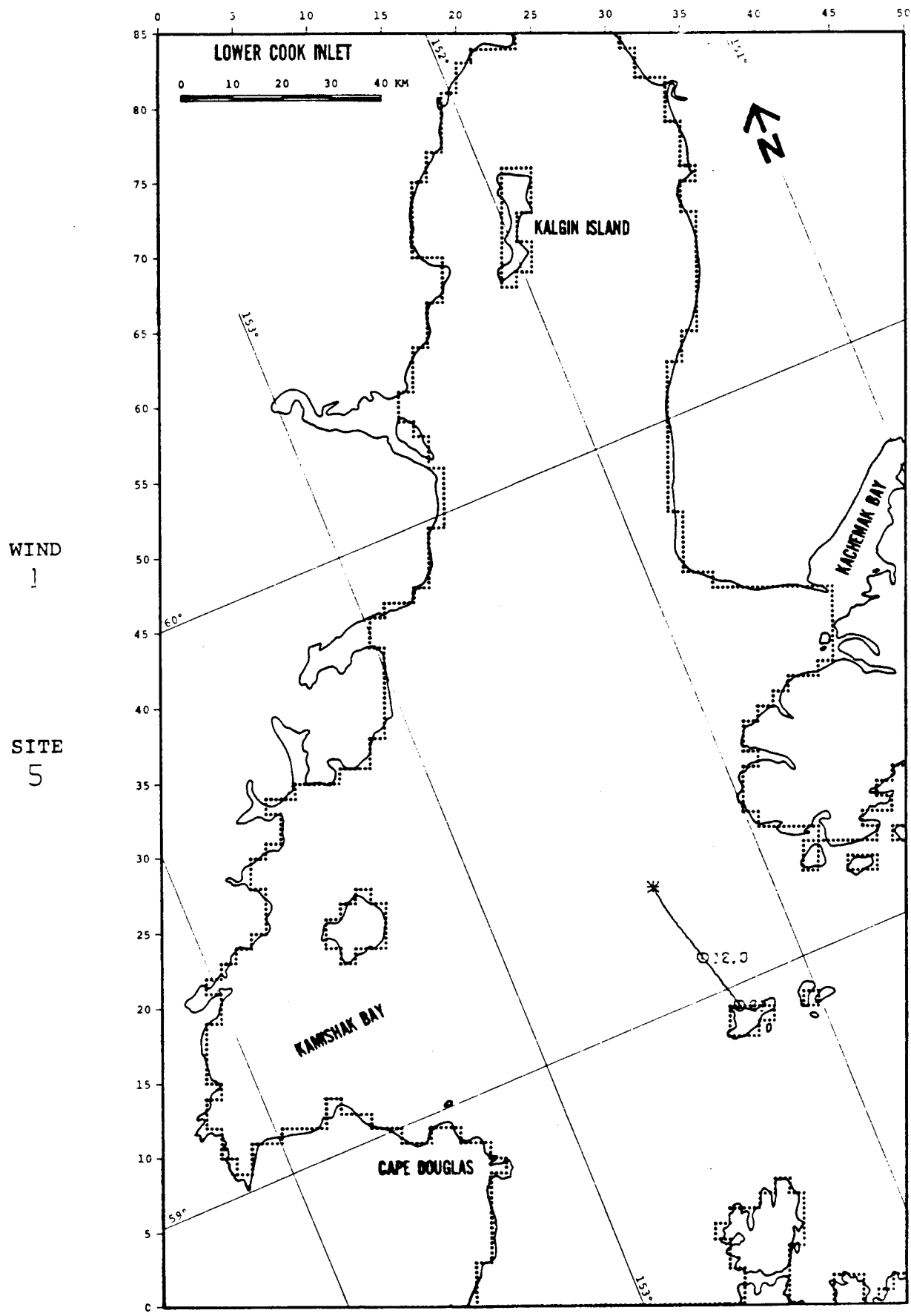


FIGURE A-5: VERIFICATION: WIND ONLY

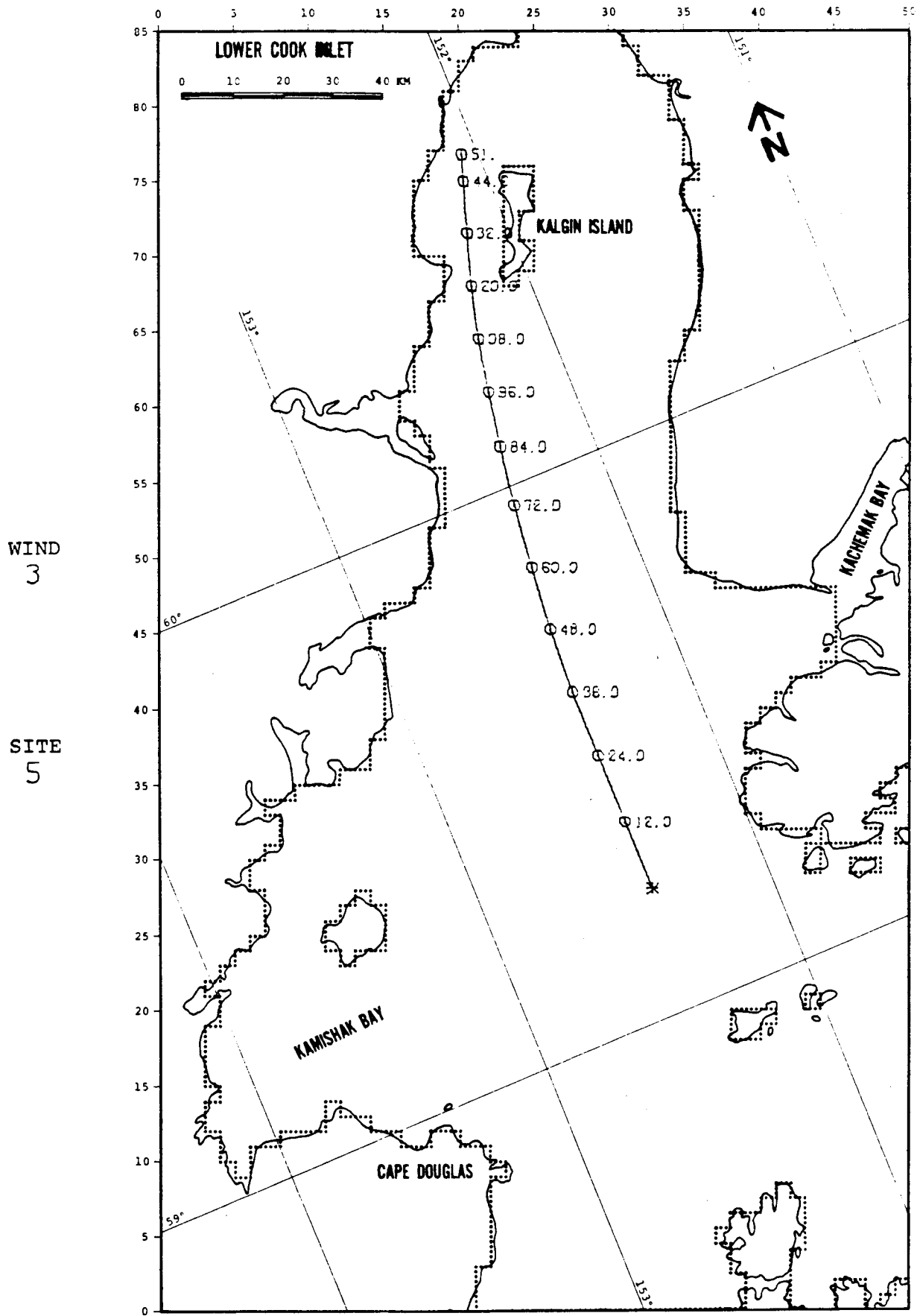


FIGURE A-6: VERIFICATION: WIND ONLY

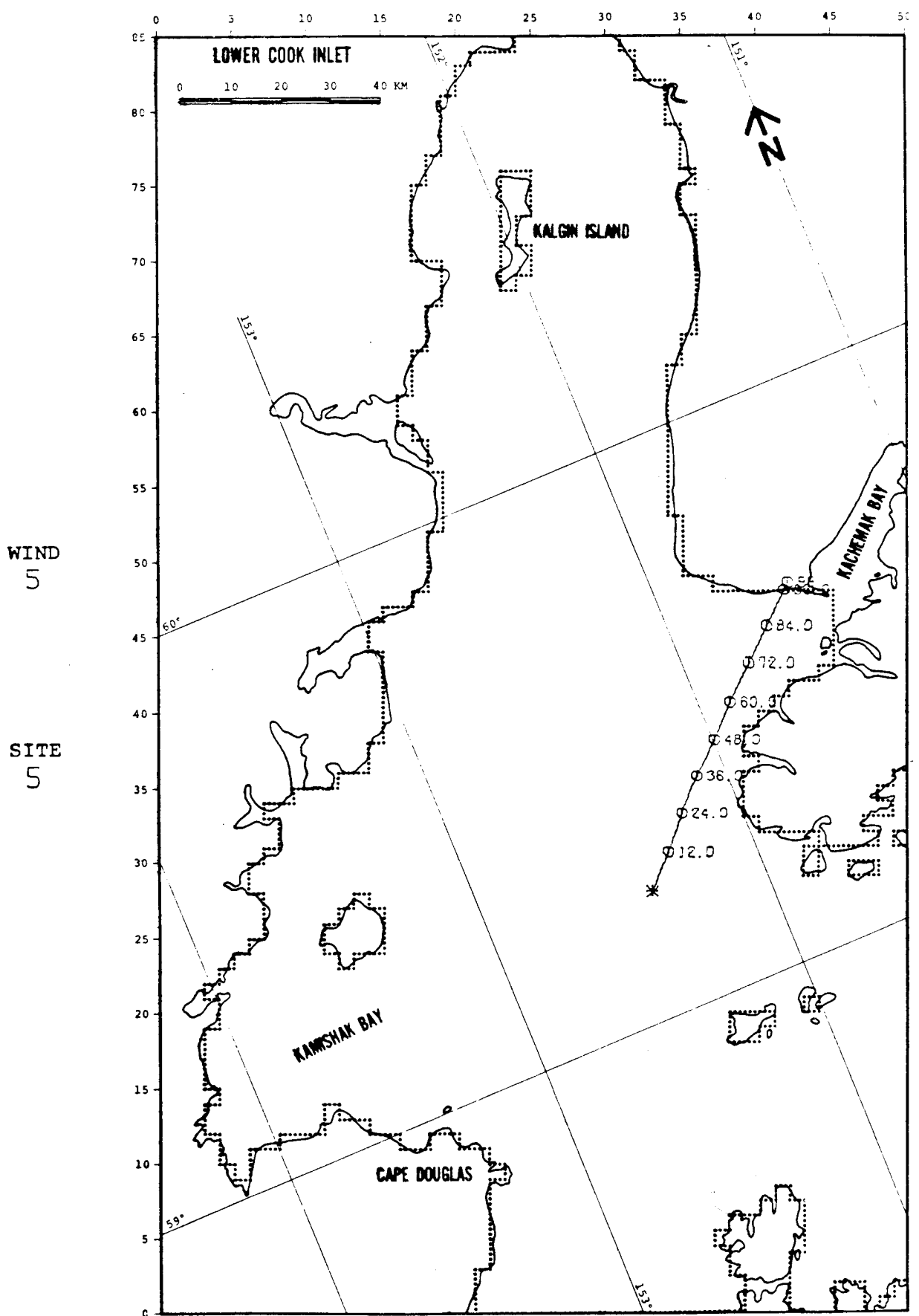


FIGURE A-7: VERIFICATION: WIND ONLY

PROGRAM LISTING

OIL SPILL PROGRAM LISTING

PROGRAM SPILL

```

1      *DECK SPILL
      PROGRAM SPILL(INPUT,OUTPUT,TAPE1,TAPE2,TAPE3,TAPE4,TAPE7,TAPE9,
      .           TAPE5=INPUT,TAPE6=OUTPUT)
      COMMON X(1)
5      C*****
      C TAPE1 - WIND DATA (INPUT) *
      C TAPE2 - TIDE DATA (INPUT) *
      C TAPE3 - NET CURRENT DATA (INPUT) *
      C TAPE4 - GEOGRAPHIC DATA (CELL DEFINITION) (INPUT) *
10     C TAPE5 - CONTROL INFORMATION (INPUT) *
      C TAPE6 - MESSAGE FILE (OUTPUT) *
      C TAPE7 - OIL DATA FILE (INPUT) *
      C TAPE9 - PLOT FILE (OUTPUT) *
      C*****
15     CALL PREP
      END
  
```

SUBROUTINE CELLIO

```

1      *DECK CELLIO
      SUBROUTINE CFLLIO(CELL,IMAX,JMAX)
      C*****
      C THIS SUBROUTINE READS THE CELLS DEFINITION. *
5      C CONVENTION USED: *
      C 1 - WATER BOUNDARY *
      C 2 - LAND *
      C 3 - INVALID WATER *
      C 4 - VALID WATER *
10     C BLANK - CELL IS OF THE SAME TYPE AS THE CELL TO ITS LEFT *
      C*****
      INTEGER CELL(IMAX,JMAX),FIRST
      IER=0
      DO 5 JJ=1,JMAX
      J=JMAX-JJ+1
15     N=0
      READ(4,1009) ID,(CELL(I,J),I=1,IMAX)
      DO 5 I=1,IMAX
      C** CHECKING VALIDITY OF CELL TYPE.
20     IF(CELL(I,J).GE.0.AND.CELL(I,J).LE.4) GO TO 1
      IFR=1
      WRITE(6,1004) ID,I,J,CELL(I,J)
      1 N=N+1
      IF(CELL(I,J).EQ.0) GO TO 5
25     IF(N.EQ.1) GO TO 4
      IF(FIRST.NE.CELL(I,J)) GO TO 2
      N=I-N
      DO 3 K=N,I
      3 CELL(K,J)=FIRST
      GO TO 4
30     2 WRITE(6,1005) ID,I,J,FIRST,CELL(I,J)
      IER=1
      4 FIRST=CELL(I,J)
      N=0
35     5 CONTINUE
      DO 8 I=1,IMAX
      DO 8 J=1,JMAX
      8 CELL(I,J)=CELL(I,J)-4
      RETURN
40     1004 FORMAT(3X,*CELL VALUF OUT OF RANGE. ID= *,A5,*I= *,I3,*J= *,I3,
      .           *CELL(I,J)= *,I1)
      1005 FORMAT(3X,*ERROR IN CELL DATA AT LINE ID *,A5,* ROW *,I4,* COL *,
      .           I4,* LABEL *,I2,* TO *,I2)
      1009 FORMAT(A5,75I1,/,/(5X,75I1))
45     END
  
```

SUBROUTINE PREP

```

1      *DECK PREP
      SUBROUTINE PREP
C*****
C      SUBROUTINE PREP READS AND PRINTS THE PROBLEM PARAMETERS *
5      AND CONVERTS THIS PARAMETERS TO THE UNITS USED BY THE PROGRAM. *
C*****
      COMMON X(1)
      INTEGER PSTEP,SOP,DOP,RUN(8),BLANK,CELLS,PROB,SALG,PLNO,WIND,TIDE
      REAL NU,MAXDOSE,MINTHK
10     COMMON /DATA/ PSTEP,DT,ST,DS,CELLS,BLANK,AGRID,ADEFL,CW,DOP,
      XSPILL,YSPILL,MFAC(3),CT(3)
      COMMON /CLOT/ XAXIS,YAXIS,XPLFAC,YPLFAC,PLNO
      DATA BLANK /10H /, IEND /3HEND/,PLNO /0/
C**   PROB - FILE OF PROBLEM PARAMETERS.
15   C**   CELLS - FILE CONTAINS CELLS DEFINITION.
      C**   WIND - FILE OF WIND DATA.
      C**   TIDE - FILE OF TIDIAL CURRENT.
      C**   NET - FILE OF NET CURRENT DATA.
      CALL PLOTS(-5.0,-200.0,9)
20     CALL PLOT(0.,3.,-3)
      1 READ(5,1001)PROB,CELLS,WIND,TIDE,NET
C**   PLNO - TRAJECTORY NUMBER.
      PLNO=PLNO+1
      IF(PROB.EQ.IEND)9,8
25     9 CALL PLOT(0.0,0.0,999)
      STOP
      8 IF(PROB.EQ.BLANK) GO TO 3
      REWIND 7
      CALL DFUR(3HGET,7,PROB,0,ISTA)
30     IF(ISTA.EQ.0) GO TO 2
      WRITE(6,1002)PROB,ISTA
      STOP 7
C**   READING PROBLEM PARAMETERS.
      2 READ(7,1001) RUN
35     READ(7,1003) RSOP,RDOP,RPSTEP,XAXIS,YAXIS
      READ(7,1003) RH20,ROIL,SIG,NU,Q,XSPILL,YSPILL,PERIOD
      READ(7,1003) CW,C1,C2,C3,ADEFL,MAXDOSE,MINTHK,ST
      READ(7,1003) RIMAX,RJMAX,DS,AGRID,DT,DCYCLE,CUTOFF,RSALG
40     READ(7,1003) CT(1),CT(2),CT(3),RMFACW,RMFACP,RMFACR,EVAPP,EVAPT
      PLNO=1
      DECODE(10,910,WIND) IWIND
      DECODE(10,910,PROB) ISPILL
50     910 FORMAT(4X,A1)
      PSTEP=RPSTEP
45     SOP=RSOP
      DOP=RDOP
      IMAX=HIMAX
      JMAX=HJMAX
      SALG=RSALG
50     MFAC(1)=RMFACW
      MFAC(2)=RMFACP
      MFAC(3)=RMFACR
C**   PRINTING PROBLEM PARAMETERS.
      WRITE(6,1006) ISPILL,IWIND,SOP,DOP,PSSTEP,RH20,ROIL,SIG,NU,Q,CW
55     ,C1,C2,C3
      WRITE(6,1007) ADEFL,MAXDOSE,MINTHK,IMAX,JMAX,DS,AGRID,DT,ST,
      CUTOFF,SALG,CT(1),CT(2),CT(3),MFAC(1),MFAC(2)
      WRITE(6,1004) MFAC(3),XSPILL,YSPILL,EVAPP,EVAPT,DCYCLE,PERIOD,
      XAXIS,YAXIS
60     IMAXP1=IMAX+1
      JMAXP1=JMAX+1
      IJ=IMAX*JMAX
      IJPI=IMAXP1*JMAXP1
C**   GRID SIZE IN METERS.
65     DS=DS*1000.

```

```

C** COORDINATES OF SPILL LOCATIONS IN METERS.
XSPILL=XSPILL*1000.
YSPILL=YSPILL*1000.
70 C** PLOTTING SCALE-FACTOR.
XPLFAC=XAXIS/FLOAT(IMAX)/DS
YPLFAC=YAXIS/FLOAT(JMAX)/DS
3 IF(CELLS.EQ.BLANK) GO TO 4
C** GETTING CELLS DEFINITION FILE.
REWIND 4
75 CALL DFUR(3HGET,4,CELLS,0,ISTA)
IF(ISTA.EQ.0) GO TO 4
WRITE(6,1002) CELLS,ISTA
STOP 3
C** GETTING WIND DATA FILE.
80 4 REWIND 1
IF(WIND.EQ.BLANK) GO TO 5
CALL DFUR(3HGET,1,WIND,0,ISTA)
IF(ISTA.EQ.0) GO TO 5
WRITE(6,1002) WIND,ISTA
STOP 1
85 C** GETTING TIDE DATA FILE
5 REWIND 2
IF(TIDE.EQ.BLANK) GO TO 6
CALL DFUR(3HGET,2,TIDE,0,ISTA)
90 IF(ISTA.EQ.0) GO TO 6
WRITE(6,1002) TIDE,ISTA
STOP 2
C** GETTING NET CURRENT DATA FILE.
95 6 REWIND 3
IF(NET.EQ.BLANK) GO TO 7
CALL DFUR(3HGET,3,NET,0,ISTA)
IF(ISTA.EQ.0) GO TO 7
WRITE(6,1002) NET,ISTA
STOP 3
100 7 N1=5
N2=N1+6*IJP1
N3=N2+6*IJP1
N4=N3+IJ
N9=LOC(X(1))+N4
105 IF (PROB.NE.BLANK) WRITE(6,1008) N9
C** FOR NOAA JOB 1978
CT(2)=FLOAT(PLNO-1)*PERIOD/10.
C** INITIALIZE TRAJECTORY PLOT.
CALL PLINIT
110 . (PLNO,XAXIS,YAXIS,XPLFAC,YPLFAC,XSPILL,YSPILL,PROB,WIND)
CALL SLICK(IMAX,JMAX,IMAXP1,JMAXP1,X(N1),X(N2),X(N3))
GO TO 1
1001 FORMAT(8A10)
1002 FORMAT(1H1,3X,*UNABLE TO GET FILE *,A7,* ISTA=*,I2)
1003 FORMAT(8F10.0)
115 1005 FORMAT(T10,*NET CURRENT GRID MULTIPLE *,I3,
. T65,*X-COORDINATE OF SPILL LOCATION *,1PE12.5,* (KM)*,/,
. T10,*Y-COORDINATE OF SPILL LOCATION *,1PE12.5,* (KM)*,/,
. T65,*MAXIMUM EVAPORATIVE LOSS *,0PF3.0,* PERCENT *,/,
120 . T10,*MAXIMUM PERIOD OF EVAPORATION *,F4.1,* (HRS)*,/,
. T65,*DRIFT COMPUTATION END TIME *,F8.4,6H (HRS),/,
. T10,*DATA CYCLE PERIOD *,F8.4,6H (HRS),/,
. T65,*X-AXIS LENGTH *,F7.2,9H (INCHES),/,
. T10,*Y-AXIS LENGTH *,F7.2,9H (INCHES))
125 1006 FORMAT(1H1,T30,*D) A M E S A N D M O O R E O I L S P I L L *,
. * M O D E L *,///,
. T20,*RUN IDENTIFICATION: *,8A10
. //T10,*SPREADING OPTION *I2,
. T65,*DISPLAY OPTION *,I2,/,
130 . T10,*PRINT FREQUENCY *,I3,
. T65,*DENSITY OF SEAWATER *,F6.3,8H (GM/CC),/,
. T10,*DENSITY OF OIL *,F6.3,8H (GM/CC),
. T65,*SPREADING COEFFICIENT *,F6.3,* (DYNES/CM)*,/,
. T10,*KINEMATIC VISCOSITY *,F6.3,12H (CM**2/SEC),
135 . T65,*SPILL VOLUME *,F8.2,* (KLS)*,/,

```

```

      .      T10,**WIND COUPLING COEFFICIENT *,F6.4,
      .      T65,**INERTIAL SPREADING COEFFICIENT *,F5.2,/,
      .      T10,**VISCOS SPREADING COEFFICIENT *,F5.2,
      .      T65,**SURFACE TENSION SPREADING COEFFICIENT *,F5.2)
140 1007 FORMAT(T10,**WIND/OIL DEFLECTION ANGLE *,F5.1,6H (DEG),
      .      T65,**MAXIMUM SHORE DOSAGE *,F6.2,*(GM/M)*,/,
      .      T10,**MINIMUM FILM THICKNESS *,1PE12.5,*(M)*,
      .      T65,**NUMBER OF HORIZONTAL CELLS *,I4,/,
      .      T10,**NUMBER OF VERTICAL CELLS *,I4,
145  .      T65,**GRID SIZE *,0PF6.2,*(KM)*,/,
      .      T10,**MAG. NORTH-HORIZONTAL AXIS ANGLE *,F6.1,6H (DEG),
      .      T65,**TIME STEP *,F8.4,6H (HRS),/,
      .      T10,**STOP TIME *,F8.1,6H (HRS),
      .      T65,**CUTOFF *,F5.2,/,
150  .      T10,**SPREADING ALGORITHM *,I2,
      .      T65,**WIND START TIME *,F8.4,6H (HRS),/,
      .      T10,**TIDE CURRENT START TIME *,F8.4,6H (HRS),
      .      T65,**NET CURRENT START TIME *,F8.4,6H (HRS),/,
      .      T10,**WIND GRID MULTIPLE *,I3,
155  .      T65,**TIDE CURRENT GRID MULTIPLE *,I3)
1008 FORMAT(/BX,* FIELD LENGTH REQUIRED IS *,06*8*//)
      END

```

SUBROUTINE SLICK

```

1  *DECK SLICK
      SUBROUTINE SLICK(IMAX,JMAX,IMAXP1,JMAXP1,SPD,DIR,CELL)
C *****
C THIS SUBROUTINE COMPUTE THE TRAJECTORY OF THE SPILL.
5 C UNITS OF CALCULATION ARE IN M.K.S
C BESIDES:
C SPEED = METERS/HR
C T,DT = HRS.
C *****
10 INTEGER PSTEP,BLANK,CELLS,DOP,CELL,PLNO
      DIMENSION CELL(IMAX,JMAX),
      .      SPD(IMAXP1,JMAXP1,6),DIR(IMAXP1,JMAXP1,6)
      COMMON /DATA/ PSTEP,DT,ST,DS,CELLS,BLANK,AGRID,ADEFL,CW,DOP,
      .      XSPILL,YSPILL,MFAC(3),CT(3)
15 COMMON /CLOT/ XAXIS,YAXIS,XPLFAC,YPLFAC,PLNO
      DIMENSION PERIOD(3),CYCLE(3),SPEED(3),DIRCT(3),TDRIFT(3,2)
      DATA PI /180./,TWOPI /360./
C** READ CELLS DEFINITION.
      IF(CELLS.NE.BLANK) CALL CELLIO(CELL,IMAX,JMAX)
20 C*** INITIALIZATION.
      T=0.
      XMAX=DS*FLOAT(IMAX)
      YMAX=DS*FLOAT(JMAX)
      XOLD=XSPILL
25      YOLD=YSPILL
      IOLD=INT(XSPILL/DS)+1
      JOLD=INT(YSPILL/DS)+1
      NSTEPS=ST/DT+1
      DO 5 K=1,3
30      K2=K+3
      TDRIFT(K,2)=-CT(K)
      TDRIFT(K,1)=9999.9
      CYCLE(K)=1.
      PERIOD(K)=0.
35      NJUMP=MFAC(K)
C** READING DRIFT INFORMATION
      DO 5 JJ=1,JMAXP1,NJUMP
      J=JMAXP1-JJ+1
      READ(K,510) (SPD(I,J,K2),DIR(I,J,K2),I=1,IMAXP1,NJUMP)
40      5 CONTINUE
C-----
C START MAIN CALCULATION LOOP
C-----
45 C*** CHECK WHETHER TO READ NEW DRIFT VALUES.

```

```

DO 40 K=1,3
10 IF (T.GE.TDRIFT(K,1).AND.T.LE.TDRIFT(K,2)) GOTO 40
C** REPLACEMENT.
K2=K+3
50 NJUMP=MFAC(K)
TDRIFT(K,1)=TDRIFT(K,2)
DO 15 J=1,JMAXP1,NJUMP
DO 15 I=1,IMAXP1,NJUMP
SPD(I,J,K)=SPD(I,J,K2)
55 15 DIR(I,J,K)=DIR(I,J,K2)
C** READING SPEED AND DIRECTION AT NEW TIME LEVEL.
READ(K,510) TIM
20 DO 25 JJ=1,JMAXP1,NJUMP
J=JMAXP1-JJ+1
60 READ(K,510) (SPD(I,J,K2),DIR(I,J,K2),I=1,IMAXP1,NJUMP)
IF (EOF(K)) 30,25
30 REWIND K
CYCLE(K)=CYCLE(K)+1.
PERIOD(K)=TIM
65 TIM=0.
GOTO 20
25 CONTINUE
TDRIFT(K,2)=(CYCLE(K)-1.)*PERIOD(K)-CT(K)+TIM
GOTO 10
70 40 CONTINUE
C** INTERPOLATING SPEED AND DIRECTION TO THE CURRENT LOCATION
DO 45 K=1,3
K2=K+3
C** WEIGHTING FACTORS.
75 TFM=(TDRIFT(K,2)-T)/(TDRIFT(K,2)-TDRIFT(K,1))
TFP=1.-TFM
NJUMP=MFAC(K)
I1=((IOLD-1)/NJUMP)*NJUMP+1
I2=I1+NJUMP
80 J1=((JOLD-1)/NJUMP)*NJUMP+1
J2=J1+NJUMP
XFM=((I2-1)*DS-XOLD)/DS/NJUMP
XFP=1.-XFM
YFM=((J2-1)*DS-YOLD)/DS/NJUMP
YFP=1.-YFM
85 C** SPEED INTERPOLATION.
SPEED(K)=TFM*(YFM*(XFM*SPD(I1,J1,K)+XFP*SPD(I2,J1,K))+
. YFP*(XFM*SPD(I1,J2,K)+XFP*SPD(I2,J2,K)))+
. TFP*(YFM*(XFM*SPD(I1,J1,K2)+XFP*SPD(I2,J1,K2))+
90 . YFP*(XFM*SPD(I1,J2,K2)+XFP*SPD(I2,J2,K2)))
C** DIRECTIN INTERPOLATION.
DUM1=DIR(I2,J1,K)
DUM2=DIR(I1,J1,K)
IF ((DUM2-DUM1).GT.PI) DUM1=DUM1+TWOPI
95 IF ((DUM1-DUM2).GT.PI) DUM2=DUM2+TWOPI
AYM=XFM*DUM2+XFP*DUM1
IF (AYM.GT.TWOPI) AYM=AYM-TWOPI
DUM1=DIR(I2,J2,K)
DUM2=DIR(I1,J2,K)
100 IF ((DUM2-DUM1).GT.PI) DUM1=DUM1+TWOPI
IF ((DUM1-DUM2).GT.PI) DUM2=DUM2+TWOPI
AYP=XFM*DUM2+XFP*DUM1
IF (AYP.GT.TWOPI) AYP=AYP-TWOPI
IF ((AYM-AYP).GT.PI) AYP=AYP+TWOPI
105 IF ((AYP-AYM).GT.PI) AYM=AYM+TWOPI
ATM=YFM*AYM+YFP*AYP
IF (ATM.GT.TWOPI) ATM=ATM-TWOPI
DUM1=DIR(I2,J1,K2)
DUM2=DIR(I1,J1,K2)
110 IF ((DUM2-DUM1).GT.PI) DUM1=DUM1+TWOPI
IF ((DUM1-DUM2).GT.PI) DUM2=DUM2+TWOPI
AYM=XFM*DUM2+XFP*DUM1
IF (AYM.GT.TWOPI) AYM=AYM-TWOPI
DUM1=DIR(I2,J2,K2)

```

```

115      DUM2=DIR(I1,J2,K2)
        IF((DUM2-DUM1).GT.PI)DUM1=DUM1+TWOPI
        IF((DUM1-DUM2).GT.PI)DUM2=DUM2+TWOPI
        AYP=XFM*DUM2+XFP*DUM1
        IF(AYP.GT.TWOPI)AYP=AYP-TWOPI
120      IF((AYM-AYP).GT.PI)AYP=AYP+TWOPI
        IF((AYP-AYM).GT.PI)AYM=AYM+TWOPI
        ATP=YFM*AYM+YFP*AYP
        IF(ATP.GT.TWOPI)ATP=ATP-TWOPI
        IF((ATM-ATP).GT.PI)ATP=ATP+TWOPI
125      IF((ATP-ATM).GT.PI)ATM=ATM+TWOPI
        C** TRANSFORMING DIRECTION TO TRIGONOMETRIC COORDINATE SYSTEM.
        DIRCT(K)=TWOPI-TFM*ATM-TFP*ATP-AGRID
        C      IF (K.EQ.1) DIRCT(1)= DIRCT(1)-ADEFL+PI
        C** DEGREES TO RADIANS.
130      DIRCT(K)=DIRCT(K)*3.14159265/PI
        45      CONTINUE
        C** TRANSFORMING SPEED TO M/HR.
        SPEED(1)=SPEFD(1)*1854.
        SPEED(2)=SPEED(2)*3600.
135      SPEED(3)=SPEED(3)*1000.
        C** RANDOMIZE NET CURRENT
        CALL RANDOM(SPEED(3),DIR(3),IOLD,JOLD,V2,D2)
        C** CALCULATE COMPONENTS OF THE DRIFT VECTOR.
        UT=CW*SPEED(1)*COS(DIRCT(1))+V2*COS(D2)+
140      .   SPEED(2)*COS(DIRCT(2))+SPEED(3)*COS(DIRCT(3))
        .   VT=CW*SPEED(1)*SIN(DIRCT(1))+V2*SIN(D2)+
        .   SPEED(2)*SIN(DIRCT(2))+SPEED(3)*SIN(DIRCT(3))
        C** CALCULATE NEW LOCATION OF THE SPILL.
        C** XNEW,YNEW NEW COORDINATES OF SPILL LOCATION.
145      XNEW=XOLD+DT*UT
        YNEW=YOLD+DT*VT
        XNEW=AMIN1(XMAX,AMAX1(XNEW,0.0))
        YNEW=AMIN1(YMAX,AMAX1(YNEW,0.0))
        C** INEW,JNEW NEW CELL OF SPILL LOCATION.
150      INEW=INT(XNEW/DS)+1
        JNEW=INT(YNEW/DS)+1
        C** CHECK IF SPILL ADVANCED MORE THAN ONE CELL.
        IF((IABS(IOLD-INEW)+IABS(JOLD-JNEW)).LE.1) GO TO 60
155      XINC=(XNEW-XOLD)/20.
        YINC=(YNEW-YOLD)/20.
        TINC=DT/20.
        XNFW=XOLD
        YNFW=YOLD
        T=T-DT
160      DO 50 N=1,20
        XNEW=XNEW+XINC
        YNEW=YNEW+YINC
        T=T+TINC
        INFW=INT(XNEW/DS)+1
        JNFW=INT(YNEW/DS)+1
165      C** CHECK IF SPILL REACHED WATER BOUNDARY.
        IF (CELL(INEW,JNEW).LT.0) GOTO 60
        50 CONTINUE
        60 CONTINUE
170      C** PREPARATION FOR NEXT TIME STEP.
        T=T+DT
        IOLD=INEW
        JOLD=JNEW
        XOLD=XNEW
        YOLD=YNEW
175      C*** XPC,YPC LOCATION OF SPILL ON THE PLOT.
        XPC=XNEW*XPLFAC
        YPC=YNEW*YPLFAC
        C** CHECK IF SPILL REACHED WATER BOUNDARY.
180      IF (CELL(INEW,JNEW).LT.0) GOTO 70
        IF (DOP.EQ.2) WRITE(6,1003) T,XNFW,YNEW,INEW,JNEW
        C*** PLOTTING A LINE IN TRAJECTORY MODE.
        C      IF (PLNO.NE.1) GOTO 2
        CALL PLOT(XPC,YPC,2)
185      IF (MOD(STEP,PSTEP).NE.0) GOTO 2

```

```

IF (DUP.EQ.1) WRITE(6,1003) T,XNEW,YNEW,INEW,JNEW
CALL SYMBOL(XPC,YPC,0.082,PLNO,0.0,-1)
CALL NUMBER(XPC,YPC-0.041,0.082,T,0.0,4HF4.0)
CALL PLOT(XPC,YPC,3)
190      2 CONTINUE
        WRITE(6,1001)
        70 WRITE(6,1002) PLNO,INEW,JNEW,T
C*** TERMINATING THE LINE IN TRAJECTORY MODE.
C      IF (PLNO.NE.1) RETURN
195      XPC=AMIN1(XPC,XAXIS)
        YPC=AMIN1(YPC,YAXIS)
        XPC=AMAX1(XPC,0.0)
        YPC=AMAX1(YPC,0.0)
        CALL PLOT(XPC,YPC,2)
200      CALL SYMBOL(XPC,YPC,0.082,PLNO,0.0,-1)
        CALL NUMBER(XPC,YPC-0.041,0.082,T,0.0,4HF4.0)
        RETURN
510  FORMAT(16F5.0)
1001 FORMAT(3X,*STOP TIME REACHED*)
205  1002 FORMAT(3X,*TRAJECTORY*,I3,* TERMINATED AT CELL *,2I5,* AT TIME *
        ,F5.0,* HOURS. *)
        1003 FORMAT(3X,*T =*,F8.3,* X =*,F8.2,* Y =*,F8.2,* AT CELL*,2I5)
        END

```

SUBROUTINE PLINIT

```

1      *DECK PLINIT
        SURROUTINE PLINIT
          (N,XAXIS,YAXIS,XPLFAC,YPLFAC,XSPILL,YSPILL,PROB,WIND)
C*****
5      C      PLOT INITIALIZATION ROUTINE.
        C      PARAMETERS:
        C      N          - TRAJECTORY NUMBER.
        C      XAXIS     - X-AXIS LENGTH IN INCHES.
        C      YAXIS     - Y-AXIS LENGTH IN INCHES.
10     C      XPLFAC    - SCALING FACTOR IN THE X DIRECTION (INCH ON PLOT/METER )
        C      YPLFAC    - SCALING FACTOR IN THE Y DIRECTION.
        C      XSPILL    - X COORDINATE OF SPILL LOCATION.
        C      YSPILL    - Y COORDINATE OF SPILL LOCATION.
C*****
15     INTEGER PROB,WIND
        DATA SPACE/4.0/
        IF (N.GT.1) GOTO 1
C*** ADVANCING PEN FOR NEW FRAME.
        CALL PLOT(XAXIS+SPACE,0.,-3)
20     C*** DRAW A BOX
        C      CALL PLOT(XAXIS,0.0,2)
        C      CALL PLOT(XAXIS,YAXIS,2)
        C      CALL PLOT(0.0,YAXIS,2)
        C      CALL PLOT(0.0,0.0,2)
25     C*** MARKERS FOR OVERLAY.
        CALL SYMBOL(-1.0,0.,0.15,3,0.0,-1)
        CALL SYMBOL(-1.0,YAXIS-1.,0.15,3,0.0,-1)
C*** PRINT RUN IDENTIFICATION.
        DECODE(10,910,WIND) I#IND
30     DECODE(10,910,PROB) ISPILL
        CALL SYMBOL(-1.,5.5,0.15,I#IND,0.0,1)
        CALL SYMBOL(-1.,4.0,0.15,ISPILL,0.0,1)
C*** DRAW A SYMBOL AT THE SPILL POINT.
        1 XPC=XSPILL*XPLFAC
35     YPC=YSPILL*YPLFAC
        IF(N.EQ.1) CALL SYMBOL(XPC,YPC,0.082,11,0.0,-1)
        CALL PLOT(XPC,YPC,3)
        RETURN
        910 FORMAT(4X,A1)
40     END

```

SUBROUTINE RANDOM

```

1          SUBROUTINE RANDOM(SPD,DIR,I,J,V2,D2)
          V2=0.
          D2=DIR+1.5/074632
          IF (J.GT.55) RETURN
5          IF (J.LT.35) GOTO 3
          V1=GAUSS(4.)
          V2=GAUSS(3.)
          GOTO 5
10         3  IF (I.GT.19) GOTO 4
          V1=GAUSS(2.)
          V2=GAUSS(2.5)
          GOTO 5
          4  V1=GAUSS(10.)
          V2=GAUSS(7.5)
15         5  SPD=SPD+V1
          RETURN
          END

```

FUNCTION GAUSS

```

1          FUNCTION GAUSS(S)
          A=0.
          DO 10 I=1,12
10         A=A+RANF(N)
5          GAUSS=(A-6.)*S*3.
          RETURN
          END

```

APPENDIX B

BASE CASE TRAJECTORIES
AND RESULTS

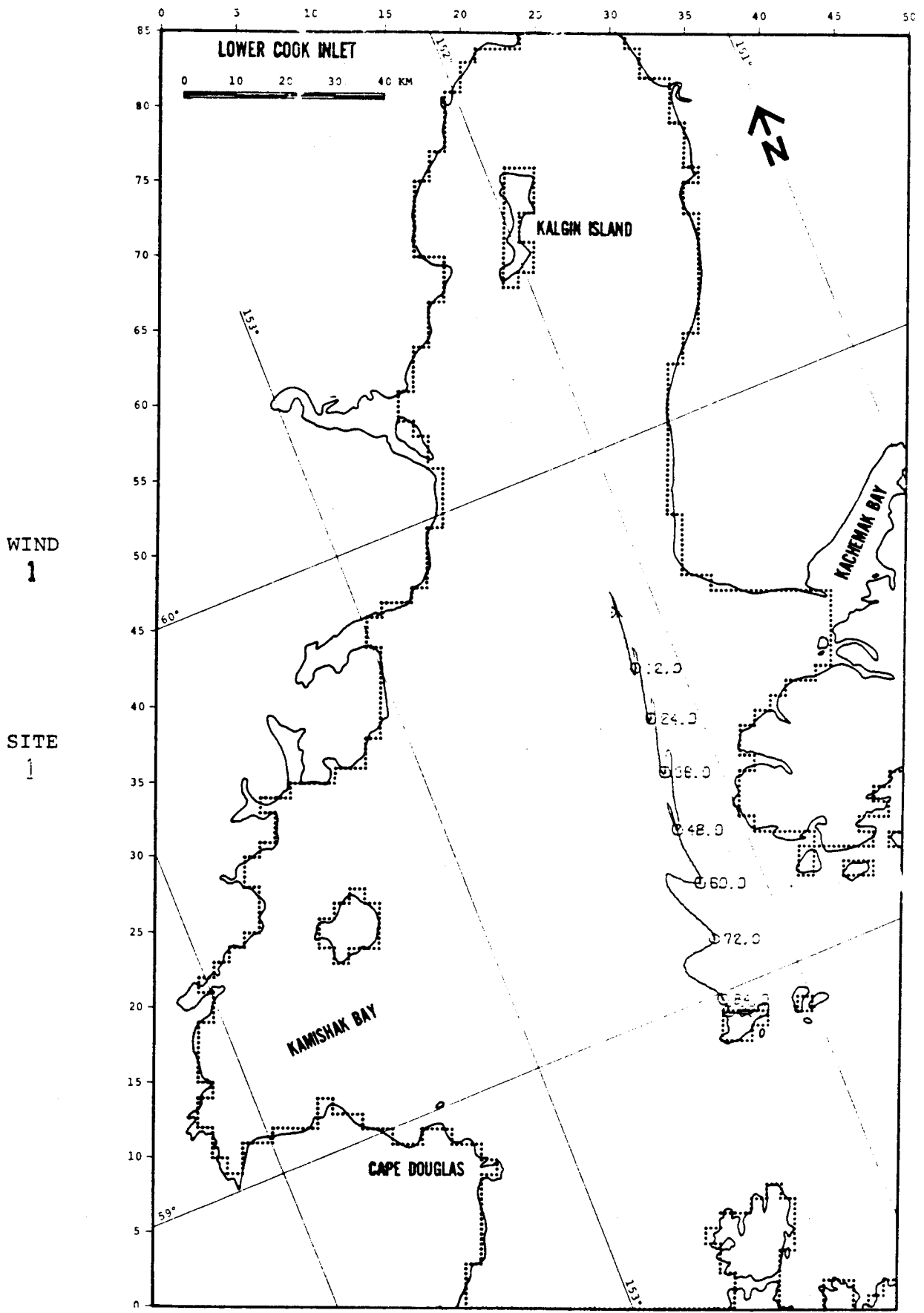


FIGURE B-1: BASE CASE

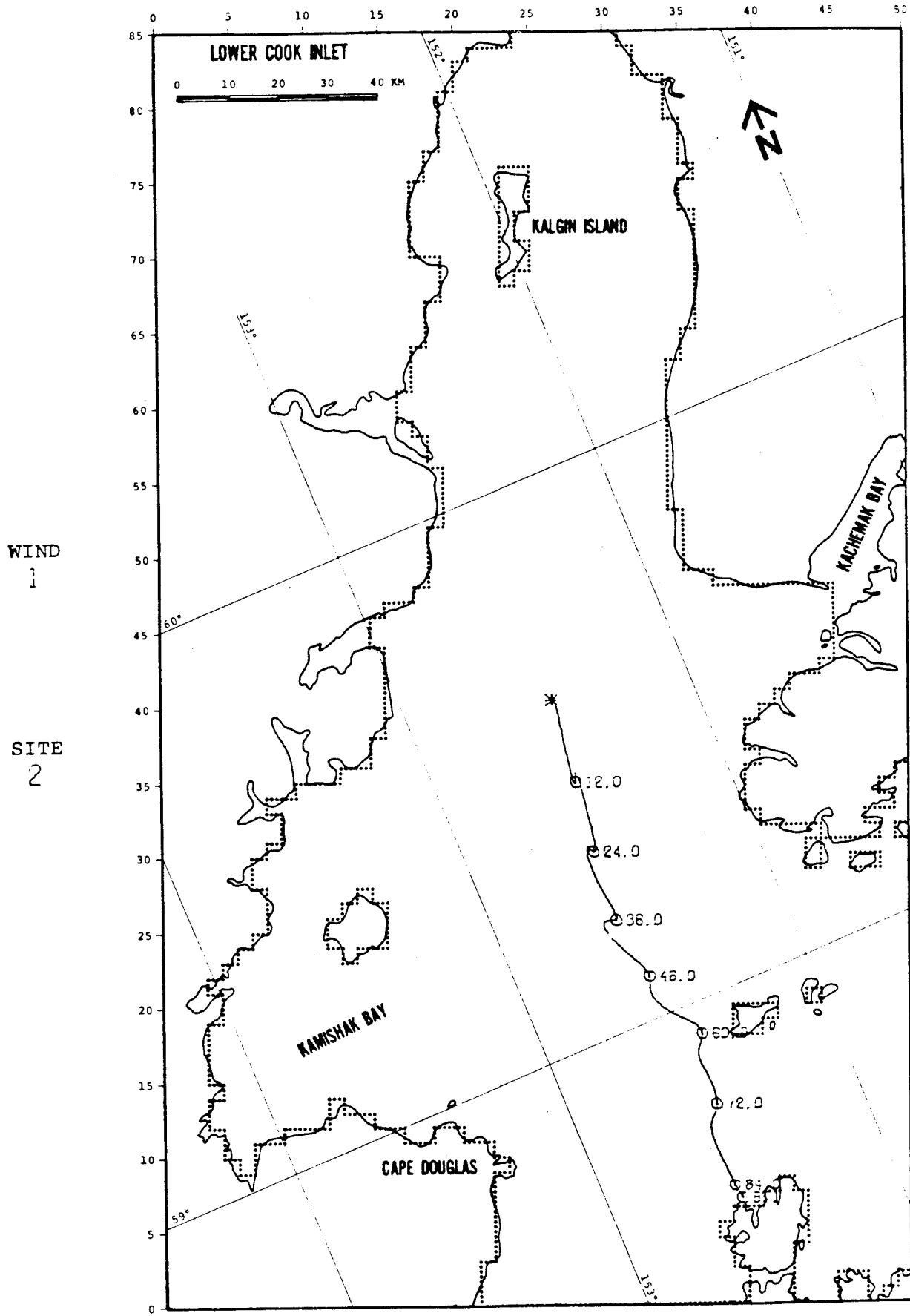


FIGURE B-2: BASE CASE

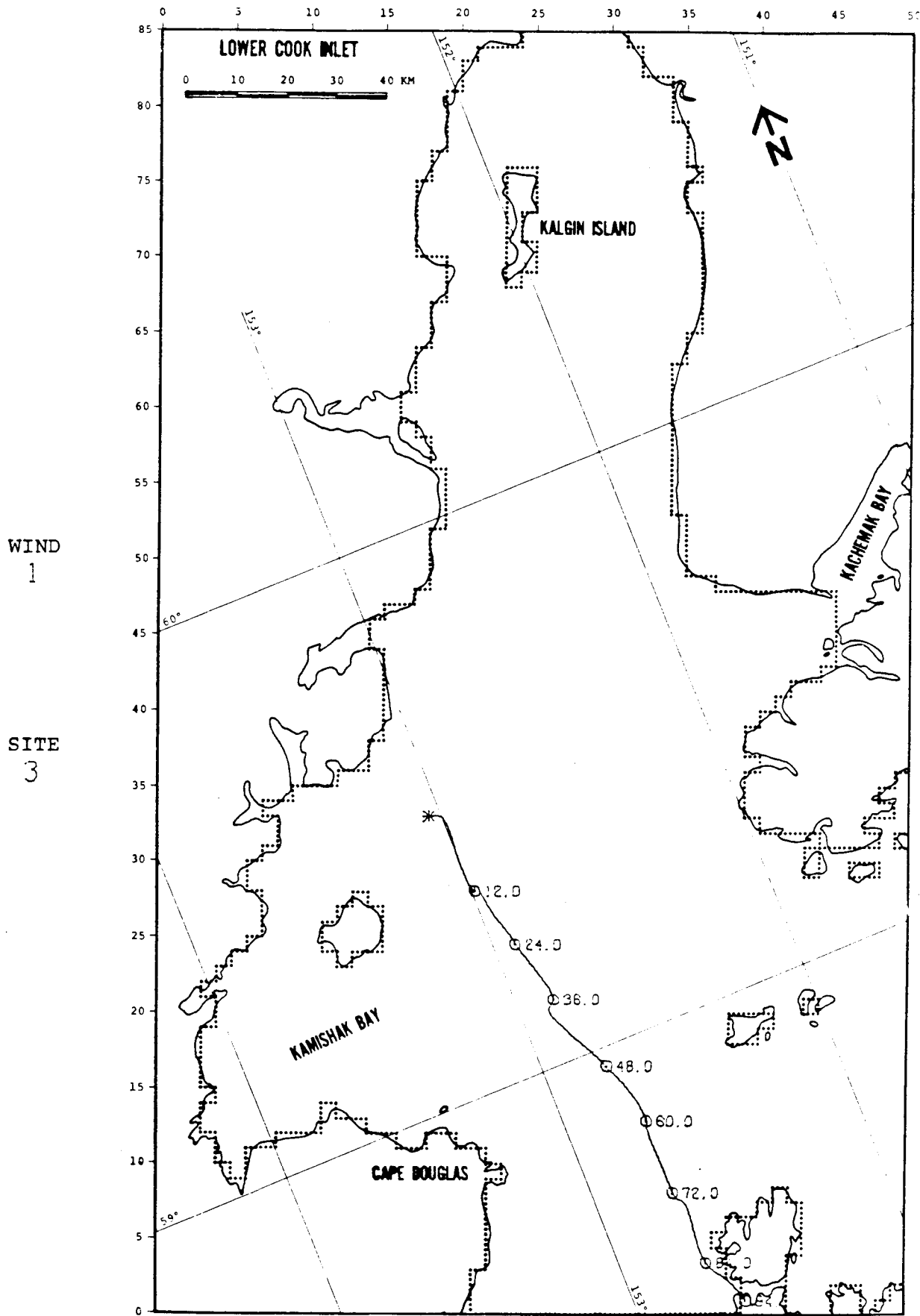


FIGURE B-3: BASE CASE

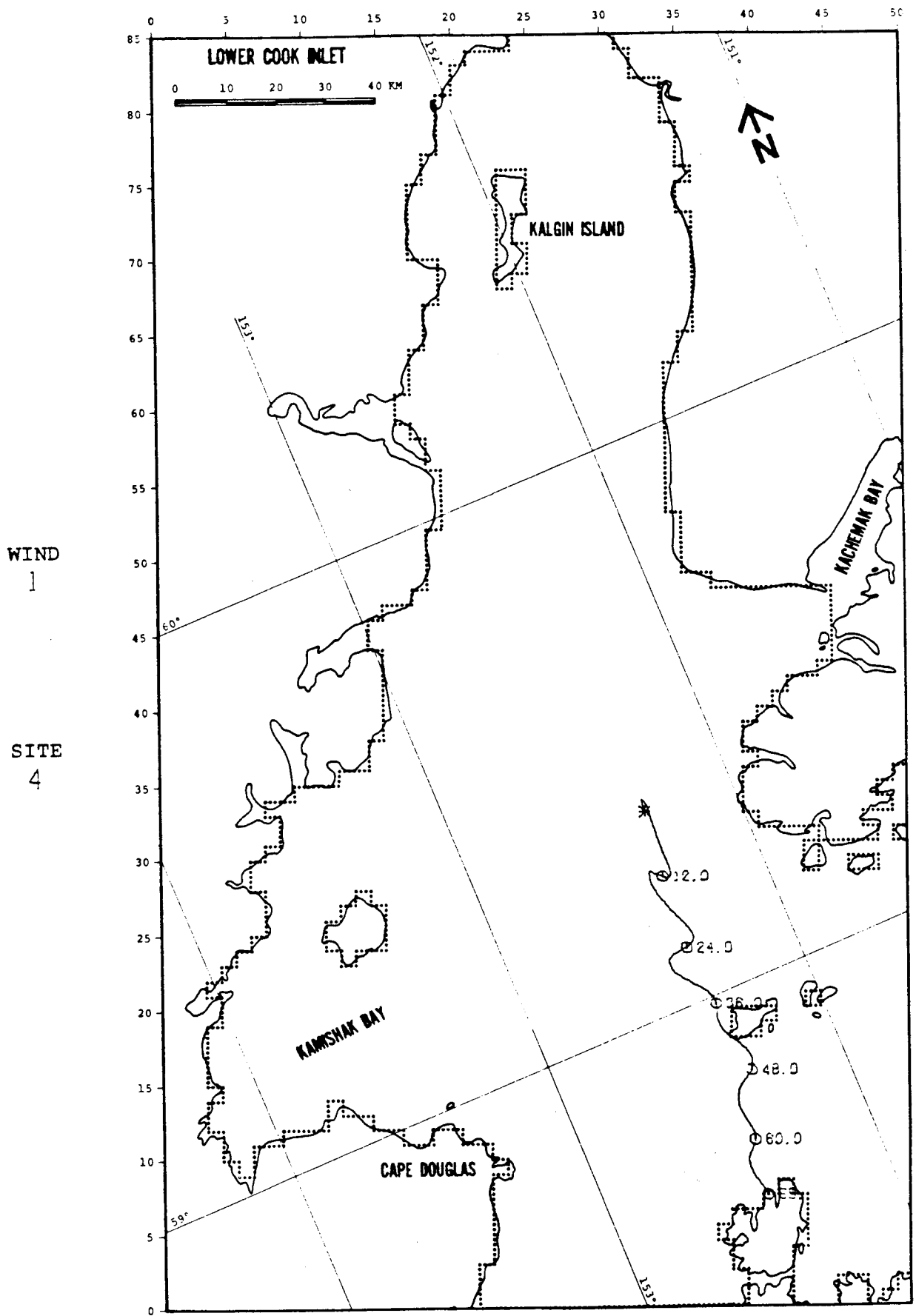


FIGURE B-4: BASE CASE

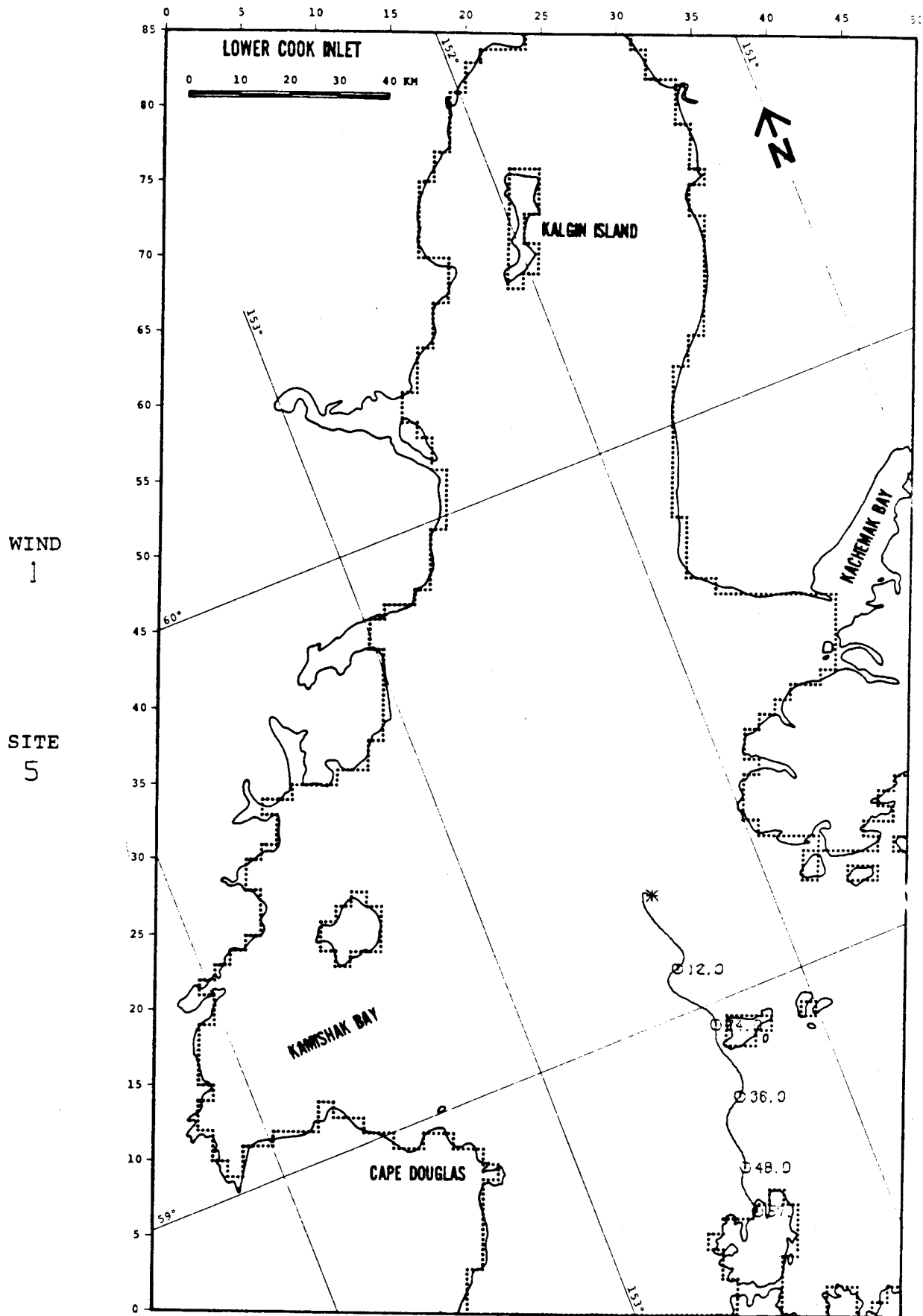


FIGURE B-5: BASE CASE

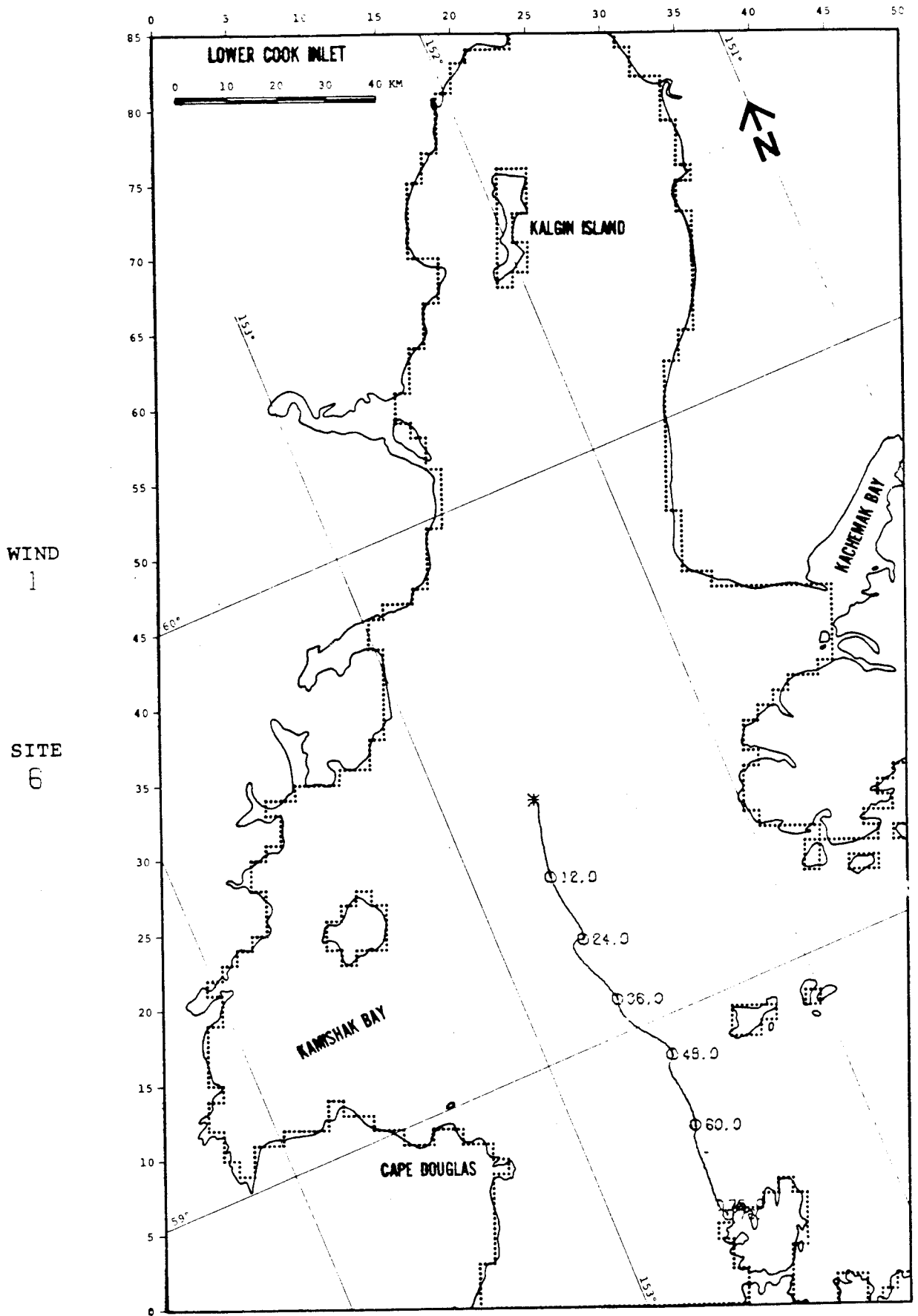


FIGURE B-6: BASE CASE

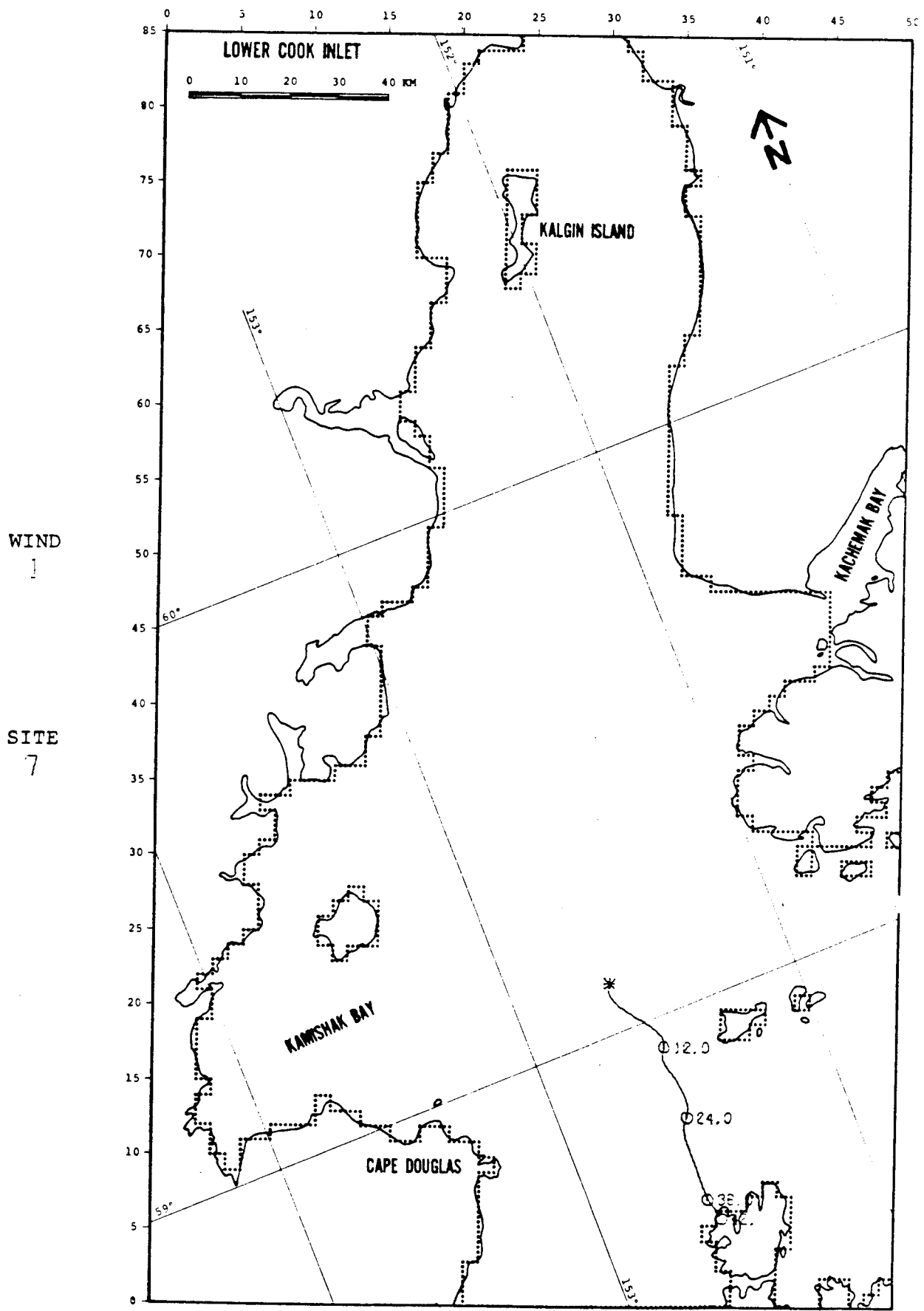


FIGURE B-7: BASE CASE

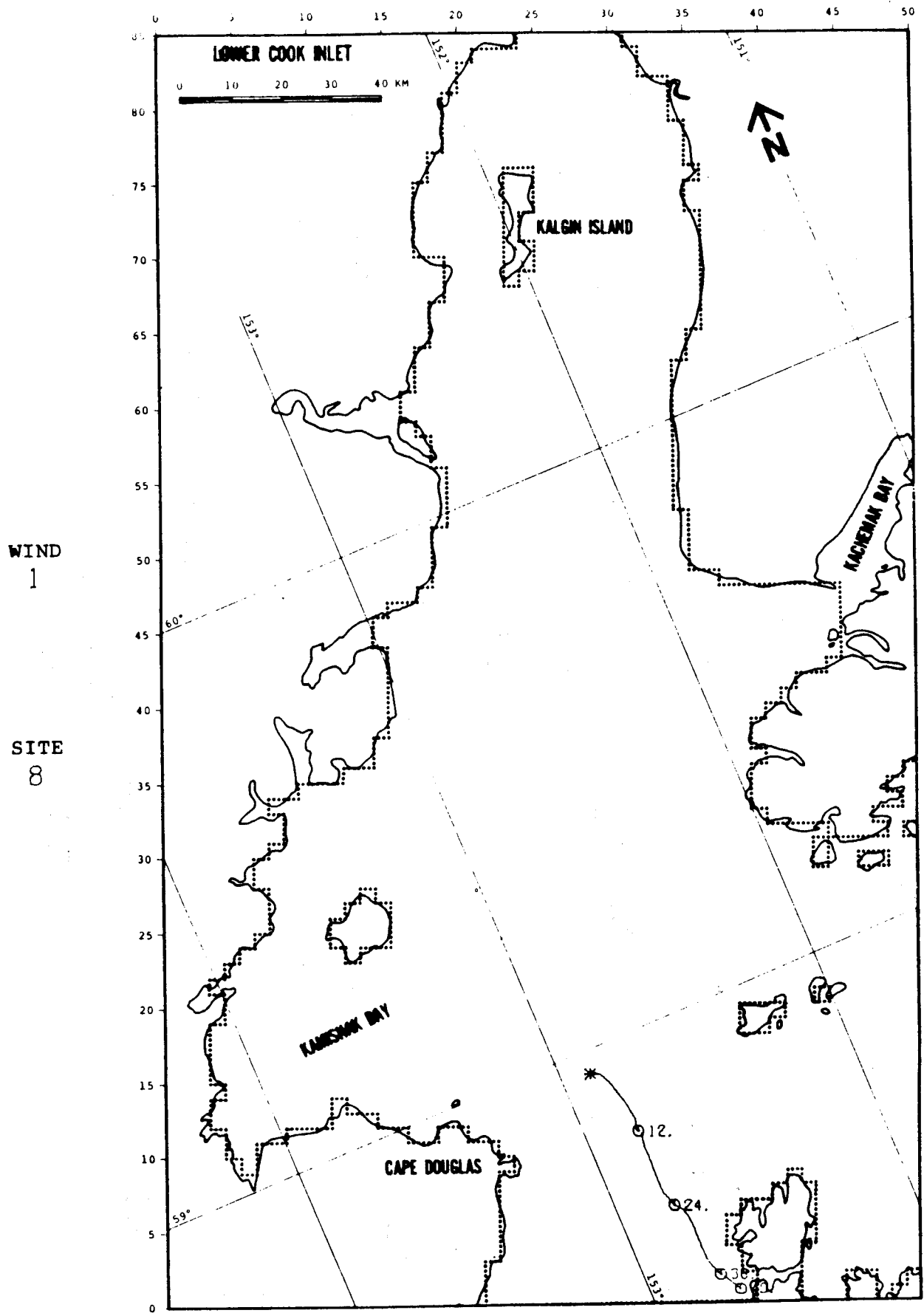
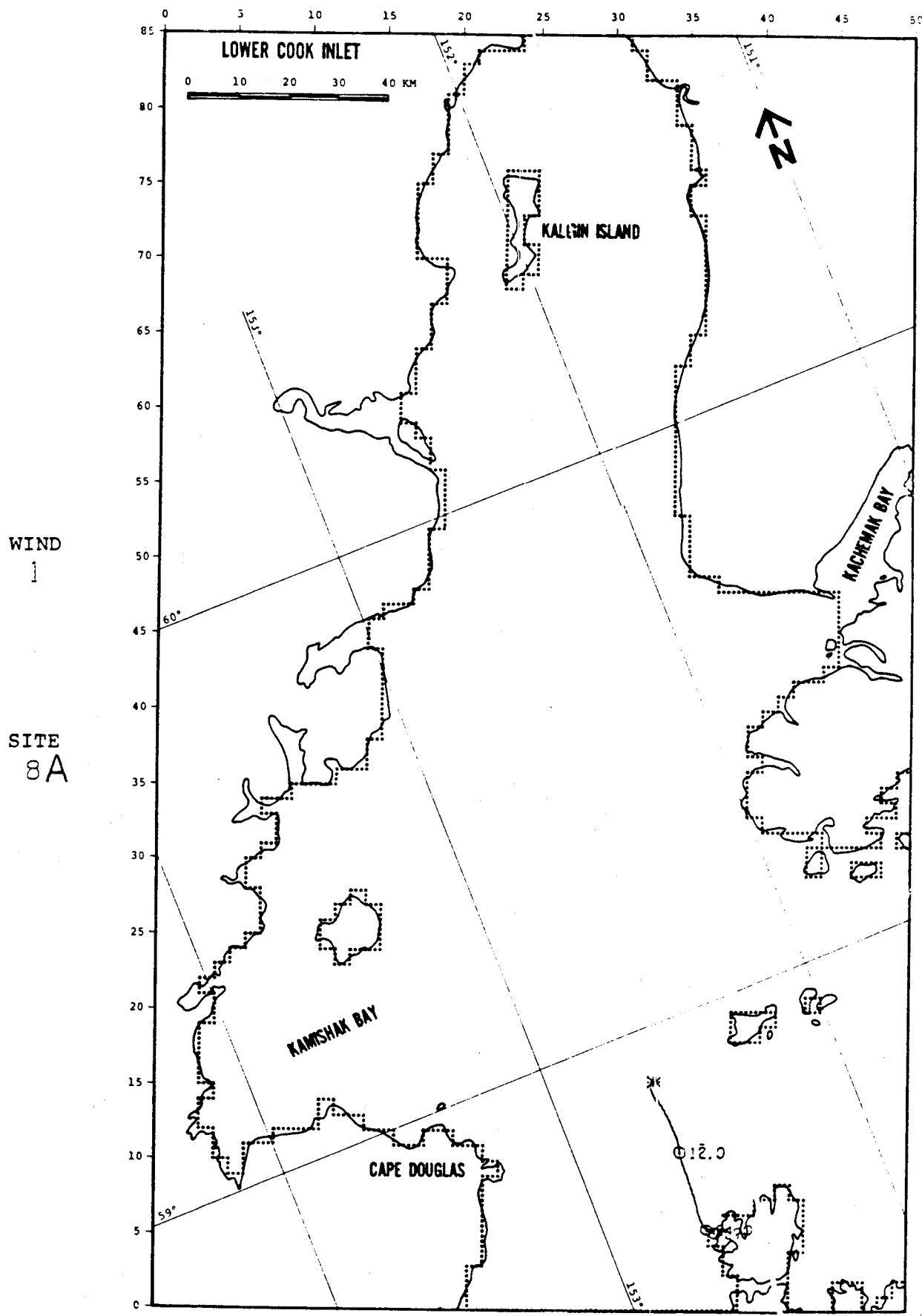


FIGURE B-8: BASE CASE



WIND
1

SITE
8A

FIGURE B-9: BASE CASE

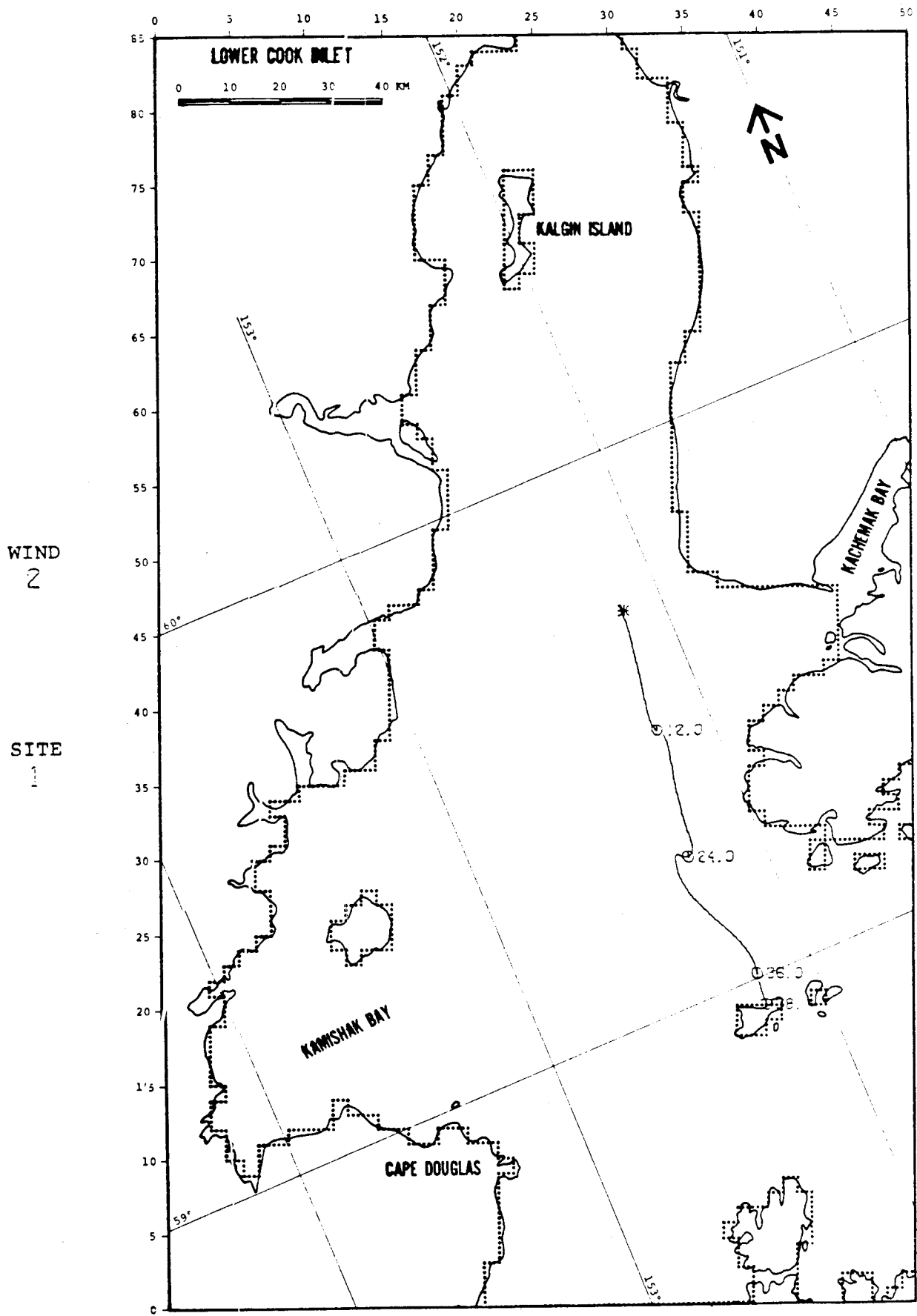


FIGURE B-10: BASE CASE

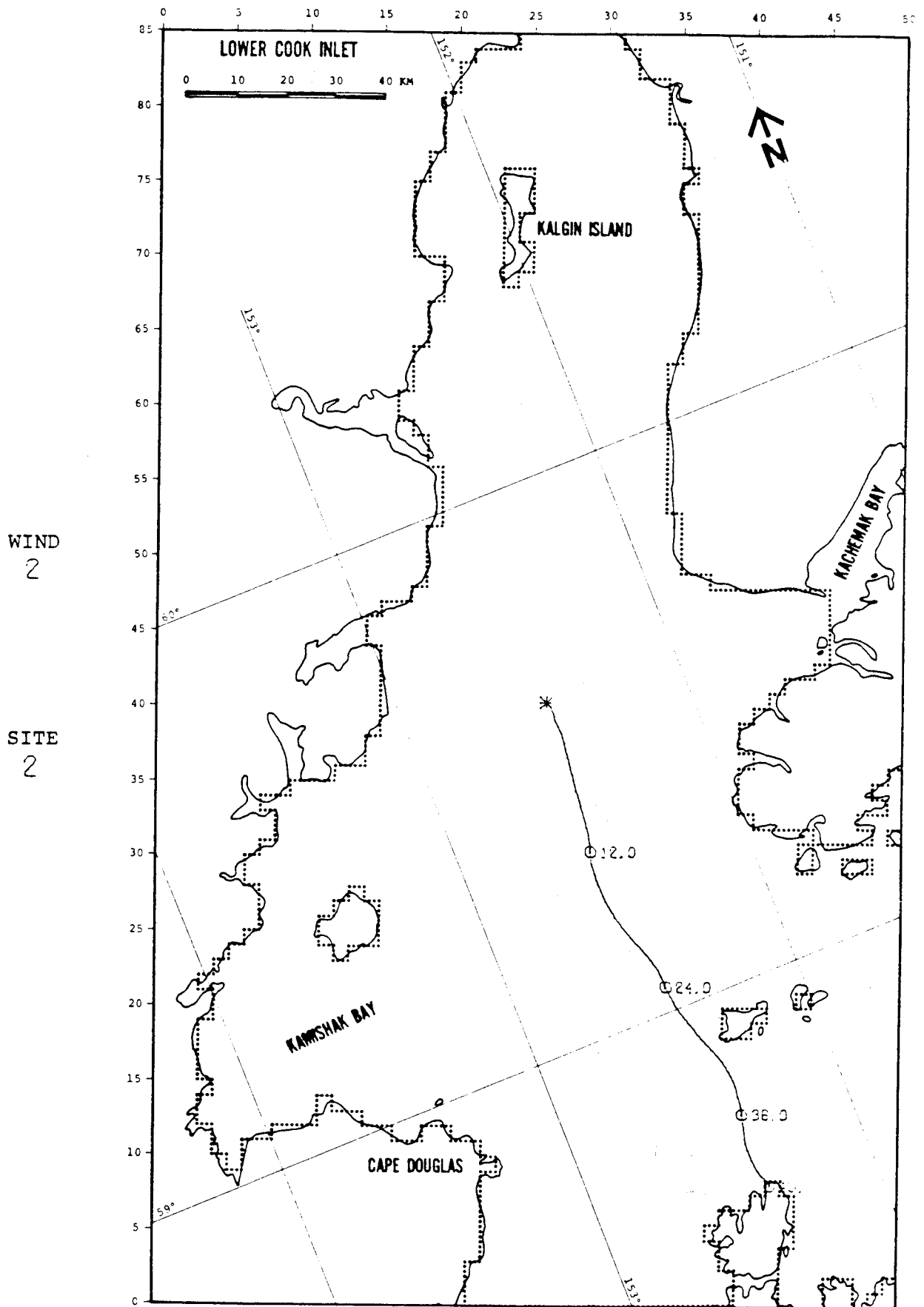


FIGURE B-11: BASE CASE

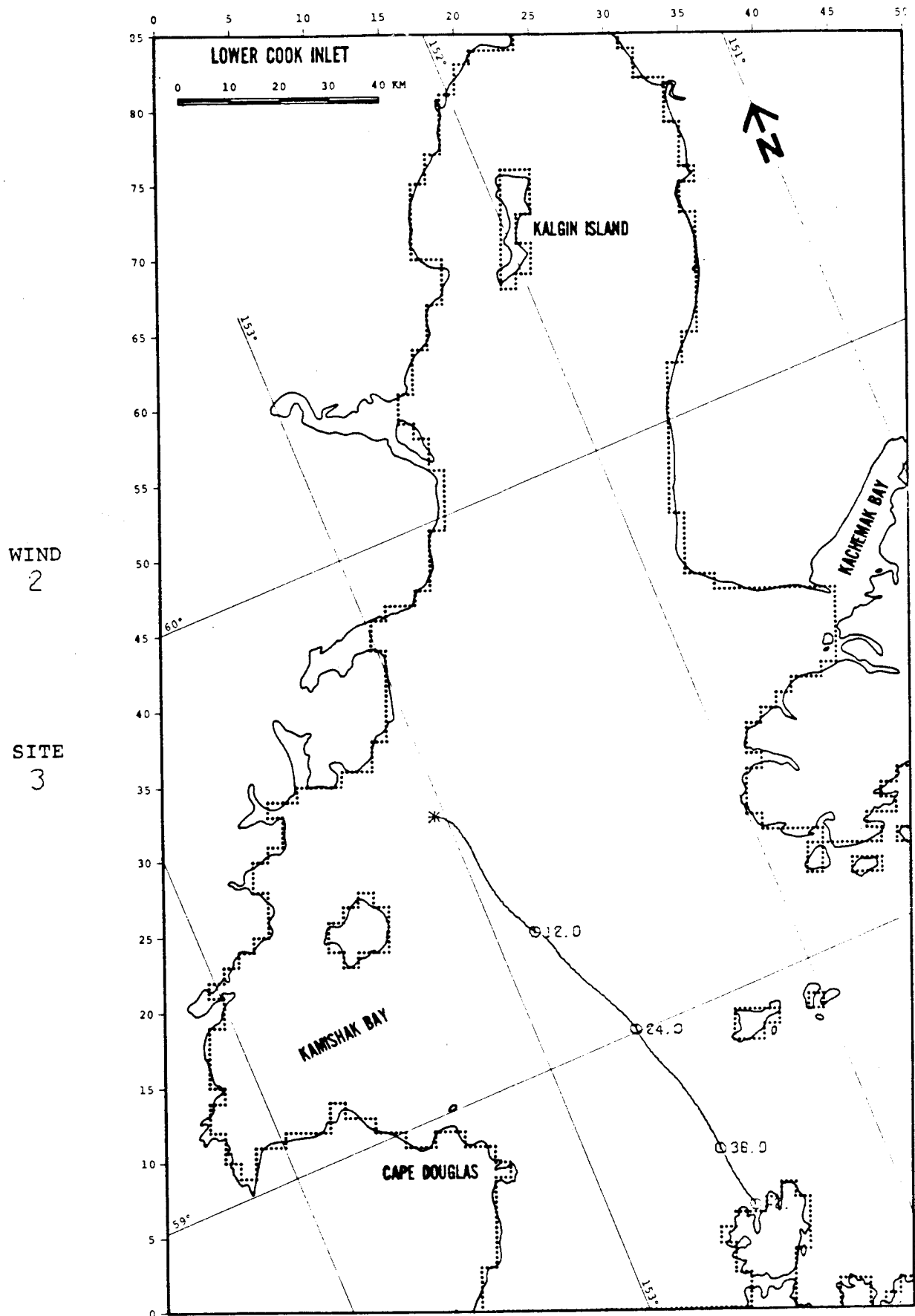


FIGURE B-12: BASE CASE

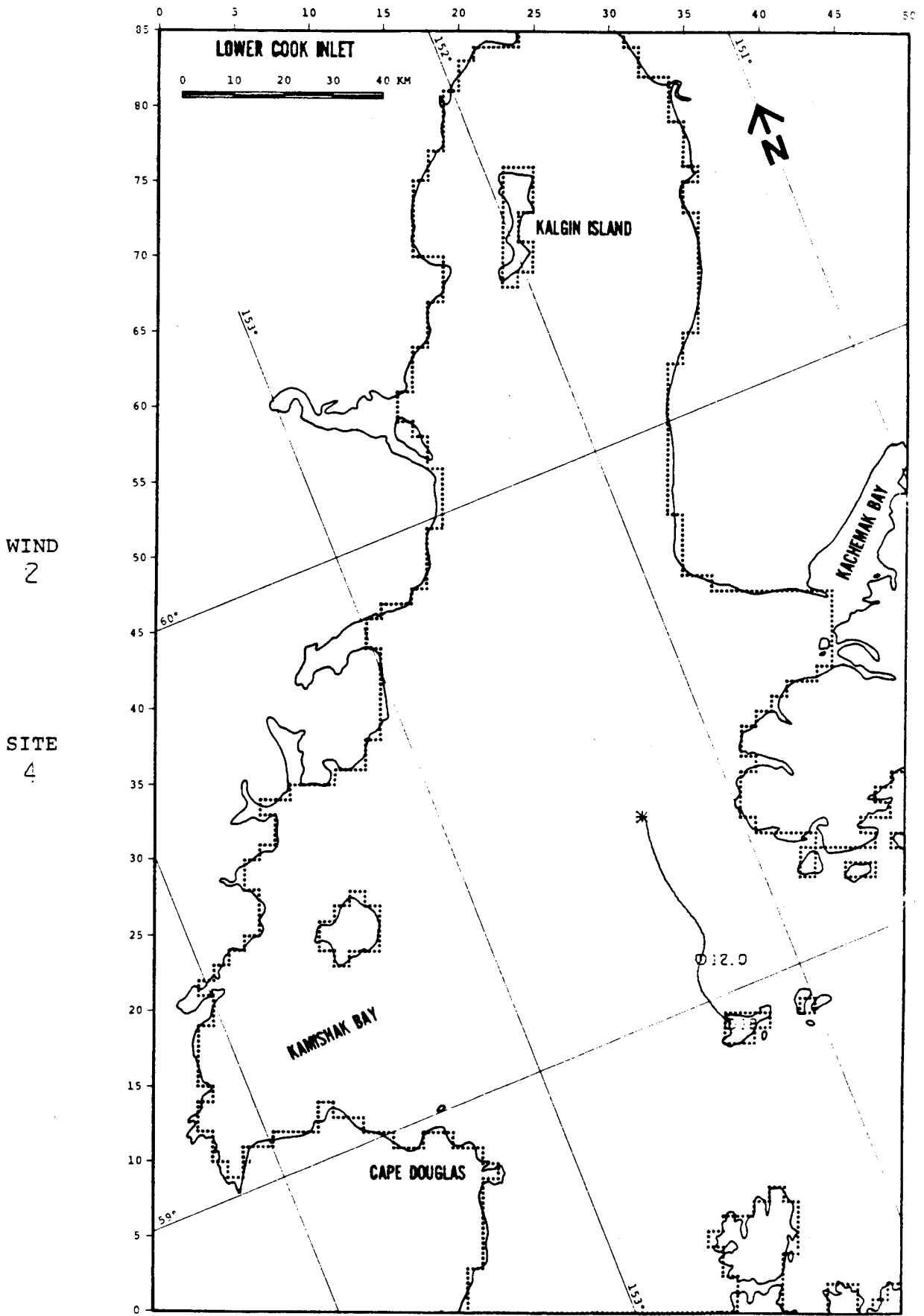


FIGURE B-13: BASE CASE

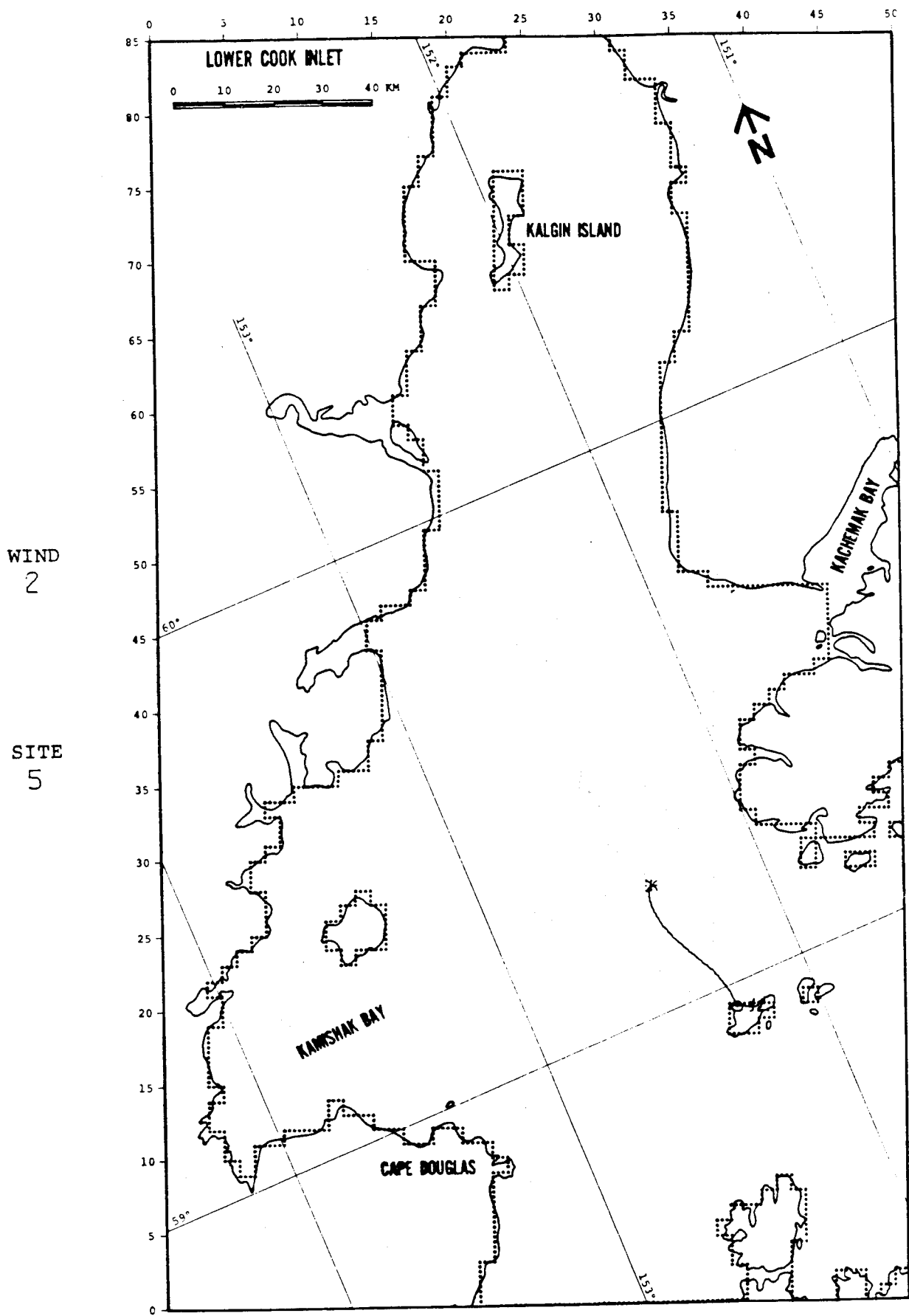


FIGURE B-14: BASE CASE

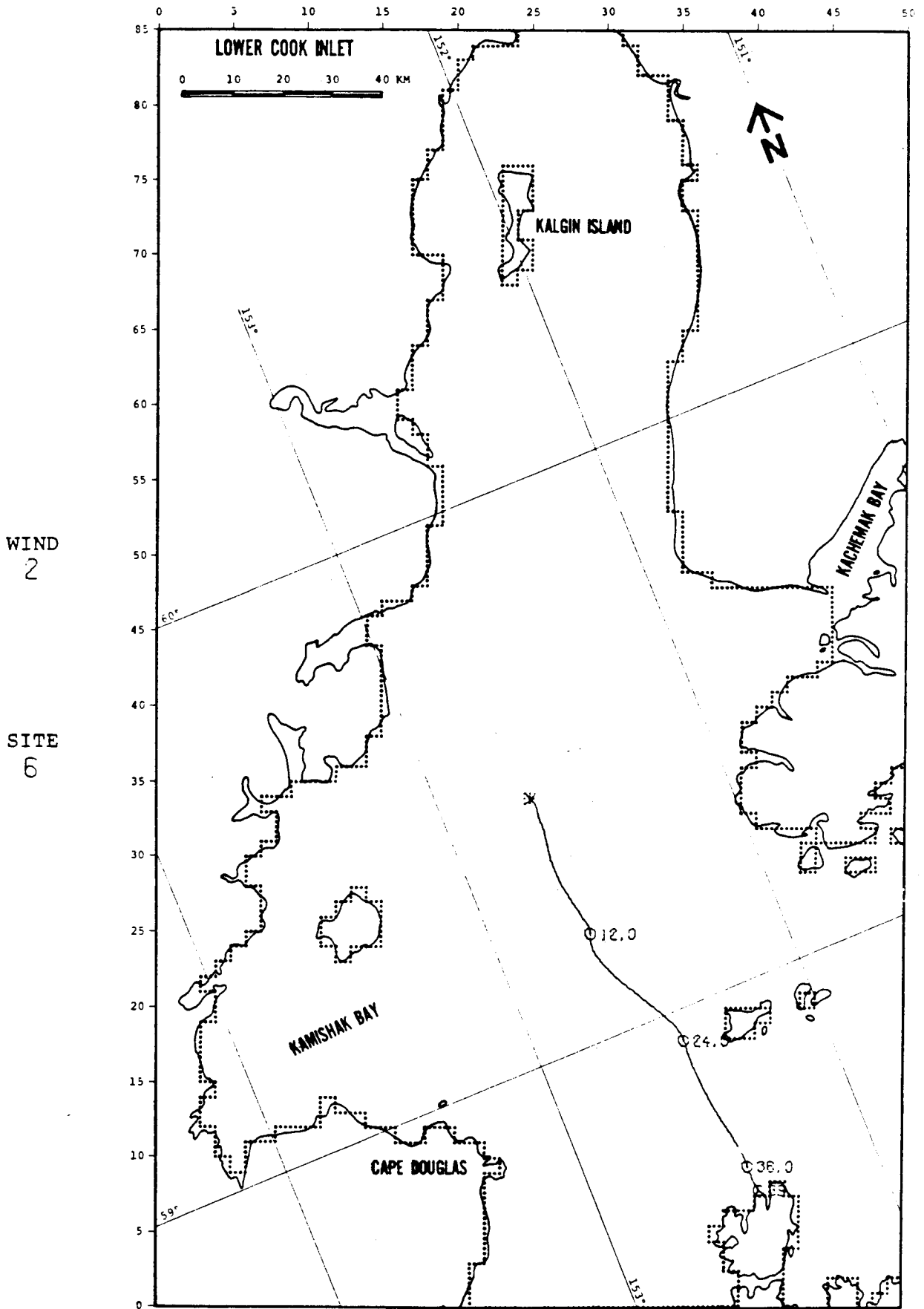


FIGURE B-15: BASE CASE

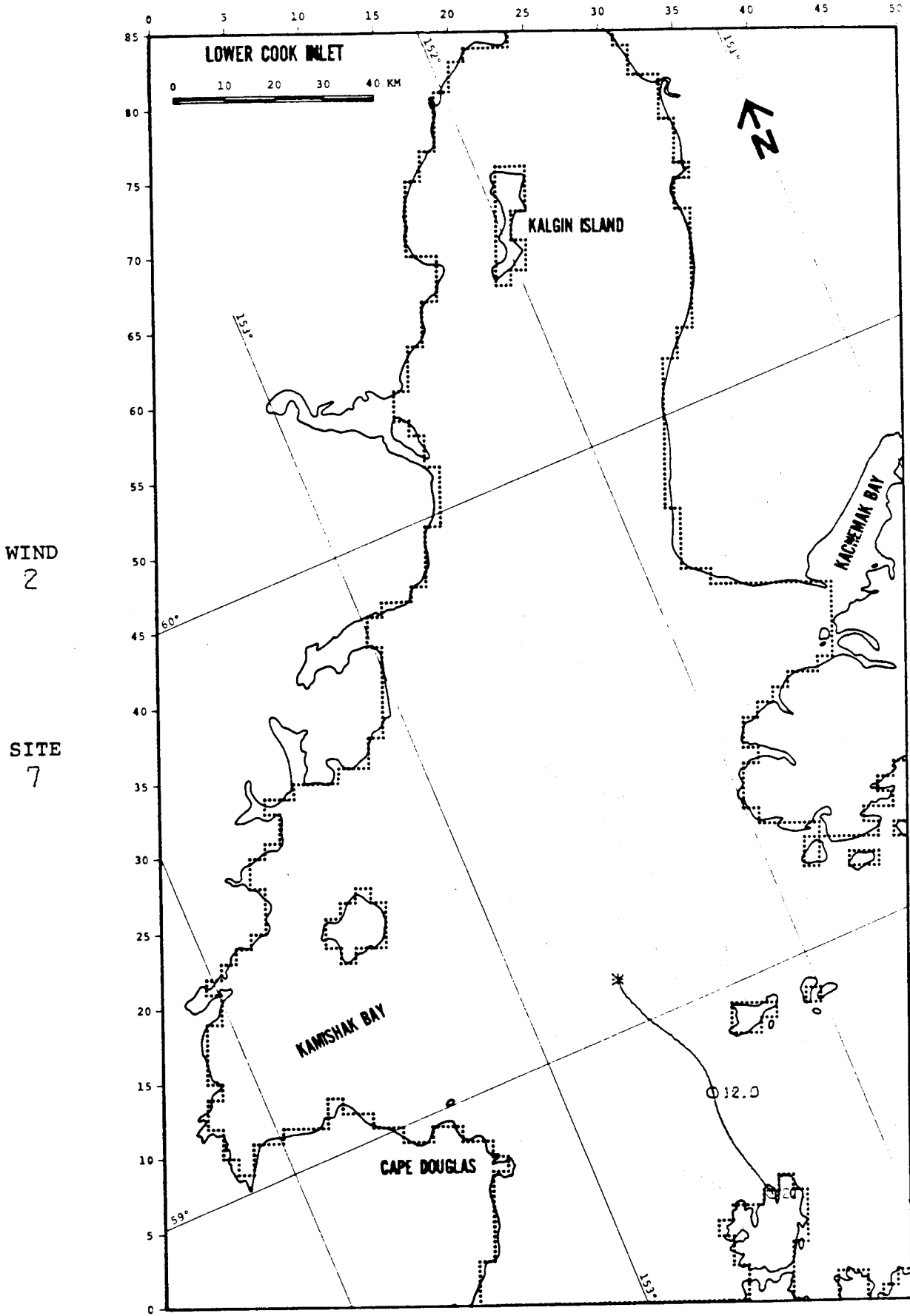


FIGURE B-16: BASE CASE

WIND
3

SITE
1

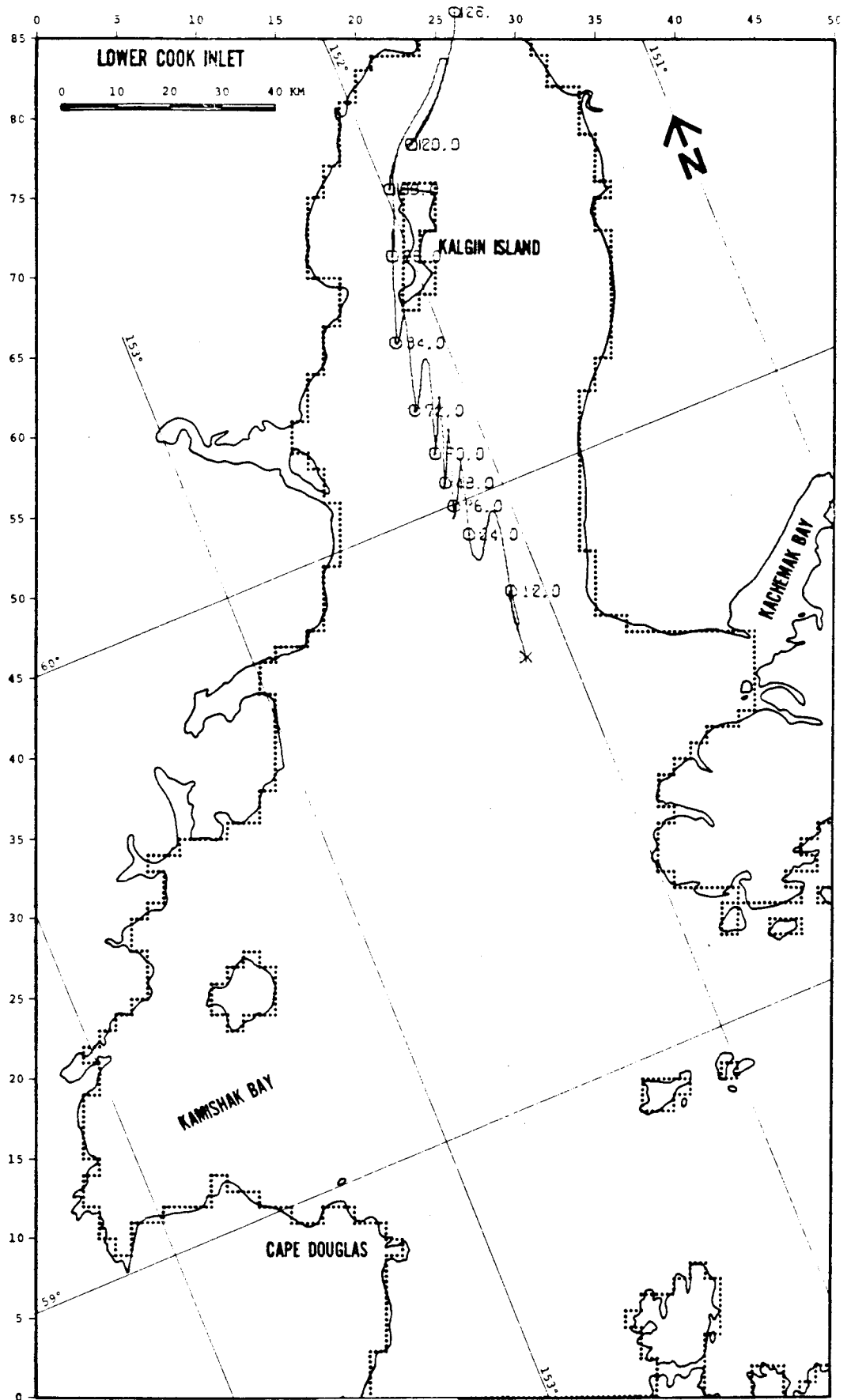


FIGURE B-19: BASE CASE

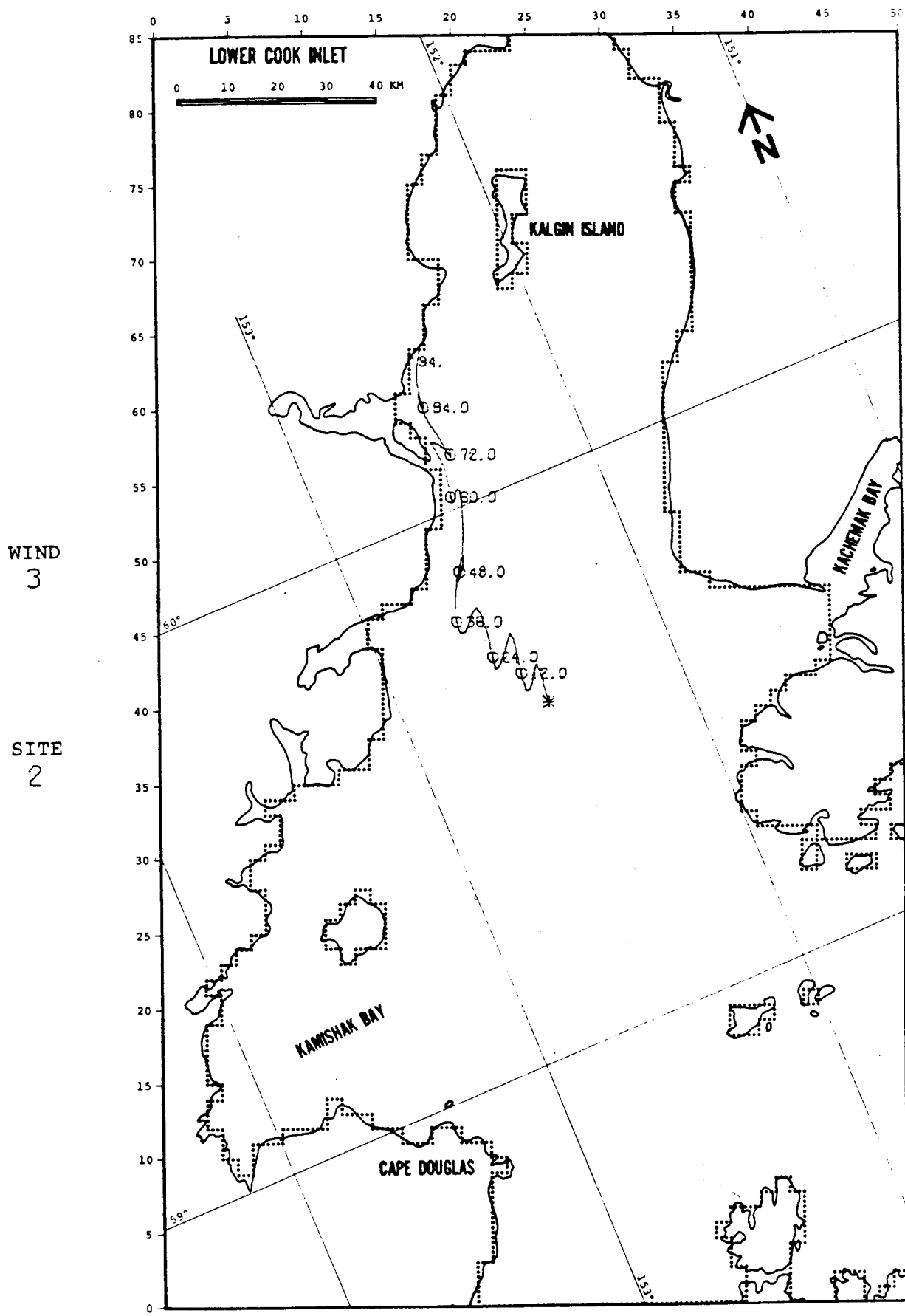
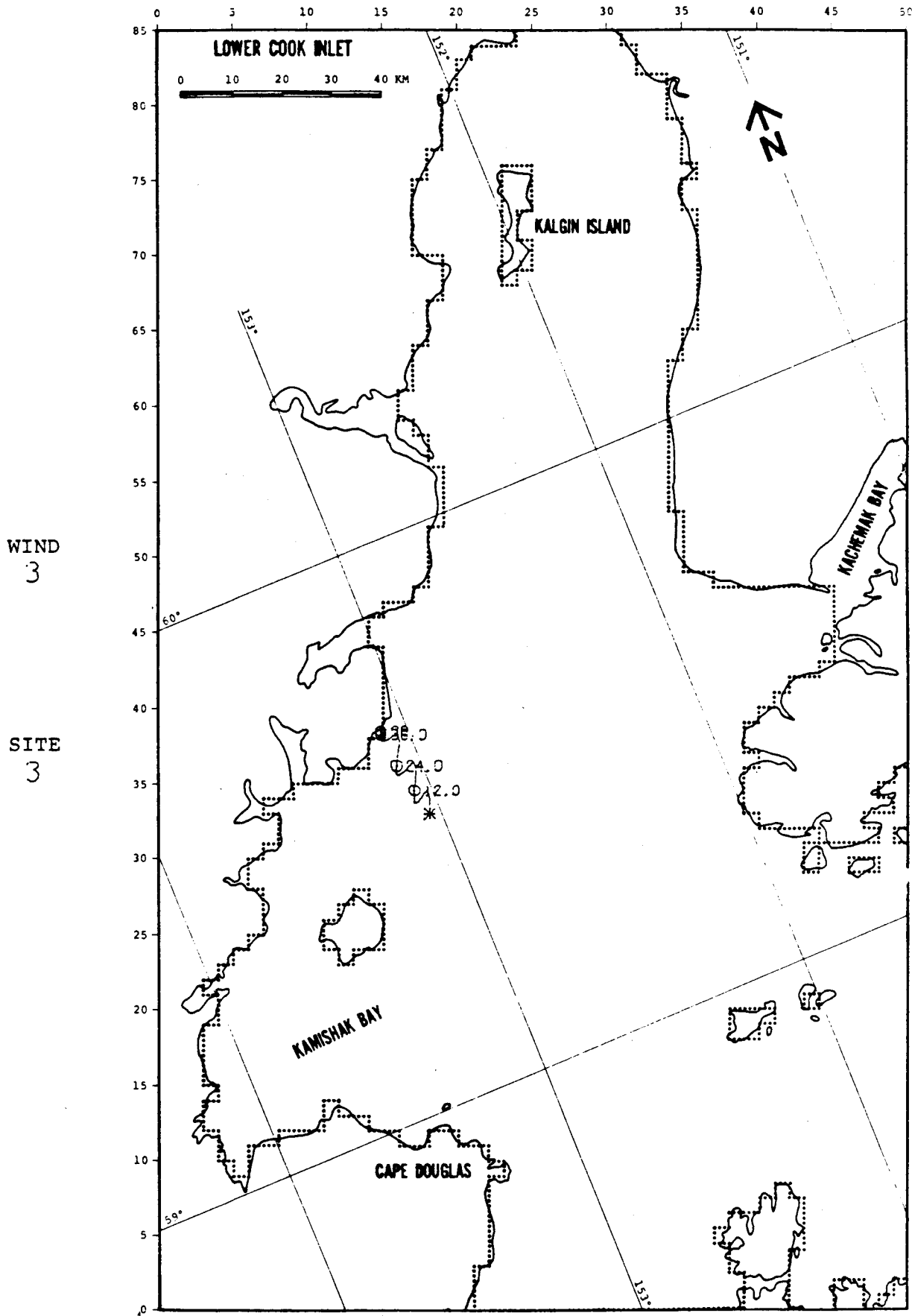


FIGURE B-20: BASE CASE



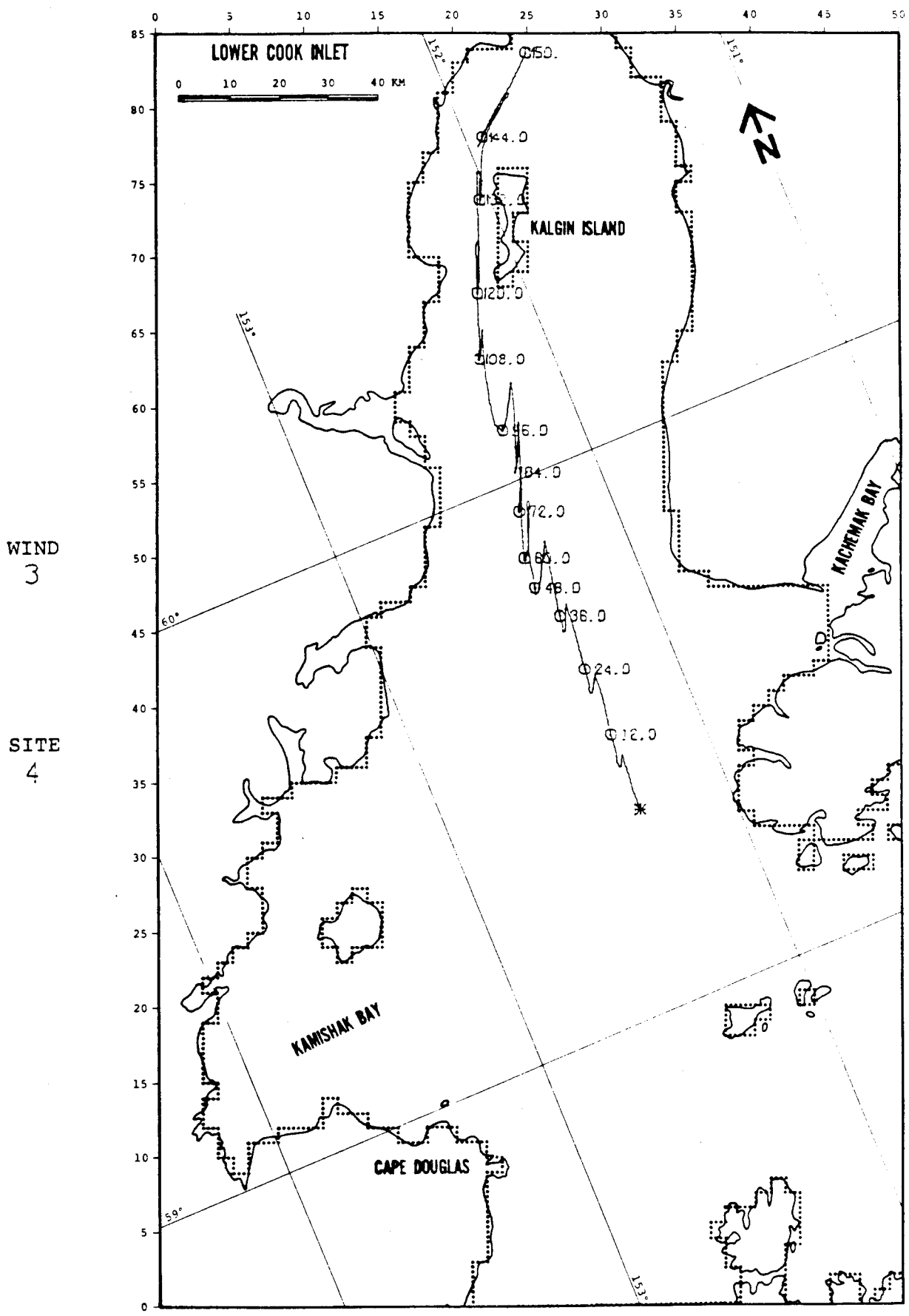


FIGURE B-22: BASE CASE

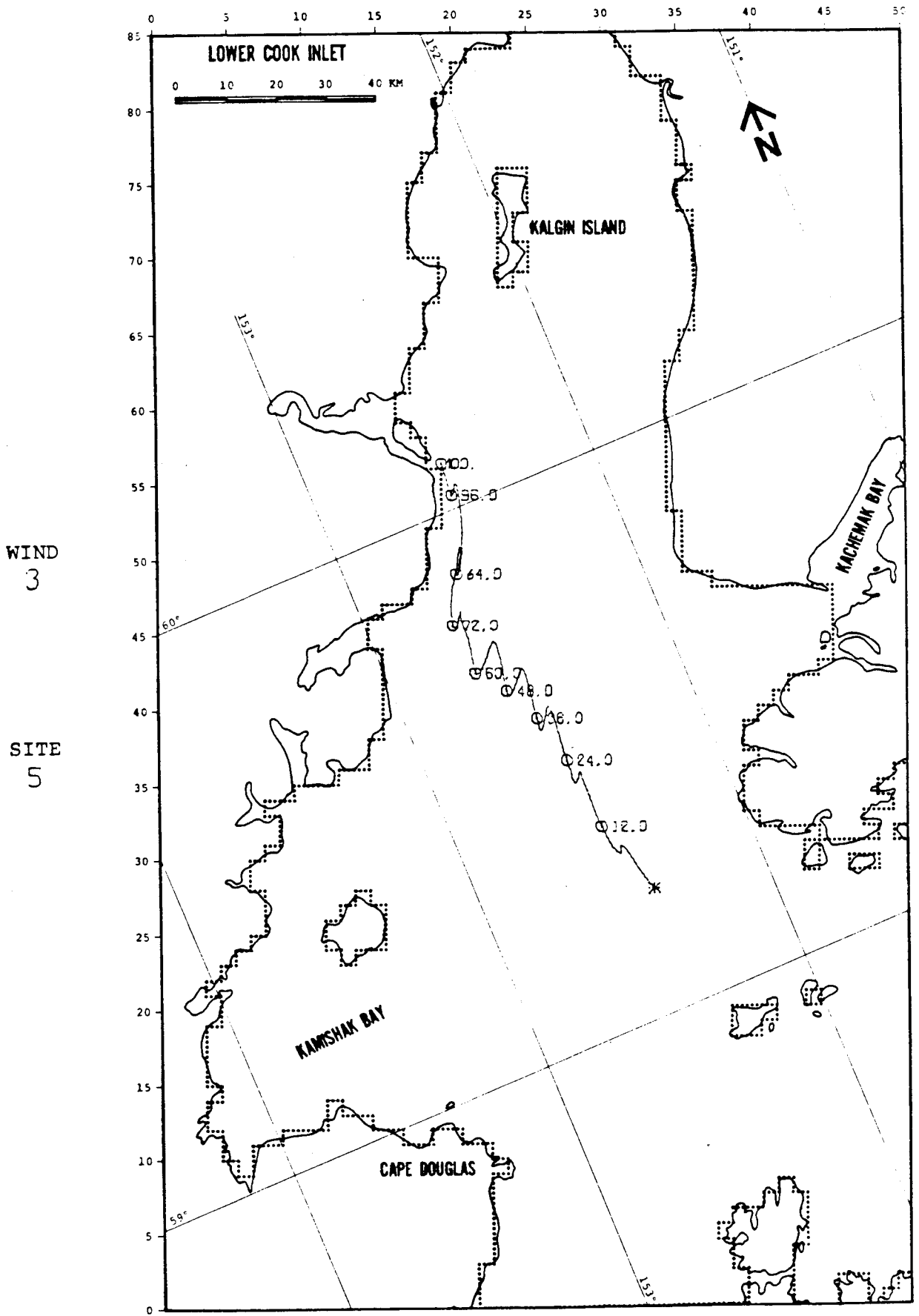


FIGURE B-23: BASE CASE

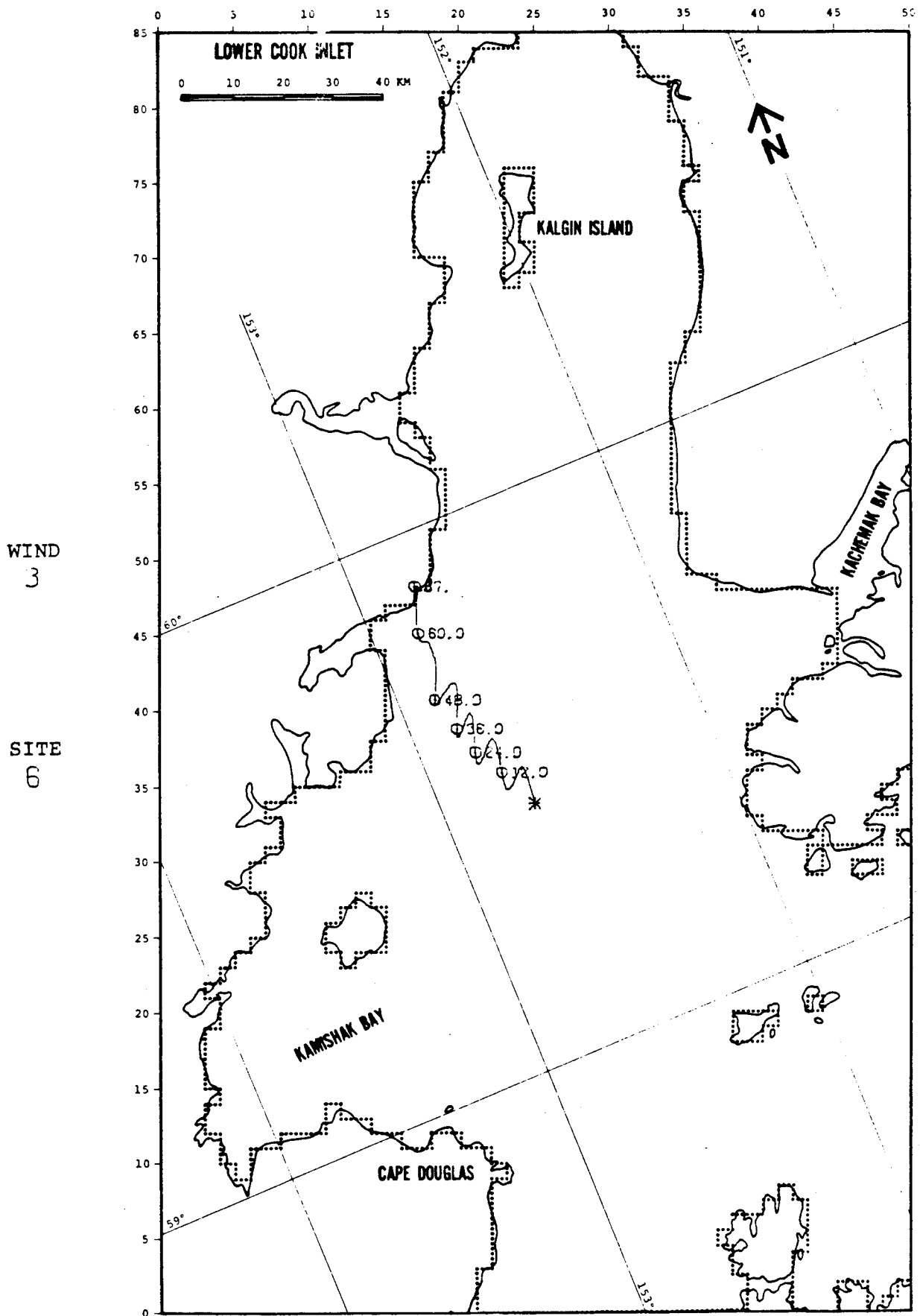


FIGURE B-24: BASE CASE

WIND
3

SITE
7

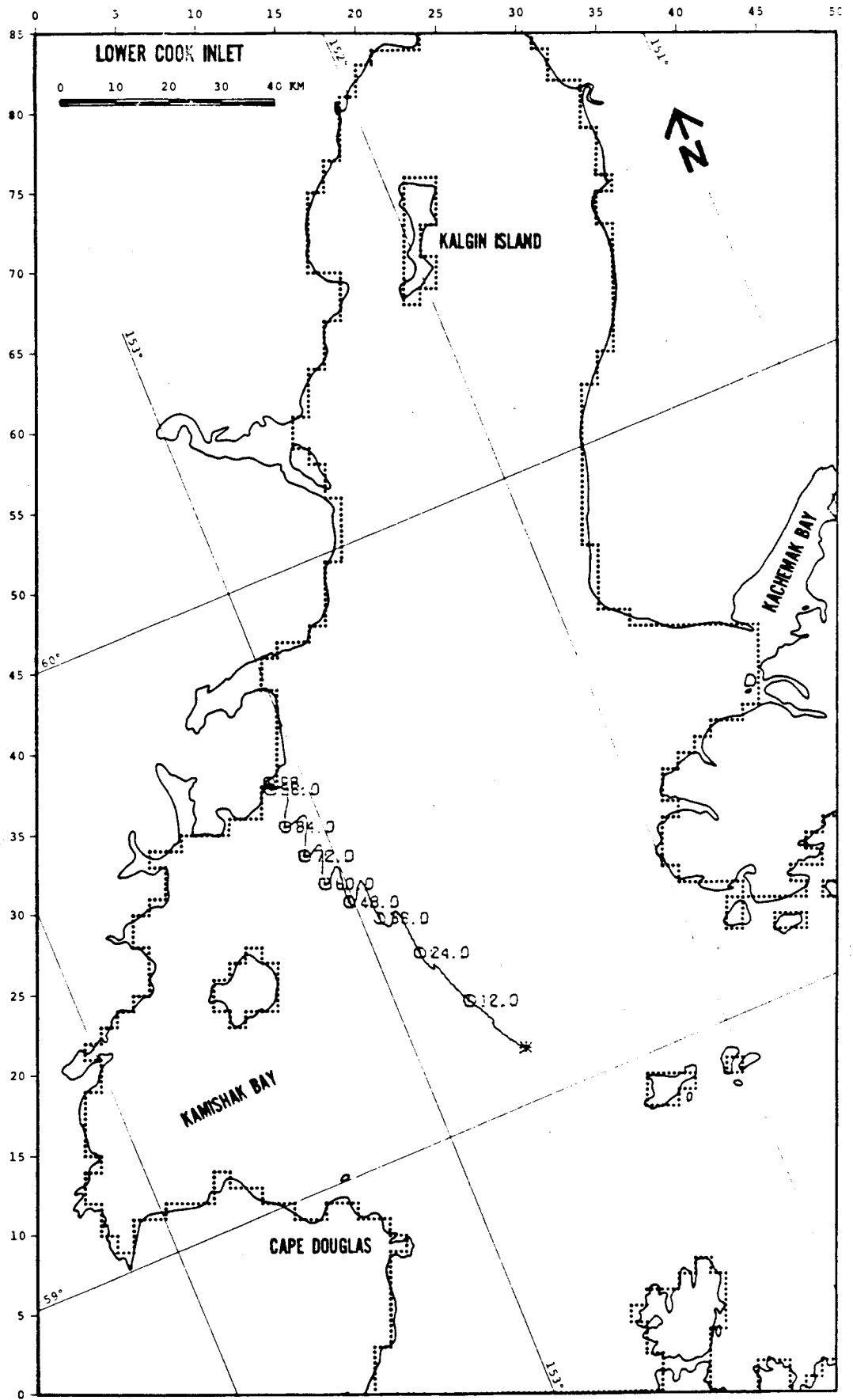
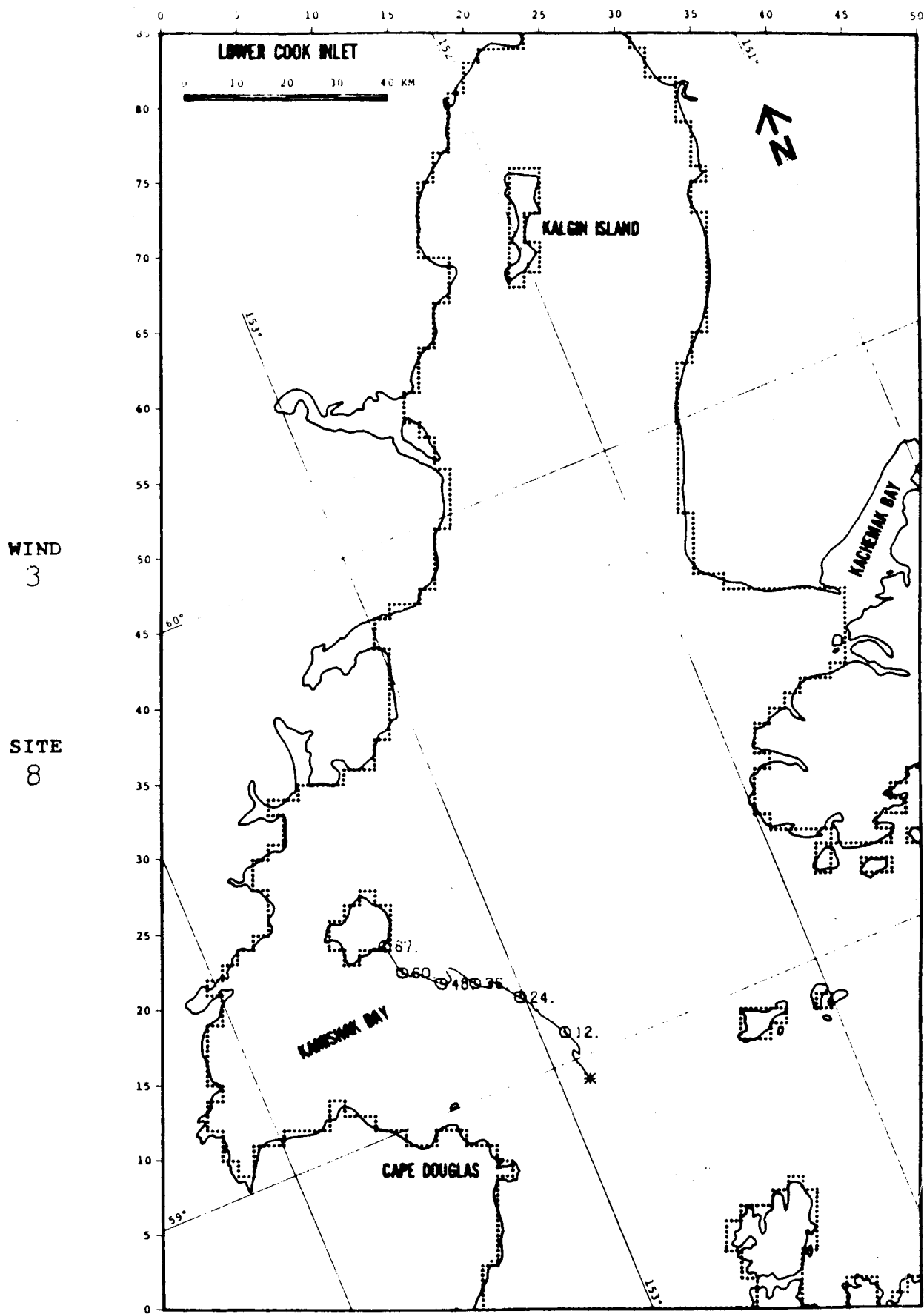


FIGURE B-25: BASE CASE



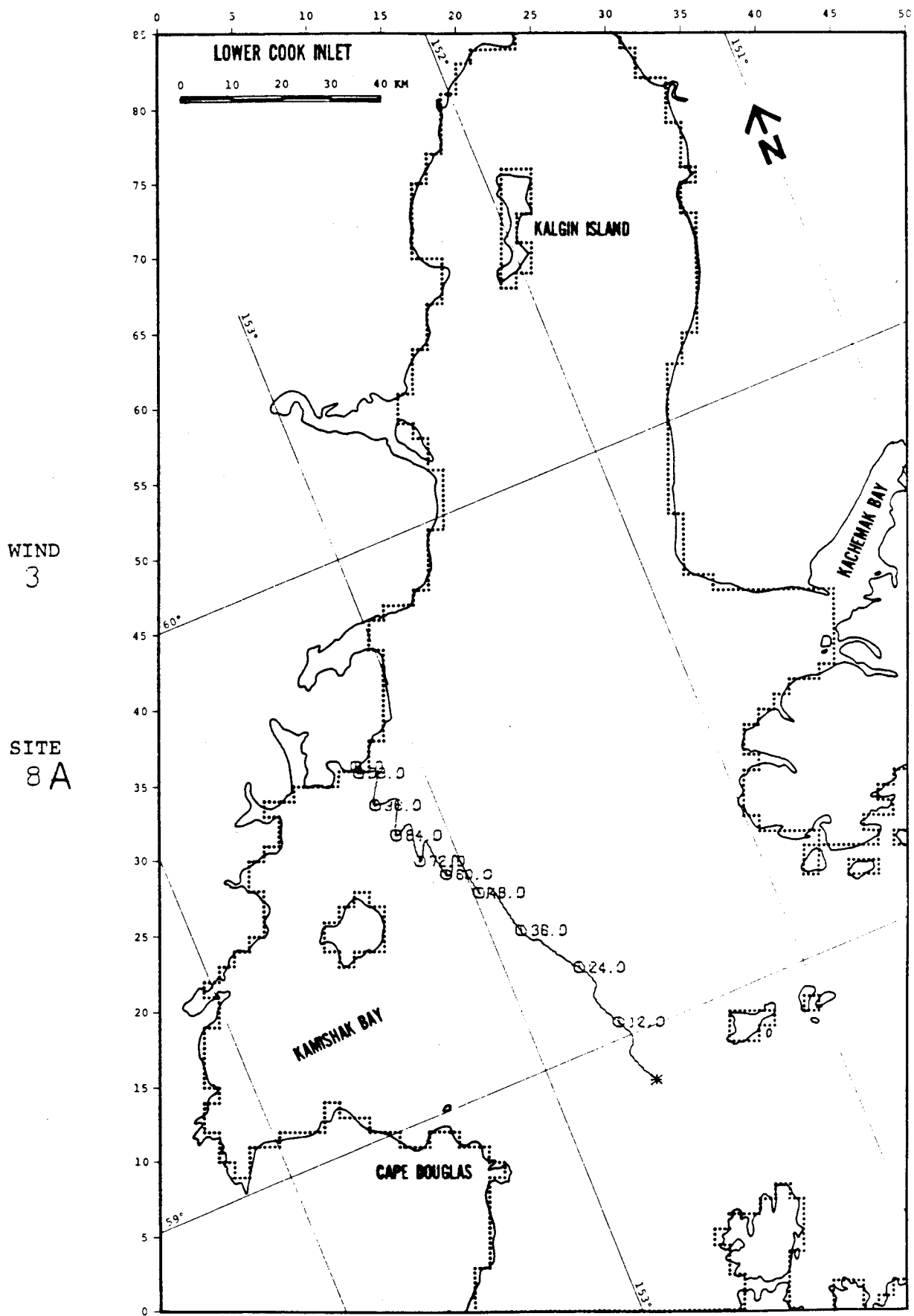


FIGURE B-27: BASE CASE

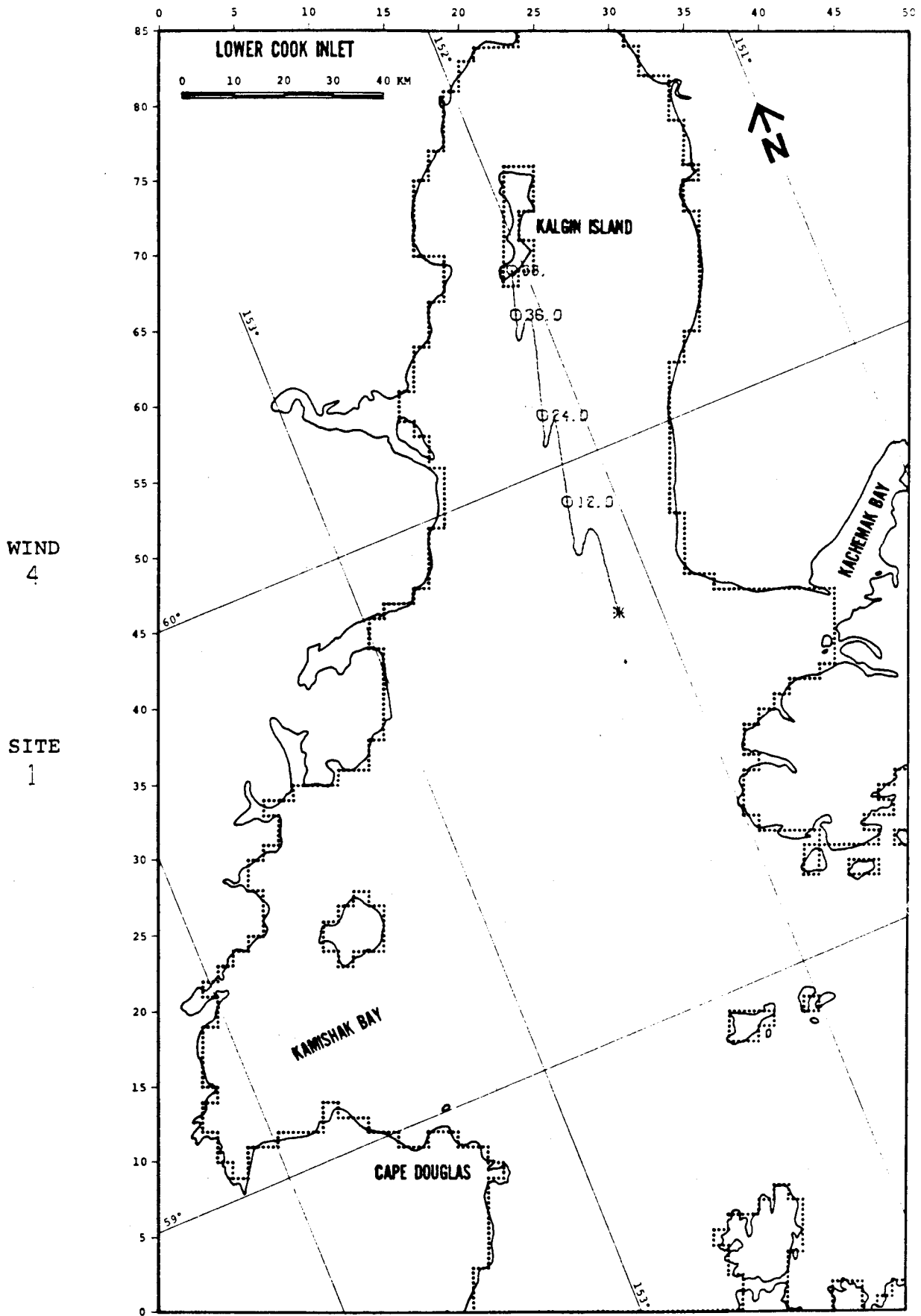


FIGURE B-28: BASE CASE

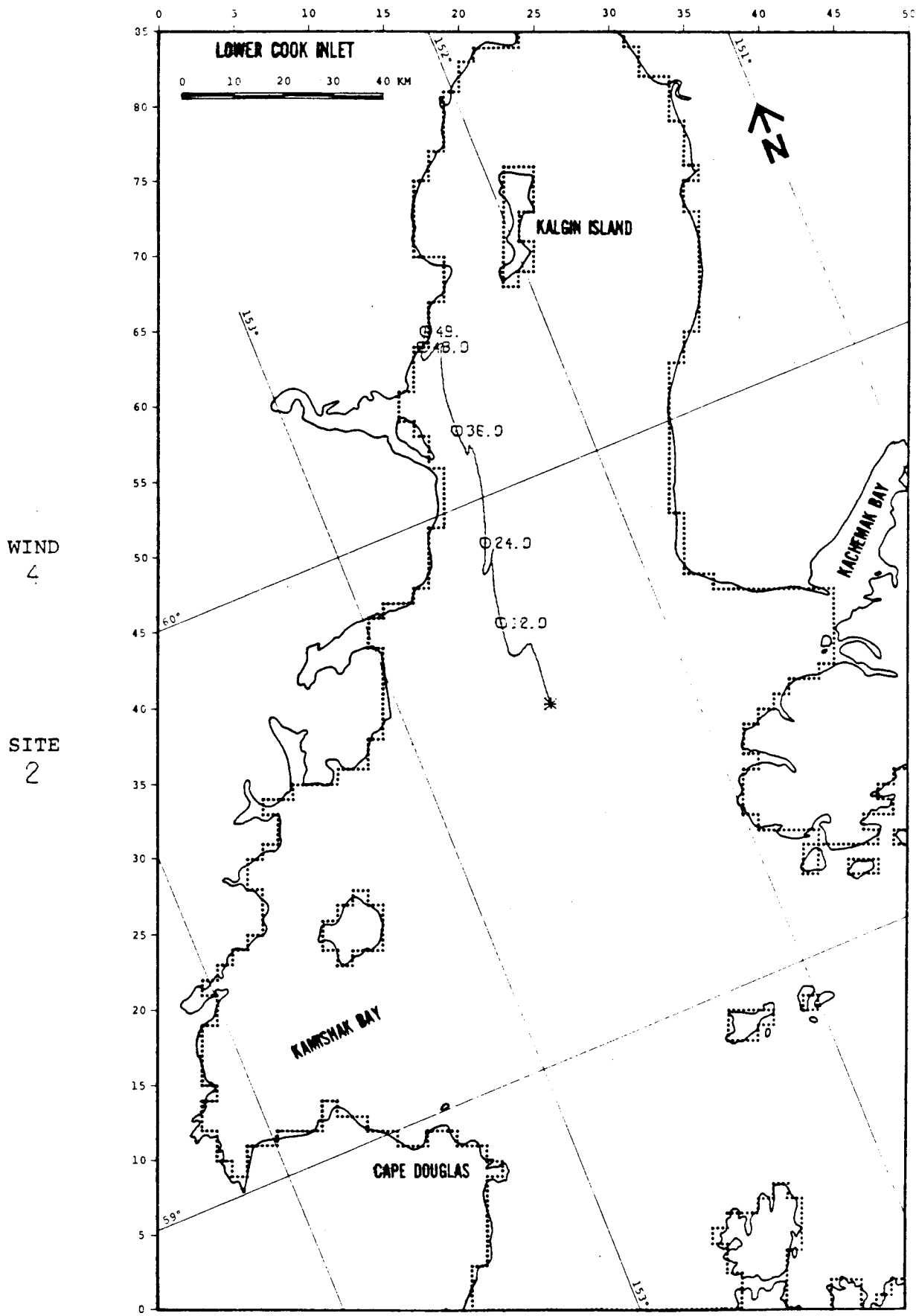


FIGURE B-29: BASE CASE

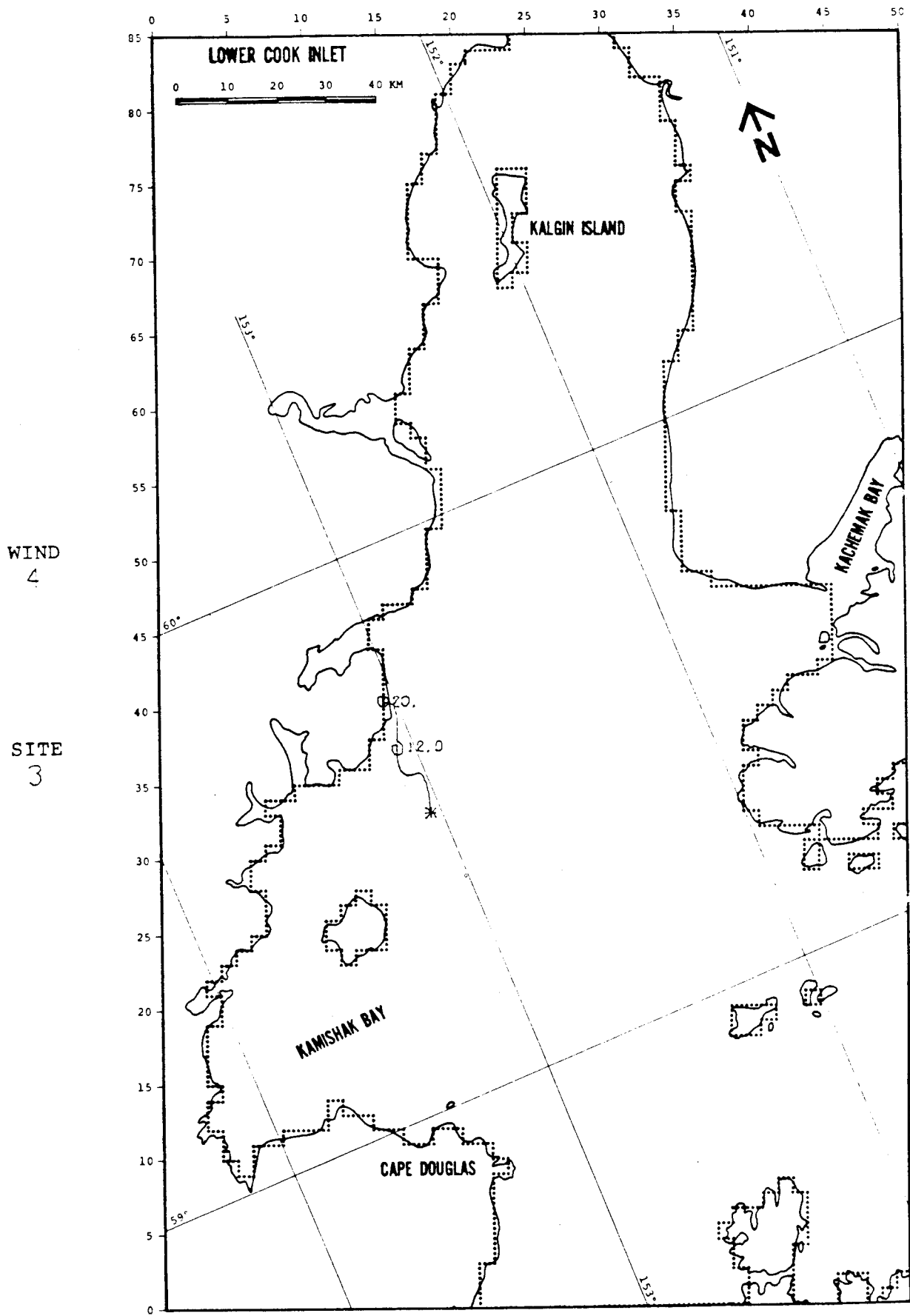


FIGURE B-30: BASE CASE

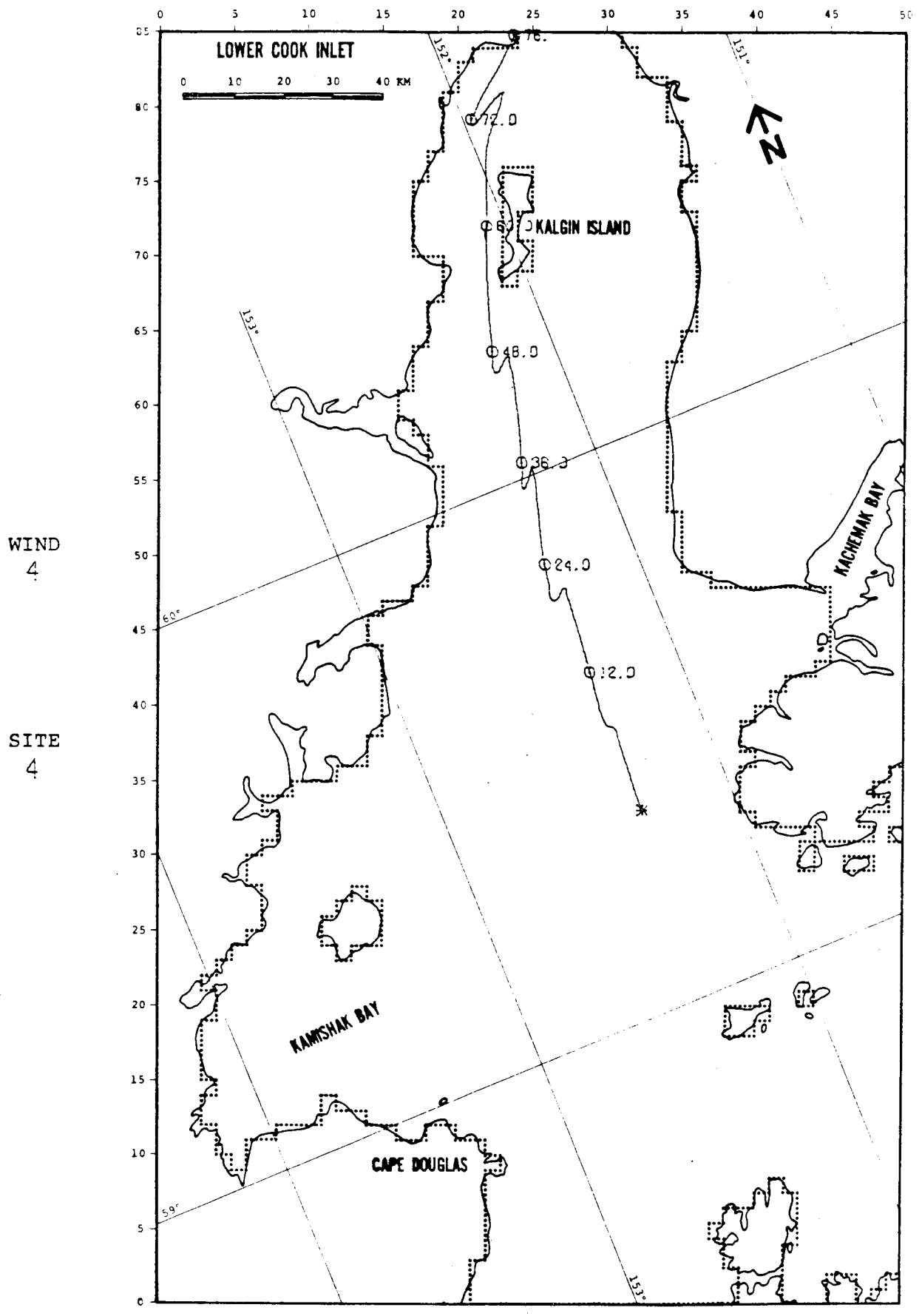


FIGURE B-31: BASE CASE

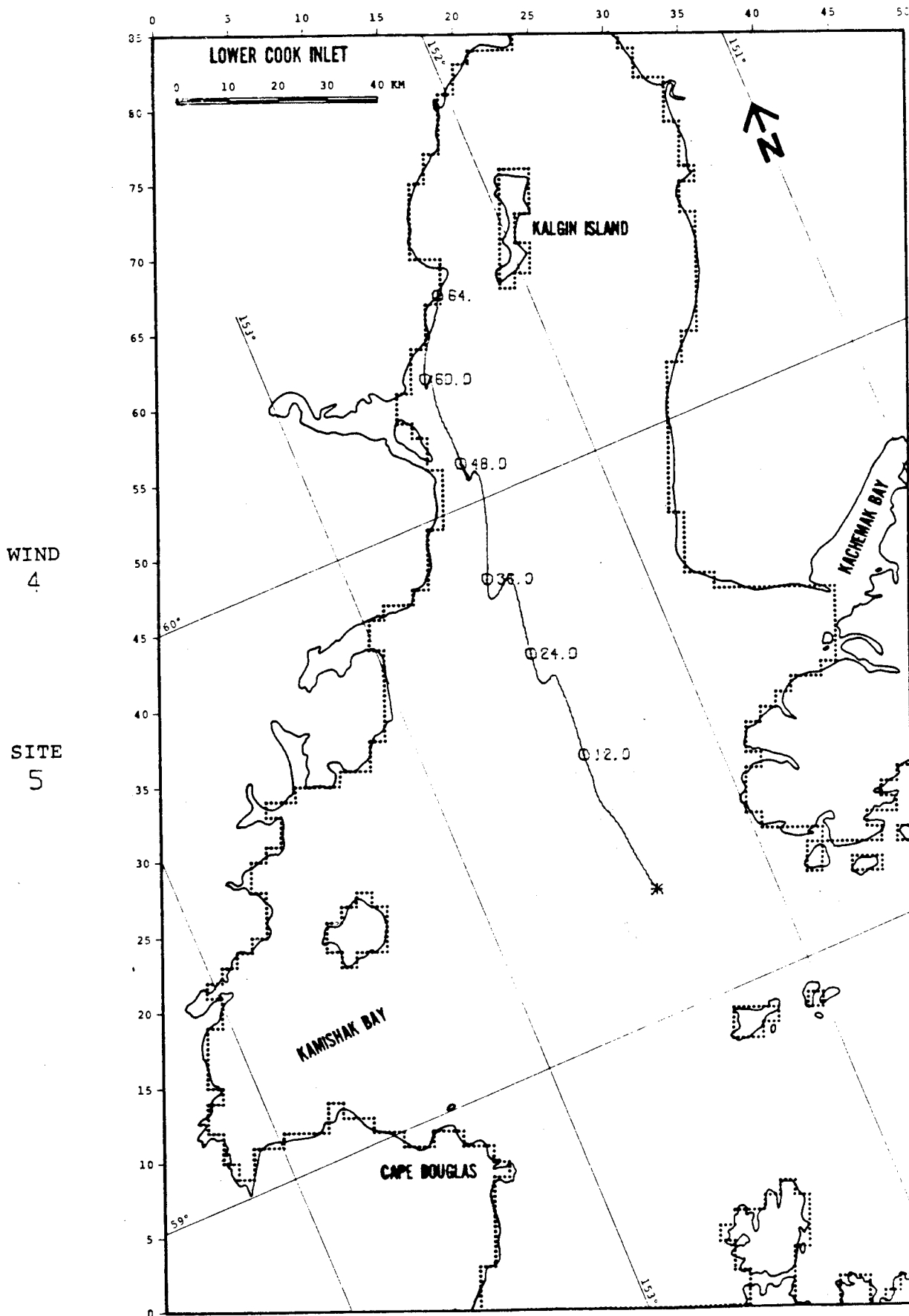


FIGURE B-32: BASE CASE

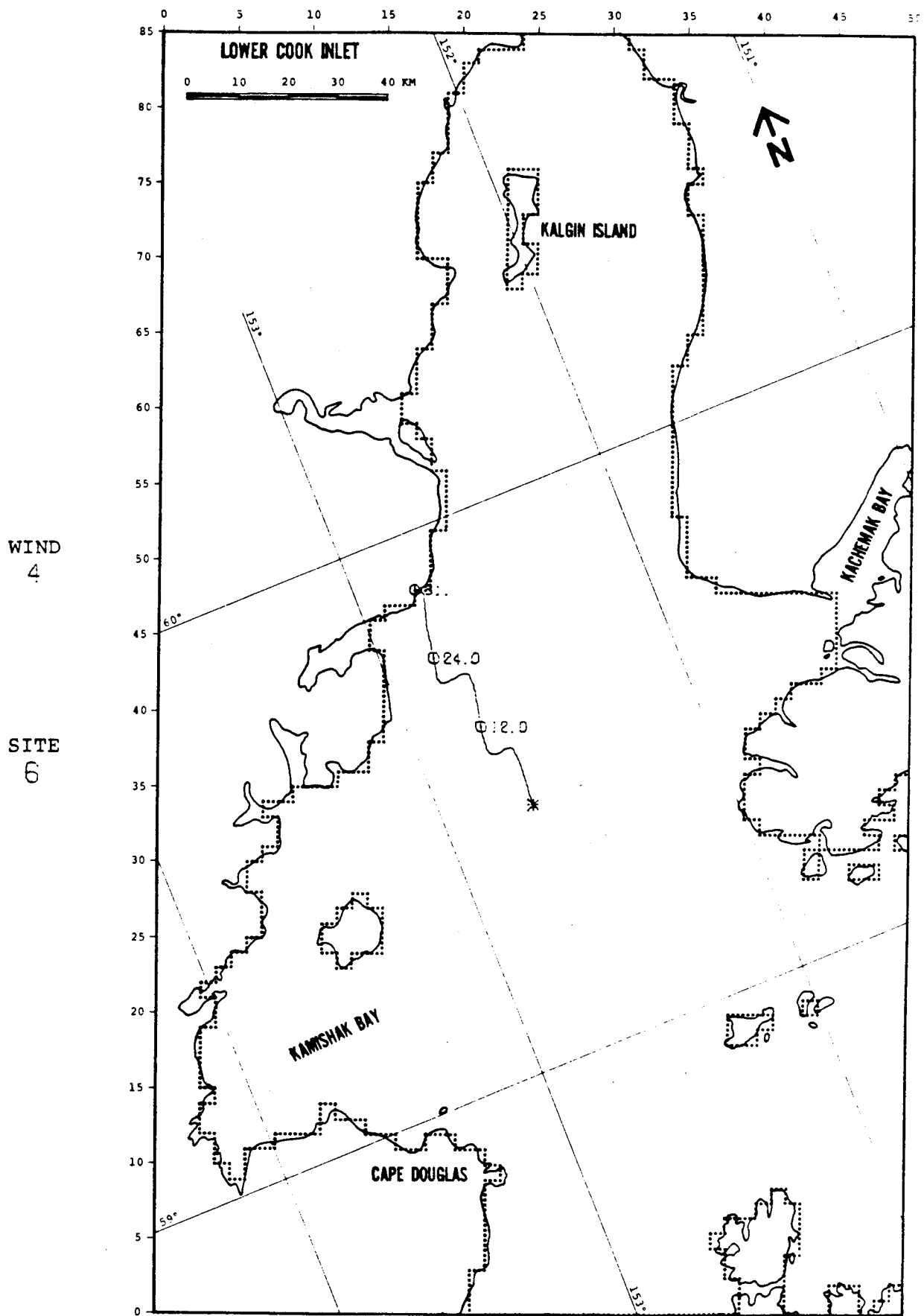


FIGURE B-33: BASE CASE

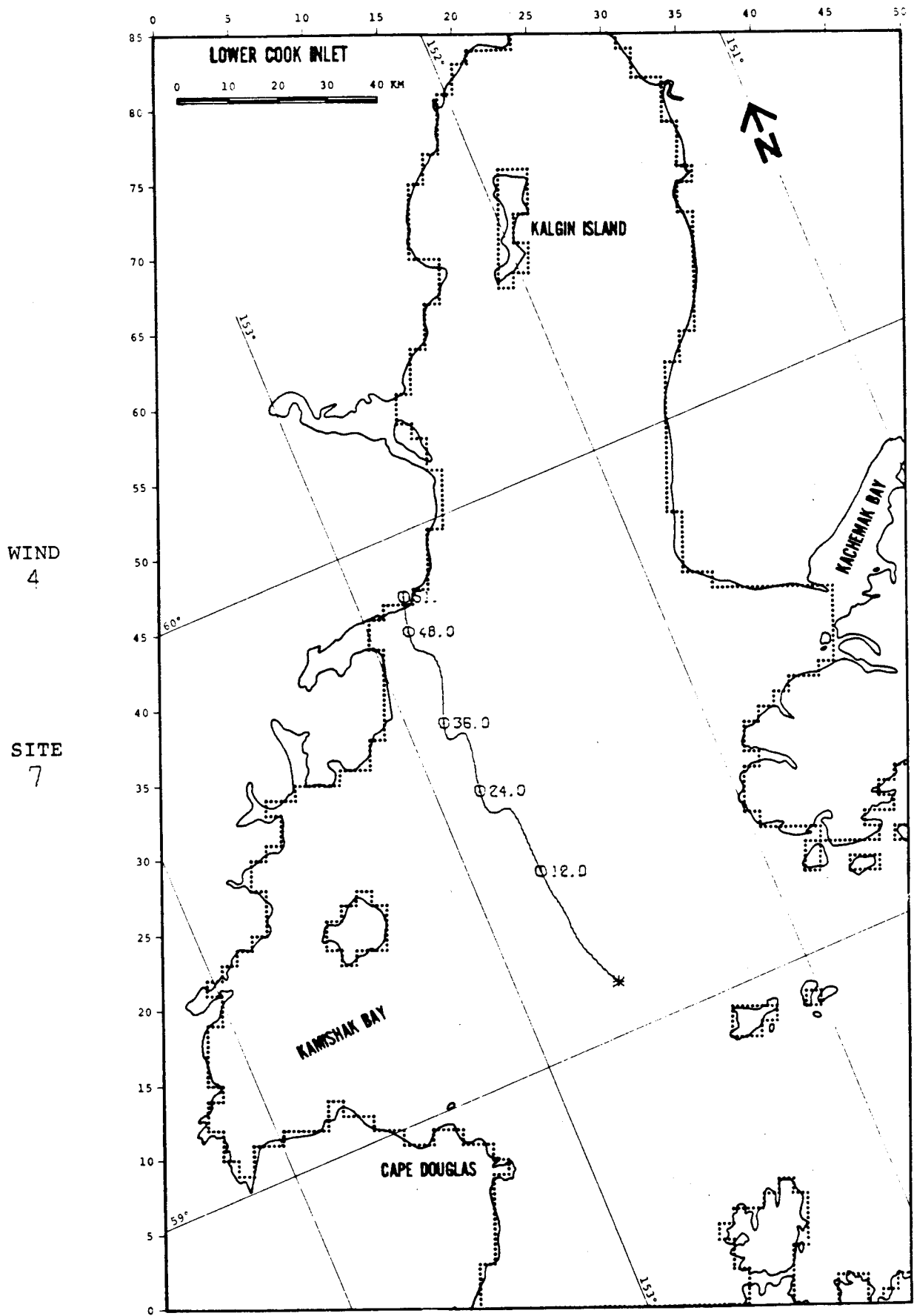


FIGURE B-34: BASE CASE

WIND
4

SITE
8

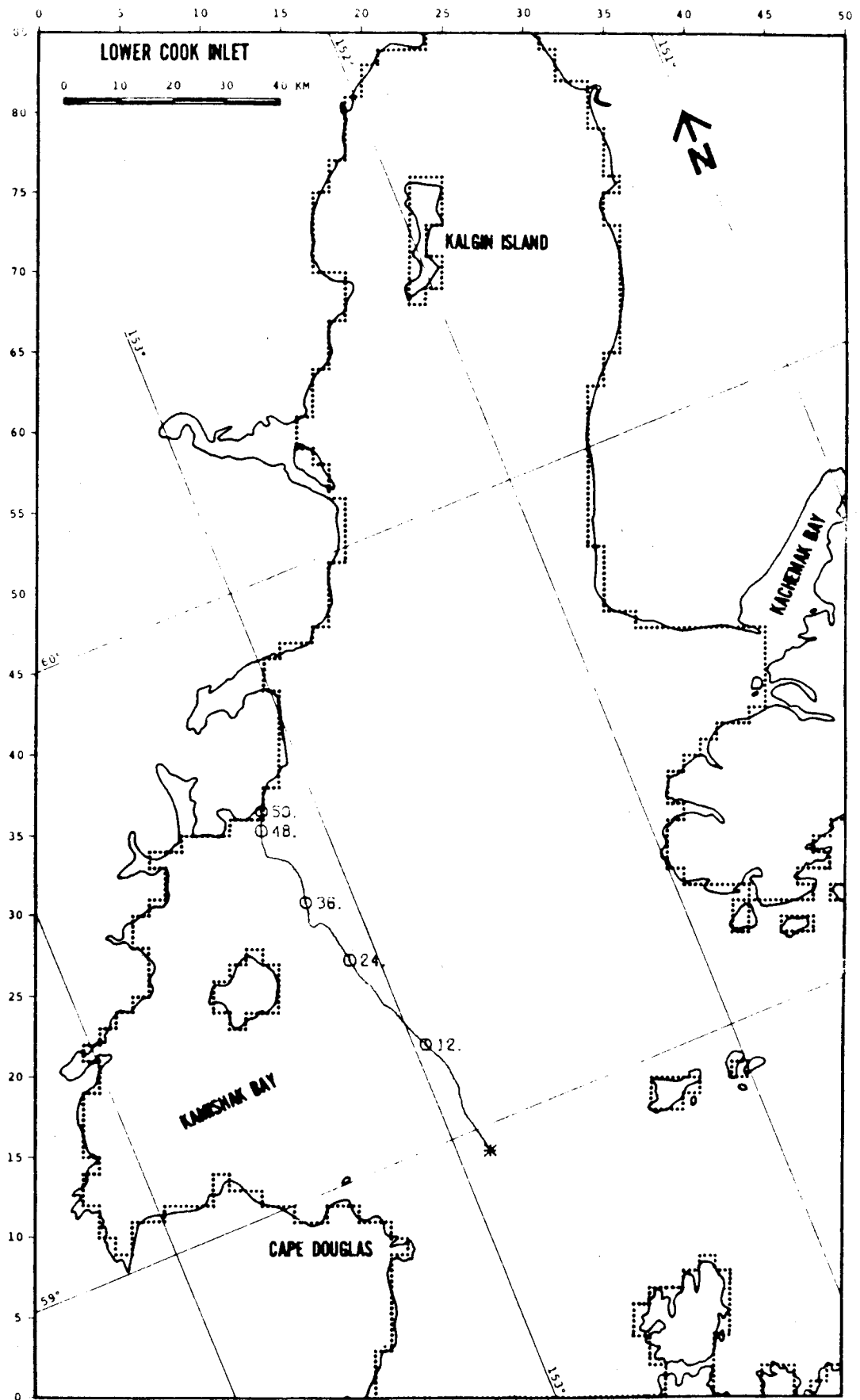


FIGURE B-35: BASE CASE

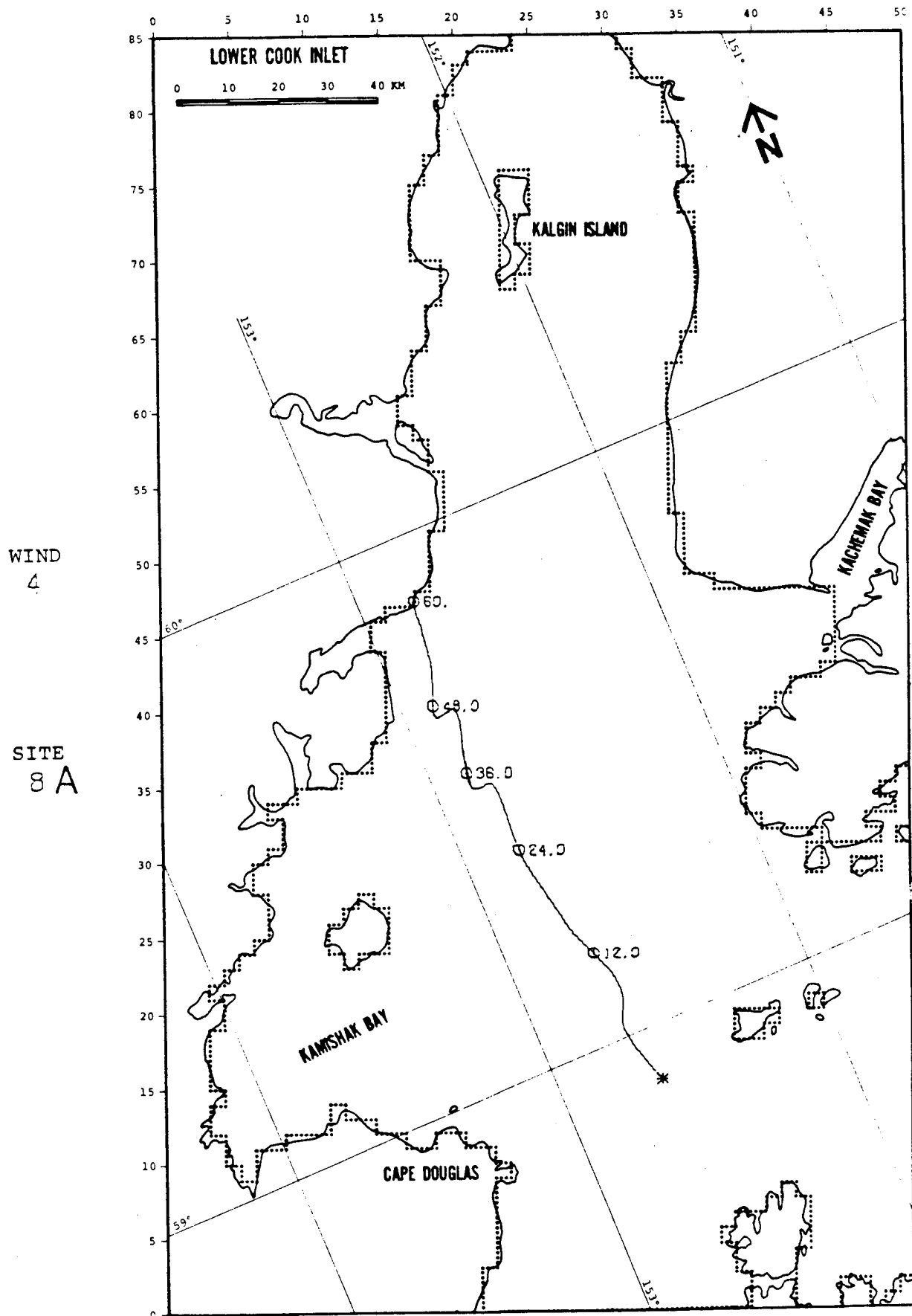


FIGURE B-36: BASE CASE

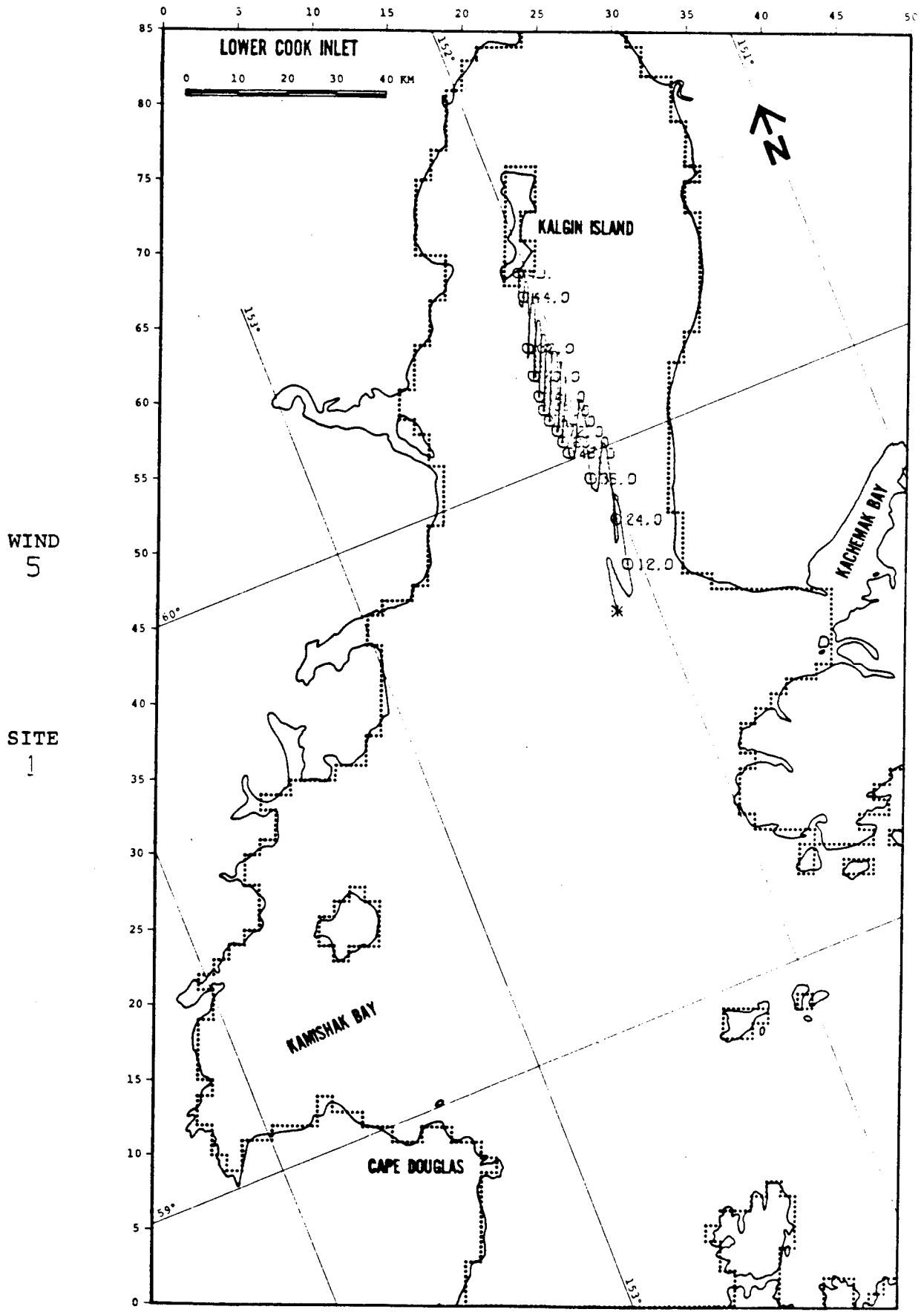


FIGURE B-37: BASE CASE

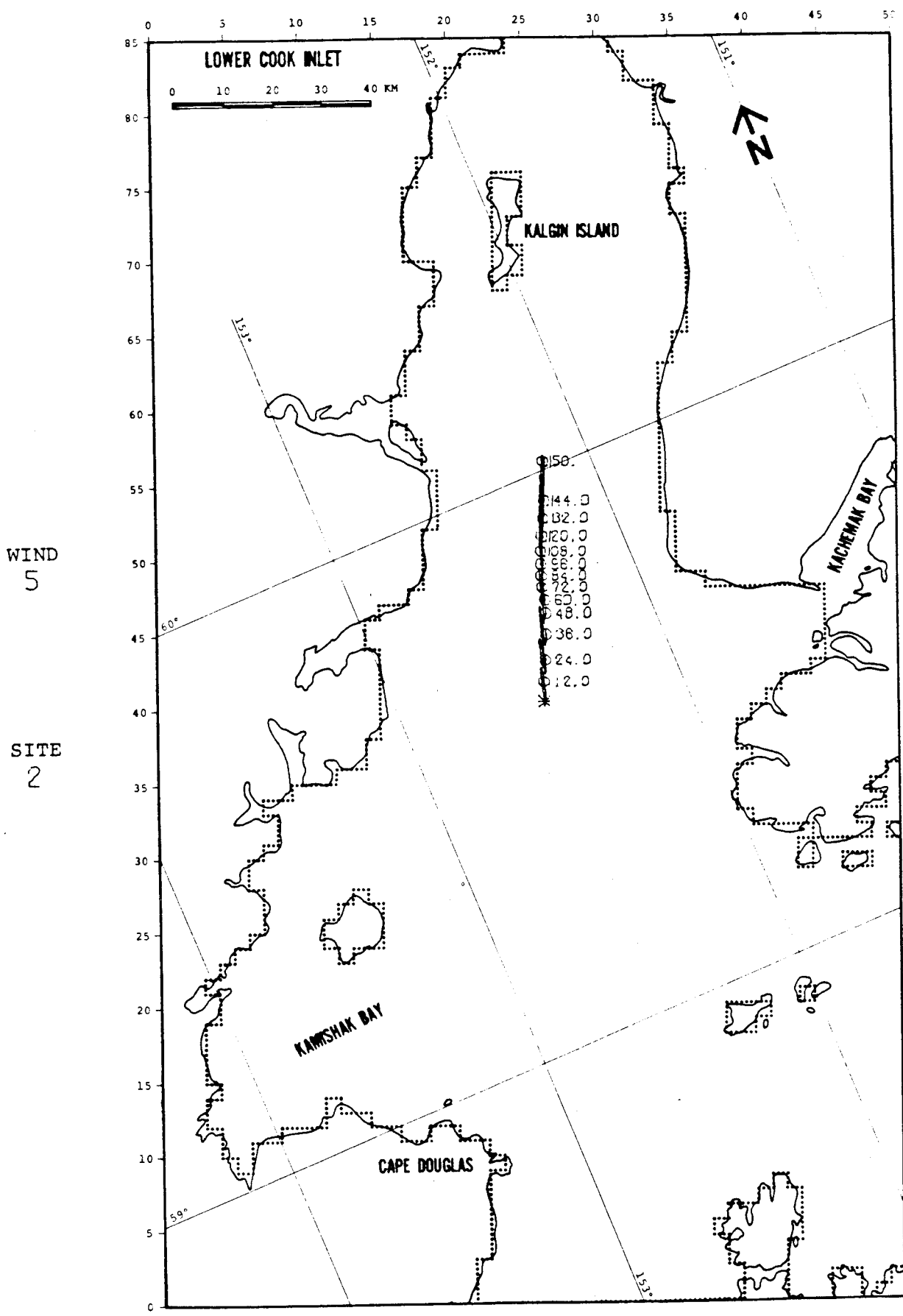


FIGURE B-38: BASE CASE

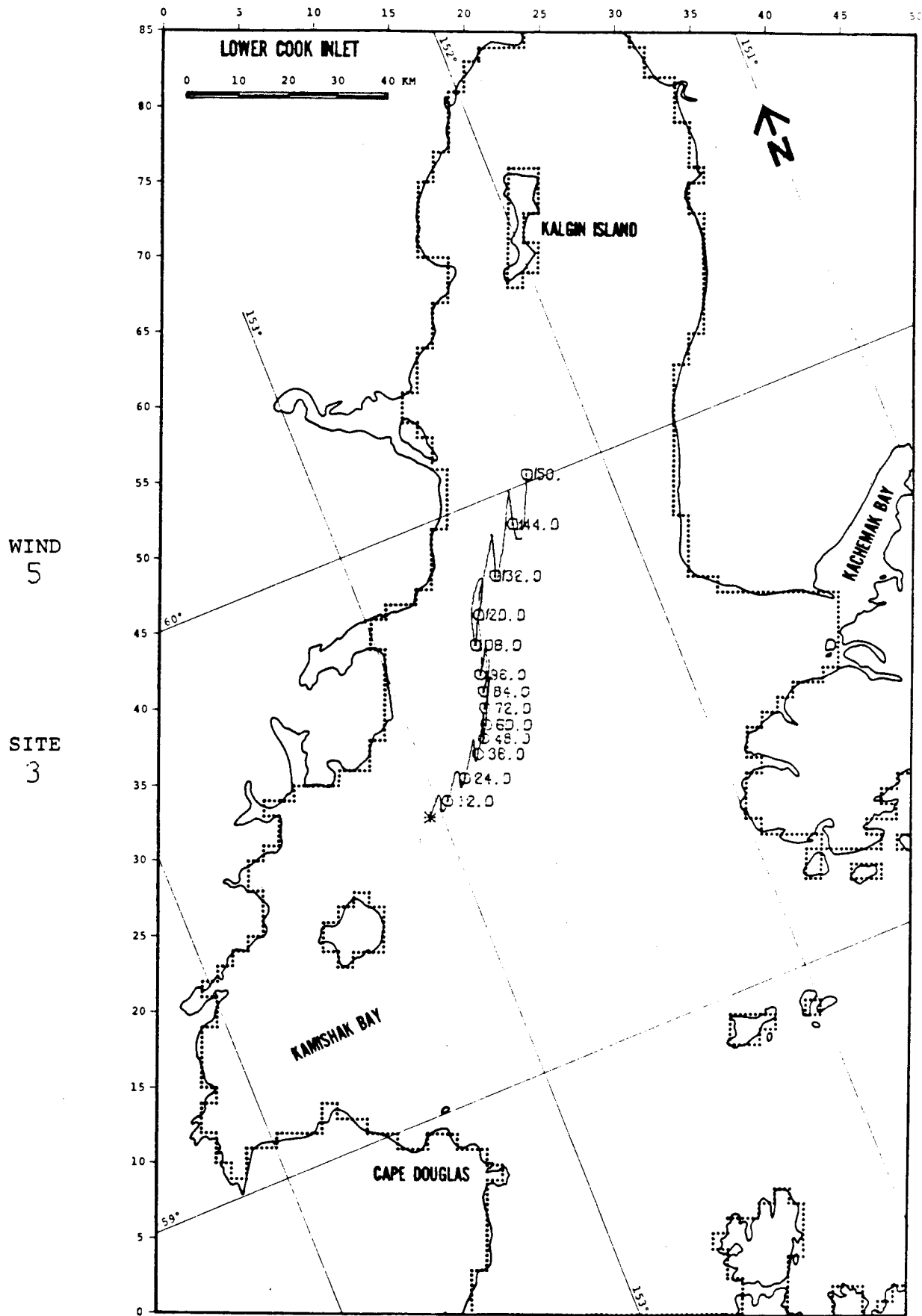


FIGURE B-39: BASE CASE

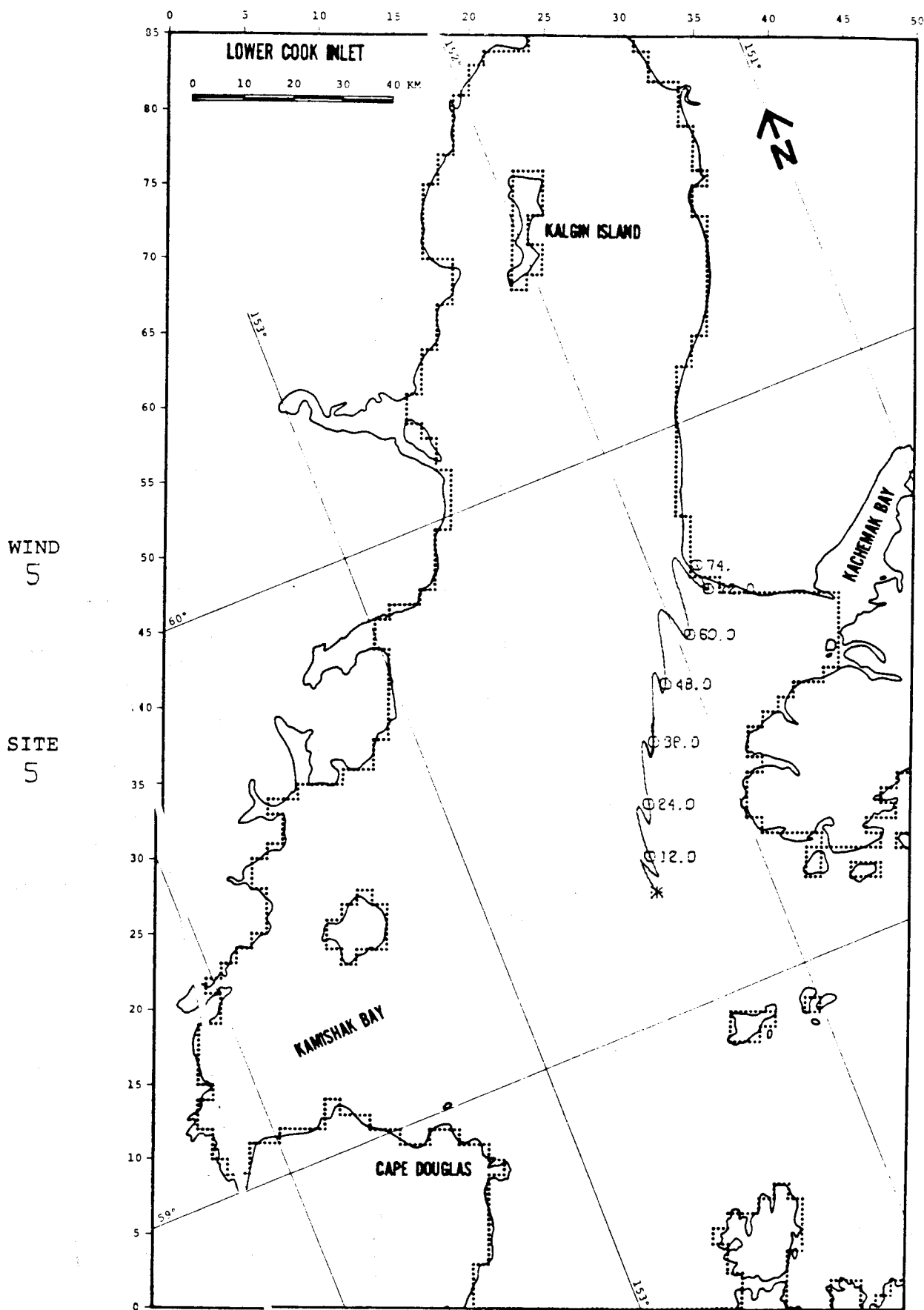


FIGURE B-41: BASE CASE

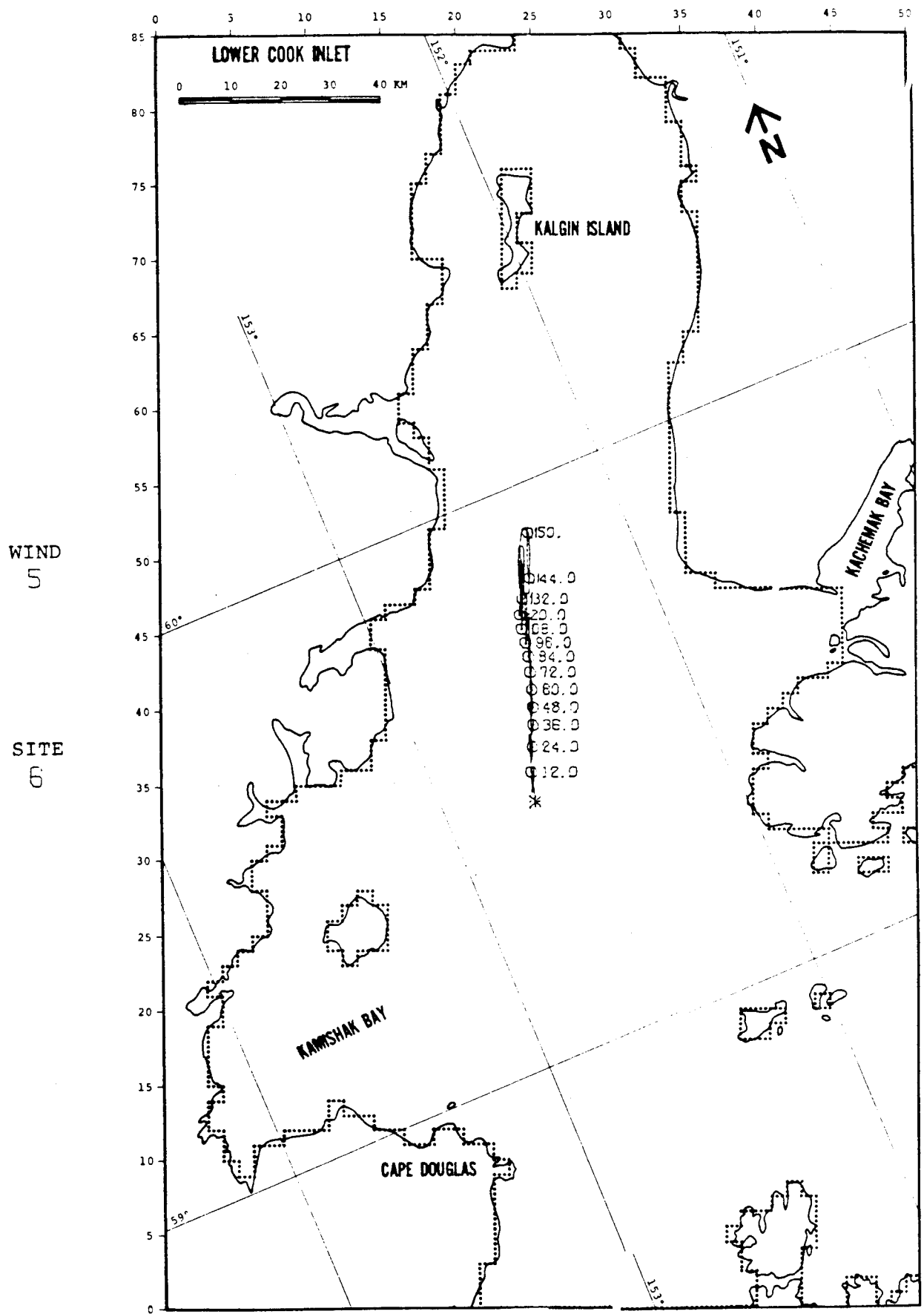


FIGURE B-42: BASE CASE

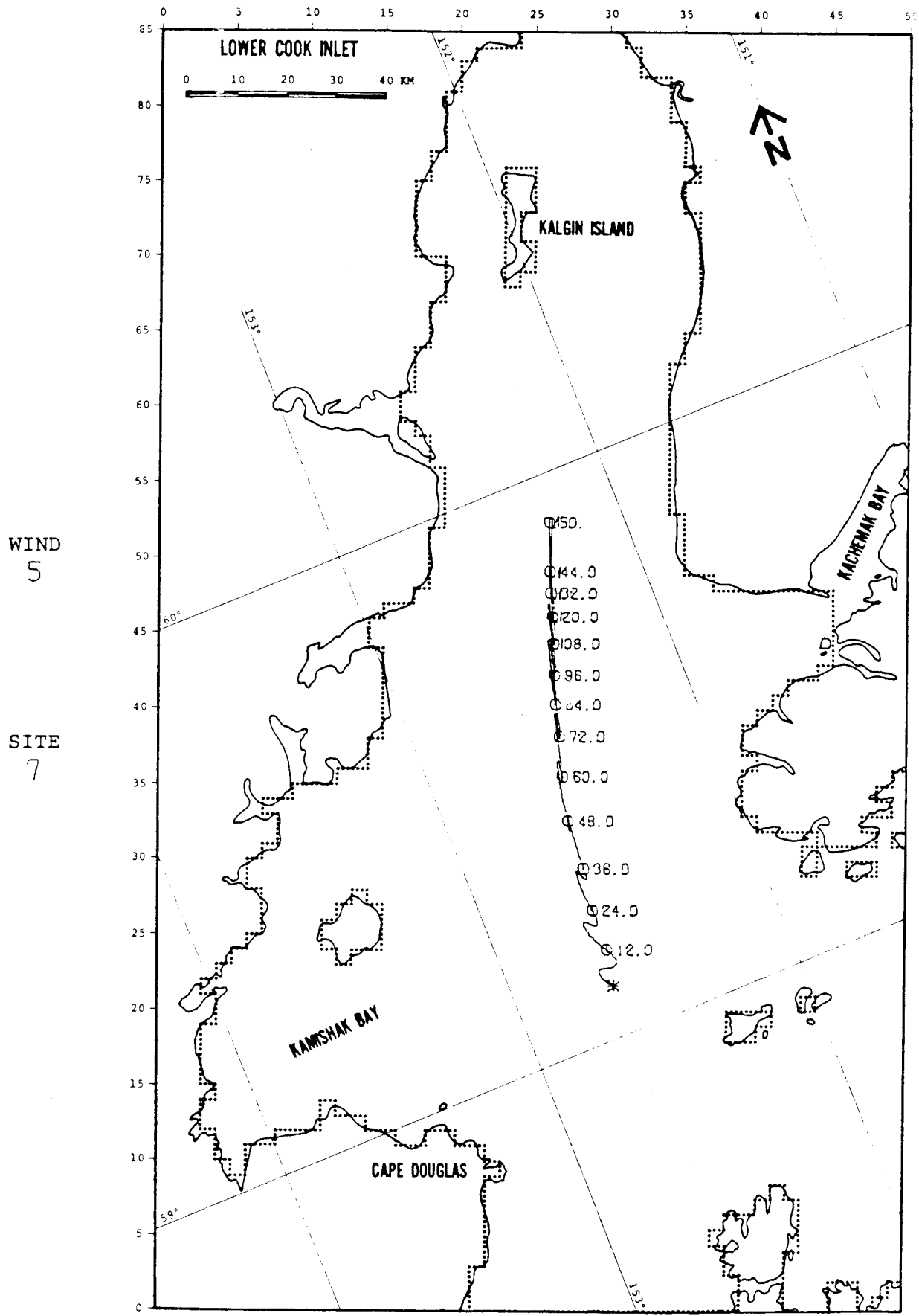


FIGURE B-43: BASE CASE

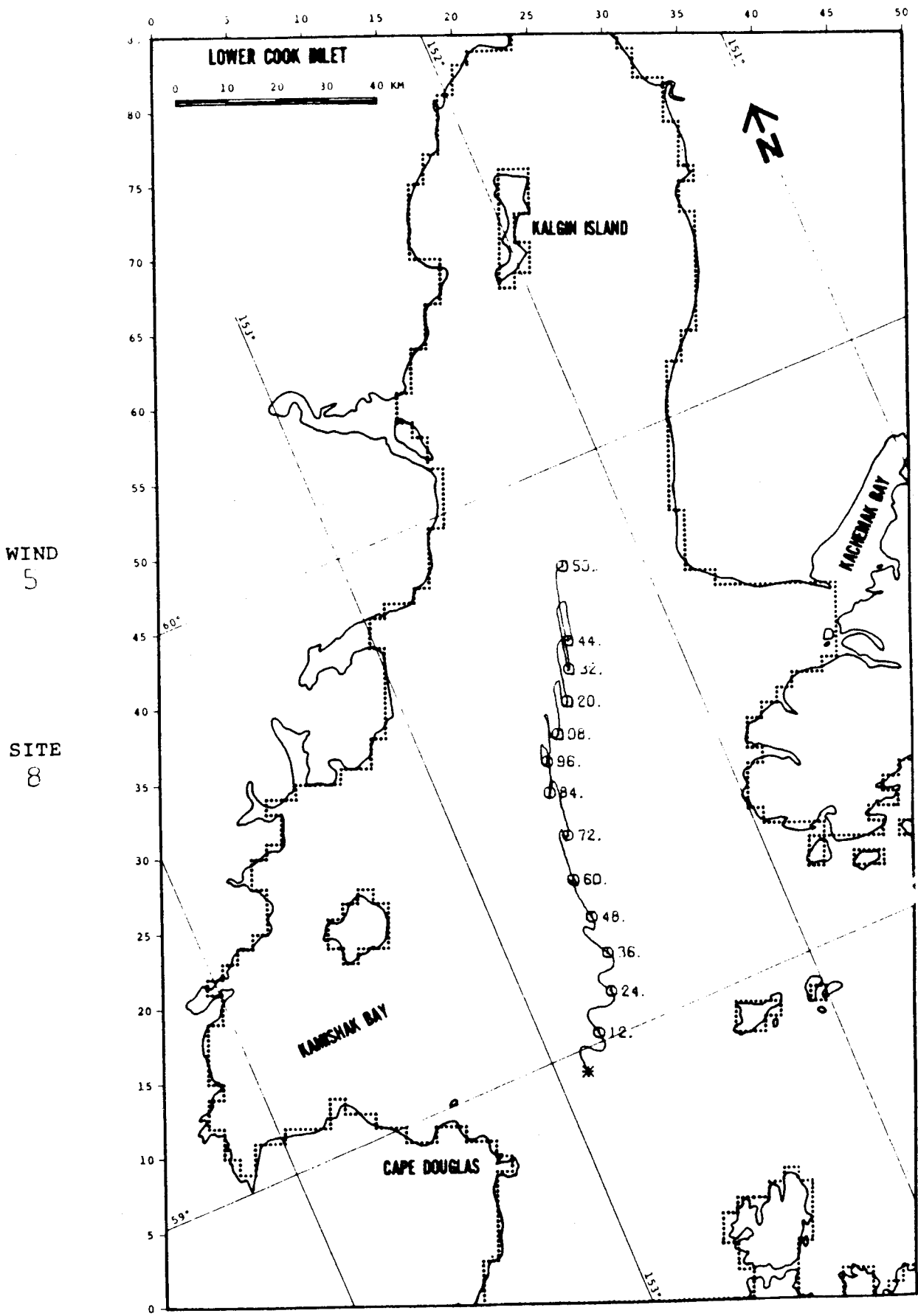


FIGURE B-44: BASE CASE

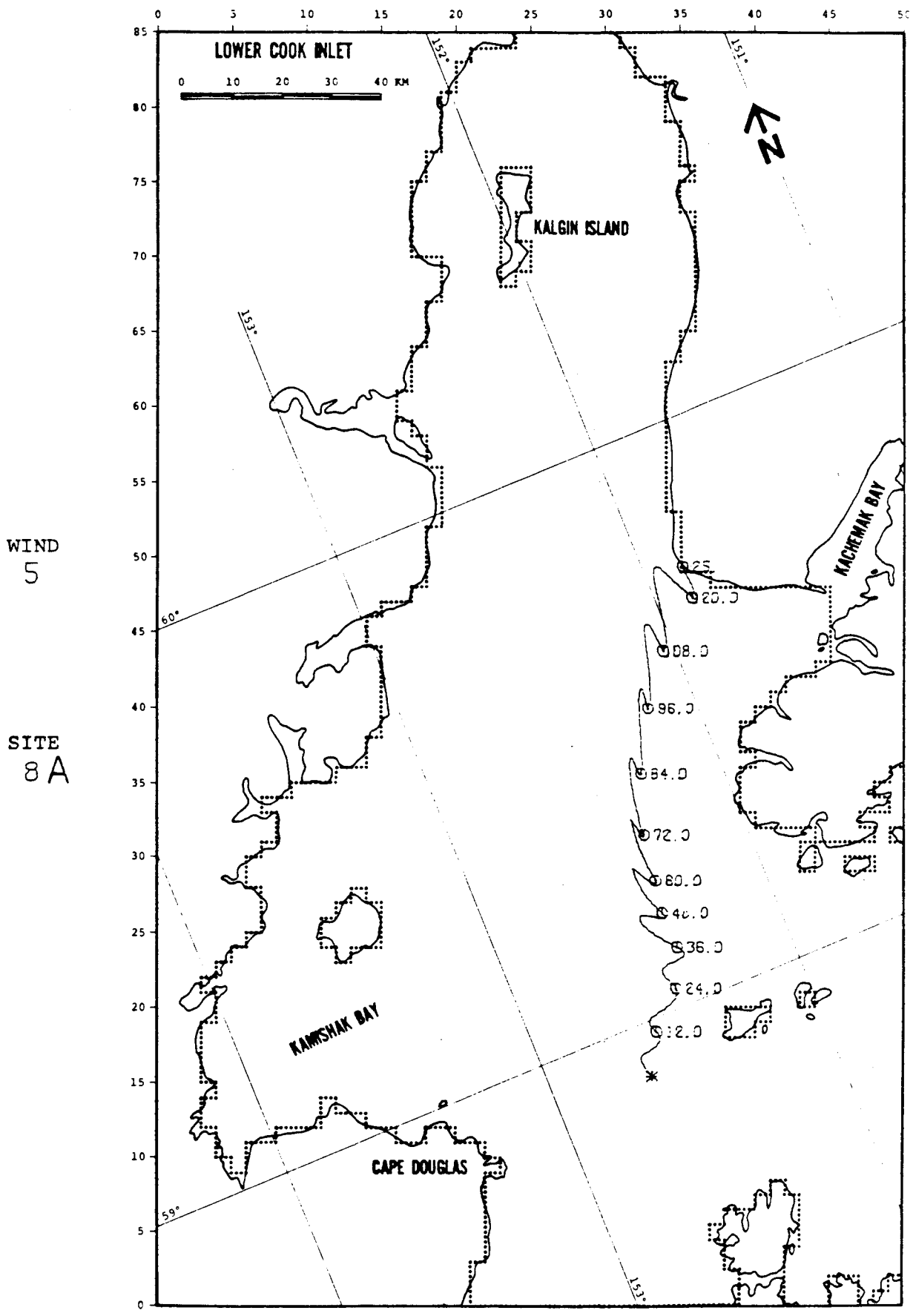


FIGURE B-45: BASE CASE

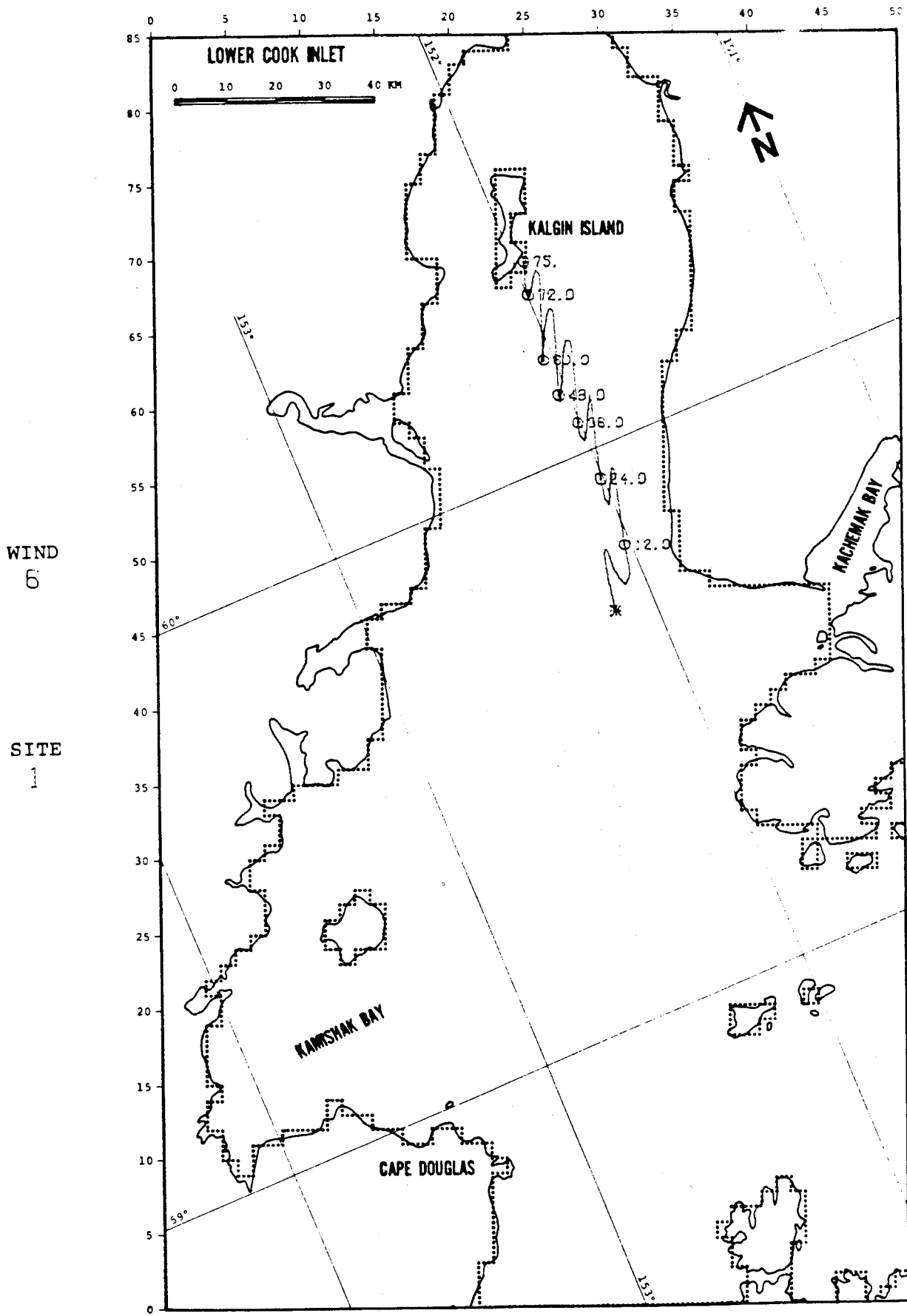


FIGURE B-46: BASE CASE

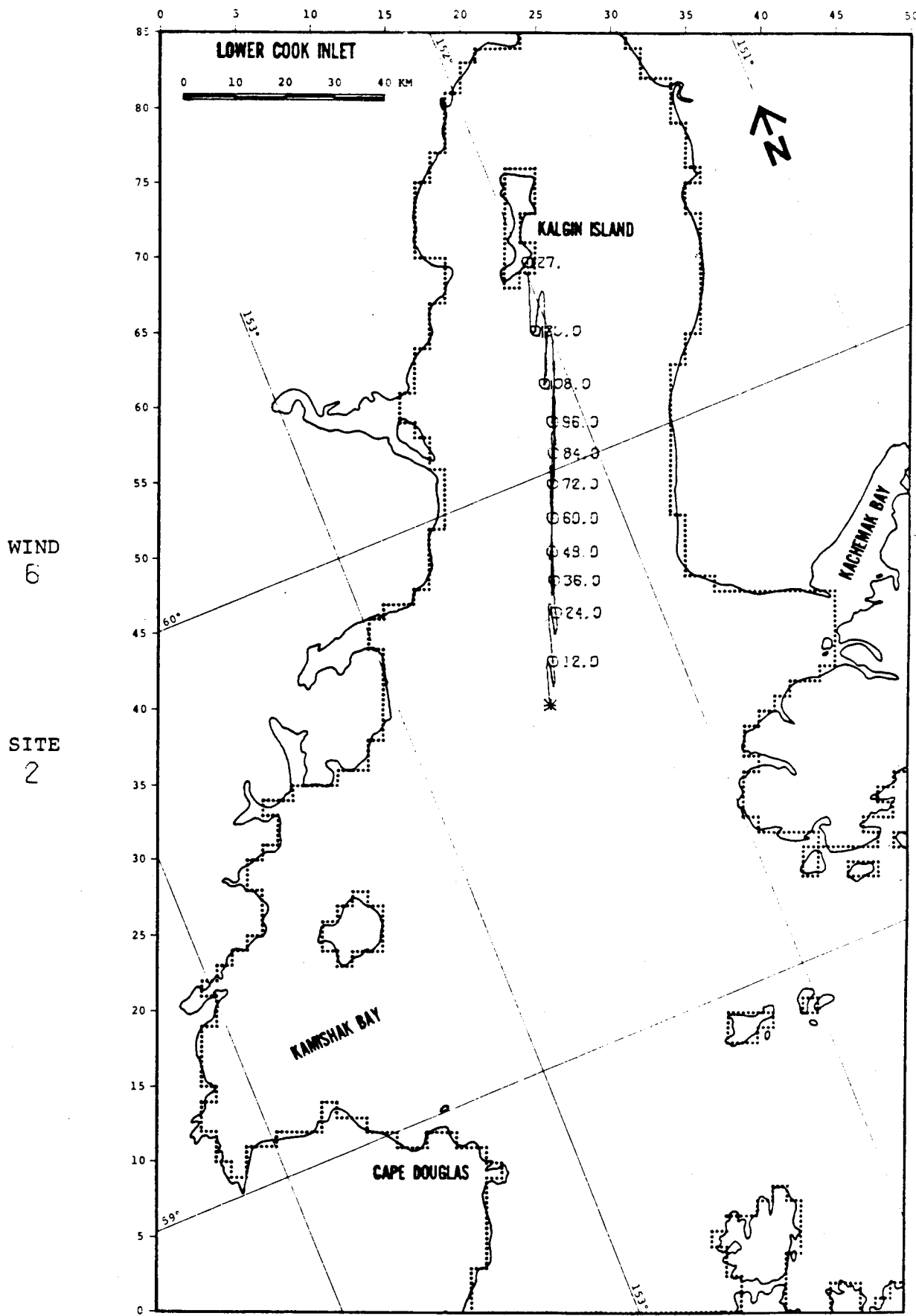


FIGURE B-47: BASE CASE

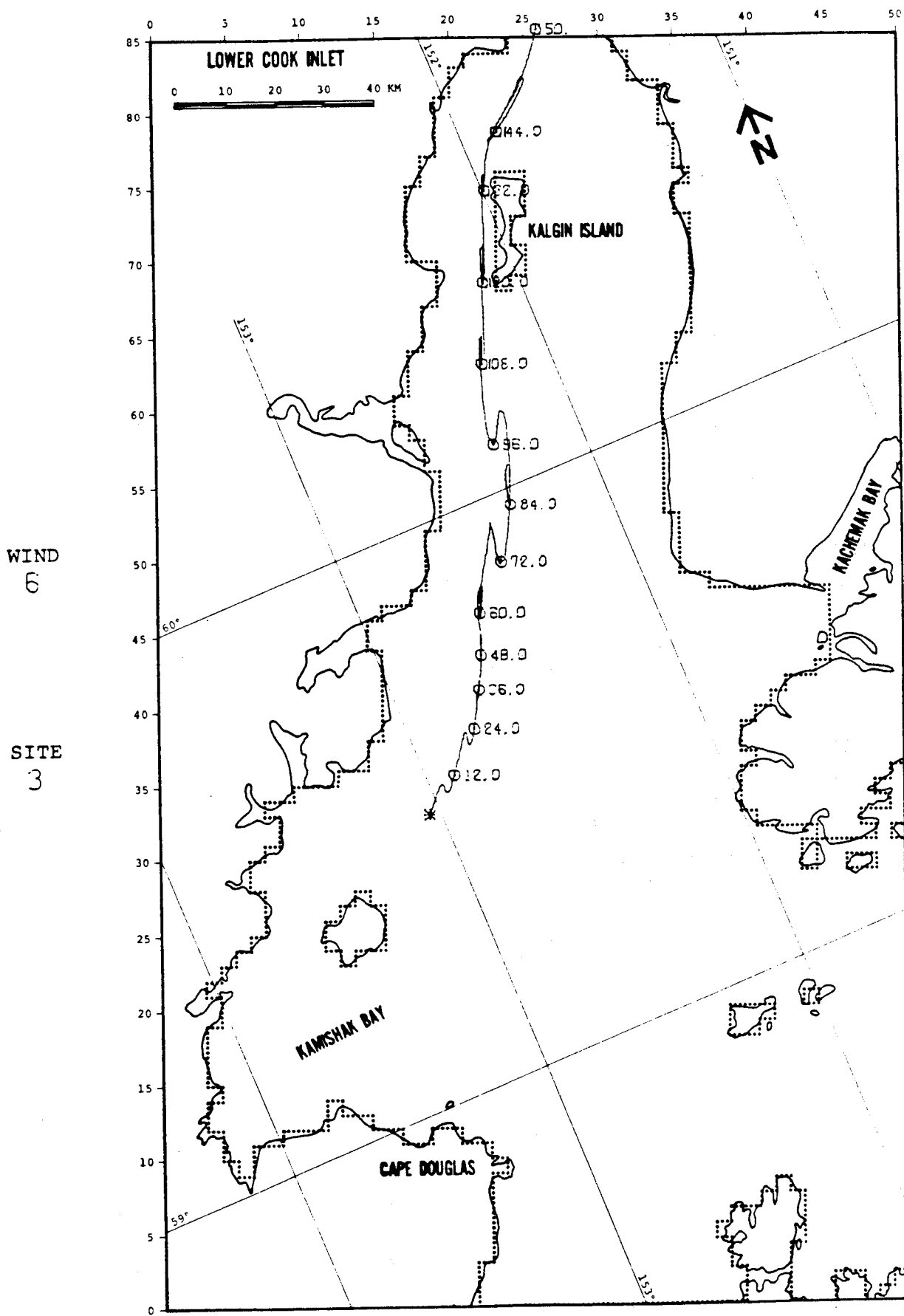


FIGURE B-48: BASE CASE

WIND
6

SITE
4

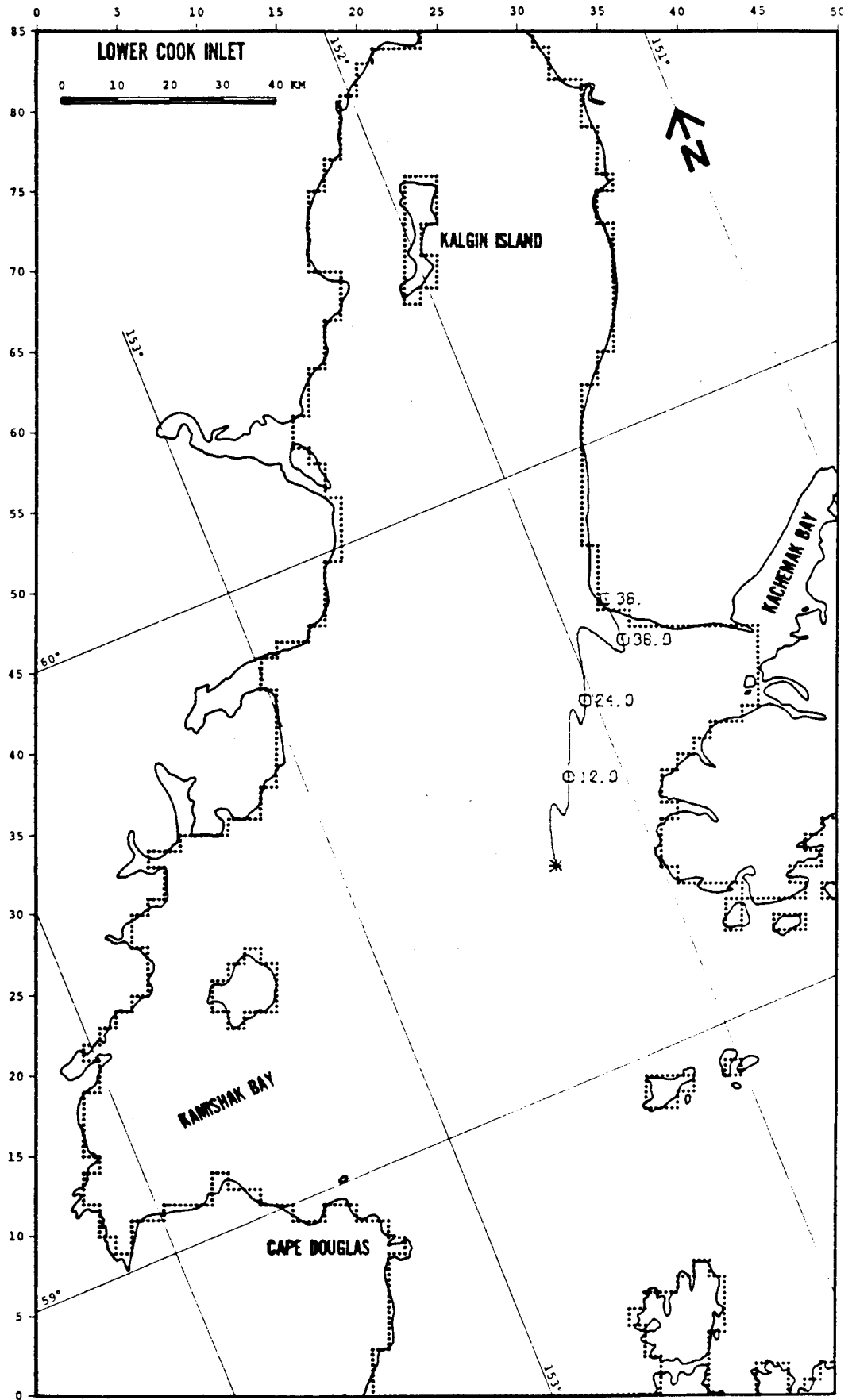


FIGURE B-49: BASE CASE

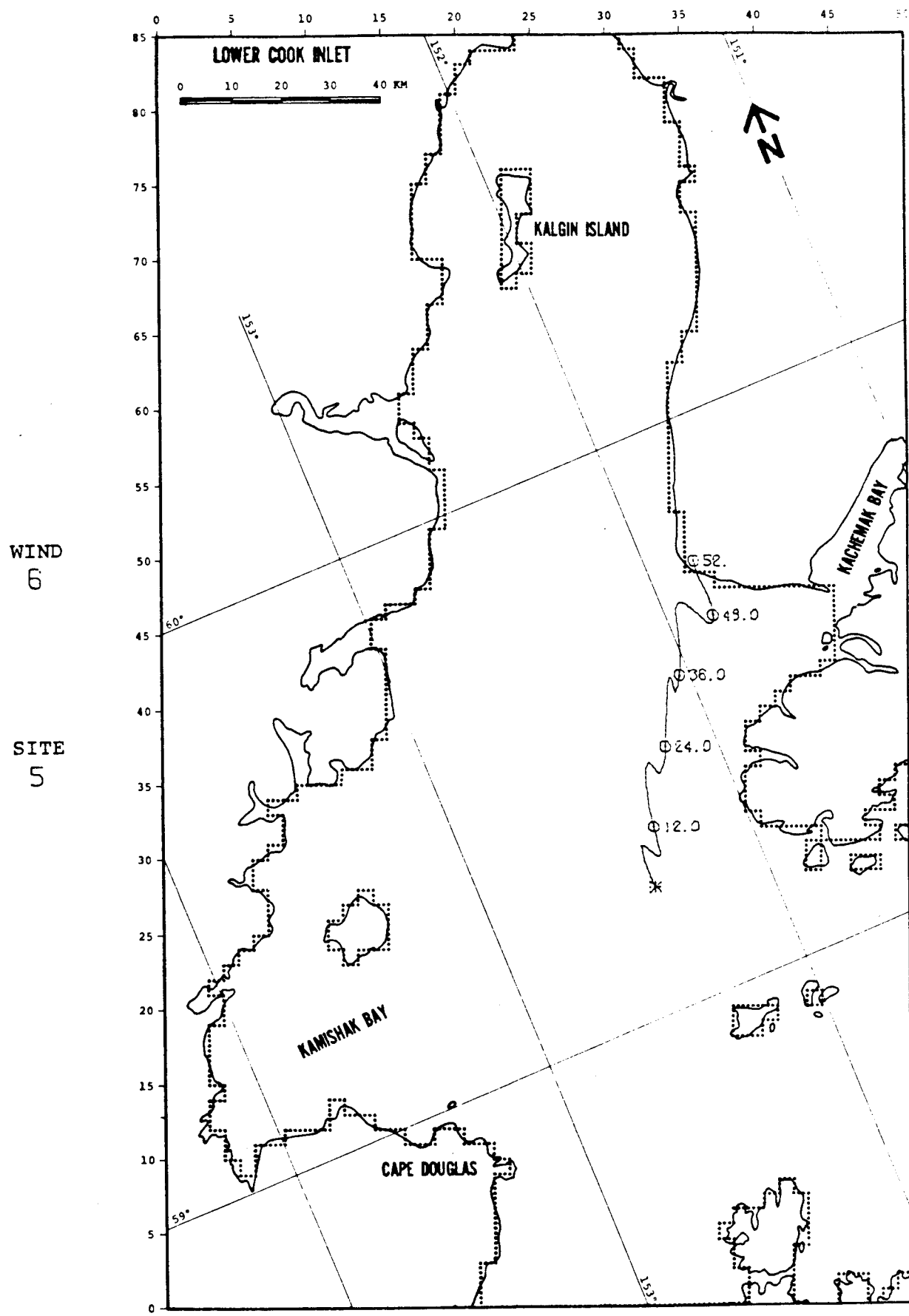


FIGURE B-50: BASE CASE

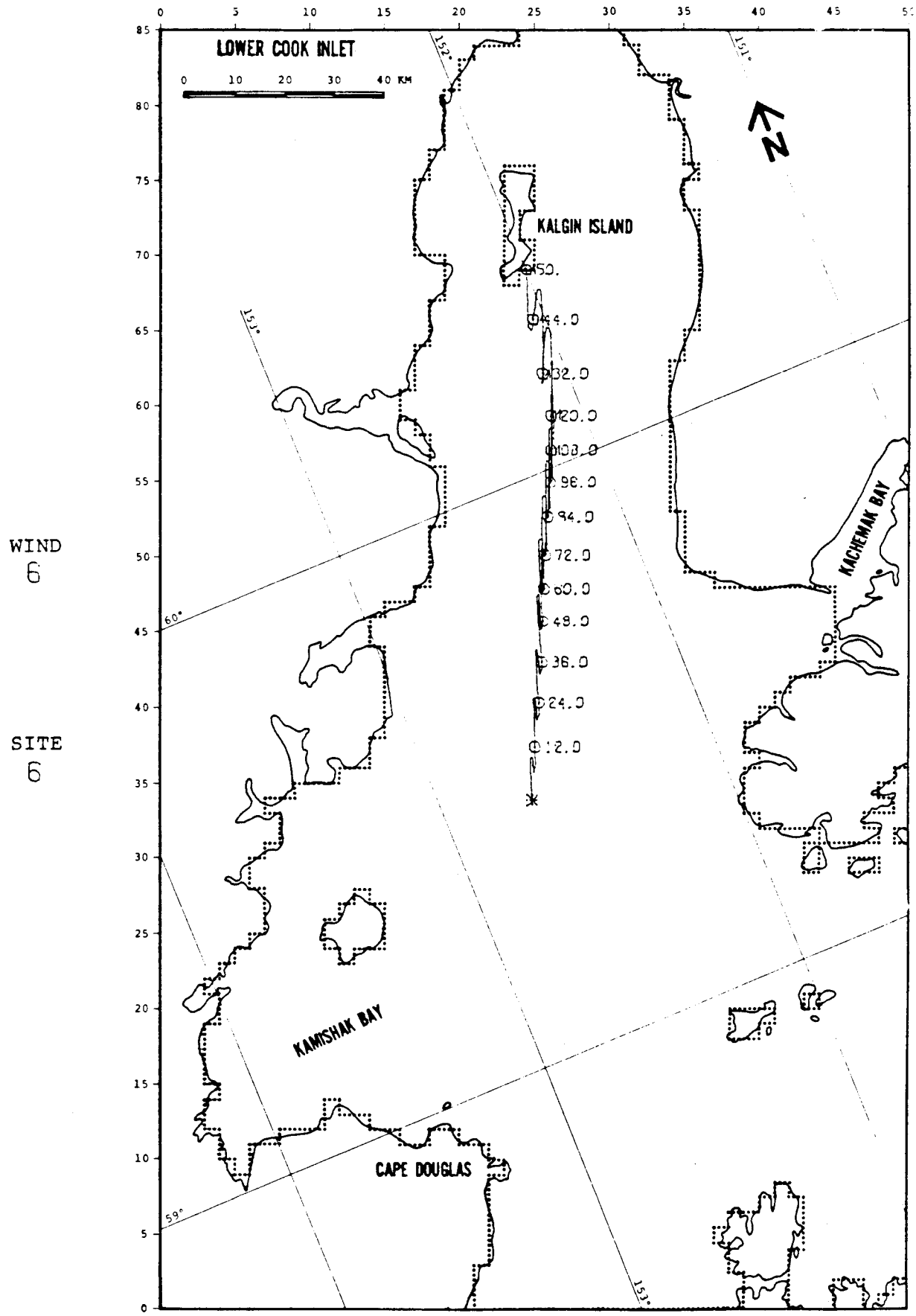


FIGURE B-51: BASE CASE

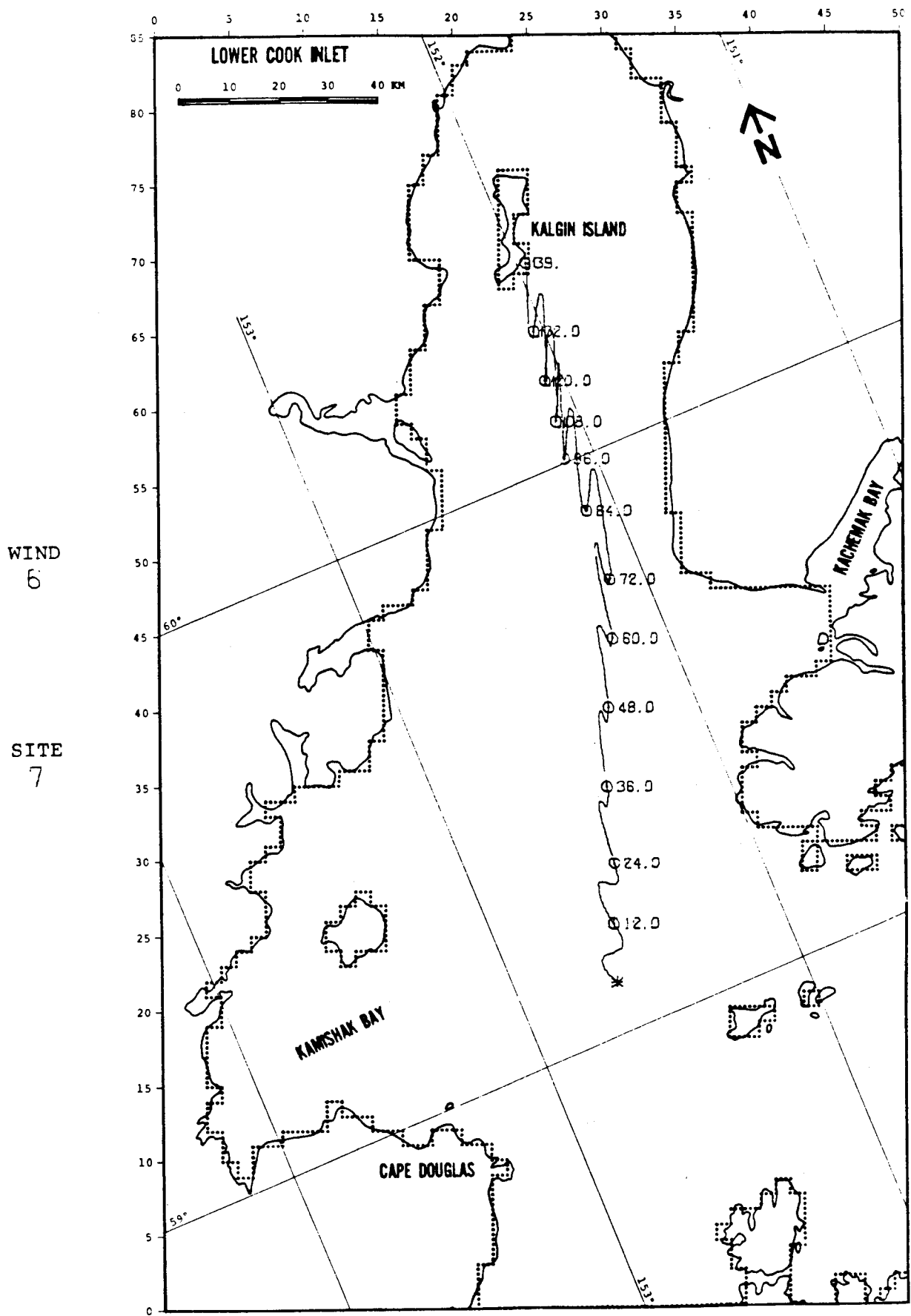
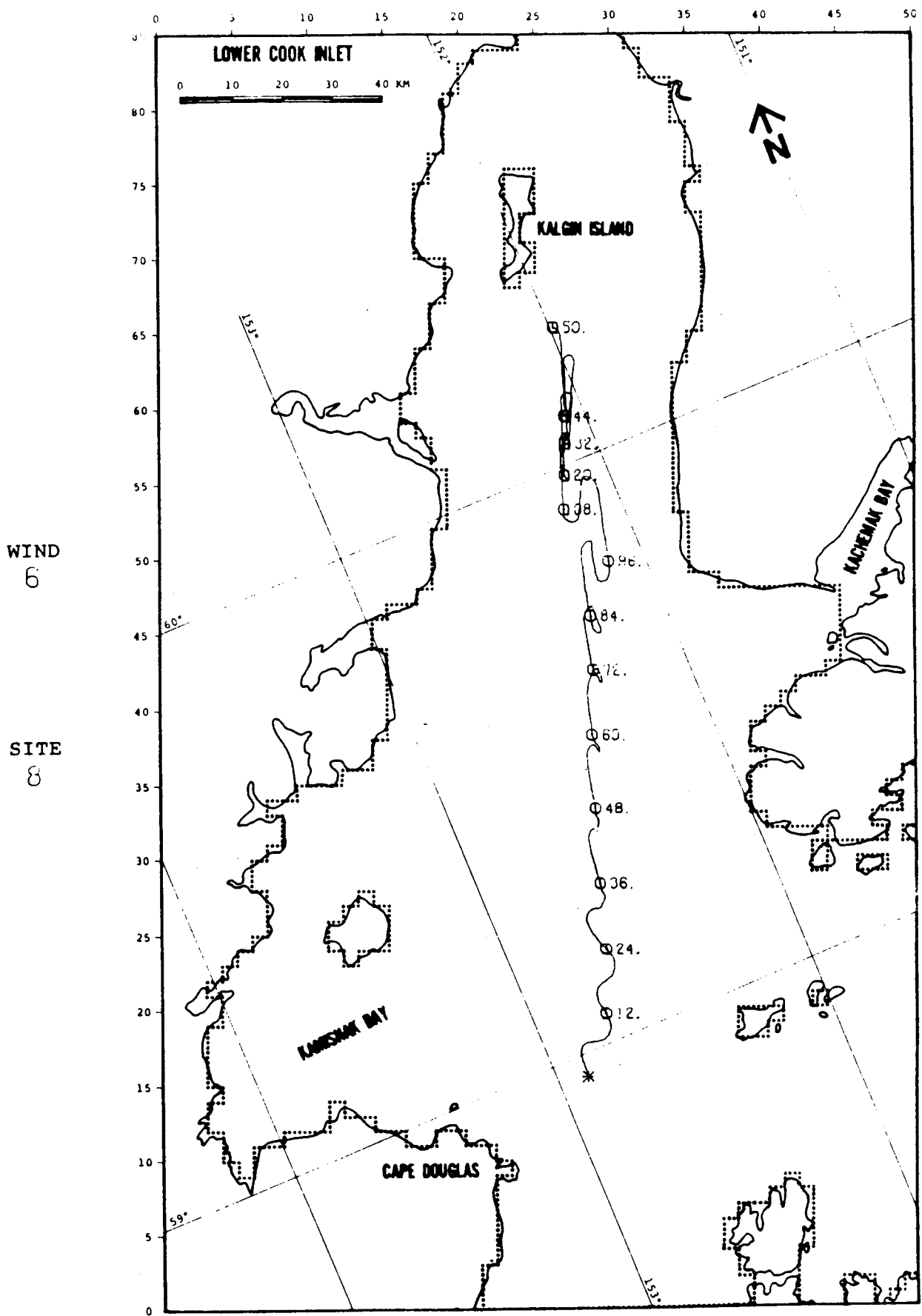


FIGURE B-52: BASE CASE



WIND
6

SITE
8

FIGURE B-53: BASE CASE

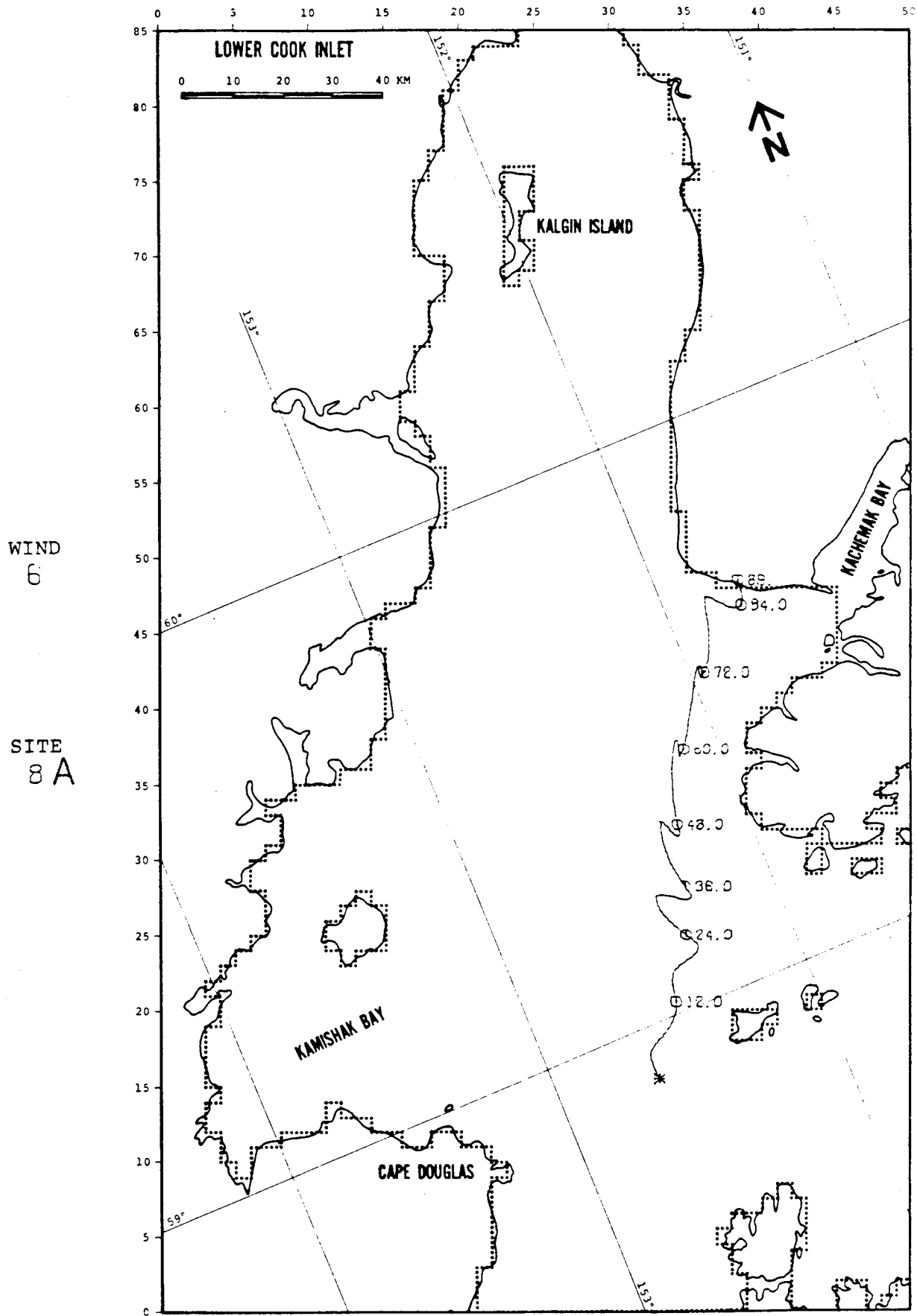


FIGURE B-54: BASE CASE

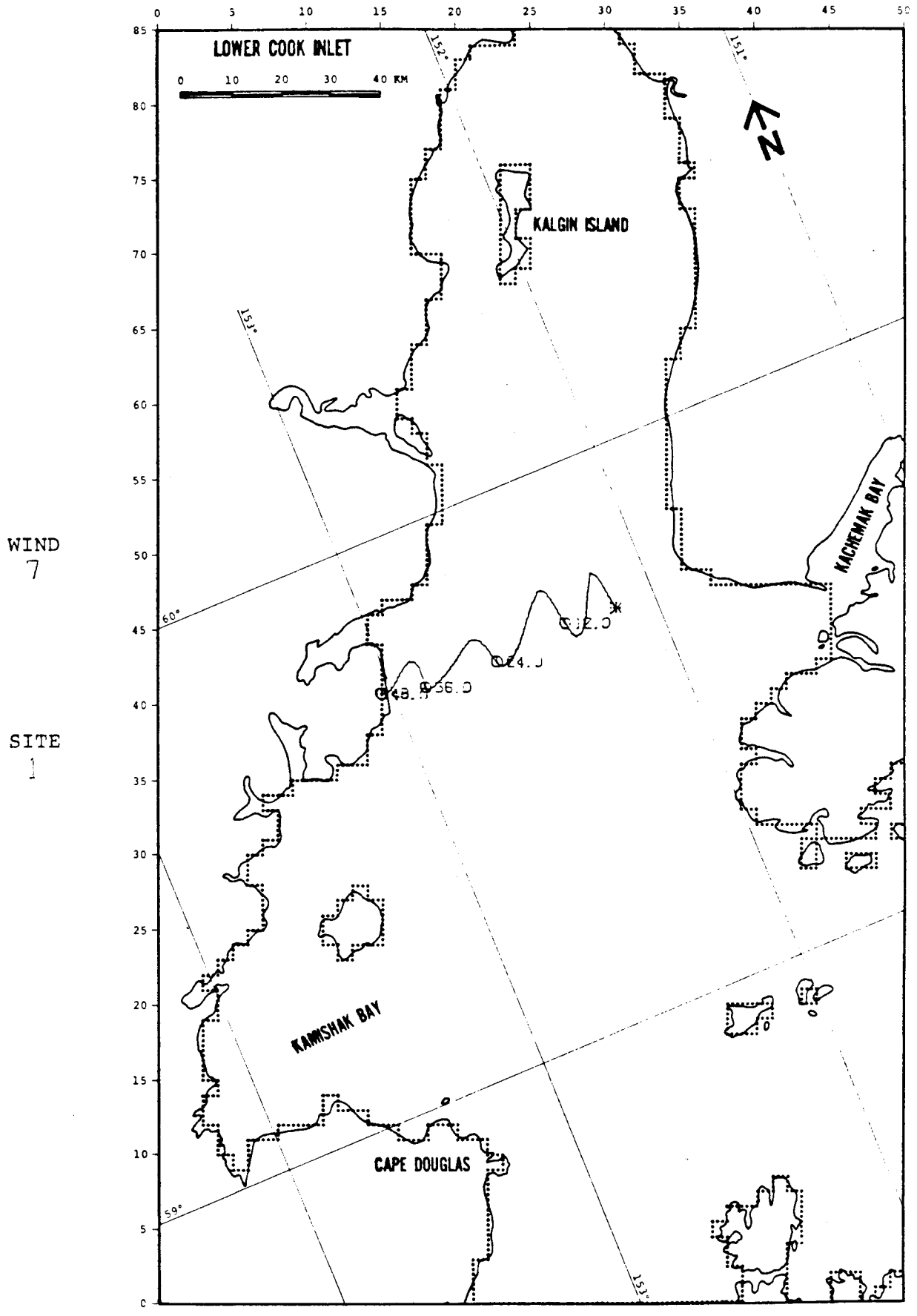


FIGURE B-55: BASE CASE

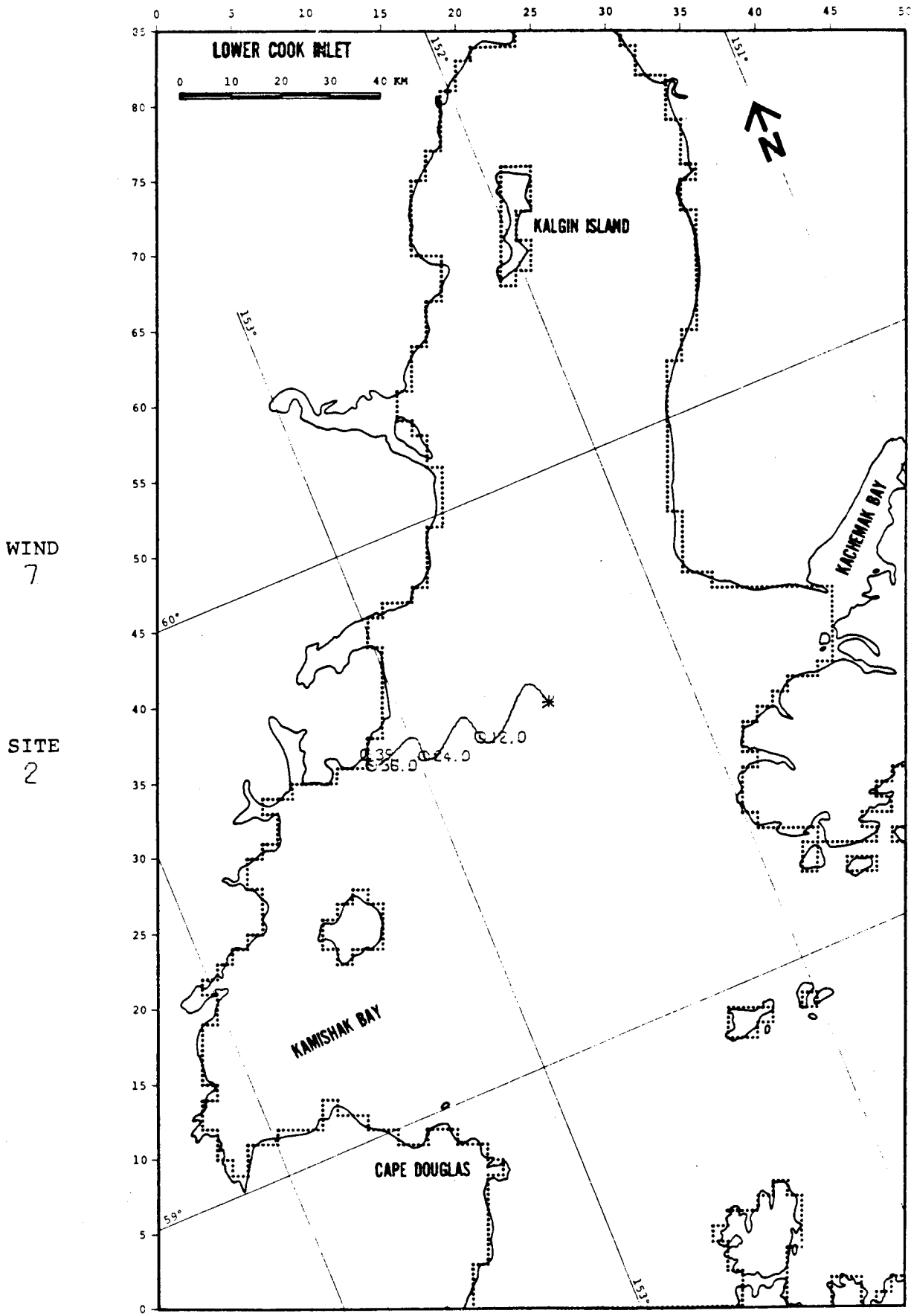


FIGURE B-56: BASE CASE

WIND
7

SITE
3

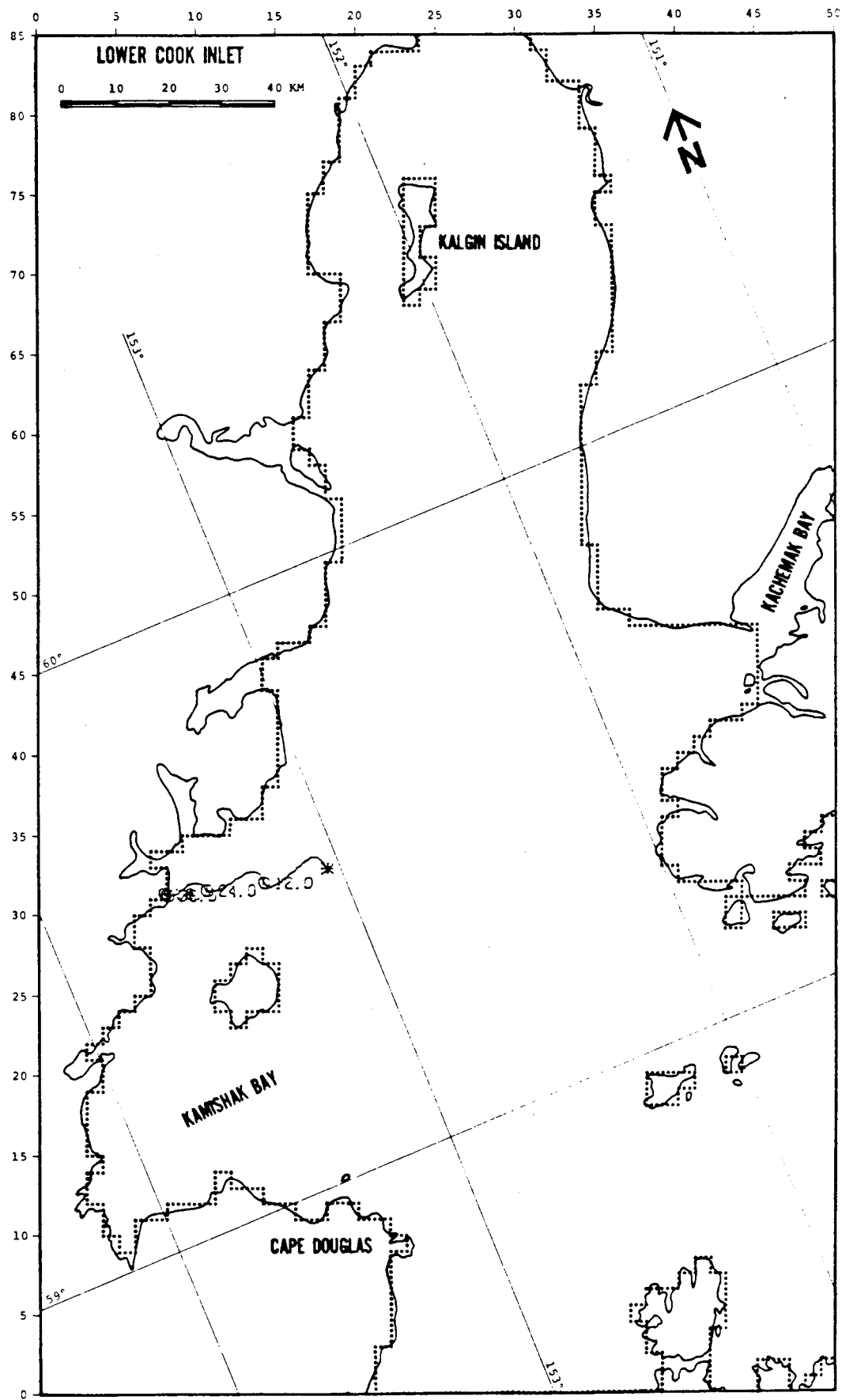


FIGURE B-57: BASE CASE

WIND
7

SITE
4

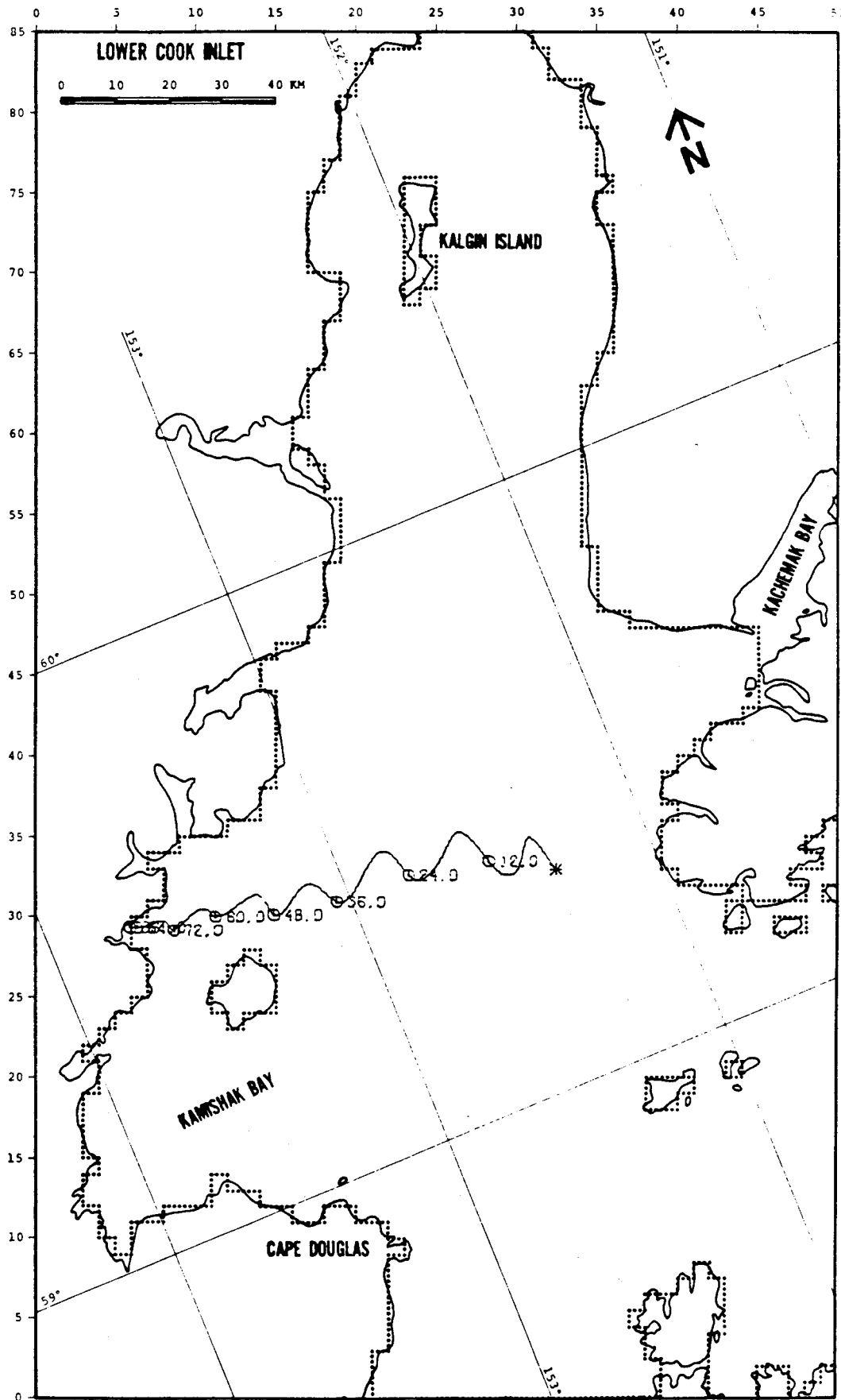


FIGURE B-58: BASE CASE

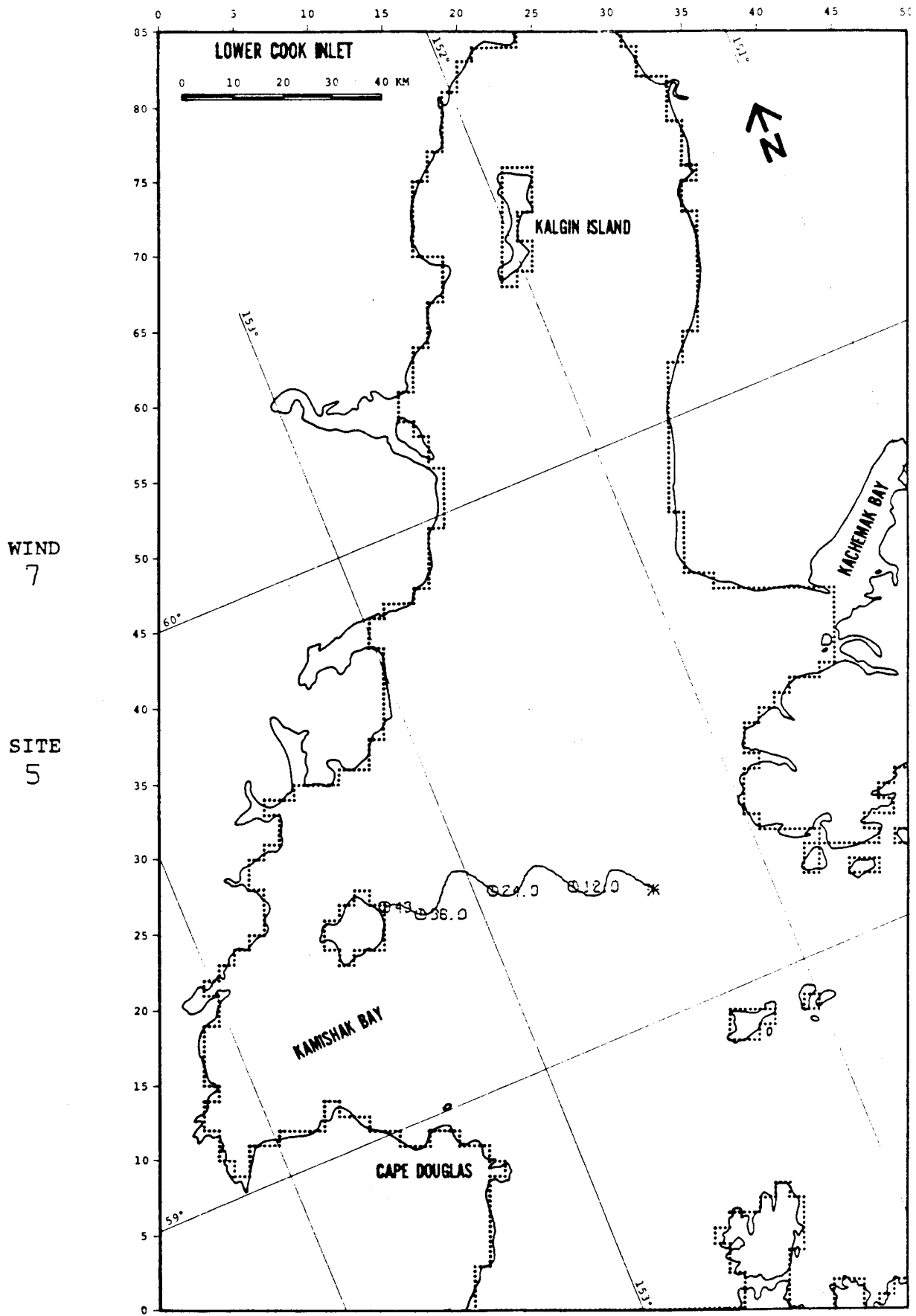


FIGURE B-59: BASE CASE

WIND
7

SITE
6

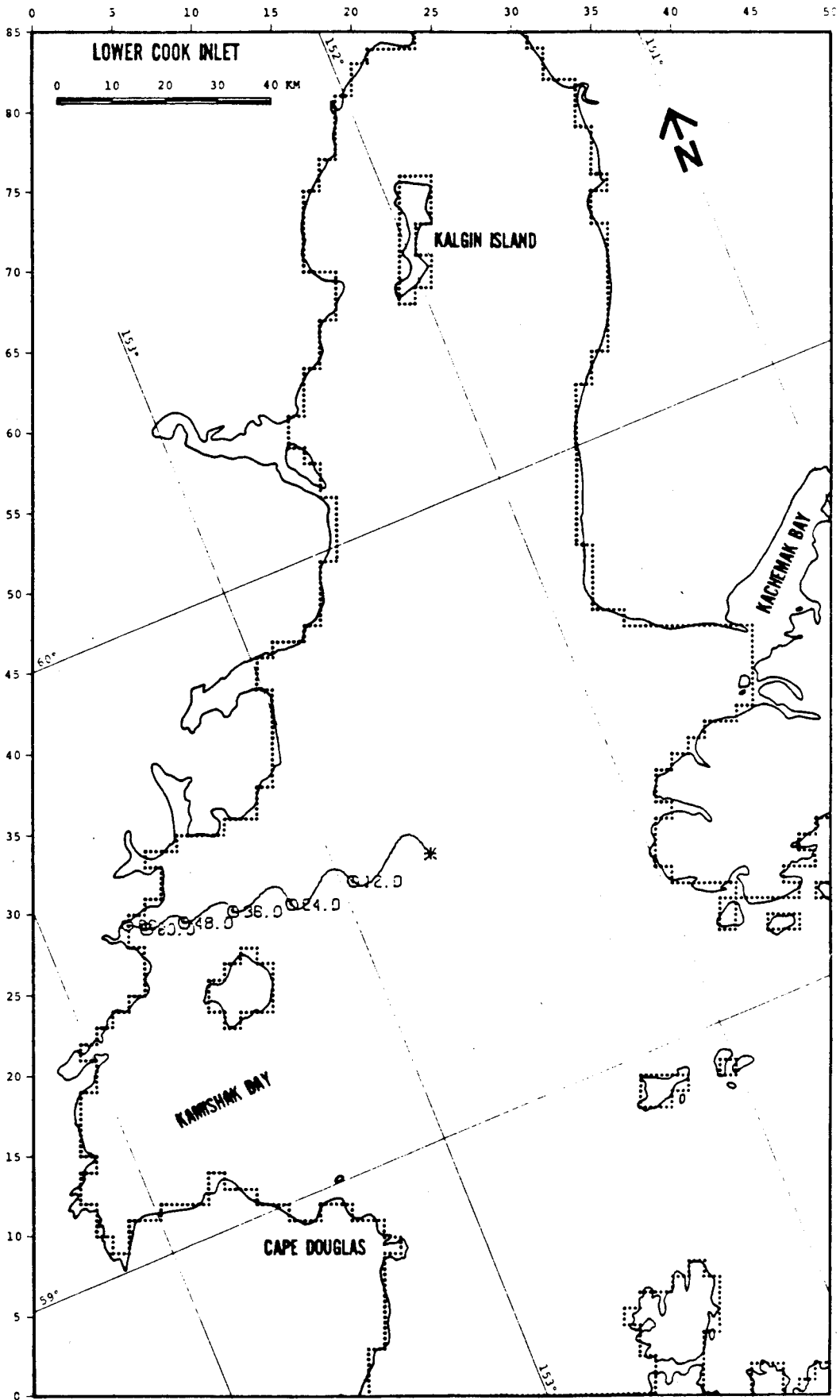


FIGURE B-60: BASE CASE

WIND
7

SITE
8

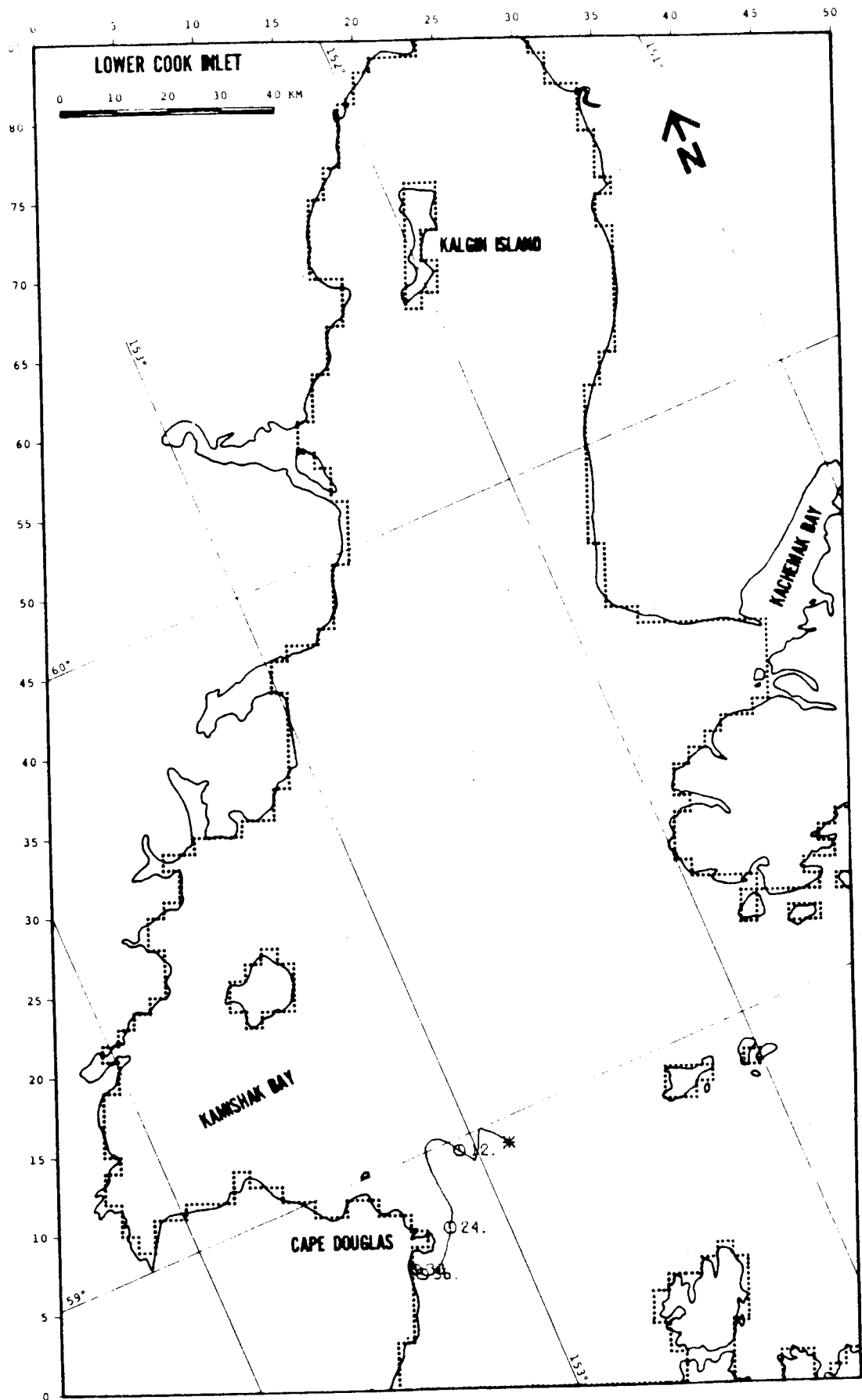
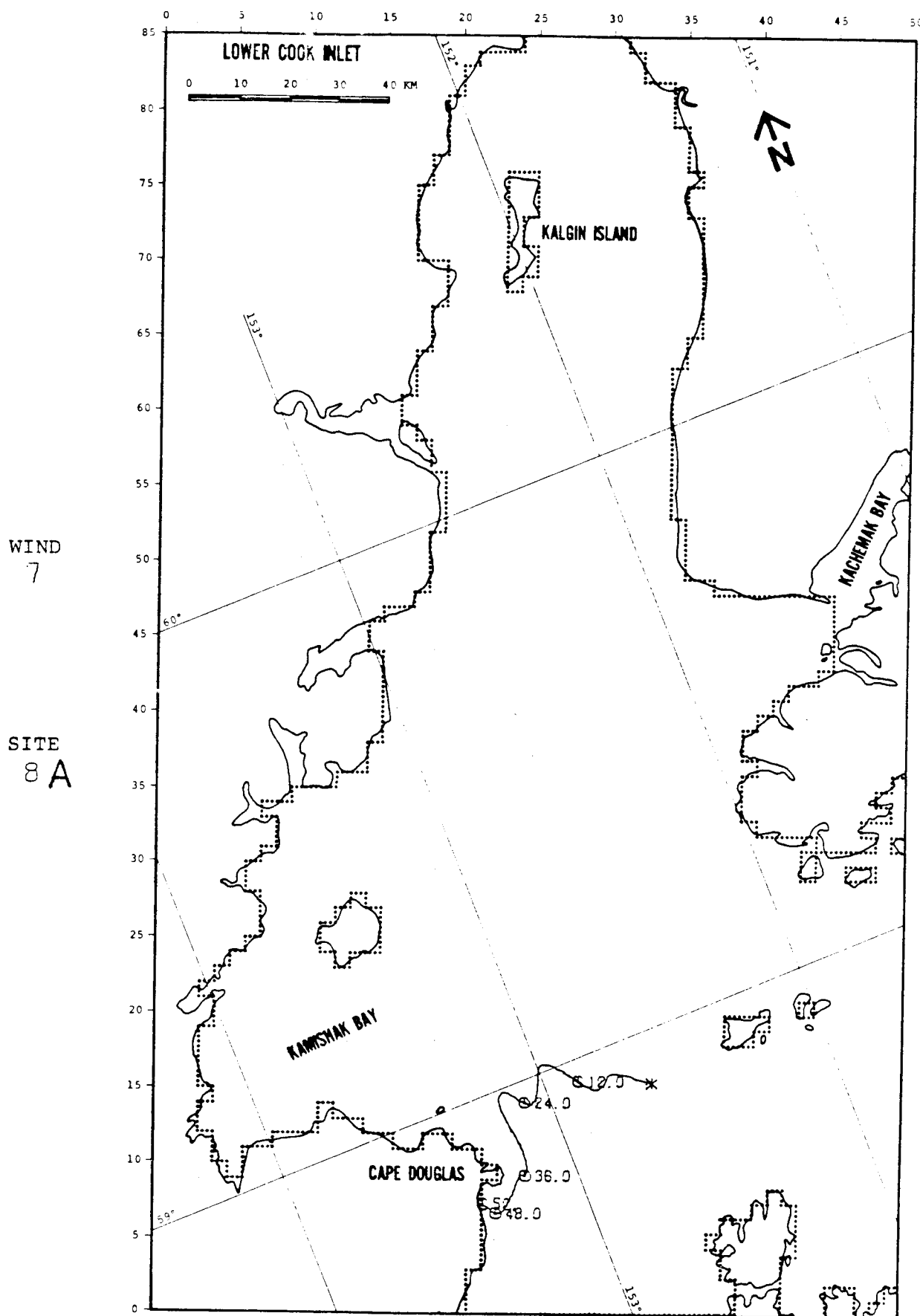


FIGURE B-62: BASE CASE



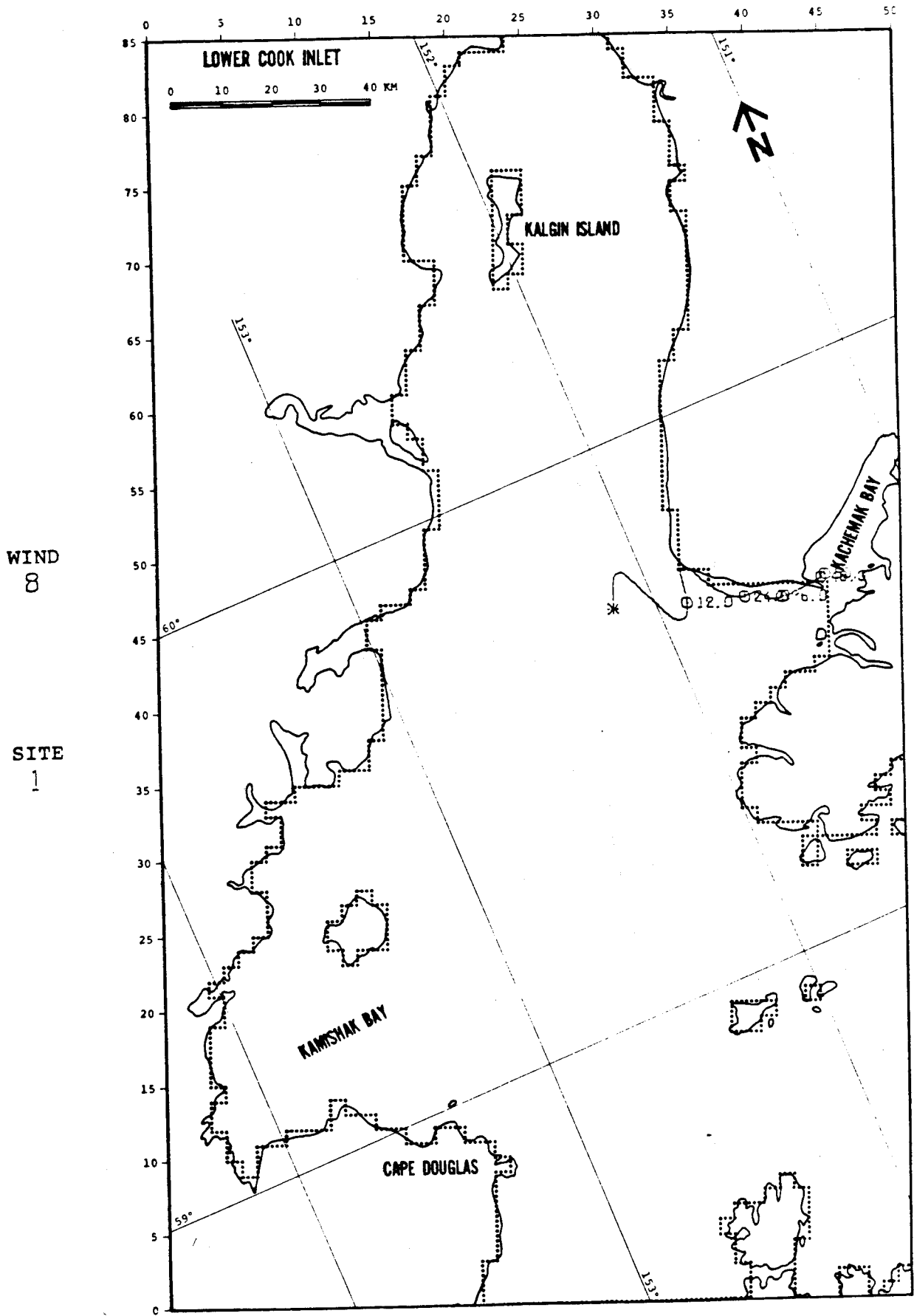


FIGURE B-64: BASE CASE

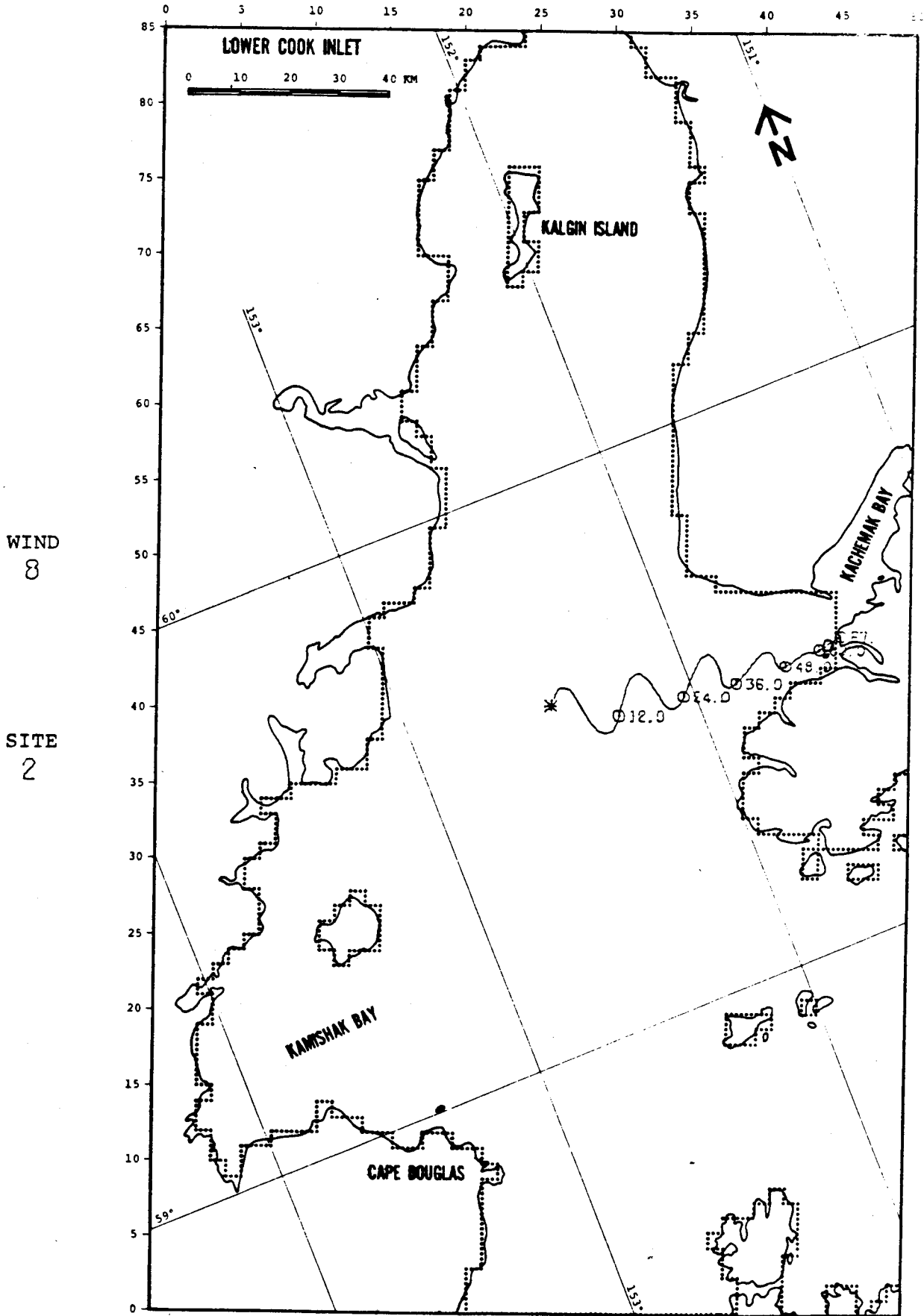


FIGURE B-65: BASE CASE

WIND
8

SITE
3

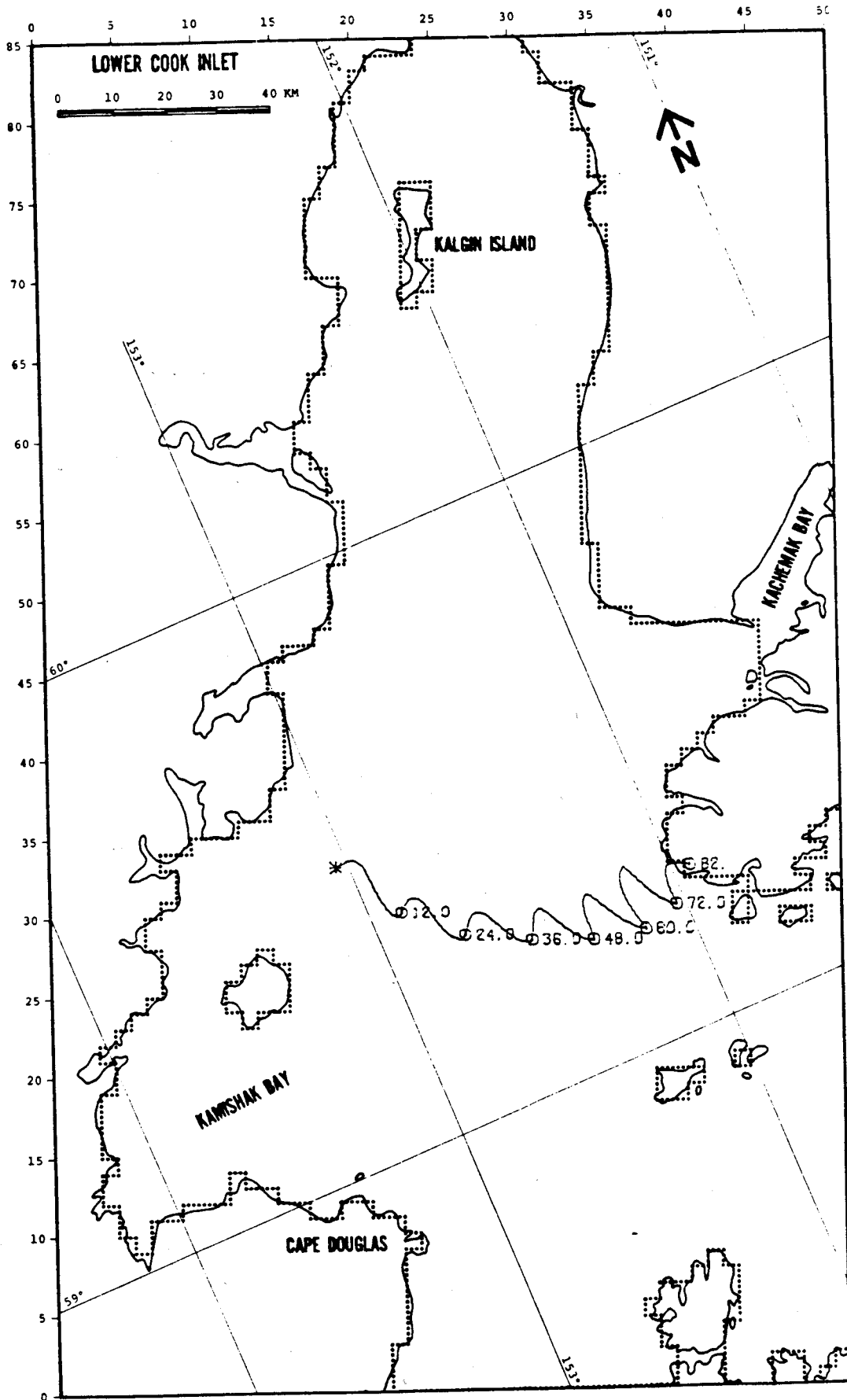


FIGURE B-66: BASE CASE

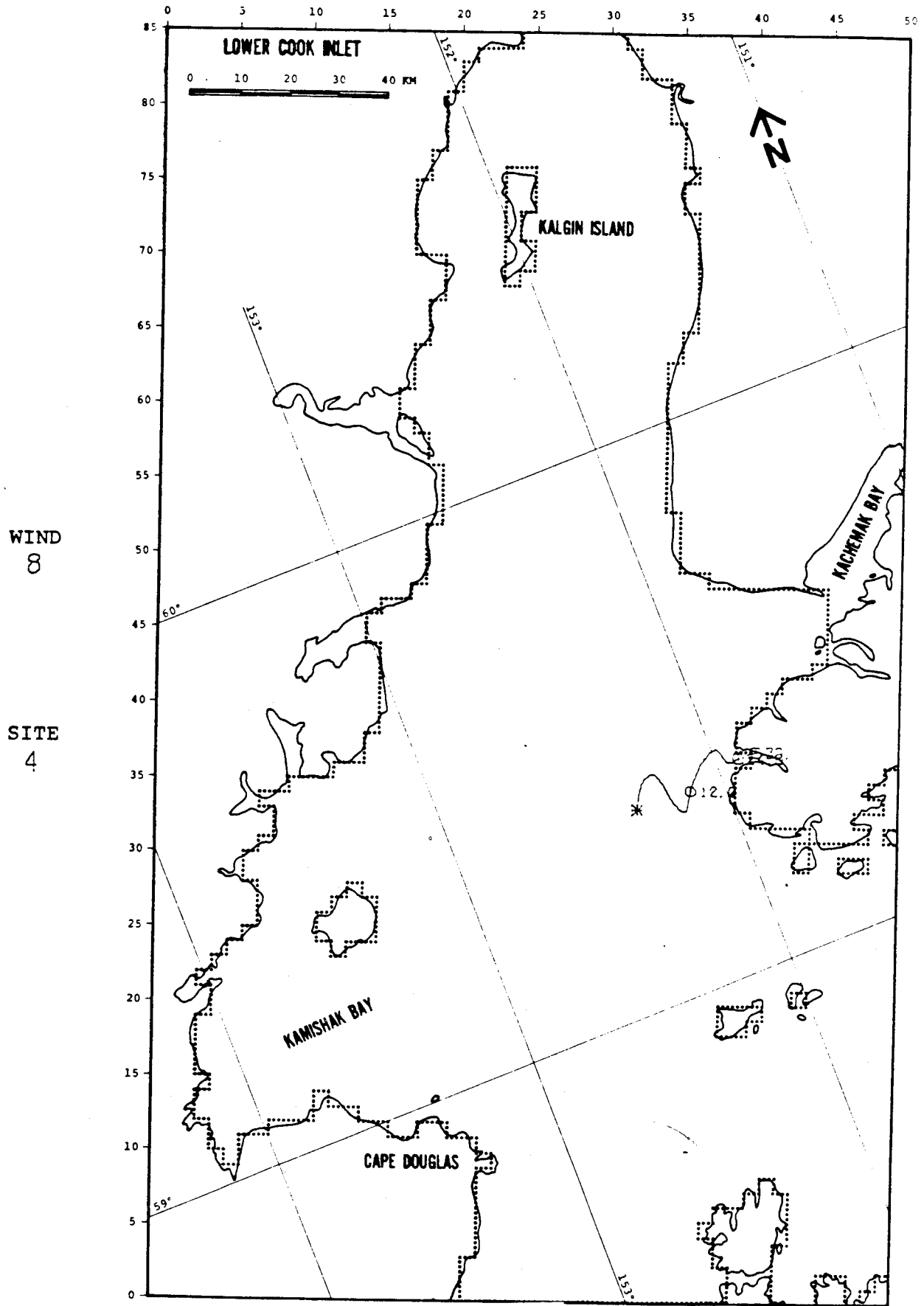


FIGURE B-67: BASE CASE

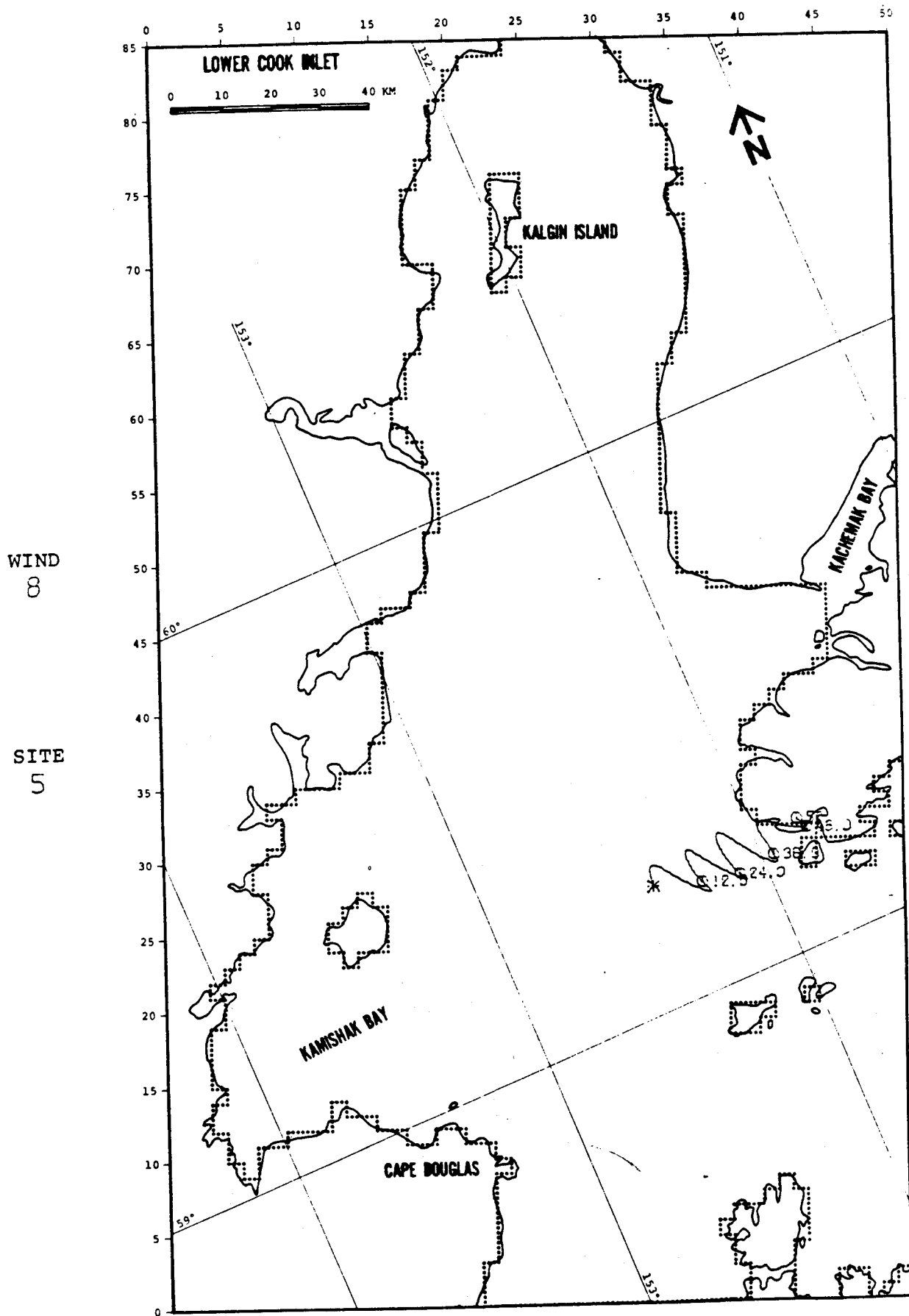


FIGURE B-68: BASE CASE

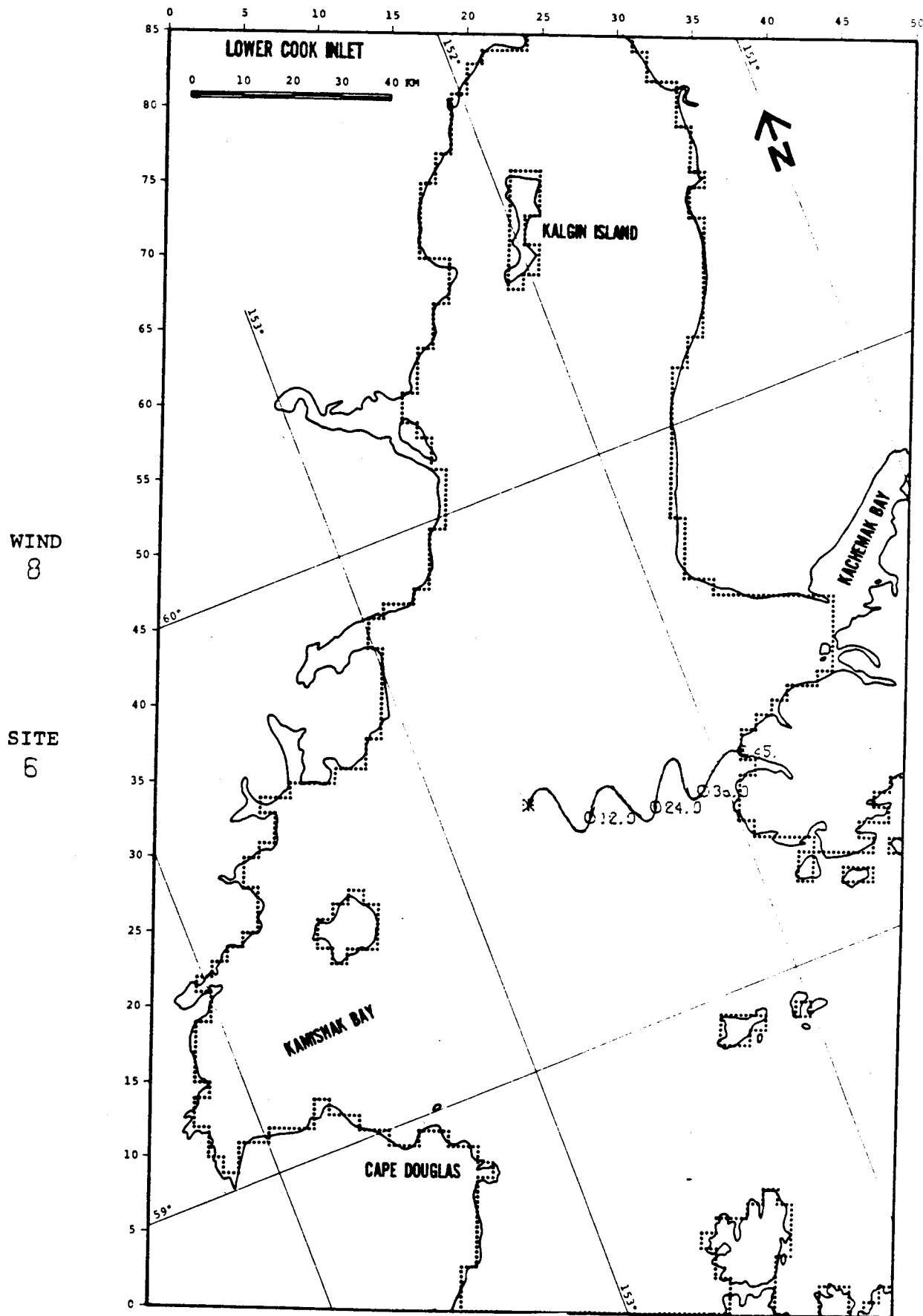


FIGURE B-69: BASE CASE

WIND
8

SITE
7

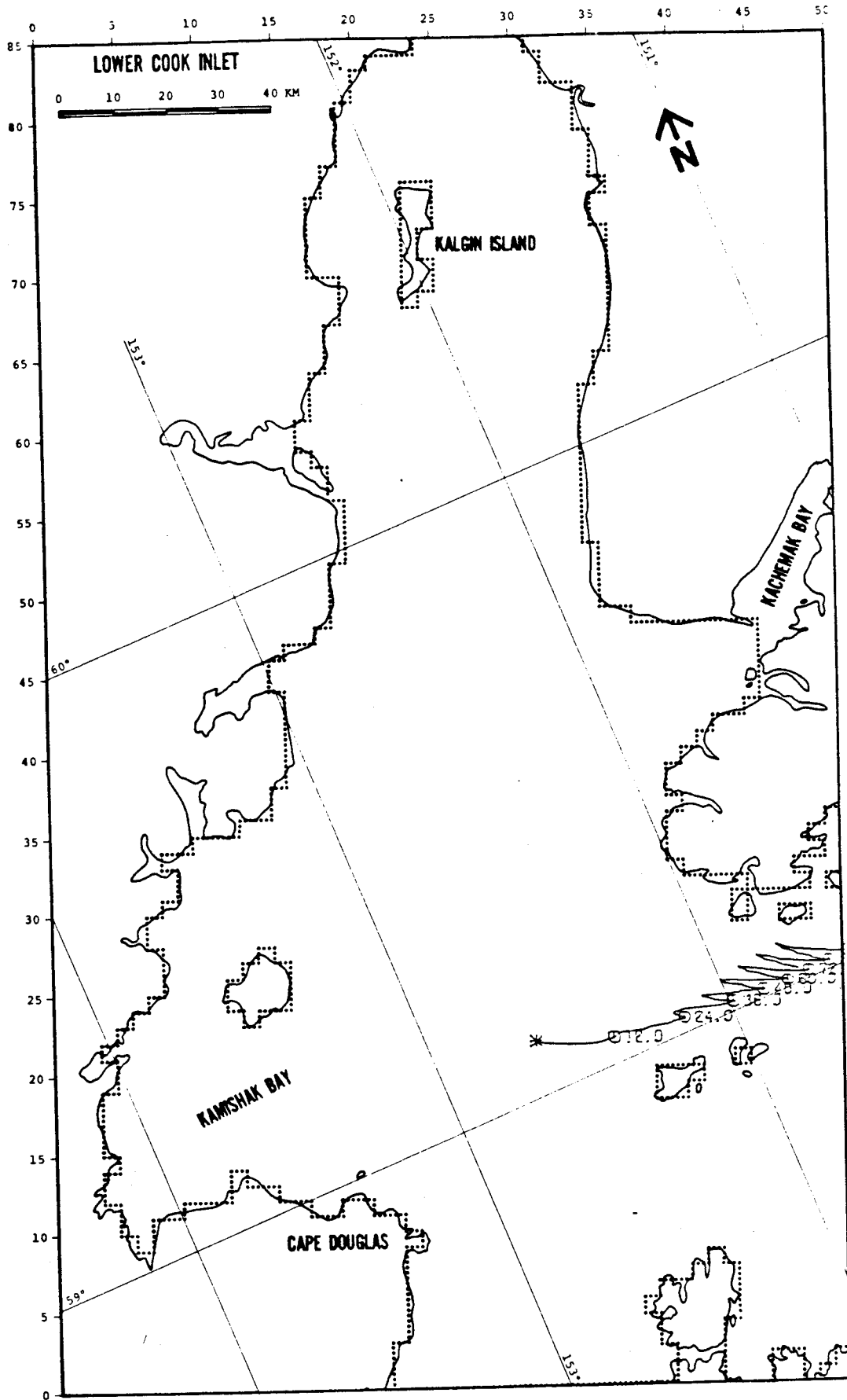


FIGURE B-70: BASE CASE

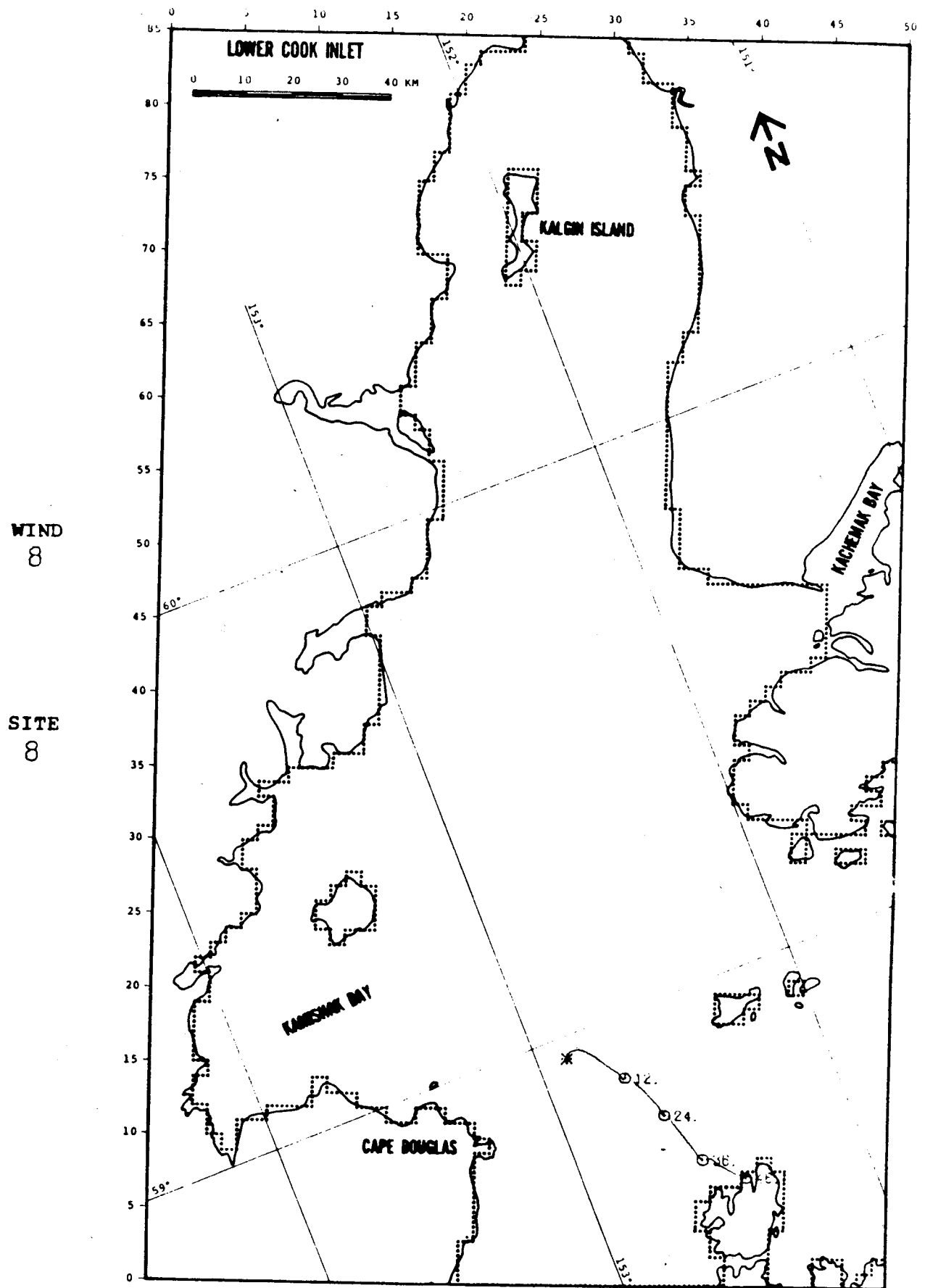


FIGURE B-71: BASE CASE

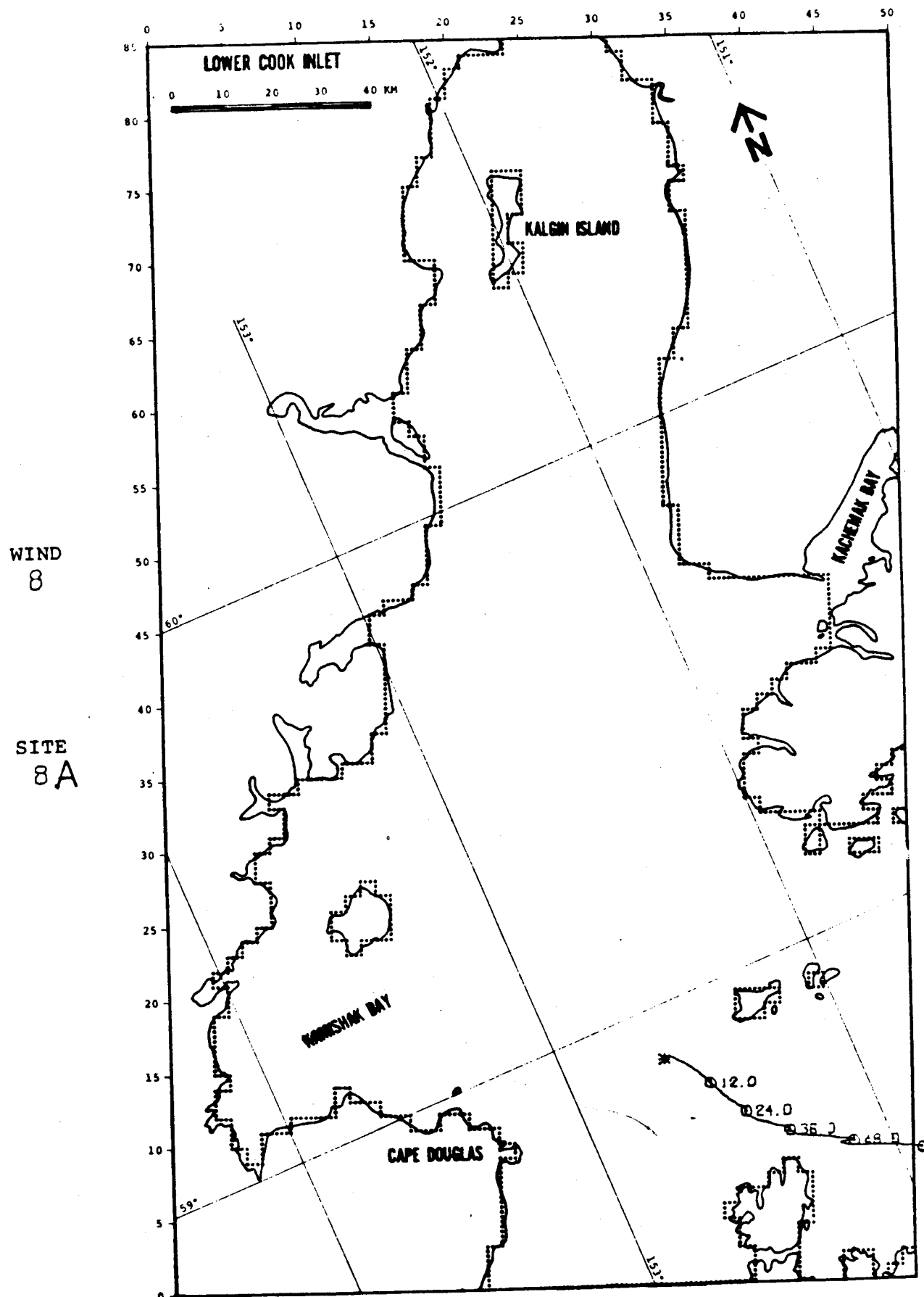


FIGURE B-72: BASE CASE

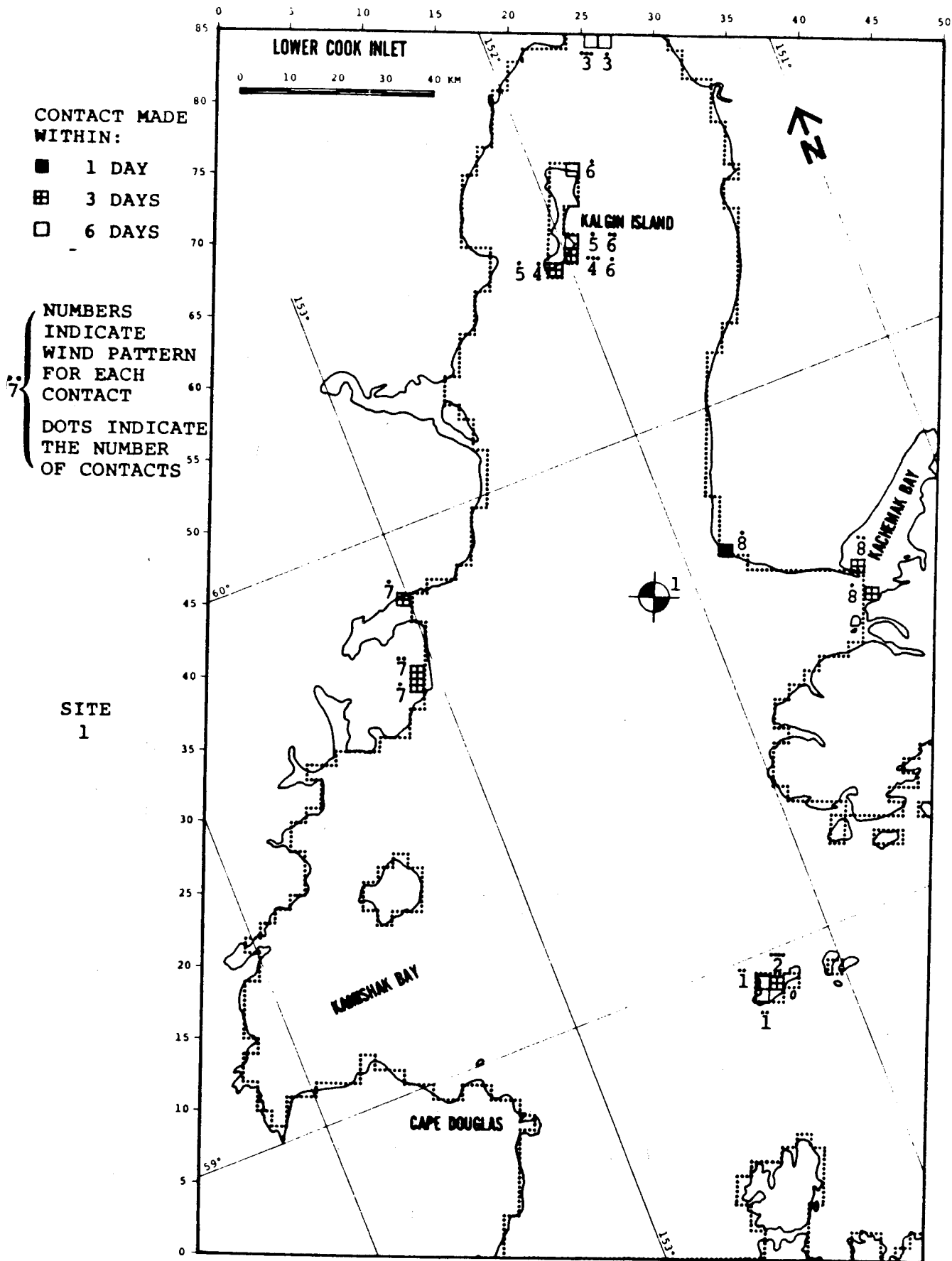


FIGURE B-73: POTENTIAL BOUNDARY CONTACT ZONES

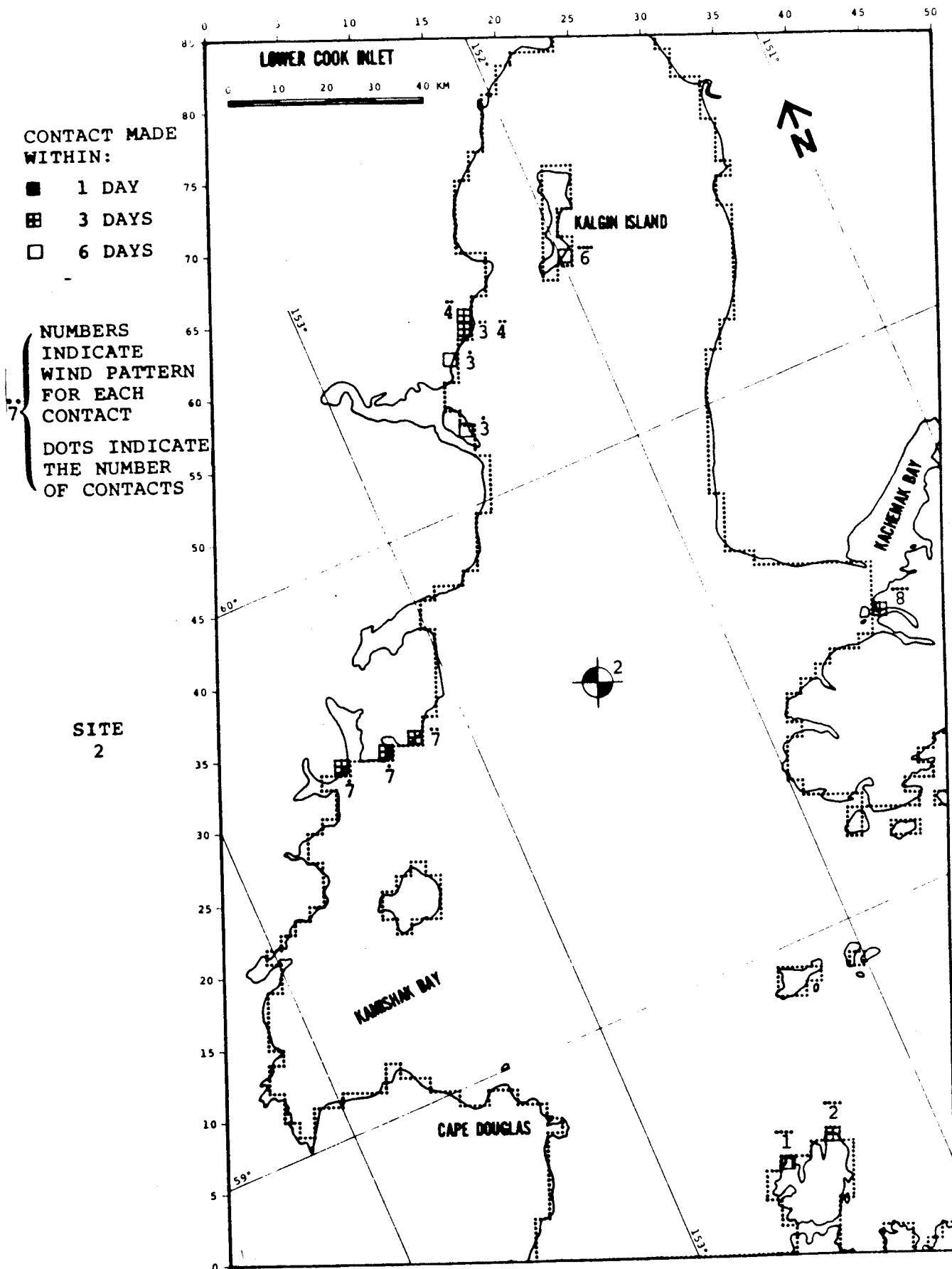


FIGURE B-74: POTENTIAL BOUNDARY CONTACT ZONES

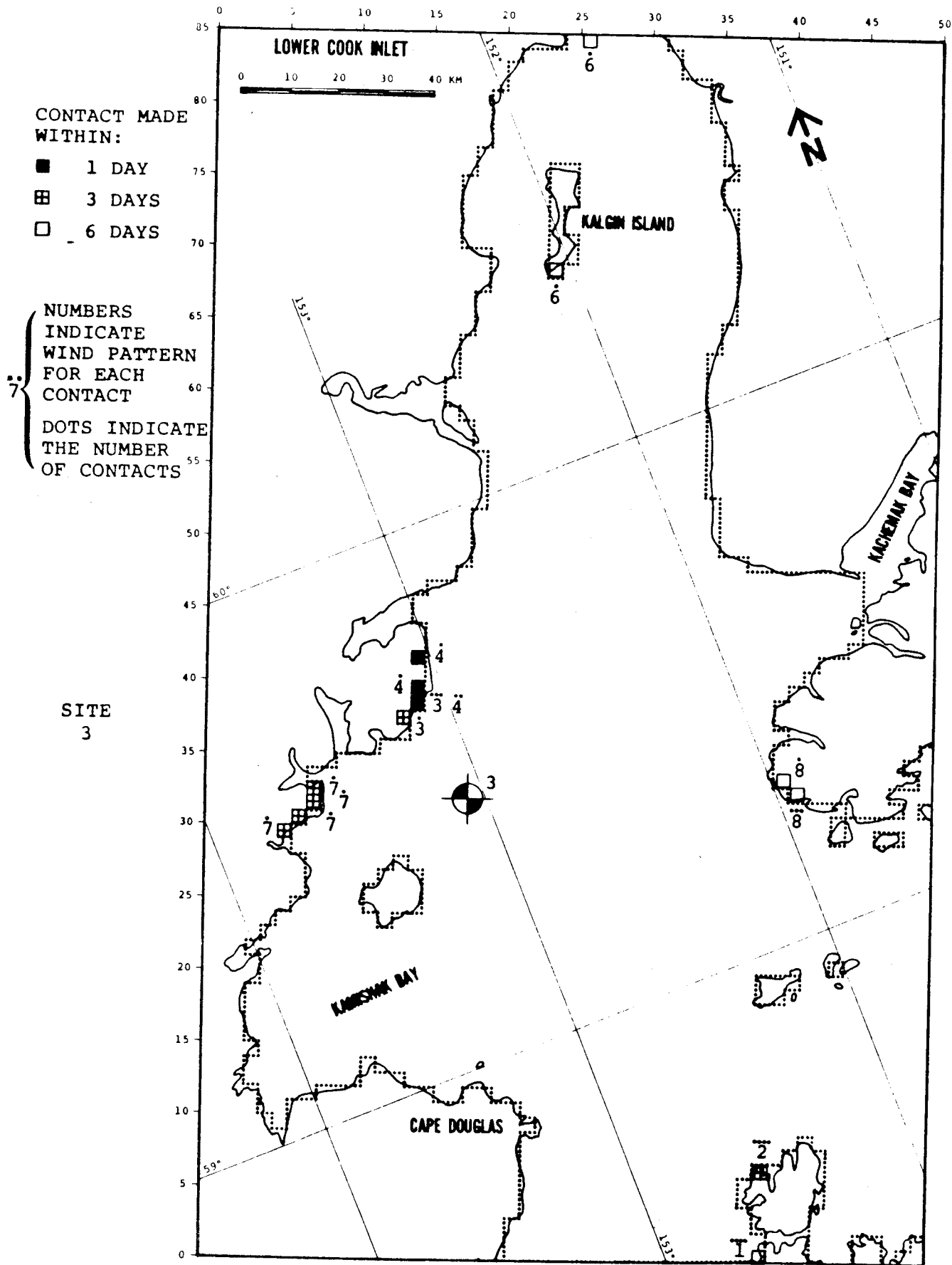


FIGURE B-75: POTENTIAL BOUNDARY CONTACT ZONES

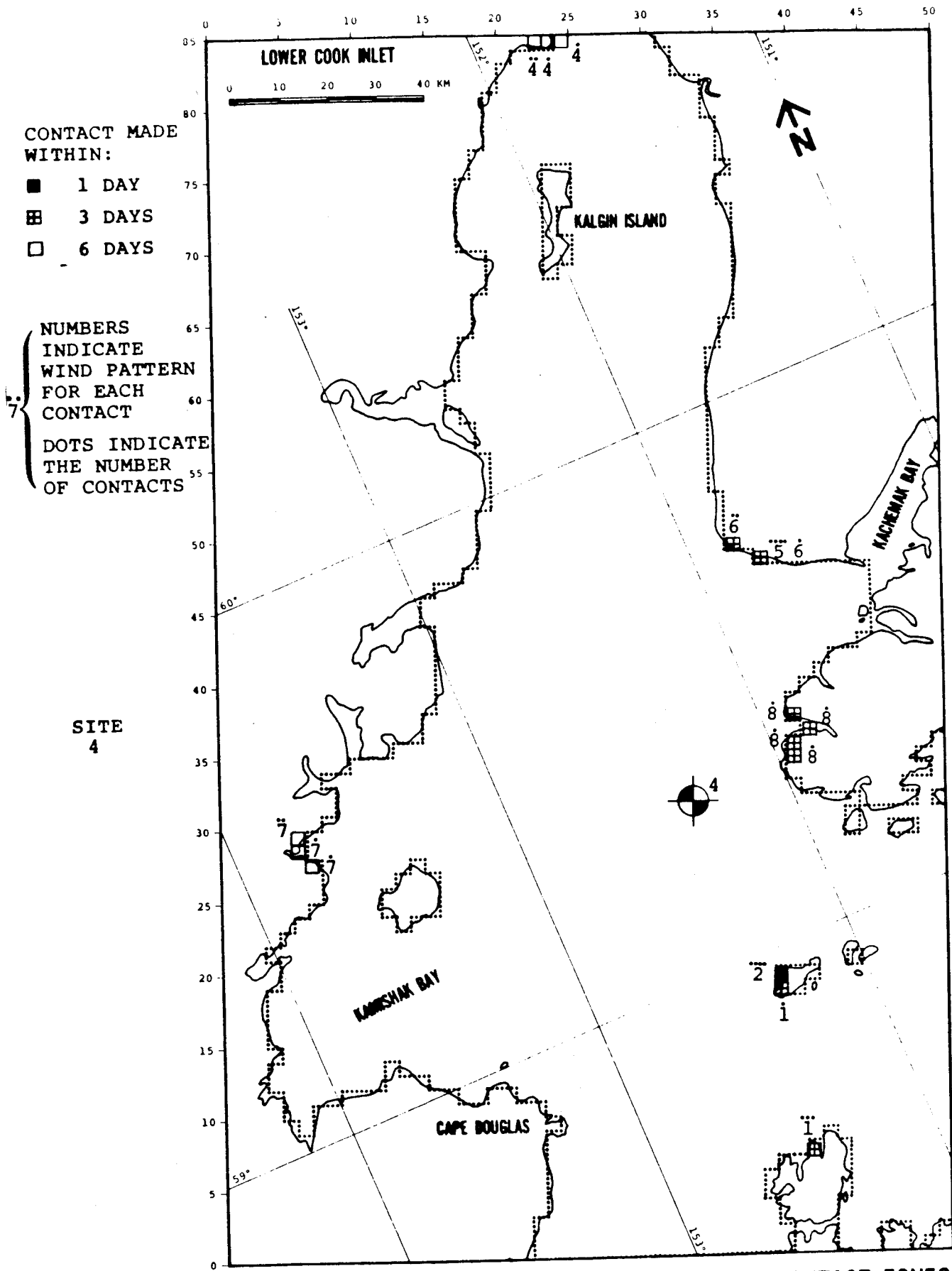


FIGURE B-76: POTENTIAL BOUNDARY CONTACT ZONES

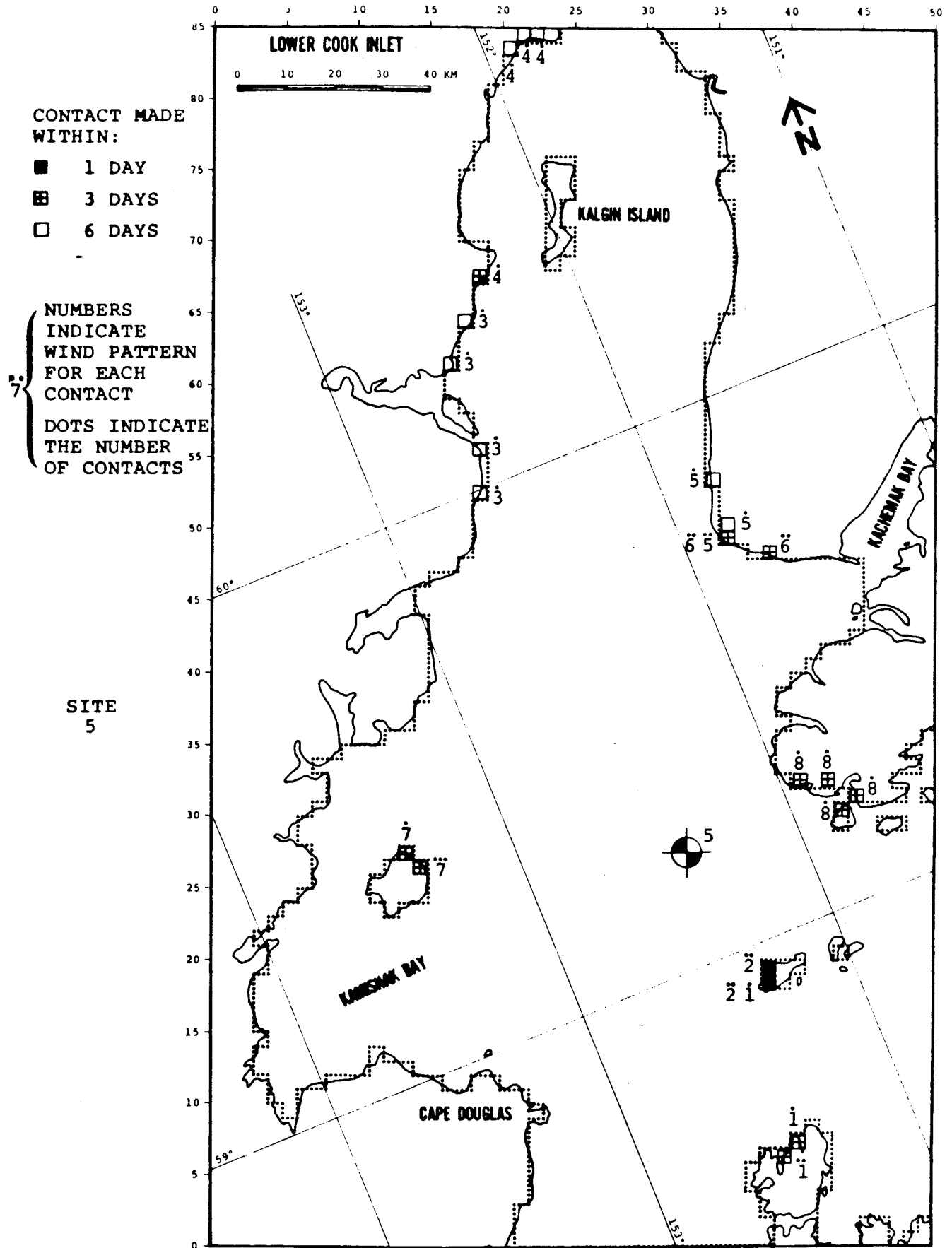


FIGURE B-77: POTENTIAL BOUNDARY CONTACT ZONES

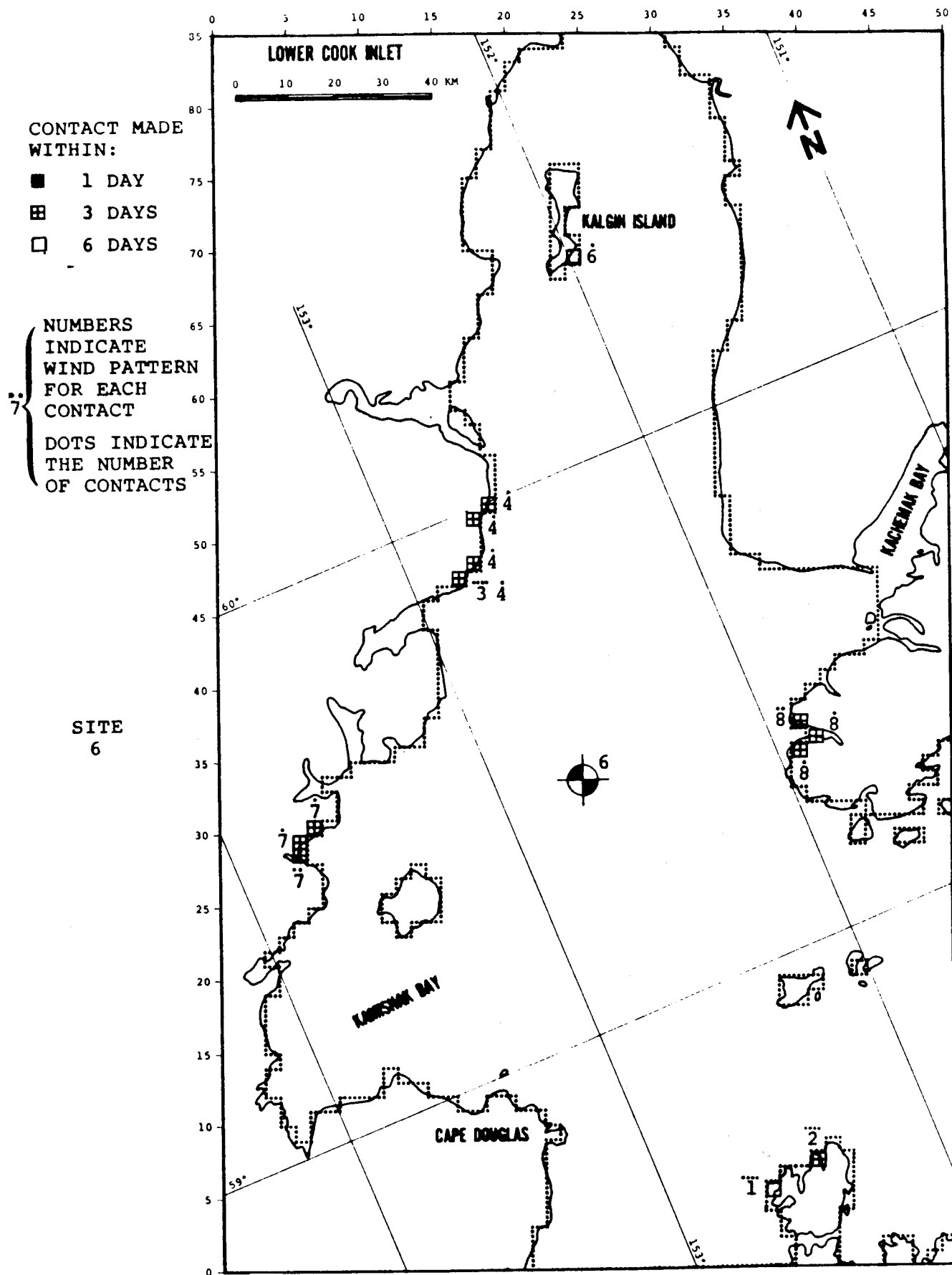


FIGURE B-78: POTENTIAL BOUNDARY CONTACT ZONES

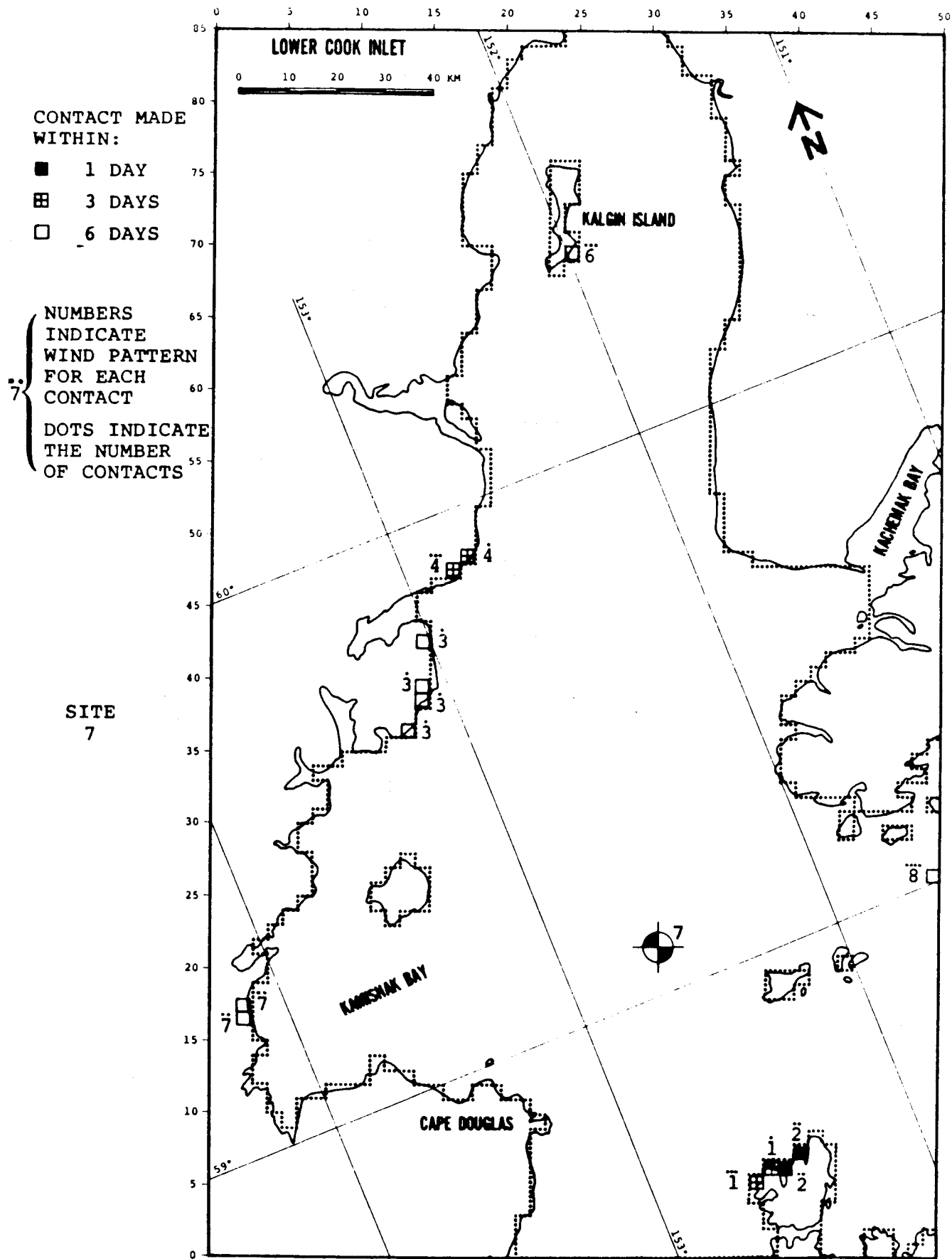


FIGURE B-79: POTENTIAL BOUNDARY CONTACT ZONES

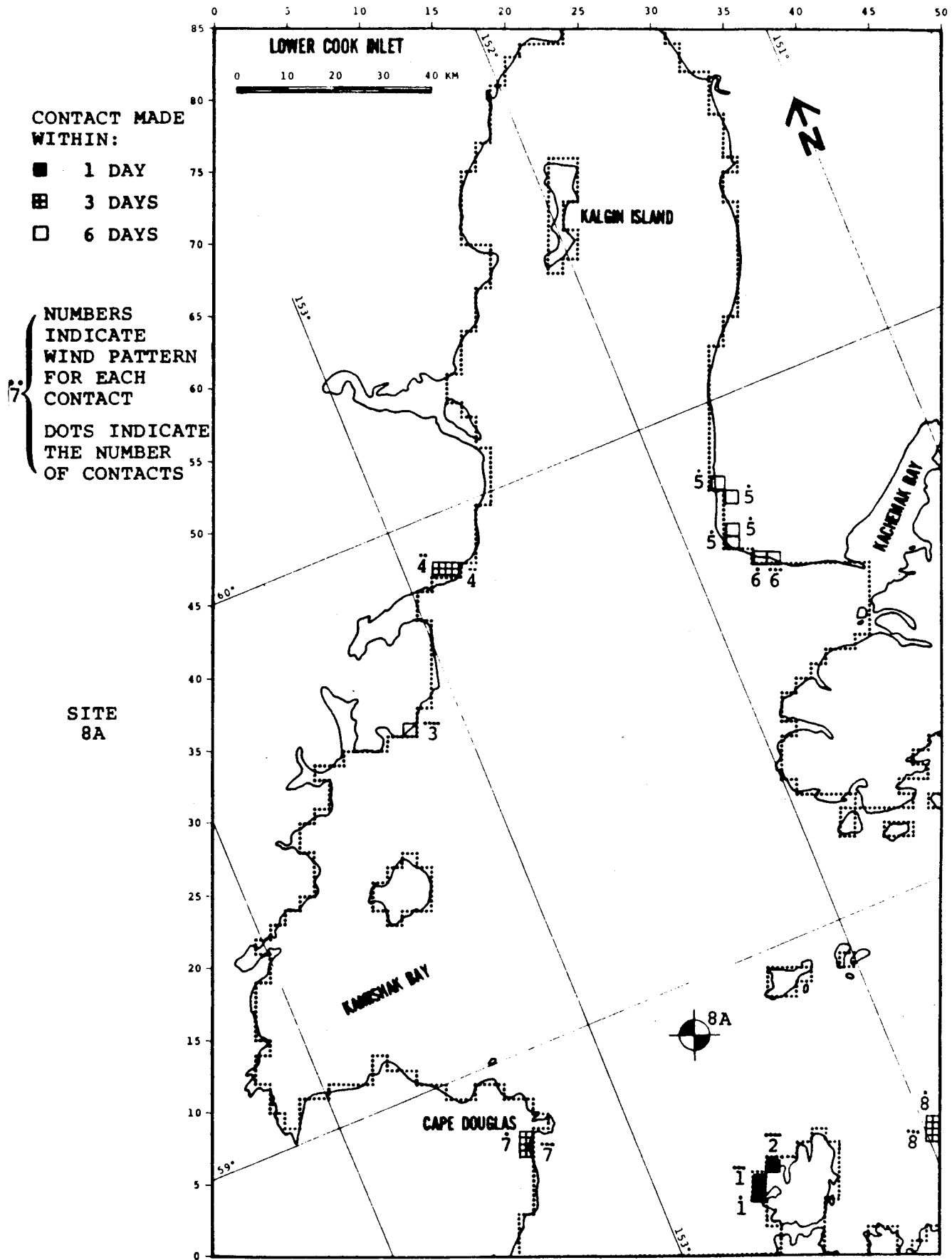


FIGURE B-81: POTENTIAL BOUNDARY CONTACT ZONES

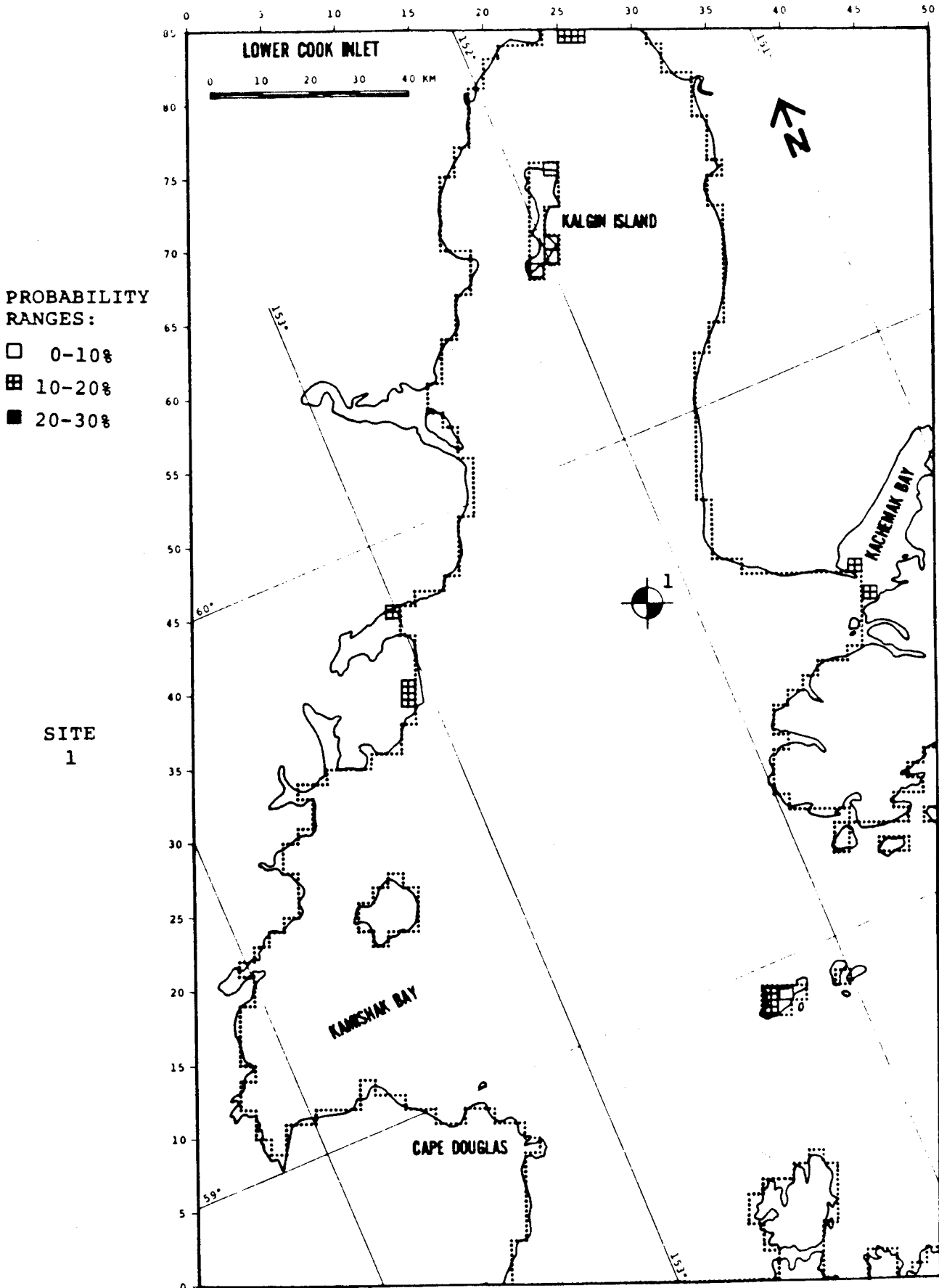


FIGURE B-82: ANNUAL PERCENT PROBABILITY OF EXPOSURE

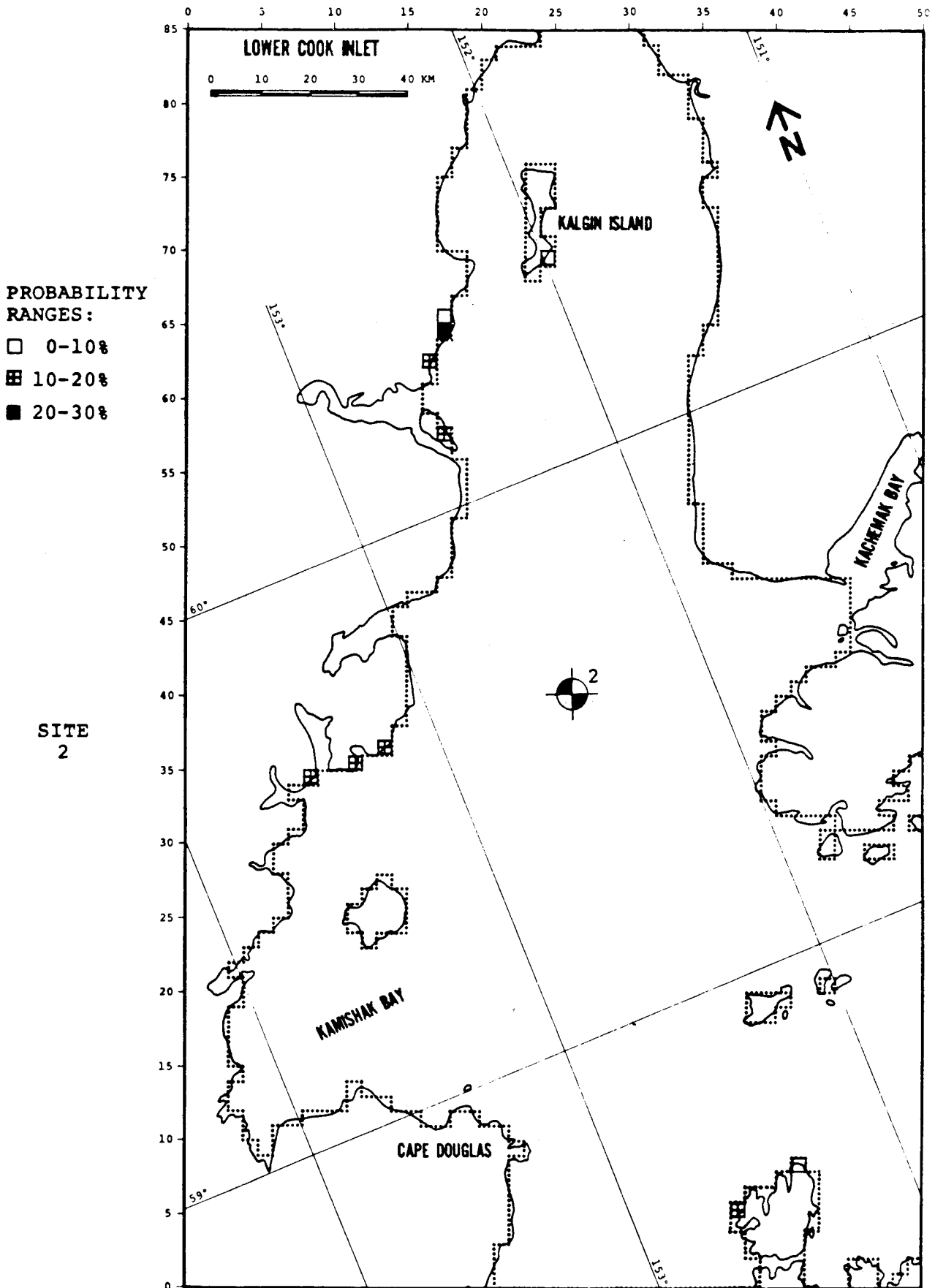


FIGURE B-83: ANNUAL PERCENT PROBABILITY OF EXPOSURE

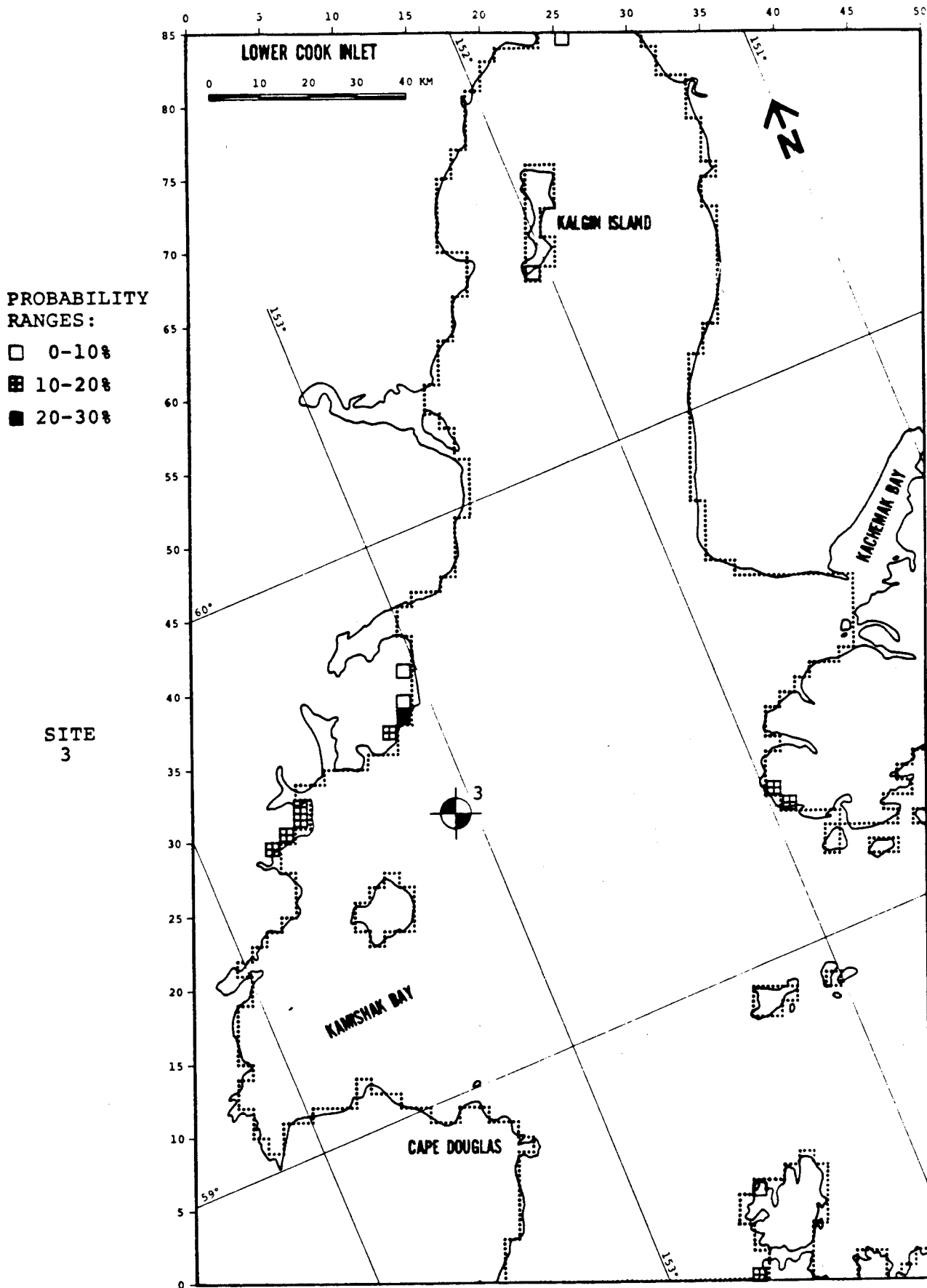


FIGURE B-84: ANNUAL PERCENT PROBABILITY OF EXPOSURE

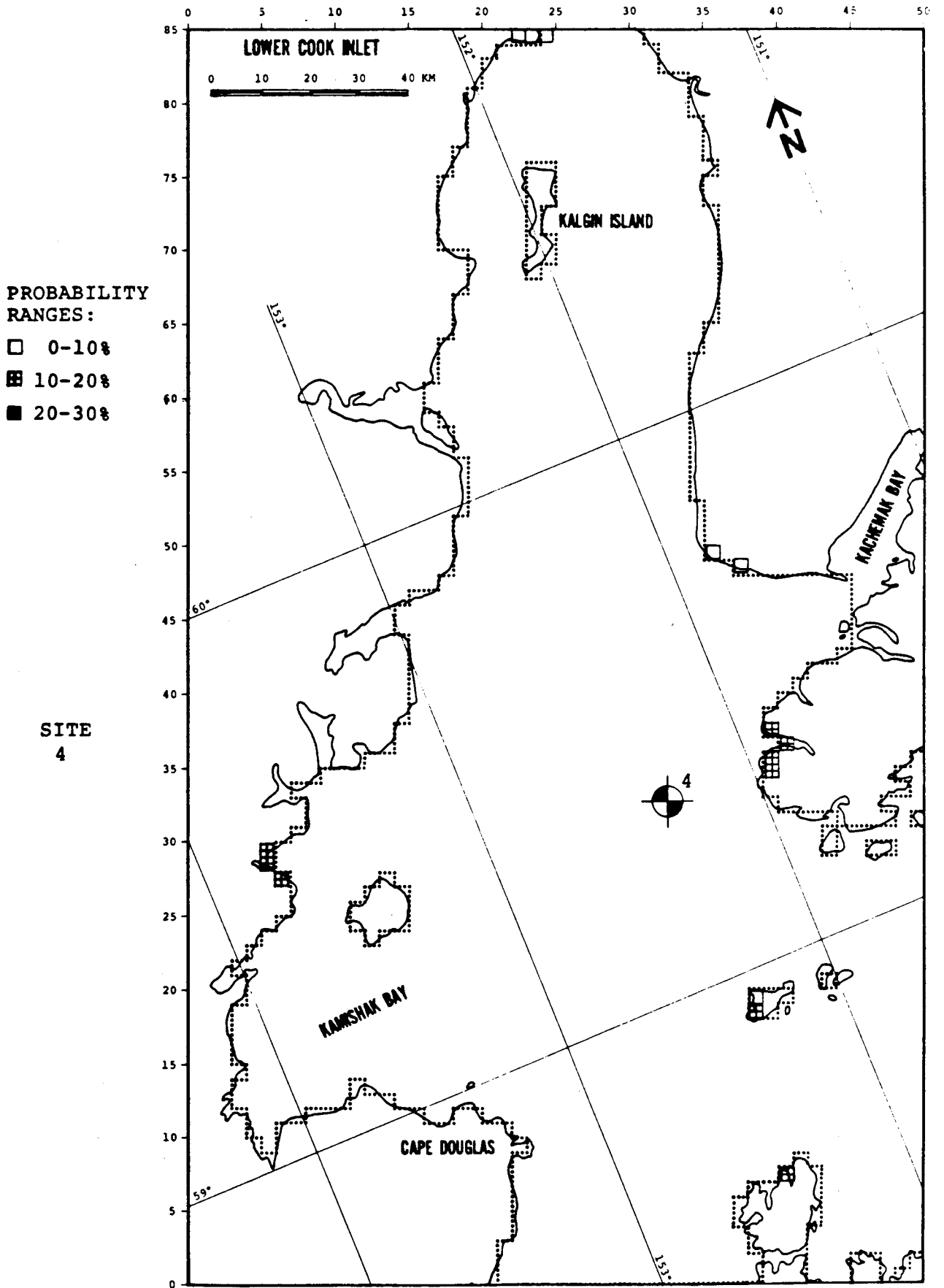


FIGURE B-85: ANNUAL PERCENT PROBABILITY OF EXPOSURE

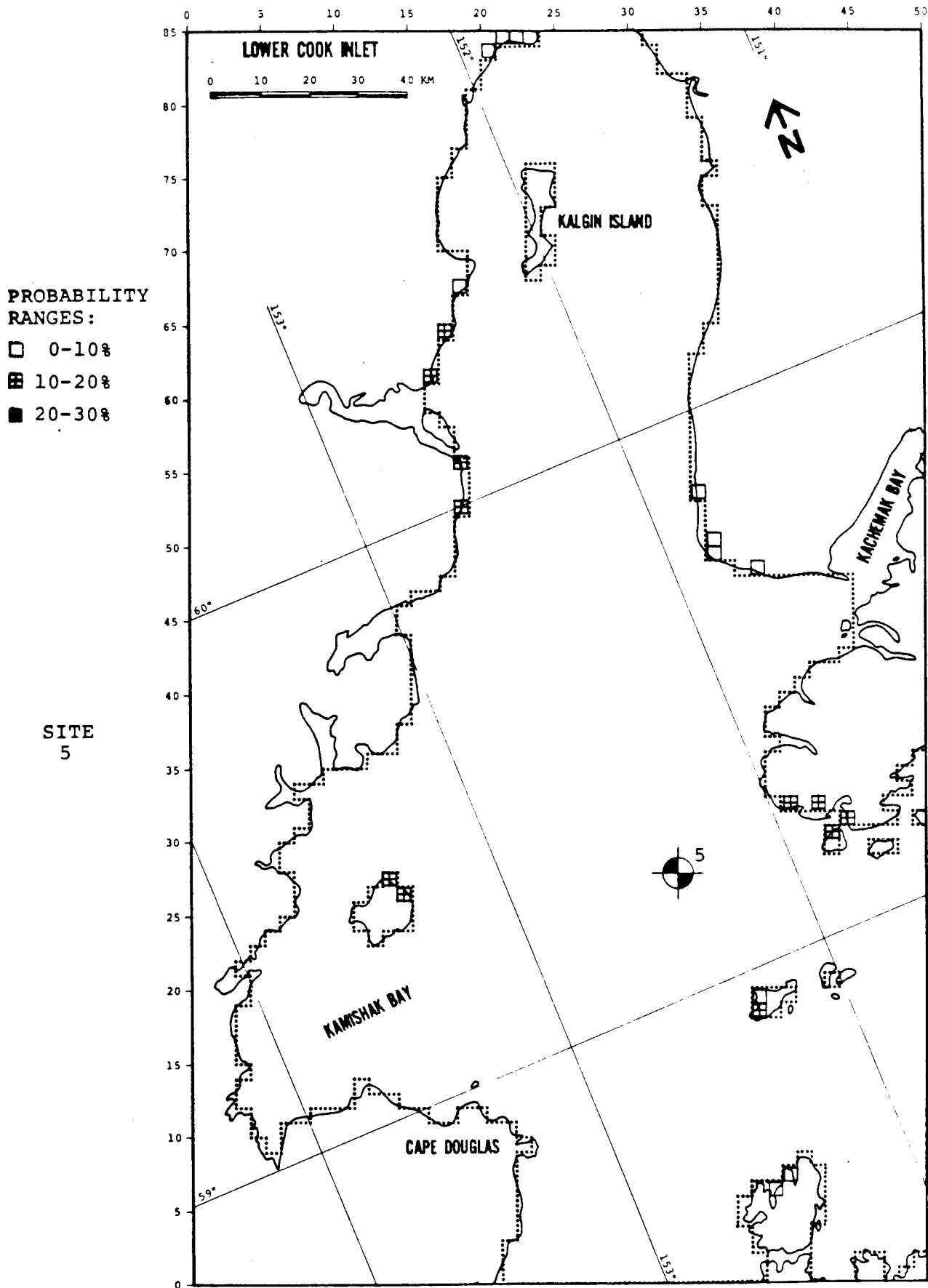


FIGURE B-86: ANNUAL PERCENT PROBABILITY OF EXPOSURE

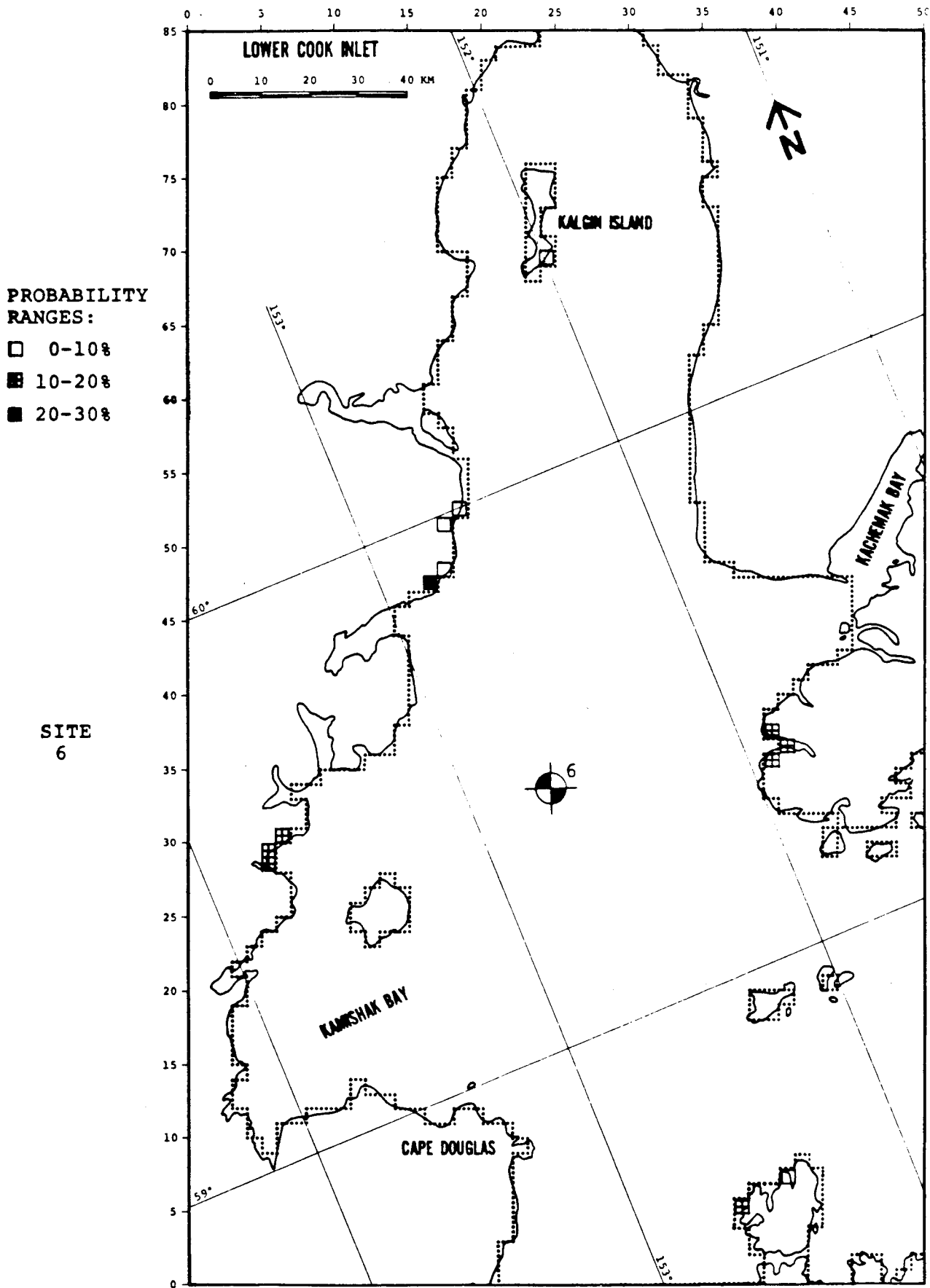


FIGURE B-87: ANNUAL PERCENT PROBABILITY OF EXPOSURE

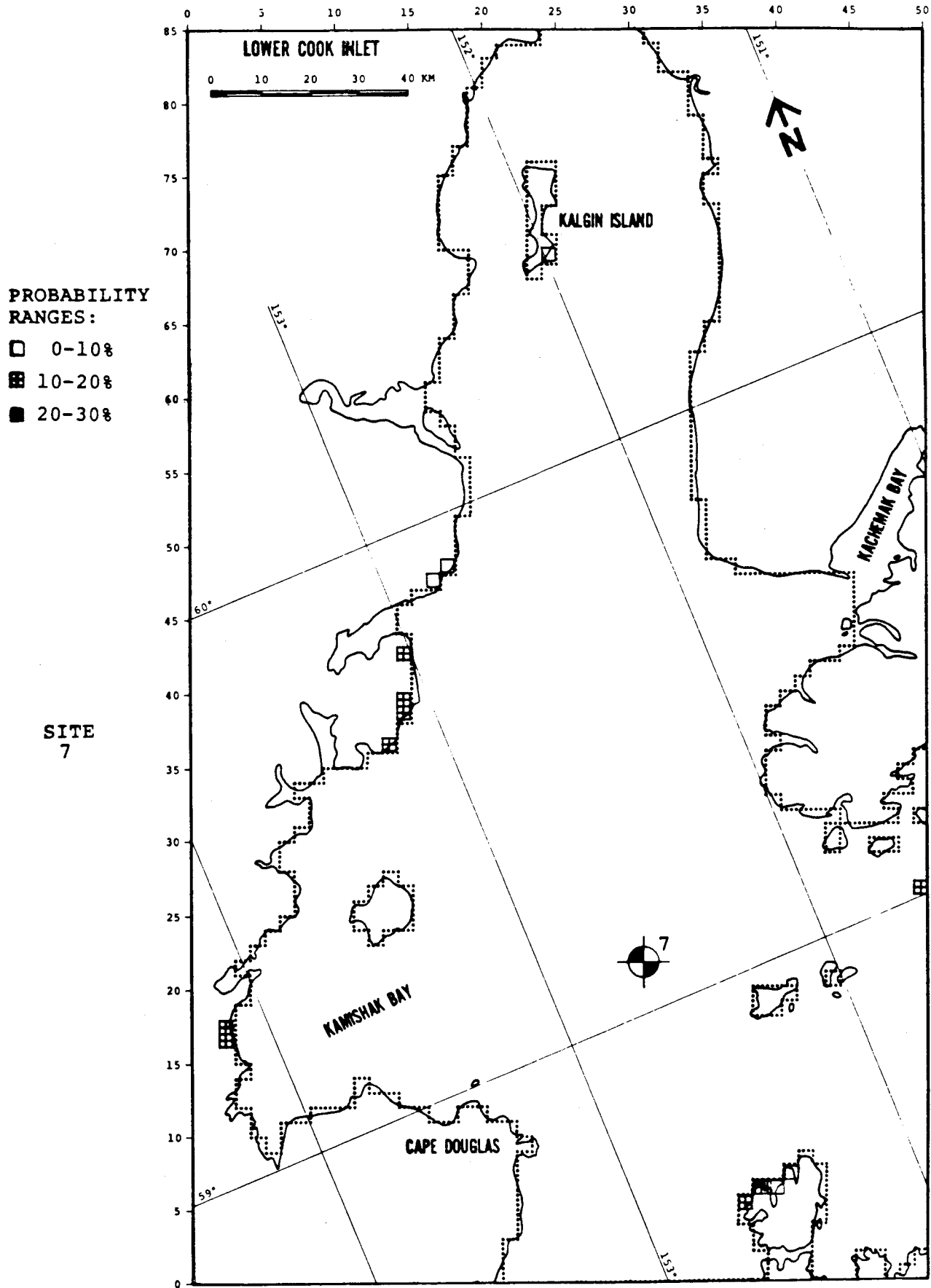


FIGURE B-88: ANNUAL PERCENT PROBABILITY OF EXPOSURE

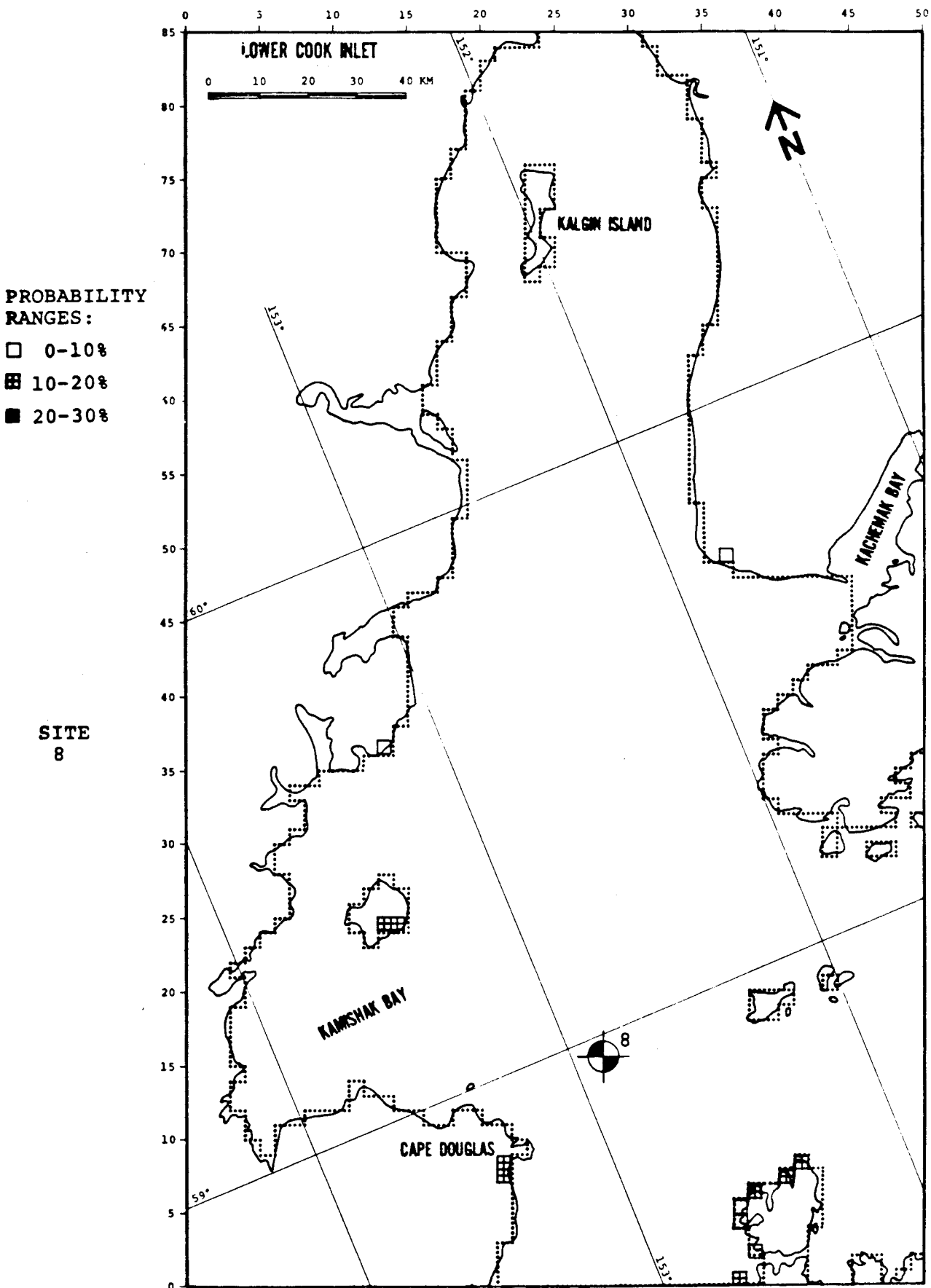


FIGURE B-89: ANNUAL PERCENT PROBABILITY OF EXPOSURE

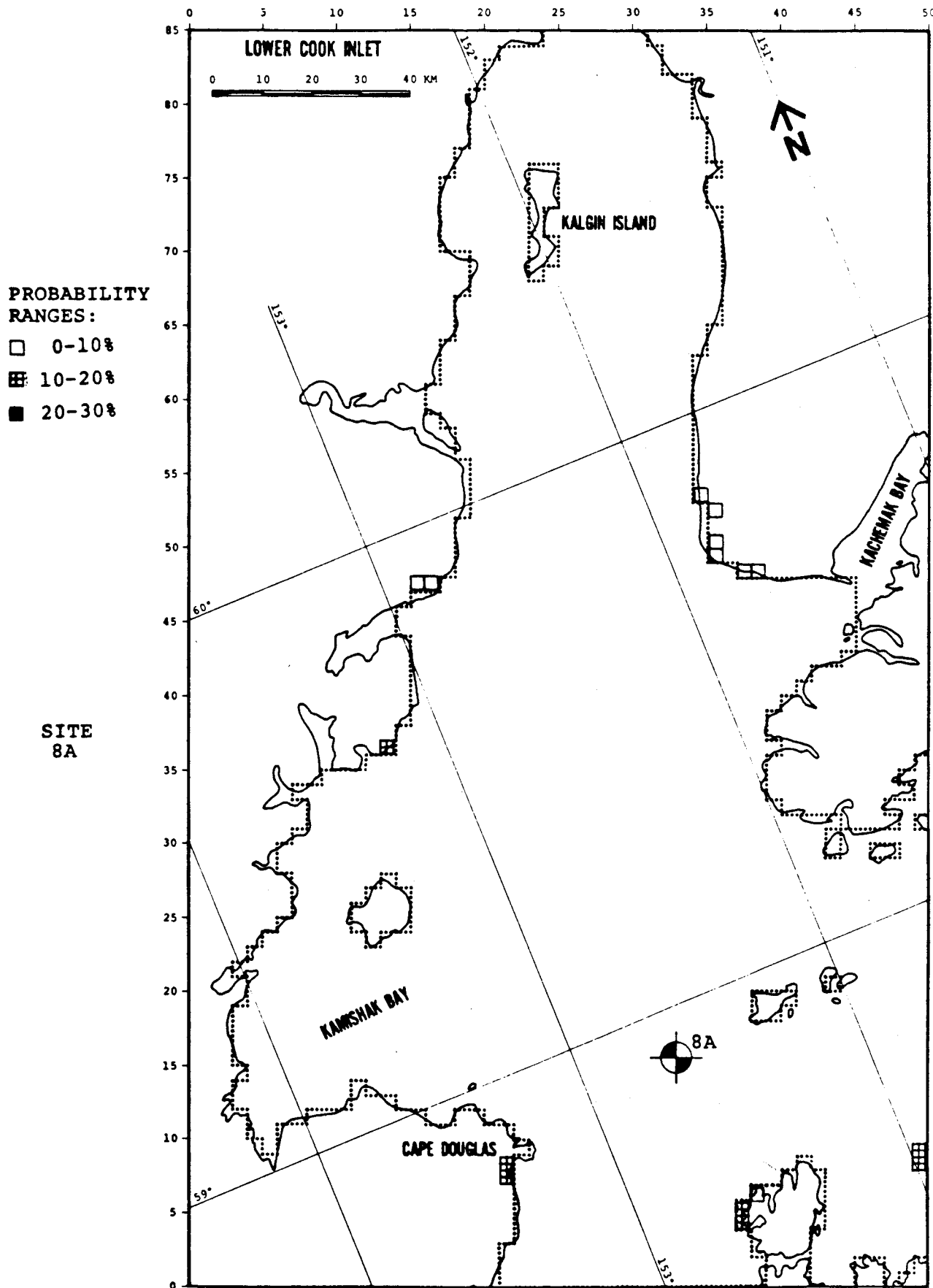


FIGURE B-90: ANNUAL PERCENT PROBABILITY OF EXPOSURE

APPENDIX C

PERTURBATION CASE TRAJECTORIES

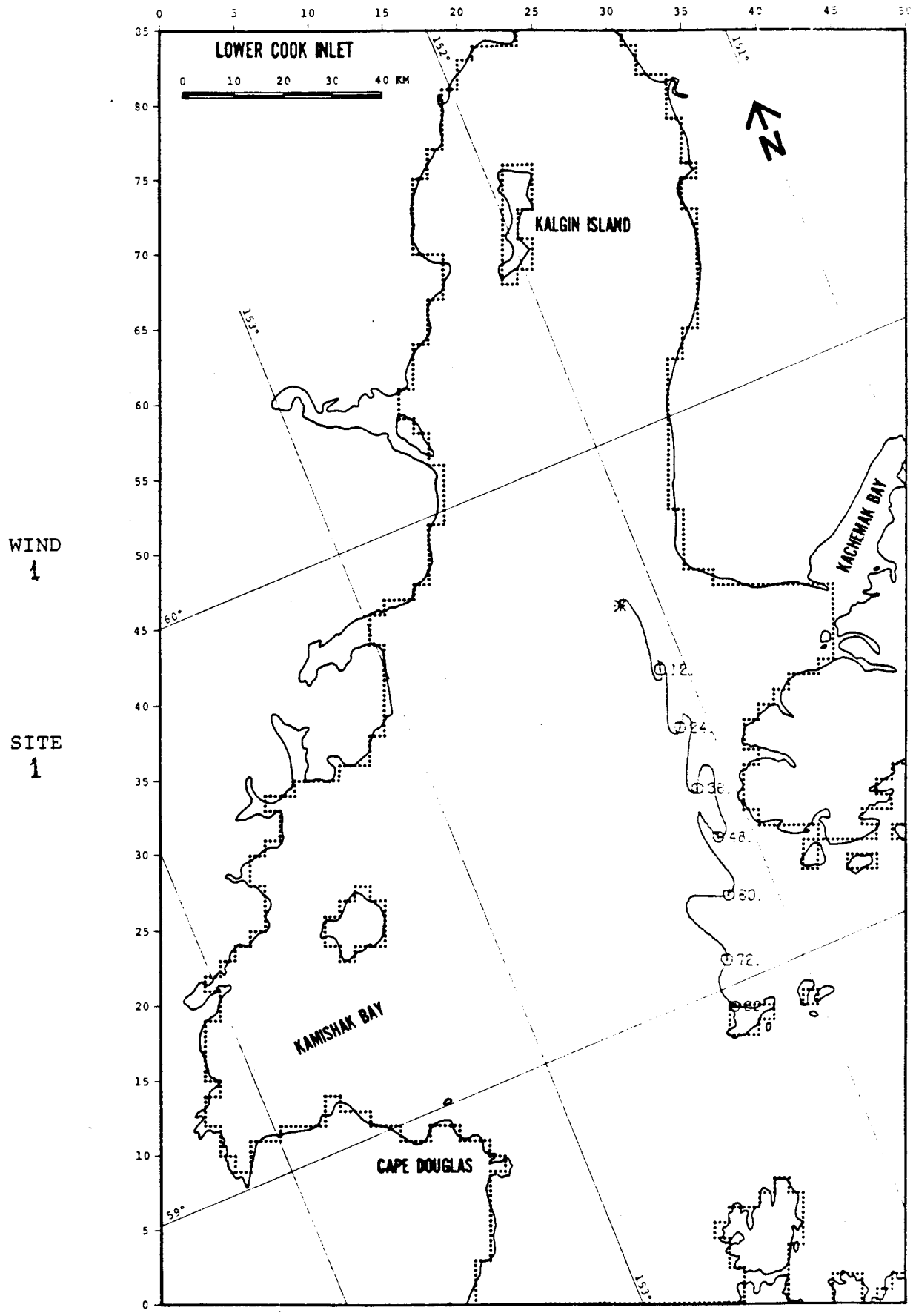


FIGURE C-1: PERTURBATION CASE: NET +25%

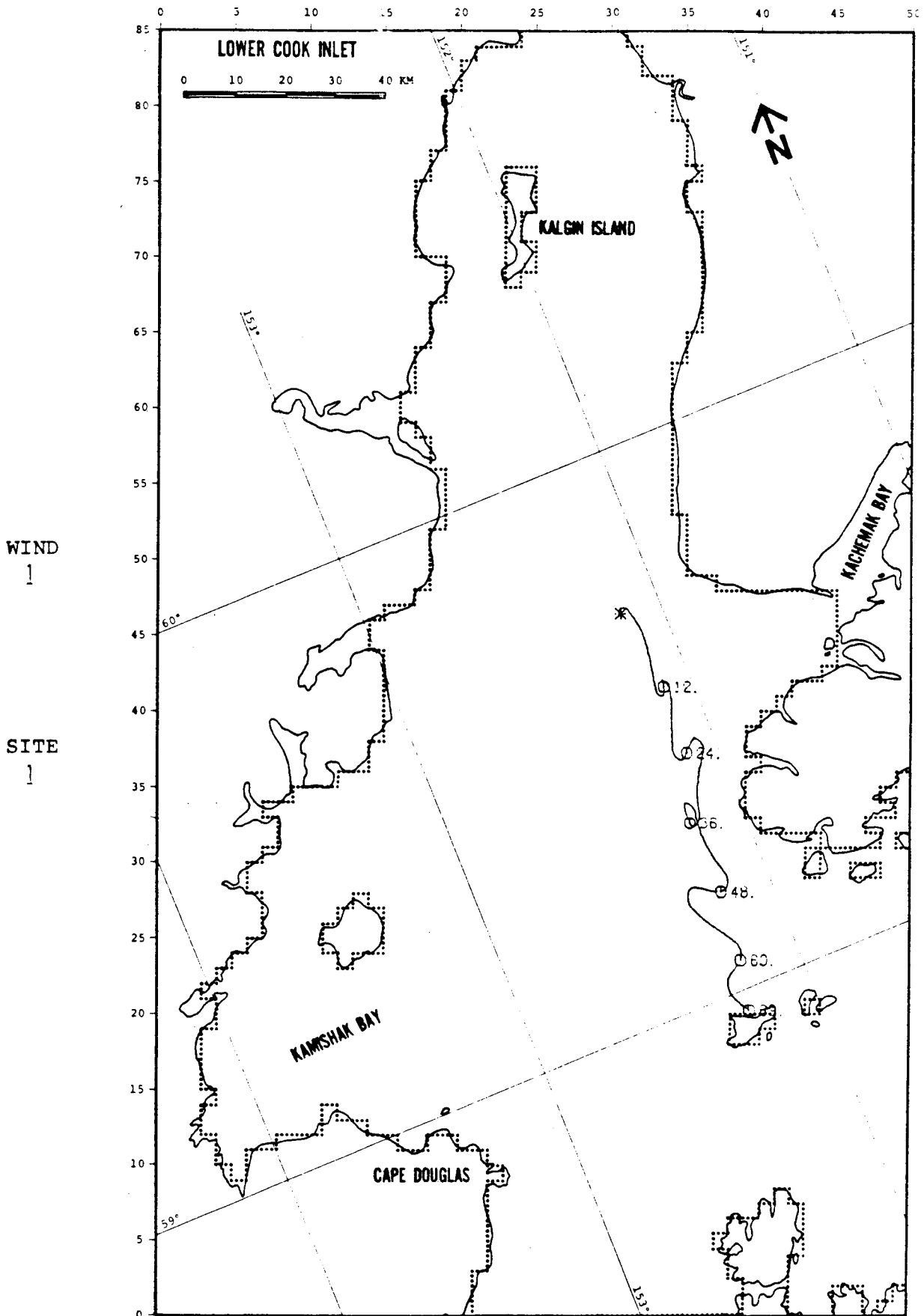


FIGURE C-2: PERTURBATION CASE: NET -25%

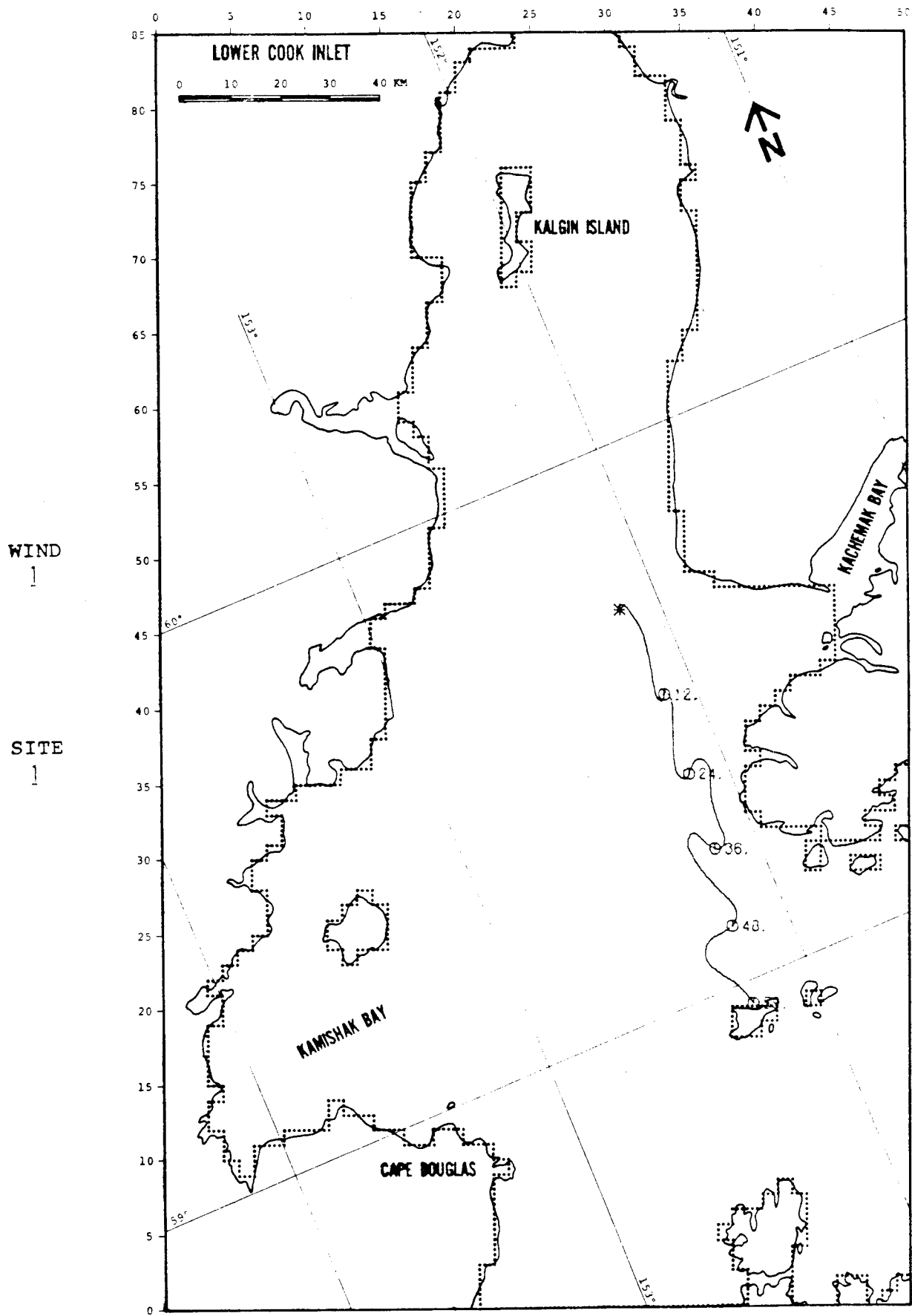


FIGURE C-3: PERTURBATION CASE: WIND +25%

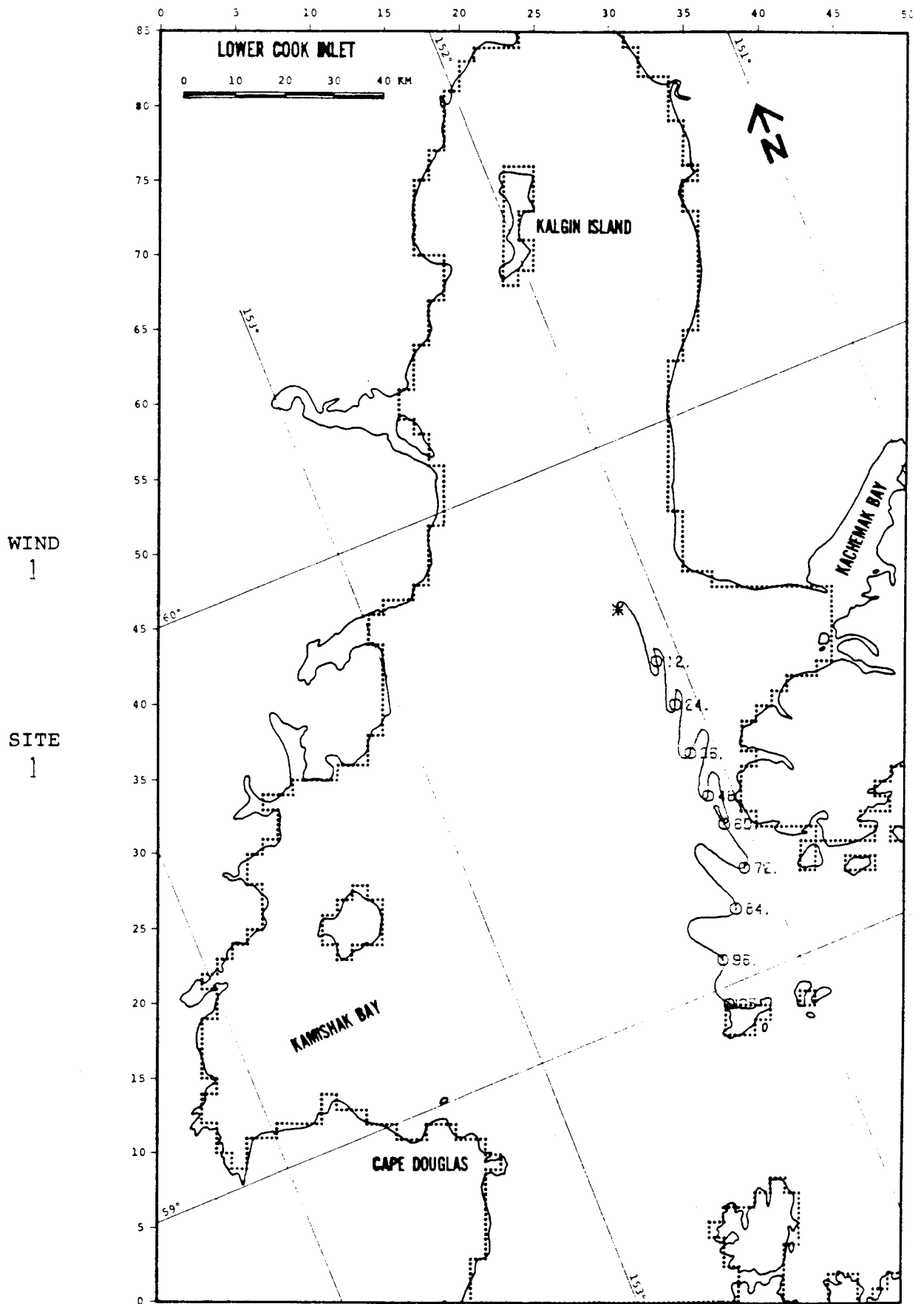


FIGURE C-4: PERTURBATION CASE: WIND -25%

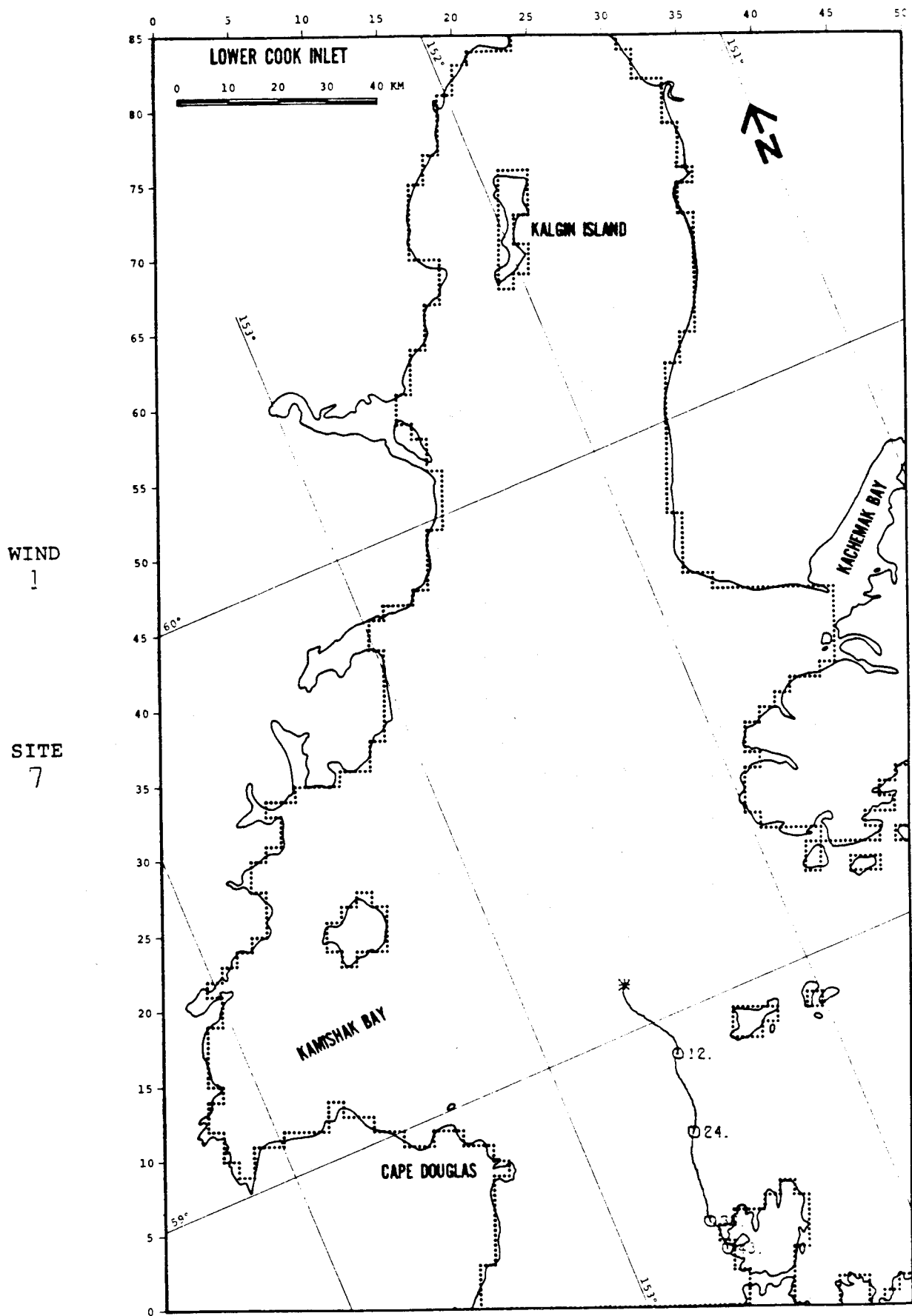


FIGURE C-5: PERTURBATION CASE: NET +25%

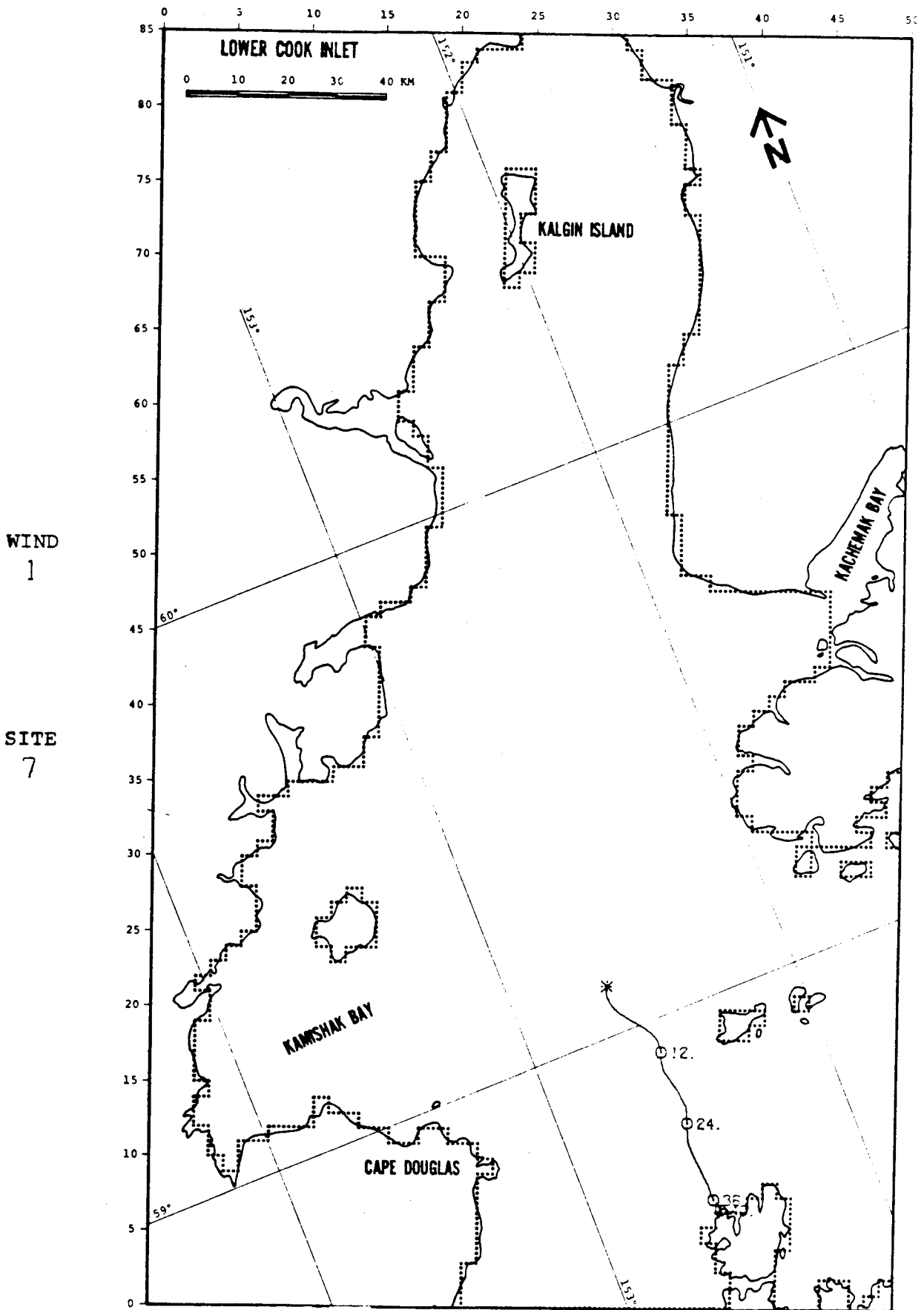


FIGURE C-6: PERTURBATION CASE: NET -25%

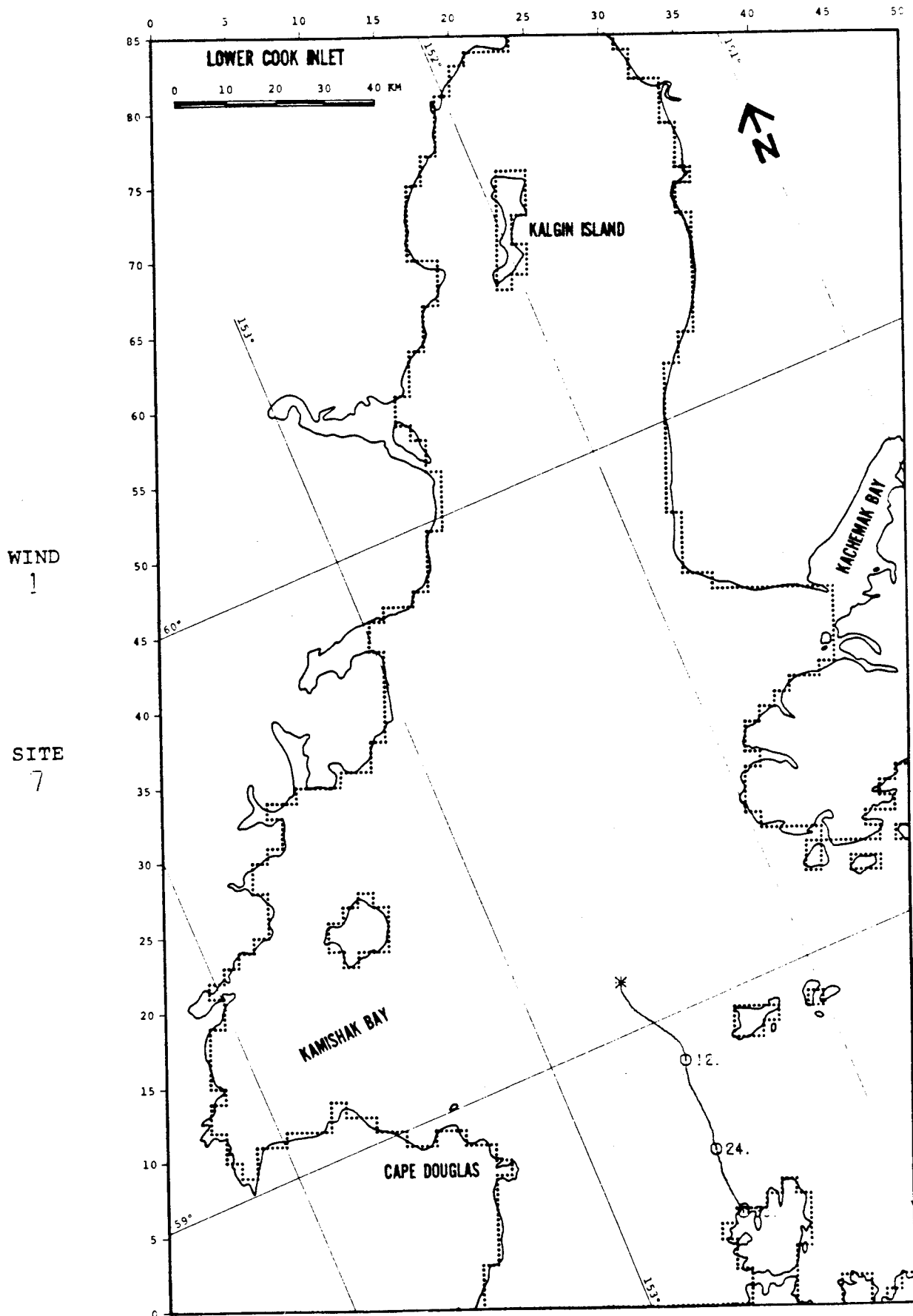


FIGURE C-7: PERTURBATION CASE: WIND +25%

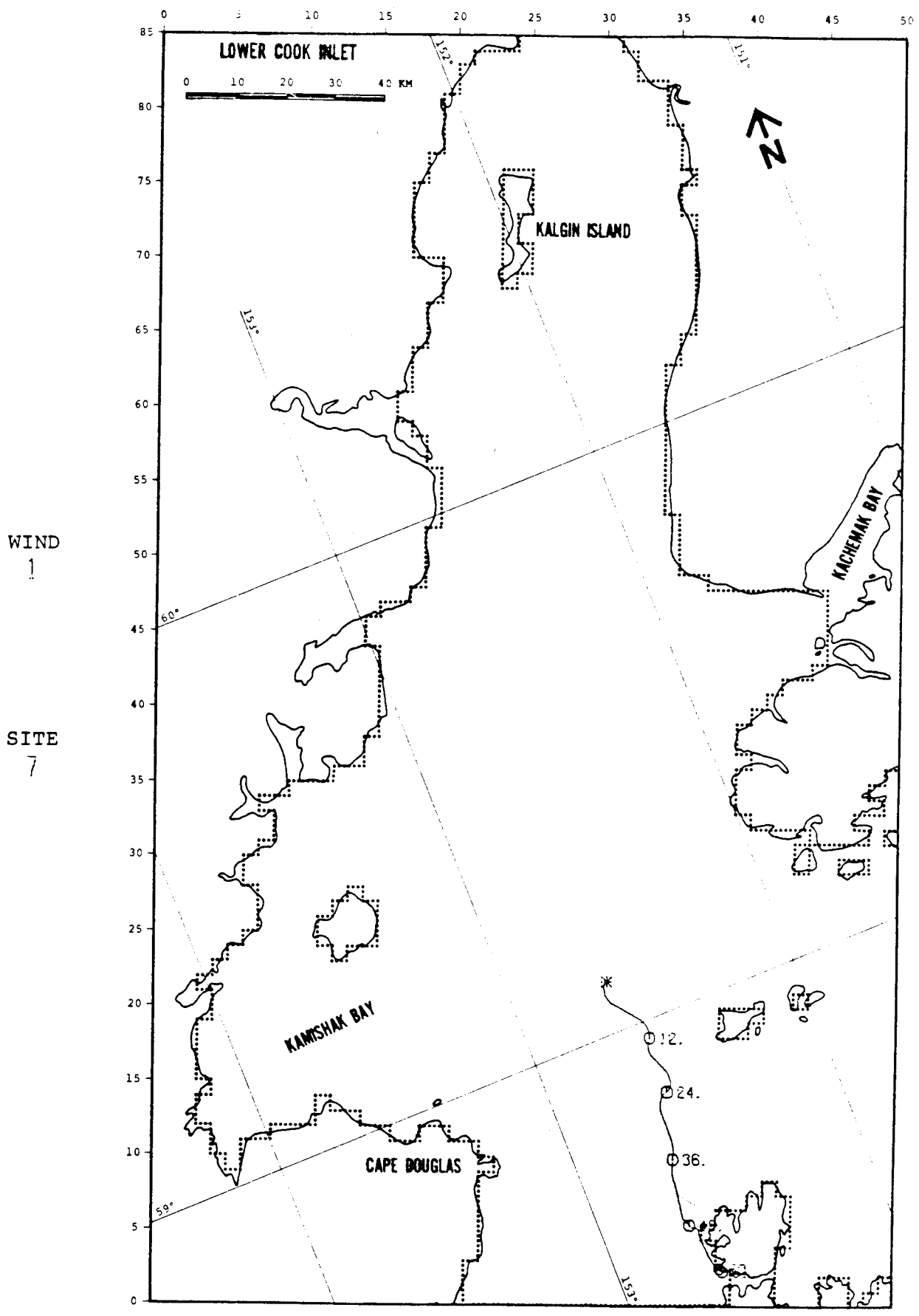


FIGURE C-8: PERTURBATION CASE: WIND -25%

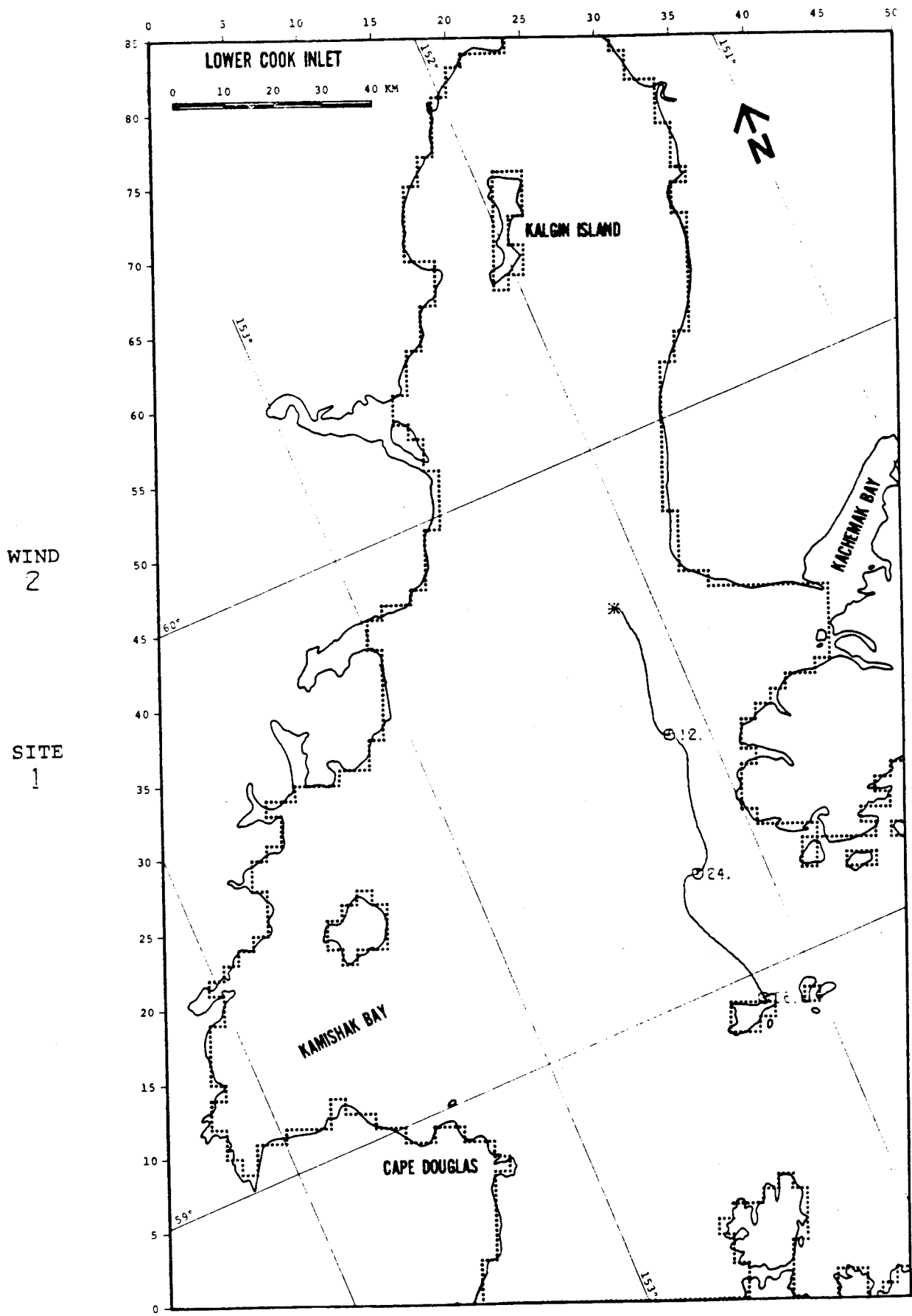


FIGURE C-9: PERTURBATION CASE: NET +25%

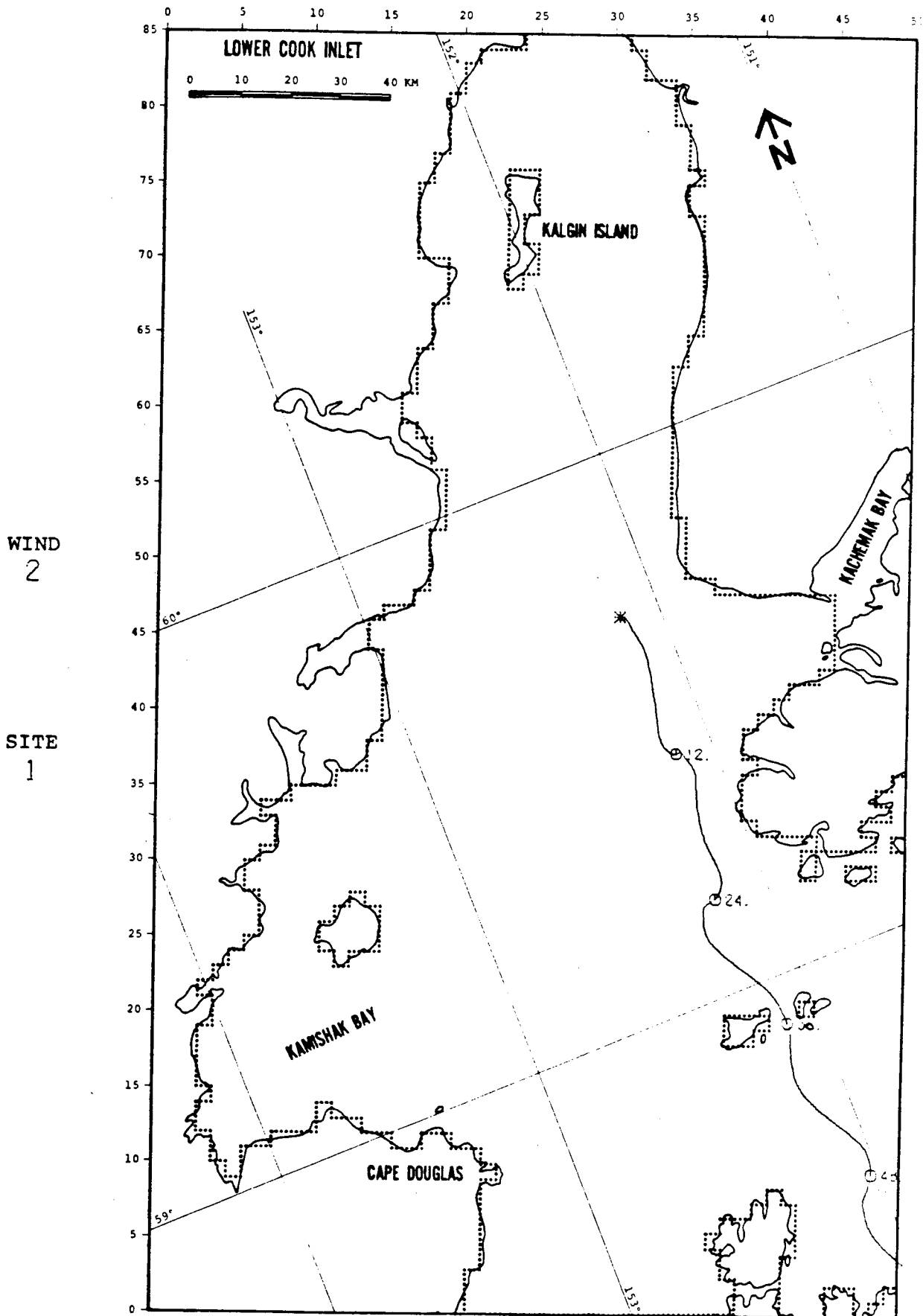


FIGURE C-10: PERTURBATION CASE: NET -25%

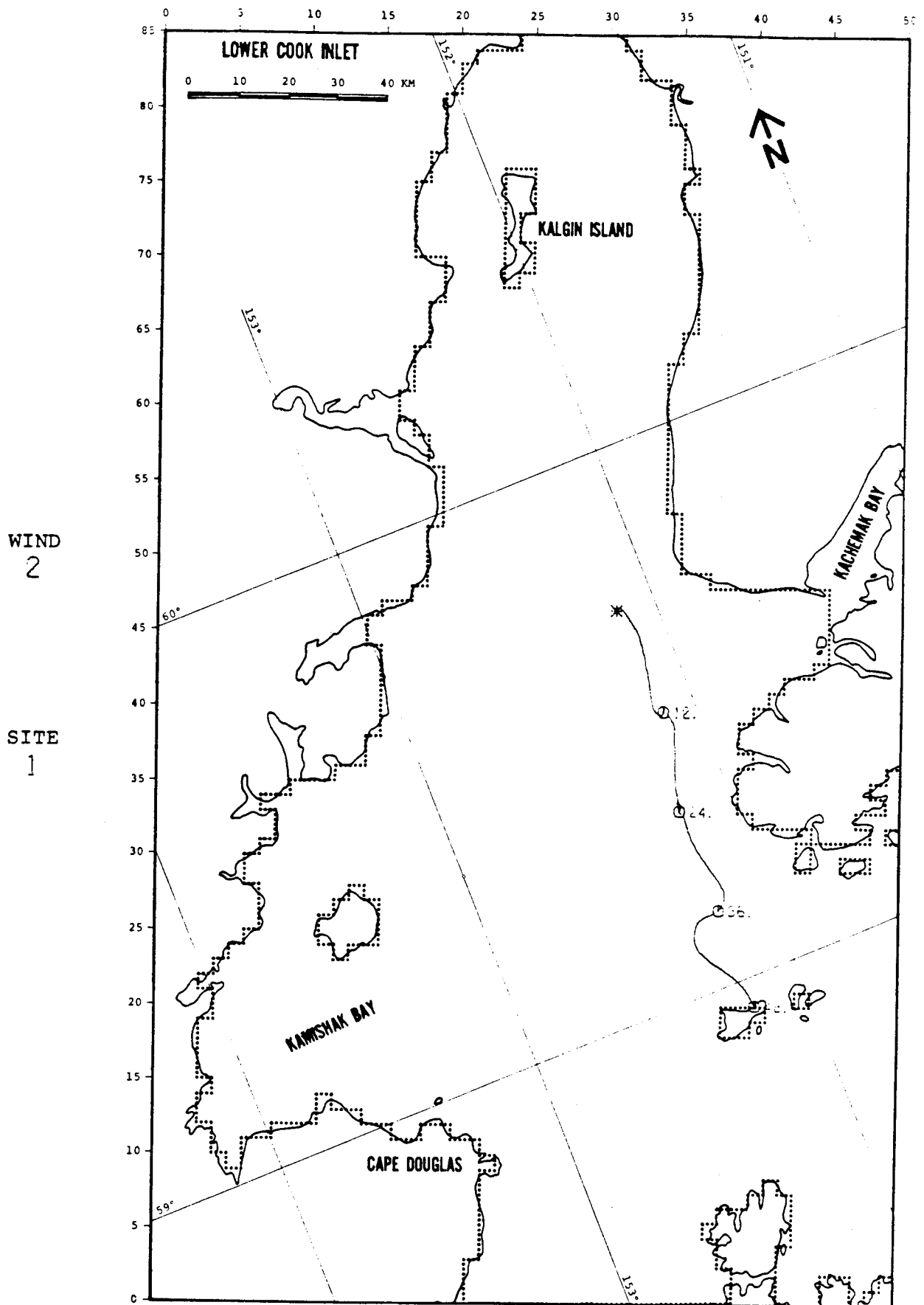


FIGURE C-12: PERTURBATION CASE: WIND -25%

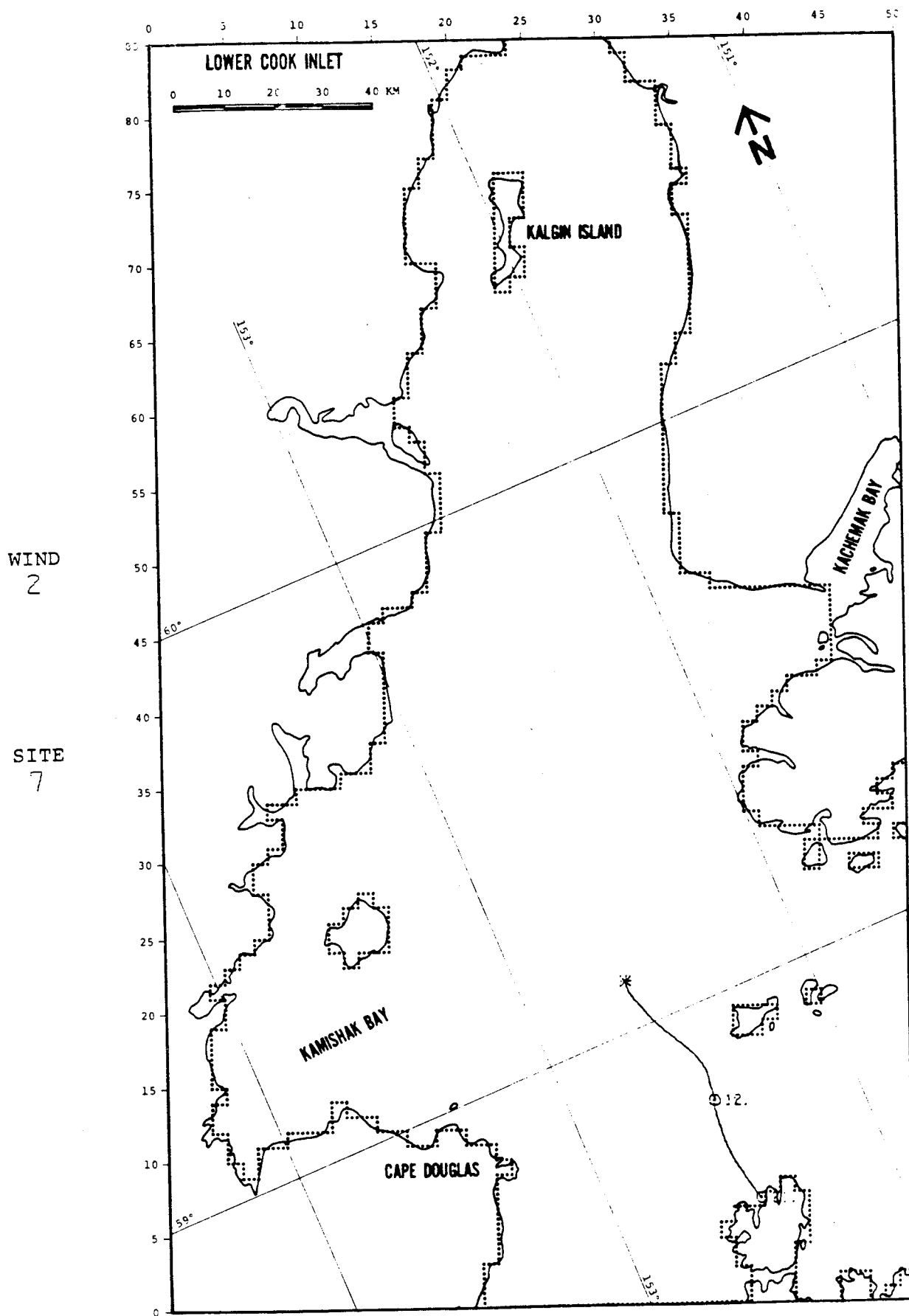


FIGURE C-13: PERTURBATION CASE: NET +25%

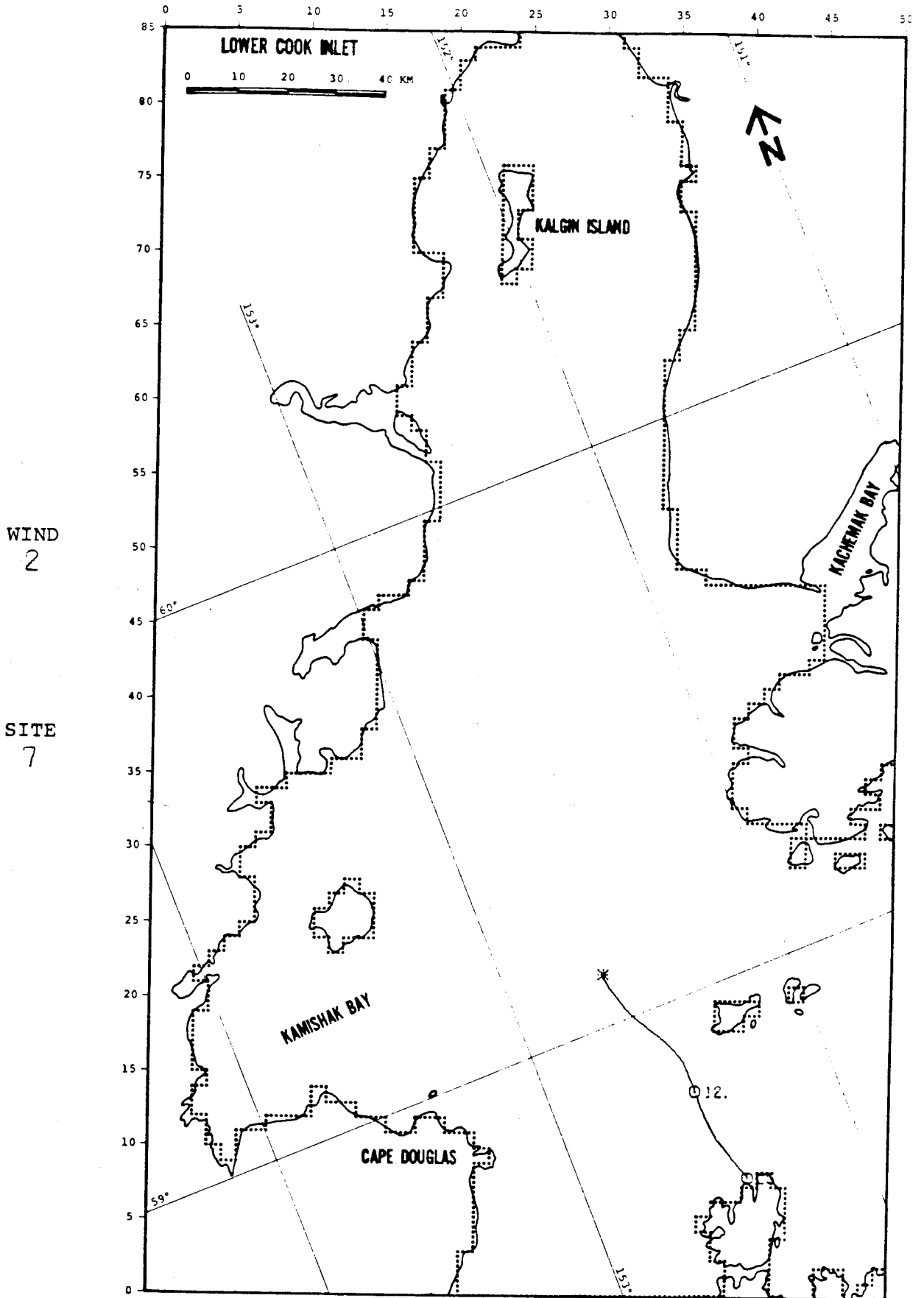


FIGURE C-14: PERTURBATION CASE: NET -25%

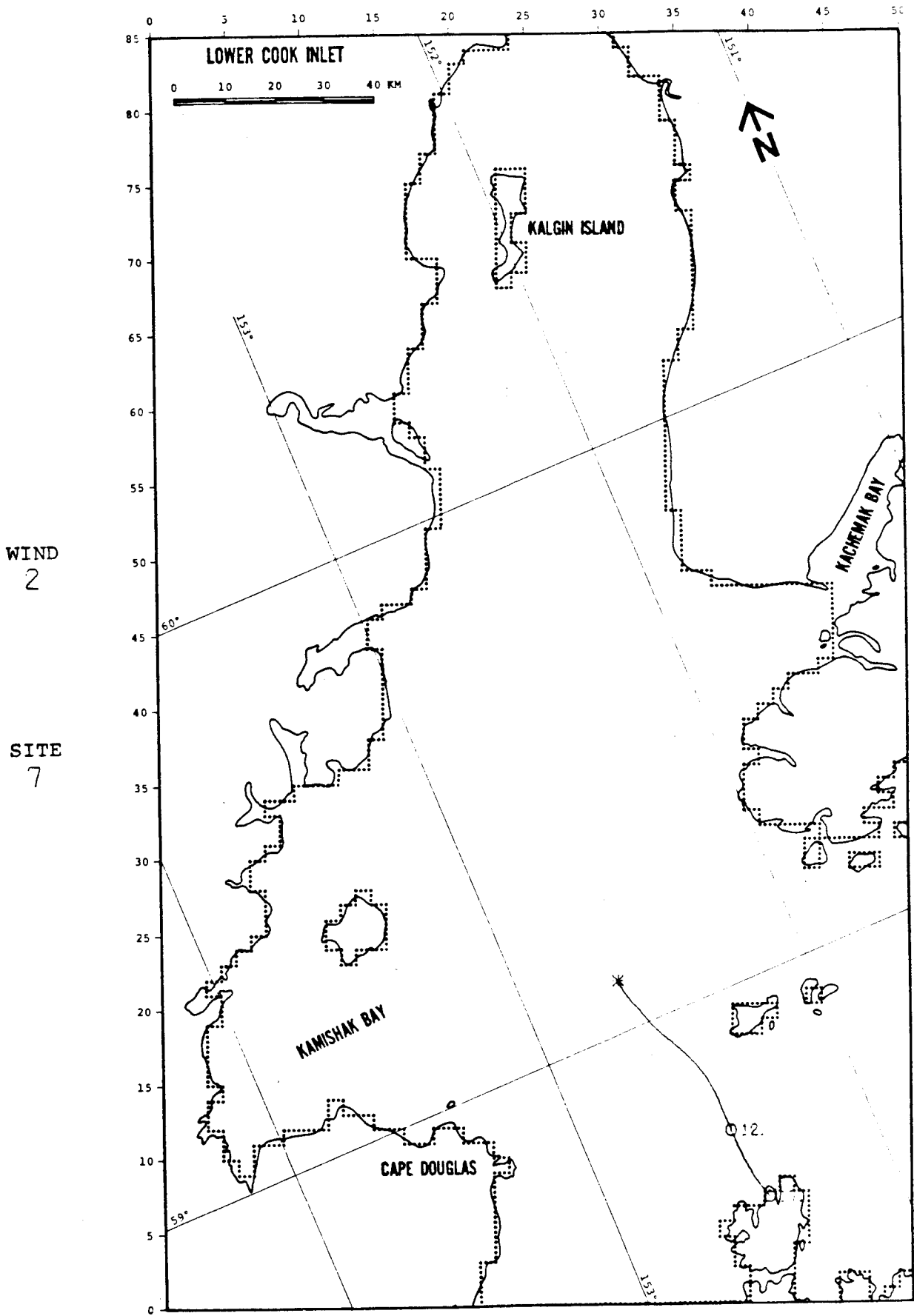


FIGURE C-15: PERTURBATION CASE: WIND +25%

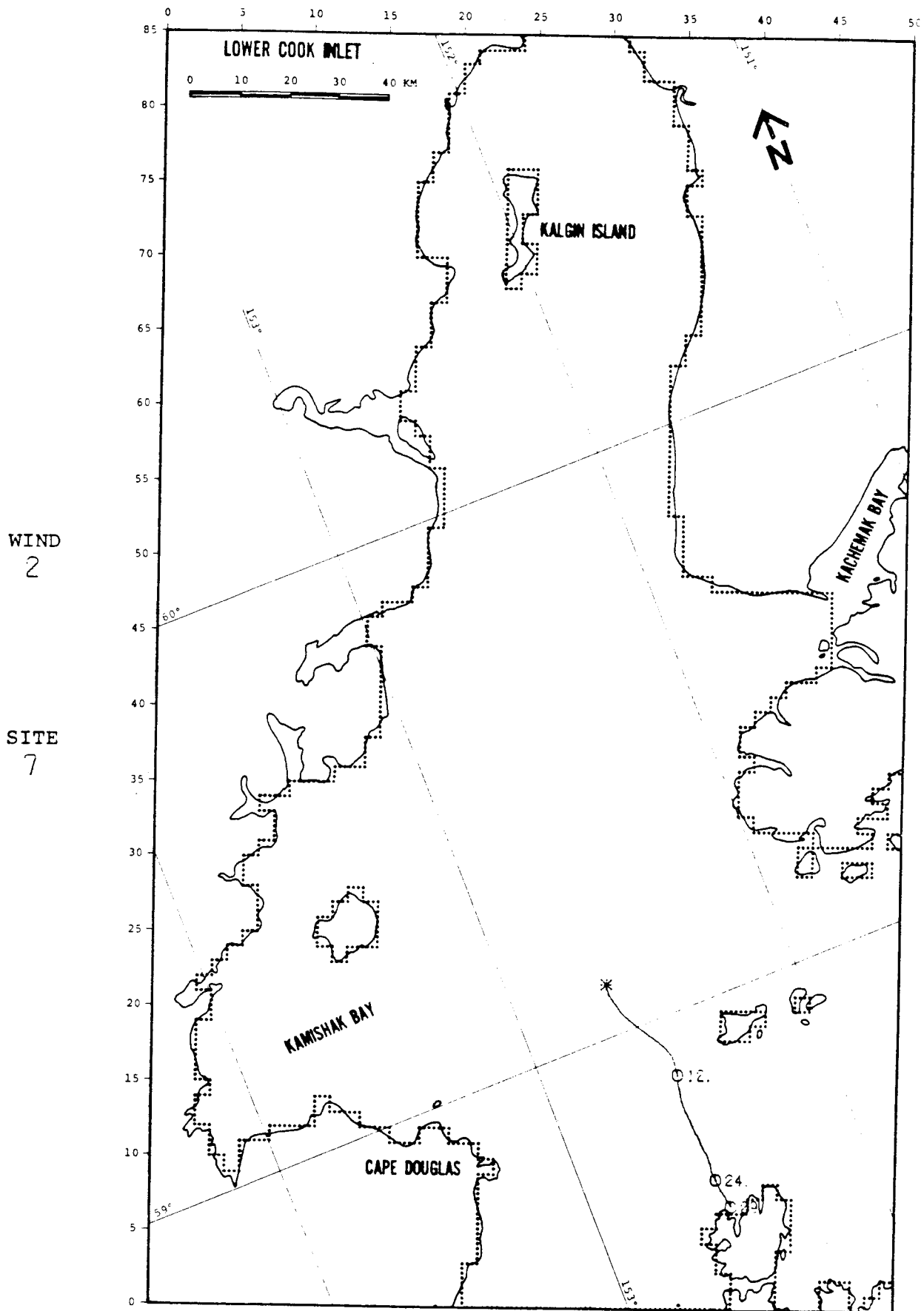


FIGURE C-16: PERTURBATION CASE: WIND -25%

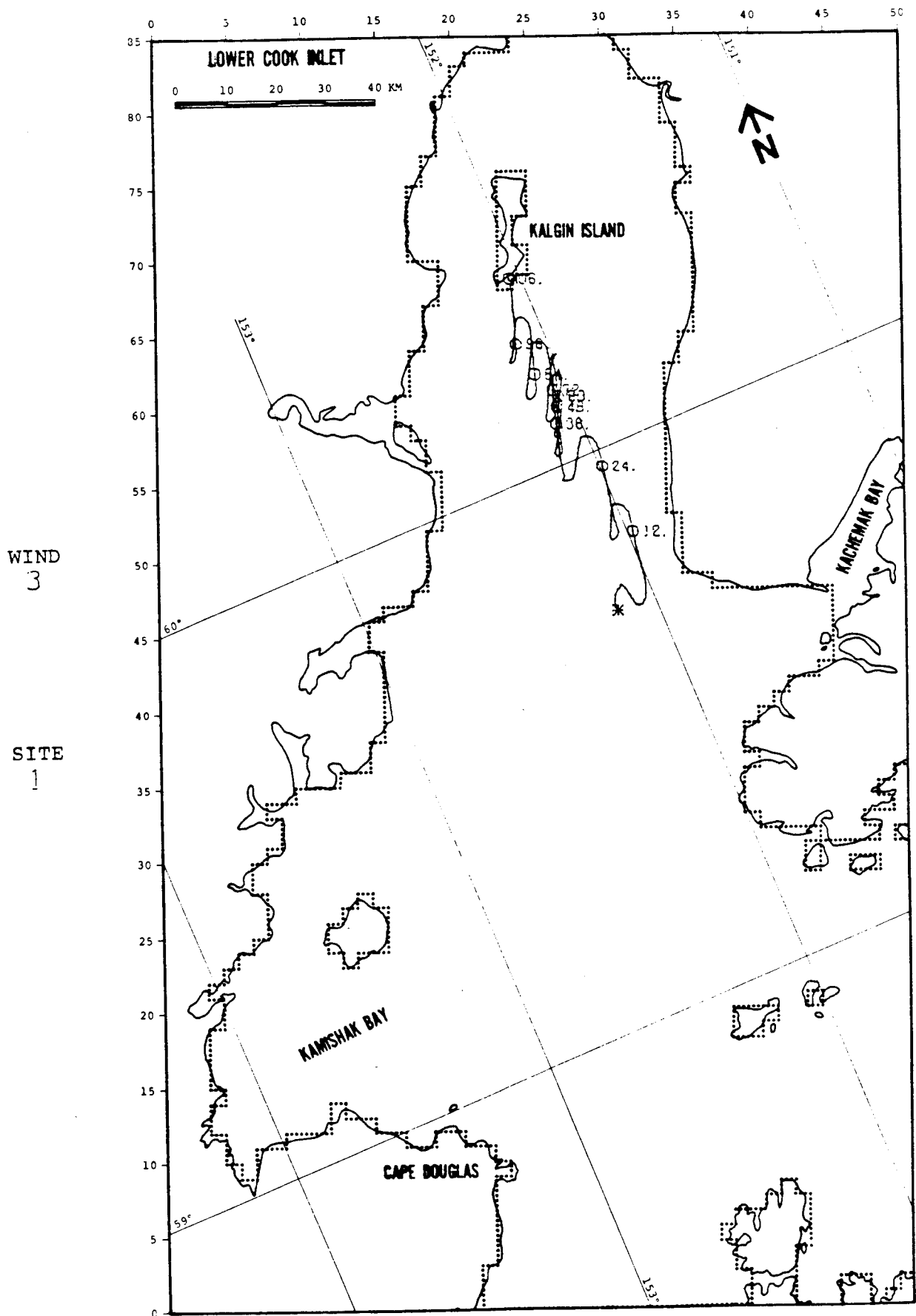


FIGURE C-17: PERTURBATION CASE: NET +25%

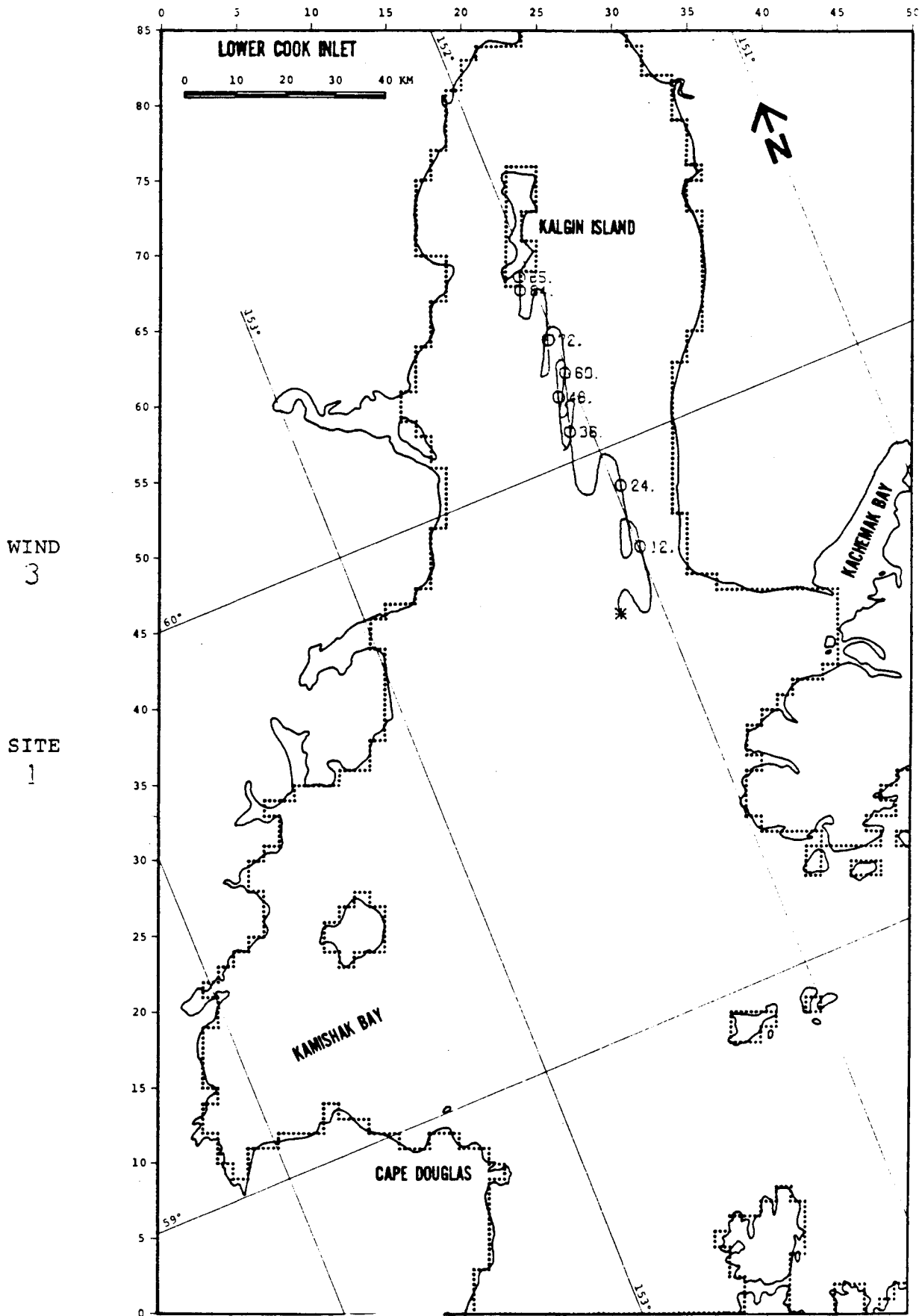


FIGURE C-18: PERTURBATION CASE: NET -25%

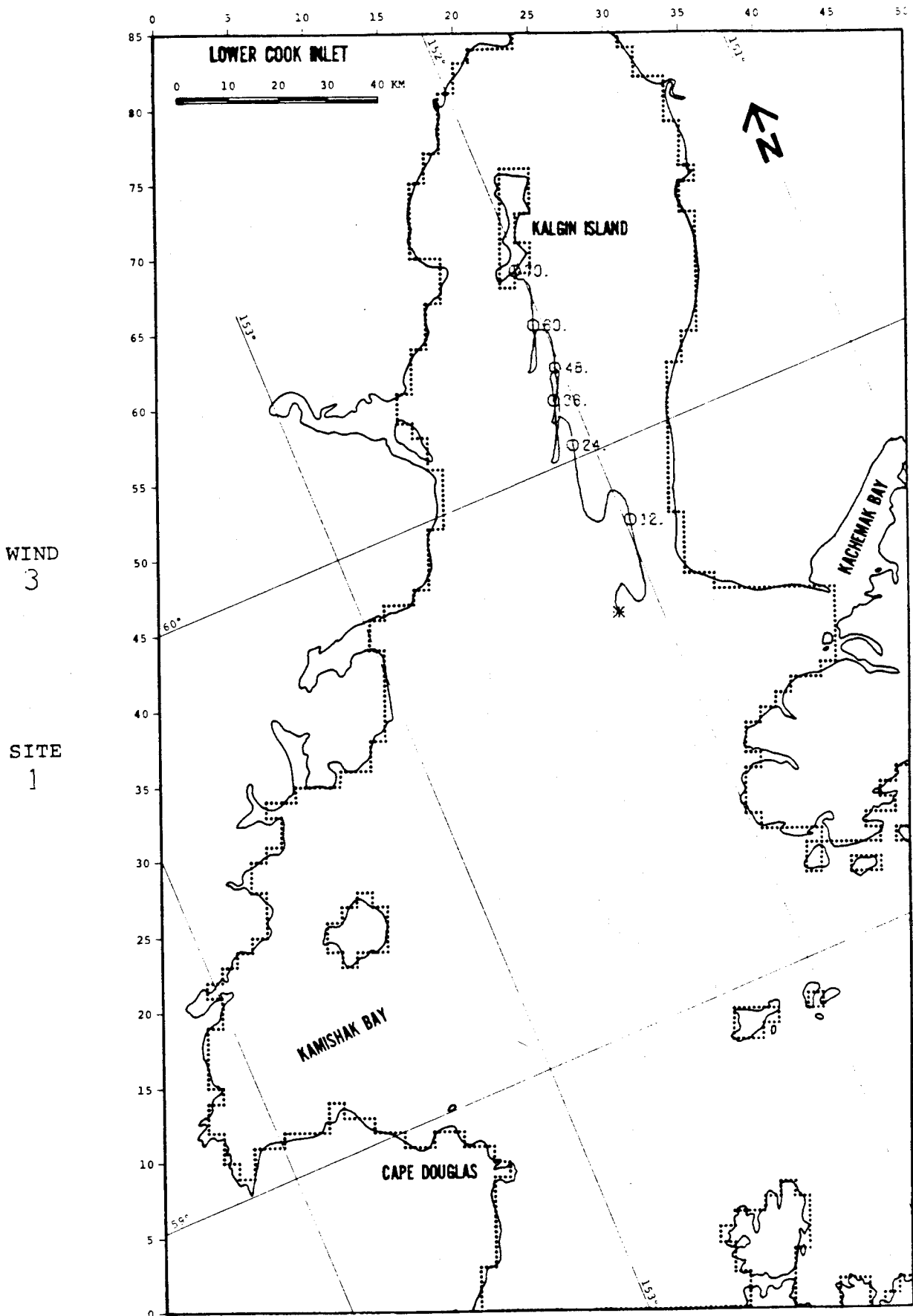


FIGURE C-19: PERTURBATION CASE: WIND +25%

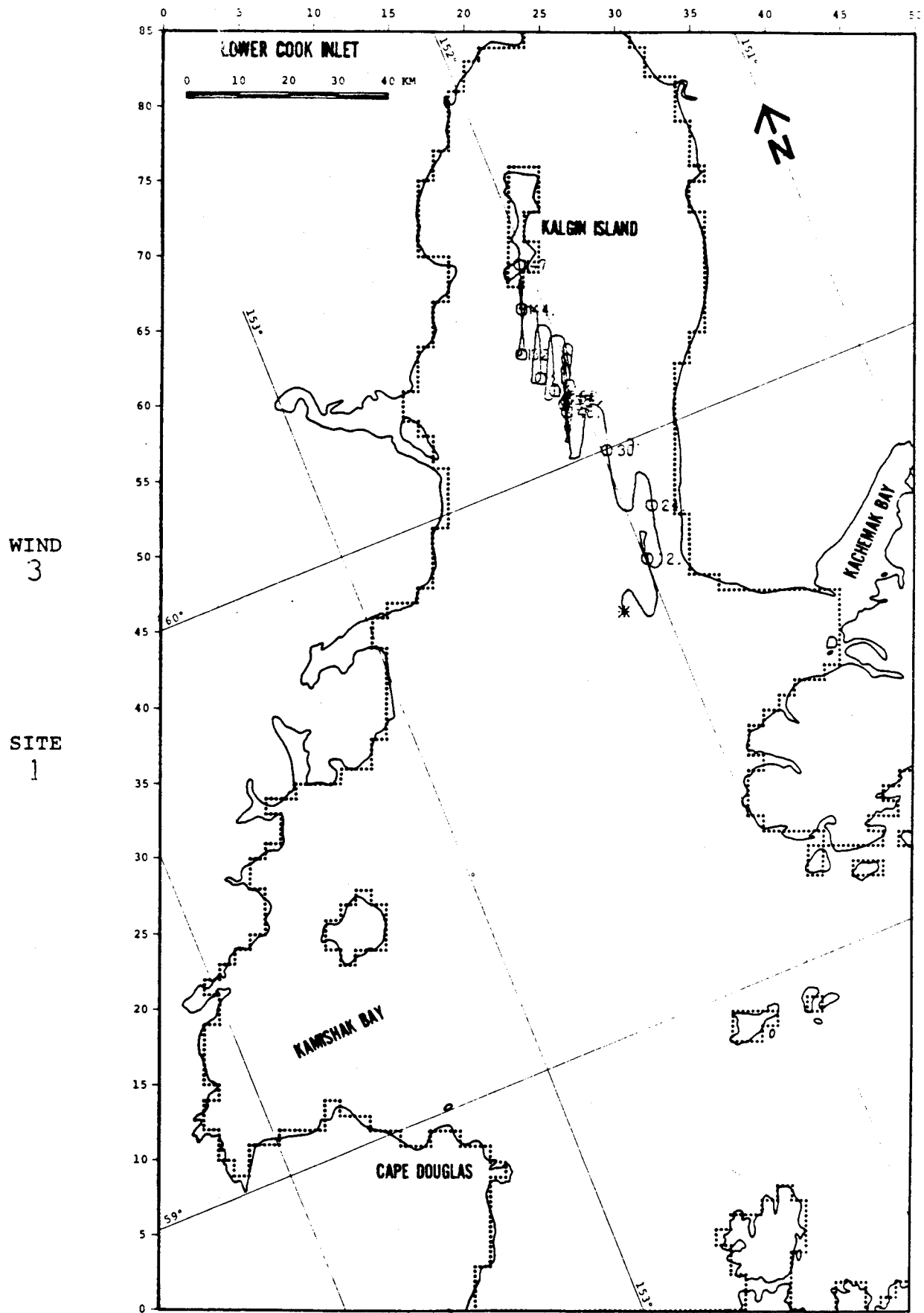


FIGURE C-20: PERTURBATION CASE: WIND -25%

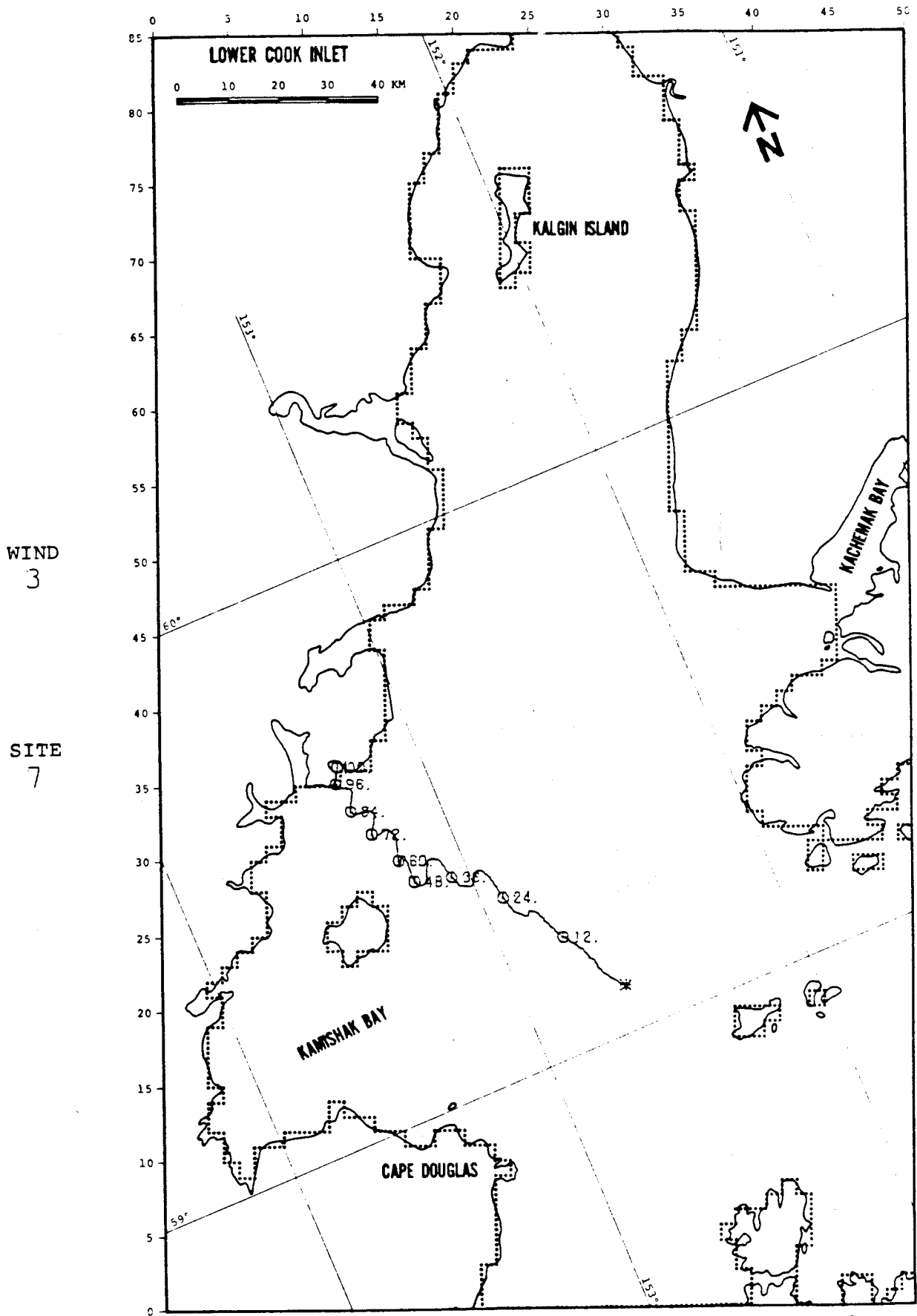


FIGURE C-21: PERTURBATION CASE: NET +25%

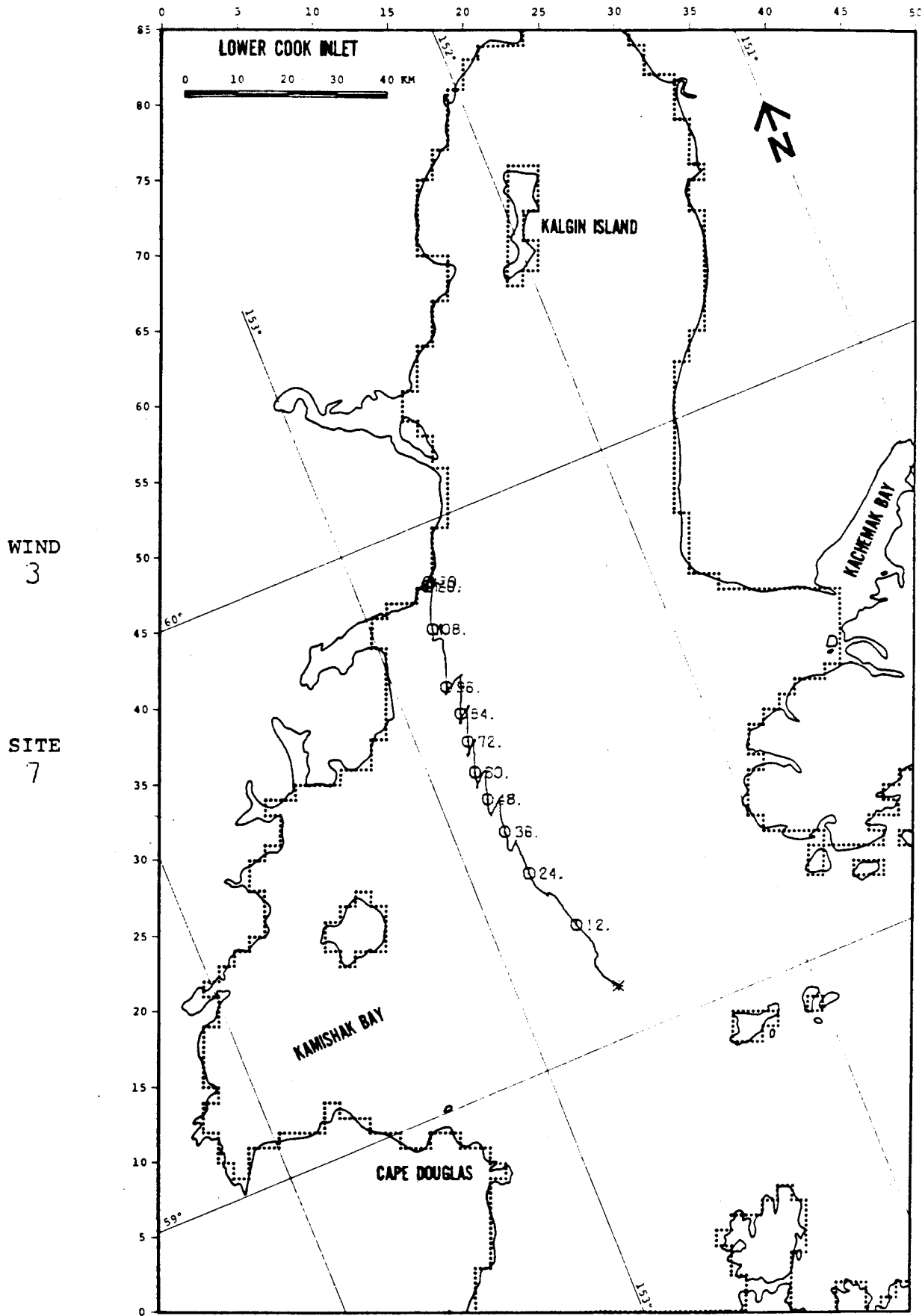


FIGURE C-22: PERTURBATION CASE: NET -25%

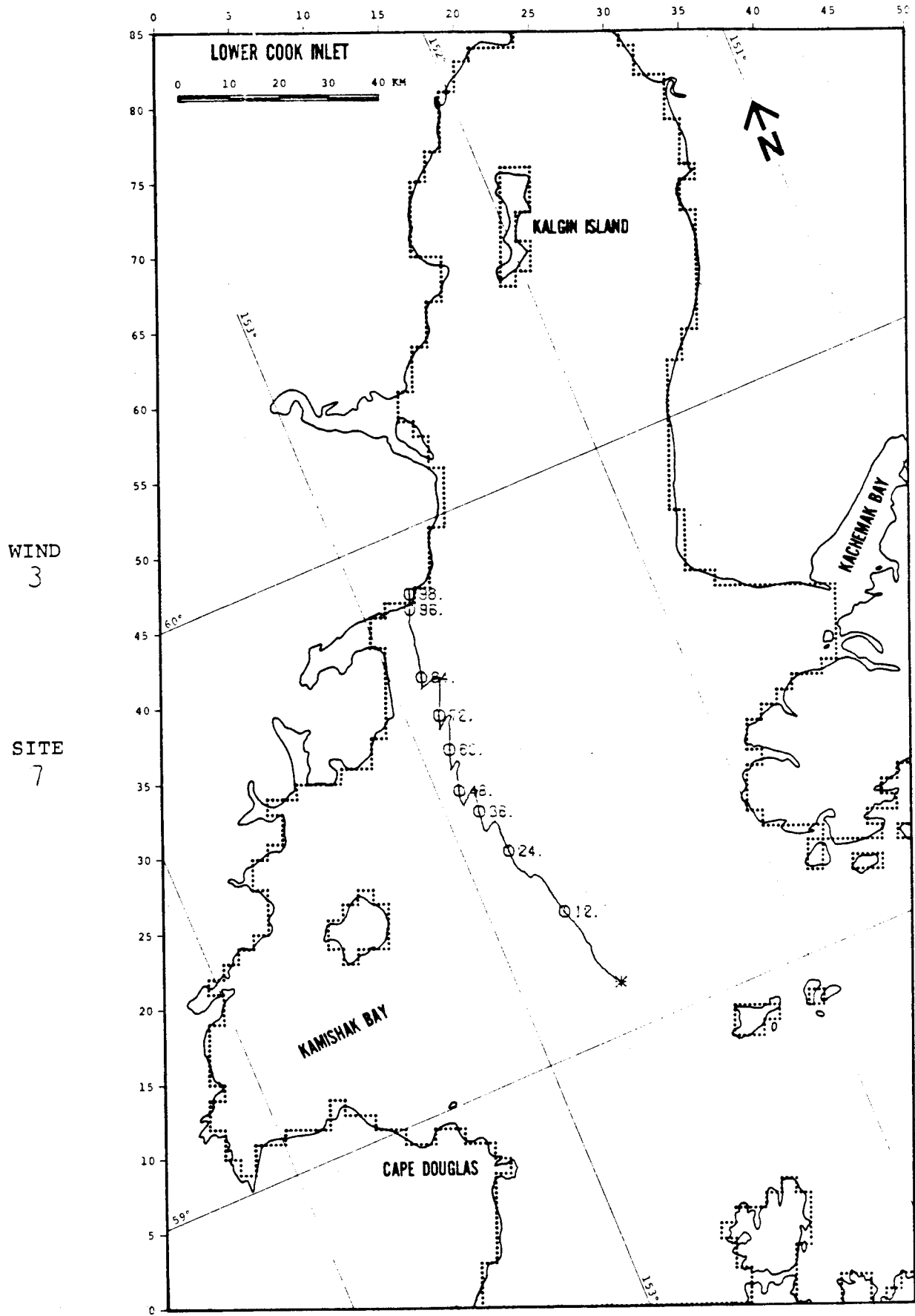


FIGURE C-23: PERTURBATION CASE: WIND +25%

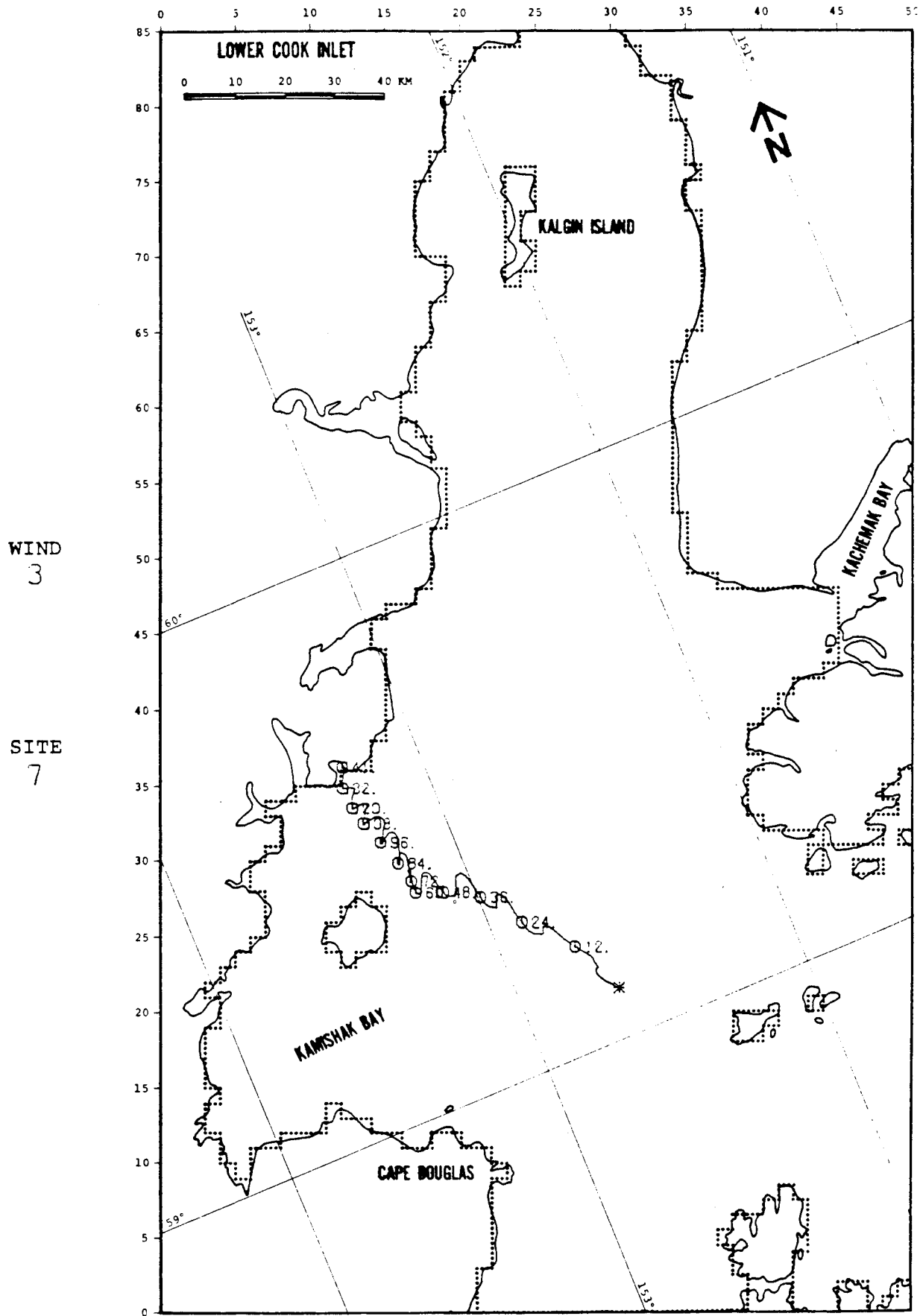


FIGURE C-24: PERTURBATION CASE: WIND -25%

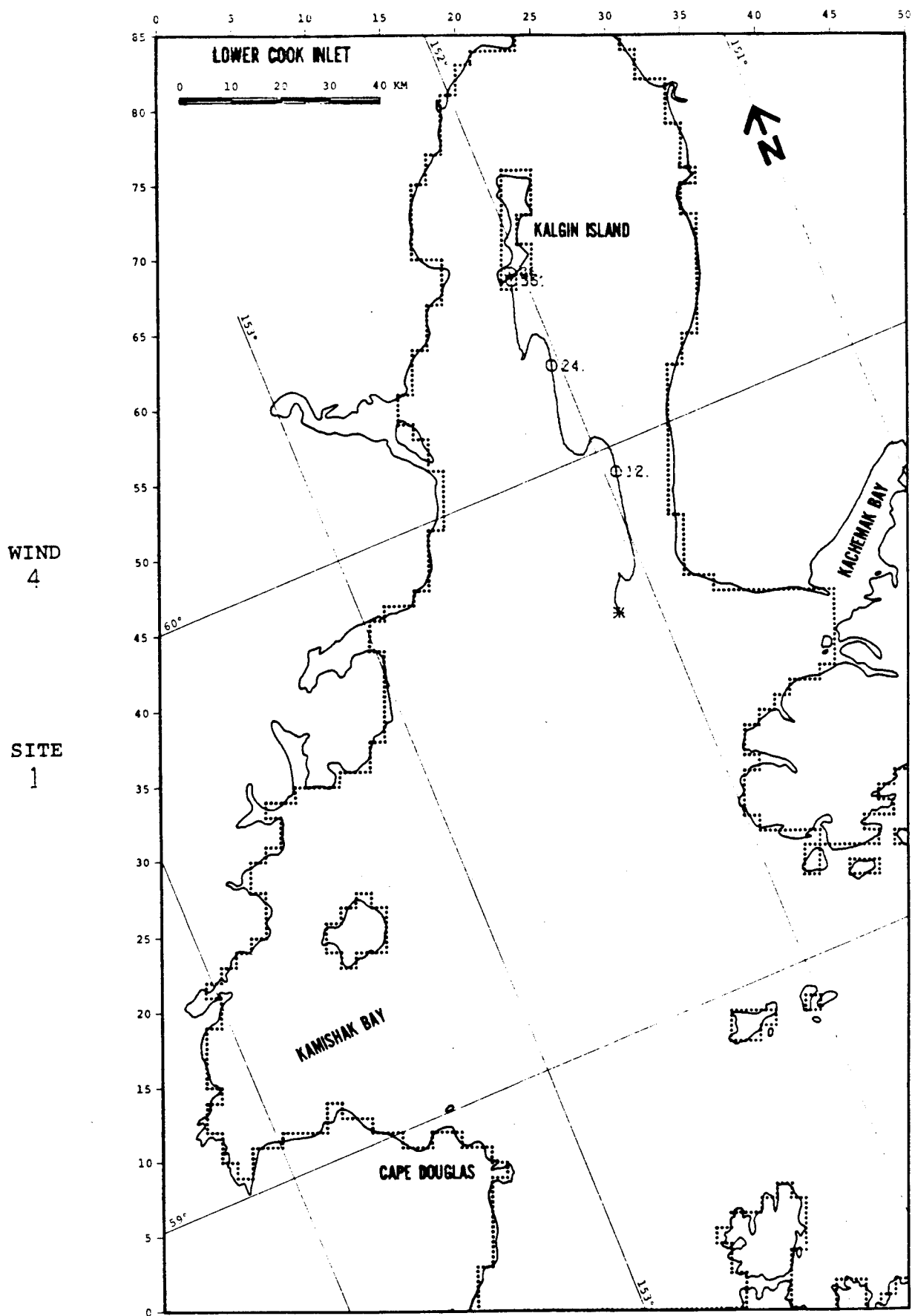


FIGURE C-25: PERTURBATION CASE: NET +25%

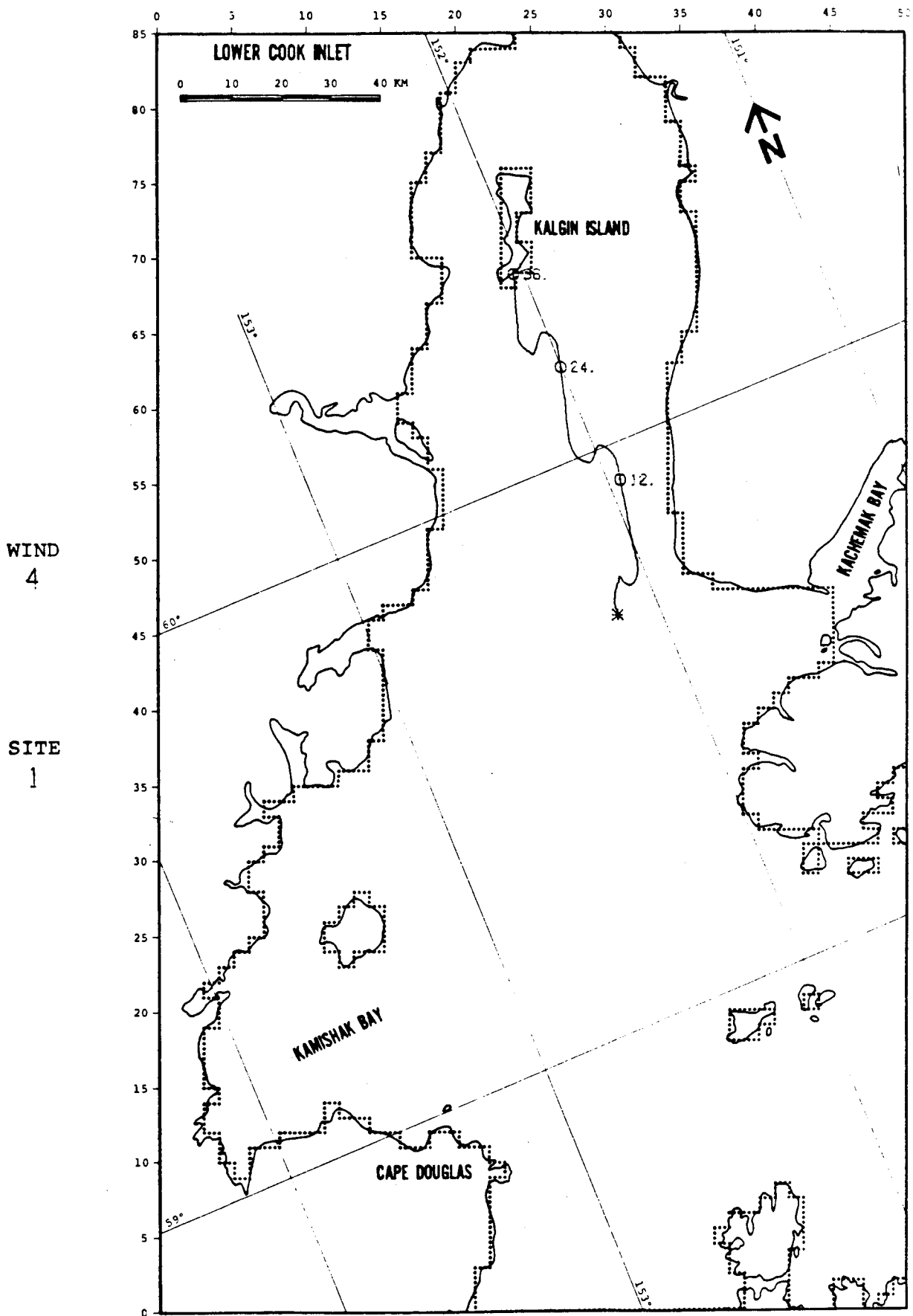


FIGURE C-26: PERTURBATION CASE: NET -25%

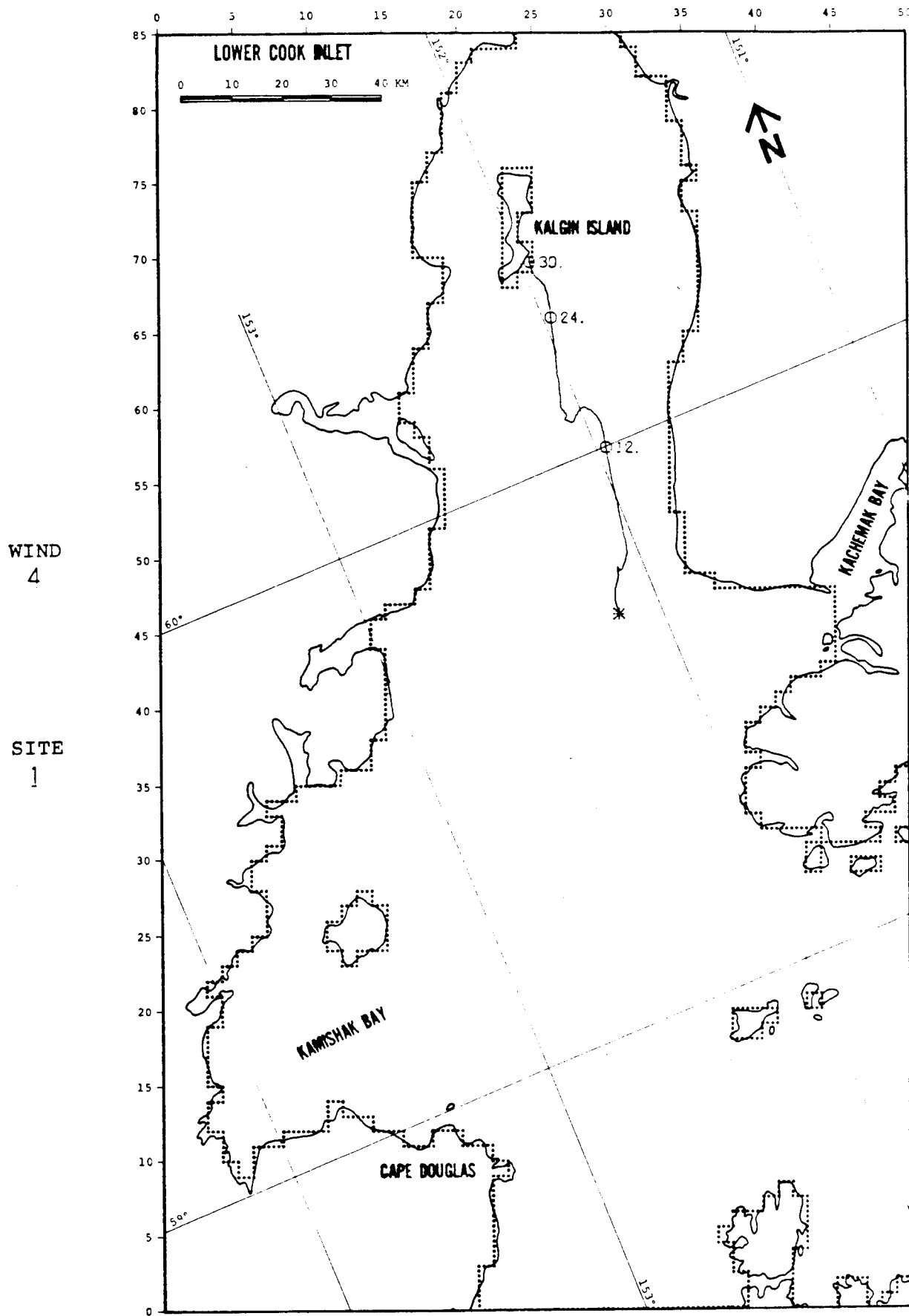


FIGURE C-27: PERTURBATION CASE: WIND +25%

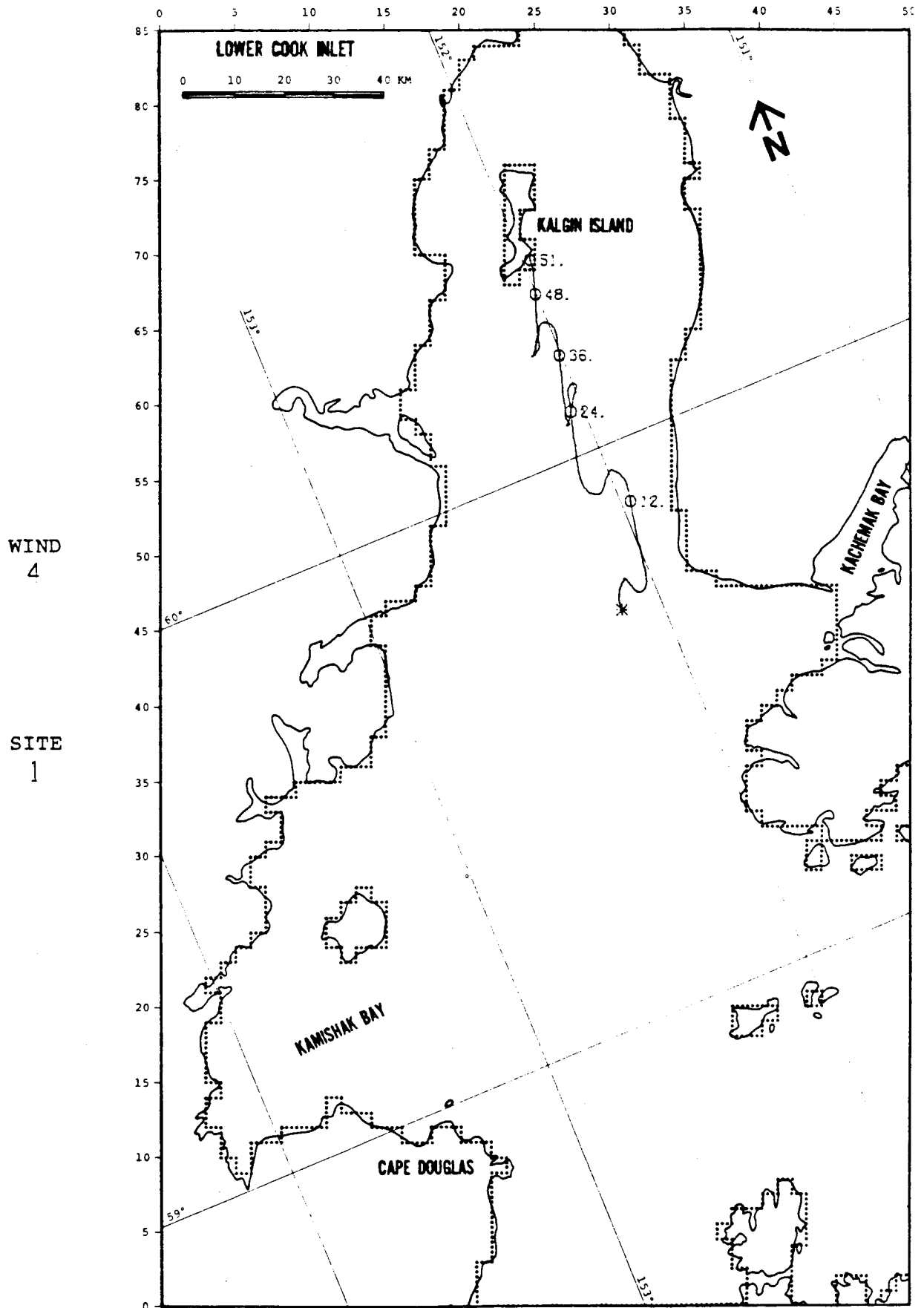


FIGURE C-28: PERTURBATION CASE: WIND -25%

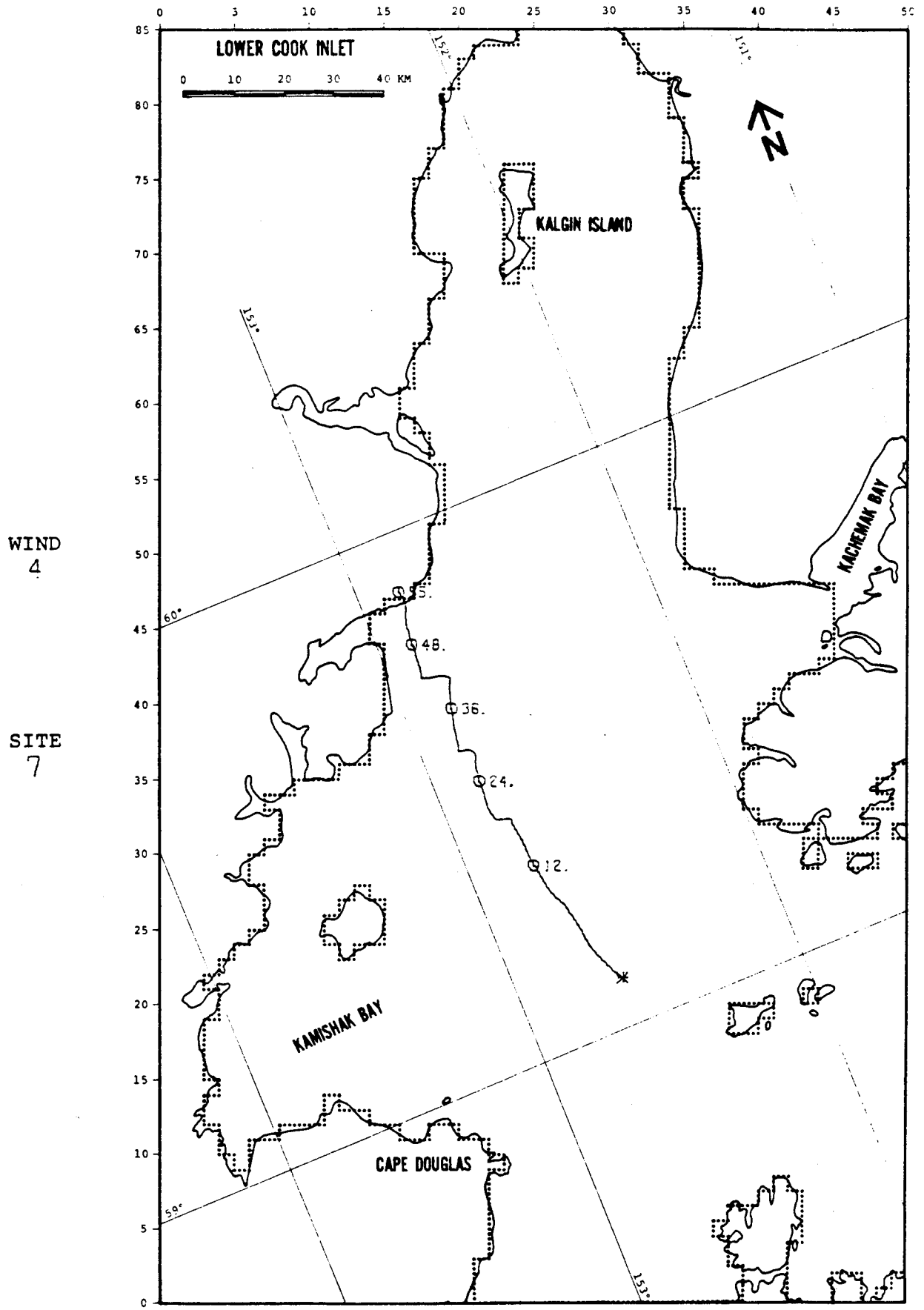


FIGURE C-29: PERTURBATION CASE: NET +25%

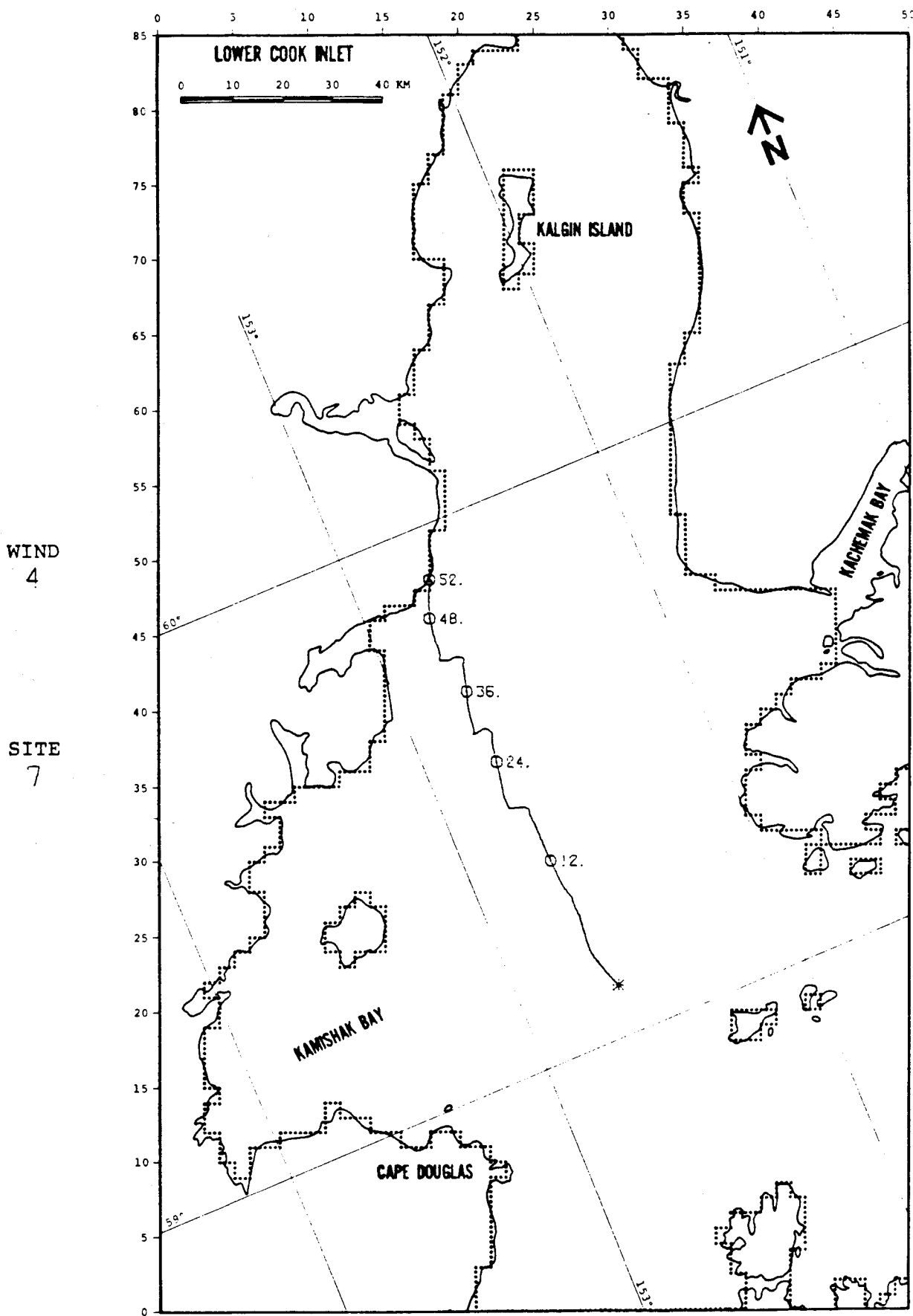


FIGURE C-30: PERTURBATION CASE: NET -25%

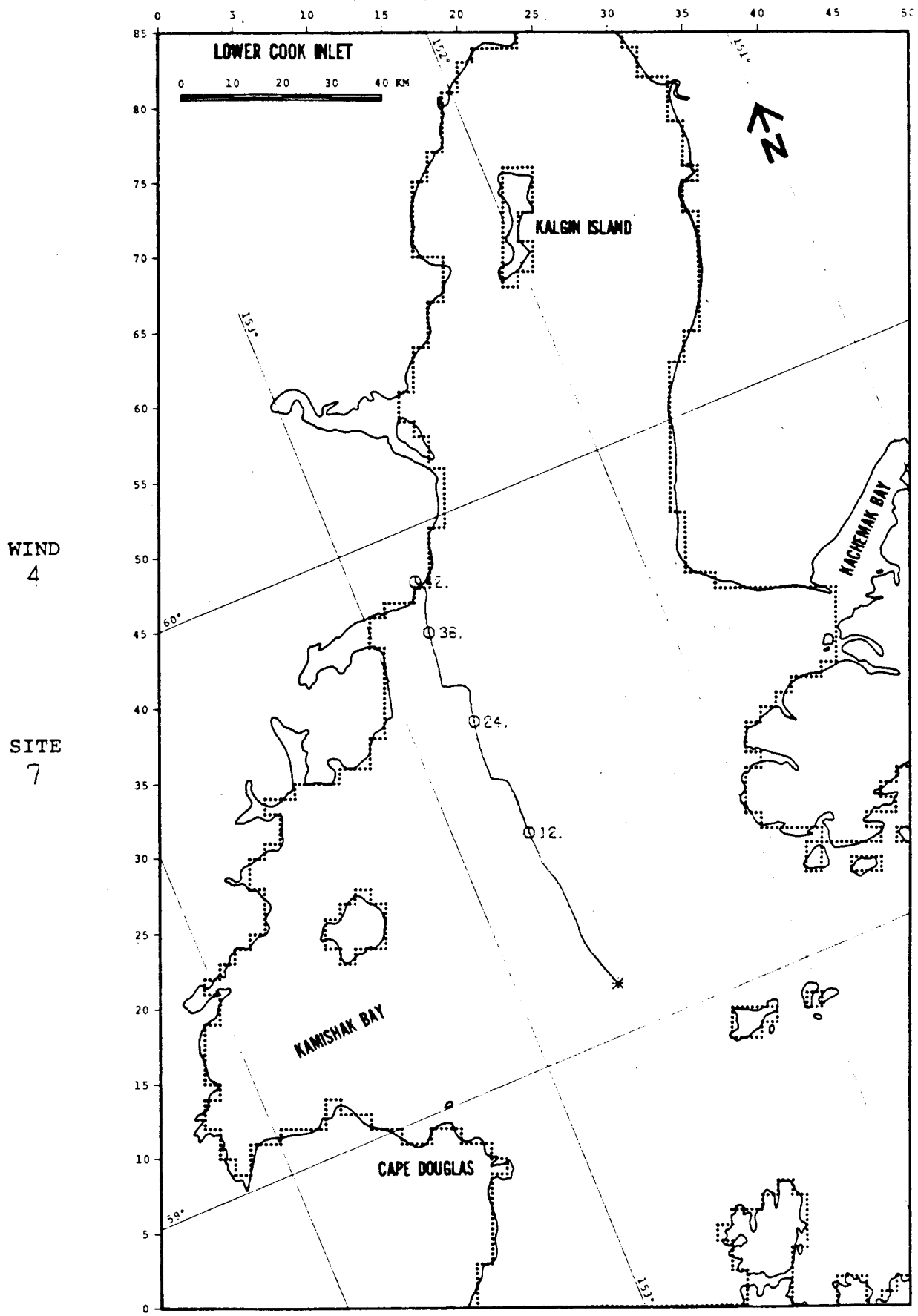


FIGURE C-31: PERTURBATION CASE: WIND +25%

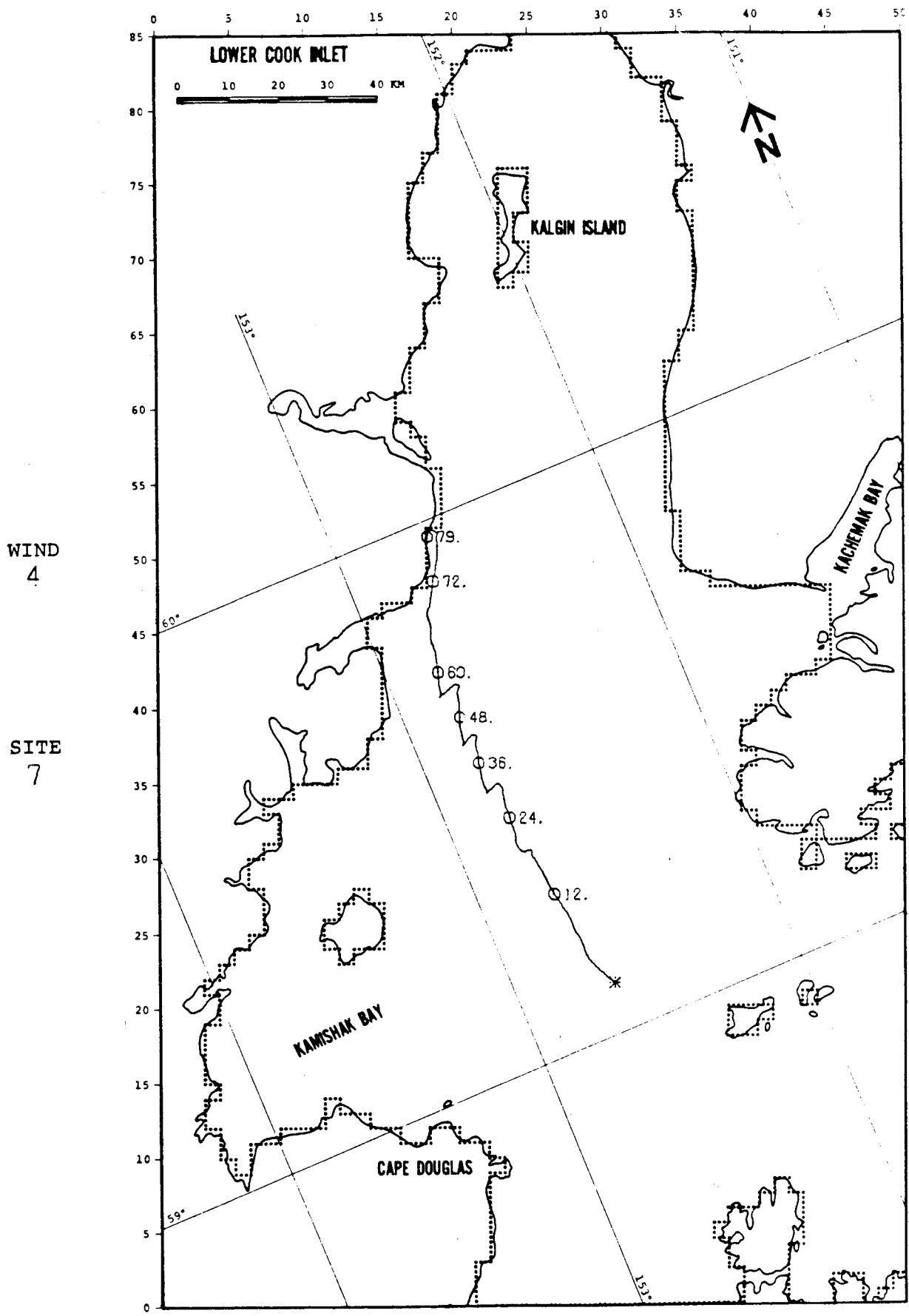


FIGURE C-32: PERTURBATION CASE: WIND -25%

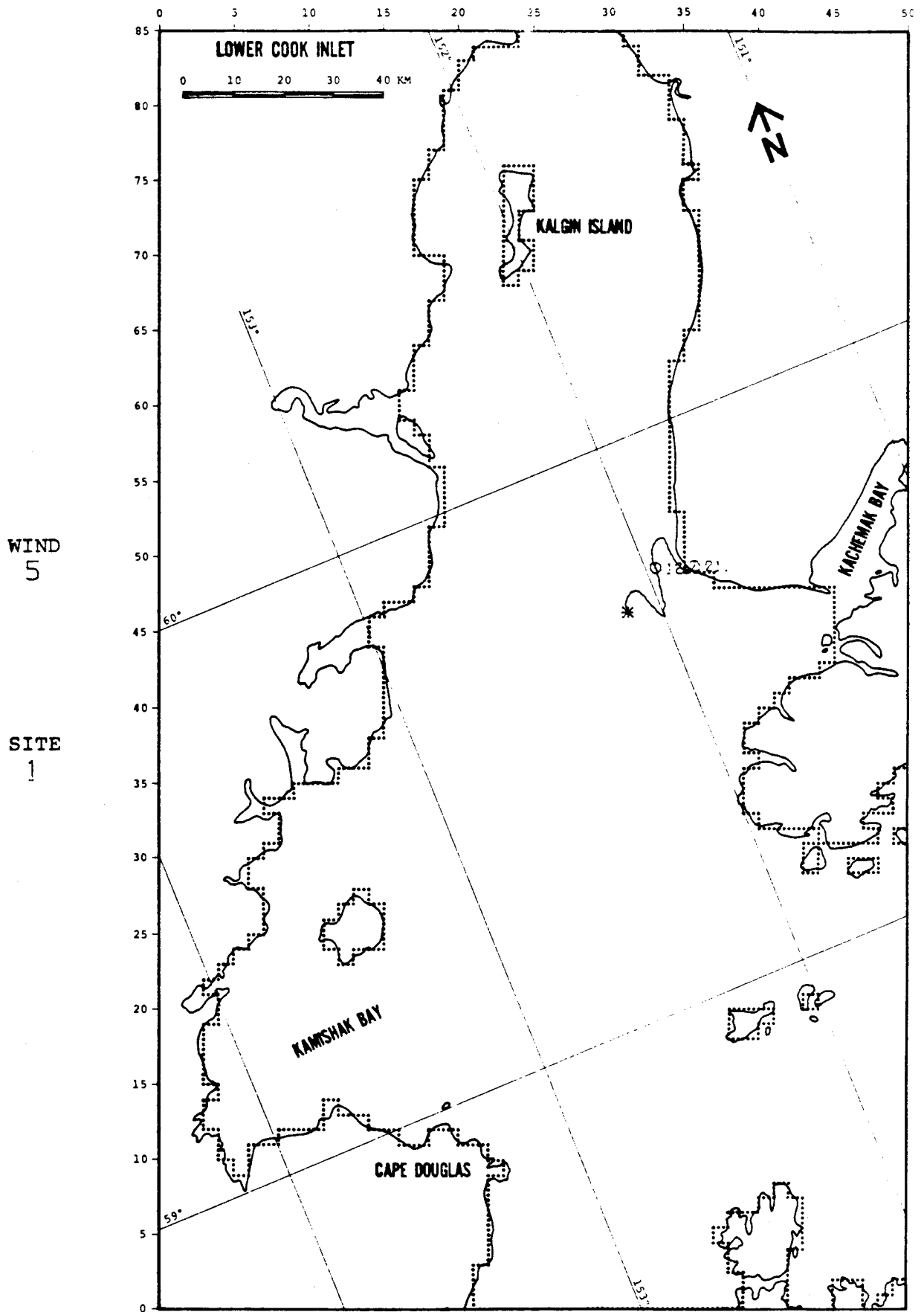


FIGURE C-33: PERTURBATION CASE: NET +25%

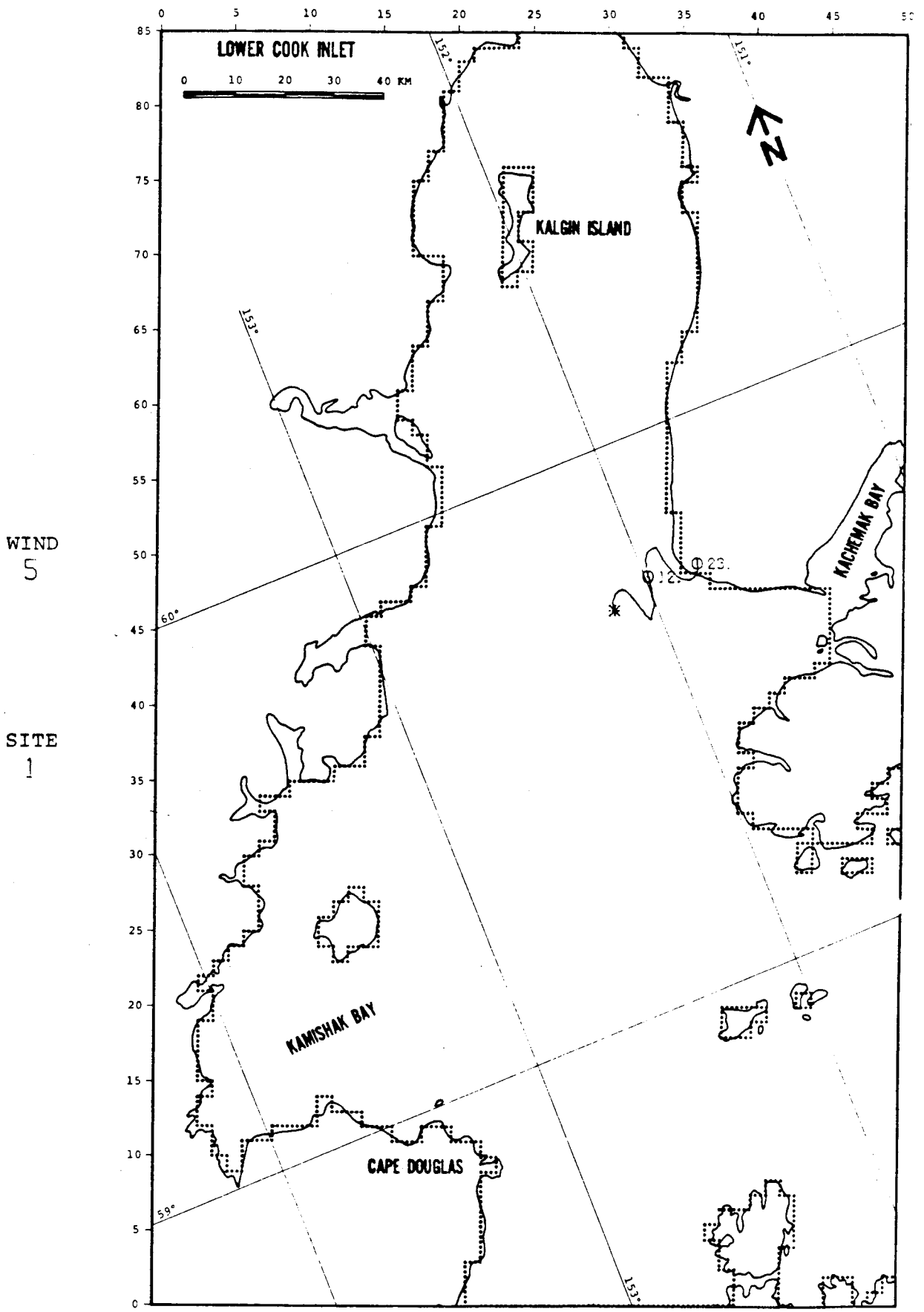


FIGURE C-34: PERTURBATION CASE: NET -25%

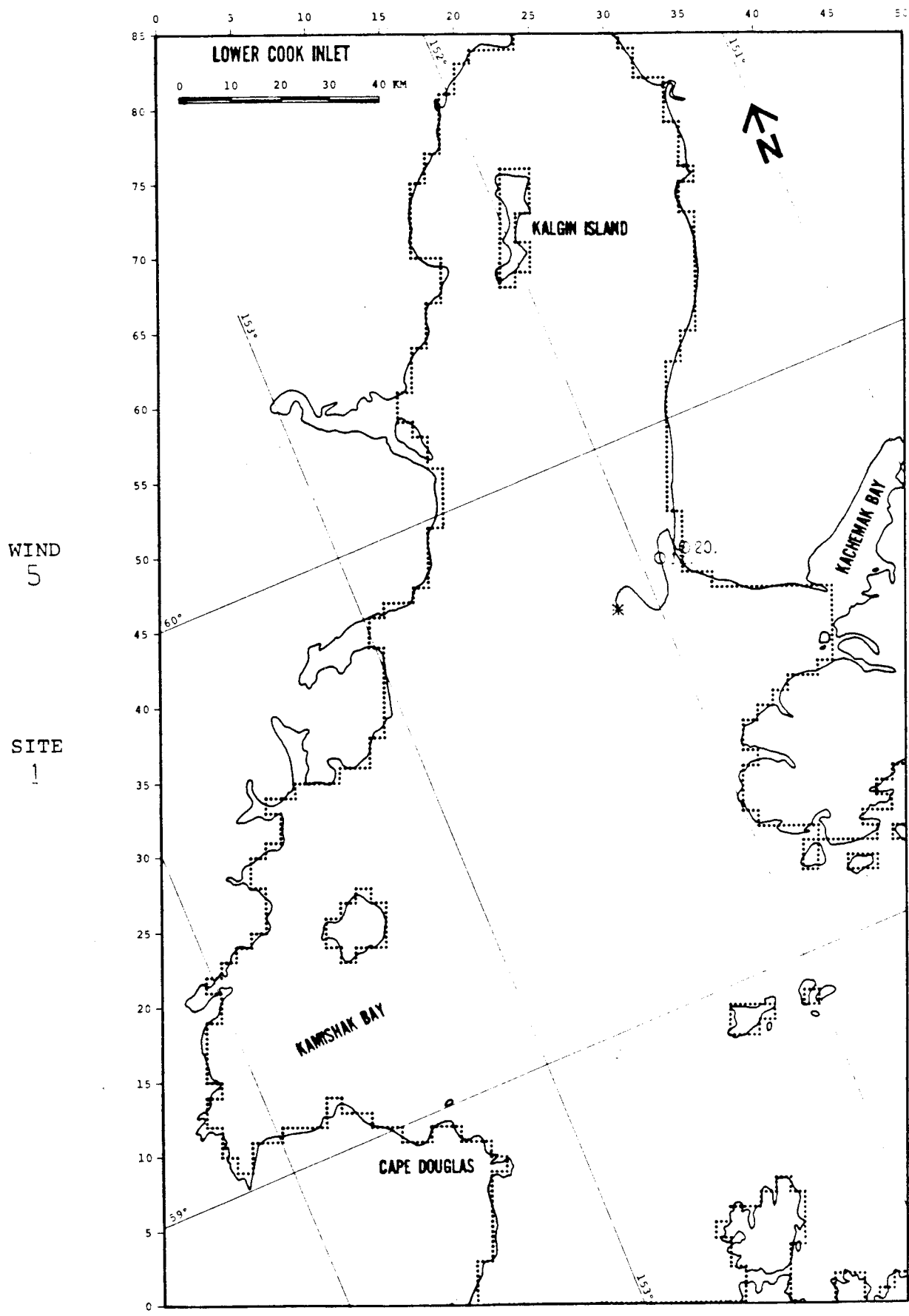


FIGURE C-35: PERTURBATION CASE: WIND +25%

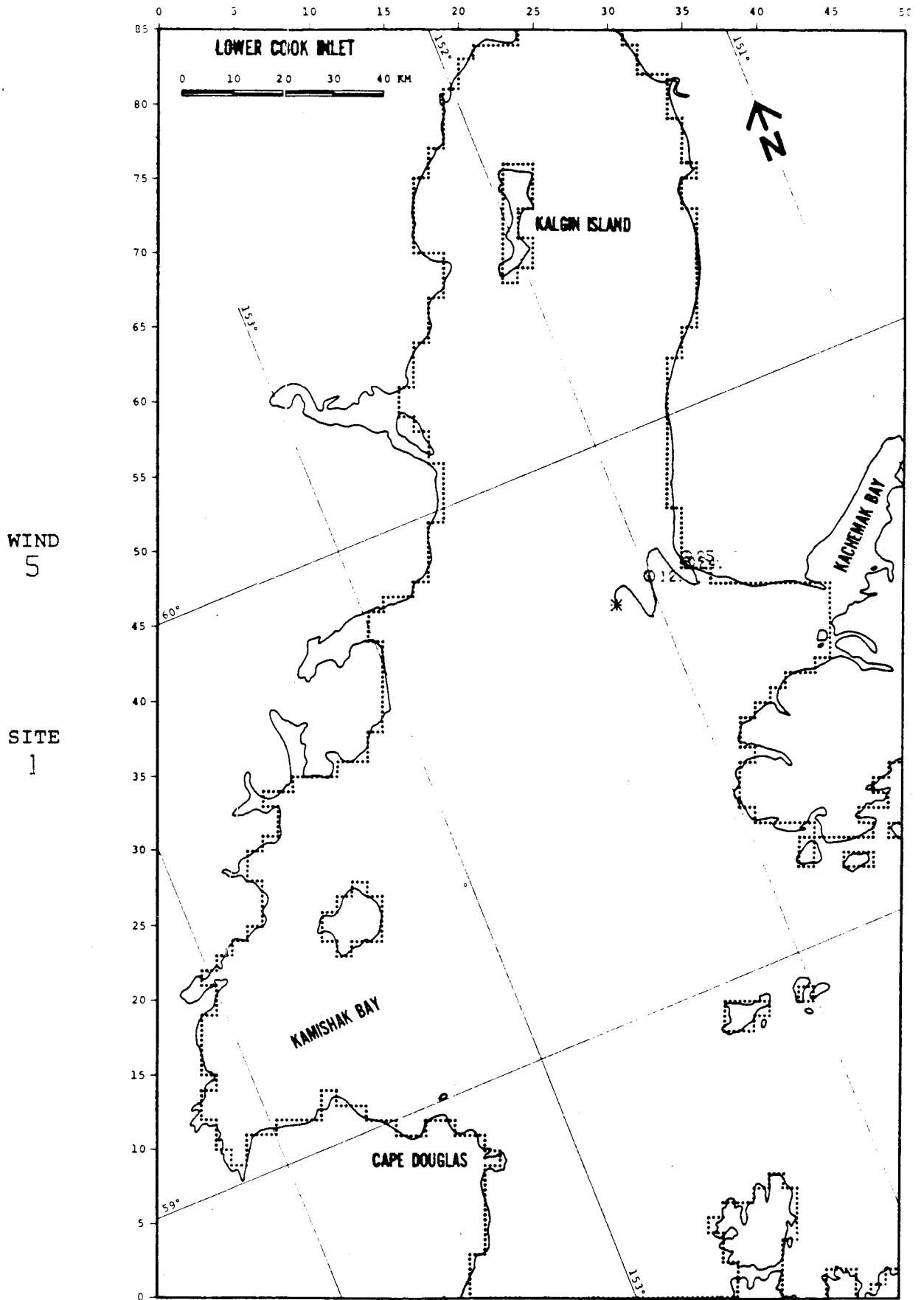


FIGURE C-36: PERTURBATION CASE: WIND -25%

WIND
5

SITE
7

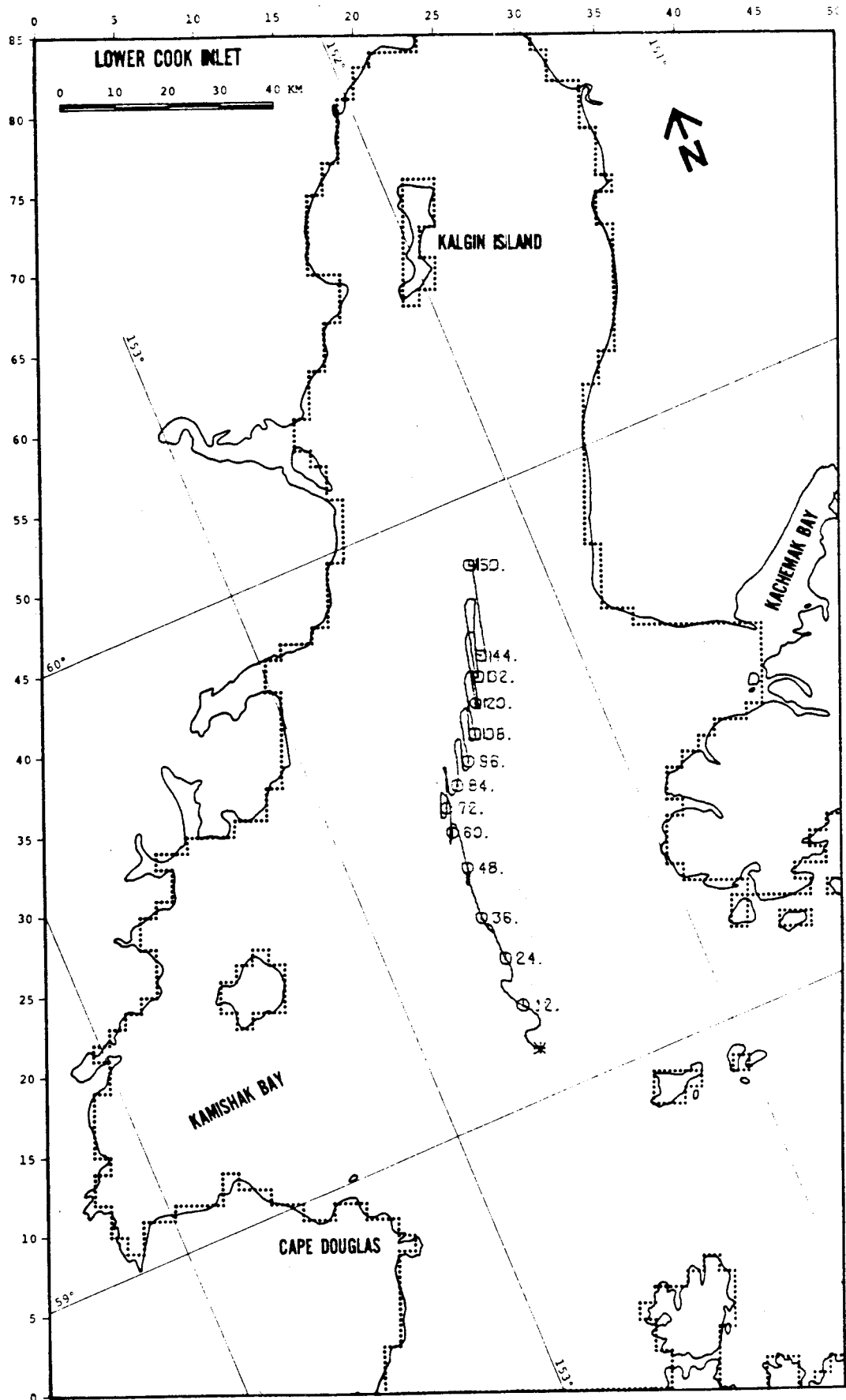


FIGURE C-37 PERTURBATION CASE: NET +25%

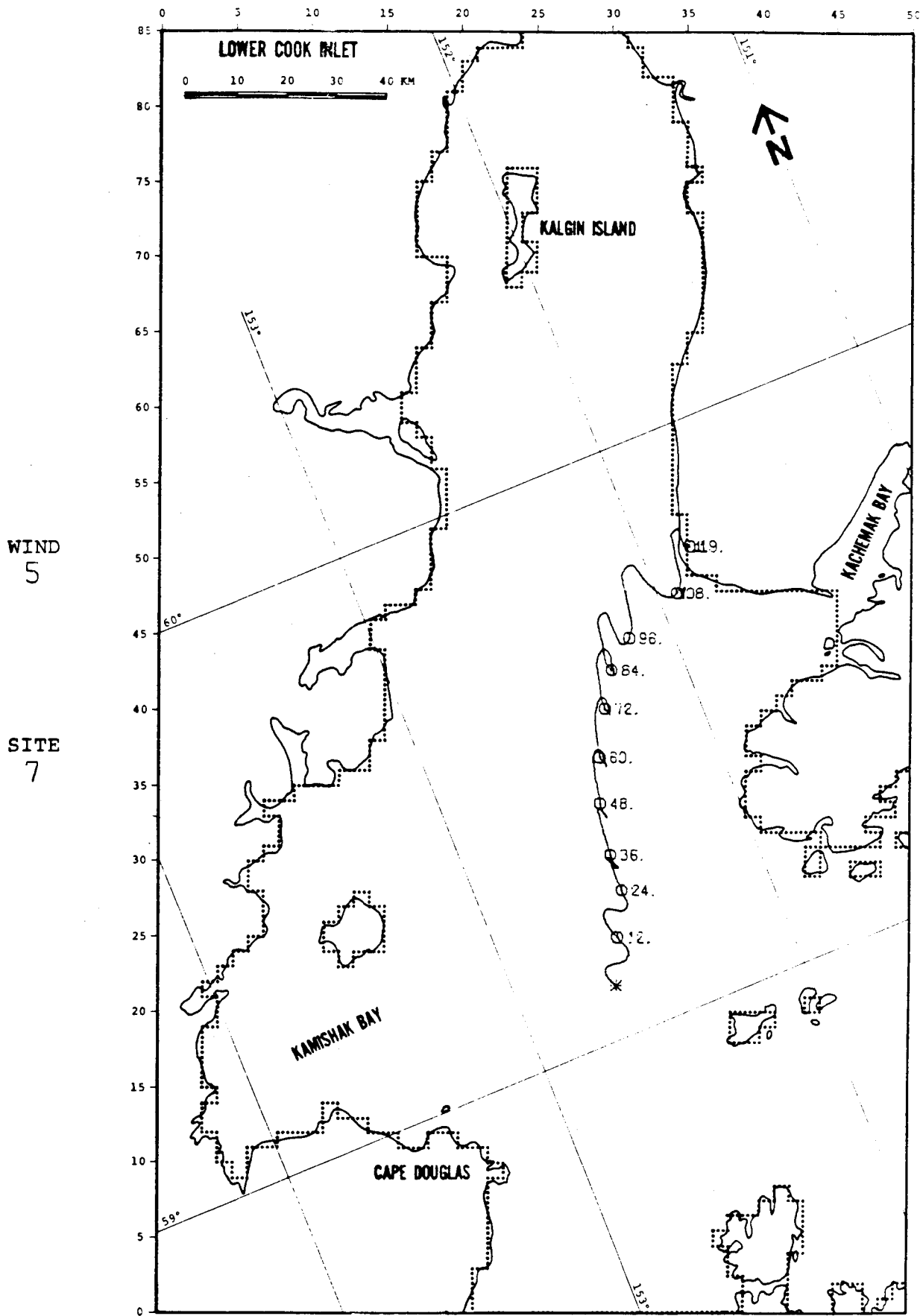


FIGURE C-38: PERTURBATION CASE: NET -25%

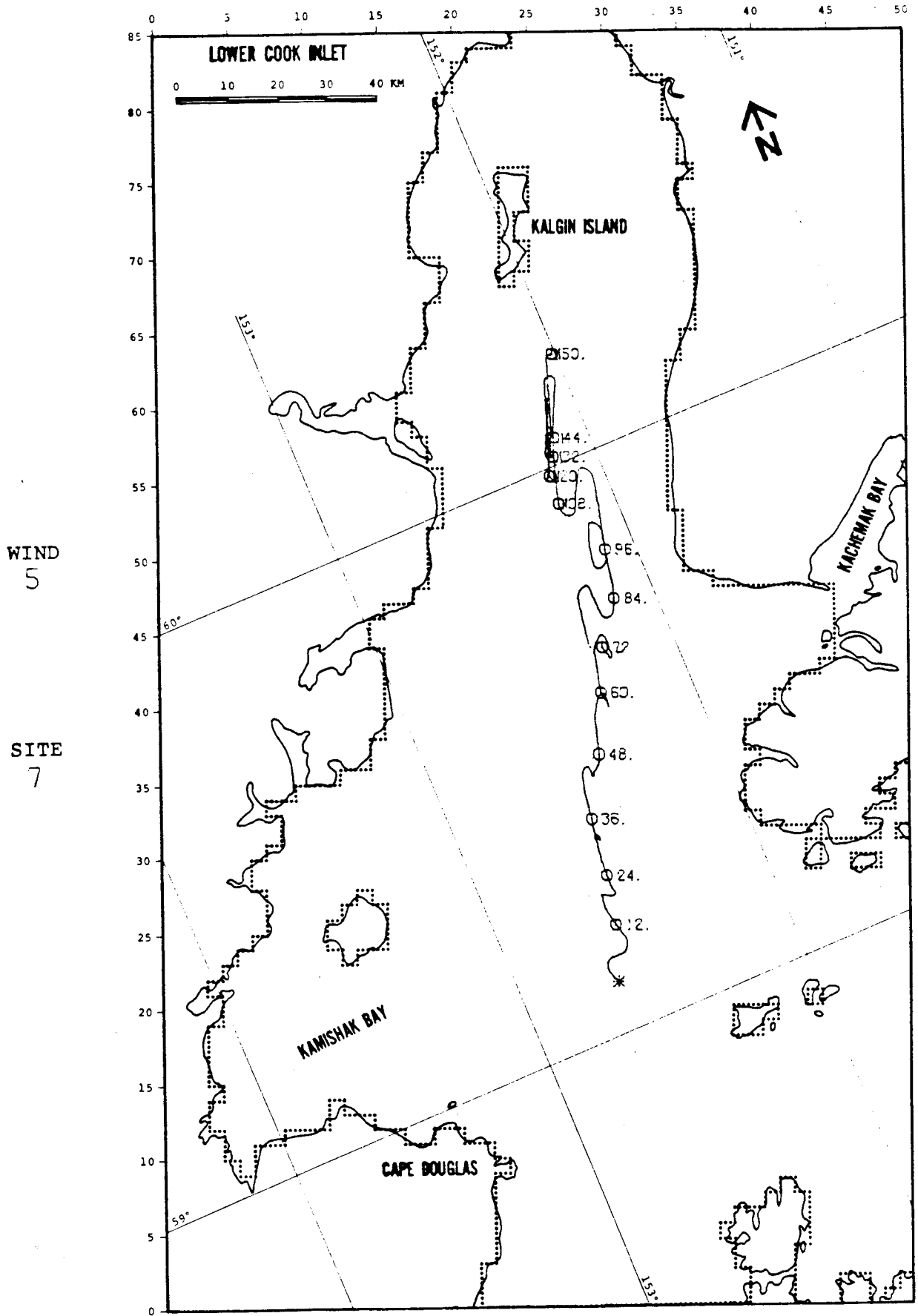


FIGURE C-39: PERTURBATION CASE: WIND +25%

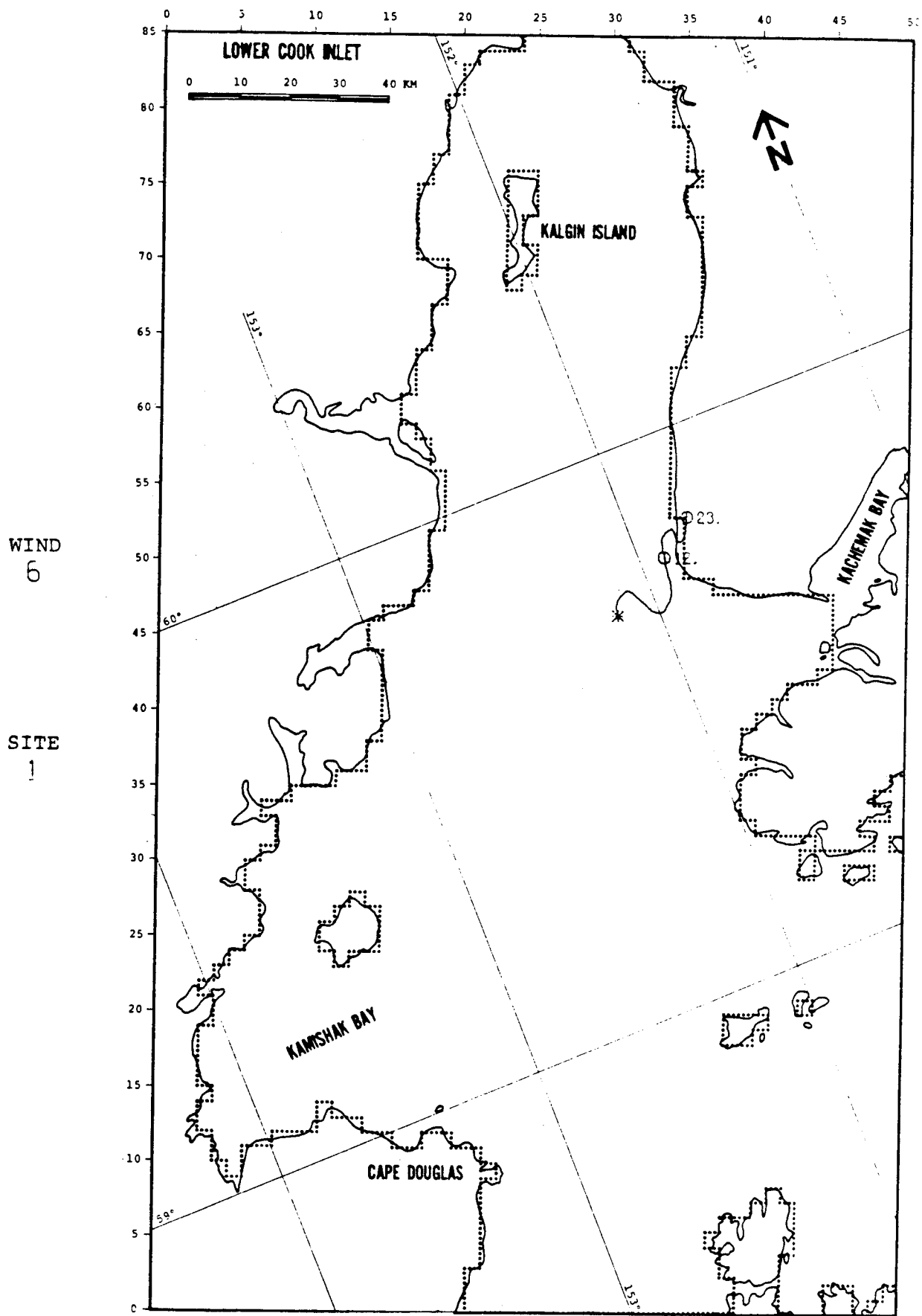


FIGURE C-42: PERTURBATION CASE: NET -25%

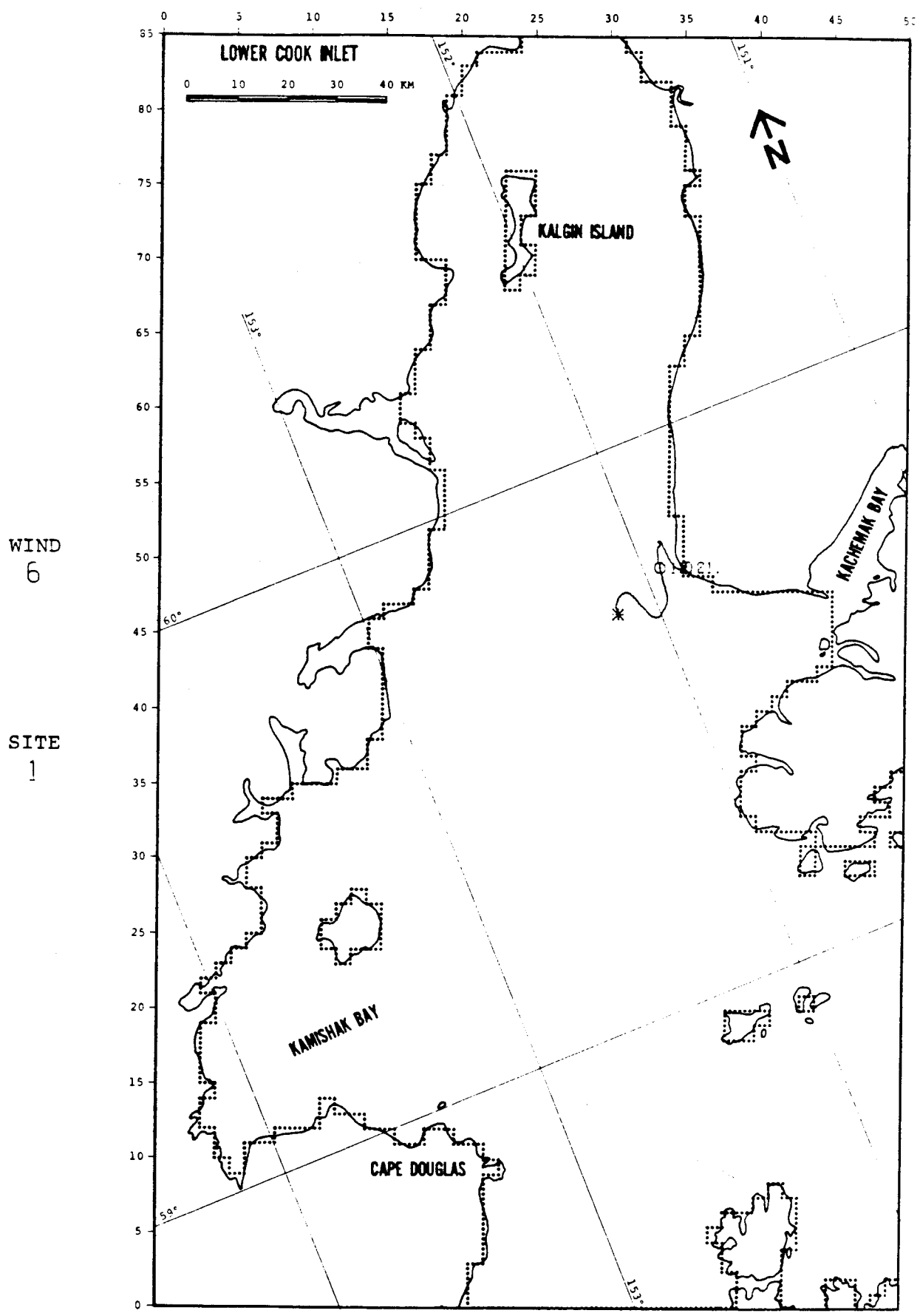


FIGURE C-44: PERTURBATION CASE: WIND -25%

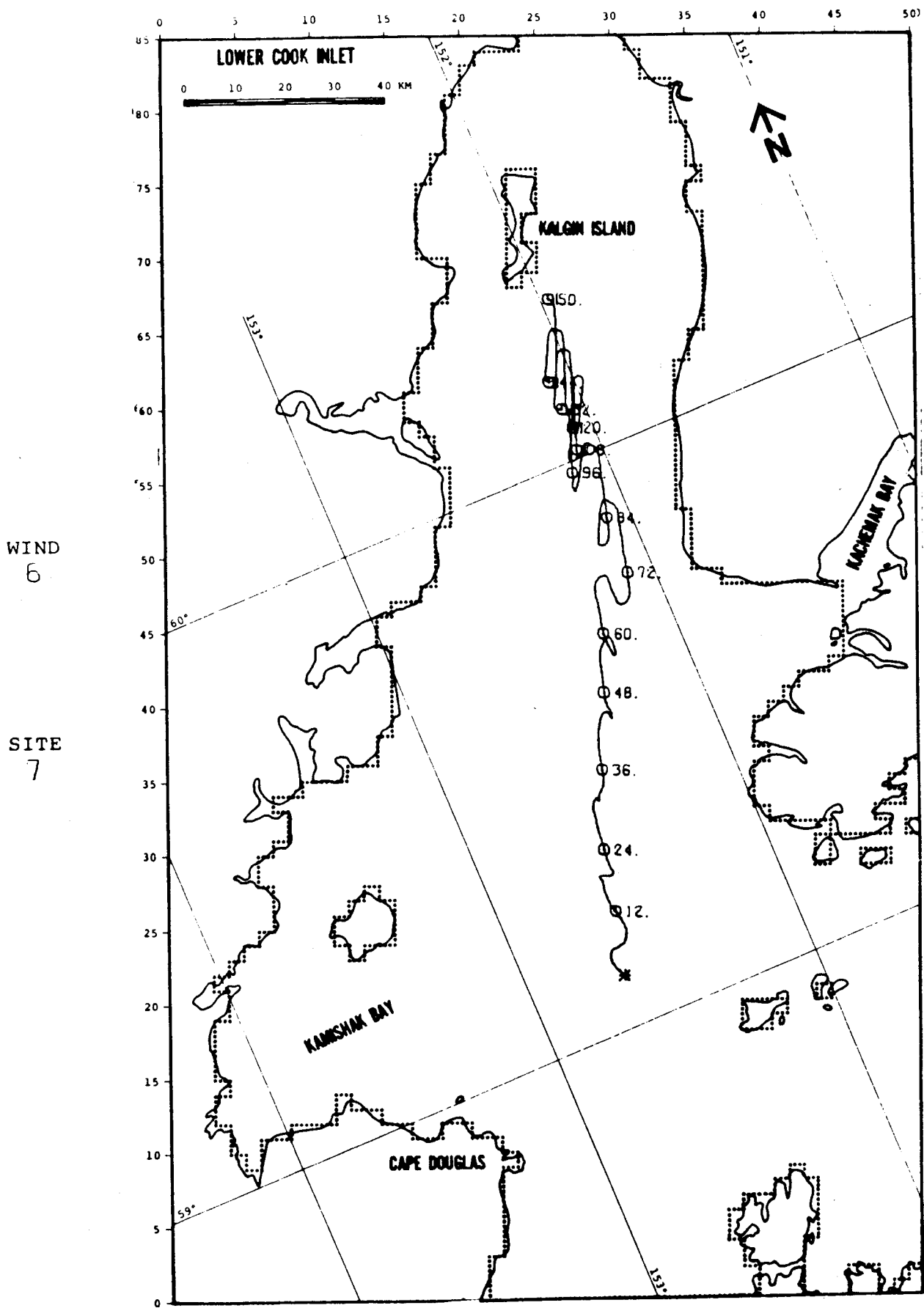


FIGURE C-45: PERTURBATION CASE: NET +25%

WIND
6

SITE
7

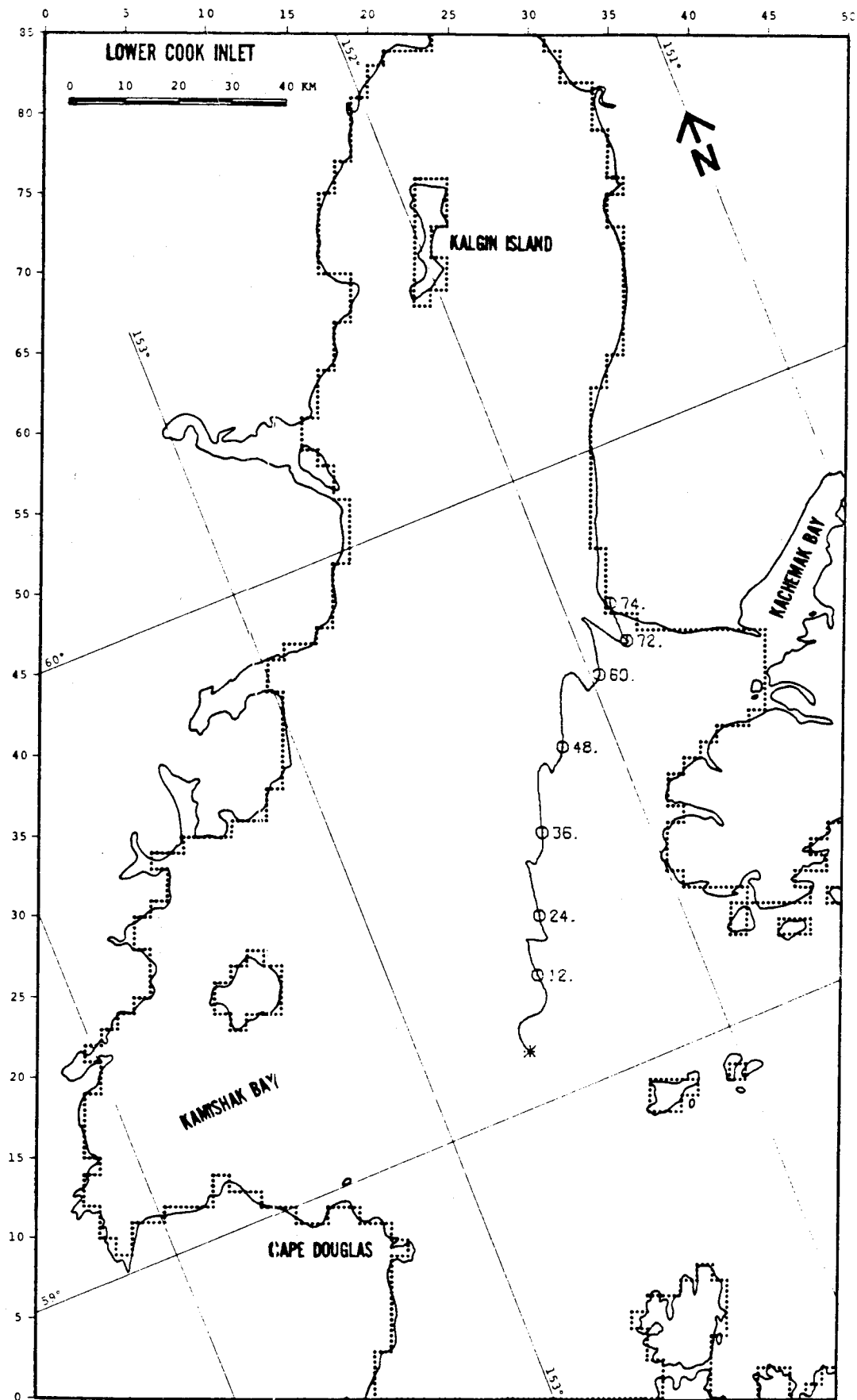


FIGURE C-46: PERTURBATION CASE: NET -25%

WIND
6

SITE
7

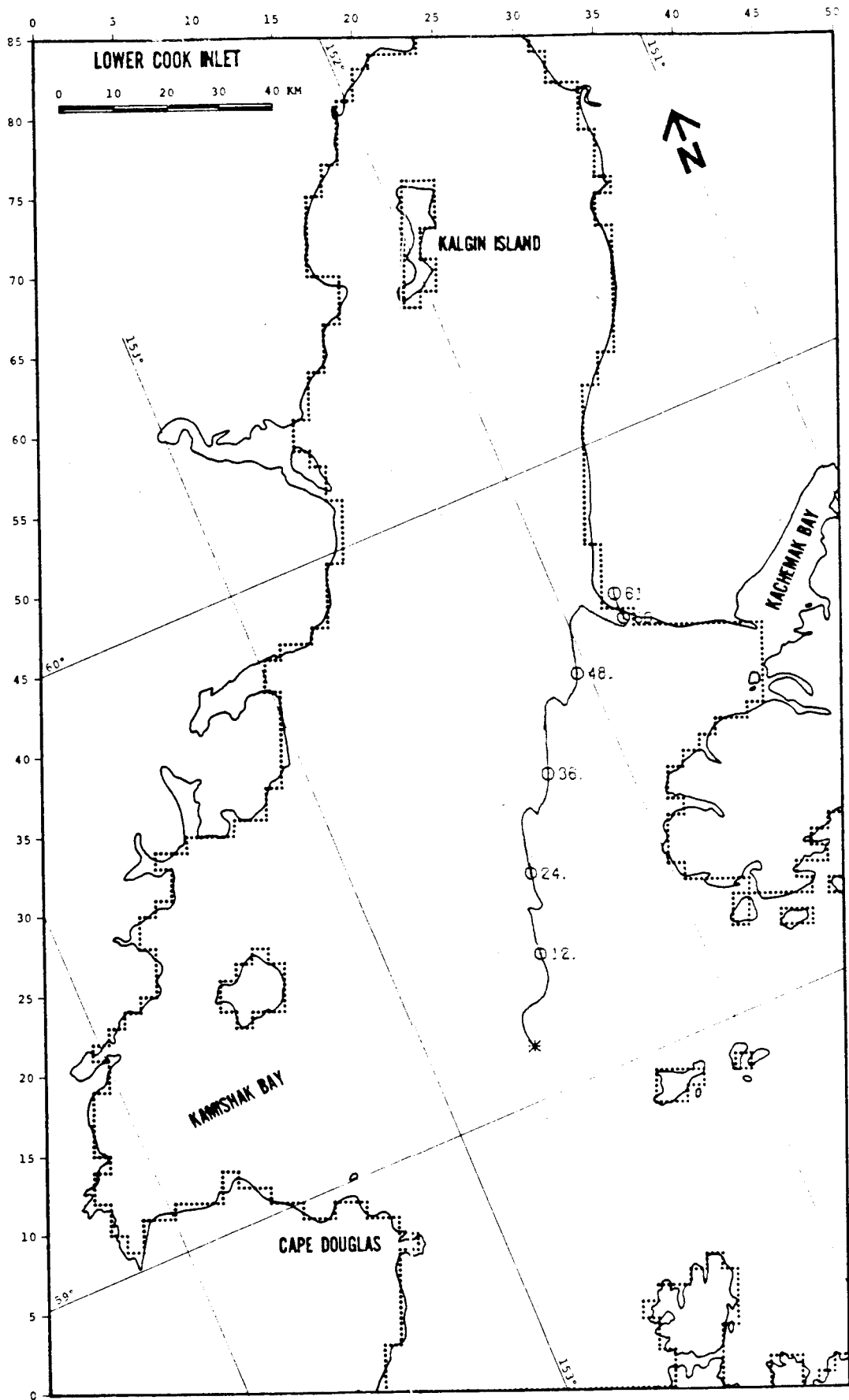


FIGURE C-47: PERTURBATION CASE: WIND +25%

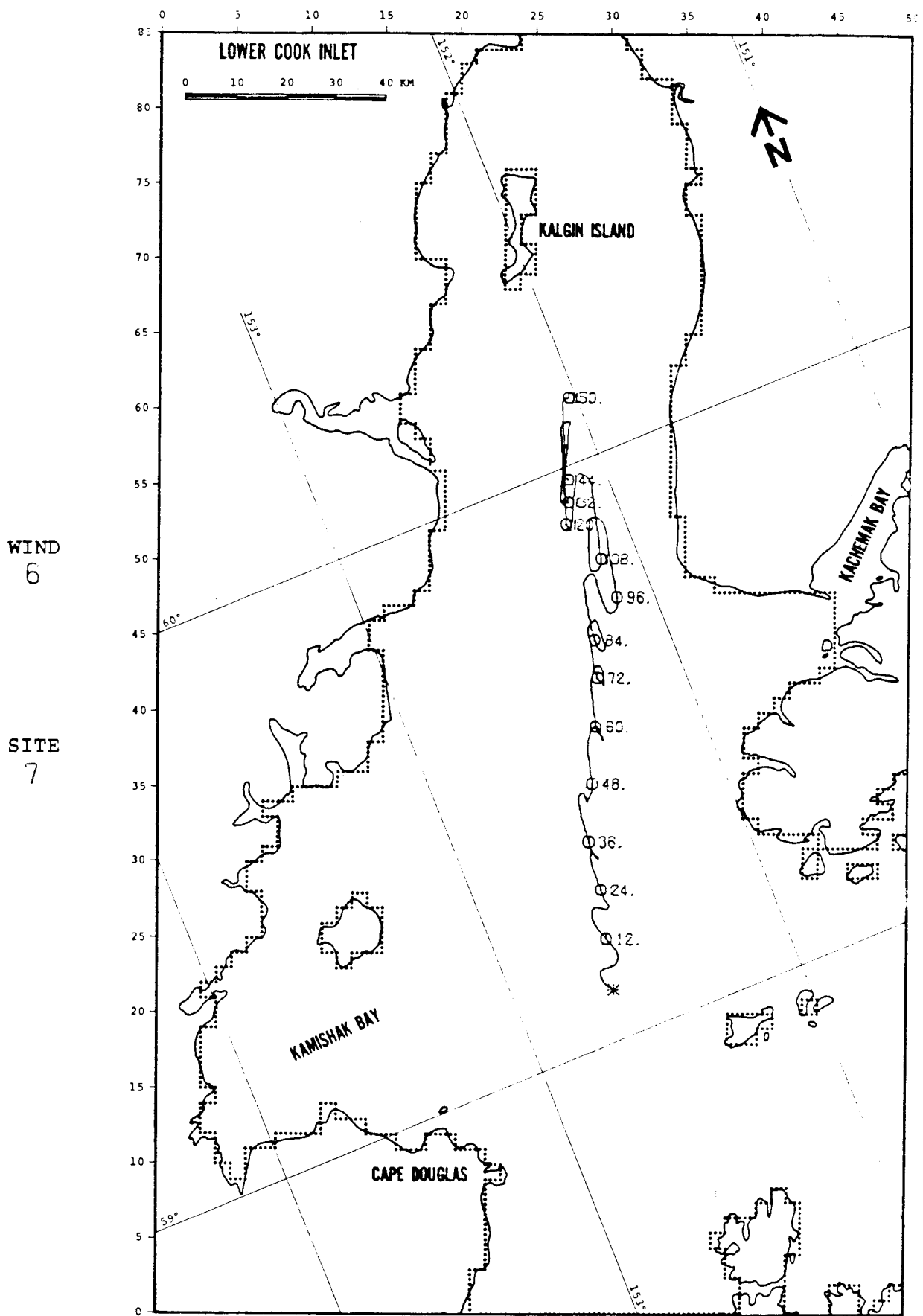


FIGURE C-48: PERTURBATION CASE: WIND -25%

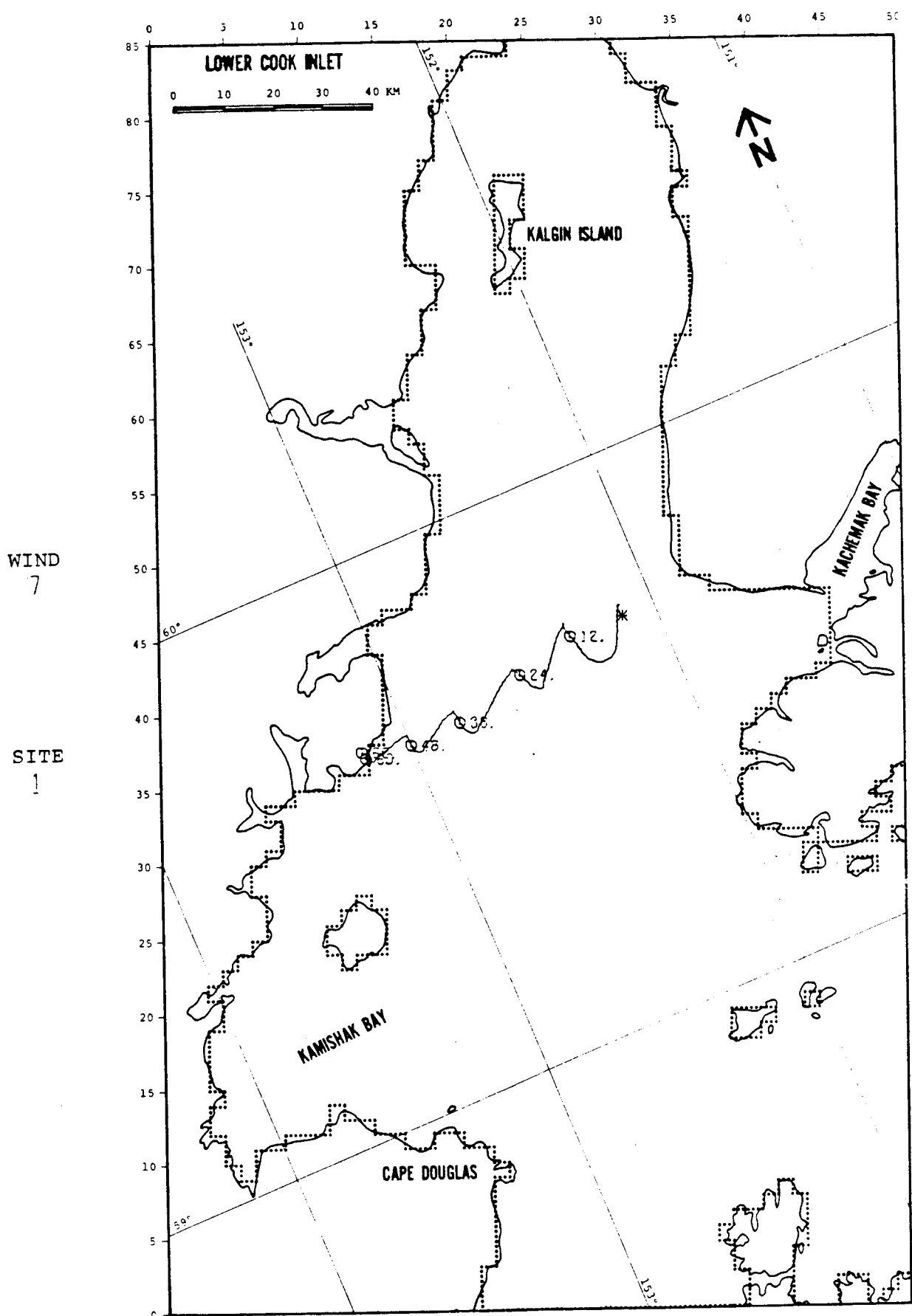


FIGURE C-49: PERTURBATION CASE: NET +25%

WIND
7

SITE
1

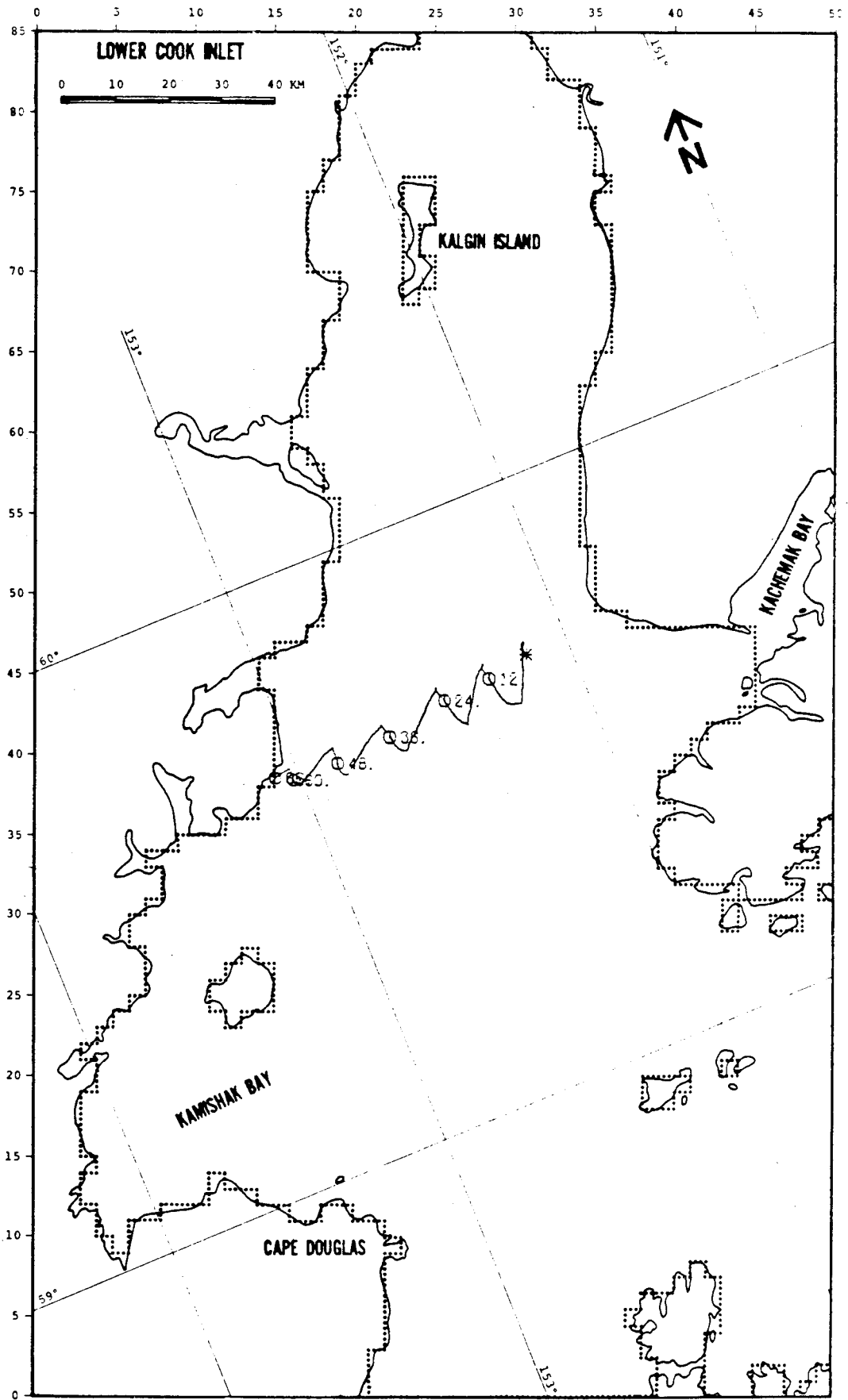


FIGURE C-50: PERTURBATION CASE: NET -25%

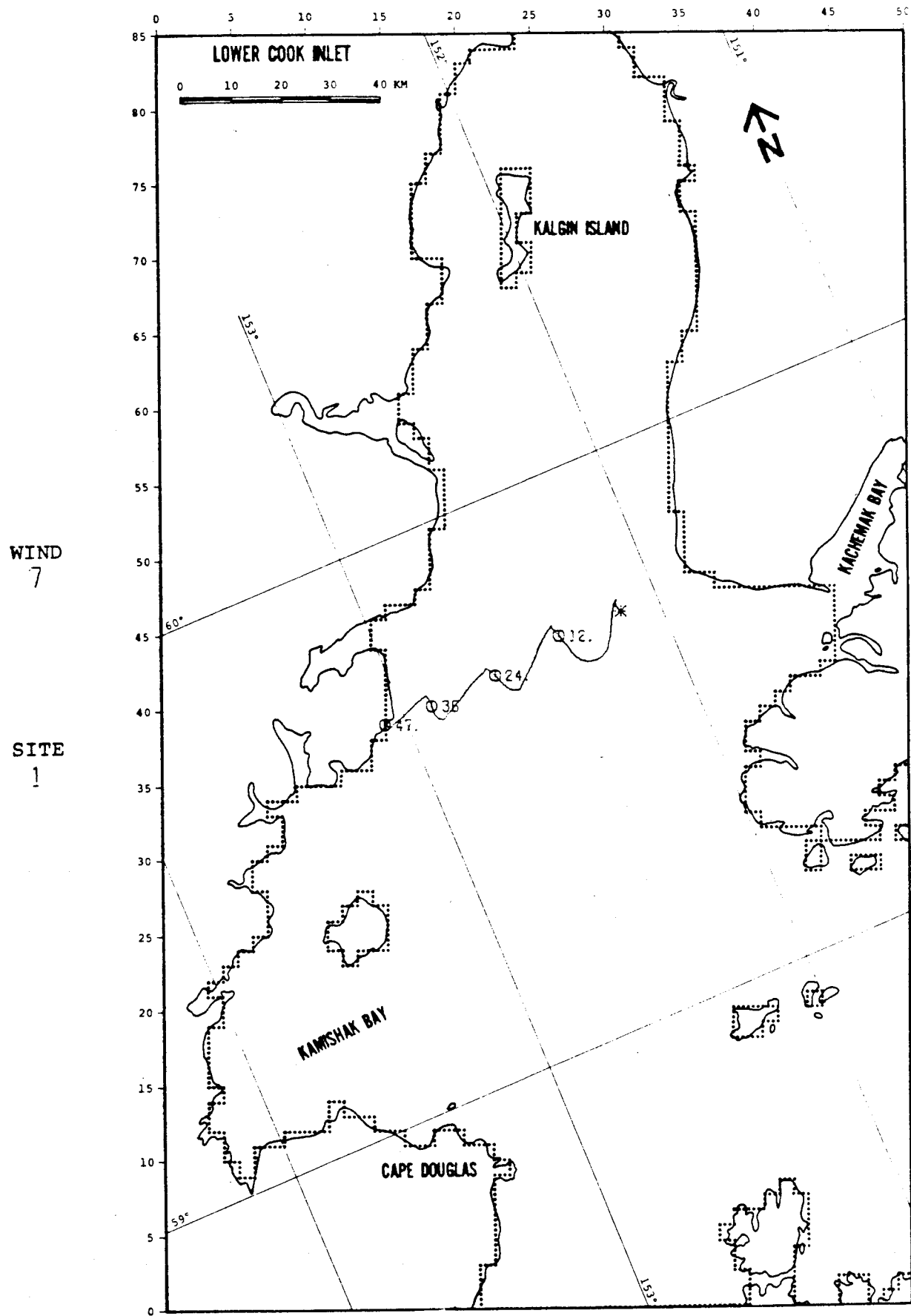


FIGURE C-51: PERTURBATION CASE: WIND +25%

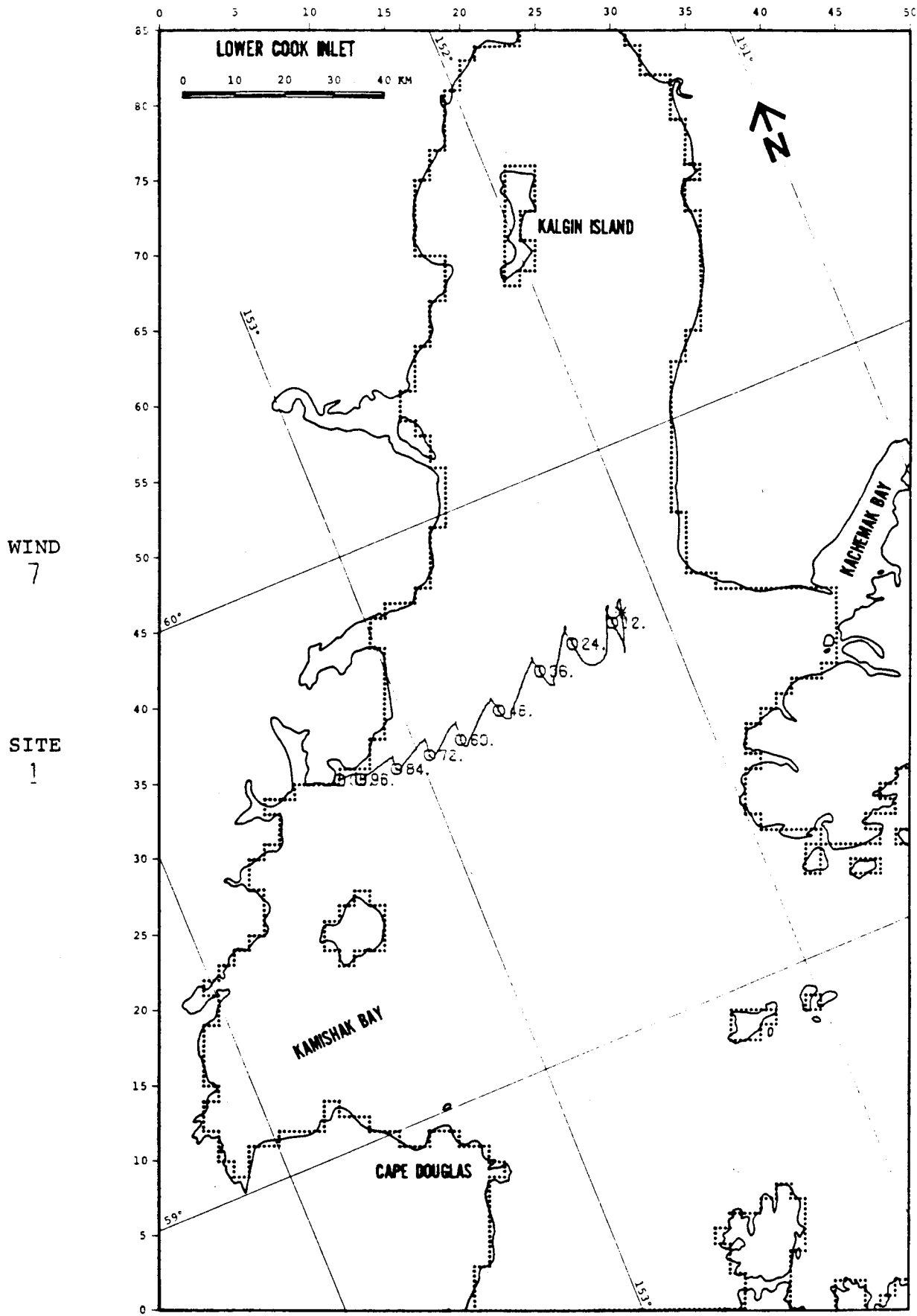
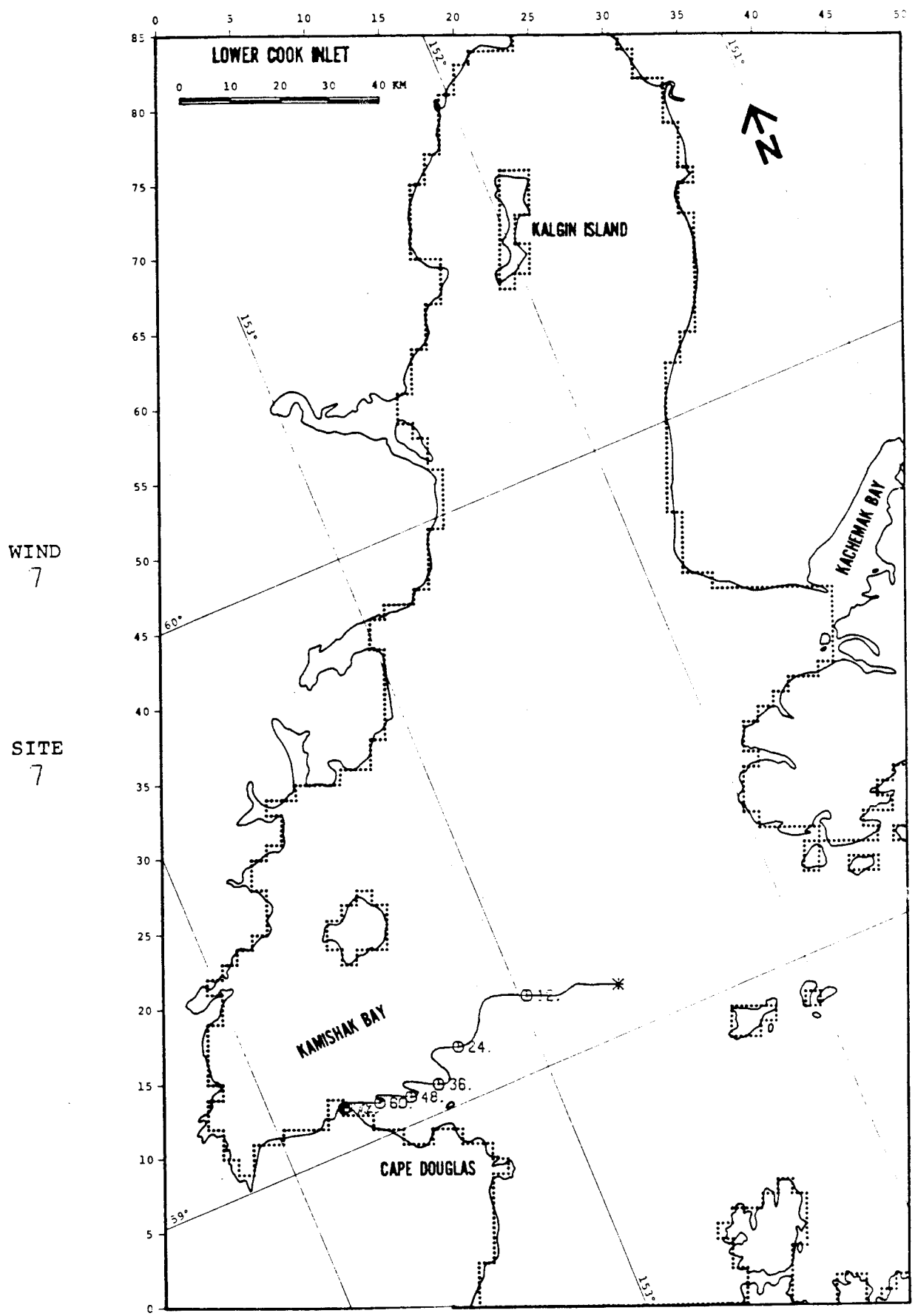


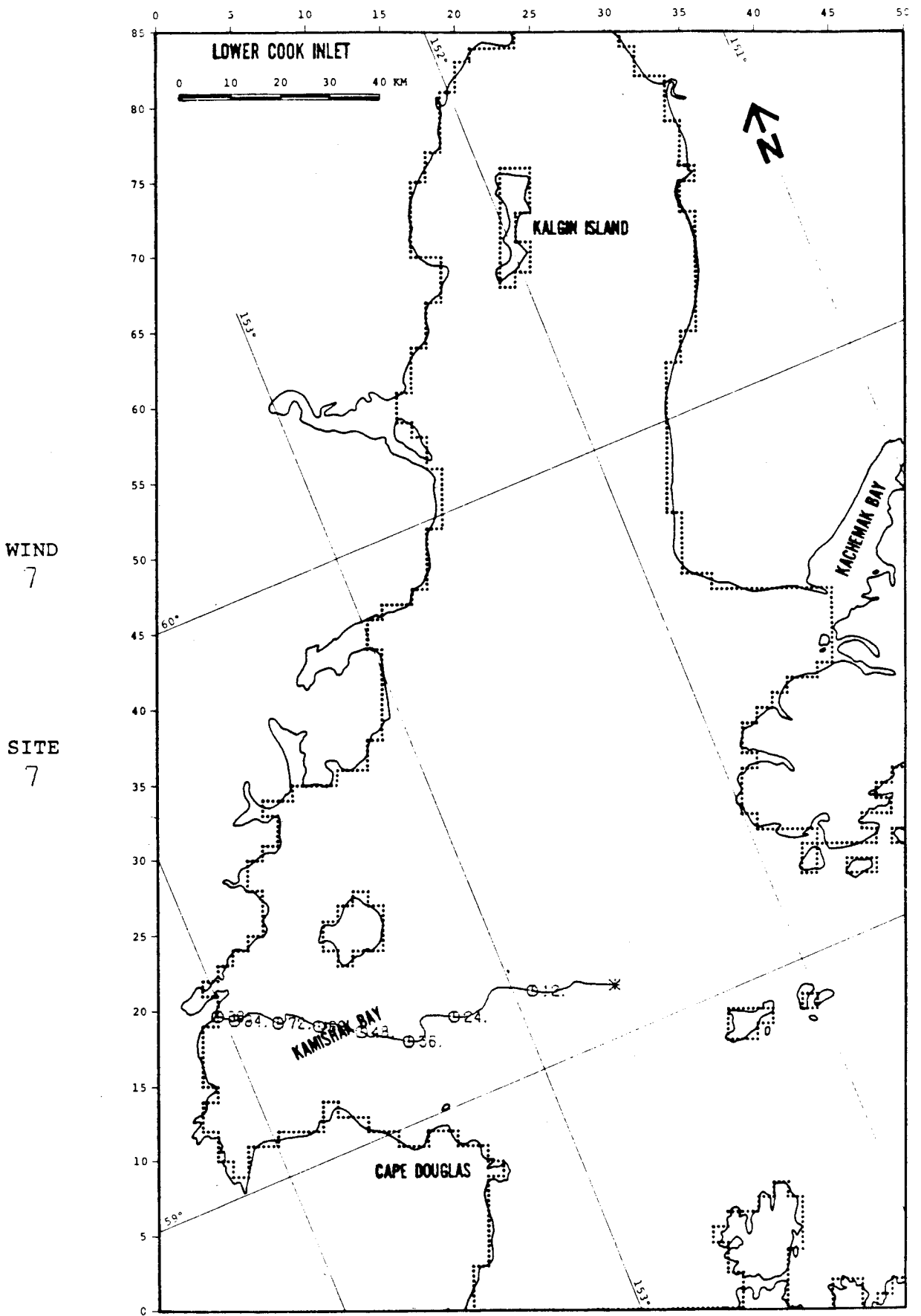
FIGURE C-52: PERTURBATION CASE: WIND -25%



WIND
7

SITE
7

FIGURE C-53: PERTURBATION CASE: NET +25%



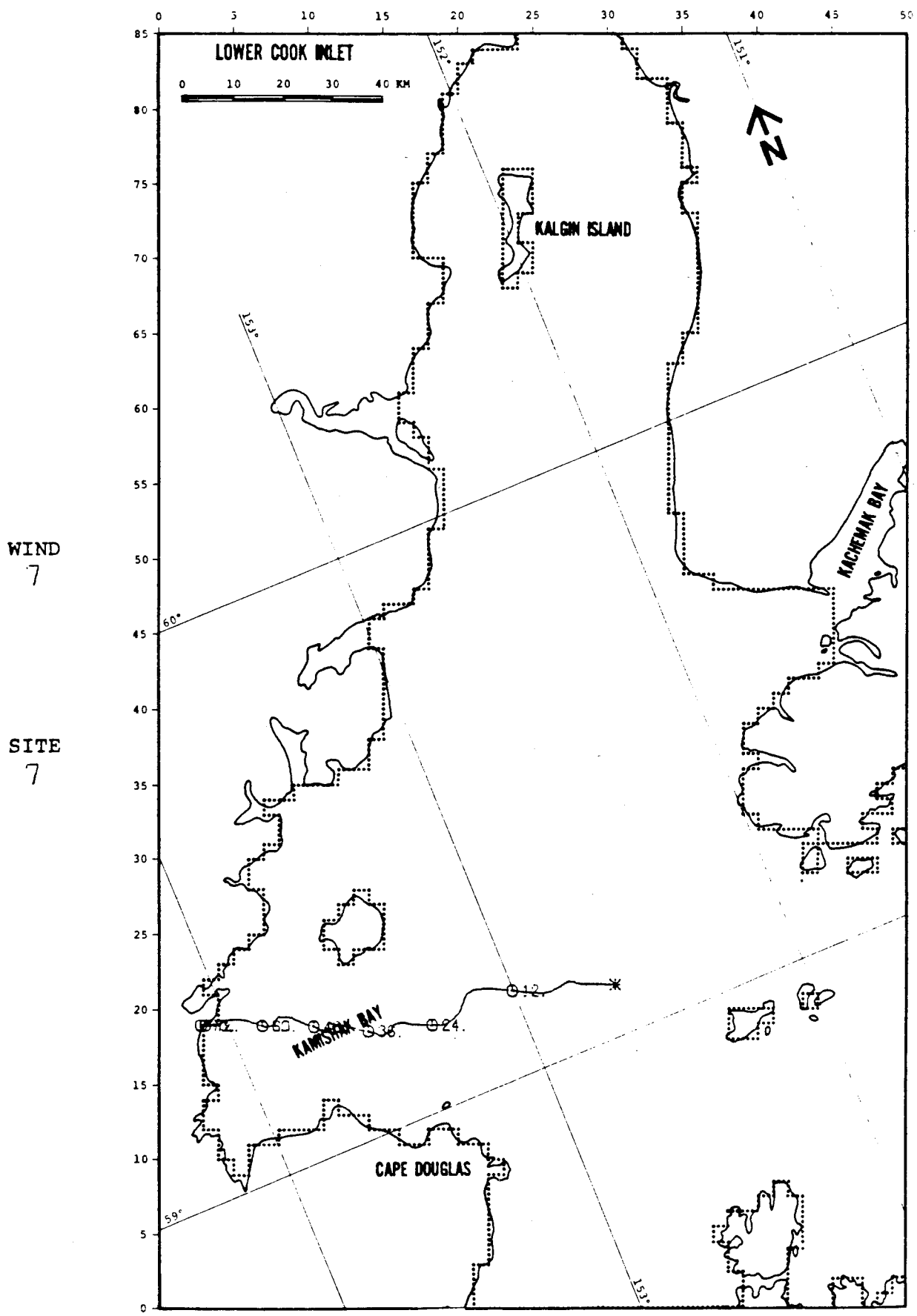


FIGURE C-55: PERTURBATION CASE: WIND +25%

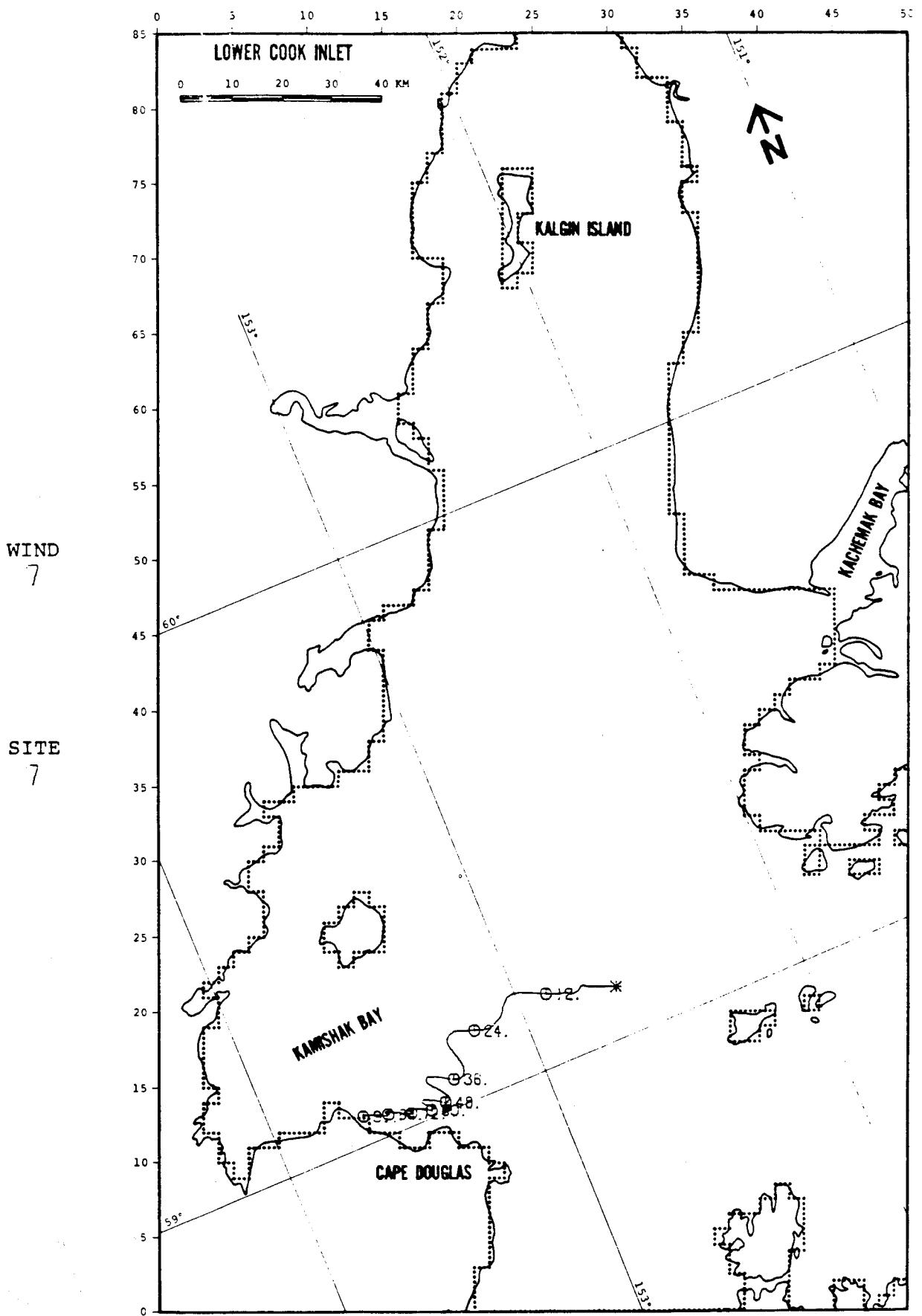


FIGURE C-56: PERTURBATION CASE: WIND -25%

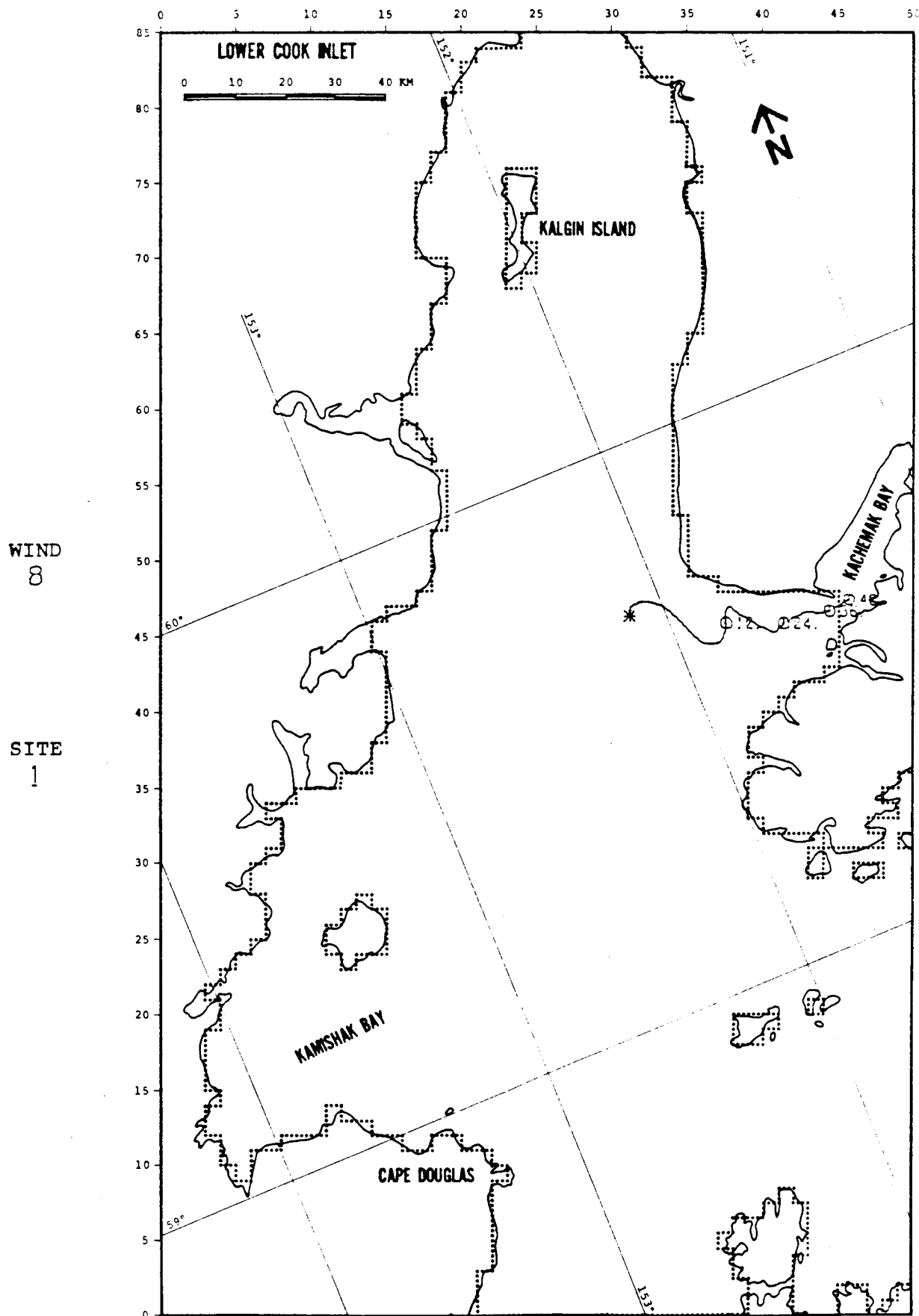


FIGURE C-57: PERTURBATION CASE: NET +25%

WIND
8

SITE
1

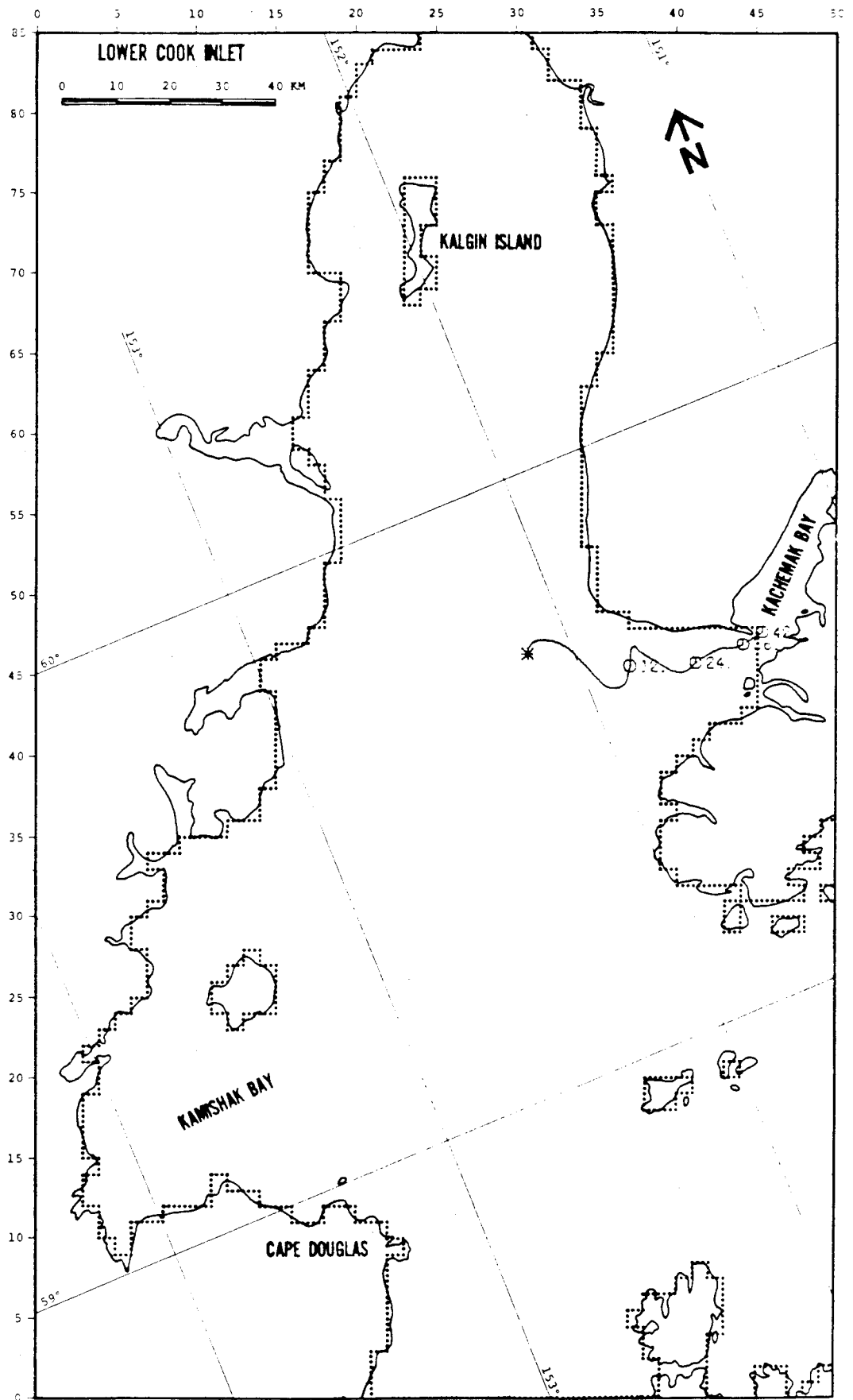


FIGURE Q-58: PERTURBATION CASE: NET -25%

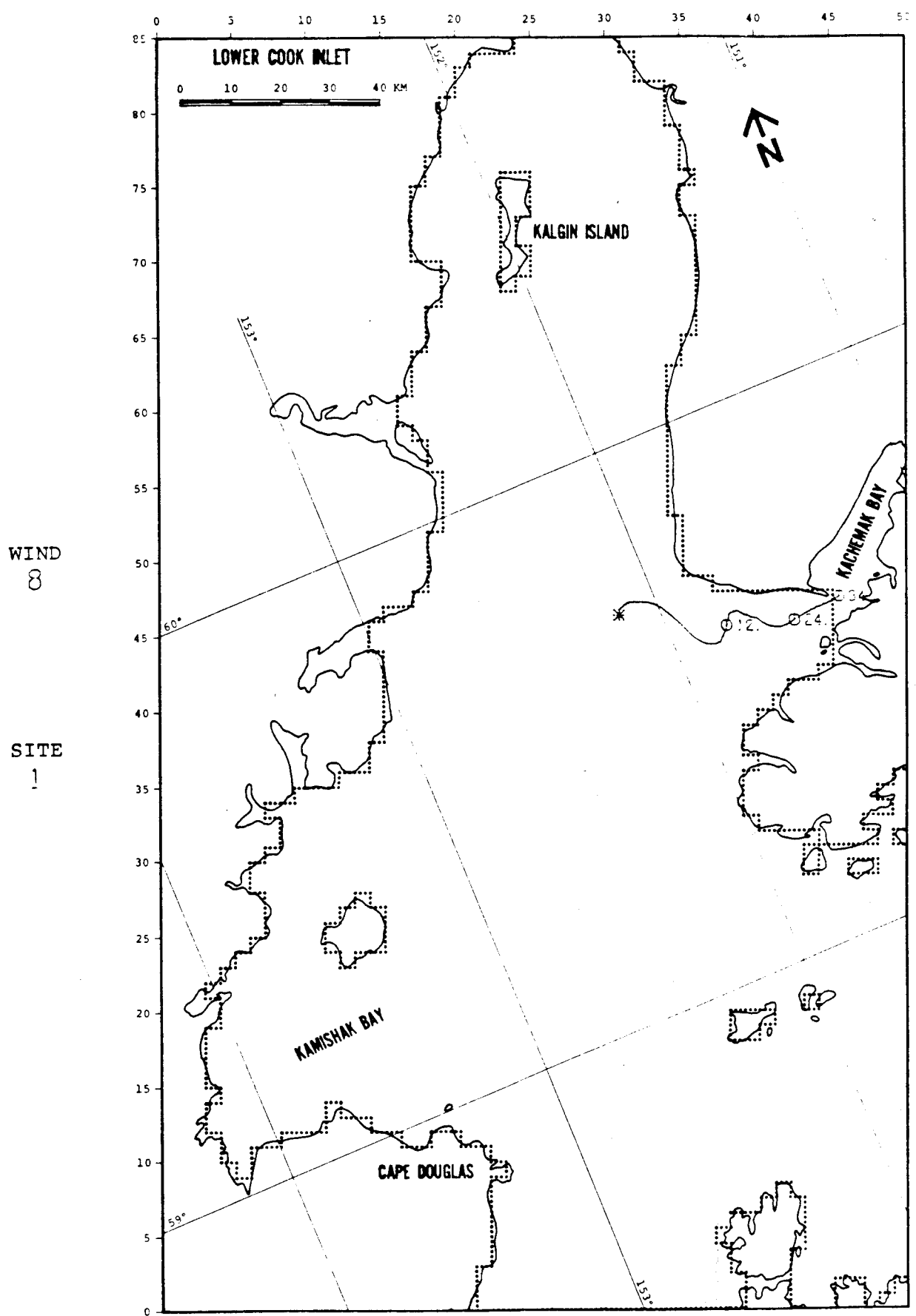


FIGURE C-59: PERTURBATION CASE: WIND +25%

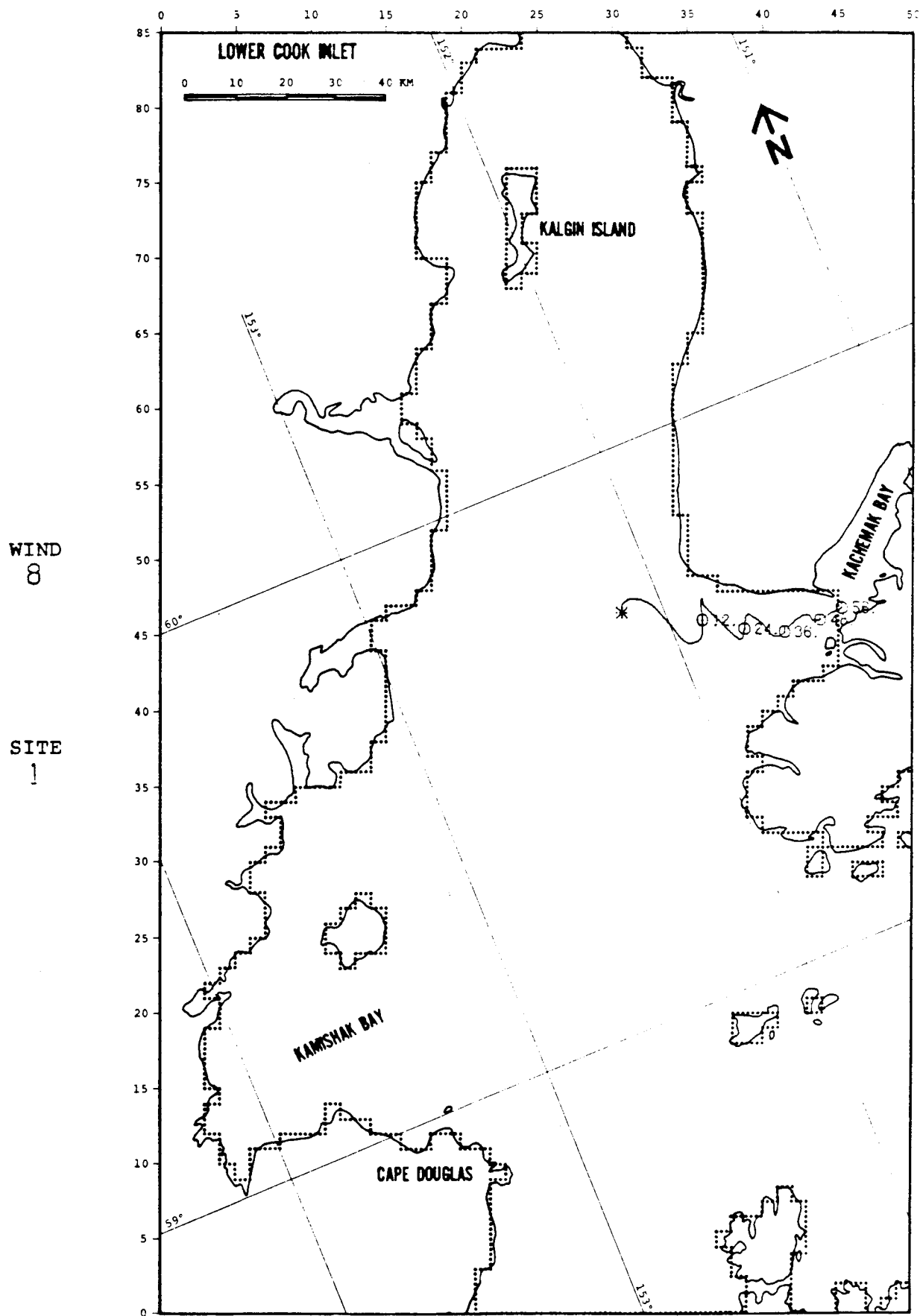


FIGURE C-60: PERTURBATION CASE: WIND -25%

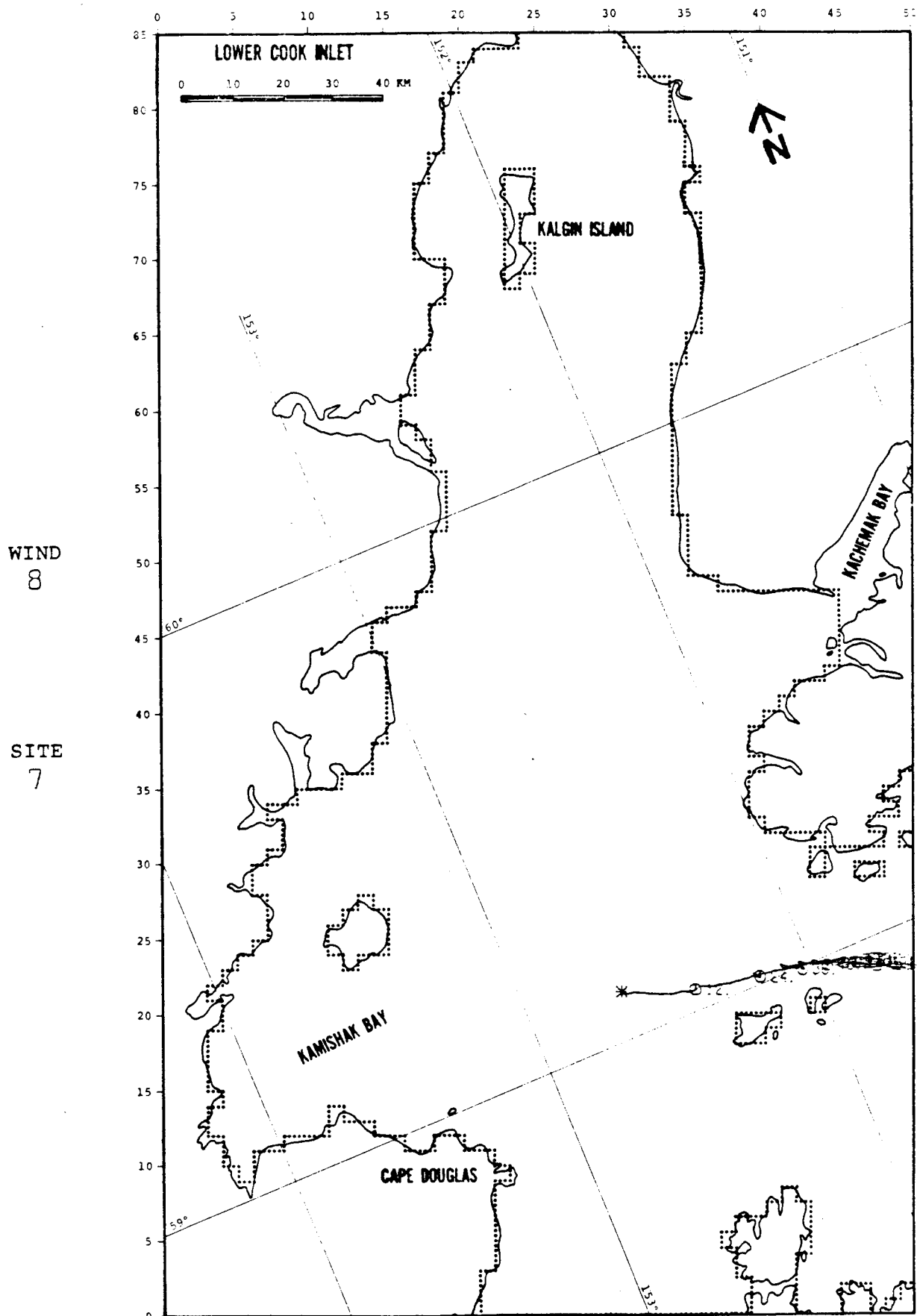


FIGURE C-61: PERTURBATION CASE: NET +25%

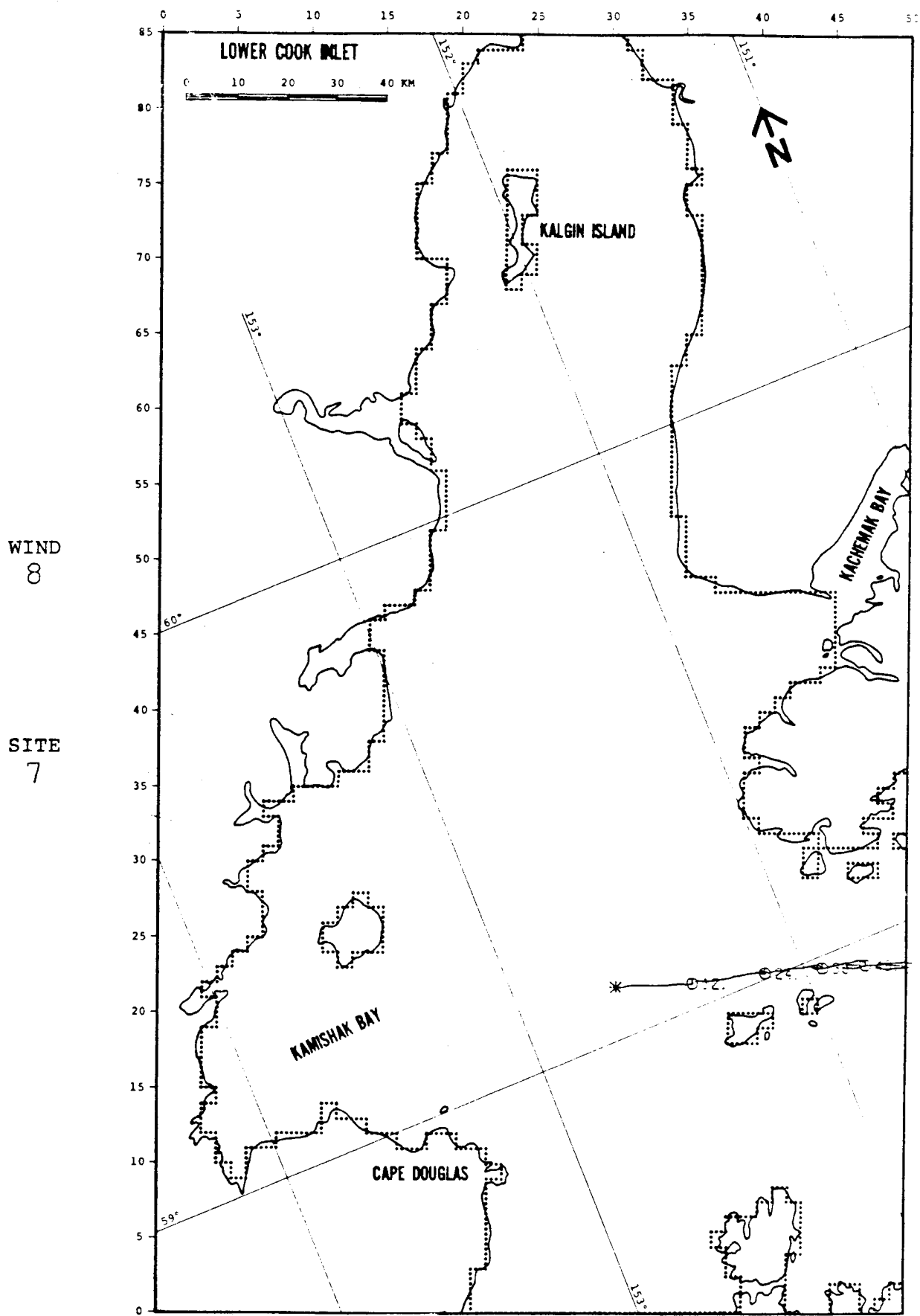


FIGURE C-62: PERTURBATION CASE: NET -25%

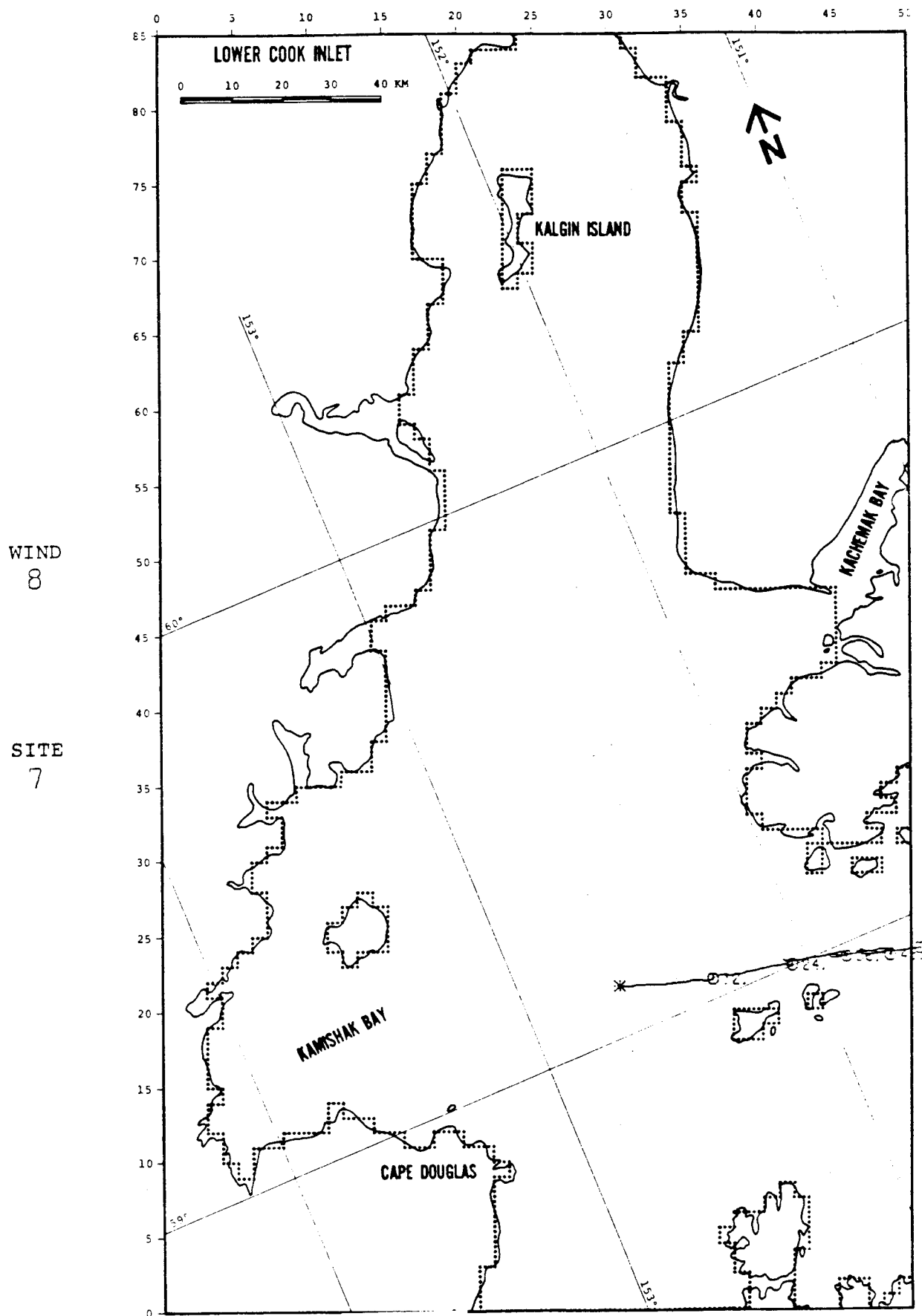


FIGURE C-63: PERTURBATION CASE: WIND +25%

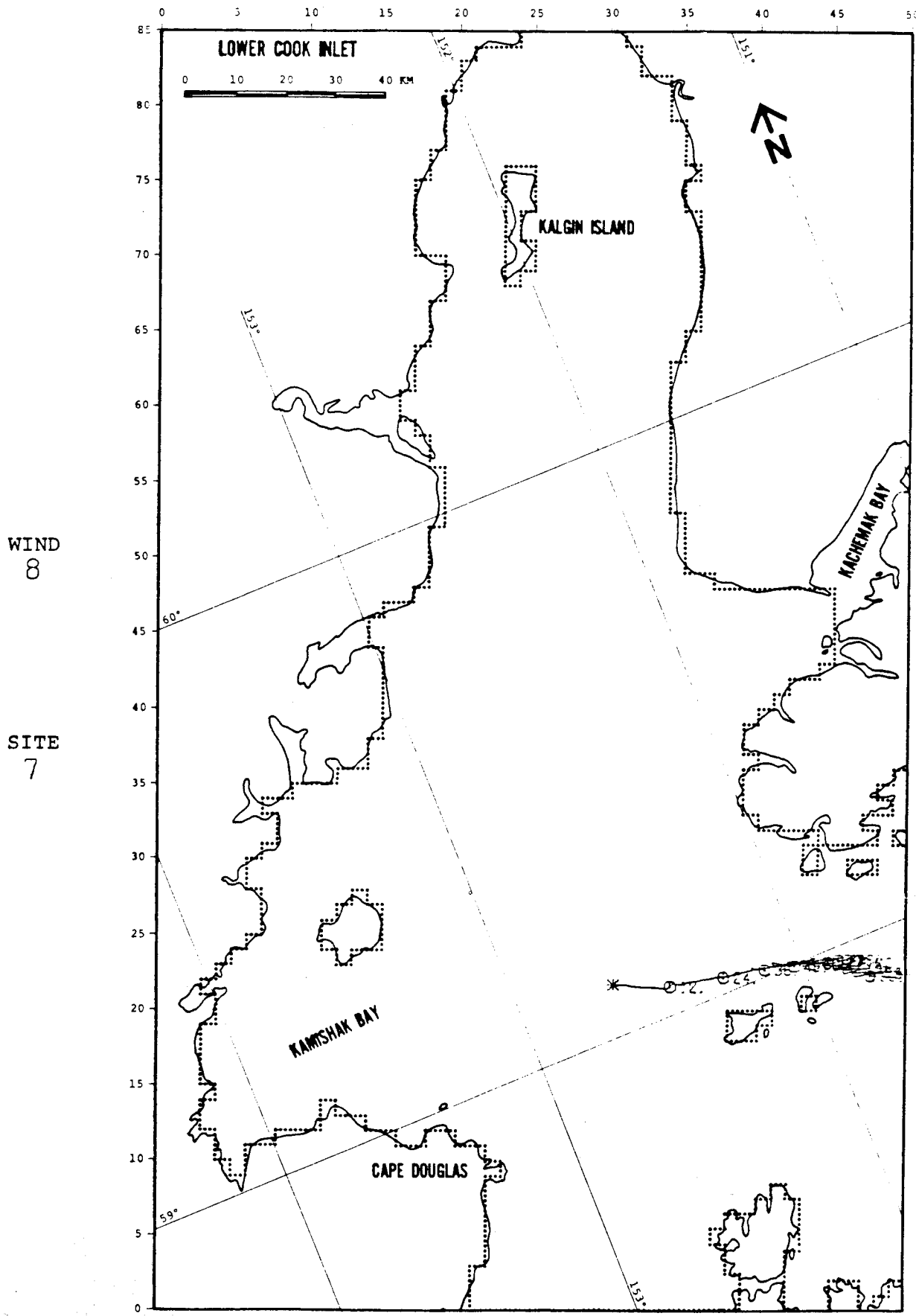


FIGURE C-64: PERTURBATION CASE: WIND -25%

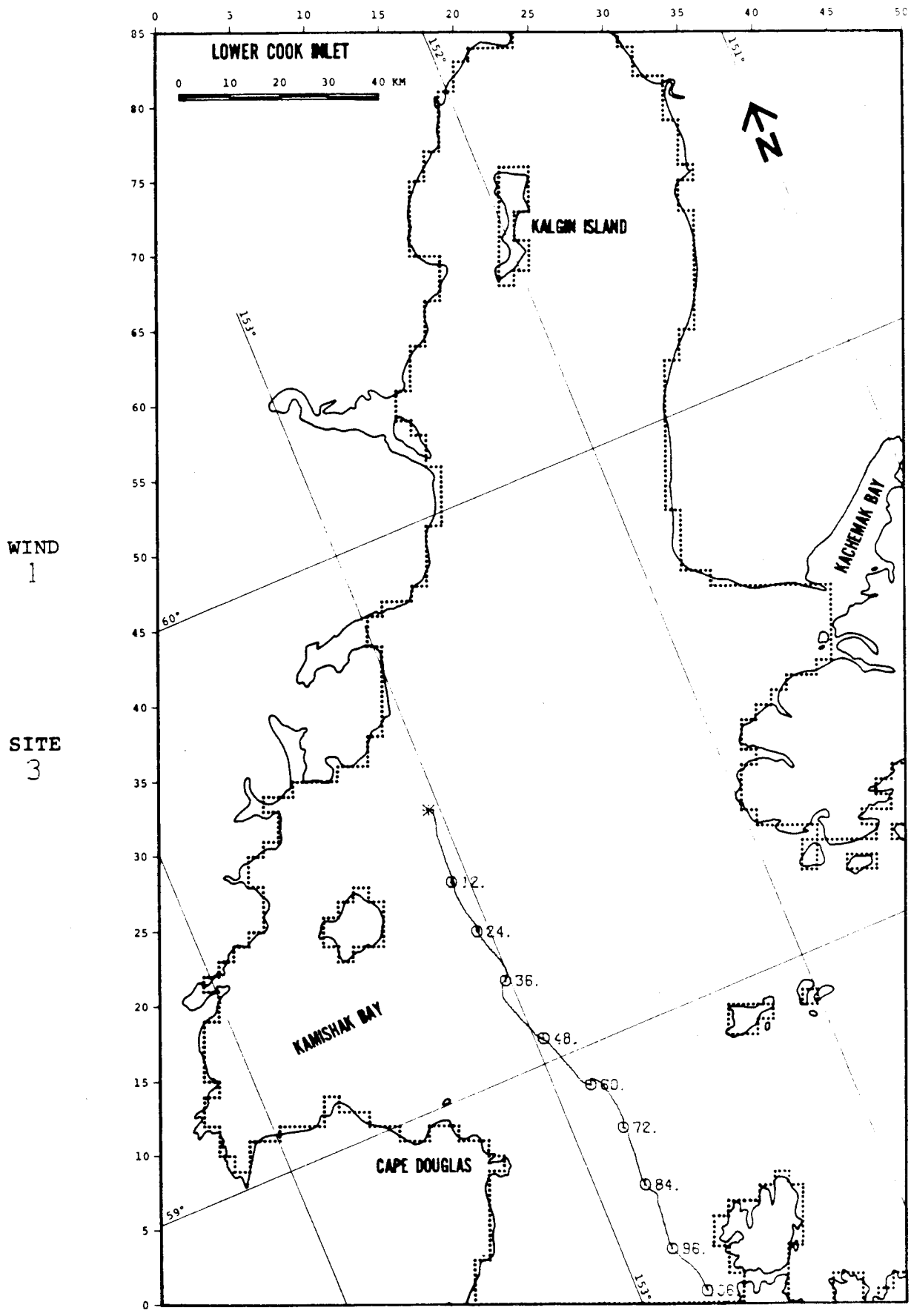


FIGURE C-65: PERTURBATION CASE: WIND -25%

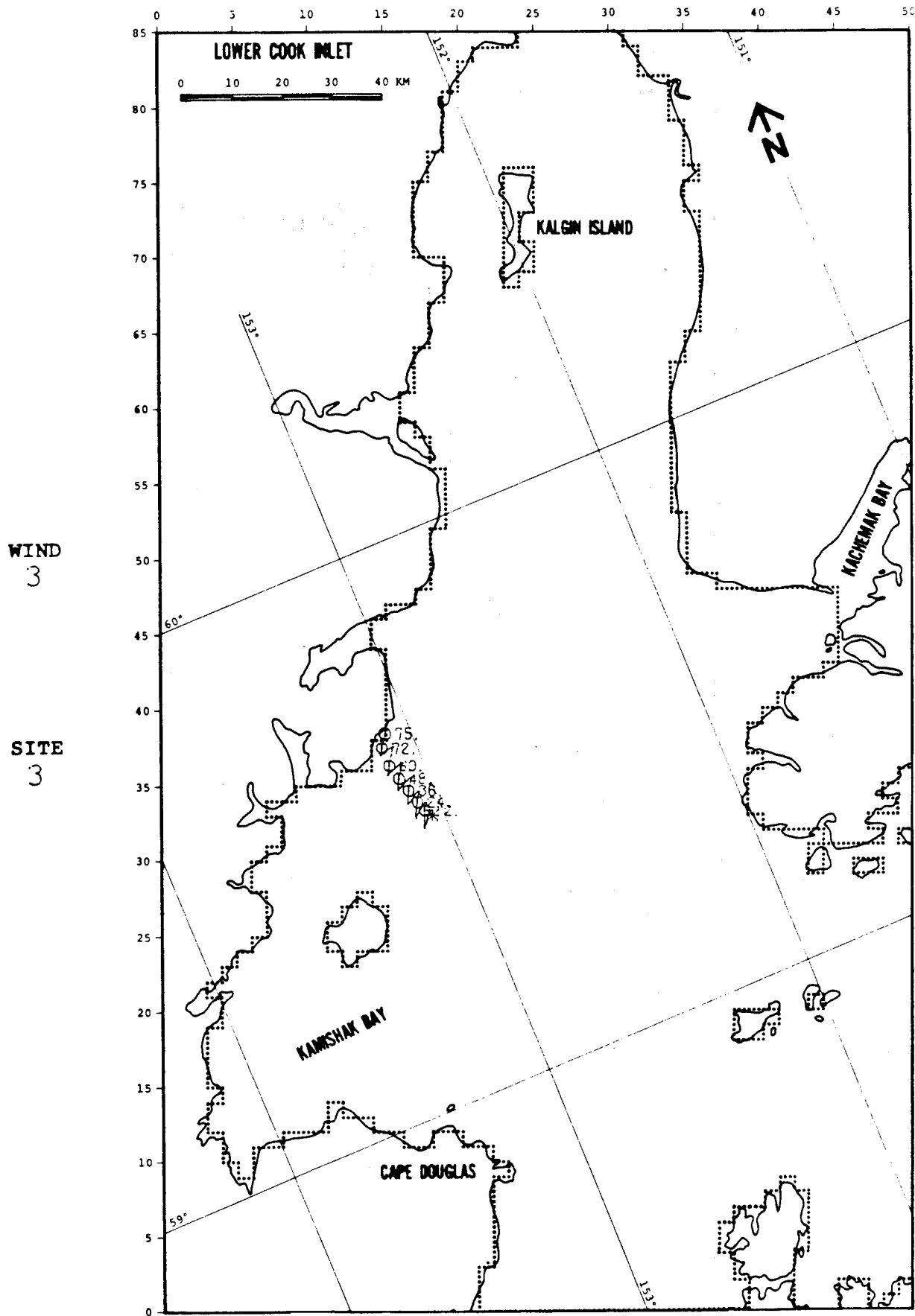


FIGURE C-67: PERTURBATION CASE: WIND -25%

WIND
5

SITE
3

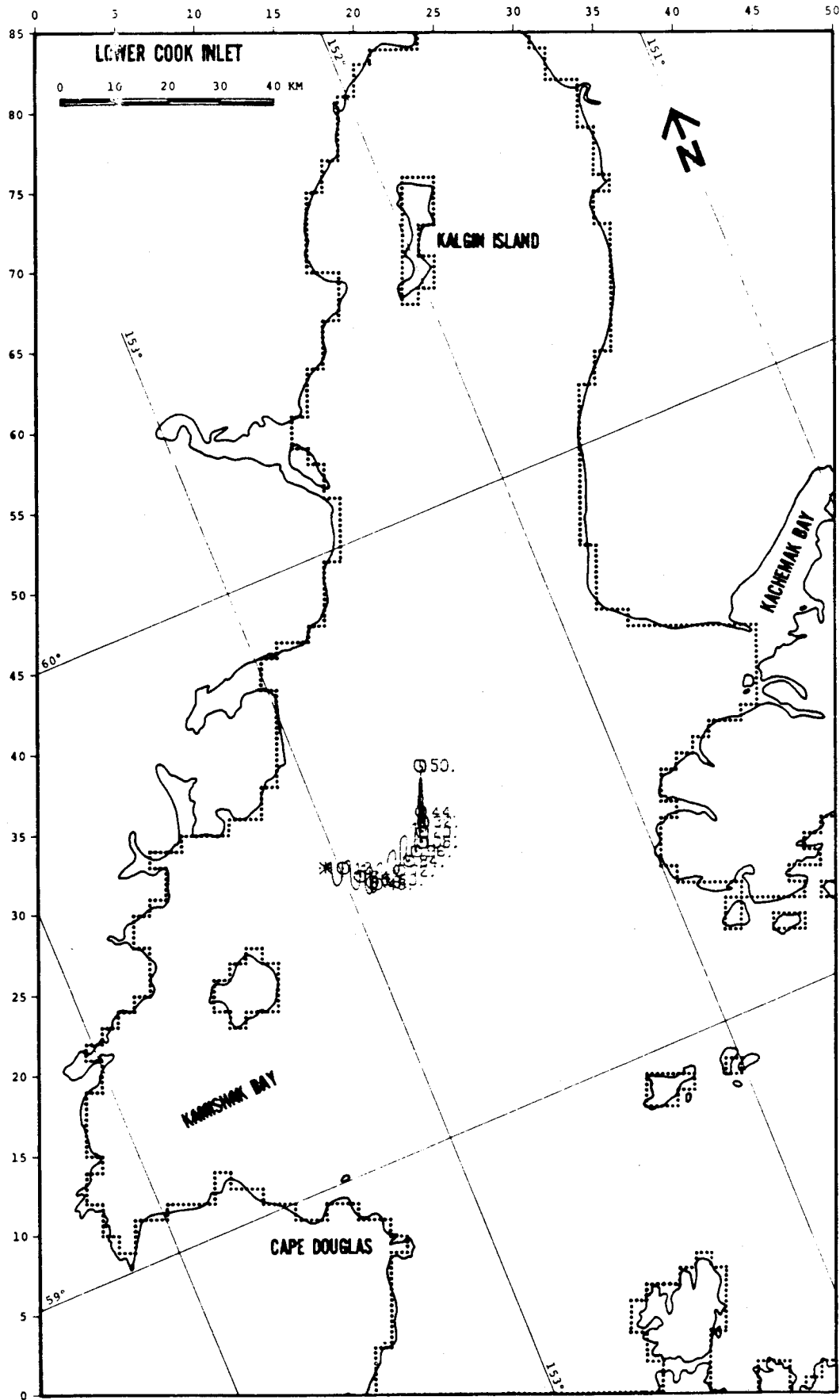


FIGURE C-69: PERTURBATION CASE: WIND -25%

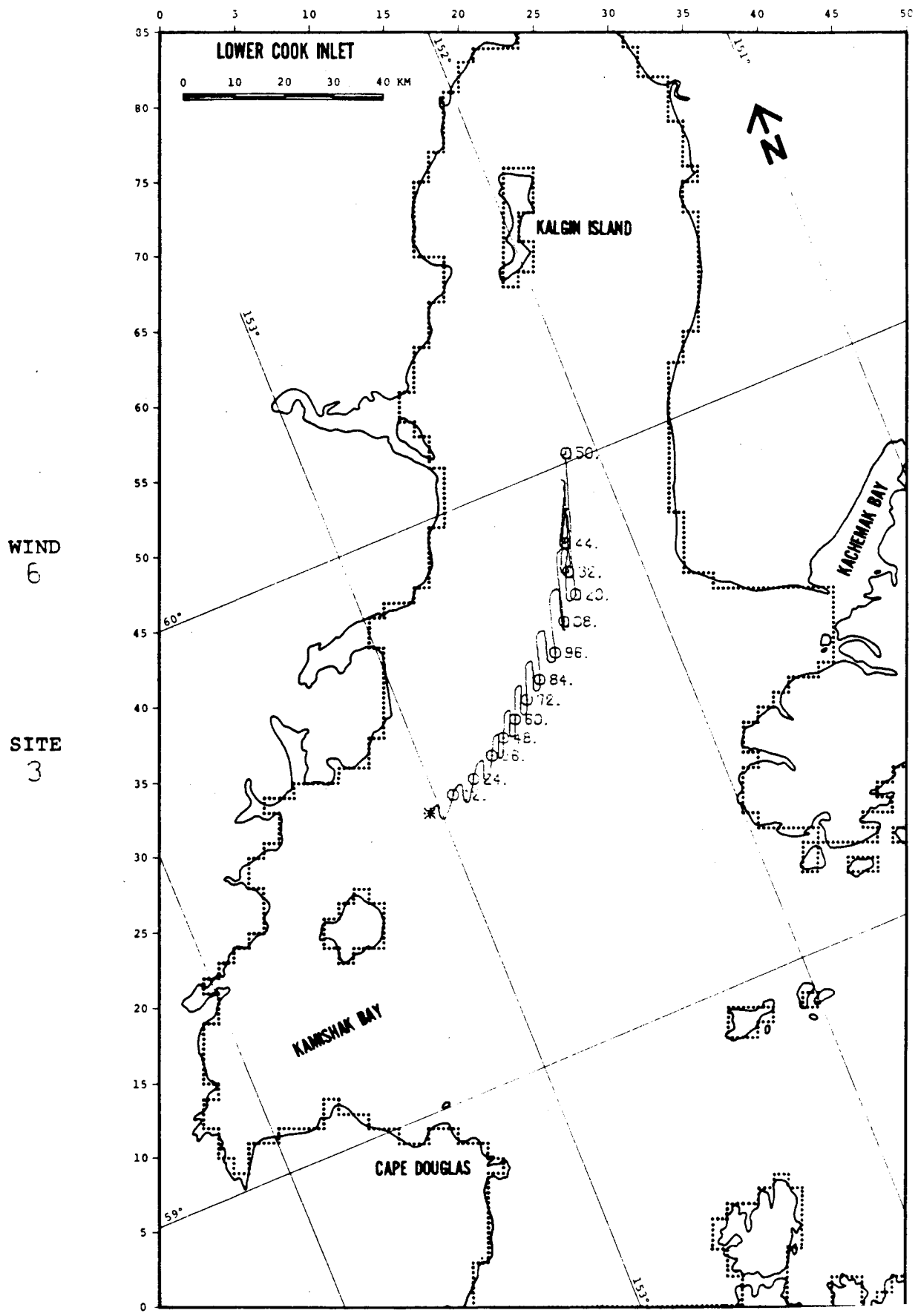


FIGURE C-70: PERTURBATION CASE: WIND -25%

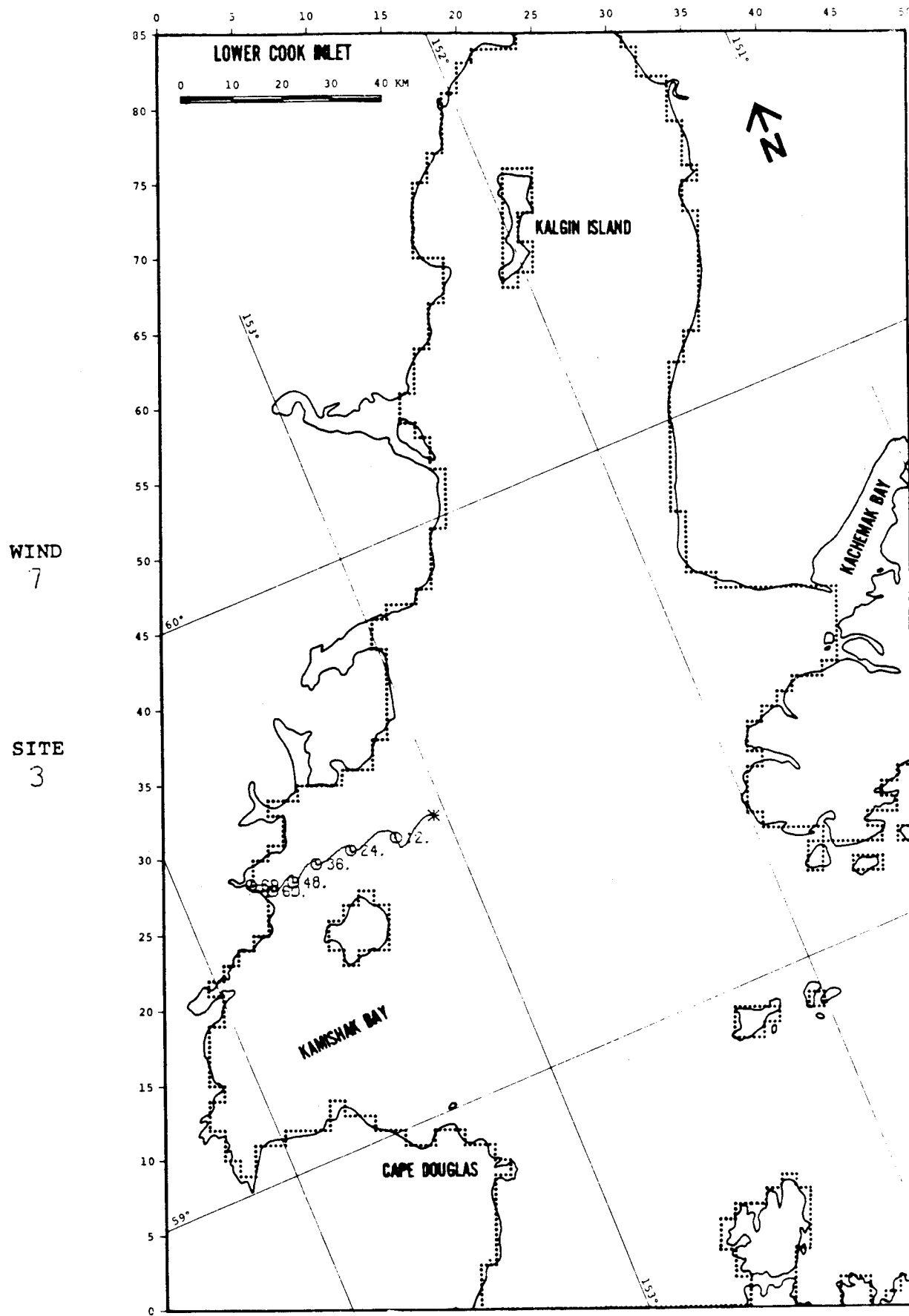


FIGURE C-71: PERTURBATION CASE: WIND -25%

WIND
8

SITE
3

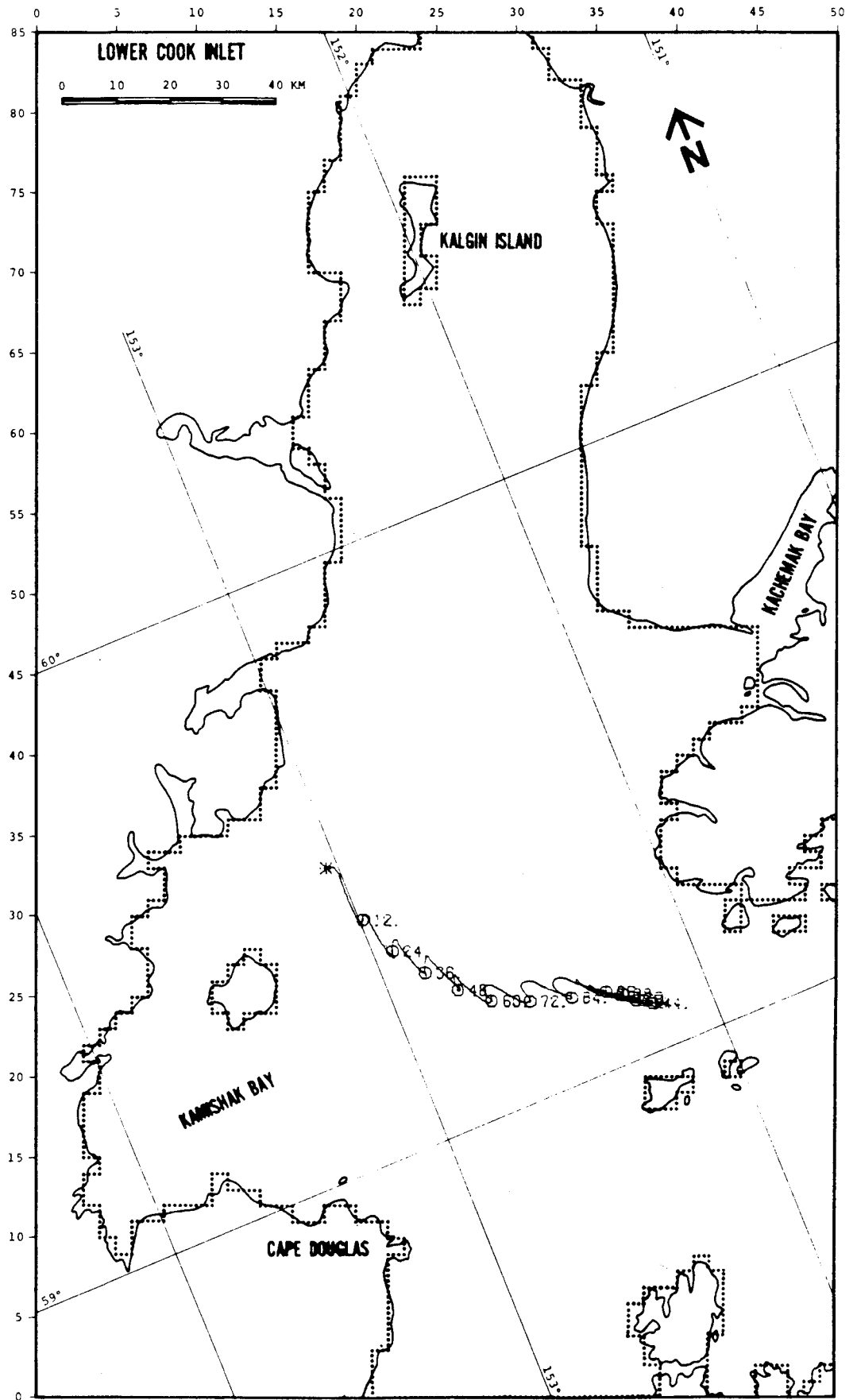


FIGURE C-72: PERTURBATION CASE: WIND -25%

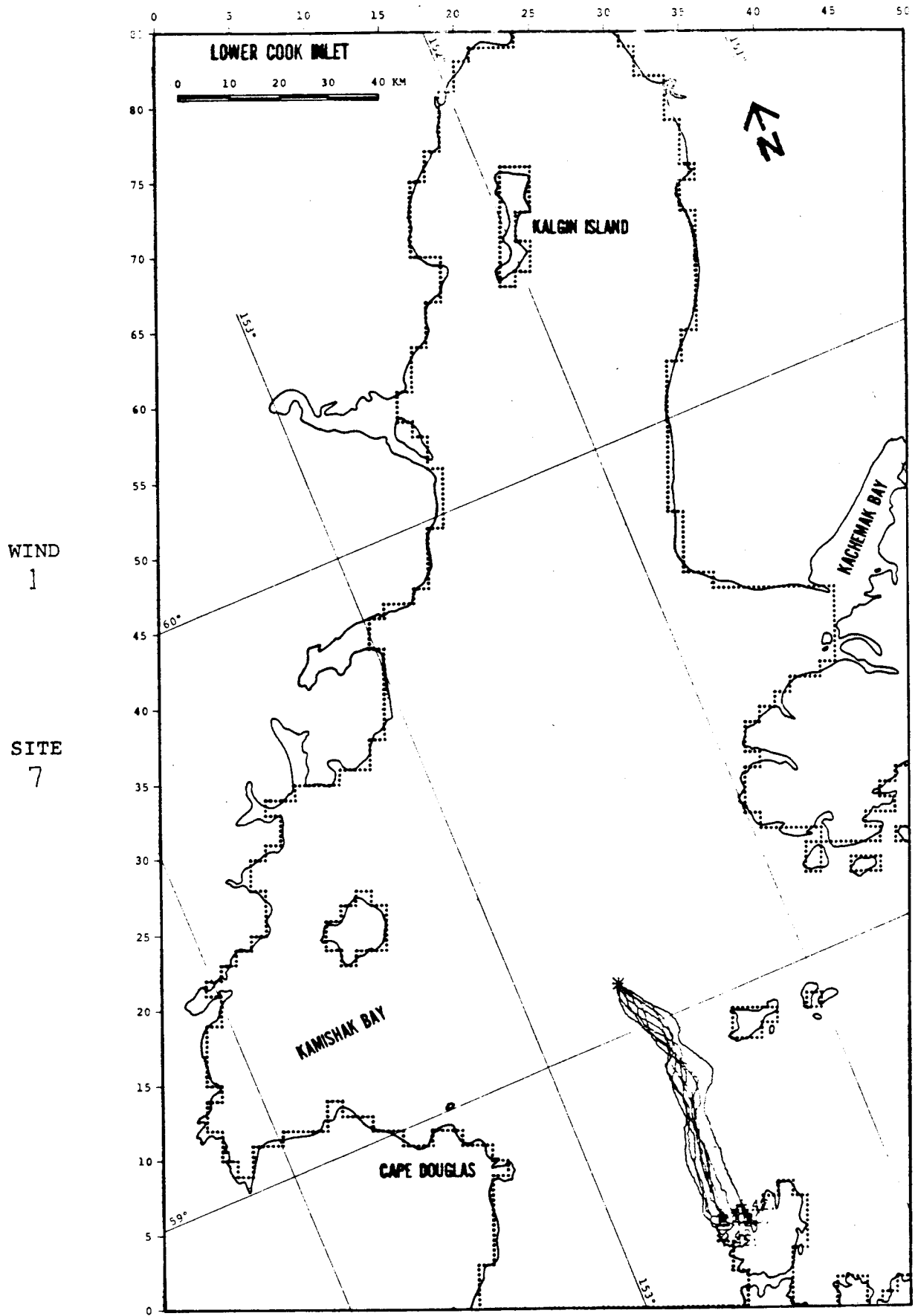


FIGURE C-73: RANDOM PERTURBATION ANALYSIS CASE

WIND
1

SITE
7

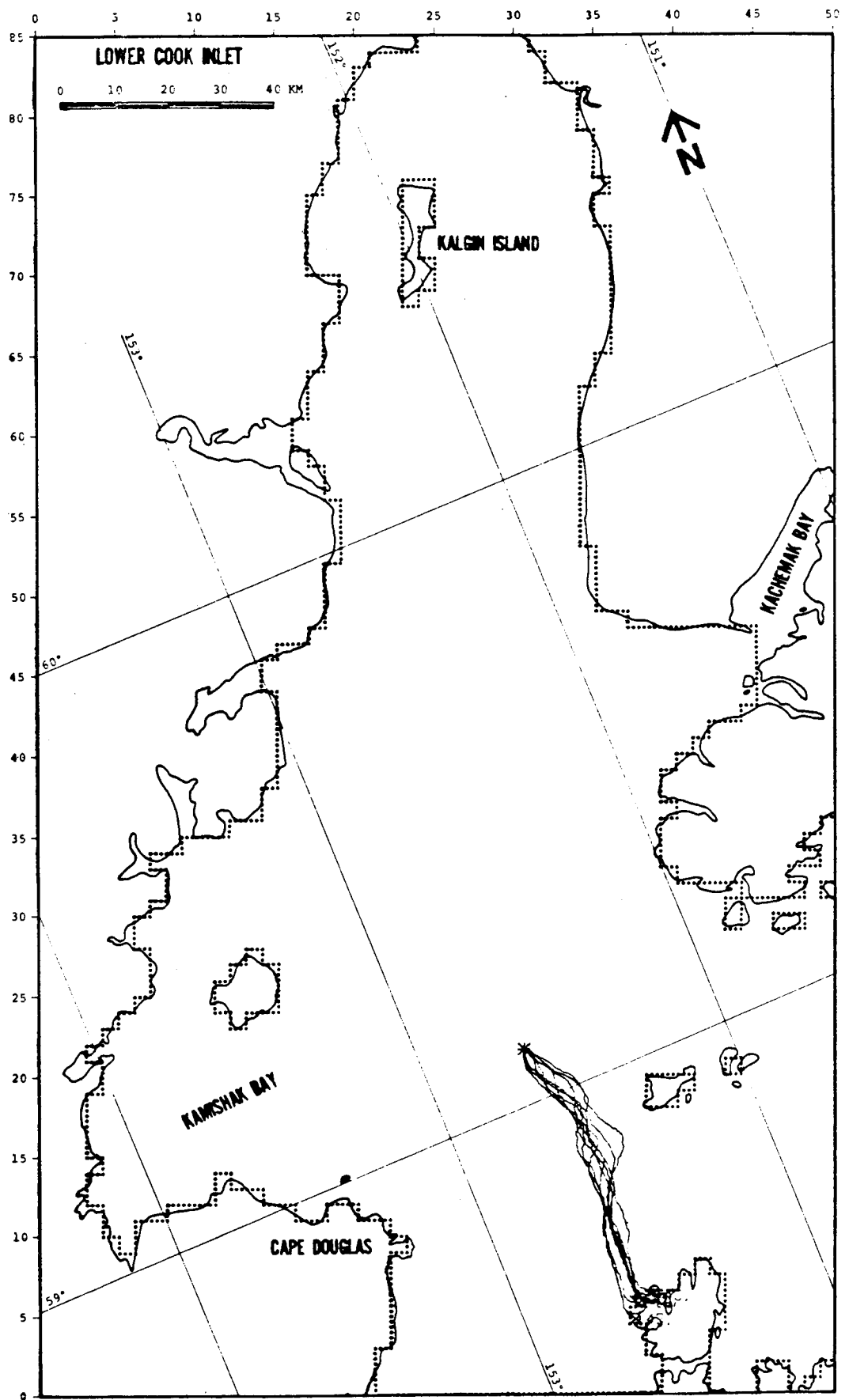


FIGURE C-74: RANDOM PERTURBATION ANALYSIS CASE

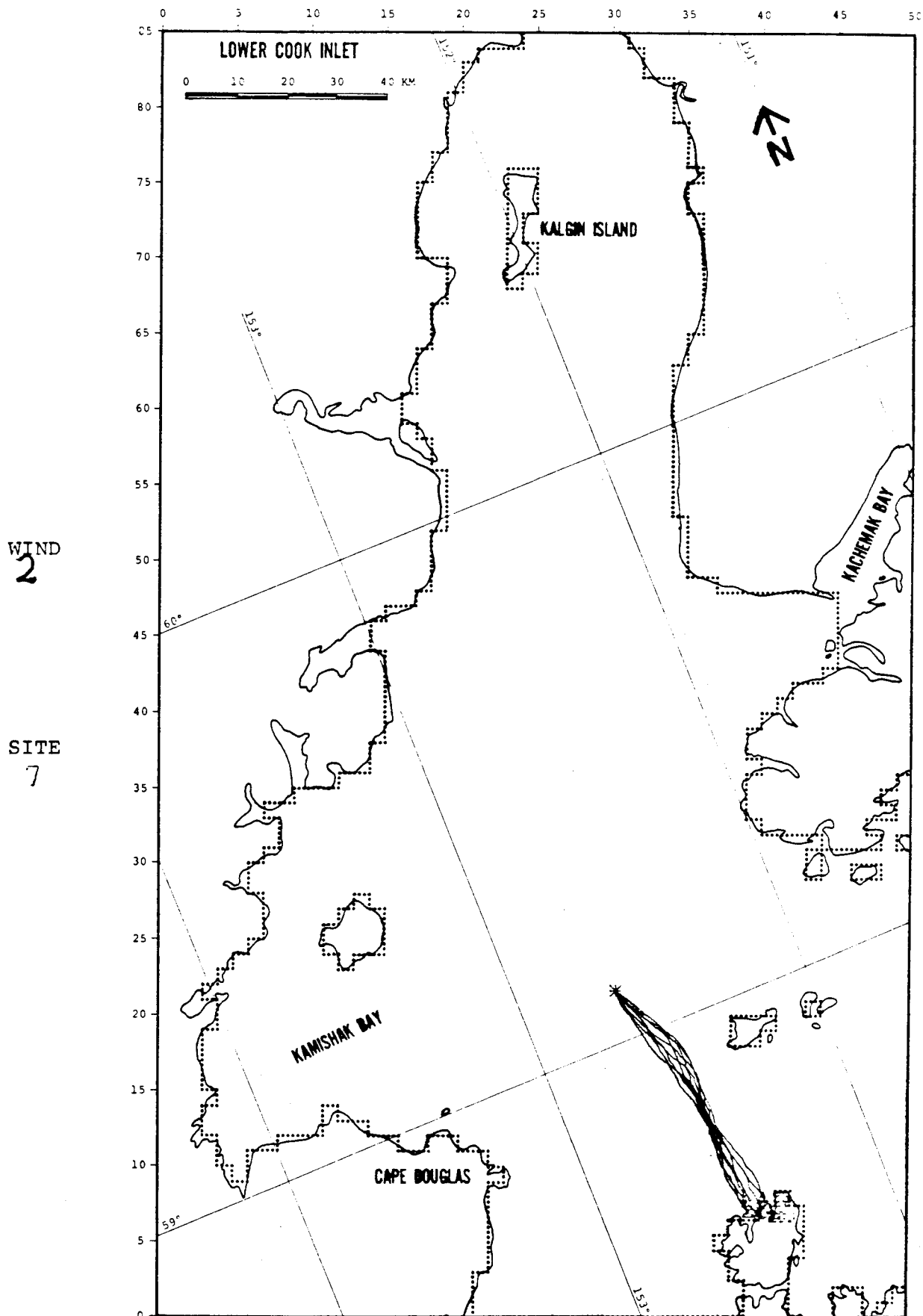


FIGURE C-75: RANDOM PERTURBATION ANALYSIS CASE

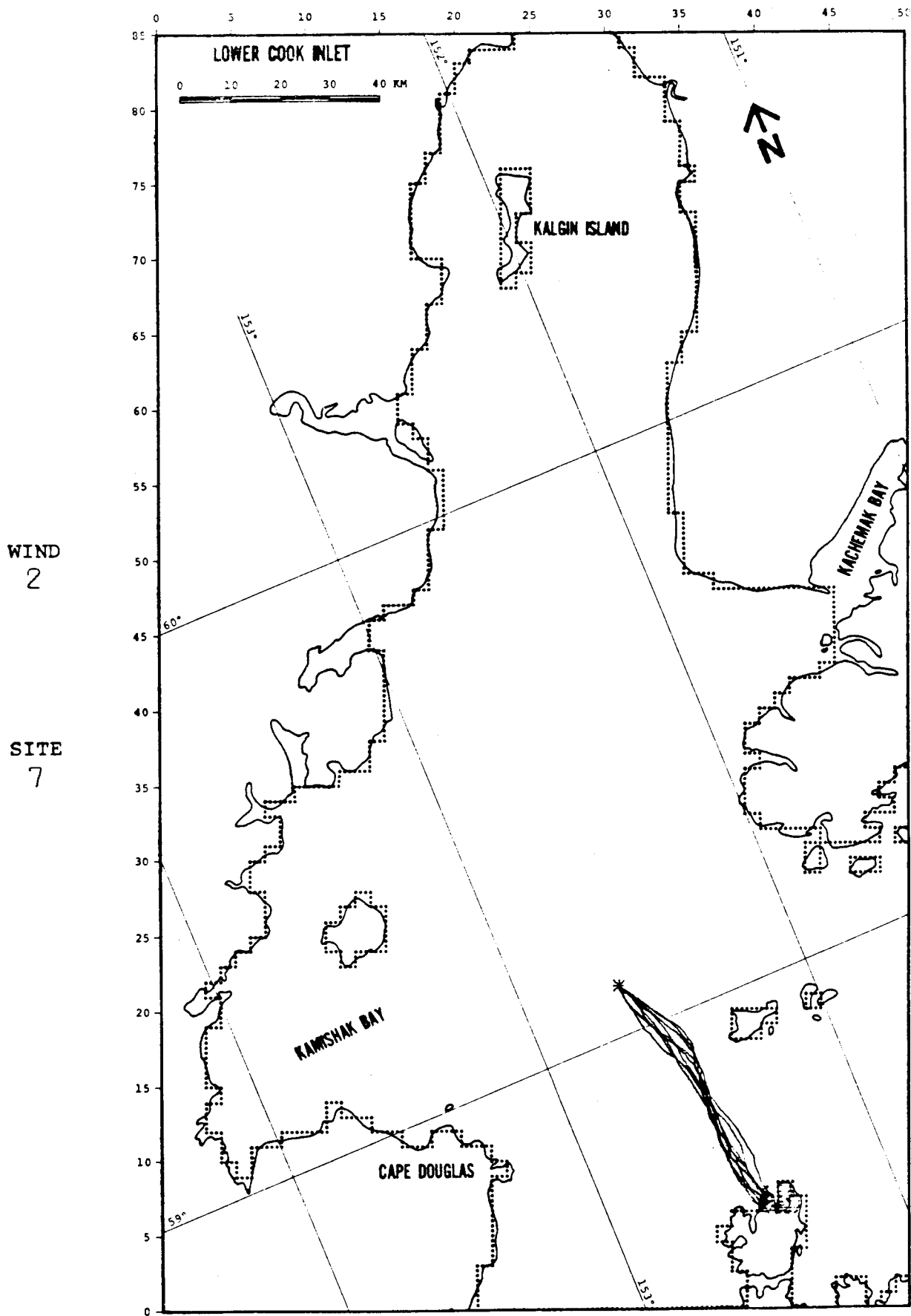


FIGURE C-76: RANDOM PERTURBATION ANALYSIS CASE
727

WIND
7

SITE
7

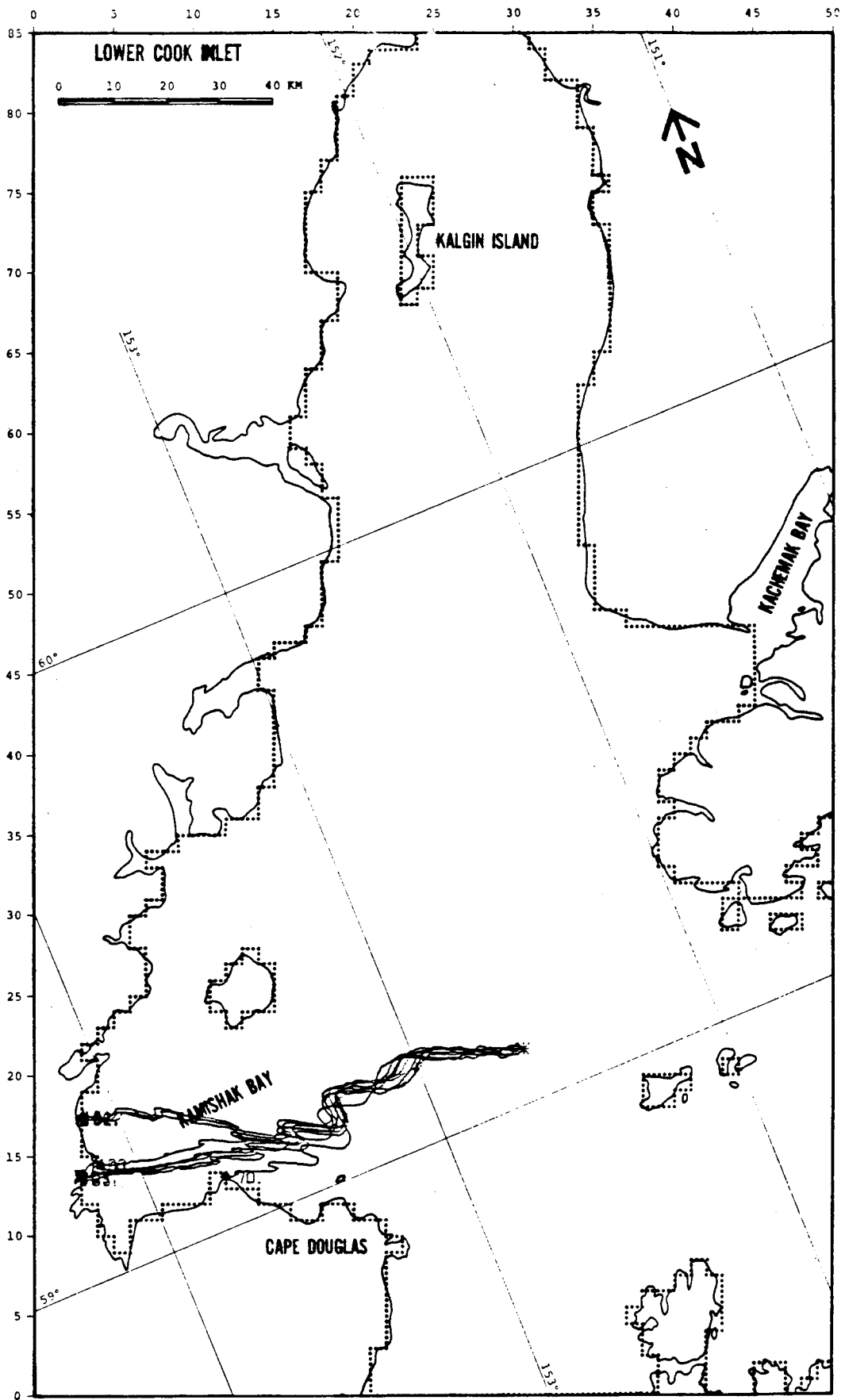


FIGURE C-77: RANDOM PERTURBATION ANALYSIS CASE

WIND
7

SITE
7

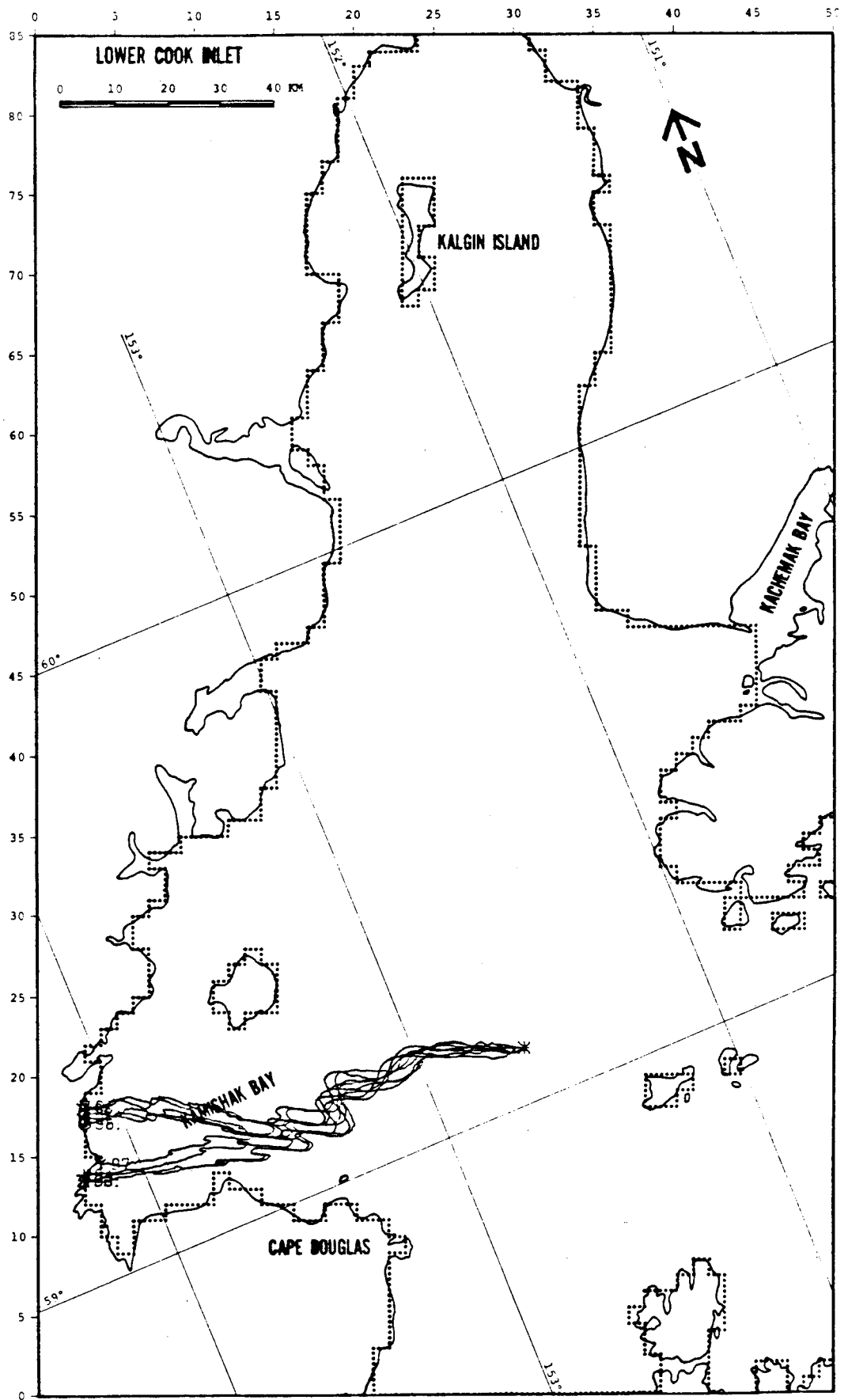


FIGURE C-78: RANDOM PERTURBATION ANALYSIS CASE

APPENDIX D

INPUT DATA FILES

Input Data Files

Input Description

Topo

- 1 water boundary
- 2 land
- 3 "invalid" water
- 4 "valid" water

Wind

- 15 wind speed in knots
- 207 wind direction in degrees
clockwise from north

Net Current

- 0.7 net current speed in km/hr
- 202 net current direction in degrees
clockwise from north

Tidal Current

- 1.3 tidal current speed in m/s
- 232 tidal current direction in degrees
clockwise from north

Y-GRID INTERSECTION

Y-GRID INTERSECTION		1.....55	
90	2	23	32
89	2	23	32
88	2	23	32
87	2	23	32
86	2	21	12
85	2	24	42
84	2	24	42
83	2	24	42
82	2	24	42
81	2	24	42
80	2	24	42
79	2	24	42
78	2	24	42
77	2	24	42
76	2	24 4224	42
75	2	24 4224	42
74	2	24 4224	42
73	2	24 424	42
72	2	24 424	42
71	2	24 4224	42
70	2	24 4224	42
69	2	24 424	42
68	2	24	42
67	2	24	42
66	2	24	42
65	2	24	42
64	2	24	42
63	2	24	42
62	2	24	42
61	2	23 32323 34	42
60	2	23 34	42
59	2	23 34	42
58	2	23 34	42
57	2	23 34	42
56	2	23 34	42
55	2	24	42
54	2	24	42
53	2	24	42
52	2	24	42
51	2	24	42
50	2	24	42
49	2	24	42
48	2	24	42
47	2	24	42
46	2	234	42
45	2	23 34	42
44	2	23 3224	42
43	2	2332 24	42
42	2	232 24	42
41	2	24	42
40	2	232 24	42
39	2	23 32 24	42
38	2	2332 24	42
37	2	232 24	432
36	2	23224	42
35	2	24	42
34	2	234	42
33	2	24	42
32	2	24	42
31	2	24	424 41
30	2	24	424422441
29	2	24	41
28	2	24 424	41
27	2	24 42224	41
26	2	24 422224	41
25	2	24 422224	41
24	2	24 424	41
23	2	24	41
22	2	24	41
21	2	24	424 41
20	2	24	42224 41
19	2	24	4224 41
18	2	24	41
17	2	24	41
16	2	24	41
15	2	24	41
14	2	24 424	41
13	2	24 42224	41
12	2	24 42 244724	41
11	2	2442 24	41
10	2	242 24	41
9	2	24	424 41
8	2	24	42 24 41
7	2	24	42 24 41
6	2	24	42 24 41
5	2	24	42 24 41
4	2	24	422224 41
3	2	732 24	422224 41
2	2	24	42224 4224421
1	2	21	1222111221221

INPUT DATA FILE: WIND PATTERN 2

Y-GRID INTERSECTION	X-GRID INTERSECTION																		
	1	4	7	10	13	16	19	22	25	28	31	34	37	40	43	46	49	52	55
91																			
88																			
85																			
82																			
79																			
76																			
73																			
70																			
67																			
64																			
61																			
58																			
55																			
52																			
49																			
46																			
43																			
40																			
37																			
34																			
31																			
28																			
25																			
22																			
19																			
16																			
13																			
10																			
7																			
4																			
1																			

INPUT DATA FILE: WIND PATTERN 3

Y-GRID INTERSECTION	X-GRID INTERSECTION																		
	1	4	7	10	13	16	19	22	25	28	31	34	37	40	43	46	49	52	55
91						10	11	12	16	19	19	16	12	17					
						16	16	18	18	18	18	25	30	40					
88						10	11	13	17	19	18	13	12	17					
						16	18	18	18	18	18	25	30	40					
85						10	12	14	19	19	17	13	12	17					
						18	18	18	18	18	18	25	30	40					
82						10	12	15	19	19	17	13	12	17					
						18	18	18	18	18	18	25	30	40					
79						10	12	15	19	19	17	14	12	17					
						18	18	18	18	18	18	25	30	40					
76						10	12	16	19	19	18	15	12	17					
						18	18	18	18	18	18	25	30	40					
73						10	12	16	19	19	18	15	12	17					
						18	18	18	18	18	18	25	30	40					
70						10	12	16	19	19	18	15	12	12					
						18	18	18	18	18	18	20	25	30					
67						10	12	16	19	19	18	15	12	17					
						15	15	15	15	15	18	20	25	30					
64						10	12	15	19	19	18	14	12	17					
						12	12	12	12	12	18	18	20	20					
61						10	10	12	15	19	18	13	12	17					
						10	10	10	10	10	10	15	15	15					
58						10	10	12	14	19	18	13	12	17	12	11	11	10	
						10	10	10	10	10	10	12	12	12	12	15	20	30	30
55						10	10	12	14	19	20	19	13	12	17	12	11	11	10
						8	8	8	8	8	8	8	10	10	10	15	20	30	30
52						10	10	12	14	19	20	19	14	12	17	12	11	11	9
						6	6	6	6	6	6	6	8	8	10	15	20	25	25
49						10	10	12	14	19	20	19	16	12	17	11	11	10	9
						6	5	5	5	6	6	8	8	8	10	15	20	25	25
46						10	10	10	12	15	18	20	19	16	12	11	10	9	9
						5	5	4	3	3	4	4	6	6	6	10	15	20	20
43						10	10	11	12	14	18	20	19	17	13	11	9	9	9
						5	5	4	2	2	2	2	2	2	2	2	2	0	0
40						10	10	11	12	14	18	20	18	14	11	9	9	9	9
						5	5	4	2	0	0	0	0	0	2	2	2	0	0
37						10	10	11	12	13	15	18	20	21	19	16	17	9	10
						4	4	4	2	0	0	0	0	0	0	355	355	350	350
34						10	10	10	11	12	13	15	18	20	21	20	17	14	11
						2	2	2	2	2	0	0	0	0	0	355	355	350	345
31						10	10	10	11	12	13	15	18	20	21	22	20	17	14
						0	2	2	2	0	0	0	0	0	0	355	350	340	345
28						10	10	11	11	12	14	16	18	21	22	22	22	20	18
						0	0	0	0	0	0	0	0	0	0	355	350	345	345
25						10	10	11	12	13	15	16	19	21	22	22	22	22	21
						355	355	355	355	355	355	355	0	0	0	0	350	345	345
22						10	10	10	11	12	14	15	17	19	20	22	22	22	22
						340	350	350	350	350	350	350	355	355	0	0	0	355	350
19						10	10	10	10	13	14	15	17	18	19	21	22	22	22
						330	330	330	340	340	340	340	350	350	355	355	0	0	355
16						10	10	10	10	12	13	14	15	16	18	19	22	22	22
						330	330	330	330	335	340	340	350	350	355	355	0	0	355
13						10	10	10	10	11	12	12	14	16	18	20	22	22	22
						330	330	330	330	335	340	345	345	350	355	355	0	0	355
10						10	10	10	10	10	11	11	12	14	16	18	21	22	22
						330	330	330	330	330	340	340	345	345	350	355	355	0	0
7																			
4																			
1																			

INPUT DATA FILE: WIND PATTERN 4

Y-GRID INTERSECTION	X-GRID INTERSECTION																			
	1	4	7	10	13	16	19	22	25	28	31	34	37	40	43	46	49	52	55	
91																				
88																				
85																				
82																				
79																				
76																				
73																				
70																				
67																				
64																				
61																				
58																				
55																				
52																				
49																				
46																				
43																				
40																				
37																				
34																				
31																				
28																				
25																				
22																				
19																				
16																				
13																				
10																				
7																				
4																				
1																				

INPUT DATA FILE: WIND PATTERN 5

Y-GRID INTERSECTION	X-GRID INTERSECTION																			
	1	4	7	10	13	16	19	22	25	28	31	34	37	40	43	46	49	52	55	
91				10	10	10	11	13	13	11	10	10								
88				15	15	15	18	20	20	25	25	30								
85				10	10	10	12	13	13	11	10	10								
82				18	18	18	20	20	20	25	25	30								
79				10	10	11	13	13	12	11	10	10								
76				20	20	20	20	20	20	25	30	35								
73				10	10	12	13	13	13	11	10	10								
70				20	20	20	20	20	20	25	30	35								
67				10	10	12	13	13	13	11	10	10								
64				22	22	20	20	20	20	25	30	35								
61				10	10	12	13	13	13	11	10	10								
58				25	25	25	23	20	20	25	30	35								
55				10	10	11	12	13	13	11	10	10								
52				0	30	30	25	23	20	30	35	40								
49				340	350	10	25	23	20	30	35	40								
46				10	10	11	12	13	13	11	10	10								
43				340	0	15	25	23	20	30	35	40								
40				10	10	11	12	13	13	12	11	10								
37				15	25	28	26	25	20	30	35	40								
34				10	10	11	13	14	13	12	11	10								
31				30	30	35	35	30	25	25	30	35								
28				10	10	10	11	13	14	13	12	11								
25				35	35	40	40	40	30	25	25	30								
22				10	10	10	12	13	14	13	12	11								
19				40	40	40	40	40	35	30	25	25								
16				10	10	11	12	14	14	14	13	13								
13				40	40	40	40	35	30	25	25	35								
10				10	10	10	12	14	14	14	13	13								
7				40	40	40	40	35	30	25	25	40								
4				10	10	10	12	13	14	14	13	12								
1				45	45	45	45	40	40	30	25	40								

INPUT DATA FILE: WIND PATTERN 6

Y-GRID INTERSECTION	1	4	7	10	13	16	19	22	25	28	31	34	37	40	43	46	49	52	55	
91						16	16	16	17	20	20	17	16	14						
						15	15	15	18	20	20	15	25	30						
88						16	16	16	18	20	20	17	16	14						
						15	15	15	18	20	20	25	25	30						
85						16	16	16	18	20	20	17	16	14						
						18	18	18	20	20	20	25	25	30						
82						16	16	17	20	20	18	17	16	14						
						20	20	20	20	20	20	25	25	30						
79						16	16	17	20	20	18	17	16	14						
						20	20	20	20	20	20	25	30	35						
76						16	16	18	20	20	20	17	16	14						
						20	20	20	20	20	20	25	30	35						
73						16	16	18	20	20	20	17	16	16						
						20	20	20	20	20	20	25	30	35						
70						16	16	18	20	20	20	17	16	16						
						20	20	20	20	20	20	25	30	35						
67						16	16	18	20	20	20	17	16	16						
						22	22	20	20	20	20	25	30	35						
64						16	16	18	20	20	20	17	19	14						
						25	25	25	23	20	20	25	30	35						
61						16	16	17	18	20	20	17	16	16						
						0	30	30	25	23	20	20	30	35	35					
58						16	16	17	18	20	20	17	16	16	16	14	17	17		
						340	350	10	25	23	20	20	30	35	40	45	45	50	50	50
55						16	16	17	18	20	20	16	17	16	16	16	17	17	16	
						340	0	15	25	23	20	20	30	35	40	45	50	50	50	
52						16	16	17	18	20	20	16	17	16	16	16	17	17	16	
						15	25	28	28	25	20	20	30	35	40	50	50	50	50	
49						16	16	17	20	21	20	18	17	16	17	18	18	17	16	
						30	30	35	35	30	25	25	30	35	45	50	50	50	50	
46						16	16	16	17	20	21	20	18	17	18	18	17	16	16	
						35	35	40	40	40	30	25	25	30	45	50	50	50	50	
43						16	16	16	16	20	21	21	20	18	20	20	17	16	16	
						40	40	40	40	35	30	25	25	35	40	50	50	50	50	
40						16	16	17	18	21	21	20	20	17	16	16	16	16		
						40	40	40	40	35	30	25	25	35	40	50	50	50	50	
37						16	16	16	18	20	21	21	20	18	16	16	16	16		
						45	45	45	40	40	30	25	25	40	50	50	50	50	50	
34						16	16	16	17	18	20	21	23	21	20	17	16	16	16	17
						50	50	50	50	50	45	40	35	25	25	45	45	45	45	45
31						16	16	16	18	18	20	21	23	21	20	17	16	16	16	17
						55	55	55	50	45	40	40	30	35	45	45	45	45	45	45
28						16	16	17	18	18	20	21	23	21	20	18	17	18	18	20
						55	55	55	50	50	45	40	30	40	45	45	45	45	45	45
25						16	17	18	18	18	20	21	23	21	20	20	20	20	20	20
						55	55	55	50	50	45	40	35	30	40	40	40	40	40	40
22						16	16	17	18	18	18	20	21	23	21	21	21	21	21	21
						55	55	60	55	50	45	45	40	30	40	40	40	40	40	40
19						16	16	17	18	18	18	20	21	23	21	21	21	21	21	21
						60	60	55	55	50	45	40	35	30	40	40	40	40	40	40
16						16	16	16	16	16	16	18	20	21	23	21	21	21	21	21
						60	60	55	55	50	45	40	30	35	40	40	40	40	40	40
13						16	16	16	16	16	16	17	20	21	23	21	21	21	21	21
						60	60	55	50	50	45	40	35	30	40	40	40	40	40	40
10						16	16	16	16	16	16	17	18	21	21	23	23	21	21	21
						60	55	55	50	50	45	40	35	35	35	35	35	35	35	35
7									16	16	17	18	21	21	21	23	21	21	21	21
									40	35	35	35	25	35	35	35	35	35	35	35
4									16	16	17	18	21	21	21	23	21	21	21	21
									35	35	35	35	25	35	35	35	35	35	35	35
1									16	16	17	18	21	21	21	23	21	21	21	21
									35	35	35	35	25	35	35	35	35	35	35	35

INPUT DATA FILE: WIND PATTERN 7

Y-GRID INTERSECTION	X-GRID INTERSECTION																			
	1	4	7	10	13	16	19	22	25	28	31	34	37	40	43	46	49	52	55	
91																				
88																				
85																				
82																				
79																				
76																				
73																				
70																				
67																				
64																				
61																				
58																				
55																				
52																				
49																				
46																				
43																				
40																				
37																				
34																				
31																				
28																				
25																				
22																				
19																				
16																				
13																				
10																				
7																				
4																				
1																				

INPUT DATA FILE: WIND PATTERN 8

91		8	9	11	12	16	18	14	11	10																		
		170	185	180	190	200	200	200	200	200	200																	
	88		8	9	11	13	18	18	13	11	10																	
			170	180	185	190	195	195	195	200	200																	
		85		8	9	11	15	18	18	12	10	10																
				170	170	180	185	190	190	195	195	195																
			82		8	9	12	15	18	18	12	10	9															
					170	170	170	180	190	190	190	190	190															
				79		8	9	12	17	18	17	12	10	9														
						170	170	170	175	180	180	180	180	185														
					76		8	9	13	17	18	16	12	10	9													
							170	170	170	170	170	170	170	170	175													
						73		8	9	14	18	18	16	12	10	9												
								165	165	165	165	165	165	165	165	165												
							70		8	9	15	18	18	15	12	10	9											
									165	160	160	160	160	160	160	160	160											
67									8	11	15	18	18	15	12	10	9											
									160	160	155	155	155	155	155	155	150											
	64								9	13	17	18	18	15	12	10	9											
									155	155	155	155	150	150	150	150	150											
		61							8	10	14	17	18	18	15	12	10	10										
									155	155	155	155	150	150	145	145	145	140										
			58						8	9	13	17	18	18	15	12	11	10	10	10	10	10	10	10	10	10	10	
									150	150	150	150	150	145	145	145	145	130	110	110	110	110	110	110	110	110	110	
				55					8	8	12	17	18	18	16	12	11	10	10	10	10	10	10	10	10	10	10	
									145	145	145	145	145	145	145	145	145	145	125	95	95	95	95	95	95	95	95	
					52				8	8	12	17	18	19	18	13	11	10	10	10	10	10	10	10	10	10	10	
									140	140	140	140	140	140	140	140	135	120	110	110	110	110	110	110	110	110	110	
						49			8	9	13	17	18	19	18	16	12	12	11	11	11	11	11	11	11	11	11	
									130	140	135	135	135	130	130	125	120	110	85	75	75	75	75	75	75	75	75	
							46		8	9	11	14	17	19	19	18	17	16	15	17	16	16	16	16	16	16	16	
									120	125	135	135	130	125	125	120	110	100	95	90	90	90	90	90	90	90	90	
43									8	10	12	15	17	20	20	19	17	16	12	9	8	8	8	8	8	8	8	
									120	130	140	140	135	130	120	110	105	100	95	90	90	90	90	90	90	90	90	
	40								8	10	11	15	18	20	21	21	19	17	16	10	8	8	8	8	8	8	8	
									120	130	135	140	140	130	120	110	105	100	95	95	90	90	90	90	90	90	90	
		37							8	9	11	13	16	19	22	22	21	20	17	11	9	8	8	8	8	8	8	
									130	130	130	130	130	130	120	110	105	100	95	95	95	95	95	95	95	95	95	
			34						8	8	10	12	16	18	21	22	22	22	20	17	17	9	9	10	11	12	12	
									130	130	130	125	125	125	125	120	110	105	100	100	100	95	95	95	95	95	95	
				31					8	9	11	14	16	18	21	22	23	22	21	18	16	15	14	14	15	15	15	
									130	130	125	125	120	120	120	115	110	105	100	100	100	100	100	95	95	95	95	
					28				8	10	12	13	15	18	20	22	23	23	22	21	19	18	18	18	18	18	18	
									125	125	125	120	120	120	115	110	110	105	100	100	100	100	100	95	95	95	95	
						25			8	11	13	13	14	18	20	22	23	24	24	24	24	22	21	21	21	21	21	
									120	120	120	115	115	115	115	110	110	110	105	100	100	100	100	100	100	95	95	
							22		8	9	12	13	15	18	20	22	23	24	25	25	25	25	25	25	25	25	25	
									120	120	120	120	115	110	110	110	100	110	105	105	105	100	100	100	100	100	100	
19									8	10	12	15	16	18	19	20	21	22	23	24	25	25	25	25	25	25	25	
									115	115	115	115	115	115	115	110	110	110	110	110	110	110	110	110	110	110	110	
	16								8	10	12	15	15	15	17	18	19	21	23	24	25	25	25	25	25	25	25	
									115	115	115	115	115	115	120	120	120	120	120	120	120	120	120	120	115	115	115	
		13							8	10	12	12	11	11	11	12	13	15	18	21	23	24	25	25	25	25	25	
									115	115	115	120	120	120	120	120	120	120	120	120	120	120	120	120	120	120	120	
			10						8	9	9	9	8	8	9	10	11	13	15	17	21	23	24	25	25	25	25	
									115	115	120	120	120	120	120	120	120	120	120	120	120	120	120	120	120	120	120	
				7					8	8	9	9	11	12	15	18	21	23	24	25	25	25	25	25	25	25	25	
									120	120	120	120	120	120	120	120	120	120	120	120	120	120	120	120	120	120	120	
					4				8	8	8	8	9	11	12	16	18	21	23	24	25	25	25	25	25	25	25	
									120	120	120	120	120	120	120	120	120	120	120	120	120	120	120	120	120	120	120	
						1			8	8	8	8	9	11	14	16	18	21	23	24	25	25	25	25	25	25	25	
									120	120	120	120	120	120	120	120	120	120	120	120	120	120	120	120	120	120	120	

INPUT DATA FILE: TIDAL CURRENT PATTERN
 PHASE = 0°
 TIME = 0.00 HRS

Y-GRID INTERSECTION	1	4	7	10	13	16	19	22	25	28	31	34	37	40	43	46	49	52	55	
85								0.0	1.3	1.6	.4	0.0								
								232	232	202	177	162								
82								0.0	.4	.5	.8	.5	.2	0.0						
								232	222	232	202	167	172	172						
79								0.0	.2	.1	.5	.4	.1	0.0						
								42	222	232	202	202	202	22						
76								0.0	.1	0.0	0.0	.2	.2	0.0	0.0					
								42	42	22	22	202	202	2	22					
73								0.0	.1	.1	0.0	0.0	0.0	.2	0.0					
								22	32	22	22	22	22	12	22					
70								0.0	.2	0.0	0.0	.1	.2	0.0						
								22	22	22	22	22	22	22						
67								0.0	.2	.2	.2	.1	.2	.4	0.0					
								52	52	22	22	22	22	32	42					
64								0.0	.3	.2	.2	.3	.4	.5	0.0					
								52	42	22	22	22	22	32	22					
61								0.0	.2	.3	.3	.4	.5	.6	0.0					
								22	7	12	22	22	22	22	22					
58								0.0	.2	.3	.4	.4	.5	.5	0.0					
								2	322	7	22	22	17	22	22					
55								0.0	.3	.4	.5	.5	.7	0.0						
								22	12	22	22	12	22	22						
52								0.0	.3	.5	.6	.6	.7	.8	0.0					
								32	22	22	22	22	15	10	22					
49								0.0	.3	.4	.6	.6	.7	.8	.8	0.0	0.0	0.0	0.0	0.0
								42	52	34	22	18	9	2	342	292	112	57		
46								0.0	.2	.4	.5	.6	.7	.7	.4	.4	0.0			
								22	13	17	22	12	4	4	1	358	53	57		
43								0.0	.2	.3	.4	.4	.6	.6	.6	.6	0.0			
								22	12	42	32	22	12	14	13	29	51	57		
40								0.0	.2	.4	.4	.5	.6	.6	.7	0.0				
								62	52	42	32	22	12	13	20	37	57			
37								0.0	.1	.3	.3	.4	.5	.5	.6	.7	.8	0.0	0.0	0.0
								82	72	52	42	32	22	12	12	12	45	22	292	292
34								0.0	.1	.2	.3	.3	.4	.5	.5	.5	.7	.8	0.0	0.0
								82	42	52	62	42	32	22	12	4	7	10	352	292
31								0.0	.2	.2	.3	.4	.4	.5	.5	.7	.9	1.0	1.0	1.5
								72	75	67	32	7	7	12	3	352	354	340	336	332
28								0.0	.4	0.0	0.0	.4	.4	.4	.4	.6	.8	.8	1.0	1.0
								22	42	52	22	352	354	356	349	342	331	320	318	312
25								0.0	.4	0.0	0.0	.3	.3	.4	.4	.5	.6	.6	.7	.7
								22	22	332	52	349	342	342	332	322	312	299	299	292
22								0.0	.1	.3	.3	.3	.3	.3	.3	.2	.2	.2	.2	0.0
								22	22	342	312	312	323	324	307	297	288	282	272	292
19								0.0	.2	.3	.3	.3	.4	.4	.5	.3	.2	.2	.2	.4
								22	342	332	322	312	322	332	333	322	282	292	292	292
16								0.0	.2	.3	.4	.5	.5	.6	.5	.4	.3	.2	.2	.4
								42	292	257	242	292	302	327	359	2	342	332	332	322
13								0.0	.1	0.0	0.0	0.0	0.0	.7	.5	.4	.3	.2	.2	.4
								332	236	242	242	292	332	342	2	2	352	342	292	292
10								0.0												
								22												
7								0.0	.3	.3	.3	.3	.3	.3	0.0	0.0	.2	.4	.6	.8
								22	22	22	22	22	22	22	332	22	342	292	292	292
4								0.0	.2	.2	.2	.2	.2	.2	0.0	0.0	.2	.2	.4	.6
								22	22	22	22	22	22	22	22	202	292	292	292	292
1								0.0	.1	.1	.1	.1	.1	.1	0.0	0.0	0.0	0.0	0.0	0.0
								22	22	22	22	22	22	22	22	202	202	292	292	292

INPUT DATA FILE: TIDAL CURRENT PATTERN

PHASE = 90°

TIME = 3.11 HRS

Y-GRID INTERSECTION	1	4	7	10	13	16	19	22	25	28	31	34	37	40	43	46	49	52	55	58	61	64	67	70	73	76	79	82	85		
85								0.0	2.3	2.8	1.5	0.0																			
								52	52	22	357	342																			
82								0.0	1.1	1.7	1.8	1.7	1.1	0.0																	
								52	72	52	22	7	352	352																	
79								0.0	1.3	1.5	1.6	1.6	1.3	0.0																	
								42	52	62	22	12	352	22																	
76								0.0	1.1	1.3	0.0	1.4	1.6	1.3	0.0																
								42	42	22	22	22	12	2	22																
73								0.0	1.1	1.3	0.0	1.4	1.5	1.1	0.0																
								22	32	22	22	22	22	12	22																
70								0.0	1.8	0.0	1.2	1.3	1.1	0.0																	
								22	22	22	22	22	22	22																	
67								0.0	.9	1.0	.9	1.0	1.1	1.0	0.0																
								52	52	22	22	22	22	32	42																
64								0.0	.8	.8	1.0	1.1	1.1	1.0	0.0																
								52	42	22	22	22	22	32	22																
61								0.0	.5	.8	1.0	1.0	1.0	.8	0.0																
								22	7	12	22	22	22	22	22																
58								0.0	.6	.8	.9	.9	1.0	.7	0.0																
								2	322	7	22	22	17	22	22																
55								0.0	.7	.9	.9	.9	.7	0.0																	
								22	12	22	22	12	22	22																	
52								0.0	.6	.9	1.0	1.1	.9	.7	0.0																
								32	22	22	22	22	15	10	22																
49								0.0	.5	.6	.8	.6	.7	.6	.5	0.0	0.0	0.0													
								42	52	34	22	18	9	2	342	292	112	57													
46								0.0	.2	.6	.6	.6	.5	.4	.2	.1	.1	0.0													
								22	13	17	22	12	4	4	1	358	53	57													
43								0.0	.2	.4	.5	.4	.5	.4	.3	.2	.1	0.0													
								22	12	42	32	22	12	14	13	29	51	57													
40								0.0	.2	.4	.4	.4	.3	.2	.1	0.0															
								62	52	42	32	22	12	13	20	37	57														
37								0.0	.1	.2	.3	.3	.3	.2	.1	0.0															
								82	72	52	42	32	22	12	12	12	45	22													
34								0.0	.1	.1	.2	.2	.3	.3	.2	.2	.1	0.0	0.0	0.0	0.0	0.0	0.0	0.0	0.0	0.0	0.0	0.0	0.0	0.0	
								82	42	52	62	42	32	22	12	4	7	10	172	112	112	72	112	112							
31								0.0	.1	.1	.2	.2	.2	.2	.1	.1	.1	0.0	0.0	0.0	0.0	0.0	0.0	0.0	0.0	0.0	0.0	0.0	0.0	0.0	
								72	75	67	32	7	7	12	3	356	354	340	156	152	172	167	132	112							
28								0.0	.2	0.0	0.0	.2	.2	.2	.2	.1	.1	.1	0.0	0.0	0.0	0.0	0.0	0.0	0.0	0.0	0.0	0.0	0.0	0.0	
								22	42	52	22	352	354	356	349	342	331	320	318	132	132	122	117	112							
25								0.0	.2	0.0	0.0	.1	.1	.1	.1	.1	.1	0.0	0.0	0.0	0.0	0.0	0.0	0.0	0.0	0.0	0.0	0.0	0.0	0.0	
								22	22	332	57	349	342	342	332	322	312	299	299	112	112	112	112	112							
22								0.0	.1	.1	.1	.1	.1	.1	0.0	0.0	0.0	0.0	0.0	0.0	0.0	0.0	0.0	0.0	0.0	0.0	0.0	0.0	0.0	0.0	
								22	22	22	342	312	317	323	329	307	297	288	282	272	112	82	112	112	112						
19								0.0	.1	.1	.1	.1	.1	.1	0.0	0.0	0.0	0.0	0.0	0.0	0.0	0.0	0.0	0.0	0.0	0.0	0.0	0.0	0.0	0.0	
								22	342	332	322	312	312	322	332	333	322	288	292	292	112	112	112	112	112						
16								0.0	.1	.1	.1	.2	.2	.1	.1	.1	.1	0.0	0.0	0.0	0.0	0.0	0.0	0.0	0.0	0.0	0.0	0.0	0.0	0.0	
								42	242	257	292	292	302	327	354	2	342	332	332	322	112	112	112	112	112						
13								0.0	.1	0.0	0.0	0.0	0.0	.1	.1	0.0	0.0	0.0	0.0	0.0	0.0	0.0	0.0	0.0	0.0	0.0	0.0	0.0	0.0	0.0	
								332	236	282	242	292	292	332	342	2	2	352	342	112	112	112	112	112	112						
10								0.0																							
								22																							
7								0.0	0.0	0.0	0.0	0.0	0.0	0.0	0.0	0.0	0.0	0.0	0.0	0.0	0.0	0.0	0.0	0.0	0.0	0.0	0.0	0.0	0.0	0.0	
								22	22	22	202	202	202	202	202	202	202	202	202	202	162	112	112	112	112						
4								0.0	0.0	0.0	0.0	0.0	0.0	0.0	0.0	0.0	0.0	0.0	0.0	0.0	0.0	0.0	0.0	0.0	0.0	0.0	0.0	0.0	0.0	0.0	
								202	202	202	202	202	202	202	202	202	202	202	202	202	22	112	112	112	112						
1								0.0	0.0	0.0	0.0	0.0	0.0	0.0	0.0	0.0	0.0	0.0	0.0	0.0	0.0	0.0	0.0	0.0	0.0	0.0	0.0	0.0	0.0	0.0	
								202	202	202	202	202	202	202	202	202	202	202	202	202	22	22	112	112	11						

INPUT DATA FILE: TIDAL CURRENT PATTERN

PHASE = 270°

TIME = 9.32 HRS

Y-GRID INTERSECTION	X-GRID INTERSECTION																			
	1	4	7	10	13	16	19	22	25	28	31	34	37	40	43	46	49	52	55	
85																				0.0 2.3 2.4 1.5 0.0 232 232 202 177 162
82																				0.0 1.1 1.7 1.8 1.7 1.1 0.0 232 222 232 202 187 172 172
79																				0.0 1.3 1.5 1.6 1.6 1.3 0.0 222 222 232 202 202 202 202
76																				0.0 1.1 1.3 0.0 1.4 1.6 1.3 0.0 222 222 202 202 202 202 202
73																				0.0 1.1 1.3 0.0 1.4 1.5 1.1 0.0 202 212 202 202 212 202 202 202
70																				0.0 1.8 0.0 1.2 1.3 1.1 0.0 202 202 202 212 202 202 202
67																				0.0 .9 1.0 .9 1.0 1.1 1.0 0.0 232 232 202 202 212 202 212 222
64																				0.0 .8 .6 1.0 1.1 1.1 1.0 0.0 232 222 202 202 202 202 212 202
61																				0.0 .5 .6 1.0 1.0 1.0 .8 0.0 202 187 192 202 202 202 202 202
58																				0.0 .6 .8 .9 .9 1.0 .7 0.0 187 142 202 202 202 202 202 202
55																				0.0 .7 .9 .9 .9 .7 0.0 202 202 202 202 202 202 202
52																				0.0 .5 .9 1.0 1.1 .9 .7 0.0 212 202 202 202 202 195 190 202
49																				0.0 .5 .6 .6 .8 .7 .6 .5 0.0 0.0 0.0 222 232 214 202 198 182 162 162 112 292 237
46																				0.0 .2 .6 .6 .6 .5 .4 .2 .1 .1 0.0 202 193 197 202 192 164 184 181 178 233 237
43																				0.0 .2 .4 .5 .4 .5 .4 .3 .2 .1 0.0 212 192 222 212 202 192 194 193 209 231 237
40																				0.0 .2 .4 .4 .4 .4 .3 .2 .1 0.0 242 232 212 202 202 192 193 200 217 237
37																				0.0 .1 .2 .3 .3 .3 .3 .2 .1 0.0 0.0 0.0 262 252 232 202 202 202 192 192 192 225 202 292 292
34																				0.0 .1 .1 .2 .2 .3 .3 .3 .2 .2 .1 0.0 0.0 0.0 0.0 0.0 0.0 262 202 232 242 202 202 202 192 184 187 190 352 292 292 252 292 292
31																				0.0 .1 .1 .2 .2 .2 .2 .2 .1 .1 .1 0.0 0.0 0.0 0.0 0.0 0.0 262 202 237 192 187 187 192 183 178 174 160 336 332 352 347 312 292
28																				0.0 .2 0.0 0.0 .2 .2 .2 .2 .1 .1 .1 0.0 0.0 0.0 0.0 0.0 0.0 202 202 232 202 187 182 176 169 162 151 140 138 312 312 302 297 292
25																				0.0 .2 0.0 0.0 .1 .1 .1 .1 .1 .1 .1 0.0 0.0 0.0 0.0 0.0 0.0 202 202 152 232 169 162 162 152 139 132 119 119 292 292 292 292 292
22																				0.0 .1 .1 .1 .1 .1 .1 .1 .1 .1 0.0 0.0 0.0 0.0 0.0 0.0 0.0 202 162 152 142 142 137 143 144 127 117 108 102 92 292 262 292 292 292
19																				0.0 .1 .1 .1 .1 .1 .1 .1 .1 .1 0.0 0.0 0.0 0.0 0.0 0.0 0.0 202 132 122 127 132 137 150 152 152 142 140 112 112 292 292 292 292 292
16																				0.0 .1 .1 .1 .2 .2 .1 .1 .1 .1 0.0 0.0 0.0 0.0 0.0 0.0 0.0 222 112 112 112 127 132 157 179 162 162 152 152 142 292 292 292 292 292
13																				0.0 .1 0.0 0.0 0.0 0.0 0.0 .1 .1 0.0 0.0 0.0 0.0 0.0 0.0 0.0 0.0 152 56 102 112 112 112 152 162 172 182 172 162 292 292 292 292 292
10																				0.0 202 0.0 0.0 0.0 0.0 0.0 0.0 0.0 0.0 0.0 0.0 0.0 0.0 0.0 0.0 0.0 202 202 202 202 187 2 322 302 292 292 292 292
7																				0.0 0.0 0.0 0.0 0.0 0.0 0.0 0.0 0.0 0.0 0.0 0.0 0.0 0.0 0.0 202 202 202 22 22 22 332 22 342 292 292 292
4																				0.0 0.0 0.0 0.0 0.0 0.0 0.0 0.0 0.0 0.0 0.0 0.0 0.0 0.0 0.0 22 22 22 22 22 22 22 202 292 292 292 292
1																				0.0 0.0 0.0 0.0 0.0 0.0 0.0 0.0 0.0 0.0 0.0 0.0 0.0 0.0 0.0 22 22 22 26 22 22 22 202 202 292 292 292

X-GRID INTERSECTION